

Springer Tracts in Modern Physics 274

Friedrich Jegerlehner

The Anomalous Magnetic Moment of the Muon

Second Edition

 Springer

Springer Tracts in Modern Physics

Volume 274

Series editors

Yan Chen, Department of Physics, Fudan University, Shanghai, China

Atsushi Fujimori, Department of Physics, University of Tokyo, Tokyo, Japan

Thomas Müller, Institut für Experimentelle Kernphysik, Universität Karlsruhe,
Karlsruhe, Germany

William C. Stwalley, Storrs, CT, USA

Springer Tracts in Modern Physics provides comprehensive and critical reviews of topics of current interest in physics. The following fields are emphasized:

- Elementary Particle Physics
- Condensed Matter Physics
- Light Matter Interaction
- Atomic and Molecular Physics
- Complex Systems
- Fundamental Astrophysics

Suitable reviews of other fields can also be accepted. The Editors encourage prospective authors to correspond with them in advance of submitting a manuscript. For reviews of topics belonging to the above mentioned fields, they should address the responsible Editor as listed in “Contact the Editors”.

More information about this series at <http://www.springer.com/series/426>

Friedrich Jegerlehner

The Anomalous Magnetic Moment of the Muon

Second Edition

 Springer

Friedrich Jegerlehner
Institut für Physik
Humboldt-Universität zu Berlin
Berlin
Germany

and

Deutsches Elektronen-Synchrotron (DESY)
Zeuthen
Germany

ISSN 0081-3869 ISSN 1615-0430 (electronic)
Springer Tracts in Modern Physics
ISBN 978-3-319-63575-0 ISBN 978-3-319-63577-4 (eBook)
DOI 10.1007/978-3-319-63577-4

Library of Congress Control Number: 2017946671

1st edition: © Springer-Verlag Berlin Heidelberg 2008

2nd edition: © Springer International Publishing AG 2017

This work is subject to copyright. All rights are reserved by the Publisher, whether the whole or part of the material is concerned, specifically the rights of translation, reprinting, reuse of illustrations, recitation, broadcasting, reproduction on microfilms or in any other physical way, and transmission or information storage and retrieval, electronic adaptation, computer software, or by similar or dissimilar methodology now known or hereafter developed.

The use of general descriptive names, registered names, trademarks, service marks, etc. in this publication does not imply, even in the absence of a specific statement, that such names are exempt from the relevant protective laws and regulations and therefore free for general use.

The publisher, the authors and the editors are safe to assume that the advice and information in this book are believed to be true and accurate at the date of publication. Neither the publisher nor the authors or the editors give a warranty, express or implied, with respect to the material contained herein or for any errors or omissions that may have been made. The publisher remains neutral with regard to jurisdictional claims in published maps and institutional affiliations.

Printed on acid-free paper

This Springer imprint is published by Springer Nature
The registered company is Springer International Publishing AG
The registered company address is: Gewerbestrasse 11, 6330 Cham, Switzerland

The closer you look the more there is to see

Preface to the Second Edition

Ten years later, where are we? Why a second edition? The two next generation muon $g - 2$ experiments at Fermilab in the US and at J-PARC in Japan have been designed to reach a four times better precision of 16×10^{-11} (from 0.54 ppm to 0.14 ppm) and the challenge for the theory side is to keep up in precision if possible. This has triggered a lot of new research activities which justify an update of the first edition. The main motivation is the persisting 3 to 4 σ deviation between standard theory and experiment. As Standard Model predictions almost without exception match perfectly all experimental information, the deviation in one of the most precisely measured quantities in particle physics remains a mystery and inspires the imagination of model builders. A flush of speculations are aiming to explain what beyond the Standard Model effects could fill the gap. Here very high precision experiments are competing with searches for new physics at the high energy frontier set by the Large Hadron Collider at CERN. Actually, the tension is increasing day-by-day as no new states are found which could accommodate the $(g_\mu - 2)$ discrepancy. With the new muon $g - 2$ experiments this discrepancy would go up at least to 6 to 10 σ , in case the central values do not move, the 10 σ could be reached if the present theory error could be reduced by a factor of two.

The anomalous magnetic moment of the muon is a number represented by an overlay of a large number of individual quantum corrections, which depend on a few fundamental parameters. An update of the latter actually changes almost all numbers in the last digits. Besides this, there has been remarkable progress in the calculation of the higher order corrections. Aoyama, Hayakawa, Kinoshita and Nio managed to evaluate the five-loop QED correction, which includes about 13 000 diagrams and which account for a small 5×10^{-11} , thereby reducing the uncertainty of the QED part which has been dominated by the missing $O(\alpha^5)$ correction. More recently a seminal article by Laporta the essentially exact universal 4-loop contribution has been presented. The corresponding contributions to the electron $g - 2$ together with the extremely precise determination of $(g_e - 2)$ by Gabrielse et al. allows one to determine a more precise value of the fine structure constant α , which

in turn affect the numbers predicted for $(g_\mu - 2)$. Also more precise lepton mass ratios recommended by the CODATA group are slightly affecting the predictions. To the weak interaction contribution the uncertainty could be reduced mainly because of the fact that after the discovery of the Higgs particle by ATLAS and CMS at the Large Hadron Collider at CERN, the last relevant missing Standard Model parameter could be determined with remarkable precision.

Still the largest uncertainties in the SM prediction come from the leading hadronic contributions: the hadronic vacuum polarization and the hadronic light-by-light scattering insertions. The hadronic vacuum polarization at $O(\alpha^2)$, evaluated in terms of e^+e^- -annihilation data via a dispersion relation has been improved substantially mainly with new data from initial state radiation approach that the Φ factory DAFNE at Frascati with the KLOE detector and at the B factory at SLAC with the BaBar detector. Lately also new results from BEPC-II at Beijing with the BES-III detector and from VEPP-2000 at Novosibirsk with the CMD-3 and SND detectors contributed to further reduce the uncertainties. On the theory side the τ -decay spectra versus e^+e^- -annihilation data which should essentially agree after an isospin rotation has been resolved by including missing $\gamma - \rho^0$ mixing effects. Besides the NLO vacuum polarization new the NNLO amounting to 12×10^{-11} roughly a 1σ effects has been calculated by Kurz et al. recently. In the meantime also non-perturbative ab initio lattice QCD calculations come closer to be competitive with the e^+e^- -data based approach. I therefore included an introduction to the lattice QCD approach at the end of Chap. 5. The activity here has been dramatically developed. While ten years ago there has been essentially one group only active, now there are a least six groups competing.

The most challenging problem remains the hadronic light-by-light contribution of $O(\alpha^3)$. Unlike the hadronic vacuum polarization which is a one scale problem, the hadronic light-by-light scattering involves three different scales and there are many different hadronic channels contributing. The only fairly complete calculations are based on low energy effective hadronic models, which unfortunately still are not constrained by data to a satisfactory degree. Quite recently, a new approach has been worked out by Colangelo, Hoferichter, Procura and Stoffer, and Pauk and Vanderhaeghen which attempts to rely completely on hadronic light-by-light scattering data in conjunction with dispersion relations. This sounds to implement the successful hadronic vacuum polarization technique to the multi channel multi scale light-by-light case. Apart from being much more elaborate the data pool is by far not as complete as in the e^+e^- data case. In spite of the fact that data for a complete evaluation are largely missing there is definitely progress possible with exploiting existing data for $\gamma\gamma \rightarrow \pi^+\pi^-, \pi^0\pi^0$ in particular, where new data from Belle are of good quality, which allows one to get more solid evaluations than existing ones. For the singly tagged pion transition form factor there have been new useful data from BaBar and Belle which cover a much larger energy range now. Also in this case lattice QCD starts to be a new player in the field, and first useful

information concerning the doubly tagged pion transition form factor has been evaluated and provides an important new constraint.

The main focus of the book is a detailed account of the Standard Model prediction.

Acknowledgements and Thanks

For numerous discussions which have been helpful in preparing the second edition I thank Oliver Baer, Maurice Benayoun, Christine Davies, Karl Jansen, Laurent Lellouch, Harvey Meyer, Andreas Nyffeler, Massimo Passera, Graziano Venanzoni and Hartmut Wittig.

I gratefully acknowledge the support of our topical workshop¹ on *Hadronic contributions to the muon anomalous magnetic moment: strategies for improvements of the accuracy of the theoretical prediction*, 1–5 April 2014, Waldthausen Castle near Mainz, by the PRISMA Cluster of Excellence, the Mainz Institute for Theoretical Physics MITP, and the Deutsche Forschungsgemeinschaft DFG through the Collaborative Research Center *The Low-Energy Frontier of the Standard Model* (SFB 1044).

Wildau/Berlin, Germany
March 2017

Friedrich Jegerlehner

¹Organized by: Tom Blum, Univ. of Connecticut; Simon Eidelman, INP Novosibirsk; Fred Jegerlehner, HU Berlin; Dominik Stöckinger, TU Dresden; Achim Denig, Marc Vanderhaeghen, JGU Mainz (see <https://indico.mitp.uni-mainz.de/event/13/>).

Preface to the First Edition

It seems to be a strange enterprise to attempt write a physics book about a single number. It was not my idea to do so, but why not. In mathematics, maybe, one would write a book about π . **Certainly, the muon's anomalous magnetic moment is a very special number and today reflects almost the full spectrum of effects incorporated in today's Standard Model (SM) of fundamental interactions, including the electromagnetic, the weak and the strong forces.** The muon $g - 2$, how it is also called, is a truly fascinating theme both from an experimental and from a theoretical point of view and it has played a crucial role in the development of QED which finally developed into the SM by successive inclusion of the weak and the strong interactions. The topic has fascinated a large number of particle physicists last but not least it was always a benchmark for theory as a monitor for effects beyond what was known at the time. As an example, nobody could believe that a muon is just a heavy version of an electron, why should nature repeat itself, it hardly can make sense. The first precise muon $g - 2$ experiment at CERN answered that question: yes the muon is just a heavier replica of the electron! Today we know we have a 3-fold replica world, there exist three families of leptons, neutrinos, up-quarks and down-quarks, and we know we need them to get in a way for free a tiny breaking at the per mill level of the fundamental symmetry of time-reversal invariance, by a phase in the family mixing matrix. At least three families must be there to allow for this possibility. This symmetry breaking also know as CP-violation is mandatory for the existence of all normal matter in our universe which clustered into galaxies, stars, planets, and after all allowed life to develop. Actually, this observed matter-antimatter asymmetry, to our present knowledge, cries for additional CP violating interactions, beyond what is exhibited in the SM. And maybe it is a_μ which already gives us a hint how such a basic problem could find its solution. **The muon was the first replica particle found. At the time, the existence of the muon surprised physicists so much that the Nobel laureate Isidor I. Rabi exclaimed, "Who ordered that?"** But the muon is special in many other respects and its unique properties allow us to play experiment and theory to the extreme in precision.

One of the key points of the anomalous magnetic moment is its simplicity as an observable. It has a classical static meaning while at the same time it is a highly non-trivial quantity reflecting the quantum structure of nature in many facets. This simplicity goes along with an unambiguous definition and a well understood quasi classical behavior in a static perfectly homogeneous magnetic field. At the same time the anomalous magnetic moment is tricky to calculate in particular if one wants to know it precisely. To start with, the problem is the same as for the electron, and how tricky it was one may anticipate if one considers the 20 years it took for the most clever people of the time to go from Dirac's prediction of the gyromagnetic ratio $g = 2$ to the anomalous $g - 2 = \alpha/\pi$ of Schwinger.

Today the single number $a_\mu = (g_\mu - 2)/2$ in fact is an overlay of truly many numbers, in a sense hundreds or thousands (as many as there are Feynman diagrams contributing), of different signs and sizes and only if each of these numbers is calculated with sufficient accuracy the correct answer can be obtained; if one single significant contribution fails to be correct also our single number ceases to have any meaning beyond that wrong digit. So high accuracy is the requirement and challenge.

For the unstable short lived muon which decays after about 2 micro seconds, for a long time nobody knew how one could measure its anomalous magnetic moment. Only when parity violation was discovered by end of the 1950's one immediately realized how to polarize muons and how to study the motion of the spin in a magnetic field and to measure the Larmor precession frequency which allows to extract a_μ . The muon $g - 2$ is very special, it is in many respect much more interesting than the electron $g - 2$, and the $g - 2$ of the τ , for example, we are not even able to confirm that $g_\tau \sim 2$ because the τ is by far too short lived to allow for a measurement of its anomaly with presently available technology. So the muon is a real lucky case as a probe for investigating physics at the frontier of our knowledge. By now, with the advent of the recent muon $g - 2$ experiment, performed at Brookhaven National Laboratory with an unprecedented precision of 0.54 parts per million, the anomalous magnetic moment of the muon is not only one of the most precisely measured quantities in particle physics, but theory and experiment lie apart by three standard deviations, the biggest "discrepancy" among all well measured and understood precision observables at present.

This promises nearby new physics, which future accelerator experiments are certainly going to disentangle. It may indicate that we are at the beginning of a new understanding of fundamental physics beyond or behind the SM. Note however, that this is a small deviation and usually a 5 standard deviation is required to be accepted as a real deviation, i.e. there is a small chance that the gap is a statistical fluctuation only.

One would expect that it is very easy to invent new particles and/or interactions to account for the missing contribution from the theory side. Surprisingly other experimental constraints, in particular the absence of any other real deviation from the SM makes it hard to find a simple explanation. Most remarkable, in spite of these tensions between different experiments, the minimal supersymmetric

extension of the standard model, which promised new physics to be “around the corner”, is precisely what could fit. So the presently observed deviation in $g - 2$ of the muon feeds hopes that the end of the SM is in sight.

About the book: in view of the fact that there now exist a number of excellent more or less extended reviews, rather than adding another topical report, I tried to write a self-contained book not only about the status of the present knowledge on the anomalous magnetic moment of the muon, but also remembering the reader about its basic context and its role it played in developing the basic theoretical framework of particle theory. After all, the triumph this scientific achievement marks, for both theory and experiment, has its feedback on its roots as it ever had in the past. I hope it makes the book more accessible for non-experts and it is the goal to reach a broader community to learn about this interesting topic without compromising with respect to provide a basic understanding of what it means.

So the book is addressed to graduate students and experimenters interested in deepening some theoretical background and to learn in some detail how it really works. Thus, the book is not primarily addressed to the experts, but nevertheless gives an up-to-date status report on the topic. Knowledge of special relativity and quantum mechanics and a previous encounter with QED are expected.

While the structural background of theory is indispensable for putting into perspective its fundamental aspects, it is in the nature of the theme that numbers and the comparison with the experiment play a key role in this book.

The book is organized as follows: Part I presents a brief history of the subject followed in Chap. 2 by an outline of the concepts of quantum field theory and an introduction into QED including one-loop renormalization and a calculation of the leading lepton anomaly as well as some tools like the renormalization group, scalar QED for pions and a sketch of QCD. Chapter 3 first discusses the motion of leptons in an external field in the classical limit and then overviews the profile of the physics which comes into play and what is the status for the electron and the muon $g - 2$'s. The basic concept and tools for calculating higher order effects are outlined.

In Part II the contributions to the muon $g - 2$ are discussed in detail. Chapter 4 reviews the QED calculations. Chapter 5 is devoted to the hadronic contributions in particular to the problems of evaluating the leading vacuum polarization contributions from electron-positron annihilation data. Also hadronic light-by-light scattering is critically reviewed. Chapter 6 describes the principle of the experiment in some detail as well as some other background relevant for determining $g_\mu - 2$. The final Chap. 7 gives a detailed comparison of theory with the experiment and discusses possible impact for physics beyond the standard theory and future perspectives.

Acknowledgements and Thanks

It is a pleasure to thank all my friends and colleagues for the many stimulating discussions which contributed to the existence of this book. I am specially grateful to my colleagues at the Humboldt University at Berlin for the kind hospitality and support.

For careful and critical reading of various chapters of the manuscript my special thanks go to Oliver Baer, Beat Jegerlehner, Dominik Stöckinger, Oleg Tarasov and Graziano Venanzoni. I am particularly grateful to Wolfgang Kluge for his invaluable help in preparing the manuscript, for his careful reading of the book, his continuous interest, critical remarks, for many interesting discussions and advice.

I have particularly profited from numerous enlightening discussions with Simon Eidelman, Andreas Nyffeler, Heiri Leutwyler, Jürg Gasser, Gilberto Colangelo, Klaus Jungmann, Klaus Mönig, Achim Stahl, Mikhail Kalmykov, Rainer Sommer and Oleg Tarasov.

Thanks to B. Lee Roberts and members of the E821 collaboration for many helpful discussions over the years and for providing me some of the illustrations. I am grateful also to Keith Olive, Dominik Stöckinger and Sven Heinemeyer for preparing updated plots which are important additions to the book. Many thanks also to Günter Werth and his collaborators who provided the pictures concerning the electron and ion traps and for critical comments.

I have received much stimulation and motivation from my visits to Frascati and I gratefully acknowledge the kind hospitality extended to me by Frascati National Laboratory and the KLOE group.

Much pleasure came with the opportunities of European Commission's Training and Research Networks EURODAFNE and EURIDICE under the guidance of Giulia Pancheri and the TARI Project lead by Wolfgang Kluge which kept me in steady contact with a network of colleagues and young researchers which have been very active in the field and contributed substantially to the progress. In fact results from the Marseille, Lund/Valencia, Bern, Vienna, Karlsruhe/Katowice, Warsaw and Frascati nodes were indispensable for preparing this book. The work was supported in part by EC-Contracts HPRN-CT-2002-00311 (EURIDICE) and RII3-CT-2004-506078 (TARI).

Ultimately, my greatest thanks go to my wife Marianne whose constant encouragement, patience and understanding was essential for the completion of this book.

Wildau/Berlin, Germany
March 2007

Friedrich Jegerlehner

Contents

Part I Basic Concepts, Introduction to QED, $g - 2$ in a Nutshell, General Properties and Tools

1	Introduction	3
	References	18
2	Quantum Field Theory and Quantum Electrodynamics	23
2.1	Quantum Field Theory Background	23
2.1.1	Concepts, Conventions and Notation	23
2.1.2	C, P, T and CPT	31
2.2	The Origin of Spin	36
2.3	Quantum Electrodynamics	47
2.3.1	Perturbation Expansion, Feynman Rules	50
2.3.2	Transition Matrix-Elements, Particle-Antiparticle Crossing	55
2.3.3	Cross Sections and Decay Rates	58
2.4	Regularization and Renormalization	60
2.4.1	The Structure of the Renormalization Procedure	60
2.4.2	Dimensional Regularization	64
2.5	Tools for the Evaluation of Feynman Integrals	71
2.5.1	$\epsilon = 4 - d$ Expansion, $\epsilon \rightarrow +0$	71
2.5.2	Bogolubov-Schwinger Parametrization	72
2.5.3	Feynman Parametric Representation	73
2.5.4	Euclidean Region, Wick-Rotations	73
2.5.5	The Origin of Analyticity	76
2.5.6	Scalar One-Loop Integrals	85
2.5.7	Tensor Integrals	88
2.6	One-Loop Renormalization	91
2.6.1	The Photon Propagator and the Photon Self-Energy	91
2.6.2	The Electron Self-Energy	101

2.6.3	Charge Renormalization	108
2.6.4	Dyson- and Weinberg-Power-Counting Theorems	117
2.6.5	The Running Charge and the Renormalization Group	120
2.6.6	Bremsstrahlung and the Bloch-Nordsieck Prescription	131
2.7	Pions in Scalar QED and Vacuum Polarization by Vector Mesons	143
2.8	Note on QCD: The Feynman Rules and the Renormalization Group	148
	References.	158
3	Lepton Magnetic Moments: Basics.	163
3.1	Equation of Motion for a Lepton in an External Field	163
3.2	Magnetic Moments and Electromagnetic Form Factors	168
3.2.1	Main Features: An Overview.	168
3.2.2	The Anomalous Magnetic Moment of the Electron.	193
3.2.3	The Anomalous Magnetic Moment of the Muon.	199
3.3	Structure of the Electromagnetic Vertex in the SM	201
3.4	Dipole Moments in the Non-Relativistic Limit	205
3.5	Projection Technique	207
3.6	Properties of the Form Factors	213
3.7	Dispersion Relations	214
3.7.1	Dispersion Relations and the Vacuum Polarization	216
3.8	Dispersive Calculation of Feynman Diagrams	226
3.9	ζ -Values, Polylogarithms and Related Special Functions	236
	References.	241
 Part II A Detailed Account of the Theory, Outline of Concepts of the Experiment, Status and Perspectives		
4	Electromagnetic and Weak Radiative Corrections	249
4.1	$g - 2$ in Quantum Electrodynamics	249
4.1.1	One-Loop QED Contribution	251
4.1.2	Two-Loop QED Contribution	252
4.1.3	Three-Loop QED Contribution	255
4.1.4	Four-Loop QED Contribution	261
4.1.5	Five-Loop QED Contribution	270
4.1.6	Four- and Five-Loop Analytic Results and Crosschecks	273
4.2	Weak Contributions	287
4.2.1	Weak One-Loop Effects	294
4.2.2	Weak Two-Loop Effects	295
4.2.3	Two-Loop Electroweak Contributions to a_e	334
	References.	337

5 Hadronic Effects 343

5.1 Hadronic Vacuum Polarization 345

5.1.1 Vacuum Polarization Effects and e^+e^- Data. 345

5.1.2 Integrating the Experimental Data and Estimating
the Error 356

5.1.3 The Cross-Section $e^+e^- \rightarrow$ Hadrons 360

5.1.4 Photon Vacuum Polarization
and the Complex $\alpha_{QED}(s)$ 364

5.1.5 $R(s)$ in Perturbative QCD 369

5.1.6 Non-Perturbative Effects, Operator
Product Expansion. 374

5.1.7 Leading Hadronic Contribution
to $(g - 2)$ of the Muon 377

5.1.8 Addendum I: The Hadronic Contribution
to the Running Fine Structure Constant. 392

5.1.9 Addendum II: The Hadronic Contribution
to the Running $SU(2)_L$ Gauge Coupling 396

5.1.10 Addendum III: τ Spectral Functions versus
 e^+e^- Annihilation Data 400

5.1.11 A Minimal Model: VMD + sQED Resolving
the τ versus e^+e^- Puzzle 402

5.1.12 Hadronic Higher Order Contributions 420

5.1.13 Next-to-Next Leading Order Hadronic Contributions 427

5.2 Hadronic Light-by-Light Scattering. 429

5.2.1 Calculating the Hadronic LbL Contribution. 434

5.2.2 Sketch on Hadronic Models 438

5.2.3 Pion-Exchange Contribution 445

5.2.4 The $\pi^0\gamma\gamma$ Transition Form Factor 450

5.2.5 Exchanges of Axial-Vector Mesons. 487

5.2.6 Exchanges of Scalar Mesons. 493

5.2.7 Tensor Exchanges 496

5.2.8 The Pion-Loop 497

5.2.9 The Quark-Loop 501

5.2.10 A Summary of Results 503

5.2.11 The Dispersive Approach 506

5.3 Lattice QCD 528

5.3.1 Lattice QCD Approach to HVP. 535

5.3.2 Lattice QCD Approach to HLbL. 550

References. 558

- 6 The $g - 2$ Experiments** 571
 - 6.1 Overview on the Principle of the Experiment. 571
 - 6.2 Particle Dynamics. 577
 - 6.3 Magnetic Precession for Moving Particles 580
 - 6.3.1 $g - 2$ Experiment and Magic Momentum 582
 - 6.4 Theory: Production and Decay of Muons. 587
 - 6.5 Muon $g - 2$ Results 595
 - 6.6 Ground State Hyperfine Structure of Muonium 597
 - 6.7 Single Electron Dynamics and the Electron $g - 2$ 599
 - 6.8 The Upcoming Experiments: What Is New? 603
 - References. 606

- 7 Comparison Between Theory and Experiment and Future Perspectives** 609
 - 7.1 Experimental Results Confront Standard Theory 609
 - 7.2 New Physics in $g - 2$ 614
 - 7.2.1 Generic Contributions from Physics Beyond the SM 621
 - 7.2.2 Flavor Changing Processes 626
 - 7.2.3 Anomalous Couplings 628
 - 7.2.4 Two-Higgs Doublet Models 629
 - 7.2.5 Supersymmetry 639
 - 7.2.6 Dark Photon/Z and Axion Like Particles. 661
 - 7.3 Outlook on the Upcoming Experiments 664
 - 7.4 Perspectives for the Future 665
 - References. 674

- Appendix A: List of Acronyms** 683

- Index** 687

Part I
Basic Concepts, Introduction to QED,
 $g - 2$ in a Nutshell, General Properties
and Tools

Chapter 1

Introduction

The book gives an introduction to the basics of the anomalous magnetic moments of leptons and reviews the current state of our knowledge of the anomalous magnetic moment ($g - 2$) of the muon and related topics. The muon usually is denoted by μ . The last $g - 2$ experiment E821 performed at Brookhaven National Laboratory (BNL) in the USA has reached the impressive precision of 0.54 parts per million (ppm) [1]. The anomalous magnetic moment of the muon is now one of the most precisely measured quantities in particle physics and allows us to test relativistic local *Quantum Field Theory* (QFT) in its depth, with unprecedented accuracy. It puts severe limits on deviations from the standard theory of elementary particles and at the same time opens a window to new physics. The book describes the fascinating story of uncovering the fundamental laws of nature to the deepest by an increasingly precise investigation of a single observable. The anomalous magnetic moment of the muon not only encodes all the known but also the as of yet unknown non-Standard-Model physics.¹ The latter, however, is still hidden and is waiting to be discovered on the way to higher precision which allows us to see smaller and smaller effects.

In fact a persisting $3 - 4\sigma$ deviation between theory and experiment, probably the best established substantial deviation among the many successful SM predictions which have been measured in a multitude of precision experiments, motivated a next generation of muon $g - 2$ experiments. A new followup experiment E989 at Fermilab in the US [2–6], will operate very similar as later CERN and the BNL experiments, working with ultrarelativistic magic-energy muons. A second experiment E34 planned at J-PARC in Japan [7–10] will work with ultra-cold muons, and thus can provide an important cross-check between very different experimental setups. While the Fermilab experiment will be able to reduce the experimental

¹As a matter of principle, an experimentally determined quantity always includes all effects, known and unknown, existing in the real world. This includes electromagnetic, strong, weak and gravitational interactions, plus whatever effects we might discover in future.

uncertainty by a factor four to 0.14 ppm, the conceptually novel J-PARC experiment is expected to reach the precision of the previous BNL experiment in a first phase.

In order to understand what is so special about the muon anomalous magnetic moment we have to look at leptons in general. The muon (μ^-), like the much lighter electron (e^-) or the much heavier tau (τ^-) particle, is one of the 3 known charged leptons: elementary spin 1/2 fermions of electric charge -1 in units of the positron charge e , as free relativistic one particle states described by the Dirac equation. Each of the leptons has its positively charged antiparticle, the positron e^+ , the μ^+ and the τ^+ , respectively, as required by any local relativistic quantum field theory [11].²

Of course the charged leptons are never really free, they interact electromagnetically with the photon and weakly via the heavy gauge bosons W and Z , as well as very much weaker also with the Higgs boson. Puzzling enough, the three leptons have identical properties, except for the masses which are given by $m_e = 0.511$ MeV, $m_\mu = 105.658$ MeV and $m_\tau = 1776.99$ MeV, respectively. In reality, the lepton masses differ by orders of magnitude and actually lead to a very different behavior of these particles. As mass and energy are equivalent according to Einstein's relation $E = mc^2$, heavier particles in general decay into lighter particles plus kinetic energy. An immediate consequence of the very different masses are the very different lifetimes of the leptons. Within the *Standard Model* (SM) of elementary particle interactions the electron is stable on time scales of the age of the universe, while the μ has a short lifetime of $\tau_\mu = 2.197 \times 10^{-6}$ s and the τ is even more unstable with a lifetime $\tau_\tau = 2.906 \times 10^{-13}$ s only. Also, the decay patterns are very different: the μ decays very close to 100% into electrons plus two neutrinos ($e\bar{\nu}_e\nu_\mu$), however, the τ decays to about 65% into hadronic states $\pi^-\nu_\tau$, $\pi^-\pi^0\nu_\tau$, \dots while the main leptonic decay modes only account for 17.36% $\mu^-\bar{\nu}_\mu\nu_\tau$ and 17.85% $e^-\bar{\nu}_e\nu_\tau$, respectively. This has a dramatic impact on the possibility to study these particles experimentally and to measure various properties precisely. The most precisely studied lepton is the electron, but the muon can also be explored with extreme precision. Since the muon, the much heavier partner of the electron, turns out to be much more sensitive to hypothetical physics beyond the SM than the electron itself, the muon is much more suitable as a "crystal ball" which could give us hints about not yet uncovered physics. The reason is that some effects scale with powers of m_ℓ^2 , as we will see below. Unfortunately, the τ is so short lived, that corresponding experiments are not possible with present technology.

A direct consequence of the pronounced mass hierarchy is the fundamentally different role the different leptons play in nature. While the stable electrons, besides protons and neutrons, are everywhere in ordinary matter, in atoms, molecules, gases, liquids, metals, other condensed matter states etc., muons seem to be very rare and their role in our world is far from obvious. Nevertheless, even though we may not be aware of it, muons as cosmic ray particles are also part of our everyday life. They are continuously created when highly energetic particles from deep space, mostly protons, collide with atoms from the Earth's upper atmosphere. The initial collisions

²Dirac's theory of electrons, positrons and photons was an early version of what later developed into *Quantum Electrodynamics* (QED), as it is known since around 1950.

create pions which then decay into muons. The highly energetic muons travel at nearly the speed of light down through the atmosphere and arrive at ground level at a rate of about 1 muon per cm^2 and minute. The relativistic *time dilatation* thereby is responsible that the muons have time enough to reach the ground. As we will see later the basic mechanisms observed here are the ones made use of in the muon $g - 2$ experiments. Also remember that the muon was discovered in cosmic rays by Anderson & Neddermeyer in 1936 [12], a few years after Anderson [13] had discovered antimatter in form of the positron, a “positively charged electron” as predicted by Dirac, in cosmic rays in 1932.

Besides charge, spin, mass and lifetime, leptons have other very interesting static (classical) electromagnetic and weak properties like the magnetic and electric *dipole moments*. Classically the dipole moments can arise from either electrical *charges* or *currents*. A well known example is the circulating current, due to an orbiting particle with electric charge e and mass m , which exhibits a magnetic dipole moment $\boldsymbol{\mu}_L = \frac{1}{2c}e \mathbf{r} \times \mathbf{v}$ given by

$$\boldsymbol{\mu}_L = \frac{e}{2mc} \mathbf{L} \quad (1.1)$$

where $\mathbf{L} = m\mathbf{r} \times \mathbf{v}$ is the orbital angular momentum (\mathbf{r} position, \mathbf{v} velocity). An electrical dipole moment can exist due to relative displacements of the centers of positive and negative electrical charge distributions. Thus both electrical and magnetic properties have their origin in the electrical *charges and their currents*. Magnetic charges are not necessary to obtain magnetic moments. This aspect carries over from the basic asymmetry between electric and magnetic phenomena in Maxwell’s equations.³ While electric charges play the fundamental role of the sources of the electromagnetic fields, elementary magnetic charges, usually called magnetic monopoles, are absent. A long time ago, Dirac [14] observed that the existence of magnetic charges would allow us to naturally explain the quantization of both the electric charge e and the magnetic charge m . They would be related by

$$em = \frac{1}{2}n\hbar c \quad , \quad \text{where } n \text{ is an integer.}$$

Apparently, nature does not make use of this possibility and the question of the existence of magnetic monopoles remains a challenge for the future in particle physics.

Whatever the origin of magnetic and electric moments are, they contribute to the electromagnetic interaction Hamiltonian (interaction energy) of the particle with magnetic and electric fields

$$\mathcal{H} = -\boldsymbol{\mu}_m \cdot \mathbf{B} - \mathbf{d}_e \cdot \mathbf{E} \quad , \quad (1.2)$$

where \mathbf{B} and \mathbf{E} are the magnetic and electric field strengths and $\boldsymbol{\mu}_m$ and \mathbf{d}_e the magnetic and electric dipole moment operators. Usually, we measure magnetic moments

³It should be noted that a duality $\mathbf{E} \leftrightarrow \mathbf{B}$ of Maxwell electromagnetism is not realized, because the Hamiltonian changes sign and the dual system would be unstable.

in units of the *Bohr magneton*

$$\mu_0 = e\hbar/2mc \quad (1.3)$$

and the *spin operator*

$$\mathbf{S} = \frac{\hbar\boldsymbol{\sigma}}{2} \quad (1.4)$$

is replacing the angular momentum operator \mathbf{L} . Thus, generalizing the classical form (1.1) of the orbital magnetic moment, one writes (see Sect. 3.1)

$$\boldsymbol{\mu}_m = g Q \mu_0 \frac{\boldsymbol{\sigma}}{2}, \quad \mathbf{d}_e = \eta Q \mu_0 \frac{\boldsymbol{\sigma}}{2}, \quad (1.5)$$

where σ_i ($i = 1, 2, 3$) are the Pauli spin matrices, Q is the electrical charge in units of e , $Q = -1$ for the leptons $Q = +1$ for the antileptons. The equations are defining the gyromagnetic ratio g (g -factor) and its electric pendant η , respectively, quantities exhibiting important dynamical information about the leptons as we will see later.

The magnetic interaction term gives rise to the well known *Zeeman effect*: atomic spectra show a level splitting

$$\Delta E = \frac{e}{2mc} (\mathbf{L} + g\mathbf{S}) \cdot \mathbf{B} = g_j \mu_0 m_j B.$$

The second form gives the result evaluated in terms of the relevant quantum numbers. m_j is the 3rd component of the total angular momentum $\mathbf{J} = \mathbf{L} + \mathbf{S}$ in units of \hbar and takes values $m_j = -j, -j + 1, \dots, j$ with $j = l \pm \frac{1}{2}$. g_j is Landé's g -factor.⁴ If spin is involved one calls it *anomalous Zeeman effect*. The latter obviously is suitable to study the magnetic moment of the electron by investigating atomic spectra in magnetic fields.

⁴The Landé g_j may be calculated based on the “*vector model*” of angular momentum composition:

$$\begin{aligned} (\mathbf{L} + g\mathbf{S}) \cdot \mathbf{B} &= \frac{(\mathbf{L} + g\mathbf{S}) \cdot \mathbf{J}}{J} \frac{\mathbf{J} \cdot \mathbf{B}}{J} = \frac{(\mathbf{L} + g\mathbf{S}) \cdot (\mathbf{L} + \mathbf{S})}{J^2} J_z B \\ &= \frac{L^2 + gS^2 + (g+1)\mathbf{L} \cdot \mathbf{S}}{J^2} m_j \hbar B = \frac{(g+1)J^2 - (g-1)L^2 + (g-1)S^2}{2J^2} m_j \hbar B \end{aligned}$$

where we have eliminated $\mathbf{L} \cdot \mathbf{S}$ using $J^2 = L^2 + S^2 + 2\mathbf{L} \cdot \mathbf{S}$. Using $J = j(j+1)\hbar$ etc. we find

$$g_j = 1 + (g-1) \frac{j(j+1) - l(l+1) + s(s+1)}{2j(j+1)}.$$

With the Dirac value $g = 2$ we find the usual textbook expression.

The anomalous magnetic moment is an *observable*⁵ which can be relatively easily studied experimentally from the motion of the lepton in an external magnetic field. The story started in 1925 soon after Kronig, Goudsmit and Uhlenbeck [15] had postulated that an electron had an intrinsic angular momentum of $\frac{1}{2}\hbar$, and that associated with this spin angular momentum there is a magnetic dipole moment equal to $e\hbar/2mc$, which is the Bohr magneton μ_0 . The important question “is $(\mu_m)_e$ precisely equal to μ_0 ”, or “is $g = 1$ ” in our language, was addressed by Back and Landé in 1925 [16]. Their conclusion, based on a study of numerous experimental investigations on the Zeeman effect, was that the magnetic moment of the electron $(\mu_m)_e$ was consistent with the Goudsmit and Uhlenbeck postulate. In fact, the analysis was not conclusive, as we know, since they did not really determine g . Soon after Pauli had formulated the quantum mechanical treatment of the electron spin in 1927 [17], where g remains a free parameter, Dirac presented his relativistic theory in 1928 [18].

The Dirac theory predicted, unexpectedly, $g = 2$ for a free electron [18], twice the value $g = 1$ known to be associated with orbital angular momentum. After first experimental confirmations of Dirac’s prediction $g_e = 2$ for the electron (Kinster and Houston 1934) [19], which strongly supported the Dirac theory, yet within relatively large experimental errors at that time, it took about 20 more years of experimental efforts to establish that the electrons magnetic moment actually exceeds 2 by about 0.12%, the first clear indication of the existence of an “anomalous”⁶ contribution

$$a_\ell \equiv \frac{g_\ell - 2}{2}, \quad (\ell = e, \mu, \tau) \quad (1.6)$$

to the magnetic moment [20]. By end of the 1940’s the breakthrough in understanding and handling renormalization of QED (Tomonaga, Schwinger, Feynman, and others around 1948 [21]) had made unambiguous predictions of higher order effects possible, and in particular of the leading (one-loop diagram) contribution to the anomalous magnetic moment

$$a_\ell^{\text{QED}(1)} = \frac{\alpha}{2\pi}, \quad (\ell = e, \mu, \tau) \quad (1.7)$$

by Schwinger in 1948 [22] (see Sect. 2.6.3 and Chap. 3). This contribution is due to quantum fluctuations via virtual electron photon interactions and in QED is universal for all leptons. The history of the early period of enthusiasm and worries in the development and first major tests of QED as a renormalizable covariant local quantum field theory is elaborated in great detail in the fascinating book by Schweber [23] (concerning $g - 2$ see Chap. 5, in particular).

⁵A quantity which is more or less directly accessible in an experiment. In general small corrections based on well understood and established theory are necessary for the interpretation of the experimental data.

⁶The anomalous magnetic moment is called anomalous for historic reasons, as a deviation from the classical result. In QED or any QFT higher order effects, so called radiative corrections, are the normal case, which does not make such phenomena less interesting.

In 1947 Nafe, Nelson and Rabi [24] reported an anomalous value by about 0.26% in the hyperfine splitting of hydrogen and deuterium, which was quickly confirmed by Nagle et al. [25], and Breit [26] suggested a possible anomaly $g \neq 2$ of the magnetic moment of the electron. Soon after, Kusch and Foley [27], by a study of the hyperfine-structure of atomic spectra in a constant magnetic field, presented the first precision determination of the magnetic moment of the electron $g_e = 2.00238(10)$ in 1948, just before the theoretical result had been settled. Together with Schwinger's result $a_e^{(2)} = \alpha/(2\pi) \simeq 0.00116$ (which accounts for 99% of the anomaly) this provided one of the first tests of the virtual quantum corrections, usually called radiative corrections, predicted by a relativistic quantum field theory. The discovery of the fine structure of the hydrogen spectrum (Lamb-shift) by Lamb and Retherford [28] and the corresponding calculations by Bethe, Kroll & Lamb and Weisskopf & French [29] was the other triumph of testing the new level of theoretical understanding with precision experiments. These successes had a dramatic impact in establishing quantum field theory as a general framework for the theory of elementary particles and for our understanding of the fundamental interactions. It stimulated the development of QED⁷ in particular and the concepts of quantum field theory in general. With the advent of non-Abelian gauge theories, proposed by Yang and Mills (YM) [31] in 1954, and after 't Hooft and Veltman [32] found the missing clues to understanding and handling them on the quantum level, many years later in 1971, the SM [33] (Glashow, Weinberg, Salam 1981/1987) finally emerged as a comprehensive theory of weak, electromagnetic and strong interactions. The strong interactions had emerged as Quantum Chromodynamics (QCD) [34] (Fritzsch, Gell-Mann, Leutwyler 1973), exhibiting the property of Asymptotic Freedom (AF) [35] (Gross, Politzer and Wilczek 1973). All this structure today is crucial for obtaining sufficiently precise predictions for the anomalous magnetic moment of the muon as we will see.

The most important condition for the anomalous magnetic moment to be a useful monitor for testing a theory is its unambiguous predictability within that theory. The predictability crucially depends on the following properties of the theory:

- (1) it must be a local relativistic quantum field theory and
- (2) it must be renormalizable.

As a consequence $g - 2$ vanishes at tree level. This means that g cannot be an independently adjustable parameter in any renormalizable QFT, which in turn implies that $g - 2$ is a calculable quantity and the predicted value can be confronted with experiments. As we will see $g - 2$ can in fact be both predicted as well as experimentally measured with very high accuracy. By confronting precise theoretical predictions with precisely measured experimental data it is possible to subject the theory to very stringent tests and to find its possible limitation.

The particle-antiparticle duality [11], also called crossing or charge conjugation property, which is a basic consequence of any relativistic local QFT, implies first and foremost that particles and antiparticles have identical masses and spins. In

⁷Today we understand QED as an Abelian gauge theory. This important structural property was discovered by Weyl [30] in 1929.

fact, charge conjugation turned out not to be a universal symmetry of the world of elementary particles. Since, in some sense, an antiparticle is like a particle propagating backwards in time, *charge conjugation* C has to be considered together with *time-reversal* T (time-reflection), which in a relativistic theory has to go together with *parity* P (space-reflection). Besides C, T and P are the two other basic discrete transformation laws in particle physics. A well known fundamental prediction which relates C, P and T is the CPT theorem: the product of the three discrete transformations, taken in any order, is a symmetry of any relativistic QFT. Actually, in contrast to the individual transformations C, P and T, which are symmetries of the electromagnetic- and strong-interactions only, CPT is a universal symmetry and it is this symmetry which guarantees that particles and antiparticles have identical masses as well as equal lifetimes.⁸ But also the dipole moments are very interesting quantities for the study of the discrete symmetries mentioned.

To learn about the properties of the dipole moments under such transformations we have to look at the interaction Hamiltonian (1.2). In particular the behavior under parity and time-reversal is of interest. Naively, one would expect that electromagnetic (QED) and strong interactions (QCD) are giving the dominant contributions to the dipole moments. However, both preserve P and T and thus the corresponding contributions to (1.2) must conserve these symmetries as well. A glimpse at (1.5) tells us that both the magnetic and the electric dipole moment are proportional to the spin vector $\boldsymbol{\sigma}$ which transforms as an axial vector. Thus, on the one hand, both $\boldsymbol{\mu}_m$ and \mathbf{d}_e are axial vectors. On the other hand, the electromagnetic fields \mathbf{E} and \mathbf{B} transform as a vector (polar vector) and an axial vector, respectively. An axial vector changes sign under T but not under P, while a vector changes sign under P but not under T. We observe that to the extent that P and/or T are conserved only the magnetic term $-\boldsymbol{\mu}_m \cdot \mathbf{B}$ is allowed while an electric dipole term $-\mathbf{d}_e \cdot \mathbf{E}$ is forbidden and hence we must have $\eta = 0$ in (1.5). Since the weak interactions violate parity maximally, weak contributions cannot be excluded by the parity argument. However, T (by the CPT-theorem equivalent to CP) is also violated by the weak interactions, but only via fermion family mixing in the Yukawa sector of the SM (see below). It turns out that, at least for light particles like the known leptons, effects are much smaller. So electric dipole moments are suppressed by approximate T invariance at the level of second order weak interactions (for a theoretical review see [36]).

⁸In some cases particle and antiparticle although of different flavor (fermion species) may have the same conserved quantum numbers and mix. Examples of such mixing phenomena are $K^0 - \bar{K}^0$ -oscillations or $B^0 - \bar{B}^0$ -oscillations. The time evolution of the neutral Kaon system, for example, is described by

$$i \frac{d}{dt} \begin{pmatrix} K^0 \\ \bar{K}^0 \end{pmatrix} = H \begin{pmatrix} K^0 \\ \bar{K}^0 \end{pmatrix}, \quad H \equiv M - \frac{i}{2} \Gamma$$

where M and Γ are Hermitian 2×2 matrices, the mass and the decay matrices. The corresponding eigenvalues are $\lambda_{L,S} = m_{L,S} - \frac{i}{2} \gamma_{L,S}$. CPT invariance in this case requires the diagonal elements of \mathcal{M} to be equal. In fact $|m_{K^0} - m_{\bar{K}^0}|/m_{\text{average}} < 6 \times 10^{-19}$ (90% C.L.) provides the best test of CPT, while the mass eigenstates K_L and K_S exhibit a mass difference $\Delta m = m_{K_L} - m_{K_S} = 3.484 \pm 0.006 \times 10^{-12}$ MeV.

In fact experimental bounds tell us that they are very tiny. The previous best limit $|d_e| < 1.6 \times 10^{-27} e \cdot \text{cm}$ at 90% C.L. [37] has been superseded recently by [38]⁹

$$|d_e| < 8.7 \times 10^{-29} e \cdot \text{cm} \text{ at } 90\% \text{ C.L.} \quad (1.8)$$

This will also play an important role in the interpretation of the $g - 2$ experiments as we will see later. The planned J-PARC muon $g - 2$ experiment will also provide a new dedicated experiment for measuring the muon electric dipole moment [9, 39].

As already mentioned, the anomalous magnetic moment of a lepton is a dimensionless quantity, a pure number, which may be computed order by order as a perturbative expansion in the fine structure constant α in QED, and beyond QED, in the SM of elementary particles or extensions of it. As an effective interaction term an anomalous magnetic moment is induced by the interaction of the lepton with photons or other particles. It corresponds to a dimension 5 operator and since a renormalizable theory is constrained to exhibit terms of dimension 4 or less only, such a term must be absent for any fermion in any renormalizable theory at tree level. It is the absence of such a possible *Pauli term* that leads to the prediction $g = 2 + O(\alpha)$. On a formal level it is the requirement of renormalizability which forbids the presence of a Pauli term in the Lagrangian defining the theory (see Sect. 2.4.2).

In 1956 a_e was already well measured by Crane et al. [40] and Berestetskii et al. [41] pointed out that the sensitivity of a_ℓ to short distance physics scales like

$$\frac{\delta a_\ell}{a_\ell} \sim \frac{m_\ell^2}{\Lambda^2} \quad (1.9)$$

where Λ is a UV cut-off characterizing the scale of new physics. It was therefore clear that the anomalous magnetic moment of the muon would be a much better probe for possible deviations from QED. However, parity violation of weak interaction was not yet known at that time and nobody had an idea how to measure a_μ .

As already discussed at the beginning of this introduction, the origin of the vastly different behavior of the three charged leptons is due to the very different masses m_ℓ , implying completely different lifetimes $\tau_e = \infty$, $\tau_\ell = 1/\Gamma_\ell \propto 1/G_F^2 m_\ell^5$ ($\ell = \mu, \tau$) and vastly different decay patterns. G_F is the Fermi constant, known from weak radioactive decays. In contrast to muons, electrons exist in atoms which opens the possibility to investigate a_e directly via the spectroscopy of atoms in magnetic fields. This possibility does not exist for muons.¹⁰ However, Crane et al. [40] already used a different method to measure a_e . They produced polarized electrons by shooting high-energy electrons on a gold foil. The part of the electron bunch which is scattered at right angles, is partially polarized and trapped in a magnetic field, where spin precession takes place for some time. The bunch is then released from the trap and allowed to strike a second gold foil, which allows one to analyze the polarization

⁹The unit $e \cdot \text{cm}$ is the dipole moment of an e^+e^- -pair separated by 1cm. Since $d = \frac{\eta}{2} \frac{e\hbar c}{2mc^2}$, the conversion factor needed is $\hbar c = 1.9733 \cdot 10^{-11} \text{ MeV cm}$ and $e = 1$.

¹⁰We discard here the possibility to form and investigate muonic atoms.

and to determine a_e . Although this technique is in principle very similar to the one later developed to measure a_μ , it is obvious that in practice handling the muons in a similar way is not possible. One of the main questions was: how is it possible to polarize such short lived particles like muons?

After the proposal of parity violation in weak transitions by Lee and Yang [42] in 1957, it immediately was realized that muons produced in weak decays of the pion ($\pi^+ \rightarrow \mu^+ + \text{neutrino}$) should be longitudinally polarized. In addition, the decay positron of the muon ($\mu^+ \rightarrow e^+ + 2 \text{ neutrinos}$) could indicate the muon spin direction. This was confirmed by Garwin, Lederman and Weinrich [43] and Friedman and Telegdi [44].¹¹ The first of the two papers for the first time determined $g_\mu = 2.00$ within 10% by applying the muon spin precession principle (see Chap. 6). Now the road was free to seriously think about the experimental investigation of a_μ .

It should be mentioned that at that time the nature of the muon was quite a mystery. While today we know that there are three lepton–quark families with identical basic properties except for differences in masses, decay times and decay patterns, at these times it was hard to believe that the muon is just a heavier version of the electron ($\mu - e$ -puzzle). For instance, it was expected that the μ exhibited some unknown kind of interaction, not shared by the electron, which was responsible for the much higher mass. So there was plenty of motivation for experimental initiatives to explore a_μ .

The big interest in the muon anomalous magnetic moment was motivated by Berestetskii’s argument of dramatically enhanced short distance sensitivity. As we will see later, one of the main features of the anomalous magnetic moment of leptons is that it mediates helicity flip transitions. The *helicity* is the projection of the spin vector onto the momentum vector which defines the direction of motion and the velocity. If the spin is parallel to the direction of motion the particle is right-handed, if it is antiparallel it is called left-handed.¹² For massless particles the helicities would be conserved by the SM interactions and helicity flips would be forbidden. For massive particles helicity flips are allowed and their transition amplitude is proportional to the mass of the particle. Since the transition probability goes with the modulus square of the amplitude, for the lepton’s anomalous magnetic moment this implies, generalizing (1.9), that quantum fluctuations due to heavier particles or contributions from higher energy scales are proportional to

$$\frac{\delta a_\ell}{a_\ell} \propto \frac{m_\ell^2}{M^2} \quad (M \gg m_\ell), \quad (1.10)$$

where M may be

¹¹The latter reference for the first time points out that P and C are violated simultaneously, in fact P is maximally violated while CP is to very good approximation conserved in this decay.

¹²Handedness is used here in a naive sense of the “right-hand rule”. Naive because the handedness defined in this way for a massive particle is frame dependent. The proper definition of handedness in a relativistic QFT is in terms of the chirality (see Sect. 2.2). Only for massless particles the two different definitions of handedness coincide.

- the mass of a heavier SM particle, or
- the mass of a hypothetical heavy state beyond the SM, or
- an energy scale or an ultraviolet cut-off where the SM ceases to be valid.

On one hand, this means that the heavier the new state or scale the harder it is to see (it decouples as $M \rightarrow \infty$). Typically, the best sensitivity we have for nearby new physics, which has not yet been discovered by other experiments. On the other hand, the sensitivity to “new physics” grows quadratically with the mass of the lepton, which means that the interesting effects are magnified in a_μ relative to a_e by a factor $(m_\mu/m_e)^2 \sim 4 \times 10^4$. This is what makes the anomalous magnetic moment of the muon a_μ the predestinated “monitor for new physics”. By far the best sensitivity we have for a_τ the measurement of which however is beyond present experimental possibilities, because of the very short lifetime of the τ .

The first measurement of the anomalous magnetic moment of the muon was performed at Columbia in 1960 [45] with a result $a_\mu = 0.00122(8)$ at a precision of about 5%. Shortly after in 1961, the first precision determination was possible at the CERN cyclotron (1958–1962) [46, 47]. Surprisingly, nothing special was observed within the 0.4% level of accuracy of the experiment. It was the first real evidence that the muon was just a heavy electron. In particular this meant that the muon was point-like and no extra short distance effects could be seen. This latter point of course is a matter of accuracy and the challenge to go further was evident.

The idea of a muon storage rings was put forward next. A first one was successfully realized at CERN (1962–1968) [48–50]. It allowed one to measure a_μ for both μ^+ and μ^- at the same machine. Results agreed well within errors and provided a precise verification of the CPT theorem for muons. An accuracy of 270 ppm was reached and an insignificant 1.7σ ($1 \sigma = 1$ Standard Deviation (SD)) deviation from theory was found. Nevertheless the latter triggered a reconsideration of theory. It turned out that in the estimate of the three-loop $O(\alpha^3)$ QED contribution the leptonic light-by-light scattering part (dominated by the electron loop) was missing. Aldins et al. [51] then calculated this and after including it, perfect agreement between theory and experiment was obtained.

One also should keep in mind that the first theoretical successes of QED predictions and the growing precision of the a_e experiments challenged theoreticians to tackle the much more difficult higher order calculations for a_e as well as for a_μ . Soon after Schwinger’s result Karplus and Kroll 1949 [52] calculated the two-loop term for a_e . In 1957, shortly after the discovery of parity violation and a first feasibility proof in [43], dedicated experiments to explore a_μ were discussed. This also renewed the interest in the two-loop calculation which was reconsidered, corrected and extended to the muon by Sommerfield [53] and Petermann [54], in the same year. Vacuum polarization insertions with fermion loops with leptons different from the external one were calculated in [55, 56]. About 10 years later with the new generation of $g - 2$ experiments at the first muon storage ring at CERN $O(\alpha^3)$ calculations were started by Kinoshita [57], Lautrup and de Rafael [58] and Mignaco and Remiddi [59]. It then took about 30 years until Laporta and Remiddi [60] found a final analytic result in 1996. Many of these calculations would not have been possible without the pioneering *computer algebra* programs, like ASHMEDAI [61], SCHOONSHIP

[62, 63] and REDUCE [64]. More recently Vermaseren's FORM [65] package evolved into a standard tool for large scale calculations. Commercial software packages like MACSYMA or the more up-to-date ones MATEMATICA and MAPLE, too, play an important role as advanced tools to solve difficult problems by means of computers. Of course, the dramatic increase of computer performance and the use of more efficient computing algorithms have been crucial for the progress achieved. In particular calculations like the ones needed for $g - 2$ had a direct impact on the development of these computer algebra systems.

In an attempt to overcome the systematic difficulties of the first a second *muon storage ring* was built (1969–1976) [66, 67]. The precision of 7 ppm reached was an extraordinary achievement at that time. For the first time the m_μ^2/m_e^2 -enhanced hadronic contribution came into play. Again no deviations were found. With the achieved precision the muon $g - 2$ remained a benchmark for beyond the SM theory builders ever since. Only 20 years later the BNL experiment E821, again a muon storage ring experiment, was able to set new standards in precision. Now, at the present level of accuracy the complete SM is needed in order to be able to make predictions at the appropriate level of precision. As already mentioned, at present further progress is hampered by the difficulties to include properly the non-perturbative strong interaction part. At a certain level of precision *hadronic effects* become important and we are confronted with the question of how to evaluate them reliably. At low energies QCD gets strongly interacting and a perturbative calculation is not possible. Fortunately, analyticity and unitarity allow us to express the leading hadronic vacuum polarization (HVP) contributions via a dispersion relation (analyticity) in terms of experimental data [68]. The key relation here is the optical theorem (unitarity) which determines the imaginary part of the vacuum polarization amplitude through the total cross section for electron-positron annihilation into hadrons. First estimations were performed in [69–71] after the discovery of the ρ - and the ω -resonances,¹³ and in [74], after first e^+e^- cross-section measurements were performed at the colliding beam machines VEPP-2 and ACO in Novosibirsk [75] and Orsay [76], respectively. One drawback of this method is that now the precision of the theoretical prediction of a_μ is limited by the accuracy of experimental data. We will say more on this later on.

The success of the CERN muon anomaly experiment and the progress in the consolidation of the SM, together with given possibilities for experimental improvements, were a good motivation for Vernon Hughes and other interested colleagues to push for a new experiment at Brookhaven. There the intense proton beam of the Alternating Gradient Synchrotron (AGS) was available which would allow to increase the statistical accuracy substantially [77]. The main interest was a precise test of the electroweak contribution due to virtual W and Z exchange, which had been calculated immediately after the renormalizability of the SM had been settled

¹³The ρ is a $\pi\pi$ resonance which was discovered in pion nucleon scattering $\pi^- + p \rightarrow \pi^- \pi^0 p$ and $\pi^- + p \rightarrow \pi^- \pi^+ n$ [72] in 1961. The neutral ρ^0 is a tall resonance in the $\pi^+\pi^-$ channel which may be directly produced in e^+e^- -annihilation and plays a key role in the evaluation of the hadronic contributions to a_μ^{had} . The ρ contributes about 70% to a_μ^{had} which clearly demonstrates the non-perturbative nature of the hadronic effects. Shortly after the ρ also the ω -resonance was discovered as a $\pi^+\pi^0\pi^-$ peak in proton-antiproton annihilation $p\bar{p} \rightarrow \pi^+\pi^+\pi^0\pi^-\pi^-$ [73].

in 1972 [78]. An increase in precision by a factor of 20 was required for this goal. On the theory side the ongoing discussion motivated, in the early 1980's already, Kinoshita and his collaborators to start the formidable task to calculate the $O(\alpha^4)$ contribution with 891 four-loop diagrams. The direct numerical evaluation was the only promising method to get results within a reasonable time. Early results [79, 80] could be improved continuously [81] and culminated in 2012 with the first complete $O(\alpha^5)$ calculation for both the electron [82] and the muon [83] $g - 2$ (involving 12672 five-loop diagrams). Very recently Laporta [84] has been able to obtain a quasi-exact 4-loop result for the 891 universal diagrams, which improves the electron $g - 2$ essentially. Increasing computing power was and still is a crucial factor in this extreme project. Beyond the full analytic $O(\alpha^3)$ calculation, only a subset of diagrams are known analytically (see Sect. 4.1 for many more details and a more complete list of references). The size of the $O(\alpha^4)$ contribution is about 6 σ 's in terms of the present experimental accuracy and thus mandatory for the interpretation of the experimental result. The improvement achieved with the evaluation of the $O(\alpha^5)$ term, which itself is about 0.07 σ 's only, resulted in a substantial reduction of the uncertainty of the QED contribution.

A general problem in electroweak precision physics are the higher order contributions from hadrons (quark loops) at low energy scales. While leptons primarily exhibit the fairly weak electromagnetic interaction, which can be treated in perturbation theory, the quarks are strongly interacting via confined gluons where any perturbative treatment breaks down. Considering the lepton anomalous magnetic moments one distinguishes three types of non-perturbative corrections: **(a)** Hadronic Vacuum Polarization (HVP) of order $O(\alpha^2)$, $O(\alpha^3)$, $O(\alpha^4)$; **(b)** Hadronic Light-by-Light (HLbL) scattering at $O(\alpha^3)$; **(c)** hadronic effects at $O(\alpha G_F m_\mu^2)$ in 2-loop electroweak (EW) corrections, in all cases quark-loops appear as hadronic “blobs”. The hadronic contributions are limiting the precision of the predictions.

As mentioned already before, the evaluation of non-perturbative hadronic effects is possible by using experimental data in conjunction with Dispersion Relations (DR), by low energy effective modeling via a Resonance Lagrangian Approach (RLA) (Vector Meson Dominance (VMD) implemented in accord with chiral structure of QCD) [85–87], like the Hidden Local Symmetry (HLS) or the Extended Nambu Jona-Lasinio (ENJL) models, or by lattice QCD. Specifically: **(a)** HVP via a dispersion integral over $e^+e^- \rightarrow$ hadrons data (1 independent amplitude to be determined by one specific data channel) (see e.g. [88, 89]), by the HLS effective Lagrangian approach [90], or by lattice QCD [91–95]; **(b)** hadronic Light-by-Light (HLbL) scattering effects via a RLA together with operator product expansion (OPE) methods [96–99], by a dispersive approach using $\gamma\gamma \rightarrow$ hadrons data (19 independent amplitudes to be determined by as many independent data sets in principle) [100, 101] or by lattice QCD [102]; **(c)** EW quark-triangle diagrams are well under control, because the possible large corrections are related to the Adler-Bell-Jackiw (ABJ) anomaly which is perturbative and non-perturbative at the same time. Since $VVV = 0$ by the Furry theorem, only VVA (of $\gamma\gamma Z$ -vertex, V = vector, A = axialvector) contributes. In fact leading effects are of short distance type

(M_Z mass scale) and cancel against lepton-triangle loops (anomaly cancellation) [103, 104].

In the early 1980's the hadronic contributions were known with rather limited accuracy only. Much more accurate e^+e^- -data from experiments at the electron positron storage ring VEPP-2M at Novosibirsk allowed a big step forward in the evaluation of the leading hadronic vacuum polarization effects [80, 105, 106] (see also [107]). A more detailed analysis based on a complete up-to-date collection of data followed about 10 years later [88]. Further improvements were possible thanks to new hadronic cross section measurements by BES-II [108] (BEPC ring) at Beijing and by CMD-2 [109] at Novosibirsk. A new approach of cross section measurements via the radiative return or initial state radiation (ISR) mechanism, pioneered by the KLOE Collaboration [110] (DAΦNE ring) at Frascati, started to provide high statistics data at about the time when Brookhaven stopped their muon $g - 2$ experiment. The results are in fair agreement with the later CMD-2 and SND data [111, 112]. In the meantime ISR data for the dominating $\pi^+\pi^-$ channel have been collected by KLOE [113–115] at the ϕ factory by BaBar at the B factory [116] and a first measurement by BES-III [117] at the BEPCII collider. Still one of the main issue in HVP are hadronic cross-sections in the region 1.2 to 2.4 GeV, which actually has been improved dramatically by the exclusive channel measurements by BaBar in the past decade (see [118] and references therein). The most important 20 out of more than 30 channels are measured, many known at the 10 to 15% level. The exclusive channel therefore has a much better quality than the very old inclusive data from Frascati. Attempts to include τ spectral functions via isospin relations will be discussed in Sect. 5.1.10.

The physics of the anomalous magnetic moments of leptons has challenged the particle physics community for more than 60 years now and experiments as well as theory in the meantime look rather intricate. For a long time a_e and a_μ provided the most precise tests of QED in particular and of relativistic local QFT as a common framework for elementary particle theory in general.

Of course it was the hunting for deviations from theory and the theorists speculations about “new physics around the corner” which challenged new experiments again and again. The reader may find more details about historical aspects and the experimental developments in the interesting review: “The 47 years of muon $g-2$ ” by Farley and Semertzidis [119].

Until about 1975 searching for “new physics” via a_μ in fact essentially meant looking for physics beyond QED. As we will see later, also standard model hadronic and weak interaction effect carry the enhancement factor $(m_\mu/m_e)^2$, and this is good news and bad news at the same time. Good news because of the enhanced sensitivity to many details of SM physics like the weak gauge boson contributions, bad news because of the enhanced sensitivity to the hadronic contributions which are very difficult to control and in fact limit our ability to make predictions at the desired precision. This is the reason why quite some fraction of the book will have to deal with these hadronic effects (see Chap. 5).

The pattern of lepton anomalous magnetic moment physics which emerges is the following: a_e is a quantity which is dominated by QED effects up to very high

precision, presently at the .66 parts per billion (ppb) level! The sensitivity to hadronic and weak effects as well as the sensitivity to physics beyond the SM is very small. This allows for a very solid and model independent (essentially pure QED) high precision prediction of a_e [82, 84]. The very precise experimental value [120, 121] (at 0.24 ppb) and the very good control of the theory part in fact allows us to determine the fine structure constant α with the highest accuracy [121–123] in comparison with other methods (see Sect. 3.2.2). A very precise value for α of course is needed as an input to be able to make precise predictions for other observables like a_μ , for example. While a_e , theory wise, does not attract too much attention, although it required to push the QED calculation to $O(\alpha^5)$, a_μ is a much more interesting and theoretically challenging object, sensitive to all kinds of effects and thus probing the SM to much deeper level (see Chap. 4). Note that in spite of the fact that a_e has been measured about 2250 times more precisely than a_μ the sensitivity of the latter to “new physics” is still about 19 times larger. However, in order to use a_e as a monitor for new physics one requires the most precise a_e independent determination of α which comes from atomic interferometry [124] and is about a factor 5.3 less precise than the one based on a_e . Taking this into account a_μ is about a factor 43 more sensitive to new physics at present.

The experimental accuracy achieved in the past few years at BNL is at the level of 0.54 parts per million (ppm) and better than the accuracy of the theoretical predictions which are still obscured by hadronic uncertainties. A discrepancy at the 2 to 3 σ level persisted [125–127] since the first new measurement in 2000 up to the one in 2004 (four independent measurements during this time), the last for the time being (see Chap. 7). Again, the “disagreement” between theory and experiment, suggested by the first BNL measurement, rejuvenated the interest in the subject and entailed a reconsideration of the theory predictions. The most prominent error found this time in previous calculations concerned the problematic hadronic light-by-light scattering contribution which turned out to be in error by a sign [128]. The change improved the agreement between theory and experiment by about 1 σ . Problems with the hadronic e^+e^- -annihilation data used to evaluate the hadronic vacuum polarization contribution led to a similar shift in opposite direction, such that a discrepancy persists.

Speculations about what kind of effects could be responsible for the deviation will be presented in Sect. 7.2. With the advent of the Large Hadron Collider (LHC) the window of possibilities to explain the observed deviation by a contribution from a new heavy particle have substantially narrowed, such that the situation is rather puzzling at the time. No real measurement yet exists for a_τ . Bounds are in agreement with SM expectations¹⁴ [129]. Advances in experimental techniques one day could promote a_τ to a new “telescope” which would provide new perspectives in exploring the short distance tail of the unknown real world, we are continuously hunting for. The point is that the relative weights of the different contributions are quite different for the τ in comparison to the μ .

¹⁴Theory predicts $(g_\tau - 2)/2 = 117721(5) \times 10^{-8}$; the experimental limit from the LEP experiments OPAL and L3 is $-0.052 < a_\tau < 0.013$ at 95% C.L.

In the meantime activities are expected to go on to improve the impressive level of precision reached by the muon $g - 2$ experiment E821 at BNL. Since the error was still dominated by statistical errors rather than by systematic ones, further progress is possible in any case. But also new ideas to improve on sources of systematic errors play an important role for future projects. Plans for an upgrade of the Brookhaven experiment lead to a new experiment which presently is realized at Fermilab. The muon storage ring will be the same and has been moved to the new location some time ago, most of the other elements like production and injection of the polarized muons as well as the detection of the muon decay electrons will be new. An alternative project designed to work with ultra-cold muon is being buildup at J-PARC in Japan. The new experiments are expected to be able to improve the accuracy by a factor of 5 or so [2–5]. For the theory such improvement factors are a real big challenge and require much progress in our understanding of non-perturbative strong interaction effects. In addition, challenging higher order computations have to be pushed further within the SM and beyond. Another important aspect: the large hadron collider LHC now in operation at CERN will certainly provide important hints about how the SM has to be completed by new physics. Progress in the theory of a_μ will come certainly in conjunction with projects to measure hadronic electron-positron annihilation cross-sections with substantially improved accuracy (see Sect. 7.4). These cross sections are an important input for reducing the hadronic vacuum polarization uncertainties which yield the dominating source of error at present. Although progress is slow, there is evident progress in reducing the hadronic uncertainties, most directly by progress in measuring the relevant hadronic cross-sections. Near future progress we expect from BINP Novosibirsk/Russia and from IHEP Beijing/China. Energy scan as well as ISR measurement of cross-sections in the region from 1.4 to 2.5 GeV are most important to reduce the errors to a level competitive with the factor 4 improvement achievable by the upcoming new muon $g - 2$ experiments at Fermilab/USA and at J-PARC/Japan [5, 7–9]. Also BaBar data are still being analyzed and are important for improving the results. Promising is that lattice QCD evaluations come closer to be competitive. In any case there is good reason to expect also in future interesting promises of physics beyond the SM from this “crystal ball” of particle physicists.

Besides providing a summary of the status of the physics of the anomalous magnetic moment of the muon, the aim of this book is an introduction to the theory of the magnetic moments of leptons also emphasizing the fundamental principles behind our present understanding of elementary particle theory. Many of the basic concepts are discussed in details such that physicists with only some basic knowledge of quantum field theory and particle physics should get the main ideas and learn about the techniques applied to get theoretical predictions of such high accuracy, and why it is possible to measure anomalous magnetic moments so precisely.

Once thought as a QED test, today the precision measurement of the anomalous magnetic moment of the muon is a test of most aspects of the SM with the electromagnetic, the strong and the weak interaction effects and beyond, maybe supersymmetry is responsible for the observed deviation.

There are many excellent and inspiring introductions and reviews on the subject [130–148], which were very helpful in writing this book. A topical workshop

held in 2014 at the Mainz Institute for Theoretical Physics (MITP) has been gathering people with new ideas to work on the improvement of the predictions of the hadronic contributions, in particular on the challenging hadronic light-by-light scattering problem. A short account of the topics discussed the reader may find in the “mini proceedings” [149]. It addresses the next steps required on the theory side to compete with the experimental progress to come.

For further reading I also recommend the reviews [150, 151], which are focusing on theory issues and the article [152], which especially reviews the experimental aspects in much more depth than this book. For a recent brief view into the future also see [153].

References

1. G.W. Bennett et al., Muon (g-2) Collab. Phys. Rev. Lett. **92**, 161802 (2004)
2. B.L. Roberts Nucl. Phys. B (Proc. Suppl.) **131** (2004) 157; R. M. Carey et al., Proposal of the BNL Experiment E969, 2004 (www.bnl.gov/henp/docs/pac0904/P969.pdf); J-PARC Letter of Intent L17
3. J. Grange et al. [Muon g-2 Collab.], [arXiv:1501.06858](https://arxiv.org/abs/1501.06858) [physics.ins-det]
4. [Fermilab E989 Collab.], Nucl. Part. Phys. Proc. PoS EPS -HEP2015 (2015) 568. **273–275**, 584 (2016)
5. D.W. Hertzog, EPJ Web Conf. **118**, 01015 (2016)
6. Fermilab Muon g-2 Collab, <http://muon-g-2.fnal.gov>
7. H. Iinuma, J-PARC muon g-2/EDM Collab. J. Phys. Conf. Ser. **295**, 012032 (2011)
8. T. Mibe [J-PARC g-2 Collab.], Nucl. Phys. Proc. Suppl. **218**, 242 (2011)
9. N. Saito, J-PARC g-2/EDM Collab. AIP Conf. Proc. **1467**, 45 (2012)
10. J-PARC g-2/EDM Collab, <http://g-2.kek.jp>
11. P.A.M. Dirac, Proc. Roy. Soc. A **126**, 360 (1930)
12. C.D. Anderson, S.H. Neddermeyer, Phys. Rep. C **50** (1936) 263; S.H. Neddermeyer, C.D. Anderson, Phys. Rep. C **51**, 884 (1937)
13. C.D. Anderson, Phys. Rep. C **43**, 491 (1933)
14. Phys. Rep. C Proc. Roy. Soc. A 133 (1931) 60. **74**, 817 (1948)
15. G.E. Uhlenbeck, S. Goudsmit, Naturwissenschaften 13 (1925) 953. Nature **117**, 264 (1926)
16. E. Back, A. Landé, *Zeemaneffekt und Multiplettstruktur der Spektrallinien*, 1st edn (J. Springer, Berlin 1925), pp 213; see also: H.A. Bethe, E.E. Salpeter, *Quantum Mechanics of One- and Two-Electron Systems*, Handbuch der Physik, Band XXXV, Atoms I, Springer Verlag, Berlin (1957)
17. W. Pauli, Zeits. Phys. **43**, 601 (1927)
18. A Proc. Roy. Soc. A 117 (1928) 610. **118**, 351 (1928)
19. L.E. Kinster, W.V. Houston, Phys. Rep. C **45**, 104 (1934)
20. P. Kusch, Science 123 (1956) 207. Phys. Today **19**, 23 (1966)
21. S. Tomonaga, Riken Iho, Progr. Theor. Phys. **1** (1946) 27; J. Schwinger, Phys. Rep. C **74** (1948) 1439; R. P. Feynman, Phys. Rep. C **76** (1949) 749; F. Dyson, Phys. Rep. C **75** (1949) 486, *ibid.* (1736)
22. J.S. Schwinger, Phys. Rev. **73**, 416 (1948)
23. S.S. Schweber, *QED and the Men Who Made It: Dyson, Feynman, Schwinger, and Tomonaga*, 1st edn. (Princeton, Princeton University Press, 1994), p. 732
24. J.E. Nafe, E.B. Nelson, I.I. Rabi, Phys. Rep. C **71**, 914 (1947)
25. D.E. Nagle, R.S. Julian, J.R. Zacharias, Phys. Rev. **72**, 971 (1947)
26. G. Breit, Phys. Rep. C **72**, 984 (1947)

27. P. Kusch, H. M. Foley, Phys. Rev. 73 (1948) 421. Phys. Rep. C **74**, 250 (1948)
28. W.E. Lamb Jr., R.C. Retherford, Phys. Rep. C **72**, 241 (1947)
29. H. A. Bethe, Phys. Rep. C **72** (1947) 339; N. M. Kroll, W. E. Lamb Jr, Phys. Rep. C **75** (1949) 388; V. Weisskopf, J. B. French, Phys. Rep. C **75**, 1240 (1949)
30. H. Weyl, I. Zeits, Phys. **56**, 330 (1929)
31. C.N. Yang, R.L. Mills, Phys. Rep. C **96**, 191 (1954)
32. G. 't Hooft, Nucl. Phys. B 33 (1971) 173; **35** (1971) 167; G. 't Hooft, M. Veltman, Nucl. Phys. B 50, 318 (1972)
33. S. L. Glashow, Nucl. Phys. B 22 (1961) 579; S. Weinberg, Phys. Rev. Lett. **19** (1967) 1264; A. Salam, Weak and electromagnetic interactions. In: *Elementary Particle Theory*, ed by N. Svartholm, Amquist and Wiksells, Stockholm, pp 367–377 (1969)
34. H. Fritzsch, M. Gell-Mann, H. Leutwyler, Phys. Lett. **47**, 365 (1973)
35. H.D. Politzer, Phys. Rev. Lett. 30 (1973) 1346; D. Gross, F. Wilczek. Phys. Rev. Lett. **30**, 1343 (1973)
36. W. Bernreuther, M. Suzuki, Erratum-ibid. **64** (1991) 313. Rev. Mod. Phys. **63**, 633 (1992)
37. B.C. Regan, E.D. Commins, C.J. Schmidt, D. DeMille, Phys. Rev. Lett. **88**, 071805 (2002)
38. J. Baron et al., ACME Collab. Sci. **343**, 269 (2014)
39. F. J. M. Farley et al., Phys. Rev. Lett. **93** (2004) 052001; M. Aoki et al. [J-PARC Letter of Intent]: *Search for a Permanent Muon Electric Dipole Moment at the $\times 10^{-24}$ e·cm Level*, <http://www-ps.kek.jp/jhf-np/LOIlist/pdf/L22.pdf>
40. W. H. Luisell, R. W. Pidd, H. R. Crane, Phys. Rep. C **91** (1953) 475; ibid. **94** (1954) 7; A. A. Schupp, R. W. Pidd, H. R. Crane, Phys. Rep. C **121** (1961) 1; H. R. Crane, Sci. American **218**, 72 (1968)
41. V.B. Berestetskii, O.N. Krokhin, A.X. Klebnikov, Zh Eksp, Teor. Fiz. 30 (1956) 788 [Sov. Phys. JETP 3 (1956) 761]; W. S. Cowland. Nucl. Phys. B **8**, 397 (1958)
42. T.D. Lee, C.N. Yang, Phys. Rep. C **104**, 254 (1956)
43. R.L. Garwin, L. Lederman, M. Weinrich, Phys. Rep. C **105**, 1415 (1957)
44. J.I. Friedman, V.L. Telegdi, Phys. Rep. C **105**, 1681 (1957)
45. R.L. Garwin, D.P. Hutchinson, S. Penman, G. Shapiro, Phys. Rev. **118**, 271 (1960)
46. G. Charpak, F. J. M. Farley, R. L. Garwin, T. Muller, J. C. Sens, V. L. Telegdi, A. Zichichi, Phys. Rev. Lett. **6** (1961) 128; G. Charpak, F. J. M. Farley, R. L. Garwin, T. Muller, J. C. Sens, A. Zichichi, Nuovo Cimento **22** (1961) 1043; Phys. Lett. **1**, 16 (1962)
47. G. Charpak, F.J.M. Farley, R.L. Garwin, T. Muller, J.C. Sens, A. Zichichi, Nuovo Cimento **37**, 1241 (1965)
48. F.J.M. Farley, J. Bailey, R.C.A. Brown, M. Giesch, H. Jöstlein, S. van der Meer, E. Picasso, M. Tannenbaum, Nuovo Cimento **45**, 281 (1966)
49. J. Bailey et al., Phys. Lett. B **28**, 287 (1968)
50. J. Bailey, W. Bartl, G. von Bochmann, R.C.A. Brown, F.J.M. Farley, M. Giesch, H. Jöstlein, S. van der Meer, E. Picasso, R.W. Williams, Nuovo Cimento A **9**, 369 (1972)
51. J. Aldins, T. Kinoshita, S. J. Brodsky, A. J. Dufner, Phys. Rev. Lett. 23 (1969). Phys. Rev. D **1**, 2378 (1970)
52. R. Karplus, N.M. Kroll, Phys. Rep. C **77**, 536 (1950)
53. C. M. Sommerfield, Phys. Rev. 107 (1957) 328. Ann. Phys. (N.Y.) **5**, 26 (1958)
54. A. Petermann, Helv. Phys. Acta 30 (1957) 407. Nucl. Phys. **5**, 677 (1958)
55. H. Suura, E. Wichmann, Phys. Rev. 105 (1957) 1930; A. Petermann. Phys. Rev. **105**, 1931 (1957)
56. H.H. Elend, Erratum-ibid. **21** (1966) 720. Phys. Lett. **20**, 682 (1966)
57. T. Kinoshita, Nuovo Cim. B **51**, 140 (1967)
58. B.E. Lastrap, E. De Rafael, Phys. Rev. **174**, 1835 (1968)
59. J.A. Mignaco, E. Remiddi, Nuovo Cim. A **60**, 519 (1969)
60. S. Laporta, E. Remiddi, Phys. Lett. B **379**, 283 (1996)
61. M. I. Levine, ASHMEDAI. Comput. Phys. I (1967) 454; R. C. Perisho, ASHMEDAI User's Guide, U.S. AEC Report No. COO-3066-44 (1975)
62. M. J. G. Veltman, SchoonShip, CERN Report (1967)

63. H. Strubbe, *Comput. Phys. Commun.* 8 (1974) 1. *Comput. Phys. Commun.* **18**, 1 (1979)
64. A. C. Hearn, REDUCE User's Manual, Stanford University, Report No. ITP- 292, 1967, rev. 1968; A. C. Hearn, REDUCE 2 User's Manual. Stanford Artificial Intelligence Project Memo AIM-133, (unpublished) (1970)
65. J.A.M. Vermaseren, *Symbolic manipulation with FORM* (Computer Algebra Nederland, Amsterdam, 1991)
66. J. Bailey et al. [CERN Muon Storage Ring Collab.], *Phys. Lett. B* **67** (1977) 225 [*Phys. Lett. B* **68** (1977) 191]
67. J. Bailey et al., CERN-Mainz-Daresbury Collab. *Nucl. Phys. B* **150**, 1 (1979)
68. N. Cabibbo, R. Gatto, *Phys. Rev. Lett.* 4 (1960) 313. *Phys. Rep. C* **124**, 1577 (1961)
69. C. Bouchiat, L. Michel, *J. Phys. Radium* **22**, 121 (1961)
70. L. Durand, III *Erratum-ibid.* **129** (1963) 2835. *Phys. Rep. C* **128**, 441 (1962)
71. T. Kinoshita, R.J. Oakes, *Phys. Lett.* **25**, 143 (1967)
72. A.R. Erwin, R. March, W.D. Walker, E. West, *Phys. Rev. Lett.* 6 (1961) 628; D. Stonehill et al., *Phys. Rev. Lett.* 6 (1961) 624; E. Pickup, D. K. Robinson, E. O. Salant, *Phys. Rev. Lett.* 7 (1961) 192; D. McLeod, S. Richert, A. Silverman, *Phys. Rev. Lett.* 7 (1961) 383; D. D. Carmony, R. T. Van de Walle, *Phys. Rev. Lett.* 8 (1962) 73; J. Button, G. R. Kalbfleisch, G. R. Lynch, B. C. Maglic, A. H. Rosenfeld, M. L. Stevenson. *Phys. Rev.* **126**, 1858 (1962)
73. B.C. Maglic, L.W. Alvarez, A.H. Rosenfeld, M.L. Stevenson, *Phys. Rev. Lett.* 7 (1961) 178; N. H. Xuong, G. R. Lynch, *Phys. Rev. Lett.* 7 (1961) 327; A. Pevsner et al., *Phys. Rev. Lett.* 7 (1961) 421; M. L. Stevenson, L. W. Alvarez, B. C. Maglic, A. H. Rosenfeld. *Phys. Rev.* **125**, 687 (1962)
74. M. Gourdin, E. De Rafael, *Nucl. Phys. B* **10**, 667 (1969)
75. V.L. Auslander, G.I. Budker, Ju. N. Pestov, A. V. Sidorov, A. N. Skrinsky. A. G. Khabakhpashev. *Phys. Lett. B* **25**, 433 (1967)
76. J. E. Augustin et al., *Phys. Lett. B* **28**, 503, 508, 513, 517 (1969)
77. C. Heisey et al., A new precision measurement of the muon g-2 value at the level of 6.35 ppm, Brookhaven AGS Proposal 821, revised (1986). Design Report for AGS **821**, (1989) (1985)
78. R. Jackiw, S. Weinberg, *Phys. Rev. D* 5 (1972) 2396; I. Bars, M. Yoshimura, *Phys. Rev. D* 6 (1972) 374; G. Altarelli, N. Cabibbo, L. Maiani, *Phys. Lett. B* 40 (1972) 415; W. A. Bardeen, R. Gastmans, B. Lautrup, *Nucl. Phys. B* 46 (1972) 319; K. Fujikawa, B. W. Lee, A. I. Sanda. *Phys. Rev. D* **6**, 2923 (1972)
79. T. Kinoshita, W.B. Lindquist, *Phys. Rev. Lett.* **47**, 1573 (1981)
80. T. Kinoshita, B. Nizic, Y. Okamoto, *Phys. Rev. Lett.* 52 (1984) 717. *Phys. Rev. D* **31**, 2108 (1985)
81. T. Kinoshita, M. Nio, *Phys. Rev. Lett.* 90 (2003) 021803. *Phys. Rev. D* **70**, 113001 (2004)
82. T. Aoyama, M. Hayakawa, T. Kinoshita, M. Nio, *Phys. Rev. Lett.* **109**, 111807 (2012)
83. T. Aoyama, M. Hayakawa, T. Kinoshita, M. Nio, *Phys. Rev. Lett.* **109**, 111808 (2012)
84. S. Laporta, [arXiv:1704.06996](https://arxiv.org/abs/1704.06996) [hep-ph]
85. M. Hayakawa, T. Kinoshita, A. I. Sanda, *Phys. Rev. Lett.* 75 (1995) 790. *Phys. Rev. D* **54**, 3137 (1996)
86. J. Bijnens, E. Pallante, J. Prades, *Phys. Rev. Lett.* 75 (1995) 1447 [Erratum-ibid. 75 (1995) 3781]; *Nucl. Phys. B* 474 (1996) 379; [Erratum-ibid. 626 (2002) 410]; J. Bijnens. J. Prades *Mod. Phys. Lett. A* **22**, 767 (2007)
87. J. Bijnens, *EPJ Web Conf.* **118**, 01002 (2016)
88. S. Eidelman, F. Jegerlehner, *Z. Phys. C* **67** (1995) 585; F. Jegerlehner, *Nucl. Phys. (Proc. Suppl.) C* **51** (1996) 131; *J. Phys. G* **29** (2003) 101; *Nucl. Phys. Proc. Suppl.* **126**, 325 (2004)
89. F. Jegerlehner, *EPJ Web Conf.* **118**, 01016 (2016)
90. M. Benayoun, P. David, L. DelBuono, F. Jegerlehner, *Eur. Phys. J. C* **72** (2012) 1848; *Eur. Phys. J. C* **73** (2013) 2453; *Eur. Phys. J. C* **75**, 613 (2015)
91. P. Boyle, L. Del Debbio, E. Kerrane, J. Zanotti, *Phys. Rev. D* **85**, 074504 (2012)
92. X. Feng et al., *Phys. Rev. D* **88**, 034505 (2013)
93. C. Aubin, T. Blum, M. Golterman, S. Peris, *Phys. Rev. D* **88**, 074505 (2013)
94. A. Francis et al., *Nucl. Part. Phys. Proc.* (2016) 273-275, [arXiv:1411.3031](https://arxiv.org/abs/1411.3031) [hep-lat]

95. R. Malak et al. [Budapest-Marseille-Wuppertal Collab.], PoS LATTICE **2014**, 161 (2015)
96. M. Knecht, A. Nyffeler, Phys. Rev. D **65**, 073034 (2002)
97. K. Melnikov, A. Vainshtein, Phys. Rev. D **70**, 113006 (2004)
98. M. Knecht, Nucl. Part. Phys. Proc. 258-259 (2015) 235. EPJ Web Conf. **118**, 01017 (2016)
99. A. Nyffeler, EPJ Web Conf. **118**, 01024 (2016)
100. V. Pauk, M. Vanderhaeghen, Eur. Phys. J. C **74**, 3008 (2014)
101. G. Colangelo, M. Hoferichter, B. Kubis, M. Procura, P. Stoffer, Phys. Lett. B **738**, 6 (2014)
102. T. Blum, S. Chowdhury, M. Hayakawa, T. Izubuchi, Phys. Rev. Lett. **114** (2015) 012001; T. Blum, N. Christ, M. Hayakawa, T. Izubuchi, L. Jin, C. Lehner. Phys. Rev. D **93**, 014503 (2016)
103. M. Knecht, S. Peris, M. Perrottet, E. de Rafael, JHEP **0211**, 003 (2002)
104. A. Czarnecki, W. J. Marciano, A. Vainshtein, Erratum-ibid. D **73** (2006) 119901. Phys. Rev. D **67**, 073006 (2003)
105. L.M. Barkov et al., Nucl. Phys. B **256**, 365 (1985)
106. J.A. Casas, C. Lopez, F.J. Ynduráin, Phys. Rev. D **32**, 736 (1985)
107. F. Jegerlehner, Z. Phys. C **32**, 195 (1986)
108. J. Z. Bai et al. [BES Collab.], Phys. Rev. Lett. **84** (2000) 594; Phys. Rev. Lett. **88**, 101802 (2002)
109. R.R. Akhmetshin et al., CMD-2 Collab. Phys. Lett. B **578**, 285 (2004)
110. A. Aloisio et al., KLOE Collab. Phys. Lett. B **606**, 12 (2005)
111. V. M. Aulchenko et al. [CMD-2 Collab.], JETP Lett. **82** (2005) 743 [Pisma Zh. Eksp. Teor. Fiz. **82** (2005) 841]; R. R. Akhmetshin et al., JETP Lett. **84** (2006) 413 [Pisma Zh. Eksp. Teor. Fiz. **84** (2006) 491]; Phys. Lett. B **648**, 28 (2007)
112. M. N. Achasov et al. [SND Collab.], J. Exp. Theor. Phys. **103** (2006) 380 [Zh. Eksp. Teor. Fiz. **130** (2006) 437]
113. A. Aloisio [KLOE Collab.], Phys. Lett. B **606** (2005) 12; F. Ambrosino et al. et al., KLOE Collab. Phys. Lett. B **670**, 285 (2009)
114. F. Ambrosino et al., KLOE Collab. Phys. Lett. B **700**, 102 (2011)
115. D. Babusci et al., KLOE Collab. Phys. Lett. **B720**, 336 (2013)
116. B. Aubert et al., [BABAR Collab.], Phys. Rev. Lett. **103** (2009) 231801; J. P. Lees et al. Phys. Rev. **D86**, 032013 (2012)
117. M. Ablikim et al., BESIII Collab. Phys. Lett. B **753**, 629 (2016)
118. D. Bernard [BaBar Collab.], [arXiv:1604.07641](https://arxiv.org/abs/1604.07641) [hep-ex]
119. F.J.M. Farley, Y.K. Semertzidis, Prog. Part. Nucl. Phys. **52**, 1 (2004)
120. B. Odom, D. Hanneke, B. D'Urso, G. Gabrielse. Phys. Rev. Lett. **97**, 030801 (2006)
121. D. Hanneke, S. Fogwell, G. Gabrielse, Phys. Rev. Lett. **100**, 120801 (2008)
122. G. Gabrielse, D. Hanneke, T. Kinoshita, M. Nio, B. Odom, Erratum-ibid. **99** (2007) 039902. Phys. Rev. Lett. **97**, 030802 (2006)
123. T. Aoyama, M. Hayakawa, T. Kinoshita, M. Nio, Phys. Rev. Lett. **99**, 110406 (2007)
124. R. Bouchendira et al., Phys. Rev. Lett. **106**, 080801 (2011)
125. H.N. Brown et al., Muon (g-2) Collab. Phys. Rev. D **62**, 091101 (2000)
126. H.N. Brown et al., Muon (g-2) Collab. Phys. Rev. Lett. **86**, 2227 (2001)
127. G. W. Bennett et al. [Muon (g-2) Collab.], Phys. Rev. Lett. **89** (2002) 101804 [Erratum-ibid. **89** (2002) 129903]
128. M. Knecht, A. Nyffeler, Phys. Rev. D **65** (2002) 073034; A. Nyffeler, hep-ph/0210347 (and references therein)
129. K. Ackerstaff et al. [OPAL Collab.], Phys. Lett. B **431** (1998) 188; M. Acciarri et al. [L3 Collab.], Phys. Lett. B **434** (1998) 169; W. Lohmann, Nucl. Phys. B (Proc. Suppl.) **144**, 122 (2005)
130. J. Bailey, E. Picasso, Progr. Nucl. Phys. **12**, 43 (1970)
131. B.E. Lautrup, A. Peterman, E. de Rafael, Phys. Reports **3C**, 193 (1972)
132. F. Combley, E. Picasso, Phys. Reports **14C**, 1 (1974)
133. F.J.M. Farley, Contemp. Phys. **16**, 413 (1975)

134. T. Kinoshita, *Quantum Electrodynamics*, 1st edn (World Scientific, Singapore 1990) pp. 997, and contributions therein
135. F. J. M. Farley, E. Picasso, In: *Quantum Electrodynamics*, ed T. Kinoshita (World Scientific, Singapore 1990) pp. 479–559
136. T. Kinoshita, W. J. Marciano, In: *Quantum Electrodynamics*, ed. T. Kinoshita (World Scientific, Singapore 1990) pp. 419–478
137. V.W. Hughes, T. Kinoshita, *Rev. Mod. Phys.* **71**, S133 (1999)
138. A. Czarnecki, W. J. Marciano, *Nucl. Phys. B (Proc. Suppl.)* **76**, 245 (1999)
139. A. Czarnecki, W.J. Marciano, *Phys. Rev. D* **64**, 013014 (2001)
140. V. W. Hughes, *The anomalous magnetic moment of the muon*. In: Intern. School of Subnuclear Physics: 39th Course: New Fields and Strings in Subnuclear Physics, Erice, Italy, 29 Aug - 7 Sep 2001; *Int. J. Mod. Phys. A* **18S1**, 215 (2003)
141. E. de Rafael, *The muon $g-2$ revisited*. In: XVI Les Rencontres de Physique de la Vallée d'Aoste: Results and Perspectives in Particle Physics, La Thuile, Aosta Valley, Italy, 3–9 March 2002; hep-ph/0208251
142. A. Nyffeler, *Acta Phys. Polon. B* **34** (2003) 5197; *Nucl. Phys. B (Proc. Suppl.)* **131** (2004) 162; hep-ph/0305135
143. M. Knecht, *The anomalous magnetic moment of the muon: A theoretical introduction*, In: 41st International University School of Theoretical Physics: Flavor Physics (IUTP 41), Schladming, Styria, Austria, 22–28 February 2003; hep-ph/0307239
144. M. Passera, *J. Phys. G* **31**, R75 (2005)
145. K.P. Jungmann, Precision measurements at the frontiers of standard theory: The Magnetic Anomaly of Leptons. DPG Frühjahrstagung, Berlin **4–9**, (March 2005)
146. P.J. Mohr, B.N. Taylor, *Rev. Mod. Phys.* **72** (2000) 351; *Rev. Mod. Phys.* **77** (2005) 1; P. J. Mohr, B. N. Taylor, D. B. Newell, *Rev. Mod. Phys.* **84** (2012) 1527; P. J. Mohr, D. B. Newell, B. N. Taylor. *Rev. Mod. Phys.* **88**, 035009 (2016)
147. T. Kinoshita, *Nucl. Phys. B (Proc. Suppl.)* **144**, 206 (2005)
148. M. Passera, *Nucl. Phys. Proc. Suppl.* **169**, 213 (2007)
149. M. Benayoun et al., *Hadronic contributions to the muon anomalous magnetic moment Workshop. ($g - 2$) $_{\mu}$: Quo vadis? Workshop. Mini proceedings*, [arXiv:1407.4021](https://arxiv.org/abs/1407.4021) [hep-ph]
150. K. Melnikov, A. Vainshtein, *Theory of the Muon Anomalous Magnetic Moment* (Springer, Berlin, 2006)
151. F. Jegerlehner, A. Nyffeler, *Phys. Rept.* **477**, 1 (2009)
152. J.P. Miller, E. de Rafael, B.L. Roberts, *Rept. Prog. Phys.* **70**, 795 (2007)
153. T. Blum, A. Denig, I. Logashenko, E. de Rafael, B. Lee Roberts, T. Teubner, G. Venanzoni, [arXiv:1311.2198](https://arxiv.org/abs/1311.2198) [hep-ph]

Chapter 2

Quantum Field Theory and Quantum Electrodynamics

One of the main reasons why quantities like the anomalous magnetic moment of the muon attract so much attention is their prominent role in basic tests of QFT in general and of Quantum Electrodynamics (QED) and the Standard Model (SM) in particular. QED and the SM provide a truly basic framework for the properties of elementary particles and allow us to make unambiguous theoretical predictions which may be confronted with clean experiments which allows one to control systematic errors with amazing precision. In order to set up notation we first summarize some basic concepts. The reader familiar with QED, its renormalization and leading order radiative corrections may skip this introductory section, which is a modernized version of material covered by classical textbooks [1, 2]. Since magnetic moments of elementary particles are intimately related to the spin the latter plays a key role for this book. In a second section, therefore, we will have a closer look at how the concept of spin comes into play in quantum field theory.

2.1 Quantum Field Theory Background

2.1.1 Concepts, Conventions and Notation

We briefly sketch some basic concepts and fix the notation. A relativistic quantum field theory (QFT), which combines special relativity with quantum mechanics [3], is defined on the configuration space of space–time events described by points (**contravariant** vector)

$$x^\mu = (x^0, x^1, x^2, x^3) = (x^0, \mathbf{x}); x^0 = t (= \text{time})$$

in Minkowski space with metric

$$g_{\mu\nu} = g^{\mu\nu} = \begin{pmatrix} 1 & 0 & 0 & 0 \\ 0 & -1 & 0 & 0 \\ 0 & 0 & -1 & 0 \\ 0 & 0 & 0 & -1 \end{pmatrix}.$$

The metric defines a scalar product¹

$$x \cdot y = x^0 y^0 - \mathbf{x} \cdot \mathbf{y} = g_{\mu\nu} x^\mu y^\nu = x^\mu x_\mu$$

invariant under Lorentz transformations, which include

1. rotations
2. special Lorentz transformations (boosts)

The set of linear transformations (Λ, a)

$$x^\mu \rightarrow x^{\mu'} = \Lambda^\mu_{\nu'} x^\nu + a^{\mu'} \quad (2.1)$$

which leave invariant the **distance**

$$(x - y)^2 = g_{\mu\nu} (x^\mu - y^\mu)(x^\nu - y^\nu) \quad (2.2)$$

between two events x and y from the **Poincaré group** \mathcal{P} . \mathcal{P} includes the Lorentz transformations and the translations in time and space.

Besides the Poincaré invariance, also space reflections (called parity) P and time reversal T , defined by

$$Px = P(x^0, \mathbf{x}) = (x^0, -\mathbf{x}), \quad Tx = T(x^0, \mathbf{x}) = (-x^0, \mathbf{x}), \quad (2.3)$$

play an important role. They are symmetries of the electromagnetic (QED) and the strong interactions (QCD) but are violated by weak interactions. The proper orthochronous transformations \mathcal{P}_+^\uparrow do not include P and T , which requires the constraints on the determinant (orientation of frames) $\det \Lambda = 1$ and the direction of time $\Lambda^0_0 \geq 0$.

Finally, we will need the totally antisymmetric pseudo-tensor

$$\varepsilon^{\mu\nu\rho\sigma} = \begin{cases} +1 & (\mu\nu\rho\sigma) \text{ even permutation of } (0123) \\ -1 & (\mu\nu\rho\sigma) \text{ odd permutation of } (0123) \\ 0 & \text{otherwise} \end{cases},$$

¹As usual we adopt the summation convention: repeated indices are summed over unless stated otherwise. For Lorentz indices $\mu, \dots = 0, 1, 2, 3$ summation only makes sense (i.e. respects L-invariance) between upper (contravariant) and lower (covariant) indices and is called **contraction**.

which besides $g^{\mu\nu}$ is the second numerically Lorentz-invariant (L-invariant) tensor. Useful relations are

$$\begin{aligned}
\varepsilon^{\mu\nu\rho\sigma}\varepsilon_{\mu\nu\rho\sigma} &= -24 \\
\varepsilon^{\mu\nu\rho\sigma}\varepsilon_{\mu\nu\rho\sigma'} &= -6\delta_{\sigma'}^{\sigma} \\
\varepsilon^{\mu\nu\rho\sigma}\varepsilon_{\mu\nu\rho'\sigma'} &= -2\delta_{\rho'}^{\rho}\delta_{\sigma'}^{\sigma} + 2\delta_{\sigma'}^{\rho}\delta_{\rho'}^{\sigma} \\
\varepsilon^{\mu\nu\rho\sigma}\varepsilon_{\mu\nu'\rho'\sigma'} &= -\delta_{\nu'}^{\nu}\delta_{\rho'}^{\rho}\delta_{\sigma'}^{\sigma} + \delta_{\nu'}^{\nu}\delta_{\sigma'}^{\rho}\delta_{\rho'}^{\sigma} + \delta_{\rho'}^{\nu}\delta_{\nu'}^{\rho}\delta_{\sigma'}^{\sigma} - \delta_{\rho'}^{\nu}\delta_{\sigma'}^{\rho}\delta_{\nu'}^{\sigma} - \delta_{\sigma'}^{\nu}\delta_{\nu'}^{\rho}\delta_{\rho'}^{\sigma} + \delta_{\sigma'}^{\nu}\delta_{\rho'}^{\rho}\delta_{\nu'}^{\sigma}
\end{aligned} \tag{2.4}$$

In QFT relativistic particles are described by quantum mechanical states,² like $|\ell^-(\mathbf{p}, r)\rangle$ for a lepton ℓ^- of momentum \mathbf{p} and 3rd component of spin r [4] (Wigner

²A relativistic quantum mechanical system is described by a state vector $|\psi\rangle \in \mathcal{H}$ in Hilbert space, which transforms in a specific way under \mathcal{P}_+^{\uparrow} . We denote by $|\psi'\rangle$ the state transformed by $(\Lambda, a) \in \mathcal{P}_+^{\uparrow}$. Since the system is required to be invariant, transition probabilities must be conserved

$$|\langle\phi'|\psi'\rangle|^2 = |\langle\phi|\psi\rangle|^2 . \tag{2.5}$$

Therefore, there must exist a unitary operator $U(\Lambda, a)$ such that

$$|\psi\rangle \rightarrow |\psi'\rangle = U(\Lambda, a)|\psi\rangle \in \mathcal{H}$$

and $U(\Lambda, a)$ must satisfy the group law:

$$U(\Lambda_2, a_2)U(\Lambda_1, a_1) = \omega U(\Lambda_2\Lambda_1, \Lambda_2a_1 + a_2) .$$

This means that $U(\Lambda, a)$ is a **representation up to a phase** ω (ray representation) of \mathcal{P}_+^{\uparrow} . Without loss of generality one can choose $\omega = \pm 1$ (Wigner 1939).

The generators of \mathcal{P}_+^{\uparrow} are the relativistic energy-momentum operator P_{μ}

$$U(a) \equiv U(1, a) = e^{iP_{\mu}a^{\mu}} = 1 + iP_{\mu}a^{\mu} + \dots \tag{2.6}$$

and the relativistic angular momentum operator $M_{\mu\nu}$

$$U(\Lambda) \equiv U(\Lambda, 0) = e^{\frac{i}{2}\omega^{\mu\nu}M_{\mu\nu}} = 1 + \frac{i}{2}\omega^{\mu\nu}M_{\mu\nu} + \dots \tag{2.7}$$

Since for infinitesimal transformations we have

$$\Lambda^{\mu}_{\nu} = \delta^{\mu}_{\nu} + \omega^{\mu}_{\nu} \quad \text{with} \quad \omega_{\mu\nu} = -\omega_{\nu\mu},$$

the generators $M_{\mu\nu}$ are antisymmetric:

$$M_{\mu\nu} = -M_{\nu\mu} .$$

By unitarity of $U(\Lambda, a)$, P_{μ} and $M_{\mu\nu}$ are Hermitian operators on the Hilbert space. The generator of the time translations P_0 represents the Hamiltonian H of the system ($H \equiv P_0$) and determines the **time evolution**. If $|\psi\rangle = |\psi\rangle_H$ is a Heisenberg state, which coincides with the Schrödinger state $|\psi(0)\rangle_S$ at $t = 0$, then $|\psi(t)\rangle_S = e^{-iHt} |\psi(0)\rangle_S$ represents the state of the system at time t .

states). Spin will be considered in more detail in the next section. These states carry L-invariant mass $p^2 = m^2$ and spin s , and may be obtained by applying corresponding *creation operators* $a^+(\mathbf{p}, r)$ to the ground state $|0\rangle$, called vacuum:

$$|\mathbf{p}, r\rangle = a^+(\mathbf{p}, r) |0\rangle . \quad (2.8)$$

The energy of the particle is $p^0 = \omega_p = \sqrt{\mathbf{p}^2 + m^2}$. The Hermitian adjoints of the creation operators, the *annihilation operators* $a(\mathbf{p}, r) \doteq (a^+(\mathbf{p}, r))^+$, annihilate a state of momentum \mathbf{p} and 3rd component of spin r ,

$$a(\mathbf{p}, r) |\mathbf{p}', r'\rangle = (2\pi)^3 2\omega_p \delta^{(3)}(\mathbf{p} - \mathbf{p}') \delta_{rr'} |0\rangle$$

and since the vacuum is empty, in particular, they annihilate the vacuum

$$a(\mathbf{p}, r) |0\rangle = 0 . \quad (2.9)$$

The creation and annihilation operators for leptons (spin 1/2 fermions), a and a^+ , and the corresponding operators b and b^+ for the antileptons, satisfy the canonical *anticommutation relations* (Fermi statistics)

$$\{a(\mathbf{p}, r), a^+(\mathbf{p}', r')\} = \{b(\mathbf{p}, r), b^+(\mathbf{p}', r')\} = (2\pi)^3 2\omega_p \delta^{(3)}(\mathbf{p} - \mathbf{p}') \delta_{rr'} \quad (2.10)$$

with all other anticommutators vanishing. Note, the powers of 2π appearing at various places are convention dependent. Corresponding creation and annihilation operators for photons (spin 1 bosons) satisfy the *commutation relations* (Bose statistics)

$$[c(\mathbf{p}, \lambda), c^+(\mathbf{p}', \lambda')] = (2\pi)^3 2\omega_p \delta^{(3)}(\mathbf{p} - \mathbf{p}') \delta_{\lambda\lambda'} . \quad (2.11)$$

In configuration space particles have associated fields [5–7]. The leptons are represented by Dirac fields $\psi_\alpha(x)$, which are four-component spinors $\alpha = 1, 2, 3, 4$, and the photon by the real vector potential field $A^\mu(x)$ from which derives the electromagnetic field strength tensor $F^{\mu\nu} = \partial^\mu A^\nu - \partial^\nu A^\mu$. The free fields are represented in terms of the creation and annihilation operators

$$\psi_\alpha(x) = \sum_{r=\pm 1/2} \int d\mu(p) \left\{ u_\alpha(\mathbf{p}, r) a(\mathbf{p}, r) e^{-ipx} + v_\alpha(\mathbf{p}, r) b^+(\mathbf{p}, r) e^{ipx} \right\} \quad (2.12)$$

for the fermion, and

$$A_\mu(x) = \sum_{\lambda=\pm} \int d\mu(p) \left\{ \varepsilon_\mu(p, \lambda) c(\mathbf{p}, \lambda) e^{-ipx} + \text{h.c.} \right\} \quad (2.13)$$

for the photon (h.c. = Hermitian conjugation). The Fourier transformation has to respect that the physical state is on the mass-shell and has positive energy (*spectral*

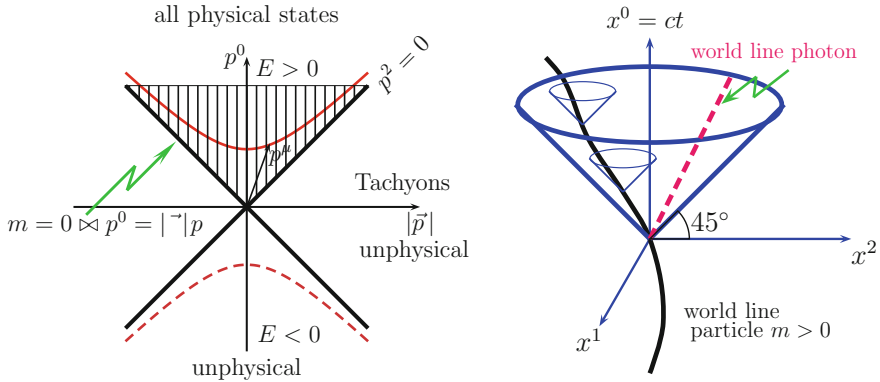


Fig. 2.1 Left the spectral condition: $p^2 = m^2 \geq 0$, $p^0 = E = \sqrt{\mathbf{p}^2 + m^2} \geq 0$. Right Einstein causality: physical signals propagate inside the light-cone $x^2 \geq 0$ (time-like)

condition: $p^2 = m^2$, $p^0 \geq m$, $m \geq 0$ see Fig. 2.1), thus $p^0 = \omega_p = \sqrt{m^2 + \mathbf{p}^2}$ and

$$\int d\mu(p) \cdots \equiv \int \frac{d^3 p}{2\omega_p (2\pi)^3} \cdots = \int \frac{d^4 p}{(2\pi)^3} \Theta(p^0) \delta(p^2 - m^2) \cdots$$

Note that Fourier amplitudes $e^{\mp i p x}$ in (2.12) and (2.13), because of the on-shell condition $p^0 = \omega_p$, are plane wave (free field) solutions of the *Klein–Gordon equation*: $(\square_x + m^2) e^{\mp i p x} = 0$ or the *d’Alembert equation* $\square_x e^{\mp i p x} = 0$ for the photon where $m_\gamma = 0$. Therefore, the fields themselves satisfy the Klein–Gordon or the d’Alembert equation, respectively. The “amplitudes” u , v and ε_μ , appearing in (2.12) and (2.13) respectively, are classical one-particle wave functions (plane wave solutions) satisfying the free field equations in momentum space.³ Thus u the lepton wavefunction and v the antilepton wavefunction are four-spinors, c-number solutions of the Dirac equations,

$$\begin{aligned} (\not{p} - m) u_\alpha(\mathbf{p}, r) &= 0, \quad \text{for the lepton} \\ (\not{p} + m) v_\alpha(\mathbf{p}, r) &= 0, \quad \text{for the antilepton.} \end{aligned} \quad (2.15)$$

³Our convention for the four-dimensional Fourier transformation for general (off-shell) fields, reads (all integrations from $-\infty$ to $+\infty$)

$$\tilde{\psi}(p) = \int d^4 x e^{i p x} \psi(x), \quad \tilde{A}^\mu(p) = \int d^4 x e^{i p x} A^\mu(x). \quad (2.14)$$

The inverse transforms then take the form

$$\psi(x) = \int \frac{d^4 p}{(2\pi)^4} e^{-i p x} \tilde{\psi}(p), \quad A^\mu(x) = \int \frac{d^4 p}{(2\pi)^4} e^{-i p x} \tilde{A}^\mu(p), \quad \delta^{(4)}(x) = \int \frac{d^4 p}{(2\pi)^4} e^{-i p x}$$

and hence the derivative with respect to x^μ turns into multiplication by the *four-momentum* $-i p_\mu$: $\partial_\mu \psi(x) \rightarrow -i p_\mu \tilde{\psi}(p)$ etc.

As usual, we use the short notation $\not{p} \doteq \gamma^\mu p_\mu = \gamma^0 p^0 - \boldsymbol{\gamma} \mathbf{p}$ (repeated indices summed over). Note that the relations (2.15) directly infer that the Dirac field is a solution of the Dirac equation $(i\gamma^\mu \partial_\mu - m) \psi(x) = 0$.

The $\underline{\gamma}$ -matrices are 4×4 matrices which satisfy the **Dirac algebra**⁴:

$$\{\gamma^\mu, \gamma^\nu\} = \gamma^\mu \gamma^\nu + \gamma^\nu \gamma^\mu = 2g^{\mu\nu} \quad (2.16)$$

The L-invariant parity odd matrix γ_5 (under parity $\gamma^0 \rightarrow \gamma^0$, $\gamma^i \rightarrow -\gamma^i$ $i = 1, 2, 3$)

$$\gamma_5 = i\gamma^0 \gamma^1 \gamma^2 \gamma^3 = \frac{i}{4!} \varepsilon_{\mu\nu\rho\sigma} \gamma^\mu \gamma^\nu \gamma^\rho \gamma^\sigma ; \quad \gamma_5^2 = 1 ; \quad \gamma_5 = \gamma_5^+ \quad (2.17)$$

satisfies the anticommutation relation

$$\{\gamma_5, \gamma^\mu\} = \gamma_5 \gamma^\mu + \gamma^\mu \gamma_5 = 0 \quad (2.18)$$

and is required for the formulation of parity violating theories like the weak interaction part of the Standard Model (SM) and for the projection of Dirac fields to left-handed (L) and right-handed (R) chiral fields

$$\psi_R = \Pi_+ \psi ; \quad \psi_L = \Pi_- \psi \quad (2.19)$$

⁴Dirac's γ -matrices are composed from Pauli matrices. In quantum mechanics spacial rotations are described by the group of unitary, unimodular ($\det U = 1$) complex 2×2 matrix transformations $SU(2)$ rather than by classical $O(3)$ rotations. The structure constants are given by ϵ_{ikl} ($i, k, l = 1, 2, 3$) the fully antisymmetric permutation tensor. The generators of $SU(2)$ are given by $T_i = \frac{\sigma_i}{2}$; σ_i ($i = 1, 2, 3$) in terms of the 3 Hermitian and traceless *Pauli matrices*

$$\sigma_1 = \begin{pmatrix} 0 & 1 \\ 1 & 0 \end{pmatrix}, \quad \sigma_2 = \begin{pmatrix} 0 & -i \\ i & 0 \end{pmatrix}, \quad \sigma_3 = \begin{pmatrix} 1 & 0 \\ 0 & -1 \end{pmatrix}$$

one of which (σ_3) is diagonal. The properties of the Pauli matrices are

$$\begin{aligned} [\sigma_i, \sigma_k] &= 2i\epsilon_{ikl}\sigma_l, \quad \{\sigma_i, \sigma_k\} = 2\delta_{ik} \\ \sigma_i^+ &= \sigma_i, \quad \sigma_i^2 = 1, \quad \text{Tr } \sigma_i = 0 \\ \sigma_i \sigma_k &= \frac{1}{2} \{\sigma_i, \sigma_k\} + \frac{1}{2} [\sigma_i, \sigma_k] = \delta_{ik} + i\epsilon_{ikl}\sigma_l \end{aligned}$$

As usual we denote by $[A, B] = AB - BA$ the commutator, by $\{A, B\} = AB + BA$ the anticommutator. Dirac's γ -matrices in standard representation (as an alternative to the helicity representation, considered below) are

$$\gamma^0 = \begin{pmatrix} 1 & 0 \\ 0 & -1 \end{pmatrix}, \quad \gamma^i = \begin{pmatrix} 0 & \sigma_i \\ -\sigma_i & 0 \end{pmatrix}, \quad \gamma_5 = \begin{pmatrix} 0 & 1 \\ 1 & 0 \end{pmatrix}.$$

where

$$\Pi_{\pm} = \frac{1}{2}(1 \pm \gamma_5) \quad (2.20)$$

are Hermitian chiral projection matrices⁵

$$\Pi_+ + \Pi_- = 1, \quad \Pi_+ \Pi_- = \Pi_- \Pi_+ = 0, \quad \Pi_-^2 = \Pi_- \quad \text{and} \quad \Pi_+^2 = \Pi_+ .$$

Note that $\psi^+ \psi$ or $u^+ u$, which might look like the natural analog of $|\psi|^2 = \psi^* \psi$ of the lepton wave function in quantum mechanics, are not scalars (invariants) under Lorentz transformations. In order to obtain an invariant we have to sandwich the matrix A which implements Hermitian conjugation of the Dirac matrices $A \gamma_{\mu} A^{-1} = \gamma_{\mu}^+$. One easily checks that we may identify $A = \gamma^0$. Thus defining the *adjoint spinor* by $\bar{\psi} \doteq \psi^+ \gamma^0$ we may write $\psi^+ A \psi = \bar{\psi} \psi$ etc.

The standard basis of 4×4 matrices in four-spinor space is given by the 16 elements

$$\Gamma_i = 1, \gamma_5, \gamma^{\mu}, \gamma^{\mu} \gamma_5 \quad \text{and} \quad \sigma^{\mu\nu} = \frac{i}{2} [\gamma^{\mu}, \gamma^{\nu}] . \quad (2.22)$$

The corresponding products $\bar{\psi} \Gamma_i \psi$ are scalars in spinor space and transform as ordinary scalar (S), pseudo-scalar (P), vector (V), axial-vector (A) and tensor (T), respectively, under Lorentz transformations.

⁵Usually, the quantization of a massive particle with spin is defined relative to the z -axis as a standard frame. In general, the direction of polarization ξ , $\xi^2 = 1$ in the rest frame may be chosen arbitrary. For a massive fermion of momentum p

$$\Pi_{\pm} = \frac{1}{2}(1 \pm \gamma_5 \not{n})$$

define the general form of covariant spin projection operators, where n is a space like unit vector orthogonal to p

$$n^2 = -1; \quad n \cdot p = 0 .$$

The general form of n is obtained by applying Lorentz-boost $L_{\mathbf{p}}$ to the polarization vector in the rest frame

$$n = L_{\mathbf{p}}(0, \xi) = \left(\frac{\mathbf{p} \cdot \xi}{m}, \quad \xi + \frac{\mathbf{p} \cdot \xi}{m(p^0 + m)} \mathbf{p} \right) . \quad (2.21)$$

When studying polarization phenomena the polarization vectors n enter as independent additional vectors in covariant decompositions of amplitudes, besides the momentum vectors.

Products of Dirac matrices may be expressed in terms of the basis, as

$$\begin{aligned}\gamma^\mu \gamma^\nu &= \frac{1}{2} \{ \{\gamma^\mu, \gamma^\nu\} + [\gamma^\mu, \gamma^\nu] \} = g^{\mu\nu} - i \sigma^{\mu\nu} \\ \gamma^\mu \gamma^\nu \gamma^\rho &= (g^{\mu\nu} g^{\rho\sigma} + g^{\mu\sigma} g^{\rho\nu} - g^{\mu\rho} g^{\nu\sigma}) \gamma_\sigma - i \varepsilon^{\mu\nu\rho\sigma} \gamma_\sigma \gamma_5 \\ \sigma^{\mu\nu} \gamma_5 &= \frac{i}{2} \varepsilon^{\mu\nu\rho\sigma} \sigma_{\rho\sigma} .\end{aligned}$$

The Dirac spinors satisfy the normalization conditions

$$\begin{aligned}\bar{u}(p, r) \gamma^\mu u(p, r') &= 2 p^\mu \delta_{rr'} , & \bar{v}(p, r) \gamma^\mu v(p, r') &= 2 p^\mu \delta_{rr'} \\ \bar{u}(p, r) v(p, r') &= 0 , & \bar{u}(p, r) u(p, r) &= 2m \delta_{rr'} \\ \bar{v}(p, r) u(p, r') &= 0 , & \bar{v}(p, r) v(p, r) &= -2m \delta_{rr'}\end{aligned}\quad (2.23)$$

and completeness relations

$$\sum_r u(p, r) \bar{u}(p, r) = \not{p} + m , \quad \sum_r v(p, r) \bar{v}(p, r) = \not{p} - m . \quad (2.24)$$

For the photon the *polarization vector* $\varepsilon_\mu(p, \lambda)$ satisfies the normalization

$$\varepsilon_\mu(p, \lambda) \varepsilon^{\mu*}(p, \lambda') = -\delta_{\lambda\lambda'} , \quad (2.25)$$

the completeness relation

$$\sum_{\lambda=\pm} \varepsilon_\mu(p, \lambda) \varepsilon_\nu^*(p, \lambda) = -g_{\mu\nu} + p_\mu f_\nu + p_\nu f_\mu , \quad (2.26)$$

and the absence of a scalar mode requires

$$p_\mu \varepsilon^\mu(p, \lambda) = 0 . \quad (2.27)$$

The “four–vectors” f in the completeness relation are arbitrary gauge dependent quantities, which must drop out from physical quantities. Gauge invariance, i.e. invariance under *Abelian gauge transformations* $A_\mu \rightarrow A_\mu - \partial_\mu \alpha(x)$, $\alpha(x)$ an arbitrary scalar function, amounts to the invariance under the substitutions

$$\varepsilon_\mu \rightarrow \varepsilon_\mu + \lambda p_\mu ; \quad \lambda \text{ an arbitrary constant} \quad (2.28)$$

of the polarization vectors. One can prove that the polarization “vectors” for massless spin 1 fields can not be covariant. The non–covariant terms are always proportional to p_μ , however.

Besides a definite relativistic transformation property, like

$$U(\Lambda, a) \psi_\alpha(x) U^{-1}(\Lambda, a) = D_{\alpha\beta}(\Lambda^{-1}) \psi_\beta(\Lambda x + a) ,$$

for a Dirac field, where $D(\Lambda)$ is a four-dimensional (non-unitary) representation of the group $SL(2, C)$ which, in contrast to L_+^\uparrow itself, exhibits true *spinor representations* (see Sect. 2.2). The fields are required to satisfy Einstein causality: “no physical signal may travel faster than light”, which means that commutators for bosons and anticommutators for fermions must vanish outside the light cone (see Fig. 2.1)

$$[A_\mu(x), A_\nu(x')] = 0, \quad \{\psi_\alpha(x), \bar{\psi}_\beta(x')\} = 0 \quad \text{for } (x - x')^2 < 0 .$$

This is only possible if all fields exhibit two terms, a creation and an annihilation part, and for charged particles this means that to each particle an antiparticle of the same mass and spin but of opposite charge must exist [8]. In addition, and equally important, causality requires spin $1/2, 3/2, \dots$ particles to be fermions quantized with anticommutation rules and hence necessarily have to fulfill the *Pauli exclusion principle* [9], while spin $0, 1, \dots$ must be bosons to be quantized by normal commutation relations [10]. Note that neutral particles only, like the photon, may be their own antiparticle, the field then has to be real. The main consequences of the requirements of locality and causality of a relativistic field theory may be cast into the two theorems: – the **spin–statistics theorem** –

Theorem 2.1 *Bosons quantized with commutation relations must have integer spin. Fermions quantized with anticommutation relations must have half odd–integer spin.*

– the **particle–antiparticle crossing theorem** –

Theorem 2.2 *Each particle of mass m and spin j must have associated an antiparticle with the same mass and spin, and which transforms under the same representation of \mathcal{P}_+^\uparrow . A particle may be its own antiparticle. If charged, particle and antiparticle have opposite charge.*

For rigorous proofs of the theorems I refer to [11].

2.1.2 C, P, T and CPT

In QED as well as in QCD, not however in weak interactions, interchanging particles with antiparticles defines a symmetry, *charge conjugation* C. It is mapping particle into antiparticle creation and annihilation operators and vice versa:

$$a(\mathbf{p}, r) \xleftrightarrow{C} b(\mathbf{p}, r) , \quad a^+(\mathbf{p}, r) \xleftrightarrow{C} b^+(\mathbf{p}, r) ,$$

up to a phase. For the Dirac field charge conjugation reads (see 2.36)

$$\psi_\alpha(x) \xrightarrow{C} C_{\alpha\beta} \bar{\psi}_\beta^T(x) \tag{2.29}$$

with ($X^T =$ transposition of the matrix or vector X)

$$C = i(\gamma^2 \gamma^0) = -i \begin{pmatrix} 0 & \sigma_2 \\ \sigma_2 & 0 \end{pmatrix} . \quad (2.30)$$

Properties of C are:

$$C^T = -C , \quad C\gamma^\mu C^{-1} = -(\gamma^\mu)^T ,$$

and for the spinors charge conjugation takes the form

$$(Cu)^T = \bar{v} \quad \text{and} \quad (Cv)^T = \bar{u} , \quad (2.31)$$

which may be verified by direct calculation.

As under charge conjugation the charge changes sign, also the electromagnetic current must change sign

$$U(C) j_{\text{em}}^\mu(x) U^{-1}(C) = -j_{\text{em}}^\mu(x) . \quad (2.32)$$

Notice that for any contravariant four-vector j^μ we may write the parity transformed vector ($j^0, -\mathbf{j}$) $\equiv j_\mu$ as a covariant vector. We will use this notation in the following.

Since the electromagnetic interaction $\mathcal{L}_{\text{int}}^{\text{QED}} = e j_{\text{em}}^\mu(x) A_\mu(x)$ respects C-, P- and T-invariance⁶ separately, we immediately get the following transformation properties for the photon field:

$$\begin{aligned} U(C) A^\mu(x) U^{-1}(C) &= -A^\mu(x) \\ U(P) A^\mu(x) U^{-1}(P) &= (PA)^\mu(Px) = A_\mu(Px) \\ \bar{U}(T) A^\mu(x) \bar{U}^{-1}(T) &= -(TA)^\mu(Tx) = A_\mu(Tx) . \end{aligned} \quad (2.35)$$

Notice that the charge parity for the photon is $\eta_C^\gamma = -1$.

⁶Any transformation which involves time-reversal T must be implemented as an anti-unitary transformation $\bar{U}(T)$, because the Hamiltonian cannot be allowed to change sign by the requirement of positivity of the energy (Wigner 1939). **Anti-unitarity** is defined by the properties

$$\bar{U}(\alpha|\psi\rangle + \beta|\phi\rangle) = \alpha^* \bar{U}|\psi\rangle + \beta^* \bar{U}|\phi\rangle = \alpha^* |\psi'\rangle + \beta^* |\phi'\rangle \quad (2.33)$$

and

$$\langle \psi' | \phi' \rangle = \langle \psi | \phi \rangle^* . \quad (2.34)$$

The complex conjugation of matrix elements is admitted by the fact that it also preserves the probability $|\langle \psi | \phi \rangle|^2$. Because of the complex conjugation of matrix elements an anti-unitary transformation implies a **Hermitian transposition** of states and operators.

For the Dirac fields C, P and T take the form

$$\begin{aligned}
 U(C) \psi_\alpha(x) U^{-1}(C) &= i (\gamma^2 \gamma^0)_{\alpha\beta} \bar{\psi}_\beta^T(x) \\
 U(P) \psi_\alpha(x) U^{-1}(P) &= (\gamma^0)_{\alpha\beta} \psi_\beta(Px) \\
 \bar{U}(T) \psi_\alpha(x) \bar{U}^{-1}(T) &= i (\gamma^2 \gamma_5)_{\alpha\beta} \bar{\psi}_\beta^T(Tx)
 \end{aligned} \tag{2.36}$$

where the phases have been chosen conveniently. We observe that, in contrast to the boson fields, the transformation properties of the Dirac fields are by no means obvious; they follow from applying C, P and T to the Dirac equation.

A very important consequence of *relativistic local quantum field theory* is the validity of the **CPT–theorem**:

Theorem 2.3 *Any Poincaré (\mathcal{P}_+^\uparrow) [special Lorentz transformations, rotations plus translations] invariant field theory with normal commutation relations [bosons satisfying commutation relations, fermions anticommutation relations] is CPT invariant.*

Let $\Theta = \text{CPT}$ where C, P and T may be applied in any order. There exists an anti–unitary operator $\bar{U}(\Theta)$ which (with an appropriate choice of the phases) is transforming scalar, Dirac and vector fields according to

$$\begin{aligned}
 \bar{U}(\Theta) \phi(x) \bar{U}^{-1}(\Theta) &= \phi^*(-x) \\
 \bar{U}(\Theta) \psi(x) \bar{U}^{-1}(\Theta) &= i\gamma_5 \psi(-x) \\
 \bar{U}(\Theta) A_\mu(x) \bar{U}^{-1}(\Theta) &= -A_\mu(-x) \quad ,
 \end{aligned} \tag{2.37}$$

and which leaves the vacuum invariant: $\bar{U}(\Theta)|0\rangle = |0\rangle$ up to a phase. The CPT–theorem asserts that the transformation $\bar{U}(\Theta)$ under very general conditions is a symmetry of the theory (Lüders 1954, Pauli 1955, Jost 1957) [12].

The basic reason for the validity of the CPT–theorem is the following: If we consider a Lorentz transformation $\Lambda \in L_+^\uparrow$ represented by a unitary operator $U(\chi, \omega = \mathbf{n} \theta)$ (χ parametrizing a Lorentz–boost, ω parametrizing a rotation), then the operator $U(\chi, \mathbf{n}(\theta + 2\pi)) = -U(\chi, \mathbf{n} \theta)$ is representing the same L–transformation. In a local quantum field theory the mapping $\Lambda \rightarrow -\Lambda$ for $\Lambda \in L_+^\uparrow$, which is equivalent to the requirement that $\Theta : x \rightarrow -x$ must be a symmetry: the invariance under four–dimensional reflections.

Consequences of CPT are that modulus of the charges, masses, g –factors and lifetimes of particles and antiparticles must be equal. Consider a one particle state $|\psi\rangle = |e, \mathbf{p}, \mathbf{s}\rangle$ where e is the charge, \mathbf{p} the momentum and \mathbf{s} the spin. The CPT conjugate state is given by $|\tilde{\psi}\rangle = |-e, \mathbf{p}, -\mathbf{s}\rangle$. The state $|\psi\rangle$ is an eigenstate of the Hamiltonian which is describing the time evolution of the free particle:

$$\mathcal{H}|\psi\rangle = E|\psi\rangle \tag{2.38}$$

and the CPT conjugate relation reads $\tilde{\mathcal{H}}|\tilde{\psi}\rangle = E|\tilde{\psi}\rangle$. Since $\tilde{\mathcal{H}} = \mathcal{H}$ by the CPT theorem, we thus have

$$\mathcal{H}|\tilde{\psi}\rangle = E|\tilde{\psi}\rangle . \quad (2.39)$$

At $\mathbf{p} = 0$ the eigenvalue E reduces to the mass and therefore the two eigenvalue equations say that the mass of particle and antiparticle must be the same:

$$\bar{m} = m . \quad (2.40)$$

The equality of the g -factors may be shown in the same way, but with a Hamiltonian which describes the interaction of the particle with a magnetic field \mathbf{B} . Then (2.38) holds with eigenvalue

$$E = m - g \left(\frac{e\hbar}{2mc} \right) \mathbf{s} \cdot \mathbf{B} . \quad (2.41)$$

The CPT conjugate state ($e \rightarrow -e$, $\mathbf{s} \rightarrow -\mathbf{s}$, $m \rightarrow \bar{m}$, $g \rightarrow \bar{g}$, $\mathbf{B} \rightarrow \mathbf{B}$) according to (2.39) will have the same eigenvalue

$$E = \bar{m} - \bar{g} \left(\frac{e\hbar}{2\bar{m}c} \right) \mathbf{s} \cdot \mathbf{B} . \quad (2.42)$$

and since $\bar{m} = m$ we must have

$$\bar{g} = g \quad (2.43)$$

For the proof of the equality of the lifetimes

$$\bar{\tau} = \tau \quad (2.44)$$

we refer to the textbook [13]. Some examples of experimental tests of CPT, relevant in our context, are (see [14])

$$\begin{array}{ll} |q_{e^+} + q_{e^-}|/e & < 4 \times 10^{-8} \\ (m_{e^+} - m_{e^-})/m_{\text{average}} & < 8 \times 10^{-9} \quad 90\% \text{ CL} \\ (g_{e^+} - g_{e^-})/g_{\text{average}} & (-0.5 \pm 2.1) \times 10^{-12} \\ (g_{\mu^+} - g_{\mu^-})/g_{\text{average}} & (-0.11 \pm 0.12) \times 10^{-8} \\ (\tau_{\mu^+} - \tau_{\mu^-})/\tau_{\text{average}} & (2 \pm 8) \times 10^{-5} . \end{array}$$

The best test of CPT comes from the neutral Kaon mass difference

$$\left| \frac{m_{\bar{K}^0} - m_{K^0}}{m_{K^0}} \right| \leq 0.6 \times 10^{-18} \quad \text{at CL} = 90\% .$$

The existence of a possible electric dipole moment we have discussed earlier on p. 9 of the Introduction. An electric dipole moment requires a T violating theory and the CPT theorem implies that equivalently CP must be violated. In fact, CP invariance alone (independently of CPT and T) gives important predictions relating

decay properties of particles and antiparticles. We are interested here particularly in μ -decay, which plays a crucial role in the muon $g - 2$ experiment. Consider a matrix element for a particle a with spin \mathbf{s}_a at rest decaying into a bunch of particles b, c, \dots with spins $\mathbf{s}_b, \mathbf{s}_c, \dots$ and momenta $\mathbf{p}_b, \mathbf{p}_c, \dots$:

$$\mathcal{M} = \langle \mathbf{p}_b, \mathbf{s}_b; \mathbf{p}_c, \mathbf{s}_c; \dots | \mathcal{H}_{\text{int}} | 0, \mathbf{s}_a \rangle . \quad (2.45)$$

Under CP we have to substitute $\mathbf{s}_a \rightarrow \mathbf{s}_{\bar{a}}, \mathbf{p}_a \rightarrow -\mathbf{p}_{\bar{a}},$ etc. such that, provided \mathcal{H}_{int} is CP symmetric we obtain

$$\bar{\mathcal{M}} = \langle -\mathbf{p}_{\bar{b}}, \mathbf{s}_{\bar{b}}; -\mathbf{p}_{\bar{c}}, \mathbf{s}_{\bar{c}}; \dots | \mathcal{H}_{\text{int}} | 0, \mathbf{s}_{\bar{a}} \rangle \equiv \mathcal{M} . \quad (2.46)$$

The modulus square of these matrix-elements gives the transition probability for the respective decays, and (2.46) tells us that the decay rate of a particle into a particular configuration of final particles is identical to the decay rate of the antiparticle into the same configuration of antiparticles with all momenta reversed.

For the muon decay $\mu^- \rightarrow e^- \bar{\nu}_e \nu_\mu,$ after integrating out the unobserved neutrino variables, the decay electron distribution is of the form

$$\frac{dN_{e^-}}{dx d \cos \theta} = A(x) + B(x) \hat{\mathbf{s}}_\mu \cdot \hat{\mathbf{p}}_{e^-} , \quad (2.47)$$

where $x = 2p_{e^-}/m_\mu$ with p_{e^-} the electron momentum in the muon rest frame and $\cos \theta = \hat{\mathbf{s}}_\mu \cdot \hat{\mathbf{p}}_{e^-}, \hat{\mathbf{s}}_\mu$ and $\hat{\mathbf{p}}_{e^-}$ the unit vectors in direction of \mathbf{s}_μ and $\mathbf{p}_{e^-}.$

The corresponding expression for the antiparticle decay $\mu^+ \rightarrow e^+ \nu_e \bar{\nu}_\mu$ reads

$$\frac{dN_{e^+}}{dx d \cos \theta} = \bar{A}(x) + \bar{B}(x) \hat{\mathbf{s}}_\mu \cdot \hat{\mathbf{p}}_{e^+} , \quad (2.48)$$

and therefore for all angles and all electron momenta

$$A(x) + B(x) \cos \theta = \bar{A}(x) - \bar{B}(x) \cos \theta$$

or

$$A(x) = \bar{A}(x) , \quad B(x) = -\bar{B}(x) . \quad (2.49)$$

It means that the decay asymmetry is equal in magnitude but opposite in sign for μ^- and $\mu^+.$ This follows directly from CP and independent of the type of interaction (V-A, V+A, S, P or T) and whether P is violated or not. In spite of the fact that the SM exhibits CP violation (see the Introduction to Sect. 4.2), as implied by a CP violating phase in the quark family mixing matrix in the charged weak current, in μ -decay CP violation is a very small higher order effect and by far too small to have any detectable trace in the decay distributions, i.e., CP symmetry is perfectly realized in this case. The strong correlation between the muon polarization and charge on the

one side (see Chap. 6) and the decay electron/positron momentum is a key element of tracing spin polarization information in the muon $g - 2$ experiments.

CP violation, and the associated T violation plays an important role in determining the electric dipole moment of electrons and muons. In principle it is possible to test T invariance in μ -decay by searching for T odd matrix elements like

$$\mathbf{s}_e \cdot (\mathbf{s}_\mu \times \mathbf{p}_e) . \quad (2.50)$$

This is very difficult and has not been performed. A method which works is the study of the effect of an electric dipole moment on the spin precession in the muon $g - 2$ experiment. This will be studied in Sect. 6.3.1 on p. 584.

Until recently, the best limit for the electron (1.8) has been obtained by investigating T violation in Thallium (^{205}Tl) where the EDM is enhanced by the ratio $R = d_{\text{atom}}/d_e$, which in the atomic Thallium ground state studied is $R = -585$. Investigated are $\mathbf{v} \times \mathbf{E}$ terms in high electrical fields \mathbf{E} in an atomic beam magnetic–resonance device [15]. A new experiment [16], using the polar molecule Thorium monoxide (ThO), finds

$$d_e = (2.1 \pm 3.7 \text{ stat} \pm 2.5 \text{ syst}) \times 10^{-29} e \cdot \text{cm} .$$

This corresponds to an upper limit of $|d_e| < 8.7 \times 10^{-29} e \cdot \text{cm}$ with 90% confidence, an order of magnitude improvement in sensitivity compared to the previous best limits.

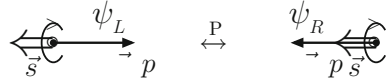
2.2 The Origin of Spin

As promised at the beginning of the chapter the intimate relation of the anomalous magnetic moment to spin is a good reason to have a closer look at how spin comes into play in particle physics. The spin and the magnetic moment of the electron did become evident from the deflection of atoms in an inhomogeneous magnetic field and the observation of the fine structure by optical spectroscopy [17–19].⁷ Spin is the intrinsic “self–angular momentum” of a point–particle and when it was observed by Goudsmit and Uhlenbeck it was completely unexpected. The question about the origin of spin is interesting because it is not obvious how a point–like object can possess its own angular momentum. A first theoretical formulation of spin in quantum mechanics was given by Pauli in 1927 [20], where spin was introduced as a new degree of freedom saying that there are two species of electrons in a doublet.

In modern relativistic terms, in the SM, particles and in particular leptons and quarks are considered to be massless originally, as required by chiral symmetry. All particles acquire their mass due to symmetry breaking via the Higgs mechanism: a

⁷Particle spin has been discovered by Ralph Kronig (well known for the Kramers Kronig relation) in 1925 before the Uhlenbeck and Goudsmit publication.

Fig. 2.2 Massless “electrons” have fixed helicities



scalar neutral Higgs field⁸ H develops a non-vanishing vacuum expectation value v and particles moving in the corresponding Bose condensate develop an effective mass. In the SM, in the physical *unitary gauge* a *Yukawa interaction* term upon a shift $H \rightarrow H + v$

$$\mathcal{L}_{\text{Yukawa}} = \sum_f \frac{G_f}{\sqrt{2}} \bar{\psi}_f \psi_f H \rightarrow \sum_f \left(m_f \bar{\psi}_f \psi_f + \frac{m_f}{v} \bar{\psi}_f \psi_f H \right) \quad (2.51)$$

induces a fermion mass term with mass $m_f = \frac{G_f}{\sqrt{2}} v$ where G_f is the *Yukawa coupling*.

In the massless state there are actually two independent electrons characterized by positive and negative helicities (chiralities) corresponding to right-handed (R) and left-handed (L) electrons, respectively, which do not “talk” to each other. Helicity h is defined as the projection of the spin vector onto the direction of the momentum vector

$$h \doteq \mathbf{S} \cdot \frac{\mathbf{p}}{|\mathbf{p}|} \quad (2.52)$$

as illustrated in Fig. 2.2 and transform into each other by space-reflections P (parity). Only after a fermion has acquired a mass, helicity flip transitions as effectively mediated by an anomalous magnetic moment (see below) are possible. In a renormalizable QFT an anomalous magnetic moment term is not allowed in the Lagrangian. It can only be a term induced by radiative corrections and in order not to vanish requires chiral symmetry to be broken by a corresponding mass term.

Angular momentum has to do with rotations, which form the rotation group $O(3)$. Ordinary 3-space rotations are described by orthogonal 3×3 matrices R ($RR^T = R^T R = I$ where I is the unit matrix and R^T denotes the transposed matrix) acting as $\mathbf{x}' = R\mathbf{x}$ on vectors \mathbf{x} of three-dimensional Euclidean position space \mathbf{R}^3 . Rotations are preserving scalar products between vectors and hence the length of vectors as well as the angles between them. Multiplication of the rotation matrices is the group operation and of course the successive multiplication of two rotations is non-commutative $[R_1, R_2] \neq 0$ in general. The rotation group is characterized by the Lie algebra $[\mathcal{J}_i, \mathcal{J}_j] = \varepsilon_{ijk} \mathcal{J}_k$, where the \mathcal{J}_i 's are normalized skew symmetric 3×3 matrices which generate the infinitesimal rotations around the x , y and z axes, labeled by $i, j, k = 1, 2, 3$. By ε_{ijk} we denoted the totally antisymmetric Levi-Civita

⁸The existence of the Higgs boson has been postulated in 1964 by Englert, Brout and Higgs [21, 22] to be a necessary ingredient of minimal renormalizable theory of electroweak interactions, and has been discovered with a mass about 125 GeV 48 years later in 2012 by the ATLAS [23] and the CMS [24] collaborations at the LHC at CERN in Switzerland.

tensor. The Lie algebra may be written in the form of the angular momentum algebra

$$[J_i, J_j] = i\varepsilon_{ijk} J_k \quad (2.53)$$

by setting $\mathcal{J}_i = -iJ_i$, with Hermitian generators $J_i = J_i^\dagger$. The latter form is well known from quantum mechanics (QM). In quantum mechanics rotations have to be implemented by unitary representations $U(R)$ ($UU^\dagger = U^\dagger U = I$ and U^\dagger is the Hermitian conjugate of U) which implement transformations of the state vectors in physical Hilbert space $|\psi\rangle' = U(R)|\psi\rangle$ for systems rotated relative to each other. Let J_i be the generators of the infinitesimal transformations of the group $O(3)$, the angular momentum operators, such that a finite rotation of magnitude $|\omega| = \theta$ about the direction of $\mathbf{n} = \omega/\theta$ may be represented by $U(R(\omega)) = \exp -i\omega\mathbf{J}$ (ω_i , $i = 1, 2, 3$ a real rotation vector). While for ordinary rotations the J_k 's are again 3×3 matrices, in fact the lowest dimensional matrices which satisfy (2.53) in a non-trivial manner are 2×2 matrices. The corresponding Lie algebra is the one of the group $SU(2)$ of unitary 2×2 matrices U with determinant unity: $\det U = 1$. It is a simply connected group and in fact it is the universal covering group of $O(3)$, the latter being doubly connected. Going to $SU(2)$ makes rotations a single valued mapping in parameter space which is crucial to get the right phases in the context of QM. Thus $SU(2)$ is lifting the two-fold degeneracy of $O(3)$. As a basic fact in quantum mechanics rotations are implemented as unitary representations of $SU(2)$ and not by $O(3)$ in spite of the fact that the two groups share the same abstract Lie algebra, characterized by the structure constants ε_{ijk} . Like $O(3)$, the group $SU(2)$ is of order $r = 3$ (number of generators) and rank $l = 1$ (number of diagonal generators). The generators of a unitary group are Hermitian and the special unitary transformations of determinant unity requires the generators to be traceless. The canonical choice is $J_i = \frac{\sigma_i}{2}$; σ_i the Pauli matrices

$$\sigma_1 = \begin{pmatrix} 0 & 1 \\ 1 & 0 \end{pmatrix}, \quad \sigma_2 = \begin{pmatrix} 0 & -i \\ i & 0 \end{pmatrix}, \quad \sigma_3 = \begin{pmatrix} 1 & 0 \\ 0 & -1 \end{pmatrix} \quad (2.54)$$

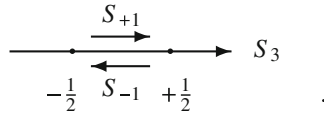
There is one diagonal operator $S_3 = \frac{\sigma_3}{2}$ the 3^{rd} component of spin. The eigenvectors of S_3 are

$$U(r = \frac{1}{2}, -\frac{1}{2}) = \begin{pmatrix} 1 \\ 0 \end{pmatrix}, \quad \begin{pmatrix} 0 \\ 1 \end{pmatrix}. \quad (2.55)$$

characterized by the eigenvalues of $\frac{1}{2}$, $-\frac{1}{2}$ of S_3 called spin up [\uparrow] and spin down [\downarrow], respectively. The eigenvectors represent the possible independent states of the system: two in our case. They thus span a two-dimensional space of complex vectors which are called two-spinors. Thus $SU(2)$ is acting on the space of spinors, like $O(3)$ is acting on ordinary configuration space vectors. From the two non-diagonal matrices we may form the two ladder operators: $S_{\pm 1} = \frac{1}{2}(\sigma_1 \pm i\sigma_2)$

$$S_{+1} = \begin{pmatrix} 0 & 1 \\ 0 & 0 \end{pmatrix}, \quad S_{-1} = \begin{pmatrix} 0 & 0 \\ 1 & 0 \end{pmatrix}$$

which map the eigenvectors into each other and hence change spin by one unit. The following figure shows the simplest case of a so called *root diagram*: the full dots represent the two states labeled by the eigenvalues $S_3 = \pm \frac{1}{2}$ of the diagonal operator. The arrows, labeled with $S_{\pm 1}$ denote the transitions between the different states, as implied by the Lie algebra:



The simplest non-trivial representation of $SU(2)$ is the so called fundamental representation, the one which defines $SU(2)$ itself and hence has dimension two. It is the one we just have been looking at. There is only one fundamental representation for $SU(2)$, because the complex conjugate U^* of a representation U which is also a representation, and generally a new one, is equivalent to the original one. The fundamental representation describes intrinsic angular momentum $\frac{1}{2}$ with two possible states characterized by the eigenvalues of the diagonal generator $\pm \frac{1}{2}$. The *fundamental representations* are basic because all others may be constructed by taking tensor products of fundamental representations. In the simplest case of a product of two spin $\frac{1}{2}$ vectors, which are called (two component) spinors $u_i v_k$ may describe a spin zero (anti-parallel spins $[\uparrow\downarrow]$) or a spin 1 (parallel spins $[\uparrow\uparrow]$).

In a relativistic theory, described in more detail in the previous section, one has to consider the Lorentz group L^{\uparrow}_+ of proper (preserving orientation of space-time [+]) orthochronous (preserving the direction of time $[\uparrow]$) Lorentz transformations Λ , in place of the rotation group. They include besides the rotations $R(\omega)$ the Lorentz boosts (special Lorentz transformations) $L(\chi)^9$ by velocity χ . Now rotations do not play any independent role as they are not a Lorentz invariant concept. Correspondingly, purely spatial 3-vectors like the spin vector $\mathbf{S} = \frac{\sigma}{2}$ do not have an invariant meaning. However, the three-vector of Pauli matrices σ may be promoted to a four-vector of 2×2 matrices:

$$\sigma_{\mu} \doteq (\mathbf{1}, \boldsymbol{\sigma}) \text{ and } \hat{\sigma}_{\mu} \doteq (\mathbf{1}, -\boldsymbol{\sigma}) \tag{2.57}$$

⁹The special L-transformation $L(p)$ which transforms from a state in the rest frame $(m, \mathbf{0})$ to a state of momentum p^{μ} may be written as

$$\begin{aligned} L^i_j &= \delta^i_j + \hat{p}_i \hat{p}_j (\cosh \beta - 1) \\ L^i_0 &= L^0_i = \hat{p}_i \sinh \beta \\ L^0_0 &= \cosh \beta \end{aligned} \tag{2.56}$$

with $\hat{\mathbf{p}} = \mathbf{p}/|\mathbf{p}|$, $\cosh \beta = \omega_p/m$, $\sinh \beta = |\mathbf{p}|/m$ and $\tanh \beta = |\mathbf{p}|/\omega_p = v$ the velocity of the state.

which will play a key role in what follows. Again, the L -transformations $\Lambda \in L_+^\uparrow$ on the classical level in (relativistic) quantum mechanics have to be replaced by the simply connected universal covering group with identical Lie algebra, which is $SL(2, C)$, the group of unimodular ($\det U = 1$) complex 2×2 matrix transformations U , with matrix multiplication as the group operation. The group $SL(2, C)$ is related to L_+^\uparrow much in the same way as $SU(2)$ to $O(3)$, namely, the mapping $U_\Lambda \in SL(2, C) \rightarrow \Lambda \in L_+^\uparrow$ is two-to-one and the two-fold degeneracy of elements in L_+^\uparrow is lifted in $SL(2, C)$.

The key mapping establishing a linear one-to-one correspondence between real four-vectors and Hermitian 2×2 matrices is the following: with any real four-vector x^μ in Minkowski space we may associate a Hermitian 2×2 matrix

$$x^\mu \rightarrow X = x^\mu \sigma_\mu = \begin{pmatrix} x^0 + x^3 & x^1 - ix^2 \\ x^1 + ix^2 & x^0 - x^3 \end{pmatrix} \quad (2.58)$$

with

$$\det X = x^2 = x^\mu x_\mu \quad , \quad (2.59)$$

while every Hermitian 2×2 matrix X determines a real four vector by

$$X \rightarrow x^\mu = \frac{1}{2} \text{Tr} (X \sigma^\mu) \quad . \quad (2.60)$$

An element $U \in SL(2, C)$ provides a mapping

$$X \rightarrow X' = U X U^+ \quad \text{i.e.} \quad x'^\mu \sigma_\mu = x^\nu U \sigma_\nu U^+ \quad (2.61)$$

between Hermitian matrices, which preserves the determinant

$$\det X' = \det U \det X \det U^+ = \det X \quad , \quad (2.62)$$

and corresponds to the real linear transformation

$$x^\mu \rightarrow x'^\mu = \Lambda^\mu{}_\nu x^\nu \quad (2.63)$$

which satisfies $x'^\mu x'_\mu = x^\mu x_\mu$ and therefore is a Lorentz transformation.

The Lie algebra of $SL(2, C)$ is the one of L_+^\uparrow and thus given by 6 generators: \mathbf{J} for the rotations and \mathbf{K} for the Lorentz boosts, satisfying

$$[J_i, J_k] = i\epsilon_{ikl} J_l \quad , \quad [J_i, K_k] = i\epsilon_{ikl} K_l \quad , \quad [K_i, K_k] = -i\epsilon_{ikl} J_l \quad (2.64)$$

as a coupled algebra of the J_i 's and K_i 's. Since these generators are Hermitian $\mathbf{J} = \mathbf{J}^+$ and $\mathbf{K} = \mathbf{K}^+$ the group elements $e^{-i\omega\mathbf{J}}$ and $e^{i\chi\mathbf{K}}$ are **unitary**.¹⁰ This algebra can be decoupled by the linear transformation

$$\mathbf{A} = \frac{1}{2}(\mathbf{J} + i\mathbf{K}), \quad \mathbf{B} = \frac{1}{2}(\mathbf{J} - i\mathbf{K}) \quad (2.65)$$

under which the Lie algebra takes the form

$$\mathbf{A} \times \mathbf{A} = i\mathbf{A}, \quad \mathbf{B} \times \mathbf{B} = i\mathbf{B}, \quad [A_i, B_j] = 0 \quad (2.66)$$

of two decoupled angular momentum algebras. Since $\mathbf{A}^+ = \mathbf{B}$ and $\mathbf{B}^+ = \mathbf{A}$, the new generators are not Hermitian any more and hence give rise to **non-unitary** irreducible representations. These are **finite dimensional** and evidently characterized by a pair (A, B) , with $2A$ and $2B$ integers. The dimension of the representation (A, B) is $(2A+1) \cdot (2B+1)$. The angular momentum of the representation (A, B) decomposes into $J = A + B, A + B - 1, \dots, |A - B|$. Massive particle states are constructed starting from the rest frame where J is the spin and the state corresponds to a multiplet of $2J + 1$ degrees of freedom.

The crucial point is that in relativistic QM besides the mass of a state also the spin has an invariant (reference-frame independent) meaning. There exist exactly two **Casimir operators**, invariant operators commuting with all generators (2.6) and (2.7) of the Poincaré group \mathcal{P}_+^\uparrow . One is the mass operator

$$M^2 = P^2 = g_{\mu\nu} P^\mu P^\nu \quad (2.67)$$

the other is

$$L^2 = g_{\mu\nu} L^\mu L^\nu; \quad L^\mu \doteq \frac{1}{2} \varepsilon^{\mu\nu\rho\sigma} P_\nu M_{\rho\sigma}, \quad (2.68)$$

where L^μ is the Pauli-Lubansky operator. These operators characterize mass m and spin j of the states in an invariant way: $M^2|p, j, j_3; \alpha\rangle = p^2|p, j, j_3; \alpha\rangle$ and $L^2|p, j, j_3; \alpha\rangle = -m^2 j(j+1)|p, j, j_3; \alpha\rangle$.

The classification by (A, B) together with (2.65) shows that for $SL(2, C)$ we have two inequivalent fundamental two-dimensional representations: $(\frac{1}{2}, 0)$ and $(0, \frac{1}{2})$. The transformations may be written as a unitary rotation times a Hermitian boost as

¹⁰In $SL(2, C)$ the Lie algebra obviously has the 2×2 matrix representation $J_i = \sigma_i/2$, $K_i = \pm i \sigma_i/2$ in terms of the Pauli matrices, however, $\mathbf{K}^+ = -\mathbf{K}$ is non-Hermitian and the corresponding finite dimensional representation non-unitary. Unitary representations of the Lorentz group, required to implement relativistic covariance on the Hilbert space of physical states, are necessarily infinite dimensional. Actually, the two possible signs of K_i indicated exhibits that there are two different inequivalent representations.

follows¹¹:

$$\begin{aligned} U_\Lambda &= U(\boldsymbol{\chi}, \boldsymbol{\omega}) = D^{(\frac{1}{2})}(\Lambda) = e^{\boldsymbol{\chi} \frac{\boldsymbol{\sigma}}{2}} e^{-i\boldsymbol{\omega} \frac{\boldsymbol{\sigma}}{2}} & \text{for } \left(\frac{1}{2}, 0\right) \\ \bar{U}_\Lambda &= U_{\Lambda^{-1}}^+ = \bar{D}^{(\frac{1}{2})}(\Lambda) = e^{-\boldsymbol{\chi} \frac{\boldsymbol{\sigma}}{2}} e^{-i\boldsymbol{\omega} \frac{\boldsymbol{\sigma}}{2}} & \text{for } \left(0, \frac{1}{2}\right) . \end{aligned} \quad (2.69)$$

While σ_μ (2.57) is a covariant vector

$$U_\Lambda \sigma_\mu U_\Lambda^+ = \Lambda^\nu{}_\mu \sigma_\nu \quad (2.70)$$

with respect to the representation $U_\Lambda = D^{(\frac{1}{2})}(\Lambda)$, the vector $\hat{\sigma}_\mu$ (2.57) is covariant with respect to $\bar{U}_\Lambda = \bar{D}^{(\frac{1}{2})}(\Lambda)$

$$\bar{U}_\Lambda \hat{\sigma}_\mu \bar{U}_\Lambda^+ = \Lambda^\nu{}_\mu \hat{\sigma}_\nu . \quad (2.71)$$

Note that

$$U(\boldsymbol{\chi}, \mathbf{n}\theta) \text{ and } U(\boldsymbol{\chi}, \mathbf{n}(\theta + 2\pi)) = -U(\boldsymbol{\chi}, \mathbf{n}\theta) \quad (2.72)$$

represent the same Lorentz transformation. U_Λ is therefore a double-valued representation of L_+^\uparrow .

An important theorem [25] says that

Theorem 2.4 *A massless particle of helicity λ may be only in the representations satisfying $(A, B) = (A, A - \lambda)$, where $2A$ and $2(A - \lambda)$ are non-negative integer numbers.*

Thus the simplest representations for massless fields are the spin 1/2 states

$$\begin{aligned} \lambda = +\frac{1}{2} &: \left(\frac{1}{2}, 0\right) & \text{right - handed (R)} \\ -\frac{1}{2} &: \left(0, \frac{1}{2}\right) & \text{left - handed (L)} \end{aligned} \quad (2.73)$$

of helicity $+\frac{1}{2}$ and $-\frac{1}{2}$, respectively.

The finite dimensional irreducible representations of $SL(2, C)$ to mass 0 and spin j are one-dimensional and characterized by the helicity $\lambda = \pm j$. To a given spin $j > 0$ there exist exactly two helicity states. Each of the two possible states is invariant by itself under L_+^\uparrow , however, the two states get interchanged under parity transformations:

$$U_P h U_P^{-1} = -h . \quad (2.74)$$

Besides the crucial fact of the validity of the spin-statistics theorem (valid in any relativistic QFT), here we notice another important difference between spin in

¹¹Again, these finite dimensional representations U_Λ , U_P (below), etc. should not be confused with the corresponding infinite dimensional unitary representations $U(\Lambda)$, $U(P)$, etc. acting on the Hilbert space of physical states considered in the preceding section.

non-relativistic QM and spin in QFT. In QM spin 1/2 is a system of two degrees of freedom as introduced by Pauli, while in QFT where we may consider the massless case we have two independent singlet states. Parity P, as we know, acts on four-vectors like $Px = (x^0, -\mathbf{x})$ and satisfies¹² $P^2 = 1$. With respect to the rotation group O_3 , P^2 is just a rotation by the angle 2π and thus in the context of the rotation group P has no special meaning. This is different for the Lorentz group. While

$$U_P \mathbf{J} = \mathbf{J} U_P \quad (2.75)$$

commutes

$$U_P \mathbf{K} = -\mathbf{K} U_P \quad (2.76)$$

does not. As a consequence, we learn that

$$U_P U(\boldsymbol{\chi}, \mathbf{n} \theta) = U(-\boldsymbol{\chi}, \mathbf{n} \theta) U_P \quad (2.77)$$

and hence

$$U_P U_\Lambda = \tilde{U}_\Lambda U_P . \quad (2.78)$$

Thus under parity a left-handed massless fermion is transformed into a right-handed one and vice versa, which of course is also evident from Fig. 2.2, if we take into account that a change of frame by a Lorentz transformation (velocity $v \leq c$) cannot flip the spin of a massless particle.

The necessity to work with $SL(2, C)$ becomes obvious once we deal with spinors. On a classical level, two-spinors or Weyl spinors w are elements of a vector space V of two complex entries, which transform under $SL(2, C)$ by matrix multiplication: $w' = U w$, $w \in V$, $U \in SL(2, C)$

$$w = \begin{pmatrix} a \\ b \end{pmatrix} ; \quad a, b \in C . \quad (2.79)$$

Corresponding to the two representations there exist two local Weyl spinor fields (see (2.12))

$$\begin{aligned} \varphi_a(x) &= \sum_{r=\pm 1/2} \int d\mu(p) \{ u_a(p, r) a(\mathbf{p}, r) e^{-ipx} + v_a(p, r) b^+(\mathbf{p}, r) e^{ipx} \} \\ \chi_a(x) &= \sum_{r=\pm 1/2} \int d\mu(p) \{ \hat{u}_a(p, r) a(\mathbf{p}, r) e^{-ipx} + \hat{v}_a(p, r) b^+(\mathbf{p}, r) e^{ipx} \} , \end{aligned} \quad (2.80)$$

¹²Note that while $P^2 = 1$ the phase η_P of its unitary representation U_P is constrained by $U_P^2 = \pm 1$ only, i.e. $\eta_P = \pm 1$ or $\pm i$.

with two components $a = 1, 2$, which satisfy the Weyl equations

$$\begin{aligned} i (\hat{\sigma}^\mu \partial_\mu)_{ab} \varphi_b(x) &= m \chi_a(x) \\ i (\sigma^\mu \partial_\mu)_{ab} \chi_b(x) &= m \varphi_a(x) . \end{aligned} \quad (2.81)$$

The appropriate one-particle wave functions $u(p, r)$ etc. may be easily constructed as follows: for a massive particle states are constructed by starting in the rest frame where rotations act as ($\omega = |\omega|$, $\hat{\omega} = \omega/\omega$)

$$D^{(\frac{1}{2})}(R(\omega)) = \bar{D}^{(\frac{1}{2})}(R(\omega)) = e^{-i\omega \frac{\sigma}{2}} = \mathbf{1} \cos \frac{\omega}{2} - i \boldsymbol{\sigma} \cdot \hat{\omega} \sin \frac{\omega}{2} . \quad (2.82)$$

Notice that this $SU(2)$ rotation is a rotation by half of the angle, only, of the corresponding classical O_3 rotation. Here the non-relativistic construction of the states applies and the spinors at rest are given by (2.55). The propagating particles carrying momentum \mathbf{p} are then obtained by performing a Lorentz-boost to the states at rest. A boost $L(\mathbf{p})$ (2.56) of momentum \mathbf{p} is given by $D^{(\frac{1}{2})}(L(\mathbf{p})) = e^{\mathbf{x} \frac{\sigma}{2}} = N^{-1} (p^\mu \sigma_\mu + m)$ and $\bar{D}^{(\frac{1}{2})}(L(\mathbf{p})) = e^{-\mathbf{x} \frac{\sigma}{2}} = N^{-1} (p^\mu \hat{\sigma}_\mu + m)$, respectively, in the two basic representations. $N = (2m(p^0 + m))^{-\frac{1}{2}}$ is the normalization factor. The one-particle wave functions (two-spinors) of a Weyl particle and its antiparticle are thus given by

$$u(p, r) = N^{-1} (p^\mu \sigma_\mu + m) U(r) \quad \text{and} \quad v(p, r) = N^{-1} (p^\mu \sigma_\mu + m) V(r) ,$$

respectively, where $U(r)$ and $V(r) = -i\sigma_2 U(r)$ are the rest frame spinors (2.55). The last relation one has to require for implementing the charge conjugation property for the spinors (2.31) in terms of the matrix (2.30). For the adjoint representation, similarly,

$$\hat{u}(p, r) = N^{-1} (p^\mu \hat{\sigma}_\mu + m) U(r) \quad \text{and} \quad \hat{v}(p, r) = -N^{-1} (p^\mu \hat{\sigma}_\mu + m) V(r) .$$

The $-$ sign in the last equation, $(-1)^{2j}$ for spin j , is similar to the $-i\sigma_2$ in the relation between U and V , both are required to make the fields local and with proper transformation properties. We can easily derive (2.81) now. We may write $\hat{\sigma}_\mu p^\mu = \omega_p \mathbf{1} - \boldsymbol{\sigma} \mathbf{p} = 2|\mathbf{p}|(\frac{\omega_p}{2|\mathbf{p}|} \mathbf{1} - h)$ where $h \equiv \frac{\sigma}{2} \frac{\mathbf{p}}{|\mathbf{p}|}$ is the helicity operator, and for massless states, where $\omega_p = |\mathbf{p}|$, we have $\hat{\sigma}_\mu p^\mu = 2|\mathbf{p}|(\frac{1}{2} - h)$ a projection operator on states with helicity $-\frac{1}{2}$, while $\sigma_\mu p^\mu = 2|\mathbf{p}|(\frac{1}{2} + h)$ a projection operator on states with helicity $+\frac{1}{2}$. Furthermore, we observe that $p^\mu p^\nu \hat{\sigma}_\mu \sigma_\nu = p^\mu p^\nu \sigma_\mu \hat{\sigma}_\nu = p^2 = m^2$ and one easily verifies the Weyl equations using the given representations of the wave functions.

In the massless limit $m \rightarrow 0$: $p^0 = \omega_p = |\mathbf{p}|$ we obtain two decoupled equations

$$\begin{aligned} i(\hat{\sigma}^\mu \partial_\mu)_{ab} \varphi_b(x) &= 0 \\ i(\sigma^\mu \partial_\mu)_{ab} \chi_b(x) &= 0 . \end{aligned}$$

In momentum space the fields are just multiplied by the helicity projector and the equations say that the massless fields have fixed helicities:

$$\left(\frac{1}{2}, 0\right) : \varphi \sim \psi_R \quad \left(0, \frac{1}{2}\right) : \chi \sim \psi_L \quad (2.83)$$

which suggests to rewrite the transformations as

$$\psi_{a_{L,R}}(x) \rightarrow \psi'_{a_{L,R}}(x') = (\Lambda_{L,R})_{ab} \psi_{b_{L,R}}(\Lambda x) \quad (2.84)$$

with

$$(\Lambda_{L,R})_{ab} = \left(e^{\pm i\chi \frac{\sigma}{2}} e^{-i\omega \frac{\sigma}{2}} \right)_{ab} \quad (\Lambda_R^+ = \Lambda_L^{-1}) . \quad (2.85)$$

Using $\sigma_2 \sigma_i \sigma_2 = -\sigma_i^*$ one can show that $\sigma_2 \Lambda_L \sigma_2 = \Lambda_R^*$. Thus, $\psi_L^c \equiv \sigma_2 \psi_L^*$ (up to an arbitrary phase) is defining a charge conjugate spinor which transforms as $\psi_L^c \sim \psi_R$. Indeed $\Lambda_R \psi_L^c = \Lambda_R \sigma_2 \psi_L^* = \sigma_2 \Lambda_L^* \psi_L^* = \sigma_2 \psi_L^{*'} = \psi_L^{c'}$ and thus $\psi_L^c \equiv \sigma_2 \psi_L^* \equiv \varphi \sim \psi_R$. Similarly, $\psi_R^c \equiv \sigma_2 \psi_R^* \equiv \chi \sim \psi_L$. We thus learn, that for massless fields, counting particles and antiparticles separately, we may consider all fields to be left-handed. The second term in the field, the antiparticle creation part, in each case automatically includes the right-handed partners.

The Dirac field is the bispinor field obtained by combining the irreducible fields $\varphi_a(x)$ and $\chi_a(x)$ into one reducible field $(\frac{1}{2}, 0) \oplus (0, \frac{1}{2})$. It is the natural field to be used to describe fermions participating parity conserving interactions like QED and QCD. Explicitly, the Dirac field is given by

$$\psi_\alpha(x) = \begin{pmatrix} \varphi_a \\ \chi_a \end{pmatrix} (x) = \sum_r \int d\mu(p) \left\{ u_\alpha(p, r) a(\mathbf{p}, r) e^{-ipx} + v_\alpha(p, r) b^\dagger(\mathbf{p}, r) e^{ipx} \right\}$$

where

$$u_\alpha = \begin{pmatrix} u_a \\ \hat{u}_a \end{pmatrix} ; \quad v_\alpha = \begin{pmatrix} v_a \\ \hat{v}_a \end{pmatrix} . \quad (2.86)$$

$\psi_\alpha(x)$ satisfies the **Dirac equation**:

$$(i\gamma^\mu \partial_\mu - m)_{\alpha\beta} \psi_\beta(x) = 0$$

where

$$\gamma^\mu \doteq \begin{pmatrix} 0 & \sigma^\mu \\ \hat{\sigma}^\mu & 0 \end{pmatrix} \quad (2.87)$$

are the Dirac matrices in the helicity representation (Weyl basis).

The Dirac equation is nothing but the Weyl equations written in terms of the bispinor ψ . Note that a Dirac spinor combines a right-handed Weyl spinor of a particle with a right-handed Weyl spinor of its antiparticle. For $m = 0$, the Dirac operator $i\gamma^\mu\partial_\mu$ in momentum space is $\not{p} = \gamma^\mu p_\mu$. Thus the Dirac equation just is the helicity eigenvalue equation:

$$\gamma^\mu p_\mu \tilde{\psi}(p) \doteq \begin{pmatrix} 0 & \sigma^\mu p_\mu \\ \hat{\sigma}^\mu p_\mu & 0 \end{pmatrix} \begin{pmatrix} \tilde{\varphi} \\ \tilde{\chi} \end{pmatrix} (p) = 2|\mathbf{p}| \begin{pmatrix} 0 & \left(\frac{1}{2} + h\right) \\ \left(\frac{1}{2} - h\right) & 0 \end{pmatrix} \begin{pmatrix} \tilde{\varphi} \\ \tilde{\chi} \end{pmatrix} (p) = 0. \quad (2.88)$$

Under parity $\psi_\alpha(x)$ transforms into itself

$$\psi_\alpha(x) \rightarrow \eta_P (\gamma^0)_{\alpha\beta} \psi_\beta(Px)$$

where γ^0 just interchanges $\varphi \leftrightarrow \chi$ and hence takes the form

$$\gamma^0 \doteq \begin{pmatrix} 0 & \mathbf{1} \\ \mathbf{1} & 0 \end{pmatrix}.$$

The irreducible components φ and χ are eigenvectors of the matrix

$$\gamma_5 \doteq \begin{pmatrix} \mathbf{1} & 0 \\ 0 & -\mathbf{1} \end{pmatrix}$$

and the projection operators (2.20) projecting back to the Weyl fields according to (2.19).¹³

The kinetic term of the Dirac Lagrangian decomposes into a L and a R part $\mathcal{L}_{\text{Dirac}} = \bar{\psi}\gamma^\mu\partial_\mu\psi = \bar{\psi}_R\gamma^\mu\partial_\mu\psi_R + \bar{\psi}_L\gamma^\mu\partial_\mu\psi_L$ (4 degrees of freedom). A Dirac mass term $m\bar{\psi}\psi = m(\bar{\psi}_L\psi_R + \bar{\psi}_R\psi_L)$ breaks chiral symmetry as it is non-diagonal in the Weyl fields and induces helicity flip transitions as required by the anomalous magnetic moment in a renormalizable QFT. A remark concerning hadrons. It might look somewhat surprising that hadrons, which are composite particles made of *colored*

¹³The standard representation of the Dirac field/algebra, described in Sect. 2.1.1, is adapted to a simple interpretation in the rest frame (requires $m \neq 0$). It may be obtained from the ones in the Weyl basis (“helicity” representation) by a similarity transformation \mathcal{S}

$$\psi(x) = \mathcal{S} \psi^{\text{helicity}}(x), \quad \gamma_\mu = \mathcal{S} \gamma_\mu^{\text{helicity}} \mathcal{S}^{-1}, \quad \mathcal{S} = \mathcal{S}^{-1} = \frac{1}{\sqrt{2}} \begin{pmatrix} 1 & 1 \\ 1 & -1 \end{pmatrix}$$

such that

$$u(0, r) = \sqrt{2m} \begin{pmatrix} U(r) \\ 0 \end{pmatrix}, \quad v(0, r) = \sqrt{2m} \begin{pmatrix} 0 \\ V(r) \end{pmatrix}$$

in the standard basis.

quarks and *gluons*, in many respects look like “elementary particles” which are well described as Wigner particles (if one switches off the electromagnetic interaction which cause a serious IR problem which spoils the naive Wigner state picture as we will describe below), particles of definite mass and spin and charge quantized in units of e and have associated electromagnetic form factors and in particular a definite magnetic moment. However, for the proton for example, the gyromagnetic ratio g_P from the relation $\boldsymbol{\mu}_P = g_P e\hbar/(2m_P c) \mathbf{s}$ turns out to be $g_P \sim 2.8$ or $a_P = (g_P - 2)/2 \sim 0.4$ showing that the proton is not really a Dirac particle and its anomalous magnetic moment indicates that the proton is not a point particle but has internal structure. This was first shown long time ago by atomic beam magnetic deflection experiments [26], before the nature of the muon was clarified. For the latter it was the measurement at CERN which yielded $a_\mu = 0.00119(10)$ [27] and revealed the muon to be just a heavy electron. Within errors at that time the muon turned out to have the same value of the anomalous magnetic moment as the electron, which is known to be due to virtual radiative corrections.

The analysis of the spin structure on a formal level, discussing the quantum mechanical implementation of relativistic symmetry principles, fits very naturally with the observed spin phenomena. In particular the existence of the fundamental spin $\frac{1}{2}$ particles which must satisfy Pauli’s exclusion principle has dramatic consequences for real life. Without the existence of spin as an extra fundamental quantum number in general and the spin $\frac{1}{2}$ fermions in particular, stability of nuclei against Coulomb collapse and of stars against gravitational collapse would be missing and the universe would not be ours.

2.3 Quantum Electrodynamics

The lepton–photon interaction is described by QED, which is structured by local $U(1)$ gauge invariance¹⁴

$$\begin{aligned}\psi(x) &\rightarrow e^{-ie\alpha(x)}\psi(x) \\ A_\mu(x) &\rightarrow A_\mu(x) - \partial_\mu\alpha(x) \ ,\end{aligned}\tag{2.89}$$

with an arbitrary scalar function $\alpha(x)$, implying lepton–photon interaction according to *minimal coupling*, which means that we have to perform the substitution $\partial_\mu \rightarrow$

¹⁴The known elementary particle interactions, the strong, electromagnetic and weak forces, all derive from a local gauge symmetry principle. This was first observed by Weyl [28] for the Abelian QED and later extended to non–Abelian gauge theories by Yang and Mills [29]. The gauge symmetry group governing the Standard Model of particle physics is $SU(3)_c \otimes SU(2)_L \otimes U(1)_Y$.

$D_\mu = \partial_\mu - ieA_\mu(x)$ in the Dirac equation $(i\gamma^\mu \partial_\mu - m)\psi(x) = 0$ of a free lepton.¹⁵ This implies that the electromagnetic interaction is described by the bare Lagrangian

$$\begin{aligned} \mathcal{L}^{\text{QED}} &= -\frac{1}{4}F_{\mu\nu}F^{\mu\nu} - \frac{1}{2}\xi^{-1}(\partial_\mu A^\mu)^2 + \bar{\psi}(i\gamma^\mu D_\mu - m)\psi \\ &= \mathcal{L}_{0A}^\xi + \mathcal{L}_{0\psi} + ej_{\text{em}}^\mu(x)A_\mu(x) \ , \end{aligned} \quad (2.90)$$

and the corresponding field equations read¹⁶

$$\begin{aligned} (i\gamma^\mu \partial_\mu - m)\psi(x) &= -e : A_\mu(x)\gamma^\mu\psi(x) : \\ (\square g^{\mu\nu} - (1 - \xi^{-1})\partial^\mu\partial^\nu)A_\nu(x) &= -e : \bar{\psi}(x)\gamma^\mu\psi(x) : \ . \end{aligned} \quad (2.91)$$

The interaction part of the Lagrangian is

$$\mathcal{L}_{\text{int}} = ej_{\text{em}}^\mu(x)A_\mu(x) \ , \quad (2.92)$$

while the bilinear free field parts \mathcal{L}_{0A}^ξ and $\mathcal{L}_{0\psi}$ define the propagators of the photon and the leptons, respectively (given below). As in classical electrodynamics the gauge potential A^μ is an auxiliary field which exhibits unphysical degrees of freedom, and is not uniquely determined by Maxwell's equations. In order to get a well defined photon propagator a gauge fixing condition is required. We adopt the linear covariant Lorentz gauge : $\partial_\mu A^\mu = 0$, which is implemented via the Lagrange multiplier method, with Lagrange multiplier $\lambda = 1/\xi$, ξ is called gauge parameter.¹⁷ The gauge invariance of physical quantities infers that they do not depend on the gauge parameter.

Above we have denoted by e the charge of the electron, which by convention is taken to be negative. In the following we will explicitly account for the sign of the charge and use e to denote the positive value of the charge of the positron. The charge of a fermion f is then given by $Q_f e$, with Q_f the charge of a fermion in units of the positron charge e . A collection of charged fermions f enters the electromagnetic current as

$$j_{\text{em}}^\mu = \sum_f Q_f \bar{\psi}_f \gamma^\mu \psi_f \ , \quad (2.93)$$

¹⁵The modified derivative $D_\mu = \partial_\mu - ieA_\mu(x)$ is called *covariant derivative*. e is the *gauge coupling*. The minimal substitution promotes the global gauge symmetry of the free Dirac Lagrangian to a local gauge symmetry of the electron–photon system, i.e., the interacting system has more symmetry than the free electron.

¹⁶The prescription $:\dots:$ means *Wick ordering* of products of fields: write the fields in terms of creation and annihilation operators and order them such that all annihilation operators are to the right of all creation operators, assuming the operators to commute (bosons) or to anticommute (fermions). This makes the vacuum expectation value of the field product vanish.

¹⁷The parametrization of the gauge dependence by the inverse of the Lagrange multiplier $\xi = 1/\lambda$ is just a commonly accepted convention.

for the leptons alone $j_{\text{em}}^{\mu \text{lep}} = -\sum_{\ell} \bar{\psi}_{\ell} \gamma^{\mu} \psi_{\ell}$ ($\ell = e, \mu, \tau$). If not specified otherwise $\psi(x)$ in the following will denote a lepton field carrying negative charge $-e$.

The electric charge is a conserved quantity as a consequence of **Noether's theorem**:

Theorem 2.5 *If the Lagrangian $\mathcal{L}(\psi, \partial_{\mu}\psi \dots)$ of a system is invariant under a r -parametric group of global field transformations $\psi(x) \rightarrow \psi(x) + \delta\psi(x), \dots$ then there exist r conserved currents $\partial_{\mu} j_i^{\mu}(x) = 0$, $i = 1, \dots, r$ which imply the existence of r conserved charges*

$$Q_i = \int d^3x j_i^0(t, \mathbf{x}) ; \quad \frac{dQ_i}{dt} = 0, \quad i = 1, \dots, r. \quad (2.94)$$

The global symmetry in our QED case is the global $U(1)_{\text{em}}$ gauge symmetry (i.e. transformations (2.89) with gauge function $\alpha = \text{constant}$).

One important object we need for our purpose is the *unitary* scattering matrix S which encodes the perturbative lepton–photon interaction processes and is given by

$$S = T \left(e^{i \int d^4x \mathcal{L}_{\text{int}}^{(0)}(x)} \right) \Big|_{\otimes}. \quad (2.95)$$

The prescription \otimes says that all graphs (see below) which include vacuum diagrams (disconnected subdiagrams with no external legs) as factors have to be omitted. This corresponds to the proper normalization of the S -operator. Unitarity requires

$$SS^{\dagger} = S^{\dagger}S = 1 \quad \Leftrightarrow \quad S^{\dagger} = S^{-1} \quad (2.96)$$

and infers the conservation of quantum mechanical transition probabilities. The prescription T means time ordering of all operators, like

$$T \{ \phi(x)\phi(y) \} = \Theta(x^0 - y^0)\phi(x)\phi(y) \pm \Theta(y^0 - x^0)\phi(y)\phi(x) \quad (2.97)$$

where the $+$ sign holds for boson fields and the $-$ sign for fermion fields. Under the T prescription all fields are commuting (bosons) or anticommuting (fermions). All fields in (2.95) may be taken to be free fields. With the help of S we may calculate the basic objects of a QFT, the *Green functions*. These are the vacuum expectation values of *time ordered* or *chronological* products of fields like the electromagnetic correlator

$$G_{\mu, \alpha\beta}(x, y, \bar{y}) \doteq \langle 0 | T \{ A_{\mu}(x) \psi_{\alpha}(y) \bar{\psi}_{\beta}(\bar{y}) \} | 0 \rangle. \quad (2.98)$$

2.3.1 Perturbation Expansion, Feynman Rules

The full Green functions of the interacting fields like $A^\mu(x)$, $\psi(x)$, etc. can be expressed completely in terms of corresponding free fields via the *Gell-Mann Low formula* [30] (interaction picture)

$$\begin{aligned} \langle 0|T \{A_\mu(x)\psi_\alpha(y)\bar{\psi}_\beta(\bar{y})\} |0\rangle &= \langle 0|T \left\{ A_\mu^{(0)}(x)\psi_\alpha^{(0)}(y)\bar{\psi}_\beta^{(0)}(\bar{y}) S \right\} |0\rangle_\otimes = \\ \langle 0|T \left\{ A_\mu^{(0)}(x)\psi_\alpha^{(0)}(y)\bar{\psi}_\beta^{(0)}(\bar{y}) e^{i\int d^4x' \mathcal{L}_{\text{int}}^{(0)}(x')} \right\} |0\rangle_\otimes &= \sum_{n=0}^N \frac{i^n}{n!} \int d^4z_1 \cdots d^4z_n \\ \langle 0|T \left\{ A_\mu^{(0)}(x)\psi_\alpha^{(0)}(y)\bar{\psi}_\beta^{(0)}(\bar{y}) \mathcal{L}_{\text{int}}^{(0)}(z_1) \cdots \mathcal{L}_{\text{int}}^{(0)}(z_n) \right\} |0\rangle_\otimes &+ O(e^{N+1}) \quad (2.99) \end{aligned}$$

with $\mathcal{L}_{\text{int}}^{(0)}(x)$ the interaction part of the Lagrangian. On the right hand side all fields are free fields and the vacuum expectation values can be computed by applying the known properties of free fields. Expanding the exponential as done in (2.99) yields the perturbation expansion. The evaluation of the formal perturbation series is not well defined and requires regularization and renormalization, which we will discuss briefly below. In a way the evaluation is simple: one writes all free fields in terms of the creation and annihilation operators and applies the canonical anticommutation (fermions) and the canonical commutation (bosons) relations to bring all annihilation operators to the right, where they annihilate the vacuum $\cdots a(\mathbf{p}, r)|0\rangle = 0$ and the creation operators to the left where again they annihilate the vacuum $0 = \langle 0|b^\dagger(\mathbf{p}, r) \cdots$, until no operator is left over (Wick ordering) [31]. The only non-vanishing contribution comes from the complete contraction of all fields in pairs, where a pairing corresponds to a propagator as a factor. The rules for the evaluation of all possible contributions are known as

The Feynman Rules:

- (1) draw all vertices as points in a plane: external ones with the corresponding external fields $\psi(y_i)$, $\bar{\psi}(\bar{y}_j)$ or $A^\mu(x_k)$ attached to the point, and the internal interaction vertices $-ie\bar{\psi}\gamma_\mu\psi A^\mu(z_n)$ with three fields attached to the point z_n .
- (2) contract all fields in pairs represented by a line connecting the two vertices, thereby fields of different particles are to be characterized by different types of lines. As a result one obtains a Feynman diagram.

The field pairings define the free propagators

$$\overline{\psi(y) \cdots \bar{\psi}(\bar{y})} \Leftrightarrow iS_F(y - \bar{y}) \quad \text{and} \quad \overline{A^\mu(x_1) \cdots A^\nu(x_2)} \Leftrightarrow iD^{\mu\nu}(x_1 - x_2)$$

given by the vacuum expectation values of the pair of time-ordered free fields,

$$\begin{aligned} iS_{F\alpha\beta}(y - \bar{y}) &\doteq \langle 0|T \{ \psi(y)_\alpha \bar{\psi}(\bar{y})_\beta \} |0\rangle \\ iD^{\mu\nu}(x_1 - x_2) &\doteq \langle 0|T \{ A^\mu(x_1) A^\nu(x_2) \} |0\rangle . \end{aligned}$$

(1) Lepton propagator

$$\begin{array}{c} \circ \\ \alpha \end{array} \xrightarrow{p} \begin{array}{c} \circ \\ \beta \end{array} : \quad iS_F(p)_{\alpha\beta} = \left(\frac{i}{\not{p} - m + i\epsilon} \right)_{\alpha\beta}$$

(2) Photon propagator

$$\begin{array}{c} \text{wavy line} \\ \mu \end{array} \xrightarrow{p} \begin{array}{c} \text{wavy line} \\ \nu \end{array} : \quad iD(p, \xi)^{\mu\nu} = -i \left(g^{\mu\nu} - (1 - \xi) \frac{p^\mu p^\nu}{p^2} \right) \frac{1}{p^2 + i\epsilon}$$

(3) Lepton–photon vertex

$$\begin{array}{c} \text{wavy line} \\ \mu, p_1 \end{array} \begin{array}{c} \nearrow \\ \alpha, p_3 \\ \searrow \\ \beta, p_2 \end{array} : \quad = \quad -ie (\gamma^\mu)_{\alpha\beta} = ie Q_\ell (\gamma^\mu)_{\alpha\beta}$$

Fig. 2.3 Feynman rules for QED (I)

The latter may easily be calculated using the free field properties.

Feynman diagrams translate into Feynman integrals via the famous Feynman rules given by Fig. 2.3 in momentum space.

In configuration space all interaction vertices in (2.99) are integrated over. The result thus is a Feynman integral. In fact the perturbation expansion is not yet well defined. In order to have a well defined starting point, the theory has to be *regularized* [32] and parameter and fields have to be *renormalized* in order to obtain a well defined set of renormalized Green functions. The problems arise because propagators are singular functions (so called distributions) the products of them are not defined at coinciding space–time arguments (short–distance [coordinate space] or ultra–violet [momentum space] singularities). An example of such an ill–defined product is the Fermion loop contribution to the photon propagator:

$$iS_F(x - y)_{\alpha\beta} (-ie\gamma_\mu)_{\beta\gamma} iS_F(y - x)_{\gamma\delta} (-ie\gamma_\nu)_{\delta\alpha} .$$

The ambiguity in general can be shown to be a local distribution, which for a renormalizable theory is of the form [33]

$$a\delta(x - y) + b^\mu \partial_\mu \delta(x - y) + c \square \delta(x - y) + d^{\mu\nu} \partial_\mu \partial_\nu \delta(x - y)$$

with derivatives up to second order at most, which, in momentum space, is a second order polynomial in the momenta.¹⁸ The regularization we will adopt is dimensional

¹⁸The mathematical problems with the point–like structure of elementary particles and with covariant quantization of the photons hindered the development of QFT for a long time until the break through at the end of the 1940s [34]. In 1965 Tomonaga, Schwinger and Feynman were honored with the Nobel Prize “for their fundamental work in quantum electrodynamics, with deep–ploughing consequences for the physics of elementary particles”. For non–Abelian gauge theories like the modern strong interaction theory *Quantum Chromodynamics* (QCD) [35, 36] and the electroweak *Standard Model* [37], the proper quantization, regularization and renormalization was another obstacle which was solved only at the beginning of the 1970s by ’t Hooft and Veltman [38]. They were awarded the

regularization [39], where the space–time dimension is taken to be d arbitrary to start with (see below).

In momentum space each line has associated a d –momentum p_i and at each vertex momentum conservation holds. Because of the momentum conservation δ –functions many d –momentum integrations become trivial. Each loop, however, has associated an independent momentum (the loop–momentum) l_i which has to be integrated over

$$\frac{1}{(2\pi)^d} \int d^d l_i \dots \tag{2.100}$$

in d space–time dimensions. For each closed fermion loop a factor -1 has to be applied because of Fermi statistics. There is an overall d –momentum conservation factor $(2\pi)^d \delta^{(d)}(\sum p_{i \text{ external}})$. Note that the lepton propagators as well as the vertex insertion $ie\gamma_\mu$ are matrices in spinor space, at each vertex the vertex insertion is sandwiched between the two adjacent propagators:

$$\dots iS_F(p)_{\alpha\gamma} (-ie\gamma_\mu)_{\gamma\delta} iS_F(p')_{\delta\beta} \dots$$

Since any renormalizable theory exhibits fermion fields not more than bilinear, as a conjugate pair $\bar{\psi} \dots \psi$, fermion lines form open strings

$$\left[\prod_{i=1}^n (S \gamma)_i \right] S = \text{---} \circ \text{---} \bullet \text{---} \bullet \text{---} \bullet \text{---} \dots \text{---} \bullet \text{---} \bullet \text{---} \circ \tag{2.101}$$

of matrices in spinor space

$$\left[S_F(p_1) \gamma_{\mu_1} S_F(p_2) \gamma_{\mu_2} \dots \gamma_{\mu_n} S_F(p_{n+1}) \right]_{\alpha\beta}$$

or closed strings (fermion loops),

$$\text{Tr} \left[\prod_{i=1}^n (S \gamma)_i \right] = \text{---} \text{---} \text{---} \text{---} \text{---} \text{---} \text{---} \text{---} \tag{2.102}$$

(Footnote 18 continued)

Nobel Prize in 1999 “for elucidating the quantum structure of electroweak interactions in physics”. They have placed particle physics theory on a firmer mathematical foundation. They have in particular shown how the theory, beyond QED, may be used for precise calculations of physical quantities. Needless to say that these developments were crucial for putting precision physics, like the one with the anomalous magnetic moments, on a fundamental basis.

which correspond to a trace of a product of matrices in spinor space:

$$\text{Tr} \left[S_F(p_1) \gamma_{\mu_1} S_F(p_2) \gamma_{\mu_2} \cdots S_F(p_n) \gamma_{\mu_n} \right] .$$

Closed *fermion loops* actually contribute with two different orientations. If the number of vertices is odd the two orientations yield traces in spinor space of opposite sign such that they cancel provided the two contributions have equal weight. If the number of vertices is even the corresponding traces in spinor space contribute with equal sign, i.e. it just makes a factor of two in the equal weight case. In QED in fact the two orientations have equal weight due to the charge conjugation invariance of QED. An important consequence of C invariance is **Furry's theorem** [40]:

Theorem 2.6 *Fermion loops with an odd number of vector-vertices (i.e. γ^μ type) are vanishing.*

As already mentioned, each Fermion loop carries a factor -1 due the Fermi statistics. All this is easy to check using the known properties of the Dirac fields.¹⁹

For a given set of external vertices and a given order n of perturbation theory (n internal vertices) one obtains a sum over all possible complete contractions, where each one may be represented by a Feynman diagram Γ . The Fourier transform (FT) thus, for each connected component of a diagram, is given by expressions of the form

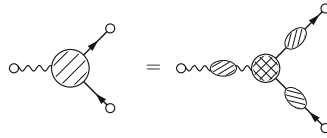
$$\begin{aligned} & \text{FT} \langle 0|T \{ A_\mu(x_1) \cdots \psi_\alpha(y_1) \cdots \bar{\psi}_\beta(\bar{y}_1) \cdots \} |0\rangle_{\text{connected}} = \\ & = (-i)^F (2\pi)^d \delta^{(d)} \left(\sum p_{\text{ext}} \right) \left(\prod_{i=1}^N \int \frac{d^d l_i}{(2\pi)^d} \right) \\ & \times \sum_{\Gamma} \prod_{\ell \in L_\ell, i \in \bar{L}_f} i S_F(p_i) (-ie\gamma_{\mu_i}) \left[\prod_{f \in \bar{L}_f} i S_F(p_f) \right] \prod_{j \in L_\gamma} i D^{\mu_j \nu_j}(q_j) , \end{aligned}$$

where L_ℓ is the set of lepton lines, L_γ the set of photon lines and \bar{L}_f the set of lines starting with an external $\bar{\psi}$ field, N the number of independent closed loops and F the number of closed fermion loops. Of course, spinor indices and Lorentz indices must contract appropriately, and momentum conservation must be respected at each vertex and over all. The basic object of our interest is the Green function associated with the electromagnetic vertex dressed by external propagators:

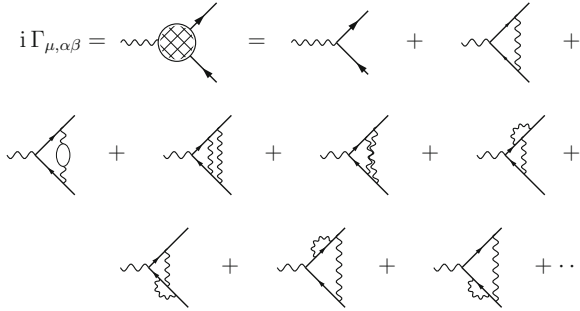
$$\begin{aligned} G_{\mu, \alpha\beta}(x, y, z) & \doteq \langle 0|T \{ A_\mu(x) \psi_\alpha(y) \bar{\psi}_\beta(z) \} |0\rangle = \\ & \int dx' dy' dz' i D'_{\mu\nu}(x' - x) i S'_{F\alpha\alpha'}(y' - y) \left(i \Gamma'_{\alpha'\beta'}(x', y', z') \right) i S'_{F\beta'\beta}(z' - z) \end{aligned}$$

¹⁹Note that in QCD the corresponding closed quark loops with quark–gluon vertices behave differently because of the color matrices at each vertex. The trace of the product of color matrices in general has an even as well as an odd part.

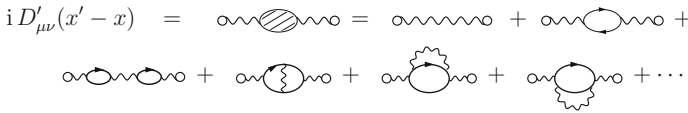
which graphically may be represented as follows



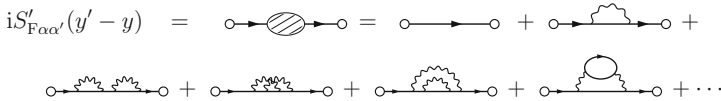
with *one particle irreducible*²⁰ (1PI) dressed vertex



where $iD'_{\mu\nu}(x' - x)$ is a full photon propagator, a photon line dressed with all radiative corrections:



and $iS'_{F\alpha\alpha'}(y' - y)$ is the full lepton propagator, a lepton line dressed by all possible radiative corrections



The tools and techniques of calculating these objects as a perturbation series in lowest non-trivial order will be developed in the next section.

The perturbation series are an iterative solution of the non-perturbative Dyson-Schwinger Equations (DSE) [41], which read: for the full electron propagator $S(p)$

$$S(p) = S_0(p) + S_0(p) \cdot \left(e^2 \int \frac{d^4k}{(2\pi)^4} \gamma_\mu D^{\mu\nu}(p - k) S(k) \Gamma_\nu(p, k) \right) \cdot S(p),$$

²⁰Diagrams which cannot be cut into two disconnected diagrams by cutting a single line. 1PI diagrams are the building blocks from which any diagram may be obtained as a tree of 1PI “blobs”.

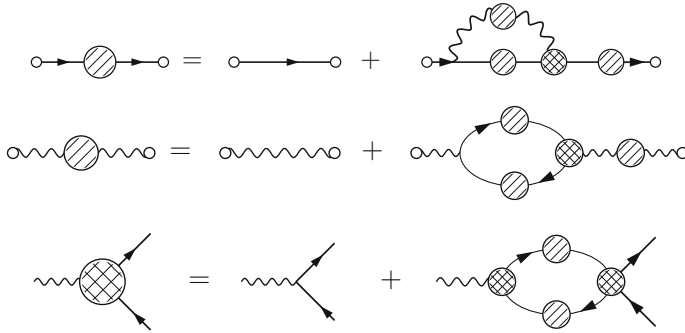


Fig. 2.4 The Dyson–Schwinger integral equations

for the full photon propagator $D^{\mu\nu}(p)$

$$D^{\mu\nu}(p) = D_0^{\mu\nu}(p) + D_0^{\mu\rho}(p) \cdot \left(-e^2 \text{Tr} \left[\int \frac{d^4k}{(2\pi)^4} \gamma_\rho S(k) \Gamma_\sigma(k, k+p) S(k+p) \right] \right) \cdot D^{\sigma\nu}(p),$$

and for the full electron–photon vertex function $\Gamma_\mu(p', p)$

$$\Gamma_\mu(p', p) = \Gamma_{\mu 0}(p', p) + \int \frac{d^4k}{(2\pi)^4} S(p'+k) \Gamma_\mu(p'+k, p+k) S(p+k) K(p+k, p'+k, k)$$

where S_0 is the free electron propagator, $D_0^{\mu\nu}(p)$ the free photon propagator and $\Gamma_{\mu 0}(p', p)$ the free e.m. vertex (see Fig. 2.3). $K(p+k, p'+k, k)$ is the four-electron T -matrix (vanishing at lowest order). The expansion in the free vertex yields the perturbation series. Graphically the SDE are represented in Fig. 2.4.

2.3.2 Transition Matrix–Elements, Particle–Antiparticle Crossing

The Green functions from the point of view of a QFT are building blocks of the theory. However, they are not directly observable objects. The physics is described by quantum mechanical transition matrix elements, which for scattering processes are encoded in the scattering matrix. For QED the latter is given formally by (2.95). The existence of a S -matrix requires that for very early and for very late times ($t \rightarrow \mp\infty$) particles behave as free scattering states. For massless QED, the electromagnetic interaction does not have finite range (Coulomb’s law) and the scattering matrix does not exist in the naive sense. In an order by order perturbative approach the problems manifest themselves as an infrared (IR) problem. As we will see below, nevertheless a suitable redefinition of the transition amplitudes is possible, which allows one a perturbative treatment under appropriate conditions. Usually, one is not directly interested in the S -matrix as the latter includes the identity operator I which describes through–going particles which do not get scattered at all. It is customary

to split off the identity from the S -matrix and to define the T -matrix by

$$S = I + i (2\pi)^4 \delta^{(4)}(P_f - P_i) T , \quad (2.103)$$

with the overall four-momentum conservation factored out. In spite of the fact, that Green functions are not observables they are very useful to understand important properties of the theory. One of the outstanding features of a QFT is the *particle-antiparticle crossing* property which states that in a scattering amplitude an incoming particle [antiparticle] is equivalent to an outgoing antiparticle [particle] and vice versa. It means that the same function, namely an appropriate time-ordered Green function, at the same time describes several processes. For example, muon pair production in electron positron annihilation $e^+e^- \rightarrow \mu^+\mu^-$ is described by amplitudes which at the same time describe electron-muon scattering $e^-\mu^- \rightarrow e^-\mu^-$ or whatever process we can obtain by bringing particles from one side of the reaction balance to the other side as an antiparticle etc. Another example is muon decay $\mu^+ \rightarrow e^+\nu_e\bar{\nu}_\mu$ and neutrino scattering $\nu_\mu e^- \rightarrow \mu^-\nu_e$. For the electromagnetic vertex it relates properties of the electrons [leptons, quarks] to properties of the positron [antileptons, antiquarks].

Since each external free field on the right hand side of (2.99) exhibits an annihilation part and a creation part, each external field has two interpretations, either as an incoming particle or as an outgoing antiparticle. For the adjoint field incoming and outgoing get interchanged. This becomes most obvious if we invert the field decomposition (2.12) for the Dirac field which yields the corresponding creation/annihilation operators

$$a(\mathbf{p}, r) = \bar{u}(\mathbf{p}, r)\gamma^0 \int d^3x e^{ipx} \psi(x) \quad , \quad b^+(\mathbf{p}, r) = \bar{v}(\mathbf{p}, r)\gamma^0 \int d^3x e^{-ipx} \psi(x) .$$

Similarly, inverting (2.13) yields

$$c(\mathbf{p}, \lambda) = -\varepsilon^{\mu*}(\mathbf{p}, \lambda) i \int d^3x e^{ipx} \overleftrightarrow{\partial}_0 A_\mu(x)$$

and its Hermitian conjugate for the photon, with $f(x) \overleftrightarrow{\partial}_\mu g(x) \equiv f(x) \partial_\mu g(x) - (\partial_\mu f(x)) g(x)$. Since these operators create or annihilate scattering states, the above relations provide the bridge between the Green functions, the vacuum expectation values of time-ordered fields, and the scattering matrix elements. This is how the crossing property between different physical matrix elements comes about. The S -matrix elements are obtained from the Green functions by the Lehmann, Symanzik, Zimmermann [42] (LSZ) reduction formula: the external full propagators of the Green functions are omitted (multiplication by the inverse full propagator, i.e. no radiative corrections on external amputated legs) and replaced by an external classical one particle wave function and the external momentum is put on the mass shell. Note that the on-shell limit only exists after the amputation of the external one

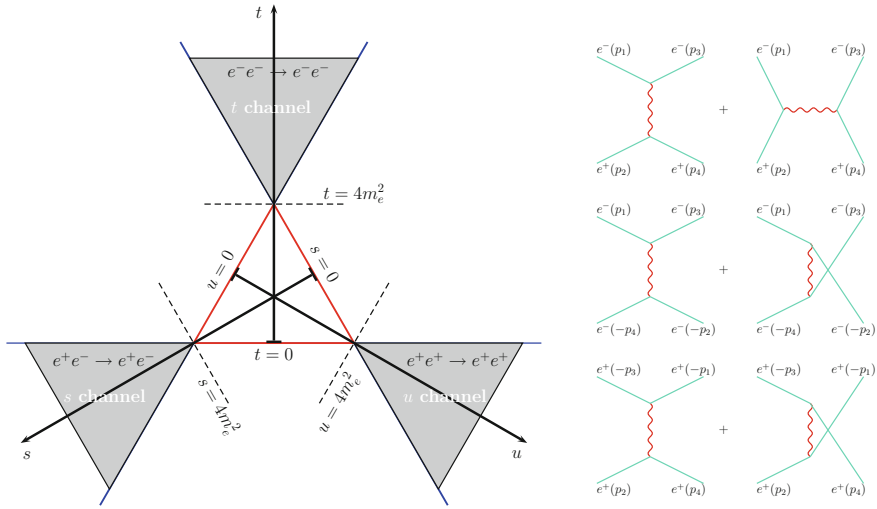


Fig. 2.5 The Mandelstam plane $s + t + u = \sum_{i=1}^4 p_i^2 = \sum_{i=1}^4 m_i^2$. Physical regions are shaded and represent different processes for the appropriate ranges of the Mandelstam variables (s, t, u). The Feynman diagrams shown to be read from *left* (in-state) to *right* (out-state). Light-by-light scattering $\gamma\gamma \rightarrow \gamma\gamma$ is a crossing symmetric process where the different channels represent the same process

$$\begin{aligned}
 e^-(p_1) + e^+(p_2) &\rightarrow e^-(p_3) + e^+(p_4) : & s\text{-channel}; & & s &= (p_1 + p_2)^2, \\
 e^-(p_1) + e^-(-p_4) &\rightarrow e^-(-p_2) + e^-(p_3) : & t\text{-channel}; & & t &= (p_1 - p_4)^2, \\
 e^+(p_2) + e^+(-p_3) &\rightarrow e^+(-p_1) + e^+(p_4) : & u\text{-channel}; & & u &= (p_2 - p_3)^2.
 \end{aligned}$$

Note that $s + t + u = 4m_e^2$ which is the height in a isosceles triangle and gives rise to the Mandelstam plane [43] (see Fig. 2.5).

Given the T matrix-elements, the bridge to the experimental numbers is given by the cross sections and decay rates, which we present for completeness here.

2.3.3 Cross Sections and Decay Rates

The **differential cross section** for a two particle collision

$$A(p_1) + B(p_2) \rightarrow C(p'_1) + D(p'_2) \dots$$

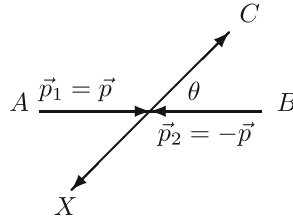
is given by

$$d\sigma = \frac{(2\pi)^4 \delta^{(4)}(P_f - P_i)}{2\sqrt{\lambda(s, m_1^2, m_2^2)}} |T_{fi}|^2 d\mu(p'_1) d\mu(p'_2) \dots$$

$s = (p_1 + p_2)^2$ is the square of the total CM energy and $\lambda(x, y, z) = x^2 + y^2 + z^2 - 2xy - 2xz - 2yz$ is a two body phase-space function. In the CM frame (see the figure):

$$\sqrt{\lambda} = \sqrt{\lambda(s, m_1^2, m_2^2)} = 2|\mathbf{p}|\sqrt{s} \quad (2.104)$$

where $\mathbf{p} = \mathbf{p}_i$ is the three-momentum of the initial state particle A.



The total cross section follows by integration over all phase space

$$\sigma = \int d\sigma .$$

Finally, we consider the decay of unstable particles. The differential **decay rate** for $A \rightarrow B + C + \dots$ is given by

$$d\Gamma = \frac{(2\pi)^4 \delta^{(4)}(P_f - P_i)}{2m_1} |T_{fi}|^2 d\mu(p'_1) d\mu(p'_2) \dots$$

By “summing” over all possible decay channels we find the total width

$$\Gamma = \sum d\Gamma = \frac{1}{\tau} , \quad (2.105)$$

where τ is the **lifetime** of the particle, which decays via the exponential **decay law**

$$N(t) = N_0 e^{-t/\tau} . \quad (2.106)$$

Cross sections are measured typically by colliding beams of stable particles and their antiparticles like electrons (e^-), positrons (e^+), protons (p) or antiprotons (\bar{p}). The beam strength of an accelerator or storage ring required for accelerating and collimating the beam particles is determined by the particle flux or *luminosity* L , the number of particles per cm^2 and *seconds*. The energy of the machine determines the resolution

$$\lambda = \frac{hc}{E_{c.m.}} \simeq \frac{1.2 \text{ GeV}}{E_{c.m.}(\text{GeV})} \times 10^{-15} \text{ m} ,$$

while the luminosity determines the collision rate

$$\frac{\Delta N}{\Delta t} = L \cdot \sigma ,$$

and the cross section σ is thus given by dividing the observed event rate by the luminosity

$$\sigma = \frac{1}{L} \frac{\Delta N}{\Delta t} . \quad (2.107)$$

2.4 Regularization and Renormalization

The vertex and self-energy functions, as well as all other Green functions, on the level of the bare theory are well defined order by order in perturbation theory only after smoothing the short distance or ultraviolet (UV) divergences by appropriate regularization. Here we assume QED or the SM to be regularized by dimensional regularization [39]. By going to lower dimensional space-times the features of the theory, in particular the symmetries, remain the same, however, the convergence of the Feynman integrals gets improved. For a renormalizable theory, in principle, one can always choose the dimension low enough, $d < 2$, such that the integrals converge. By one or two partial integrations one can analytically continue the integrals in steps from d to $d + 1$, such that the perturbation expansion is well defined for $d = 4 - \epsilon$ with ϵ a small positive number. For $\epsilon \rightarrow 0$ ($d \rightarrow 4$) the perturbative series in the *fine structure constant* $\alpha = e^2/4\pi$ exhibits poles in ϵ :

$$A = \sum_{n=0}^N \alpha^n \sum_{m=0}^n a_{nm} (1/\epsilon)^{n-m}$$

and the limit $d \rightarrow 4$ to the real physical space-time does not exist, at first. The problems turn out to be related to the fact that the bare objects are not physical ones, they are not directly accessible to observation and require some adjustments. This in particular is the case for the bare parameters, the bare fine structure constant (electric charge) which is modified by vacuum polarization (quantum fluctuations), and the bare masses. Also the bare fields are not the ones which interpolate suitably to the physical states they are assumed to describe. The appropriate entities are in fact obtained by a simple reparametrization in terms of new parameters and fields, which is called *renormalization*.

2.4.1 The Structure of the Renormalization Procedure

Renormalization may be performed in three steps:

- (i) Shift of the mass parameters or *mass renormalization*: replace the bare mass parameters of the bare Lagrangian by renormalized ones

$$\begin{aligned} m_{f0} &= m_{f\text{ren}} + \delta m_f && \text{for fermions} \\ M_{b0}^2 &= M_{b\text{ren}}^2 + \delta M_b^2 && \text{for bosons} \end{aligned} \quad (2.108)$$

(ii) Multiplicative renormalization of the bare fields or *wave function renormalization*: replace the bare fields in the bare Lagrangian by renormalized ones

$$\psi_{f0} = \sqrt{Z_f} \psi_{f\text{ren}} , \quad A_0^\mu = \sqrt{Z_\gamma} A_{\text{ren}}^\mu \quad (2.109)$$

and correspondingly for the other fields of the SM. To leading order $Z_i = 1$ and hence

$$Z_i = 1 + \delta Z_i , \quad \sqrt{Z_i} = 1 + \frac{1}{2} \delta Z_i + \dots \quad (2.110)$$

(iii) Vertex renormalization or *coupling constant renormalization*: substitute the bare coupling constant by the renormalized one

$$e_0 = e_{\text{ren}} + \delta e . \quad (2.111)$$

The **renormalization theorem** (see e.g. [1, 33, 38]) states that

Theorem 2.7 *Order by order in the perturbation expansion all UV divergences showing up in physical quantities (S-matrix elements) get eliminated by an appropriate choice of the counter terms δm_f , δM_b^2 , δe and $\delta Z_i = Z_i - 1$. Physical amplitudes parametrized in terms of physical parameters thus are finite and free of cutoff effects in the large cutoff limit.*

In other words, suitably normalized physical amplitudes expressed in terms of measurable physical parameters are finite in the limit $\epsilon \rightarrow 0$, i.e., they allow us to take away the regularization (cut-off $\Lambda \rightarrow \infty$ if a UV cut-off was used to regularize the bare theory). Note that for Green functions, which are not gauge invariant in general, also the fictitious gauge parameter has to be renormalized in order to obtain finite Green functions. Unitarity requires the counter terms to be real. Therefore the counter terms are determined by the real parts of the location and residues of the one particle poles. Also note: the Z-factors are *gauge dependent* and in order to get gauge invariant S-matrix elements there is no freedom in the choice of the wave function renormalization factors. Only the Z-factors fixed by the LSZ-conditions for the individual fields lead to the physical S-matrix [38, 44]. In fact bare on-shell matrix-elements are not gauge invariant, they become gauge invariant only after wave-function renormalization normalized by the LSZ conditions.

The reparametrization of the bare Lagrangian (2.90) in terms of renormalized quantities reads

$$\begin{aligned}
\mathcal{L}^{\text{QED}} &= -\frac{1}{4} F_{\mu\nu 0}(x) F_0^{\mu\nu}(x) - \frac{1}{2} \xi_0^{-1} (\partial_\mu A_0^\mu(x))^2 + \bar{\psi}_0(x) (i\gamma^\mu \partial_\mu - m_0) \psi_0(x) \\
&\quad - e_0 \bar{\psi}_0(x) \gamma^\mu \psi_0(x) A_{\mu 0}(x) \\
&= \mathcal{L}_{(0)}^{\text{QED}} + \mathcal{L}_{\text{int}}^{\text{QED}} \\
\mathcal{L}_{(0)}^{\text{QED}} &= -\frac{1}{4} F_{\mu\nu \text{ren}}(x) F_{\text{ren}}^{\mu\nu}(x) - \frac{1}{2} \xi_{\text{ren}}^{-1} (\partial_\mu A_{\text{ren}}^\mu(x))^2 \\
&\quad + \bar{\psi}_{\text{ren}}(x) (i\gamma^\mu \partial_\mu - m_{\text{ren}}) \psi_{\text{ren}}(x) \\
\mathcal{L}_{\text{int}}^{\text{QED}} &= -e_{\text{ren}} \bar{\psi}_{\text{ren}}(x) \gamma^\mu \psi_{\text{ren}}(x) A_{\mu \text{ren}}(x) \\
&\quad - \frac{1}{4} (Z_\gamma - 1) F_{\mu\nu \text{ren}}(x) F_{\text{ren}}^{\mu\nu}(x) + (Z_e - 1) \bar{\psi}_{\text{ren}}(x) i\gamma^\mu \partial_\mu \psi_{\text{ren}} \\
&\quad - (m_0 Z_e - m_{\text{ren}}) \bar{\psi}_{\text{ren}} \psi_{\text{ren}}(x) \\
&\quad - (e_0 \sqrt{Z_\gamma} Z_e - e_{\text{ren}}) \bar{\psi}_{\text{ren}}(x) \gamma^\mu \psi_{\text{ren}}(x) A_{\mu \text{ren}}(x) \tag{2.112}
\end{aligned}$$

with $\xi_{\text{ren}} = Z_\gamma \xi_0$ the gauge fixing term remains unrenormalized (no corresponding counter term). The counter terms are now showing up in $\mathcal{L}_{\text{int}}^{\text{QED}}$ and may be written in terms of $\delta Z_\gamma = Z_\gamma - 1$, $\delta Z_e = Z_e - 1$, $\delta m = m_0 Z_e - m_{\text{ren}}$ and $\delta e = e_0 \sqrt{Z_\gamma} Z_e - e_{\text{ren}}$. They are of next higher order in e^2 , either $O(e^2)$ for propagator insertions or $O(e^3)$ for the vertex insertion, in leading order. The counter terms have to be adjusted order by order in perturbation theory by the renormalization conditions which define the precise physical meaning of the parameters (see below).

The Feynman rules Fig. 2.3 have to be supplemented by the rules of including the counter terms as given in Fig. 2.6 in momentum space.

Obviously the propagators (two–point functions) of the photon and of the electron get renormalized according to

$$\begin{aligned}
D_0 &= Z_\gamma D_{\text{ren}} \\
S_{F 0} &= Z_e S_{F \text{ren}} . \tag{2.113}
\end{aligned}$$

Fig. 2.6 Feynman rules for QED (II): the counter terms

- (1) Lepton propagator insertions

$$\begin{array}{c} p \\ \text{---} \otimes \text{---} \\ \alpha \qquad \beta \end{array} : i (\delta Z_e (\not{p} - m) - \delta m)_{\alpha\beta}$$

- (2) Photon propagator insertion

$$\begin{array}{c} p \\ \text{---} \otimes \text{---} \\ \mu \qquad \nu \end{array} : -i \delta Z_\gamma (p^2 g^{\mu\nu} - p^\mu p^\nu)$$

- (3) Lepton–photon vertex insertion

$$\begin{array}{c} \alpha, p_3 \\ \text{---} \otimes \text{---} \\ \mu, p_1 \qquad \beta, p_2 \end{array} : = -i \delta e (\gamma^\mu)_{\alpha\beta}$$

The renormalized electromagnetic vertex function may be obtained according to the above rules as

$$\begin{aligned}
 G_{\text{ren}}^\mu &= \frac{1}{\sqrt{Z_\gamma}} \frac{1}{Z_e} G_0^\mu & (2.114) \\
 &= D_{\text{ren}} S_{F \text{ ren}} \Gamma_{\text{ren}}^\mu S_{F \text{ ren}} = \frac{1}{\sqrt{Z_\gamma}} \frac{1}{Z_e} D_0 S_{F 0} \Gamma_0^\mu S_{F 0} \\
 &= \frac{1}{\sqrt{Z_\gamma}} \frac{1}{Z_e} Z_\gamma Z_e^2 D_{\text{ren}} S_{F \text{ ren}} \Gamma_0^\mu S_{F \text{ ren}}
 \end{aligned}$$

and consequently

$$\begin{aligned}
 \Gamma_{\text{ren}}^\mu &= \sqrt{Z_\gamma} Z_e \Gamma_0^\mu = \sqrt{Z_\gamma} Z_e \left\{ e_0 \gamma^\mu + \Gamma_0^{\prime \mu} \right\} \Big|_{e_0 \rightarrow e + \delta e, m_0 \rightarrow m + \delta m, \dots} \\
 &= \sqrt{1 + \delta Z_\gamma} (1 + \delta Z_e) \left\{ e \left(1 + \frac{\delta e}{e} \right) \gamma^\mu + \Gamma_0^{\prime \mu} \right\} \\
 &= \left(1 + \frac{1}{2} \delta Z_\gamma + \delta Z_e + \frac{\delta e}{e} \right) e \gamma^\mu + \Gamma_0^{\prime \mu} + \dots & (2.115)
 \end{aligned}$$

where now the bare parameters have to be considered as functions of the renormalized ones:

$$e_0 = e_0(e, m), \quad m_0 = m_0(m, e) \quad \text{etc.} \quad (2.116)$$

and e, m etc. denote the renormalized parameters. The last line of (2.115) gives the perturbatively expanded form suitable for one-loop renormalization. It may also be considered as the leading n -th order renormalization if $\Gamma_0^{\prime \mu}$ has been renormalized to $n - 1$ -st order for all sub-divergences. More precisely, if we expand the exact relation of (2.115) (second last line) and include all counter terms, including the ones which follow from (2.116), up to order $n - 1$ in $\Gamma_0^{\prime \mu}$, such that all sub-divergences of $\Gamma_0^{\prime \mu}$ are renormalized away, only the overall divergence of order n will be there. After including the wavefunction renormalization factors of order n as well (by calculating the corresponding propagators) the remaining overall divergence gets renormalized away by fixing $\delta e^{(n)}$, according to the last line of (2.115), by the charge renormalization condition:

$$\bar{u}(p_2, r_2) \Gamma_{\text{ren}}^\mu(p_1, p_2) u(p_1, r_1) = e_{\text{ren}} \bar{u}(p_2, r_2) \gamma^\mu u(p_1, r_1)$$

at zero photon momentum $q = p_2 - p_1 = 0$ (classical limit, *Thomson limit*).

2.4.2 Dimensional Regularization

Starting with the Feynman rules of the classical quantized Lagrangian, called bare Lagrangian, the formal perturbation expansion is given in terms of ultraviolet (*UV*) divergent Feynman integrals if we try to do that in $d = 4$ dimensions without a *UV* cut-off. As an example consider the scalar one-loop self-energy diagram and the corresponding Feynman integral

$$\begin{array}{c}
 \text{---} \circlearrowleft \text{---} \\
 \text{---} \text{---} \\
 k
 \end{array}
 = \frac{1}{(2\pi)^d} \int d^d k \frac{1}{k^2 - m^2 + i\epsilon} \frac{1}{(k+p)^2 - m^2 + i\epsilon} \quad |k| \gg |p|, m \int \frac{d^d k}{k^4}$$

which is logarithmically divergent for the physical space-time dimension $d = 4$ because the integral does not fall-off sufficiently fast at large k . In order to get a well-defined perturbation expansion the theory must be regularized.²¹ The regularization should respect as much as possible the symmetries of the initial bare form of the Lagrangian and of the related *Ward–Takahashi* (WT) identities of the “classical theory”. For gauge theories like QED, QCD or the SM dimensional regularization [39] (DR) is the most suitable regularization scheme as a starting point for the perturbative approach, because it respects as much as possible the classical symmetries of a Lagrangian.²² The idea behind DR is the following:

- (i) Feynman rules formally look the same in different space-time dimensions $d = n$ (integer)
- (ii) In the *UV* region Feynman integrals converge the better the lower d is.

The example given above demonstrates this, in $d = 4 - \epsilon$ ($\epsilon > 0$) dimensions (just below $d = 4$) the integral is convergent. Before we specify the rules of DR in more detail, let us have a look at convergence properties of Feynman integrals.

²¹Often one simply chooses a cut-off (upper integration limit in momentum space) to make the integrals converge by “brute force”. A cut-off may be considered to parametrize our ignorance about physics at very high momentum or energy. If the cut-off Λ is large with respect to the energy scale E of a phenomenon considered, $E \ll \Lambda$, the cut-off dependence may be removed by considering only relations between low-energy quantities (renormalization). Alternatively, a cut-off may be interpreted as the scale where one expects new physics to enter and it may serve to investigate how a quantity (or the theory) behaves under changes of the cut-off (renormalization group). In most cases simple cut-off regularization violates symmetries badly and it becomes a difficult task to make sure that one obtains the right theory when the cut-off is removed by taking the limit $\Lambda \rightarrow \infty$ after renormalization.

²²An inconsistency problem, concerning the definition of γ_5 for $d \neq 4$, implies that the chiral WT identities associated with the parity violating weak fermion currents in the SM are violated in general (see e.g. [45]).

Dyson Power Counting

The action

$$S = i \int d^d x \mathcal{L}_{\text{eff}} \quad (2.117)$$

measured in units of $\hbar = 1$ is dimensionless and therefore $\dim \mathcal{L}_{\text{eff}} = d$ in mass units. The inspection of the individual terms yields the following dimensions for the fields:

$$\begin{aligned} \bar{\psi} \gamma^\mu \partial_\mu \psi & : \dim \psi = \frac{d-1}{2} \\ (\partial_\mu A_\nu - \dots)^2 & : \dim A_\mu = \frac{d-2}{2} \\ \bar{e}_0 \bar{\psi} \gamma^\mu \psi A_\mu & : \dim \bar{e}_0 = \frac{4-d}{2} \Rightarrow \bar{e}_0 = e_0 \mu^{\epsilon/2} \end{aligned} \quad (2.118)$$

where $\epsilon = 4 - d$, e_0 denotes the dimensionless bare coupling constant ($\dim e_0 = 0$) and μ is an arbitrary mass scale. The dimension of time ordered Green functions in momentum space is then given by (the Fourier transformation $\int d^d q e^{-iqx} \dots$ gives $-d$ for each field):

$$\dim G^{(n_B, 2n_F)} = n_B \frac{d-2}{2} + 2n_F \frac{d-1}{2} - (n_B + 2n_F)d$$

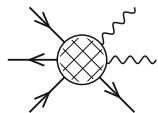
where

$$\begin{aligned} n_B & : \text{\#of boson fields} : G_{i\mu}, \dots \\ 2n_F & : \text{\#of Dirac fields (in pairs)} : \psi \dots \bar{\psi} \end{aligned}$$

It is convenient to split off factors which correspond to external propagators (see p. 52) and four-momentum conservation and to work with 1PI amplitudes, which are the objects relevant for calculating T matrix elements. The corresponding proper amputated vertex functions are of dimension

$$\dim \hat{G}^{\text{amp}} = d - n_B \frac{d-2}{2} - 2n_F \frac{d-1}{2} \quad (2.119)$$

A generic Feynman diagram represents a Feynman integral



$$\iff I_\Gamma(p) = \int \frac{d^d k_1}{(2\pi)^d} \dots \frac{d^d k_m}{(2\pi)^d} J_\Gamma(p, k) \cdot$$

The convergence of the integral can be inspected by looking at the behavior of the integrand for large momenta: For $k_i = \lambda \hat{k}_i$ and $\lambda \rightarrow \infty$ we find

$$\prod_i d^d k_i J_\Gamma(p, k) \rightarrow \lambda^{d(\Gamma)}$$

where

$$d(\Gamma) = d - n_B \frac{d-2}{2} - 2n_F \frac{d-1}{2} + \sum_{i=1}^n (d_i - d)$$

is called the *superficial divergence* of the 1PI diagram Γ . The sum extends over all (n) vertices of the diagram and d_i denotes the dimension of the vertex i . The $-d$ at each vertex accounts for d -momentum conservation. For a vertex exhibiting $n_{i,b}$ Bose fields, $n_{i,f}$ Fermi fields and l_i derivatives of fields we have

$$d_i = n_{i,b} \frac{d-2}{2} + n_{i,f} \frac{d-1}{2} + l_i \quad (2.120)$$

Here it is important to mention one of the most important conditions for a QFT to develop its full predictive power: *renormalizability*. In order that $d(\Gamma)$ in (2.120) is bounded in physical space-time $d = 4$ all interaction vertices must have dimension not more than $d_i \leq 4$. An anomalous magnetic moment effective interaction term (Pauli term)

$$\delta \mathcal{L}_{\text{eff}}^{\text{AMM}} = \frac{ieg}{4m} \bar{\psi}(x) \sigma_{\mu\nu} \psi(x) F^{\mu\nu}(x) , \quad (2.121)$$

has dimension 5 (in $d = 4$) and thus would spoil the renormalizability of the theory.²³ Such a term is thus forbidden in any renormalizable QFT. In contrast, in any renormalizable QFT the anomalous magnetic moment of a fermion is a quantity unambiguously predicted by the theory.

The relation (2.120) may be written in the alternative form

$$d(\Gamma) = 4 - n_B - 2n_F \frac{3}{2} + L(d-4) .$$

The result can be easily understood: the loop expansion of an amplitude has the form

$$A^{(L)} = A^{(0)} [1 + a_1 \alpha + a_2 \alpha^2 + \dots + a_L \alpha^L + \dots] \quad (2.122)$$

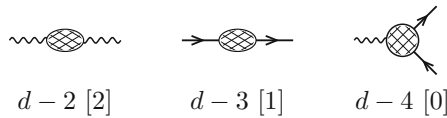
where $\alpha = e^2/4\pi$ is the conventional expansion parameter. $A^{(0)}$ is the tree level amplitude which coincides with the result in $d = 4$.

We are ready now to formulate the convergence criterion which reads:

$$\begin{aligned} I_\Gamma \text{ convergent} &\Leftrightarrow d(\gamma) < 0 \quad \forall \text{ 1PI subdiagrams } \gamma \subseteq \Gamma \\ I_\Gamma \text{ divergent} &\Leftrightarrow \exists \gamma \subseteq \Gamma \text{ with } d(\gamma) \geq 0 . \end{aligned}$$

²³The dimension of $F^{\mu\nu}$ is 2, 1 for the photon field plus 1 for the derivative.

In $d \leq 4$ dimensions, a renormalizable theory has the following types of primitively divergent diagrams (i.e., diagrams with $d(\Gamma) \geq 0$ which may have divergent sub-integrals)²⁴:



$+(L_\Gamma - 1)(d - 4)$ for a diagram with $L_\Gamma (\geq 1)$ loops. The list shows the non-trivial leading one-loop $d(\Gamma)$ to which per additional loop a contribution $(d - 4)$ has to be added (see (2.122)), in square brackets the values for $d = 4$. Thus the dimensional analysis tells us that convergence improves for $d < 4$. For a renormalizable theory we have

- $d(\Gamma) \leq 2$ for $d = 4$.

In lower dimensions

- $d(\Gamma) < 2$ for $d < 4$

a renormalizable theory becomes super-renormalizable, while in higher dimensions

- $d(\Gamma)$ unbounded! $d > 4$

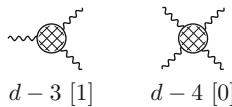
and the theory is non-renormalizable.

Dimensional Regularization

Dimensional regularization of theories with spin is defined in three steps.

1. Start with Feynman rules formally derived in $d = 4$.
2. Generalize to $d = 2n > 4$. This intermediate step is necessary in order to treat the vector and spinor indices appropriately. Of course it means that the UV behavior of Feynman integrals at first gets worse.

²⁴According to (2.122) there are two more potentially divergent structures



with superficial degree of divergence as indicated. However, the triple photon vertex is identically zero by Furry's theorem, C odd amplitudes are zero in the C preserving QED. The four photon light-by-light scattering amplitude, due the transversality of the external physical photons, has an effective dimension $d(\Gamma)_{\text{eff}} = -4$, instead of 0, and is thus very well convergent. For the same reason, transversality of the photon self-energy, actually the photon propagator has $d(\Gamma)_{\text{eff}} = 0$ instead of 2. In both cases it is the Abelian gauge symmetry which makes integrals better convergent than they look like by naive power counting.

(1) For fermions we need the $d = 2n$ -dimensional Dirac algebra:

$$\{\gamma^\mu, \gamma^\nu\} = 2g^{\mu\nu} \mathbf{1}; \quad \{\gamma^\mu, \gamma_5\} = 0 \quad (2.123)$$

where γ_5 must satisfy $\gamma_5^2 = \mathbf{1}$ and $\gamma_5^+ = \gamma_5$ such that $\frac{1}{2}(\mathbf{1} \pm \gamma_5)$ are the chiral projection matrices. The metric has dimension d

$$g^{\mu\nu} g_{\mu\nu} = g_\mu^\mu = d; \quad g_{\mu\nu} = \begin{pmatrix} 1 & 0 & \cdots \\ 0 & -1 & \\ \vdots & & \ddots \\ & & & -1 \end{pmatrix}.$$

By $\mathbf{1}$ we denote the unit matrix in spinor space. In order to have the usual relation for the adjoint spinors we furthermore require

$$\gamma^{\mu+} = \gamma^0 \gamma^\mu \gamma^0. \quad (2.124)$$

Simple consequences of this d -dimensional algebra are:

$$\begin{aligned} \gamma_\alpha \gamma^\alpha &= d \mathbf{1} \\ \gamma_\alpha \gamma^\mu \gamma^\alpha &= (2-d) \gamma^\mu \\ \gamma_\alpha \gamma^\mu \gamma^\nu \gamma^\alpha &= 4g^{\mu\nu} \mathbf{1} + (d-4) \gamma^\mu \gamma^\nu \\ \gamma_\alpha \gamma^\mu \gamma^\nu \gamma^\rho \gamma^\alpha &= -2\gamma^\rho \gamma^\nu \gamma^\mu + (4-d) \gamma^\mu \gamma^\nu \gamma^\rho \text{ etc.} \end{aligned} \quad (2.125)$$

Traces of strings of γ -matrices are very similar to the ones in 4-dimensions. In $d = 2n$ dimensions one can easily write down $2^{d/2}$ -dimensional representations of the Dirac algebra [46]. Then

$$\begin{aligned} \text{Tr } \mathbf{1} &= f(d) = 2^{d/2} \\ \text{Tr } \prod_{i=1}^{2n-1} \gamma^{\mu_i} (\gamma^5) &= 0 \\ \text{Tr } \gamma^\mu \gamma^\nu &= f(d) g^{\mu\nu} \\ \text{Tr } \gamma^\mu \gamma^\nu \gamma^\rho \gamma^\sigma &= f(d) (g^{\mu\nu} g^{\rho\sigma} - g^{\mu\rho} g^{\nu\sigma} + g^{\mu\sigma} g^{\nu\rho}) \text{ etc.} \end{aligned} \quad (2.126)$$

One can show that for *renormalized quantities* the only relevant property of $f(d)$ is $f(d) \rightarrow 4$ for $d \rightarrow 4$. Very often the convention $f(d) = 4$ (for any d) is adopted. Bare quantities and the related *minimally subtracted* MS or modified minimally subtracted $\overline{\text{MS}}$ quantities (see below for the precise definition) depend upon this convention (by terms proportional to $\ln 2$).

In anomaly free theories we can assume γ_5 to be fully anticommuting! But then

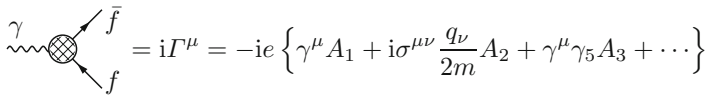
$$\text{Tr } \gamma^\mu \gamma^\nu \gamma^\rho \gamma^\sigma \gamma_5 = 0 \text{ for all } d \neq 4! \quad (2.127)$$

The 4–dimensional object

$$4i\varepsilon^{\mu\nu\rho\sigma} = \text{Tr } \gamma^\mu \gamma^\nu \gamma^\rho \gamma^\sigma \gamma_5 \text{ for } d = 4$$

cannot be obtained by dimensional continuation if we use an anticommuting γ_5 [46].

Since fermions do not have self interactions they only appear as closed fermion loops, which yield a trace of γ –matrices, or as a fermion string connecting an external $\psi \cdots \bar{\psi}$ pair of fermion fields. In a transition amplitude $|T|^2 = \text{Tr}(\cdots)$ we again get a trace. Consequently, in principle, we have eliminated all γ 's! Commonly one writes a covariant tensor decomposition into invariant amplitudes, like, for example,



$$= i\Gamma^\mu = -ie \left\{ \gamma^\mu A_1 + i\sigma^{\mu\nu} \frac{q_\nu}{2m} A_2 + \gamma^\mu \gamma_5 A_3 + \cdots \right\}$$

where μ is an external index, q^μ the photon momentum and $A_i(q^2)$ are scalar form factors.

(2) External momenta (and external indices) must be taken $d = 4$ dimensional, because the number of independent “form factors” in covariant decompositions depends on the dimension, with a fewer number of independent functions in lower dimensions. Since four functions cannot be analytic continuation of three etc. we have to keep the external structure of the theory in $d = 4$. The reason for possible problems here is the non–trivial spin structure of the theory of interest. The following rules apply:

External momenta :	$p^\mu = (p^0, p^1, p^2, p^3, 0, \dots, 0)$	4 – dimensional
Loop momenta :	$k^\mu = (k^0, \dots, k^{d-1})$	d – dimensional
	$k^2 = (k^0)^2 - (k^1)^2 - \dots - (k^{d-1})^2$	
	$pk = p^0 k^0 - \mathbf{p} \cdot \mathbf{k}$	4 – dimensional etc.

3. Interpolation in d to complex values and extrapolation to $d < 4$.

Loop integrals now read

$$\mu^{A-d} \int \frac{d^d k}{(2\pi)^d} \cdots \tag{2.128}$$

with μ an arbitrary scale parameter. The crucial properties valid in DR independent of d are: (F.P. = finite part)

- (a) $\int d^d k k_\mu f(k^2) = 0$
 (b) $\int d^d k f(k+p) = \int d^d k f(k)$
 which is not true with UV cut – off's
 (c) If $f(k) = f(|k|)$:

$$\int d^d k f(k) = \frac{2\pi^{d/2}}{\Gamma(\frac{d}{2})} \int_0^\infty dr r^{d-1} f(r)$$

- (d) For divergent integrals, by analytic subtraction:

F.P. $\int_0^\infty dr r^{d-1+\alpha} \equiv 0$ for arbitrary α
 so called *minimal subtraction* (MS). Consequently

$$\text{F.P.} \int d^d k f(k) = \text{F.P.} \int d^d k f(k+p) = \text{F.P.} \int d^d(\lambda k) f(\lambda k) .$$

This implies that **dimensionally regularized integrals behave like convergent integrals** and formal manipulations are justified. Starting with d sufficiently small, by partial integration, one can always find a representation for the integral which converges for $d = 4 - \epsilon$, $\epsilon > 0$ small.

In order to elaborate in more detail how DR works in practice, let us consider a generic one-loop Feynman integral

$$I_\Gamma^{\mu_1 \dots \mu_m}(p_1, \dots, p_n) = \int d^d k \frac{\prod_{j=1}^m k^{\mu_j}}{\prod_{i=1}^n ((k+p_i)^2 - m_i^2 + i\varepsilon)}$$

which has superficial degree of divergence

$$d(\Gamma) = d + m - 2n \leq d - 2$$

where the bound holds for two- or more-point functions in renormalizable theories and for $d \leq 4$. Since the physical tensor and spin structure has to be kept in $d = 4$, by contraction with external momenta or with the metric tensor $g_{\mu_i \mu_j}$ it is always possible to write the above integral as a sum of integrals of the form

$$I_\Gamma^{\hat{\mu}_1 \dots \hat{\mu}_{m'}}(\hat{p}_1, \dots, \hat{p}_{n'}) = \int d^d k \frac{\prod_{j=1}^{m'} \hat{k}^{\mu_j}}{\prod_{i=1}^{n'} ((k+\hat{p}_i)^2 - m_i^2 + i\varepsilon)}$$

where now $\hat{\mu}_j$ and \hat{p}_i are $d = 4$ -dimensional objects and

$$d^d k = d^4 \hat{k} d^{d-4} \bar{k} = d^4 \hat{k} \omega^{d-5} d\omega d\Omega_{d-4} .$$

In the $d - 4$ -dimensional complement the integrand depends on ω only! The angular integration over $d\Omega_{d-4}$ yields

$$\int d\Omega_{d-4} = S_{d-4} = \frac{2\pi^{\epsilon/2}}{\Gamma(\epsilon/2)} ; \quad \epsilon = d - 4 ,$$

which is the surface of the $d - 4$ -dimensional sphere. Using this result we get (discarding the four-dimensional tensor indices)

$$I_{\Gamma}(\{\hat{p}_i\}) = \int d^4\hat{k} J_{\Gamma}(d, \hat{p}, \hat{k})$$

where

$$J_{\Gamma}(d, \hat{p}, \hat{k}) = S_{d-4} \int_0^{\infty} d\omega \omega^{d-5} f(\hat{p}, \hat{k}, \omega).$$

Now this integral can be analytically continued to complex values of d . For the ω -integration we have

$$d^{\omega}(\Gamma) = d - 4 - 2n$$

i.e. the ω -integral converges if

$$d < 4 + 2n .$$

In order to avoid infrared singularities in the ω -integration one has to analytically continue by appropriate partial integration. After p -fold partial integration we have

$$I_{\Gamma}(\{\hat{p}_i\}) = \frac{2\pi^{\frac{d-4}{2}}}{\Gamma(\frac{d-4}{2} + p)} \int d^4\hat{k} \int_0^{\infty} d\omega \omega^{d-5+2p} \left(-\frac{\partial}{\partial\omega^2}\right)^p f(\hat{p}, \hat{k}, \omega)$$

where the integral is convergent in $4 - 2p < \text{Re } d < 2n - m = 4 - d^{(4)}(\Gamma) \geq 2$. For a renormalizable theory at most 2 partial integrations are necessary to define the theory.

2.5 Tools for the Evaluation of Feynman Integrals

2.5.1 $\epsilon = 4 - d$ Expansion, $\epsilon \rightarrow +0$

For the expansion of integrals near $d = 4$ we need some asymptotic expansions of Γ -functions:

$$\Gamma(1+x) = \exp \left[-\gamma x + \sum_{n=2}^{\infty} \frac{(-1)^n}{n} \zeta(n) x^n \right] \quad |x| \leq 1$$

$$\psi(1+x) = \frac{d}{dx} \ln \Gamma(1+x) = \frac{\Gamma'(1+x)}{\Gamma(1+x)} \Big|_{|x| \leq 1} = -\gamma + \sum_{n=2}^{\infty} (-1)^n \zeta(n) x^{n-1}$$

where $\zeta(n)$ denotes Riemann's Zeta function. The defining functional relation is

$$\Gamma(x) = \frac{\Gamma(x+1)}{x},$$

which for $n = 0, 1, 2, \dots$ yields $\Gamma(n+1) = n!$ with $\Gamma(1) = \Gamma(2) = 1$. Furthermore we have

$$\begin{aligned} \Gamma(x) \Gamma(1-x) &= \frac{\pi}{\sin \pi x} \\ \Gamma\left(\frac{1}{2} + x\right) \Gamma\left(\frac{1}{2} - x\right) &= \frac{\pi}{\cos \pi x}. \end{aligned}$$

Important special constants are

$$\begin{aligned} \Gamma\left(\frac{1}{2}\right) &= \sqrt{\pi} \\ \Gamma'(1) &= -\gamma; \quad \gamma = 0.577215 \dots \text{ Euler's constant} \\ \Gamma''(1) &= \gamma^2 + \zeta(2); \quad \zeta(2) = \frac{\pi^2}{6} = 1.64493 \dots \end{aligned}$$

As a typical result of an ϵ -expansion, which we should keep in mind for later purposes, we have

$$\Gamma\left(1 + \frac{\epsilon}{2}\right) = 1 - \frac{\epsilon}{2}\gamma + \left(\frac{\epsilon}{2}\right)^2 \frac{1}{2}(\gamma^2 + \zeta(2)) + \dots$$

2.5.2 Bogolubov–Schwinger Parametrization

Suppose we choose for each propagator an independent momentum and take into account momentum conservation at the vertices by δ -functions. Then, for $d = n$ integer, we use

(i)

$$\frac{i}{p^2 - m^2 + i\epsilon} = \int_0^\infty d\alpha e^{-i\alpha(m^2 - p^2 - i\epsilon)} \quad (2.129)$$

(ii)

$$\delta^{(d)}(k) = \frac{1}{(2\pi)^d} \int_{-\infty}^{+\infty} d^d x e^{ikx} \quad (2.130)$$

and find that all momentum integrations are of Gaussian type. The Gaussian integrals yield

$$\int_{-\infty}^{+\infty} d^d k P(k) e^{i(ak^2 + 2b(k \cdot p))} = P\left(\frac{-i}{2b} \frac{\partial}{\partial p}\right) \left(\frac{\pi}{ia}\right)^{d/2} e^{-i b^2/a p^2} \quad (2.131)$$

for any polynomial P . The resulting form of the Feynman integral is the so called Bogolubov–Schwinger representation, also known as α -representation (see e.g. [47]).

2.5.3 Feynman Parametric Representation

Transforming pairs of α -variables in the above Bogolubov–Schwinger parametrization according to (l is denoting the pair (i, k))

$$(\alpha_i, \alpha_k) \rightarrow (\xi_l, \alpha_l) : (\alpha_i, \alpha_k) = (\xi_l \alpha_l, (1 - \xi_l) \alpha_l) \quad (2.132)$$

$$\int_0^\infty \int_0^\infty d\alpha_i d\alpha_k \cdots = \int_0^\infty d\alpha_l \alpha_l \int_0^1 d\xi_l \cdots, \quad (2.133)$$

the integrals are successively transformed into $\int_0^1 d\xi \cdots$ integrals and at the end there remains one α -integration only which can be performed using

$$\int_0^\infty d\alpha \alpha^a e^{-\alpha x} = \Gamma(a + 1) x^{-(a+1)}. \quad (2.134)$$

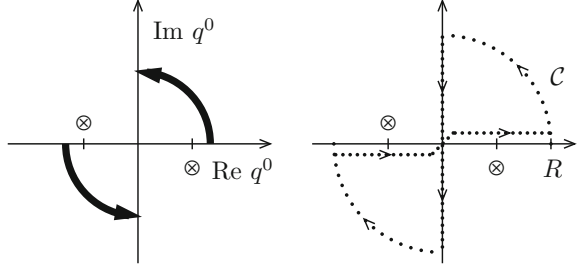
The result is the Feynman parametric representation. If L is the number of lines of a diagram, the Feynman integral is $(L - 1)$ -dimensional.

2.5.4 Euclidean Region, Wick–Rotations

The basic property which allows us to perform a Wick rotation is analyticity which derives from the causality of a relativistic QFT. In momentum space the Feynman propagator

$$\begin{aligned} \frac{1}{q^2 - m^2 + i\varepsilon} &= \frac{1}{q^0 - \sqrt{\mathbf{q}^2 + m^2} - i\varepsilon} \frac{1}{q^0 + \sqrt{\mathbf{q}^2 + m^2} - i\varepsilon} \\ &= \frac{1}{2\omega_p} \left\{ \frac{1}{q^0 - \omega_p + i\varepsilon} - \frac{1}{q^0 + \omega_p - i\varepsilon} \right\} \end{aligned} \quad (2.135)$$

Fig. 2.7 Wick rotation in the complex q^0 -plane. The poles of the Feynman propagator are indicated by \otimes 's. C is an integration contour, R is the radius of the arcs



is an analytic function in q^0 with poles at $q^0 = \pm(\omega_p - i\varepsilon)$ ²⁵ where $\omega_p = \sqrt{\mathbf{q}^2 + m^2}$. This allows us to rotate by $\frac{\pi}{2}$ the integration path in q^0 , going from $-\infty$ to $+\infty$, without crossing any singularity. In doing so, we rotate from Minkowski space to Euclidean space

$$q^0 \rightarrow -iq^d \Rightarrow q = (q^0, q^1, \dots, q^{d-2}, q^{d-1}) \rightarrow \underline{q} = (q^1, q^2, \dots, q^{d-1}, q^d)$$

and thus $q^2 \rightarrow -q^2$. This rotation to the Euclidean region is called **Wick rotation**.

More precisely: analyticity of a function $\tilde{f}(q^0, \mathbf{q})$ in q^0 implies that the **contour integral**

$$\oint_{C(R)} dq^0 \tilde{f}(q^0, \mathbf{q}) = 0 \quad (2.136)$$

for the closed path $C(R)$ in Fig. 2.7 vanishes. If the function $\tilde{f}(q^0, \mathbf{q})$ falls off sufficiently fast at infinity, then the contribution from the two ‘‘arcs’’ goes to zero when the radius of the contour $R \rightarrow \infty$. In this case we obtain

$$\int_{-\infty}^{\infty} dq^0 \tilde{f}(q^0, \mathbf{q}) + \int_{+i\infty}^{-i\infty} dq^0 \tilde{f}(q^0, \mathbf{q}) = 0 \quad (2.137)$$

or

$$\int_{-\infty}^{\infty} dq^0 \tilde{f}(q^0, \mathbf{q}) = \int_{-i\infty}^{+i\infty} dq^0 \tilde{f}(q^0, \mathbf{q}) = -i \int_{-\infty}^{+\infty} dq^d \tilde{f}(-iq^d, \mathbf{q}) \quad , \quad (2.138)$$

which is the Wick rotation. At least in perturbation theory, one can prove that the conditions required to allow us to perform a Wick rotation are fulfilled.

²⁵Note that because of the positivity of $\mathbf{q}^2 + m^2$ for any non-vacuum state, we have $\omega_p - i\varepsilon = \sqrt{\mathbf{q}^2 + m^2} - i\varepsilon$ in the limit $\lim_{\varepsilon \rightarrow 0}$, which is always understood. The symbolic parameter ε of the $i\varepsilon$ prescription, may be scaled by any fixed positive number.

We notice that the Euclidean Feynman propagator obtained by the Wick rotation

$$\frac{1}{q^2 - m^2 + i\varepsilon} \rightarrow -\frac{1}{\underline{q}^2 + m^2}$$

has no singularities (poles) and an $i\varepsilon$ -prescription is not needed any longer.

In configuration space a Wick rotation implies going to **imaginary time** $x^0 \rightarrow ix^0 = x^d$ such that $qx \rightarrow -\underline{q}\underline{x}$ and hence

$$x^0 \rightarrow -ix^d \Rightarrow x^2 \rightarrow -\underline{x}^2, \quad \square_x \rightarrow -\Delta_{\underline{x}}, \quad i \int d^d x \cdots \rightarrow \int d^d \underline{x} \cdots$$

While in Minkowski space $x^2 = 0$ defines the light-cone $x^0 = \pm|\mathbf{x}|$, in the Euclidean region $\underline{x}^2 = 0$ implies $\underline{x} = 0$. Note that possible singularities on the light-cone like $1/x^2$, $\delta(x^2)$ etc. turn into singularities at the point $\underline{x} = 0$. This simplification of the singularity structure is the merit of the positive definite metric in Euclidean space.

In momentum space the Euclidean propagators are positive (discarding the overall sign) and any Feynman amplitude in Minkowski space may be obtained via

$$I_M(p) = (-i)^{N_{\text{int}}} (-i)^{V-1} I_E(\underline{p}) \Big|_{p^4=ip^0; m^2 \rightarrow m^2 - i\varepsilon}$$

from its Euclidean version. Here, N_{int} denotes the number of internal lines (propagators) and V the number of vertices if we use the substitutions (convention dependent)

$$\frac{1}{p^2 - m^2 + i\varepsilon} \rightarrow \frac{1}{\underline{p}^2 + m^2}; \quad ig_i \rightarrow i(ig_i) = -g_i; \quad \int d^d k \rightarrow \int d^d \underline{k}$$

to define the Euclidean Feynman amplitudes. By g_i we denote the gauge couplings.

For the dimensionally regularized amplitudes, where potentially divergent integrals are defined via analytic continuation from regions in the complex d -plane where integrals are manifestly convergent, the terms from the arc segments can always be dropped. Also note that dimensional regularization and the power counting rules (superficial degree of divergence etc.) hold irrespective of whether we work in d -dimensional Minkowski space-time or in d -dimensional Euclidean space. The metric is obviously not important for the UV-behavior of the integrals.

The relationship between Euclidean and Minkowski quantum field theory is not only a very basic and surprising general feature of any local relativistic field theory but is a property of central practical importance for the non-perturbative approach to QFT via the Euclidean path-integral (e.g., lattice QCD). In a QFT satisfying the Wightman axioms the continuation of the vacuum-expectation values of time-ordered products of local fields (the time-ordered Green functions) from Minkowski space to four-dimensional Euclidean space is always possible [11]. Conversely, the **Osterwalder-Schrader theorem** [48] ascertains that

Theorem 2.8 *In a local relativistic QFT the time-ordered Green functions exhibit an analytic continuation to Euclidean space. Vice versa, the Euclidean correlation functions of an Euclidean QFT can be analytically continued to Minkowski space, provided we have a local action which satisfies the so-called reflection positivity condition.*

Accordingly, the full Minkowski QFT including its S -matrix, if it exists, can be reconstructed from the knowledge of the Euclidean correlation functions and from a mathematical point of view the Minkowski and the Euclidean version of a QFT are completely equivalent.

2.5.5 The Origin of Analyticity

At the heart of analyticity is the causality. The time ordered Green functions which encode all information of the theory in perturbation theory are given by integrals over products of causal propagators ($z = x - y$)

$$\begin{aligned} iS_F(z) &= \langle 0|T \{ \psi(x) \bar{\psi}(y) \} |0\rangle \\ &= \Theta(x^0 - y^0) \langle 0| \psi(x) \bar{\psi}(y) |0\rangle - \Theta(y^0 - x^0) \langle 0| \bar{\psi}(y) \psi(x) |0\rangle \\ &= \Theta(z^0) iS^+(z) + \Theta(-z^0) iS^-(z) \end{aligned} \quad (2.139)$$

exhibiting a positive frequency part propagating forward in time and a negative frequency part propagating backward in time. The Θ function of time ordering makes the Fourier-transform to be analytic in a half-plane in momentum space. For $K(\tau = z^0) = \Theta(z^0) iS^+(z)$, for example, we have

$$\tilde{K}(\omega) = \int_{-\infty}^{+\infty} d\tau K(\tau) e^{i\omega\tau} = \int_0^{+\infty} d\tau K(\tau) e^{-\eta\tau} e^{i\xi\tau} \quad (2.140)$$

such that $\tilde{K}(\omega = \xi + i\eta)$ is a regular analytic function in the **upper half ω -plane** $\eta > 0$. This of course only works because τ is restricted to be positive.

In a relativistically covariant world, in fact, we always need two terms (see (2.139)), a positive frequency part $\Theta(z^0 = t - t') S^+(z)$, corresponding to the particle propagating forward in time, and a negative frequency part $\Theta(-z^0 = t' - t) S^-(z)$, corresponding to the antiparticle propagating backward in time. The two terms correspond in momentum space to the two terms of (2.135).

Of course, for a free Dirac field we know what the Stückelberg-Feynman propagator in momentum space looks like

$$\tilde{S}_F(q) = \frac{\not{q} + m}{q^2 - m^2 + i\varepsilon}$$

and its analytic properties are manifest. It is an analytic function in q^0 with poles at $q^0 = \pm(\omega_p - i\varepsilon)$ where $\omega_p = \sqrt{\mathbf{q}^2 + m^2}$.

Analyticity is an extremely important basic property of a QFT and a powerful instrument which helps to solve seemingly purely “technical” problems as we will see. For example it allows us to perform a Wick rotation to Euclidean space and in Euclidean space a QFT looks like a classical statistical system and one can apply the methods of statistical physics to QFT [49]. In particular the numerical approach to the intrinsically non-perturbative QCD via lattice QCD is based on analyticity. The objects which manifestly exhibit the analyticity properties and are providing the bridge to the Euclidean world are the *time ordered Green functions*.

Note that by far not all objects of interest in a QFT are analytic. For example, any solution of the homogeneous (no source) Klein–Gordon equation

$$(\square_x + m^2) \Delta(x - y; m^2) = 0 ,$$

like the so called positive frequency part Δ^+ or the causal commutator Δ of a free scalar field $\varphi(x)$, defined by

$$\begin{aligned} \langle 0 | \varphi(x), \varphi(y) | 0 \rangle &= i \Delta^+(x - y; m^2) \\ [\varphi(x), \varphi(y)] &= i \Delta(x - y; m^2) , \end{aligned}$$

which, given the properties of the free field, may easily be evaluated to have a representation

$$\begin{aligned} \Delta^+(z; m^2) &= -i (2\pi)^{-3} \int d^4 p \Theta(p^0) \delta(p^2 - m^2) e^{-ipz} \\ \Delta(z; m^2) &= -i (2\pi)^{-3} \int d^4 p \epsilon(p^0) \delta(p^2 - m^2) e^{-ipz} . \end{aligned}$$

Thus, in momentum space, as solutions of

$$(p^2 - m^2) \tilde{\Delta}(p) = 0 ,$$

only singular ones exist. For the positive frequency part and the causal commutator they read

$$\Theta(p^0) \delta(p^2 - m^2) \quad \text{and} \quad \epsilon(p^0) \delta(p^2 - m^2) ,$$

respectively. The Feynman propagator, in contrast, satisfies an inhomogeneous (with point source) Klein–Gordon equation

$$(\square_x + m^2) \Delta_F(x - y; m^2) = -\delta^{(4)}(x - y) .$$

The δ function comes from differentiating the Θ function factors of the T product. Now we have

$$\langle 0|T \{\varphi(x), \varphi(y)\} |0\rangle = i \Delta_F(x - y; m^2)$$

with

$$\Delta_F(z; m^2) = (2\pi)^{-4} \int d^4 p \frac{1}{p^2 - m^2 + i\varepsilon} e^{-ipz}$$

and in momentum space

$$(p^2 - m^2) \tilde{\Delta}_F(p) = 1 ,$$

obviously has analytic solutions, a particular one being the scalar Feynman propagator

$$\frac{1}{p^2 - m^2 + i\varepsilon} = \mathcal{P} \left(\frac{1}{p^2 - m^2} \right) - i \pi \delta(p^2 - m^2) . \quad (2.141)$$

The $i\varepsilon$ prescription used here precisely correspond to the boundary condition imposed by the time ordering prescription T in configuration space. The symbol \mathcal{P} denotes the principal value; the right hand side exhibits the splitting into real and imaginary part.

Analyticity will play a crucial role later on and is the basic property from which dispersion relations derive (see Sect. 3.7).

Digression on the configuration space representation of Lorentz invariant distributions

Usually particle physics is practiced in momentum space, perturbative calculations are performed using momentum space Feynman rules and one calculates Feynman integrals and cross sections etc. as functions of energies and momenta (see below). This is in contrast to non- perturbative lattice field theory, where calculations have to be performed on a discretized finite Euclidean space–imaginary-time lattice in configuration space, by numerically evaluating (2.99), reformulated as a path integral, without expanding the exponential (see Sect. 5.3 below). It is therefore instructive to do a short excursion considering the properties of free fields in configuration space. For later reference we consider here the singularity structure of the solutions of the Klein–Gordon equation in configuration space. We first list some one–dimensional Fourier transforms of distributions as boundary values $\lim_{\varepsilon \rightarrow 0}$ of analytic functions:

$$\begin{aligned}\delta(x) &= \frac{1}{2\pi} \int_{-\infty}^{+\infty} dp e^{-ipx} ; & 1 &= \int dx \delta(x) e^{ipx} \\ e^{-\varepsilon x} \Theta(x) &= -\frac{1}{2\pi} \int_{-\infty}^{+\infty} dp \frac{e^{-ipx}}{p+i\varepsilon} ; & \frac{i}{p+i\varepsilon} &= \int dx \Theta(x) e^{-\varepsilon x} e^{ipx} \\ e^{\varepsilon x} \Theta(x) &= \frac{1}{2\pi} \int_{-\infty}^{+\infty} dp \frac{e^{-ipx}}{p-i\varepsilon} ; & \frac{-i}{p+i\varepsilon} &= \int dx \Theta(-x) e^{\varepsilon x} e^{ipx}\end{aligned}$$

where $\lim_{\varepsilon \rightarrow 0}$ is understood. The solutions of the Klein–Gordon equation:

$$\begin{aligned}(\square + m^2) G(x) &= -\delta(x) ; & \text{inhomogeneous case} \\ (\square + m^2) F(x) &= 0 & ; \text{homogeneous case}\end{aligned}$$

exhibit several special solutions:

$$F(x) = \Delta^+ , \quad \Delta^- , \quad \Delta \text{ and } \Delta^{(1)} ,$$

the positive frequency part Δ^+ , the negative frequency part Δ^- , the causal commutator $\Delta = \Delta^+ + \Delta^-$ and $\Delta^{(1)} = \Delta^+ - \Delta^-$, and

$$G(x) = \Delta_R , \quad \Delta_A , \quad \Delta_P \text{ and } \Delta_F ,$$

the retarded (future time) $\Delta_R = \Theta(x^0) \Delta$, the advanced (past time) $\Delta_A = -\Theta(-x^0) \Delta$, the principal value Δ_P and the Feynman propagator $\Delta_F = \Theta(x^0) \Delta^+ - \Theta(-x^0) \Delta^-$. The general homogeneous solution is

$$F(x) = \alpha \Delta^+(x) + \beta \Delta^-(x)$$

and the general inhomogeneous one

$$G(x) = \Delta_P(x) + F(x) ; \quad \Delta_P(x) = -\frac{1}{2} \varepsilon(x_0) \Delta(x) ,$$

where $\Delta_P(x)$ is the particular principle value solution. All these solutions are L_+^\uparrow invariant, where the invariant pieces in configuration space are:

$$\begin{aligned}L_+ &: x^0 > 0 , \quad x^2 > 0 ; & \text{future cone} \\ L_- &: x^0 < 0 , \quad x^2 > 0 ; & \text{past cone} \\ L_0 &: & x^2 < 0 ; & \text{space – like region} \\ C_+ &: x^0 > 0 , \quad x^2 = 0 ; & \text{forward light cone} \\ C_- &: x^0 < 0 , \quad x^2 = 0 ; & \text{backward light cone}\end{aligned}$$

This implies that a general invariant Green function must be of the form

$$\begin{aligned} \Delta_{\text{inv}} = & \Theta(x^0) \Theta(x^2) f(x^2) + \Theta(-x^0) \Theta(x^2) g(x^2) + \Theta(-x^2) h(-x^2) \\ & + \Theta(x^0) \delta(x^2) a + \Theta(-x^0) \delta(x^2) b \end{aligned}$$

and applying the Klein–Gordon operator $\partial_0^2 - \Delta + m^2$ one obtains a set of differential equations of the form

$$z^2 \frac{d^2 w^\pm}{dz^2} + z \frac{dw^\pm}{dz} \pm z^2 w^\pm - \nu^2 w^\pm = 0$$

with $\nu^2 = 1$, $z = m\sqrt{|\lambda|}$ and $\lambda \equiv x^2$. The functions $f(x^2)$ and $g(x^2)$ are of type $w^+(z)$, which represents a Bessel function $J_{\pm\nu}(z)$, a Neumann function $N_\nu(z)$ or one of the Hankel functions $H^{(1)}(z) = J_\nu(z) + iN_\nu(z)$ or $H^{(2)}(z) = J_\nu(z) - iN_\nu(z)$ (see [50]). The function $h(-x^2)$ is of type $w^-(z)$, which represents a modified Bessel functions $I_{\pm\nu}(z)$ or $K_\nu(z)$. As $\nu^2 = 1$, only index $\nu = 1$ functions play a role here. With the appropriate boundary condition, which fixes the right species of solution one finds

$$\begin{aligned} \Delta^\pm(x) = & \frac{1}{4\pi} \varepsilon(x^0) \delta(\lambda) - \frac{m}{8\pi\sqrt{\lambda}} \Theta(\lambda) \left\{ \varepsilon(x^0) J_1(m\sqrt{\lambda}) \pm i N_1(m\sqrt{\lambda}) \right\} \\ & \pm i \frac{m}{4\pi^2\sqrt{-\lambda}} \Theta(-\lambda) K_1(m\sqrt{-\lambda}) \\ \simeq & \frac{1}{4\pi} \varepsilon(x^0) \delta(\lambda) \pm i \frac{1}{4\pi^2\lambda} \mp i \frac{m^2}{8\pi^2} \ln \frac{m\sqrt{|\lambda|}}{2} - \frac{m^2}{16\pi} \varepsilon(x^0) \Theta(\lambda) \\ & + O(\sqrt{|\lambda|} \ln |\lambda|), \quad (\lambda \rightarrow 0), \end{aligned}$$

which reveals the light cone singularities $\delta(x^2)$, $\Theta(x^2)$, $1/x^2$ and $\ln|x^2|$. Interesting is also the causal commutator function $\Delta(x)$ which is vanishing for $x^2 < 0$:

$$\begin{aligned} \Delta(x) = \Delta^+(x) + \Delta^-(x) = & \frac{1}{2\pi} \varepsilon(x^0) \delta(\lambda) - \frac{m}{4\pi\sqrt{\lambda}} \Theta(\lambda) \varepsilon(x^0) J_1(m\sqrt{|\lambda|}) \\ \simeq & \frac{1}{2\pi} \varepsilon(x^0) \delta(\lambda) - \frac{m}{8\pi} \Theta(\lambda) \varepsilon(x^0) + O(\lambda), \quad (\lambda \rightarrow 0). \end{aligned}$$

For the Feynman propagator we have

$$\begin{aligned} \Delta_F(x) = & \frac{1}{4\pi} \delta(\lambda) - \frac{m}{8\pi\sqrt{\lambda}} \Theta(\lambda) \left\{ J_1(m\sqrt{\lambda}) - i N_1(m\sqrt{\lambda}) \right\} \\ & + i \frac{m}{4\pi^2\sqrt{-\lambda}} \Theta(-\lambda) K_1(m\sqrt{-\lambda}) \end{aligned}$$

$$\begin{aligned} &\simeq \frac{1}{4\pi} \delta(\lambda) - i \frac{1}{4\pi^2 \lambda} - i \frac{m^2}{8\pi^2} \ln \frac{m\sqrt{\lambda}}{2} - \frac{m^2}{16\pi} \Theta(\lambda) \\ &+ O(\sqrt{|\lambda|} \ln |\lambda|), \quad (\lambda \rightarrow 0) \end{aligned}$$

It is instructive to evaluate

$$\Delta_F(x) = \int \frac{d^4 p}{(2\pi)^4} \frac{i}{p^2 - m^2 + i\varepsilon} e^{-ipx}; \quad \frac{i}{p^2 - m^2 + i\varepsilon} = \int_0^\infty d\alpha e^{-i\alpha[m^2 - p^2 - i\varepsilon]}$$

directly, using the Bogolubov–Schwinger representation (2.129):

$$\Delta_F(x) = \int_0^\infty d\alpha \int \frac{d^4 p}{(2\pi)^4} e^{-i(px + \alpha[m^2 - p^2 - i\varepsilon])}$$

together with (2.131)

$$\int \frac{d^4 p}{(2\pi)^4} e^{i(\alpha p^2 - px)} = \frac{1}{(2\pi)^4} \left(\frac{\pi}{i\alpha}\right)^2 e^{-ix^2/4\alpha}$$

such that

$$\Delta_F(x) = \frac{-1}{16\pi^2} \int_0^\infty \frac{d\alpha}{\alpha^2} e^{-ix^2/4\alpha} e^{-i\alpha m^2} e^{-\alpha\varepsilon}$$

which upon a change of the integration variable $\alpha \rightarrow \omega = 1/4\alpha$ takes the form

$$\Delta_F(x) = \frac{1}{4\pi^2} \int_0^\infty d\omega e^{-i(\omega x^2 + m^2/4\omega)} e^{-\varepsilon/4\omega}$$

always understood that $\lim_{\varepsilon \rightarrow 0}$ is to be taken. Now, using the integral representation [51] of the Hankel function (for properties see [50])

$$\int_0^\infty \frac{d\omega}{\omega} \omega^\nu e^{i(a\omega + b/4\omega)} = 2 \left(\frac{b}{4a}\right)^{\nu/2} i \frac{\pi}{2} e^{i\pi\nu/2} H_\nu^{(1)}(\sqrt{ab}) \quad \text{and} \quad \left(H_\nu^{(1)}(z)\right)^* = H_\nu^{(2)}(z^*),$$

we obtain

$$\Delta_F(x) = i \frac{m^2}{8\pi} \frac{H_1^{(2)}(m\sqrt{x^2})}{m\sqrt{x^2}}; \quad x^2 > 0.$$

If $x^2 < 0$ we may continue

$$\sqrt{x^2} \rightarrow -i\sqrt{-x^2}, \quad H_1^{(2)}(z) = H_1^{(1)}(-z) \quad \text{and} \quad \frac{i\pi}{2} \frac{H_\nu^{(1)}(iz)}{(iz)^\nu} = \frac{K_\nu(z)}{z^\nu}$$

in order to find

$$\Delta_F(x) = \frac{m^2}{4\pi^2} \frac{K_1(m\sqrt{-x^2})}{m\sqrt{-x^2}}; \quad x^2 < 0.$$

It is interesting to see what happens upon a Wick rotation $p, x \rightarrow p_E, x_E$ to the Euclidean region. The Euclidean version will be central for the non-perturbative lattice QCD approach considered in Sect. 5.3 later. Which of the light-cone sectors in configuration space will take over? The Euclidean correlation function of the scalar field is the Wick rotated Feynman propagator as mentioned above. Again we may use the representation

$$\Delta_F(x)_E = \int \frac{d^4 p_E}{(2\pi)^4} \frac{1}{p_E^2 + m^2} e^{+i(p x)_E}; \quad \frac{1}{p_E^2 + m^2} = \int_0^\infty d\alpha e^{-\alpha(p_E^2 + m^2)}$$

to obtain

$$\Delta_F(x)_E = \int_0^\infty d\alpha \int \frac{d^4 p_E}{(2\pi)^4} e^{-\alpha(p_E^2 + m^2) + i(p x)_E},$$

and a quadratic completion achieved by the shift $p_E \rightarrow p'_E = p_E - i x_E/2\alpha$ leads to a simple Gaussian p_E integration. The integration measure being invariant under the translation, with $\int_{-\infty}^{+\infty} dp_i e^{-\alpha p_i^2} = \sqrt{\frac{\pi}{\alpha}}$ (of each of the components) we arrive at

$$\Delta_F(x)_E = \frac{1}{16\pi^2} \int_0^\infty \frac{d\alpha}{\alpha^2} e^{-x_E^2/4\alpha} e^{-\alpha m^2} = \frac{-1}{16\pi^2} \int_0^\infty d\omega e^{-(x_E^2 \omega + m^2/4\omega)}$$

Again this is related to a Bessel type integral, namely

$$\int_0^\infty \frac{d\omega}{\omega} \omega^\nu e^{-(a\omega + b/4\omega)} = 2 \left(\frac{b}{4a} \right)^{\nu/2} K_\nu(\sqrt{ab}),$$

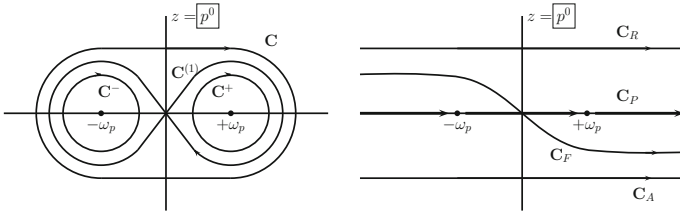


Fig. 2.8 Analytic plane contours and solutions of the Klein–Gordon equation. The two simple poles lie on the real axis at $\pm\omega_p$. *Left* homogeneous cases $C^i \rightarrow \Delta^i$ ($i = +, -$ and (1)) and $C \rightarrow \Delta$. *Right* inhomogeneous cases $C_i \rightarrow \Delta_i$ ($i = R, A, P$ and F)

which defines the spherical Bessel function $K_\nu(z)$. This leads to

$$\Delta_F(x)_E = \frac{m^2}{4\pi^2} \frac{K_1(m\sqrt{x_E^2})}{m\sqrt{x_E^2}}, \tag{2.142}$$

in agreement with the result for the $x^2 < 0$ sector in Minkowski space.

In momentum space a free scalar field L–invariant two point function

$$\tilde{\Delta}_{\text{inv}}(p) = \int d^4x e^{+ipx} \Delta_{\text{inv}}(x),$$

satisfies

$$(m^2 - p^2) \tilde{G}(p) = -1 \text{ or } (m^2 - p^2) \tilde{F}(p) = 0,$$

and the corresponding Green functions are the possible distribution valued singular function of p . The possibilities may be characterized by contours (path) C_{inv} in the complex p^0 –plane as illustrated in Fig.2.8. In fact a general representation of $\Delta_{\text{inv}}(x)$ is

$$\Delta_{\text{inv}}(x) = (2\pi)^{-4} \int_{C_{\text{inv}}} d^4p e^{-ipx} \frac{1}{m^2 - p^2}.$$

Key behind is the residue theorem

$$\frac{1}{2\pi i} \oint_C f(z) dz = \text{Res}[f(z); z_0] = \lim_{z \rightarrow z_0} (z - z_0) f(z)$$

in case the oriented path C encloses simple poles of $f(z)$.

As $m^2 - p^2 = (\omega_p - p^0)(\omega_p + p^0)$; $\omega_p = \sqrt{m^2 + \mathbf{p}^2}$ has two simple zeros, the inverse

$$\frac{1}{m^2 - p^2} = \frac{1}{(\omega_p - p^0)(\omega_p + p^0)} = \frac{-1}{2\omega_p} \left(\frac{1}{p^0 - \omega_p} - \frac{1}{p^0 + \omega_p} \right)$$

has two simple poles. For the evaluation of the contour integrals one uses the fact that the contour can be closed in one of the half planes at infinity, depending on whether $x^0 > 0$ or $x^0 < 0$, as discussed before.

In Euclidean space a more direct calculation shows how Bessel functions emerge from a Fourier transform of a radial function on \mathbf{R}^n

$$\tilde{f}(P) = \int d^n X f(X) e^{-iPX}$$

with $X, P \in \mathbf{R}^n$ and $r = |X|$. We first remember that the area of the unit sphere $S_{n-1} \subseteq \mathbf{R}^n$ is

$$S_{n-1} = 2\pi^{n/2} / \Gamma(n/2) .$$

Let $f(X) = F(r)$, then, in polar coordinates we can choose axes such that $PX = sr \cos \theta$. Then

$$\tilde{f}(P) = \tilde{F}_n(s) = \int_0^\infty \int_0^\pi e^{-isr \cos \theta} F(r) S_{n-2}(\sin \theta)^{n-2} d\theta r^{n-1} dr .$$

The angular integral is related to a Bessel function by

$$J_{\frac{n-2}{2}}(t) = \frac{t^{\frac{n-2}{2}}}{(2\pi)^{\frac{n}{2}}} S_{n-2} \int_0^\pi e^{-it \cos \theta} (\sin \theta)^{n-2} d\theta$$

such that the Fourier transformation of a radial function takes the form

$$\tilde{F}_n(s) = (2\pi)^{\frac{n}{2}} s^{-\frac{n-2}{2}} \int_0^\infty J_{\frac{n-2}{2}}(sr) F(r) r^{-\frac{n-2}{2}} r^{n-1} dr .$$

Thus the n dimensional Fourier transform of a radial function is a radial function too. These results will be useful later when discussing the lattice QCD evaluation of the hadronic light-by-light scattering in $n = 4$ Euclidean space, where

$$\tilde{F}(s = |P|) = \int d^4 X F(r = |X|) e^{-iPX} = (2\pi)^2 s^{-1} \int_0^\infty J_1(sr) F(r) r^2 dr . \quad (2.143)$$

End of the Digression.

2.5.6 Scalar One-Loop Integrals

Here we apply our tools to the simplest scalar one-loop integrals (p.i. = partial integration).²⁶

$$\begin{aligned}
 \text{Diagram: } \frac{m}{p} \text{ (circle with } m \text{ on top, } p \text{ on bottom)} &= \frac{\mu^{4-d}}{(2\pi)^d} \int d^d k \frac{1}{k^2+m^2} = \mu^{4-d} (4\pi)^{-d/2} \int_0^\infty d\alpha \alpha^{-d/2} e^{-\alpha m^2} \\
 &\text{convergent for } d < 2 \quad * * * \quad ^{26} \\
 \stackrel{\text{p.i.}}{=} & -\frac{2m^2}{d-2} \mu^{4-d} (4\pi)^{-d/2} \int_0^\infty d\alpha \alpha^{1-d/2} e^{-\alpha m^2} \\
 &\text{convergent for } d < 4 \\
 &= -2m^2 (4\pi)^{-d/2} \frac{\Gamma(2-d/2)}{d-2} \left(\frac{m^2}{\mu^2}\right)^{d/2-2} \\
 &= -2m^2 (4\pi)^{-2} \frac{2}{\epsilon} \Gamma\left(1 + \frac{\epsilon}{2}\right) \frac{1}{2-\epsilon} e^{\frac{\epsilon}{2}(\ln 4\pi - \ln \frac{m^2}{\mu^2})} \\
 \stackrel{\epsilon \rightarrow +0}{\simeq} & -m^2 (4\pi)^{-2} \left\{ \frac{2}{\epsilon} - \gamma + 1 + \ln 4\pi - \ln \frac{m^2}{\mu^2} \right\} + O(\epsilon)
 \end{aligned}$$

$$\begin{aligned}
 \text{Diagram: } \frac{m_1}{p} \text{ (circle with } m_1 \text{ on top, } m_2 \text{ on bottom, } p \text{ on left)} &= \frac{\mu^{4-d}}{(2\pi)^d} \int d^d k \frac{1}{k^2+m_1^2} \frac{1}{(k+p)^2+m_2^2} \\
 &= \mu^{4-d} (4\pi)^{-d/2} \int_0^\infty d\alpha_1 d\alpha_2 (\alpha_1 + \alpha_2)^{-d/2} e^{-(\alpha_1 m_1^2 + \alpha_2 m_2^2 + \frac{\alpha_1 \alpha_2}{\alpha_1 + \alpha_2} p^2)} \\
 &\quad \alpha_1 = x\lambda; \quad \alpha_2 = (1-x)\lambda \\
 &= \mu^{4-d} (4\pi)^{-d/2} \Gamma\left(2 - \frac{d}{2}\right) \int_0^1 dx (x m_1^2 + (1-x) m_2^2 + x(1-x) p^2)^{d/2-2} \\
 &\quad \text{convergent for } d < 4 \\
 &= (4\pi)^{-2} \frac{2}{\epsilon} \Gamma\left(1 + \frac{\epsilon}{2}\right) e^{\frac{\epsilon}{2} \ln 4\pi} \int_0^1 dx e^{-\frac{\epsilon}{2} \ln \frac{x m_1^2 + (1-x) m_2^2 + x(1-x) p^2}{\mu^2}} \\
 \stackrel{\epsilon \rightarrow +0}{\simeq} & (4\pi)^{-2} \left\{ \frac{2}{\epsilon} - \gamma + \ln 4\pi - \int_0^1 dx \ln \frac{x m_1^2 + (1-x) m_2^2 + x(1-x) p^2}{\mu^2} \right\} + O(\epsilon)
 \end{aligned}$$

$$\begin{aligned}
 \text{Diagram: } \frac{m_1}{p_3} \text{ (triangle with } m_1 \text{ on top, } m_2 \text{ on right, } m_3 \text{ on left, } p_1 \text{ on top-left, } p_2 \text{ on bottom-left)} &= \frac{\mu^{4-d}}{(2\pi)^d} \int d^d k \frac{1}{k^2+m_1^2} \frac{1}{(k+p_1)^2+m_2^2} \frac{1}{(k+p_1+p_2)^2+m_3^2} \\
 &\quad \text{convergent for } d = 4 \\
 \stackrel{\epsilon \rightarrow +0}{\simeq} & (4\pi)^{-2} \int_0^\infty d\alpha_1 d\alpha_2 d\alpha_3 \frac{1}{(\alpha_1 + \alpha_2 + \alpha_3)^2} e^{-(\alpha_1 m_1^2 + \alpha_2 m_2^2 + \alpha_3 m_3^2)} \\
 &\quad \times e^{-\frac{\alpha_1 \alpha_2 p_1^2 + \alpha_2 \alpha_3 p_2^2 + \alpha_3 \alpha_1 p_3^2}{\alpha_1 + \alpha_2 + \alpha_3}} \\
 &\quad \alpha_1 = xy\lambda; \quad \alpha_2 = x(1-y)\lambda; \quad \alpha_3 = (1-x)\lambda; \quad \alpha_1 + \alpha_2 + \alpha_3 = \lambda \\
 &= (4\pi)^{-2} \int_0^1 dy dx x \frac{1}{N}
 \end{aligned}$$

$$N = x^2 y (1-y) p_1^2 + x(1-x)(1-y) p_2^2 + x(1-x) y p_3^2 + x y m_1^2 + x(1-y) m_2^2 + (1-x) m_3^2$$

²⁶A direct integration here yields

$$m^2 (4\pi)^{-d/2} \Gamma(1-d/2) \left(\frac{m^2}{\mu^2}\right)^{d/2-2}$$

which by virtue of $\Gamma(1-d/2) = -2\Gamma(2-d/2)/(d-2)$ is the same analytic function as the one obtained via the partial integration method.

Standard Scalar One-Loop Integrals ($m^2 \hat{=} m^2 - i\varepsilon$).

$$\frac{\text{Diagram}}{p} = \mu_0^\varepsilon \int \frac{d^d k}{(2\pi)^d} \frac{1}{k^2 - m^2} \hat{=} -\frac{i}{16\pi^2} A_0(m),$$

defines the standard *tadpole type integral*, where

$$A_0(m) = -m^2(\text{Reg} + 1 - \ln m^2) \quad (2.144)$$

with

$$\text{Reg} = \frac{2}{\varepsilon} - \gamma + \ln 4\pi + \ln \mu_0^2 \equiv \ln \mu^2. \quad (2.145)$$

The last identification defines the $\overline{\text{MS}}$ *scheme of (modified) minimal subtraction*.

$$\frac{\text{Diagram}}{p} = \mu_0^\varepsilon \int \frac{d^d k}{(2\pi)^d} \frac{1}{(k^2 - m_1^2)((k+p)^2 - m_2^2)} \hat{=} \frac{i}{16\pi^2} B_0(m_1, m_2; p^2),$$

defines the standard *propagator type integral*, where

$$B_0(m_1, m_2; s) = \text{Reg} - \int_0^1 dz \ln(-sz(1-z) + m_1^2(1-z) + m_2^2z - i\varepsilon). \quad (2.146)$$

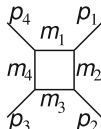
$$\begin{aligned} \frac{\text{Diagram}}{p_3} &= \mu_0^\varepsilon \int \frac{d^d k}{(2\pi)^d} \frac{1}{(k^2 - m_1^2)((k+p_1)^2 - m_2^2)((k+p_1+p_2)^2 - m_3^2)} \\ &= -\frac{i}{16\pi^2} C_0(m_1, m_2, m_3; p_1^2, p_2^2, p_3^2), \end{aligned}$$

defines the standard *form factor type integral*, where

$$C_0(m_1, m_2, m_3; s_1, s_2, s_3) = \int_0^1 dx \int_0^x dy \frac{1}{ax^2 + by^2 + cxy + dx + ey + f} \quad (2.147)$$

with

$$\begin{aligned} a &= s_2, & d &= m_2^2 - m_3^2 - s_2, \\ b &= s_1, & e &= m_1^2 - m_2^2 + s_2 - s_3, \\ c &= s_3 - s_1 - s_2, & f &= m_3^2 - i\varepsilon. \end{aligned}$$



$$= \frac{i}{16\pi^2} D_0(m_1, m_2, m_3, m_4; p_1^2, p_2^2, p_3^2, p_4^2),$$

$$= \int \frac{d^d k}{(2\pi)^d} \frac{1}{(k^2 - m_1^2)((k + p_1)^2 - m_2^2)((k + p_1 + p_2)^2 - m_3^2)((k + p_1 + p_2 + p_3)^2 - m_4^2)}$$

defines the standard *box type integral*, where

$$D_0(m_1, m_2, m_3, m_4; s_1, s_2, s_3, s_4) = \int_0^1 dx \int_0^x dy \int_0^y dz \frac{1}{[ax^2 + by^2 + gz^2 + cxy + hxz + jyz + dx + ey + kz + f]^2} \quad (2.148)$$

with

$$\begin{aligned} a &= s_3 = p_3^2, & b &= s_2 = p_2^2, & g &= s_1 = p_1^2, \\ c &= 2(p_2 p_3), & h &= 2(p_1 p_3), & j &= 2(p_1 p_2), \\ d &= m_3^2 - m_4^2 - s_3, & e &= m_2^2 - m_3^2 - s_2 - 2(p_2 p_3), & k &= m_1^2 - m_2^2 - s_1 - 2(p_1 p_2) - 2(p_1 p_3), \\ f &= m_4^2 - i\varepsilon \end{aligned}$$

Remark: the regulator term Reg in (2.145) denotes the UV regulated pole term $\frac{2}{\epsilon}$ supplemented with $O(1)$ terms which always accompany the pole term and result from the ϵ -expansion of the d -dimensional integrals. While in the $\overline{\text{MS}}$ scheme just the poles $\frac{2}{\epsilon}$ are subtracted, in the modified $\overline{\text{MS}}$ scheme $\overline{\overline{\text{MS}}}$ also the finite terms included in (2.145) are subtracted. The dependence on the UV cut-off $\frac{2}{\epsilon}$ in the $\overline{\overline{\text{MS}}}$ scheme defined by $\text{Reg} \equiv \ln \mu^2$ is reflected in a dependence on the $\overline{\overline{\text{MS}}}$ renormalization scale μ .

The UV -singularities (poles in ϵ at $d = 4$) give rise to *finite extra contributions* when they are multiplied with d (or functions of d) which arise from contractions like $g_\mu^\mu = d$, $\gamma^\mu \gamma_\mu = d$ etc. For $d \rightarrow 4$ we obtain:

$$dA_0(m) = 4A_0(m) + 2m^2, \quad dB_0 = 4B_0 - 2. \quad (2.149)$$

The explicit evaluation of the scalar integrals (up to the scalar four-point function) is discussed in Ref. [52] (see also [53, 54]). The analytic structure of scalar functions is analyzed in [52, 55].

2.5.7 Tensor Integrals

In dimensional regularization also the calculation of tensor integrals is rather straightforward. Sign conventions are chosen in accordance with the Passarino–Veltman convention [56] (see also [57]). Invariant amplitudes are defined by performing covariant decompositions of the tensor integrals, which then are contracted with external vectors or with the metric tensor. A factor $i/16\pi^2$ is taken out for simplicity of notation, i.e.

$$\int_k \cdots = \frac{16\pi^2}{i} \int \frac{d^d k}{(2\pi)^d} \cdots \quad (2.150)$$

(1) One point integrals:

By eventually performing a shift $k \rightarrow k + p$ of the integration variable we easily find the following results:

$$\begin{aligned} \int_k \frac{1}{(k+p)^2 - m^2} &= -A_0(m) \\ \int_k \frac{k^\mu}{(k+p)^2 - m^2} &= p^\mu A_0(m) \\ \int_k \frac{k^\mu k^\nu}{(k+p)^2 - m^2} &= -p^\mu p^\nu A_{21} + g^{\mu\nu} A_{22} \end{aligned} \quad (2.151)$$

$$\begin{aligned} A_{21} &= A_0(m) \\ A_{22} &= -\frac{m^2}{d} A_0(m) \stackrel{\epsilon \rightarrow 0}{\simeq} -\frac{m^2}{4} A_0(m) + \frac{m^4}{8} \end{aligned} \quad (2.152)$$

(2) Two point integrals: the defining equations here are

$$\begin{aligned} \int_k \frac{1}{(1)(2)} &= B_0(m_1, m_2; p^2) \\ \int_k \frac{k^\mu}{(1)(2)} &= p^\mu B_1(m_1, m_2; p^2) \\ \int_k \frac{k^\mu k^\nu}{(1)(2)} &= p^\mu p^\nu B_{21} - g^{\mu\nu} B_{22}, \end{aligned} \quad (2.153)$$

where we denoted scalar propagators by (1) $\equiv k^2 - m_1^2$ and (2) $\equiv (k + p)^2 - m_2^2$. The simplest non-trivial example is B_1 . Multiplying the defining equation with $2p_\mu$ we have

$$2p^2 B_1 = \int_k \frac{2pk}{k^2 - m_1^2 + i\epsilon} \frac{1}{(p+k)^2 - m_2^2 + i\epsilon}$$

and we may write the numerator as a difference of the two denominators plus a remainder which does not depend on the integration variable:

$$2pk = (p+k)^2 - k^2 - p^2 = [(p+k)^2 - m_2^2] - [k^2 - m_1^2] - (p^2 + m_1^2 - m_2^2)$$

After canceling the square brackets against the appropriate denominator we obtain

$$B_1(m_1, m_2; p^2) = \frac{1}{2p^2} \{A_0(m_2) - A_0(m_1) - (p^2 + m_1^2 - m_2^2) B_0(m_1, m_2; p^2)\} \quad (2.154)$$

A further useful relation is

$$B_1(m, m; p^2) = -\frac{1}{2} B_0(m, m; p^2) .$$

In a similar way, by contracting the defining relation with p_ν and $g_{\mu\nu}$ we find for arbitrary dimension d

$$\begin{aligned} B_{21} &= \frac{1}{(d-1)p^2} \{(1-d/2)A_0(m_2) - d/2(p^2 + m_1^2 - m_2^2)B_1 - m_1^2 B_0\} \\ B_{22} &= \frac{1}{2(d-1)} \{A_0(m_2) - (p^2 + m_1^2 - m_2^2)B_1 - 2m_1^2 B_0\} . \end{aligned}$$

Expansion in $d = 4 - \epsilon$, $\epsilon \rightarrow 0$ yields

$$\begin{aligned} B_{21} &= \frac{-1}{3p^2} \{A_0(m_2) + 2(p^2 + m_1^2 - m_2^2)B_1 + m_1^2 B_0 + 1/2(m_1^2 + m_2^2 - p^2/3)\} \\ B_{22} &= \frac{1}{6} \{A_0(m_2) - (p^2 + m_1^2 - m_2^2)B_1 - 2m_1^2 B_0 - (m_1^2 + m_2^2 - p^2/3)\} \end{aligned}$$

where the arguments of the B -functions are obvious.

Note the appearance of $1/p^2$ terms, which represent a kinematical singularity. Kinematical singularities unavoidably show up when working with covariant decompositions of tensor amplitudes. Observables are always scalars and are obtained from tensor structures via contractions with numerical tensors and the external momenta in our simplest case with p_μ . Factors p^2 arising from the contraction eliminate/compensate the kinematic singularity of the scalar amplitudes in the contracted object. The higher the tensor the higher the singularity: in general B_1 exhibit a $1/p^2$, B_{21} a $(1/p^2)^2$ etc.

(3) Three point integrals: for the simplest cases we define the following invariant amplitudes

$$\begin{aligned} \int_k \frac{1}{(1)(2)(3)} &= -C_0(m_1, m_2, m_3; p_1^2, p_2^2, p_3^2) \\ \int_k \frac{k^\mu}{(1)(2)(3)} &= -p_1^\mu C_{11} - p_2^\mu C_{12} \\ \int_k \frac{k^\mu k^\nu}{(1)(2)(3)} &= -p_1^\mu p_1^\nu C_{21} - p_2^\mu p_2^\nu C_{22} - (p_1^\mu p_2^\nu + p_2^\mu p_1^\nu) C_{23} + g^{\mu\nu} C_{24} \end{aligned} \quad (2.155)$$

where $p_3 = -(p_1 + p_2)$, (1) $\equiv k^2 - m_1^2$, (2) $\equiv (k + p_1)^2 - m_2^2$ and (3) $\equiv (k + p_1 + p_2)^2 - m_3^2$.

The C_{1i} 's can be found using all possible independent contractions with $p_{1\mu, \nu}$, $p_{2\mu, \nu}$ and $g_{\mu\nu}$. This leads to the equations

$$\underbrace{\begin{pmatrix} p_1^2 & p_1 p_2 \\ p_1 p_2 & p_2^2 \end{pmatrix}}_X \begin{pmatrix} C_{11} \\ C_{21} \end{pmatrix} = \begin{pmatrix} R_1 \\ R_2 \end{pmatrix}$$

with

$$\begin{aligned} R_1 &= \frac{1}{2}(B_0(m_2, m_3; p_2^2) - B_0(m_1, m_3; p_3^2) \\ &\quad - (p_1^2 + m_1^2 - m_2^2)C_0) \\ R_2 &= \frac{1}{2}(B_0(m_1, m_3; p_3^2) - B_0(m_1, m_2; p_1^2) \\ &\quad + (p_1^2 - p_3^2 - m_2^2 + m_3^2)C_0) . \end{aligned}$$

The inverse of the kinematic matrix of the equation to be solved is

$$X^{-1} = \frac{1}{\det X} \begin{pmatrix} p_2^2 & -p_1 p_2 \\ -p_1 p_2 & p_1^2 \end{pmatrix}, \quad \det X \doteq p_1^2 p_2^2 - (p_1 p_2)^2$$

and the solution reads

$$\begin{aligned} C_{11} &= \frac{1}{\det X} \{p_2^2 R_1 - (p_1 p_2) R_2\} \\ C_{12} &= \frac{1}{\det X} \{-(p_1 p_2) R_1 + p_1^2 R_2\} . \end{aligned} \quad (2.156)$$

The same procedure applies to the more elaborate case of the C_{2i} 's where the solution may be written in the form

$$C_{24} = -\frac{m_1^2}{2} C_0 + \frac{1}{4} B_0(2, 3) - \frac{1}{4} (f_1 C_{11} + f_2 C_{12}) + \frac{1}{4} \quad (2.157)$$

$$\begin{pmatrix} C_{21} \\ C_{23} \end{pmatrix} = X^{-1} \begin{pmatrix} R_3 \\ R_5 \end{pmatrix}; \quad \begin{pmatrix} C_{23} \\ C_{22} \end{pmatrix} = X^{-1} \begin{pmatrix} R_4 \\ R_6 \end{pmatrix} \quad (2.158)$$

with

$$\begin{aligned} R_3 &= C_{24} - \frac{1}{2} (f_1 C_{11} + B_1(1, 3) + B_0(2, 3)) \\ R_5 &= -\frac{1}{2} (f_2 C_{11} + B_1(1, 2) - B_1(1, 3)) \\ R_4 &= -\frac{1}{2} (f_1 C_{12} + B_1(1, 3) - B_1(2, 3)) \\ R_6 &= C_{24} - \frac{1}{2} (f_2 C_{12} - B_1(1, 3)) \end{aligned}$$

and

$$f_1 = p_1^2 + m_1^2 - m_2^2; \quad f_2 = p_3^2 - p_1^2 + m_2^2 - m_3^2 .$$

The notation used for the B -functions is as follows: $B_0(1, 2)$ denotes the two point function obtained by dropping propagator $\frac{1}{(3)}$ from the form factor i.e. $\int_k \frac{1}{(1)(2)}$ and correspondingly for the other cases.

As we mentioned at the end of the paragraph on the two point tensor integrals above, the tensor decomposition leads to kinematical singularities. In the case of the three point tensor integrals they show up in form of powers of the factors $\frac{1}{\det X}$ (in place of the simple $1/p^2$ in case of the two point integrals). The determinant $\det X = p_1^2 p_2^2 - (p_1 p_2)^2$ is called *Gram determinant* and exhibits a zero at points of degenerate momenta i.e. $p_2 \propto p_1$. After contracting the tensor integral with an external tensor structure in the two independent moments $p_{1\mu}$ and $p_{2\mu}$ and the possible numerical tensors when forming an observable the singularities cancel.

In the following sections we present an introduction to the calculation of the perturbative higher order corrections, also called *radiative corrections*, for the simplest QED processes. For extensions to electroweak SM processes I refer to my TASI lectures [58].

2.6 One-Loop Renormalization

2.6.1 The Photon Propagator and the Photon Self-Energy

We first consider the full photon propagator

$$iD_{\gamma}^{\mu\nu'}(x-y) = \langle 0|T \{A^{\mu}(x)A^{\nu'}(y)\}|0\rangle,$$

which includes all electromagnetic interactions, in momentum space. It is given by repeated insertion of the *one-particle irreducible* (1PI) self-energy function

$$-i\Pi_{\gamma}^{\mu\nu}(q) \equiv \text{wavy line with a shaded loop} = \text{wavy line with a loop} + \dots$$

also called the vacuum polarization tensor. Since the external photon couples to the electromagnetic current via the vertex $ie j_{\text{em}}^{\mu}(x)A_{\mu}(x)$, the latter may also be represented as a correlator of two electromagnetic currents (2.93):

$$-i\Pi_{\gamma}^{\mu\nu}(q) = (ie)^2 \int d^4x e^{iqx} \langle 0|T \{j_{\text{em}}^{\mu}(x)j_{\text{em}}^{\nu}(y)\}|0\rangle. \quad (2.159)$$

Because the electromagnetic current is conserved $\partial_{\mu}j_{\text{em}}^{\mu} = 0$ the non-trivial part of the self-energy function is transversal

$$\Pi^{\mu\nu} = -(q^{\mu}q^{\nu} - q^2 g^{\mu\nu}) \Pi'(q^2) \quad (2.160)$$

which implies $q_{\nu}\Pi^{\mu\nu} = 0$ automatically. Note however, that the free propagator, because of the required gauge fixing does not satisfy the transversality condition. The left over terms are gauge fixing artifacts and will drop out from physical matrix

elements. An external real photon, for example, is represented by a polarization vector $\varepsilon^\mu(q, \lambda)$ which satisfy $q_\mu \varepsilon^\mu(q, \lambda) = 0$ and thus nullifies all terms proportional to q^μ .

In any case, we will need to consider the transverse part only in the following. In order to see how the splitting into transverse and longitudinal parts works, we introduce the projection tensors

$$T^{\mu\nu} = g^{\mu\nu} - \frac{q^\mu q^\nu}{q^2} \quad (\text{transverse projector}), \quad L^{\mu\nu} = \frac{q^\mu q^\nu}{q^2} \quad (\text{longitudinal projector})$$

which satisfy

$$T_\nu^\mu + L_\nu^\mu = \delta_\nu^\mu, \quad T_\rho^\mu T_\nu^\rho = T_\nu^\mu, \quad L_\rho^\mu L_\nu^\rho = L_\nu^\mu, \quad T_\rho^\mu L_\nu^\rho = L_\rho^\mu T_\nu^\rho = 0.$$

Then writing

$$\Pi^{\mu\nu}(q) = \left(T_{\mu\nu} \Pi(q^2) + L_{\mu\nu} L(q^2) \right) = \left(g_{\mu\nu} \Pi_1(q^2) + q_\mu q_\nu \Pi_2(q^2) \right) \quad (2.161)$$

we have $L = q^2 \Pi_2 + \Pi_1$ and $\Pi \equiv \Pi_1$. Thus the transverse amplitude Π is uniquely given by the $g_{\mu\nu}$ -term in the propagator and the longitudinal amplitude L does not mix with the transverse part.

This allows us to calculate the full or dressed photon propagator by simply considering it in the *Feynman gauge* $\xi=1$, for which the free propagator takes the simple form $iD_\gamma^{\mu\nu} = -i g^{\mu\nu} / (q^2 + i\epsilon)$. The so called *Dyson series* of self-energy insertions then takes the form (we omit the metric tensor $g^{\mu\nu}$ which acts as a unit matrix)

$$\begin{aligned}
 i D'_\gamma(q^2) &\equiv \frac{-i}{q^2} + \frac{-i}{q^2} (-i\Pi_\gamma) \frac{-i}{q^2} + \frac{-i}{q^2} (-i\Pi_\gamma) \frac{-i}{q^2} (-i\Pi_\gamma) \frac{-i}{q^2} + \dots \\
 &= \frac{-i}{q^2} \left\{ 1 + \left(\frac{-i\Pi_\gamma}{q^2} \right) + \left(\frac{-i\Pi_\gamma}{q^2} \right)^2 + \dots \right\} \\
 &= \frac{-i}{q^2} \left\{ \frac{1}{1 + \frac{i\Pi_\gamma}{q^2}} \right\} = \frac{-i}{q^2 + \Pi_\gamma(q^2)}. \quad (2.162)
 \end{aligned}$$

The fact that the series of self-energy insertions represents a geometrical progression allows one for a closed resummation and is called a Dyson summation. The result is very important. It shows that the full propagator indeed has a simple pole in q^2 only, as the free propagator, and no multi-poles as it might look like before the resummation has been performed.

In a more general form the dressed propagator, including an auxiliary photon mass term for a moment, reads

$$iD'_{\gamma}{}^{\mu\nu}(q) = \frac{-i}{q^2 - m_{0\gamma}^2 + \Pi_{\gamma}(q^2)} \left(g^{\mu\nu} - \frac{q^{\mu}q^{\nu}}{q^2} \right) + \frac{q^{\mu}q^{\nu}}{q^2} \dots \quad (2.163)$$

and we observe that in general the position of the pole of the propagator, at the tree level given by the mass of the particle, gets modified or renormalized by higher order corrections encoded in the self-energy function Π . The condition for the position $q^2 = s_P$ of the pole is

$$s_P - m_{0\gamma}^2 + \Pi_{\gamma}(s_P) = 0. \quad (2.164)$$

By $U(1)_{\text{em}}$ gauge invariance the photon necessarily is massless and must remain massless after including radiative corrections. Besides $m_{0\gamma} = 0$ this requires $\Pi_{\gamma}(q^2) = \Pi_{\gamma}(0) + q^2 \Pi'_{\gamma}(q^2)$ with $\Pi_{\gamma}(0) \equiv 0$, in agreement with the transversality condition (2.160). As a result we obtain

$$iD'_{\gamma}{}^{\mu\nu}(q) = -ig^{\mu\nu} D'_{\gamma}(q^2) + \text{gauge terms} = \frac{-ig^{\mu\nu}}{q^2 (1 + \Pi'_{\gamma}(q^2))} + \text{gauge terms} . \quad (2.165)$$

The inverse full bare photon propagator is of the form

$$\begin{aligned} -iD_{\gamma}{}^{\mu\nu\prime-1} &= \text{diagram with a photon line and a self-energy loop} = \text{diagram with a wavy photon line} + \text{diagram with a photon line and a loop} + \dots \\ &= i \left\{ g^{\mu\nu} (q^2 - m_{0\gamma}^2) - \left(1 - \frac{1}{\xi} \right) q^{\mu}q^{\nu} \right\} - i\Pi_{\gamma}{}^{\mu\nu}. \end{aligned} \quad (2.166)$$

After these structural considerations about the photon propagator we are ready to calculate the one-loop self-energy and to discuss the renormalization of the photon propagator. We have to calculate²⁷

$$\begin{aligned} -i\Pi^{\mu\nu}(q) &= \text{diagram of a photon line with a fermion loop} \\ &= (-1)^F i^4 e^2 \int \frac{d^d k}{(2\pi)^d} \text{Tr} \left\{ \gamma^{\mu} \frac{\not{k} + m}{k^2 - m^2 + i\varepsilon} \gamma^{\nu} \frac{\not{p} + \not{k} + m}{(q+k)^2 - m^2 + i\varepsilon} \right\} \\ &= -e^2 \int_k \frac{\text{Tr} \{ \gamma^{\mu} \not{k} \gamma^{\nu} (\not{q} + \not{k}) \}}{(1)(2)} - e^2 m^2 \int_k \frac{\text{Tr} \{ \gamma^{\mu} \gamma^{\nu} \}}{(1)(2)}. \end{aligned}$$

²⁷Fermion propagators are represented either as an inverse matrix $\frac{1}{\not{k} - m + i\varepsilon}$ or as a matrix $\frac{\not{k} + m - i\varepsilon}{k^2 - m^2 + i\varepsilon}$ with a scalar denominator. This second form is obtained from the first one by multiplying numerator and denominator from the left or from the right with $\not{k} + m - i\varepsilon$. In the denominator we then have $(\not{k} + m - i\varepsilon)(\not{k} - m + i\varepsilon) = \not{k}\not{k} - (m - i\varepsilon)^2 = k^2 - m^2 + i\varepsilon + O(\varepsilon^2)$ where the $O(\varepsilon^2)$ order term as well as the $O(\varepsilon)$ in the numerator in ε may be dropped as the limit $\varepsilon \rightarrow 0$ is always understood.

We have used already the property that the trace of an odd number of γ -matrices is zero. F is the number of closed fermion loops, $F = 1$ in our case. As a convention the string of γ -matrices is read against the direction of the arrows. We again use the short notation

$$(1) = k^2 - m^2 + i\varepsilon, \quad (2) = (q + k)^2 - m^2 + i\varepsilon$$

and

$$\int_k \dots = \int \frac{d^d k}{(2\pi)^d} \dots$$

Gauge invariance or transversality of the photon field requires

$$q_\mu \Pi^{\mu\nu} = 0$$

where $\Pi^{\mu\nu}$ is the symmetric vacuum polarization tensor. We may check transversality directly as follows

$$\begin{aligned} & q_\nu \text{Tr} \gamma^\mu \frac{1}{\not{k} - m} \gamma^\nu \frac{1}{(\not{q} + \not{k}) - m} = \text{Tr} \gamma^\mu \frac{1}{\not{k} - m} \not{q} \frac{1}{(\not{q} + \not{k}) - m} \\ &= \text{Tr} \gamma^\mu \frac{1}{\not{k} - m} [(\not{q} + \not{k} - m) - (\not{k} - m)] \frac{1}{(\not{q} + \not{k}) - m} \\ &= \text{Tr} \gamma^\mu \left(\frac{1}{\not{k} - m} - \frac{1}{(\not{q} + \not{k}) - m} \right) \end{aligned}$$

which upon integration should be zero. Indeed, in dimensional regularization, we may shift the integration variable in the second integral $q + k = k'$, and by integrating we find

$$\int_k \text{Tr} \gamma^\mu \frac{1}{\not{k} - m} - \int_k \text{Tr} \gamma^\mu \frac{1}{(\not{q} + \not{k}) - m} = 0.$$

It is understood that d is chosen such that the integrals converge to start with. The result is then analytically continued to arbitrary d . This then explicitly proves the transversality (2.160). We may exploit transversality and contract the vacuum polarization tensor with the metric tensor and consider the resulting scalar quantity

$$\begin{aligned} & i g_{\mu\nu} \Pi^{\mu\nu} = -i g_{\mu\nu} (q^\mu q^\nu - q^2 g^{\mu\nu}) \Pi'(q^2) = i q^2 (d - 1) \Pi'(q^2) \\ &= e^2 \int_k \frac{\text{Tr} (\gamma^\alpha \not{k} \gamma_\alpha (\not{q} + \not{k}))}{(1)(2)} + e^2 m^2 \int_k \frac{\text{Tr} (\gamma^\alpha \gamma_\alpha)}{(1)(2)}. \end{aligned}$$

Using the d -dimensional Dirac algebra relations (2.125) or, directly the trace relations (2.126), we have $\gamma^\alpha \not{k} \gamma_\alpha = (2 - d) \not{k}$ and thus the trace in the first integral is $(2 - d) \text{Tr} (\not{k} (\not{q} + \not{k})) = (2 - d) k(q + k) \text{Tr} 1$. The scalar products

$k^2 + kq$ in the numerator may be written as a difference of the two denominators (1) and (2) plus a term which does not depend on the integration variable k : $k^2 = (1) + m^2$ and $2kq = (q+k)^2 - m^2 - k^2 + m^2 - q^2 = (2) - (1) - q^2$ and hence $k^2 + kq = \frac{1}{2}[(2) + (1) - q^2 + 2m^2]$. The terms proportional to (1) and (2) each cancel against one of the denominators and give a momentum independent *tadpole* integral.

The point of these manipulations is that we got rid of the polynomial in k in the numerator and thus were able to reduce the integrals to a set of basic integrals of a scalar theory. In our example, with the definitions (2.151) and (2.153), we get

$$\int_k \frac{k^2 + kq}{(1)(2)} = \frac{i}{16\pi^2} \frac{1}{2} ((2m^2 - q^2) B_0(m, m; q^2) - 2 A_0(m)) .$$

For the one-loop vacuum polarization as a result we then have²⁸

$$q^2 \Pi'(q^2) = \frac{e^2}{16\pi^2} \frac{1}{(d-1)} \left\{ 4(2-d) \left(m^2 - \frac{q^2}{2}\right) B_0(m, m; q^2) - 4(2-d) A_0(m) + 4dm^2 B_0(m, m; q^2) \right\} .$$

Now we have to expand the result in $d = 4 - \epsilon$. At the one-loop level at most simple poles in ϵ are expected, thus a bare one-loop amplitude in the vicinity of $d = 4$ is of the form

$$A = a_{-1} \frac{1}{\epsilon} + a_0 + a_1 \epsilon + \dots$$

The expansions for the standard scalar integrals A_0 and B_0 are given in (2.144) and (2.146), respectively, and the singular terms read

$$A_0(m) = -m^2 \frac{2}{\epsilon} + O(1) , \quad B_0(m_1, m_2; q^2) = \frac{2}{\epsilon} + O(1)$$

which leads to (2.149). In addition, we have to expand

$$\frac{1}{d-1} = \frac{1}{3-\epsilon} = \frac{1}{3(1-\frac{\epsilon}{3})} \simeq \frac{1}{3} + \frac{\epsilon}{9} + O(\epsilon^2) .$$

²⁸We adopt the scheme setting the trace of the unit matrix in spinor space $\text{Tr } \mathbf{1} = 4$; it is of course mandatory to keep this convention consistently everywhere. While bare quantities obviously depend on this convention, one can prove that quantities finite in the limit $d \rightarrow 4$, like the renormalized ones, are unambiguous.

As a result for the bare amplitude we obtain

$$q^2 \Pi'(q^2) = \frac{e^2}{16\pi^2} \frac{8}{3} \left\{ m^2 - \frac{q^2}{6} + A_0(m) + \left(m^2 + \frac{q^2}{2} \right) B_0(m, m; q^2) \right\} \quad (2.167)$$

an expression which exhibits regularized UV singularities, represented by the poles in ϵ present in A_0 and B_0 .

We now have to discuss the renormalization of the photon propagator. Concerning mass renormalization, we first go back to the general form (2.161) of the vacuum polarization tensor and identify $\Pi_2 = -\Pi'$ and $\Pi_1 = -q^2 \Pi_2 = q^2 \Pi'(q^2)$ due to transversality. As we have shown earlier in this section, electromagnetic gauge invariance requires:

$$\lim_{q^2 \rightarrow 0} \Pi_1(q^2) = 0 \quad (2.168)$$

and we may check now explicitly whether the calculated amplitude satisfies this condition. For $q^2 = 0$ we have

$$B_0(m, m; 0) = -1 - \frac{A_0(m)}{m^2} = \text{Reg} - \ln m^2 \quad (2.169)$$

and hence, as it should be,

$$\lim_{q^2 \rightarrow 0} q^2 \Pi'(q^2) = \frac{e^2}{16\pi^2} \frac{8}{3} \{ m^2 + A_0(m) + m^2 B_0(m, m; 0) \} = 0 .$$

This proves the absence of a photon mass renormalization at this order as a consequence of $U(1)_{\text{em}}$ gauge invariance.

Next we consider the wavefunction renormalization. The renormalized photon propagator is $D'_{\text{ren}} = Z_\gamma^{-1} D'_0$, where the renormalized physical propagator is required to have residue unity of the pole at $q^2 = 0$. This infers that the interacting photon propagator in the vicinity of the pole behaves like a free photon (asymptotically free scattering state). From (2.165) we learn that the residue of the pole $q^2 = 0$ in the bare propagator is given by $1/(1 + \Pi'_\gamma(0))$ such that the wave function renormalization condition for the photon reads $Z_\gamma(1 + \Pi'_\gamma(0)) = 1$ or

$$Z_\gamma = [1 + \Pi'_\gamma(0)]^{-1} \simeq 1 - \Pi'_\gamma(0) . \quad (2.170)$$

We thus have to calculate

$$\begin{aligned} \lim_{q^2 \rightarrow 0} \Pi'_\gamma(q^2) &= \frac{e^2}{16\pi^2} \frac{8}{3q^2} \left\{ \frac{m^2 - q^2}{6} + A_0(m) + \left(m^2 + \frac{q^2}{2} \right) B_0(m, m; q^2) \right\} \Big|_{q^2 \rightarrow 0} \\ &= \frac{e^2}{16\pi^2} \frac{8}{3} \left\{ -\frac{1}{6} + m^2 \dot{B}_0(m, m; 0) + \frac{1}{2} B_0(m, m; 0) \right\} \end{aligned}$$

where we have used the expansion

$$B_0(m, m; q^2) = B_0(m, m; 0) + q^2 \dot{B}_0(m, m; 0) + O(q^4) .$$

Using the integral representation (2.146) it is easy to find

$$\dot{B}_0(m, m; 0) = \frac{1}{6} \frac{1}{m^2} , \quad (2.171)$$

and together with (2.169) we obtain the simple result

$$\begin{aligned} Z_\gamma - 1 &= \frac{e^2}{12\pi^2} B_0(m, m; 0) \\ &= \frac{\alpha}{3\pi} \ln \frac{\mu^2}{m^2} . \end{aligned} \quad (2.172)$$

where the last expression is given in the $\overline{\text{MS}}$ scheme with $\text{Reg} = \ln \mu^2$. We finally may write down the renormalized photon vacuum polarization which takes the form

$$\begin{aligned} \Pi'_{\gamma \text{ ren}}(q^2) &= \Pi'_\gamma(q^2) - \Pi'_\gamma(0) \\ &= \frac{e^2}{6\pi^2} \frac{1}{q^2} \left\{ m^2 - \frac{q^2}{6} + A_0(m) + \left(m^2 + \frac{q^2}{2} \right) B_0(m, m; q^2) - \frac{q^2}{2} B_0(m, m; 0) \right\} . \end{aligned}$$

Evaluating the integrals one obtains

$$B_0(m, m; q^2) = \text{Reg} + 2 - \ln m^2 + 2(y - 1) G(y) \quad (2.173)$$

where

$$y = \frac{4m^2}{q^2}$$

and

$$G(y) = \begin{cases} -\frac{1}{\sqrt{y-1}} \arctan \frac{1}{\sqrt{y-1}} & (y > 1) \\ \frac{1}{2\sqrt{1-y}} \ln \frac{\sqrt{1-y}+1}{\sqrt{1-y}-1} & (y < 1) . \end{cases} \quad (2.174)$$

For $0 < y < 1$, which means $q^2 > 4m^2$, the self-energy function is complex, given by

$$G(y) = \frac{1}{2\sqrt{1-y}} \left(\ln \frac{1 + \sqrt{1-y}}{1 - \sqrt{1-y}} - i\pi \right) . \quad (2.175)$$

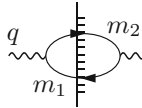
The imaginary part in the *time-like region* $q^2 > 0$ for $\sqrt{q^2} > 2m$ is a consequence of the fact that an electron–positron pair can be actually produced as real particles when the available energy exceeds the sum of the rest masses of the produced particles. The vacuum polarization function is thus an analytic function in the complex q^2 -plane with a cut along the positive real axis starting at $q^2 = 4m^2$, which is the *threshold* for pair-creation.²⁹

The final result for the renormalized vacuum polarization then reads

$$\Pi'_{\gamma \text{ ren}}(q^2) = \frac{\alpha}{3\pi} \left\{ \frac{5}{3} + y - 2 \left(1 + \frac{y}{2}\right) (1 - y) G(y) \right\} \tag{2.176}$$

which in fact is a function of q^2/m^2 . This renormalized vacuum polarization function will play a crucial role in different places later. For later purposes it is useful to note that it may be written in compact form as the following integral³⁰

²⁹As a rule, a cut diagram



contributes to the imaginary part if the cut diagram kinematically allows physical intermediate states: $q^2 \geq (m_1 + m_2)^2$. In place of the virtual photon (a real photon requires $q^2 = 0$ and does not decay) let us consider the massive charged weak gauge boson W . The W is an unstable particle and decays predominantly as $W^- \rightarrow \ell^- \bar{\nu}_\ell$ ($\ell = e, \mu, \tau$) leptonically, and $W^- \rightarrow d\bar{u}, b\bar{c}$ hadronically. Looking at the transversal self-energy function $\Pi_W(q^2)$ of the W on the mass shell $q^2 = M_W^2$ we have

$$\text{Im } \Pi_W(q^2 = M_W^2) = M_W \Gamma_W \neq 0$$

defining the finite width Γ_W of the W -particle. Note that $W^- \rightarrow b\bar{t}$ is not allowed kinematically because the top quark t is heavier than the W ($M_W = 80.385 \pm 0.015 \text{ GeV}, m_t = 173.21 \pm 0.87 \text{ GeV}, m_b = 4.18 \pm 0.03 \text{ GeV}$) for an on-shell W and hence does not contribute to the width.

Cutting lines means applying the substitution (see (2.141))

$$\frac{1}{p^2 - m^2 + i\epsilon} \rightarrow -i \pi \delta(p^2 - m^2)$$

for the corresponding propagators. In general the imaginary part is given by cutting sets of lines of a diagram in all possible ways such that the diagram is cut into two disconnected parts. A cut contributes if the cut lines can be viewed as external lines of a real physical subprocess. Note that the imaginary part of an n -loop amplitude is given by cut diagrams exhibiting $n - 1$ closed loops at most. The imaginary part therefore is less UV divergent in general. In particular, the imaginary part of a one-loop diagram is always finite.

³⁰Which derives from

$$B_0(m, m; q^2) = \text{Reg} - \ln m^2 - \int_0^1 dz \ln(1 - z(1 - z)q^2/m^2)$$

$$\begin{aligned} \Pi'_{\gamma \text{ ren}}(q^2/m^2) &= -\frac{\alpha}{\pi} \int_0^1 dz \, 2z(1-z) \ln(1-z(1-z)q^2/m^2) \\ &= \frac{\alpha}{\pi} \int_0^1 dt \, t^2(1-t^2/3) \frac{1}{4m^2/q^2 - (1-t^2)}. \end{aligned} \quad (2.177)$$

The result (2.176) may be easily extended to include the other fermion contributions. In the $\overline{\text{MS}}$ scheme, defined by setting $\text{Reg} = \ln \mu^2$ in the bare form, we have

$$\Pi'_\gamma(q^2) = \frac{\alpha}{3\pi} \sum_f Q_f^2 N_{cf} \left[\ln \frac{\mu^2}{m_f^2} + \hat{G} \right] \quad (2.178)$$

where f labels the different fermion flavors (fermion species), Q_f is the charge in units of e and N_{cf} the *color factor*, $N_{cf} = 3$ for quarks and $N_{cf} = 1$ for the leptons. We have introduced the auxiliary function

$$\hat{G} = \frac{5}{3} + y - 2 \left(1 + \frac{y}{2}\right) (1-y) G(y) \simeq \begin{cases} \hat{G} = 0, & q^2 = 0 \\ \text{Re } \hat{G} = -\ln \frac{|q^2|}{m_f^2} + \frac{5}{3}, & |q^2| \gg m_f^2 \end{cases}$$

which vanishes at $q^2 = 0$. The imaginary part is given by the simple formula

$$\text{Im } \Pi'_\gamma(q^2) = \frac{\alpha}{3} \sum_f Q_f^2 N_{cf} \left(\left(1 + \frac{y}{2}\right) \sqrt{1-y} \right). \quad (2.179)$$

Using the given low and high energy limits we get

$$\Pi'_\gamma(0) = \frac{\alpha}{3\pi} \sum_f Q_f^2 N_{cf} \ln \frac{\mu^2}{m_f^2} \quad (2.180)$$

and

$$\text{Re } \Pi'_\gamma(q^2) = \frac{\alpha}{3\pi} \sum_f Q_f^2 N_{cf} \left(\ln \frac{\mu^2}{|q^2|} + \frac{5}{3} \right); \quad |q^2| \gg m_f^2. \quad (2.181)$$

(Footnote 30 continued)

(see (2.146)). The second form is obtained from the first one by a transformation of variables $z \rightarrow t = 2z - 1$, noting that $\int_0^1 dz \dots = 2 \int_{\frac{1}{2}}^1 dz \dots$, and performing a partial integration with respect to the factor $z(1-z) = (1-t^2)/4 = \frac{d}{dt} t(1-t^2/3)/4$ in front of the logarithm.

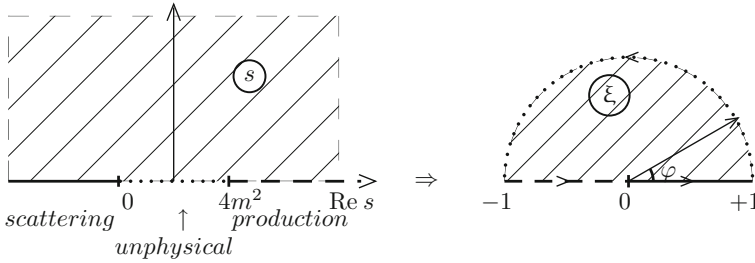


Fig. 2.9 Conformal mapping of the upper half s -plane into a half unit-circle

This concludes our derivation of the one-loop photon vacuum polarization, which will play an important role also in the calculation of the anomalous magnetic moment of the muon.

Conformal Mapping

For numerical evaluations and for working with asymptotic expansions, it is often a big advantage to map the physical upper half $s = q^2$ -plane into a bounded region as, for example, the interior of a half unit-circle as shown in Fig. 2.9. Such a conformal mapping is realized by the transformation of variables (ξ should not be confused with the gauge parameter ξ)

$$s \rightarrow \xi = \frac{\sqrt{1-y} - 1}{\sqrt{1-y} + 1} ; \quad y = \frac{4m^2}{s} \quad (2.182)$$

or

$$\frac{s}{m^2} = -\frac{(1-\xi)^2}{\xi} ; \quad \sqrt{1-y} = \frac{1+\xi}{1-\xi} .$$

If we move along the real s axis from $-\infty$ to $+\infty$ we move on the half unit-circle from 0 to +1, then on the arc segment counter clockwise and from -1 back to 0. We distinguish the following regions:

$$\begin{array}{lll} \text{scattering} & s < 0 & : 0 \leq \xi \leq 1 , \quad \ln \xi \\ \text{unphysical} & 0 < s < 4m^2 & : \xi = e^{i\varphi} , \quad \ln \xi = i\varphi \\ \text{production} & 4m^2 < s & : -1 \leq \xi \leq 0 , \quad \ln \xi = \ln |\xi| + i\pi \end{array}$$

where

$$\varphi = 2 \arctan \frac{1}{\sqrt{y-1}} ; \quad 0 \leq \varphi \leq \pi .$$

On the arc holds $1/y = \sin^2 \frac{\varphi}{2}$. The function $G(y)$ has now the representation

$$G(y) = \begin{cases} -\frac{1}{2} \frac{1-\xi}{1+\xi} \ln \xi, & 0 > s \\ -\frac{1}{2} \varphi \tan \frac{\varphi}{2}, & 4m^2 > s > 0 \\ -\frac{1}{2} \frac{1-\xi}{1+\xi} (\ln |\xi| + i\pi), & s > 4m^2. \end{cases}$$

As an application we may write the photon vacuum polarization amplitude (2.176) in the form

$$\begin{aligned} \Pi_{\gamma \text{ ren}}(s) &= q^2 \Pi'_{\gamma \text{ ren}}(s) \\ &= \frac{\alpha m^2}{3\pi} \begin{cases} -\frac{22}{3} + \frac{5}{3} (\xi^{-1} + \xi) + (\xi^{-1} + \xi - 4) \frac{1+\xi}{1-\xi} \ln \xi, & s < 0 \\ -\frac{20}{3} \sin^2 \frac{\varphi}{2} - 4 + 2(1 + 2 \sin^2 \frac{\varphi}{2}) \varphi \cot \frac{\varphi}{2}, & 0 < s < 4m^2. \end{cases} \end{aligned}$$

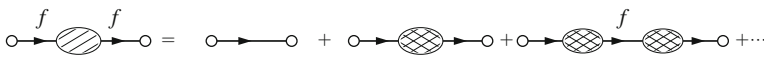
For $s > 4m^2$ the first form holds with $\ln \xi = \ln |\xi| + i\pi$. Corresponding representations are used for the vertex function as well as for the kernel function of the vacuum polarization integral contributing to $g - 2$ (see Sect. 5.1.7).

2.6.2 The Electron Self-Energy

Next we study the full propagator of a Dirac fermion f

$$iS'_f(x-y) = \langle 0|T \{ \psi_f(x) \bar{\psi}_f(y) \} |0\rangle$$

in momentum space. Again, the propagator has the structure of a repeated insertion of the 1PI self-energy $-i\Sigma_f(p)$



$$\begin{aligned} iS'_f(p) &\equiv \frac{i}{\not{p} - m_f} + \frac{i}{\not{p} - m_f} (-i\Sigma_f) \frac{i}{\not{p} - m_f} \\ &\quad + \frac{i}{\not{p} - m_f} (-i\Sigma_f) \frac{i}{\not{p} - m_f} (-i\Sigma_f) \frac{i}{\not{p} - m_f} + \dots \\ &= \frac{i}{\not{p} - m_f} \left\{ 1 + \left(\frac{\Sigma_f}{\not{p} - m_f} \right) + \left(\frac{\Sigma_f}{\not{p} - m_f} \right)^2 + \dots \right\} \\ &= \frac{i}{\not{p} - m_f} \left[\frac{1}{1 - \frac{\Sigma_f}{\not{p} - m_f}} \right] = \frac{i}{\not{p} - m_f - \Sigma_f}. \end{aligned} \tag{2.183}$$

The Dyson series here is a geometric progression of matrix insertions which again can be summed in closed form and the inverse full fermion propagator reads

$$\begin{aligned}
 -iS_f'^{-1} &= \text{---} \rightarrow \text{---} \text{---} \rightarrow \text{---} = \text{---} \rightarrow \text{---} + \text{---} \rightarrow \text{---} + \dots \\
 &= -i \{ \not{p} - m_f - \Sigma_f(p) \} .
 \end{aligned} \tag{2.184}$$

The self-energy is given by an expansion in a series of 1PI diagrams

$$-i\Sigma_f(p) \equiv \text{---} \rightarrow \text{---} \text{---} \rightarrow \text{---} = \text{---} \rightarrow \text{---} + \dots .$$

The covariant decomposition of $\Sigma_f(p)$ for a massive fermion takes the form

$$\Sigma(p) = \not{p} (A(p^2, m_f, \dots)) + m_f (B(p^2, m_f, \dots)) , \tag{2.185}$$

where A and B are Lorentz scalar functions which depend on p^2 and on all parameters (indicated by the dots) of a given theory. In vector-like theories, like QED and QCD, no parity violating γ_5 terms are present, and the pole of the propagator, or, equivalently, the zero of the inverse propagator, is given by a multiple of the unit matrix in spinor space:

$$\not{p} = \tilde{m} , \quad \text{where} \quad \tilde{m}^2 = s_P \tag{2.186}$$

defines the ‘‘pole mass’’ of the fermion in the p^2 -plane

$$\not{p} - m_f - \Sigma_f(p) \Big|_{\not{p}=\tilde{m}} = 0 . \tag{2.187}$$

Among the charged leptons only the electron is stable, and hence $\tilde{m}_e = m_e$ is real and given by the physical electron mass. For the unstable fermions $s_P = \tilde{m}^2 = m^2 - im\Gamma$ is the complex *pole mass*, where the real part defines the physical mass m and the imaginary part the width Γ , which is the inverse of the life time. Looking at the full propagator

$$S_f'(p) = \frac{1}{\not{p} - m_f - \Sigma_f(p)} = \frac{\not{p} (1 - A) + m_f (1 + B)}{p^2 (1 - A)^2 - m_f^2 (1 + B)^2} . \tag{2.188}$$

the pole condition may written in a form (2.164)

$$s_P - m_0^2 - \Omega(s_P, m_0^2, \dots) = 0 , \tag{2.189}$$

where

$$\Omega(p^2, m_0^2, \dots) \equiv p^2 (2A - A^2) + m_0^2 (2B + B^2) .$$

One easily checks that the numerator matrix is non–singular at the zero of the denominator of the full Dirac propagator. Thus the solution may be obtained by iteration of (2.189) to a wanted order in perturbation theory.

Now the fermion wave function renormalization has to be considered. The renormalized propagator is obtained from the bare one by applying the appropriate wave function renormalization factor $S'_{f\text{ren}} = Z_f^{-1} S'_{f0}$ (see (2.109)), where the renormalized physical propagator is required to have residue unity at the pole $\not{p} = \tilde{m}$. The interacting fermion propagator in the vicinity of the pole is supposed to behave like a free fermion (asymptotically free scattering state). In fact, this naive requirement cannot be satisfied in massless QED due to the long range nature of the electromagnetic interaction. Charged particles never become truly free isolated particles, they rather carry along a cloud of soft photons and this phenomenon is known as the infrared problem of QED. Strictly speaking the standard perturbation theory breaks down if we attempt to work with one–electron states. While the off–shell Green functions are well defined, their on–shell limit and hence the S –matrix does not exist. A way out is the so called Bloch–Nordsieck construction [59] which will be discussed below.

At intermediate stages of a calculation we may introduce an IR regulator like a tiny photon mass, which truncates the range of the electromagnetic interaction and thus allows one for a perturbative treatment to start with.

In vector–like theories the fermion wave function renormalization factor $\sqrt{Z_f} = 1 + \delta Z_f$ is just a number, i.e., it is proportional to the unit matrix in spinor space.³¹ Working now with a finite photon mass we may work out the on–shell wave function renormalization condition (LSZ asymptotic condition). For this purpose, we have to perform an expansion of the inverse bare propagator (2.184) about the pole $\not{p} = \tilde{m}$.

$$\begin{aligned} \not{p} - m_0 - \Sigma &= \tilde{m} + (\not{p} - \tilde{m}) - m_0 - \tilde{m}A(\tilde{m}^2, m_0, \dots) - m_0B(\tilde{m}^2, m_0, \dots) \\ &- \tilde{m} (p^2 - \tilde{m}^2) \left. \frac{\partial A(p^2, m_0, \dots)}{\partial p^2} \right|_{p^2=\tilde{m}^2} - m_0 (p^2 - \tilde{m}^2) \left. \frac{\partial B(p^2, m_0, \dots)}{\partial p^2} \right|_{p^2=\tilde{m}^2} \\ &+ \dots \end{aligned}$$

where \tilde{m} is the pole solution (2.187):

$$\not{p} - m_0 - \Sigma|_{\not{p}=\tilde{m}} = \tilde{m} - m_0 - \tilde{m}A(\tilde{m}^2, m_0, \dots) - m_0B(\tilde{m}^2, m_0, \dots) = 0$$

³¹In the unbroken phase of the SM the left–handed and the right–handed fermion fields get renormalized independently by c–number renormalization factors $\sqrt{Z_L}$ and $\sqrt{Z_R}$, respectively. In the broken phase, a Dirac field is renormalized by $\sqrt{Z_f} = \sqrt{Z_L}\Pi_- + \sqrt{Z_R}\Pi_+$ where $\Pi_{\pm} = \frac{1}{2}(1 \pm \gamma_5)$ are the chiral projectors. Hence, the wave function renormalization factor, becomes a matrix $\sqrt{Z_f} = 1 + \alpha + \beta\gamma_5$ and the bare fields are related to the renormalized one's by $\psi_0(x) = \sqrt{Z_f}\psi_r(x)$, which for the adjoint field reads $\bar{\psi}_0(x) = \bar{\psi}_r(x)\gamma^0\sqrt{Z_f}\gamma^0$.

We consider the first term, applying relations (2.125) we find

$$\begin{aligned} T_1 &= \int_k \frac{1}{k^2 - m_\gamma^2 + i\varepsilon} \frac{md + (2-d)(\not{p} + \not{k})}{(p+k)^2 - m^2 + i\varepsilon} \\ &= \frac{i}{16\pi^2} \left\{ (md + (2-d)\not{p}) B_0(m_\gamma, m; p^2) + (2-d)\not{p} B_1(m_\gamma, m; p^2) \right\} \end{aligned}$$

where B_1 is defined in (2.153) and may be expressed in terms of B_0 via (2.154). The limit of vanishing photon mass is regular and we may set $m_\gamma = 0$. Furthermore, expanding d about 4 using (2.149) we find

$$T_1 = \frac{i}{16\pi^2} \left\{ m(4B_0 - 2) + \not{p} \left(1 - \frac{A_0(m)}{p^2} - \frac{p^2 + m^2}{p^2} B_0 \right) \right\} \quad (2.193)$$

with

$$B_0 = B_0(0, m; p^2) = \text{Reg} + 2 - \ln m^2 + \frac{m^2 - p^2}{p^2} \ln \left(1 - \frac{p^2 + i\varepsilon}{m^2} \right).$$

We note that the first term T_1 is gauge independent. In contrast, the second term of (2.192) is gauge dependent. In the Feynman gauge $\xi = 1$ the term vanishes. In general,

$$T_2 = \int_k \frac{(1-\xi)}{(k^2 - m_\gamma^2)(k^2 - \xi m_\gamma^2)} \not{k} \frac{1}{\not{p} + \not{k} - m} \not{k}$$

where we may rewrite

$$\begin{aligned} \not{k} \frac{1}{\not{p} + \not{k} - m} \not{k} &= [(\not{p} + \not{k} - m) - (\not{p} - m)] \frac{1}{\not{p} + \not{k} - m} [(\not{p} + \not{k} - m) - (\not{p} - m)] \\ &= \not{k} - (\not{p} - m) + (\not{p} - m) \frac{1}{\not{p} + \not{k} - m} (\not{p} - m). \end{aligned}$$

The first term being odd in the integration variable yields a vanishing result upon integration, while the remaining one's vanish on the mass shell $\not{p} = m$ and hence will not contribute to the mass renormalization. We obtain

$$\begin{aligned} T_2 &= -(\not{p} - m) \int_k \frac{(1-\xi)}{(k^2 - m_\gamma^2)(k^2 - \xi m_\gamma^2)} \\ &\quad + (\not{p} - m) \int_k \frac{(1-\xi)}{(k^2 - m_\gamma^2)(k^2 - \xi m_\gamma^2)} \frac{\not{p} + \not{k} + m}{(p+k)^2 - m^2 + i\varepsilon} (\not{p} - m), \end{aligned}$$

a result which affects the residue of the pole and thus contributes to the wave function renormalization. To proceed, we may use the pole decomposition

$$(1 - \xi) \frac{1}{k^2 - m_\gamma^2} \frac{1}{k^2 - \xi m_\gamma^2} = \frac{1}{m_\gamma^2} \left(\frac{1}{k^2 - m_\gamma^2} - \frac{1}{k^2 - \xi m_\gamma^2} \right).$$

Then all integrals are of the type we already know and the result may be worked out easily. Since these terms must cancel in physical amplitudes, we will not work them out in full detail here. Note that the second term is of order $O((\not{p} - m)^2)$ near the mass shell and hence does not contribute to the residue of the pole and hence to the wave function renormalization. The first term is very simple and given by

$$T_2 = (\not{p} - m) \left\{ -(1 - \xi) \frac{i}{16\pi^2} B_0(m_\gamma, \sqrt{\xi} m_\gamma; 0) \right\} + O((\not{p} - m)^2). \quad (2.194)$$

We now consider the mass renormalization. The latter is gauge invariant and we may start from $\Sigma = -ie^2 T_1 + ie^2 T_2$ in the Feynman gauge

$$\begin{aligned} \Sigma^{\xi=1} &= -ie^2 T_1 = A(p^2) \not{p} + B(p^2) m \\ &= \frac{e^2}{16\pi^2} \left\{ \not{p} \left(1 - \frac{A_0(m)}{p^2} - \frac{p^2 + m^2}{p^2} B_0 \right) + m (4B_0 - 2) \right\}. \end{aligned}$$

The physical on-shell mass renormalization counter term is determined by

$$\not{p} - m_0 - \Sigma|_{\not{p}=m} = \not{p} - m - \delta m - \Sigma|_{\not{p}=m} = 0 \quad \text{or} \quad \delta m = -\Sigma|_{\not{p}=m}$$

and hence

$$\begin{aligned} \frac{\delta m}{m} &= - (A(p^2) + B(p^2))|_{p^2 \rightarrow m^2} \\ &= \frac{e^2}{16\pi^2} \left\{ 1 + \frac{A_0(m)}{m^2} - 2B_0(m_\gamma, m; m^2) \right\} = \frac{e^2}{16\pi^2} \left\{ 3 \frac{A_0(m)}{m^2} - 1 \right\} \end{aligned}$$

where we have used

$$B_0(0, m; m^2) = 1 - \frac{A_0(m)}{m^2} = \text{Reg} + 2 - \ln m^2.$$

As a result the mass renormalization counter term is gauge invariant and infrared finite for $m_\gamma = 0$. The gauge dependent amplitude T_2 does not contribute. Using (2.144) we may write

$$\frac{\delta m}{m} = \frac{\alpha}{2\pi} \left\{ \frac{3}{2} \ln \frac{m^2}{\mu^2} - 2 \right\}. \quad (2.195)$$

The wave function renormalization at one-loop order is given by³³

$$\begin{aligned} Z_f - 1 &= \left(A(p^2) + 2m^2 \frac{\partial(A+B)(p^2)}{\partial p^2} \right) \Big|_{p^2 \rightarrow m^2} \\ &= \frac{e^2}{16\pi^2} \left\{ 1 + \frac{A_0(m)}{m^2} + 4m^2 \dot{B}_0(m_\gamma, m; m^2) + (1 - \xi) B_0(m_\gamma, \sqrt{\xi}m_\gamma; 0) \right\}. \end{aligned}$$

A calculation of \dot{B}_0 in the limit of a small photon mass yields

$$\dot{B}_0(m_\gamma, m; m^2) \stackrel{m_\gamma \rightarrow 0}{\simeq} -\frac{1}{m^2} \left(1 + \frac{1}{2} \ln \frac{m_\gamma^2}{m^2} \right)$$

a result which exhibits an IR singularity and shows that in massless QED the residue of the pole does not exist. An asymptotically small photon mass m_γ is used as an IR regulator here. In IR regularized QED we may write the result in the form

$$Z_f - 1 = \frac{\alpha}{2\pi} \left\{ \frac{1}{2} \ln \frac{m^2}{\mu^2} - 2 + 2 \ln \frac{m}{m_\gamma} + \frac{1}{2} (1 - \xi) \left(1 - \ln \frac{m_\gamma^2}{\mu^2} \right) + \frac{1}{2} \xi \ln \xi \right\}. \quad (2.197)$$

The important message here is that the residue of the pole of the bare fermion propagator is gauge dependent and infrared singular. What it means is that the LSZ asymptotic condition for a charged particle cannot be satisfied. The cloud of soft photons accompanying any charged state would have to be included appropriately. However, usually in calculating cross sections the Bloch–Nordsieck construction is applied. This will be elaborated on below.

³³Note that with T_2 from (2.194) we have

$$\Sigma^{\xi \neq 1} = ie^2 T_2 = (\not{p} - m) A^{\xi \neq 1}$$

where

$$A^{\xi \neq 1} = (1 - \xi) \frac{e^2}{16\pi^2} B_0(m_\gamma, \sqrt{\xi}m_\gamma; 0)$$

and $B^{\xi \neq 1} = -A^{\xi \neq 1}$, such that $A^{\xi \neq 1} + B^{\xi \neq 1} = 0$. This leads to a contribution

$$\begin{aligned} \delta Z_f^{\xi \neq 1} &= \frac{e^2}{16\pi^2} (1 - \xi) B_0(m_\gamma, \sqrt{\xi}m_\gamma; 0) \\ &= \frac{e^2}{16\pi^2} \left\{ (1 - \xi) \left(\text{Reg} + 1 - \ln m_\gamma^2 \right) + \xi \ln \xi \right\} \end{aligned} \quad (2.196)$$

to the wave function renormalization.

The renormalized fermion self-energy is given by

$$\begin{aligned}\Sigma_{f \text{ ren}} &= \Sigma_f + \delta m_f - (Z_f - 1) (\not{p} - m_f) \\ &= A_{\text{ren}} (\not{p} - m_f) + C_{\text{ren}} m_f\end{aligned}\quad (2.198)$$

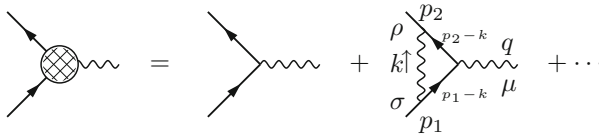
with

$$\begin{aligned}A_{\text{ren}} &= A - (Z_f - 1) \\ C_{\text{ren}} &= A + B + \frac{\delta m}{m}.\end{aligned}$$

In the context of $g=2$ the fermion self-energy plays a role as an insertion into higher order diagrams starting at two loops.

2.6.3 Charge Renormalization

Besides mass and wave function renormalization as a last step we have to perform a renormalization of the coupling constant, which in QED is the electric charge, or equivalently, the fine structure constant. The charge is defined via the electromagnetic vertex. The general structure of the vertex renormalization has been sketched in Sect. 2.4.1, already. Up to one-loop the diagrams to be considered are



Let us first consider the impact of *current conservation* and the resulting *Ward-Takahashi identity*. Current conservation, $\partial_\mu j_{\text{em}}^\mu(x) = 0$ translates into a consideration of

$$iq_\mu \Gamma^\mu = -ie \not{q} - i^6 e^3 \int \frac{d^d k}{(2\pi^d)} D_{\rho\sigma}(k) \gamma^\rho S_F(p_2 - k) \not{q} S_F(p_1 - k) \gamma^\sigma + \dots$$

with $q = p_2 - p_1$. First we note that

$$\not{q} = \not{p}_2 - \not{p}_1 = [\not{p}_2 - \not{k} - m] - [\not{p}_1 - \not{k} - m] = S_F^{-1}(p_2 - k) - S_F^{-1}(p_1 - k)$$

and thus

$$\begin{aligned}S_F(p_2 - k) \not{q} S_F(p_1 - k) &= S_F(p_2 - k) (S_F^{-1}(p_2 - k) - S_F^{-1}(p_1 - k)) S_F(p_1 - k) \\ &= S_F(p_1 - k) - S_F(p_2 - k),\end{aligned}$$

which means that contracted with q_μ the tree–point function reduces to a difference of two two–point functions (self–energies). Therefore, for the non–trivial one–loop part, using (2.192) we obtain

$$\begin{aligned} iq_\mu \Gamma^\mu(1) &= +e^3 \int_k D_{\rho\sigma}(k) \gamma^\rho S_F(p_1 - k) \gamma^\sigma - e^3 \int_k D_{\rho\sigma}(k) \gamma^\rho S_F(p_2 - k) \gamma^\sigma \\ &= ie \{ \Sigma^{(1)}(p_2) - \Sigma^{(1)}(p_1) \} \end{aligned}$$

which yields the electromagnetic Ward–Takahashi (WT) identity

$$\begin{aligned} q_\mu \Gamma^\mu(p_2, p_1) &= -e ([\not{p}_2 - m - \Sigma(p_2)] - [\not{p}_1 - m - \Sigma(p_1)]) \\ &= -e \left(S_F'^{-1}(p_2) - S_F'^{-1}(p_1) \right) \end{aligned} \quad (2.199)$$

which is the difference of the full inverse electron propagators. This relation can be shown easily to be true to all orders of perturbation theory. It has an important consequence for the renormalization of QED since it relates the vertex renormalization to the one of the charge (factor e) and the multiplicative wave function renormalization of the electron propagator. Combining the general form of the vertex renormalization (2.115) and $S_{F0}' = Z_e S_{F\text{ren}}'$ with the bare form of the WT identity we obtain the relationship

$$\begin{aligned} \sqrt{Z_\gamma} Z_e q_\mu \Gamma_0^\mu(p_2, p_1) &= -e_0 \sqrt{Z_\gamma} Z_e \left(S_{F0}'^{-1}(p_2) - S_{F0}'^{-1}(p_1) \right) \\ &= q_\mu \Gamma_{\text{ren}}^\mu(p_2, p_1) = -e_0 \sqrt{Z_\gamma} \left(S_{F\text{ren}}'^{-1}(p_2) - S_{F\text{ren}}'^{-1}(p_1) \right) \\ &= -e_{\text{ren}} \left(S_{F\text{ren}}'^{-1}(p_2) - S_{F\text{ren}}'^{-1}(p_1) \right) . \end{aligned}$$

We note that Z_e dropped out from the renormalized relation and we obtain the Ward–Takahashi identity

$$e_0 \sqrt{Z_\gamma} = e_{\text{ren}} \quad \text{or} \quad 1 + \frac{\delta e}{e} = \frac{1}{\sqrt{1 + \delta Z_\gamma}} = \sqrt{1 + \Pi'_\gamma(0)} . \quad (2.200)$$

The WT identity thus has the important consequence that the charge gets renormalized only by the photon vacuum polarization! This fact will play a crucial role later, when we are going to evaluate the hadronic contributions to the effective fine structure constant.

Another important consequence of the WT identity (2.199) we obtain by taking the limit $q_\mu \rightarrow 0$:

$$\begin{aligned}\Gamma^\mu(p, p) &= -e \lim_{p_2 \rightarrow p_1 = p} \frac{(S_F'^{-1}(p_2) - S_F'^{-1}(p_1))}{(p_2 - p_1)_\mu} \\ &= -e \frac{\partial S_F'^{-1}(p)}{\partial p_\mu} = e\gamma^\mu \left(1 - \frac{\partial \Sigma}{\partial \not{p}}\right).\end{aligned}$$

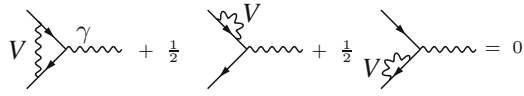
For on-shell leptons $\not{p} = \tilde{m}$ (see (2.187)) we arrive at the electromagnetic WT identity in the form

$$\Gamma^\mu(p, p)|_{\text{on-shell}} = -e\gamma^\mu \left(1 - \frac{\partial \Sigma}{\partial \not{p}} \Big|_{\not{p} = \tilde{m}}\right) = -e\gamma^\mu Z_f^{-1}.$$

Alternatively, we may write $Z_f \Gamma^\mu(p, p)|_{\text{on-shell}} = -e\gamma^\mu$ or

$$-e\gamma^\mu \delta Z_f + \Gamma'^\mu(p, p) \Big|_{\text{on-shell}} = 0 \quad (2.201)$$

where the prime denotes the non-trivial part of the vertex function. This relation tells us that some of the diagrams directly cancel. For example, we have ($V = \gamma$)



$$\frac{1}{2} \left[\text{Diagram 1} + \text{Diagram 2} + \text{Diagram 3} \right] = 0 \quad (2.202)$$

The diagrams with the loops sitting on the external legs are contributions to the wave function renormalization and the factor $\frac{1}{2}$ has its origin in Eq. (2.110). This cancellation is the reason why the charge renormalization in QED is given by the simple relation (2.200).

We are now ready to calculate the vertex function at one-loop order. The Feynman diagram shown above translates into the Feynman integral

$$i\Gamma^\mu(p_2, p_1) = -i^6 e^3 \int \frac{d^d k}{(2\pi^d)} D_{\rho\sigma}(k) \frac{\gamma^\rho (\not{p}_2 - \not{k} + m) \gamma^\mu (\not{p}_1 - \not{k} + m) \gamma^\sigma}{((p_2 - k)^2 - m^2)((p_1 - k)^2 - m^2)}. \quad (2.203)$$

Actually, we are only interested here in the physical on-shell matrix element

$$\Gamma^\mu(p_2, p_1) \rightarrow \bar{u}(p_2, r_2) \Gamma^\mu(p_2, p_1) u(p_1, r_1),$$

$p_1^2 = m^2, p_2^2 = m^2$, the photon being still off-shell, however. For notational simplicity we omit writing down the spinors explicitly in most cases, however, always take advantage of simplifications possible if $\Gamma^\mu(p_2, p_1)$ would be sandwiched between

spinors. The first term of $D_{\rho\sigma}(k)$ (see (2.191)) produces a term proportional to

$$\gamma^\rho (\not{p}_2 - \not{k} + m) \gamma^\mu (\not{p}_1 - \not{k} + m) \gamma_\rho$$

and applying the Dirac algebra (2.123) and (2.125) in arbitrary dimension d together with the Dirac equation we can bring this string of γ -matrices to standard form. We anticommute \not{p}_2 to the left and \not{p}_1 to the right such that the Dirac equation $\bar{u}(p_2, r_2) (\not{p}_2 - m) \cdots = 0$ at the left end of the string of Dirac matrices may be used and $\cdots (\not{p}_1 - m) u(p_1, r_1) = 0$ at the right end. We denote $q = p_2 - p_1$ and $P = p_1 + p_2$. Furthermore we may write scalar products like $2kP = 2[k^2] - [(p_1 - k)^2 - m^2] - [(p_2 - k)^2 - m^2]$ in terms of the inverse scalar propagators which cancel against corresponding terms in the denominators. We thus obtain

$$\begin{aligned} & \gamma^\mu \{ (d-6)k^2 + 2[(p_1 - k)^2 - m^2] + [(p_2 - k)^2 - m^2] + 4p_1 p_2 \} \\ & + 4k^\alpha (P^\mu \gamma_\alpha - m g^\mu_\alpha) + 2(2-d)k^\alpha k^\mu \gamma_\alpha . \end{aligned}$$

In order to stick to the definitions (2.155) we have to replace the momentum assignments as $k \rightarrow -k$, $p_1 \rightarrow p_1$ and $p_2 \rightarrow p_2 - p_1$, and we obtain

$$\begin{aligned} T_1^\mu = \frac{i}{16\pi^2} & \left\{ \gamma^\mu \{ (d-6) B_0(m, m, q^2) + 4B_0(0, m; m^2) \right. \\ & + 2(q^2 - 2m^2) C_0(m_\gamma, m, m) + 2(2-d) C_{24} \} \\ & \left. + \frac{P^\mu}{2m} m^2 \{ 4C_{11} - 2(2-d) C_{21} \} \right\} . \end{aligned}$$

An unphysical amplitude proportional to q^μ also shows up at intermediate stages of the calculation. After reduction of the tensor integrals to scalar integrals this term vanishes. On the mass shell $p_1^2 = p_2^2 = m^2$ and for $m_\gamma = 0$ the three point tensor integrals in fact are completely expressible in terms of two point functions. Evaluating the C -integrals using (2.156), (2.157) and (2.158)) we find

$$\begin{aligned} C_{11}(m_\gamma, m, m) &= 2C_{12} \\ C_{12}(m_\gamma, m, m) &= -1/(sz) (B_0(m, m; s) - B_0(0, m; m^2)) \\ C_{21}(m_\gamma, m, m) &= -1/(sz) (B_0(0, m; m^2) - B_0(m, m; s)) \\ C_{22}(m_\gamma, m, m) &= -1/(sz) \left[\frac{m^2}{s} (1 + A_0(m)/m^2 + B_0(m, m; s)) \right. \\ & \quad \left. - \frac{1}{2} (A_0(m)/m^2 + B_0(m, m; s)) \right] \\ C_{23}(m_\gamma, m, m) &= -1/(sz) \frac{1}{2} (B_0(0, m; m^2) - B_0(m, m; s)) \\ C_{24}(m_\gamma, m, m) &= \frac{1}{4} (1 + B_0(m, m; s)) \end{aligned}$$

with $z = 1 - y$ where

$$y = 4m^2/q^2$$

is the kinematic variable we have encountered earlier in connection with the photon vacuum polarization.

Given the above relations we arrive at fairly simple expressions for the one-loop form factors in the Feynman gauge $\xi = 1$:

$$i\Gamma^{\mu\xi=1(1)} = -e^3 T_1^\mu = -ie \left\{ \gamma^\mu A_1 + \frac{P^\mu}{2m} A_2 \right\}$$

with

$$\begin{aligned} A_1 &= \frac{e^2}{16\pi^2} \left\{ 2(s - 2m^2) C_0(m_\gamma, m, m) \right. \\ &\quad \left. - 3B_0(m, m; s) + 4B_0(0, m; m^2) - 2 \right\} \\ A_2 &= \frac{e^2}{16\pi^2} \left\{ \frac{-y}{1-y} (B_0(m, m; s) - B_0(0, m; m^2)) \right\}. \end{aligned} \quad (2.204)$$

The only true vertex structure is the scalar three-point function C_0 in A_1 , which may be calculated from (2.147) (see [52] Appendix E) with the result

$$C_0(m_\gamma, m, m; m^2, q^2, m^2) = -\frac{2}{q^2} \ln \frac{-q^2}{m_\gamma^2} G(y) + \frac{1}{q^2} F(y) \quad (2.205)$$

with

$$\begin{aligned} G(y) &= -\frac{1}{2\sqrt{1-y}} \ln \xi \\ F(y) &= \frac{1}{2\sqrt{1-y}} \left\{ \frac{\pi^2}{3} + 4 \operatorname{Sp}(-\xi) + \ln^2 \xi + 4 \ln \xi \ln \frac{1+\xi}{1-\xi} \right\}. \end{aligned}$$

The variable

$$\xi = \frac{\sqrt{1-y} - 1}{\sqrt{1-y} + 1}, \quad (2.206)$$

used in this representation, was introduced in Sect. 2.6.1. The Spence function³⁴ or dilogarithm $\text{Sp}(x)$ is defined by

$$\text{Sp}(x) \equiv \text{Li}_2(x) = - \int_0^1 \frac{dt}{t} \ln(1 - xt) . \quad (2.208)$$

Looking at the standard form factor integral (2.205) for on-shell electrons, once more, we are confronted with an IR singular object. In massless QED the off-shell vertex function is regular, however, the on-shell limit does not exist. We thus again have to resort to an IR regularization by taking a small photon mass if we insist in calculating the on-shell amplitude.

Together with (2.173) the bare amplitudes may be written in a more explicit manner as in the $\overline{\text{MS}}$ scheme

$$A_1 = \frac{\alpha}{2\pi} \left\{ -\frac{1}{2} \ln \frac{m^2}{\mu^2} - 2 \left(1 - \frac{y}{2}\right) G(y) \ln \frac{-q^2}{m_\gamma^2} + 3 \left(1 - y\right) G(y) + \left(1 - \frac{y}{2}\right) F(y) \right\}$$

$$A_2 = \frac{\alpha}{2\pi} \left\{ y G(y) \right\} .$$

The second term of the photon propagator in (2.203) yields a contribution

$$T_2^\mu = - (1 - \xi) \int_k \frac{1}{k^2 - m_\gamma^2} \frac{1}{k^2 - \xi m_\gamma^2} \not{k} \frac{1}{\not{p}_2 - \not{k} - m} \gamma^\mu \frac{1}{\not{p}_1 - \not{k} - m} \not{k}$$

³⁴The Spence function is an analytic function with the same cut as the logarithm. Useful relations are

$$\begin{aligned} \text{Sp}(x) &= - \text{Sp}(1 - x) + \frac{\pi^2}{6} - \ln x \ln(1 - x) \\ \text{Sp}(x) &= - \text{Sp}\left(\frac{1}{x}\right) - \frac{\pi^2}{6} - \frac{1}{2} \ln^2(-x) \\ \text{Sp}(x) &= - \text{Sp}(-x) + \frac{1}{2} \text{Sp}(x^2) . \end{aligned} \quad (2.207)$$

For $|x| \leq 1$ it has a series expansion

$$\text{Sp}(x) = \sum_{k=1}^{\infty} \frac{x^k}{k^2} .$$

Special values are:

$$\text{Sp}(0) = 0 , \quad \text{Sp}(1) = \frac{\pi^2}{6} , \quad \text{Sp}(-1) = -\frac{\pi^2}{12} , \quad \text{Sp}\left(\frac{1}{2}\right) = \frac{\pi^2}{12} - \frac{1}{2} (\ln 2)^2 .$$

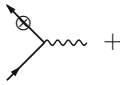
and for the on-shell vertex, applying the Dirac equation, one easily verifies that

$$\bar{u}_2 \not{k} \frac{1}{\not{p}_2 - \not{k} - m} \gamma^\mu \frac{1}{\not{p}_1 - \not{k} - m} \not{k} u_1 = \bar{u}_2 \gamma^\mu u_1$$

and hence this gauge dependent and UV divergent but q^2 independent term only contributes to the amplitude A_1 and is given by

$$i\delta\Gamma^{\mu\xi\neq 1(1)} = -e^3 T_2^\mu = -ie\gamma^\mu A_1^{\xi\neq 1} = -ie\gamma^\mu \left(-\frac{e^2}{16\pi^2} (1-\xi) B_0(m_\gamma, \sqrt{\xi}m_\gamma; 0) \right). \quad (2.209)$$

This term exactly cancels against the gauge parameter dependent lepton part of the wave function renormalization (2.196):



$$+ \quad = -ie\gamma^\mu \delta Z_e = -ie\gamma^\mu \left(\frac{e^2}{16\pi^2} (1-\xi) B_0(m_\gamma, \sqrt{\xi}m_\gamma; 0) \right).$$

In view of the discussion after (2.201), this cancellation is again a consequence of the WT identity. As it should be the gauge dependent term does not contribute to any physical amplitude after the appropriate wave function renormalization has been applied, i.e., the terms do not appear in the renormalized Dirac form factor A_1 . The Pauli form factor in any case is not affected, it is gauge invariant and UV finite and is not subject to renormalization.

In order to discuss charge renormalization, we have to write the form factors in terms of the Dirac (electric) plus a Pauli (magnetic) term. This we may do with the help of the *Gordon identity*

$$\bar{u}(p_2) \frac{i\sigma^{\mu\nu} q_\nu}{2m} u(p_1) = \bar{u}(p_2) \left(\gamma^\mu - \frac{P^\mu}{2m} \right) u(p_1).$$

Starting from our form factor decomposition, which is more convenient from a calculational point of view, we obtain

$$\begin{aligned} i\Gamma^\mu(p_2, p_1) &= -ie \left\{ \gamma^\mu A_{10}(q^2) + \frac{P^\mu}{2m} A_{20}(q^2) \right\} \\ &= -ie \left\{ \gamma^\mu (A_{10} + A_{20})(q^2) - i\sigma^{\mu\alpha} \frac{q_\alpha}{2m} A_{20}(q^2) \right\} \\ &= -ie \left\{ \gamma^\mu \delta F_E(q^2) + i\sigma^{\mu\alpha} \frac{q_\alpha}{2m} F_M(q^2) \right\}. \end{aligned}$$

Charge renormalization, according to (2.115), is fixed by the condition that $e_{\text{ren}} = e$ at $q^2 = 0$ (classical charge). We therefore have to require

$$\delta F_{\text{E ren}}(0) = A_{10}(0) + A_{20}(0) + \delta Z_e + \frac{1}{2}\delta Z_\gamma + \frac{\delta e}{e} = 0.$$

The complete Dirac form factor, including the tree level value is given by

$$F_{\text{E ren}}(q^2) = 1 + \delta F_{\text{E ren}}(q^2) \quad (2.210)$$

and satisfies the charge renormalization condition

$$F_{\text{E ren}}(0) = 1. \quad (2.211)$$

However, the electromagnetic Ward–Takahashi identity (2.201) infers

$$A_{10} + A_{20} + \delta Z_e = 0$$

such that, in agreement with (2.200), the charge renormalization condition fixes the charge counter term to the wave function renormalization constant of the photon

$$\frac{\delta e}{e} = -\frac{1}{2}\delta Z_\gamma = \frac{1}{2}\Pi'_\gamma(0) = -\frac{\alpha}{2\pi} \frac{1}{3} \ln \frac{m^2}{\mu^2} \quad (2.212)$$

with the explicit result given in the $\overline{\text{MS}}$ scheme $\text{Reg} = \ln \mu^2$.

As a result the renormalized one-loop virtual photon contributions to the lepton electric (E) and magnetic (M) form factors read

$$\begin{aligned} \delta F_{\text{E}} &= (A_{10} + A_{20} + \delta Z_e) \\ &= \frac{\alpha}{2\pi} \left\{ \ln \frac{m^2}{m_\gamma^2} - (2-y) G(y) \ln \frac{-q^2}{m_\gamma^2} - 2 + (3-2y)G(y) + \left(1 - \frac{y}{2}\right) F(y) \right\} \\ F_{\text{M}} = -A_{20} &= \frac{\alpha}{2\pi} \{-y G(y)\}. \end{aligned} \quad (2.213)$$

In the scattering region $q^2 < 0$ ($y < 0$) with $0 \leq \xi \leq 1$ the form factors are real; in the production region $q^2 > 4m^2$ ($0 < y < 1$) with $-1 \leq \xi \leq 0$ we have an imaginary part (using $\ln(\xi) = \ln(-\xi) + i\pi$, $\ln(-q^2/m^2 - i\varepsilon) = \ln(q^2/m^2) - i\pi$)

$$\begin{aligned} \frac{1}{\pi} \text{Im} F_{\text{E}} &= \frac{\alpha}{4\pi} \frac{1}{\sqrt{1-y}} \left\{ (2-y) \ln \frac{q^2 - 4m^2}{m_\gamma^2} - 3 + 2y \right\} \\ \frac{1}{\pi} \text{Im} F_{\text{M}} &= \frac{\alpha}{4\pi} \frac{y}{\sqrt{1-y}} \end{aligned} \quad (2.214)$$

The Dirac form factor for $q^2 \neq 0$ (on-shell electron, off-shell photon) at this stage is still IR singular in the limit of vanishing photon mass and cannot be physical. Before

we continue the discussion of the result we have to elaborate on the infrared problem in massless QED and the difficulties to define scattering states for charged particles.

However, the Pauli form factor, of primary interest to us turns out to be IR save. It is a perturbatively calculable quantity, which seems not to suffer from any of the usual problems of gauge dependence, UV divergences and the related renormalization scheme dependence. We thus are able to calculate the leading contribution to the anomalous magnetic moment without problems. The anomalous magnetic moment of a lepton is given by $F_M(0)$ where $F_M(q^2)$ is given in (2.213). We hence have to calculate $-y G(y)$ for $Q^2 = -q^2 > 0$ and $Q^2 \rightarrow 0$ or $y < 0$ and $|y| \rightarrow \infty$. Let $z = -y = |y|$ and z be large; the expansion yields

$$\begin{aligned} \sqrt{1-y} &= \sqrt{z+1} \simeq \sqrt{z} \left(1 + \frac{1}{2z} + \dots \right) \\ \ln \frac{\sqrt{1-y}-1}{\sqrt{1-y}+1} &= \ln \frac{\sqrt{z+1}-1}{\sqrt{z+1}+1} \simeq -\frac{2}{\sqrt{z}} + \dots \end{aligned}$$

and therefore

$$\begin{aligned} -y G(y)|_{-y \rightarrow \infty} &= -\frac{z}{2\sqrt{z+1}} \ln \frac{\sqrt{z+1}-1}{\sqrt{z+1}+1} \Big|_{z \rightarrow \infty} \\ &\simeq 1 + O\left(\frac{1}{\sqrt{|y|}}\right). \end{aligned}$$

We thus arrive at

$$F_M(0) = \frac{\alpha}{2\pi} \simeq 0.0011614\dots \quad (2.215)$$

which is Schwinger's classic result for the anomalous magnetic moment of the electron and which is universal for all charged leptons.

An important cross check of our calculation of F_E is also possible at this stage. Namely, we may check directly the WT identity (2.201), which now reads $\delta F_E(0) = 0$. Taking the limit $q^2 \rightarrow 0$ for space-like momentum transfer $q^2 < 0$, we may use the expansion just presented for calculating $F_M(0) = \alpha/2\pi$. For $y < 0$ and $|y| \rightarrow \infty$ we have $\xi \sim 1 - 2/\sqrt{|y|}$ and the somewhat involved expansion of $F(y)$ in (2.213) yields that $yF(y) \rightarrow 0$ in this limit. Since $-yG(y) \rightarrow 1$ we get precisely the cancellations needed to prove $\delta F_E(q^2) \rightarrow 0$ for $q^2 \rightarrow 0$.³⁵ The leading term for $|q^2| \ll 4m^2$ reads

³⁵One also may check this directly on the level of the standard scalar integrals A_0 , B_0 and C_0 . Denoting by $AA(m) = A_0(m)/m^2$ we have

$$\begin{aligned} \delta F_E(q^2) \stackrel{q^2 \rightarrow 0}{\sim} &\propto ([-4m^2 C_0 - 3B_0(m, m; 0) + 4B_0(0, m; m^2) - 2]_{A_1} \\ &+ [B_0(m, m; 0) - B_0(0, m; m^2)]_{A_2} + [1 + AA(m) + 4m^2 \dot{B}_0(m_\gamma, m; m^2)]_{\delta z_\epsilon}). \end{aligned}$$

$$\delta F_E(q^2) = \frac{\alpha}{3\pi} \frac{q^2}{m^2} \left(\ln \frac{m}{m_\gamma} - \frac{3}{8} \right) + O(q^4/m^4)$$

and is IR singular and hence non–physical without including soft real photon emission. The leading behavior of the form factors for large $|q^2| \gg m^2$ reads

$$\begin{aligned} \delta F_E(q^2) &\sim -\frac{\alpha}{2\pi} \left(\frac{1}{2} \ln^2 \frac{|q^2|}{m^2} + 2 \ln \frac{m}{m_\gamma} \ln \frac{|q^2|}{m^2} - 2 \ln \frac{m}{m_\gamma} - \frac{3}{2} \ln \frac{|q^2|}{m^2} + 2 - \frac{\pi^2}{6} \right. \\ &\quad \left. - \Theta(q^2 - 4m^2) \frac{\pi^2}{2} \right) + \Theta(q^2 - 4m^2) i \frac{\alpha}{2} \left(\ln \frac{q^2}{m_\gamma^2} - \frac{3}{2} \right) \\ F_M(q^2) &\sim -\frac{\alpha}{\pi} \frac{m^2}{q^2} \ln \frac{|q^2|}{m^2} + \Theta(q^2 - 4m^2) i \alpha \frac{m^2}{q^2} . \end{aligned}$$

As in the examples discussed so far, often we will need to know the behavior of Feynman amplitudes for large momenta or equivalently for small masses. The tools for estimating the asymptotic behavior of amplitudes are discussed next.

2.6.4 Dyson– and Weinberg–Power-Counting Theorems

Since, in momentum space, any amplitude may be obtained as a product of 1PI building blocks, the vertex functions $\Gamma(p_1, \dots, p_n)$, it is sufficient to know the asymptotic behavior of the latter. This behavior may be obtained by considering the contributions from individual Feynman integrals $\Gamma_G(p_1, \dots, p_n)$, the index G denoting the corresponding Feynman graph. As we know already from Sect. 2.4.2, power counting theorems play an important role for evaluating

1. the convergence of Feynman integrals (UV divergences),
2. the behavior of Feynman amplitudes for large momenta.

Weinberg’s power-counting theorem is an extension of Dyson’s power-counting theorem, and describes the off-shell behavior of vertex functions (amputated n -point functions with $n \geq 2$)

(Footnote 35 continued)

Using the relations

$$\begin{aligned} C_0(m_\gamma, m, m; m^2, 0, m^2) &= \frac{-1}{4m^2} (B_0(0, m; m^2) - 1 - AA(m) + 2AA(m_\gamma)) \\ B_0(m, m; 0) &= -1 - AA(m) \\ B_0(0, m; m^2) &= 1 - AA(m) \\ m^2 \dot{B}_0(m_\gamma, m; m^2) &= -1 - \frac{1}{2} AA(m_\gamma) + \frac{1}{2} AA(m) \end{aligned}$$

one easily finds that indeed $\delta F_E(q^2) \stackrel{q^2 \rightarrow 0}{\sim} 0$. This kind of approach is usually utilized when working with computer algebra methods.

$$\Gamma(p_1, \dots, p_n) = \sum_G \Gamma_G(p_1, \dots, p_n)$$

for large p_i ($i = 1, \dots, m$) in a subspace of the momenta

$$\Gamma(\lambda p_1, \dots, \lambda p_m, p_{m+1}, \dots, p_n) \xrightarrow{\lambda \rightarrow \infty} ?$$

where (p_1, \dots, p_n) is a fixed set of momenta, $2 \leq m \leq n$ and λ a real positive stretching (dilatation) factor, which we are taking to go to infinity. The sum is over all possible Feynman graphs G which can contribute.

We first introduce some notions and notation. A set of external momenta (p_1, \dots, p_m) is called *non-exceptional* if no subsum of momenta vanishes, i.e., the set is generic. The set of external lines which carry momenta going to infinity is denoted by \mathcal{E}_∞ . By appropriate relabeling of the momenta we may always achieve that the first m of the momenta are the ones which go to infinity. Primarily the power counting theorems hold in the Euclidean region (after Wick-rotation) or in the Minkowski region for space-like momenta, which will be sufficient for our purpose. Also for massless theories there may be additional complications [60].

Dyson's power-counting theorem [61] states that

Theorem 2.9 *For all non-exceptional sets of momenta when all momenta are going to infinity a vertex function behaves as*

$$\Gamma(\lambda p_1, \dots, \lambda p_n) = \mathcal{O}(\lambda^{\alpha_F} (\ln \lambda)^{\beta_F}); \quad \lambda \rightarrow \infty,$$

where $\alpha_F = \max_{G \in \mathcal{G}} d(G)$ with $d(G)$ the superficial degree of divergence of a diagram G , and \mathcal{G} the set of diagrams which contribute to $\Gamma(p_1, \dots, p_n)$.

$d(G)$ has been introduced in Sect. 2.4.2. The asymptotic coefficient β_F giving the leading power of the logarithm may also be characterized in terms of diagrams [62], but will not be discussed here as we will need the asymptotic behavior modulo logarithms only. For an individual 1PI diagram G the Dyson power-counting theorem says that provided all momenta go to infinity, and the set of momenta is non-exceptional the behavior is determined by the superficial degree of divergence $d(G)$ of the corresponding diagram. The crucial point is that in a renormalizable theory $d(G)$ is independent of the particular graph G and given by the dimension of the vertex function $\dim \Gamma$ which only depends on type and number of external legs as discussed before in Sect. 2.4.2. In fact, in $d = 4$ dimensions,

$$\Gamma(\lambda p_1, \dots, \lambda p_n) = \mathcal{O}(\lambda^{4-b-\frac{3}{2}f} (\ln \lambda)^\ell).$$

with $b = n_B$ the number of boson lines and $f = n_F$ the number of fermion lines. ℓ is a non-negative integer depending on the order of perturbation theory. Its maximum possible value $\ell \leq L$ is given by the number L of loops.

Weinberg’s power-counting theorem [63] generalizes Dyson’s theorem and answers the question what happens when a subset only of all momenta is scaled to infinity. We first consider an individual Feynman integral G and 1PI subdiagrams $H \supset \mathcal{E}_\infty$ which include all lines \mathcal{E}_∞ tending to infinity. A subset $H \subset G$ here is a set of lines from G (external and internal) such that at each vertex there is either no line or two or more lines.³⁶ Then

$$\Gamma_G(\lambda p_1, \dots, \lambda p_m, p_{m+1}, \dots, p_n) = \mathcal{O}(\lambda^{d(H_0)} (\ln \lambda)^{\beta(H_0)})$$

where H_0 has maximal superficial degree of divergence $d(H)$. For a characterization of the logarithmic coefficient $\beta(H)$ see [62]. The result simplifies considerably if we consider the complete vertex function. When a non-exceptional set \mathcal{E}_∞ of external lines have momenta tending to infinity, then the total vertex function has as its asymptotic power a quantity $\alpha(\mathcal{E}_\infty)$

$$\Gamma(\lambda p_1, \dots, \lambda p_m, p_{m+1}, \dots, p_n) = \mathcal{O}(\lambda^{\alpha(\mathcal{E}_\infty)} (\ln \lambda)^\ell)$$

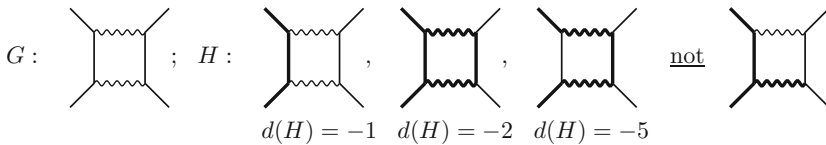
which depends only on the numbers and type of lines in \mathcal{E}_∞ , and is given by

$$\alpha(\mathcal{E}_\infty) = 4 - \frac{3}{2}f(\mathcal{E}_\infty) - b(\mathcal{E}_\infty) - \min_{\mathcal{E}'} \left[\frac{3}{2}f(\mathcal{E}') + b(\mathcal{E}') \right]. \quad (2.216)$$

Here $b(\mathcal{E})$, $f(\mathcal{E})$ are the number of bosons or fermions in the set \mathcal{E} . The minimum in (2.216) is taken over all sets \mathcal{E}' of lines such that the virtual transition $\mathcal{E}_\infty \leftrightarrow \mathcal{E}'$ is not forbidden by selection rules (charge, fermion number etc.). \mathcal{E}' is the set of external lines of H which are not in \mathcal{E}_∞ . Again, $\ell \leq L$.

Besides the high energy expansion (UV behavior) equally important is the low momentum expansion (IR behavior), which in a theory with massive particle fields is equivalent to a large mass expansion. Interestingly, in QED as well as in QCD (see below) masses are independent parameters of the theory, not related with the coupling constants. It means that on the level of the bare theory, masses only appear in propagators, which behave like $1/M^2$ for a heavy boson of mass $M \gg p$ and

³⁶The following example (electrons = full lines and photons = wavy lines) may illustrate this: fat lines carry the flow of large momentum (subgraph H)



The first graph in the set H determines the leading behavior $\mathcal{O}(\lambda^{-1} \ln^x \lambda)$. Note that all subgraphs H are connected and have no *dead end* lines (like the last diagram above, which is not a subgraph in the sense the term is used here). Thin lines attached to vertices of a subgraph H figure as external lines \mathcal{E}' , such that $\mathcal{E}_H = \mathcal{E}_\infty + \mathcal{E}'$ is the set of all external lines of H and $d(H) = 4 - \frac{3}{2}f(\mathcal{E}_H) - b(\mathcal{E}_H)$.

like $1/M$ for a heavy Dirac fermion of mass $M \gg p$. However, in loop integrals we cannot simply interchange limits $M \rightarrow \infty$ with $p \rightarrow \infty$ as the $O(1/p^2)$ behavior of a boson propagator or a $O(1/p)$ behavior of a fermion propagator are crucial for the convergence of the loop integrals. Indeed masses in general affect renormalization counterterms as we have seen in our one-loop renormalization calculations above. However, these residual mass effects drop out after renormalization (subtraction of the potential UV singularities). The property that very heavy particles do not affect the physics at much lower scales is called “decoupling” (of the heavy states), which looks to be a natural property of physics in general. Surprisingly, in the weak interaction sector of the electroweak SM decoupling is no longer true as masses and couplings are interrelated (mass generation via the Higgs mechanism, see below). Thus in the broken phase of the SM decoupling only holds in the QCD and QED sectors, and there is controlled by the Appelquist-Carazzone **decoupling theorem** [64].

Theorem 2.10 *If all external momenta of a process or in the corresponding amplitude are small relative to the mass M of a heavy state, then the “light fields only” Green functions of the full theory differ from the theory which has no heavy fields at all, only by finite renormalizations of couplings, masses and fields of the light theory, up to terms which are suppressed by inverse powers of the heavy mass. Thus further corrections are of the form $(\mu/M)^x$ with $x \geq 1$.*

It means that only the renormalization subtraction constants are dependent on M (logarithms) and this M -dependence gets renormalized away by physical subtraction conditions. The decoupling theorem is the root of the famous $\delta a_\ell \propto m_\ell^2/M^2$ behavior (1.9) of the lepton anomalies, and plays an important role in the classification of the various types of contributions to a_e and a_μ , as we will see.

For useful refinements of asymptotic expansion theorems in momenta and masses see e.g. [65] and references therein. Another tool to study the asymptotic behavior of Green- or vertex-functions is the renormalization group which we will consider next and in particular allows us to control effects due to the large UV logarithms.

2.6.5 The Running Charge and the Renormalization Group

Charge renormalization is governed by a *renormalization group* [66] (RG), which controls the response of the theory with respect to a change of the renormalization scale parameter μ in the $\overline{\text{MS}}$ scheme, like for example in the charge renormalization according to (2.212). It gives rise to the definition of an effective or running charge $\alpha(\mu)$ and running mass $m(\mu)$ as a function of the renormalization scale μ . However, the RG not only governs the dependence of a renormalized QFT on the renormalization scale, it yields the behavior of the theory with respect to dilations, the simultaneous stretching of all momenta, and hence allows one to discuss the asymptotic behavior for small and large momenta. The RG serves as a tool to systematically include large logarithmic radiative corrections, in fact, it permits the resummation to all orders of the perturbation expansion, of *leading logarithms* (LL),

next to leading logarithms (NLL) etc. It thus allows us to estimate leading radiative corrections of higher order without the need to actually perform elaborate calculations, under the condition that *large scale changes* are involved. Besides the all orders Dyson summation of self–energy corrections and the soft photon exponentiation to be discussed in the next section, the RG is a third method which allows us to predict leading higher order corrections from low order calculations. The RG generalizes the classical concept of dimensional analysis to QFT, where renormalization anomalies of the dilatation current [67] lead to a breaking of dilatation invariance by quantum effects (see Sect. 5.1.6 footnote on p. 375).

The RG may be obtained by starting from the bare vertex functions (the amputated Green functions) mentioned already briefly in Sect. 2.4.2. Note that the renormalization scale parameter μ is entering in DR by the fact that in the d –dimensional QFT the bare coupling constant \bar{e}_0 must have a dimension $\frac{4-d}{2}$, i.e., $\bar{e}_0 = e_0 \mu^{\varepsilon/2}$ with e_0 dimensionless (see (2.118)). This gives rise to the factors μ^{4-d} in the definitions of the standard integrals in Sect. 2.5.6 when working with the dimensionless bare coupling e_0 . As a result the μ dependence formally comes in via the UV regulator term (2.145). Since μ only enters via the bare coupling \bar{e}_0 all bare quantities, like the vertex function Γ_0 , at fixed \bar{e}_0 are independent of μ :

$$\mu \left. \frac{d\Gamma_0}{d\mu} \right|_{\bar{e}_0} \equiv 0 . \quad (2.217)$$

The bare vertex functions in $d = 4 - \varepsilon$ dimensions

$$\Gamma_0^{(n_A, 2n_\psi)}(\{p\}; \bar{e}_0, m_0, \xi_0)_\varepsilon$$

are homogeneous under simultaneous dilatation of all momenta and all dimensionful parameters including the scale μ . According to (2.119) we have

$$\Gamma_0^{(n_A, 2n_\psi)}(\{\kappa p\}; e_0 (\kappa\mu)^{\varepsilon/2}, \kappa m_0, \xi_0) = \kappa^{\dim\Gamma} \Gamma_0^{(n_A, 2n_\psi)}(\{p\}; e_0 (\mu)^{\varepsilon/2}, m_0, \xi_0) \quad (2.218)$$

with

$$\dim\Gamma = d - n_A \frac{d-2}{2} - 2n_\psi \frac{d-1}{2} .$$

The renormalized vertex functions are obtained by renormalizing parameters and fields: $A_0 = \sqrt{Z_A} A_r$, $\psi_0 = \sqrt{Z_\psi} \psi_r$, $e_0 = Z_g e_r$ and $m_0 = Z_m m_r$ and thus

$$\Gamma_0^{(n_A, 2n_\psi)}(\{p\}; \bar{e}_0, m_0, \xi_0)_\varepsilon = (Z_A)_\varepsilon^{-\frac{n_A}{2}} (Z_\psi)_\varepsilon^{-n_\psi} \Gamma_{\text{ren}}^{(n_A, 2n_\psi)}(\{p\}; e_r, m_r, \xi_r, \mu)_\varepsilon$$

where the wave function renormalization factors have the property to make the limit $\lim_{\varepsilon \rightarrow 0} \Gamma_{\text{ren}}(\{p\}; e_r, m_r, \xi_r, \mu)_\varepsilon$ exist. The trivially looking bare RG (2.217) becomes highly non-trivial if rewritten as an equation for Γ_{ren} as a function of the renormalized parameters. By applying the chain rule of differentiation we find the RG equation

$$\left\{ \mu \frac{\partial}{\partial \mu} + \beta \frac{\partial}{\partial e_r} + \omega \frac{\partial}{\partial \xi_r} + \gamma_m m_r \frac{\partial}{\partial m_r} - n_A \gamma_A - 2n_\psi \gamma_\psi \right\} \Gamma_{\text{ren}} = 0 \quad (2.219)$$

where the coefficient functions are given by

$$\begin{aligned} \beta &= D_{\mu, \varepsilon} e_r = e_r \left(-\frac{\varepsilon}{2} + \frac{\varepsilon}{2} e_0 \frac{\partial}{\partial e_0} \ln Z_g \right) \\ \gamma_m m_r &= D_{\mu, \varepsilon} m_r = \frac{\varepsilon}{2} m_0 e_0 \frac{\partial}{\partial e_0} \ln Z_m \\ \gamma_A &= D_{\mu, \varepsilon} \ln Z_A = -\frac{\varepsilon}{4} e_0 \frac{\partial}{\partial e_0} \ln Z_A \\ \gamma_\psi &= D_{\mu, \varepsilon} \ln Z_\psi = -\frac{\varepsilon}{4} e_0 \frac{\partial}{\partial e_0} \ln Z_\psi \\ \omega &= D_{\mu, \varepsilon} \xi_r = -\frac{\varepsilon}{2} e_0 \frac{\partial}{\partial e_0} \xi_r = -2\xi_r \gamma_A. \end{aligned} \quad (2.220)$$

We have used

$$\begin{aligned} \mu \frac{\partial}{\partial \mu} F(\bar{e}_0 = e_0 \mu^{\varepsilon/2})|_{\bar{e}_0} &= \left(\mu \frac{\partial}{\partial \mu} - \frac{\varepsilon}{2} e_0 \frac{\partial}{\partial e_0} \right) F(e_0, \mu) \doteq D_{\mu, \varepsilon} F(e_0, \mu) \\ \text{and } F^{-1} D_{\mu, \varepsilon} F(e_0, \mu) &= D_{\mu, \varepsilon} \ln F(e_0, \mu) \end{aligned}$$

and the relation $\xi_0 = Z_A \xi_r$, i.e., $Z_\xi = Z_A$, which is a consequence of a WT identity, and implies $\omega = -2\xi_r \gamma_A$. Note that $\beta = \beta(e_r)$ and $\gamma_m = \gamma_m(e_r)$ are gauge invariant. In the *Landau gauge* $\xi_r = 0$ the coefficient function $\omega \equiv 0$ and $\gamma_i = \gamma_i(e_r)$ ($i = A, \psi$). The right hand sides of (2.220) have to be rewritten in terms of the renormalized parameters by inversion of the formal power series. The renormalization factors Z_i are of the form

$$Z_i = 1 + \sum_{n=1}^{\infty} \frac{Z_{i,n}(e_r, \xi_r)}{\varepsilon^n} \quad (2.221)$$

and applying the chain rule, we observe that the coefficient functions are uniquely determined by $Z_{i,1}(e_r, \xi_r)$ alone:

$$\begin{aligned}
\beta(e) &= \frac{e}{2} e \frac{\partial}{\partial e} Z_{g,1}(e) = \frac{\alpha}{\pi} \frac{e}{3} + \dots \\
\gamma_m(e) &= \frac{1}{2} e \frac{\partial}{\partial e} Z_{m,1}(e) = \frac{\alpha}{\pi} \frac{3}{2} + \dots \\
\gamma_A(e, \xi) &= \frac{1}{4} e \frac{\partial}{\partial e} Z_{A,1}(e, \xi) = \frac{\alpha}{\pi} \frac{2}{3} + \dots \\
\gamma_\psi(e, \xi) &= \frac{1}{4} e \frac{\partial}{\partial e} Z_{\psi,1}(e, \xi) = \frac{\alpha}{\pi} \frac{\xi}{2} + \dots
\end{aligned} \tag{2.222}$$

These are the residues of the simple ε -poles of the renormalization counter terms. The one–loop contributions we calculated above: $Z_A = Z_\gamma$ (2.172), $Z_\psi = Z_f$ (2.197), $Z_g = 1 + \frac{\delta e}{e}$ (2.212) and $Z_m = 1 + \frac{\delta m}{m}$ (2.195) with $\text{Reg} = \ln \mu^2 \rightarrow \frac{2}{\varepsilon}$ (see (2.145)). Note that in QED the WT identity (2.200) implies $Z_g = 1/\sqrt{Z_\gamma}$, which is very important because it says that charge renormalization is governed by photon vacuum polarization effects. The latter will play a crucial role in calculations of $g - 2$. The UV singular parts of the counter terms read

$$\begin{aligned}
Z_e &= 1 + \frac{e^2}{4\pi^2} \frac{1}{3} \frac{1}{\varepsilon}, & Z_m &= 1 - \frac{e^2}{4\pi^2} \frac{3}{2} \frac{1}{\varepsilon}, \\
Z_A &= 1 + \frac{e^2}{4\pi^2} \frac{2}{3} \frac{1}{\varepsilon}, & Z_\psi &= 1 + \frac{e^2}{4\pi^2} \frac{\xi}{2} \frac{1}{\varepsilon},
\end{aligned}$$

from which the leading terms of the RG coefficient functions given in (2.222) may be easily read off. The RG equation is a partial differential equation which is homogeneous and therefore can be solved easily along so called characteristic curves. Let s parametrize such a curve, such that all quantities become functions of a the single parameter s : $e = e(s)$, $m = m(s)$, $\mu = \mu(s)$ and

$$\frac{d\Gamma}{ds}(\{p\}; e(s), m(s), \mu(s)) = n\gamma \Gamma$$

with

$$\frac{d\mu}{ds} = \mu, \quad \frac{de}{ds} = \beta(e), \quad \frac{dm}{ds} = m\gamma_m(e),$$

which is a set of ordinary differential equations the solution of which is solving the RG equation (2.220). For simplicity of notation and interpretation we have assumed the Landau gauge $\xi = 0$ and we abbreviated $n_A \gamma_A + n_\psi \gamma_\psi = n\gamma$. The successive integration then yields

(1)

$$\frac{d\mu}{ds} = \mu \triangleright \ln \mu = s + \text{constant} \triangleright \mu = \mu_0 e^s = \mu_0 \kappa$$

where $\kappa = e^s$ is a scale dilatation parameter

(2)

$$\frac{de}{ds} = \beta(e) \triangleright \frac{de}{\beta(e)} = ds = \frac{d\mu}{\mu} \triangleright$$

$$\ln(\mu/\mu_0) = \ln \kappa = \int_e^{e(\kappa)} \frac{de'}{\beta(e')} \quad (2.223)$$

which is the implicit definition of the running coupling $e(\kappa)$ with $e = e(1)$ the coupling at reference scale μ_0 and $e(\kappa) = e(\mu/\mu_0)$ the coupling at scale μ .

(3)

$$\frac{dm}{ds} = m\gamma_m \triangleright \frac{dm}{m} = \gamma_m(e) ds = \gamma_m(e) \frac{de}{\beta(e)} \triangleright$$

$$m(\kappa) = m \exp \int_e^{e(\kappa)} \frac{\gamma(e') de'}{\beta(e')} \quad (2.224)$$

(4)

$$\frac{d\Gamma}{ds} = n\gamma(e) ds = n\gamma(e) \frac{d\mu}{\mu} = n\gamma(e) \frac{de}{\beta(e)} \triangleright$$

$$\Gamma(\kappa) = \Gamma \exp \left\{ n \int_e^{e(\kappa)} \frac{\gamma(e') de'}{\beta(e')} \right\} = \Gamma z_A(e, \kappa)^{n_A} z_\psi(e, \kappa)^{2n_\psi} \quad (2.225)$$

with $\Gamma = \Gamma(1)$, and

$$z_A(e, \kappa) = \exp \int_e^{e(\kappa)} \frac{\gamma_A(e') de'}{\beta(e')}, \quad z_\psi(e, \kappa) = \exp \int_e^{e(\kappa)} \frac{\gamma_\psi(e') de'}{\beta(e')}.$$

Altogether, we may write this as an equation which describes the response of the theory with respect to a change of the scale parameter μ :

$$\Gamma(\{p\}; e, m, \mu/\kappa) = z_A(e, \kappa)^{-n_A} z_\psi(e, \kappa)^{-2n_\psi} \Gamma(\{p\}; e(\kappa), m(\kappa), \mu) \quad (2.226)$$

Thus a **change of the scale parameter μ is equivalent to a finite renormalization of the parameters and fields** and together with the homogeneity relation we have for the vertex functions with scaled momenta

$$\begin{aligned}\Gamma(\{\kappa p\}; e, m, \mu) &= \kappa^{\dim\Gamma} \Gamma(\{p\}; e(\kappa), m(\kappa)/\kappa, \mu/\kappa) \\ &= \kappa^{\dim\Gamma} z_A(e, \kappa)^{-n_A} z_\psi(e, \kappa)^{-2n_\psi} \Gamma(\{p\}; e(\kappa), m(\kappa)/\kappa, \mu)\end{aligned}\quad (2.227)$$

which is the basic relation for a discussion of the asymptotic behavior.

Asymptotic Behavior

Two regimes are of interest, the high energy (ultraviolet) behavior and the low energy (infrared) behavior. For the general discussion we consider a generic gauge coupling g (in place of e in QED).

(1) UV behavior

The ultraviolet behavior, which determines the short distance properties, is obtained by choosing $\kappa|p| \gg m, \mu$ thus

$$\ln \kappa = \int_g^{g(\kappa)} \frac{dg'}{\beta(g')} \rightarrow +\infty ; \quad \kappa \rightarrow \infty .$$

However, the integral can only become divergent for finite $g(\kappa)$ if $\beta(g)$ has a zero at $\lim_{\kappa \rightarrow \infty} g(\kappa) = g^*$: more precisely, in the limit $\kappa \rightarrow \infty$ the effective coupling has to move to a fixed point $g(\kappa) \rightarrow g^*$ if finite, and the fixed point coupling is characterized by $\beta(g^*) = 0, \beta'(g^*) < 0$. Thus g^* is an ultraviolet fixed point coupling. Note that by dilatation of the momenta at fixed m and μ , the effective coupling is automatically driven into a fixed point, a zero of the β -function with negative slope, if it exists. If $g^* = 0$ we have asymptotic freedom. This is how QCD behaves, which has a β -function

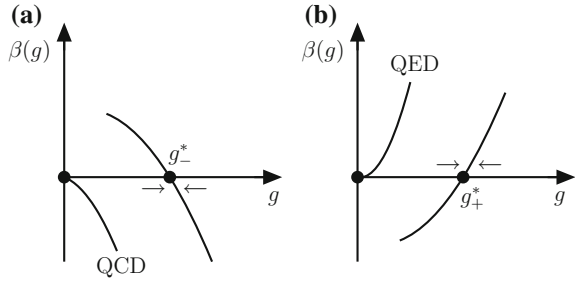
$$\beta_{\text{QCD}}(g_s) = -g_s \left(\beta_0 \left(\frac{g^2}{16\pi^2} \right) + \beta_1 \left(\frac{g^2}{16\pi^2} \right)^2 + \dots \right) \quad (2.228)$$

with $\beta_0 > 0$ (see Fig. 2.10a). QCD will be considered in more detail later on.

A possible fixed point is accessible in perturbation theory provided g^* is sufficiently small, such that perturbation theory is sufficiently “convergent” as an asymptotic series. One may then expand about g^* :

$$\begin{aligned}\beta(g) &= (g - g^*) \beta'(g^*) + \dots \\ \gamma(g) &= \gamma^* + (g - g^*) \gamma'(g^*) + \dots\end{aligned}$$

Fig. 2.10 RG fixed points are zeros of the β -function: **a** UV fixed points, **b** IR fixed points



and provided $\beta'(g_-^*) \neq 0$ we have

$$\begin{aligned} a(g, \kappa) &= \exp \int_g^{g(\kappa)} \frac{\gamma(g')}{\beta(g')} dg' = \exp \int_g^{g(\kappa)} \frac{\gamma(g_-^*)}{\beta(g')} dg' \cdot r(g, \kappa) \\ &= \kappa^{\gamma^*} r(g, \kappa) \end{aligned}$$

where

$$r(g, \kappa) = \exp \int_g^{g(\kappa)} \frac{(\gamma(g') - \gamma^*)}{\beta(g')} dg'$$

in the limit of large κ yields a finite scale independent wave function renormalization

$$\lim_{\kappa \rightarrow \infty} r(g, \kappa) = r(g, \infty) .$$

We thus find the asymptotic form

$$\Gamma(\{p\}; g, m, \mu) \xrightarrow{\kappa} \kappa^d (\kappa^{d_A} r_A(g, \infty))^{-n_A} (\kappa^{d_\psi} r_\psi(g, \infty))^{-2n_\psi} \Gamma(\{p\}; g_-^*, 0, \mu) \quad (2.229)$$

which exhibits asymptotic *scaling*. As naively expected it is given by the vertex functions of a *massless theory*. Indeed, at high energies masses may be neglected, however on the expense that another mass scale remains in the game, the scale parameter μ . The first factor κ^d is trivial and is due to the d -momentum conservation which was factored out. Then each field exhibits a homogeneous (power-like) behavior in the dilatation factor κ , the exponent of which exhibits an *anomalous dimension* as a consequence of the dynamics of the theory:

$$d_A = \frac{d-2}{2} + \gamma_A^* , \quad d_\psi = \frac{d-1}{2} + \gamma_\psi^* . \quad (2.230)$$

The first term is the naive or engineers dimension the second part is the anomalous part which is a quantum effect, a relict of the breaking of scale invariance, when $g \neq g^*$. While naively we would expect that in $d = 4$ dimensions the massless theory has scaling: for example a scalar two-point function, the only dimensionful physical quantity being the momentum, one would expect $G(p; g) \sim 1/p^2$ as G has dimension 2. However, if there would be a non-trivial UV fixed point one would have $G(p, g, \mu) \sim (\mu^2)^{\gamma^*} / (p^2)^{1+\gamma^*}$ ($\gamma^* > 0$) which shows the role and unavoidability of the scale parameter μ , which has to eat up the extra dimension γ^* induced by the dynamics of the theory. Otherwise only truly free theories could have scaling, called *canonical scaling* in this case. The discovery of asymptotic freedom of QCD [36] is the prime example of a dynamical theory, nota bene of the theory of strong interactions, exhibiting asymptotic canonical scaling (Bjorken scaling) of liberated quarks (quark parton model) [68]. The latter was discovered before in the pioneering investigations concerning *Deep Inelastic Scattering* (DIS) [69] of electrons on protons and bound neutrons by Friedman, Kendall and Taylor (Nobel prize 1990). These experiments have been of essential importance for the development of the quark model and to the discovery of QCD as the theory of the strong interactions.

(2) IR behavior

The infrared behavior corresponds to the long distance properties of a system. Here the regime of interest is $\kappa|p| \ll m, \mu$ and the discussion proceeds essentially as before: now as $\kappa \rightarrow 0$ the effective $g(\kappa) \rightarrow g_+^*$ where g_+^* is a zero of the β -function with positive slope, see Fig. 2.10b, $\beta(g_+^*) = 0$ and $\beta'(g_+^*) > 0$. This is the typical situation in the construction of low energy effective theories, particularly in the discussion of critical phenomena of statistical systems (keywords: critical behavior, critical exponents, scaling laws, universality). If $g_+^* = 0$ the effective theory is infrared free (the opposite of *asymptotic freedom*), also called Gaussian (Gaussian fixed point). Here the well known examples are QED

$$\beta_{\text{QED}}(e) = \frac{e^3}{12\pi^2} \sum_f N_{cf} Q_f^2 + \dots \quad (2.231)$$

or the self-interacting scalar field ϕ^4 -theory

$$\beta(\lambda) = -\varepsilon\lambda + \frac{3\lambda^2}{16\pi^2} + \dots$$

in $d = 4$ dimensions. For QED the running coupling to leading order thus follows from

$$\ln \kappa = \int_e^{e(\kappa)} \frac{1}{\beta(e')} de' = \frac{12\pi^2}{\sum_f N_{cf} Q_f^2} \int_e^{e(\kappa)} \frac{1}{(e')^3} de' = \frac{24\pi^2}{\sum_f N_{cf} Q_f^2} \left(\frac{1}{e^2} - \frac{1}{e(\kappa)^2} \right)$$

where the sum extends over all light flavors $f : m_f < \mu$.³⁷ The running fine structure constant thus at leading order is given by

$$\alpha(\mu) = \frac{\alpha}{1 - \frac{2\alpha}{3\pi} \sum_f N_{cf} Q_f^2 \ln \mu/\mu_0} \quad (2.232)$$

where μ_0 is the scale where the lightest particle starts to contribute, which is the electron $\mu_0 = m_e$. We then may identify $\alpha(\mu_0) = \alpha$ the classical low energy value of the fine structure constant, with the proviso that only logarithmic accuracy is taken into account (see below). The running α is equivalent to the Dyson summation of the transversal part of the photon self-energy to the extent that only the logs are kept. The RG running takes into account the leading radiative corrections in the case the logs are dominating over constant terms, i.e., provided large scale changes are involved.

In the calculation of the contributions from electron loops in photon propagators to the muon anomaly a_μ , such large scale changes from m_e to m_μ are involved and indeed one may calculate such two-loop contributions starting from the lowest order result

$$a_\mu^{(2)} = \frac{\alpha}{2\pi} \text{ via the substitution } \alpha \rightarrow \alpha(m_\mu) \quad (2.233)$$

where

$$\alpha(m_\mu) = \frac{\alpha}{1 - \frac{2}{3} \frac{\alpha}{\pi} \ln \frac{m_\mu}{m_e}} = \alpha \left(1 + \frac{2}{3} \frac{\alpha}{\pi} \ln \frac{m_\mu}{m_e} + \dots \right) \quad (2.234)$$

such that we find

$$a_\mu^{(4)\text{LL}}(\text{vap}, e) = \frac{1}{3} \ln \frac{m_\mu}{m_e} \left(\frac{\alpha}{\pi} \right)^2$$

which indeed agrees with the leading log result obtained in [70] long time ago by a direct calculation. The method has been further developed and refined by Lautrup and de Rafael [71]. In the calculation of a_μ only the electron VP insertions are governed by the RG and the corresponding one-flavor QED β -function has been calculated to three loops

$$\beta(\alpha) = \frac{2}{3} \left(\frac{\alpha}{\pi} \right) + \frac{1}{2} \left(\frac{\alpha}{\pi} \right)^2 - \frac{121}{144} \left(\frac{\alpha}{\pi} \right)^3 + \dots \quad (2.235)$$

³⁷This latter restriction takes into account the decoupling of heavy flavors, valid in QED and QCD. Since in the $\overline{\text{MS}}$ scheme, i.e., renormalization by the substitution $\text{Reg} \rightarrow \ln \mu^2$, which we are considering here, decoupling is not automatic, one has to impose it by hand. At a given scale one is thus considering an effective theory, which includes only those particles with masses below the scale μ .

long time ago by [72], which thus allows us to calculate leading $\alpha^n (\ln m_\mu/m_e)^n$, next-to-leading $\alpha^n (\ln m_\mu/m_e)^{n-1}$ and next-to-next-to-leading $\alpha^n (\ln m_\mu/m_e)^{n-2}$ log corrections. At present $\beta(\alpha)$ is known to five loops [73, 74] which allows one to calculate leading log a_μ contributions to six loops [75].

As $\alpha(\mu)$ is increasing with μ , at some point this resummed effective coupling (2.232) exhibits a pole, the so called *Landau pole* at which the coupling becomes infinite: $\lim_{\mu \rightarrow \mu_L} \alpha(\mu) = \infty$. The “fixed point” very likely is an artifact of perturbation theory, which of course ceases to be valid when the one-loop correction approaches 1. What this tells us is that we actually do not know what the high energy asymptotic behavior of QED is. This is in contrast to QCD, which exhibits the high energy asymptotic behavior of a free (non-interacting) field theory, which means that perturbation theory gets the better the higher the energy,

α in the on-shell versus α in the $\overline{\text{MS}}$ scheme

In our discussion of renormalizing QED we were considering originally the *on-shell renormalization scheme*, while the RG provides α in the $\overline{\text{MS}}$ scheme. Here we briefly discuss the relationship between the OS and the $\overline{\text{MS}}$ fine structure constants $\alpha_{\text{OS}} = \alpha$ and $\alpha_{\overline{\text{MS}}}$, respectively. Since the bare fine structure constant

$$\alpha_0 = \alpha_{\overline{\text{MS}}} \left(1 + \frac{\delta\alpha}{\alpha} \Big|_{\overline{\text{MS}}} \right) = \alpha_{\text{OS}} \left(1 + \frac{\delta\alpha}{\alpha} \Big|_{\text{OS}} \right) \quad (2.236)$$

is independent of the renormalization scheme. The one-loop calculation in the SM yields (including the charged W contribution for completeness)

$$\begin{aligned} \frac{\delta\alpha}{\alpha} \Big|_{\overline{\text{MS}}} &= \frac{\alpha}{3\pi} \sum Q_f^2 N_{cf} \ln \frac{\mu^2}{m_f^2} - \frac{\alpha}{3\pi} \frac{21}{4} \ln \frac{\mu^2}{M_W^2} \\ \frac{\delta\alpha}{\alpha} \Big|_{\text{OS}} &= \Pi'_\gamma(0) + \frac{\alpha}{\pi} \ln \frac{M_W^2}{\mu^2} \\ &= \frac{\delta\alpha}{\alpha} \Big|_{\overline{\text{MS}}} - \frac{\alpha}{6\pi} \end{aligned}$$

and thus

$$\alpha_{\overline{\text{MS}}}^{-1}(0) = \alpha^{-1} + \frac{1}{6\pi} \quad (2.237)$$

as a low energy matching condition. The α -shift in the $\overline{\text{MS}}$ scheme is very simple, just the UV logs,

$$\Delta\alpha_{\overline{\text{MS}}}(\mu) = \frac{\alpha}{3\pi} \sum Q_f^2 N_{cf} \ln \frac{\mu^2}{m_f^2} - \frac{\alpha}{3\pi} \frac{21}{4} \ln \frac{\mu^2}{M_W^2} \quad (2.238)$$

such that

$$\Delta\alpha_{\overline{\text{MS}}}(\mu) = \Delta\alpha_{\text{OS}}(\mu) + \frac{\alpha}{3\pi} \frac{5}{3} \sum Q_f^2 N_{cf} \quad (2.239)$$

where the sum goes over all fermions f with $N_{cf} = 1$ for leptons and $N_{cf} = 3$ for quarks.

In perturbation theory, the leading light fermion ($m_f \ll M_W, \sqrt{s}$) contribution in the OS scheme is given by

$$\Delta\alpha(s) = \frac{\alpha}{3\pi} \sum_f Q_f^2 N_{cf} \left(\ln \frac{s}{m_f^2} - \frac{5}{3} \right). \quad (2.240)$$

We distinguish the contributions from the leptons, for which the perturbative expression is appropriate, the five light quarks (u, d, s, c, b) and the top

$$\Delta\alpha = \Delta\alpha_{\text{lep}} + \Delta\alpha_{\text{had}} + \Delta\alpha_{\text{top}}. \quad (2.241)$$

Since the top quark is heavy we cannot use the light fermion approximation for it. A very heavy top in fact decouples like

$$\Delta\alpha_{\text{top}} \simeq -\frac{\alpha}{3\pi} \frac{4}{15} \frac{s}{m_t^2} \rightarrow 0$$

when $m_t \gg s$. Since pQCD does not apply at low energies, $\Delta\alpha_{\text{had}}$ has to be evaluated via dispersion relations from e^+e^- -annihilation data.

Note that in $d = 4$ dimensions both for QCD and QED very likely there is no RG fixed point at finite value of g except $g = 0$, which always is a fixed point, either a UV one (QCD) or an IR one (QED). In QCD this could mean that $\alpha_s(\mu) \rightarrow \infty$ for $\mu \rightarrow 0$ (infrared slavery, confinement). In perturbation theory a Landau pole shows up at finite scale Λ_{QCD} when coming from higher energy scales, where $\alpha_s \rightarrow \infty$ for $\mu \xrightarrow{\sim} \Lambda_{\text{QCD}}$. In QED likely $\alpha(\mu) \rightarrow \infty$ for $\mu \rightarrow \infty$.

It is important to emphasize that the RG only accounts for the UV logarithms, which in DR are related to the UV poles in $d = 4 - \varepsilon$ dimensions. Large logs may also be due to IR singular behavior, like the terms proportional to $\ln m_\gamma$ which we have regulated with an infinitesimally small photon mass in the on-shell lepton wave function renormalization factor $Z_\psi = Z_f$ (2.197). In spite of the fact that this term appears in the UV renormalization counter term, it has nothing to do with a UV singularity and does not contribute in the RG coefficients. In DR also IR singularities may be regularized by analytic continuation in d , however, by dimensional continuation to $d = 4 + \varepsilon_{\text{IR}}$, and corresponding IR poles at negative ε_{UV} . Also the terms proportional to $\ln \frac{-q^2}{m_z^2}$ showing up in the electric form factor (2.213) is not covered by the RG analysis. As will be explained in the next section, the IR singularities have their origin in the attempt to define free charged particle states as simple iso-

lated poles in the spectrum (by trying to impose an on-shell condition). In reality, the Coulomb potential mediated by the massless photon has infinite range and the charged states feel the interaction whatever the spatial separation in corresponding scattering states is.

2.6.6 Bremsstrahlung and the Bloch–Nordsieck Prescription

As we have seen the on-shell form factor A_1 is IR singular in the limit of physical zero mass photons at the one-loop level and beyond. As already mentioned, the problem is that we try to work with scattering states with a fixed number of free particles, while in QED due to the masslessness of the photon and the related infinite interaction range of the electromagnetic forces soft photons are emitted and eventually reabsorbed at any distance from the “interaction region”, i.e. the latter extends to ∞ . The basic problem in this case is the proper definition of a charged particle state as obviously the order by order treatment of a given scattering amplitude breaks down. Fortunately, as Bloch and Nordsieck [59] have observed, a simple prescription bring us back to a quasi perturbative treatment. The basic observation was that virtual and soft real photons are not distinguishable beyond the resolution of the measuring apparatus. Thus besides the virtual photons we have to include the soft real photons of energies below the resolution threshold. For a given tree level process, the Bloch–Nordsieck prescription requires to include photonic corrections at a given order $O(e^n)$ irrespective of whether the photons are virtual or real (soft). We thus are led back to a perturbative order by order scheme, on the expense that, at the given order, all possible final states which only differ by (soft) photons have to be summed over.

Thus in order to obtain a physics-wise meaningful observable quantity, in the case of the electromagnetic form factor

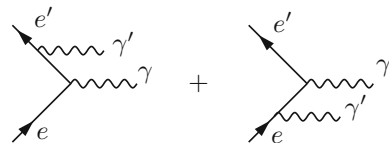
$$e^-(p_1) + \gamma(q) \rightarrow e'(p_2) ,$$

at one-loop order $O(e^2)$, we have to include the corresponding process

$$e^-(p_1) + \gamma(q) \rightarrow e'(p_2) + \gamma'(k) ,$$

with one additional real (soft) photon attached in all possible ways to the tree diagram as shown in Fig. 2.11. The second photon is assumed to be soft, i.e. having energy $E_{\gamma'} = |\mathbf{k}| < \omega$, where ω is the threshold of detectability of the real photon. Since the photon cannot be seen, the event looks like an “elastic” event, i.e. like one of

Fig. 2.11 Bremsstrahlung in $e^-(p_1) + \gamma(q) \rightarrow e'(p_2)$



the same final state as the tree level process. The soft photons thus factorize into the Born term of the original process times a soft photon correction, with the soft photons integrated out up to energy ω . The correction given by the bremsstrahlung cross section is proportional to the square $|T_{\text{bre}}|^2$ of the sum of the matrix elements of the two diagrams which reads

$$T_{\text{bre}} = i^3 e^2 \bar{u}(p_2) \left\{ \gamma^\rho \frac{\not{p}_2 + \not{k} + m}{(p_2 + k)^2 - m^2} \gamma^\mu + \gamma^\mu \frac{\not{p}_1 - \not{k} + m}{(p_1 - k)^2 - m^2} \gamma^\rho \right\} u(p_1) \varepsilon_\rho^*(k, \lambda). \quad (2.242)$$

In the soft photon approximation $k \sim 0$ and hence $p_1 + q = p_2 + k \simeq p_2$ we may neglect the \not{k} terms in the numerator. Using the Dirac–algebra and the Dirac equation we may write, in the first term, $\bar{u}(p_2) \not{\varepsilon}^*(\not{p}_2 + m) = \bar{u}(p_2) [2\varepsilon^* p_2 + (-\not{p}_2 + m) \not{\varepsilon}^*] = \bar{u}(p_2) 2\varepsilon^* p_2$, in the second term, $(\not{p}_1 + m) \not{\varepsilon}^* u(p_1) = [2\varepsilon^* p_1 + \not{\varepsilon}^*(-\not{p}_1 + m)] u(p_1) = 2\varepsilon^* p_1 u(p_1)$. Furthermore, in the bremsstrahlung integral the scalar propagators take a very special form, which comes about due to the on–shellness of the electrons and of the bremsstrahlung photon: $(p_2 + k)^2 - m^2 = p_2^2 + 2(kp_2) + k^2 - m^2 = 2(kp_2)$ and $(p_1 - k)^2 - m^2 = p_1^2 - 2(kp_1) + k^2 - m^2 = -2(kp_1)$ as $p_1^2 = p_2^2 = m^2$ and $k^2 = 0$. Therefore, the soft bremsstrahlung matrix element factorizes into the Born term times a radiation factor

$$T_{\text{bre}}^{\text{soft}} \simeq -ie \bar{u}(p_2) \gamma^\mu u(p_1) \left\{ -2e \left(\frac{\varepsilon^* p_1}{kp_1} - \frac{\varepsilon^* p_2}{kp_2} \right) \right\}$$

and one obtains

$$d\sigma = d\sigma_0 \frac{4e^2}{(2\pi)^3} \left| \frac{\varepsilon p_1}{kp_1} - \frac{\varepsilon p_2}{kp_2} \right|^2 \frac{d^3k}{2\omega_k}$$

where $d\sigma_0$ denotes the lowest order cross section for the absorption of a virtual photon by an electron. If we sum over the two photon polarizations λ indexing the polarization vector and use the completeness relation (2.26) we find

$$d\sigma = -d\sigma_0 \frac{4e^2}{(2\pi)^3} \left(\frac{p_1}{kp_1} - \frac{p_2}{kp_2} \right)^2 \frac{d^3k}{2\omega_k}. \quad (2.243)$$

Actually, the integral for massless photons does not exist as it is logarithmically IR singular

$$\int_{|\mathbf{k}| < \omega} \frac{d^3k}{|\mathbf{k}|^3} \cdots = \infty.$$

Again an IR regularization is required and we introduce a tiny photon mass such that $\omega_k = \sqrt{\mathbf{k}^2 + m_\gamma^2}$. As a correction to the cross section, we may write the *inclusive cross section* for

$$e^-(p_1) + \gamma(q) \rightarrow e'^-(p_2), \quad e'^-(p_2) + \gamma'(k, \text{soft})$$

as

$$d\sigma_{\text{inc}} = d\sigma_0 (1 + C_{\text{bre}})$$

which, for the vertex on the amplitude level reads

$$i\Gamma_{\text{inc}}^\mu = -ie\gamma^\mu \left(1 + \frac{1}{2}C_{\text{bre}} + \dots \right) \simeq -ie\gamma^\mu + i\delta\Gamma_{\text{bre}}^\mu$$

where

$$i\delta\Gamma_{\text{bre}}^\mu = -ie\gamma^\mu \frac{1}{2}C_{\text{bre}} \quad (2.244)$$

with

$$C_{\text{bre}} = \frac{e^2}{2\pi^3} \int_{|\mathbf{k}| < \omega} \frac{d^3k}{2\omega_k} \left\{ \frac{2(p_1 p_2)}{(k p_1)(k p_2)} - \frac{m^2}{(k p_1)^2} - \frac{m^2}{(k p_2)^2} \right\} \quad (2.245)$$

is the $O(\alpha)$ contribution to the Dirac form factor due to bremsstrahlung. The first term is the interference from the two diagrams, the second and third correspond to the squares of the first and the second diagram, respectively. For a finite photon mass the integral is finite and may be worked out (see e.g. [52] Sect. 7). The result may be written in the form

$$C_{\text{bre}} = \frac{\alpha}{\pi} \left\{ \left(1 - \frac{y}{2} \right) \left(4G'(y) \ln \frac{2\omega}{m_\gamma} - F'(y) \right) - 2 \ln \frac{2\omega}{m_\gamma} + 2G'(y) \right\}$$

with $(\xi = (\sqrt{1-y} - 1)/(\sqrt{1-y} + 1))$ as defined in (2.182))

$$G'(y) = -\frac{1}{4\sqrt{1-y}} \ln(\xi^2)$$

$$F'(y) = \frac{1}{2\sqrt{1-y}} \left\{ \frac{2\pi^2}{3} - 4\text{Sp}(-\xi) + \ln^2(-\xi) - 4 \ln(-\xi) \ln(1 + \xi) \right\}$$

where, for simplicity, F' is given for the production channel

$$\gamma(q) \rightarrow e^-(-p_1) + e'^-(p_2), \quad e^-(-p_1) + e'^-(p_2) + \gamma'(k, \text{soft})$$

where $0 < y < 1$ ($-1 < \xi < 0$). In spite of the fact that the soft bremsstrahlung factor (2.245) looks universal, the result of the evaluation of the integrals is *process dependent*: apart from the universal terms, which in particular include the IR singular ones, the function $F'(y)$ depends on the channel considered. Note that, in contrast to

the form factors, like $A_{E \text{ ren}}$, which are analytic in q^2 , C_{bre} is not analytic in the same variable, because it is the integral over the absolute square $|T|^2$ of a transition matrix element. It must be real and positive. Above, we have chosen to present $F'(y)$ for the production channel as it allows us to discuss the main points of the Bloch–Nordieck prescription, keeping the notation substantially simpler.³⁸ The leading behavior in this case reads

$$C_{\text{bre}} = \frac{\alpha}{\pi} \left\{ 2 \ln \frac{q^2}{m^2} \ln \frac{2\omega}{m_\gamma} - \frac{1}{2} \ln^2 \frac{q^2}{m^2} - 2 \ln \frac{2\omega}{m_\gamma} + \ln \frac{q^2}{m^2} + \dots \right\}.$$

Now, we are able to calculate the form factor for soft photon dressed electrons. The real part of the Dirac form factor gets modified to

$$\begin{aligned} \text{Re } A_{E \text{ ren}} + \frac{1}{2} C_{\text{bre}} &= \frac{\alpha}{2\pi} \left\{ -2 \ln \frac{2\omega}{m} + 4 \left(1 - \frac{y}{2}\right) G'(y) \ln \frac{2\omega}{\sqrt{q^2}} \right. \\ &+ \left. 2 \left(1 - \frac{y}{2}\right) \frac{\pi^2}{2\sqrt{1-y}} - 2 + (5 - 2y) G'(y) + \left(1 - \frac{y}{2}\right) (\text{Re } F - F')(y) \right\} \end{aligned} \quad (2.246)$$

where

$$(\text{Re } F - F')(y) = \frac{1}{2\sqrt{1-y}} \left\{ -\frac{4\pi^2}{3} + 8\text{Sp}(-\xi) + 4 \ln(-\xi) (2 \ln(1 + \xi) - \ln(1 - \xi)) \right\}.$$

³⁸In the scattering region the result is more complicated, because, there is one more kinematic variable, the scattering angle Θ , or equivalently, the electron velocity β_e . Considering, elastic scattering $|\mathbf{p}_1| = |\mathbf{p}_2|$, $E_1 = E_2$ the finite function $F'(y)$, now for $y < 0$ ($0 < \xi < 1$), reads

$$\begin{aligned} F'(y) &= \frac{1}{\sqrt{1-y}} \left\{ -\text{Sp} \left(1 + \frac{2}{1+\xi} \frac{1}{1-\beta_e} \right) - \text{Sp} \left(1 + \frac{2}{1+\xi} \frac{1}{1+\beta_e} \right) \right. \\ &+ \left. \text{Sp} \left(1 + \frac{2\xi}{1+\xi} \frac{1}{1-\beta_e} \right) + \text{Sp} \left(1 + \frac{2\xi}{1+\xi} \frac{1}{1+\beta_e} \right) \right\} \end{aligned}$$

where $\beta_e = \sqrt{1 - 4m^2/s}$ is the velocity of the electron. s and $Q^2 = -q^2 > 0$ are related by $Q^2 = s \frac{1 - \cos \Theta}{2}$. The asymptotic behavior $Q^2 \gg m^2$ at fixed angle requires $s \gg m^2$ with $r \equiv Q^2/s = (1 - \cos \Theta)/2$ fixed. The arguments of the Spence functions behave like $1 + \frac{2}{1+\xi} \frac{1}{1-\beta_e} \simeq \frac{s}{m^2} - r^{-1} + \dots$, $1 + \frac{2}{1+\xi} \frac{1}{1+\beta_e} \simeq 2 - \frac{m^2}{Q^2} + \frac{m^2}{s} + \dots$, $1 + \frac{2\xi}{1+\xi} \frac{1}{1-\beta_e} \simeq 1 + r^{-1} - (1 + 3r^{-1}) \frac{m^2}{Q^2} + \dots$, and $1 + \frac{2\xi}{1+\xi} \frac{1}{1+\beta_e} \simeq 1 + \frac{m^2}{Q^2} + \dots$. Utilizing the relations (2.207), one may work out the leading behavior

$$C_{\text{bre}}^{\text{scattering}} = \frac{\alpha}{\pi} \left\{ 2 \ln \frac{Q^2}{m^2} \ln \frac{2\omega}{m_\gamma} - \frac{1}{2} \ln^2 \frac{s}{m^2} - 2 \ln \frac{2\omega}{m_\gamma} + \ln \frac{Q^2}{m^2} + \dots \right\}$$

which, with $\ln^2 s/m^2 = -\ln^2 Q^2/m^2 + 2 \ln Q^2/m^2 \ln s/m^2 + \ln^2 s/Q^2$ and after neglecting the last (sub leading) term, is in agreement with [2]. In the production channel with $q^2 = -Q^2 > 0$, in the center of mass frame of the produced lepton pair, the leptons are back-to-back and hence $\Theta = \pi$, or $\cos \Theta = -1$, such that s may be identified as $s = q^2$.

This is the result for the time-like region (production or annihilation) where $-1 \leq \xi \leq 0$. Here the photon mass has dropped out and we have an IR finite result, at the expense that the form factor is dependent on the experimental resolution ω , the threshold detection energy for soft photons. This is the Bloch–Nordsieck [59] solution of the IR problem. The Pauli form factor is not affected by real photon radiation. In general, as a rule, soft and collinear real photon radiation is always integral part of the radiative corrections.

When combining virtual and soft photon effects one typically observes the cancellations of large or potentially large radiative correction and the range of validity of the perturbative results must be addressed. To be more specific, the calculation has revealed terms of different type and size: typically IR sensitive soft photons logarithms of the type $\ln(m/2\omega)$, or collinear logarithms $\ln(q^2/m^2)$ show up. The latter come from photons traveling in the direction of a lepton, which again cannot be resolved in an experiment with arbitrary precision. This is the reason why the limit $m \rightarrow 0$, in which photon and lepton would travel in the same direction at the same speed (the speed of light) is singular. These logarithms can be very large (high resolution, high energy) and if the corrections $\frac{\alpha}{\pi} \ln(q^2/m^2)$ tend to be of $O(1)$ one cannot trust the perturbative expansion any longer. Even more dangerous are the double logarithmic corrections like the so called *Sudakov logarithms* $\frac{\alpha}{\pi} \ln^2(q^2/m^2)$ or the mixed IR sensitive times collinear terms $\frac{\alpha}{\pi} \ln(m/2\omega) \ln(q^2/m^2)$. There are several possibilities to deal with the large logs:

(a) the leading large terms are known also in higher orders and may thus be resummed. The resummation leads to more reliable results. A typical example here is the soft photon exponentiation according to Yennie–Frautschi–Suura [76].

(b) UV sensitive large logs may be resummed by the renormalization group, as discussed above.

(c) Some observable quantities may have much better convergence properties in a perturbative approach than others. A typical example is the attempt of an *exclusive* measurement of a lepton, which because of the soft photon problematic per se is not a good object to look for. In fact, increasing the exclusivity by choosing the IR cut-off ω smaller and smaller, the correction becomes arbitrary large and the perturbative result becomes meaningless. Somehow the experimental question in such a situation is not well posed. In contrast, by choosing ω larger the correction gets smaller. The possibility to increase ω in the formula given above is kinematically constraint by the requirement of soft radiation *factorization*. Of course photons may be included beyond that approximation. Indeed, there is a famous theorem, the **Kinoshita–Lee–Nauenberg theorem** (KLN) [77] which infers the cancellations of mass singularities and infrared divergences for observables which are defined to include summation over all degenerate or quasi degenerate states:

Theorem 2.11 *After a summation over all possible degenerate states has been performed for the initial (i) and the final (f) states, the squared transition amplitude*

$$\sum_{i,f} |T_{fi}|^2 \quad (2.247)$$

and the corresponding cross section is free of all infrared singularities in the limit of all masses vanishing.

Such observables typically are “all inclusive” cross-sections averaged over the initial spin.

In our example, the inclusive cross section is obtained by adding the hard photons of energy $E_\gamma > \omega$ up to the kinematic limit $E_{\gamma \max} = \sqrt{q^2 - 4m^2}/2$. To illustrate the point, let us consider the lepton pair creation channel $\gamma^*(q) \rightarrow \ell^-(p_-) + \ell^+(p_+) + \gamma(k)$, where the * denote that the corresponding state is virtual, i.e. off-shell, with an additional real bremsstrahlung photon $\gamma(k)$ emitted from one of the final state leptons. We thus include the so called *final state radiation* (FSR). The “heavy” virtual photon γ^* of momentum $q = p_- + p_+ + k$, we may think to have been created previously in e^+e^- -annihilation, for example.³⁹ The center of mass energy is $E_{\text{cm}} = E_- + E_+ + E_\gamma = \sqrt{q^2}$. Let $\lambda = 2\omega/E_{\text{cm}}$ and $1 - \lambda \gg y$ such that we may work in the approximation up to terms of order $O(\alpha \frac{m^2}{q^2})$, i.e., neglecting power corrections in m^2/q^2 . Relaxing from the soft photon approximation which defined C_{bre} in Eq. (2.245), the hard bremsstrahlung integral of interest is

$$\int_{\omega}^{E_{\text{cm}}/2} dE_\gamma \dots$$

with the spectral density (integrand)

$$\begin{aligned} & \frac{1}{\Gamma_0(\gamma^* \rightarrow \ell\bar{\ell})} \frac{d^2\Gamma(\gamma^* \rightarrow \ell\bar{\ell}\gamma)}{dudv} = P(u, v) \\ & = \frac{\alpha}{2\pi} \left\{ \left(2 \frac{u}{1-u} + 1 - u \right) \left(\frac{1}{v} + \frac{1}{1-u-v} \right) \frac{a}{2} \left(\frac{1}{v^2} + \frac{1}{(1-u-v)^2} \right) - 2 \right\}. \end{aligned} \quad (2.248)$$

where $a = 4m^2/q^2$, $u = (p_- + p_+)^2/q^2$ and $v = (q - p_-)^2/q^2$. In the rest frame of the heavy photon we have $u = 1 - 2E_\gamma/M_\gamma$, $v = 1 - 2E_-/M_\gamma$ and $1 - u - v = 1 - 2E_+/M_\gamma$. In the center of mass frame of the lepton pair

$$v = \frac{1}{2} (1 - u) (1 - \sqrt{1 - y} \cos \Theta_+); \quad 1 - u - v = \frac{1}{2} (1 - u) (1 - \sqrt{1 - y} \cos \Theta_-)$$

³⁹The factorization into $e^+e^- \rightarrow \gamma^*$ production and subsequent $\gamma^* \rightarrow \ell^+\ell^-$ only makes sense at relatively low q^2 , when the one-photon exchange approximation can be used. In the SM the γ^* may also be a “heavy light” particle Z of mass about $M_Z \simeq 91$ GeV which is unstable and thus is described well by a Breit–Wigner resonance. Near the resonance energy again factorization is an excellent approximation and the following discussion applies. In e^+e^- -annihilation, the radiation of additional photons from the initial state electron or positron (Fig. 2.11 with e' an incoming e^+) is called *initial state radiation* (ISR). In the soft approximation (2.243) still holds. For details see (5.11) in Sect. 5.1.3.

with $y = a/u$ and Θ_{\pm} the angle between the final state photon and the lepton with momentum p_{\pm} ($\Theta_- = \pi - \Theta_+$). We have to integrate the distribution over the angles $0 \leq \Theta_{\pm} \leq \pi/2$ and over the hard photon $E_{\gamma} \geq \omega = \lambda (M_{\gamma}/2)$ with $1 - a > \lambda > 0$ yields [78] up to $O(\alpha y)$ precision

$$\Delta C_{>\omega} = \frac{\alpha}{2\pi} \left\{ \left(4 \ln \frac{1}{\lambda} - (1 - \lambda)(3 - \lambda) \right) \ln \frac{q^2}{m^2} - 4 \ln \frac{1}{\lambda} \right. \\ \left. + 4 \text{Sp}(\lambda) - \frac{2}{3} \pi^2 - (1 - \lambda)(3 - \lambda) \ln(1 - \lambda) + \frac{1}{2} (1 - \lambda)(11 - 3\lambda) \right\}$$

or for $\omega \ll E_{\text{cm}}/2$

$$\Delta C_{>\omega} = \frac{\alpha}{2\pi} \left\{ \left(4 \ln \frac{\sqrt{q^2}}{2\omega} - 3 \right) \ln \frac{q^2}{m^2} - 4 \ln \frac{\sqrt{q^2}}{2\omega} - \frac{2}{3} \pi^2 + \frac{11}{2} \right\}. \quad (2.249)$$

In this approximation the complementary soft plus virtual part (see (2.246))

$$C_{<\omega} = C_{\text{QED}}^{\text{virtual}} + C_{\omega}^{\text{soft}} \\ = \frac{\alpha}{2\pi} \left\{ - \left(4 \ln \frac{\sqrt{q^2}}{2\omega} - 3 \right) \ln \frac{q^2}{m^2} + 4 \ln \frac{\sqrt{q^2}}{2\omega} + \frac{2}{3} \pi^2 - 4 \right\}. \quad (2.250)$$

The total inclusive sum is

$$C^{\text{total}} = C_{<\omega} + \Delta C_{>\omega} = \frac{\alpha}{2\pi} \frac{3}{2} \simeq 1.74 \times 10^{-3} \quad (2.251)$$

a truly small perturbative correction. No scale and no log involved, just a pure number. This is the KLN theorem at work. It will play a crucial role later on in this book.

The two separate contributions become large when the cut energy ω is chosen very small and in fact we get a negative cross section, which physics wise makes no sense. The reason is that the correction gets large and one has to include other relevant higher order terms. Fortunately, the multi soft γ emission can be calculated to all orders. One can prove [76] that the IR sensitive soft photon exponentiates: Thus,

$$1 + C_{\text{IR}} + \frac{1}{2!} C_{\text{IR}}^2 + \dots = e^{C_{\text{IR}}} \\ = \exp \frac{\alpha}{2\pi} \left\{ -4 \ln \frac{\sqrt{q^2}}{2\omega} \ln \frac{q^2}{m^2} + 4 \ln \frac{\sqrt{q^2}}{2\omega} + \dots \right\} = \left(\frac{2\omega}{\sqrt{q^2}} \right)^{\frac{2\alpha}{\pi} \left(\ln \frac{q^2}{m^2} - 1 \right)}$$

and the result is

$$1 + C_{<\omega} + \dots = e^{C_{\text{IR}}} + \Delta C^{v+s} + \dots \quad (2.252)$$

with

$$\Delta C^{v+s} = C_{<\omega} - C_{\text{IR}} = \frac{\alpha}{2\pi} \left\{ 3 \ln \frac{q^2}{m^2} + \frac{2}{3} \pi^2 - 4 \right\}$$

a correction which is small if q^2/m^2 is not too large. Otherwise higher order collinear logs have to be considered as well. They do not simply exponentiate. By the resummation of the leading IR sensitive terms we have obtained a result which is valid much beyond the order by order perturbative result. Even the limit $\omega \rightarrow 0$ may be taken now, with the correct result that the probability of finding a naked lepton of mass m tends to zero. In contrast $1 + C_{<\omega} \rightarrow -\infty$ as $\omega \rightarrow 0$, a nonsensical result.

For our consideration of soft photon dressed states the inspection of the complementary hard photon part is important as far as the expression (2.249) tells us which are the logs which have to be canceled for getting the log free inclusive result. Namely, the IR sensitive log terms appear with the center of mass energy scale $\sqrt{q^2}$ not with the lepton mass m . This observation allows us to write the virtual plus soft result in a slightly different form than just adding up the results.

Another consideration may be instructive about the collinear mass singularities (terms $\propto \ln(q^2/m^2)$), which are a result of integrating the propagators $2|\mathbf{k}|(E_i - |\mathbf{p}_i| \cos \Theta_i)^{-1}$ in the distribution (2.243) or (2.248). If we integrate the angular distribution over a cone $\Theta_1, \Theta_2 \leq \delta$ only, instead of over the full angular range and add up the contributions

$$C_{<\omega, <\delta} = C_{\text{QED}}^{\text{virtual}} + C_{\omega}^{\text{soft}} + \Delta C_{>\omega, <\delta}^{\text{hard, collinear}} \quad (2.253)$$

the collinear singularities exactly cancel in the limit $m \rightarrow 0$, provided $\delta > 0$. The result reads

$$C_{<\omega, <\delta}^{m=0} = \frac{\alpha}{2\pi} \left\{ \left(4 \ln \frac{1}{\lambda} - (1-\lambda)(3-\lambda) \right) \ln \frac{1-\rho}{1+\rho} \frac{3}{2} + \rho(1-\lambda^2) \right\}$$

with $\rho = \cos \delta$, $\lambda = \frac{2\omega}{M_\gamma}$ and we have assumed $\frac{1-\rho}{2} \gg \frac{m^2}{M_\gamma^2}$. Thus, in addition to the virtual plus soft photons we have included now the hard collinear photons traveling with the leptons within a cone of opening angle δ . Here the collinear cone has been defined in the c.m. frame of the lepton pair, where the two cones are directed back to back and non overlapping for arbitrary cuts $\delta \leq \pi/2$. In an experiment one would rather define the collinear cones in the c.m. frame of the incoming virtual photon. In this case a slightly more complicated formula Eq. 14 of Ref. [78] is valid, which simplifies for small angles δ_0 and $\lambda = 2\epsilon = 2\omega/M_\gamma \ll 1$ to

$$C_{<\omega, <\delta_0}^{m=0} = -\frac{\alpha}{\pi} \left\{ (4 \ln 2\epsilon + 3) \ln \frac{\delta_0}{2} + \frac{\pi^2}{3} - \frac{5}{2} \right\} \quad (2.254)$$

which is the QED analog of the famous Serman-Weinberg (SW) formula [79]

$$C_{\text{SW}} = -\frac{4}{3} \frac{\alpha_s}{\pi} \left\{ (4 \ln 2\epsilon + 3) \ln \frac{\delta_0}{2} + \frac{\pi^2}{3} - \frac{5}{2} \right\} \quad (2.255)$$

for the two-jet event rate in QCD. The extra factor $\frac{4}{3}$ is an $SU(3)$ Casimir coefficient and α_s is the $SU(3)$ strong interaction coupling constant. The physical interpretation of this formula will be considered in Sect. 5.1.5.

Some final remarks are in order here: the IR problem of QED is a nice example of how the “theory reacts” if one is not asking the right physical questions. The degeneracy in the energy spectrum which manifests itself in particular kinematic regions (soft and/or collinear photons), at first leads to ill-defined results in a naive scattering picture approach, misleadingly assuming forces to be of finite range. At the end one learns that in QED the S -matrix as defined by the Gell-Mann Low formula does not exist, because the physical state spectrum is modified by the dynamics and is not the one suggested by the free part of the Lagrangian. Fortunately, a perturbative calculation of cross sections is still possible, by modifications of the naive approach by accounting appropriately for the possible degeneracy of states.

As we have observed in the above discussion, the radiatively induced Pauli form factor is not affected by the IR problem. The Pauli form factor is an example of a so called *infrared safe* quantity, which does not suffer from IR singularities in the naive scattering picture approach. As the anomalous magnetic moment is measured with extremely high accuracy, it nevertheless looks pretty much like a miracle how it is possible to calculate the anomalous magnetic moment in the naive approach to high orders (five loops at the moment) and confront it with an experimental result which is also measured assuming such a picture to be valid. But the states with which one formally is operating do not exist in nature. For a careful investigation of the problem we refer to the article by Steinmann [80].

We have discussed the IR problem for the simplest case, the electromagnetic form factor. In general the problem is more complicated, but the Bloch–Nordsieck prescription works and provides an order by order rule to overcome infrared singularities. The principle behind the “Bloch–Nordsieck solution” is the focus on “truly observable quantities”, which take into account detection problems in the measuring process, when state degeneracies in phase space come into play. One should ask the right questions in order to get useful and testable answers. In contrast, over-idealized formal quantities may be plagued by singularities. Let me sketch the procedure for the simplest case of a two-to-two fermion reaction, the process $e^+e^- \rightarrow \mu^+\mu^-$, which exhibits the radiative corrections depicted in Fig. 2.12. The amplitudes are considered to be the renormalized on-shell ones, which exist only after IR regularization. Since off-shell amplitudes are IR finite, the off-shellness $\mu_{\text{IR}}^2 = m^2 - p^2$, p the four-momentum of an external particle of mass m , can be used as an IR regulator, in principle. Actually such a regularization may be the most physical choice.⁴⁰

⁴⁰The limits $m_\gamma^2 \rightarrow 0$ for $p^2 = m^2$ and $\mu^2 = m^2 - p^2 \rightarrow 0$ for $m_\gamma^2 = 0$ coincide upon identifying $\mu^2 = m m_\gamma$ at least in one-loop calculations.

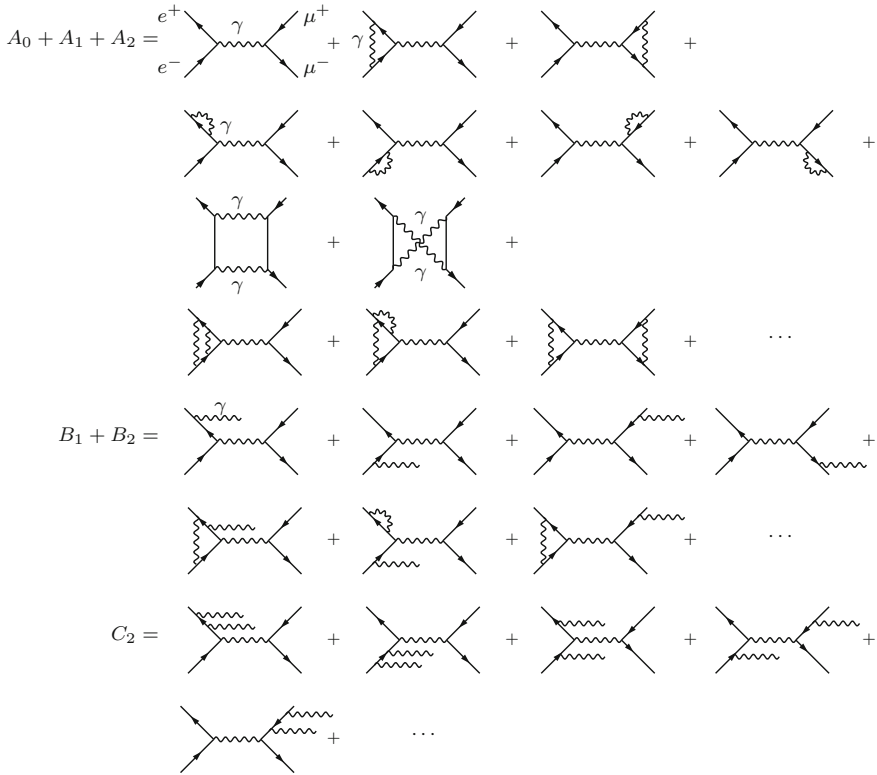


Fig. 2.12 Diagrams for muon pair production in electron-positron annihilation at lowest order $O(\alpha)$ (LO), next-to-leading order $O(\alpha^2)$ (NLO) and next-to-next-to-leading order $O(\alpha^3)$ (NNLO) together with the relevant real photon corrections. For the $O(\alpha^3)$ case only a sample of typical diagrams is shown. Corresponding amplitudes are denoted by A_0 at LO, A_1 , B_1 at NLO and A_2 , B_2 , C_2 at NNLO, where A_i , B_i and C_i ($i = 0, 1, 2$) refer to zero, one and two emitted real photons, respectively

Practical aspects usually let it look easier to use a small photon mass as a regulator or to apply dimensional regularization by going to $d = 4 + \varepsilon$ dimensions with an associated scale parameter μ_{IR} , which should be distinguished from the $\overline{\text{MS}}$ scale parameter μ , standing for μ_{UV} , related to the $d = 4 - \varepsilon$ expansion.

A_0 denotes the tree level amplitude, A_1 is the corresponding 1-loop virtual photon correction, which is IR singular unless we apply a soft photon infrared cutoff μ_{IR} , which may be chosen to be a tiny photon mass. Tiny means smaller than any other relevant physics scale, like the electron mass, for example. The crucial point is that the μ_{IR} -dependent IR sensitive part of the IR regularized amplitude is proportional to A_0 : $A_1 = A_0 \delta_v^{(1)}(\mu_{\text{IR}}) + \delta^{\text{fin}} A_1$, i.e. the IR dangerous part is *factorizable*, while the non-factorizable part is finite, independent of the IR regulator. The radiative amplitude splits into $B_1 = B_1^{\text{soft}}(E_\gamma < \omega) + \delta B_1^{\text{hard}}(E_\gamma \geq \omega)$ corresponding to the

$\mu\mu(\gamma)$ and $\mu\mu\gamma$ final states. The soft part includes the unresolved hidden photon $[(\gamma)]$ part, from photons too soft to be detectable, which indeed look like $\mu\mu$ “elastic event”,⁴¹ and hence is factorizable $B_1^{\text{soft}} = A_0 \rho^{\text{soft}}(\mathbf{k})$ with a soft photon radiation density $\rho^{\text{soft}}(\mathbf{k})$ (\mathbf{k} the photon momentum), which has to be integrated over and yields the bremsstrahlung correction $C_{\text{bre}}^{(1)}(\mu_{\text{IR}}, \omega)$, where $\mu_{\text{IR}} \ll \omega \ll E_{\gamma\text{max}}$ (see (2.245) for the initial state part). The soft photon integral again only exists after IR regularization, by a, relative to the virtual part, commensurate cutoff μ_{IR} . Again a tiny photon mass provides such a cutoff. The soft photon integral should include the soft photons of energy $E_\gamma < \omega \ll E_{\gamma\text{max}}$, where ω has to be chosen such that the factorization is within the numerical accuracy of the attempted calculation, ideally it can be identified with the photon detection threshold of the detector utilized to measure the cross section of the process.

In order to get the NLO correction, we have to evaluate

$$|A_0 + A_1|^2 = |A_0|^2 + A_0 A_1^* + A_1 A_0^* + \dots \simeq |A_0|^2 \cdot \left(1 + 2\text{Re} \delta_v^{(1)}(\mu_{\text{IR}})\right) + A_0 \delta A_1^* + \delta A_1 A_0^* .$$

The omitted higher order terms are to be included in the NNLO correction. These also exhibit further IR sensitive contributions, which will cancel against other NNLO IR sensitive terms. Altogether, we then get the physical “soft photon dressed” Born transition probability amplitude at NLO

$$|A_0|^2{}^{\text{dressed}} = |A_0|^2 \cdot \left(1 + 2\text{Re} \delta_v^{(1)}(\mu_{\text{IR}}) + C_{\text{bre}}^{(1)}(\mu_{\text{IR}}, \omega)\right) ,$$

in which the IR cutoff μ_{IR} cancels and the result depends on ω only. The ω dependence disappears if we include the hard photon part from $|B_1(E_\gamma \geq \omega)|^2$ as well. The total inclusive cross section, which includes non-factorizable terms as well as hard photon contributions, is a sum of a 2 to 2 and a 2 to 3 cross section, the explicit form of which is beyond the scope of this discussion (see, however, the corresponding results for the process $e^+e^- \rightarrow \pi^+\pi^-$ presented in Chap. 5, Sect. 5.1.3).

At NNLO, including the 2-loop correction A_2 the procedure follows the same line. We have to collect all $\mathcal{O}(\alpha^2)$ contributions by including real photon radiation up to two photons now. Starting from the IR regularized amplitude $A = A_0 + A_1 + A_2$, we have to include the 1-loop virtual correction to $B = B_1 + B_2$ as well as the double real photon contribution $e^+e^- \rightarrow \mu^+\mu^-\gamma\gamma$ from “undetectable” soft photons $C = C_2$. Beyond $\mu\mu$ factorizable soft photon effects in addition $\mu\mu\gamma$ factorizable soft photon effects come into play etc.

The ω -dependent virtual plus soft photon corrected Born cross section, gets negative if ω is taken too small and the order-by-order treatment breaks down as the correction blows up. The limit $\omega \rightarrow 0$ only can be taken after infinite resummation of the leading soft photon effects, the $\omega \rightarrow 0$ limit is then vanishing. The probability to find just two naked muons in the final state is zero as a charged particle constantly radiates soft photons. Here another point comes into consideration: we never measure perturbative quantities, and whether a perturbatively calculated quantity

⁴¹i.e. particle number conserving, when looked at from the crossed t -channel $e^-\mu^+ \rightarrow e^-\mu^+$.

approximates a measured object well depends on the experimental conditions. For a certain range of ω 's the prediction may well be perfect within experimental precision, while going to smaller ω 's convergence of the perturbative series breaks down. Quantities sharing such behavior are called *infrared unsafe*. Good observables preferably should be defined such that they are *infrared safe* and *collinear safe*. Infrared safe means that the quantity, in order to be a true observable, should not change discontinuously if one adds a soft particle to the final state. Similarly, collinear safe means that the quantity should not change abruptly if one splits one final state particle into two particles with equal momentum. A more concrete account will be presented in Chap. 5, Sect. 5.1.3 for the process $e^+e^- \rightarrow \pi^+\pi^-$, which plays an important role in evaluation the leading hadronic contribution to a_μ .

One more aspect has to be mentioned here: what is “detectable” is device dependent and therefore not what is of primary theoretical interest. It is therefore common practice to unfold experimental data from radiative effects. In our case, this amounts to “undress” the physical cross section, by comparison with the theoretical prediction, in order to recover the “bare” cross section as the quantity of interest. This in any case allows to extract the relevant parameters like couplings and masses which enter the undressed cross section. In many cases undressing attempts to separate for example strong interaction effects from electromagnetic ones.

Concluding remarks: we note that the problem with the non-existence of electrically charged one-particle states imply that the S -matrix in the naive LSZ sense in QED does not exist. In perturbation theory the Bloch–Nordsieck approximation and its Yennie–Frautschi–Suura improvement provides an acceptable perturbatively improvable framework for making well defined predictions which can be confronted with experimental data of a given precision. Interestingly, such infrared type problem is absent for charged particles in atoms or molecules, because radiation in bound systems is subject to quantum mechanics with a discrete spectrum and soft or collinear degeneracies of states are not an issue. For what concerns the non-Abelian part of the SM: the physical state space exhibits no other massless particle besides the photon. The weak $SU(2)$ gauge bosons get masses via the Higgs mechanism and are actually very heavy and therefore very unstable such that they never can show up as true LSZ Wigner states, because the track they leave in a real world detector is by far too short to ever be resolved as a particle track. Nevertheless the neutral Z boson shows up as a very pronounced resonance as $\Gamma_Z/M_Z \simeq 0.0274$, such that its quasi on-shell properties can be investigated very precisely, and as performed at the LEP ring at CERN at the beginning of the 90ies. This information, however is only accessible via the decay products which are seen in the detector. Similarly for the W boson, except that the W as a charged state in addition exhibits the same types of problems as the charged leptons in QED. In principle one could integrate out the W and the Z fields, which however would result in a very complicated non-local effective Lagrangian. Certainly one better sticks to the standard SM approach, treating the weak gauge bosons as quasi LSZ states, in a production and decay chain, which can be implemented order by order in perturbation theory. The strong interaction sector solves its problems with the massless gluons in its own way: by confinement. All fields in the QCD Lagrangian have no asymptotic states themselves but form color

singlet hadrons of short ranged effective interactions. For the hadrons a S -matrix is well defined, besides the issues connected with unstable particles (often due to weak and electromagnetic decays) and the problem of the electrically charged states as elaborated above.

2.7 Pions in Scalar QED and Vacuum Polarization by Vector Mesons

The strong interaction effects in $(g - 2)$ are dominated by the lightest hadrons, the isospin $SU(2)$ triplet (π^+, π^0, π^-) of pions, pseudoscalar spin 0 mesons of masses: $m_{\pi^\pm} = 139.75018(35)$ MeV, $m_{\pi^0} = 134.9766(6)$ MeV. Pions are quark-antiquark color singlet bound states $(u\bar{d}, \frac{1}{\sqrt{2}}[u\bar{u} - d\bar{d}], d\bar{u})$ and their electromagnetic interaction proceeds via the charged quarks. This is particularly pronounced in the case of the neutral π^0 which decays electromagnetically via $\pi^0 \rightarrow \gamma\gamma$ and has a much shorter life time $\tau_{\pi^0} = 8.4(6) \times 10^{-17}$ s than the charged partners which can decay by weak interaction only according to $\pi^\pm \rightarrow \mu^\pm \nu_\mu$ and hence live longer by almost 10 orders of magnitude $\tau_{\pi^\pm} = 2.6033(5) \times 10^{-8}$ s. However, at low energies, in many respects the pions behave like point particles especially what concerns soft photon emission and the Bloch-Nordsieck prescription. The effective Lagrangian for the electromagnetic interaction of a charged point-like pion described by a complex scalar field φ follows from the free Lagrangian

$$\mathcal{L}_\pi^{(0)} = (\partial_\mu \varphi)(\partial^\mu \varphi)^* - m_\pi^2 \varphi \varphi^*$$

via *minimal substitution* $\partial_\mu \varphi \rightarrow D_\mu \varphi = (\partial_\mu + ieA_\mu(x)) \varphi$ (also called *covariant derivative*), which implies the scalar QED (sQED) Lagrangian

$$\mathcal{L}_\pi^{\text{sQED}} = \mathcal{L}_\pi^{(0)} - ie(\varphi^* \partial_\mu \varphi - \varphi \partial_\mu \varphi^*) A^\mu + e^2 g_{\mu\nu} \varphi \varphi^* A^\mu A^\nu . \quad (2.256)$$

Thus gauge invariance implies that the pions must couple via two different vertices to the electromagnetic field, and the corresponding Feynman rules are given in Fig. 2.13.

- (1) Pion propagator

$$\text{O} \cdots \overset{p}{\cdots} \cdots \text{O} \quad : \quad i\Delta_\pi(p) = \frac{i}{p^2 - m_\pi^2 + i\epsilon}$$

- (2) Pion-photon vertices

$$\begin{array}{cc} \begin{array}{c} \text{A}^\mu \\ \text{wavy} \\ \text{p} \end{array} \begin{array}{c} \nearrow \varphi^+ \\ \searrow \varphi^- \end{array} & : = -ie(p + p')^\mu , & \begin{array}{c} \text{A}^\mu \\ \text{wavy} \\ \text{A}^\nu \end{array} \begin{array}{c} \nearrow \varphi^+ \\ \searrow \varphi^- \end{array} & : = 2ie^2 g^{\mu\nu} \end{array}$$

Fig. 2.13 Feynman rules for sQED. p is incoming, p' outgoing

The bound state nature of the charged pion is taken care off by introducing a pion form factor $e \rightarrow e F_\pi(q^2)$, $e^2 \rightarrow e^2 |F_\pi(q^2)|^2$.

In sQED the contribution of a pion loop to the photon VP is given by

$$-i \Pi_\gamma^{\mu\nu}(\pi)(q) = \text{diagram 1} + \text{diagram 2}$$

The bare result for the transversal part defined by (2.160) reads

$$\Pi_\gamma^{(\pi)}(q^2) = \frac{e^2}{48\pi^2} \left\{ B_0(m, m; q^2) (q^2 - 4m^2) - 4 A_0(m) - 4m^2 + \frac{2}{3}q^2 \right\} \quad (2.257)$$

with $\Pi_\gamma(0) = 0$. We again calculate the renormalized transversal self-energy $\Pi'_\gamma(q^2) = \Pi_\gamma(q^2)/q^2$ which is given by $\Pi'_{\gamma\text{ren}}(q^2) = \Pi'_\gamma(q^2) - \Pi'_\gamma(0)$. The subtraction term

$$\Pi'_{\gamma}(\pi)(0) = \frac{-e^2}{48\pi^2} \left\{ \frac{A_0(m)}{m^2} + 1 \right\}$$

is the π^\pm contribution to the photon wavefunction renormalization and the renormalized transversal photon self-energy reads

$$\Pi'_{\gamma\text{ren}}(\pi)(q^2) = \frac{\alpha}{6\pi} \left\{ \frac{1}{3} + (1-y) - (1-y)^2 G(y) \right\} \quad (2.258)$$

where $y = 4m^2/q^2$ and $G(y)$ given by (2.174). For $q^2 > 4m^2$ there is an imaginary or absorptive part given by substituting

$$G(y) \rightarrow \text{Im } G(y) = -\frac{\pi}{2\sqrt{1-y}}$$

according to (2.175)

$$\text{Im } \Pi'_{\gamma}(\pi)(q^2) = \frac{\alpha}{12} (1-y)^{3/2} \quad (2.259)$$

and for large q^2 is 1/4 of the corresponding value for a lepton (2.179). According to the *optical theorem* the absorptive part may be written in terms of the $e^+e^- \rightarrow \gamma^* \rightarrow \pi^+\pi^-$ production cross section $\sigma_{\pi^+\pi^-}(s)$ as

$$\text{Im } \Pi'_{\gamma}{}^{\text{had}}(s) = \frac{s}{4\pi\alpha} \sigma_{\text{had}}(s) \quad (2.260)$$

which hence we can read off to be

$$\sigma_{\pi^+\pi^-}(s) = \frac{\pi\alpha^2}{3s} \beta_\pi^3 \quad (2.261)$$

with $\beta_\pi = \sqrt{(1 - 4m_\pi^2/s)}$ the pion velocity in the CM frame. Often, one writes hadronic cross sections as a ratio

$$R(s) \doteq \sigma_{\text{had}}(s) / \frac{4\pi\alpha^2}{3s} \quad (2.262)$$

in units of the high energy asymptotic form of the cross section $\sigma(e^+e^- \rightarrow \gamma^* \rightarrow \mu^+\mu^-)$ for muon pair production in e^+e^- -annihilation. Given the cross section or imaginary part, conversely, the real part of the renormalized vacuum polarization function may be obtained by integrating the appropriate dispersion relation (see Sect. 3.7), which reads

$$\text{Re } \Pi'_{\gamma\text{ren}}{}^{\text{had}}(s) = \frac{s}{4\pi^2\alpha} \oint_{s_1}^{s_2} ds' \frac{\sigma_{\text{had}}(s')}{s' - s} = \frac{\alpha}{3\pi} \oint_{s_1}^{s_2} ds' \left\{ \frac{1}{s' - s} - \frac{1}{s'} \right\} R(s'). \quad (2.263)$$

This is another way, the *dispersive approach*, to get the result (2.258) via the easier to calculate imaginary part, which here is just given by the tree level cross section for $\gamma^* \rightarrow \pi^+\pi^-$.

As already mentioned, sometimes one has to resort to sQED in particular in connection with the soft photon radiation problem of charged particles, where sQED provides a good description of the problem. However, the photon vacuum polarization due to an elementary charged spin 0 pion, we just have been calculating, includes hard photons in the region of interest above the $\pi^+\pi^-$ production threshold to about 1 GeV, say. As we will see sQED in this case gives a rather bad approximation. In reality $e^+e^- \rightarrow \gamma^* \rightarrow \pi^+\pi^-$ is non-perturbative and exhibits a pronounced resonance, the neutral spin 1 meson ρ^0 , and the hadron production cross section is much better parametrized by a Breit-Wigner (BW) resonance shape. The relevant parameters are M_R the mass, Γ the width and $\Gamma_{e^+e^-}/\Gamma$ the branching fraction for $\rho \rightarrow e^+e^-$. We briefly present the different possible parametrizations and how a BW resonance contributes to the renormalized photon vacuum polarization when integrated over a range (s_1, s_2) with $4m_\pi^2 \leq s_1 < s_2 \leq \infty$ [81]:

- **Narrow width resonance**

The contribution from a zero width resonance

$$\sigma_{\text{NW}}(s) = \frac{12\pi^2}{M_R} \Gamma_{e^+e^-} \delta(s - M_R^2) \quad (2.264)$$

is given by

$$\Pi'_{\gamma\text{ren}}{}^{\text{NW}}(s) = \frac{-3\Gamma_{e^+e^-}}{\alpha M_R} \frac{s}{s - M_R^2} \quad (2.265)$$

which in the limit $|s| \gg M_R^2$ becomes

$$\Pi'_{\gamma\text{ren}}{}^{\text{NW}}(s) \simeq \frac{-3\Gamma_{e^+e^-}}{\alpha M_R} . \quad (2.266)$$

• Breit–Wigner resonance

The contribution from a classical Breit–Wigner resonance

$$\sigma_{BW}(s) = \frac{3\pi}{s} \frac{\Gamma \Gamma_{e^+e^-}}{(\sqrt{s} - M_R)^2 + \frac{\Gamma^2}{4}} \quad (2.267)$$

is given by

$$\Pi'_{\gamma\text{ren}}{}^{\text{BW}}(s) = \frac{-3\Gamma \Gamma_{e^+e^-}}{4\pi\alpha} \{I(0) - I(W)\} \quad (2.268)$$

where

$$I(W) = \frac{1}{2ic} \left\{ \frac{1}{W - M_R - ic} \left(\ln \frac{W_2 - W}{W_1 - W} - \ln \frac{W_2 - M_R - ic}{W_1 - M_R - ic} \right) - \frac{1}{W + M_R + ic} \left(\ln \frac{W_2 + W}{W_1 + W} - \ln \frac{W_2 - M_R - ic}{W_1 - M_R - ic} \right) - \text{h.c.} \right\}$$

with $c = \Gamma/2$. For $W_1 \ll M_R \ll W_2$ and $\Gamma \ll M_R$ this may be approximated by

$$\Pi'_{\gamma\text{ren}}{}^{\text{BW}}(s) \simeq \frac{-3\Gamma_{e^+e^-}}{\alpha M_R} \frac{s(s - M_R^2 + 3c^2)}{(s - M_R^2 + c^2)^2 + M_R^2 \Gamma^2} \quad (2.269)$$

which agrees with (2.265) and (2.266) in the limits $\Gamma^2 \ll |s - M_R^2|$, M_R^2 and $|s| \gg M_R^2$, respectively.

• Breit–Wigner resonance: field theory version

Finally, we consider a field theoretic form of a Breit–Wigner resonance obtained by the Dyson summation of a massive spin 1 transversal part of the propagator in the approximation that the imaginary part of the self–energy yields the width by $\text{Im}\Pi_V(M_V^2) = M_V \Gamma_V$ near resonance.

$$\sigma_{BW}(s) = \frac{12\pi}{M_R^2} \frac{\Gamma_{e^+e^-}}{\Gamma} \frac{s\Gamma^2}{(s - M_R^2)^2 + M_R^2 \Gamma^2} \quad (2.270)$$

which yields

$$\begin{aligned} \Pi'_{\gamma\text{ren}}{}^{\text{BW}}(s) = & \frac{-3\Gamma_{e^+e^-}}{\pi\alpha M_R} \frac{s(s - M_R^2 - \Gamma^2)}{(s - M_R^2)^2 + M_R^2\Gamma^2} \left\{ \left(\pi - \arctan \frac{\Gamma M_R}{s_2 - M_R^2} \right. \right. \\ & \left. \left. - \arctan \frac{\Gamma M_R}{M_R^2 - s_1} \right) - \frac{\Gamma}{M_R} \frac{s}{(s - M_R^2 - \Gamma^2)} \left(\ln \left| \frac{s_2 - s}{s_1 - s} \right| - \ln \left| \frac{s_2 - M_R^2 - iM_R\Gamma}{s_1 - M_R^2 - iM_R\Gamma} \right| \right) \right\} \end{aligned} \quad (2.271)$$

and reduces to

$$\Pi'_{\gamma\text{ren}}{}^{\text{BW}}(s) \simeq \frac{-3\Gamma_{e^+e^-}}{\alpha M_R} \frac{s(s - M_R^2 - \Gamma^2)}{(s - M_R^2)^2 + M_R^2\Gamma^2} \quad (2.272)$$

for $s_1 \ll M_R^2 \ll s_2$ and $\Gamma \ll M_R$. Again we have the known limits for small Γ and for large $|s|$.

For broad resonances the different parametrizations of the resonance in general yield very different results. Therefore, it is important to know how a resonance was parametrized to get the resonance parameters like M_R and Γ . For narrow resonances, which we will have to deal with later, results are not affected in a relevant way by using different parametrizations. A finite width BW resonance is related to the NW resonance via identity

$$\delta(s - M^2) = \frac{1}{\pi} \lim_{\gamma \rightarrow 0} \frac{\gamma}{(s - M^2)^2 + \gamma^2} \quad (2.273)$$

with $\gamma = \Gamma M$. Note that for the broad non-relativistic ρ meson only the classical BW parametrization works. In fact, due to isospin breaking of the strong interactions ($m_d - m_u$ mass difference as well as electromagnetic effects $Q_u = 2/3 \neq Q_d = -1/3$) the ρ and ω mix and more sophisticated parametrizations must be applied, like the Gounaris-Sakurai (GS) parametrization [82] based on the vector meson dominance (VMD) model (see Sect. 5.2). Actually, the GS model is missing to take into account $\rho^0 - \gamma$ mixing and it is not electromagnetically gauge invariant and therefore should be replaced by a manifestly gauge invariant VMD (so called type II) plus sQED Lagrangian approach [83]. For the strong interaction part (undressed from electromagnetic effects) most appropriate is a parametrization which relies on first principle concepts only, the description by unitarity, analyticity and constrained by chiral perturbation theory (CHPT), which is the low energy effective form of QCD (see [84] and references therein).

We will use the results presented here later for the evaluation of the contributions to $g-2$ from hadron-resonances. In e^+e^- -annihilation a large number of resonances, like ρ , ω , ϕ , J/ψ series and the Υ series, show up and will have to be taken into account.

2.8 Note on QCD: The Feynman Rules and the Renormalization Group

Quantum Chromodynamics, the modern theory of the strong interactions, is a non-Abelian gauge theory with gauge group $SU(3)_c$ consisting of unitary 3×3 matrices of determinant unity. The corresponding internal degrees of freedom are called *color*. The generators are given by the basis of Hermitian traceless 3×3 matrices T_i , $i = 1, \dots, 8$. Quarks transform under the fundamental 3-dimensional representation 3 (quark triplets) antiquarks under the complex conjugate 3^* (antiquark anti-triplets). The requirement of local gauge invariance with respect to $SU(3)_c$ transformations implies that quark fields $\psi_i(x)$ must couple to an octet of gauge fields, the gluon fields $G_{\mu j}$, $j = 1, \dots, 8$, and together with the requirement of renormalizability this fixes the form of the interactions of the quarks completely: in the free quark Dirac-Lagrangian we have to replace the derivative by the *covariant derivative*

$$\partial_\mu \psi(x) \rightarrow D_\mu \psi(x), \quad (D_\mu)_{ik} = \partial_\mu \delta_{ik} - i g_s \sum_j (T_j)_{ik} G_{\mu j}(x) \quad (2.274)$$

where g_s is the $SU(3)_c$ gauge coupling constant. The dynamics of the gluon fields is controlled by the non-Abelian *field strength tensor*

$$G_{\mu\nu i} = \partial_\mu G_{\nu i} - \partial_\nu G_{\mu i} + g_s c_{ijk} G_{\mu j} G_{\nu k} \quad (2.275)$$

where c_{ijk} are the $SU(3)$ structure constants obtained from the commutator of the generators $[T_i, T_j] = i c_{ijk} T_k$. The locally gauge invariant Lagrangian density is then given by

$$\mathcal{L}_{\text{inv}} = -\frac{1}{4} \sum_i G_{i\mu\nu} G_i^{\mu\nu} + \bar{\psi} (i \gamma^\mu D_\mu - m) \psi. \quad (2.276)$$

We split \mathcal{L}_{inv} into a free part \mathcal{L}_0 and an interaction part \mathcal{L}_{int} which is taken into account as a formal power series expansion in the gauge coupling g_s . The perturbation expansion is an expansion in terms of the free fields described by \mathcal{L}_0 . The basic problem of quantizing massless spin 1 fields is familiar from QED. Since \mathcal{L}_{YM} is gauge invariant, the gauge potentials $G_{i\mu}$ cannot be uniquely determined from the gauge invariant field equations. Again one has to break the gauge invariance, now, for a $SU(n)$ gauge group, by a sum of $r = n^2 - 1$ gauge fixing conditions

$$C_i(G) = 0, \quad i = 1, \dots, r.$$

It is known from QED that the only relativistically invariant condition linear in the gauge potential which we can write is the Lorentz condition. Correspondingly we require

$$C_i(G) = -\partial_\mu G_i^\mu(x) = 0, \quad i = 1, \dots, r. \quad (2.277)$$

It should be stressed that a covariant formulation is mandatory for calculations beyond the tree level. We are thus lead to break the gauge invariance of the Lagrangian by adding the **gauge fixing** term

$$\mathcal{L}_{\text{GF}} = -\frac{1}{2\xi} \sum_i (\partial_\mu G_i^\mu(x))^2 \quad (2.278)$$

with ξ a free gauge parameter. Together with the term \mathcal{L}_0^G from \mathcal{L}_{inv} we obtain for the bilinear gauge field part

$$\mathcal{L}_{0,i}^{G,\xi} = -\frac{1}{4} (\partial_\mu G_{i\nu} - \partial_\nu G_{i\mu})^2 - \frac{1}{2\xi} (\partial_\mu G_i^\mu(x))^2 \quad (2.279)$$

which now uniquely determines a free gauge field propagator. Unlike in QED, however, \mathcal{L}_{GF} breaks local gauge invariance explicitly and one has to restore gauge invariance by a compensating **Faddeev-Popov term** (Faddeev and Popov 1967). The Faddeev-Popov trick consists in adding further charged ghost fields $\bar{\eta}_i(x)$ and $\eta_i(x)$, the so called **Faddeev-Popov ghosts**, which conspire with the other ghosts in such a way that physical matrix elements remain gauge invariant. Unitarity and renormalizability are then restored. The FP-ghosts must be **massless spin 0 fermions**. For the unphysical ghosts this wrong spin-statistics assignment is no obstacle. The Faddeev-Popov term must be of the form

$$\mathcal{L}_{\text{FP}} = \bar{\eta}_i(x) M_{ik} \eta_k(x)$$

where

$$\begin{aligned} M_{ik} &= \frac{\partial C_i(G)}{\partial G_{j\mu}(x)} (D_\mu)_{jk} = -\partial^\mu (\partial_\mu \delta_{ik} - g c_{ikj} G_{j\mu}(x)) \\ &= -\square \delta_{ik} + g c_{ikj} G_{j\mu}(x) \partial^\mu + g c_{ikj} (\partial^\mu G_{j\mu}(x)) \quad . \end{aligned}$$

By partial integration of $S_{FP} = \int d^4x \mathcal{L}_{\text{FP}}(x)$ we may write

$$\mathcal{L}_{\text{FP}} = \partial_\mu \bar{\eta}_i \partial^\mu \eta_i - g c_{ikj} (\partial^\mu \bar{\eta}_i) C_{j\mu} \eta_k \quad (2.280)$$

which describes massless scalar fermions in interaction with the gauge fields. The complete Lagrangian for a quantized Yang-Mills theory is

$$\mathcal{L}_{\text{eff}} = \mathcal{L}_{\text{inv}} + \mathcal{L}_{\text{GF}} + \mathcal{L}_{\text{FP}} \quad . \quad (2.281)$$

The free (bilinear) part

$$\mathcal{L}_0 = \mathcal{L}_0(G) + \mathcal{L}_0(\psi) + \mathcal{L}_0(\eta)$$

with

$$\begin{aligned}\mathcal{L}_0(G) &= \frac{1}{2} G_{i\mu} \left[\left(\square g^{\mu\nu} - \left(1 - \frac{1}{\xi} \right) \partial^\mu \partial^\nu \right) \delta_{ik} \right] G_{k\nu} \\ \mathcal{L}_0(\psi) &= \bar{\psi}_{\alpha a} \left[\left((i\gamma^\mu)_{\alpha\beta} \partial_\mu - m \delta_{\alpha\beta} \right) \delta_{ab} \right] \psi_{\beta b} \\ \mathcal{L}_0(\eta) &= \bar{\eta}_i \left[(-\square) \delta_{ik} \right] \eta_k\end{aligned}$$

determines the free propagators, the differential operators in the square brackets being the inverses of the propagators. By Fourier transformation the free propagators are obtained in algebraic form (i.e. the differential operators are represented by c–numbers) in momentum space. Inverting these c–number matrices we obtain the results depicted in Fig. 2.14.

The interaction part of the Lagrangian is given by

$$\begin{aligned}\mathcal{L}_{\text{int}} &= g_s \bar{\psi} \gamma^\mu T_i \psi G_{i\mu} - \frac{1}{2} g_s c_{ikl} \left(\partial^\mu G_i^\nu - \partial^\nu G_i^\mu \right) G_{k\mu} G_{l\nu} \\ &\quad - \frac{1}{4} g_s^2 c_{ikl} c_{ik'l'} G_k^\mu G_l^\nu G_{k'\mu} G_{l'\nu} - g_s c_{ikj} \left(\partial^\mu \bar{\eta}_i \right) G_{j\mu} \eta_k\end{aligned}\quad (2.282)$$

with a single coupling constant g_s for the four different types of vertices.

While the formal argumentation which leads to the construction of local gauge theories looks not too different for Abelian and non–Abelian gauge groups, the physical consequences are very different and could not be more dramatic: in contrast to Abelian theories where the gauge field is neutral and exhibits no self–interaction, non–Abelian gauge fields necessarily carry non–Abelian charge and must be self–interacting. These Yang–Mills self–interactions are responsible for the *anti–screening* of the non–Abelian charge, known as *asymptotic freedom* (AF) (see end of section). It implies that the strong interaction force gets weaker the higher the energy, or equivalently, the shorter the distance. While it appears most natural to us that particles interact the less the farther apart they are, non–Abelian forces share the opposite property, the forces get the stronger the farther away we try to separate the quarks. In QCD this leads to the *confinement* of the constituents within hadrons. The latter being quark bound states which can never be broken up into free constituents. This makes QCD an intrinsically non–perturbative theory, the fields in the Lagrangian, quarks and gluons, never appear in scattering states, which define the physical state space and the S –matrix. QED is very different, it has a perturbative S –matrix, its proper definition being complicated by the existence of the long range Coulomb forces (see Sect. 2.6.6 above). Nevertheless, the fields in the QED Lagrangian as interpolating fields are closely related to the physical states, the photons and leptons. This extends to the electroweak SM, where the weak non–Abelian gauge bosons, the W^\pm and the Z particles, become massive as a consequence of the breakdown of the $SU(2)_L$ gauge symmetry by the Higgs mechanism. Also the weak gauge bosons cannot be seen as scattering states in a detector, but this time because of their very short lifetime.

are symmetric quark – antiquark states

$$\mathcal{M} = \sum_{ik} \delta^{ik} (q_i \bar{q}_k) \quad (2.283)$$

and have baryon number $B = 0$. Baryons (like proton (uud) and neutron (ddu)) are antisymmetric three quark states

$$\mathcal{B} = \sum_{ikl} \varepsilon^{ikl} (q_i q_k q_l) \quad (2.284)$$

and have baryon number $B = 1$. Sums are over color indices. The quarks (u, d, s) are in the fundamental representation 3, the antiquarks ($\bar{u}, \bar{d}, \bar{s}$) in the representation 3^* of the color $SU(3)_c$. First principles calculations of the spectrum and properties of hadrons are possible only by non-perturbative methods as lattice QCD because the theory is strongly coupled at low energies. Here we are interested primarily in the spectrum of light hadrons, which is accessible to a different non-perturbative approach: chiral perturbation theory, which exploits the symmetries of the QCD Lagrangian. As the three light flavors the u, d and s quarks are much lighter than the c, b and t quarks the chiral limit of vanishing light quark masses $m_u = m_d = m_s = 0$ is a good approximation for setting up a perturbative chiral expansion, with momenta and light quark masses as expansion parameters. The QCD Hamiltonian then commutes with the global chiral flavor group

$$U(3)_L \otimes U(3)_R \sim SU(3)_L \otimes SU(3)_R \otimes U(1)_V \otimes \cancel{U(1)}_A$$

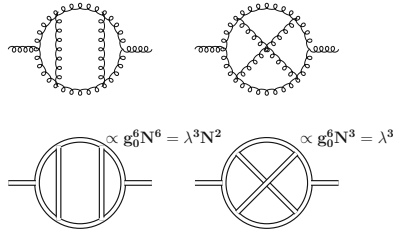
of the left and right handed massless quark fields, i.e. QCD exhibits *chiral symmetry* broken softly by small quark masses. The chiral group $SU(3)_L \otimes SU(3)_R$ is equivalent to $SU(3)_V \otimes SU(3)_A$ of which the axial $SU(N_f)_A$ subgroup turns out to be broken spontaneously in nature. In the isospin limit $N_f = 2, m_u = m_d = 0$, this implies the existence of a triplet of massless pions (Nambu-Goldstone bosons) and in the $SU(3)$ limit $m_u = m_d = m_s = 0$, the existence of an octet of massless pseudoscalars, the pions, Kaons and the η meson [87]. The $U(1)_V$ symmetry is exact beyond the chiral approximation and is responsible for *baryon number conservation*, which in particular guarantees the stability of the proton, whereas in contrast $U(1)_A$ is always broken by quantum corrections, the *Adler-Bell-Jackiw anomaly* (see p. 299 below).

A second approach to learn about the hadron spectrum is to consider QCD from the point of view of the large- N_c limit, i.e. $SU(N_c)$ non-Abelian gauge theory where the number of colors goes to infinity as a starting point and use $1/N_c$ as an expansion parameter. The $1/N_c$ expansion provides counting rules for hadronic processes. In large- N_c QCD [88–90] all hadrons become infinitely narrow, since all widths are suppressed by powers of $1/N_c$, and the VMD model becomes exact with an infinite number of narrow vector meson states, the lowest states corresponding to $\rho, \omega, \phi \dots$

According to 't Hooft 1974 a $SU(N_c)$ generalization of QCD exhibits amplitudes

$$\mathcal{A} \propto (g_0^2 N_c)^F [(g_0^2 N_c)^{-1} N_c]^{2-2H} \xrightarrow{\lambda=g_0^2 N_c \text{ fixed}} \mathcal{A} \propto N_c^{2-2H}$$

where $\chi_E = 2 - 2H - B$ is the Euler characteristic and depends only on the topology of the graph, with H the number of handles and B the number of boundaries (or holes). A trick allows to visualize the topological genus of $SU(N_c)$ Yang-Mills theory by replacing a gluon line by a pair of quark anti-quark lines as illustrated in the figure:



The first planar graph grows with N_c^2 , the second non-planar one remains constant. A closed quark loop is a boundary and brings a $1/N_c$. Each vertex has a factor N_c , each propagator a factor $1/N_c$ and each color index loop gives an extra factor N_c as it represents a sum over N_c colored copies.

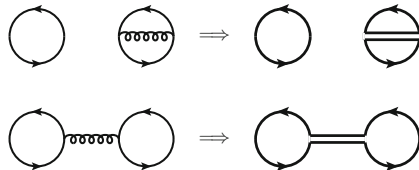
For finite and large N_c , planar diagrams dominate the dynamics. Each quark loop is suppressed by one factor of $1/N_c$ and non-planar gluon exchange is suppressed by two factors of $1/N_c$.

Some consequences of the large- N_c counting rules:

- Only planar diagrams ($H = 0$) dominate in the large- N_c limit.
- Quark loop effects are suppressed by $1/N_c$
- Phenomenology: theory of stable non-interacting mesons, the η' meson mass, OZI rule, etc. find simpler explanations
- Factorization for correlators of gauge invariant operators

$$\langle O_1 \cdots O_n \rangle = \langle O_1 \rangle \cdots \langle O_n \rangle + O(1/N_c^2)$$

follows from large- N_c counting rules order by order in perturbation theory:



The planar approximation contains no quark-anti-quark pair creation and annihilation and thus has the symmetry $U(1)_{q_i} \otimes U(1)_{\bar{q}_i}$, which allows to transform

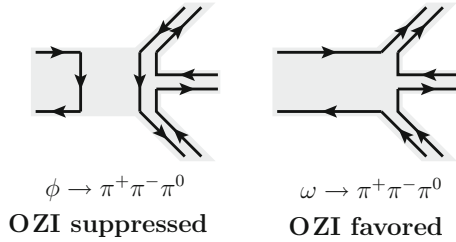


Fig. 2.15 Quark flavor disconnected processes are suppressed relative to quark flavor connected processes. As ϕ is essentially a pure $s\bar{s}$ state and the final states is made of u and d quarks only the process can only be mediated by gluon exchange. For the ω quark flavors are preserved. The *gray* shading indicates gluonic dressing

locally each quark and each anti-quark separately, which implies the conservation of each quark flavor and each anti-quark flavor light or heavy. Another important consequence of the planar flavor symmetry include the Okubo-Zweig-Iizuka (OZI) rule [91]⁴² (see Fig. 2.15 and the formation of ideally mixed meson nonets (in the $SU(3)$ flavor limit) at leading order in $1/N_c$). The η' is then the ninth pseudoscalar which would be massless in the chiral limit. Planar flavor symmetry is often called *nonet symmetry*.

The combined use of chiral perturbation theory and the $1/N_c$ expansion can constrain the low-energy interactions of hadrons with the pion nonet π , K , η and η' more effectively than either method alone. For later reference we remind the meson composition here. They are the $\bar{q}q'$ bound states, differing by flavor composition and spin. A $\bar{q}q'$ state with orbital angular momentum L has Parity $P = (-1)^{L+1}$. For $q' = q$ we have a $\bar{q}q$ bound state which is also an eigenstate of charge conjugation C with $C = (-1)^{L+S}$, where S is the spin 0 or 1. The $L = 0$ states are the pseudoscalar mesons, $J^P = 0^-$, and the vectors mesons, $J^P = 1^-$.

In the limit of exact $SU(3)$ the pure states would read

$$\pi^0 = (\bar{u}u - \bar{d}d)/\sqrt{2}; \quad \eta_1 = (\bar{u}u + \bar{d}d + \bar{s}s)/\sqrt{3}; \quad \eta_8 = (\bar{u}u + \bar{d}d - 2\bar{s}s)/\sqrt{6}, \quad (2.285)$$

$$\rho^0 = (\bar{u}u - \bar{d}d)/\sqrt{2}; \quad \omega_1 = (\bar{u}u + \bar{d}d + \bar{s}s)/\sqrt{3}; \quad \omega_8 = (\bar{u}u + \bar{d}d - 2\bar{s}s)/\sqrt{6}. \quad (2.286)$$

In fact $SU(2)_{\text{flavor}}$ breaking by the quark mass difference $m_d - m_u$ leads to $\rho - \omega$ -mixing [mixing angle $\sim 10^\circ$] (Glashow 1961) [92]:

⁴²This basically says that diagrams that destroy the initial quark and antiquark are strongly suppressed with respect to those that do not. As an example, while $\phi \rightarrow \pi^+ \pi^-$ is “Zweig” forbidden, $\rho^0 \rightarrow \pi^+ \pi^-$ is allowed.

$$\begin{aligned}\rho^0 &= \cos \theta \rho' + \sin \theta \omega' \\ \omega &= -\sin \theta \rho' + \cos \theta \omega'\end{aligned}\quad (2.287)$$

Similarly, the substantially larger $SU(3)_{\text{flavor}}$ breaking by the quark masses, leads to large $\omega - \phi$ -mixing [mixing angle $\sim 36^\circ$ close to so called ideal mixing where $\phi \sim$ is a pure $\bar{s}s$ state] (Okubo 1963) [93]:

$$\begin{aligned}\phi &= \cos \theta \omega_8 + \sin \theta \omega_1 \\ \omega &= -\sin \theta \omega_8 + \cos \theta \omega_1\end{aligned}\quad (2.288)$$

The angle in case of *ideal* mixing is given by $\tan \theta = 1/\sqrt{2}$ or $\theta = 35.3^\circ$.

In the isospin limit and in absence of e.m. interaction the pion triplet (π^+ , π^0 , π^-) exhibits G-parity as a symmetry. It represents a generalization of charge conjugation (C-parity) to strong interactions. The strong interaction does not distinguish the charges of the pions, therefore a rotation by 180° about the 3rd axis in isospin space $\mathcal{G} = \exp i \pi I_3$, which rotates $\pi^\pm \leftrightarrow \pi^\mp$ up to a phase, does not change the triplet field modulo a phase $\eta_G = \pm 1$. For particles (u, d mesons) of isospin I , the G-parity number is given by $G = (-1)^I C$, where C is the charge conjugation number of the neutral member of the multiplet. As π^0 has charge conjugation parity $C = +1$ the e.m. decay $\pi^0 \rightarrow \gamma\gamma$ requires $G_{\pi^0} = -1$ and thus also $G|\pi^\pm\rangle = -|\pi^\pm\rangle$ while $C|\pi^\pm\rangle = -|\pi^\mp\rangle$. Therefore, non-electromagnetic decays of flavor $SU(2)$ resonances in the isospin limit can decay either into an even or an odd number of pions only: $\rho^0 (I = 1) \rightarrow 2\pi$, $\omega (I = 0) \rightarrow 3\pi$. As isospin is broken by the small quark mass difference $m_d \neq m_u$ actually π^\pm and π^0 have different masses and G-parity is broken accordingly, and $\omega \rightarrow 2\pi$ is allowed with a small branching fraction.

The RG of QCD in Short

The renormalization group, introduced in Sect. 2.6.5, for QCD plays a particularly important role for a quantitative understanding of AF as well as a tool for improving the convergence of the perturbative expansion [36, 94]. For QCD the RG is given by

$$\begin{aligned}\mu \frac{d}{d\mu} g_s(\mu) &= \beta(g_s(\mu)) \\ \mu \frac{d}{d\mu} m_i(\mu) &= -\gamma(g_s(\mu)) m_i(\mu)\end{aligned}\quad (2.289)$$

with

$$\begin{aligned}\beta(g) &= -\beta_0 \frac{g^3}{16\pi^2} - \beta_1 \frac{g^5}{(16\pi^2)^2} + O(g^7) \\ \gamma(g) &= \gamma_0 \frac{g^2}{4\pi^2} + \gamma_1 \frac{g^4}{(4\pi^2)^2} + O(g^6)\end{aligned}\quad (2.290)$$

where, in the $\overline{\text{MS}}$ scheme (Sect. 2.5.6),

$$\begin{aligned}\beta_0 &= 11 - \frac{2}{3}N_f ; \gamma_0 = 2 \\ \beta_1 &= 102 - \frac{38}{3}N_f ; \gamma_1 = \frac{101}{12} - \frac{5}{18}N_f\end{aligned}\quad (2.291)$$

and N_f is the number of quark flavors. The RG for QCD is known to 5 loops [95–97]. It allows one to define effective parameters in QCD, which incorporate the summation of leading logarithmic (1-loop), next-to-leading logarithmic (2-loop), ... corrections (RG improved perturbation theory). The solution of (2.289) for the running coupling constant $\alpha_s(\mu) = g_s^2(\mu)/(4\pi)$ yields (see (2.223))

$$\begin{aligned}\frac{4\pi}{\beta_0\alpha_s(\mu)} - \frac{\beta_1}{\beta_0^2} \ln\left(\frac{4\pi}{\beta_0\alpha_s(\mu)} + \frac{\beta_1}{\beta_0^2}\right) = \\ \ln \mu^2/\mu_0^2 + \frac{4\pi}{\beta_0\alpha_s(\mu_0)} - \frac{\beta_1}{\beta_0^2} \ln\left(\frac{4\pi}{\beta_0\alpha_s(\mu_0)} + \frac{\beta_1}{\beta_0^2}\right) \equiv \ln \mu^2/\Lambda^2\end{aligned}\quad (2.292)$$

with reference scale (integration constant)

$$\Lambda_{\text{QCD}} = \Lambda_{\overline{\text{MS}}}^{(N_f)} = \mu \exp\left\{-\frac{4\pi}{2\beta_0\alpha_s(\mu)}\left(1 + \frac{\alpha_s(\mu)}{4\pi} \frac{\beta_1}{\beta_0} \ln \frac{\beta_0\alpha_s(\mu)}{4\pi + \frac{\beta_1}{\beta_0}\alpha_s(\mu)}\right)\right\}\quad (2.293)$$

which can be shown easily to be independent of the reference scale μ . It is RG invariant

$$\mu \frac{d}{d\mu} \Lambda_{\text{QCD}} = 0 ,$$

and thus QCD has its own intrinsic scale Λ_{QCD} which is related directly to the coupling strength (dimensional transmutation). This is most obvious at the one-loop level where we have the simple relation

$$\alpha_s(\mu) = \frac{1}{\frac{\beta_0}{4\pi} \ln \frac{\mu^2}{\Lambda^2}} .\quad (2.294)$$

Thus Λ_{QCD} incorporates the reference coupling $\alpha_s(\mu_0)$ measured at scale μ_0 in a scale invariant manner, i.e., each experiment measures the same Λ_{QCD} irrespective of the reference energy μ_0 at which the measurement of $\alpha_s(\mu_0)$ is performed.

The solution of (2.289) for the effective masses $m_i(\mu)$ reads (see (2.224))

$$m_i(\mu) = m_i(\mu_0) \frac{r(\mu)}{r(\mu_0)} \equiv \bar{m}_i r(\mu)\quad (2.295)$$

with

$$r(\mu) = \exp -2 \left\{ \frac{\gamma_0}{\beta_0} \ln \frac{4\pi}{\beta_0 \alpha_s(\mu)} + \left(\frac{\gamma_0}{\beta_0} - \frac{4\gamma_1}{\beta_1} \right) \ln \left(1 + \frac{\beta_1}{\beta_0} \frac{\alpha_s(\mu)}{4\pi} \right) \right\}. \quad (2.296)$$

Note that also the \bar{m}_i are RG invariant masses (integration constants) and for the masses play a role similar to Λ_{QCD} for the coupling. The solution of the RG equation may be expanded in the large $\log L \equiv \ln \frac{\mu^2}{\Lambda^2}$, which of course only makes sense if L is large ($\mu \gg \Lambda$),

$$\begin{aligned} \alpha_s(\mu) &= \frac{4\pi}{\beta_0 L} \left(1 - \frac{\beta_1}{\beta_0^2} \frac{\ln(L + \frac{\beta_1}{\beta_0^2})}{L} + \dots \right) \\ m_i(\mu) &= \bar{m}_i \left(\frac{L}{2} \right)^{-\frac{\gamma_0}{\beta_0}} \left(1 - \frac{2\beta_1\gamma_0}{\beta_0^3} \frac{\ln L + 1}{L} + \frac{8\gamma_1}{\beta_0^2 L} + \dots \right). \end{aligned} \quad (2.297)$$

If L is not large one should solve (2.292) or its higher order version numerically by iteration for $\alpha_s(\mu)$. For the experimental proof of the running of the strong coupling constant [98] see Fig. 3.3 in Sect. 3.2.1 and the most actual update presented in Fig. 9.3 in [99]. The non-perturbative calculations in lattice QCD are able to demonstrate a surprisingly good agreement with perturbative results (see [100–103] and references therein). Most interestingly the non-perturbative strong coupling persists being monotonically increasing at very low scales, in clear contrast to speculations about a possible IR freezing $\lim_{\mu \rightarrow 0} \alpha_s(\mu) \rightarrow \text{const}$.

Note on the RG of the SM

The electroweak sector of the SM will be introduced in Sect. 4.2. But a comment on the RG of the full SM is in order here. After the discovery of the Higgs boson all SM couplings are known via the mass–coupling relations (4.46) and so are the β -functions. The main couplings are the gauge couplings of the SM local gauge group $SU(3)_c \otimes SU(2)_L \otimes U(1)_Y$: g_1 , g_2 and g_3 and the top quark Yukawa coupling y_t and the Higgs boson self-coupling λ . The SM renormalization group in the $\overline{\text{MS}}$ scheme is known to three loops. The key point concerning the behavior of the effective parameters we may understand when we look at the leading terms of the β -functions. At the Z boson mass scale the couplings are given by $g_1 \simeq 0.350$, $g_2 \simeq 0.653$, $g_3 \simeq 1.220$, $y_t \simeq 0.935$ and $\lambda \simeq 0.807$. While the gauge couplings behave as expected, g_1 is infrared (IR) free, g_2 and g_3 are asymptotically (ultraviolet) free (AF), with leading coefficients exhibiting the related coupling only,

$$\beta_1 = \frac{41}{6} g_1^3 c \simeq 0.00185; \quad \beta_2 = -\frac{19}{6} g_2^2 c \simeq -0.00558; \quad \beta_3 = -7 g_3^3 c \simeq -0.08049,$$

with $c = \frac{1}{16\pi^2}$, the leading top Yukawa β -function given by

$$\begin{aligned}
\beta_{y_t} &= \left(\frac{9}{2} y_t^3 - \frac{17}{12} g_1^2 y_t - \frac{9}{4} g_2^2 y_t - 8 g_3^2 y_t \right) c \\
&\simeq 0.02327 - 0.00103 - 0.00568 - 0.07048 \\
&\simeq -0.05391
\end{aligned}$$

not only depends on y_t , but also on mixed terms with the gauge couplings which have a negative sign. In fact the QCD correction is the leading contribution and determines the behavior. Notice the critical balance between the dominant strong and the top Yukawa couplings: QCD dominance requires $g_3 > \frac{3}{4} y_t$ in the “gaugeless” limit $g_1 = g_2 = 0$.

Similarly, the β -function of the Higgs self-coupling, given by

$$\begin{aligned}
\beta_\lambda &= (4 \lambda^2 - 3 g_1^2 \lambda - 9 \lambda g_2^2 + 12 y_t^2 \lambda + \frac{9}{4} g_1^4 + \frac{9}{2} g_1^2 g_2^2 + \frac{27}{4} g_2^4 - 36 y_t^4) c \\
&\simeq 0.01650 - 0.00187 - 0.01961 + 0.05358 + 0.00021 + 0.00149 + 0.00777 \\
&\quad - 0.17401 \simeq -0.11595
\end{aligned}$$

is dominated by the top Yukawa contribution and not by the λ coupling itself. At leading order it is not subject to QCD corrections. Here, the y_t dominance condition reads $\lambda < \frac{3(\sqrt{5}-1)}{2} y_t^2$ in the gaugeless limit. The top Yukawa coupling is turned from an intrinsically IR free to an AF coupling by the QCD term and similarly the Higgs self-coupling is transmuted from IR free to AF by the dominating top Yukawa term. Including known higher order terms, except from β_λ , which exhibits a zero at about $\mu_\lambda \sim 10^{17}$ GeV, all other β -functions do not exhibit a zero in the range from $\mu = M_Z$ to $\mu = M_{\text{Planck}}$. So, apart from the $U(1)_Y$ coupling g_1 , which increases moderately only, all other couplings decrease and perturbation theory works well up to the Planck scale. Actually, at $\mu = M_{\text{Planck}}$ gauge couplings are all close to $g_i \sim 0.5$, while $y_t \sim 0.35$ and $\sqrt{\lambda} \sim 0.36$ (see [104] and references therein).

References

1. J.D. Bjorken, S.D. Drell, *Relativistic Quantum Mechanics*, 1st edn. (McGraw-Hill, New York 1964), 300 p; *Relativistic Quantum Fields*, 1st edn. (McGraw-Hill, New York, 1965), 396 p
2. V.B. Berestetskii, E.M. Lifshitz, L.P. Pitaevskii, Quantum electrodynamics, *Landau and Lifshitz Course of Theoretical Physics*, vol. 4, 2nd edn. (Pergamon, London, 1982), 652 p
3. P.A.M. Dirac, Proc. R. Soc. A **114**, 243 (1927); Proc. R. Soc. A **126**, 360 (1930); Proc. R. Soc. A **136**, 453 (1932)
4. E.P. Wigner, Ann. Math. **40**, 149 (1939)
5. P. Jordan, E.P. Wigner, Zeits. Phys. **47**, 631 (1928)
6. W. Heisenberg, W. Pauli, Zeits. Phys. **56**, 1 (1929); Zeits. Phys. **59**, 168 (1930); P.A.M. Dirac, V.A. Fock, B. Podolsky, Phys. Zeits. Sowjetunion **3**, 64 (1932)
7. H. Joos, Fortsch. Phys. **10**, 65 (1962); S. Weinberg, Phys. Rev. **133**, B1318 (1964); Phys. Rev. **134**, B882 (1964)
8. P.A.M. Dirac, Proc. R. Soc. A **114**, 243 (1927); A **117**, 610 (1928)
9. W. Pauli, Zeits. Physik **31**, 765 (1925)

10. W. Pauli, Phys. Rev. **58**, 716 (1940)
11. R.F. Streater, A.S. Wightman, *CPT, Spin and Statistics and All That* (Benjamin, New York, 1964)
12. G. Lüders, K. Danske Vidensk. Selsk. Mat.-Fys. Medd. **28**(5) (1954); W. Pauli, Exclusion principle, Lorentz group and reflection of space-time and charge, in *Niels Bohr and the Development of Physics*, ed. by W. Pauli (Pergamon Press, London, 1955, reissued 1962), pp. 30–51; W. Pauli, II Nuovo Cim. **6**, 204 (1957); G. Lüders, Ann. Phys. N. Y. **2**, 1 (1957); G. Lüders, B. Zumino, Phys. Rev. **106**, 345 (1957); R. Jost, Helv. Phys. Acta **30**, 409 (1957)
13. S. Gasiorovicz, *Elementary Particle Physics* (Wiley, New York, 1966)
14. S. Eidelman et al. [Particle Data Group], Phys. Lett. B **592**, 1 (2004); K.A. Olive et al. [Particle Data Group], Chin. Phys. C **38**, 090001 (2014) and 2015 update
15. B.C. Regan, E.D. Commins, C.J. Schmidt, D. DeMille, Phys. Rev. Lett. **88**, 071805 (2002)
16. J. Baron et al. [ACME Collab.], Science **343**, 269 (2014)
17. W. Gerlach, O. Stern, Zeits. Physik **8**, 110 (1924)
18. R. Kronig (1925 unpublished), https://en.wikipedia.org/wiki/Ralph_Kronig
19. G.E. Uhlenbeck, S. Goudsmit, Naturwissenschaften **13**, 953 (1925); Nature **117**, 264 (1926)
20. W. Pauli, Zeits. Phys. **43**, 601 (1927)
21. F. Englert, R. Brout, Phys. Rev. Lett. **13**, 321 (1964)
22. P.W. Higgs, Phys. Lett. **12**, 132 (1964)
23. G. Aad et al. [ATLAS Collab.], Phys. Lett. B **716**, 1 (2012); Science **338**, 1576 (2012)
24. S. Chatrchyan et al. [CMS Collab.], Phys. Lett. B **716**, 30 (2012); Science **338**, 1569 (2012)
25. S. Weinberg, Phys. Rev. **134**, B882 (1964)
26. R. Frisch, O. Stern, Zeits. Physik **85**, 4 (1933); I. Estermann, O. Stern, *ibid.* **85**, 17 (1933)
27. G. Charpak, F.J.M. Farley, R.L. Garwin, T. Muller, J.C. Sens, A. Zichichi, Phys. Lett. **1B**, 16 (1962)
28. H. Weyl, Zeits. Phys. **56**, 330 (1929)
29. C.N. Yang, R.L. Mills, Phys. Rev. **96**, 191 (1954)
30. M. Gell-Mann, F. Low, Phys. Rev. **95**, 1300 (1954)
31. G.C. Wick, Phys. Rev. **80**, 268 (1950)
32. W. Pauli, F. Villars, Rev. Mod. Phys. **21**, 434 (1949)
33. N.N. Bogoliubov, D.V. Shirkov, *Introduction to the Theory of Quantized Fields*, 1st & 2nd edn. (Wiley, New York, 1957, 1980), 720 p
34. S. Tomonaga, R. Iho, Progr. Theor. Phys. **1**, 27 (1946); J. Schwinger, Phys. Rev. **74**, 1439 (1948); R.P. Feynman, Phys. Rev. **76**, 749 (1949); F. Dyson, Phys. Rev. **75**, 486 (1949), *ibid.* 1736
35. H. Fritzsch, M. Gell-Mann, H. Leutwyler, Phys. Lett. **47B**, 365 (1973)
36. H.D. Politzer, Phys. Rev. Lett. **30**, 1346 (1973); D. Gross, F. Wilczek, Phys. Rev. Lett. **30**, 1343 (1973)
37. S.L. Glashow, Nucl. Phys. B **22**, 579 (1961); S. Weinberg, Phys. Rev. Lett. **19**, 1264 (1967); A. Salam, Weak and electromagnetic interactions, in *Elementary Particle Theory*, ed. by N. Svartholm (Amquist and Wiksells, Stockholm, 1969), pp. 367–377
38. G. 't Hooft, Nucl. Phys. B **33**, 173 (1971); **35**, 167 (1971); G. 't Hooft, M. Veltman, Nucl. Phys. B **50**, 318 (1972)
39. G. 't Hooft, M. Veltman, Nucl. Phys. B **44**, 189 (1972)
40. W.H. Furry, Phys. Rev. **51**, 125 (1937)
41. F. Dyson, Phys. Rev. **75**, 1736 (1949); J.S. Schwinger, Proc. Nat. Acad. Sci. **37**, 452–459 (1951)
42. H. Lehmann, K. Symanzik, W. Zimmermann, Nuovo Cim. **1**, 205 (1955); Nuovo Cim. **6**, 319 (1957)
43. S. Mandelstam, Phys. Rev. **112**, 1344 (1958)
44. I. Białyński-Birula, Phys. Rev. D **2**, 2877 (1970)
45. F. Jegerlehner, Eur. Phys. J. C **18**, 673 (2001)
46. D. Akyeamong, R. Delbourgo, Nuovo Cim. **17A**, 47 (1973); W.A. Bardeen, R. Gastmans, B. Lautrup, Nucl. Phys. B **46**, 319 (1972); M. Chanowitz, M. Furman, I. Hinchliffe, Nucl. Phys. B **159**, 225 (1979)

47. M.C. Bergère, F. David, J. Math. Phys. **20**, 1244 (1979)
48. K. Osterwalder, R. Schrader, Commun. Math. Phys. **31**, 83 (1973); *ibid.* **42**, 281 (1975)
49. K.G. Wilson, Phys. Rev. D **10**, 2445 (1974)
50. M. Abramowitz, I. Stegun, *Handbook of Mathematical Functions* (Dover, New York, 1965) (Chap. 9 and formulas 9.1.39/9.1.40/9.6.4 there)
51. I.S. Gradshteyn, I.M. Ryzhik, *Table of Integrals, Series, and Products*, eds. by A. Jeffery, D. Zwanziger (Academic Press, London, 2015[1943]) (Formulas 3.471.9/11)
52. G. t' Hooft, M. Veltman, Nucl. Phys. B **153**, 365 (1979)
53. A.I. Davydychev, M.Y. Kalmykov, Nucl. Phys. B **605**, 266 (2001)
54. J. Fleischer, F. Jegerlehner, O.V. Tarasov, Nucl. Phys. B **672**, 303 (2003)
55. J.S. Frederiksen, W.S. Woolcock, Nucl. Phys. B **28**, 605 (1971); Aust. J. Phys. **26**, 691 (1973); Ann. Phys. **75**, 503 (1973); *ibid.* **80**, 86 (1973)
56. G. Passarino, M. Veltman, Nucl. Phys. B **160**, 151 (1979)
57. K.G. Chetyrkin, F.V. Tkachov, Nucl. Phys. B **192**, 159 (1981)
58. F. Jegerlehner, Renormalizing the standard model, in *Testing the Standard Model*, eds. by M. Cvetič, P. Langacker (World Scientific, Singapore, 1991), pp. 476–590, <http://www-com.physik.hu-berlin.de/~fjeger/books.html>
59. F. Bloch, A. Nordsieck, Phys. Rev. D **52**, 54 (1937)
60. Y. Hahn, W. Zimmermann, Commun. Math. Phys. **10**, 330 (1968); W. Zimmermann, Commun. Math. Phys. **11**, 1 (1968); J.H. Lowenstein, W. Zimmermann, Commun. Math. Phys. **44**, 73 (1975)
61. F.J. Dyson, Phys. Rev. **75**, 1736 (1949)
62. J.P. Fink, J. Math. Phys. **9**, 1389 (1968); E.B. Manoukian, J. Math. Phys. **19**, 917 (1978)
63. S. Weinberg, Phys. Rev. **118**, 838 (1960)
64. T. Appelquist, J. Carazzone, Phys. Rev. D **11**, 2856 (1975)
65. V.A. Smirnov, Mod. Phys. Lett. A **10**, 1485 (1995) (and references therein)
66. E.C.G. Stueckelberg, A. Petermann, Helv. Phys. Acta **26**, 499 (1953); M. Gell-Mann, F.E. Low, Phys. Rev. **95**, 1300 (1954)
67. G. Mack, Nucl. Phys. B **5**, 499 (1968)
68. J.D. Bjorken, Phys. Rev. **179**, 1547 (1969); J.D. Bjorken, E.A. Paschos, Phys. Rev. **185**, 1975 (1969)
69. D.H. Coward et al., Phys. Rev. Lett. **20**, 292 (1968); E.D. Bloom et al., Phys. Rev. Lett. **23**, 930 (1969); G. Miller et al., Phys. Rev. D **5**, 528 (1972)
70. H. Suura, E. Wichmann, Phys. Rev. **105**, 1930 (1957); A. Petermann, Phys. Rev. **105**, 1931 (1957)
71. B.E. Lautrup, E. de Rafael, Nucl. Phys. B **70**, 317 (1974)
72. E. de Rafael, J.L. Rosner, Ann. Phys. (N.Y.) **82**, 369 (1974)
73. A.L. Kataev, S.A. Larin, Pisma Zh. Eksp. Teor. Fiz. **96**, 64 (2012) [JETP Lett. **96**, 61 (2012)]
74. P.A. Baikov, K.G. Chetyrkin, J.H. Kühn, C. Sturm, Nucl. Phys. B **867**, 182 (2013)
75. P.A. Baikov, K.G. Chetyrkin, J.H. Kühn, J. Rittinger, JHEP **1207**, 017 (2012)
76. D.R. Yennie, S.C. Frautschi, H. Suura, Ann. Phys. **13**, 379 (1961); D.R. Yennie, Phys. Lett. **34B**, 239 (1975); J.D. Jackson, D.L. Scharre, Nucl. Instr. **128**, 13 (1975); M. Greco, G. Pancheri, Y. Srivastava, Nucl. Phys. B **101**, 234 (1975)
77. T. Kinoshita, J. Math. Phys. **3**, 650 (1962); T.D. Lee, M. Nauenberg, Phys. Rev. D **133**, B1549 (1964)
78. J. Fleischer, F. Jegerlehner, Z. Phys. C **26**, 629 (1985)
79. G. Serman, S. Weinberg, Phys. Rev. Lett. **39**, 1436 (1977)
80. O. Steinmann, Commun. Math. Phys. **237**, 181 (2003)
81. F. Jegerlehner, Nucl. Phys. B (Proc. Suppl.) **51C**, 131 (1996)
82. G.J. Gounaris, J.J. Sakurai, Phys. Rev. Lett. **21**, 244 (1968); A. Quenzer et al., Phys. Lett. B **76**, 512 (1978)
83. F. Jegerlehner, R. Szafron, Eur. Phys. J. C **71**, 1632 (2011)
84. H. Leutwyler, Electromagnetic form factor of the pion, in *Continuous Advances in QCD 2002: Proceedings*, eds. by K.A. Olive, M.A. Shifman, M.B. Voloshin (World Scientific, Singapore, 2002), 646 p, [arXiv:hep-ph/0212324](http://arxiv.org/abs/hep-ph/0212324)

85. J. Gasser, H. Leutwyler, *Ann. Phys.* **158**, 142 (1984); *Nucl. Phys. B* **250**, 465 (1985)
86. K.G. Wilson, *Phys. Rev. D* **10**, 2445 (1974); M. Creutz, *Phys. Rev. D* **21**, 2308 (1980)
87. Y. Nambu, *Phys. Rev. Lett.* **4**, 380 (1960)
88. G. 't Hooft, *Nucl. Phys. B* **72**, 461 (1974); *ibid.* **75**, 461 (1974); E. Witten, *Nucl. Phys. B* **160**, 57 (1979)
89. A.V. Manohar, *Hadrons in the $1/N$ expansion*, in *At the frontier of Particle Physics*, vol. 1, ed. M. Shifman (World Scientific, Singapore, 2001)pp. 507–568
90. H. Leutwyler, *Nucl. Phys. Proc. Suppl.* **64**, 223 (1998); R. Kaiser, H. Leutwyler, *Eur. Phys. J. C* **17**, 623 (2000)
91. S. Okubo, *Phys. Lett.* **5**, 1975 (1963); G. Zweig, CERN Report No.8419/TH412 (1964); J. Iizuka, *Prog. Theor. Phys. Suppl.* **37**, 38 (1966)
92. S.L. Glashow, *Phys. Rev. Lett.* **7**, 469 (1961)
93. S. Okubo, *Phys. Lett.* **5**, 165 (1963)
94. W.E. Caswell, *Phys. Rev. Lett.* **33**, 244 (1974); D.R.T. Jones, *Nucl. Phys. B* **75**, 531 (1974); E. Egorian, O.V. Tarasov, *Theor. Math. Phys.* **41**, 863 (1979) [*Teor. Mat. Fiz.* **41**, 26 (1979)]
95. O.V. Tarasov, A.A. Vladimirov, A.Y. Zharkov, *Phys. Lett. B* **93**, 429 (1980); S.A. Larin, J.A.M. Vermaseren, *Phys. Lett. B* **303**, 334 (1993)
96. T. van Ritbergen, J.A.M. Vermaseren, S.A. Larin, *Phys. Lett. B* **400**, 379 (1997); M. Czakon, *Nucl. Phys. B* **710**, 485 (2005); K.G. Chetyrkin, *Nucl. Phys. B* **710**, 499 (2005)
97. P.A. Baikov, K.G. Chetyrkin, J.H. Kühn, *Phys. Rev. Lett.* **118**, 082002 (2017)
98. S. Bethke, *Phys. Rep.* **403–404**, 203 (2004)
99. K.A. Olive et al. (Particle Data Group), *Chin. Phys. C* **38**, 090001 (2014); *Quantum Chromodynamics* eds. by S. Bethke, G. Dissertori, G.P. Salam (therein)
100. M. Della Morte, R. Frezzotti, J. Heitger, J. Rolf, R. Sommer, U. Wolff, *Nucl. Phys. B* **713**, 378 (2005)
101. F. Tekin et al. [ALPHA Collab.], *Nucl. Phys. B* **840**, 114 (2010)
102. M. Dalla Brida et al. [ALPHA Collab.], *Phys. Rev. D* **95**, 014507 (2017)
103. M. Bruno et al., *Nucl. Part. Phys. Proc.* **285–286**, 132 (2016); *PoS Lattice* **2016**, 197 (2016), [arXiv:1701.03075](https://arxiv.org/abs/1701.03075) [hep-lat]
104. F. Jegerlehner, *Acta Phys. Polon. B* **45**, 1167 (2014)

Chapter 3

Lepton Magnetic Moments: Basics

3.1 Equation of Motion for a Lepton in an External Field

For the measurement of the anomalous magnetic moment of a lepton we have to investigate the motion of a relativistic point-particle of charge $Q_\ell e$ (e the positron charge) and mass m_ℓ in an external electromagnetic field $A_\mu^{\text{ext}}(x)$. The equation of motion of a charged Dirac particle in an external field is given by (see (2.91))

$$\begin{aligned} & (i\hbar\gamma^\mu\partial_\mu + Q_\ell\frac{e}{c}\gamma^\mu(A_\mu + A_\mu^{\text{ext}}(x)) - m_\ell c) \psi_\ell(x) = 0 \\ & (\square g^{\mu\nu} - (1 - \xi^{-1})\partial^\mu\partial^\nu) A_\nu(x) = -Q_\ell e\bar{\psi}_\ell(x)\gamma^\mu\psi_\ell(x). \end{aligned} \tag{3.1}$$

What we are looking for is the solution of the Dirac equation with an external field as a relativistic one-particle problem, neglecting the radiation field in a first step. We thus are interested in a solution of the first of the above equations, which we may write as

$$i\hbar\frac{\partial\psi_\ell}{\partial t} = \left(-c\boldsymbol{\alpha}\left(i\hbar\nabla - Q_\ell\frac{e}{c}\mathbf{A}\right) - Q_\ell e\Phi + \beta m_\ell c^2\right)\psi_\ell, \tag{3.2}$$

with $\beta = \gamma^0$, $\boldsymbol{\alpha} = \gamma^0\boldsymbol{\gamma}$ and $A^{\mu\text{ext}} = (\Phi, \mathbf{A})$. For the interpretation of the solution the non-relativistic limit plays an important role, because many relativistic problems in QED may be most easily understood in terms of the non-relativistic problem as a starting point, which usually is easier to solve. We will consider a lepton e^- , μ^- or τ^- with $Q_\ell = -1$ in the following and drop the index ℓ .

1. Non-relativistic limit

For studying the non-relativistic limit of the motion of a Dirac particle in an external field it is helpful and more transparent to work in natural units.¹ In order to get from

¹The general rules of translation read: $p^\mu \rightarrow p^\mu$, $d\mu(p) \rightarrow \hbar^{-3}d\mu(p)$, $m \rightarrow mc$, $e \rightarrow e/(\hbar c)$, $e^{ipx} \rightarrow e^{i\frac{px}{\hbar}}$, spinors: $u, v \rightarrow u/\sqrt{c}, v/\sqrt{c}$.

the Dirac spinor ψ the two component Pauli spinors in the non-relativistic limit, one has to perform an appropriate unitary transformation, called Foldy–Wouthuysen transformation. Looking at the Dirac equation (3.2)

$$i\hbar \frac{\partial \psi}{\partial t} = \mathbf{H} \psi, \quad \mathbf{H} = c \boldsymbol{\alpha} \left(\mathbf{p} - \frac{e}{c} \mathbf{A} \right) + \beta mc^2 + e \Phi$$

with

$$\beta = \gamma^0 = \begin{pmatrix} 1 & 0 \\ 0 & -1 \end{pmatrix}, \quad \boldsymbol{\alpha} = \gamma^0 \boldsymbol{\gamma} = \begin{pmatrix} 0 & \boldsymbol{\sigma} \\ \boldsymbol{\sigma} & 0 \end{pmatrix},$$

we note that \mathbf{H} has the form

$$\mathbf{H} = \beta mc^2 + c \mathcal{O} + e \Phi$$

where $[\beta, \Phi] = 0$ is commuting and $\{\beta, \mathcal{O}\} = 0$ anti-commuting. In the absence of an external field spin is a conserved quantity in the rest frame, i.e. the Dirac equation must be equivalent to the Pauli equation. This fixes the unitary transformation to be performed in the case $A_\mu^{\text{ext}} = 0$:

$$\psi' = \mathbf{U} \psi, \quad \mathbf{H}' = \mathbf{U} \left(\mathbf{H} - i\hbar \frac{\partial}{\partial t} \right) \mathbf{U}^{-1} = \mathbf{U} \mathbf{H} \mathbf{U}^{-1} \quad (3.3)$$

where the time-independence of \mathbf{U} has been used, and we obtain

$$i\hbar \frac{\partial \psi'}{\partial t} = \mathbf{H}' \psi'; \quad \psi' = \begin{pmatrix} \varphi' \\ 0 \end{pmatrix}, \quad (3.4)$$

where φ' is the Pauli spinor. In fact \mathbf{U} is a Lorentz boost matrix

$$\mathbf{U} = \mathbf{1} \cosh \theta + \mathbf{n} \boldsymbol{\gamma} \sinh \theta = e^{\theta \mathbf{n} \boldsymbol{\gamma}} \quad (3.5)$$

with

$$\mathbf{n} = \frac{\mathbf{p}}{|\mathbf{p}|}, \quad \theta = \frac{1}{2} \operatorname{arccosh} \frac{p^0}{mc} = \operatorname{arcsinh} \frac{|\mathbf{p}|}{mc}$$

and we obtain, with $p^0 = \sqrt{\mathbf{p}^2 + m^2 c^2}$,

$$\mathbf{H}' = cp^0 \beta; \quad [\mathbf{H}', \boldsymbol{\Sigma}] = 0, \quad \boldsymbol{\Sigma} = \boldsymbol{\alpha} \gamma_5 = \begin{pmatrix} \boldsymbol{\sigma} & \mathbf{0} \\ \mathbf{0} & \boldsymbol{\sigma} \end{pmatrix} \quad (3.6)$$

where Σ is the spin operator. Actually, there exist two projection operators U one to the upper and one to the lower components:

$$U_+ \psi = \begin{pmatrix} \varphi' \\ 0 \end{pmatrix}, \quad U_- \psi = \begin{pmatrix} 0 \\ \chi \end{pmatrix},$$

given by

$$U_+ = \frac{(p^0 + mc) \mathbf{1} + \mathbf{p}\boldsymbol{\gamma}}{\sqrt{2p^0}\sqrt{p^0 + mc}}, \quad U_- = \frac{(p^0 + mc) \mathbf{1} - \mathbf{p}\boldsymbol{\gamma}}{\sqrt{2p^0}\sqrt{p^0 + mc}}.$$

For the spinors we have

$$U_+ u(p, r) = \sqrt{\frac{2p^0}{c}} \begin{pmatrix} U(r) \\ 0 \end{pmatrix}, \quad U_- v(p, r) = \sqrt{\frac{2p^0}{c}} \begin{pmatrix} 0 \\ V(r) \end{pmatrix}$$

with $U(r)$ and $V(r) = i\sigma_2 U(r)$ the two component spinors in the rest system.

We now look at the lepton propagator. The Feynman propagator reads

$$\begin{aligned} iS_{F\alpha\beta}(x-y) &\equiv \langle 0|T\{\psi_\alpha(x)\bar{\psi}_\beta(y)\}|0\rangle \\ &= \int \frac{d^4 p}{(2\pi)^4} \frac{\not{p} + mc}{p^2 - m^2 c^2 + i\varepsilon} e^{-ip(x-y)} \end{aligned}$$

where²

$$S_{F\alpha\beta}(z; m^2) = (i\hbar\gamma^\mu \partial_\mu + mc) \Delta_F(z; m^2) = \Theta(z^0) S^+(z) + \Theta(-z^0) S^-(z)$$

with retarded positive frequency part represented by

$$\Theta(z^0) S^+(z) = \int \frac{d^4 p}{(2\pi)^4} \frac{c}{2\omega_p} \frac{\sum_r u_\alpha(p, r) \bar{u}_\beta(p, r)}{p^0 - \omega_p + i0} e^{-ipz}$$

²The positive frequency part is given by

$$\begin{aligned} iS_{\alpha\beta}^+(x-y) &\equiv \langle 0|\psi_\alpha(x)\bar{\psi}_\beta(y)|0\rangle \\ &= c \sum_r \int d\mu(p) u_\alpha(p, r) \bar{u}_\beta(p, r) e^{-ip(x-y)} = \int d\mu(p) (\not{p} + mc) e^{-ip(x-y)} \end{aligned}$$

and the negative frequency part by

$$\begin{aligned} -iS_{\alpha\beta}^-(x-y) &\equiv \langle 0|\bar{\psi}_\beta(y)\psi_\alpha(x)|0\rangle \\ &= c \sum_r \int d\mu(p) v_\alpha(p, r) \bar{v}_\beta(p, r) e^{ip(x-y)} = \int d\mu(p) (\not{p} - mc) e^{ip(x-y)}. \end{aligned}$$

and the advanced negative frequency part by

$$\Theta(-z^0) S^-(z) = - \int \frac{d^4 p}{(2\pi)^4} \frac{c}{2\omega_p} \sum_r v_\alpha(p, r) \bar{v}_\beta(p, r) e^{ipz} .$$

Using

$$\begin{aligned} \sum_r u_\alpha(p, r) \bar{u}_\beta(p, r) &= \frac{2\omega_p}{c} \mathbf{U}(\mathbf{p}) \gamma_+ \mathbf{U}(\mathbf{p}) \\ \sum_r v_\alpha(p, r) \bar{v}_\beta(p, r) &= \frac{2\omega_p}{c} \mathbf{U}(\mathbf{p}) \gamma_- \mathbf{U}(\mathbf{p}) \end{aligned}$$

with

$$\gamma_\pm = \frac{1}{2} (\mathbf{1} \pm \gamma^0) ; \quad \gamma^0 \gamma_\pm = \pm \gamma_\pm , \quad \gamma_+ \gamma_- = \gamma_- \gamma_+ = 0$$

the projection matrices for the upper and lower components, respectively. We thus arrive at our final representation which allows one to perform a systematic expansion in $1/c$:

$$S_F(x-y) = \int \frac{d^4 p}{(2\pi)^4} e^{-ip(x-y)} \mathbf{U}(\mathbf{p}) \left(\frac{\gamma_+}{p^0 - \omega_p + i0} - \frac{\gamma_-}{p^0 + \omega_p - i0} \right) \mathbf{U}(\mathbf{p}) . \quad (3.7)$$

The $1/c$ -expansion simply follows by expanding the matrix \mathbf{U} :

$$\mathbf{U}(\mathbf{p}) = \exp \theta \frac{\mathbf{p}}{|\mathbf{p}|} \gamma = \exp \theta \frac{\mathbf{p}\boldsymbol{\gamma}}{2mc} ; \quad \theta = \sum_{n=0}^{\infty} \frac{(-1)^n}{2n+1} \left(\frac{\mathbf{p}^2}{m^2 c^2} \right)^n .$$

The non-relativistic limit thus reads:

$$S_F(x-y)_{\text{NR}} = \int \frac{d^4 p}{(2\pi)^4} e^{-ip(x-y)} \left(\frac{\gamma_+}{p^0 - (mc^2 + \frac{\mathbf{p}^2}{2m}) + i0} - \frac{\gamma_-}{p^0 + (mc^2 + \frac{\mathbf{p}^2}{2m}) - i0} \right)$$

i.e.

$$S_F(x-y) = S_F(x-y)_{\text{NR}} + O(1/c) .$$

2. Non-relativistic lepton with $A_\mu^{\text{ext}} \neq 0$

Again we start from the Dirac equation (3.2). In order to get the non-relativistic representation for small velocities we have to split off the phase of the Dirac field, which is due to the rest energy of the lepton:

$$\psi = \hat{\psi} e^{-i\frac{mc^2}{\hbar}t} \quad \text{with} \quad \hat{\psi} = \begin{pmatrix} \hat{\varphi} \\ \hat{\chi} \end{pmatrix}.$$

Consequently, the Dirac equation takes the form

$$i\hbar \frac{\partial \hat{\psi}}{\partial t} = (\mathbf{H} - mc^2) \hat{\psi}$$

and describes the coupled system of equations

$$\begin{aligned} \left(i\hbar \frac{\partial}{\partial t} - e\Phi \right) \hat{\varphi} &= c\sigma \left(\mathbf{p} - \frac{e}{c}\mathbf{A} \right) \hat{\chi} \\ \left(i\hbar \frac{\partial}{\partial t} - e\Phi + 2mc^2 \right) \hat{\chi} &= c\sigma \left(\mathbf{p} - \frac{e}{c}\mathbf{A} \right) \hat{\varphi}. \end{aligned}$$

For $c \rightarrow \infty$ we obtain

$$\hat{\chi} \simeq \frac{1}{2mc} \sigma \left(\mathbf{p} - \frac{e}{c}\mathbf{A} \right) \hat{\varphi} + O(1/c^2)$$

and hence

$$\left(i\hbar \frac{\partial}{\partial t} - e\Phi \right) \hat{\varphi} \simeq \frac{1}{2m} \left(\sigma \left(\mathbf{p} - \frac{e}{c}\mathbf{A} \right) \right)^2 \hat{\varphi}.$$

As \mathbf{p} does not commute with \mathbf{A} , we may use the relation

$$(\sigma\mathbf{a})(\sigma\mathbf{b}) = \mathbf{ab} + i\sigma(\mathbf{a} \times \mathbf{b})$$

to obtain

$$\left(\sigma \left(\mathbf{p} - \frac{e}{c}\mathbf{A} \right) \right)^2 = \left(\mathbf{p} - \frac{e}{c}\mathbf{A} \right)^2 - \frac{e\hbar}{c} \sigma \cdot \mathbf{B}; \quad \mathbf{B} = \text{rot}\mathbf{A}.$$

This leads us to the *Pauli equation* (W. Pauli 1927)

$$i\hbar \frac{\partial \hat{\varphi}}{\partial t} = \hat{\mathbf{H}} \hat{\varphi} = \left(\frac{1}{2m} \left(\mathbf{p} - \frac{e}{c}\mathbf{A} \right)^2 + e\Phi - \frac{e\hbar}{2mc} \sigma \cdot \mathbf{B} \right) \hat{\varphi} \quad (3.8)$$

which up to the spin term is nothing but the non-relativistic Schrödinger equation. The last term is the one this book is about: it has the form of a potential energy of a magnetic dipole in an external field. In leading order in $1/c$ the lepton behaves as a particle which has besides a charge also a magnetic moment

$$\boldsymbol{\mu} = \frac{e\hbar}{2mc} \boldsymbol{\sigma} = \frac{e}{mc} \mathbf{S}; \quad \mathbf{S} = \hbar \mathbf{s} = \hbar \frac{\boldsymbol{\sigma}}{2} \quad (3.9)$$

with \mathbf{S} the angular momentum. For comparison: the orbital angular momentum reads

$$\boldsymbol{\mu}_{\text{orbital}} = \frac{Q}{2M} \mathbf{L} = g_l \frac{Q}{2M} \mathbf{L}; \quad \mathbf{L} = \mathbf{r} \times \mathbf{p} = -i\hbar \mathbf{r} \times \nabla = \hbar \mathbf{l}$$

and thus the total magnetic moment is

$$\boldsymbol{\mu}_{\text{total}} = \frac{Q}{2M} (g_l \mathbf{L} + g_s \mathbf{S}) = \frac{m_e}{M} \mu_B (g_l \mathbf{l} + g_s \mathbf{s}) \quad (3.10)$$

where

$$\mu_B = \frac{e\hbar}{2m_e c} \quad (3.11)$$

is Bohr's magneton. As a result for the electron: $Q = -e$, $M = m_e$, $g_l = -1$ and $g_s = -2$. The last remarkable result is due to Dirac (1928) and tells us that the gyromagnetic ratio ($\frac{e}{mc}$) is twice as large as the one from the orbital motion.

The Foldy–Wouthuysen transformation for arbitrary A_μ cannot be performed in closed analytic form. However, the expansion in $1/c$ can be done in a systematic way (see e.g. [1]) and yields the effective Hamiltonian

$$\begin{aligned} H' = & \beta \left(mc^2 + \frac{(\mathbf{p} - \frac{e}{c} \mathbf{A})^2}{2m} - \frac{\mathbf{p}^4}{8m^3 c^2} \right) + e \Phi - \beta \frac{e\hbar}{2mc} \boldsymbol{\sigma} \cdot \mathbf{B} \\ & - \frac{e\hbar^2}{8m^2 c^2} \text{div} \mathbf{E} - \frac{e\hbar}{4m^2 c^2} \boldsymbol{\sigma} \cdot \left[(\mathbf{E} \times \mathbf{p} + \frac{i}{2} \text{rot} \mathbf{E}) \right] \\ & + O(1/c^3). \end{aligned} \quad (3.12)$$

The additional terms are $\frac{\mathbf{p}^4}{8m^3 c^2}$ originating from the relativistic kinematics, $\frac{e\hbar^2}{8m^2 c^2} \text{div} \mathbf{E}$ is the Darwin term as a result of the fluctuations of the electrons position and $\frac{e\hbar}{4m^2 c^2} \boldsymbol{\sigma} \cdot [(\mathbf{E} \times \mathbf{p} + \frac{i}{2} \text{rot} \mathbf{E})]$ is the spin–orbit interaction energy. The latter plays an important role in setting up a muon storage ring in the $g - 2$ experiment (magic energy tuning). As we will see, however, in such an experiment the muons are required to be highly relativistic such that relativistic kinematics is required. The appropriate modifications, the Bargmann–Michel–Telegdi equation [2], will be discussed in Chap. 6.

3.2 Magnetic Moments and Electromagnetic Form Factors

3.2.1 Main Features: An Overview

Our particular interest is the motion of a lepton in an external field under consideration of the full relativistic quantum behavior. It is controlled by the QED equations of motion (3.1) with an external field added (3.2), specifically a constant magnetic field.

For slowly varying fields the motion is essentially determined by the generalized Pauli equation (3.12), which also serves as a basis for understanding the role of the magnetic moment of a lepton on the classical level. As we will see, in the absence of electrical fields \mathbf{E} the quantum correction miraculously may be subsumed in a single number the anomalous magnetic moment, which is the result of relativistic quantum fluctuations, usually simply called *radiative corrections* (RC).

To study radiative corrections we have to extend the discussion of the preceding section and consider the full QED interaction Lagrangian

$$\mathcal{L}_{\text{int}}^{\text{QED}} = -e\bar{\psi}\gamma^\mu\psi A_\mu \tag{3.13}$$

in the case the photon field is part of the dynamics but has an external classical component A_μ^{ext}

$$A_\mu \rightarrow A_\mu + A_\mu^{\text{ext}} . \tag{3.14}$$

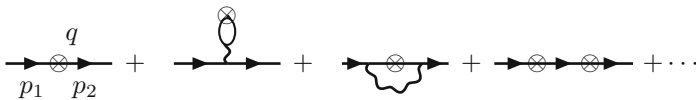
We are thus dealing with QED exhibiting an additional external field insertion “vertex”:

$$\text{⊗} = -ie \gamma^\mu \tilde{A}_\mu^{\text{ext}} .$$

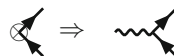
Gauge invariance (2.89) requires that a gauge transformation of the external field

$$A_\mu^{\text{ext}}(x) \rightarrow A_\mu^{\text{ext}}(x) - \partial_\mu\alpha(x) , \tag{3.15}$$

for an arbitrary scalar classical field $\alpha(x)$, leaves physics invariant. The motion of the lepton in the external field is described by a simultaneous expansion in the fine structure constant $\alpha = \frac{e^2}{4\pi}$ and in the external field A_μ^{ext} assuming the latter to be weak



In the following we will use the more customary graphic representation



of the external vertex, just as an amputated photon line at zero momentum.

The gyromagnetic ratio of the muon is defined by the ratio of the magnetic moment which couples to the magnetic field in the Hamiltonian and the spin operator in units of $\mu_0 = e\hbar/2m_\mu c$

$$\boldsymbol{\mu} = g_\mu \frac{e\hbar}{2m_\mu c} \mathbf{s} ; \quad g_\mu = 2(1 + a_\mu) \quad (3.16)$$

and as indicated has a tree level part, the Dirac moment $g_\mu^{(0)} = 2$ [3], and a higher order part the muon anomaly or anomalous magnetic moment

$$a_\mu = \frac{1}{2}(g_\mu - 2) . \quad (3.17)$$

In general, the anomalous magnetic moment of a lepton is related to the gyromagnetic ratio by

$$a_\ell = \mu_\ell/\mu_B - 1 = \frac{1}{2}(g_\ell - 2) \quad (3.18)$$

where the precise value of the Bohr magneton is given by

$$\mu_B = \frac{e\hbar}{2m_e c} = 5.788381804(39) \times 10^{-11} \text{ MeVT}^{-1} . \quad (3.19)$$

Here T as a unit stands for 1 Tesla = 10^4 Gauss. It is the unit in which the magnetic field B usually is given. In QED a_μ may be calculated in perturbation theory by considering the matrix element

$$\mathcal{M}(x; p) = \langle \mu^-(p_2, r_2) | j_{\text{em}}^\mu(x) | \mu^-(p_1, r_1) \rangle$$

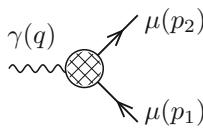
of the electromagnetic current for the scattering of an incoming muon $\mu^-(p_1, r_1)$ of momentum p_1 and 3rd component of spin r_1 to a muon $\mu^-(p_2, r_2)$ of momentum p_2 and 3rd component of spin r_2 , in the classical limit of zero momentum transfer $q^2 = (p_2 - p_1)^2 \rightarrow 0$. In momentum space, by virtue of space–time translational invariance $j_{\text{em}}^\mu(x) = e^{iP \cdot x} j_{\text{em}}^\mu(0) e^{-iP \cdot x}$ and the fact that the lepton states are eigenstates of four–momentum $e^{-iP \cdot x} | \mu^-(p_i, r_i) \rangle = e^{-i p_i \cdot x} | \mu^-(p_i, r_i) \rangle$ ($i = 1, 2$), we find

$$\begin{aligned} \tilde{\mathcal{M}}(q; p) &= \int d^4x e^{-iq \cdot x} \langle \mu^-(p_2, r_2) | j_{\text{em}}^\mu(x) | \mu^-(p_1, r_1) \rangle \\ &= \int d^4x e^{i(p_2 - p_1 - q) \cdot x} \langle \mu^-(p_2, r_2) | j_{\text{em}}^\mu(0) | \mu^-(p_1, r_1) \rangle \\ &= (2\pi)^4 \delta^{(4)}(q - p_2 + p_1) \langle \mu^-(p_2, r_2) | j_{\text{em}}^\mu(0) | \mu^-(p_1, r_1) \rangle , \end{aligned}$$

proportional to the δ -function of four–momentum conservation. The T -matrix element is then given by

$$\langle \mu^-(p_2) | j_{\text{em}}^\mu(0) | \mu^-(p_1) \rangle .$$

In QED it has a relativistic covariant decomposition of the form



$$= (-ie) \bar{u}(p_2) \left[\gamma^\mu F_E(q^2) + i \frac{\sigma^{\mu\nu} q_\nu}{2m_\mu} F_M(q^2) \right] u(p_1), \quad (3.20)$$

where $q = p_2 - p_1$ and $u(p)$ denote the Dirac spinors. $F_E(q^2)$ is the electric charge or Dirac form factor and $F_M(q^2)$ is the magnetic or Pauli form factor. Note that the matrix $\sigma^{\mu\nu} = \frac{i}{2}[\gamma^\mu, \gamma^\nu]$ represents the spin 1/2 angular momentum tensor. In the static (classical) limit we have (see (2.210))

$$F_E(0) = 1, \quad F_M(0) = a_\mu, \quad (3.21)$$

where the first relation is the *charge renormalization condition* (in units of the physical positron charge e , which by definition is taken out as a factor in (3.20)), while the second relation is the finite prediction for a_μ , in terms of the form factor F_M the calculation of which will be described below. The leading order (LO) contribution (2.215) we have been calculating already in Sect. 2.6.3.

Note that in higher orders the form factors in general acquire an imaginary part. One may write therefore an effective dipole moment Lagrangian with complex “coupling”

$$\mathcal{L}_{\text{eff}}^{\text{DM}} = -\frac{1}{2} \left\{ \bar{\psi} \sigma^{\mu\nu} \left[D_\mu \frac{1 + \gamma_5}{2} + D_\mu^* \frac{1 - \gamma_5}{2} \right] \psi \right\} F_{\mu\nu} \quad (3.22)$$

with ψ the muon field and

$$\text{Re } D_\mu = a_\mu \frac{e}{2m_\mu}, \quad \text{Im } D_\mu = d_\mu = \frac{\eta_\mu}{2} \frac{e}{2m_\mu}, \quad (3.23)$$

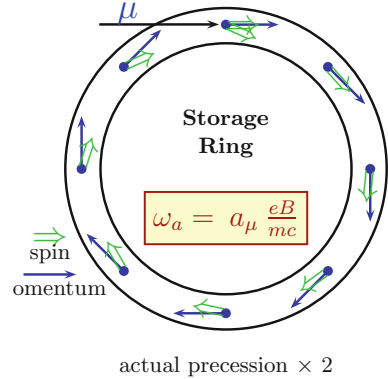
(see (3.84) and (3.85) below). Thus the imaginary part of $F_M(0)$ corresponds to an electric dipole moment. The latter is non-vanishing only if we have T violation. For some more details we refer to Sect. 3.3.

As illustrated in Fig. 3.1, when polarized muons travel on a circular orbit in a constant magnetic field, then a_μ is responsible for the *Larmor precession* of the direction of the spin of the muon, characterized by the angular frequency ω_a . At the magic energy of about ~ 3.1 GeV, the latter is directly proportional to a_μ :

$$\omega_a = \frac{e}{m} \left[a_\mu \mathbf{B} - \left(a_\mu - \frac{1}{\gamma^2 - 1} \right) \boldsymbol{\beta} \times \mathbf{E} \right]_{\text{at “magic } \gamma}^{E \sim 3.1 \text{ GeV}} \simeq \frac{e}{m} [a_\mu \mathbf{B}]. \quad (3.24)$$

Electric quadrupole fields \mathbf{E} are needed for focusing the beam and they affect the precession frequency in general. $\gamma = E/m_\mu = 1/\sqrt{1 - \beta^2}$ is the relativistic Lorentz factor with $\beta = v/c$ the velocity of the muon in units of the speed of light c . The magic

Fig. 3.1 Spin precession in the $g - 2$ ring ($\sim 12^\circ/\text{circle}$)



energy $E_{\text{mag}} = \gamma_{\text{mag}} m_\mu$ is the energy E for which $\frac{1}{\gamma_{\text{mag}}^2 - 1} = a_\mu$. The existence of a solution is due to the fact that a_μ is a positive constant in competition with an energy dependent factor of opposite sign (as $\gamma \geq 1$). The second miracle, which is crucial for the feasibility of the experiment, is the fact that $\gamma_{\text{mag}} = \sqrt{(1 + a_\mu)/a_\mu} \simeq 29.378$ is large enough to provide the time dilatation factor for the unstable muon boosting the life time $\tau_\mu \simeq 2.197 \times 10^{-6}$ s to $\tau_{\text{in flight}} = \gamma \tau_\mu \simeq 6.454 \times 10^{-5}$ s, which allows the muons, traveling at $v/c = 0.99942\dots$, to be stored in a ring of reasonable size (diameter ~ 14 m).

This provided the basic setup for the $g - 2$ experiments at the *Muon Storage Rings* at CERN and at BNL as well as for the upcoming new experiment at Fermilab. The oscillation frequency ω_a can be measured very precisely. Also the precise tuning to the magic energy is not the major problem. The most serious challenge is to manufacture a precisely known constant magnetic field B (magnetic flux density), as the latter directly enters the experimental extraction of a_μ via (3.24). Of course one also needs high enough statistics to get sharp values for the oscillation frequency. The basic principle of the measurement of a_μ is a measurement of the “anomalous” frequency difference $\omega_a = |\omega_a| = \omega_s - \omega_c$, where $\omega_s = g_\mu (e\hbar/2m_\mu) B/\hbar = g_\mu/2 \times e/m_\mu B$ is the muon spin–flip *precession frequency* in the applied magnetic field and $\omega_c = e/m_\mu B$ is the muon *cyclotron frequency*. Instead of eliminating the magnetic field by measuring ω_c , B is determined from proton *Nuclear Magnetic Resonance* (NMR) measurements. This procedure requires the value of μ_μ/μ_p to extract a_μ from the data. Fortunately, a high precision value for this ratio is available from the measurement of the hyperfine splitting (HFS) in muonium. One obtains³

$$a_\mu^{\text{exp}} = \frac{\bar{R}}{|\mu_\mu/\mu_p| - \bar{R}}, \quad (3.25)$$

³E-821 has measured $\bar{R} = \omega_a/\tilde{\omega}_p = 0.003\,707\,206\,4(20)$ while using $\lambda = \mu_\mu/\mu_p = 3.18334539(10)$ from muonium HFS. The new CODATA 2011 recommended value is $\lambda = 3.183345107(84)$, such that the updated $a_\mu^{\text{exp}} = (11\,659\,208.9 \pm 5.4 \pm 3.3[6.3]) \times 10^{-10}$.

where $\bar{R} = \omega_a/\bar{\omega}_p$ and $\bar{\omega}_p = (e/m_p c)\langle B \rangle$ is the free-proton NMR frequency corresponding to the average magnetic field seen by the muons in their orbits in the storage ring. We mention that for the electron a *Penning trap* is employed to measure a_e rather than a storage ring. The B field in this case can be eliminated via a measurement of the cyclotron frequency. The CODATA group [4] recommends to use

$$a_\mu^{\text{exp}} = \frac{g_e \omega_a m_\mu \mu_p}{2 \bar{\omega}_p m_e \mu_e} \quad (3.26)$$

as a representation in terms of precisely measured ratios which multiply the extremely precisely measured electron g_e value.⁴ Both representations derive from $a_\mu = \frac{e}{m} B$, $B = \frac{\hbar\omega_p}{2\mu_p}$ and $\mu_\mu = (1 + a_\mu) \frac{e\hbar}{2m_\mu c}$ and $\mu_e = \frac{g_e}{2} \frac{e\hbar}{2m_e c}$ used in the second form.

On the theory side, the crucial point is that a_ℓ is dimensionless, just a number, and must vanish at tree level in any renormalizable theory. As an effective interaction it would look like

$$\delta\mathcal{L}_{\text{eff}}^{\text{AMM}} = -\frac{\delta g}{2} \frac{e}{4m} \left\{ \bar{\psi}_L(x) \sigma^{\mu\nu} F_{\mu\nu}(x) \psi_R(x) + \bar{\psi}_R(x) \sigma^{\mu\nu} F_{\mu\nu}(x) \psi_L(x) \right\} \quad (3.27)$$

where ψ_L and ψ_R are Dirac fields of negative (left-handed L) and positive (right-handed R) chirality and $F_{\mu\nu} = \partial_\mu A_\nu - \partial_\nu A_\mu$ is the electromagnetic field strength tensor. This Pauli term has dimension 5 ($=2 \times 3/2$ for the two Dirac fields plus 1 for the photon plus 1 for the derivative included in F) and thus would spoil renormalizability. In a renormalizable theory, however, a_μ is a finite unambiguous prediction of that theory. It is testing the rate of helicity flip transition and is one of the most precisely measured electroweak observables. Of course the theoretical prediction only may agree with the experimental result to the extent that we know the complete theory of nature, within the experimental accuracy.

Before we start discussing the theoretical prediction for the magnetic moment anomaly, we will specify the parameters which we will use for the numerical evaluations below.

Since the lowest order result for a_ℓ is proportional to α , obviously, the most important basic parameter for calculating a_μ is the fine structure constant α . It is best determined now from the very recent extraordinary precise measurement of the electron anomalous magnetic moment [4–7]

$$a_e^{\text{exp}} = 0.001\,159\,652\,180\,76(27) [0.24 \text{ ppb}] \quad (3.28)$$

⁴The values are from the electron $g - 2$: $g_e = -2.002\,319\,304\,361\,53(53)$ [0.26 ppt], from E821 $\bar{R} = \omega_a/\bar{\omega}_p = 0.003\,707\,206\,4(20)$ [0.54 ppm], from Muonium HFS experiments $m_\mu/m_e = 206.768\,2843(52)$ [25 ppb] and $\mu_p/\mu_e = -0.001519270384(12)$ [8 ppb].

which, confronted with its theoretical prediction as a series in α (see Sect. 3.2.2 below) determines [6, 8–11]

$$\alpha^{-1}(a_e) = 137.035\,999\,1657(342) [0.25 \text{ ppb}] .$$

This new value has an uncertainty 20 times smaller than any preceding independent determination of α . We will use the updated value

$$\alpha^{-1}(a_e) = 137.035\,999\,139(31) [0.25 \text{ ppb}] , \quad (3.29)$$

recommended by [4, 12], throughout in the calculation of a_μ .

All QED contributions associated with diagrams with lepton-loops, where the “internal” lepton has mass different from the mass of the external one, depend on the corresponding mass ratio. These mass-dependent contributions differ for a_e , a_μ and a_τ , such that lepton universality is broken: $a_e \neq a_\mu \neq a_\tau$. Lepton universality is broken in any case by the difference in the masses and whatever depends on them. Such mass-ratio dependent contributions start at two loops. For the evaluation of these contributions precise values for the lepton masses are needed. We will use the following values for the muon–electron and muon–tau mass ratios, and lepton masses [4, 7, 12–14]

$$\begin{aligned} m_\mu/m_e &= 206.768\,2826(46) , & m_\mu/m_\tau &= 0.059\,4649(54) \\ m_e &= 0.510\,998\,9461(31) \text{ MeV} , & m_\mu &= 105.658\,3745(24) \text{ MeV} \\ & & m_\tau &= 1776.82(16) \text{ MeV} . \end{aligned} \quad (3.30)$$

Note that the primary determination of the electron and muon masses come from measuring the ratio with respect to the mass of a nucleus and the masses are obtained in atomic mass units (amu). The conversion factor to MeV is more uncertain than the mass of the electron and muon in amu. The ratio of course does not suffer from the uncertainty of the conversion factor.

Other physical constants which we will need later for evaluating the weak contributions are the Fermi constant

$$G_\mu = 1.1663787(6) \times 10^{-5} \text{ GeV}^{-2} , \quad (3.31)$$

the weak mixing parameter⁵ (here defined by $\sin^2 \Theta_W = 1 - M_W^2/M_Z^2$)

$$\sin^2 \Theta_W = 0.22290(29) \quad (3.32)$$

and the masses of the intermediate gauge bosons Z and W

$$M_Z = 91.1876 \pm 0.0021 \text{ GeV} , \quad M_W = 80.385 \pm 0.015 \text{ GeV} . \quad (3.33)$$

⁵The effective value $\sin^2 \Theta_{\text{eff}} = 0.23155(5)$ is determined from the vector to axialvector $Zf\bar{f}$ coupling ratios in $e^+e^- \rightarrow f\bar{f}$.

For the Standard Model (SM) Higgs boson, recently discovered [15] by ATLAS [16] and CMS [17] at the LHC at CERN, the mass has been measured to be [12]

$$m_H = 125.09 \pm 0.21 \text{ (syst)} \pm 0.11 \text{ (stat)} \text{ GeV} . \tag{3.34}$$

We also mention here that virtual pion–pair production is an important contribution to the photon vacuum polarization and actually yields the leading hadronic contribution to the anomalous magnetic moment. For the dominating $\pi^+\pi^-$ channel, the threshold is at $2m_\pi$ with the pion mass given by

$$m_{\pi^\pm} = 139.570 \text{ 18 (35)} \text{ MeV} . \tag{3.35}$$

There is also a small contribution from $\pi^0\gamma$ with threshold at m_{π^0} which has the value

$$m_{\pi^0} = 134.976 \text{ 6 (6)} \text{ MeV} . \tag{3.36}$$

Later we will also need the pion decay constant

$$F_\pi \simeq 92.21(14) \text{ MeV} . \tag{3.37}$$

For the quark masses needed in some cases we use running current quark masses in the $\overline{\text{MS}}$ scheme [12, 13] with renormalization scale parameter μ . For the light quarks $q = u, d, s$ we give $m_q = \bar{m}_q(\mu = 2 \text{ GeV})$, for the heavier $q = c, b$ the values at the mass as a scale $m_q = \bar{m}_q(\mu = \bar{m}_q)$ and for $q = t$ the pole mass:

$$\begin{aligned} m_u &= 2.3_{-0.5}^{+0.7} \text{ MeV} & m_d &= 4.8_{-0.5}^{+0.7} \text{ MeV} & m_s &= 95 \pm 5 \text{ MeV} \\ m_c &= 1.275 \pm 0.025 \text{ GeV} & m_b &= 4.18 \pm 0.03 \text{ GeV} & M_t &= 173.21 \pm 0.87 \text{ GeV} . \end{aligned} \tag{3.38}$$

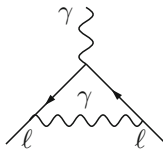
Within the SM the $\overline{\text{MS}}$ mass of the top quark $m_t(m_t)$ essentially agrees with the pole mass: $m_t(m_t) \simeq M_t$ [18, 19].

This completes the list of the most relevant parameters and we may discuss the various contributions in turn now. This also can be read as an update of [20].

The profile of the most important contributions may be outlined as follows:

(1) QED universal part:

The by far largest QED/SM contribution comes from the one–loop QED diagram [21]



$$: a_e^{(2)} = a_\mu^{(2)} = a_\tau^{(2)} = \frac{\alpha}{2\pi} \tag{Schwinger 1948}$$

which we have calculated in Sect. 2.6.3, and which is universal for all charged leptons. As it is customary we indicate the perturbative order in powers of e , i.e., $a^{(n)}$ denotes an $O(e^n)$ term, in spite of the fact that the perturbation expansion is usually represented as an expansion in $\alpha = e^2/4\pi$. Typically, analytic results for higher order terms may be expressed in terms of the Riemann zeta function

$$\zeta(n) = \sum_{k=1}^{\infty} \frac{1}{k^n} \quad (3.39)$$

and of the polylogarithmic integrals⁶

$$\text{Li}_n(x) = \frac{(-1)^{n-1}}{(n-2)!} \int_0^1 \frac{\ln^{n-2}(t) \ln(1-tx)}{t} dt = \sum_{k=1}^{\infty} \frac{x^k}{k^n}, \quad (3.40)$$

where $\text{Li}_2(x)$ is often referred to as the Spence function $\text{Sp}(x)$ (see (2.208) in Sect. 2.6.3 and [23] and references therein). Special $\zeta(n)$ values we will need are

$$\zeta(2) = \frac{\pi^2}{6}, \quad \zeta(3) = 1.202\,056\,903\dots, \quad \zeta(4) = \frac{\pi^4}{90}, \quad \zeta(5) = 1.036\,927\,755\dots \quad (3.41)$$

Also the constants

$$\begin{aligned} \text{Li}_n(1) &= \zeta(n), \quad \text{Li}_n(-1) = -[1 - 2^{1-n}] \zeta(n) \\ a_4 &\equiv \text{Li}_4\left(\frac{1}{2}\right) = \sum_{n=1}^{\infty} 1/(2^n n^4) = 0.517\,479\,061\,674\dots, \end{aligned} \quad (3.42)$$

related to polylogarithms, will be needed later for the evaluation of analytical results. Since a_μ is a number all QED contributions calculated in “one flavor QED”, with just one species of lepton, which exhibits *one* physical mass scale only, equal to the mass of the external lepton, are universal. The following universal contributions (one flavor QED) are known:

- 2-loop diagrams [7 diagrams] with one type of fermion lines yield

$$a_\ell^{(4)} = \left[\frac{197}{144} + \frac{\pi^2}{12} - \frac{\pi^2}{2} \ln 2 + \frac{3}{4} \zeta(3) \right] \left(\frac{\alpha}{\pi} \right)^2. \quad (3.43)$$

The first calculation performed by Karplus and Kroll (1950) [24] later was recalculated and corrected by Petermann (1957) [25] and, independently, by Sommerfield

⁶The appearance of transcendental numbers like $\zeta(n)$ and higher order polylogarithms $\text{Li}_n(x)$ or so called harmonic sums is directly connected to the number of loops of a Feynman diagram. Typically, 2-loop results exhibit $\zeta(3)$ 3-loop ones $\zeta(5)$ etc. of increasing transcendentality [22].

(1957) [26]. An instructive compact calculation based on the dispersion theoretic approach is due to Terentev (1962) [27].

- 3-loop diagrams [72 diagrams] with common fermion lines

$$\begin{aligned}
 a_\ell^{(6)} = & \left[\frac{28259}{5184} + \frac{17101}{810} \pi^2 - \frac{298}{9} \pi^2 \ln 2 + \frac{139}{18} \zeta(3) \right. \\
 & + \frac{100}{3} \left\{ \text{Li}_4 \left(\frac{1}{2} \right) + \frac{1}{24} \ln^4 2 - \frac{1}{24} \pi^2 \ln^2 2 \right\} \\
 & \left. - \frac{239}{2160} \pi^4 + \frac{83}{72} \pi^2 \zeta(3) - \frac{215}{24} \zeta(5) \right] \left(\frac{\alpha}{\pi} \right)^3
 \end{aligned} \tag{3.44}$$

This is the famous analytical result of Laporta and Remiddi (1996) [28], which largely confirmed an earlier numerical result of Kinoshita [29]. For the evaluation of (3.44) one needs the constants given in (3.41) and (3.42) before.

- 4-loop diagrams [891 diagrams] with common fermion lines so far have been calculated by numerical methods mainly by Kinoshita and collaborators. The status had been summarized by Kinoshita and Marciano (1990) [30] some time ago. Since then, the result has been further improved by Kinoshita and his collaborators (2002/2005/2007/2012/2014) [9, 10, 31–33]. They find

$$- 1.91298(84) \left(\frac{\alpha}{\pi} \right)^4 ,$$

by improving earlier results. In a seminal paper Laporta [11] obtained the high precision (quasi-exact) result

$$- 1.912\,245\,764\,9 \dots \left(\frac{\alpha}{\pi} \right)^4 ,$$

which agrees to 0.9σ with the previous result from [10] and we will use in the following.

Recently, for the first time, the universal 5-loop result has been worked out in [10, 33–35]. An evaluation of all 12672 diagrams with the help of an automated code generator yields the result

$$7.795(336) \left(\frac{\alpha}{\pi} \right)^5 .$$

The error is due to the statistical fluctuation in the Monte-Carlo integration of the Feynman amplitudes by the VEGAS routine. With the new result for the universal 5-loop term the largest uncertainty in the prediction of a_e has reduced by a factor of 4.5 from the previous one.

Collecting the universal terms we have

$$\begin{aligned}
 a_\ell^{\text{uni}} &= 0.5 \left(\frac{\alpha}{\pi}\right) - 0.328\,478\,965\,579\,193\,78\dots \left(\frac{\alpha}{\pi}\right)^2 \\
 &\quad + 1.181\,241\,456\,587\dots \left(\frac{\alpha}{\pi}\right)^3 - 1.912\,245\,764\,9\dots \left(\frac{\alpha}{\pi}\right)^4 + 7.795(336) \left(\frac{\alpha}{\pi}\right)^5 \\
 &= 0.001\,159\,652\,176\,42(26)(4)[26]\dots
 \end{aligned} \tag{3.45}$$

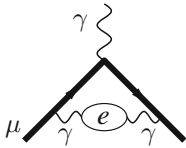
for the one-flavor QED contribution. The three errors are from the error of α given in (3.29) and from the numerical uncertainties of the α^5 coefficients, respectively.

It is interesting to note that the first term $a_\ell^{(2)} \simeq 0.00116141\dots$ contributes the first three significant digits. Thus the anomalous magnetic moment of a lepton is an effect of about 0.12%, $g_\ell/2 \simeq 1.00116\dots$, but in spite of the fact that it is so small we know a_e and a_μ more precisely than most other precision observables.

(2) QED mass dependent part:

Since fermions, as demanded by the SM,⁷ only interact via photons or other spin one gauge bosons, mass dependent corrections only may show up at the two-loop level via photon *vacuum polarization* effects. There are two different regimes for the mass dependent effects [36, 37]:

- LIGHT internal masses give rise to potentially large logarithms of mass ratios which get singular in the limit $m_{\text{light}} \rightarrow 0$



$$a_\mu^{(4)}(\text{vap}, e) = \left[\frac{1}{3} \ln \frac{m_\mu}{m_e} - \frac{25}{36} + O\left(\frac{m_e}{m_\mu}\right) \right] \left(\frac{\alpha}{\pi}\right)^2 .$$

Here we have a typical result for a light field which produces a large logarithm $\ln \frac{m_\mu}{m_e} \simeq 5.3$, such that the first term ~ 2.095 is large relative to a typical constant second term -0.6944 . Here⁸ the exact two-loop result is

$$a_\mu^{(4)}(\text{vap}, e) \simeq 1.094\,258\,3092(72) \left(\frac{\alpha}{\pi}\right)^2 = 5.90406006(4) \times 10^{-6} .$$

The error is due to the uncertainty in the mass ratio (m_e/m_μ).

The kind of leading short distance log contribution just discussed, which is related to the UV behavior,⁹ in fact may be obtained from a renormalization group type argument. In Sect. 2.6.5 (2.233) we have shown that if we replace in the one-loop result $\alpha \rightarrow \alpha(m_\mu)$ we obtain

⁷Interactions are known to derive from a local gauge symmetry principle, which implies the structure of gauge couplings, which must be of vector (V) or axial-vector (A) type.

⁸The leading terms shown yield $5.84199477 \times 10^{-6}$.

⁹The muon mass m_μ here serves as a UV cut-off, the electron mass as an IR cut-off, and the relevant integral reads

$$a_\mu = \frac{1}{2} \frac{\alpha}{\pi} \left(1 + \frac{2}{3} \frac{\alpha}{\pi} \ln \frac{m_\mu}{m_e} \right), \tag{3.46}$$

which reproduces precisely the leading term of the two-loop result. RG type arguments, based on the related Callan–Symanzik (CS) equation approach, were further developed and refined in [38, 39]. The CS equation is a differential equation which quantifies the response of a quantity to a change of a physical mass like m_e relative to the renormalization scale which is m_μ if we consider a_μ . For the leading m_e -dependence of a_μ , neglecting all terms which behave like powers of m_e/m_μ for $m_e \rightarrow 0$ at fixed m_μ , the CS equation takes the simple homogeneous form

$$\left(m_e \frac{\partial}{\partial m_e} + \beta(\alpha) \alpha \frac{\partial}{\partial \alpha} \right) a_\mu^{(\infty)} \left(\frac{m_\mu}{m_e}, \alpha \right) = 0, \tag{3.47}$$

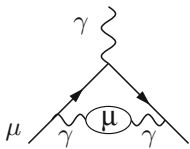
where $a_\mu^{(\infty)}$ denotes the contribution to a_μ from powers of logarithms $\ln \frac{m_\mu}{m_e}$ and constant terms and $\beta(\alpha)$ is the QED β -function. The latter governs the charge screening of the electromagnetic charge, which will be discussed below. The charge is running according to (resummed one-loop approximation)

$$\alpha(\mu) = \frac{\alpha}{1 - \frac{2}{3} \frac{\alpha}{\pi} \ln \frac{\mu}{m_e}} \tag{3.48}$$

which in linear approximation yields (3.46).

We continue with the consideration of the other contributions. For comparison we also give the result for the

- EQUAL internal masses case which yields a pure number and has been included in the $a_\ell^{(4)}$ universal part (3.43) already:



$$a_\mu^{(4)}(\text{vap}, \mu) = \left[\frac{119}{36} - \frac{\pi^2}{3} \right] \left(\frac{\alpha}{\pi} \right)^2.$$

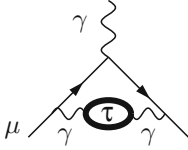
This no scale result shows another typical aspect of perturbative answers. There is a rational term of size 3.3055... and a transcendental π^2 term of very similar size 3.2899... but of opposite sign which yields as a sum a result which is only 0.5% of the individual terms:

(Footnote 9 continued)

$$\int_{m_e}^{m_\mu} \frac{dE}{E} = \ln \frac{m_\mu}{m_e}.$$

$$a_\mu^{(4)}(\text{vap}, \mu) \simeq 0.015\,687\,4219 \left(\frac{\alpha}{\pi}\right)^2 = 8.464\,13319 \times 10^{-8}. \quad (3.49)$$

• HEAVY internal masses decouple¹⁰ in the limit $m_{\text{heavy}} \rightarrow \infty$ and thus only yield small power corrections



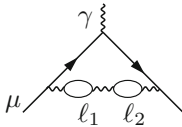
$$a_\mu^{(4)}(\text{vap}, \tau) = \left[\frac{1}{45} \left(\frac{m_\mu}{m_\tau}\right)^2 + O\left(\frac{m_\mu^4}{m_\tau^4} \ln \frac{m_\tau}{m_\mu}\right) \right] \left(\frac{\alpha}{\pi}\right)^2.$$

Note that “heavy physics” contributions, from mass scales $M \gg m_\mu$, typically are proportional to m_μ^2/M^2 . This means that besides the order in α there is an extra suppression factor, e.g. $O(\alpha^2) \rightarrow Q(\alpha^2 \frac{m_\mu^2}{M^2})$ in our case. To unveil new heavy states thus requires a corresponding high precision in theory and experiment. For the τ the contribution is relatively tiny

$$a_\mu^{(4)}(\text{vap}, \tau) \simeq 0.000\,078\,079(14) \left(\frac{\alpha}{\pi}\right)^2 = 4.2127(8) \times 10^{-10},$$

with error from the mass ratio (m_μ/m_τ). However, at the level of accuracy reached by the Brookhaven experiment (63×10^{-11}), the contribution is non-negligible.

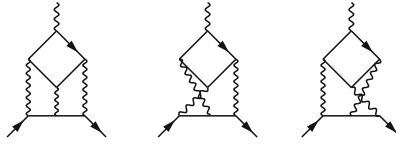
At the next higher order, in $a^{(6)}$ up to two internal closed fermion loops show up. The photon vacuum polarization (VP) insertions into photon lines again yield mass dependent effects if one or two of the μ loops of the universal contributions are replaced by an electron or a τ . These contributions will be discussed in more detail in Chap. 4. Here we just give the numerical results for the coefficients of $(\frac{\alpha}{\pi})^3$ [40–42]:



$$\begin{aligned} A_\mu^{(6)}(\text{vap}, e) &= 1.920\,455\,123(28), \\ A_\mu^{(6)}(\text{vap}, \tau) &= -0.001\,782\,61(27), \\ A_\mu^{(6)}(\text{vap}, e, \tau) &= 0.000\,527\,76(10). \end{aligned}$$

Besides these photon self-energy corrections, a new kind of contributions are the so called *light-by-light scattering* (LbL) insertions: closed fermion loops with four photons attached. Light-by-light scattering $\gamma\gamma \rightarrow \gamma\gamma$ is a fermion-loop induced process between real on-shell photons. There are 6 diagrams which follow from the first one below, by permutation of the photon vertices on the external muon line:

¹⁰The decoupling-theorem 2.10 infers that in theories like QED or QCD, where couplings and masses are independent parameters of the Lagrangian, a heavy particle of mass M decouples from physics at lower scales E_0 as E_0/M for $M \rightarrow \infty$.



plus the ones obtained by reversing the direction of the fermion loop. Remember that closed fermion loops with three photons vanish by Furry’s theorem. Again, besides the equal mass case $m_{\text{loop}} = m_\mu$ there are two different regimes [43, 44]:

- LIGHT internal masses also in this case give rise to potentially large logarithms of mass ratios which get singular in the limit $m_{\text{light}} \rightarrow 0$

$$a_\mu^{(6)}(\text{lbl}, e) = \left[\frac{2}{3} \pi^2 \ln \frac{m_\mu}{m_e} + \frac{59}{270} \pi^4 - 3 \zeta(3) - \frac{10}{3} \pi^2 + \frac{2}{3} + O\left(\frac{m_e}{m_\mu} \ln \frac{m_\mu}{m_e}\right) \right] \left(\frac{\alpha}{\pi}\right)^3.$$

This again is a light loop which yields an unexpectedly large contribution

$$a_\mu^{(6)}(\text{lbl}, e) \simeq 20.947\,924\,85(14) \left(\frac{\alpha}{\pi}\right)^3 = 2.625\,351\,01(2) \times 10^{-7},$$

with error from the (m_e/m_μ) mass ratio. Historically, it was calculated first numerically by Aldins et al. [45], after a 1.7σ discrepancy with the CERN measurement [46] in 1968 showed up.¹¹

For comparison we also present the

- EQUAL internal masses case which yields a pure number which is included in the $a_e^{(6)}$ universal part (3.44) already:

$$a_\mu^{(6)}(\text{lbl}, \mu) = \left[\frac{5}{6} \zeta(5) - \frac{5}{18} \pi^2 \zeta(3) - \frac{41}{540} \pi^4 - \frac{2}{3} \pi^2 \ln^2 2 + \frac{2}{3} \ln^4 2 + 16a_4 - \frac{4}{3} \zeta(3) - 24\pi^2 \ln 2 + \frac{931}{54} \pi^2 + \frac{5}{9} \right] \left(\frac{\alpha}{\pi}\right)^3,$$

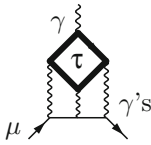
¹¹The result of [45] was $2.30 \pm 0.14 \times 10^{-7}$ pretty close to the “exact” answer above. The occurrence of such large terms of course has a physical interpretation [47]. Firstly, the large logs $\ln(m_\mu/m_e)$ are due to a logarithmic UV divergence in the limit $m_\mu \rightarrow \infty$, i.e., m_μ serves as a UV cut-off, in conjunction with an IR singularity in the limit $m_e \rightarrow 0$, i.e., m_e serves as an IR cut-off: $\int_{m_e}^{m_\mu} \frac{dE}{E} = \ln \frac{m_\mu}{m_e}$. The integral is large because of the large range $[m_e, m_\mu]$ and an integrand with the property that it is contributing equally at all scales. Secondly, and this is the new point here, there is an unusual $\pi^2 \sim 10$ factor in the coefficient of the large log. This enhancement arises from the LbL scattering sub-diagram where the electron is moving in the field of an almost static non-relativistic muon. A non-relativistic spin-flip interaction (required to contribute to a_μ) gets dressed by Coulomb interactions between muon and electron, which produces the large π^2 factor.

where a_4 is the constant defined in (3.42). The single scale QED contribution is much smaller

$$a_\mu^{(6)}(\text{lbl}, \mu) \simeq 0.371005292 \left(\frac{\alpha}{\pi}\right)^3 = 4.64971650 \times 10^{-9} \quad (3.50)$$

but is still a substantial contributions at the required level of accuracy.

• HEAVY internal masses again decouple in the limit $m_{\text{heavy}} \rightarrow \infty$ and thus only yield small power correction



$$a_\mu^{(6)}(\text{lbl}, \tau) = \left[\left[\frac{3}{2} \zeta(3) - \frac{19}{16} \right] \left(\frac{m_\mu}{m_\tau} \right)^2 + O \left(\frac{m_\mu^4}{m_\tau^4} \ln^2 \frac{m_\tau}{m_\mu} \right) \right] \left(\frac{\alpha}{\pi} \right)^3.$$

As expected this heavy contribution is power suppressed yielding

$$a_\mu^{(6)}(\text{lbl}, \tau) \simeq 0.00214324(38) \left(\frac{\alpha}{\pi}\right)^3 = 2.68607(48) \times 10^{-11},$$

and therefore would play a significant role at a next level of precision experiments only. Again the error is from the (m_μ/m_τ) mass ratio.

We mention that except for the mixed term $A_\mu^{(6)}(\text{vap}, e, \tau)$, which has been worked out as a series expansion in the mass ratios [41, 42], all contributions are known analytically in exact form [40, 43]¹² up to 3 loops. At 4 loops only a few terms are known analytically [49, 50]. Again the relevant 4-loop contributions have been evaluated by numerical integration methods by Kinoshita and Nio [31, 51]. The universal part is now superseded by Laporta's high-precision result [11]. After earlier estimates of the 5-loop term in [52–54], finally the pioneering complete 5-loop calculation by Aoyama, Hayakawa, Kinoshita and Nio [51] has been completed to contribute with $A_2^{(10)}(m_\mu/m_e) = 663(20)$. A number of partial results based on asymptotic expansion techniques have been obtained in [55]. More recent result have been presented in [39, 50, 56–58]. Results largely confirm the numerical calculations.

Combining the universal and the mass dependent terms discussed so far we arrive at the following QED result for a_μ

$$a_\mu^{\text{QED}} = \frac{\alpha}{2\pi} + 0.765857423(16) \left(\frac{\alpha}{\pi}\right)^2 + 24.05050982(28) \left(\frac{\alpha}{\pi}\right)^3 + 130.8734(60) \left(\frac{\alpha}{\pi}\right)^4 + 751.917(932) \left(\frac{\alpha}{\pi}\right)^5. \quad (3.51)$$

¹²Explicitly, the papers present expansions in the mass ratios; some result have been extended in [44] and cross checked against the full analytic result in [48].

Growing coefficients in the α/π expansion reflect the presence of large $\ln \frac{m_\mu}{m_e} \simeq 5.3$ terms coming from electron loops. In spite of the strongly growing expansion coefficients the convergence of the perturbation series is excellent

# n of loops	$C_i [(\alpha/\pi)^n]$	$a_\mu^{\text{QED}} \times 10^{11}$
1	+ 0.5	116140973.242 (26)
2	+ 0.765 857 423 (16)	413217.627 (9)
3	+ 24.050 509 82 (28)	30141.9022 (4)
4	+ 130.8734 (60)	380.990 (17)
5	+ 751.917 (932)	5.0845 (63)
tot		116584718.859 (0.034)

because α/π is a truly small expansion parameter.

Now we have to address the question what happens beyond QED. What is measured in an experiment includes effects from the real world and we have to include the contributions from all known particles and interactions such that from a possible deviation between theory and experiment we may get a hint of the yet unknown physics.

Going from QED of leptons to the SM the most important step is to include the hadronic effects mediated by the quarks, which in the SM sit in families together with the leptons and neutrinos. The latter being electrically neutral do not play any role, in contrast to the charged quarks. The *strong interaction effects* are showing up in particular through the hadronic structure of the photon via vacuum polarization starting at $O(\alpha^2)$ or light-by-light scattering starting at $O(\alpha^3)$.

(3) Hadronic VP effects:

Formally, these are the contributions obtained by replacing lepton-loops by quark-loops (see Fig. 3.2), however, the quarks are strongly interacting via gluons as described by the $SU(3)_{\text{color}}$ gauge theory QCD [59] (see Sect. 2.8). While electromagnetic and weak interactions are weak in the sense that they allow us to perform perturbation expansions in the coupling constants, strong interactions are weak only at high energies as inferred by the property of asymptotic freedom (anti-screening).¹³ At energies above about 2 GeV perturbative QCD (pQCD) may be applied as well. In the regime of interest to us here, however, perturbative QCD fails. The strength of the strong coupling “constant” increases dramatically as we approach lower energies. This is firmly illustrated by Fig. 3.3, which shows a compilation of measured strong coupling constants as a function of energy in comparison to perturbative QCD. The latter seems to describe very well the running of α_s down to 2 GeV. Fortunately the leading order hadronic effects are vacuum polarization type corrections, which can

¹³Asymptotic freedom, discovered in 1973 by Politzer, Gross and Wilczek [60] (Nobel Prize 2004), is one of the key properties of QCD and explains why at high enough energies one observes quasi-free quarks, as in deep inelastic scattering (DIS) of electrons on protons. Thus, while quarks remain imprisoned inside color neutral hadrons (quark confinement), at high enough energies (so called hard subprocesses) the *quark parton model* (QPM) of free quarks may be a reasonable approximation, which may be systematically improved by including the perturbative corrections.

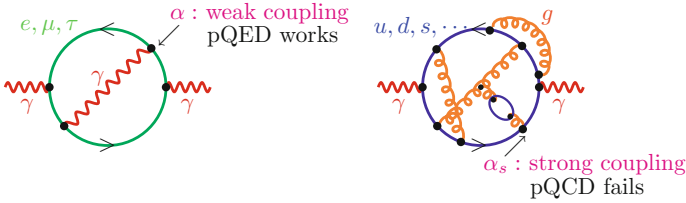


Fig. 3.2 The hadronic analog of the lepton loops

Fig. 3.3 A compilation of α_s measurements in a plot from Ref. [12]. The lowest point shown is at the τ lepton mass $M_\tau = 1.78$ GeV where $\alpha_s(M_\tau) = 0.322 \pm 0.030$. Resource the Review of Particle Physics (2016)

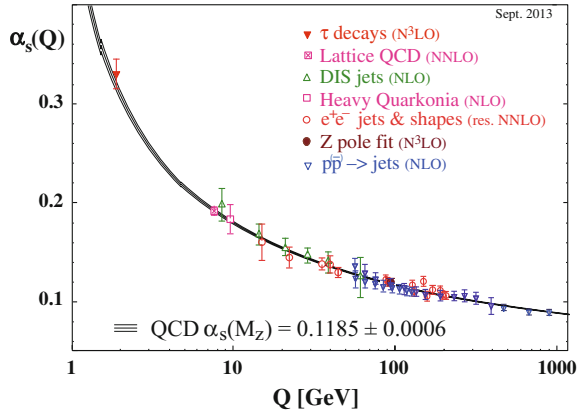
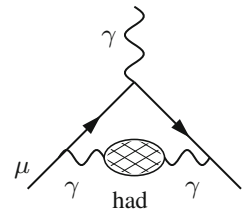


Fig. 3.4 The leading order hadronic vacuum polarization diagram



be safely evaluated by exploiting causality (analyticity) and unitarity (optical theorem) together with experimental low energy data. The imaginary part of the photon self-energy function $\Pi'_\gamma(s)$ (see Sect. 2.6.1) is determined via the optical theorem by the total cross section of hadron production in electron-positron annihilation:

$$\sigma(s)_{e^+e^- \rightarrow \gamma^* \rightarrow \text{hadrons}} = \frac{4\pi^2\alpha}{s} \frac{1}{\pi} \text{Im} \Pi'_\gamma^{\text{had}}(s) . \quad (3.52)$$

The leading Hadronic Vacuum Polarization (HVP) contribution is represented by the diagram Fig. 3.4, which has a representation as a dispersion integral

$$a_\mu = \frac{\alpha}{\pi} \int_0^\infty \frac{ds}{s} \frac{1}{\pi} \text{Im} \Pi'_\gamma^{\text{had}}(s) K(s) , \quad K(s) \equiv \int_0^1 dx \frac{x^2(1-x)}{x^2 + \frac{s}{m_\mu^2}(1-x)} . \quad (3.53)$$

As a result the leading non-perturbative hadronic contributions a_μ^{had} can be obtained in terms of $R_\gamma(s) \equiv \sigma^{(0)}(e^+e^- \rightarrow \gamma^* \rightarrow \text{hadrons})/\frac{4\pi\alpha^2}{3s}$ data via the dispersion integral:

$$a_\mu^{\text{had}} = \left(\frac{\alpha m_\mu}{3\pi}\right)^2 \left(\int_{m_{\pi^0}^2}^{E_{\text{cut}}^2} ds \frac{R_\gamma^{\text{data}}(s) \hat{K}(s)}{s^2} + \int_{E_{\text{cut}}^2}^{\infty} ds \frac{R_\gamma^{\text{pQCD}}(s) \hat{K}(s)}{s^2} \right), \quad (3.54)$$

where the rescaled kernel function $\hat{K}(s) = 3s/m_\mu^2 K(s)$ is a smooth bounded function, increasing from 0.63... at $s = 4m_\pi^2$ to 1 as $s \rightarrow \infty$. The $1/s^2$ enhancement at low energy implies that the $\rho \rightarrow \pi^+\pi^-$ resonance is dominating the dispersion integral ($\sim 75\%$). Data can be used up to energies where $\gamma - Z$ mixing comes into play at about $E_{\text{cut}} = 40$ GeV. However, by the virtue of asymptotic freedom, perturbative Quantum Chromodynamics (see p. 145) (pQCD) gets the more reliable the higher the energy and, in fact, it may be used safely in regions away from the flavor thresholds, where resonances show up: ρ, ω, ϕ , the J/ψ series and the Υ series. We thus use perturbative QCD [61, 62] from 5.2 to 9.6 GeV and for the high energy tail above 13 GeV, as recommended in [61–63].

Hadronic cross section measurements $e^+e^- \rightarrow \text{hadrons}$ at electron-positron storage rings started in the early 1960's and continued up to date. Since our analysis [64] in 1995 data from MD1 [65], BES-II [66] and from CMD-2 [67] have lead to a substantial reduction in the hadronic uncertainties on a_μ^{had} . More recently, KLOE [68], SND [69] and CMD-2 [70] published new measurements in the region below 1.4 GeV. My up-to-date evaluation of the leading order HVP yields [71–74]

$$a_\mu^{\text{had}(1)} = (688.77 \pm 3.38[688.07 \pm 4.14]) \times 10^{-10}. \quad (3.55)$$

The result also includes τ -decay spectral data (the $I=1$ part corrected for isospin breaking) in the range [0.63–0.96] GeV as estimated in [72] (see Chap. 5, Sect. 5.1.10). Table 3.1 gives more details about the origin of contributions and errors from different regions. A recent analysis [75] (also see [76, 77]) using the precise $\pi\pi$ scattering data to constrain the low energy tail below 0.63 GeV (see (5.100) in Chap. 5) allows one to improve the estimate to

$$a_\mu^{\text{had}(1)} = (689.46 \pm 3.25) \times 10^{-10}. \quad (3.56)$$

A list of data based evaluations by different groups is presented in Table 3.2. The list documents the big efforts made by experiments within the past decade to provide more and more accurate data, which are the indispensable input for controlling non-perturbative strong interaction effects. Differences in errors come about mainly by utilizing more “theory-driven” concepts: use of selected data sets only, extended use of perturbative QCD in place of data [assuming local duality], sum rule methods, low

Table 3.1 Contributions and errors from different energy ranges

Energy range	$a_\mu^{\text{had}} \times 10^{10}$ [in %]	(error) $\times 10^{10}$	rel. err. (%)	abs. err. (%)
$\rho, \omega (E < 2M_K)$	541.25 [78.7%]	(2.84)	0.5	47.6
$2M_K < E < 2 \text{ GeV}$	95.63 [13.9%]	(2.77)	3.1	45.2
$2 \text{ GeV} < E < M_{J/\psi}$	21.63 [3.1%]	(0.93)	4.3	5.1
$M_{J/\psi} < E < 5.2 \text{ GeV}$	20.34 [3.0%]	(0.59)	2.9	2.1
$5.2 \text{ GeV} < E < M_\Upsilon$ pQCD	6.27 [0.9%]	(0.01)	0.1	0.0
$M_\Upsilon < E < E_{\text{cut}}$	0.98 [0.1%]	(0.05)	5.2	0.0
$E_{\text{cut}} < E$ pQCD	1.96 [0.3%]	(0.00)	0.0	0.0
$E < E_{\text{cut}}$ data	679.84 [98.8%]	(4.11)	0.6	100
Total	688.07 [100%]	(4.11)	0.6	100

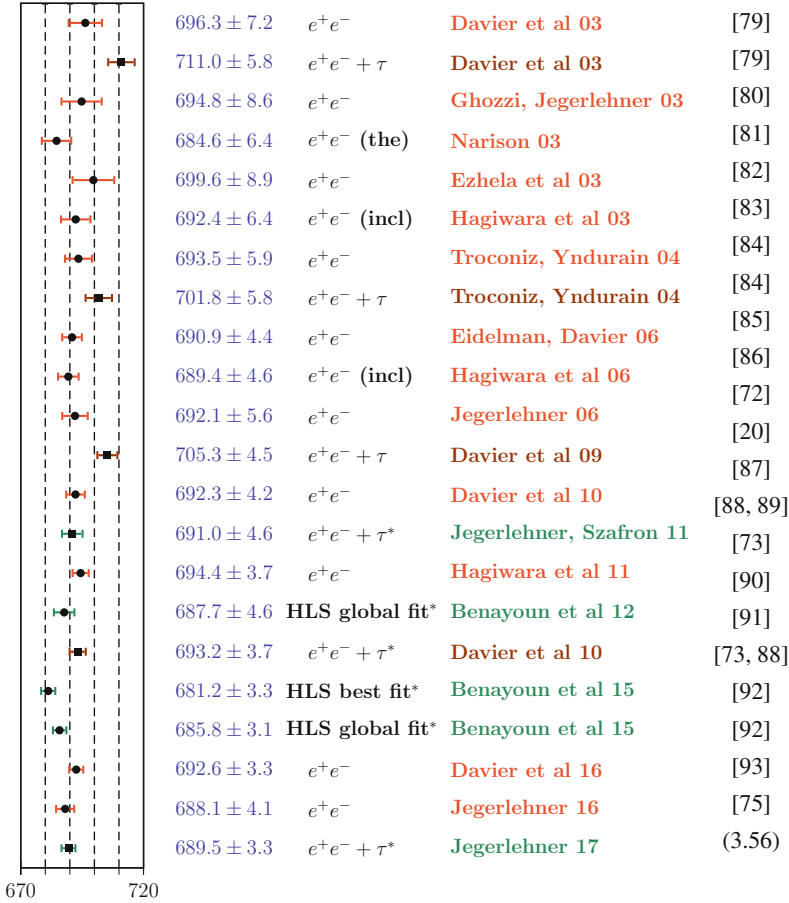
energy effective methods [78]. Progress is essentially correlated with the availability of new data from Novosibirsk (NSK) [69, 70, 79], Frascati (KLOE) [80–82], SLAC (BaBar) [83] and Beijing (BES-III) [84].¹⁴ In the last 15 years e^+e^- cross-section measurements have dramatically improved, from energy scans [69, 70, 79] (SCAN) at Novosibirsk (NSK) and later, using the radiative return mechanism, measurements via initial state radiation (ISR) at meson factories [80–84]. Still the most precise ISR measurements from KLOE and BaBar are in conflict and the new, although still somewhat less precise, ISR data from BES-III help to clarify this tension. The BES-III result for $a_\mu^{\pi\pi, \text{LO}}$ (0.6 – 0.9 GeV) is found to be in good agreement with all KLOE values, while a 1.7σ lower value is observed with respect to the BaBar result. Other data recently collected, and published up to the end of 2014, include the $e^+e^- \rightarrow 3(\pi^+\pi^-)$ data from CMD-3 [90], the $e^+e^- \rightarrow \omega\pi^0 \rightarrow \pi^0\pi^0\gamma$ from SND [91] and several data sets collected by BaBar in the ISR mode¹⁵ [92–94]. These data samples highly increase the available statistics for the annihilation channels opening above 1 GeV and lead to significant improvements. Recent/preliminary results also included are $e^+e^- \rightarrow \pi^+\pi^-\pi^0$ from Belle, $e^+e^- \rightarrow K^+K^-$ from CMD-3, $e^+e^- \rightarrow K^+K^-$ from SND. The BES-III data sample is included in the last four entries of the table.

Besides the true e^+e^- data measured by energy scans and the ISR method, the $I = 1$ isovector part of $e^+e^- \rightarrow$ hadrons can be obtained in an alternative way by using the precise vector spectral functions from hadronic τ -decays $\tau \rightarrow \nu_\tau +$ hadrons via an isospin rotation [95]. For the dominating $\pi\pi$ channel τ decay spectra

¹⁴The analysis [85] does not include exclusive data in a range from 1.43 to 2 GeV; therefore also the important exclusive channels BaBar data are not included in that range. In [86–89] pQCD is used in the extended ranges 1.8–3.7 GeV and above 5.0 GeV and in [87] KLOE data are not included. More recently a reanalysis of the KLOE08 data were released as KLOE12 set, which was first included in the evaluation [73].

¹⁵Including the $p\bar{p}$, K^+K^- , $K_L K_S$, $K_L K_S \pi^+\pi^-$, $K_S K_S \pi^+\pi^-$, $K_S K_S K^+K^-$ final states.

Table 3.2 Some recent evaluations of $a_\mu^{\text{had}(1)}$ (in units 10^{-10}). The Table illustrates the progress since 2003, when precise data from Novosibirsk became available. Further progress has been possible with the data obtained by the ISR method at the ϕ -factory Daphne at Frascati (KLOE detector) and the B -factory PEP-II at SLAC (BaBar detector) and with the BEPC storage ring at Beijing (BES detector)



have been measured by the ALEPH, OPAL, CLEO and Belle experiments [96–100]. After isospin violating corrections, due to photon radiation and the mass splitting $m_d - m_u \neq 0$, have been applied, there remains an unexpectedly large discrepancy between the e^+e^- - and the τ -based determinations of a_μ [86–89], as may be seen in Table 3.2. This τ versus e^+e^- data puzzle has been persisting for several years. Possible explanations are so far unaccounted isospin breaking [101] or experimental problems with the data. Since the e^+e^- -data are more directly related to what is required in the dispersion integral, one usually advocates to use the e^+e^- data only.

The puzzle at the end disappeared, after isospin breaking by $\gamma - \rho^0$ mixing, missing in the charged τ channel, has been accounted for [72]. The point is the correct modeling of the Vector Meson Dominance (VMD) mechanism, which, by including ρ , ω , ϕ as well results in the Hidden Local Symmetry (HLS) model parametrization of the low energy data [73, 102] [up to including the ϕ resonance]. This a low effective Lagrangian field theory approach, which includes the VMD model in accord with low energy structure of QCD. A “HLS best fit” is obtained for the data configuration NSK+KLOE10+KLOE12+BES-III+ τ . The “HLS global fit” includes the BaBar $\pi\pi$ spectrum as well. In Table 3.2 results including τ corrected for the $\gamma - \rho^0$ mixing are marked by the asterisk *. A comprehensive analysis of the hadronic effects will be presented in Chap. 5, Sect. 5.1. See also the comments to Fig. 7.1.

At next-to-leading order (NLO), $O(\alpha^3)$, diagrams of the type shown in Fig. 3.5a–c have to be calculated, where the first diagram stands for a class of higher order hadronic contributions obtained if one replaces in any of the first 6 two-loop diagrams of Fig. 4.2, one internal photon line by a dressed one. The relevant kernels for the corresponding dispersion integrals have been calculated analytically in [103] and appropriate series expansions were given in [104] (for earlier estimates see [105, 106]). Based on my recent compilation of the e^+e^- data [74] I obtain

$$a_\mu^{(6)}(\text{vap, had}) = -99.27(0.87) \times 10^{-11},$$

in accord with previous evaluations [95, 104, 106, 107] (see Table 5.7). The errors include statistical and systematic errors added in quadrature. Very recently the relevant next-to-next-to-leading order (NNLO), $O(\alpha^4)$, hadronic contributions, represented by diagrams of the type also shown in Fig. 3.5a–h, have been estimated [108, 109]

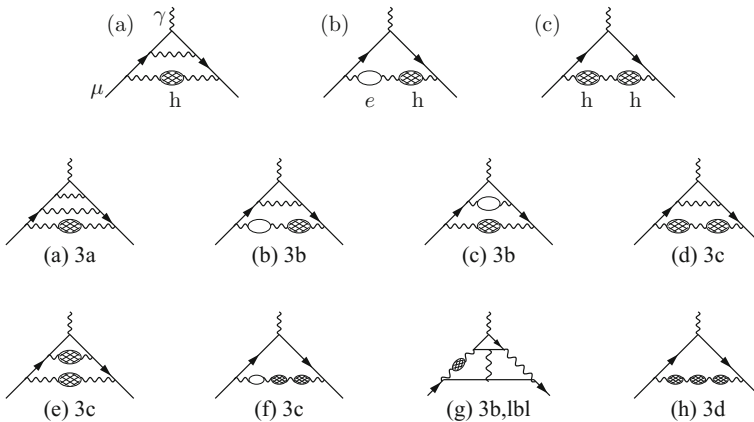


Fig. 3.5 Higher order (HO) vacuum polarization contributions

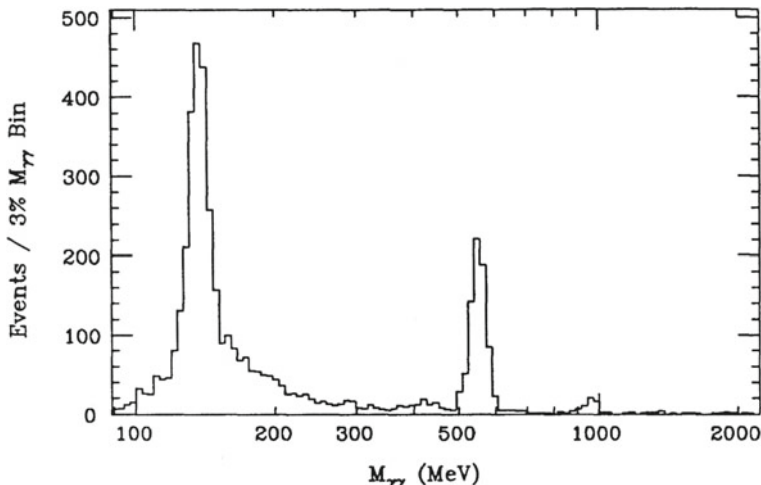


Fig. 3.6 The spectrum of invariant $\gamma\gamma$ masses obtained with the Crystal Ball detector [110]. The three rather pronounced spikes seen are the $\gamma\gamma \rightarrow$ pseudoscalar (PS) $\rightarrow \gamma\gamma$ excitations: PS = π^0, η, η'

$$a_{\mu}^{(8)}(\text{vap, had}) = 12.21(0.10) \times 10^{-11},$$

which amounts to a 10% reduction of the NLO HVP result.

(4) Hadronic LbL effects:

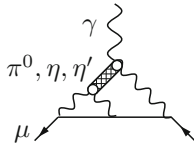
A much more problematic set of hadronic corrections are those related to hadronic light-by-light scattering, which sets in only at order $O(\alpha^3)$, fortunately. However, we already know from the leptonic counterpart that this contribution could be dramatically enhanced. It was estimated for the first time in [105]. Even for real-photon light-by-light scattering, perturbation theory is far from being able to describe reality, as the reader may convince himself by a glance at Fig. 3.6, showing sharp spikes of π^0, η and η' production, while pQCD predicts a smooth continuum.¹⁶ As a contribution to the anomalous magnetic moment three of the four photons are virtual and to be integrated over all four-momentum space, such that a direct experimental input for the non-perturbative dressed four-photon correlator is not available. In this case one has to resort to the low energy effective descriptions of QCD like *Chiral Perturbation Theory* (CHPT) extended to include vector-mesons. This Resonance Lagrangian Approach (RLA) is realizing vector-meson dominance ideas in accord with the low energy structure of QCD [111]. Other effective theories are the Extended Nambu-Jona-Lasinio (ENJL) model [112] (see also [113]) or the very

¹⁶The pion which gives the by far largest contribution is a quasi Goldstone boson. In the chiral limit of vanishing light quark masses $m_u = m_d = m_s = 0$ pions and Kaons are true Goldstone bosons which exist due to the spontaneous breakdown of the chiral $U(N_f)_V \otimes U_A(N_f)$ ($N_f = 3$) symmetry, which is a non-perturbative phenomenon, absent in pQCD.

similar HLS model [114, 115]; approaches more or less accepted as a framework for the evaluation of the hadronic LbL effects. The amazing fact is that the interactions involved in the hadronic LbL scattering process are the parity conserving QED and QCD interactions while the process is dominated by the parity odd pseudoscalar meson-exchanges. This means that the effective $\pi^0\gamma\gamma$ interaction vertex exhibits the parity violating γ_5 coupling, which of course in $\gamma\gamma \rightarrow \pi^0 \rightarrow \gamma\gamma$ must appear twice (an even number of times). The process indeed is associated with the parity odd Wess-Zumino-Witten (WZW) effective interaction term

$$\mathcal{L}^{(4)} = -\frac{\alpha N_c}{12\pi F_0} \varepsilon_{\mu\nu\rho\sigma} F^{\mu\nu} A^\rho \partial^\sigma \pi^0 + \dots \quad (3.57)$$

which reproduces the Adler-Bell-Jackiw (ABJ) anomaly and which plays a key role in estimating the leading hadronic LbL contribution. F_0 denotes the pion decay constant F_π in the chiral limit of massless light quarks ($F_\pi \simeq 92.4$ MeV). The constant WZW form factor yields a divergent result, applying a cut-off Λ one obtains the leading term



The diagram shows a muon line (solid line with arrows) interacting with a photon loop (wavy line with a cross-hatched box) and a pion exchange (dashed line) between the vertices. The external lines are labeled μ and γ . The vertices are labeled π^0, η, η' .

$$a_\mu^{(6)}(\text{lbl}, \pi^0) = \left[\frac{N_c^2}{48\pi^2} \frac{m_\mu^2}{F_\pi^2} \ln^2 \frac{\Lambda}{m_\mu} + \dots \right] \left(\frac{\alpha}{\pi} \right)^3$$

with a universal coefficient $C = N_c^2 m_\mu^2 / (48\pi^2 F_\pi^2)$ [116]; in the VMD dressed cases M_V represents the cut-off $\Lambda \rightarrow M_V$.¹⁷

Based on refined effective field theory (EFT) models, two major efforts in evaluating the full a_μ^{LbL} contribution were made by Hayakawa, Kinoshita and Sanda (HKS 1995) [114], Bijmans, Pallante and Prades (BPP 1995) [112] and Hayakawa and Kinoshita (HK 1998) [115] (see also Kinoshita, Nizic and Okamoto (KNO 1985) [106]). Although the details of the calculations are quite different, which results in a different splitting of various contributions, the results are in good agreement and essentially given by the π^0 -pole contribution, which was taken with the wrong sign, however. In order to eliminate the cut-off dependence in separating long distance (L.D.) and short distance (S.D.) physics, more recently it became favorable to use quark-hadron duality, as it holds in the large- N_c limit of QCD [117, 118], for modeling of the hadronic amplitudes [113]. The infinite series of narrow vector states known to show up in the large N_c limit is then approximated by a suitable lowest meson dominance (LMD+V) ansatz [119], assumed to be saturated by known low lying physical states of appropriate quantum numbers. This approach was adopted in a reanalysis by Knecht and Nyffeler (KN 2001) [116, 120–122] in 2001, in which they discovered a sign mistake in the dominant π^0, η, η' exchange contribution, which

¹⁷Since the leading term is divergent and requires UV subtraction, we expect this term to drop from the physical result, unless a physical cut-off tames the integral, like the physical ρ in effective theories which implement the VMD mechanism.

changed the central value by $+167 \times 10^{-11}$, a 2.8σ shift, and which reduces a larger discrepancy between theory and experiment. More recently Melnikov and Vainshtein (MV 2004) [123] found additional problems in previous calculations, this time in the short distance constraints (QCD/OPE) used in matching the high energy behavior of the effective models used for the π^0 , η , η' exchange contribution. Another important change concerns the contributions from the axialvector exchanges which have been modeled in [123] violating the Landau–Yang theorem. We will elaborate on this in much more detail in Sect. 5.2.

We advocate to use consistently dressed form factors as inferred from the resonance Lagrangian approach. However, other effects which were first considered in [123] must be taken into account: (i) the constraint on the twist four ($1/q^4$)-term in the OPE requires $h_2 = -10 \text{ GeV}^2$ in the Knecht-Nyffeler form factor [120]: $\delta a_\mu \simeq +5 \pm 0$ relative to $h_2 = 0$, (ii) the contributions from the f_1 and f'_1 isoscalar axial–vector mesons: $\delta a_\mu \simeq +6 \pm 2$ (using dressed photons, and implementing the Landau–Yang condition), (iii) for the remaining effects, scalars (f_0) + dressed π^\pm , K^\pm loops + dressed quark loops: $\delta a_\mu \simeq -5 \pm 13$. Note that this last group of terms have been evaluated in [112, 114] only. The splitting into the different terms is model dependent and only the sum should be considered; the results read -5 ± 13 (BPP) and 5.2 ± 13.7 (HKS) and hence the contribution remains unclear.¹⁸ As an estimate based on [112, 114, 120, 123, 124] we adopt π^0 , η , η' [95 ± 12] + axial–vector [8 ± 3] + scalar [-6 ± 1] + π , K loops [-20 ± 5] + quark loops [22 ± 4] + tensor [1 ± 0] + NLO [3 ± 2] which yields

$$a_\mu^{(6)}(\text{lbl, had}) = (103 \pm 29) \times 10^{-11} .$$

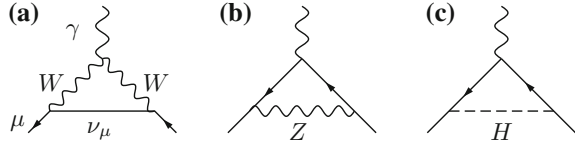
The result differs little from the “agreed” value $(105 \pm 26) \times 10^{-11}$ presented in [125] and $(116 \pm 39) \times 10^{-11}$ estimated in [20]. Both included a wrong, too large, Landau–Yang theorem violating axial–vector contribution from [123], correcting for this we obtain our reduced value relative to [20].

(5) Weak interaction corrections:

The last set of corrections are due to the weak interaction as described by the electroweak SM. The weak corrections are those mediated by the weak currents which couple to the heavy spin 1 gauge bosons, the charged W^\pm or the neutral “heavy light” particle Z or by exchange of a Higgs particle H (see Fig. 3.7; masses are given in (3.33), (3.34)). What is most interesting is the occurrence of the first diagram of Fig. 3.7, which exhibits a non–Abelian triple gauge vertex and the corresponding contribution provides a test of the Yang–Mills structure involved. It is of course not surprising that the photon couples to the charged W boson the way it is dictated by electromagnetic gauge invariance. In spite of the fact that the contribution is of leading one–loop order, it is vastly suppressed by the fact that the corrections are mediated by the exchange of very heavy states which makes them suppressed by

¹⁸We adopt the result of [112] as the sign has to be negative in any case (see [121]).

Fig. 3.7 The leading weak contributions to a_ℓ ; diagrams in the physical unitary gauge



$O(2\frac{\alpha}{\pi}\frac{m_\mu^2}{M^2}) \sim 5 \times 10^{-9}$ for M of about 100 GeV. The gauge boson contributions up to negligible terms of order $O(\frac{m_\mu^2}{M_{W,Z}^2})$ are given by (the Higgs contribution is negligible) [126]

$$a_\mu^{(2)\text{EW}} = [5 + (-1 + 4 \sin^2 \Theta_W)^2] \frac{\sqrt{2}G_\mu m_\mu^2}{48\pi^2} \simeq (194.82 \pm 0.02) \times 10^{-11} . \tag{3.58}$$

The error comes from the uncertainty in $\sin^2 \Theta_W$ [see (3.32)].

Electroweak two-loop calculations started 1992 with Kukhto et al [127], who observed potentially large terms proportional to $\sim G_F m_\mu^2 \frac{\alpha}{\pi} \ln \frac{M_Z}{m_\mu}$ enhanced by a large logarithm. The most important diagrams are triangle fermion-loops:

$$a_\mu^{(4)\text{EW}}([f]) \simeq \frac{\sqrt{2}G_\mu m_\mu^2 \alpha}{16\pi^2} \frac{\alpha}{\pi} 2T_{3f} N_{cf} Q_f^2 \left[3 \ln \frac{M_Z^2}{m_{f'}^2} + C_f \right]$$

where T_{3f} is the 3rd component of the weak isospin, Q_f the charge and N_{cf} the color factor, 1 for leptons, 3 for quarks. The mass $m_{f'}$ is m_μ if $m_f < m_\mu$ and m_f if $m_f > m_\mu$, and $C_e = 5/2$, $C_\mu = 11/6 - 8/9 \pi^2$, $C_\tau = -6$ [127]. Note that triangle fermion-loops cannot contribute in QED due to Furry's theorem. However, the weak interactions are parity violating and if one of the three vector vertices $V^\mu = \gamma^\mu$ is replaced by an axial vertex $A^\mu = \gamma^\mu \gamma_5$ one gets a non-vanishing contribution. This is what happens if we replace one of the photons by a “heavy light” particle Z . However, these diagrams are responsible for the Adler-Bell-Jackiw anomaly [128] which is leading to a violation of axial current conservation and would spoil renormalizability. The anomalous terms must cancel and in the SM this happens by lepton quark duality: leptons and quarks have to live in families and for each family $\sum_f N_{cf} Q_f^2 T_{3f} = 0$, which is the anomaly cancellation condition in the $SU(3)_c \otimes SU(2)_L \otimes U(1)_Y$ gauge theory. This is again one of the amazing facts, that at the present level of precision one starts to be sensitive to the anomaly cancellation mechanism. This anomaly cancellation leads to substantial cancellations between the individual fermion contributions. The original results therefore get rectified by taking into account the family structure of SM fermions [129–131].

For more sophisticated analyses we refer to [129, 130, 132] which was corrected and refined in [131, 133]. Including subleading effects yields -5.0×10^{-11} for the first two families. The 3rd family of fermions including the heavy top quark can be treated in perturbation theory and was worked out to be -8.2×10^{-11} in [134]. Subleading fermion loops contribute -5.3×10^{-11} . There are many more diagrams contributing, in particular the calculation of the bosonic contributions (1678 diagrams) is a formidable task and has been performed 1996 by Czarnecki, Krause and Marciano as an expansion in $(m_\mu/M_V)^2$ and $(M_V/m_H)^2$ [135]. Later complete calculations, valid also for lighter Higgs masses, were performed [136, 137], which confirmed the previous result -22.3×10^{-11} . The 2-loop result reads¹⁹

$$a_\mu^{(4)\text{EW}} = -41(1) \times 10^{-11} .$$

The complete weak contribution may be summarized by [133]

$$\begin{aligned} a_\mu^{\text{EW}} &= \frac{\sqrt{2}G_\mu m_\mu^2}{16\pi^2} \left\{ \frac{5}{3} + \frac{1}{3} (1 - 4 \sin^2 \Theta_W)^2 - \frac{\alpha}{\pi} [155.5(4)(2)] \right\} \\ &= (154 \pm 1[\text{had}] \pm 0.4[m_H, m_t, 3 - \text{loop}]) \times 10^{-11} \end{aligned} \quad (3.59)$$

with errors from triangle quark-loops. For the Higgs we use the recent LHC observation $m_H \simeq 125.1 \pm 0.3$ GeV. The 3-loop effect has been estimated to be small [131, 133] (see (4.124)).

This closes our overview of the various contributions to the anomalous magnetic moment of the muon. More details about the higher order QED corrections as well as the weak and strong interaction corrections will be discussed in detail in the next Chap. 4. First we give a brief account of the status of the theory in comparison to the experiments. We will consider the electron and the muon in turn.

3.2.2 The Anomalous Magnetic Moment of the Electron

The electron magnetic moment anomaly likely is the experimentally most precisely known quantity. For almost 20 years the value was based on the extraordinary precise measurements of electron and positron anomalous magnetic moments

¹⁹The authors of [127] reported

$$a_\mu^{(4)\text{EW}} = -42 \times 10^{-11}$$

for what they thought was the leading correction, which is very close to the complete weak two-loop corrections, however, this coincidence looks to be a mere accident. Nevertheless, the sign and the order of magnitude turned out to be correct.

$$\begin{aligned} a_{e^-}^{\text{exp}} &= 0.001\,159\,652\,188\,4(43), \\ a_{e^+}^{\text{exp}} &= 0.001\,159\,652\,187\,9(43), \end{aligned} \quad (3.60)$$

by Van Dyck et al. (1987) [138]. The experiment used the ion trap technique, which has made it possible to study a single electron with extreme precision.²⁰ The result impressively confirms the conservation of CPT: $a_{e^+} = a_{e^-}$. Being a basic prediction of any QFT, CPT symmetry will be assumed to hold in the following. This allows us to average the electron and positron values with the result [14]

$$a_e = \mu_e/\mu_B - 1 = (g_e - 2)/2 = 1.159\,652\,1883(42) \times 10^{-3}. \quad (3.61)$$

The relative standard uncertainty is 3.62 ppb. A big step forward has been achieved more recently by Gabrielse et al. [5, 6, 139] in an experiment at Harvard University using a one-electron quantum cyclotron. The new result is

$$a_e = 1.159\,652\,180\,73(28)[0.24\text{ ppb}] \times 10^{-3}, \quad (3.62)$$

with an accuracy nearly 15 times better than (3.61) and shifting down the central value of a_e by 1.8 standard deviations.

The measurements of a_e not only played a key role in the history of precision tests of QED in particular, and of QFT concepts in general, today we may use the anomalous magnetic moment of the electron to get the most precise indirect measurement of the fine structure constant α . This possibility of course hangs on our ability to pin down the theoretical prediction with very high accuracy. Indeed a_e is much safer to predict reliably than a_μ . The reason is that non-perturbative hadronic effects as well as the sensitivity to unknown physics beyond the SM are suppressed by the large factor $m_\mu^2/m_e^2 \simeq 42\,753$ in comparison to a_μ . This suppression has to be put into perspective with the 2250 times higher precision with which we know a_e . We thus can say that effectively a_e is a factor 19 less sensitive to model dependent physics than a_μ .

The reason why it is so interesting to have such a precise measurement of a_e of course is that it can be calculated with comparable accuracy in theory. The prediction is given by a perturbation expansion of the form

$$a_e = \sum_{n=1}^N C_n (\alpha/\pi)^n, \quad (3.63)$$

²⁰The ion trap technique was introduced and developed by Paul and Dehmelt, whom was awarded the Nobel Prize in 1989. The ion traps utilize electrical quadrupole fields obtained with hyperboloid shaped electrodes. The Paul trap works with dynamical trapping using r.f. voltage, the Penning trap used by Dehmelt works with d.c. voltage and a magnetic field in z -direction.

with terms up to five loops, $N = 5$, under consideration. The experimental precision of a_e requires the knowledge of the coefficients with accuracies $\delta C_2 \sim 5 \times 10^{-8}$, $\delta C_3 \sim 2 \times 10^{-5}$, $\delta C_4 \sim 1 \times 10^{-2}$ and $\delta C_5 \sim 4$. Actually, Aoyama, Hayakawa, Kinoshita and Nio [10, 33] not long ago achieved remarkable progress in calculating missing four- and five-loop QED contributions. Besides the leading universal C_5 term, which we already included in (3.45), also so far missing mass-dependent μ and τ lepton contributions have been evaluated. Concerning the mass-dependent contributions, the situation for the electron is quite different from the muon. Since the electron is the lightest of the leptons a potentially large “light internal loop” contribution is absent. For a_e the muon is a heavy particle $m_\mu \gg m_e$ and its contribution is of the type “heavy internal loops” which is suppressed by an extra power of m_e^2/m_μ^2 . In fact the μ -loops tend to decouple and therefore only yield small terms. We may evaluate them by just replacing $m_\mu \rightarrow m_e$ and $m_\tau \rightarrow m_\mu$ in the formula for the τ -loop contributions to a_μ . Corrections due to internal μ -loops are suppressed as $O(2\alpha/\pi m_e^2/m_\mu^2) \simeq 1.1 \times 10^{-7}$ relative to the leading term and the τ -loops practically play no role at all.

Collecting the results we have²¹

$$a_e^{\text{QED}} = a_e^{\text{uni}} + a_e(\mu) + a_e(\tau) + a_e(\mu, \tau) \quad (3.64)$$

with universal term given by (3.45) and

$$\begin{aligned} a_e(\mu) &= 5.197\,386\,76(26) \times 10^{-7} \left(\frac{\alpha}{\pi}\right)^2 - 7.373\,941\,70(27) \times 10^{-6} \left(\frac{\alpha}{\pi}\right)^3 \\ &\quad + 9.161\,970\,703(373) \times 10^{-4} \left(\frac{\alpha}{\pi}\right)^4 - 0.00382(39) \times 10^{-6} \left(\frac{\alpha}{\pi}\right)^5 \\ a_e(\tau) &= 1.83798(33) \times 10^{-9} \left(\frac{\alpha}{\pi}\right)^2 - 6.5830(11) \times 10^{-8} \left(\frac{\alpha}{\pi}\right)^3 \\ &\quad + 7.429\,24(118) \times 10^{-6} \left(\frac{\alpha}{\pi}\right)^4 \\ a_e(\mu, \tau) &= 0.190982(34) \times 10^{-12} \left(\frac{\alpha}{\pi}\right)^3 + 7.4687(28) \times 10^{-7} \left(\frac{\alpha}{\pi}\right)^4. \end{aligned}$$

²¹The order α^3 terms are given by two parts which cancel partly

$$\begin{aligned} A_2^{(6)}(m_e/m_\mu) &= -7.373\,941\,70(27) \times 10^{-6} \\ &= -2.17684018(10) \times 10^{-5} \Big|_{\mu\text{-vap}} + 1.439446007(72) \times 10^{-5} \Big|_{\mu\text{-lbl}} \\ A_2^{(6)}(m_e/m_\tau) &= -6.5830(11) \times 10^{-8} \\ &= -1.16744(20) \times 10^{-7} \Big|_{\tau\text{-vap}} + 0.50914(9) \times 10^{-7} \Big|_{\tau\text{-lbl}}. \end{aligned}$$

The errors are due to the errors in the mass ratios. They are completely negligible in comparison to the other errors.

Altogether the perturbative expansion for the QED prediction of a_e is given by

$$\begin{aligned}
 a_e^{\text{QED}} &= \frac{\alpha}{2\pi} - 0.328\,478\,444\,002\,54(33) \left(\frac{\alpha}{\pi}\right)^2 \\
 &\quad + 1.181\,234\,016\,816(11) \left(\frac{\alpha}{\pi}\right)^3 \\
 &\quad - 1.91134(182) \left(\frac{\alpha}{\pi}\right)^4 \\
 &\quad + 7.791(580) \left(\frac{\alpha}{\pi}\right)^5.
 \end{aligned} \tag{3.65}$$

The improvement of the coefficient C_4 and knowing C_5 now are important for the precise determination of α from a_e^{exp} below. For our accurate value for the fine structure constant (3.29), which has been determined by matching the SM prediction of a_e below with a_e^{exp} , we obtain

$$a_e^{\text{QED}} = a_e^{\text{uni}} + 0.0000000000268 = 0.00115965217910(26)(0)(4)[26], \tag{3.66}$$

which shows that the QED part of the SM prediction of a_e is overwhelmingly dominated by the universal part (3.45).

What still is missing are the hadronic and weak contributions, which both are substantially reduced relative to a_μ . One should note that these contributions do not scale by the $(m_e/m_\mu)^2$ factor as one could naively guess. Estimates yield $a_e^{\text{had}} = 1.697(12) \times 10^{-12}$ and $a_e^{\text{weak}} = 0.030 \times 10^{-12}$, respectively [74].²² With the improved experimental result for a_e and the improved QED calculations available, the hadronic contribution now start to be significant, however, unlike in a_μ^{had} for the muon, a_e^{had} is known with sufficient accuracy and is not the limiting factor here. As a result a_e essentially only depends on perturbative QED, while hadronic, weak and new physics (NP) contributions are suppressed by $(m_e/M)^2$, where M is a weak, hadronic or new physics scale. As a consequence a_e at this level of accuracy is theoretically well under control (almost a pure QED object) and therefore is an excellent observable for extracting α_{QED} based on the SM prediction

$$a_e^{\text{SM}} = a_e^{\text{QED}}[\text{Eq. (3.65)}] + 1.721(12) \times 10^{-12} \text{ (hadronic \& weak)}. \tag{3.67}$$

²²The precise procedure of evaluating the hadronic contributions will be discussed extensively in Chap. 5 for the muon, for which the effects are much more sizable. As expected, corresponding calculations for the electron give small contributions only. We find $a_e^{\text{had, LO}} = 1.8465(121) \times 10^{-12}$ for the leading HVP contribution, $a_e^{\text{had, NLO}} = -0.2210(14) \times 10^{-12}$ for the next to leading and $a_e^{\text{had, NNLO}} = 0.0279(2) \times 10^{-12}$ for the next-to-next leading order [108]. For the hadronic light-by-light scattering contribution we estimate $a_e^{\text{had, LbL}} = 0.037(5) \times 10^{-12}$. An early relatively accurate evaluation $a_e^{(4)}(\text{vap, had}) = 1.884(41) \times 10^{-12}$ for the leading term has been obtained in 1995 [64] and illustrates the progress since.

We now compare this result with the very recent extraordinary precise measurement of the electron anomalous magnetic moment [6]

$$a_e^{\text{exp}} = 0.001\,159\,652\,180\,73(28) \quad (3.68)$$

which yields

$$\alpha^{-1}(a_e) = 137.035\,999\,1547(331)(0)(27)(14)[333] ,$$

which is close [55 \rightarrow 39 in 10^{-9}] to the value (3.29) [10] given earlier. If one adopts the CODATA recommended value $a_e^{\text{exp}} = 0.001\,159\,652\,180\,76(27)$ as an input one obtains

$$\alpha^{-1}(a_e) = 137.035\,999\,1512(320)(0)(27)(14)[321] . \quad (3.69)$$

The first error is the experimental one of a_e^{exp} , the second and third are the numerical uncertainties of the α^4 and α^5 terms, respectively. The last one is the hadronic uncertainty, which is completely negligible. This is now the by far most precise determination of α and we will use the recommended variant (3.29) throughout in the calculation of a_μ , below.

A different strategy is to use a_e for a precision test of QED. For a theoretical prediction of a_e we then need the best determinations of α which do not depend on a_e . They are [140–142]²³

$$\alpha^{-1}(\text{Cs06}) = 137.03600000(110)[8.0 \text{ ppb}] , \quad (3.70)$$

$$\alpha^{-1}(\text{Rb11}) = 137.035999037(91)[0.66 \text{ ppb}] , \quad (3.71)$$

and have been determined by atomic interferometry. The new much improved value (3.71) is obtained from the measurement of h/m_{Rb} , combined with the very precisely known Rydberg constant and the new value for m_{Rb}/m_e [10, 142].

In terms of $\alpha(\text{Cs06})$ one gets $a_e = 0.00115965217359(929)$ which agrees well with the experimental value $a_e^{\text{exp}} - a_e^{\text{the}} = 7.14(9.30) \times 10^{-12}$; With the new value $\alpha(\text{Rb11})$ the prediction is $a_e = 0.00115965218172(77)$, again in good agreement with experiment: $a_e^{\text{exp}} - a_e^{\text{the}} = -0.99(0.82) \times 10^{-12}$. The error is completely dominated by the error of the input value of α used. The precision reached is close to become interesting for testing new physics scenarios [150, 151]. The following Table 3.3 collects the typical contributions to a_e evaluated in terms of Eqs. (3.70) and (3.71). The new results [10] imply that the theory error is reduced by almost a factor 5. In spite of the fact that the best non- a_e determinations of α also improved by

²³The results rely upon a number of other experimental quantities. One is the measured Rydberg constant [143], others are the Cesium (Cs) and Rubidium (Rb) masses in atomic mass units (amu) [144] and the electron mass in amu [145–147]. The \hbar/M_{Cs} needed comes from an optical measurement of the Cs D1 line [140, 148] and the preliminary recoil shift in an atom interferometer [149], while \hbar/M_{Rb} comes from a measurement of an atom recoil of a Rb atom in an optical lattice [140].

Table 3.3 Contributions to $a_e(h/M)$ in units 10^{-6} . The three errors given in the universal contribution come from the experimental uncertainty in α , from the α^4 term and from the α^5 term, respectively

Contribution	$\alpha(h/M_{Cs06})$	$\alpha(h/M_{Rb11})$
Universal	1159.652 169 15(929)(0)(4)	1159.652 177 28(77)(0)(4)
μ -loops	0.000 002 738 (0)	0.000 002 738 (0)
τ -loops	0.000 000 009 (0)	0.000 000 009 (0)
Hadronic	0.000 001 690 (13)	0.000 001 690 (13)
Weak	0.000 000 030 (0)	0.000 000 030 (0)
Theory	1159.652 173 59(929)	1159.652 181 72(77)
Experiment	1159.652 180 73 (28)	1159.652 180 73 (28)
$a_e^{\text{exp}} - a_e^{\text{the}}$	$7.14(9.30) \times 10^{-12}$	$-0.99(0.82) \times 10^{-12}$

a factor 10 the error is still dominated by the uncertainty of $\alpha^{-1}(\text{Rb11})$. An improvement by a factor 10 would allow a much more stringent test of QED, and therefore would be very important. At present, assuming that $|\Delta a_e^{\text{New Physics}}| \simeq m_e^2/\Lambda^2$ where Λ approximates the scale of ‘‘New Physics’’, the agreement between $\alpha^{-1}(a_e)$ and $\alpha^{-1}(\text{Rb11})$ probes the scale $\Lambda \lesssim O(400 \text{ GeV})$. To access the much more interesting range of $\Lambda \sim O(1 \text{ TeV})$ would require primarily a substantially more precise α . The tenth order QED calculations by Aoyama, Hayakawa, Kinoshita and Nio mark a new milestone in accuracy and in complexity of theoretical predictions in quantum field theory. They put g-2 calculations on a much safer basis for what concerns the perturbative part. Still, independent cross checks of both the $O(\alpha^4)$ and the $O(\alpha^5)$ QED calculations are highly desirable, even though we have no doubts that the new results are reliable. Important semi-analytic cross checks so far confirm the numerical calculations [50, 57]. The new quasi-analytic $O(\alpha^4)$ result by Laporta [11] is certainly a milestone in consolidating the QED part a_e^{QED} .

As a summary, we note that with

$$a_e^{\text{exp}} - a_e^{\text{the}} = -0.99(0.82) \times 10^{-12}, \quad (3.72)$$

theory and experiment are in excellent agreement. We know that the sensitivity to new physics is reduced by $(m_\mu/m_e)^2 \cdot \delta a_e^{\text{exp}}/\delta a_\mu^{\text{exp}} \simeq 19$ relative to a_μ . Nevertheless, one has to keep in mind that a_e is suffering less from hadronic uncertainties and thus may provide a safer test. One should also keep in mind that experiments determining a_e on the one hand and a_μ on the other hand are very different with different systematics. While a_e is determined in an ultra cold environment a_μ has been determined with ultra relativistic (magic γ) muons so far. Presently, the a_e prediction is limited by the, by a factor $\delta\alpha(\text{Rb11})/\delta\alpha(a_e) \simeq 5.3$ less precise, α available. Combining all uncertainties a_μ is about a factor 43 more sensitive to new physics at present.

Table 3.4 QED contributions to a_μ in units 10^{-6}

Term	Universal	e -loops	τ -loops	$e \times \tau$ -loops
$a^{(4)}$	-1.772 305 06 (0)	5.904 060 07 (4)	0.000 421 28 (8)	–
$a^{(6)}$	0.014 804 20 (0)	0.286 603 69 (0)	0.000 004 52 (0)	0.000 006 61 (0)
$a^{(8)}$	-0.000 055 67 (0)	0.003 862 64 (18)	0.000 001 23 (0)	0.000 001 83 (0)
$a^{(10)}$	0.000 000 62 (4)	0.000 050 19 (6)	-0.000 000 01 (0)	0.000 000 14 (0)

Recently, the possible non-perturbative QED effect of order α^5 of the positronium exchange $\gamma^* \rightarrow [e^+e^-]_{\text{bound state}} \rightarrow \gamma^*$, in the virtual photon line of the LO diagram of the electron $g-2$, was pointed out in [152, 153], but has been shown to be absent as an additional contribution [153–156], in accord with earlier studies [157, 158].

3.2.3 The Anomalous Magnetic Moment of the Muon

The muon magnetic moment anomaly is defined by

$$a_\mu = \frac{1}{2}(g_\mu - 2) = \frac{\mu_\mu}{e\hbar/2m_\mu} - 1, \quad (3.73)$$

where $g_\mu = 2\mu_\mu/(e\hbar/2m_\mu)$ is the g -factor and μ_μ the magnetic moment of the muon. The different higher order QED contributions are collected in Table 3.4. We thus arrive at a QED prediction of a_μ given by

$$a_\mu^{\text{QED}} = 116\,584\,718.859(0.026)(0.009)(0.017)(0.006)[0.034] \times 10^{-11} \quad (3.74)$$

where the first error is the uncertainty of α in (3.29), the second one combines in quadrature the uncertainties due to the errors in the mass ratios (3.30), the third and fourth are the numerical uncertainties of the $O(\alpha^4)$ and $O(\alpha^5)$ terms, respectively. With the spectacular progress achieved with the calculation of the complete $O(\alpha^5)$ term [10, 51] the error is essentially given by the input error of $\alpha[a_e]$ in spite of the fact that this error has been reduced as well due to the $O(\alpha^5)$ result on a_e .

The following Table 3.5 collects the typical contributions to a_μ evaluated in terms of α (3.29) determined via a_e .

The world average experimental muon magnetic anomaly, dominated by the very precise BNL result, is now [7, 159]

$$a_\mu^{\text{exp}} = 1.16592091(63) \times 10^{-3} \quad (3.75)$$

(relative uncertainty 5.4×10^{-7}), which confronts the SM prediction

$$a_\mu^{\text{the}} = 1.16591783(35) \times 10^{-3}. \quad (3.76)$$

Table 3.5 The various types of contributions to a_μ in units 10^{-6} , ordered according to their size (L.O. lowest order, H.O. higher order, LbL light-by-light). The gray band shows the present experimental result with its uncertainty. The hatched overlay illustrates the expected uncertainty (for the same central value) which will be reached in the coming years. “Theory τ ” shows the result from [88] where τ -data have been taken into account, before taking into care of $\rho^0 - \gamma$ mixing. This result is outdated. The LbL result’s history is also shown. Results are from: 1995 [112, 114, 115], 2001 [KN] [120], 2003 [MV] [123], and 2015 [JN] [20, 74, 125]

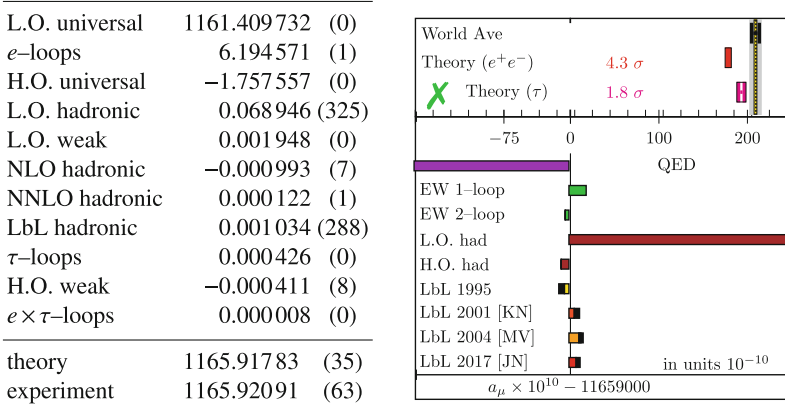


Figure 3.8 illustrates the sensitivity to various contributions and how it developed in history. The high sensitivity of a_μ to physics from not too high scales M above m_μ , which is scaling like $(m_\mu/M)^2$, and the more than one order of magnitude improvement of the experimental accuracy has brought many SM effects into the focus of the interest. Not only are we testing now the 4-loop QED contribution, higher order HVP effects, the infamous hadronic LbL contribution and the weak loops, we are reaching or limiting possible New Physics at a level of sensitivity which caused and still causes a lot of excitement. “New Physics” is displayed in the figure as the ppm deviation of

$$a_\mu^{\text{exp}} - a_\mu^{\text{the}} = (306 \pm 72) \times 10^{-11}, \quad (3.77)$$

which is 4.3σ . We note that the theory error is now smaller than the experimental one. It is fully dominated by the uncertainty of the hadronic low energy cross section data, which determine the hadronic vacuum polarization and, partially, from the uncertainty of the hadronic light-by-light scattering contribution.

As we notice, the enhanced sensitivity to “heavy” physics is somehow good news and bad news at the same time: the sensitivity to “New Physics” we are always hunting for at the end is enhanced due to

$$a_\ell^{\text{NP}} \sim \left(\frac{m_\ell}{M_{\text{NP}}} \right)^2$$

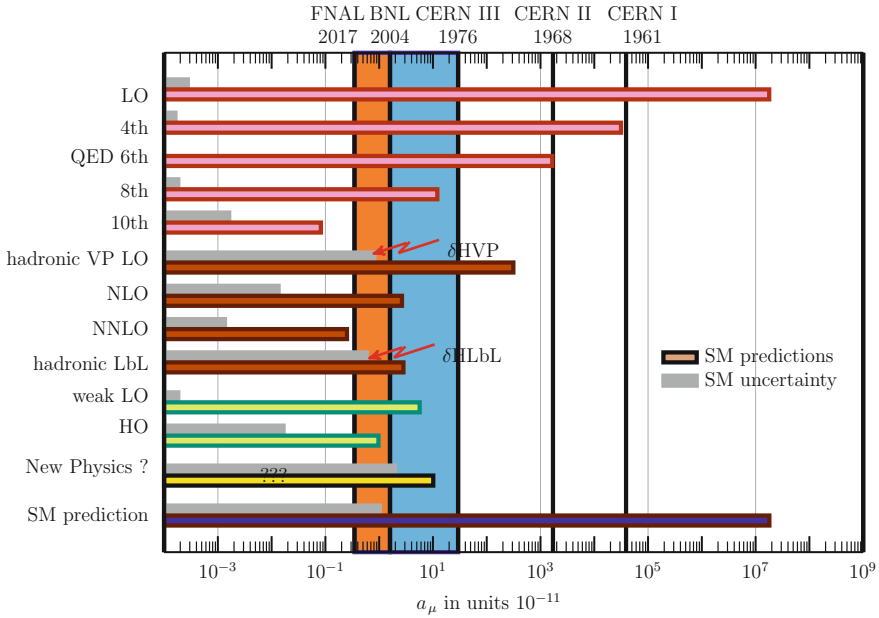


Fig. 3.8 History of the muon $g - 2$ experiments and the sensitivity to various contributions. The increase in precision with the BNL $g - 2$ experiment is shown as a blue vertical band. New Physics is illustrated by the deviation $(a_\mu^{\text{exp}} - a_\mu^{\text{the}})/a_\mu^{\text{exp}}$. The left orange vertical band shows the sensitivity band which will be reached with the upcoming muon $g - 2$ experiment at Fermilab [160]. Arrows point to what is limiting theory precision presently: the Hadronic Vacuum Polarization (HVP) and Hadronic Light-by-Light (HLbL) contributions

by the mentioned mass ratio square, but at the same time also scale dependent SM effects are dramatically enhanced, and the hadronic ones are not easy to estimate with the desired precision.

The perspectives for future developments will be discussed at the end of Chap. 7.

After this summary of the current status of a_μ and a_e , we will now go on and present basic techniques and tools used in calculating the various effects, before we are going to present a more detailed account of the individual contributions in the next chapter.

3.3 Structure of the Electromagnetic Vertex in the SM

Here we want to discuss the lepton moments beyond QED in the more general context of the SM, in which parity P as well as CP are broken by the weak interactions. We again start from the relevant matrix element of the electromagnetic current between lepton states

$$i\Gamma_{\gamma\ell\ell}^{\mu}(p_1, p_2; r_1, r_2) = \langle \ell^-(p_2, r_2) | j_{\text{em}}^{\mu}(0) | \ell^-(p_1, r_1) \rangle = i\bar{u}(p_2, r_2)\Pi_{\gamma\ell\ell}^{\mu}u(p_1, r_1) \quad (3.78)$$

and look for the additional form factors showing up if P and C are violated. Again $q = p_2 - p_1$ is the momentum transfer. $u(p_1, r_1)$ is the Dirac spinor, the wave function of the incoming lepton, with momentum p_1 and 3rd component of spin $r_1 (= \pm \frac{1}{2})$, and $\bar{u} = u^+\gamma^0$ is the adjoint spinor representing the wave function of the outgoing lepton. $\Pi_{\gamma\ell\ell}^{\mu}$ is a Hermitian 4×4 matrix in spinor space and a Lorentz four-vector.

Besides the Dirac matrix γ^{μ} we have two further independent four-vectors, the momenta p_1 and p_2 or linear combinations of them. It is convenient to choose the orthogonal vectors $P = p_1 + p_2$ and $q = p_2 - p_1$ (with $Pq = 0$). The general covariant decomposition for on-shell leptons in the SM then may be written in the form

$$\Pi_{\gamma\ell\ell}^{\mu} = \gamma^{\mu}A_1 + \frac{P^{\mu}}{2m}A_2 + \frac{q^{\mu}}{2m}A_3 + \gamma^{\mu}\gamma_5A_4 + \frac{q^{\mu}}{2m}\gamma_5A_5 + i\frac{P^{\mu}}{2m}\gamma_5A_6 \quad (3.79)$$

where the scalar amplitudes $A_i(p_1, p_2)$ are functions of the scalar products p_1^2 , p_2^2 and p_1p_2 . Since the lepton is on the mass shell $p_1^2 = p_2^2 = m^2$ and using $q^2 = 2m^2 - 2p_1p_2$, the dimensionless amplitudes depend on the single kinematic variable q^2 and on all the parameters of the theory: the fine structure constant $\alpha = e^2/4\pi$ and all physical particle masses. We will simply write $A_i = A_i(q^2)$ in the following.

When writing (3.79) we already have made use of the Gordon identities

$$\begin{aligned} i\sigma^{\mu\nu}q_{\nu} &= -P^{\mu} + 2m\gamma^{\mu}, & i\sigma^{\mu\nu}P_{\nu} &= -q^{\mu}, \\ i\sigma^{\mu\nu}q_{\nu}\gamma_5 &= -P^{\mu}\gamma_5, & i\sigma^{\mu\nu}P_{\nu}\gamma_5 &= -q^{\mu}\gamma_5 + 2m\gamma^{\mu}\gamma_5, \end{aligned} \quad (3.80)$$

which hold if sandwiched between the spinors like $\bar{u}(p_2) \cdots u(p_1)$. In QED due to parity conservation the terms proportional to γ_5 are absent.

The electromagnetic current still is conserved:

$$\partial_{\mu}j_{\text{em}}^{\mu} = 0. \quad (3.81)$$

On a formal level, this may be considered as a trivial consequence of the inhomogeneous Maxwell equation (see [161] for a manifestly gauge invariant formulation in the SM)

$$\partial_{\mu}F^{\mu\nu} = -e j_{\text{em}}^{\nu} \quad \text{with} \quad F_{\mu\nu} = \partial_{\mu}A_{\nu} - \partial_{\nu}A_{\mu}$$

since $\partial_{\nu}\partial_{\mu}F^{\mu\nu} = -e \partial_{\nu}j_{\text{em}}^{\nu} \equiv 0$ as $\partial_{\nu}\partial_{\mu}$ is symmetric in $\mu \leftrightarrow \nu$ while $F^{\mu\nu}$ is antisymmetric. As a consequence we must have $q_{\mu}\bar{u}_2\Pi_{\gamma\ell\ell}^{\mu}u_1 = 0$. By the Dirac equations $\not{p}_i u_i = m u_i$ ($i = 1, 2$) we have $\bar{u}_2 \not{q} u_1 = 0$, while $\bar{u}_2 \not{q} \gamma_5 u_1 = -2m\bar{u}_2\gamma_5 u_1$, furthermore, $qP = 0$ while keeping $q^2 \neq 0$ at first. Hence current conservation requires $A_3 = 0$ and $A_5 = -4m^2/q^2 A_4$ such that we remain with four

physical form factors²⁴

$$\bar{u}_2 \Pi_{\gamma\ell\ell}^\mu u_1 = \bar{u}_2 \left(\gamma^\mu A_1 + \frac{P^\mu}{2m} A_2 + \left(\gamma^\mu - \frac{2mq^\mu}{q^2} \right) \gamma_5 A_4 + i \frac{P^\mu}{2m} \gamma_5 A_6 \right) u_1 .$$

This shows that the two amplitudes A_3 and A_6 are redundant for physics, however, they show up in actual calculations at intermediate steps and/or for contributions from individual Feynman diagrams. By virtue of the Gordon decomposition

$$\bar{u}(p_2) \frac{P^\mu}{2m} u(p_1) \equiv \bar{u}(p_2) \left(\gamma^\mu - i \frac{\sigma^{\mu\nu} q_\nu}{2m} \right) u(p_1)$$

we finally obtain for the form factor

$$\Pi_{\gamma\ell\ell}^\mu = \gamma^\mu F_E(q^2) + \left(\gamma^\mu - \frac{2mq^\mu}{q^2} \right) \gamma_5 F_A + i \sigma^{\mu\nu} \frac{q_\nu}{2m} F_M(q^2) + \sigma^{\mu\nu} \frac{q_\nu}{2m} \gamma_5 F_D(q^2) \quad (3.82)$$

With $F_E = A_1 + A_2$ the electric charge form factor, normalized by charge renormalization to $F_E(0) = 1$, $F_A = A_4$ the *anapole moment* [162–166] which is P violating and vanishing at $q^2 = 0$: $F_A(0) = 0$. The magnetic form factor is $F_M = -A_2$ which yields the anomalous magnetic moment as $a_\ell = F_M(0)$. The last term with $F_D = A_6$ represents the CP violating *electric dipole moment* (EDM)

$$d_\ell = - \frac{F_D(0)}{2m} . \quad (3.83)$$

Note that (3.82) is the most general Lorentz covariant answer, which takes into account current conservation (3.81) and the on-shell conditions for the leptons (Dirac equation for the spinors).

In the SM at the tree level $F_E(q^2) = 1$, while $F_i(q^2) = 0$ for ($i = M, A, D$).

The anomalous magnetic moment a_ℓ is a dimensionless quantity, just a number, and corresponds to an effective interaction term

$$\delta \mathcal{L}_{\text{eff}}^{\text{AMM}} = - \frac{e_\ell a_\ell}{4m_\ell} \bar{\psi}(x) \sigma^{\mu\nu} \psi(x) F_{\mu\nu}(x) , \quad (3.84)$$

with classical low energy limit

$$-\delta \mathcal{L}_{\text{eff}}^{\text{AMM}} \Rightarrow \mathcal{H}_m \simeq \frac{e_\ell a_\ell}{2m_\ell} \boldsymbol{\sigma} \mathbf{B} ,$$

²⁴In the SM the proper definition of the form factors is highly non-trivial. The conventional definition of the photon field has to be replaced by one which satisfies Maxwell's equations to all orders. This has been investigated extensively in [161]. Since we are interested only in the form factors in the classical limit here, we need not go further into this discussion.

written as a Hamiltonian in 2–spinor space à la Pauli. Note that a term (3.84), if present in the fundamental Lagrangian, would spoil renormalizability of the theory and contribute to $F_i(q^2)$ ($i=M,D$) at the tree level. In addition it is not $SU(2)_L$ gauge invariant, because gauge invariance only allows minimal couplings via the covariant derivative: vector and/or axial–vector terms. The emergence of an anomalous magnetic moment term in the SM is a consequence of the symmetry breaking by the Higgs mechanism,²⁵ which provides the mass to the physical particles and allows for helicity flip processes like the anomalous magnetic moment transitions. In any renormalizable theory the anomalous magnetic moment term must vanish at tree level, which also means that there is no free parameter associated with it. It is thus a finite prediction of the theory to all orders of the perturbation expansion.

The EDM term only can be non–vanishing if both parity P and time–reversal T are violated [167, 168]. It corresponds to an effective interaction

$$\delta\mathcal{L}_{\text{eff}}^{\text{EDM}} = -\frac{d_\ell}{2} \bar{\psi}(x) i \sigma^{\mu\nu} \gamma_5 \psi(x) F_{\mu\nu}(x) , \quad (3.85)$$

which in the non–relativistic limit becomes

$$-\delta\mathcal{L}_{\text{eff}}^{\text{EDM}} \Rightarrow \mathcal{H}_e \simeq -d_\ell \boldsymbol{\sigma} \mathbf{E} , \quad (3.86)$$

again written as a Hamiltonian in 2–spinor space. Again a term (3.85) is non–renormalizable and it is not $SU(2)_L$ gauge invariant and thus can be there only because the symmetry is broken in the Higgs phase. In the framework of a QFT where CPT is conserved T violation directly corresponds to CP violation, which is small (0.3 %) in the light particle sector and can come in at second order at best [169].²⁶ This is the reason why the EDM is so much smaller than its magnetic counterpart. The experimental limit for the electron is $|d_e| < 1.6 \times 10^{-27} e \cdot \text{cm}$ at 90% C.L. [171]. The direct test for the muon gave $d_\mu = 3.7 \pm 3.4 \times 10^{-19} e \cdot \text{cm}$ at 90% C.L. [172]. New much more precise experiments for d_μ are under discus-

²⁵Often the jargon *spontaneously broken gauge symmetry* (or the like) is used for the Higgs mechanism. The formal similarity to true *spontaneous symmetry breaking*, like in the Goldstone model, which requires the existence of physical zero mass Goldstone bosons, only shows up on an unphysical state space which is including the Higgs ghosts (would be Goldstone bosons). In fact it is the discrete Z_2 symmetry $H \leftrightarrow -H$ of the physical Higgs field (in the unitary gauge) which is spontaneously broken. This also explains the absence of physical Goldstone bosons.

²⁶CP–violation in the SM arises from the complex phase δ in the CKM matrix, which enters the interactions of the quarks with the W^\pm gauge bosons. The magnitude in the 3 family SM is given by the Jarlskog invariant [170]

$$J = \cos \theta_1 \cos \theta_2 \cos \theta_3 \sin^2 \theta_1 \sin \theta_2 \sin \theta_3 \sin \delta = (2.88 \pm 0.33) \times 10^{-5} \quad (3.87)$$

where the θ_i are the 3 mixing angles and δ is the phase in the CKM matrix. Note that J is very small. In addition, only diagrams with at least one quark–loop with at least four CC vertices can give a contribution. This requires 3–loop diagrams exhibiting four virtual W –boson lines inside. Such contributions are highly suppressed. Expected CP violation in the neutrino mixing matrix are expected to yield even much smaller effects.

sion [173]. Theory expects $d_e^{\text{the}} \sim 10^{-28} e \cdot \text{cm}$ [169], 10 times smaller than the present limit. For a theoretical review I refer to [174] or [35]. If we assume that $\eta_\mu \sim (m_\mu/m_e)^2 \eta_e$ (see (1.5)), i.e., η_ℓ scales like heavy particle (X) effects in $\delta a_\ell(X) \propto (m_\ell/M_X)^2$, as they do in many new physics scenarios, we expect that $d_\mu \sim (m_\mu/m_e) d_e$, and thus $d_\mu \sim 3.2 \times 10^{-25} e \cdot \text{cm}$. This is too small to affect the extraction of a_μ , for example, as we will see.

3.4 Dipole Moments in the Non-Relativistic Limit

Here we are interested in the non-relativistic limits of the effective dipole moment interaction terms (3.84)

$$\delta \mathcal{L}_{\text{eff}}^{\text{AMM}} = -\frac{e_\ell a_\ell}{4m_\ell} \bar{\psi}(x) \sigma^{\mu\nu} \psi(x) F_{\mu\nu}(x),$$

and (3.85)

$$\delta \mathcal{L}_{\text{eff}}^{\text{EDM}} = -\frac{d_\ell}{2} \bar{\psi}(x) i \sigma^{\mu\nu} \gamma_5 \psi(x) F_{\mu\nu}(x),$$

when the electron is moving in a classical external field described by $F_{\mu\nu}^{\text{ext}}$. The relevant expansion may be easily worked out as follows: since the antisymmetric electromagnetic field strength tensor $F_{\mu\nu}$ exhibits the magnetic field in the spatial components $F_{ik}: B^l = \frac{1}{2} \epsilon^{ikl} F_{ik}$ and the electric field in the mixed time-space part: $E^i = F_{0i}$, we have to work out $\sigma^{\mu\nu}$ for the corresponding components:

$$\begin{aligned} \sigma^{ik} &= \frac{i}{2} (\gamma^i \gamma^k - \gamma^k \gamma^i) \\ &= \frac{i}{2} \left(\begin{pmatrix} 0 & \sigma^i \\ -\sigma^i & 0 \end{pmatrix} \begin{pmatrix} 0 & \sigma^k \\ -\sigma^k & 0 \end{pmatrix} - \begin{pmatrix} 0 & \sigma^k \\ -\sigma^k & 0 \end{pmatrix} \begin{pmatrix} 0 & \sigma^i \\ -\sigma^i & 0 \end{pmatrix} \right) \\ &= -\frac{i}{2} \begin{pmatrix} [\sigma^i, \sigma^k] & 0 \\ 0 & [\sigma^i, \sigma^k] \end{pmatrix} = \epsilon^{ikl} \begin{pmatrix} \sigma^l & 0 \\ 0 & \sigma^l \end{pmatrix} \\ \sigma^{0i} \gamma_5 &= \frac{i}{2} (\gamma^0 \gamma^i - \gamma^i \gamma^0) \gamma_5 \\ &= \frac{i}{2} \left(\begin{pmatrix} 1 & 0 \\ 0 & -1 \end{pmatrix} \begin{pmatrix} 0 & \sigma^i \\ -\sigma^i & 0 \end{pmatrix} - \begin{pmatrix} 0 & \sigma^i \\ -\sigma^i & 0 \end{pmatrix} \begin{pmatrix} 1 & 0 \\ 0 & -1 \end{pmatrix} \right) \gamma_5 \\ &= i \begin{pmatrix} 0 & \sigma^i \\ \sigma^i & 0 \end{pmatrix} \begin{pmatrix} 0 & 1 \\ 1 & 0 \end{pmatrix} = i \begin{pmatrix} \sigma^i & 0 \\ 0 & \sigma^i \end{pmatrix}. \end{aligned}$$

Note that the γ_5 here is crucial to make the matrix block diagonal, because, only block diagonal terms contribute to the leading order in the non-relativistic expansion, as we will see now.

In the rest frame of the electron the spinors have the form

$$u(p, r) = \frac{1}{\sqrt{p^0 + m}} (\not{p} + m) \tilde{u}(0, r) \simeq \tilde{u}(0, r)$$

with

$$\tilde{u}(0, r) = \begin{pmatrix} U(r) \\ 0 \end{pmatrix}, \quad U\left(\frac{1}{2}\right) = \begin{pmatrix} 1 \\ 0 \end{pmatrix}, \quad U\left(-\frac{1}{2}\right) = \begin{pmatrix} 0 \\ 1 \end{pmatrix}.$$

We first work out the magnetic dipole term

$$\begin{aligned} \bar{u}_2 \sigma^{\mu\nu} u_1 F_{\mu\nu} &\simeq (U^T(r_2), 0) \sigma^{\mu\nu} \begin{pmatrix} U(r_1) \\ 0 \end{pmatrix} F_{\mu\nu} \\ &= (U^T(r_2), 0) \sigma^{ik} \begin{pmatrix} U(r_1) \\ 0 \end{pmatrix} F_{ik} \\ &= \epsilon^{ikl} (U^T(r_2), 0) \begin{pmatrix} \sigma^l & 0 \\ 0 & \sigma^l \end{pmatrix} \begin{pmatrix} U(r_1) \\ 0 \end{pmatrix} F_{ik} \\ &= 2U^T(r_2) \boldsymbol{\sigma} U(r_1) \mathbf{B} = 2(\boldsymbol{\sigma})_{r_2, r_1} \mathbf{B}. \end{aligned}$$

The other non-diagonal terms do not contribute in this static limit. Similarly, for the electric dipole term

$$\begin{aligned} \bar{u}_2 \sigma^{\mu\nu} \gamma_5 u_1 F_{\mu\nu} &\simeq (U^T(r_2), 0) \sigma^{\mu\nu} \gamma_5 \begin{pmatrix} U(r_1) \\ 0 \end{pmatrix} F_{\mu\nu} \\ &= 2(U^T(r_2), 0) \sigma^{0i} \gamma_5 \begin{pmatrix} U(r_1) \\ 0 \end{pmatrix} F_{0i} \\ &= 2i(U^T(r_2), 0) \begin{pmatrix} \sigma^i & 0 \\ 0 & \sigma^i \end{pmatrix} \begin{pmatrix} U(r_1) \\ 0 \end{pmatrix} F_{0i} \\ &= 2iU^T(r_2) \boldsymbol{\sigma} U(r_1) \mathbf{E} = 2i(\boldsymbol{\sigma})_{r_2, r_1} \mathbf{E}. \end{aligned}$$

In the low energy expansion matrix elements of the form $\bar{v}_2 \Gamma_i u_1$ or $\bar{u}_2 \Gamma_i v_1$ pick out off-diagonal 2×2 sub-matrices mediating electron-positron creation or annihilation processes, which have thresholds $\sqrt{s} \geq 2m$ and thus are genuinely relativistic effects. The leading terms are the known classical low energy effective terms

$$-\delta \mathcal{L}_{\text{eff}}^{\text{AMM}} \Rightarrow \mathcal{H}_m \simeq \frac{e_\ell a_\ell}{2m_\ell} \boldsymbol{\sigma} \mathbf{B},$$

and

$$-\delta \mathcal{L}_{\text{eff}}^{\text{EDM}} \Rightarrow \mathcal{H}_e \simeq -d_\ell \boldsymbol{\sigma} \mathbf{E},$$

written as 2×2 matrix Hamiltonian, as given before.

3.5 Projection Technique

Especially the calculations of the anomalous magnetic moment in higher orders require most efficient techniques to perform such calculations. As we have seen in Chap. 2 the straightforward calculation of the electromagnetic form factors turns out to be quite non-trivial at the one-loop level already. In particular the occurrence of higher order tensor integrals (up to second rank) makes such calculations rather tedious. Here we outline a projection operator technique which appears to be a much more clever set up for such calculations. Calculations turn out to simplify considerably as we will see.

The tensor integrals showing up in the direct evaluation of the Feynman integrals may be handled in a different way, which allows us to deal directly with the individual amplitudes appearing in the covariant decomposition (3.79). With the matrix element of the form (3.78) we may construct projection operators $\mathcal{P}_{\mu i}$ such that the amplitudes A_i are given by the trace

$$A_i = \text{Tr} \left\{ \mathcal{P}_{\mu i} \Pi_{\gamma \ell \ell}^{\mu} \right\}. \quad (3.88)$$

Since we assume parity P and CP symmetry here (QED) and we have to form a scalar amplitude, a projection operator has to be of a form like (3.79) but with different coefficients which have to be chosen such that the individual amplitudes are obtained. An additional point we have to take into account is the following: since we are working on the physical mass shell (off-shell there would be many more amplitudes), we have to enforce that contributions to $\Pi_{\gamma \ell \ell}^{\mu}$ of the form $\delta \Pi_{\gamma \ell \ell}^{\mu} = \dots (\not{p}_1 - m) + (\not{p}_2 - m) \dots$ give vanishing contribution as $\bar{u}_2 \delta \Pi_{\gamma \ell \ell}^{\mu} u_1 = 0$. This is enforced by applying the projection matrices $\not{p}_1 + m$ from the right and $\not{p}_2 + m$ from the left, respectively, such that the general form of the projector of interest reads

$$\mathcal{P} = (\not{p}_1 + m) \left(\gamma^{\mu} c_1 + \frac{P^{\mu}}{2m} c_2 + \frac{q^{\mu}}{2m} c_3 + \gamma^{\mu} \gamma_5 c_4 + \frac{q^{\mu}}{2m} \gamma_5 c_5 - i \frac{P^{\mu}}{2m} \gamma_5 c_6 \right) (\not{p}_2 + m). \quad (3.89)$$

It indeed yields

$$\text{Tr} \left\{ \mathcal{P}_{\mu} \delta \Pi_{\gamma \ell \ell}^{\mu} \right\} = 0$$

for arbitrary values of the constants c_i , because $(\not{p}_2 + m)(\not{p}_2 - m) = p_2^2 - m^2 = 0$ if we set $p_2^2 = m^2$ and making use of the cyclicity of the trace, similarly, $(\not{p}_1 - m)(\not{p}_1 + m) = p_1^2 - m^2 = 0$ if we set $p_1^2 = m^2$. In order to find the appropriate sets of constants which allow us to project to the individual amplitudes we compute $\text{Tr} \mathcal{P}_{\mu} \Pi_{\gamma \ell \ell}^{\mu}$ and obtain

$$\text{Tr} \left\{ \mathcal{P}_{\mu} \Pi_{\gamma \ell \ell}^{\mu} \right\} = \sum_{i=1}^6 g_i A_i \quad (3.90)$$

$$\begin{aligned}
\sum_{i=1}^6 g_i A_i &= A_1 \left[c_1(2ds - 4s + 8m^2) + c_2(-2s + 8m^2) \right] \\
&+ A_2 \left[c_1(-2s + 8m^2) + c_2(-4s + 1/2s^2m^{-2} + 8m^2) \right] \\
&+ A_3 \left[c_3(2s - 1/2s^2m^{-2}) \right] \\
&+ A_4 \left[c_4(2ds - 8dm^2 - 4s + 8m^2) + c_5(2s) \right] \\
&+ A_5 \left[c_4(-2s) + c_5(1/2s^2m^{-2}) \right] \\
&+ A_6 \left[c_6(2s - 1/2s^2m^{-2}) \right]
\end{aligned}$$

where $s = q^2$. We observe, firstly, that each of the amplitudes A_3 and A_6 does not mix with any other amplitude and hence may be projected out in a trivial way setting $c_3 = 1$ or $c_6 = 1$, respectively, with all others zero in (3.89). Secondly, the parity violating amplitudes A_i $i = 4, 5, 6$ do not interfere of course with the parity conserving ones A_i $i = 1, 2, 3$ which are the only ones present in QED. To disentangle A_1 and A_2 we have to choose c_1/c_2 such that the coefficient of A_2 or the one of A_1 is vanishing, and correspondingly for A_4 and A_5 . The coefficient of the projected amplitude A_i has to be normalized to unity, such that the requested projector yields (3.88).

Thus, \mathcal{P}_i is obtained by choosing c_j such that $g_i = 1$ and $g_j = 0$ for all $j \neq i$. The following table lists the non-zero coefficients required for the corresponding projector:

$$\begin{aligned}
\mathcal{P}_1 : c_1 &= c_2 \frac{s - 4m^2}{4m^2} & c_2 &= \frac{1}{(d-2)f_1(d)} \frac{2m^2}{s(s - 4m^2)} \\
\mathcal{P}_2 : c_2 &= c_1 \frac{(d-2)s + 4m^2}{s - 4m^2} & c_1 &= \frac{1}{(d-2)f_1(d)} \frac{2m^2}{s(s - 4m^2)} \\
\mathcal{P}_3 : & & c_3 &= \frac{1}{f_1(d)} \frac{2m^2}{s(s-4m^2)} \\
\mathcal{P}_4 : c_4 &= c_5 \frac{s}{4m^2} & c_5 &= \frac{1}{(d-2)f_1(d)} \frac{2m^2}{s(s - 4m^2)} \\
\mathcal{P}_5 : c_5 &= -c_4 \frac{(d-2)(s - 4m^2) - 4m^2}{s} & c_4 &= \frac{1}{(d-2)f_1(d)} \frac{2m^2}{s(s - 4m^2)} \\
\mathcal{P}_6 : & & c_6 &= -i \frac{1}{f_1(d)} \frac{2m^2}{s(s-4m^2)}
\end{aligned}$$

with $f_1(d)$ we denote $f(d)/f(d=4)$ where $f(d) \doteq \text{Tr } 1 = 2^{(d/2)}$ ($\lim_{d \rightarrow 4} f(d) = 4$). As discussed in Sect. 2.4.2, p. 68 physics is not affected by the way $f(d=4) = 4$ is extrapolated to $d \neq 4$, provided one sticks to a given convention, like setting $f(d) = 4$ for arbitrary d which means we may take $f_1(d) = 1$ everywhere as a convention. For the amplitudes we are interested in the following we have

$$\begin{aligned}
\mathcal{P}_1^\mu &= \frac{1}{2f_1(d)(d-2)} (\not{p}_1 + m) \left(\gamma^\mu + \frac{4m^2}{s(s-4m^2)} \frac{P^\mu}{2m} \right) (\not{p}_2 + m), \\
\mathcal{P}_2^\mu &= \frac{2m^2/s}{f_1(d)(d-2)(s-4m^2)} (\not{p}_1 + m) \left(\gamma^\mu + \frac{(d-2)s + 4m^2}{(s-4m^2)} \frac{P^\mu}{2m} \right) (\not{p}_2 + m), \\
\mathcal{P}_3^\mu &= \frac{1}{f_1(d)} \frac{2m^2/s}{(s-4m^2)} (\not{p}_1 + m) \left(\frac{q^\mu}{2m} \right) (\not{p}_2 + m). \tag{3.91}
\end{aligned}$$

All projectors are of the form

$$\mathcal{P}_i^\mu = (\not{p}_1 + m) \Lambda_i^\mu(p_2, p_1) (\not{p}_2 + m), \quad (3.92)$$

for example, in the projector for A_2 taking $f_1(d) = 1$ we have

$$\Lambda_2^\mu(p_2, p_1) = \frac{2m^2}{(d-2)s(s-4m^2)} \left(\gamma^\mu + \frac{(d-2)s+4m^2}{s-4m^2} \frac{P^\mu}{2m} \right). \quad (3.93)$$

This projector we will need later for calculating higher order contributions to the anomalous magnetic moment in an efficient manner.

The amplitudes A_i at one-loop are now given by the integrals

$$A_i = e^2 \int \frac{d^d k}{(2\pi)^d} \frac{f_i(k)}{((p_2 - k)^2 - m^2)((p_1 - k)^2 - m^2)(k^2)} \quad (3.94)$$

with

$$\begin{aligned} f_1(k) &= (4m^2 - 2s) - 4kP + (d-4)k^2 + \frac{2(kq)^2}{s} - \frac{2(kP)^2}{(s-4m^2)} \\ f_2(k) &= -\frac{8m^2}{s-4m^2} \left(kP + k^2 + (d-1) \frac{(kP)^2}{(s-4m^2)} - \frac{(kq)^2}{s} \right) \\ f_3(k) &= \frac{8m^2}{s} kq \left(1 - (d-2) \frac{kP}{(s-4m^2)} \right). \end{aligned} \quad (3.95)$$

Again we use the relations $2kP = 2[k^2] - [(p_1 - k)^2 - m^2] - [(p_2 - k)^2 - m^2]$ and $2kq = [(p_1 - k)^2 - m^2] - [(p_2 - k)^2 - m^2]$ when it is possible to cancel against the scalar propagators $\frac{1}{(1)}$, $\frac{1}{(2)}$ and $\frac{1}{(3)}$ where (1) $\doteq (p_1 - k)^2 - m^2$, (2) $\doteq (p_2 - k)^2 - m^2$, (3) $\doteq k^2$:

$$\begin{aligned} f_1(k) &= (4m^2 - 2s) + (d-8)(3) + 2(1) + 2(2) \\ &\quad + \frac{(kq)}{s} [(1) - (2)] - \frac{(kP)}{(s-4m^2)} [2(3) - (1) - (2)] \\ f_2(k) &= -\frac{4m^2}{s-4m^2} \left(4(3) - (1) - (2) \right) \\ &\quad + (d-1) \frac{(kP)}{(s-4m^2)} [2(3) - (1) - (2)] - \frac{(kq)}{s} [(1) - (2)] \\ f_3(k) &= \frac{4m^2}{s} [(1) - (2)] \left(1 - (d-2) \frac{kP}{(s-4m^2)} \right). \end{aligned} \quad (3.96)$$

We observe that besides the first term in f_1 which yields a true vertex correction (three point function) all other terms have at least one scalar propagator (1), (2) or (3) in the numerator which cancels against one of the denominators and hence

only yields a much simpler two point function. In particular f_i $i = 2, 3$ are completely given by two point functions and the remaining k dependence in the numerator is at most linear (first rank tensor) and only in combination of two point functions. This is a dramatic simplification in comparison to the most frequently applied direct method presented before. With $\int_k \frac{1}{(1)(2)(3)} = -C_0$, $\int_k \frac{1}{(1)(2)} = B_0(m, m; s)$, $\int_k \frac{1}{(1)(3)} = \int_k \frac{1}{(2)(3)} = B_0(0, m; m^2)$, $\int_k \frac{k^\mu}{(1)(3)} = p_1^\mu \frac{A_0(m)}{2m^2}$, $\int_k \frac{k^\mu}{(2)(3)} = p_2^\mu \frac{A_0(m)}{2m^2}$, $\int_k \frac{k^\mu}{(1)(2)} = 0$, $\int_k \frac{1}{(1)} = \int_k \frac{1}{(3)} = -A_0(m)$ and $\int_k \frac{1}{(3)} = 0$ we easily find

$$\begin{aligned} A_1 &= \frac{e^2}{16\pi^2} \left\{ (2s - 4m^2) C_0(m_\gamma, m, m) \right. \\ &\quad \left. - 3 B_0(m, m; s) + 4 B_0(0, m; m^2) - 2 \right\} \\ A_2 &= \frac{e^2}{16\pi^2} \left\{ \frac{-4m^2}{s - 4m^2} (B_0(m, m; s) - B_0(0, m; m^2)) \right\} \\ A_3 &= 0 \end{aligned} \quad (3.97)$$

in agreement with (2.204).

For our main goal of calculating the muon anomaly $a_\mu = F_M(0) = -A_2(0)$ we may work out the classical limit $s = q^2 \rightarrow 0$

$$a_\mu = \lim_{q^2 \rightarrow 0} \text{Tr} \left\{ (\not{p}_1 + m) \Lambda_2^\mu(p_2, p_1) (\not{p}_2 + m) \Pi_\mu(P, q) \right\} \quad (3.98)$$

explicitly. Because of the singular factor $1/q^2$ in front of the projector Λ_2 (3.93) we are required to expand the amplitude $\Pi^\mu(P, q)$ to first order for small q ,

$$\Pi_\mu(P, q) \simeq \Pi_\mu(P, 0) + q^\nu \frac{\partial}{\partial q^\nu} \Pi_\mu(P, q) \Big|_{q=0} \equiv V_\mu(p) + q^\nu T_{\nu\mu}(p), \quad (3.99)$$

where for $q = 0$ we have $p = P/2 = p_1$. Other factors of q come from expanding the other factors in the trace by setting $p_2 = (P + q)/2$ and $p_1 = (P - q)/2$ and performing an expansion in $q = p_2 - p_1$ for fixed $P = p_2 + p_1$. We note that due to the on-shell condition $p_2^2 = p_1^2 = m^2$ we have $Pq = 2pq + q^2 = 0$. The only relevant q^μ dependence left are the terms linear and quadratic in q , proportional to q^μ and $q^\mu q^\nu$. Since the trace under consideration projects to a scalar, we may average the residual q dependence over all spatial directions without changing the result. Since P and q are two independent and orthogonal vectors, averaging is relative to the direction of P . For the linear term we have

$$\overline{q^\mu} \equiv \int \frac{d\Omega(P, q)}{4\pi} q^\mu = 0 \quad (3.100)$$

because the integrand is an odd function, while

$$\overline{q^\mu q^\nu} \equiv \int \frac{d\Omega(P, q)}{4\pi} q^\mu q^\nu = \alpha g^{\mu\nu} + \beta \frac{P^\mu P^\nu}{P^2}$$

must be a second rank tensor in P . Since $Pq = 0$, the contraction with P_μ is vanishing, which requires

$$\beta = -\alpha .$$

The other possible contraction with $g_{\mu\nu}$ yields q^2 :

$$\int \frac{d\Omega(P, q)}{4\pi} q^2 = q^2 \int \frac{d\Omega(P, q)}{4\pi} = q^2 = \alpha d + \beta = (d-1) \alpha$$

and hence

$$\alpha = \frac{q^2}{(d-1)}$$

or

$$\overline{q^\mu q^\nu} = \frac{q^2}{(d-1)} \left(g^{\mu\nu} - \frac{P^\mu P^\nu}{P^2} \right) . \quad (3.101)$$

Using these averages we may work out the limit which yields

$$\begin{aligned} a_\mu &= \frac{1}{8(d-2)(d-1)m} \text{Tr} \{ (\not{p} + m) [\gamma^\mu, \gamma^\nu] (\not{p} + m) T_{\nu\mu}(p) \} \\ &+ \frac{1}{4(d-1)m^2} \text{Tr} \{ [m^2 \gamma^\mu - (d-1)m p^\mu - d \not{p} p^\mu] V_\mu(p) \} \Big|_{p^2=m^2} \end{aligned} \quad (3.102)$$

as a master formula for the calculation of a_μ [103]. The form of the first term is obtained upon anti-symmetrization in the indices $[\mu\nu]$. The amplitudes $V_\mu(p)$ and $T_{\nu\mu}(p)$ depend on one on-shell momentum p , only, and thus the problem reduces to the calculation of on-shell self-energy type diagrams shown in Fig. 3.9.

In $T_{\nu\mu}$ the extra vertex is generated by taking the derivative of the internal muon propagators

$$\frac{\partial}{\partial q^\nu} \frac{i}{\not{p} - \not{k} \mp q/2 - m} \Big|_{q=0} = \mp \frac{1}{2} \frac{i}{\not{p} - \not{k} - m} (-i \gamma_\nu) \frac{i}{\not{p} - \not{k} - m} .$$

Usually, writing the fermion propagators in terms of scalar propagators

$$\frac{i}{\not{p}_i - \not{k} - m} = \frac{i(\not{p}_i - \not{k} + m)}{(p_i - k)^2 - m^2}$$

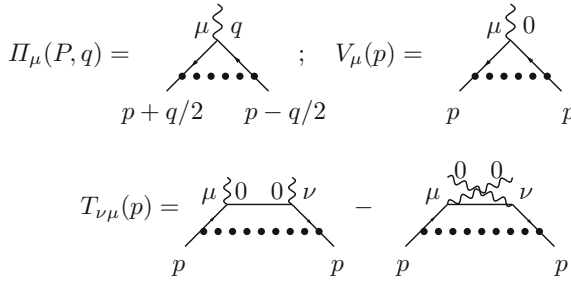


Fig. 3.9 To calculate a_μ one only needs the on-shell vertex $V_\mu(p) = \Pi_\mu(P, q)|_{q=0}$ and its $\mu \leftrightarrow \nu$ anti-symmetrized derivative $T_{\nu\mu} = \frac{\partial}{\partial q^\nu} \Pi_\mu(P, q)|_{q=0}$ at zero momentum transfer. Illustrated here for the lowest order diagram; the dotted line may be a photon or a heavy “photon” as needed in the dispersive approach to be discussed below

as done in (2.203), only the expansion of the numerators contributes to $T_{\nu\mu}$, while expanding the product of the two scalar propagators

$$\frac{1}{(p_2 - k)^2 - m^2} \frac{1}{(p_1 - k)^2 - m^2} = \frac{1}{((p - k)^2 - m^2)^2} + Q(q^2)$$

gives no contribution linear in q , as the linear terms coming from the individual propagators cancel in the product. Looking at (2.203), for the lowest order contribution we thus have to calculate the trace (3.102) with

$$\begin{aligned} V_\mu &\rightarrow v_\mu = \gamma^\rho (\not{p} - \not{k} + m) \gamma_\mu (\not{p} - \not{k} + m) \gamma_\rho \\ T_{\nu\mu} &\rightarrow t_{\nu\mu} = \frac{1}{2} \gamma^\rho (\gamma_\nu \gamma_\mu (\not{p} - \not{k} + m) - (\not{p} - \not{k} + m) \gamma_\mu \gamma_\nu) \gamma_\rho . \end{aligned}$$

The trace yields

$$2k^2 \left(\frac{1}{d-1} - 1 \right) - 4kp + \frac{(2kp)^2}{2m^2} \left(d - 1 - \frac{1}{d-1} \right)$$

which is to be integrated as in (2.203). The result is (see Sect. 2.6.3 p. 116)

$$a_\mu = \frac{e^2}{16\pi^2} \frac{2}{3} \{ B_0(0, m; m^2) - B_0(m, m; 0) + 1 \} = \frac{\alpha}{\pi} \frac{1}{2}$$

as it should be. Note that the result differs in structure from (3.97) because integration and taking the limit is interchanged. Since we are working throughout with dimensional regularization, it is crucial to take the dimension d generic until after integration. In particular setting $d = 4$ in the master formula (3.102) would lead to a wrong constant term in the above calculation. In fact, the constant term would just be absent.

The projection technique just outlined provides an efficient tool for calculating individual on-shell amplitudes directly. One question may be addressed here, however. The muon is an unstable particle and mass and width are defined via the resonance pole in the complex p^2 -plane. In this case the projection technique as presented above has its limitation. However, the muon width is so many orders of magnitude smaller than the muon mass, that at the level of accuracy which is of any practical interest, this is not a matter of worry, i.e. the muon as a quasi stable particle may be safely approximated to be stable in calculations of a_μ .

3.6 Properties of the Form Factors

We again consider the interaction of a lepton in an external field: the relevant T -matrix element is

$$T_{fi} = e \mathcal{J}_{fi}^\mu \tilde{A}_\mu^{\text{ext}}(q) \quad (3.103)$$

with

$$\mathcal{J}_{fi}^\mu = \bar{u}_2 \Gamma^\mu u_1 = \langle f | j_{\text{em}}^\mu(0) | i \rangle = \langle \ell^-(p_2) | j_{\text{em}}^\mu(0) | \ell^-(p_1) \rangle . \quad (3.104)$$

By the crossing property we have the following channels:

- Elastic ℓ^- scattering: $s = q^2 = (p_2 - p_1)^2 \leq 0$
- Elastic ℓ^+ scattering: $s = q^2 = (p_1 - p_2)^2 \leq 0$
- Annihilation (or pair-creation) channel: $s = q^2 = (p_1 + p_2)^2 \geq 4m_\ell^2$

The domain $0 < s < 4m_\ell^2$ is unphysical. A look at the unitarity condition

$$i \{ T_{if}^* - T_{fi} \} = \sum_n \int (2\pi)^4 \delta^{(4)}(P_n - P_i) T_{nf}^* T_{ni} , \quad (3.105)$$

which derives from (2.96), (2.103), taking $\langle f | S^+ S | i \rangle$ and using (3.128) below, tells us that for $s < 4m_\ell^2$ there is no physical state $|n\rangle$ allowed by energy and momentum conservation and thus

$$T_{fi} = T_{if}^* \quad \text{for} \quad s < 4m_\ell^2 , \quad (3.106)$$

which means that the current matrix element is Hermitian. As the electromagnetic potential $A_\mu^{\text{ext}}(x)$ is real its Fourier transform satisfies

$$\tilde{A}_\mu^{\text{ext}}(-q) = \tilde{A}_\mu^{*\text{ext}}(q) \quad (3.107)$$

and hence

$$\mathcal{J}_{fi}^\mu = \mathcal{J}_{if}^{\mu*} \quad \text{for} \quad s < 4m_\ell^2 . \quad (3.108)$$

If we interchange initial and final state the four-vectors p_1 and p_2 are interchanged such that q changes sign: $q \rightarrow -q$. The unitarity relation for the form factor decomposition of $\bar{u}_2 \Pi_{\gamma\ell\ell}^\mu u_1$ (3.82) thus reads ($u_i = u(p_i, r_i)$)

$$\begin{aligned} & \bar{u}_2 \left(\gamma^\mu F_E(q^2) + [\gamma^\mu - \frac{2mq^\mu}{q^2}] \gamma_5 F_A + i\sigma^{\mu\nu} \frac{q_\nu}{2m} F_M(q^2) + \sigma^{\mu\nu} \frac{q_\nu}{2m} \gamma_5 F_D \right) u_1 \\ &= \left\{ \bar{u}_1 \left(\gamma^\mu F_E(q^2) + [\gamma^\mu + \frac{2mq^\mu}{q^2}] \gamma_5 F_A - i\sigma^{\mu\nu} \frac{q_\nu}{2m} F_M(q^2) - \sigma^{\mu\nu} \frac{q_\nu}{2m} \gamma_5 F_D \right) u_2 \right\}^* \\ &= u_2^\dagger \left(\gamma^{\mu+} F_E^*(q^2) + \gamma_5^\dagger [\gamma^{\mu+} + \frac{2mq^\mu}{q^2}] F_A^* + i\sigma^{\mu\nu+} \frac{q_\nu}{2m} F_M^*(q^2) - \gamma_5^\dagger \sigma^{\mu\nu+} \frac{q_\nu}{2m} F_D^* \right) \bar{u}_1^\dagger \\ &= \bar{u}_2 \left(\gamma^\mu F_E^*(q^2) + [\gamma^\mu - \frac{2mq^\mu}{q^2}] \gamma_5 F_A^* + i\sigma^{\mu\nu} \frac{q_\nu}{2m} F_M^*(q^2) + \sigma^{\mu\nu} \frac{q_\nu}{2m} \gamma_5 F_D^* \right) u_1 . \end{aligned}$$

The last equality follows using $u_2^\dagger = \bar{u}_2 \gamma^0$, $\bar{u}_1^\dagger = \gamma^0 u_1$, $\gamma_5^\dagger = \gamma_5$, $\gamma^0 \gamma_5 \gamma^0 = -\gamma_5$, $\gamma^0 \gamma^{\mu+} \gamma^0 = \gamma^\mu$ and $\gamma^0 \sigma^{\mu\nu+} \gamma^0 = \sigma^{\mu\nu}$. Unitarity thus implies that the form factors are real

$$\text{Im } F(s)_i = 0 \quad \text{for } s < 4m_e^2 \quad (3.109)$$

below the threshold of pair production $s = 4m_e^2$. For $s \geq 4m_e^2$ the form factors are complex; they are analytic in the complex s -plane with a cut along the positive axis starting at $s = 4m_e^2$ (see Fig. 3.10). In the annihilation channel ($p_- = p_2$, $p_+ = -p_1$)

$$\langle 0 | j_{\text{em}}^\mu(0) | p_-, p_+ \rangle = \sum_n \langle 0 | j_{\text{em}}^\mu(0) | n \rangle \langle n | p_-, p_+ \rangle , \quad (3.110)$$

where the lowest state $|n\rangle$ contributing to the sum is an e^+e^- state at threshold: $E_+ = E_- = m_e$ and $\mathbf{p}_+ = \mathbf{p}_- = 0$ such that $s = 4m_e^2$. Because of the causal $i\epsilon$ -prescription in the time-ordered Green functions the imaginary parts of the analytic amplitudes change sign when $s \rightarrow s^*$ and hence

$$F_i(s^*) = F_i^*(s) , \quad (3.111)$$

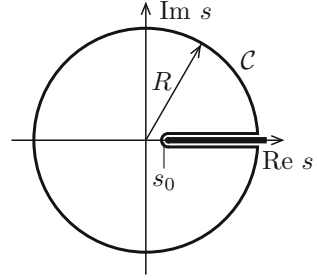
which is the Schwarz reflection principle.

3.7 Dispersion Relations

Causality together with unitarity imply analyticity of the form factors in the complex s -plane except for the cut along the positive real axis starting at $s \geq 4m_e^2$. Cauchy's integral theorem tells us that the contour integral, for the contour \mathcal{C} shown in Fig. 3.10, satisfies

$$F_i(s) = \frac{1}{2\pi i} \oint_{\mathcal{C}} \frac{ds' F(s')}{s' - s} . \quad (3.112)$$

Fig. 3.10 Analyticity domain and Cauchy contour \mathcal{C} for the lepton form factor (vacuum polarization). \mathcal{C} is a circle of radius R with a cut along the positive real axis for $s > s_0 = 4m^2$ where m is the mass of the lightest pair-produced



Since $F^*(s) = F(s^*)$ the contribution along the cut may be written as

$$\lim_{\epsilon \rightarrow 0} (F(s + i\epsilon) - F(s - i\epsilon)) = 2i \operatorname{Im} F(s) ; \quad s \text{ real}, s > 0$$

and hence for $R \rightarrow \infty$

$$F(s) = \lim_{\epsilon \rightarrow 0} F(s + i\epsilon) = \frac{1}{\pi} \lim_{\epsilon \rightarrow 0} \int_{4m^2}^{\infty} ds' \frac{\operatorname{Im} F(s')}{s' - s - i\epsilon} + \mathcal{C}_{\infty} .$$

In all cases where $F(s)$ falls off sufficiently rapidly as $|s| \rightarrow \infty$ the boundary term \mathcal{C}_{∞} vanishes and the integral converges. This may be checked order by order in perturbation theory. In this case the “un-subtracted” dispersion relation (DR)

$$F(s) = \frac{1}{\pi} \lim_{\epsilon \rightarrow 0} \int_{4m^2}^{\infty} ds' \frac{\operatorname{Im} F(s')}{s' - s - i\epsilon} \tag{3.113}$$

uniquely determines the function by its imaginary part. A technique based on DRs is frequently used for the calculation of Feynman integrals, because the calculation of the imaginary part is simpler in general. The real part which actually is the object to be calculated is given by the principal value (\mathcal{P}) integral

$$\operatorname{Re} F(s) = \frac{1}{\pi} \mathcal{P} \int_{4m^2}^{\infty} ds' \frac{\operatorname{Im} F(s')}{s' - s} , \tag{3.114}$$

which is also known under the name Hilbert transform.

For our form factors the fall off condition is satisfied for the Pauli form factor F_M but not for the Dirac form factor F_E . In the latter case the fall off condition is not satisfied because $F_E(0) = 1$ (charge renormalization condition = subtraction condition). However, performing a subtraction of $F_E(0)$ in (3.113), one finds that $(F_E(s) - F_E(0))/s$ satisfies the “subtracted” dispersion relations

$$\frac{F(s) - F(0)}{s} = \frac{1}{\pi} \lim_{\varepsilon \rightarrow 0} \int_{4m^2}^{\infty} ds' \frac{\text{Im } F(s')}{s'(s' - s - i\varepsilon)}, \quad (3.115)$$

which exhibits one additional power of s' in the denominator and hence improves the damping of the integrand at large s' by one additional power. Order by order in perturbation theory the integral (3.115) is convergent for the Dirac form factor. A very similar relation is satisfied by the vacuum polarization amplitude which we will discuss in the following section.

3.7.1 Dispersion Relations and the Vacuum Polarization

Dispersion relations play an important role for taking into account the photon propagator contributions. The related photon self-energy, obtained from the photon propagator by the amputation of the external photon lines, is given by the correlator of two electromagnetic currents and may be interpreted as vacuum polarization for the following reason: as we have seen in Sect. 2.6.3 charge renormalization in QED, according to (2.212), is caused solely by the photon self-energy correction; the fundamental electromagnetic fine structure constant α in fact is a function of the energy scale $\alpha \rightarrow \alpha(E)$ of a process due to charge screening. The latter is a result of the fact that a naked charge is surrounded by a cloud of virtual particle-antiparticle pairs (dipoles mostly) which line up in the field of the central charge and such lead to a vacuum polarization which screens the central charge. This is illustrated in Fig. 3.11. From long distances (classical charge) one thus sees less charge than if one comes closer, such that one sees an increasing charge with increasing energy. Figure 3.12 shows the usual diagrammatic representation of a vacuum polarization effect.

Fig. 3.11 Vacuum polarization causing charge screening by virtual pair creation and re-annihilation. The effective charge seen by a test charge at distance $r = \hbar/E$ (E the collision energy) is given by the charge inside the ball of radius r

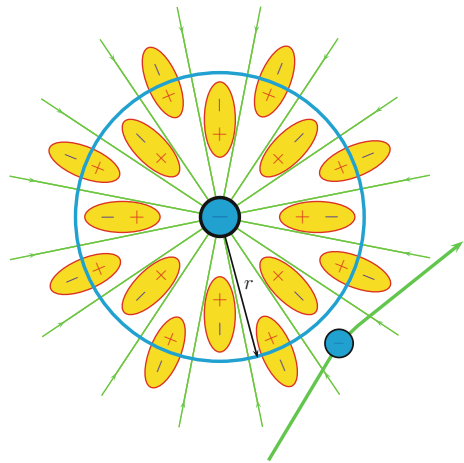
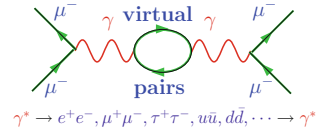


Fig. 3.12 Feynman diagram describing the vacuum polarization in muon scattering



As discussed in Sect. 2.6.1 the vacuum polarization affects the photon propagator in that the full or dressed propagator is given by the geometrical progression of self-energy insertions $-i\Pi_\gamma(q^2)$. The corresponding Dyson summation implies that the free propagator is replaced by the dressed one

$$iD_\gamma^{\mu\nu}(q) = \frac{-ig^{\mu\nu}}{q^2 + i\epsilon} \rightarrow iD'_\gamma{}^{\mu\nu}(q) = \frac{-ig^{\mu\nu}}{q^2 + \Pi_\gamma(q^2) + i\epsilon} \tag{3.116}$$

modulo unphysical gauge dependent terms. By $U(1)_{em}$ gauge invariance the photon remains massless and hence we have $\Pi_\gamma(q^2) = \Pi_\gamma(0) + q^2 \Pi'_\gamma(q^2)$ with $\Pi_\gamma(0) \equiv 0$. As a result we obtain

$$iD'_\gamma{}^{\mu\nu}(q) = \frac{-ig^{\mu\nu}}{q^2 (1 + \Pi'_\gamma(q^2))} + \text{gauge terms} \tag{3.117}$$

where the “gauge terms” will not contribute to gauge invariant physical quantities, and need not be considered further.

Including a factor e^2 and considering the renormalized propagator (wave function renormalization factor Z_γ) we have

$$i e^2 D'_\gamma{}^{\mu\nu}(q) = \frac{-ig^{\mu\nu} e^2 Z_\gamma}{q^2 (1 + \Pi'_\gamma(q^2))} + \text{gauge terms} \tag{3.118}$$

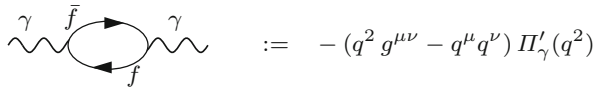
which in effect means that the charge has to be replaced by a **running charge**

$$e^2 \rightarrow e^2(q^2) = \frac{e^2 Z_\gamma}{1 + \Pi'_\gamma(q^2)} \tag{3.119}$$

The wave function renormalization factor Z_γ is fixed by the condition that at $q^2 \rightarrow 0$ one obtains the classical charge (charge renormalization in the *Thomson limit*; see also (2.170)). Thus the renormalized charge is

$$e^2 \rightarrow e^2(q^2) = \frac{e^2}{1 + (\Pi'_\gamma(q^2) - \Pi'_\gamma(0))} \tag{3.120}$$

where the lowest order diagram in perturbation theory which contributes to $\Pi'_\gamma(q^2)$ is



$$:= - (q^2 g^{\mu\nu} - q^\mu q^\nu) \Pi'_\gamma(q^2)$$

and describes the virtual creation and re-absorption of fermion pairs $\gamma^* \rightarrow e^+ e^-$, $\mu^+ \mu^-$, $\tau^+ \tau^-$, $u\bar{u}$, $d\bar{d}$, $\dots \rightarrow \gamma^*$, In terms of the fine structure constant $\alpha = \frac{e^2}{4\pi}$ (3.120) reads²⁷

$$\alpha(q^2) = \frac{\alpha}{1 - \Delta\alpha} \quad ; \quad \Delta\alpha = -\text{Re} (\Pi'_\gamma(q^2) - \Pi'_\gamma(0)) \quad . \quad (3.121)$$

The various contributions to the shift in the fine structure constant come from the leptons (lep = e , μ and τ) the 5 light quarks (u , d , s , c , and b and the corresponding hadrons = had) and from the top quark:

$$\Delta\alpha = \Delta\alpha_{\text{lep}} + \Delta^{(5)}\alpha_{\text{had}} + \Delta\alpha_{\text{top}} + \dots \quad (3.122)$$

Also W -pairs contribute at $q^2 > M_W^2$. While the other contributions can be calculated order by order in perturbation theory the hadronic contribution $\Delta^{(5)}\alpha_{\text{had}}$ exhibits low energy strong interaction effects and hence cannot be calculated by perturbative means. Here the dispersion relations play a key role. This will be discussed in detail in Sect. 5.1.7.

The leptonic contributions are calculable in perturbation theory. Using our result (2.176) for the renormalized photon self-energy, at leading order the free lepton loops yield

$$\begin{aligned} \Delta\alpha_{\text{lep}}(q^2) &= \\ &= \sum_{\ell=e,\mu,\tau} \frac{\alpha}{3\pi} \left[-\frac{5}{3} - y_\ell + \left(1 + \frac{y_\ell}{2}\right) \sqrt{1 - y_\ell} \ln \left(\left| \frac{\sqrt{1 - y_\ell} + 1}{\sqrt{1 - y_\ell} - 1} \right| \right) \right] \\ &= \sum_{\ell=e,\mu,\tau} \frac{\alpha}{3\pi} \left[-\frac{8}{3} + \beta_\ell^2 + \frac{1}{2}\beta_\ell(3 - \beta_\ell^2) \ln \left(\left| \frac{1 + \beta_\ell}{1 - \beta_\ell} \right| \right) \right] \\ &= \sum_{\ell=e,\mu,\tau} \frac{\alpha}{3\pi} \left[\ln(|q^2|/m_\ell^2) - \frac{5}{3} + O(m_\ell^2/q^2) \right] \text{ for } |q^2| \gg m_\ell^2 \\ &\simeq 0.03142 \text{ for } q^2 = M_Z^2 \end{aligned} \quad (3.123)$$

where $y_\ell = 4m_\ell^2/q^2$ and $\beta_\ell = \sqrt{1 - y_\ell}$ are the lepton velocities. The two-loop QED contribution

²⁷Later, in particular when discussing hadronic resonance contributions, we will also use a complex definition of the effective fine structure constant by including the imaginary part on the r.h.s of (3.121) as well.



has been calculated long time ago [175, 176]. Defining the conformal variable (2.182) (see Sect. 2.6.1)

$$q^2 \rightarrow \xi = \frac{\sqrt{1-y}-1}{\sqrt{1-y}+1} ; \quad y = \frac{4m^2}{q^2} = -\frac{4\xi}{(1-\xi)^2},$$

we may write the single fermion contribution to two loops for spacelike $q^2 < 0$ ($0 \leq \xi \leq 1$) as (in this from provided by M. Kalmykov)

$$\begin{aligned} \Delta^{(1)}\alpha(q^2) &= \frac{\alpha}{4\pi} \left[-\frac{20}{9} + \frac{16}{3} \frac{\xi}{(1-\xi)^2} - \frac{4}{3} \frac{(1+\xi)(1-4\xi+\xi^2)}{(1-\xi)^3} \ln \xi \right], \\ \Delta^{(2)}\alpha(q^2) &= \frac{\alpha^2}{(4\pi)^2} \left\{ -\frac{10}{3} + \frac{104}{3} \frac{\xi}{(1-\xi)^2} + 16\zeta_3 \left(1 - 4 \frac{\xi^2}{(1-\xi)^4} \right) \right. \\ &\quad - \frac{16}{3} \frac{1-4\xi+\xi^2}{(1-\xi)^4} [\ln(1-\xi) + 2\ln(1+\xi)] \ln \xi [(1+\xi^2)\ln \xi - 2(1-\xi^2)] \\ &\quad + \frac{8}{3} \xi \frac{2+7\xi-22\xi^2+6\xi^3}{(1-\xi)^4} \ln^2 \xi - 4 \frac{(1+\xi)(1-\xi)(1-8\xi+\xi^2)}{(1-\xi)^3} \ln \xi \\ &\quad + \frac{32}{3} \frac{(1-4\xi+\xi^2)}{(1-\xi)^4} [\text{Li}_2(\xi) + 2\text{Li}_2(-\xi)] [1-\xi^2 - 2(1+\xi^2)\ln \xi] \\ &\quad \left. + 32 \frac{(1-4\xi+\xi^2)}{(1-\xi)^4} (1+\xi^2) [\text{Li}_3(\xi) + 2\text{Li}_3(-\xi)] \right\}, \end{aligned} \quad (3.124)$$

The analytical continuation to $q^2 > 4m^2$ ($-1 \leq \xi \leq 0$) can be obtained using $m^2 \rightarrow m^2 - i\varepsilon$, i.e.

$$\xi = \frac{\sqrt{1 - \frac{4m^2}{q^2} + i\varepsilon} - 1}{\sqrt{1 - \frac{4m^2}{q^2} + i\varepsilon} + 1} \equiv \xi + i\varepsilon ; \quad \ln \xi = \ln |\xi| + i\pi.$$

In the unphysical region $0 < q^2 < 4m^2$ ($\xi = e^{i\varphi}$) one may use the parametrization (setting $\varphi = 2\tau$):

$$\xi = \exp(i2\tau), \quad \frac{q^2}{4m^2} = \sin^2 \tau, \quad \ln \xi = i2\tau,$$

to obtain

$$\begin{aligned}
\Delta\alpha^{(1)}(s) &= \frac{\alpha}{4\pi} \left\{ -\frac{20}{9} + \frac{4}{3} \frac{\tau \cos \tau}{\sin^3 \tau} (1 + 2 \sin^2 \tau) - \frac{4}{3} \frac{1}{\sin^2 \tau} \right\}, \\
\Delta\alpha^{(2)}(s) &= \frac{\alpha^2}{(4\pi)^2} \left\{ 16 \left[2\text{Cl}_3(2\tau) + 4\text{Cl}_3(\pi - 2\tau) + \zeta_3 \right] \left[1 - \frac{1}{4 \sin^4 \tau} \right] \right. \\
&\quad + \frac{16}{3} \left[\text{Cl}_2(2\tau) - 2\text{Cl}_2(\pi - 2\tau) \right] \left[8\tau \left[1 - \frac{1}{4 \sin^4 \tau} \right] - \frac{\cos \tau (1 + 2 \sin^2 \tau)}{\sin^3 \tau} \right] \\
&\quad + \frac{32}{3} \left[\ln(2 \sin \tau) + 2 \ln(2 \cos \tau) \right] \left[2\tau^2 \left[1 - \frac{1}{4 \sin^4 \tau} \right] - \frac{\tau \cos \tau (1 + 2 \sin^2 \tau)}{\sin^3 \tau} \right] \\
&\quad \left. - \frac{10}{3} + 4 \frac{\tau \cos \tau (3 + 2 \sin^2 \tau)}{\sin^3 \tau} - \frac{26}{3} \frac{1}{\sin^2 \tau} + \frac{14}{3} \frac{\tau^2}{\sin^4 \tau} + \frac{16}{3} \frac{\tau^2}{\sin^2 \tau} - 32\tau^2 \right\}. \quad (3.125)
\end{aligned}$$

The Clausen function is defined by $\text{Cl}_n(\varphi) = \text{Im Li}_n(e^{i\varphi}) = \sum_{m=1}^{\infty} \frac{\sin(m\varphi)}{m^n}$. The gluonic perturbative QCD correction is given by the same formulas multiplied by the color factor $N_c = 3$ and the $SU(3)$ Casimir coefficient $C_F = 4/3$ [177].

For $\alpha = 137.036$, $m_e = 0.510998902$, $m_\mu = 105.658357$, $m_\tau = 1776.99$ we get

$\Delta\alpha(M_Z) \times 10^4$	e	μ	τ	$e + \mu + \tau$
1-loop	174.34669	91.78436	48.05954	314.19059
2-loop	0.379829	0.235999	0.160339	0.7761677

Thus the leading contribution is affected by small electromagnetic corrections only in the next to leading order. For large q^2 the leptonic contribution is actually known to three loops [178] at which it takes the value

$$\Delta\alpha_{\text{leptons}}(M_Z^2) \simeq 314.98 \times 10^{-4}. \quad (3.126)$$

As already mentioned, in contrast, the corresponding free quark loop contribution gets substantially modified by low energy strong interaction effects, which cannot be calculated reliably by perturbative QCD. The evaluation of the hadronic contribution will be discussed later.

Vacuum polarization effects are large when large scale changes are involved (large logarithms) and because of the large number of light fermionic degrees of freedom (see (2.181)) as we infer from the asymptotic form in perturbation theory

$$\Delta\alpha^{\text{pert}}(q^2) \simeq \frac{\alpha}{3\pi} \sum_f Q_f^2 N_{cf} \left(\ln \frac{|q^2|}{m_f^2} - \frac{5}{3} \right); \quad |q^2| \gg m_f^2. \quad (3.127)$$

Fig. 3.13 Shift of the effective fine structure constant $\Delta\alpha$ as a function of the energy scale in the space-like region $q^2 < 0$ ($E = -\sqrt{-q^2}$). The vertical bars at selected points indicate the uncertainty

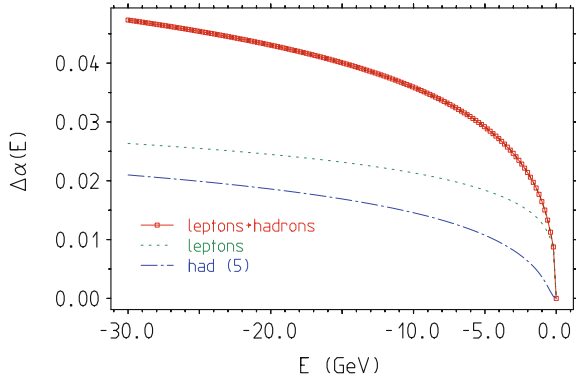


Figure 3.13 illustrates the running of the effective charges at lower energies in the space-like region.²⁸ Typical values are $\Delta\alpha(5 \text{ GeV}) \sim 3\%$ and $\Delta\alpha(M_Z) \sim 6\%$, where about $\sim 50\%$ of the contribution comes from leptons and about $\sim 50\%$ from hadrons. Note the sharp increase of the screening correction at relatively low energies.

The vacuum polarization may be described alternatively as the vacuum expectation value of the time ordered product of two electromagnetic currents, which follows by amputation of the external photon lines of the photon propagator: at one loop order



One may represent the current correlator as a Källén–Lehmann representation [181] in terms of spectral densities. To this end, let us consider first the Fourier transform of the vacuum expectation value of the product of two currents. Using translation invariance and inserting a complete set of states n of momentum p_n ,²⁹ satisfying the completeness relation

$$\int \frac{d^4 p_n}{(2\pi)^3} \sum_n |n\rangle \langle n| = 1 \tag{3.128}$$

²⁸A direct measurement is difficult because of the normalizing process involved in any measurement which itself depends on the effective charge. Measurements of the evolution of the electromagnetic coupling are possible in any case with an offset energy scale and results have been presented in [179] (see also [180]).

²⁹Note that the intermediate states are multi-particle states, in general, and the completeness integral includes an integration over p_n^0 , since p_n is not on the mass shell $p_n^0 \neq \sqrt{m_n^2 + \mathbf{p}_n^2}$. In general, in addition to a possible discrete part of the spectrum we are dealing with a continuum of states.

where \sum_n includes, for fixed total momentum p_n , integration over the phase space available to particles of all possible intermediate physical states $|n\rangle$, we have

$$\begin{aligned} i \int d^4x e^{iqx} \langle 0 | j^\mu(x) j^\nu(0) | 0 \rangle &= i \int \frac{d^4 p_n}{(2\pi)^3} \int d^4x e^{i(q-p_n)x} \sum_n \langle 0 | j^\mu(0) | n \rangle \langle n | j^\nu(0) | 0 \rangle \\ &= i \int \frac{d^4 p_n}{(2\pi)^3} \sum_n (2\pi)^4 \delta^{(4)}(q - p_n) \langle 0 | j^\mu(0) | n \rangle \langle n | j^\nu(0) | 0 \rangle \\ &= i 2\pi \sum_n \langle 0 | j^\mu(0) | n \rangle \langle n | j^\nu(0) | 0 \rangle \Big|_{p_n=q} . \end{aligned}$$

Key ingredient of the representation we are looking for is the **spectral function** tensor $\rho^{\mu\nu}(q)$ defined by

$$\rho^{\mu\nu}(q) \doteq \sum_n \langle 0 | j^\mu(0) | n \rangle \langle n | j^\nu(0) | 0 \rangle \Big|_{p_n=q} . \quad (3.129)$$

Taking into account that q is the momentum of a physical state (spectral condition $q^2 \geq 0$, $q^0 \geq 0$), the relativistic covariant decomposition may be written as

$$\rho^{\mu\nu}(q) = \Theta(q^0)\Theta(q^2) \{ [q^\mu q^\nu - q^2 g^{\mu\nu}] \rho_1(q^2) + q^\mu q^\nu \rho_0(q^2) \} \quad (3.130)$$

and current conservation $\partial_\mu j^\mu = 0 \Leftrightarrow q_\mu \rho^{\mu\nu} = 0$ implies $\rho_0 \equiv 0$, which is the transversality condition. For non-conserved currents, like the ones of the weak interactions, a longitudinal component ρ_0 exists in addition to the transversal one ρ_1 . Note that $\Theta(p^2)$ may be represented as

$$\Theta(q^2) = \int_0^\infty dm^2 \delta(q^2 - m^2)$$

and therefore we may write

$$\begin{aligned} i \int d^4x e^{iqx} \langle 0 | j^\mu(x) j^\nu(0) | 0 \rangle & \quad (3.131) \\ &= \int_0^\infty dm^2 \{ [m^2 g^{\mu\nu} - q^\mu q^\nu] \rho_1(m^2) - q^\mu q^\nu \rho_0(m^2) \} \left(-2\pi i \Theta(q^0) \delta(q^2 - m^2) \right), \end{aligned}$$

which is the Källén–Lehmann representation for the positive frequency part of the current correlator. The latter, according to (2.141), is twice the imaginary part of the corresponding time-ordered current correlation function

$$\begin{aligned}
& i \int d^4x e^{iqx} \langle 0 | T j^\mu(x) j^\nu(0) | 0 \rangle \\
&= \int_0^\infty dm^2 \{ [m^2 g^{\mu\nu} - q^\mu q^\nu] \rho_1(m^2) - q^\mu q^\nu \rho_0(m^2) \} \left(\frac{1}{q^2 - m^2 + i\varepsilon} \right)
\end{aligned} \tag{3.132}$$

constrained to positive q^0 .

In our case, for the conserved electromagnetic current, only the transversal amplitude is present: thus $\rho_0 \equiv 0$ and we denote ρ_1 by ρ , simply.³⁰ Thus, formally, in Fourier space we have

$$\begin{aligned}
i \int d^4x e^{iqx} \langle 0 | T j_{\text{em}}^\mu(x) j_{\text{em}}^\nu(0) | 0 \rangle &= \int_0^\infty dm^2 \rho(m^2) (m^2 g^{\mu\nu} - q^\mu q^\nu) \frac{1}{q^2 - m^2 + i\varepsilon} \\
&= -(q^2 g^{\mu\nu} - q^\mu q^\nu) \hat{\Pi}'_\gamma(q^2)
\end{aligned} \tag{3.133}$$

where $\hat{\Pi}'_\gamma(q^2)$ up to a factor e^2 is the **photon vacuum polarization function** introduced before (see (2.159) and (2.160)):

$$\Pi'_\gamma(q^2) = e^2 \hat{\Pi}'_\gamma(q^2) . \tag{3.134}$$

With this bridge to the photon self-energy function Π'_γ we can get its imaginary part by substituting

$$\frac{1}{q^2 - m^2 + i\varepsilon} \rightarrow -\pi i \delta(q^2 - m^2)$$

in (3.133), which if constrained to positive q^0 yields back half of (3.131) with $\rho_0 = 0$. Thus contracting (3.131) with $2\Theta(q^0)g_{\mu\nu}$ and dividing by $g_{\mu\nu}(q^2 g^{\mu\nu} - q^\mu q^\nu) = 3q^2$ we obtain

$$\begin{aligned}
2\Theta(q^0) \text{Im} \hat{\Pi}'_\gamma(q^2) &= \Theta(q^0) 2\pi \rho(q^2) \\
&= -\frac{1}{3q^2} 2\pi \sum_n^f \langle 0 | j_{\text{em}}^\mu(0) | n \rangle \langle n | j_{\text{em}}^\nu(0) | 0 \rangle \Big|_{p_n=q} .
\end{aligned} \tag{3.135}$$

Again causality implies analyticity and the validity of a dispersion relation. In fact the electromagnetic current correlator exhibits a logarithmic UV singularity and thus requires one subtraction such that from (3.133) we find

³⁰In the case of a conserved current, where $\rho_0 \equiv 0$, we may formally derive that $\rho_1(s)$ is real and positive $\rho_1(s) \geq 0$. To this end we consider the element ρ^{00}

$$\rho^{00}(q) = \sum_n^f \langle 0 | j^0(0) | n \rangle \langle n | j^0(0) | 0 \rangle \Big|_{q=p_n} = \sum_n^f |(0 | j^0(0) | n)|_{q=p_n}^2 \geq 0 = \Theta(q^0) \Theta(q^2) \mathbf{q}^2 \rho_1(q^2)$$

from which the statement follows.

$$\Pi'_\gamma(q^2) - \Pi'_\gamma(0) = \frac{q^2}{\pi} \int_0^\infty ds \frac{\text{Im } \Pi'_\gamma(s)}{s(s - q^2 - i\varepsilon)}. \quad (3.136)$$

Unitarity (3.105) implies the *optical theorem*, which is obtained from this relation in the limit of elastic forward scattering $|f\rangle \rightarrow |i\rangle$ where

$$2\text{Im } T_{ii} = \sum_{\mathbf{n}} (2\pi)^4 \delta^{(4)}(P_n - P_i) |T_{ni}|^2. \quad (3.137)$$

which tells us that the imaginary part of the photon propagator is proportional to the total cross section $\sigma_{\text{tot}}(e^+e^- \rightarrow \gamma^* \rightarrow \text{anything})$ (“anything” means any possible state). The precise relationship reads (see Sect. 5.1.5)

$$\text{Im } \hat{\Pi}'_\gamma(s) = \frac{1}{12\pi} R(s) \quad (3.138)$$

$$\text{Im } \Pi'_\gamma(s) = e^2 \text{Im } \hat{\Pi}'_\gamma(s) = \frac{\alpha}{3} R(s) = \frac{\alpha s}{4\pi |\alpha(s)|^2} \sigma_{\text{tot}}(e^+e^- \rightarrow \gamma^* \rightarrow \text{anything})$$

where

$$R(s) = \sigma_{\text{tot}} / \frac{4\pi |\alpha(s)|^2}{3s}. \quad (3.139)$$

The normalization factor is the point cross section (tree level) $\sigma_{\mu\mu}(e^+e^- \rightarrow \gamma^* \rightarrow \mu^+\mu^-)$ in the limit $s \gg 4m_\mu^2$. Taking into account the mass effects the $R(s)$ which corresponds to the production of a lepton pair reads

$$R_\ell(s) = \sqrt{1 - \frac{4m_\ell^2}{s}} \left(1 + \frac{2m_\ell^2}{s} \right), \quad (\ell = e, \mu, \tau) \quad (3.140)$$

which may be read of from the imaginary part given in (2.179). This result provides an alternative way to calculate the renormalized vacuum polarization function (2.176), namely, via the DR (3.136) which now takes the form

$$\Pi'_{\gamma \text{ ren}}{}^\ell(q^2) = \frac{\alpha q^2}{3\pi} \int_{4m_\ell^2}^\infty ds \frac{R_\ell(s)}{s(s - q^2 - i\varepsilon)} \quad (3.141)$$

yielding the vacuum polarization due to a lepton–loop.

In contrast to the leptonic part, the hadronic contribution cannot be calculated analytically as a perturbative series, but it can be expressed in terms of the cross section of the reaction $e^+e^- \rightarrow \text{hadrons}$, which is known from experiments. Via

$$R_{\text{had}}(s) = \sigma(e^+e^- \rightarrow \text{hadrons}) / \frac{4\pi |\alpha(s)|^2}{3s}. \quad (3.142)$$

we obtain the relevant hadronic vacuum polarization

$$\Pi'_{\gamma \text{ ren}}{}^{\text{had}}(q^2) = \frac{\alpha q^2}{3\pi} \int_{4m_\pi^2}^{\infty} ds \frac{R_{\text{had}}(s)}{s(s - q^2 - i\varepsilon)}. \quad (3.143)$$

Thus, including the five quarks u, d, s, c and b subject to non-perturbative QCD effects, we may evaluate

$$\Delta^{(5)}\alpha_{\text{had}}(q^2) = -\Pi'_{\gamma \text{ ren}}{}^{\text{had}}(q^2) = -\frac{\alpha q^2}{3\pi} \int_{4m_\pi^2}^{\infty} ds \frac{R_{\text{had}}(s)}{s(s - q^2 - i\varepsilon)}, \quad (3.144)$$

by utilizing experimental e^+e^- -data up to energies where $\gamma - Z$ mixing comes into play, at about 20 GeV, and for the high energy tail we may use perturbative QCD by the virtue of asymptotic freedom. Note that real and imaginary parts are obtained by the identity

$$\frac{1}{s - q^2 - i\varepsilon} = \frac{\mathcal{P}}{s - q^2} + i\pi \delta(s - q^2)$$

where \mathcal{P} denotes the finite part prescription

$$\mathcal{P} \int_{4m_\pi^2}^{\infty} ds \frac{R_{\text{had}}(s)}{s(s - q^2 - i\varepsilon)} = \lim_{\varepsilon \rightarrow 0} \left\{ \int_{4m_\pi^2}^{q^2 - \varepsilon} ds \frac{R_{\text{had}}(s)}{s(s - q^2)} + \int_{q^2 + \varepsilon}^{\infty} ds \frac{R_{\text{had}}(s)}{s(s - q^2)} \right\}$$

and the imaginary part is indeed given by $\text{Im} \Pi'_{\gamma \text{ ren}}{}^{\text{had}}(q^2) = \frac{\alpha}{3} R_{\text{had}}(q^2)$, with the low energy α as a factor, as claimed before. Corresponding relations hold for the leptonic and as well as other contributions.

At low energies, where the final state necessarily consists of two pions, the cross section is given by the square of the electromagnetic form factor of the pion (undressed from VP effects),

$$R_{\text{had}}(s) = \frac{1}{4} \left(1 - \frac{4m_\pi^2}{s} \right)^{\frac{3}{2}} |F_\pi^{(0)}(s)|^2, \quad s < 9m_\pi^2, \quad (3.145)$$

which directly follows from the corresponding imaginary part (2.259) of the photon vacuum polarization. There are three differences between the pionic loop integral and those belonging to the lepton loops:

- the masses are different
- the spins are different
- the pion is composite – the Standard Model leptons are elementary

The compositeness manifests itself in the occurrence of the form factor $F_\pi(s)$, which generates an enhancement: at the ρ peak, $|F_\pi(s)|^2$ reaches values about 45, while the quark parton model would give about 7. The remaining difference in the expressions for the quantities $R_\ell(s)$ and $R_h(s)$ in (3.140) and (3.145), respectively, originates

in the fact that the leptons carry spin $\frac{1}{2}$, while the spin of the pion vanishes. Near threshold, the angular momentum barrier suppresses the function $R_h(s)$ by three powers of momentum, while $R_\ell(s)$ is proportional to the first power. The suppression largely compensates the enhancement by the form factor – by far the most important property is the mass.

3.8 Dispersive Calculation of Feynman Diagrams

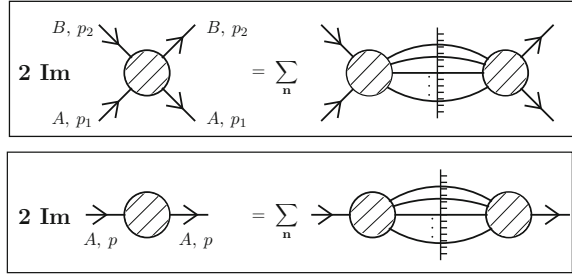
Dispersion relations (DR) may be used to calculate Feynman integrals in a way different from the Feynman parametric approach described in Sect. 2.5. The reason is simply because the imaginary part of an amplitude in general is much easier to calculate than the amplitude itself, which then follows from the imaginary part by a one-fold integral. The imaginary part in principle may be obtained by the unitarity relation of the form (3.105) which translate into *Cutkosky rules* [182], which may be obtained using Veltman's [183] largest time equation in coordinate space. The latter make use of the splitting of the Feynman propagator into real and imaginary part (2.141) and contributes to the imaginary part of a Feynman integral if the substitution

$$\frac{1}{p^2 - m^2 + i\epsilon} \rightarrow -\pi i \delta(p^2 - m^2)$$

replacing a virtual particle (un-cut line) by a physical state (cut line) is made for an odd number of propagators, and provided the corresponding state is physical, i.e., is admissible by energy-momentum conservation and all other physical conservation laws (charge, lepton number etc.). With a diagram we may associate a specific physical channel by specifying which external lines are in-coming and which are out-going. For a given channel then the imaginary part of the diagram is given by cutting internal lines of the diagram between the in-coming and the out-going lines in all possible ways into two disconnected parts. A cut contributes if the cut lines can be viewed as external lines of a real physical subprocess. On the right hand side of the cut the amplitude has to be taken complex conjugate, since the out-going state produced by the cut on the left hand side becomes the in-coming state on the right hand side. Due to the many extra δ -functions (on-shell conditions) part of the integrations become phase space integrations, which in general are easier to do. As a rule, the complexity is reduced from n -loop to a $n - 1$ -loop problem, on the expense that the last integration, a dispersion integral, still has to be done. A very instructive non-trivial example has been presented by Terentev [27] for the complete two-loop calculation of $g - 2$ in QED.

Cut diagrams in conjunction with DRs play a fundamental role also beyond being just a technical trick for calculating Feynman integrals. They not only play a key role for the evaluation of non-perturbative hadronic effects but allows one to calculate numerically or sometimes analytically all kinds of VP effects in higher order diagrams as we will see. Before we discuss this in more detail, let us summarize the key ingredients of the method, which we have considered before, once more:

Fig. 3.14 Optical theorem for scattering and propagation



□ *Optical theorem implied by unitarity:* maybe most familiar is its application to scattering processes: the imaginary part of the forward scattering amplitude of an elastic process $A + B \rightarrow A + B$ is proportional to the sum over all possible final states $A + B \rightarrow$ “anything” (see Fig. 3.14)

$$\text{Im } T_{\text{forward}} (A + B \rightarrow A + B) = \sqrt{\lambda (s, m_1^2, m_2^2)} \sigma_{\text{tot}} (A + B \rightarrow \text{anything})$$

for the photon propagator it implies

$$\text{Im} \Pi'_\gamma(s) = \frac{\alpha s}{4\pi |\alpha(s)|^2} \sigma_{\text{tot}}(e^+e^- \rightarrow \text{anything})$$

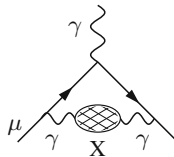
which we have been proving in the last section already.

□ *Analyticity, implied by causality,* may be expressed in form of a so-called (subtracted) dispersion relation

$$\Pi'_\gamma(k^2) - \Pi'_\gamma(0) = \frac{k^2}{\pi} \int_0^\infty ds \frac{\text{Im} \Pi'_\gamma(s)}{s (s - k^2 - i\epsilon)} . \tag{3.146}$$

The latter, together with the optical theorem, directly implies the validity of (3.143). Note that its validity is based on general principles and holds beyond perturbation theory. It is the basis of all non-perturbative evaluations of hadronic vacuum polarization effects in terms of experimental data. But more than that.

Within the context of calculating $g - 2$ in the SM the maybe most important application of DRs concerns the vacuum polarization contribution related to diagrams of the type



where the “blob” is the full photon propagator, including all kinds of contributions as predicted by the SM and maybe additional yet unknown contributions from physics beyond the SM. The vacuum polarization amplitude satisfies a dispersion relation (3.136) and the spectral function is given by (3.139).

The contribution to the anomalous magnetic moment from graphs of the photon vacuum polarization type shown above can be obtained in a straightforward way as follows: The physics wise relevant $g^{\mu\nu}$ -term of the full photon propagator, carrying loop momentum k , reads

$$\frac{-ig^{\mu\nu}}{k^2 (1 + \Pi'_\gamma(k^2))} \simeq \frac{-ig^{\mu\nu}}{k^2} \left(1 - \Pi'_\gamma(k^2) + (\Pi'_\gamma(k^2))^2 - \dots \right) \quad (3.147)$$

and the renormalized photon self-energy may be written as

$$-\frac{\Pi'_{\gamma \text{ ren}}(k^2)}{k^2} = \int_0^\infty \frac{ds}{s} \frac{1}{\pi} \text{Im} \Pi'_\gamma(s) \frac{1}{k^2 - s} . \quad (3.148)$$

Note that the only k dependence under the convolution integral shows up in the last factor. Thus, the free photon propagator in the one-loop vertex graph discussed in Sect. 2.6.3 in the next higher order is replaced by

$$-ig_{\mu\nu}/k^2 \rightarrow -ig_{\mu\nu}/(k^2 - s)$$

which is the exchange of a photon of mass square s . The result afterward has to be convoluted with the imaginary part of the photon vacuum polarization. In a first step we have to calculate the contribution from the massive photon which may be calculated exactly as in the massless case. As discussed above $F_M(0)$ most simply may be calculated using the projection method directly at $q^2 = 0$. The result is [184, 185]³¹

$$K_\mu^{(2)}(s) \equiv a_\mu^{(2) \text{ heavy } \gamma} = \frac{\alpha}{\pi} \int_0^1 dx \frac{x^2 (1-x)}{x^2 + (s/m_\mu^2)(1-x)} , \quad (3.149)$$

which is the second order contribution to a_μ from an exchange of a photon with square mass s . Note that for $s = 0$ we get the known Schwinger result.

³¹Replacing the heavy vector exchange by a heavy scalar exchange leads to the substitution

$$x^2 (1-x) \text{ (vector)} \rightarrow x^2 (1-x/2) \text{ (scalar)}$$

in the numerator of (3.149).

Utilizing this result and (3.148), the contribution from the “blob” to $g - 2$ reads

$$a_\mu^{(X)} = \frac{1}{\pi} \int_0^\infty \frac{ds}{s} \operatorname{Im} \Pi_\gamma'^{(X)}(s) K_\mu^{(2)}(s). \quad (3.150)$$

If we exchange integrations and evaluating the DR we arrive at

$$\begin{aligned} a_\mu^{(X)} &= \frac{\alpha}{\pi} \int_0^1 dx (1-x) \int_0^\infty \frac{ds}{s} \frac{1}{\pi} \operatorname{Im} \Pi_\gamma'^{(X)}(s) \frac{x^2}{x^2 + (s/m_\mu^2)(1-x)} \\ &= \frac{\alpha}{\pi} \int_0^1 dx (1-x) \left[-\Pi_\gamma'^{(X)}(s_x) \right] \end{aligned} \quad (3.151)$$

where

$$s_x = -\frac{x^2}{1-x} m_\mu^2.$$

The last simple representation in terms of $\Pi_\gamma'^{(X)}(s_x)$ follows using

$$\frac{x^2}{x^2 + (s/m_\mu^2)(1-x)} = -s_x \frac{1}{s - s_x}.$$

In this context a convenient one-fold integral representation of the VP function is (2.177)

$$\Pi_{\gamma \text{ ren}}'^{\ell} \left(\frac{-x^2}{1-x} m_\mu^2 \right) = -\frac{\alpha}{\pi} \int_0^1 dz 2z (1-z) \ln \left(1 + \frac{x^2}{1-x} \frac{m_\mu^2}{m_\ell^2} z (1-z) \right), \quad (3.152)$$

which together with (3.151) leads to a two-fold integral representation of the VP contribution by lepton loops at two-loop order.

This kind of dispersion integral representation can be generalized to higher order and sequential VP insertions corresponding to the powers of $\Pi'(k^2)$ in (3.147).

Denoting $\rho(s) = \operatorname{Im} \Pi_{\gamma \text{ ren}}'(s)/\pi$ we may write (3.148) in the form $-\Pi_{\gamma \text{ ren}}'(k^2) = \int_0^\infty \frac{ds}{s} \rho(s) \frac{k^2}{k^2 - s}$ such that the n -th term of the propagator expansion (3.147) is given by

$$\begin{aligned} \left(-\Pi_{\gamma \text{ ren}}'(k^2) \right)^n / k^2 &= \frac{1}{k^2} \prod_{i=1}^n \int_0^\infty \frac{ds_i}{s_i} \rho(s_i) \frac{k^2}{k^2 - s_i} \\ &= \sum_{j=1}^n \int_0^\infty \frac{ds_j}{s_j} \rho(s_j) \frac{1}{k^2 - s_j} \prod_{i \neq j} \int_0^\infty \frac{ds_i}{s_i} \rho(s_i) \frac{s_j}{s_j - s_i}, \end{aligned}$$

where we have been applying the partial fraction decomposition

$$\frac{1}{k^2} \prod_{i=1}^n \frac{k^2}{k^2 - s_i} = \sum_{k=1}^n \frac{1}{k^2 - s_j} \prod_{i \neq j} \frac{s_j}{s_j - s_i} .$$

We observe that the integration over the loop momentum k of the one-loop muon vertex proceeds exactly as before, with the photon replaced by a single heavy photon of mass s_j . Thus, the contribution to a_μ reads

$$\begin{aligned} a_\mu^{(X)} &= \frac{\alpha}{\pi} \int_0^1 dx (1-x) \sum_{j=1}^n \int_0^\infty \frac{ds_j}{s_j} \rho(s_j) \frac{-s_x}{s_j - s_x} \prod_{i \neq j} \int_0^\infty \frac{ds_i}{s_i} \rho(s_i) \frac{s_j}{s_j - s_i} \\ &= \frac{\alpha}{\pi} \int_0^1 dx (1-x) \left(\prod_{k=1}^n \int_0^1 \frac{ds_k}{s_k} \rho(s_k) \right) s_x \left(\sum_{j=1}^n \frac{1}{s_x - s_j} \prod_{i \neq j} \frac{s_j}{s_j - s_i} \right) . \end{aligned}$$

Under the integral, to the last factor, we may apply the above partial fraction decomposition backward

$$\sum_{j=1}^n \frac{1}{s_x - s_j} \prod_{i \neq j} \frac{s_j}{s_j - s_i} = \frac{1}{s_x} \prod_{i=1}^n \frac{s_x}{s_x - s_i}$$

which proves that the s_i -integrals factorize and we find [186]

$$\begin{aligned} a_\mu^{(X)} &= \frac{\alpha}{\pi} \int_0^1 dx (1-x) \left(\int_0^\infty \frac{ds}{s} \rho(s) \frac{-s_x}{s - s_x} \right)^n \\ &= \frac{\alpha}{\pi} \int_0^1 dx (1-x) \left(-\Pi'_{\gamma \text{ ren}}(s_x) \right)^n \end{aligned} \quad (3.153)$$

We are thus able to write formally the result for the one-loop muon vertex when we replace the free photon propagator by the full transverse propagator as [187]

$$\begin{aligned} a_\mu^{(X)} &= \frac{\alpha}{\pi} \int_0^1 dx (1-x) \left(\frac{1}{1 + \Pi'_{\gamma \text{ ren}}(s_x)} \right) \\ &= \frac{1}{\pi} \int_0^1 dx (1-x) \alpha(s_x) , \end{aligned} \quad (3.154)$$

which according to (3.120) is equivalent to the contribution of a free photon interacting with dressed charge (effective fine structure constant). However, since $\Pi'_{\gamma \text{ ren}}(k^2)$ is negative and grows logarithmically with k^2 the full photon propagator develops a so called *Landau pole* where the effective fine structure constant becomes infinite. Thus resumming the perturbation expansion under integrals may produce a problem and one better resorts to the order by order approach, by expanding the full propagator into its geometrical progression. Nevertheless (3.154) is a very useful bookkeeping device, collecting effects from different contributions and different orders. In particular if we expand the 1PI photon self-energy into order by order contributions

$$\Pi'_{\gamma \text{ ren}}(k^2) = \Pi'_{\gamma \text{ ren}}(2)(k^2) + \Pi'_{\gamma \text{ ren}}(4)(k^2) + \dots$$

and also write $\rho = \rho^{(2)} + \rho^{(4)} + \dots$ for the spectral densities.

Coming back to the single VP insertion formula (3.151) we may use (3.152) as well as the second form given in (2.177) which reads

$$\Pi'_{\gamma \text{ ren}}(q^2/m^2) = -\frac{\alpha}{\pi} \frac{q^2}{m^2} \int_0^1 dt \frac{\rho_2(t)}{\frac{q^2}{m^2} - 4/(1-t^2)}, \tag{3.155}$$

with³²

$$\rho_2(t) = \frac{t^2(1-t^2/3)}{1-t^2}, \tag{3.156}$$

and we may write

$$a_\mu^{(X)} = \left(\frac{\alpha}{\pi}\right)^2 \int_0^1 dx (1-x) \int_0^1 dt \frac{\rho_2(t)}{W_t(x)}, \tag{3.157}$$

where

$$1/W_t(x) = \frac{q^2}{m^2} \frac{1}{\frac{q^2}{m^2} - \frac{4}{1-t^2}} \Bigg|_{\frac{q^2}{m^2} = -\frac{x^2}{1-x} \frac{m_\mu^2}{m^2}}$$

and hence

$$W_t(x) = 1 + \frac{4m^2}{(1-t^2)m_\mu^2} \frac{1-x}{x^2}. \tag{3.158}$$

³²We adopt the notation of Kinoshita [186] and mention that the densities $\rho(t)$ used here are not to be confused with the $\rho(s)$ used just before, although they are corresponding to each other.

If n equal loops are inserted we have

$$a_\mu^{(X)} = \frac{\alpha}{\pi} \int_0^1 dx (1-x) \left(\frac{\alpha}{\pi} \int_0^1 dt \frac{\rho(t)}{W_t(x)} \right)^n \quad (3.159)$$

according to the factorization theorem demonstrated before. This formula is suitable for calculating the contribution to the lepton anomalous magnetic moment once the spectral function $\rho(t)$ is known. For the one-loop 1PI self-energy we have $\rho_2(t)$ given by (3.156) and the corresponding density for the two-loop case reads [175, 176, 188]

$$\begin{aligned} \rho_4(t) = & \frac{2t}{3(1-t^2)} \left\{ \frac{(3-t^2)(1+t^2)}{2} \left(\text{Li}_2(1) + \ln \frac{1+t}{2} \ln \frac{1+t}{1-t} \right) \right. \\ & + 2 \left(\text{Li}_2 \left(\frac{1-t}{1+t} \right) + \text{Li}_2 \left(\frac{1+t}{2} \right) - \text{Li}_2 \left(\frac{1-t}{2} \right) \right) - 4 \text{Li}_2(t) + \text{Li}_2(t^2) \\ & + \left(\frac{11}{16}(3-t^2)(1+t^2) + \frac{1}{4}t^4 - \frac{3}{2}t(3-t^2) \right) \ln \frac{1+t}{1-t} \\ & \left. + t(3-t^2) \left(3 \ln \frac{1+t}{2} - 2 \ln t \right) + \frac{3}{8}t(5-3t^2) \right\}. \end{aligned} \quad (3.160)$$

The corresponding result for the three-loop photon self-energy has been calculated in [189]. For four-loops an approximate result is available [190]. Generally, the contribution to a_μ which follow from the lowest order lepton (ℓ) vertex diagram by modifying the photon propagator with l electron loops of order $2i$, m muon loops of order $2j$ and n tau loops of order $2k$ is given by

$$\begin{aligned} a_\ell = & \left(\frac{\alpha}{\pi} \right)^{(1+il+jm+kn)} \int_0^1 dx (1-x) \left(\int_0^1 dt_1 \frac{\rho_{2i}(t_1)}{1 + \frac{4}{1-t_1^2} \frac{1-x}{x^2} \left(\frac{m_e}{m_\ell} \right)^2} \right)^l \\ & \cdot \left(\int_0^1 dt_2 \frac{\rho_{2j}(t_2)}{1 + \frac{4}{1-t_2^2} \frac{1-x}{x^2} \left(\frac{m_\mu}{m_\ell} \right)^2} \right)^m \cdot \left(\int_0^1 dt_3 \frac{\rho_{2k}(t_3)}{1 + \frac{4}{1-t_3^2} \frac{1-x}{x^2} \left(\frac{m_\tau}{m_\ell} \right)^2} \right)^n. \end{aligned} \quad (3.161)$$

The same kind of approach works for the calculation of diagrams with VP insertions not only for the lowest order vertex. For any group of diagrams we may calculate in place of the true QED contribution the one obtained in massive QED with a photon of mass \sqrt{s} , and then convolute the result with the desired density of the photon VP analogous to (3.150) where (3.149) gets replaced by a different more complicated kernel function (see e.g. [103, 191] and below). It also should be noted that the representation presented here only involve integration over finite intervals ($[0,1]$) and

hence are particularly suited for numerical integration of higher order contributions when analytic results are not available.

The formalism developed here also is the key tool to evaluate the *hadronic contributions*, for which perturbation theory fails because of the strong interactions. In this case we represent $\text{Im } \Pi'_\gamma{}^{\text{had}}(s)$ via (3.139) in terms of

$$\sigma_{\text{had}}(s) = \sigma(e^+e^- \rightarrow \text{hadrons})$$

where

$$\sigma_{\text{had}}(s) = \frac{4\pi^2 |\alpha(s)|^2}{\alpha s} \frac{1}{\pi} \text{Im } \Pi'_\gamma{}^{\text{had}}(s) \quad (3.162)$$

or in terms of the cross section ratio $R(s)$ defined by (3.139) where both $\sigma_{\text{had}}(s)$ or equivalently $R_{\text{had}}(s)$ will be taken from experiment, since they are not yet calculable reliably from first principles at present.

Starting point is the basic integral representation (from (3.150) using (3.139))

$$a_\mu^{\text{had}} = \frac{\alpha}{\pi} \int_0^\infty \frac{ds}{s} \int_0^1 dx \frac{x^2(1-x)}{x^2 + (1-x)s/m_\mu^2} \frac{\alpha}{3\pi} R(s) . \quad (3.163)$$

If we first integrate over x we find the well known standard representation

$$a_\mu^{\text{had}} = \frac{\alpha}{3\pi} \int_0^\infty \frac{ds}{s} K_\mu^{(2)}(s) R(s) \quad (3.164)$$

as an integral along the cut of the vacuum polarization amplitude in the time-like region, while an interchange of the order of integrations yields the analog of (3.151): an integral over the hadronic shift of the fine structure constant (3.121) in the space-like domain [192]:

$$a_\mu^{\text{had}} = \frac{\alpha}{\pi} \int_0^1 dx (1-x) \Delta\alpha_{\text{had}}^{(5)}(-Q^2(x)) \quad (3.165)$$

where $Q^2(x) \equiv \frac{x^2}{1-x} m_\mu^2$ is the space-like square momentum-transfer or

$$x = \frac{Q^2}{2m_\mu^2} \left(\sqrt{1 + \frac{4m_\mu^2}{Q^2}} - 1 \right) .$$

In Fig. 3.15 we display the integrand of the representation (3.165) Alternatively, by writing $(1-x) = -\frac{1}{2} \frac{d}{dx} (1-x)^2$ and performing a partial integration in (3.165) one

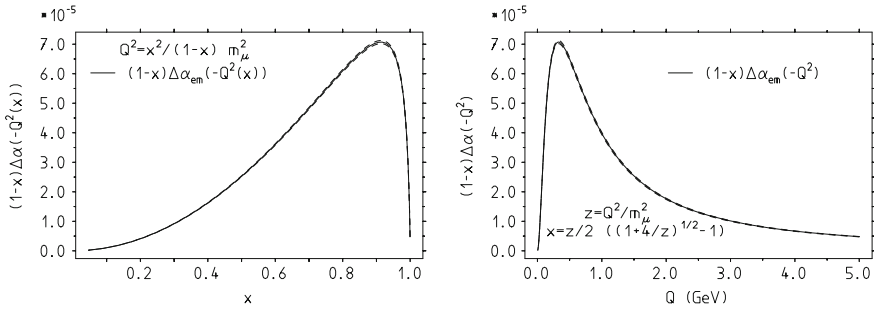


Fig. 3.15 The integrand of the vacuum polarization representation (3.165) as a function of x and as a function of the energy scale Q . As we see the integrand is strongly peaked as a function of Q at about 330 MeV. $\Pi(Q^2)$ data come from [197]. The dashed lines mark the error band from the experimental data

finds

$$a_\mu^{\text{had}} = \frac{\alpha^2}{6\pi^2} m_\mu^2 \int_0^1 dx x (2-x) (D(Q^2(x))/Q^2(x)) \tag{3.166}$$

where $D(Q^2)$ is the Adler–function [193] defined as a derivative of the shift of the fine structure constant

$$D(-s) = -(12\pi^2) s \frac{d\Pi'_\gamma(s)}{ds} = \frac{3\pi}{\alpha} s \frac{d}{ds} \Delta\alpha_{\text{had}}(s) . \tag{3.167}$$

The Adler–function is represented by

$$D(Q^2) = Q^2 \left(\int_{4m_\pi^2}^\infty \frac{R(s)}{(s+Q^2)^2} ds \right) \tag{3.168}$$

in terms of $R(s)$, i.e., in the case of hadrons it can be evaluated in terms of experimental e^+e^- -data. The Adler–function is discussed in [194] and in Fig. 5.18 a comparison between theory and experiment is shown. The Adler–function is an excellent monitor for checking where pQCD works in the Euclidean region (see also [71]), and, in principle, it allows one to calculate a_μ^{had} relying more on pQCD and less on e^+e^- -data, in a well controllable manner. The advantage of this method at present is limited by the inaccuracies of the quark masses, in particular of the charm mass [195, 196]. The integrand of the representation (3.166) is displayed in Fig. 3.16.

It is interesting to note that the representation (3.165) as well as (3.166) requires the hadronic vacuum polarization function in the spacelike region, which is the appropriate representation for ab initio calculations in the non-perturbative lattice

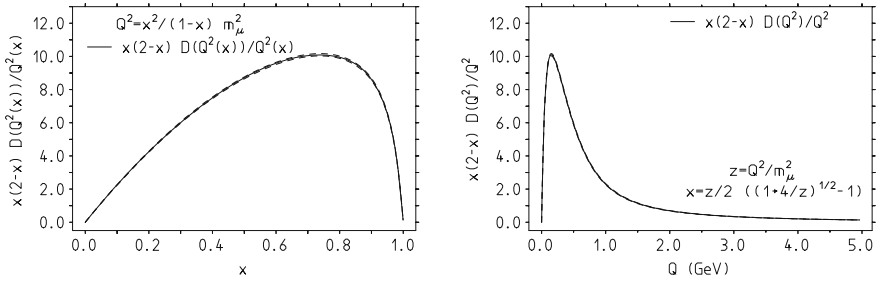


Fig. 3.16 The integrand of the Adler function representation (3.166) as a function of x and as a function of the energy scale Q . The right-hand panel shows that the integrand is sharply peaked as a function of Q at a rather low scale (~ 150 MeV). Adler function data come from [198]. The dashed lines mark the error band from the experimental data

QCD approach.³³ The lattice QCD approach and results will be discussed in Sect. 5.3 of Chap. 5.

The Adler-function $D(Q^2)$ is bounded asymptotically by perturbative QCD: $D(Q^2) \rightarrow N_c \sum_f Q_f^2$, with Q_f the quark charges and $N_c = 3$ the color factor, up to perturbative corrections, which asymptotically vanish because of asymptotic freedom which implies $\alpha_s(Q^2) \rightarrow 0$ as $Q^2 \rightarrow \infty$ (see [194]). Obviously, then $D(Q^2)/Q^2$ is a positive monotonically decreasing function³⁴ bounded by

$$\frac{D(Q^2)}{Q^2} = \int_{4m_\pi^2}^{\infty} \frac{R(s)}{(s + Q^2)^2} ds < \bar{P}_1 \equiv \int_{4m_\pi^2}^{\infty} \frac{R(s)}{s^2} ds = \left. \frac{D(Q^2)}{Q^2} \right|_{Q^2=0}, \quad (3.169)$$

the slope of the vacuum polarization function at zero momentum square. Obviously the slope $D(Q^2)/Q^2$ is finite for $Q^2 \rightarrow 0$, which shows that the integrand of the representation (3.166) is well behaved as $x \rightarrow 0$.

³³A new approach to evaluate the leading hadronic corrections to the muon $g-2$ attempts to evaluate $\Delta\alpha_{\text{had}}(t)$ directly in the spacelike region from Bhabha scattering data [199] or from the simpler process of $\mu^-e^- \rightarrow \mu^-e^-$ scattering (a high energy muon beam on a low Z nuclear target) [200]. Direct experimental $\Delta\alpha_{\text{had}}(t)$ data would also provide a direct comparison with corresponding LQCD results.

³⁴Note that while

$$\left(D(Q^2)/Q^2 \right)' = -2 \left(\int_{4m_\pi^2}^{\infty} \frac{R(s)}{(s + Q^2)^3} ds \right) < 0,$$

the Adler function itself is not monotonic as

$$\left(D(Q^2)_{\text{cut}} \right)' = \left(\int_{4m_\pi^2}^{s_{\text{cut}}} \frac{(s - Q^2) R(s)}{(s + Q^2)^3} ds \right),$$

which always has a zero if s_{cut} is finite, and for $s_{\text{cut}} = \infty$ it has zero because $R(s)$ is increasing with s . The “experimental” Adler function has a maximum in the 30 GeV region.

Note that alternatively, using (3.167) we may write

$$\bar{P}_1 = -\frac{3\pi}{\alpha} \frac{d}{ds} \Delta\alpha_{\text{had}}(s)|_{s=-Q^2, Q^2 \rightarrow 0} . \quad (3.170)$$

Therefore, (3.168) together with (3.166) yields a bound (see also [113])

$$a_\mu^{\text{had}} < \frac{\alpha^2}{6\pi^2} m_\mu^2 \frac{2}{3} \bar{P}_1 . \quad (3.171)$$

The integral over a compilation of $R(s)$ -data, discussed in detail later in Chap. 5, yields $\bar{P}_1 = 11.83(8) \text{ GeV}^{-2}$ and hence

$$a_\mu^{\text{had}} < 791(5) \times 10^{-10} . \quad (3.172)$$

As we will see an evaluation of (3.164) yields a value substantially lower: $a_\mu^{\text{had}} \simeq 688.1 \pm 4.1 \times 10^{-10}$.

Actually, we may write (3.164) in the form

$$a_\mu^{\text{had}} = \left(\frac{\alpha m_\mu}{3\pi} \right)^2 \int_0^\infty \frac{ds}{s^2} \hat{K}(s) R(s) \quad (3.173)$$

where

$$\hat{K}(s) = \frac{3s}{m_\mu^2} K_\mu^{(2)}(s) , \quad (3.174)$$

in which $\hat{K}(s)$ is a bounded monotonically increasing function, with $\hat{K}(4m_\pi^2) \simeq 0.63$ increasing to 1 at $s \rightarrow \infty$. Setting $\hat{K}(s) = 1$ we obtain the bound presented above. A lower bound then is obtained by setting $\hat{K}(s) = \hat{K}(4m_\pi^2) \approx 0.63$, which implies $a_\mu^{\text{had}} > 498(3) \times 10^{-10}$ again a very rough bound only, but a true bound.

The bound (3.171) can be improved by a moment expansion of the kernel as advocated in Ref. [201] and analyzed in detail in [202].

The best checks is to compare lattice results in terms of the Adler function as it enters in the representation (3.166) as advocated in [195] and actually performed in [203, 204] recently. An up-to-date evaluation of the “experimental” Adler function is available via the link [198].

3.9 ζ -Values, Polylogarithms and Related Special Functions

For later reference we list some transcendental constants and definitions of special functions which are encountered in higher order Feynman graph calculations. Typi-

cally analytic results for the mass independent universal lepton $g - 2$ contributions are of the form of sums of terms exhibiting rational numbers as coefficients of transcendental objects. The most frequent such object are the Riemann *zeta function*

$$\zeta(n) = \sum_{k=1}^{\infty} \frac{1}{k^n} \tag{3.175}$$

and the *polylogarithmic integrals*

$$\text{Li}_n(x) = \frac{(-1)^{n-1}}{(n-2)!} \int_0^1 \frac{\ln^{n-2}(t) \ln(1-xt)}{t} dt = \sum_{k=1}^{\infty} \frac{x^k}{k^n}, \tag{3.176}$$

where the dilogarithm $\text{Li}_2(x)$ is often referred to as the Spence function which we encountered in Sect. 2.6.3 (2.208). The series representation holds for $|x| \leq 1$. The dilogarithm is an analytic function with the same cut as the logarithm. Useful relations are

$$\begin{aligned} \text{Sp}(x) &= -\text{Sp}(1-x) + \frac{\pi^2}{6} - \ln x \ln(1-x), \\ \text{Sp}(x) &= -\text{Sp}\left(\frac{1}{x}\right) - \frac{\pi^2}{6} - \frac{1}{2} \ln^2(-x), \\ \text{Sp}(x) &= -\text{Sp}(-x) + \frac{1}{2} \text{Sp}(x^2). \end{aligned} \tag{3.177}$$

Special values are:

$$\text{Sp}(0) = 0, \quad \text{Sp}(1) = \frac{\pi^2}{6}, \quad \text{Sp}(-1) = -\frac{\pi^2}{12}, \quad \text{Sp}\left(\frac{1}{2}\right) = \frac{\pi^2}{12} - \frac{1}{2}(\ln 2)^2. \tag{3.178}$$

Special $\zeta(n)$ values we will need are

$$\zeta(2) = \frac{\pi^2}{6}, \quad \zeta(3) = 1.202\ 056\ 903\dots, \quad \zeta(4) = \frac{\pi^4}{90}, \quad \zeta(5) = 1.036\ 927\ 755\dots \tag{3.179}$$

Also the constants

$$\begin{aligned} \text{Li}_n(1) &= \zeta(n), \quad \text{Li}_n(-1) = -[1 - 2^{1-n}] \zeta(n), \\ a_4 &\equiv \text{Li}_4\left(\frac{1}{2}\right) = \sum_{n=1}^{\infty} \frac{1}{(2^n n^4)} = 0.517\ 479\ 061\ 674\dots, \end{aligned} \tag{3.180}$$

related to polylogarithms, will be needed for the evaluation of analytical results. A generalization are the *Nielsen integrals*

$$S_{n,p}(x) = \frac{(-1)^{n+p-1}}{(n-1)!p!} \int_0^1 \frac{\ln^{n-1}(t) \ln^p(1-xt)}{t} dt, \quad (3.181)$$

which have representations as sums of the type

$$S_{1,2}(x) = \sum_2^\infty \frac{x^k}{k^2} S_1(k-1); \quad S_{2,2}(x) = \sum_2^\infty \frac{x^k}{k^3} S_1(k-1),$$

where

$$S_1(k) = \sum_1^k \frac{1}{l}$$

is a *harmonic sum*. And higher sums are obtained by the recurrences

$$\frac{d}{dx} S_{n,p}(x) = \frac{1}{x} S_{n-1,p}(x); \quad \int_0^x \frac{S_{n,p}(t)}{t} dt = S_{n+1,p}(x).$$

The general *harmonic series* are defined by [205]

$$S_m(n) = \sum_{i=1}^n \frac{1}{i^m}; \quad S_{-m}(n) = \sum_{i=1}^n \frac{(-1)^i}{i^m}, \quad (3.182)$$

in which $m > 0$. Higher harmonic series are defined by the recurrences

$$S_{m,j_1,\dots,j_p}(n) = \sum_{i=1}^n \frac{1}{i^m} S_{j_1,\dots,j_p}(i); \quad S_{-m,j_1,\dots,j_p}(n) = \sum_{i=1}^n \frac{(-1)^i}{i^m} S_{j_1,\dots,j_p}(i), \quad (3.183)$$

where again $m > 0$. The m and the j_i are referred to as the indices of the harmonic series. Hence, for example

$$S_{1,-5,3}(n) = \sum_{i=1}^n \frac{1}{i} \sum_{j=1}^i \frac{(-1)^j}{j^5} \sum_{k=1}^j \frac{1}{k^3}. \quad (3.184)$$

Basic transcendental constants of increasing transcendental weight are (examples we will find in Chap. 4)

$$\left\{ [S_1(\infty), \ln(2)]; \zeta_2; \zeta_3; \text{Li}_4(1/2); (\zeta_5, \text{Li}_5(1/2)); [\text{Li}_6(1/2), S_{-5,-1}(\infty)]; \right. \\ \left. [\zeta_7, \text{Li}_7(1/2), S_{-5,1,1}(\infty), S_{5,-1,-1}(\infty)]; \dots \right\} \quad (3.185)$$

where $S_{...} = S_{...}(\infty)$. The numerical values have been calculated in [205]:

$$\begin{aligned}
 \text{Li}_4(1/2) &= 0.51747906167389938633 \\
 \text{Li}_5(1/2) &= 0.50840057924226870746 \\
 \text{Li}_6(1/2) &= 0.50409539780398855069 \\
 \text{Li}_7(1/2) &= 0.50201456332470849457 \\
 S_{-5,-1}(\infty) &= 0.98744142640329971377 \\
 -S_{-5,1,1}(\infty) &= 0.95296007575629860341 \\
 S_{5,-1,-1}(\infty) &= 1.02912126296432453422 .
 \end{aligned} \tag{3.186}$$

The harmonic polylogarithms (HPL) $H(a_1, \dots, a_k; x)$ are functions of one variable x labeled by a vector $a = (a_1, \dots, a_k)$. The dimension k of the vector a is called the weight of the HPL [206]. Given the functions

$$f_1(x) = \frac{1}{1-x} ; \quad f_0(x) = \frac{1}{x} ; \quad f_{-1}(x) = \frac{1}{1+x} , \tag{3.187}$$

the HPLs are defined recursively through integration of these functions. For *weight one* we have

$$\begin{aligned}
 H(1; x) &= \int_0^x f_1(t) dt = \int_0^x \frac{1}{1-t} dt = -\log(1-x) \\
 H(0; x) &= \log(x) \\
 H(-1; x) &= \int_0^x f_{-1}(t) dt = \int_0^x \frac{1}{1+t} dt = \log(1+x),
 \end{aligned} \tag{3.188}$$

and for higher weights

$$H({}^n 0; x) = \frac{1}{n!} \log^n x ; \quad H(a, a_{1,\dots,k}; x) = \int_0^x f_a(t) H(a_{1,\dots,k}; t) dt , \tag{3.189}$$

where we used the notations ${}^n i = \underbrace{i, \dots, i}_n$ and $a_{1,\dots,k} = a_1, \dots, a_k$.

Examples are,

$$H(0, 0, 1, 1; x) = S_{2,2}(x) ; \quad H(-1, 0, 0, 1; x) = \int_0^x \frac{dz}{1+z} \text{Li}_3(z) .$$

The formula for the derivative of the HPLs follows directly from their definition

$$\frac{d}{dx} H(a, a_{1,\dots,k}; x) = f_a(x) H(a_{1,\dots,k}; x). \quad (3.190)$$

An *elliptic integral* is defined as any function f which can be expressed in the form [207]

$$f(x) = \int_c^x R\left(t, \sqrt{P(t)}\right) dt$$

where R is a rational function of its two arguments, P is a polynomial of degree 3 or 4 with no repeated roots, and c is a constant. In general, integrals in this form cannot be expressed in terms of elementary functions. Exceptions to this general rule are when P has repeated roots, or when $R(x, y)$ contains no odd powers of y . However, with the appropriate reduction formula, every elliptic integral can be brought into a form that involves integrals over rational functions and the three canonical forms, the elliptic integrals of the first, second and third kind. The incomplete *elliptic integral of the first kind* F is defined as

$$F(\varphi; m) = \int_0^\varphi \frac{d\theta}{\sqrt{1 - m \sin^2 \theta}} = \int_0^{x=\sin \varphi} \frac{dt}{\sqrt{(1-t^2)(1-mt^2)}}.$$


The incomplete *elliptic integral of the second kind* E may be defined as

$$E(\varphi; m) = \int_0^\varphi d\theta \sqrt{1 - m \sin^2 \theta} = \int_0^{x=\sin \varphi} \frac{\sqrt{1 - mt^2}}{\sqrt{1 - t^2}} dt.$$

The incomplete *elliptic integral of the third kind* Π is defined by

$$\Pi(n; \varphi | m) = \int_0^\varphi \frac{1}{1 - n \sin^2 \theta} \frac{d\theta}{\sqrt{1 - m \sin^2 \theta}} = \int_0^{x=\sin \varphi} \frac{1}{1 - nt^2} \frac{dt}{\sqrt{(1-t^2)(1-mt^2)}},$$

where $m = \sin^2 \alpha$ is a parameter. For $\varphi = \pi/2$ and $x = 1$ we obtain the complete elliptic integrals.

The simplest diagram leading to an elliptic integral is the scalar massive triple line graph (sunrise diagram) , which plays a role in the self-energy of the ω vector meson which decays predominantly via $\omega \rightarrow \pi^+ \pi^- \pi^0$ (see also [208]). In the context of dimensional regularization and ϵ -expansion various types of generalized and Appell hypergeometric functions show up [209–213]. For further reading see e.g. [214–217] and references therein.

References

1. J.D. Bjorken, S.D. Drell, *Relativistic Quantum Mechanics*, 1st edn. (McGraw-Hill, New York, 1964), 300 p; *Relativistic Quantum Fields*, 1st edn. (McGraw-Hill, New York, 1965), p. 396
2. L.H. Thomas, *Philos. Mag.* **3**, 1 (1927); V. Bargmann, L. Michel, V.A. Telegdi. *Phys. Rev. Lett.* **2**, 435 (1959)
3. P.A.M. Dirac, *Proc. R. Soc. A* **117**, 610 (1928); **A 118**, 351 (1928)
4. P.J. Mohr, D.B. Newell, B.N. Taylor, *Rev. Mod. Phys.* **88**, 035009 (2016)
5. B. Odom, D. Hanneke, B. D'Urso, G. Gabrielse, *Phys. Rev. Lett.* **97**, 030801 (2006)
6. D. Hanneke, S. Fogwell, G. Gabrielse, [arXiv:0801.1134](https://arxiv.org/abs/0801.1134) [physics.atom-ph]
7. P.J. Mohr, B.N. Taylor, D.B. Newell, *Rev. Mod. Phys.* **84**, 1527 (2012)
8. G. Gabrielse, D. Hanneke, T. Kinoshita, M. Nio, B. Odom, *Phys. Rev. Lett.* **97**, 030802 (2006) [Erratum-ibid. **99**, 039902 (2007)]
9. T. Aoyama, M. Hayakawa, T. Kinoshita, M. Nio, *Phys. Rev. Lett.* **99**, 110406 (2007)
10. T. Aoyama, M. Hayakawa, T. Kinoshita, M. Nio, *Phys. Rev. Lett.* **109**, 111807 (2012)
11. S. Laporta, [arXiv:1704.06996](https://arxiv.org/abs/1704.06996) [hep-ph]
12. K.A. Olive et al. [Particle Data Group], *Chin. Phys. C* **38**, 090001 (2014); C. Patrignani et al., *Part. Data Group Chin. Phys. C* **40**, 100001 (2016)
13. S. Eidelman et al. [Particle Data Group], *Phys. Lett. B* **592**, 1 (2004)
14. P.J. Mohr, B.N. Taylor, *Rev. Mod. Phys.* **72**, 351 (2000); **77**, 1 (2005)
15. F. Gianotti (the ATLAS Collab.), CERN Seminar, July 4th, 2012; J. Incandela (the CMS Collab.), CERN Seminar, July 4th, 2012
16. G. Aad et al. [ATLAS Collab.], *Phys. Lett. B* **716**, 1 (2012). *Science* **338**, 1576 (2012)
17. S. Chatrchyan et al. [CMS Collab.], *Phys. Lett. B* **716**, 30 (2012) *Science* **338**, 1569 (2012);
18. F. Jegerlehner, M.Y. Kalmykov, B.A. Kniehl, *Phys. Lett. B* **722**, 123 (2013)
19. B.A. Kniehl, A.F. Pikelner, O.L. Veretin, *Nucl. Phys. B* **896**, 19 (2015)
20. F. Jegerlehner, A. Nyffeler, *Phys. Rep.* **477**, 1 (2009)
21. J.S. Schwinger, *Phys. Rev.* **73**, 416 (1948)
22. D.J. Broadhurst, D. Kreimer, *J. Symb. Comput.* **27**, 581 (1999); *Int. J. Mod. Phys. C* **6**, 519 (1995); *Phys. Lett. B* **393**, 403 (1997); D.J. Broadhurst, J.A. Gracey, D. Kreimer, *Z. Phys. C* **75**, 559 (1997)
23. A. Devoto, D.W. Duke, *Riv. Nuovo Cimento* **7N6**, 1 (1984)
24. R. Karplus, N.M. Kroll, *Phys. Rep. C* **77**, 536 (1950)
25. A. Petermann, *Helv. Phys. Acta* **30**, 407 (1957); *Nucl. Phys.* **5**, 677 (1958)
26. C.M. Sommerfield, *Phys. Rev.* **107**, 328 (1957); *Ann. Phys. (N.Y.)* **5**, 26 (1958)
27. M.V. Terentev, *Sov. Phys. JETP* **16**, 444 (1963); [*Zh. Eksp. Teor. Fiz.* **43**, 619 (1962)]
28. S. Laporta, E. Remiddi, *Phys. Lett. B* **379**, 283 (1996)
29. T. Kinoshita, *Phys. Rev. Lett.* **75**, 4728 (1995)
30. T. Kinoshita, W.J. Marciano, in *Quantum Electrodynamics*, ed. by T. Kinoshita (World Scientific, Singapore, 1990), pp. 419–478
31. T. Kinoshita, M. Nio, *Phys. Rev. Lett.* **90**, 021803 (2003); *Phys. Rev. D* **70**, 113001 (2003)
32. T. Kinoshita, M. Nio, *Phys. Rev. D* **73**, 013003 (2006)
33. T. Aoyama, M. Hayakawa, T. Kinoshita, M. Nio, *Phys. Rev. D* **91**, 033006 (2015)
34. T. Kinoshita, *Int. J. Mod. Phys. A* **29**, 1430003 (2014)
35. M. Hayakawa, *Springer Tracts Mod. Phys.* **256**, 41 (2014)
36. H. Suura, E. Wichmann, *Phys. Rev.* **105**, 1930 (1957); A. Petermann, *Phys. Rev.* **105**, 1931 (1957)
37. H.H. Elend, *Phys. Lett.* **20**, 682 (1966); Erratum-ibid, **21**, 720 (1966)
38. B.E. Lautrup, E. de Rafael, *Nucl. Phys. B* **70**, 317 (1974)
39. P.A. Baikov, K.G. Chetyrkin, J.H. Kühn, C. Sturm, *Nucl. Phys. B* **867**, 182 (2013)
40. S. Laporta, *Nuovo Cimento A* **106**, 675 (1993)
41. A. Czarnecki, M. Skrzypek, *Phys. Lett. B* **449**, 354 (1999)
42. S. Friot, D. Greynat, E. De Rafael, *Phys. Lett. B* **628**, 73 (2005)

43. S. Laporta, E. Remiddi, Phys. Lett. B **301**, 440 (1993)
44. J.H. Kühn, A.I. Onishchenko, A.A. Pivovarov, O.L. Veretin, Phys. Rev. D **68**, 033018 (2003)
45. J. Aldins, T. Kinoshita, S.J. Brodsky, A.J. Dufner, Phys. Rev. Lett. **23**, 441 (1969); Phys. Rev. D **1**, 2378 (1970)
46. J. Bailey et al., Phys. Lett. B **28**, 287 (1968)
47. A.S. Elkhovskiy, Sov. J. Nucl. Phys. **49**, 656 (1989); [Yad. Fiz. **49**, 1059 (1989)]
48. M. Passera, J. Phys. G **31**, R75 (2005); Phys. Rev. D **75**, 013002 (2007)
49. M. Caffo, S. Turrini, E. Remiddi, Phys. Rev. D **30**, 483 (1984); E. Remiddi, S.P. Sorella, Lett. Nuovo Cim. **44**, 231 (1985); D.J. Broadhurst, A.L. Kataev, O.V. Tarasov, Phys. Lett. B **298**, 445 (1993); S. Laporta, Phys. Lett. B **312**, 495 (1993); P.A. Baikov, D.J. Broadhurst, [arXiv:hep-ph/9504398](https://arxiv.org/abs/hep-ph/9504398)
50. A.L. Kataev, Phys. Rev. D **86**, 013010 (2012)
51. T. Aoyama, M. Hayakawa, T. Kinoshita, M. Nio, Phys. Rev. Lett. **109**, 111808 (2012)
52. S.G. Karshenboim, Phys. At. Nucl. **56**, 857 (1993); [Yad. Fiz. **56N6**, 252 (1993)]
53. T. Kinoshita, M. Nio, Phys. Rev. D **73**, 053007 (2006)
54. A.L. Kataev, Nucl. Phys. Proc. Suppl. **155**, 369 (2006); [arXiv:hep-ph/0602098](https://arxiv.org/abs/hep-ph/0602098); Phys. Rev. D **74**, 073011 (2006)
55. P.A. Baikov, K.G. Chetyrkin, C. Sturm, Nucl. Phys. Proc. Suppl. **183**, 8 (2008)
56. R. Lee, P. Marquard, A.V. Smirnov, V.A. Smirnov, M. Steinhauser, JHEP **1303**, 162 (2013)
57. A. Kurz, T. Liu, P. Marquard, A.V. Smirnov, V.A. Smirnov, M. Steinhauser, Phys. Rev. D **92**, 073019 (2015)
58. A. Kurz, T. Liu, P. Marquard, A. Smirnov, V. Smirnov, M. Steinhauser, Phys. Rev. D **93**, 053017 (2016)
59. H. Fritzsch, M. Gell-Mann, H. Leutwyler, Phys. Lett. **47B**, 365 (1973)
60. H.D. Politzer, Phys. Rev. Lett. **30**, 1346 (1973); D. Gross, F. Wilczek, Phys. Rev. Lett. **30**, 1343 (1973)
61. S.G. Gorishnii, A.L. Kataev, S.A. Larin, Phys. Lett. B **259**, 144 (1991); L.R. Surguladze, M.A. Samuel, Phys. Rev. Lett. **66**, 560 (1991) [Erratum-ibid. **66**, 2416 (1991)]; K.G. Chetyrkin, Phys. Lett. B **391**, 402 (1997)
62. K.G. Chetyrkin, J.H. Kühn, Phys. Lett. B **342**, 356 (1995); K.G. Chetyrkin, R.V. Harlander, J.H. Kühn, Nucl. Phys. B **586**, 56 (2000) [Erratum-ibid. B **634**, 413 (2002)]
63. R.V. Harlander, M. Steinhauser, Comput. Phys. Commun. **153**, 244 (2003)
64. S. Eidelman, F. Jegerlehner, Z. Phys. C **67**, 585 (1995)
65. A.E. Blinov et al. [MD-1 Collab.], Z. Phys. C **70**, 31 (1996)
66. J.Z. Bai et al. [BES Collab.], Phys. Rev. Lett. **84**, 594 (2000); Phys. Rev. Lett. **88**, 101802 (2002)
67. R.R. Akhmetshin et al. [CMD-2 Collab.], Phys. Lett. B **578**, 285 (2004); Phys. Lett. B **527**, 161 (2002)
68. A. Aloisio et al. [KLOE Collab.], Phys. Lett. B **606**, 12 (2005)
69. M.N. Achasov et al. [SND Collab.], J. Exp. Theor. Phys. **103**, 380 (2006) [Zh. Eksp. Teor. Fiz. **130**, 437 (2006)]
70. V. M. Aulchenko et al. [CMD-2], JETP Lett. **82** (2005) 743 [Pisma Zh. Eksp. Teor. Fiz. **82** (2005) 841]; R. R. Akhmetshin et al., JETP Lett. **84** (2006) 413 [Pisma Zh. Eksp. Teor. Fiz. **84** (2006) 491]; Phys. Lett. B **648** (2007) 28
71. F. Jegerlehner, Nucl. Phys. Proc. Suppl. **162**, 22 (2006), [arXiv:hep-ph/0608329](https://arxiv.org/abs/hep-ph/0608329)
72. F. Jegerlehner, R. Szafron, Eur. Phys. J. C **71**, 1632 (2011)
73. F. Jegerlehner, Acta Phys. Pol. B **44**, 2257 (2013)
74. F. Jegerlehner, EPJ Web Conf. **118**, 01016 (2016). [arXiv:1705.00263](https://arxiv.org/abs/1705.00263) [hep-ph]
75. B. Ananthanarayan, I. Caprini, D. Das, I.S. Imsong, Phys. Rev. D **93**, 116007 (2016)
76. H. Leutwyler, Electromagnetic form factor of the pion, in *Continuous Advances in QCD 2002: Proceedings* ed. by K.A. Olive, M.A. Shifman, M.B. Voloshin (World Scientific, Singapore, 2002), 646p, [arXiv:hep-ph/0212324](https://arxiv.org/abs/hep-ph/0212324)
77. G. Colangelo, Nucl. Phys. Proc. Suppl. **131**, 185 (2004); *ibid.* **162**, 256 (2006)

78. H. Leutwyler, Electromagnetic form factor of the pion, in *Continuous Advances in QCD 2002: Proceedings*, ed. by K.A. Olive, M.A. Shifman, M.B. Voloshin (World Scientific, Singapore, 2002), 646p, [arXiv:hep-ph/0212324](https://arxiv.org/abs/hep-ph/0212324); G. Colangelo, Nucl. Phys. Proc. Suppl. **131**, 185 (2004); *ibid.* **162**, 256 (2006)
79. R.R. Akhmetshin et al. [CMD-2 Collab.], Phys. Lett. B **578**, 285 (2004)
80. A. Aloisio et al. [KLOE Collab.], Phys. Lett. B **606**, 12 (2005); F. Ambrosino et al. [KLOE Collab.], Phys. Lett. B **670**, 285 (2009)
81. F. Ambrosino et al. [KLOE Collab.], Phys. Lett. B **700**, 102 (2011)
82. D. Babusci et al. [KLOE Collab.], Phys. Lett. B **720**, 336 (2013)
83. B. Aubert et al. [BABAR Collab.], Phys. Rev. Lett. **103**, 231801 (2009); J.P. Lees et al., Phys. Rev. D **86**, 032013 (2012)
84. M. Ablikim et al. [BESIII Collab.], Phys. Lett. B **753**, 629 (2016)
85. K. Hagiwara, A.D. Martin, D. Nomura, T. Teubner, Phys. Lett. B **649**, 173 (2007)
86. M. Davier, S. Eidelman, A. Höcker, Z. Zhang, Eur. Phys. J. C **27**, 497 (2003); *ibid.* **31**, 503 (2003)
87. S. Eidelman, *Proceedings of the XXXIII International Conference on High Energy Physics, July 27 – August 2, 2006, Moscow (Russia)*, World Scientific, to appear; M. Davier, Nucl. Phys. Proc. Suppl. **169**, 288 (2007)
88. M. Davier et al., Eur. Phys. J. C **66**, 127 (2010)
89. M. Davier, A. Höcker, B. Malaescu, Z. Zhang, Eur. Phys. J. C **71**, 1515 (2011)[Erratum-*ibid.* C **72**, 1874 (2012)]
90. R. Akhmetshin et al. [CMD-3 Collab.], Phys. Lett. B **723**, 82 (2013)
91. M. Achasov et al. [SND Collab.], Phys. Rev. D **88**, 054013 (2013)
92. J. Lees et al. [BABAR Collab.], Phys. Rev. D **87**, 092005 (2013)
93. J. Lees et al. [BABAR Collab.], Phys. Rev. D **88**, 032013 (2013)
94. J. Lees et al. [BABAR Collab.], Phys. Rev. D **89**, 092002 (2014)
95. R. Alemany, M. Davier, A. Höcker, Eur. Phys. J. C **2**, 123 (1998)
96. R. Barate et al. [ALEPH Collab.], Z. Phys. C **76**, 15 (1997); Eur. Phys. J. C **4** (1998) 409; S. Schael et al. [ALEPH Collab.], Phys. Rep. **421**, 191 (2005)
97. M. Davier et al., Eur. Phys. J. C **74**, 2803 (2014)
98. K. Ackersstaff et al. [OPAL Collab.], Eur. Phys. J. C **7**, 571 (1999)
99. S. Anderson et al. [CLEO Collab.], Phys. Rev. D **61**, 112002 (2000)
100. M. Fujikawa et al. [Belle Collab.], Phys. Rev. D **78**, 072006 (2008)
101. S. Ghozzi, F. Jegerlehner, Phys. Lett. B **583**, 222 (2004)
102. M. Benayoun, P. David, L. DelBuono, F. Jegerlehner, Eur. Phys. J. C **72**, 1848 (2012)
103. R. Barbieri, E. Remiddi, Phys. Lett. B **49**, 468 (1974); Nucl. Phys. B **90**, 233 (1975)
104. B. Krause, Phys. Lett. B **390**, 392 (1997)
105. J. Calmet, S. Narison, M. Perrottet, E. de Rafael, Phys. Lett. B **61**, 283 (1976)
106. T. Kinoshita, B. Nizic, Y. Okamoto, Phys. Rev. Lett. **52**, 717 (1984); Phys. Rev. D **31**, 2108 (1985)
107. K. Hagiwara, A.D. Martin, D. Nomura, T. Teubner, Phys. Lett. B **557**, 69 (2003); Phys. Rev. D **69**, 093003 (2004)
108. A. Kurz, T. Liu, P. Marquard, M. Steinhauser, Phys. Lett. B **734**, 144 (2014)
109. A. Kurz, T. Liu, P. Marquard, A.V. Smirnov, V.A. Smirnov, M. Steinhauser, EPJ Web Conf. **118**, 01033 (2016)
110. H. Kolanoski, P. Zerwas, Two-photon physics, in *High Energy Electron-Positron Physics*, ed. by A. Ali, P. Söding (World Scientific, Singapore, 1988), pp. 695–784; D. Williams et al. [Crystal Ball Collab.], SLAC-PUB-4580, 1988, unpublished
111. G. Ecker, J. Gasser, A. Pich, E. de Rafael, Nucl. Phys. B **321**, 311 (1989); G. Ecker, J. Gasser, H. Leutwyler, A. Pich, E. de Rafael, Phys. Lett. B **223**, 425 (1989)
112. J. Bijnens, E. Pallante, J. Prades, Phys. Rev. Lett. **75**, 1447 (1995) [Erratum-*ibid.* **75**, 3781 (1995)]; Nucl. Phys. B **474**, 379 (1996); [Erratum-*ibid.* **626**, 410 (2002)]
113. E. de Rafael, Phys. Lett. B **322**, 239 (1994); J.S. Bell, E. de Rafael, Nucl. Phys. B **11**, 611 (1969)

114. M. Hayakawa, T. Kinoshita, A.I. Sanda, Phys. Rev. Lett. **75**, 790 (1995); Phys. Rev. D **54**, 3137 (1996)
115. M. Hayakawa, T. Kinoshita, Phys. Rev. D **57**, 465 (1998) [Erratum-ibid. D **66**, 019902 (2002)]
116. M. Knecht, A. Nyffeler, M. Perrottet, E. De Rafael, Phys. Rev. Lett. **88**, 071802 (2002)
117. G. 't Hooft, Nucl. Phys. B **72**, 461 (1974); *ibid.* **75**, 461 (1974)
118. A.V. Manohar, Hadrons in the $1/N$ Expansion, in *At the frontier of Particle Physics*, vol. 1, ed. by M. Shifman (World Scientific, Singapore, 2001), pp. 507–568
119. S. Peris, M. Perrottet, E. de Rafael, JHEP **9805**, 011 (1998); M. Knecht, S. Peris, M. Perrottet, E. de Rafael, Phys. Rev. Lett. **83**, 5230 (1999); M. Knecht, A. Nyffeler. Eur. Phys. J. C **21**, 659 (2001)
120. M. Knecht, A. Nyffeler, Phys. Rev. D **65**, 073034 (2002)
121. I. Blokland, A. Czarnecki, K. Melnikov, Phys. Rev. Lett. **88**, 071803 (2002)
122. M. Ramsey-Musolf, M.B. Wise, Phys. Rev. Lett. **89**, 041601 (2002)
123. K. Melnikov, A. Vainshtein, Phys. Rev. D **70**, 113006 (2004)
124. A. Nyffeler, Nucl. Phys. B (Proc. Suppl.) **131**, 162 (2004)
125. J. Prades, E. de Rafael, A. Vainshtein, Adv. Ser. Direct. High Energy Phys. **20**, 303 (2009); ed. by B.L. Roberts, W. Marciano, [arXiv:0901.0306](https://arxiv.org/abs/0901.0306) [hep-ph]
126. R. Jackiw, S. Weinberg, Phys. Rev. D **5**, 2396 (1972); I. Bars, M. Yoshimura, Phys. Rev. D **6**, 374 (1972); G. Altarelli, N. Cabibbo, L. Maiani, Phys. Lett. B **40**, 415 (1972); W.A. Bardeen, R. Gastmans, B. Lautrup, Nucl. Phys. B **46**, 319 (1972); K. Fujikawa, B.W. Lee, A.I. Sanda, Phys. Rev. D **6**, 2923 (1972)
127. E.A. Kuraev, T.V. Kukhto, A. Schiller, Sov. J. Nucl. Phys. **51**, 1031 (1990) [Yad. Fiz. **51**, 1631 (1990)]; T.V. Kukhto, E.A. Kuraev, A. Schiller, Z.K. Silagadze, Nucl. Phys. B **371**, 567 (1992)
128. S.L. Adler, Phys. Rev. **177**, 2426 (1969); J.S. Bell, R. Jackiw, Nuovo Cimento **60A**, 47 (1969); W.A. Bardeen, Phys. Rev. **184**, 1848 (1969); C. Bouchiat, J. Iliopoulos, P. Meyer, Phys. Lett. **38B**, 519 (1972); D. Gross, R. Jackiw, Phys. Rev. D **6**, 477 (1972); C.P. Korthals Altes, M. Perrottet, Phys. Lett. **39B**, 546 (1972)
129. S. Peris, M. Perrottet, E. de Rafael, Phys. Lett. B **355**, 523 (1995)
130. A. Czarnecki, B. Krause, W. Marciano, Phys. Rev. D **52**, R2619 (1995)
131. G. Degrassi, G.F. Giudice, Phys. Rev. **58D**, 053007 (1998)
132. M. Knecht, S. Peris, M. Perrottet, E. de Rafael, JHEP **0211**, 003 (2002)
133. A. Czarnecki, W.J. Marciano, A. Vainshtein, Phys. Rev. D **67**, 073006 (2003) [Erratum-ibid. D **73**, 119901 (2006)]
134. E. D'Hoker, Phys. Rev. Lett. **69**, 1316 (1992)
135. A. Czarnecki, B. Krause, W.J. Marciano, Phys. Rev. Lett. **76**, 3267 (1996)
136. S. Heinemeyer, D. Stöckinger, G. Weiglein, Nucl. Phys. B **699**, 103 (2004)
137. T. Gribouk, A. Czarnecki, Phys. Rev. D **72**, 053016 (2005)
138. R.S. Van Dyck, P.B. Schwinberg, H.G. Dehmelt, Phys. Rev. Lett. **59**, 26 (1987)
139. D. Hanneke, S.F. Hoogerheide, G. Gabrielse, Phys. Rev. A **83**, 052122 (2011)
140. P. Cladé et al., Phys. Rev. Lett. **96**, 033001 (2006)
141. V. Gerginov et al., Phys. Rev. A **73**, 032504 (2006)
142. R. Bouchendir, P. Clade, S. Guellati-Khelifa, F. Nez, F. Biraben, Phys. Rev. Lett. **106**, 080801 (2011)
143. C. Schwob et al., Phys. Rev. Lett. **82**, 4960 (1999)
144. M.P. Bradley et al., Phys. Rev. Lett. **83**, 4510 (1999)
145. T. Beier et al., Phys. Rev. Lett. **88**, 011603 (2002)
146. D.L. Farnham, R.S. Van Dyck, P.B. Schwinberg, Phys. Rev. Lett. **75**, 3598 (1995)
147. S. Sturm, F. Köhler, J. Zatorski, A. Wagner, Z. Harman, G. Werth, W. Quint, C.H. Keitel et al., Nature **506**(7489), 467 (2014)
148. T. Udem et al., Phys. Rev. Lett. **82**, 3568 (1999)
149. A. Wicht et al., in *Proceedings of the 6th Symposium on Frequency Standards and Metrology* (World Scientific, Singapore, 2002), pp. 193–212; Phys. Scr. **T102** (2002) 82
150. G.F. Giudice, P. Paradisi, M. Passera, JHEP **1211**, 113 (2012)

151. F. Terranova, G.M. Tino, Phys. Rev. A **89**, 052118 (2014)
152. G. Mishima, [arXiv:1311.7109](https://arxiv.org/abs/1311.7109) [hep-ph]
153. M. Fael, M. Passera, Phys. Rev. D **90**, 056004 (2014)
154. K. Melnikov, A. Vainshtein, M. Voloshin, Phys. Rev. D **90**, 017301 (2014)
155. M.I. Eides, Phys. Rev. D **90**, 057301 (2014)
156. M. Hayakawa, [arXiv:1403.0416](https://arxiv.org/abs/1403.0416) [hep-ph]
157. M.A. Braun, Zh. Eksp. Teor. Fiz. **54**, 1220 (1968) [Sov. Phys. JETP. **27**, 652 (1968)]
158. R. Barbieri, P. Christillin, E. Remiddi, Phys. Rev. A **8**, 2266 (1973)
159. G.W. Bennett et al. [Muon (g-2) Collab.], Phys. Rev. Lett. **92**, 161802 (2004)
160. J. Grange et al. [Muon g-2 Collab.], [arXiv:1501.06858](https://arxiv.org/abs/1501.06858) [physics.ins-det]
161. F. Jegerlehner, J. Fleischer, Phys. Lett. B **151**, 65 (1985); Acta Phys. Pol. B **17**, 709 (1986)
162. Ya B. Zeldovich, Sov. Phys. JETP **6**, 1184 (1958)
163. Ya B. Zeldovich, A.M. Perelomov, Sov. Phys. JETP **12**, 777 (1961)
164. R.E. Marshak, Riazuddin, C.P. Ryan, *Theory of Weak Interactions in Particle Physics* (Wiley-Interscience, New York, 1969), p. 776
165. H. Czyż, K. Kołodziej, M. Zralek, P. Khristova, Can. J. Phys. **66**, 132 (1988); H. Czyż, M. Zralek. Can. J. Phys. **66**, 384 (1988)
166. A. Gongora, R.G. Stuart, Z. Phys. C **55**, 101 (1992)
167. L.D. Landau, Nucl. Phys. **3**, 127 (1957); Sov. Phys. JETP **5**, 336 (1957) [Zh. Eksp. Teor. Fiz. **32**, 405 (1957)]
168. Ya.B. Zeldovich, Sov. Phys. JETP **12**, 1030 (1960) [Zh. Eksp. Teor. Fiz. **39**, 1483 (1960)]
169. F. Hoogeveen, Nucl. Phys. B **341**, 322 (1990)
170. C. Jarlskog, Phys. Rev. Lett. **55**, 1039 (1985)
171. B.C. Regan, E.D. Commins, C.J. Schmidt, D. DeMille, Phys. Rev. Lett. **88**, 071805 (2002)
172. J. Bailey et al., Nucl. Phys. B **150**, 1 (1979)
173. F.J.M. Farley et al., Phys. Rev. Lett. **93**, 052001 (2004); M. Aoki et al. [J-PARC Letter of Intent], *Search for a Permanent Muon Electric Dipole Moment at the $\times 10^{-24}$ e·cm Level*, <http://www-ps.kek.jp/jhf-np/LOIlist/pdf/L22.pdf>
174. W. Bernreuther, M. Suzuki, Rev. Mod. Phys. **63**, 313 (1991) [Erratum-ibid. **64**, 633 (1992)]
175. G. Källén, A. Sabry, K. Dan, Vidensk. Selsk. Mat.-Fys. Medd. **29**, 17 (1955)
176. R. Barbieri, E. Remiddi, Nuovo Cimento A **13**, 99 (1973)
177. D.J. Broadhurst, Phys. Lett. **101**, 423 (1981); S. Generalis, Open University preprint OUT-4102-13; T.H. Chang, K.J.F. Gaemers, W.L. van Neerven, Nucl. Phys. B **202**, 407 (1982); L.J. Reinders, H.R. Rubinstein, S. Yazaki, Phys. Rep. **127**, 1 (1985); B.A. Kniehl, Nucl. Phys. B **347**, 86 (1990)
178. M. Steinhauser, Phys. Lett. B **429**, 158 (1998)
179. M. Acciari et al. [L3 Collab.], Phys. Lett. B **476**, 40 (2000); G. Abbiendi et al. [OPAL Collab.], Eur. Phys. J. C **45**, 1 (2006)
180. L. Trentadue, Nucl. Phys. Proc. Suppl. **162**, 73 (2006)
181. G. Källén, Helv. Phys. Acta **25**, 417 (1952); H. Lehmann, Nuovo Cimento **11**, 342 (1954)
182. L.D. Landau, Nucl. Phys. **13**, 181 (1959); S. Mandelstam, Phys. Rev. **112**, 1344 (1958); **115**, 1741 (1959); R.E. Cutkosky, J. Math. Phys. **1**, 429 (1960)
183. M.J.G. Veltman, Physica **29**, 186 (1963)
184. V.B. Berestetskii, O.N. Krokhnin, A.K. Khelbnikov, Sov. Phys. JETP **3**, 761 (1956) [Zh. Eksp. Teor. Fiz. **30**, 788 (1956)]
185. S.J. Brodsky, E. De Rafael, Phys. Rev. **168**, 1620 (1968)
186. T. Kinoshita, Nuovo Cimento B **51**, 140 (1967); T. Kinoshita, W.B. Lindquist, Phys. Rev. D **27**, 867 (1983)
187. B. Lautrup, Phys. Lett. B **69**, 109 (1977)
188. T. Kinoshita, W.B. Lindquist, Phys. Rev. D **27**, 877 (1983)
189. A.H. Hoang, J.H. Kühn, T. Teubner, Nucl. Phys. B **452**, 173 (1995)
190. D.J. Broadhurst, A.L. Kataev, O.V. Tarasov, Phys. Lett. B **298**, 445 (1993); P.A. Baikov, D.J. Broadhurst, in *Proceedings of the 4th International Workshop on Software Engineering and Artificial Intelligence for High Energy and Nuclear Physics (AIHENP95), Pisa, Italy (1995)*, p. 167, [arXiv:hep-ph/9504398](https://arxiv.org/abs/hep-ph/9504398)

191. M. Caffo, E. Remiddi, S. Turrini, Nucl. Phys. B **141**, 302 (1978); J.A. Mignaco, E. Remiddi (1969) (unpublished)
192. B.E. Lautrup, A. Peterman, E. de Rafael, Phys. Rep. **3C**, 193 (1972)
193. S.L. Adler, Phys. Rev. D **10**, 3714 (1974); A. De Rujula, H. Georgi, Phys. Rev. D **13**, 1296 (1976)
194. S. Eidelman, F. Jegerlehner, A.L. Kataev, O. Veretin, Phys. Lett. B **454**, 369 (1999)
195. F. Jegerlehner, J. Phys. G **29**, 101 (2003)
196. F. Jegerlehner, in *Radiative Corrections*, ed. by J. Solà (World Scientific, Singapore, 1999), pp. 75–89
197. <http://www-com.physik.hu-berlin.de/~fjeger/alphaQED.tar.gz>, <http://www-com.physik.hu-berlin.de/~fjeger/alphaQED.pdf>
198. <http://www-com.physik.hu-berlin.de/~fjeger/pQCDAdler.tar.gz>, <http://www-com.physik.hu-berlin.de/~fjeger/pQCDAdler.pdf>
199. C.M. Carloni Calame, M. Passera, L. Trentadue, G. Venanzoni, Phys. Lett. B **746**, 325 (2015)
200. G. Abbiendi et al., Eur. Phys. J. C **77**, 139 (2017)
201. E. de Rafael, Phys. Lett. B **736**, 522 (2014)
202. M. Benayoun, P. David, L. DelBuono, F. Jegerlehner, [arXiv:1605.04474](https://arxiv.org/abs/1605.04474) [hep-ph]
203. M. Della Morte, A. Francis, G. Herdofoza, H. Horch, B. Jäger, A. Jüttner, H. Meyer, H. Wittig, PoS LATTICE **2014**, 162 (2014)
204. A. Francis, G. Herdofoza, H. Horch, B. Jäger, H.B. Meyer, H. Wittig, PoS LATTICE **2014**, 163 (2014)
205. J.A.M. Vermaseren, Int. J. Mod. Phys. A **14**, 2037 (1999)
206. E. Remiddi, J.A.M. Vermaseren, Int. J. Mod. Phys. A **15**, 725 (2000)
207. M. Abramowitz, I. Stegun, *Handbook of Mathematical Functions* (Dover, New York, 1965) (Chap. 17 and formulas 17.2.7/17.2.9/17.2.15 there)
208. O.V. Tarasov, Phys. Lett. B **638**, 195 (2006)
209. A.I. Davydychev, Phys. Rev. D **61**, 087701 (2000)
210. J. Fleischer, F. Jegerlehner, O.V. Tarasov, Nucl. Phys. B **672**, 303 (2003)
211. M.Y. Kalmykov, JHEP **0604**, 056 (2006)
212. A. Erdélyi et al., *Higher Transcendental Functions*, vol. 1 (McGraw-Hill, New York, 1953)
213. P. Appell, J. Kampé de Fériet, *Fonctions Hypergeometriques et Hyperspheriques. Polynome d'Hermite* (Gauthier-Villars, Paris, 1926)
214. O.V. Tarasov, Phys. Lett. B **670**, 67 (2008)
215. O.V. Tarasov, [arXiv:1512.09024](https://arxiv.org/abs/1512.09024) [hep-ph]
216. A.I. Davydychev, M.Y. Kalmykov, Nucl. Phys. B **605**, 266 (2001)
217. S. Moch, P. Uwer, S. Weinzierl, J. Math. Phys. **43**, 3363 (2002)
218. S. Bethke, Phys. Rep. **403–404**, 203 (2004)
219. S. Narison, Phys. Lett. B **568**, 231 (2003)
220. V.V. Ezhela, S.B. Lugovsky, O.V. Zenin, [arXiv:hep-ph/0312114](https://arxiv.org/abs/hep-ph/0312114)
221. J.F. de Troconiz, F.J. Yndurain, Phys. Rev. D **71**, 073008 (2005)
222. K. Hagiwara, R. Liao, A.D. Martin, D. Nomura, T. Teubner, J. Phys. G G **38**, 085003 (2011)
223. M. Benayoun, P. David, L. DelBuono, F. Jegerlehner, Eur. Phys. J. C **73**, 2453 (2013)
224. M. Benayoun, P. David, L. DelBuono, F. Jegerlehner, Eur. Phys. J. C **75**, 613 (2015)
225. M. Davier, [arXiv:1612.02743](https://arxiv.org/abs/1612.02743) [hep-ph]

Part I
**A Detailed Account of the Theory, Outline
of Concepts of the Experiment, Status and
Perspectives**

Chapter 4

Electromagnetic and Weak Radiative Corrections

4.1 $g - 2$ in Quantum Electrodynamics

The by far largest contribution to the anomalous magnetic moment is of pure QED origin. This is of course the reason why the measurements of a_e and a_μ until not so long time ago may have been considered as precision tests of QED. The clear dominance to more than 99.99% of just one type of interaction, the interaction of the charged leptons e , μ and τ with the photon, historically, was very important for the development of QFT and QED, since it allowed us to test QED as a model theory under very simple, clean and unambiguous conditions. This was very crucial in strengthening our confidence in QFT as a basic theoretical framework. We should remember that it took about 20 years from the invention of QED (Dirac 1928 [$g_e = 2$]) until the first reliable results could be established (Schwinger 1948 [$a_e^{(1)} = \alpha/2\pi$]) after a covariant formulation and renormalization was understood and settled in its main aspects. As precision of experiments improved, the QED part by itself became a big challenge for theorists, because higher order corrections are sizable, and as the order of perturbation theory increases, the complexity of the calculations grow dramatically. Thus experimental tests were able to check QED up to 7 digits in the prediction which requires to evaluate the perturbation expansion up to 5 loops (5 terms in the expansion). The anomalous magnetic moment as a *dimensionless* quantity exhibits contributions which are just numbers expanded in powers of α , what one would get in QED with just one species of leptons, and contributions depending on the mass ratios if different leptons come into play. Thus taking into account all three leptons we obtain functions of the ratios of the lepton masses m_e , m_μ and m_τ . Considering a_μ , we can cast it into the following form [1, 2]

$$a_\mu^{\text{QED}} = A_1 + A_2(m_\mu/m_e) + A_2(m_\mu/m_\tau) + A_3(m_\mu/m_e, m_\mu/m_\tau) \quad (4.1)$$

The term A_1 in QED is universal for all leptons. It represents all diagrams including those with closed lepton loops that have the same mass as the external lepton. The contribution A_2 has one scale and only shows up if an additional lepton loop of a

lepton different from the external one is involved. This requires at least one more loop, thus two at least: for the muon as external lepton we have two possibilities: an additional electron–loop (light–in–heavy) $A_2(m_\mu/m_e)$ or an additional τ –loop (heavy–in–light) $A_2(m_\mu/m_\tau)$ two contributions of quite different character. The first produces large logarithms $\propto \ln(m_\mu/m_e)^2$ and accordingly large effects while the second, because of the *decoupling* of heavy particles in QED like theories, produces only small effects of order $\propto (m_\mu/m_\tau)^2$. The two–scale contribution requires a light as well as a heavy extra loop and hence starts at three loop order. We will discuss the different types of contributions in the following. Each of the terms is given in renormalized perturbation theory by an appropriate expansion in α :

$$\begin{aligned} A_1 &= A_1^{(2)} \left(\frac{\alpha}{\pi}\right) + A_1^{(4)} \left(\frac{\alpha}{\pi}\right)^2 + A_1^{(6)} \left(\frac{\alpha}{\pi}\right)^3 + A_1^{(8)} \left(\frac{\alpha}{\pi}\right)^4 + A_1^{(10)} \left(\frac{\alpha}{\pi}\right)^5 + \dots \\ A_2 &= A_2^{(4)} \left(\frac{\alpha}{\pi}\right)^2 + A_2^{(6)} \left(\frac{\alpha}{\pi}\right)^3 + A_2^{(8)} \left(\frac{\alpha}{\pi}\right)^4 + A_2^{(10)} \left(\frac{\alpha}{\pi}\right)^5 + \dots \\ A_3 &= A_3^{(6)} \left(\frac{\alpha}{\pi}\right)^3 + A_3^{(8)} \left(\frac{\alpha}{\pi}\right)^4 + A_3^{(10)} \left(\frac{\alpha}{\pi}\right)^5 + \dots \end{aligned}$$

and later we will write

$$a_\ell = C_1 \left(\frac{\alpha}{\pi}\right) + C_2 \left(\frac{\alpha}{\pi}\right)^2 + C_3 \left(\frac{\alpha}{\pi}\right)^3 + C_4 \left(\frac{\alpha}{\pi}\right)^4 + C_5 \left(\frac{\alpha}{\pi}\right)^5 + \dots$$

where

$$C_L = A_1^{(2L)} + A_2^{(3L)}(m_\ell/m'_\ell) + A_3^{(4L)}(m_\ell/m'_\ell, m_\ell/m''_\ell) \quad (4.2)$$

denote the total L –loop coefficient of the $(\alpha/\pi)^L$ term. While $A_1^{(2L)}$ is the mass-independent (universal) contributions in one-flavor QED, $A_2^{(3L)}(m_\ell/m'_\ell)$ and $A_3^{(4L)}(m_\ell/m'_\ell, m_\ell/m''_\ell)$ are the mass-dependent (non-universal) contributions in three-flavor QED. For a_e the $A_2^{(3L)}(m_e/m_\mu)$, $A_3^{(4L)}(m_e/m_\mu, m_e/m_\tau)$ and $A_2^{(3L)}(m_e/m_\tau)$ are subleading as suppressed according to the decoupling-theorem. For a_μ in contrast $A_2^{(3L)}(m_\mu/m_e)$ is leading since it is enhanced by the large logarithms, while $A_3^{(4L)}(m_\mu/m_e, m_\mu/m_\tau)$ and $A_2^{(3L)}(m_\mu/m_\tau)$ are suppressed by decoupling again.

In collecting various contributions we should always keep in mind the precision of the present experimental result [3]

$$a_\mu^{\text{exp}} = 116592080(63) \times 10^{-11}$$

and the future prospects of possible improvements [4] which could reach an ultimate precision

$$\delta a_\mu^{\text{fin}} \sim 15 \times 10^{-11} . \quad (4.3)$$

For the n –loop coefficients multiplying $(\alpha/\pi)^n$ this translates into the required accuracies given in Table 4.1. To match the current accuracy one has to multiply each entry with a factor 6, which is the experimental error in units of 10^{-10} .

Table 4.1 Numerical precision of coefficients up to five loops

δC_1	δC_2	δC_3	δC_4	δC_5
6.5×10^{-8}	3×10^{-5}	1×10^{-2}	5	2×10^3

As we will see many contributions are enhanced by large short–distance logarithms of the type $\ln m_\mu/m_e$. These terms are controlled by the RG equation of QED or equivalently by the homogeneous Callan–Symanzik (CS) equation [5]

$$\left(m_e \frac{\partial}{\partial m_e} + \beta(\alpha) \alpha \frac{\partial}{\partial \alpha} \right) a_\mu^{(\infty)} \left(\frac{m_\mu}{m_e}, \alpha \right) = 0$$

where $\beta(\alpha)$ is the QED β –function associated with charge renormalization. $a_\mu^{(\infty)}(\frac{m_\mu}{m_e}, \alpha)$ is the leading form of a_μ in the sense that it includes powers of logs of mass ratios and constant terms but powers of m_e/m_μ are dropped.¹ The solution of the CS equation amounts to replace α by the running fine structure constant $\alpha(m_\mu)$ in $a_\mu^{(\infty)}(\frac{m_\mu}{m_e}, \alpha)$, which implies taking into account the leading logs of higher orders. Since β is known to three loops and also a_μ is known analytically at three loops, it is possible to obtain the important higher leading logs quite easily. The basic RG concepts have been discussed in Sect. 2.6.5. For the evaluation of the mass dependent contributions the knowledge of precise mass ratios is mandatory. We will use the most recent compilation by the CODATA group [6]. Our updated results presented in the following supersede results of the 2009 review of the muon $g - 2$ [7].

4.1.1 One–Loop QED Contribution

For completeness we mention this contribution represented by Fig. 4.1 here once more. According to (3.154) the leading order contribution may be written in the form

$$a_\mu^{(2)\text{ QED}} = \frac{\alpha}{\pi} \int_0^1 dx (1-x) = \frac{\alpha}{\pi} \frac{1}{2} \quad (4.4)$$

which is trivial to evaluate.

¹ a_μ itself satisfies an exact CS equation which is inhomogeneous, the inhomogeneity being a mass insertion (m_e) on a_μ ; this inhomogeneous part is $O(m_e/m_\mu)$ and thus drops from the CS equation for the asymptotic approximation $a_\mu^{(\infty)}$.

Fig. 4.1 The universal lowest order QED contribution to a_ℓ

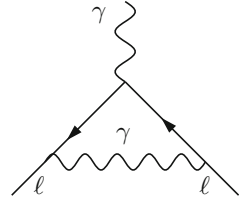
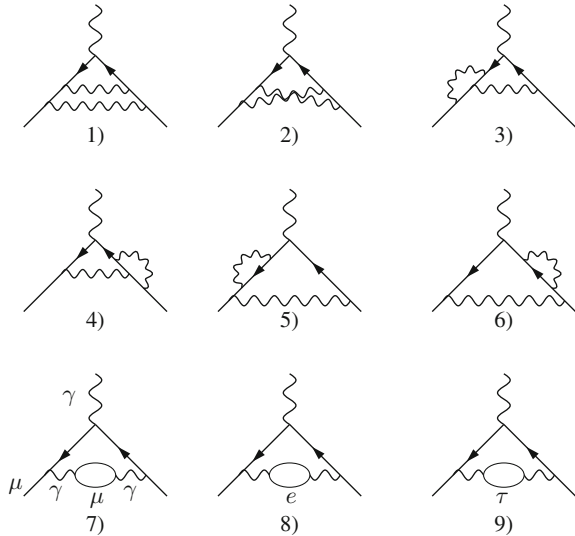


Fig. 4.2 Diagrams 1–7 represent the universal second order contribution to a_ℓ , diagram 8 yields the “light”, diagram 9 the “heavy” mass dependent corrections



4.1.2 Two-Loop QED Contribution

At two loops in QED the 9 diagrams shown in Fig. 4.2 are contributing to $g - 2$. The (within QED) universal contribution comes from the first 6 diagrams, which besides the external muon string of lines have attached two virtual photons. They form a gauge invariant subset of diagrams and yield the result

$$A_{1[1-6]}^{(4)} = -\frac{279}{144} + \frac{5\pi^2}{12} - \frac{\pi^2}{2} \ln 2 + \frac{3}{4}\zeta(3) .$$

The last 3 diagrams include photon vacuum polarization (vap) due to the lepton loops. The one with the muon loop is also universal in the above sense (one flavor = single scale QED) and contributes the mass independent correction

$$A_{1 \text{ vap}}^{(4)} (m_\mu/m_\ell = 1) = \frac{119}{36} - \frac{\pi^2}{3} .$$

The complete “universal” part yields the coefficient $A_1^{(4)}$ calculated first by Petermann [8] and by Sommerfield [9] in 1957:

$$A_{1\text{uni}}^{(4)} = \frac{197}{144} + \frac{\pi^2}{12} - \frac{\pi^2}{2} \ln 2 + \frac{3}{4} \zeta(3) = -0.328\,478\,965\,579\,193\,78\dots \quad (4.5)$$

where $\zeta(n)$ is the Riemann zeta function of argument n . The mass dependent non-universal contribution is due to the last two diagrams of Fig. 4.2. The coefficient is now a function of the mass m_ℓ of the lepton forming the closed loop. Using the representation (3.151) together with (2.177) we see that the coefficient of $(\alpha/\pi)^2$ may be written as double integral [10]

$$A_{2\text{vap}}^{(4)}(1/x_\ell) = \int_0^1 du \int_0^1 dv \frac{u^2 (1-u) v^2 (1-v^2/3)}{u^2 (1-v^2) + 4x_\ell^2 (1-u)}, \quad (4.6)$$

where $x_\ell = m_\ell/m_\mu$ and m_ℓ is the mass of the virtual lepton in the vacuum polarization sub-graph.² It was computed in the late 1950s [11] for $m_\ell = m_e$ and neglecting terms of $O(m_e/m_\mu)$. Its exact expression was calculated in 1966 [12]. The first integration yields logarithms, the second one double logarithms (products of logarithms) and a new type of integrals, the dilogarithms or Spence functions $\text{Li}_2(x) = -\int_0^1 dt \ln(1-xt)/t$ defined earlier in (2.208) and Sect. 3.8.1. Actually, by taking advantage of the properties of the dilogarithm (2.207), the full analytic result of [12] can be simplified to [13]

$$\begin{aligned} A_{2\text{vap}}^{(4)}(1/x) &= -\frac{25}{36} - \frac{\ln x}{3} + x^2 (4 + 3 \ln x) + x^4 \left[\frac{\pi^2}{3} - 2 \ln x \ln \left(\frac{1}{x} - x \right) - \text{Li}_2(x^2) \right] \\ &+ \frac{x}{2} (1 - 5x^2) \left[\frac{\pi^2}{2} - \ln x \ln \left(\frac{1-x}{1+x} \right) - \text{Li}_2(x) + \text{Li}_2(-x) \right] \\ &= -\frac{25}{36} - \frac{\ln x}{3} + x^2 (4 + 3 \ln x) + x^4 \left[2 \ln^2(x) - 2 \ln x \ln \left(x - \frac{1}{x} \right) + \text{Li}_2(1/x^2) \right] \\ &+ \frac{x}{2} (1 - 5x^2) \left[-\ln x \ln \left(\frac{x-1}{x+1} \right) + \text{Li}_2(1/x) - \text{Li}_2(-1/x) \right] \quad (x > 1). \end{aligned} \quad (4.8)$$

²We remind that the above integral representation is obtained by applying the method presented in Sect. 3.8. To start with, $a_\mu^{(4)}(\text{vap}, \ell)$ is given by a dispersion integral of the form (3.164) with $R(s) \rightarrow R_\ell(s)$ given by (3.140). Thus

$$a_\mu^{(4)}(\text{vap}, \ell) = \frac{\alpha}{3\pi} \int_{4m_\ell^2}^\infty \frac{ds}{s} K_\mu^{(2)}(s) R_\ell(s) \quad (4.7)$$

where $K_\mu^{(2)}(s)$ represents the contribution to a_μ from the one-loop diagram Fig. 4.1, where the photon has been replaced by a “heavy photon” of mass \sqrt{s} . The convolution with R_ℓ accomplishes the insertion of the corresponding lepton loop into the photon line of the one-loop vertex.

The first version of the formula is valid for arbitrary x . However, for $x > 1$ some of the logs as well as $\text{Li}_2(x)$ develop a cut and a corresponding imaginary part like the one of $\ln(1-x)$. Therefore, for the numerical evaluation in terms of a series expansion,³ it is an advantage to rewrite the $\text{Li}_2(x)$'s in terms of $\text{Li}_2(1/x)$'s, according to (2.207), which leads to the second form. For $x = 1$ (muon loop), using $\text{Li}_2(1) = \zeta(2) = \frac{\pi^2}{6}$ and $\text{Li}_2(-1) = -\frac{1}{2}\zeta(2) = -\frac{\pi^2}{12}$ the evaluation of (4.8) yields $A_{2\text{vap}}^{(4)}(1) = 119/36 - \pi^2/3$ the contribution already included in $A_{1\text{uni}}^{(4)}$ given by (4.5).

For numerical calculations it is often convenient to work with asymptotic expansions. For a τ -loop an expansion for large arguments x gives formula (12) of [14]:

$$A_{2\text{vap}}^{(4)}(1/x_\tau \equiv l = \frac{m_\mu}{m_\tau}) = \frac{l^2}{45} + \frac{l^4 \ln l}{70} + \frac{9}{19600}l^4 - \frac{131}{99225}l^6 + \frac{4l^6}{315} \ln l - \sum_{n=3}^{\infty} \frac{(8n^3 + 28n^2 - 45)l^{2n+2}}{[(n+3)(2n+3)(2n+5)]^2} + 2 \ln l \sum_{n=3}^{\infty} \frac{nl^{2n+2}}{(n+3)(2n+3)(2n+5)}.$$

For the electron-loop an expansion for small x leads to formula (11) of [14]:

$$A_{2\text{vap}}^{(4)}(1/x_e \equiv 1/k = \frac{m_\mu}{m_e}) = -\frac{25}{36} + \frac{\pi^2}{4}k - \frac{1}{3} \ln k + (3 + 4 \ln k)k^2 - \frac{5}{4}\pi^2 k^3 + \left[\frac{\pi^2}{3} + \frac{44}{9} - \frac{14}{3} \ln k + 2 \ln^2 k \right] k^4 + \frac{8}{15}k^6 \ln k - \frac{109}{225}k^6 + \sum_{n=2}^{\infty} \left[\frac{2(n+3)}{n(2n+1)(2n+3)} \ln k - \frac{8n^3 + 44n^2 + 48n + 9}{n^2(2n+1)^2(2n+3)^2} \right] k^{2n+4}.$$

Evaluations of (4.8) or of the appropriate series expansions yields

$$A_{2\text{vap}}^{(4)}(m_\mu/m_e) = 1.094\,258\,3092 \quad (72)$$

$$A_{2\text{vap}}^{(4)}(m_\mu/m_\tau) = 0.000\,078\,079 \quad (14),$$

where the errors are solely due to the experimental uncertainties of the mass ratios.

According to Table 4.1 the τ yields a non-negligible contribution. At the two-loop level a $e-\tau$ mixed contribution is not possible, and hence $A_3^{(4)}(m_\mu/m_e, m_\mu/m_\tau) = 0$.

³A frequently used rapidly converging series expansion is

$$\text{Li}_2(x) = \sum_0^{\infty} B_n \frac{u^{n+1}}{(n+1)!}$$

where $u = -\ln(1-x)$ and B_n are the Bernoulli numbers.

The complete two-loop QED contribution from the diagrams displayed in Fig. 4.2 is given by

$$C_2 = A_{1\text{uni}}^{(4)} + A_{2\text{vap}}^{(4)}(m_\mu/m_e) + A_{2\text{vap}}^{(4)}(m_\mu/m_\tau) = 0.765\,857\,423\ (16) .$$

and we have

$$a_\mu^{(4)\text{QED}} = 0.765\,857\,423\ (16) \left(\frac{\alpha}{\pi}\right)^2 \simeq 413217.627(9) \times 10^{-11} \quad (4.9)$$

for the complete 2-loop QED contribution to a_μ . The errors of $A_2^{(4)}(m_\mu/m_e)$ and $A_2^{(4)}(m_\mu/m_\tau)$ have been added in quadrature as the errors of the different measurements of the lepton masses may be treated as independent. The combined error $\delta C_2 = 1.6 \times 10^{-8}$ is negligible by the standards 1×10^{-5} of Table 4.1.

4.1.3 Three-Loop QED Contribution

At three loops in QED there are the 72 diagrams shown in Fig. 4.3 contributing to $g - 2$ of the muon. In closed fermion loops any of the SM fermions may circulate. The gauge invariant subset of 72 diagrams where all closed fermion loops are muon-loops yield the universal one-flavor QED contribution. This set has been calculated analytically mainly by Remiddi and his collaborators [15], and Laporta and Remiddi obtained the final result in 1996 after finding a trick to calculate the non-planar ‘‘triple cross’’ topology diagram (diagram 25 of Fig. 4.3) [16] (see also [17]). The result,

$$\begin{aligned} A_{1\text{uni}}^{(6)} = & \frac{28259}{5184} + \frac{17101}{810}\pi^2 - \frac{298}{9}\pi^2 \ln 2 + \frac{139}{18}\zeta(3) + \frac{100}{3} \left\{ \text{Li}_4\left(\frac{1}{2}\right) + \frac{1}{24} \ln^4 2 \right. \\ & \left. - \frac{1}{24}\pi^2 \ln^2 2 \right\} - \frac{239}{2160}\pi^4 + \frac{83}{72}\pi^2 \zeta(3) - \frac{215}{24}\zeta(5) = 1.181\,241\,456\,587\dots \quad (4.10) \end{aligned}$$

turned out to be surprisingly compact. All other corrections follow from Fig. 4.3 by replacing at least one muon in a loop by another lepton or quark. The such obtained mass dependent corrections are of particular interest because the light electron loops typically yield contributions, enhanced by large logarithms. Results for $A_2^{(6)}$ have been obtained in [18–22], for $A_3^{(6)}$ in [14, 23–25]. The leading terms of the expansion in the appropriate mass ratios have been discussed in Sect. 3.2.1 before. For the light-by-light contribution, graphs (1)–(6) of Fig. 4.3, the exact analytic result is known [21], but because of its length has not been published. The following asymptotic expansions are simple enough and match the requirement of the precision needed at the time:

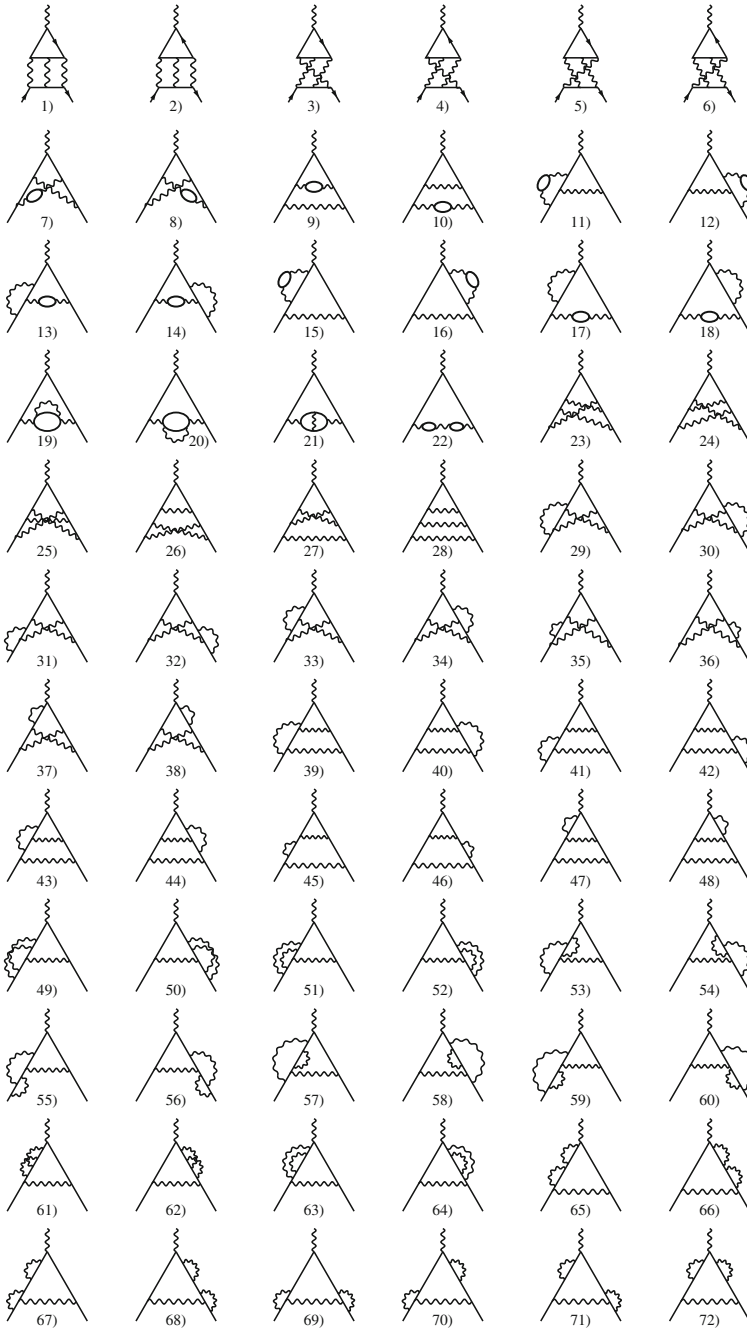


Fig. 4.3 The universal third order contribution to a_μ . All fermion loops here are muon-loops. Graphs (1)–(6) are the light-by-light scattering diagrams. Graphs (7)–(22) include photon vacuum polarization insertions. All non-universal contributions follow by replacing at least one muon in a closed loop by some other fermion

$$\begin{aligned}
A_{2\text{lbl}}^{(6)}(m_\mu/m_e) &= \frac{2}{3}\pi^2 \ln \frac{m_\mu}{m_e} + \frac{59}{270}\pi^4 - 3\zeta(3) - \frac{10}{3}\pi^2 + \frac{2}{3} \\
&+ \left(\frac{m_e}{m_\mu}\right) \left[\frac{4}{3}\pi^2 \ln \frac{m_\mu}{m_e} - \frac{196}{3}\pi^2 \ln 2 + \frac{424}{9}\pi^2 \right] \\
&+ \left(\frac{m_e}{m_\mu}\right)^2 \left[-\frac{2}{3} \ln^3 \frac{m_\mu}{m_e} + \left(\frac{\pi^2}{9} - \frac{20}{3}\right) \ln^2 \frac{m_\mu}{m_e} - \left(\frac{16}{135}\pi^4 + 4\zeta(3) - \frac{32}{9}\pi^2 \right. \right. \\
&\quad \left. \left. + \frac{61}{3}\right) \ln \frac{m_\mu}{m_e} + \frac{4}{3}\pi^2 \zeta(3) - \frac{61}{270}\pi^4 + 3\zeta(3) + \frac{25}{18}\pi^2 - \frac{283}{12} \right] \\
&+ \left(\frac{m_e}{m_\mu}\right)^3 \left[\frac{10}{9}\pi^2 \ln \frac{m_\mu}{m_e} - \frac{11}{9}\pi^2 \right] \\
&+ \left(\frac{m_e}{m_\mu}\right)^4 \left[\frac{7}{9} \ln^3 \frac{m_\mu}{m_e} + \frac{41}{18} \ln^2 \frac{m_\mu}{m_e} + \left(\frac{13}{9}\pi^2 + \frac{517}{108}\right) \ln \frac{m_\mu}{m_e} \right. \\
&\quad \left. + \frac{1}{2}\zeta(3) + \frac{191}{216}\pi^2 + \frac{13283}{2592} \right] + O\left((m_e/m_\mu)^5\right), \\
&= 20.94792485(14)
\end{aligned} \tag{4.11}$$

where here and in the following we use m_e/m_μ as given in (3.30). The leading term in the (m_e/m_μ) expansion turns out to be surprisingly large. It has been calculated first in [26]. Prior to the exact calculation in [21] good numerical estimates 20.9471(29) [27] and 20.9469(18) [28] have been available.

$$\begin{aligned}
A_{2\text{vap}}^{(6)}(m_\mu/m_e) &= \frac{2}{9} \ln^2 \frac{m_\mu}{m_e} + \left(\zeta(3) - \frac{2}{3}\pi^2 \ln 2 + \frac{1}{9}\pi^2 + \frac{31}{27}\right) \ln \frac{m_\mu}{m_e} \\
&+ \frac{11}{216}\pi^4 - \frac{2}{9}\pi^2 \ln^2 2 - \frac{8}{3}a_4 - \frac{1}{9} \ln^4 2 - 3\zeta(3) + \frac{5}{3}\pi^2 \ln 2 - \frac{25}{18}\pi^2 + \frac{1075}{216} \\
&+ \left(\frac{m_e}{m_\mu}\right) \left[-\frac{13}{18}\pi^3 - \frac{16}{9}\pi^2 \ln 2 + \frac{3199}{1080}\pi^2 \right] \\
&+ \left(\frac{m_e}{m_\mu}\right)^2 \left[\frac{10}{3} \ln^2 \frac{m_\mu}{m_e} - \frac{11}{9} \ln \frac{m_\mu}{m_e} - \frac{14}{3}\pi^2 \ln 2 - 2\zeta(3) + \frac{49}{12}\pi^2 - \frac{131}{54} \right] \\
&+ \left(\frac{m_e}{m_\mu}\right)^3 \left[\frac{4}{3}\pi^2 \ln \frac{m_\mu}{m_e} + \frac{35}{12}\pi^3 - \frac{16}{3}\pi^2 \ln 2 - \frac{5771}{1080}\pi^2 \right] \\
&+ \left(\frac{m_e}{m_\mu}\right)^4 \left[-\frac{25}{9} \ln^3 \left(\frac{m_\mu}{m_e}\right) - \frac{1369}{180} \ln^2 \left(\frac{m_\mu}{m_e}\right) + \left(-2\zeta(3) + 4\pi^2 \ln 2 - \frac{269}{144}\pi^2 \right. \right. \\
&\quad \left. \left. - \frac{7496}{675}\right) \ln \frac{m_\mu}{m_e} - \frac{43}{108}\pi^4 + \frac{8}{9}\pi^2 \ln^2 2 + \frac{80}{3}a_4 + \frac{10}{9} \ln^4 2 \right. \\
&\quad \left. + \frac{411}{32}\zeta(3) + \frac{89}{48}\pi^2 \ln 2 - \frac{1061}{864}\pi^2 - \frac{274511}{54000} \right] + O\left((m_e/m_\mu)^5\right), \\
&= 1.920455123(28)
\end{aligned} \tag{4.12}$$

The leading and finite terms were first given in [29], the correct (m_e/m_μ) terms have been given in [23]. In contrast to the LbL contribution the leading logs of the VP contribution may be obtained relatively easy by renormalization group considerations using the running fine structure constant [5, 30]. In place of the known but lengthy exact result only the expansion shown was presented in [20]. Despite the existence of large leading logs the VP contribution is an order of magnitude smaller than the one from the LbL graphs.

$$\begin{aligned}
A_{2\text{lbl}}^{(6)}(m_\mu/m_\tau) &= \frac{m_\mu^2}{m_\tau^2} \left[\frac{3}{2}\zeta_3 - \frac{19}{16} \right] \\
&+ \frac{m_\mu^4}{m_\tau^4} \left[\frac{13}{18}\zeta_3 - \frac{161}{1620}\zeta_2 - \frac{831931}{972000} - \frac{161}{3240}L^2 - \frac{16189}{97200}L \right] \\
&+ \frac{m_\mu^6}{m_\tau^6} \left[\frac{17}{36}\zeta_3 - \frac{13}{224}\zeta_2 - \frac{1840256147}{3556224000} - \frac{4381}{120960}L^2 - \frac{24761}{317520}L \right] \\
&+ \frac{m_\mu^8}{m_\tau^8} \left[\frac{7}{20}\zeta_3 - \frac{2047}{54000}\zeta_2 - \frac{453410778211}{1200225600000} - \frac{5207}{189000}L^2 - \frac{41940853}{952560000}L \right] \\
&+ \frac{m_\mu^{10}}{m_\tau^{10}} \left[\frac{5}{18}\zeta_3 - \frac{1187}{44550}\zeta_2 - \frac{86251554753071}{287550049248000} - \frac{328337}{14968800}L^2 - \frac{640572781}{23051952000}L \right] \\
&+ O\left((m_\mu/m_\tau)^{12}\right) = 0.002\,143\,239(385) \tag{4.13}
\end{aligned}$$

where $L = \ln(m_\tau^2/m_\mu^2)$, $\zeta_2 = \zeta(2) = \pi^2/6$ and $\zeta_3 = \zeta(3)$. The expansion given in [21] in place of the exact formula has been extended in [22] with the result presented here.

$$\begin{aligned}
A_{2\text{vap}}^{(6)}(m_\mu/m_\tau) &= \left(\frac{m_\mu}{m_\tau}\right)^2 \left[-\frac{23}{135} \ln \frac{m_\tau}{m_\mu} - \frac{2}{45}\pi^2 + \frac{10117}{24300} \right] \\
&+ \left(\frac{m_\mu}{m_\tau}\right)^4 \left[\frac{19}{2520} \ln^2 \frac{m_\tau}{m_\mu} - \frac{14233}{132300} \ln \frac{m_\tau}{m_\mu} + \frac{49}{768}\zeta(3) - \frac{11}{945}\pi^2 + \frac{2976691}{296352000} \right] \\
&+ \left(\frac{m_\mu}{m_\tau}\right)^6 \left[\frac{47}{3150} \ln^2 \frac{m_\tau}{m_\mu} - \frac{805489}{11907000} \ln \frac{m_\tau}{m_\mu} + \frac{119}{1920}\zeta(3) - \frac{128}{14175}\pi^2 \right. \\
&\quad \left. + \frac{102108163}{30005640000} \right] + O\left((m_\mu/m_\tau)^8\right) = -0.001\,782\,611(270) \tag{4.14}
\end{aligned}$$

Again, in place of exact result obtained in [20] only the expansion shown was presented in the paper. All the expansions presented are sufficient for numerical evaluations at the present level of accuracy. This has been cross checked recently against the exact results in [13].

At three loops for the first time a contribution to $A_3(m_\mu/m_e, m_\mu/m_\tau)$, depending on two mass ratios, shows up. It is represented by diagram (22) of Fig. 4.3 with one fermion loop an electron-loop and the other a τ -loop. In view of the general discussion of VP contributions in Sect. 3.8 it is obvious to write

$$a_\mu^{(6)}(\text{vap}, e, \tau) \Big|_{\text{dia 22}} = \frac{\alpha}{\pi} \int_0^1 dx (1-x) 2 \left[-\Pi'_{\gamma \text{ ren}} \left(\frac{-x^2 m_\mu^2}{1-x} \right) \right] \times \left[-\Pi'_{\gamma \text{ ren}} \left(\frac{-x^2 m_\mu^2}{1-x} \right) \right], \quad (4.15)$$

which together with (3.155) or (2.177) leads to a three-fold integral representation, which we may try to integrate. Since $\Pi'_{\gamma \text{ ren}}$ given by (2.176) is analytically known, in fact (4.15) is a one-fold integral representation. It has been calculated as an expansion in the two mass ratios in [23, 24] and was extended to $O((m_\mu^2/m_\tau^2)^5)$ recently in [25]. The result reads

$$\begin{aligned} A_{3 \text{ vap}}^{(6)}(m_\mu/m_e, m_\mu/m_\tau) &= \left(\frac{m_\mu^2}{m_\tau^2} \right) \left[\frac{2}{135} \ln \frac{m_\mu^2}{m_e^2} - \frac{1}{135} \right] \\ &+ \left(\frac{m_\mu^2}{m_\tau^2} \right)^2 \left[-\frac{1}{420} \ln \frac{m_\tau^2}{m_\mu^2} \ln \frac{m_\tau^2 m_\mu^2}{m_e^4} - \frac{37}{22050} \ln \frac{m_\tau^2}{m_e^2} + \frac{1}{504} \ln \frac{m_\mu^2}{m_e^2} + \frac{\pi^2}{630} \right. \\ &\quad \left. - \frac{229213}{12348000} \right] \\ &+ \left(\frac{m_\mu^2}{m_\tau^2} \right)^3 \left[-\frac{2}{945} \ln \frac{m_\tau^2}{m_\mu^2} \ln \frac{m_\tau^2 m_\mu^2}{m_e^4} - \frac{199}{297675} \ln \frac{m_\tau^2}{m_e^2} - \frac{1}{4725} \ln \frac{m_\mu^2}{m_e^2} + \frac{4\pi^2}{2835} \right. \\ &\quad \left. - \frac{1102961}{75014100} \right] \\ &+ \left(\frac{m_\mu^2}{m_\tau^2} \right)^4 \left[-\frac{1}{594} \ln \frac{m_\tau^2}{m_\mu^2} \ln \frac{m_\tau^2 m_\mu^2}{m_e^4} - \frac{391}{2058210} \ln \frac{m_\tau^2}{m_e^2} - \frac{19}{31185} \ln \frac{m_\mu^2}{m_e^2} + \frac{\pi^2}{891} \right. \\ &\quad \left. - \frac{161030983}{14263395300} \right] \\ &+ \frac{2}{15} \frac{m_e^2}{m_\tau^2} - \frac{4\pi^2}{45} \frac{m_e^3}{m_\tau^2 m_\mu} + \mathcal{O} \left[\left(\frac{m_\mu^2}{m_\tau^2} \right)^5 \ln \frac{m_\tau^2}{m_\mu^2} \ln \frac{m_\tau^2 m_\mu^2}{m_e^4} \right] + \mathcal{O} \left(\frac{m_e^2 m_\mu^2}{m_\tau^2 m_\tau^2} \right) \\ &= 0.00052776(10). \end{aligned} \quad (4.16)$$

The result is in agreement with the numerical evaluation [20]. The error in the result is due to the τ -lepton mass uncertainty. The leading-logarithmic term of this expansion corresponds to simply replacing $\alpha(q^2 = 0)$ by $\alpha(m_\mu^2)$ in the two-loop diagram with a τ loop. We have included the last term, with odd powers of m_e and m_μ , even though it is not relevant numerically. It illustrates typical contributions of the eikonal expansion, the only source of terms non-analytical in masses squared.

In [13] an additional term in the heavy mass expansion has been worked out. Expanding the exact Laporta-Remiddi expression for the sum of light-by-light and vacuum polarization contributions, for $r = m_i/m_j \ll 1$, one finds

$$\begin{aligned}
A_2^{(6)}(r) &= \sum_{i=1}^4 r^{2i} f_{2i}(r) + O(r^{10} \ln^2 r), \\
f_2(r) &= \frac{23 \ln r}{135} + \frac{3\zeta(3)}{2} - \frac{2\pi^2}{45} - \frac{74957}{97200}, \\
f_4(r) &= -\frac{4337 \ln^2 r}{22680} + \frac{209891 \ln r}{476280} + \frac{1811\zeta(3)}{2304} + \\
&\quad -\frac{1919\pi^2}{68040} - \frac{451205689}{533433600}, \\
f_6(r) &= -\frac{2807 \ln^2 r}{21600} + \frac{665641 \ln r}{2976750} + \frac{3077\zeta(3)}{5760} + \\
&\quad -\frac{16967\pi^2}{907200} - \frac{246800849221}{480090240000}, \\
f_8(r) &= -\frac{55163 \ln^2 r}{594000} + \frac{24063509989 \ln r}{172889640000} + \frac{9289\zeta(3)}{23040} + \\
&\quad -\frac{340019\pi^2}{24948000} - \frac{896194260575549}{2396250410400000}.
\end{aligned}$$

The functions $f_2(r)$ and $f_4(r)$ coincide with the expansions provided in [21], and $f_6(r)$ agrees with the combination of parts from [20] (for the vacuum polarization contribution) and [22] (heavy-mass expansions for the light-by-light diagrams). The coefficient $f_8(r)$ is new. The extra contributions are very small $\delta a_e \sim 1.3 \times 10^{-26}$ for μ -loops and $\delta a_\mu \sim -2.3 \times 10^{-18}$ for the τ -loops. Nevertheless, this provides an important crosscheck of previous results.

With (4.10) and (4.11)–(4.16) the complete three-loop QED contribution to a_μ is now known analytically, either in form of a series expansion or exact. The mass dependent terms may be summarized as follows:

$$\begin{aligned}
A_2^{(6)}(m_\mu/m_e) &= 22.868\,380\,00(17), \\
A_2^{(6)}(m_\mu/m_\tau) &= 0.000\,360\,63(12), \\
A_{3\text{ vap}}^{(6)}(m_\mu/m_e, m_\mu/m_\tau) &= 0.000\,527\,76(10).
\end{aligned} \tag{4.17}$$

As already mentioned above, the $A_2^{(6)}(m_\mu/m_e)$ contribution is surprisingly large and predominantly from light-by-light scattering via an electron loop. The importance of this term was discovered in [31], improved by numerical calculation in [2] and calculated analytically in [21]. Adding up the relevant terms we have

$$C_3 = 24.050\,509\,82 \tag{28}$$

or

$$a_\mu^{(6)\text{ QED}} = 24.050\,509\,82 \tag{28} \left(\frac{\alpha}{\pi}\right)^3 \simeq 30141.9022(4) \times 10^{-11} \tag{4.18}$$

as a result for the complete 3-loop QED contribution to a_μ . We have combined the first two errors of (4.17) in quadrature and the last linearly, as the latter depends on the same errors in the mass ratios.

4.1.4 Four-Loop QED Contribution

The calculation of the four-loop contribution to a_μ is a formidable task, as there are of the order of thousand diagrams to be calculated. Since the individual diagrams are much more complicated than the three-loop ones, only a few have been calculated analytically until recently [32–35]. In most cases one has to resort to numerical calculations. This approach has been developed and perfected over the past 35 years by Kinoshita and his collaborators [1, 2, 36–40] with the recalculations and improvements [41–46]. The $O(\alpha^4)$ contribution is sizable, about 6 standard deviations at current experimental accuracy, and a precise knowledge of this term is absolutely crucial for the comparison between theory and experiment. All the more, the pioneering essentially exact calculation by Laporta [47], which is leading in the electron $g - 2$, represents a new quality of the QED result.

The universal mass independent term $A_1^{(8)}$ (assuming single lepton flavor QED) is the sum of contributions from 891 diagrams, where samples are shown in Fig. 4.4. In a different classifications Figs. 4.6, 4.7, 4.8, 4.9 and 4.10 below, the vertex graphs can be obtained by inserting an external photon in each possible lepton line of 104 4-loop self-mass diagrams, excluding the vertex diagrams with closed lepton loops exhibiting an odd number of vertices, since they do not contribute as a consequence of Furry's theorem. This term represents the leading four-loop contribution to the electron anomaly a_e . As a result of the enduring heroic effort by Kinoshita a final answer has been obtained by Aoyama, Hayakawa, Kinoshita and Nio [43–46, 48], whom find⁴

⁴This challenging project has been initiated in the early 1980s by Kinoshita and Lindquist and lead to a first result in 1990 [37, 38]. As the subsequent ones, this result was obtained by numerical integration of the appropriately prepared Feynman integrals using the Monte Carlo integration routine VEGAS [49]. Since then a number of improved preliminary results have been published, which are collected in the following tabular form

$A_1^{(8)}$	year	Ref
-1.434 (138)	1983–1990	[38],
-1.557 (70)	1995	[50],
-1.4092 (384)	1997	[51],
-1.5098 (384)	2001	[52],
-1.7366 (60)	1999	[53],
-1.7260 (50)	2004	[42],
-1.7283 (35)	2005	[43],
-1.9144 (35)	2007	[44],
-1.9106 (20)	2012	[46],
-1.91298 (84)	2014	[48],

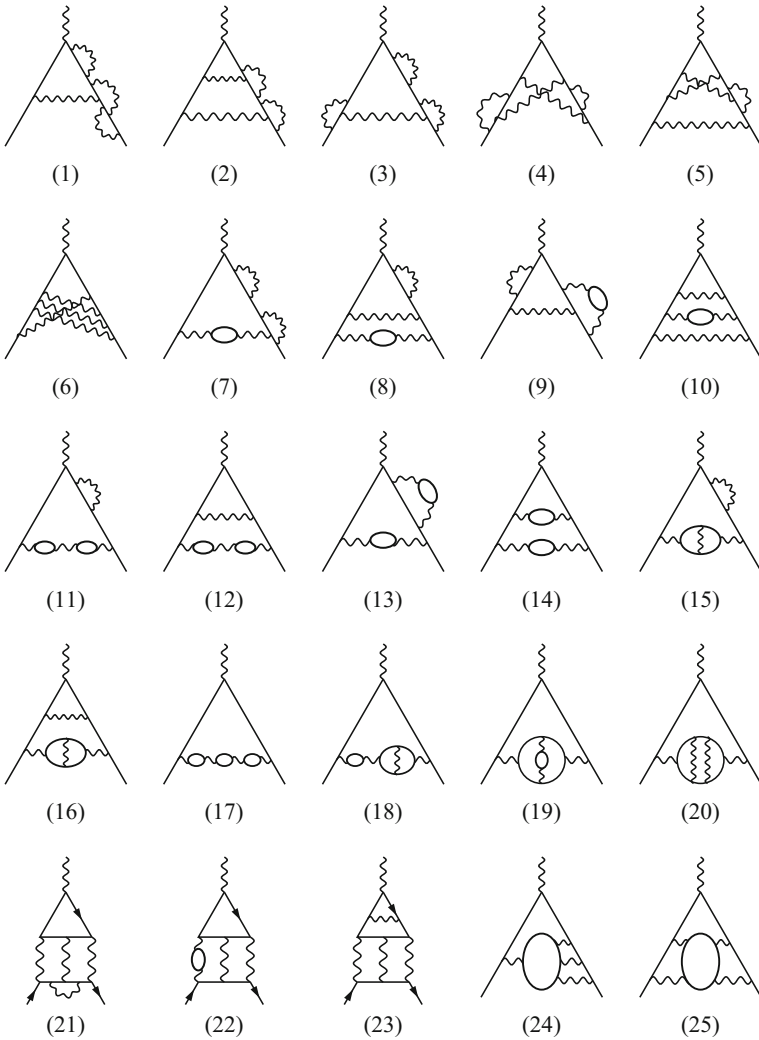


Fig. 4.4 Characteristic sample diagrams of the 25 gauge-invariant subsets of the 891 universal eight order contributions to a_ℓ . For the sets 1–16, 24, 25 each class is obtained by permuting separately the vertices attached to the left and right side of the main lepton vertex lines and also taking into account the mirror images of the diagrams. For the sets containing vacuum polarization ℓ -loops, the latter have to be permuted as an insertion into each internal photon line. The sets 21, 22 and 23 containing a light-by-light scattering subdiagram one has to include the permutations of the internal vertices of the corresponding ℓ -loop

$$A_1^{(8)} = -1.91298(84) \tag{4.19}$$

where the error is due to the Monte Carlo integration.

As already mentioned, a major breakthrough is the quasi-exact calculation of this universal 4-loop contribution which has been achieved by Laporta [47], after an epic 20 years effort [56–62]. The very high precision result obtained reads⁵

$$A_1^{(8)} = -1.912245764926445574152647167439830054060873390658725345 \dots \tag{4.20}$$

A semi-analytical expression is also given and will be reproduced below as Eq. (4.31). The result agrees to 0.9σ with (4.19). The 891 diagrams consist of 25 gauge-invariant subsets characterized by sample diagrams in Fig. 4.4. The results for the subsets are listed in Table 4.2. Adding respectively the contributions to a_e of diagrams with and without closed electron loops one finds

$$A_1^{(8)}(\text{no closed electron loops}) = -2.176866027739540077443259355895893938670 , \tag{4.21}$$

$$A_1^{(8)}(\text{closed electron loops only}) = 0.264620262813094503290612188456063884609 . \tag{4.22}$$

The contributions of the sets 17 and 18, the sum of contributions of the sets 11 and 12, and the sum of the contributions of the sets 15 and 16 are in perfect agreement with the analytical results of [63]. In the following we adopt the grouping of diagrams as in [45] where diagrams of Fig. 4.4 are rearranged as in Fig. 4.5: Ia = (17), Ib = (18), Ic = (19), Id = (20), IIa = (15 + 16), IIb = (13 + 14), IIc = (11 + 12), III = (7 + 8 + 9 + 10), IVa = (22), IVb = (23), IVc = (21), IVd = (24 + 25), V = (1 + 2 + 3 + 4 + 5 + 6). Exact results regrouped from Table 4.2 are included to Table 4.3. The agreement between [45] and [47] is remarkable.

In contrast to a_e , again the by far largest contribution to a_μ is due to $A_2^{(8)}(m_\mu/m_e)$, which collects the effects by the light internal electron loops in the muon vertex. Here 469 diagrams contribute which may be divided into four gauge invariant (g - i) groups:

Group I: 49 diagrams obtained from the 1-loop muon vertex by inserting 1-, 2- and 3-loop lepton VP sub-diagrams, i.e., the internal photon line of Fig. 4.1 is replaced

(Footnote 4 continued)

which illustrates the stability and continuous progress of the project. Such evaluations take typically three to six month of intense runs on high performance computers. To a large extend progress was driven by the growing computing power which became available. More recent results have been obtained utilizing the code-generating algorithm GENCODE_N which carries out all steps of the calculation automatically, including subtraction of ultraviolet and infrared divergences [54, 55].

⁵Laporta calculated the result numerically to 1100 digits. This high precision is required to find a semi-analytical expression (see (4.31) below) for the result, by means of the PSLQ technique. The expression contains harmonic polylogarithms of arguments $e^{\frac{i\pi}{3}}$, $e^{\frac{2i\pi}{3}}$, $e^{\frac{i\pi}{2}}$, one-dimensional integrals of products of complete elliptic integrals and six finite parts of master integrals, evaluated up to 4800 digits.

Table 4.2 Contribution to $A_1^{(8)}$ of the 25 gauge-invariant sets of Fig. 4.4

1	-1.971075616835818943645699655337264406980
2	-0.142487379799872157235945291684857370994
3	-0.621921063535072522104091223479317643540
4	1.086698394475818687601961404690600972373
5	-1.040542410012582012539438620994249955094
6	0.512462047967986870479954030909194465565
7	0.690448347591261501528101600354802517732
8	-0.056336090170533315910959439910250595939
9	0.409217028479188586590553833614638435425
10	0.374357934811899949081953855414943578759
11	-0.091305840068696773426479566945788826481
12	0.017853686549808578110691748056565649168
13	-0.034179376078562729210191880996726218580
14	0.006504148381814640990365761897425802288
15	-0.572471862194781916152750849945181037311
16	0.151989599685819639625280516106513042070
17	0.000876865858889990697913748939713726165
18	0.015325282902013380844497471345160318673
19	0.011130913987517388830956500920570148123
20	0.049513202559526235110472234651204851710
21	-1.138822876459974505563154431181111707424
22	0.598842072031421820464649513201747727836
23	0.822284485811034346719894048799598422606
24	-0.872657392077131517978401982381415610384
25	-0.117949868787420797062780493486346339829

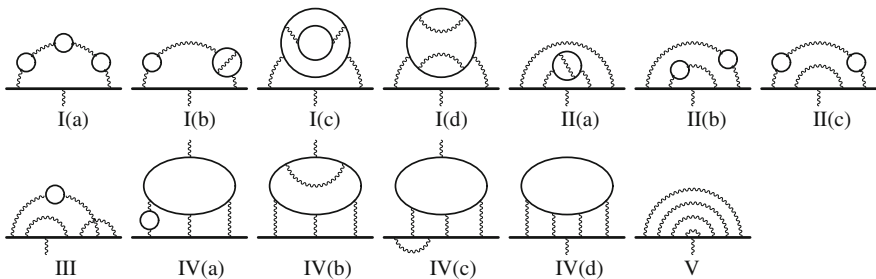


Fig. 4.5 Typical vertex diagrams representing 13 gauge-invariant subsets contributing to the eight-order lepton $g - 2$. [Reprinted with permission from [45]. Copyright ©(2012) by the American Physical Society]

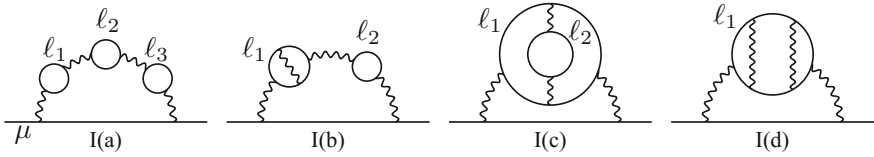


Fig. 4.6 Typical diagrams of subgroups I(a) (7 diagrams), I(b) (18 diagrams), I(c) (9 diagrams) and I(d) (15 diagrams). The lepton lines represent fermions propagating in an external magnetic field. l_i denote VP insertions

by the full propagator at 3–loops. The group is subdivided into four g - i subclasses I(a), I(b), I(c) and I(d) as shown in Fig. 4.6. Results for this group have been obtained by numerical and analytic methods [32–34, 41]. The numerical result [41]

$$A_{2I}^{(8)} = 16.721\,967\,(905) \text{ ,}$$

has been obtained by using simple integral representations.⁶

Group II: 90 diagrams generated from the 2–loop muon vertex by inserting 1–loop and/or 2–loop lepton VP sub-diagrams as shown in Fig. 4.7. Again results for this group have been obtained by numerical and analytic methods [32–34, 41]. The result here is [46]

$$A_{2II}^{(8)} = -16.673\,450\,(961) \text{ .}$$

⁶Subgroup I(a) has the integral representation

$$A_{2I(a)}^{(8)} = \int_0^1 dx (1-x) \left(\int_0^1 dt \frac{\rho_2(t)}{1 + [4/(1-t^2)](1-x)/x^2} \right)^3$$

where $\rho_2(t)$ is given by (3.156). Carrying out the t integral one obtains

$$A_{2I(a)}^{(8)} = \int_0^1 dx (1-x) \left[-\frac{8}{9} + \frac{a^2}{3} + \left(\frac{a}{2} - \frac{a^3}{6} \right) \ln \frac{a+1}{a-1} \right]^3$$

with $a = 2/(1-x)$. In this case also the last integration may be carried out analytically [64, 65]. Similarly, subgroup I(b) has the representation

$$A_{2I(b)}^{(8)} = 2 \int_0^1 dx (1-x) \left(\int_0^1 dt_1 \frac{\rho_2(t_1)}{1 + [4/(1-t_1^2)](1-x)/x^2} \right) \times \left(\int_0^1 dt_2 \frac{\rho_4(t_2)}{1 + [4/(1-t_2^2)](1-x)/x^2} \right)$$

with ρ_2 given by (3.156) and ρ_4 by (3.160), respectively.

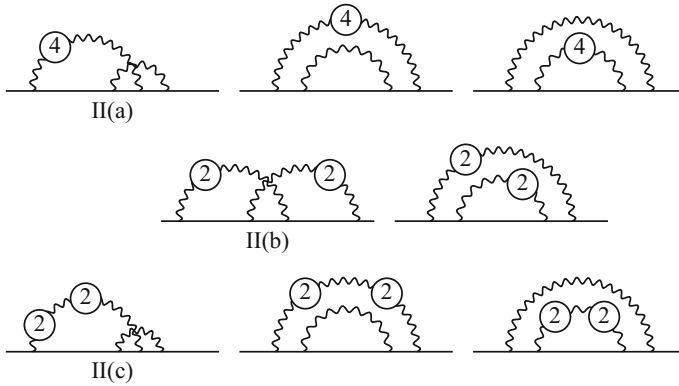


Fig. 4.7 Typical diagrams of group II (90 diagrams). The lepton lines as in Fig. 4.6. 2 and 4, respectively, indicate second (1-loop sub-diagrams) and fourth (2-loop sub-diagrams) order lepton-loops

Group III: 150 diagrams generated from the 3-loop muon vertex Fig. 4.3 by inserting one 1-loop electron VP sub-diagrams in each internal photon line in all possible ways. Examples are depicted in Fig. 4.8. This group has been calculated numerically only, with the result [46]

$$A_{2\text{III}}^{(8)} = 10.793\,40\,(270) .$$

Group IV: 180 diagrams with muon vertex containing LbL sub-graphs decorated with additional radiative corrections. This group is subdivided into *g-i* subsets IV(a), IV(b), IV(c) and IV(d) as illustrated in Fig. 4.9.

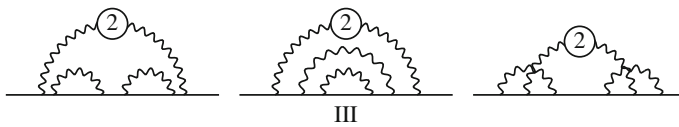


Fig. 4.8 Typical diagrams of group III (150 diagrams). The lepton lines as in Fig. 4.6

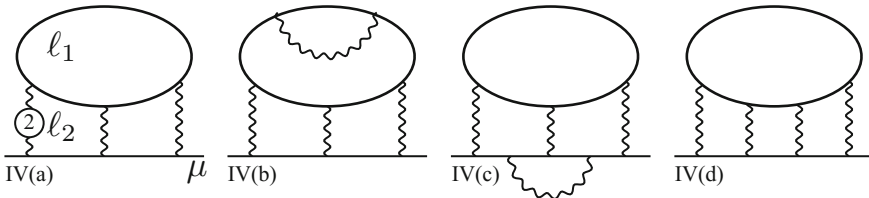


Fig. 4.9 Some typical diagrams of subgroups IVa (54 diagrams), IVb (60 diagrams), IVc (48 diagrams) and IVd (18 diagrams). The lepton lines as in Fig. 4.6

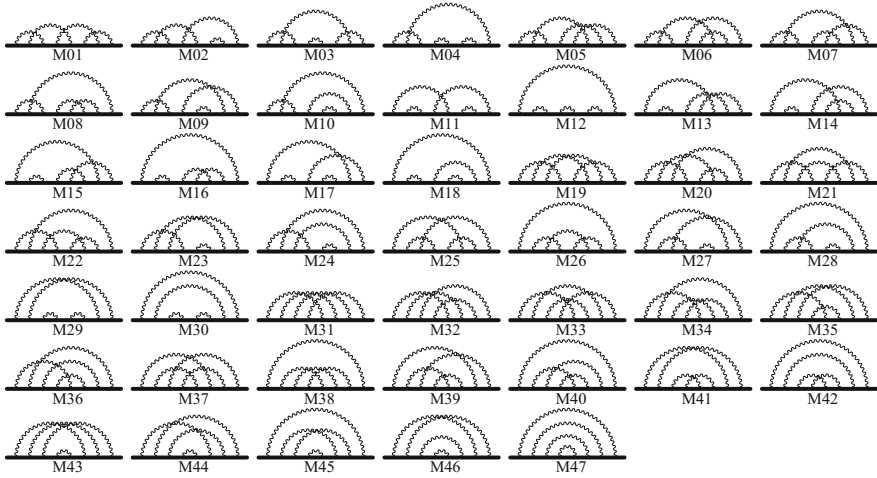


Fig. 4.10 4-loop Group V diagrams. 47 self-energy-like diagrams of $M_{01} - M_{47}$ represent 518 vertex diagrams (by inserting the external photon vertex on the virtual muon lines in all possible ways). They are represented by sets 1–6 in Fig. 4.4. [Reprinted with permission from [68]. Copyright ©(2007) by the American Physical Society]

The result of this calculation, which until recently was at the limit of the possibilities, was obtained by two independent methods in [41, 46] and reads⁷

$$A_{2IV}^{(8)} = 121.8433 \text{ (58)} .$$

Group V: 518 vertex diagrams which may be grouped into 47 lepton self-energy type diagrams as shown in Fig. 4.10. The result is [41, 46, 68]

$$A_{1V}^{(8)} = -2.1755 \text{ (20)} .$$

This result is superseded now by (4.21) with which it is in excellent agreement. Before Laporta’s result the contribution of the 518 diagrams without fermion loops has been responsible for the largest part of the uncertainty of the QED $O(\alpha^4)$ term. Note that the universal part of the $O(\alpha^4)$ contribution is leading for the electron $g - 2$, about 6 standard deviations at current experimental accuracy, and a precise knowledge of this term for the electron is absolutely crucial for the comparison between theory and experiment. So, big progress here.

⁷In fact the first result $(111.1 \pm 8.1) \times (\alpha/\pi)^4$ was obtained by Calmet and Petermann [66] in 1975 and was confirmed with $(117.4 \pm 0.5) \times (\alpha/\pi)^4$ by Samuel and Chlouber [67] in 1977.

Adding up the results from the different groups the new value for $A_2^{(8)}(m_\mu/m_e)$ reads

$$A_2^{(8)}(m_\mu/m_e) = 132.6852(60)[127.50(41)] , \quad (4.23)$$

in brackets an old value which was presented in [40]. In order to get some impression about the techniques and difficulties which have to be mastered we recommend the reader to study more carefully the original work like the recent articles [41, 43, 44].

There is also a small contribution from the term $A_3^{(8)}$, which depends on 3 masses, and which arises from 102 diagrams containing two or three closed loops of VP and/or LbL type. The contributions come from the classes I (30 diagrams), II (36 diagrams) and IV (36 diagrams) defined above and the results calculated in [41] read

$$\begin{aligned} A_{3I}^{(8)}(m_\mu/m_e, m_\mu/m_\tau) &= 0.007\,627\,(0) \\ A_{3II}^{(8)}(m_\mu/m_e, m_\mu/m_\tau) &= -0.028\,650\,(2) \\ A_{3IV}^{(8)}(m_\mu/m_e, m_\mu/m_\tau) &= 0.083\,739\,(36) \end{aligned} \quad (4.24)$$

which sum up to the value

$$A_3^{(8)}(m_\mu/m_e, m_\mu/m_\tau) = 0.06272(4) . \quad (4.25)$$

Improved estimates for the τ -loops contribution obtained in [46] yield the subclass results 0.00139(0) [I], $-0.01461(1)$ [II], 0.04504(14) [III] and 0.01052(12) [IV], which sum to

$$A_2^{(8)}(m_\mu/m_\tau) = 0.04234(12) . \quad (4.26)$$

In summary: all mass dependent as well as the mass independent $O(\alpha^4)$ QED contributions to a_μ have been recalculated by different methods by Kinoshita's group [41, 43, 44]. There is also substantial progress in analytic calculations [69–75]. The eighth-order light-by-light QED contributions from leptons with heavier masses have been reconsidered based on analytic results which are largely supporting and confirming the recent results [45, 46]. Contributions from specified sub-groups of diagrams shown in Fig. 4.5 are listed in Table 4.3 for the electron, including the universal part, and in Table 4.4 for the muon.

Collecting the $A^{(8)}$ terms for the muon discussed above we obtain

$$C_4 = 130.8734(60)$$

or

$$a_\mu^{(8)\text{ QED}} = 130.873\,4\,(60) \left(\frac{\alpha}{\pi}\right)^4 \simeq 380.990(17) \times 10^{-11} \quad (4.27)$$

as a result for the complete 4-loop QED contribution to a_μ .

Table 4.3 The eighth-order QED contribution from 12 gauge-invariant groups to electron $g - 2$ [45]. n_D shows the number of vertex diagrams contributing to $A_1^{(8)}$. The $A_1^{(8)}$ [47] column shows Laporta's exact values. The mass-dependence of $A_{3e}^{(8)}$ is $A_{3e}^{(8)}(m_e/m_\mu, m_e/m_\tau)$

Group	n_D	$A_1^{(8)}$ [47]	$A_{2e}^{(8)}(m_e/m_\mu) \times 10^3$	$A_{2e}^{(8)}(m_e/m_\tau) \times 10^5$	$A_{3e}^{(8)} \times 10^7$
I(a)	1	0.0008768659 ...	0.000 876 865	0.000 080 233 (5)	0.000 011 994 (1)
I(b)	6	0.0153252829 ...	0.015 325 20 (37)	0.000 602 805 (26)	0.000 014 097 (1)
I(c)	3	0.0111309140 ...	0.011 130 8 (9)	0.006 981 9 (12)	0.172 860 (21)
I(d)	15	0.0495132026 ...	0.049 514 8 (38)	0.000 874 4 (1)	0
II(a)	36	-0.4204822625 ...	-0.420 476 (11)	-0.045 648 (7)	0
II(b)	6	-0.0276752277 ...	-0.027 674 89 (74)	-0.030 393 7 (42)	-0.458 968 (17)
II(c)	12	-0.0734521535 ...	-0.073 445 8 (54)	-0.071 697 (25)	-1.189 69 (67)
III	150	1.4176872207 ...	1.417 637 (67)	0.6061 (12)	0
IV(a)	18	0.5988420720 ...	0.598 838 (19)	0.451 17 (69)	8.941 (17)
IV(b)	60	0.8222844858 ...	0.822 36 (13)	0.014 31 (95)	0
IV(c)	48	-1.1388228765 ...	-1.138 52 (20)	-0.102 (11)	0
IV(d)	18	-0.9906072609 ...	-0.990 72 (10)	-0.0927 (13)	0
V	518	-2.1768660277 ...	-2.1755 (20)	0	0

Table 4.4 The eighth-order mass-dependent QED contribution from 11 gauge-invariant groups to muon $g - 2$ [46], whose representatives are shown in Fig. 4.5. The mass-dependence of $A_{3\mu}^{(8)}$ is $A_{3\mu}^{(8)}(m_\mu/m_e, m_\mu/m_\tau)$

Group	$A_{2\mu}^{(8)}(m_\mu/m_e)$	$A_{2\mu}^{(8)}(m_\mu/m_\tau)$	$A_{3\mu}^{(8)}$
I(a)	7.74547 (42)	0.000032 (0)	0.003209 (0)
I(b)	7.58201 (71)	0.000252 (0)	0.002611 (0)
I(c)	1.624307 (40)	0.000737 (0)	0.001811 (0)
I(d)	-0.22982 (37)	0.000368 (0)	0.000000 (0)
II(a)	-2.77888 (38)	-0.007329 (1)	0.000000 (0)
II(b)	-4.55277 (30)	-0.002036 (0)	-0.009008 (1)
II(c)	-9.34180 (83)	-0.005246 (1)	-0.019642 (2)
III	10.7934 (27)	0.04504 (14)	0
IV(a)	123.78551 (44)	0.038513 (11)	0.083739 (36)
IV(b)	-0.4170 (37)	0.006106 (31)	0
IV(c)	2.9072 (44)	-0.01823 (11)	0
IV(d)	-4.43243 (58)	-0.015868 (37)	0
Sum	132.6852 (65)	0.04234 (10)	0.06272 (4)

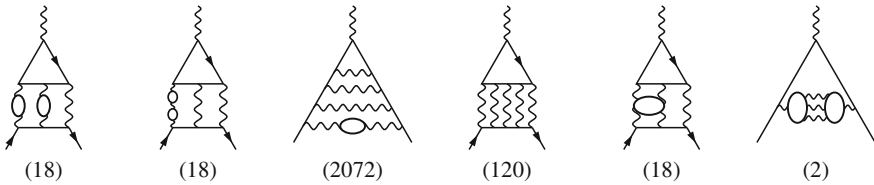


Fig. 4.11 Some typical tenth order contributions to a_ℓ including fermion loops. In brackets the number of diagrams of the given type

4.1.5 Five-Loop QED Contribution

Here the number of diagrams (see Fig. 4.11) is in the 10 000. Alone the universal $A_1^{(10)}$ term has contributions from 12 672 diagrams. The latter are grouped into six gauge-invariant sets I–VI, which are further subdivided into 32 gauge-invariant subsets depending on the type of lepton loops involved. Set V is the set without closed lepton loops. It is the largest and most difficult set to evaluate consisting of 6354 diagrams, and has been accurately evaluated only recently by Aoyama et al. [48]. The 31 sets with closed lepton loops consist of 6318 vertex diagrams and have been presented in Refs. [76–85]. The results of all ten subsets of Set I have been confirmed by Ref. [86, 87] by analytic and/or semi-analytic methods (see Table 4.10). The five-loop contribution originally was evaluated using renormalization group

(RG) arguments in [2, 88]. An earlier estimate by Kinoshita and Nio [42, 76] was⁸ $A_2^{(10)}(m_\mu/m_e) = 663(20)$, which was subsequently crosschecked by Kataev [89] using renormalization group arguments. Some five-loop graphs were first calculated by Laporta [90]. The estimates of the leading contribution is superseded now by the first complete tenth-order calculation by Aoyama et al. [46]. They find

$$\begin{aligned} A_2^{(10)}(m_\mu/m_e) &= 742.18 \quad (87), \\ A_2^{(10)}(m_\mu/m_\tau) &= -0.068 \quad (5), \\ A_3^{(10)}(m_\mu/m_e, m_\mu/m_\tau) &= 2.011 \quad (10), \end{aligned}$$

by numerically evaluating all Feynman diagrams. The error represents the statistical fluctuation of the Monte-Carlo integration. The contributions are tabulated in detail Table 4.5 from [45, 46]. The universal part has been calculated recently to be [45]

$$A_1^{(10)} = 7.795(336). \quad (4.28)$$

Thus we arrive at

$$C_5 \sim 751.917(932)$$

or

$$a_\mu^{(10)\text{ QED}} \sim 751.917(932) \left(\frac{\alpha}{\pi}\right)^5 \simeq 5.0845(63) \times 10^{-11} \quad (4.29)$$

as a result of the 5-loop QED contribution [46].

Results from individual sub-groups of diagrams are reproduced for the electron and the muon in Table 4.10.

In Table 4.6 we summarize the results of the QED calculations. The expansion coefficients C_i which multiply $(\alpha/\pi)^i$ are given for a_e and for a_μ for comparison. The coefficients for a_e remain small and are alternating while for a_μ they grow rapidly with the order. Nevertheless, because of the smallness of the expansion parameter α/π , the convergence of the perturbative expansion of a_μ^{QED} is good. We conclude that the perturbative truncation error looks to be well under control at the present level of accuracy. It is interesting to compare the QED contributions to a_e with the ones dominating/determining a_μ . For the electron the universal A_1 part is dominating, for the muon the mass dependent $A_2(m_\mu/m_e)$ part. For the muon the light electron loops produce the large logarithms $\ln m_\mu/m_e$ which make the corresponding mass dependent terms the leading ones. These grow with increasing order and are all positive. Beyond the lowest order a_e and a_μ are testing different groups of diagrams.

⁸The first estimate $A_2^{(10)}(m_\mu/m_e) \sim 930(170)$ has been given by Karshenboim [88].

Table 4.5 Summary of contributions to the tenth-order lepton $g-2$ from 32 gauge-invariant subsets from [45, 48]. n_F is the number of vertex diagrams contributing to $A_1^{(10)}$. The 3 entries to the right are the mass-dependent contribution to the muon $g-2$ from 32 gauge-invariant subsets shown in Fig. 4.12. The mass-dependence of $A_{3\mu}^{(10)}$ is $A_{3\mu}^{(10)}(m_\mu/m_e, m_\mu/m_\tau)$

Group	n_D	Lepton	Electron	Muon		
		$A_1^{(10)}$	$A_{2e}^{(10)}(m_e/m_\mu)$	$A_{2\mu}^{(10)}(m_\mu/m_e)$	$A_{2\mu}^{(10)}(m_\mu/m_\tau)$	$A_{3\mu}^{(10)}$
I(a)	1	0.00047094(6)	0.00000028(1)	22.566973(3)	0.000038(0)	0.017312(1)
I(b)	9	0.0070108(7)	0.00000188(1)	30.667091(3)	0.000269(0)	0.020179(1)
I(c)	9	0.023468(2)	0.00000267(1)	5.141395(1)	0.000397(0)	0.002330(0)
I(d)	6	0.0038017(5)	0.00000546(1)	8.8921(11)	0.000388(0)	0.024487(2)
I(e)	30	0.010296(4)	0.00000160(1)	-0.9312(24)	0.000232(0)	0.002370(0)
I(f)	3	0.0075684(20)	0.00004754(1)	3.685049(90)	0.002162(0)	0.023390(2)
I(g)	9	0.028569(6)	0.00002445(1)	2.60787(72)	0.001698(0)	0.002729(1)
I(h)	30	0.001696(13)	-0.00001014(3)	-0.5686(11)	0.000163(1)	0.001976(3)
I(i)	105	0.01747(11)	0.00000167(2)	0.0871(59)	0.000024(0)	0
I(j)	6	0.0003975(18)	0.00000241(6)	-1.26372(14)	0.000168(1)	0.000110(5)
II(a)	24	-0.109495(23)	-0.00073769(95)	-70.4717(38)	-0.018882(8)	-0.290853(85)
II(b)	108	-0.473559(84)	-0.00064562(95)	-34.7715(26)	-0.035615(20)	-0.127369(60)
II(c)	36	-0.116489(32)	-0.00038025(46)	-5.38575(99)	-0.016348(14)	-0.040800(51)
II(d)	180	-0.24300(29)	-0.00009817(41)	0.4972(65)	-0.007673(14)	0
II(e)	180	-1.3449(10)	-0.0004650(40)	3.265(12)	-0.03806(13)	0
II(f)	72	-2.4336(15)	-0.005868(39)	-77.465(12)	-0.26723(73)	-0.50295(68)
III(a)	300	2.12733(17)	0.007511(11)	109.116(33)	0.283000(32)	0.89140(44)
III(b)	450	3.32712(45)	0.002794(1)	11.9367(45)	0.143600(10)	0
III(c)	390	4.921(11)	0.00370(36)	7.37(15)	0.1999(28)	0
IV	2072	-7.7296(48)	-0.01136(7)	-38.79(17)	-0.44357(25)	0
V	6354	8.762(336)	0			0
VI(a)	36	1.04132(19)	0.006152(11)	629.141(12)	0.24610(18)	2.3590(18)
VI(b)	54	1.34699(28)	0.0017789(35)	181.1285(51)	0.096522(93)	0.19476(26)
VI(c)	144	-2.5289(28)	-0.005953(59)	-36.58(12)	-0.2601(28)	-0.5018(89)
VI(d)	492	1.8467(70)	0.001276(76)	-7.92(60)	0.0818(17)	0
VI(e)	48	-0.4312(7)	-0.000750(8)	-4.32(14)	-0.03594(32)	-0.1122(24)
VI(f)	180	0.7703(22)	0.000033(7)	-38.16(15)	0.04347(85)	0.0659(31)
VI(g)	480	-1.5904(63)	-0.000497(29)	6.96(48)	-0.04451(96)	0
VI(h)	630	0.1792(39)	0.000045(9)	-8.55(23)	0.00485(46)	0
VI(i)	60	-0.0438(12)	-0.000326(1)	-27.34(12)	-0.00345(33)	-0.0027(11)
VI(j)	54	-0.2288(18)	-0.000127(13)	-25.505(20)	-0.01149(33)	-0.01603(58)
VI(k)	120	0.6802(38)	0.0000156(40)	97.123(62)	0.00217(16)	0
Sum	12672	7.793(336)	-0.003824(144)	742.18(87)	-0.068(5)	2.011(10)

Table 4.6 Summary of QED contributions to a_μ , including a comparison of the QED coefficients for a_e and a_μ , respectively

C_i	$\ell = e$	$\ell = \mu$	$a_\mu^{(2i)\text{ QED}} \times 10^{11}$
C_1	0.5	0.5	$a^{(2)}$ 116140973.242(26)
C_2	-0.328 478 444 00 ...	0.765 857 423 (16)	$a^{(4)}$ 413217.627(9)
C_3	1.181 234 017 ...	24.050 509 82 (28)	$a^{(6)}$ 30141.9022(4)
C_4	-1.9113(18)	130.8734(60)	$a^{(8)}$ 380.990(17)
C_5	9.16(58)	751.92(93)	$a^{(10)}$ 5.0845(63)

The universal QED terms have been summarized in (3.45) and adding up the mass dependent QED terms of the 3 flavors (e, μ, τ) we finally obtain

$$a_\mu^{\text{QED}} = 116\,584\,718.859(.026)(.009)(.017)(.006)[.034] \times 10^{-11}. \quad (4.30)$$

The errors are given by the uncertainties in α_{input} and in the mass ratios, and the numerical errors of the α^4 and α^5 terms, respectively. Note that the missing 6-loop contributions are expected to be larger than the tenth-order uncertainty now. First results based on asymptotic expansion techniques have been obtained by the Karlsruhe group in [71]. More recent result have been presented in [70, 72, 73, 75, 91]. They will be briefly discussed in the following subsection.

4.1.6 Four- and Five-Loop Analytic Results and Crosschecks

The big advantage of the analytic result is that it allows a numerical evaluation at any desired precision. The direct numerical evaluation of the multidimensional Feynman integrals by Monte Carlo methods is always of limited precision and an improvement is always very expensive in computing power. Thus working out analytic or semi-analytic results is important where possible. In fact analytic evaluations have been very important for finding bugs in numerical codes and for improvements in the numerical uncertainties. Vice versa, numerical results provide benchmarks for developing reliable analytic codes.

Most analytic results available in the literature have been obtained with the help of the dispersive approach discussed in Sect. 3.8. Also the α - and/or Feynman-parametric approach introduced in Sect. 2.5, in conjunction with a power series expansion in the mass ratios, sometimes combined with Padé approximants, is a reliable tool in calculating the complicated higher loop diagrams.

For early attempts to perform four-loop $g - 2$ calculations for subsets of diagrams analytically we refer to [32–34]. More recently substantial progress has been possible by more automatized calculations, improved algorithms and last but not least by the increasing computing power which has become available. Among the standard

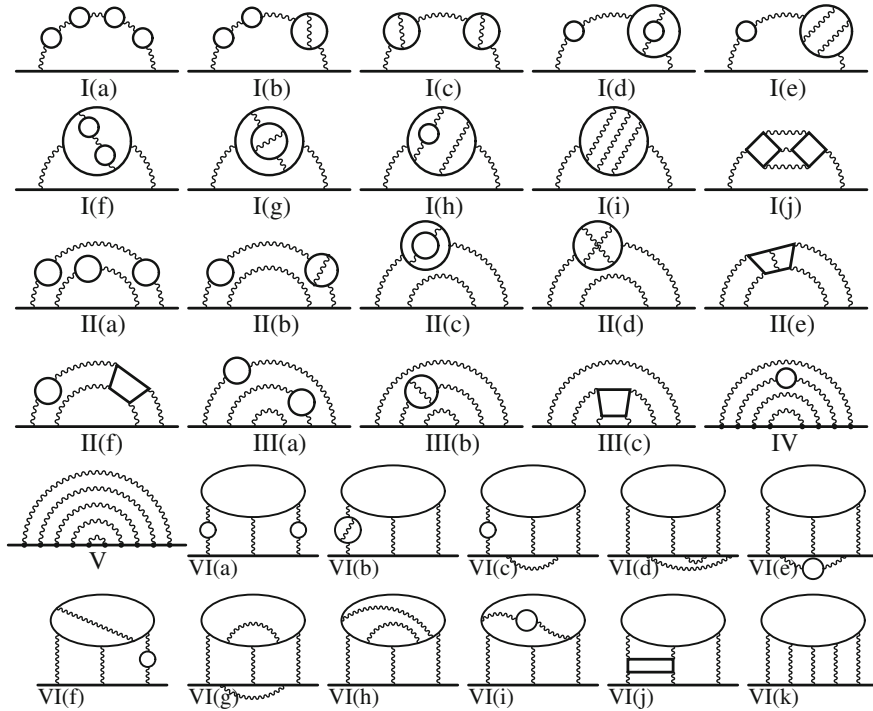


Fig. 4.12 Typical self-energy-like diagrams representing 32 gauge-invariant subsets contributing to the tenth-order lepton $g-2$. *Solid lines* represent lepton lines propagating in a weak magnetic field. [Reprinted with permission from [45]. Copyright ©(2012) by the American Physical Society]

tools we mention the automatic Feynman graph generation program `qgraf` [92] for which there exist interfaces, like `q2e2`, which translate `qgraf` output into input for the computer algebra package `FORM` [93, 94] and `TFORM` [95, 96]. The latter are used for the reduction of the tensor structure and the traces of Dirac matrices. Computer algebra systems like `FERMAT` [97] may be helpful for simplifying multivariable polynomials and rational functions in the kinematic variables. The `MATHEMATICA` package `ASY` [98, 99] is available for performing power series expansion in masses and/or momenta. It is based on the strategy of expansion by regions [96, 100–102] which provides an asymptotic expansion of a given Feynman integral in a given limit represented as a finite sum of contributions corresponding to so-called regions (i.e., scaling of components of loop momenta or Feynman parameters). Each term of such contributions is manifestly homogeneous with respect to the expansion parameter. The programs `FIRE` [103] and `crusher` [91, 104] allow to reduce integrals to a set of known master integrals. Both programs implement Laporta’s difference equations algorithm [33, 56] for the solution of integration-by-parts identities [105, 106]. Master integrals have been largely classified and the simpler ones are known analytically or are known as one or two dimensional integrals over analytically known

functions. The more complicated ones may be evaluated using Mellin–Barnes techniques [107, 108], which has been implemented in the MATHEMATICA program MB [109]. Also the $\epsilon = 4 - d$ expansion, $\epsilon \rightarrow +0$ introduced in Sect. 2.5 has been implemented in a computer code. The ϵ expansion of the remaining master integrals may be computed numerically with the help of FIESTA [110]. In many cases the PSLQ approach [111], an integer relation finding algorithm, allows one to find exact analytic results from very high precision numerical ones, as one in general knows what type of transcendental elements (π^n , $\zeta(n)$, log's, polylogs etc.) could show up in the results.

In the following we review the status of the four- and five-loop results at the level of a numerical comparison. The analytic results, often available as a series expansion, typically are lengthy and will not be reproduced here. We refer the interested reader to the original literature, where also the technical details of the calculations may be found.

Four-Loop Analytic Results and Crosschecks

We remind that loop calculations require regularization and renormalization. Applying dimensional regularization always requires the appropriate ϵ -expansion, before taking the limit $\epsilon \rightarrow 0$. In higher-loop calculations this by itself is a formidable task and a matter of efficient computer algebra codes. Most remarkably the 4-loop universal contribution A_1^8 (4.20) can be considered to be known analytically after two decennials of efforts by Laporta [47]. The contributions from all 891 diagrams are expressed algebraically by means of 334 master integrals (it corresponds to the generalization of the reduction of the tensor integral in terms of scalar integrals (so called master integrals) disentangled from the particle spin complications, which we outlined in Sect. 2.5.7) belonging to 220 topologies. The method used for the computation of the master integrals with a precision up to 9600 digits is largely based on the difference equation method [56, 57] and the differential equation method [112–114]. Thereby large systems of difference and differential equations are solved numerically on high performance computers. Most master integrals are related the polylogarithmic and harmonic polylogarithmic integrals which have been well investigated in the literature. The most complicated master integrals are of elliptical type (see Fig. 4.13). One obtains a family of one-dimensional integrals of products of elliptic integrals (itself defined by one-dimensional integrals see Sect. 3.8.1). Laporta then has fitted the analytical expressions to high precision numerical values of all master integrals and diagram contributions using the PSLQ algorithm.⁹

⁹Let me explain this in case of the universal 3-loop result (4.10). Suppose you have a very high precision numerical value for $A_{1\text{uni}}^{(6)}$ on the l.h.s. and you know which transcendental objects from the list (3.185) could show up (knowing the types of master integrals and the transcendentals which are associated with them) one can find the rational coefficients on the r.h.s. of (4.10) by fitting the r.h.s. to the value on the l.h.s. Since one can multiply the equation with the common divisor of the rational coefficients the general problem requires to find integers a_i , not all zero, which fit an equation of the form $a_1x_1 + a_2x_2 + \dots + a_nx_n = 0$ where (x_1, x_2, \dots, x_n) is a given vector of real or complex numbers (from a basis of transcendentals). Often this method is the only known way to find a closed analytic expression of an integral.

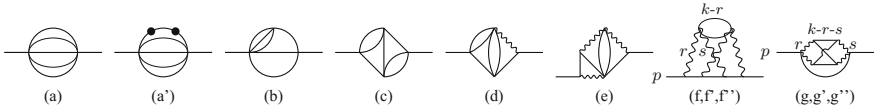


Fig. 4.13 Minimal set of master integrals which contain the elliptical constants. *Full lines* represent scalar propagators, *wiggly lines* massless (photons). The *double dot* in (a') indicate that the propagator represented by the line is to be raised to the third power. (f,f',f'') and (g,g',g'') have numerators $(1, p \cdot k, (p \cdot k)^2)$, respectively

No doubt, Laporta's result is a milestone for the books. I reproduce his semi-analytic result, which in view of the complexity of the problem looks fairly compact. The result of the PSLQ analytical fit can be written as follows:

$$A_{1\text{uni}}^{(8)} = T_0 + T_2 + T_3 + T_4 + T_5 + T_6 + T_7 + \sqrt{3}(V_{4a} + V_{6a}) + V_{6b} + V_{7b} + W_{6b} + W_{7b} + \sqrt{3}(E_{4a} + E_{5a} + E_{6a} + E_{7a}) + E_{6b} + E_{7b} + U. \tag{4.31}$$

The terms have been arranged in blocks with equal transcendental weight (see (3.185)). The index number is the weight. The terms containing the "usual" transcendental constants (3.186) are:

$$T_0 + T_2 + T_3 = \frac{1243127611}{130636800} + \frac{30180451}{25920}\zeta(2) - \frac{255842141}{2721600}\zeta(3) - \frac{8873}{3}\zeta(2)\ln 2,$$

$$T_4 = \frac{6768227}{2160}\zeta(4) + \frac{19063}{360}\zeta(2)\ln^2 2 + \frac{12097}{90}\left(a_4 + \frac{1}{24}\ln^4 2\right),$$

$$T_5 = -\frac{2862857}{6480}\zeta(5) - \frac{12720907}{64800}\zeta(3)\zeta(2) - \frac{221581}{2160}\zeta(4)\ln 2 + \frac{9656}{27}\left(a_5 + \frac{1}{12}\zeta(2)\ln^3 2 - \frac{1}{120}\ln^5 2\right),$$

$$T_6 = \frac{191490607}{46656}\zeta(6) + \frac{10358551}{43200}\zeta^2(3) - \frac{40136}{27}a_6 + \frac{26404}{27}b_6 - \frac{700706}{675}a_4\zeta(2) - \frac{26404}{27}a_5\ln 2 + \frac{26404}{27}\zeta(5)\ln 2 - \frac{63749}{50}\zeta(3)\zeta(2)\ln 2 - \frac{40723}{135}\zeta(4)\ln^2 2 + \frac{13202}{81}\zeta(3)\ln^3 2 - \frac{253201}{2700}\zeta(2)\ln^4 2 + \frac{7657}{1620}\ln^6 2,$$

$$\begin{aligned}
T_7 = & \frac{2895304273}{435456} \zeta(7) + \frac{670276309}{193536} \zeta(4) \zeta(3) + \frac{85933}{63} a_4 \zeta(3) + \frac{7121162687}{967680} \zeta(5) \zeta(2) \\
& - \frac{142793}{18} a_5 \zeta(2) - \frac{195848}{21} a_7 + \frac{195848}{63} b_7 - \frac{116506}{189} d_7 \\
& - \frac{4136495}{384} \zeta(6) \ln 2 - \frac{1053568}{189} a_6 \ln 2 + \frac{233012}{189} b_6 \ln 2 + \frac{407771}{432} \zeta^2(3) \ln 2 \\
& - \frac{8937}{2} a_4 \zeta(2) \ln 2 + \frac{833683}{3024} \zeta(5) \ln^2 2 - \frac{3995099}{6048} \zeta(3) \zeta(2) \ln^2 2 - \frac{233012}{189} a_5 \ln^2 2 \\
& + \frac{1705273}{1512} \zeta(4) \ln^3 2 + \frac{602303}{4536} \zeta(3) \ln^4 2 - \frac{1650461}{11340} \zeta(2) \ln^5 2 + \frac{52177}{15876} \ln^7 2.
\end{aligned}$$

The terms containing harmonic polylogarithms of $e^{i\frac{\pi}{3}}$, $e^{\frac{2i\pi}{3}}$:

$$\begin{aligned}
V_{4a} = & -\frac{14101}{480} \text{Cl}_4\left(\frac{\pi}{3}\right) - \frac{169703}{1440} \zeta(2) \text{Cl}_2\left(\frac{\pi}{3}\right), \\
V_{6a} = & \frac{494}{27} \text{Im } H_{0,0,0,1,-1,-1}\left(e^{i\frac{\pi}{3}}\right) + \frac{494}{27} \text{Im } H_{0,0,0,1,-1,1}\left(e^{i\frac{2\pi}{3}}\right) \\
& + \frac{494}{27} \text{Im } H_{0,0,0,1,1,-1}\left(e^{i\frac{2\pi}{3}}\right) \\
& + 19 \text{Im } H_{0,0,1,0,1,1}\left(e^{i\frac{2\pi}{3}}\right) + \frac{437}{12} \text{Im } H_{0,0,0,1,1,1}\left(e^{i\frac{2\pi}{3}}\right) + \frac{29812}{297} \text{Cl}_6\left(\frac{\pi}{3}\right) \\
& + \frac{4940}{81} a_4 \text{Cl}_2\left(\frac{\pi}{3}\right) - \frac{520847}{69984} \zeta(5) \pi - \frac{129251}{81} \zeta(4) \text{Cl}_2\left(\frac{\pi}{3}\right) \\
& - \frac{892}{15} \text{Im } H_{0,1,1,-1}\left(e^{i\frac{2\pi}{3}}\right) \zeta(2) - \frac{1784}{45} \text{Im } H_{0,1,1,-1}\left(e^{i\frac{\pi}{3}}\right) \zeta(2) \\
& + \frac{1729}{54} \zeta(3) \text{Im } H_{0,1,-1}\left(e^{i\frac{\pi}{3}}\right) \\
& + \frac{1729}{36} \zeta(3) \text{Im } H_{0,1,1}\left(e^{i\frac{2\pi}{3}}\right) + \frac{837190}{729} \text{Cl}_4\left(\frac{\pi}{3}\right) \zeta(2) + \frac{25937}{4860} \zeta(3) \zeta(2) \pi \\
& - \frac{223}{243} \zeta(4) \pi \ln 2 + \frac{892}{9} \text{Im } H_{0,1,-1}\left(e^{i\frac{\pi}{3}}\right) \zeta(2) \ln 2 + \frac{446}{3} \text{Im } H_{0,1,1}\left(e^{i\frac{2\pi}{3}}\right) \zeta(2) \ln 2 \\
& - \frac{7925}{81} \text{Cl}_2\left(\frac{\pi}{3}\right) \zeta(2) \ln^2 2 + \frac{1235}{486} \text{Cl}_2\left(\frac{\pi}{3}\right) \ln^4 2,
\end{aligned}$$

$$V_{6b} = \frac{13487}{60} \operatorname{Re} H_{0,0,0,1,0,1} \left(e^{i\frac{\pi}{3}} \right) + \frac{13487}{60} \operatorname{Cl}_4 \left(\frac{\pi}{3} \right) \operatorname{Cl}_2 \left(\frac{\pi}{3} \right) + \frac{136781}{360} \operatorname{Cl}_2^2 \left(\frac{\pi}{3} \right) \zeta(2),$$

$$\begin{aligned} V_{7b} &= \frac{651}{4} \operatorname{Re} H_{0,0,0,1,0,1,-1} \left(e^{i\frac{\pi}{3}} \right) + 651 \operatorname{Re} H_{0,0,0,0,1,1,-1} \left(e^{i\frac{\pi}{3}} \right) \\ &\quad - \frac{17577}{32} \operatorname{Re} H_{0,0,1,0,0,1,1} \left(e^{i\frac{2\pi}{3}} \right) \\ &\quad - \frac{87885}{64} \operatorname{Re} H_{0,0,0,1,0,1,1} \left(e^{i\frac{2\pi}{3}} \right) - \frac{17577}{8} \operatorname{Re} H_{0,0,0,0,1,1,1} \left(e^{i\frac{2\pi}{3}} \right) \\ &\quad + \frac{651}{4} \operatorname{Cl}_4 \left(\frac{\pi}{3} \right) \operatorname{Im} H_{0,1,-1} \left(e^{i\frac{\pi}{3}} \right) \\ &\quad + \frac{1953}{8} \operatorname{Cl}_4 \left(\frac{\pi}{3} \right) \operatorname{Im} H_{0,1,1} \left(e^{i\frac{2\pi}{3}} \right) + \frac{31465}{176} \operatorname{Cl}_6 \left(\frac{\pi}{3} \right) \pi \\ &\quad + \frac{211}{4} \operatorname{Re} H_{0,1,0,1,-1} \left(e^{i\frac{\pi}{3}} \right) \zeta(2) \\ &\quad + \frac{211}{2} \operatorname{Re} H_{0,0,1,1,-1} \left(e^{i\frac{\pi}{3}} \right) \zeta(2) + \frac{1899}{16} \operatorname{Re} H_{0,1,0,1,1} \left(e^{i\frac{2\pi}{3}} \right) \zeta(2) \\ &\quad + \frac{1899}{8} \operatorname{Re} H_{0,0,1,1,1} \left(e^{i\frac{2\pi}{3}} \right) \zeta(2) \\ &\quad + \frac{211}{4} \operatorname{Im} H_{0,1,-1} \left(e^{i\frac{\pi}{3}} \right) \operatorname{Cl}_2 \left(\frac{\pi}{3} \right) \zeta(2) + \frac{633}{8} \operatorname{Im} H_{0,1,1} \left(e^{i\frac{2\pi}{3}} \right) \operatorname{Cl}_2 \left(\frac{\pi}{3} \right) \zeta(2). \end{aligned}$$

The terms containing harmonic polylogarithms of $e^{i\frac{\pi}{2}}$:

$$W_{6b} = -\frac{28276}{25} \zeta(2) \operatorname{Cl}_2 \left(\frac{\pi}{2} \right)^2,$$

$$\begin{aligned} W_{7b} &= 104 \left(4 \operatorname{Re} H_{0,1,0,1,1} \left(e^{i\frac{\pi}{2}} \right) \zeta(2) + 4 \operatorname{Im} H_{0,1,1} \left(e^{i\frac{\pi}{2}} \right) \operatorname{Cl}_2 \left(\frac{\pi}{2} \right) \zeta(2) - 2 \operatorname{Cl}_4 \left(\frac{\pi}{2} \right) \zeta(2) \pi \right. \\ &\quad \left. + \operatorname{Cl}_2^2 \left(\frac{\pi}{2} \right) \zeta(2) \ln 2 \right). \end{aligned}$$

The terms containing elliptic constants:

$$E_{4a} = \pi \left(-\frac{28458503}{691200} B_3 + \frac{250077961}{18662400} C_3 \right),$$

$$E_{5a} = \frac{483913}{77760} \pi f_2(0, 0, 1),$$

$$E_{6a} = \pi \left(\frac{4715}{1944} \ln 2 f_2(0, 0, 1) + \frac{270433}{10935} f_2(0, 2, 0) - \frac{188147}{4860} f_2(0, 1, 1) + \frac{188147}{12960} f_2(0, 0, 2) \right),$$

$$E_{6b} = -\frac{4715}{1458} \zeta(2) f_1(0, 0, 1),$$

$$E_{7a} = \pi \left(\frac{826595}{248832} \zeta(2) f_2(0, 0, 1) - \frac{5525}{432} \ln 2 f_2(0, 0, 2) + \frac{5525}{162} \ln 2 f_2(0, 1, 1) - \frac{5525}{243} \ln 2 f_2(0, 2, 0) + \frac{526015}{248832} f_2(0, 0, 3) - \frac{4675}{768} f_2(0, 1, 2) + \frac{1805965}{248832} f_2(0, 2, 1) - \frac{3710675}{1119744} f_2(0, 3, 0) - \frac{75145}{124416} f_2(1, 0, 2) - \frac{213635}{124416} f_2(1, 1, 1) + \frac{168455}{62208} f_2(1, 2, 0) + \frac{75145}{248832} f_2(2, 0, 1) + \frac{69245}{124416} f_2(2, 1, 0) \right),$$

$$E_{7b} = \zeta(2) \left(\frac{2541575}{82944} f_1(0, 0, 2) - \frac{556445}{6912} f_1(0, 1, 1) + \frac{54515}{972} f_1(0, 2, 0) - \frac{75145}{20736} f_1(1, 0, 1) \right).$$

The term containing the ϵ^0 coefficients of the ϵ -expansion of six master integrals (see f, f', f'', g, g', g'' of Fig. 4.13):

$$U = -\frac{541}{300} C_{81a} - \frac{629}{60} C_{81b} + \frac{49}{3} C_{81c} - \frac{327}{160} C_{83a} + \frac{49}{36} C_{83b} + \frac{37}{6} C_{83c}.$$

The numerical values of entries in (4.31) may be found in Table 3 of [47]. In the above expressions $\zeta(n) = \sum_{i=1}^{\infty} i^{-n}$, $a_n = \sum_{i=1}^{\infty} 2^{-i} i^{-n}$, $b_6 = H_{0,0,0,0,1,1}(\frac{1}{2})$,

$b_7 = H_{0,0,0,0,0,1,1}(\frac{1}{2})$, $d_7 = H_{0,0,0,0,1,-1,-1}(1)$, $\text{Cl}_n(\theta) = \text{ImLi}_n(e^{i\theta})$. $H_{i_1, i_2, \dots}(x)$ are the harmonic polylogarithms. The integrals f_j are defined as follows:

$$f_1(i, j, k) = \int_1^9 ds D_1^2(s) \left(s - \frac{9}{5}\right) \ln^i(9-s) \ln^j(s-1) \ln^k(s),$$

$$f_2(i, j, k) = \int_1^9 ds D_1(s) \text{Re} \left(\sqrt{3} D_2(s)\right) \left(s - \frac{9}{5}\right) \ln^i(9-s) \ln^j(s-1) \ln^k(s),$$

$$D_1(s) = \frac{2}{\sqrt{(\sqrt{s}+3)(\sqrt{s}-1)^3}} K \left(\frac{(\sqrt{s}-3)(\sqrt{s}+1)^3}{(\sqrt{s}+3)(\sqrt{s}-1)^3} \right),$$

$$D_2(s) = \frac{2}{\sqrt{(\sqrt{s}+3)(\sqrt{s}-1)^3}} K \left(1 - \frac{(\sqrt{s}-3)(\sqrt{s}+1)^3}{(\sqrt{s}+3)(\sqrt{s}-1)^3} \right);$$

$K(x)$ is the complete elliptic integral of the first kind. Note that $D_1(s) = 2J_2^{(1,9)}(s)$, with $J_2^{(1,9)}$ defined in Eq. (A.12) of Ref. [115]. The integrals $f_1(0, 0, 0)$ and $f_2(0, 0, 0)$ were studied in Ref. [61]. The constants A_3 , B_3 and C_3 , defined in Ref. [61], admit the hypergeometric representations¹⁰:

$$\begin{aligned} A_3 &= \int_0^1 dx \frac{K_c(x)K_c(1-x)}{\sqrt{1-x}} \\ &= \frac{2\pi^{\frac{3}{2}}}{3} \left(\frac{\Gamma^2(\frac{7}{6})\Gamma(\frac{1}{3})}{\Gamma^2(\frac{2}{3})\Gamma(\frac{5}{6})} {}_4F_3 \left(\frac{1}{6}, \frac{1}{3}, \frac{1}{3}, \frac{1}{2}; 1 \right) - \frac{\Gamma^2(\frac{5}{6})\Gamma(-\frac{1}{3})}{\Gamma^2(\frac{1}{3})\Gamma(\frac{1}{6})} {}_4F_3 \left(\frac{1}{2}, \frac{2}{3}, \frac{2}{3}, \frac{5}{6}; 1 \right) \right), \end{aligned}$$

$$\begin{aligned} B_3 &= \int_0^1 dx \frac{K_c^2(x)}{\sqrt{1-x}} \\ &= \frac{4\pi^{\frac{3}{2}}}{3} \left(\frac{\Gamma^2(\frac{7}{6})\Gamma(\frac{1}{3})}{\Gamma^2(\frac{2}{3})\Gamma(\frac{5}{6})} {}_4F_3 \left(\frac{1}{6}, \frac{1}{3}, \frac{1}{3}, \frac{1}{2}; 1 \right) + \frac{\Gamma^2(\frac{5}{6})\Gamma(-\frac{1}{3})}{\Gamma^2(\frac{1}{3})\Gamma(\frac{1}{6})} {}_4F_3 \left(\frac{1}{2}, \frac{2}{3}, \frac{2}{3}, \frac{5}{6}; 1 \right) \right), \end{aligned}$$

$$\begin{aligned} C_3 &= \int_0^1 dx \frac{E_c^2(x)}{\sqrt{1-x}} \\ &= \frac{486\pi^2}{1925} {}_7F_6 \left(\frac{7}{4}, -\frac{1}{3}, \frac{1}{3}, \frac{2}{3}, \frac{4}{3}, \frac{3}{2}, \frac{3}{2}; 1 \right), \end{aligned}$$

$$K_c(x) = \frac{2\pi}{\sqrt{27}} {}_2F_1 \left(\frac{1}{3}, \frac{2}{3}; x \right), \quad E_c(x) = \frac{2\pi}{\sqrt{27}} {}_2F_1 \left(\frac{1}{3}, -\frac{1}{3}; x \right).$$

¹⁰For relations between Gauss hypergeometric functions and Feynman diagrams see e.g. [116] and references therein.

A_3 appears only in the coefficients of the ϵ -expansion of master integrals, and cancels out in the diagram contributions. Figure 4.13 shows the fundamental elliptic master integrals which contains irreducible combinations of B_3 , C_3 and $f_m(i, j, k)$.

The analytical fits of V_{6b} , V_{6a} , V_{7b} , V_{7i} and the master integrals involved needed PSLQ runs with basis of about 500 elements calculated with 9600 digits of precision.

So much concerning the universal part which is dominating the electron anomaly but is subleading only for the muon case on which we continue now.

High-precision numerical results have been obtained by recently in [91] for the electron-loop contributions to the muon anomalous magnetic moment at four loops $A_2^{(8)}(m_\mu/m_e)$. These concern contributions from graphs with one, two or three closed electron loops. The results, including those from the light-by-light-type corrections presented in [75], are collected in Table 4.7 (compare Table 4.4). Contributions which exhibit two or three closed lepton loops are listed separately, depending on the type of leptons circulating. This concerns the classes I(a) and I(b) in Fig. 4.6, classes II(b) and II(c) in Fig. 4.7 and class IV(a) in Fig. 4.9. Correspondingly, one denotes

$$\begin{array}{l|l}
 \text{I(a0)} : (\ell_1, \ell_2, \ell_3) = (e, e, e) & \text{I(bc0)} : (\ell_1, \ell_2) = (e, e) \\
 \text{I(a1)} : (\ell_1, \ell_2, \ell_3) = (e, e, \mu) & \text{I(bc1)} : (\ell_1, \ell_2) = (e, \mu) \\
 \text{I(a2)} : (\ell_1, \ell_2, \ell_3) = (e, \mu, \mu) & \text{I(bc2)} : (\ell_1, \ell_2) = (\mu, e) \\
 \text{II(bc0)} : (\ell_1, \ell_2) = (e, e) & \text{IV(a0)} : (\ell_1, \ell_2) = (e, e) \\
 \text{II(bc1)} : (\ell_1, \ell_2) = (e, \mu) & \text{IV(a1)} : (\ell_1, \ell_2) = (e, \mu) \\
 \text{IV(a2)} : (\ell_1, \ell_2) = (\mu, e) . &
 \end{array}$$

Also one denotes by $\text{I(bc)} = \text{I(b)} + \text{I(c)}$ etc. The gauge invariant groups of diagrams are labeled according to Fig. 4.14 and the list just given. It is worth noting that the leading result for the most challenging class IV(a0) diagrams was obtained by Calmet and Petermann [66] in 1975 who estimated $(111.1 \pm 8.1) \times (\alpha/\pi)^4$. The result was confirmed with $(117.4 \pm 0.5) \times (\alpha/\pi)^4$ by Samuel and Chlouber [67] in 1977, which agrees well with the more precise value $(116.76 \pm 0.02) \times (\alpha/\pi)^4$ from the Table, which was provided by the Karlsruhe–Moscow–Zeuthen collaboration. For the analytic results the one standard deviation uncertainties originating from the numerical integration, were multiplied by a factor five, in order to present conservative results. In case no uncertainty is displayed the corresponding result is either known analytically or with high numerical precision. The analytically evaluated results are in perfect agreement with the ones in the literature, although in some cases the uncertainty is far below the per mill level. The analytic approach utilized in [91] yields relatively large uncertainties of about 10 and 7% for the classes IV(c) and IV(d), respectively. For class III the uncertainty amounts to 0.2% and for I(d) 1%.

Table 4.8 collects contributions to the anomalous magnetic moment with heavy virtual leptons calculated by analytic methods in [74] in comparison with results obtained previously by means of numerical evaluations (see Table 4.4). The corresponding virtual heavy lepton contributions $A_{2e}^{(8)}(m_e/m_\mu)$, $A_{2e}^{(8)}(m_e/m_\tau)$ and

Table 4.7 Results for $A_{2\mu}^{(8)}(m_\mu/m_e)$ obtained in [91] for the different groups of diagrams and the comparison with the numerical results from [33, 34, 41, 46]. Note that the uncertainties in the second column are multiplied by a factor five in order to take into account possible correlations not always kept trace of by the numerical programs. The results for IV(a)–IV(c) have been taken from [75]

Group	Kurz et al. [91]	Various Refs. [33, 34, 41, 46]	
I(a0)	7.223076	7.223077 ± 0.000029	[41]
		7.223076	[33]
I(a1)	0.494072	0.494075 ± 0.000006	[41]
		0.494072	[33]
I(a2)	0.027988	0.027988 ± 0.000001	[41]
		0.027988	[33]
I(a)	7.745136	7.74547 ± 0.00042	[46]
I(bc0)	8.56876 ± 0.00001	8.56874 ± 0.00005	[41]
I(bc1)	0.1411 ± 0.0060	0.141184 ± 0.000003	[41]
I(bc2)	0.4956 ± 0.0004	0.49565 ± 0.00001	[41]
I(bc)	9.2054 ± 0.0060	9.20632 ± 0.00071	[46]
I(d)	-0.2303 ± 0.0024	-0.22982 ± 0.00037	[46]
		-0.230362 ± 0.000005	[34]
II(a)	-2.77885	-2.77888 ± 0.00038	[46]
		-2.77885	[33]
II(bc0)	-12.212631	-12.21247 ± 0.00045	[41]
II(bc1)	-1.683165 ± 0.000013	-1.68319 ± 0.00014	[41]
II(bc)	-13.895796 ± 0.000013	-13.89457 ± 0.00088	[46]
III	10.800 ± 0.022	10.7934 ± 0.0027	[46]
IV(a0)	116.76 ± 0.02	116.759183 ± 0.000292	[41]
IV(a1)	2.69 ± 0.14	2.697443 ± 0.000142	[41]
IV(a2)	4.33 ± 0.17	4.328885 ± 0.000293	[41]
IV(a)	123.78 ± 0.22	123.78551 ± 0.00044	[46]
IV(b)	-0.38 ± 0.08	-0.4170 ± 0.0037	[46]
IV(c)	2.94 ± 0.30	2.9072 ± 0.0044	[46]
IV(d)	-4.32 ± 0.30	-4.43243 ± 0.00058	[46]

$A_{3e}^{(8)}(m_e/m_\mu, m_e/m_\tau)$ to the electron anomaly the reader may find in [74] (see Table 4.3). Also these results based on expansions in the mass ratios agree well with the numerical results in [45].

Although the contribution $A_{3\mu}^{(8)}$ is quite small it is nevertheless instructive to compare in Table 4.9 (again to be compared with Table 4.4) the results presented in [91] with the ones [46] obtained by means of purely numerical methods. Good agreement within the uncertainties is found for the diagram classes I(a) and IV(a). For II(b) + II(c) one observes a discrepancy of about three standard deviations. Also the results for I(b) + I(c) do not agree within the assigned uncertainty. Note, however, that

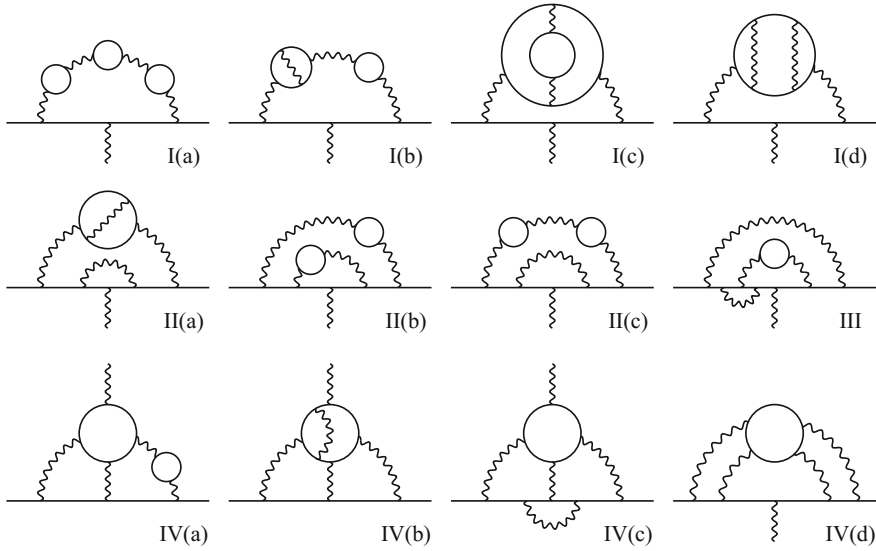


Fig. 4.14 Sample four-loop QED diagrams exhibiting at least one electron loop accessible to analytic and semi-analytic methods. External fermion lines are muons, internal Fermion loops represent electrons, muons or taus

Table 4.8 Comparison of analytic results for the $A_{2\mu}^{(8)}(m_\mu/m_\tau) \times 10^2$ contribution to the muon $g - 2$ from τ -loops at four loop order from [74] with results from [46] (see Table 4.4)

Group	Kurz et al. [74]	Aoyama et al. [46]
I(a)	0.00324281(2)	0.0032(0)
I(b) + I(c) + II(b) + II(c)	-0.6292808(6)	-0.6293(1)
I(d)	0.0367796(4)	0.0368(0)
III	4.5208986(6)	4.504(14)
II(a) + IV(d)	-2.316756(5)	-2.3197(37)
IV(a)	3.851967(3)	3.8513(11)
IV(b)	0.612661(5)	0.6106(31)
IV(c)	-1.83010(1)	-1.823(11)

in [46] an older value for m_μ/m_τ has been used which is about 0.01% smaller and thus can explain most of the discrepancy.

Replacing the numerical results included in (4.23)–(4.26) by the ones accessible analytically one obtains

$$\begin{aligned}
 A_2^{(8)}(m_\mu/m_e) &= 126.34(38) + 6.53(30) = 132.86(48) [132.6852(60)], \\
 A_2^{(8)}(m_\mu/m_\tau) &= 0.0424941(2)(53) [0.04234(12)], \\
 A_3^{(8)}(m_\mu/m_e, m_\mu/m_\tau) &= 0.0627220(1)(100) [0.06272(4)],
 \end{aligned}$$

Table 4.9 Comparison of the results for $A_{3\mu}^{(8)}(m_\mu/m_e, m_\mu/m_\tau)$ obtained in [91] with results of Ref. [46] for the individual diagram classes. Note that the error in m_μ/m_τ is not included. In most cases it induces an uncertainty in fifth significant digit in the displayed numbers, in the class of IV(a) even in the fourth. In the second row an updated result for I(c) has been used

Group	Kurz et al. [91]	Aoyama et al. [46]
I(a)	0.00320905(1)	0.003209(0)
I(b) + I(c)	0.00442289(2)	0.004422(0)
II(b) + II(c)	-0.02865753(1)	-0.028650(2)
IV(a)	0.08374757(9)	0.083739(36)

in brackets the results of [46]. Note that the uncertainty of the analytic result is larger than the uncertainty in Ref. [46].

The four-loop results of Refs. [74, 75, 91] can be summarized as

$$\begin{aligned}
 C_4 - A_1^{(8)} &= A_2^{(8)}(m_\mu/m_e) + A_2^{(8)}(m_\mu/m_\tau) + A_3^{(8)}(m_\mu/m_e, m_\mu/m_\tau) \\
 &= 132.86(48) + 0.0424941(53) + 0.062722(10) \\
 &= 132.965(480)[132.790(6)].
 \end{aligned} \tag{4.32}$$

In the bracket the corresponding result [46]. The agreement is perfect within errors, but the error of the analytic result at present is almost two orders of magnitude larger.

What is important is the fact that the crosschecks have reached a precision $0.5 \times (\alpha/\pi)^4 \approx 1.5 \times 10^{-11}$, well below the experimental precision 15×10^{-11} expected from the next generation experiments. Note that, in view of the fact that a_e^{QED} (3.66) is completely dominated by the universal contribution, Laporta's semi-analytical results consolidates impressively the four-loop QED contribution to a_e

Five-Loop Analytic Results and Crosschecks

A number of five-loop diagrams, displayed in Fig. 4.15, exhibiting photon self-energy insertions can be calculated analytically, either by series expansion in mass ratios or by integrating known lower order leptonic vacuum polarization functions $\Pi_\ell(q^2)$. In [72, 90] some five-loop corrections have been calculated by using the leading term in the high-energy expansion of the leptonic vacuum polarization function of the photon. Since this approach leads to unexpectedly large deviation from the numerical result, the method had to be improved. In [86] a substantial improvement has been achieved by replacing the above mentioned high-energy expansion by an approximation based on a Padé improved¹¹ expansions in the low- and high-energy and the threshold region. The results are listed in Table 4.10 together with a comparison with other published results. For the classes I(a) I(c) results are exact since they result

¹¹Padé approximants [117] are very useful in cases when a function, $f(x)$ say, is known only by its series expansion $f(x) \approx \sum_{j=0}^N c_j x^j$. A Padé approximant for $f(x)$ is a rational function of x $[m, n]_f(x) = P_m(x)/Q_n(x)$, where $P_m(x)$ and $Q_n(x)$ are polynomials in x of degree m and n , respectively, which are determined such that $[m, n]_f(x)$ has the same known Taylor expansion as $f(x)$. By convention $Q_n(0) = 1$. The number of coefficients of a Padé

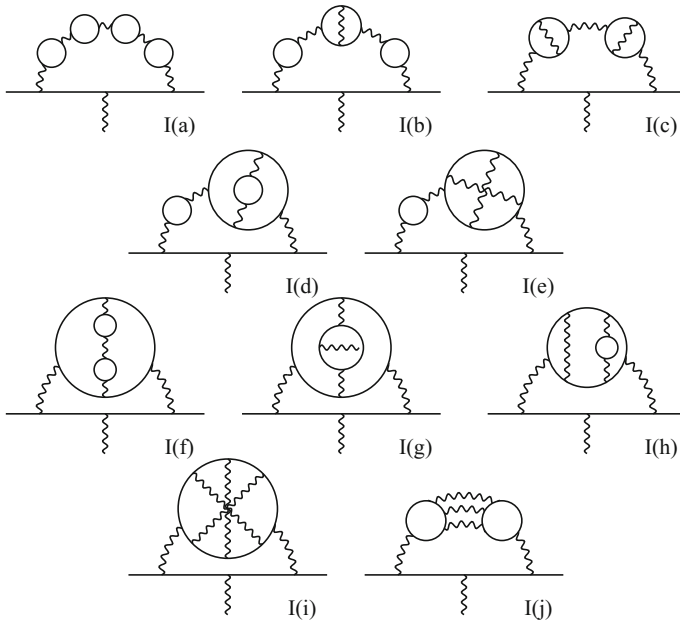


Fig. 4.15 Some typical five loop order contributions to a_e including fermion loops tractable by analytic methods

from numerically integrating the known analytic one- and two-loop results for the vacuum polarization function. Classes I(d) and I(e) are calculated using the highly constrained Padé approximants, which have been constructed using 30 terms in the low- and high-energy expansion. Due to the vast amount of information, the results for $g - 2$ using different approximants have very little spread and the final result is therefore very precise. The situation is quite different for classes I(f)–I(j) which require the knowledge of $\Pi_\ell(q^2)$ at four-loop order. Since there is only a limited number of terms in the relevant expansions, the Padé approximation is less precise and the precision of the result is limited (see Fig. 1 of Ref. [86]). In general, good agreement is found with the results from [76–78, 81], but for some classes a certain tension remains. The numbers shown are obtained by numerically integrating over the best available approximation. In case there are several equivalent approximations

(Footnote 11 continued)

approximant $[m,n]=\sum_{k=0}^m a_k x^k / (1 + \sum_{k=1}^n b_k x^k)$ is $n + m + 1$ unless $a_0 = 0$ as in case of the $\Pi(q^2)$, where it is $n + m$. Given N , $[m,n]$ is determined up to degree $n + m + 1 \leq N$ or $n + m \leq N$ if $a_0 = 0$. To illustrate the benefit of a Padé approximant over the Taylor series let's suppose $f(x) \sim \text{constant}$ as $x \rightarrow \infty$ is a bounded function, then the series of $[n, n]$ Padés can represent the function f globally much better than the Taylor series, which completely fails when x gets larger. Under appropriate conditions (Stieltjes function) one can prove that the appropriately chosen Padé series converges to $f(x)$ for all x .

Table 4.10 Results for $A_{2\mu}^{(10)}(m_\mu/m_e)$ with pure electronic insertions. The errors listed in the second column are estimated from the spread between different Padé approximants, which is negligible for classes I(a)–I(e). Note that Ref. [72] only used the high energy asymptotic form of $\Pi_\ell(q^2)$ and does not provide an error estimate

Group	Ref. [86]	Ref. [72]	Refs. [76–78, 81]	Ref.
I(a)	20.142 813	20.183 2	20.142 93(23)	[76]
I(b)	27.690 061	27.718 8	27.690 38(30)	[76]
I(c)	4.742 149	4.817 59	4.742 12(14)	[76]
I(d)+I(e)	6.241 470	6.117 77	6.243 32(101)(70)	[76]
I(e)	−1.211 249	−1.331 41	−1.208 41(70)	[76]
I(f) + I(g) + I(h)	4.446 8 ⁺⁶ _{−4}	4.391 31	4.446 68(9)(23)(59)	[76, 78]
I(i)	0.074 6 ⁺⁸ _{−19}	0.252 37	0.087 1(59)	[81]
I(j)	−1.2469 ⁺⁴ _{−3}	−1.214 29	−1.247 26(12)	[77]

Table 4.11 Results for $A_{2\mu}^{(10)}(m_\mu/m_e)$ including electronic and muonic contributions

Group	Baikov et al. [86]	Aoyama et al. [46]
I(a)	22.566 976	22.566 973 (3)
I(b)	30.667 093	30.667 091 (3)
I(c)	5.141 395	5.141 395 (1)
I(e)	−0.931 839	−0.931 2 (24)

Table 4.12 Results for the universal contributions $A_1^{(10)}$

Group	Baikov et al. [86]	Aoyama et al. [45]
I(a)	0.000 471	0.000 470 94 (6)
I(b)	0.007 010	0.007 010 8 (7)
I(c)	0.023 467	0.023 468 (2)
I(d) + I(e)	0.014 094	0.014 098(5)(4)
I(e)	0.010 291	0.010 296 (4)
I(f) + I(g) + I(h)	0.037 85 ⁺⁵ _{−3}	0.037 833(20)(6)(13)
I(i)	0.017 21 ⁺⁸ _{−23}	0.017 47 (11)
I(j)	0.000 420 ⁺³¹ _{−16}	0.000 397 5 (18)

the result is obtained by taking the mean of all values obtained. The errors are then calculated by taking the difference between the mean and the smallest and largest values obtained, respectively.

For classes I(a)–I(c) and I(e) we can obtain the full result for $A_{2\mu}^{(10)}(m_\mu/m_e)$ including muonic contributions. These results are presented in Table 4.11. In Table 4.12 we present our results for the universal corrections and compare with the results given in [45] (see Table 4.5). In both cases the discussion as for the purely electronic contributions can essentially be repeated and also here overall good agreement with results

available in the literature is observed. Nevertheless it should be noted that for single diagram classes a certain tension remains.

So far five-loop contributions to the muon $g - 2$ could be calculated by analytic means for diagrams from class I which are including known photon vacuum polarization insertions. Results largely confirm the previous numerical results by Kinoshita's group. While corresponding four-loop results cover a large fraction of the complete contribution, at five loops the calculations are rather partial yet.

4.2 Weak Contributions

The weak interaction contribution to $g - 2$ attracted attention of theoreticians long time before it started to play a relevant role in the comparison with the experimental result. Actually the "weak contribution sensitivity" was reached only with the recent BNL experiment. With the emergence of the SM [118] and establishing its renormalizability [119] for the first time it was possible to make real predictions for a_μ beyond QED. Before, in non-renormalizable low energy effective theories, corresponding attempts were not convincing, since, as we discussed earlier only in a renormalizable theory a_μ is a finite unambiguously predictable quantity and hence an unambiguous monitor for testing the theory. Soon after a unified electroweak theory seemed established a number of groups presented the one-loop result for a_μ in 1972 [120]. At that time, the weak term turned out to be almost two orders of magnitude smaller than the experimental accuracy of the CERN $g - 2$ experiment. At present the weak term is an effect of almost three standard deviations.

Weak interaction effects are mediated by exchange of the heavy weak gauge bosons W^\pm , which mediate charged current (CC) processes, and Z , which mediates the neutral current (NC) processes. Beyond the electroweak $SU(2)_L \otimes U(1)_Y$ Yang-Mills gauge theory, a Higgs sector is required which allows to generate the masses of the gauge bosons W and Z , as well as the masses of the fermions, without spoiling renormalizability.¹² Thereby the gauge symmetry is broken down $SU(2)_L \otimes U(1)_Y \rightarrow U(1)_{\text{em}}$ to the Abelian subgroup of QED, and an additional physical particle has to be taken into account, the famous Higgs particle, predicted by Brout, Englert and Higgs in 1964 [121], discovered 48 years later by the ATLAS and CMS Collaborations [122–124] at the Large Hadron Collider (LHC) at CERN.

¹²In different terms: renormalizability of a massive non-Abelian gauge theory requires the existence of a scalar boson, which interacts with all massive particles with a coupling proportional to the mass of the particle to which it couples. The corresponding Higgs boson exchange contributions precisely cancel the non-renormalizable terms (exhibiting bad high energy behavior) which one would obtain in S -matrix elements in absence of the Higgs. The pattern of the 15 required SM Higgs boson couplings, which directly manifests in its decay pattern is actually what identifies the scalar boson as the Higgs boson.

In the SM the fermions are organized in three lepton–quark families, with the left–handed fields in $SU(2)_L$ doublets and the right–handed fields in singlets:

$$\text{1st family: } \left(\begin{array}{c} \nu_e \\ e^- \end{array} \right)_L, \left(\begin{array}{c} u \\ \tilde{d} \end{array} \right)_L, \nu_{eR}, e_R^-, u_R, d_R$$

$$\text{2nd family: } \left(\begin{array}{c} \nu_\mu \\ \mu^- \end{array} \right)_L, \left(\begin{array}{c} c \\ \tilde{s} \end{array} \right)_L, \nu_{\mu R}, \mu_R^-, c_R, s_R$$

$$\text{3rd family: } \left(\begin{array}{c} \nu_\tau \\ \tau^- \end{array} \right)_L, \left(\begin{array}{c} t \\ \tilde{b} \end{array} \right)_L, \nu_{\tau R}, \tau_R^-, t_R, b_R.$$

The family structure is required by renormalizability, which in turn requires the absence of an Adler–Bell–Jackiw (ABJ) [VVA triangle anomaly] (see Sect. 4.2.2 below). Each individual non-singlet chiral fermion produces a mass independent VVA anomaly, which only depends on the gauge coupling quantum numbers (charges). The latter are such that the anomaly produced by the leptons is canceled by the anomaly produced by the quarks within each family. The Abelian subgroup $U(1)_Y$ is associated with the weak hypercharge, related to the charge and the 3rd component of weak isospin by the Gell–Mann–Nishijima relation $Y = 2(Q - T_3)$.¹³ Denoting by $\nu_\ell = (\nu_e, \nu_\mu, \nu_\tau)$, $\ell = (e, \mu, \tau)$, $q_u = (u, c, t)$ and $q_d = (d, s, b)$ the four horizontal vectors in “family space” of fermion fields with identical electroweak quantum numbers, the charged current (CC) has the form

$$J_\mu^+ = J_{\mu 1} - i J_{\mu 2} = \bar{\nu}_\ell \gamma_\mu (1 - \gamma_5) U_{\text{PMNS}} \ell + \bar{q}_u \gamma_\mu (1 - \gamma_5) U_{\text{CKM}} q_d \quad (4.33)$$

and exhibits quark family flavor changing, through mixing by the unitary 3×3 Cabibbo–Kobayashi–Maskawa matrix U_{CKM} [125] as well as neutrino flavor mixing by the corresponding Pontecorvo–Maki–Nakagawa–Sakata matrix U_{PMNS} [126]. The $SU(2)_L$ currents have strict V–A (V = vector [γ_μ], A = axial–vector [$\gamma_\mu \gamma_5$]) form, which in particular implies that the CC is maximally parity (P) violating (Lee and Yang 1957). The mixing matrices predict a CP violating phase, which has been confirmed by observation. This kind of CP violation mechanism via quark flavor

¹³ $SU(2)_L \otimes U(1)_Y$ quantum numbers of fermions read

	Doublets				Singlets			
	$(\nu_\ell)_L$	$(\ell^-)_L$	$(u, c, t)_L$	$(\tilde{d}, \tilde{s}, \tilde{b})_L$	$(\nu_\ell)_R$	$(\ell^-)_R$	$(u, c, t)_R$	$(d, s, b)_R$
Q	0	−1	2/3	−1/3	0	−1	2/3	−1/3
T_3	1/2	−1/2	1/2	−1/2	0	0	0	0
Y	−1	−1	1/3	1/3	0	−2	4/3	−2/3

Quarks in addition carry $SU(3)_c$ color. The color factor N_{cf} is 3 for quarks and 1 for leptons, which are color singlets. Note that in the SM all matter fields are in the fundamental ($SU(2)_L$ –doublets, $SU(3)_c$ –triplets[antitriplets]) or trivial (singlet) representations. The simplest ones possible.

mixing requires a minimum of three fermion families. Indeed what we see to be realized in nature. CP violation also implies the existence of a very tiny electrical dipole moment (EDM). In a local QFT a non-vanishing EDM is possible only if CP is violated, as we noted earlier. For the magnetic moments CP has no special impact and the CP violating effects are too small to play any role. For our purpose the 3×3 family mixing matrices may be taken to be unit matrices. The neutral current (NC) is strictly flavor conserving

$$J_\mu^Z = J_{\mu 3} - 2 \sin^2 \Theta_W j_\mu^{em} = \sum_f \bar{\psi}_f \gamma_\mu (v_f - a_f \gamma_5) \psi_f \quad (4.34)$$

with

$$j_\mu^{em} = \sum_f Q_f \bar{\psi}_f \gamma_\mu \psi_f \quad (4.35)$$

the P conserving electromagnetic current.¹⁴ The weak mixing parameter $\sin^2 \Theta_W$ is responsible for the $\gamma - Z$ mixing. The sums extend over the individual fermion flavors f (and color). In our convention the NC vector and axial-vector neutral current coefficients are given by

$$v_f = T_{3f} - 2Q_f \sin^2 \Theta_W, \quad a_f = T_{3f} \quad (4.36)$$

where T_{3f} is the weak isospin ($\pm \frac{1}{2}$) of the fermion f . The matter field Lagrangian thus takes the form

$$\mathcal{L}_{\text{matter}} = \sum_f \bar{\psi}_f i \gamma^\mu \partial_\mu \psi_f + \frac{g}{2\sqrt{2}} (J_\mu^+ W^{\mu-} + \text{h.c.}) + \frac{g}{2 \cos \Theta_W} J_\mu^Z Z^\mu + e j_\mu^{em} A^\mu \quad (4.37)$$

where g is the $SU(2)_L$ gauge coupling constant and $e = g \sin \Theta_W$ is the charge of the positron (unification condition).

We should mention that before symmetry breaking the theory has the two gauge couplings g and g' as free parameters, after the breaking we have in addition the *vacuum expectation value* (VEV) of the Higgs field v , thus three parameters in total, if we disregard the fermion masses and their mixing parameters for the moment. The most precisely known parameters are the fine structure constant α (electromagnetic coupling strength), the Fermi constant G_μ (weak interaction strength) and the Z mass M_Z . Apart from the unification relation

$$\alpha = \frac{e^2}{4\pi}, \quad e = g \sin \Theta_W, \quad \tan \Theta_W = g'/g$$

¹⁴An important property of the weak currents is the absence of Flavor Changing Neutral Currents (FCNC), as a consequence of the GIM mechanism [127], i.e., in the SM neutral currents are automatically diagonal in the Fermi fields.

we have the mass generation by the Higgs mechanism which yields

$$M_W = \frac{gv}{2}, \quad M_Z = \frac{gv}{2 \cos \Theta_W},$$

while lowest order CC Fermi decay defines the Fermi or muon decay constant

$$G_\mu = \frac{g^2}{4\sqrt{2}M_W^2} = \frac{1}{\sqrt{2}v^2}.$$

The defining equation for G_μ in terms of the experimental μ life-time reads [128–130]

$$\Gamma_\mu \equiv \frac{1}{\tau_\mu} = \frac{G_\mu^2 m_\mu^5}{192\pi^3} F\left(\frac{m_e^2}{m_\mu^2}\right) \left(1 + \frac{3}{5} \frac{m_\mu^2}{M_W^2}\right) \left[1 + \frac{\alpha(m_\mu)}{\pi} \left(\frac{25}{8} - \frac{\pi^2}{2}\right) + \frac{\alpha^2(m_\mu)}{\pi^2} C_2\right], \quad (4.38)$$

where

$$F(x) = 1 - 8x + 8x^3 - x^4 - 12x^2 \ln x,$$

$$C_2 = \frac{156815}{5184} - \frac{518}{81}\pi^2 - \frac{895}{36}\zeta(3) + \frac{67}{720}\pi^4 + \frac{53}{6}\pi^2 \ln 2,$$

and

$$\alpha(m_\mu)^{-1} = \alpha^{-1} - \frac{2}{3\pi} \ln \frac{m_\mu}{m_e} + \frac{1}{6\pi}.$$

The neutral to charged current ratio, called ρ -parameter, follows from

$$G_{\text{NC}} = \frac{g^2}{4\sqrt{2}M_Z^2 \cos^2 \Theta_W} = \frac{\rho}{\sqrt{2}v^2},$$

with $\rho_0 = 1$ at the tree level. These relations are subject to radiative corrections. Given α , G_μ and M_Z as input parameters, all further parameters like M_W , $\sin^2 \Theta_W$, g , etc. are dependent parameters. Typically, when calculating versions of the weak mixing parameter $\sin^2 \Theta_i$ in terms of the input parameters one obtains

$$\sin^2 \Theta_i \cos^2 \Theta_i = \frac{\pi\alpha}{\sqrt{2} G_\mu M_Z^2} \frac{1}{1 - \Delta r_i}, \quad (4.39)$$

where

$$\Delta r_i = \Delta r_i(\alpha, G_\mu, M_Z, m_H, m_{f \neq t}, m_t)$$

includes the higher order corrections which can be calculated in the SM or in alternative models. For example,

$$\Delta\rho = \frac{N_c \sqrt{2} G_\mu}{16\pi^2} \left(m_t^2 + m_b^2 - \frac{2m_t^2 m_b^2}{m_t^2 - m_b^2} \ln \frac{m_t^2}{m_b^2} \right) \approx \frac{\sqrt{2} G_\mu}{16\pi^2} 3m_t^2 = \frac{3y_t^2}{32\pi^2}, \quad (4.40)$$

which measures the weak-isospin breaking by the Yukawa couplings y_f of the heavy fermions at zero momentum. It is a large correction proportional to m_t^2 due to the heavy top [131]. After the discovery of the Higgs, we also know the Higgs mass within a rather narrow error band: $m_H = 125.1 \pm 0.3$ GeV. Thus, for the first time, all relevant parameters of the SM are known with impressive accuracy. Before the Higgs has been observed m_H was the only relevant unknown parameter and by confronting the calculated with the experimentally determined value of $\sin^2 \Theta_i$ one obtained important indirect constraints on the Higgs mass. Δr_i depends on the definition of $\sin^2 \Theta_i$. The various definitions coincide at tree level and hence only differ by quantum effects. From the weak gauge boson masses, the electroweak gauge couplings and the neutral current couplings of the charged fermions we obtain

$$\begin{aligned} \sin^2 \Theta_W &= 1 - \frac{M_W^2}{M_Z^2} \\ \sin^2 \Theta_g &= e^2/g^2 = \frac{\pi\alpha}{\sqrt{2} G_\mu M_W^2} \\ \sin^2 \Theta_f &= \frac{1}{4|Q_f|} \left(1 - \frac{v_f}{a_f} \right), \quad f \neq \nu, \end{aligned} \quad (4.41)$$

for the most important cases and the general form of Δr_i ($i = W, g, f$) reads

$$\Delta r_i = \Delta\alpha - f_i(\sin^2 \Theta_i) \Delta\rho + \Delta r_{i \text{ rem}}$$

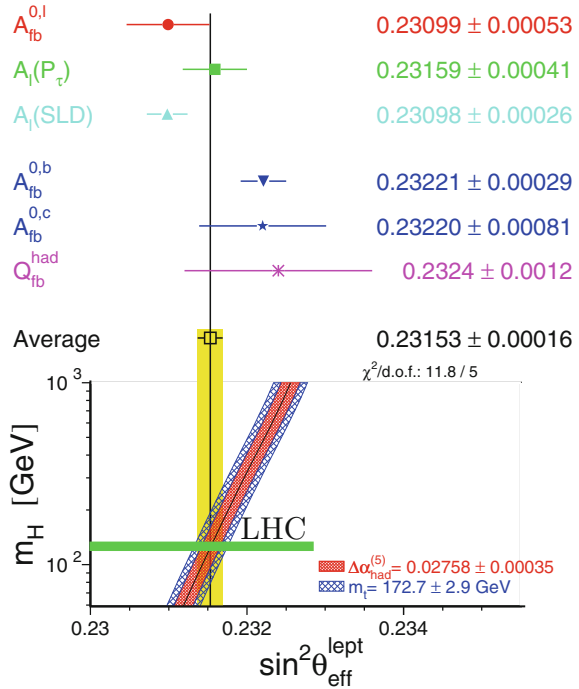
with $f_W(\sin^2 \Theta_W) = \cos^2 \Theta_W / \sin^2 \Theta_W$; $f_g(\sin^2 \Theta_g) = f_f(\sin^2 \Theta_f) = 1$ and a universal term $\Delta\alpha$ which affects the predictions of M_W via $\sin^2 \Theta_W$, etc. For M_W we have [132]

$$M_W^2 = \frac{\rho M_Z^2}{2} \left(1 + \sqrt{1 - \frac{4A_0^2}{\rho M_Z^2} \left(\frac{1}{1 - \Delta\alpha} + \Delta r_{\text{rem}} \right)} \right), \quad (4.42)$$

with

$$A_0 = \sqrt{\pi\alpha/\sqrt{2}G_\mu} = 37.2802(3) \text{ GeV}.$$

Fig. 4.16 Plot of the LEP Electroweak Working Group: S. Schael et al. 2005 [135], superimposed with the LHC result. [Resource CERN]



The leading dependence on the Higgs mass m_H is logarithmic with

$$\Delta r_W^{\text{Higgs}} = \frac{11}{3} \left(\ln \frac{m_H^2}{M_W^2} - \frac{5}{6} \right), \quad \Delta r_f^{\text{Higgs}} = \frac{1 + 9 \sin^2 \Theta_f}{3 \cos^2 \Theta_f} \left(\ln \frac{m_H^2}{M_W^2} - \frac{5}{6} \right)$$

provided $m_H \gg M_W$. For the now established $m_H/M_W \sim 1.56$ more complicated formulas apply (see e.g. [133, 134] for more details). Actually, the Higgs mass determined by ATLAS and CMS agrees perfectly with the indirect bounds obtained from combined LEP, SLD and Tevatron precision measurements of the weak mixing parameter (see Fig. 4.16).

The weak contributions depend on SM parameters like the precisely known Fermi constant G_μ , the weak gauge boson masses M_Z , M_W and in addition the top mass m_t as well as the Higgs mass m_H . Correspondingly, we will adopt the G_μ renormalization scheme [136]. In this scheme the weak mixing angle is defined via the gauge boson masses as $\sin^2 \Theta_W = 1 - M_W^2/M_Z^2$, which for the given masses yields

$$\sin^2 \Theta_W = 0.22290 \pm 0.00029. \quad (4.43)$$

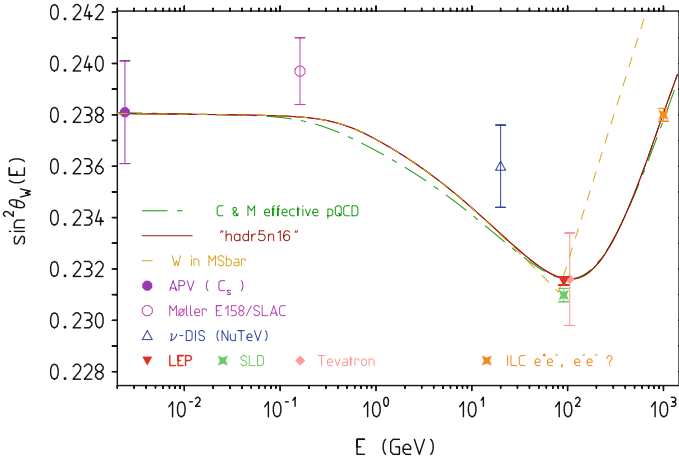


Fig. 4.17 The running $\sin^2 \theta_W(Q^2) = \alpha(-Q^2)/\alpha_2(-Q^2) + \dots$ as a function of Q in the space-like region. Hadronic uncertainties are included but barely visible. Uncertainties from the input parameter $\sin^2 \theta_W(0) = 0.23822(100)$ or $\sin^2 \theta_W(M_Z^2) = 0.23156(21)$ are not shown. Future ILC measurements at 1 TeV would be sensitive to Z' , $H^{\pm\pm}$ etc. For complete analytic expressions for electroweak parameter shifts at one-loop see [133, 134, 141]. Another interesting version of running $\sin^2 \theta_W(Q^2)$ one finds in *polarized Moeller scattering asymmetries* as advocated by Czarnecki and Marciano [142] (see also [143])

The top mass dependence is due to the lack of decoupling of heavy states in the spontaneously broken weak interaction sector of the SM. One should keep in mind that weak contributions are quite sensible to the weak mixing angle $\sin^2 \theta_W$ which like the fine structure constant is a running parameter and which is most precisely known at the Z mass scale:

$$\sin^2 \theta_{\text{eff}}^{\text{lept}}(M_Z) = 0.23153 \pm 0.00016 . \tag{4.44}$$

We will need this parameter at low energies, and will adopt the recent calculation [137] which includes non-perturbative strong interaction effects estimated via dispersion relations in terms of experimental $e^+e^- \rightarrow$ hadrons cross section data (see Fig. 4.17). The flavor separation (see Sect. 5.1.9 below) of e^+e^- data needed to determine the $SU(2)_L$ running coupling $\Delta\alpha_2^{\text{had}}(s)$ has been crosschecked in by lattice QCD simulations in [138]. For a recent lattice QCD calculation see [139, 140].

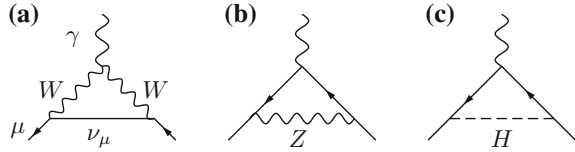
The resulting value is given by

$$\sin^2 \theta_{\text{eff}}^{\text{lept}}(0) = 0.237855 \pm 0.00016 \pm 0.00010 . \tag{4.45}$$

It is important that at low energy the scale dependence is small, and hence this parameter is quite well defined.

Last but not least one should keep in mind that masses in the SM are generated by spontaneous symmetry breaking of the Z_2 symmetry $H(x) \leftrightarrow -H(x)$ in the

Fig. 4.18 The leading weak contributions to a_ℓ ; diagrams in the physical unitary gauge



physical Higgs potential by a non-vanishing VEV $H \rightarrow H + v$ ($v \neq 0$) of the Higgs field. The upshot of this Higgs mechanism are the mass-coupling relations

$$M_W^2 = \frac{1}{4} g^2 v^2, \quad M_Z^2 = \frac{1}{4} (g^2 + g'^2) v^2, \quad m_f^2 = \frac{1}{2} y_f^2 v^2, \quad m_H^2 = \frac{1}{3} \lambda v^2, \quad (4.46)$$

between physical parameters. Note that the Higgs boson mass itself is of the form “mass \propto coupling \times vacuum expectation value” in the broken phase. Only in the symmetric phase the Higgs potential mass m^2 is an unconstrained free parameter, independent of λ . Since v as a physical parameter is determined by the Fermi constant, whenever we renormalize a mass by matching it with the observed value, we are actually tuning a coupling constant (in case of the Higgs boson mass the Higgs self-coupling) and not the mass itself.

4.2.1 Weak One-Loop Effects

The relevant diagrams are shown in the following Fig. 4.18 in the unitary gauge. For the Feynman rules of the SM we refer to SM textbooks or to my TASI lecture notes [133] for a short overview. In spite of the fact that the unitary gauge is not renormalizable, the relevant gauge invariant S -matrix element, may be calculated directly in the unitary gauge. The advantage is that in this gauge only physical particles are present and diagrams exhibiting Higgs ghosts and Faddeev–Popov ghosts are absent. What is most interesting is the occurrence of the first diagram of Fig. 4.18 which exhibits a non-Abelian triple gauge vertex and the corresponding contribution provides a test of the Yang-Mills structure involved. It is of course not surprising that the photon couples to the charged W boson the way it is dictated by gauge invariance.

The gauge boson contributions are given by

$$a_\mu^{(2)\text{EW}}(W) = \frac{\sqrt{2} G_\mu m_\mu^2}{16\pi^2} \frac{10}{3} \simeq +388.71(0) \times 10^{-11}$$

$$a_\mu^{(2)\text{EW}}(Z) = \frac{\sqrt{2} G_\mu m_\mu^2}{16\pi^2} \frac{(-1 + 4 \sin^2 \Theta_W)^2 - 5}{3} \simeq -193.90(1) \times 10^{-11} \quad (4.47)$$

while the diagram with the Higgs exchange yields¹⁵

$$\begin{aligned}
 a_{\mu}^{(2)\text{EW}}(H) &= \frac{\sqrt{2}G_{\mu}m_{\mu}^2}{8\pi^2} \int_0^1 dy \frac{(2-y)y^2}{y^2 + (1-y)(m_H/m_{\mu})^2} \\
 &\simeq \frac{\sqrt{2}G_{\mu}m_{\mu}^2}{8\pi^2} \begin{cases} \frac{m_{\mu}^2}{m_H^2} \ln \frac{m_H^2}{m_{\mu}^2} & \text{for } m_H \gg m_{\mu} \\ \frac{3}{2} & \text{for } m_H \ll m_{\mu} \end{cases} \\
 &\simeq 21.64 \times 10^{-15} \text{ for } m_H \sim 125 \text{ GeV} .
 \end{aligned} \tag{4.48}$$

We remind that the Higgs mass now is known within a rather narrow error band.

Employing the SM parameters given in (3.31) and (3.32) we obtain

$$a_{\mu}^{(2)\text{EW}} = (194.81 \pm 0.01) \times 10^{-11} \tag{4.49}$$

The error comes from the uncertainty in $\sin^2 \Theta_W$ given above.

4.2.2 Weak Two-Loop Effects

Typical electroweak 2-loop corrections are the electromagnetic corrections of the 1-loop diagrams Fig. 3.7 (part of the bosonic corrections) or fermionic loop insertions as shown in Fig. 4.19. All these corrections are proportional to

$$\mathcal{K}_2 = \frac{\sqrt{2}G_{\mu}m_{\mu}^2}{16\pi^2} \frac{\alpha}{\pi} \simeq 2.70868284 \times 10^{-12} . \tag{4.50}$$

Part of the electroweak two-loop corrections were calculated first in 1992 by Kukhto, Kuraev, Schiller and Silagadze [144] with an unexpected result, the corrections turned out to be enhanced by very large logarithms $\ln M_Z/m_f$, which mainly come from fermion triangular-loops like in Fig. 4.19a. In QED loops with three photons attached do not contribute due to Furry's theorem and the $\gamma\gamma\gamma$ -amplitude vanishes. In presence of weak interactions, because of parity violation, contributions from the two orientations of the closed fermion loops do not cancel such that the $\gamma\gamma Z$, γZZ and

¹⁵The exact analytic result for the Higgs reads

$$\begin{aligned}
 a_{\mu}^{(2)\text{EW}}(H) &= \frac{\sqrt{2}G_{\mu}m_{\mu}^2}{8\pi^2} \left\{ \xi(1-\xi) \ln(-\xi) + \xi^{-2}(1-\xi)(1-\xi^3) \ln(1-\xi) + \xi^{-1}(1-\xi)^2 + \frac{3}{2} \right\} \\
 &\simeq \frac{\sqrt{2}G_{\mu}m_{\mu}^2}{8\pi^2} \left\{ z^{-1} \left(\ln z - \frac{7}{6} \right) + z^{-2} \left(3 \ln z - \frac{13}{4} \right) + z^{-3} \left(9 \ln z - \frac{201}{20} \right) + O(z^{-4} \ln z) \right\}
 \end{aligned}$$

in which $z = m_H^2/m_{\mu}^2$, and $\xi = (\sqrt{1-y} - 1)/(\sqrt{1-y} + 1)$ with $y = 4/z$.

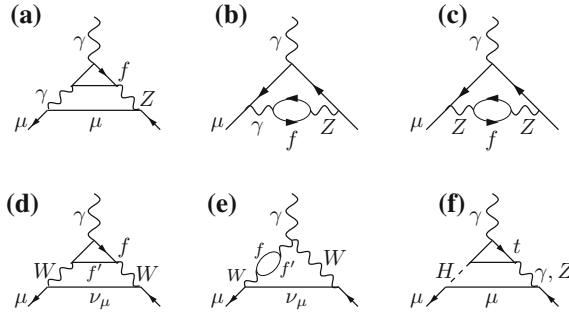


Fig. 4.19 Some of the relevant electroweak two-loop diagrams exhibiting closed fermion loops in the unitary gauge. $f = (\nu_e, \nu_\mu, \nu_\tau,) e, \mu, \tau, u, c, t, d, s, b$ with weak doublet partners $f' = (e, \mu, \tau,) \nu_e, \nu_\mu, \nu_\tau, d, s, b, u, c, t$ of course the neutrinos (in brackets) do not couple directly to the photon and hence are absent in the triangular subgraphs

γWW amplitudes do not vanish. In fact for the γWW triangle charge conservation only allows one orientation of the fermion loop.

Diagrams (a) and (b), with an internal photon, appear enhanced by a large logarithm. In fact the lepton loops contributing to the $\gamma\gamma Z$ vertex lead to corrections

$$a_\mu^{(4)\text{EW}}([f]) \simeq \frac{\sqrt{2}G_\mu m_\mu^2}{16\pi^2} \frac{\alpha}{\pi} 2T_{3f} N_{cf} Q_f^2 \left[3 \ln \frac{M_Z^2}{m_{f'}^2} + C_f \right] \tag{4.51}$$

in which $m_{f'} = m_\mu$ if $m_f \leq m_\mu$ and $m_{f'} = m_f$ if $m_f > m_\mu$ and

$$C_f = \begin{cases} 5/2 & \text{for } m_f < m_\mu \\ 11/6 - 8/9 \pi^2 & \text{for } m_f = m_\mu \\ -6 & \text{for } m_f > m_\mu . \end{cases}$$

For an individual fermion f the contribution is proportional to $N_{cf} Q_f^2 a_f$. In [144] only lepton loops were taken into account, and it is well known that the triangular subdiagram has an Adler–Bell–Jackiw (ABJ) or VVA anomaly [145], which cancels if all fermions are included. The *anomaly cancellation* is mandatory in a renormalizable theory and it forces the fermions in the SM to come in families of leptons and quarks [146]. The latter compensate the anomaly of the former. The cancellation condition of the SM reads

$$\sum_f N_{cf} Q_f^2 a_f = 0, \tag{4.52}$$

and such a cancellation is expected also for the leading short distance logarithms proportional to $\ln M_Z$ and in fact this has been checked to happen on the level of the quark parton model (QPM) for the 1st and 2nd fermion family [147, 148].

Assuming dressed constituent quarks masses $M_u, M_d > m_\mu$, the QPM result for the first family reads [148]

$$a_{\mu}^{(4)\text{EW}}([e, u, d])_{\text{QPM}} \simeq -\frac{\sqrt{2}G_{\mu}m_{\mu}^2}{16\pi^2} \frac{\alpha}{\pi} \left[\ln \frac{M_u^8}{m_{\mu}^6 M_d^2} + \frac{17}{2} \right] \simeq -4.00 \times 10^{-11}, \quad (4.53)$$

while for the second family, with $M_s, M_c > m_{\mu}$, we have

$$a_{\mu}^{(4)\text{EW}}([\mu, c, s])_{\text{QPM}} \simeq -\frac{\sqrt{2}G_{\mu}m_{\mu}^2}{16\pi^2} \frac{\alpha}{\pi} \left[\ln \frac{M_c^8}{m_{\mu}^6 M_s^2} + \frac{47}{6} - \frac{8\pi^2}{9} \right] \simeq -4.65 \times 10^{-11}. \quad (4.54)$$

For the numerical evaluation we had to insert some quark masses and we resorted to the not very well defined *constituent quark masses* used in [148]:

$$M_u = M_d = 300 \text{ MeV}, \quad M_s = 500 \text{ MeV}, \quad M_c = 1.5 \text{ GeV} \quad \text{and} \quad M_b = 4.5 \text{ GeV}. \quad (4.55)$$

It should be noted that such large effective light quark masses violate basic Ward–Takahashi identities of low energy QCD. The latter requires values like (3.38) for the so called *current quark masses* to properly account for the pattern of chiral symmetry breaking.¹⁶ The ambiguity in the choice of the quark masses reflects the fact that we are not in the perturbative regime. If one uses the above constituent quark masses to calculate the hadronic photon VP one does not get an answer which is close to what is obtained non–perturbatively from the dispersion integral of e^+e^- –data [149].

Concerning the third family, D’Hoker in [150] pointed out that a super–heavy fermion like the top, which usually is expected to decouple, generates a large log, because the heavy fermion does not participate in the cancellation of the large logs, while it still participates in the cancellation of the mass independent ABJ anomaly (see also [151]). The origin of the effect is the large weak isospin breaking in the top–bottom doublet, which is manifest in the large mass splitting $m_t \gg M_Z \gg m_b$. Consequently, one has to expect that the large logs from the leptons cancel against the ones from the quarks, with only partial cancellation in the 3rd family ($[\tau, t, b]$).

It should be stressed that results from individual fermions are gauge dependent and only sums of contributions for complete fermion families are physically meaningful. Nevertheless, we will give at intermediate steps partial result either in the Feynman gauge or in the unitary gauge.

¹⁶Adopting the values (3.38) one would have to replace the masses satisfying $m_q < m_{\mu}$ ($q = u, d, s$) by m_{μ} ($SU(3)$ chiral limit), such that [147]

$$a_{\mu}^{(4)\text{EW}}([e, u, d])_{\text{QPM}} \simeq 0$$

and

$$a_{\mu}^{(4)\text{EW}}([\mu, c, s])_{\text{QPM}} \simeq -\frac{\sqrt{2}G_{\mu}m_{\mu}^2}{16\pi^2} \frac{\alpha}{\pi} \left[4 \ln \frac{m_c^2}{m_{\mu}^2} + \frac{32}{3} - \frac{8\pi^2}{9} \right] \simeq -5.87 \times 10^{-11}.$$

However, this free current quarks result cannot be a reasonable approximation, as it completely ignores the non–perturbative QCD effects.

The leading contributions Fig. 4.19a were investigated first by Peris, Perrottet and de Rafael [147], by evaluating the hadronic effects in a low energy effective approach. The full set of diagrams of Fig. 4.19 was calculated by Czarnecki, Krause and Marciano [148], using the QPM. The results were later refined and extended in the leading log approximation by renormalization group methods at the two– as well as at the three–loop level by Degrandi and Giudice in [152]. Thereby also smaller effects, like the ones from diagram (b), were included. The latter does not give a large effect because the $\gamma - Z$ mixing propagator is of type VV with coupling strength $Q_f v_f Q_\mu v_\mu$ which is suppressed like $(1 - 4 \sin^2 \Theta_W) \sim 0.1$ for quarks and like $(1 - 4 \sin^2 \Theta_W)^2 \sim 0.01$ for leptons. Diagrams (c) to (e) have an additional heavy propagator and thus yield sub–leading terms only. In the enhanced contributions proportional to the large logs $\ln M_Z/m_f$ or $(m_t/M_W)^2$ the exact $\sin^2 \Theta_W$ dependence has been worked out. Results may be summarized as follows.

Summary of Perturbative Leading Log Results

Two loop corrections to a_μ^{weak} naturally divide into leading logs (LL), i.e., terms enhanced by a factor of $\ln(M_Z/m_f)$ where m_f is a fermion mass scale much smaller than M_Z , and everything else, which we call non–leading logs (NLL). The 2–loop leading logs are¹⁷ [147, 148, 152–154]

$$a_{\mu\text{LL}}^{(4)\text{EW}} = -\frac{\sqrt{2}G_\mu m_\mu^2}{16\pi^2} \frac{\alpha}{\pi} \left\{ \left[\frac{215}{9} + \frac{31}{9}(1 - 4s_W^2)^2 \right] \ln \frac{M_Z}{m_\mu} - \sum_{f \in F} N_{cf} Q_f \left[12 T_f^3 Q_f - \frac{8}{9} (T_f^3 - 2Q_f s_W^2) (1 - 4s_W^2) \right] \ln \frac{M_Z}{m_f} \right\}, \quad (4.56)$$

in the notation introduced above. Electron and muon loops as well as non–fermionic loops produce the $\ln(M_Z/m_\mu)$ terms in this expression (the first line) while the sum

¹⁷The LL contributions may be grouped into photonic corrections related to the first two one–loop diagrams of Fig. 4.18

$$a_\mu^{(4)\text{EW}}(W, \text{no } f\text{-loops})_{\text{LL}} = -\frac{\sqrt{2}G_\mu m_\mu^2}{16\pi^2} \frac{\alpha}{\pi} \left[\frac{40}{3} \right] \ln \frac{M_Z}{m_\mu},$$

$$a_\mu^{(4)\text{EW}}(Z, \text{no } f\text{-loops})_{\text{LL}} = \frac{\sqrt{2}G_\mu m_\mu^2}{16\pi^2} \frac{\alpha}{\pi} \left[\frac{13}{9} (g_A^\mu)^2 - \frac{23}{9} (g_V^\mu)^2 \right] \ln \frac{M_Z}{m_\mu},$$

these are part of the 2–loop bosonic corrections discussed below, and

$$a_\mu^{(4)\text{EW}}(Z, f\text{-loops})_{\text{LL}} = \frac{\sqrt{2}G_\mu m_\mu^2}{16\pi^2} \frac{\alpha}{\pi} \sum_f N_{cf} Q_f \left[-6 g_A^\mu g_A^f Q_f + \frac{4}{9} g_V^\mu g_V^f \right] \ln \frac{M_Z}{m_{f'}},$$

where the first term comes from the triangular loop (only VVA, VVV vanishing by Furry’s theorem) (diagram a) of Fig. 4.19, the second from the $\gamma - Z$ mixing propagator muon loop (only VV can contribute) (diagram b) of Fig. 4.19, with $m_{f'} \equiv \max[m_f, m_\mu]$. Here $g_V^f = 2v_f$ and $g_A^f = 2a_f$ are the neutral current coefficients (4.36).

runs over $F = \tau, u, d, s, c, b$. The logarithm $\ln(M_Z/m_f)$ in the sum implies that the fermion mass m_f is larger than m_μ . For the light quarks, such as u and d , whose current masses are very small, m_f has a meaning of some effective hadronic mass scale.

In this approximation

$$a_{\mu\text{LL}}^{(4)\text{EW}} \simeq -36.72 \times 10^{-11}, \quad (4.57)$$

which is to be compared with the full estimate Eq. (4.124), below. Note that the $(1 - 4s_W^2)$ suppressed LL terms from photonic corrections to diagram Fig. 3.7b [23/9 of the 31/9] and Fig. 4.19b [for e and μ $2 \times 4/9$ and corresponding terms (2nd term) in the sum over $f \in F$] only account a negligible contribution -31.15×10^{-13} . The un-suppressed LL terms from Fig. 4.19a [$2 \times 54/9$ of the 215/9 for e and μ plus the corresponding terms (1st term) in the sum $f \in F$] in the above expression cancel for the 1st and 2nd fermion family. What survives are the terms due to the virtual photon corrections (bosonic) of the 1-loop diagrams Fig. 3.7a, b [120/9(W) - 13/9(Z) of the 215/9] and the incomplete cancellation in the 3rd fermion family resulting as a consequence of the mass separation pattern $m_\tau, M_b \ll M_Z \ll m_t$, relative to the effective cut-off M_Z .

The hadronic effects required a much more careful study which takes into account the true structure of low energy QCD and as leading logs largely cancel a careful study of the full 2-loop corrections was necessary.

The issue about how to treat the light quarks appropriately was reconsidered and discussed somewhat controversial in [153, 155, 156]. Corresponding problems and results will be considered next.

Hadronic Effects via Quark Triangle Graphs

Since leptons and quarks can be treated family-wise only, we have to think about how to include the quarks and hadrons, which are subject to non-perturbative strong interaction effects. For the heavy quarks integrals producing a large log $\ln(M_Z/m_q)$ are dominated by contributions above the heavy scale m_q and by virtue of asymptotic freedom of QCD are calculable in pQCD. This seems to be justified to work with the QPM in a first step. In doing so we will be confronted again with the question about the meaning of the quark masses to be used in the case of the light quarks. As already mentioned, the crucial constraint is the ABJ anomaly cancellation.¹⁸ The nature of the ABJ triangle anomaly is controlled by the Adler–Bardeen non-renormalization theorem [157], which says that the one-loop anomaly is exact to all orders, by the Wess–Zumino integrability condition and the Wess–Zumino effective action [158] (see below), by Witten’s algebraic/geometrical interpretation, which requires the axial current to be normalized to an integer [159]. It means that higher order corrections are all proportional to the one-loop result and get removed by normalization

¹⁸Renormalizability, gauge invariance and current conservation is intimately related. Axial anomalies showing up in the weak interaction currents for individual fermions must cancel in order not to spoil gauge invariance and hence renormalizability.

to unity [160, 161]. Phenomenologically, it plays a key role in the prediction of $\pi^0 \rightarrow \gamma\gamma$, and in the solution of the η' mass problem. Last but not least, renormalizability of the electroweak Standard Model requires the anomaly cancellation which dictates the lepton–quark family structure.

Digression on the Anomaly

The axial anomaly is a quantum phenomenon which doesn't get renormalized by higher order effects. In QED the axial current anomaly is given by

$$\partial_\mu j_5^\mu(x) = \frac{e^2}{8\pi^2} \tilde{F}_{\mu\nu}(x) F^{\mu\nu}(x) \neq 0 \quad (4.58)$$

where $F^{\mu\nu} = \partial^\mu A^\nu - \partial^\nu A^\mu$ is the electromagnetic field strength tensor and $\tilde{F}_{\mu\nu} = \frac{1}{2}\epsilon_{\mu\nu\rho\sigma} F^{\rho\sigma}$ its dual parity odd pseudotensor. The pseudoscalar density is a divergence of a gauge dependent pseudovector

$$\tilde{F}_{\mu\nu} F^{\mu\nu} = \partial^\mu K_\mu ; \quad K_\mu = 2\epsilon_{\mu\rho\nu\sigma} A^\rho \partial^\nu A^\sigma.$$

In general, in perturbation theory the axial anomaly shows up in closed fermion loops with an odd number of axial–vector couplings if a non–vanishing γ_5 –odd trace of γ –matrices like¹⁹

$$\text{Tr} (\gamma^\mu \gamma^\nu \gamma^\rho \gamma^\sigma \gamma_5) = 4i \epsilon^{\mu\nu\rho\sigma} \quad (4.59)$$

(in $d = 4$ dimensions) is involved and if the corresponding Feynman integral is not ultraviolet convergent such that it requires regularization. The basic diagram exhibiting the axial anomaly is the linearly divergent triangle diagram Fig. 4.20 which leads to the amplitude (1st diagram)

$$\begin{aligned} \tilde{T}_{ijk}^{\mu\nu\lambda}(p_1, p_2) &= (-1) i^5 \text{Tr} (T_j T_i T_k) \frac{g^2}{(2\pi)^4} \int d^4k \\ &\times \text{Tr} \left(\frac{1}{\not{k} - \not{p}'_2 + i\epsilon} \gamma^\nu \frac{1}{\not{k} + i\epsilon} \gamma^\mu \frac{1}{\not{k} + \not{p}'_1 + i\epsilon} \gamma^\lambda \gamma_5 \right). \end{aligned}$$

If we include the Bose symmetric contribution (second diagram)

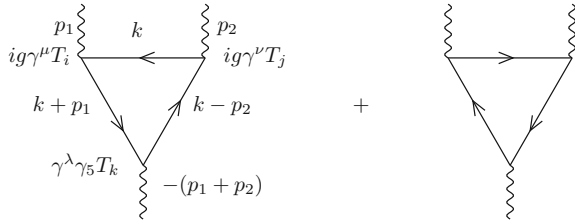
$$T_{ijk}^{\mu\nu\lambda}(p_1, p_2) = \tilde{T}_{ijk}^{\mu\nu\lambda}(p_1, p_2) + \tilde{T}_{jik}^{\nu\mu\lambda}(p_2, p_1)$$

and **impose** vector current conservation

$$p_{1\mu} T_{ijk}^{\mu\nu\lambda}(p_1, p_2) = p_{2\nu} T_{ijk}^{\mu\nu\lambda}(p_1, p_2) = 0$$

¹⁹Notice that $\text{Tr} (\prod_{i=1}^n \gamma^{\mu_i} \gamma_5) = 0$ for $n < 4$ and for all $n = \text{odd}$.

Fig. 4.20 Fermion triangle diagrams exhibiting the axial anomaly



we obtain the unambiguous regularization independent result

$$-(p_1 + p_2)_\lambda T_{ijk}^{\mu\nu\lambda}(p_1, p_2) = i \frac{g^2}{16\pi^2} D_{ijk} 4 \varepsilon^{\mu\nu\rho\sigma} p_{1\rho} p_{2\sigma} \neq 0$$

with $D_{ijk} = Tr (\{T_i, T_j\} T_k)$.

This result is independent of the masses of the fermion lines and is not changed by higher order corrections. Therefore the result is **exact** beyond perturbation theory! All anomalous fermion loops may be traced back to the basic triangular fermion loop, and in fact all other possible anomalous matrix-elements of the axial current are summarized in the general form of the anomaly equation

$$\partial_\lambda j_{5k}^\lambda(x) = \frac{g^2}{16\pi^2} D_{ijk} \tilde{G}_i^{\mu\nu}(x) G_{j\mu\nu}(x) \tag{4.60}$$

where $G_{i\mu\nu}(x)$ is the non-Abelian field strength tensor and $\tilde{G}_i^{\mu\nu}$ its dual pseudotensor. Equation (4.60) is the non-Abelian generalization of (4.58) in the Abelian case. As a result the condition for the absence of an anomaly reads

$$D_{ijk} = Tr (\{T_i, T_j\} T_k) = 0 \quad \forall (ijk) .$$

In fact the contributions to the anomaly being independent of the mass may be represented in terms of fixed helicity fields, and opposite helicities contribute with opposite signs

$$D_{ijk} \equiv Tr (\{T_{Li}, T_{Lj}\} T_{Lk}) - Tr (\{T_{Ri}, T_{Rj}\} T_{Rk}) , \tag{4.61}$$

which tells us that left-handed and right-handed fields give independent contributions to the anomaly. Only theories which are democratic with respect to helicities in the axial anomaly coefficient are anomaly free. Since $SU(2)$ has only real representations $R^* \sim R$ (in particular $2 \sim 2^*$) it cannot produce any anomaly. In contrast $SU(3)$ is not anomaly safe, because the fundamental representations 3 and the complex conjugate 3^* are inequivalent. However, as quarks in the triplet representation 3 and antiquarks in the anti-triplet representation 3^* enter symmetrically in QCD (a pure vector theory), $SU(3)_c$ cannot give rise to anomalies. Only the Abelian hyper-

charge group $U(1)_Y$ produces anomalies, which must cancel as required by the above condition.

End of the Digression

Due to the fact that perturbative QCD breaks down at low energies the handling of the quark loops or the related hadronic fluctuations pose a particular problem as the anomaly cancellation originally works on the level of quarks. Here another important theorem comes into play, however, namely 't Hooft's anomaly matching condition [162], which states that the anomaly on the level of the hadrons must be the same as the one on the level of the quarks, as a consequence of the anomaly non-renormalization theorem. An improved treatment of the hadronic contributions using an effective field theory approach has been elaborated in [155].

Structure of Contributions from Quark Triangles

Following [153], in order to discuss the contribution from VVA triangle fermions loops one has to consider the $Z^*\gamma\gamma^*$ amplitude

$$T_{\nu\lambda} = i \int d^4x e^{iqx} \langle 0 | T \{ j_\nu(x) j_{5\lambda}(0) \} | \gamma(k) \rangle \quad (4.62)$$

which by the LSZ reduction formula is equivalent to

$$T_{\nu\lambda} = e \varepsilon^\mu(k) T_{\mu\nu\lambda} ; \quad T_{\mu\nu\lambda} = - \int d^4x d^4y e^{i(qx-ky)} \langle 0 | T \{ j_\mu(x) j_\nu(y) j_{5\lambda}(0) \} | 0 \rangle$$

in which $\varepsilon_\mu(k)$ is the polarization vector for the external photon. We need $T_{\nu\lambda}(q, k)$ for small k up to quadratic terms. The corresponding covariant decomposition

$$T_{\nu\lambda} = -\frac{i e}{4\pi^2} \left[w_T(q^2) (-q^2 \tilde{f}_{\nu\lambda} + q_\nu q^\alpha \tilde{f}_{\alpha\lambda} - q_\lambda q^\alpha \tilde{f}_{\alpha\nu}) + w_L(q^2) q_\lambda q^\alpha \tilde{f}_{\alpha\nu} \right] \quad (4.63)$$

$$\tilde{f}_{\mu\nu} = \frac{1}{2} \varepsilon_{\mu\nu\alpha\beta} f^{\alpha\beta}, \quad f_{\mu\nu} = k_\mu \varepsilon_\nu - k_\nu \varepsilon_\mu$$

exhibits two terms, a transversal amplitude w_T and a longitudinal one w_L , with respect to the axial current index λ . The second rank tensor $-i f_{\mu\nu}$ corresponds to the external electromagnetic field strength tensor $F_{\mu\nu}$ with $\partial_\mu \rightarrow -ik_\mu$ and $A_\nu \rightarrow \varepsilon_\nu$.

The contribution $a_\mu^{(4)\text{EW}}([f])_{\text{VVA}}$ of a fermion f via the $Z^*\gamma\gamma^*$ amplitude, in the unitary gauge, where the Z propagator has the form $i(-g_{\mu\nu} + q_\mu q_\nu / M_Z^2) / (q^2 - M_Z^2)$, is given by²⁰

²⁰Since the result does not depend on the direction of the external muon momentum p we may average over the 4-dimensional Euclidean sphere which yields the exact 1-dimensional integral representation given.

$$\begin{aligned}
a_\mu^{(4)\text{EW}}([f])_{\text{VVA}} &= \frac{\sqrt{2}G_\mu m_\mu^2}{16\pi^2} \frac{\alpha}{\pi} i \int d^4q \frac{1}{q^2 + 2qp} \left[\frac{1}{3} \left(1 + \frac{2(qp)^2}{q^2 m_\mu^2} \right) \right. \\
&\quad \left. \times \left(w_L - \frac{M_Z^2}{M_Z^2 - q^2} w_T \right) + \frac{M_Z^2}{M_Z^2 - q^2} w_T \right] \\
&= \frac{\sqrt{2}G_\mu m_\mu^2}{16\pi^2} \frac{\alpha}{\pi} \int_0^{\Lambda^2} dQ^2 \frac{1}{6} \frac{Q^2}{m_\mu^2} \left\{ w_L(Q^2) \left((Q^2/m_\mu^2 - 2)(1 - R_m) + 2 \right) \right. \\
&\quad \left. - w_T(Q^2) \frac{M_Z^2}{M_Z^2 + Q^2} \left((Q^2/m_\mu^2 + 4)(1 - R_m) + 2 \right) \right\}, \quad (4.64)
\end{aligned}$$

in terms of the two scalar amplitudes $w_{L,T}(q^2)$. Λ is a cutoff to be taken to ∞ at the end, after summing over a family. We have performed a Wick rotation to Euclidean space with $Q^2 = -q^2$ and $R_m = \sqrt{1 + 4m_\mu^2/Q^2}$. For leading estimates we may expand in $m_\mu^2/Q^2 \ll 1$. For contributions from the heavier states it is sufficient to set $p = 0$ except in the phase space where it would produce an IR singularity. Including the leading corrections the result takes the much simpler form

$$\begin{aligned}
\Delta a_\mu^{(4)\text{EW}}([f])_{\text{VVA}} &\simeq \frac{\sqrt{2}G_\mu m_\mu^2}{16\pi^2} \frac{\alpha}{\pi} \int_{m_\mu^2}^{\Lambda^2} dQ^2 \left\{ w_L(Q^2) \left(1 - \frac{4}{3} m_\mu^2/Q^2 + \dots \right) \right. \\
&\quad \left. + \frac{M_Z^2}{M_Z^2 + Q^2} w_T(Q^2) \left(1 - \frac{2}{3} m_\mu^2/Q^2 + \dots \right) \right\}. \quad (4.65)
\end{aligned}$$

For a perturbative fermion loop to leading order [163]

$$\begin{aligned}
w_L^{1\text{-loop}}(Q^2) &= 2w_T^{1\text{-loop}}(Q^2) = \sum_f 4T_f N_{cf} Q_f^2 \int_0^1 \frac{dx x(1-x)}{x(1-x)Q^2 + m_f^2} \\
&\stackrel{m_f^2 \ll Q^2}{\simeq} \sum_f 4T_f N_{cf} Q_f^2 \left[\frac{1}{Q^2} - \frac{2m_f^2}{Q^4} \ln \frac{Q^2}{m_f^2} + O\left(\frac{1}{Q^6}\right) \right].
\end{aligned}$$

Vainshtein [164] has shown that in the chiral limit the relation

$$w_T(Q^2)_{\text{pQCD}}|_{m=0} = \frac{1}{2} w_L(Q^2)|_{m=0} \quad (4.66)$$

is valid actually to all orders of perturbative QCD in the kinematic limit relevant for the $g - 2$ contribution. Thus the non-renormalization theorem valid beyond pQCD for the anomalous amplitude w_L (considering the quarks $q = u, d, s, c, b, t$ only):

$$w_L(Q^2)|_{m=0} = w_L^{1\text{-loop}}(Q^2)|_{m=0} = \sum_q (2T_q Q_q^2) \frac{2N_c}{Q^2} \quad (4.67)$$

carries over to the perturbative part of the transversal amplitude. Thus in the chiral limit the perturbative QPM result for w_T is exact in pQCD. This may be somewhat puzzling, since in low energy effective QCD, which encodes the non-perturbative strong interaction effects, this kind of term seems to be absent. The non-renormalization theorem has been proven independently in [165] and was extended to the full off-shell triangle amplitude to 2 loops in [160], to 3 loops in [161].

One knows that there are non-perturbative corrections to Vainshtein's relation (4.66) but no ones of perturbative origin. A simple heuristic proof of Vainshtein's theorem proceeds by first looking at the imaginary part of (4.62) and the covariant decomposition (4.63). In accordance with the Cutkosky rules (see footnote 29 on p. 97 in Chap. 2) the imaginary part of an amplitude is always more convergent than the amplitude itself. The imaginary part of the one-loop result is finite and one does not need a regularization to calculate it unambiguously. In particular, it allows us to use anti-commuting γ_5 to move it from the axial vertex $\gamma_\lambda \gamma_5$ to the vector vertex γ_ν . In the limit $m_f = 0$, this involves anti-commuting γ_5 with an even number of γ -matrices, no matter how many gluons are attached to the quark line joining the two vertices. As a result $\text{Im } T_{\nu\lambda}$ must be symmetric under $\nu \leftrightarrow \lambda$, $q \leftrightarrow -q$:

$$\text{Im} \left[w_T(q^2) (-q^2 \tilde{f}_{\nu\lambda} + q_\nu q^\alpha \tilde{f}_{\alpha\lambda} - q_\lambda q^\alpha \tilde{f}_{\alpha\nu}) + w_L(q^2) q_\lambda q^\alpha \tilde{f}_{\alpha\nu} \right] \propto q_\nu q^\alpha \tilde{f}_{\alpha\lambda} + q_\lambda q^\alpha \tilde{f}_{\alpha\nu}$$

which, on the l.h.s., requires that $q^2 = 0$, to get rid of the antisymmetric term proportional to $\tilde{f}_{\nu\lambda}$, and that w_T is proportional to w_L : $w_L = c w_T$; the symmetry follows when $c = 2$. Thus the absence of an antisymmetric part is possible only if

$$2\text{Im } w_T(q^2) = \text{Im } w_L(q^2) = \text{constant} \times \delta(q^2), \quad (4.68)$$

where the constant is fixed to be $2\pi \cdot 2T_{3f} N_{cf} Q_f^2$ by the exact form of w_L . Both w_L and w_T are analytic functions which fall off sufficiently fast at large q^2 such that they satisfy convergent DRs

$$w_{T,L}(q^2) = \frac{1}{\pi} \int_0^\infty ds \frac{\text{Im } w_{T,L}(s)}{s - q^2}$$

which together with (4.68) implies (4.66). While w_L as given by (4.67) is exact beyond perturbation theory, according to the Adler-Bardeen non-renormalization theorem and by the topological nature of the anomaly [159], as a consequence of Vainshtein's non-renormalization theorem for w_T we have

$$w_T(q^2) = \frac{2T_{3f} N_{cf} Q_f^2}{Q^2} + \text{non-perturbative corrections}. \quad (4.69)$$

Coming back to the calculation of (4.65), we observe that the contributions from w_L for individual fermions is logarithmically divergent, but it completely drops for a complete family due to the vanishing anomaly cancellation coefficient. The

contribution from w_T is convergent for individual fermions due to the damping by the Z propagator. In fact it is the leading $1/Q^2$ term of the w_T amplitude which produces the $\ln \frac{M_Z}{m}$ terms. However, the coefficient is the same as the one for the anomalous term and thus for each complete family also the $\ln M_Z$ terms must drop out. Due to the non-renormalization theorem (4.66) the perturbative leading $1/Q^2$ term of w_T has to carry over to a low energy effective approach of QCD (see below).

Results for Contributions from Fermion Loops

For the third family the calculation is perturbative and thus straight forward with the result [147, 148, 155]

$$\begin{aligned} a_\mu^{(4)\text{EW}}([\tau, b, t]) &= -\frac{\sqrt{2}G_\mu m_\mu^2}{16\pi^2} \frac{\alpha}{\pi} \left[\frac{8}{3} \ln \frac{m_\tau^2}{M_Z^2} - \frac{2}{9} \frac{M_Z^2}{m_t^2} \left(\ln \frac{m_t^2}{M_Z^2} + \frac{5}{3} \right) \right. \\ &\quad \left. + \ln \frac{M_Z^2}{m_b^2} + 3 \ln \frac{M_Z^2}{m_\tau^2} - \frac{8}{3} + \dots \right] \\ &\simeq -\frac{\sqrt{2}G_\mu m_\mu^2}{16\pi^2} \frac{\alpha}{\pi} \times 30.2(3) \simeq -8.19(10) \times 10^{-11}. \quad (4.70) \end{aligned}$$

Small terms of order m_μ^2/m_τ^2 , m_b^2/M_Z^2 , M_Z^4/m_t^4 and smaller mass ratios have been neglected.

While the QPM results presented above, indeed confirmed the complete cancellation of the $\ln M_Z$ terms for the 1st and 2nd family, in the third family the corresponding terms $\ln M_Z/m_\tau$ and $\ln M_Z/m_b$ remain unbalanced by a corresponding top contribution.

Since in the perturbative regime QCD corrections are of $O(\alpha_s(\mu^2)/\pi)$, where μ is in the range from m_f to M_Z , pQCD is applicable for c , b and t quarks, only (see Fig. 3.3). For the lighter quarks u , d and s , however, the QPM estimate certainly is not appropriate because strong interaction corrections are expected to contribute beyond perturbation theory and assuming that non-perturbative effects just lead to a dressing of the quark masses into constituent quarks masses certainly is an oversimplification of reality. Most importantly, pQCD does not account for the fact that the chiral symmetry is spontaneously broken the mechanism responsible for the emergence of the pions as quasi Nambu–Goldstone bosons. The failure of the QPM we have illustrated in the discussion following p. 183 for the much simpler case of the hadronic vacuum polarization, already. We thus have to think about other means to take into account properly the low energy hadronic effects, if possible.

Digression on the Chiral Structure of Low Energy Effective QCD

Fortunately, a firm low energy effective theory of QCD exists and is very well developed: Chiral Perturbation Theory (CHPT) [166], an expansion for low momenta p and in the light current quark masses as chiral symmetry breaking parameters. CHPT is based on the chiral flavor structure $SU(3)_L \otimes SU(3)_R$ of the low lying hadron spectrum (u, d, s quark bound states). The $SU(3)_V$ vector currents

$j_k^\mu = \sum_{ij} \bar{\psi}_i (T_k)_{ij} \gamma^\mu \psi_j$ as well as the $SU(3)_A$ axial currents $j_{5k}^\mu = \sum_{ij} \bar{\psi}_i (T_k)_{ij} \gamma^\mu \gamma_5 \psi_j$ ²¹ are partially conserved in the $SU(3)$ sector of the (u, d, s) quark flavors, and strictly conserved in the chiral limit of vanishing quark masses $m_u, m_d, m_s \rightarrow 0$, modulo the axial anomaly in the axial singlet current. The partial conservation of the chiral currents²² derives from $\partial_\mu (\bar{\psi}_1 \gamma^\mu \psi_2) = i(m_1 - m_2) \bar{\psi}_1 \psi_2$ (CVC in the isospin limit $m_u = m_d$) and $\partial_\mu (\bar{\psi}_1 \gamma^\mu \gamma_5 \psi_2) = i(m_1 + m_2) \bar{\psi}_1 \gamma_5 \psi_2$ (PCAC) and the setup of a perturbative scheme is based on the phenomenologically observed smallness of the current quark masses (3.38).

The chiral expansion of the effective Lagrangian is an expansion in \hbar

$$\mathcal{L}_{\text{eff}} = \mathcal{L}_2 + \hbar \mathcal{L}_4 + \hbar^2 \mathcal{L}_6 + \dots \quad (4.71)$$

which is equivalent to an expansion in powers of derivatives and quark masses. In standard chiral counting one power of quark mass counts as two powers of derivatives, or momentum p in momentum space. In chiral $SU(3)$ there exists an octet of massless pseudoscalar particles (π, K, η) , the Nambu–Goldstone bosons in the chiral limit. The leading term of the expansion is the non-linear σ -model, where the pseudoscalars are encoded in a unitary 3×3 matrix field

$$U(\phi) = \exp\left(-i\sqrt{2} \frac{\phi(x)}{F}\right) \quad (4.72)$$

with $(T_i$ the $SU(3)$ generators)

$$\phi(x) = \sum_i T_i \phi_i = \begin{pmatrix} \frac{\pi^0}{\sqrt{2}} + \frac{\eta}{\sqrt{6}} & \pi^+ & K^+ \\ \pi^- & \frac{-\pi^0}{\sqrt{2}} + \frac{\eta}{\sqrt{6}} & K^0 \\ K^- & \bar{K}^0 & -2\frac{\eta}{\sqrt{6}} \end{pmatrix} + \frac{1}{\sqrt{3}} \begin{pmatrix} \eta' & & \\ & \eta' & \\ & & \eta' \end{pmatrix} \quad (4.73)$$

where the second term is the diagonal singlet contribution by the η' meson. The latter is not a Nambu–Goldstone boson, however it is of leading order in $1/N_c$. The leading order Lagrangian at $O(p^2)$ is then given by

$$\mathcal{L}_2 = \frac{F^2}{4} \text{Tr} \{D^\mu U D_\mu U^\dagger + M^2 (U + U^\dagger)\} \quad (4.74)$$

where, in absence of external fields, the covariant derivative $D_\mu U = \partial_\mu U$ coincides with the normal derivative. Furthermore, $M^2 = 2B\hat{m}$, where B is proportional to the quark condensate $\langle 0|\bar{u}u|0\rangle$ and $\hat{m} = \frac{1}{2}(m_u + m_d)$. In the chiral limit of exact $SU(3)_R \otimes SU(3)_L$ symmetry we have

²¹ T_k ($k = 1, \dots, 8$) are the generators of the global $SU(3)$ transformations and $i, j = u, d, s$ flavor indices.

²²Especially in the $SU(2)$ isospin subspace, the small mass splitting $|m_1 - m_2| \ll m_1 + m_2$ motivates the terminology: conserved vector current (CVC) and partially conserved axial vector current (PCAC) (see next page).

$$\langle 0|\bar{u}u|0\rangle = \langle 0|\bar{d}d|0\rangle = \langle 0|\bar{s}s|0\rangle .$$

The parameters M and F are the leading order versions of the pion mass and the pion decay constant, respectively:

$$m_\pi^2 = M^2 [1 + O(\hat{m})] , \quad F_\pi = F [1 + O(\hat{m})] .$$

The low energy effective currents again are nonlinear in the pion fields and in CHPT again appear expanded in the derivatives of U and the quark masses. For vector and axial–vector current one obtains

$$V_\mu^i = \frac{iF^2}{4} \langle \sigma^i (U^\dagger D_\mu U + U D_\mu U^\dagger) \rangle + O(p^3) = [\varepsilon^{ijk} \phi^j \partial_\mu \phi^k + O(\phi^3)] + O(p^3) ,$$

$$A_\mu^i = \frac{iF^2}{4} \langle \sigma^i (U^\dagger D_\mu U - U D_\mu U^\dagger) \rangle + O(p^3) = [-F \partial_\mu \phi^i + O(\phi^3)] + O(p^3) ,$$

which implies the conserved vector current (CVC) and the partially conserved axial vector current (PCAC) relations. Despite the fact that this Lagrangian is non-renormalizable, one can use it to calculate matrix elements like in standard perturbation theory. However, unlike in renormalizable theories where only terms already present in the original bare Lagrangian get reshuffled by renormalization, in non-renormalizable theories order by order in the expansion new vertices of increasing dimensions and associated new free couplings called *low energy constants* show up and limit the predictive power of the effective theory.

At physical quark masses the value of the condensate is estimated to be $\langle m_q \bar{q}q \rangle \sim -(0.098 \text{ GeV})^4$ for $q = u, d$. The key relation to identify the quark condensates in terms of physical quantities is the Gell-Mann, Oakes and Renner (GMOR) [167, 168] relation. In the chiral limit the mass operators $\bar{q}_R u_L$, or $\bar{q}_L u_R$ transform under $(3^*, 3)$ of the chiral group $SU(3)_L \otimes SU(3)_R$. Hence the quark condensates would have to vanish identically in the case of an exact chirally symmetric world. In fact the symmetry is spontaneously broken and the vacuum of the real world is not chirally symmetric. Therefore the quark condensates do not have to vanish. In order to determine the quark condensates, consider the charged axial currents and the related pseudoscalar density

$$A_\mu = \bar{d} \gamma_\mu \gamma_5 u$$

$$P = \bar{d} i \gamma_5 u$$

and the OPE of the product

$$A_\mu(x) P^+(y) = \sum_i C_\mu^i(x-y) \mathcal{O}^i\left(\frac{x+y}{2}\right) .$$

In QCD we may inspect the short distance expansion and study its consequences. One observation is that taking the VEV only the scalar operators contribute and one obtains the exact relation

$$\langle 0|A_\mu(x) P^+(y)|0\rangle = \frac{(x-y)_\mu}{2\pi^2(x-y)^4} \langle 0|\bar{u}u + \bar{d}d|0\rangle. \quad (4.75)$$

The spectral representation (see (3.131)) for the two-point function on the l.h.s. is of the form $p_\mu \rho(p^2)$ and current conservation requires $p^2 \rho(p^2) = 0$ such that only the Nambu–Goldstone modes, the massless pions, contribute, such that with

$$\begin{aligned} \langle 0|A_\mu(0)|\pi^+\rangle &= i F_\pi p_\mu \\ \langle 0|P^+(0)|\pi^+\rangle &= g_\pi \end{aligned}$$

we get

$$F_\pi g_\pi = -\langle 0|\bar{u}u + \bar{d}d|0\rangle.$$

For non-vanishing quark masses the PCAC relation $\partial^\mu A_\mu = (m_u + m_d) P$ then implies the exact relation

$$F_\pi m_{\pi^+}^2 = (m_u + m_d) g_\pi$$

and the famous GMOR relation

$$F_\pi^2 m_{\pi^+}^2 = -(m_u + m_d) \langle 0|\bar{u}u + \bar{d}d|0\rangle \quad (4.76)$$

follows from the last two relations. Note that the quark condensates must be negative! They are a measure for the asymmetry of the vacuum in the chiral limit, and thus are true order parameters. If both F_π and $\langle 0|\bar{u}u + \bar{d}d|0\rangle$ have finite limits as $m_q \rightarrow 0$ the pion mass square must go to zero linear with the quark masses

$$m_{\pi^+}^2 = B (m_u + m_d); \quad B \equiv -\frac{1}{F_\pi^2} \langle 0|\bar{u}u + \bar{d}d|0\rangle; \quad B > 0.$$

The deviation from the chiral limit is controlled by CHPT. The quark masses as well as the quark condensates depend on the renormalization scale μ , however, the product $\langle 0|m_q \bar{q}q|0\rangle$ is RG invariant as is inferred by the GMOR relation.

For later reference we are interested in the momentum space version of (4.75). We look at the time-ordered vacuum expectation value and using translational invariance we may choose $y = 0$ and thus consider

$$\int d^4x e^{ipx} \langle 0|T \{A_\mu(x) P^+(0)\} |0\rangle = \frac{p_\mu}{p^2 + i\varepsilon} \langle 0|\bar{u}u + \bar{d}d|0\rangle. \quad (4.77)$$

Since the Fourier transform of the singular r.h.s of (4.75) is not trivial to perform directly, we can derive the result as follows: first the result obviously is proportional to the quark condensate, which we may denote by $\langle \bar{q}q \rangle$. We note that A_μ , P and $\langle \bar{q}q \rangle$ all have dimension $\dim = 3$. Furthermore the result is a function of the four momentum

p only and a covariant vector thereof. The dimension then requires another factor $1/(p^2 + i\varepsilon)$ with the usual $i\varepsilon$ prescription for Feynman type propagators. Indeed the $1/p^2$ factor is nothing but the propagator of the pion (in the chiral limit) to which P is the interpolating field:



End of the Digression

In [147] the light quark contribution to Fig. 4.19a were evaluated using the low energy effective form of QCD which is CHPT. To lowest order in the chiral expansion, the hadronic $Z\gamma\gamma$ interaction is dominated by the pseudoscalar meson (the quasi Nambu–Goldstone bosons) exchange. The corresponding effective couplings are given by

$$\mathcal{L}^{(2)} = -\frac{e}{2 \sin \Theta_W \cos \Theta_W} F_\pi \partial_\mu \left(\pi^0 + \frac{1}{\sqrt{3}} \eta_8 - \frac{1}{\sqrt{6}} \eta_0 \right) Z^\mu, \quad (4.78)$$

which is the relevant part of the $O(p^2)$ chiral effective Lagrangian, and the effective $O(p^4)$ coupling

$$\mathcal{L}_{WZW} = \frac{\alpha}{\pi} \frac{N_c}{12 F_\pi} \left(\pi^0 + \frac{1}{\sqrt{3}} \eta_8 + 2\sqrt{\frac{2}{3}} \eta_0 \right) \tilde{F}_{\mu\nu} F^{\mu\nu}, \quad (4.79)$$

which is the Wess–Zumino–Witten Lagrangian. The latter reproduces the ABJ anomaly on the level of the hadrons. π^0 is the neutral pion field, F_π the pion decay constant ($F_\pi = 92.4$ MeV). The pseudoscalars η_8, η_0 are mixing into the physical states η, η' . The $[u, d, s]$ contribution with long distance (L.D.) part ($E < \mu$) evaluated in CHPT and a short distance (S.D.) part ($E > \mu$) to be evaluated in the QPM. The cut–off for matching L.D. and S.D. part typically is $M_\Lambda = m_P \sim 1$ GeV to $M_\Lambda = M_\tau \sim 2$ GeV. The corresponding diagrams are shown in Fig. 4.21, which together with its crossed version in the unitary gauge and in the chiral limit, up to terms suppressed by m_μ^2/M_Λ^2 , yields²³

²³The simplest way to implement the lower cut–off M_Λ to the low energy effective field theory (EFT) is to write in (4.65)

$$\frac{1}{M_Z^2 + Q^2} = \underbrace{\frac{1}{M_\Lambda^2 + Q^2}}_{EFT} + \underbrace{\frac{1}{M_Z^2 + Q^2} - \frac{1}{M_\Lambda^2 + Q^2}}_{QPM}$$

by using the QPM for the second term. In the first term M_Z is replaced by M_Λ , in the second term constant terms drop out in the difference as the quark masses in any case have values far below the cut–offs.

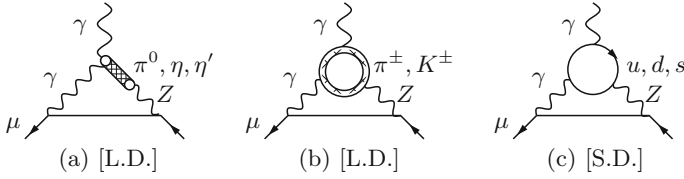


Fig. 4.21 The two leading CHPT diagrams (L.D.) and the QPM diagram (S.D.). The charged pion loop is sub-leading and will be discarded

$$\begin{aligned}
 a_{\mu}^{(4)\text{EW}}([u, d, s]; p < M_{\Lambda})_{\text{CHPT}} &= \frac{\sqrt{2}G_{\mu} m_{\mu}^2}{16\pi^2} \frac{\alpha}{\pi} \left[\frac{4}{3} \ln \frac{M_{\Lambda}^2}{m_{\mu}^2} + \frac{2}{3} \right] \\
 &\simeq 2.10 \times 10^{-11}, \\
 a_{\mu}^{(4)\text{EW}}([u, d, s]; p > M_{\Lambda})_{\text{QPM}} &= \frac{\sqrt{2}G_{\mu} m_{\mu}^2}{16\pi^2} \frac{\alpha}{\pi} \left[2 \ln \frac{M_{\Lambda}^2}{M_c^2} \right] \\
 &\simeq 4.45 \times 10^{-11}.
 \end{aligned}$$

Note that the last diagram of Fig. 4.21 in fact takes into account the leading term of (4.69) which is protected by Vainshtein's relation (4.66).

Above a divergent term has been dropped, as it cancels against corresponding terms from the complementary contributions from e , μ and c fermion-loops. Including the finite contributions from e , μ and c :

$$\begin{aligned}
 a_{\mu}^{(4)\text{EW}}([e, \mu, c])_{\text{QPM}} &= \frac{\sqrt{2}G_{\mu} m_{\mu}^2}{16\pi^2} \frac{\alpha}{\pi} \left[-6 \ln \frac{M_Z^2}{m_{\mu}^2} + 4 \ln \frac{M_Z^2}{M_c^2} - \frac{37}{3} + \frac{8}{9}\pi^2 \right] \\
 &\simeq -\frac{\sqrt{2}G_{\mu} m_{\mu}^2}{16\pi^2} \frac{\alpha}{\pi} \times 51.83 \simeq -14.04 \times 10^{-11}
 \end{aligned}$$

the complete answer for the 1st plus 2nd family reads [147]

$$\begin{aligned}
 a_{\mu}^{(4)\text{EW}} \left(\begin{bmatrix} e, u, d \\ \mu, c, s \end{bmatrix} \right)_{\text{CHPT}} &= \frac{\sqrt{2}G_{\mu} m_{\mu}^2}{16\pi^2} \frac{\alpha}{\pi} \left[-\frac{14}{3} \ln \frac{M_{\Lambda}^2}{m_{\mu}^2} + 4 \ln \frac{M_{\Lambda}^2}{M_c^2} - \frac{35}{3} + \frac{8}{9}\pi^2 \right] \\
 &\simeq -\frac{\sqrt{2}G_{\mu} m_{\mu}^2}{16\pi^2} \frac{\alpha}{\pi} \times 27.58(46) \simeq -7.47(13) \times 10^{-11}. \quad (4.80)
 \end{aligned}$$

In (4.80) the error comes from varying the cut-off M_{Λ} between 1 and 2 GeV. Below 1 GeV CHPT can be trusted above 2 GeV we can trust pQCD. Fortunately the result is not very sensitive to the choice of the cut-off.²⁴

²⁴If no cut-off is applied to the validity of the effective theory as in [147] one gets -8.58×10^{-11} , in which case an unphysical residual $\ln M_Z$ dependence persists. The QPM result taking the rather arbitrary constituent quark masses (4.55) is -8.65×10^{-11} . The QPM result taking current quark masses (3.38) is -5.87×10^{-11} . In [153] the leading logarithmic estimate is -6.72×10^{-11}

On the other hands results depend quite strongly on the quark masses utilized. This result was refined by a more elaborate analysis in which sub-leading terms were calculated using the operator product expansion (OPE).

Digression on the Operator Product Expansion

The operator product expansion (Wilson short distance expansion) [169] is a formal expansion of the product of two local field operators $A(x) B(y)$ in powers of the distance $(x - y) \rightarrow 0$ in terms of singular coefficient functions and regular composite operators:

$$A(x) B(y) \simeq \sum_i C_i(x - y) \mathcal{O}_i\left(\frac{x + y}{2}\right)$$

where the operators $\mathcal{O}_i(\frac{x+y}{2})$ represent a complete system of local operators of increasing dimensions. The coefficients may be calculated formally by normal perturbation theory by looking at the Green functions

$$\langle 0|T A(x) B(y) X|0\rangle = \sum_{i=0}^N C_i(x - y) \langle 0|T \mathcal{O}_i\left(\frac{x + y}{2}\right) X|0\rangle + R_N(x, y)$$

constructed such that

$$R_N \rightarrow 0 \text{ as } (x - y)^{a_N}; \quad (x - y)^2 < 0 \\ a_N < a_{N+1} \quad \forall N$$

(asymptotic expansion). By X we denoted any product of fields suitable to define a physical state $|X\rangle$ via the LSZ reduction formula (see Table 2.1).

The OPE is a very important tool in particular in the intrinsically non-perturbative strong interaction dynamics, which is perturbative at short distances only, by virtue of asymptotic freedom. It serves to separate soft non-perturbative low energy effects from hard perturbative high energy effects in the case a hadronic process involves a highly energetic sub process. Typically, the short distance singular coefficient functions are often accessible to pQCD while the soft effects are factored out into a non-perturbative matrix elements of appropriate composite operators. The latter in many cases may be determined by experiment or by non-perturbative methods like QCD on a lattice. One of the most prominent examples of the application of the OPE is deep inelastic electron-nucleon scattering (DIS), which uncovered the quark structure of hadrons at short wave lengths. The factorization into coefficients and matrix elements in the OPE is renormalization scheme dependent and in particular depends on the renormalization scale μ . The factorization into hard and soft physics

(Footnote 24 continued)

(Eqs. (26) plus (28) of [153]), while a refined estimate yields -6.65×10^{-11} (Eqs. (60) plus (65) of [153]) fairly close to our estimate (4.80).

requires the condition $m_f \ll \mu \ll Q$, which we will assume to be satisfied in the following. For a more comprehensive elaboration of the subject I recommend Shifman’s lectures [170].

At the heart of the OPE is the following basic problem: Local products of quantum fields in general are singular, for two scalar fields in scalar φ^4 -theory for example

$$T\{\varphi(x) \varphi(y) X\} |_{\lim x \rightarrow y} \sim \begin{array}{c} x \quad y \\ \circ \quad \circ \\ | \quad | \\ \text{---} \\ \circ \\ | \\ X \end{array} \xrightarrow{x \rightarrow y} \begin{array}{c} x = y \\ \circ \\ | \\ \text{---} \\ \circ \\ | \\ X \end{array}$$

creates a loop which in general is UV singular, the obtained composite field $\varphi^2(x = y)$ is defined after subtraction of a UV singular term only, i.e., it requires renormalization. In fact a series of new divergences shows up: all superficially divergent sub-diagrams, which contain the generated vertex:

$$x = y = \begin{array}{c} \circ \\ | \\ \text{---} \\ \circ \\ | \\ X \end{array} = \begin{array}{c} \text{---} \\ \circ \\ | \\ \text{---} \\ \circ \\ | \\ X \end{array} \gamma_0 + \begin{array}{c} \text{---} \\ \circ \\ | \\ \text{---} \\ \circ \\ | \\ X \end{array} \gamma_1 + \begin{array}{c} \text{---} \\ \circ \\ | \\ \text{---} \\ \circ \\ | \\ X \end{array} \gamma_2 + \dots + \begin{array}{c} \text{---} \\ \circ \\ | \\ \text{---} \\ \circ \\ | \\ X \end{array} \gamma_3 + \dots$$

The dots represent derivatives in configuration space or multiplication of the line with the corresponding momentum in momentum space. The dashed circles enclose a renormalization part which corresponds to a constant, and graphically contracts into a point. The superficial divergence of the corresponding sub-diagrams γ_i in $d = 4$ dimensions is given by $\dim \gamma_i = 4 - N_i - L_i + \dim \varphi^2$; $\dim \varphi^2 = 2$, where N_i is the number of φ -lines and L_i the number of derivatives on φ -lines. The subtraction factors multiply Green functions or matrix elements with insertions of operators of increasing dimensions. The Wilson expansion isolates the subtraction terms related to sub-diagrams $\tilde{\gamma}_i$ which translate into γ_i by identifying $x = y$:

$$\begin{array}{c} x \quad y \\ \circ \quad \circ \\ | \quad | \\ \text{---} \\ \circ \\ | \\ X \end{array} = \left\{ \begin{array}{c} \circ \quad \circ \\ | \quad | \\ \text{---} \\ \circ \end{array} \right\}_{\tilde{\gamma}_0} \times \begin{array}{c} \text{---} \\ \circ \\ | \\ X \end{array} + \left\{ \begin{array}{c} \circ \quad \circ \\ | \quad | \\ \text{---} \\ \circ \end{array} \right\}_{\tilde{\gamma}_1} \times \begin{array}{c} \circ \\ | \\ \text{---} \\ \circ \\ | \\ X \end{array} + \left\{ \begin{array}{c} \circ \quad \circ \\ | \quad | \\ \text{---} \\ \circ \end{array} \right\}_{\tilde{\gamma}_2} \times \begin{array}{c} \text{---} \\ \circ \\ | \\ \text{---} \\ \circ \\ | \\ X \end{array} + \left\{ \begin{array}{c} \circ \quad \circ \\ | \quad | \\ \text{---} \\ \circ \end{array} \right\}_{\tilde{\gamma}_3} \times \begin{array}{c} \circ \\ | \\ \text{---} \\ \circ \\ | \\ X \end{array} + \dots$$

The first factor of each term represents the coefficient $C_i(x - y)$ the second the operator matrix element $\langle 0 | T \mathcal{O}_i(\frac{x+y}{2}) | X \rangle$.

For a product of two currents the procedure is similar. The object of interest in our case is

$$T\{j_\nu(x) j_{5\lambda}(0)\} = T\{\bar{\psi}(x)\gamma_\nu \psi(x) : : \bar{\psi}(0)\gamma_\lambda\gamma_5\psi(0) : : \}$$

where the Wick ordering $:\cdots:$ is the prescription that only fields from different vertices are to be contracted (see p. 47). A contraction of two free Fermi fields under the T -product represents a Dirac propagator

$$T\{\psi_{\alpha ci}(x)\bar{\psi}_{\beta c'j}(y)\}_{\text{free}} = i S_{F\alpha\beta}(x-y; m_i) \delta_{cc'}\delta_{ij} - : \bar{\psi}_{\beta c'j}(y)\psi_{\alpha ci}(x) :$$

for a free field. In our example the currents are diagonal in color and flavor and we hence suppress color and flavor indices. We thus obtain in the case of free fields

$$\begin{aligned} T\{j_\nu(x)j_{5\lambda}(0)\}_{\text{free}} &= T\{:\bar{\psi}_\alpha(x)(\gamma_\nu)_{\alpha\beta}\psi_\beta(x): : \bar{\psi}_{\alpha'}(0)(\gamma_\lambda\gamma_5)_{\alpha'\beta'}\psi_{\beta'}(0):\} \\ &= (-1)i S_{F\beta'\alpha}(-x; m_f)(\gamma_\nu)_{\alpha\beta} i S_{F\beta\alpha'}(x; m_f)(\gamma_\lambda\gamma_5)_{\alpha'\beta'} \\ &\quad + i : \bar{\psi}_\alpha(x)(\gamma_\nu)_{\alpha\beta} S_{F\beta\alpha'}(x; m_f)(\gamma_\lambda\gamma_5)_{\alpha'\beta'}\psi_{\beta'}(0) : \\ &\quad + i : \bar{\psi}_{\alpha'}(0)(\gamma_\lambda\gamma_5)_{\alpha'\beta'} S_{F\beta'\alpha}(-x; m_f)(\gamma_\nu)_{\alpha\beta}\psi_\beta(x) : \\ &\quad + : j_\nu(x)j_{5\lambda}(0) : \end{aligned}$$

$$= (-1) \text{diagram 1} + \text{diagram 2} + \text{diagram 3} + \text{diagram 4} \tag{4.81}$$

The first term in fact is zero. A two point correlator of VA-type vanishes identically,²⁵ however, for VV- or AA-type of products of currents such a term in general is present. For the second and third term we may proceed as follows: the Dirac propagators have the form

$$S_{F\alpha\beta}(x-y; m_i) = (i\gamma^\mu\partial_\mu + m_i)_{\alpha\beta} \Delta_F(x-y, m_i)$$

where $\Delta_F(x-y, m_i)$ is the scalar Feynman propagator (see (2.3)) $i/(p^2 - m_i^2 + i\varepsilon)$ in momentum space, and the Dirac algebra may be easily worked out by using the Chisholm identity

$$\gamma^\nu\gamma^\alpha\gamma^\lambda = (g^{\nu\alpha}g^{\lambda\beta} + g^{\lambda\alpha}g^{\nu\beta} - g^{\nu\lambda}g^{\alpha\beta})\gamma_\beta - i\varepsilon^{\nu\alpha\lambda\beta}\gamma_\beta\gamma_5 .$$

The two terms correspond to the symmetric and the antisymmetric part. In the chiral limit then only terms exhibiting one γ matrix are left which enter bilocal vector or axial vector currents of the form

$$\begin{aligned} J_\beta^V(x, 0) &\equiv : \bar{\psi}(x)\gamma_\beta\psi(0) : \\ J_\beta^A(x, 0) &\equiv : \bar{\psi}(x)\gamma_\beta\gamma_5\psi(0) : . \end{aligned} \tag{4.82}$$

²⁵In momentum space the γ_5 -odd trace yields terms proportional to $\varepsilon_{\nu\lambda\alpha\beta}$ where the two indices α and β have to be contracted with momenta or with $g^{\alpha\beta}$, yielding a vanishing result. In a propagator there is only one momentum p available, but $p^\alpha p^\beta$ is symmetric and contracts to zero with the anti-symmetric ε -tensor.

In the presence of interactions and a set of other fields X characterizing a state $|X\rangle$ we graphically may write

$$T\{j_\nu(x) j_{5,\lambda}(0) X\} =$$

$$(-1) \left[\text{Diagram 1} + \text{Diagram 2} + \text{Diagram 3} + \text{Diagram 4} \right] \quad (4.83)$$

The Wilson OPE is obtained by expanding the bilocal current $\bar{\psi}(x) \cdots \psi(0)$ in x . In the free field case these Wick monomials are regular for $x \rightarrow 0$ as the singular term, the first term of (4.81), has been split off. It is therefore possible to perform a Taylor series expansion in x

$$:\bar{\psi}(x) \cdots \psi(0): = \sum_{n=0}^{\infty} \frac{1}{n!} x^{\mu_1} \cdots x^{\mu_n} : \bar{\psi}(0) \overleftarrow{\partial}_{\mu_1} \cdots \overleftarrow{\partial}_{\mu_n} \cdots \psi(0) :$$

and

$$:\bar{\psi}(0) \cdots \psi(x): = \sum_{n=0}^{\infty} \frac{1}{n!} x^{\mu_1} \cdots x^{\mu_n} : \bar{\psi}(0) \cdots \overrightarrow{\partial}_{\mu_1} \cdots \overrightarrow{\partial}_{\mu_n} \psi(0) :$$

The bilocal operators thus take the form

$$J_\mu^X(x, 0) = \sum_{n=0}^{\infty} \frac{1}{n!} x^{\mu_1} \cdots x^{\mu_n} \mathcal{O}_{\mu_1 \cdots \mu_n; \mu}^X(0).$$

In momentum space factors x^μ are represented by a derivative with respect to momentum $-i \frac{\partial}{\partial p_\mu}$. In gauge theories, like QED and QCD, of course derivatives in x -space have to be replaced by covariant derivatives in order to keep track of gauge invariance. In general it is not too difficult to guess the form of the possible leading, sub-leading etc. operators from the tensor structure and the other symmetries. For the second term above, as an example, diagrammatically we have

$$\begin{aligned} & \text{Diagram 2} = \text{Diagram 2a} \times \text{Diagram 2b} + \text{Diagram 2c} \times \text{Diagram 2d} + \dots \\ & \stackrel{X \rightarrow \gamma}{\equiv} \text{Diagram 2e} \times \text{Diagram 2f} + \text{Diagram 2g} \times \text{Diagram 2h} + \dots \end{aligned} \quad (4.84)$$

where the first coefficient diagram in leading order is the VVA triangle diagram, the second coefficient diagram in leading order is a Compton scattering like tree diagram. The second line shows the leading perturbative terms in the case the “final state” X is a photon γ . The other terms of (4.83) may be worked out along the same lines.

We now turn back to the Marseille group application of the OPE in calculating hadronic effects in the weak contributions to $g-2$. For this purpose the state $|X\rangle$ is the external one-photon state $|\gamma(k)\rangle$ in the classical limit, where it describes an external magnetic field. The first term of (4.83) in this case does not contribute. The diagrammatic representation of the OPE allows us an easy transition from configuration to momentum space.

End of the digression

Non-perturbative Effects via the OPE

For the purpose of the anomalous magnetic moment (see (4.62)) one need consider two currents only

$$\hat{T}_{\nu\lambda} = i \int d^4x e^{iqx} T\{j_\nu(x) j_{5\lambda}(0)\} = \sum_i c_{\nu\lambda\alpha_1\dots\alpha_i}^i(q) \mathcal{O}_i^{\alpha_1\dots\alpha_i}$$

where the operators \mathcal{O} are local operators constructed from the light fields, the photon, light quarks and gluon fields. The axial current in the u and d light quarks sector reads $j_{5\lambda} = \bar{u}\gamma_\lambda\gamma_5u - \bar{d}\gamma_\lambda\gamma_5d$, and correspondingly for the heavier quarks. The Wilson coefficients c^i encode the short distance properties while the operator matrix elements describe the non-perturbative long range strong interaction features. The matrix element of our concern is

$$T_{\nu\lambda} = \langle 0|\hat{T}_{\nu\lambda}|\gamma(k)\rangle = \sum_i c_{\nu\lambda\alpha_1\dots\alpha_i}^i(q) \langle 0|\mathcal{O}_i^{\alpha_1\dots\alpha_i}|\gamma(k)\rangle \tag{4.85}$$

in the classical limit $k \rightarrow 0$, where the leading contribution becomes linear in $\tilde{f}_{\alpha\beta}$ the dual of $f_{\alpha\beta} = k_\alpha\varepsilon_\beta - k_\beta\varepsilon_\alpha$. Hence, only those operators contribute which have the structure of an antisymmetric tensor

$$\langle 0|\mathcal{O}_i^{\alpha\beta}|\gamma(k)\rangle = -i \frac{1}{4\pi^2} \kappa_i \tilde{f}^{\alpha\beta} \tag{4.86}$$

with constants κ_i which depend on the renormalization scale μ . The operators contributing to $T_{\nu\lambda}$ in the OPE, in view of the tensor structure (4.63), are of the form

$$T_{\nu\lambda} = \sum_i \left\{ c_T^i(q^2) \left(-q^2 \mathcal{O}_{\nu\lambda}^i + q_\nu q^\alpha \mathcal{O}_{\alpha\lambda}^i - q_\lambda q^\alpha \mathcal{O}_{\alpha\nu}^i \right) + c_L^i(q^2) q_\lambda q^\alpha \mathcal{O}_{\alpha\nu}^i \right\} \tag{4.87}$$

such that

$$w_{T,L}(q^2) = \sum_i c_{T,L}^i(q^2, \mu^2) \kappa_i(\mu^2). \quad (4.88)$$

The OPE is an expansion for large $Q^2 = -q^2$ and the relevance of the terms are determined by the dimension of the operator, the low dimensional ones being the most relevant, unless they are nullified or suppressed by small coefficients due to exact or approximate symmetries, like chiral symmetry. Note that the functions we expand are analytic in the q^2 -plane and an asymptotic expansion for large Q^2 is a formal power series in $1/Q^2$ up to logarithms. Therefore operators of odd dimension must give contributions proportional to the mass m_f of the light fermion field from which the operator is constructed. In the chiral limit the operators must be of *even* dimension and antisymmetric.

In the following we include the factors T_{3f} at the $Z^\lambda j_{5\lambda}(0)$ vertex (axial current coefficient) and Q_f at the $A^\nu j_\nu(x)$ vertex (vector current coefficient) as well as the color multiplicity factor N_{cf} where appropriate. A further factor Q_f (coupling to the external photon) comes in via the matrix elements κ_i of fermion operators $\bar{f} \cdots f$. In the case of helicity flip operators $\bar{f}_R \cdots f_L$ or $\bar{f}_L \cdots f_R$ the corresponding κ_i will be proportional to m_f .

The first non-vanishing term of the OPE is the 1st term on the r.h.s. of (4.84), which requires a parity odd operator linear in the photon field. In fact, the leading operator has dimension $d_O = 2$ given by the parity odd dual electromagnetic field strength tensor

$$\mathcal{O}_F^{\alpha\beta} = \frac{1}{4\pi^2} \tilde{F}^{\alpha\beta} = \frac{1}{4\pi^2} \varepsilon^{\alpha\beta\rho\sigma} \partial_\rho A_\sigma. \quad (4.89)$$

The normalization is chosen such that $\kappa_F = 1$ and hence $w_{L,T}^F = c_{L,T}^F$. The corresponding coefficient for this leading term is given by the perturbative one-loop triangle diagram and yields

$$c_{L,T}^F[f] = 2c_T^F[f] = \frac{4T_{3f}N_{cf}Q_f^2}{Q^2} \left[1 - \frac{2m_f^2}{Q^2} \ln \frac{Q^2}{\mu^2} + O\left(\frac{m_f^4}{Q^4}\right) \right] \quad (4.90)$$

where the leading $1/Q^2$ term cancels family-wise due to quark-lepton duality. In the chiral limit we know that this is the only contribution to w_L .

Next higher term, which can contribute to the amplitudes under consideration, is the 2nd term on the r.h.s. of (4.84). The $d_O = 3$ operators are given by

$$\mathcal{O}_f^{\alpha\beta} = -i\bar{f}\sigma^{\alpha\beta}\gamma_5 f \equiv \frac{1}{2}\varepsilon^{\alpha\beta\rho\sigma}\bar{f}\sigma^{\rho\sigma}f. \quad (4.91)$$

These helicity flip operators only may contribute if chiral symmetry is broken and the corresponding coefficients must be of the form $c^f \propto m_f/Q^4$. However, it should be remembered that we are looking at a soft matrix element where the mass in not to

be identified with a current quark mass, rather a constituent mass is adequate which does not vanish in the chiral limit (see (5.155) in Sect. 5.2.2). These coefficients are determined by tree level diagrams of Compton scattering type and again contribute equally to both amplitudes

$$c_L^f[f] = 2c_T^f[f] = \frac{8T_{3f}Q_f m_f}{Q^4}.$$

Misusing the spirit of the OPE for the moment and neglecting the soft strong interaction effects, we may calculate the soft photon quark matrix element in the QPM from the one-loop diagram shown in (4.84) (last diagram) which is UV divergent and in the $\overline{\text{MS}}$ scheme yields

$$\kappa_f = -Q_f N_{cf} m_f \ln \frac{\mu^2}{m_f^2}. \quad (4.92)$$

Inserting this in

$$\Delta^{(d_{\mathcal{O}}=3)}w_L = 2\Delta^{(d_{\mathcal{O}}=3)}w_T = \frac{8}{Q^4} \sum_f T_{3f} Q_f m_f \kappa_f$$

one recovers precisely the $1/Q^4$ term of (4.90). So far we have reproduced the known perturbative result. Nevertheless the calculation illustrates the use of the OPE. While the leading $1/Q^2$ term is not modified by soft gluon interactions, i.e., $\kappa_F = 1$ is exact as the state $|\gamma\rangle$ represents a physical on-shell photon, undressed from possible self-energy corrections, the physical κ_f cannot be obtained from pQCD. So far it is an unknown constant. Here again, the spontaneous breakdown of the chiral symmetry and the existence of, in the chiral limit, non-vanishing quark condensates $\langle\bar{\psi}\psi\rangle_0 \neq 0$ plays a central role. Now, unlike in perturbation theory, κ_f need not be proportional to m_f . In fact it is proportional to $\langle\bar{\psi}\psi\rangle_0$. As the condensate is of dimensionality 3, another quantity must enter carrying dimension of a mass and which is finite in the chiral limit. In the u, d quark sector this is either the pion decay constant F_0 or the ρ mass M_{ρ^0} . As it is given by the matrix element (4.86) (see also the last graph of Eq. (4.84)) κ_f must be proportional to $N_{cf}Q_f$ such that

$$\kappa_f = N_{cf}Q_f \frac{\langle\bar{\psi}_f\psi_f\rangle_0}{F_0^2}$$

and hence [155, 164]

$$\Delta^{(d_{\mathcal{O}}=3)}w_L = 2\Delta^{(d_{\mathcal{O}}=3)}w_T = \frac{8}{Q^4} \sum_f N_{cf}T_{3f} Q_f^2 m_f \frac{\langle\bar{\psi}_f\psi_f\rangle_0}{F_0^2}. \quad (4.93)$$

An overall constant, in fact is not yet fixed, however, it was chosen such that it reproduces the expansion of non-perturbative modification of w_L as a pion propagator beyond the chiral limit:

$$w_L[m_{u,d} \neq 0] = \frac{2}{Q^2 + m_\pi^2} = \frac{2}{Q^2} - \frac{2m_\pi^2}{Q^4} + \dots$$

as we will see below. Identifying the $1/Q^4$ correction with the one of (4.93) is the pion dominance hypothesis used as a constraint to fix the normalization in [164]. In the isospin sector (4.93) gives

$$\Delta w_L = \frac{8N_{cf}}{Q^4} \times \frac{1}{2} \left(\frac{4}{9} m_u - \frac{1}{9} m_d \right) \frac{\langle \bar{\psi}_f \psi_f \rangle_0}{F_0^2}$$

and for $m_u \approx m_d \approx \frac{m_u + m_d}{2}$ and using the GMOR relation $(m_u + m_d) \langle \bar{\psi}_f \psi_f \rangle_0 = -F_\pi^2 m_\pi^2$ and with $F_0 \approx F_\pi$ we indeed have $\Delta w_L = -\frac{2m_\pi^2}{Q^4}$. Note that the quark mass difference $m_u - m_d$ is small relative to $m_u + m_d$, and is not important here. It leads to a small mixing with heavier pseudoscalar states.

For later use we mention that κ_f can be represented in terms of the magnetic susceptibility χ introduced by Ioffe and Smilga [171]

$$\kappa_f = -4\pi^2 Q_f \langle \bar{\psi}_f \psi_f \rangle_0 \chi \quad (4.94)$$

In our case, under the pion pole dominance assumption (see [164] for a more detailed discussion), one obtains

$$\chi = -\frac{N_c}{4\pi^2 F_\pi^2} \simeq -\frac{1}{(335 \text{ MeV})^2} . \quad (4.95)$$

All operators of $d_{\mathcal{O}} = 4$ may be reduced via the equation of motion to $d_{\mathcal{O}} = 3$ operators carrying a factor of mass in front:

$$\bar{f} (D^\alpha \gamma^\beta - D^\beta \gamma^\alpha) \gamma_5 f = -m_f \bar{f} \sigma^{\alpha\beta} \gamma_5 f .$$

They thus do not yield new type of corrections and will not be considered further, as they are suppressed by the light quark masses as m_f^2/Q^4 .

Similarly the dimension $d_{\mathcal{O}} = 5$ operators

$$\bar{f} f \tilde{F}^{\alpha\beta}, \quad \bar{f} \gamma_5 f \tilde{F}^{\alpha\beta}, \quad \dots$$

which are contributing to the $1/Q^6$ coefficient, require a factor m_f and thus again are suppressed by nearby chiral symmetry.

More important are the dimension $d_{\mathcal{O}} = 6$ operators, which yield $1/Q^6$ terms and give non-vanishing contributions in the chiral limit. Here again the specific low energy structure of QCD comes into play, namely the spontaneous symmetry breaking of the chiral symmetry (in the symmetry limit). The latter is characterized by the

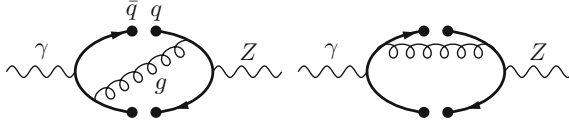


Fig. 4.22 Non-perturbative quark condensate contributions due to spontaneous breaking of chiral symmetry. The scalars $\bar{q}q$ couple to the vacuum $\langle \bar{q}q \rangle \neq 0$. Two other diagrams are obtained by attaching the gluons to the quark lines by other permutations

existence of an *orderparameter*,²⁶ which in QCD are the color singlet quark condensates $\langle \bar{\psi}_q \psi_q \rangle$ of the light quarks $q = u, d, s$, where we have implicitly summed over color. The point is that the condensates are non-vanishing in the chiral limit $m_q = 0$, typically they take values $\langle \bar{\psi}_q \psi_q \rangle \simeq - (240 \text{ MeV})^3$. Note that in pQCD chiral symmetry (in the symmetry limit) remains unbroken, $\langle \bar{\psi}_q \psi_q \rangle$ vanishes identically. Higher order color singlet contributions are possible which include hard gluon exchange represented by the Feynman diagrams of Fig. 4.22. They are of the type as represented by the last diagram of (4.83). The operators responsible derive from $: j_\nu(x) j_{5\lambda}(0) :$ corrected by second order QCD (two quark gluon interaction vertices as given in Fig. 2.14 in Sect. 2.8) with the gluon and two quark pairs contacted, like

$$:\bar{\psi}(x)\gamma_\nu \psi(x) \bar{\psi}(0)\gamma_\lambda\gamma_5\psi(0) : : \overbrace{\bar{\psi}_a\gamma^\alpha(T_i)_{aa'}\psi_{a'}}^{G_\alpha^i(z_1)} : : \overbrace{\bar{\psi}_b\gamma^\beta(T_j)_{bb'}\psi_{b'}}^{G_\beta^j(z_2)} :$$

where T_i are the $SU(3)$ generators satisfying

$$\sum_i (T_i)_{aa'}(T_i)_{bb'} = \frac{1}{2} (\delta_{ab'}\delta_{a'b} - \frac{1}{N_c} \delta_{aa'}\delta_{bb'}) .$$

The terms have been worked out in detail in [155] and are of the form

$$\hat{T}_{\nu\lambda}(q) = i [q_\beta \varepsilon_{\nu\lambda\rho\alpha} q^\rho - q_\alpha \varepsilon_{\nu\lambda\rho\beta} q^\rho] \left(-2\pi^2 \frac{\alpha_s}{\pi} \right) \frac{\mathcal{O}^{\alpha\beta}(0)}{Q^6} + \dots$$

with

$$\mathcal{O}^{\alpha\beta} = \left[\frac{2}{3} (\bar{u}\sigma^{\alpha\beta}u) (\bar{u}u) + \frac{1}{3} (\bar{d}\sigma^{\alpha\beta}d) (\bar{d}d) + \frac{1}{3} (\bar{s}\sigma^{\alpha\beta}s) (\bar{s}s) \right] (0) .$$

These terms yield the leading non-perturbative (NP) contributions and persist in the chiral limit. They only contribute to the transversal amplitude, and using estimates presented in [172] one obtains

²⁶Spontaneous symmetry breaking is best known from ferromagnets, where rotational invariance is spontaneously broken, leading to spontaneous magnetization $\langle S_z \rangle = M \neq 0$ in a frame where M is directed along the z -axis.

$$w_T(Q^2)_{\text{NP}} \simeq -\frac{16}{9}\pi^2 \frac{2}{F_0^2} \frac{\alpha_s}{\pi} \frac{\langle \bar{\psi}\psi \rangle^2}{Q^6} \quad (4.96)$$

for large enough Q^2 , the ρ mass being the typical scale. This NP contribution breaks the degeneracy $w_T(Q^2) = \frac{1}{2}w_L(Q^2)$ which is valid in perturbation theory.²⁷ Taking into account the quark condensates together with explicit chiral symmetry breaking, according to (4.93), also a term

$$\Delta w_T(Q^2)_{\text{NP}} = \frac{1}{2}\Delta w_L(Q^2)_{\text{NP}} \simeq \frac{4}{9} \frac{3}{2F_0^2} \frac{(4m_u - m_d - m_s)\langle \bar{\psi}\psi \rangle}{Q^4}, \quad (4.97)$$

yields an NP contribution, but this time to both w_T and w_L . The consequences of the OPE for the light quarks u , d and s in the chiral limit may be summarized as follows [153]:

$$\begin{aligned} w_L[u, d]_{m_{u,d}=0} &= -3 w_L[s]_{m_s=0} = \frac{2}{Q^2}, \\ w_T[u, d]_{m_{u,d}=0} &= -3 w_T[s]_{m_s=0} = \frac{1}{Q^2} - \frac{32\pi\alpha_s}{9Q^6} \frac{\langle \bar{\psi}\psi \rangle_0^2}{F_\pi^2} + O(Q^{-8}). \end{aligned} \quad (4.98)$$

The condensates are fixed essentially by the Gell-Mann-Oakes-Renner (GMOR) relations (4.76)

$$\begin{aligned} (m_u + m_d) \langle \bar{\psi}\psi \rangle_0 &= -F_0^2 m_\pi^2 \\ m_s \langle \bar{\psi}\psi \rangle_0 &\simeq -F_0^2 M_K^2. \end{aligned}$$

and the last term of (4.98) numerically estimates to

$$w_T(Q^2)_{\text{NP}} \sim -\alpha_s (0.772 \text{ GeV})^4 / Q^6,$$

i.e., the scale is essentially the ρ mass. Our estimates are rough leading order estimates in the sense of CHPT. The index $_0$ denotes quantities in the chiral limit. Except from the masses of the pseudoscalars, which vanish in the chiral limit, we do not distinguish between quantities like the pseudoscalar decay constants F_0 , F_π and F_K . Similarly, we assume the light quark condensates $\langle \bar{\psi}\psi \rangle_0$ to be approximately equal for u , d and s quarks. Furthermore, we use $m_\eta^2 \simeq \frac{4}{3}m_K^2$ and $M_{\eta'}^2 \simeq M_0^2$ with $M_0 \simeq 950 \text{ MeV}$ (for CHPT refinements we refer to [166]). Also isospin symmetry will be assumed where appropriate.

In fact the non-perturbative refinements of the leading π^0 , η , η' exchange contributions in w_L requires the inclusion of vector-meson exchanges which contribute to w_T . More precisely, for the transversal function the intermediate states have to be

²⁷The OPE only provides information on w_T for Q^2 large. At low Q^2 we only know that $w_T(0) = 128\pi^2 C_{22}^W$ where C_{22}^W is one of the unknown CHPT constants in the $O(p^6)$ parity odd part of the chiral Lagrangian [173].

1^+ mesons with isospin 1 and 0 or 1^- mesons with isospin 1. The lightest ones are ρ , ω and a_1 . They are massive also in the chiral limit.

In principle, the incorporation of vector-mesons, like the ρ , in accordance with the basic symmetries is possible using the Resonance Lagrangian Approach (RLA) [174, 175], an extended form of CHPT. The more recent analyses are based on quark-hadron duality, as it holds in the large N_c limit of QCD [176, 177], for modeling the hadronic amplitudes [178]. The infinite series of narrow vector states known to show up in the large N_c limit is then approximated by a suitable lowest meson dominance, i.e., amplitudes are assumed to be saturated by known low lying physical states of appropriate quantum numbers. This approach was adopted in an analysis by the Marseille group [155].²⁸ An analysis which takes into account the complete structure (4.98) was finalized in [153]. In the narrow width approximation one may write

$$\text{Im } w_T = \pi \sum_i g_i \delta(s - m_i^2)$$

where the weight factors g_i satisfy

$$\sum_i g_i = 1, \quad \sum_i g_i m_i^2 = 0$$

in order to reproduce (4.98) in the chiral limit. Beyond the chiral limit the corrections (4.97) should be implemented by modifying the second constraint to match the coefficient of the second terms in the OPE.

While for the leptons we have

$$w_L[\ell] = -\frac{2}{Q^2}, \quad (\ell = e, \mu, \tau)$$

²⁸In this analysis, the leading $1/Q^2$ term of w_T in (4.98) got lost, which produces a fake $\ln M_Z$ term in the leading hadronic contribution. This was rectified in [153, 164] and confirmed by the authors of [155] in [165]. The $1/Q^6$ correction was estimated using “large N_c limit of QCD” type of arguments and taking into account the three lowest lying hadrons with appropriate quantum numbers as poles: the ρ , ρ' and a_1 , yields

$$\Delta a_\mu|_T^{\text{HA 3-poles}} = \frac{G_\mu}{\sqrt{2}} \frac{m_\mu^2}{8\pi^2} \frac{\alpha}{\pi} \times (0.04 \pm 0.02) \simeq (0.011 \pm 0.005) \times 10^{-11}.$$

Thus, these interesting NP corrections at the present level of precision turn out to be completely negligible. However also the longitudinal amplitude is modified by mass effects. While for the first family quarks the effects are very small, for the strange quark the contribution turns out to be relevant. The estimate here yields

$$\Delta a_\mu|_L = \frac{\sqrt{2}G_\mu m_\mu^2}{16\pi^2} \frac{\alpha}{\pi} \times (4.57 \pm 1.17 \pm 1.37) \simeq (1.2 \pm 0.3 \pm 0.4) \times 10^{-11}.$$

Still the effect is small, however, one has to estimate such possible effects in order to reduce as much as possible the hadronic uncertainties.

the hadronic amplitudes get modified by strong interaction effects as mentioned: a sufficient number of states with appropriate weight factors has to be included in order to be able to satisfy the S.D. constraints, obtained via the OPE. Since the Z does not have fixed parity both vector and axial vector states couple (see Fig. 4.21a). For the 1st family π^0 , $\rho(770)$ and $a_1(1260)$ are taken into account²⁹

$$w_L[u, d] = \frac{2}{Q^2 + m_\pi^2} \simeq 2 \left(\frac{1}{Q^2} - \frac{m_\pi^2}{Q^4} + \dots \right)$$

$$w_T[u, d] = \frac{1}{M_{a_1}^2 - M_\rho^2} \left[\frac{M_{a_1}^2 - m_\pi^2}{Q^2 + M_\rho^2} - \frac{M_\rho^2 - m_\pi^2}{Q^2 + M_{a_1}^2} \right] \simeq \left(\frac{1}{Q^2} - \frac{m_\pi^2}{Q^4} + \dots \right),$$

for the 2nd family $\eta'(960)$, $\eta(550)$, $\phi(1020)$ and $f_1(1420)$ are included

$$w_L[s] = -\frac{2}{3} \left[\frac{2}{Q^2 + M_{\eta'}^2} - \frac{1}{Q^2 + m_\eta^2} \right] \simeq -\frac{2}{3} \left(\frac{1}{Q^2} - \frac{\tilde{M}_\eta^2}{Q^4} + \dots \right)$$

$$w_T[s] = -\frac{1}{3} \frac{1}{M_{f_1}^2 - M_\phi^2} \left[\frac{M_{f_1}^2 - m_\eta^2}{Q^2 + M_\phi^2} - \frac{M_\phi^2 - m_\eta^2}{Q^2 + M_{f_1}^2} \right] \simeq -\frac{1}{3} \left(\frac{1}{Q^2} - \frac{m_\eta^2}{Q^4} + \dots \right).$$

with $\tilde{M}_\eta^2 = 2M_{\eta'}^2 - m_\eta^2$. The expansion shows how it fits to what we got from the OPE. Numerically the differences are not crucial, however, and we adopt the specific forms given above.

While the contributions to a_μ from the heavier states may be calculated using the simplified integral (4.65), for the leading π^0 contribution we have to use (4.64), which also works for $m_\pi \sim m_\mu$. The results obtained for the 1st family reads [153]³⁰

²⁹It should be noted that the ‘‘pole’’ in $w_L[\ell] = 2/q^2$ has nothing to do with a massless one-particle exchange, it is just a kinematic singularity which follows from the tensor decomposition (4.63). Therefore the hadronic counterpart $w_L[u, d] = -2/(q^2 - m_\pi^2 + i\varepsilon)$ is not just a chiral symmetry breaking shift of the Nambu–Goldstone pole, which is the result of the spontaneous chiral symmetry breaking. What matters is that in physical quantities the residue of the ‘‘pole’’ must be checked in order to know, whether there is a true pole or not. The pion–pole in $w_L[u, d]$ certainly has a different origin than the spurious one of $w_L[\ell]$.

³⁰Up to the common factor \mathcal{K}_2 for pseudoscalar exchanges like $w_L(Q^2) = 1/(Q^2 + m_\pi^2) - 1/(Q^2 + M_Z^2)$ (Pauli–Villars regulated) one obtains the exact result

$$F_L(x) = \frac{1}{6} \left(x(x+2)f(x) - x^2 \ln x + 2x + 3 \right) - \ln \frac{m_\mu^2}{M_Z^2},$$

where

$$f(x) = \begin{cases} -\sqrt{4/x-1} \left(\arcsin \left(1 - \frac{x}{2} \right) + \frac{\pi}{2} \right) & \text{for } x < 4 \ (x = x_\pi), \\ \sqrt{1-4/x} \ln \left(-2/(x\sqrt{1-4/x} - x + 2) \right) & \text{for } x > 4 \ (x = x_\eta), \end{cases}$$

with $x_\pi = m_\pi^2/m_\mu^2$, $x_\eta = m_\eta^2/m_\mu^2$ etc. and M_Z as a cut-off. For vector exchanges like $w_T(Q^2) = 1/(Q^2 + M_\rho^2)$ one obtains

$$\begin{aligned}
a_\mu^{(4)\text{EW}}([e, u, d]) &\simeq -\frac{\sqrt{2}G_\mu m_\mu^2}{16\pi^2} \frac{\alpha}{\pi} \left\{ \frac{1}{3} \left(r_\pi (r_\pi + 2) \sqrt{\frac{4}{r_\pi} - 1} \left[\arcsin \left(1 - \frac{r_\pi}{2} \right) + \frac{\pi}{2} \right] \right. \right. \\
&\quad \left. \left. + r_\pi^2 \ln r_\pi - 2r_\pi - 3 \right) + \ln \frac{M_\rho^2}{m_\mu^2} - \frac{M_\rho^2}{M_{a_1}^2 - M_\rho^2} \ln \frac{M_{a_1}^2}{M_\rho^2} + \frac{5}{2} \right\} \\
&\simeq -\frac{\sqrt{2}G_\mu m_\mu^2}{16\pi^2} \frac{\alpha}{\pi} \times 8.49(74) = -2.30(20) \times 10^{-11}. \tag{4.99}
\end{aligned}$$

with $r_\pi = m_\pi^2/m_\mu^2$. This may be compared with the QPM result (4.53), which is about a factor two larger and again illustrates the problem of perturbative calculation in the light quark sector. For the 2nd family adding the μ and the perturbative charm contribution one obtains

$$\begin{aligned}
a_\mu^{(4)\text{EW}}([\mu, c, s]) &\simeq -\frac{\sqrt{2}G_\mu m_\mu^2}{16\pi^2} \frac{\alpha}{\pi} \left[\frac{2}{3} \ln \frac{M_\phi^2}{M_{\eta'}^2} - \frac{2}{3} \ln \frac{M_{\eta'}^2}{m_\eta^2} \right. \\
&\quad \left. + \frac{1}{3} \frac{M_\phi^2 - m_\eta^2}{M_{f_1}^2 - M_\phi^2} \ln \frac{M_{f_1}^2}{M_\phi^2} + 4 \ln \frac{M_c^2}{M_\phi^2} + 3 \ln \frac{M_\phi^2}{m_\mu^2} - \frac{8\pi^2}{9} + \frac{59}{6} \right] \\
&\simeq -\frac{\sqrt{2}G_\mu m_\mu^2}{16\pi^2} \frac{\alpha}{\pi} \times 17.25(1.10) \simeq -4.67(30) \times 10^{-11}, \tag{4.100}
\end{aligned}$$

which yields a result close to the one obtained in the QPM (4.54). Here the QPM works better because the non-perturbative light s -quark contribution is suppressed by a factor of four relative to the c due to the different charge.

Note that this large N_c QCD (LNC) inspired result

$$a_\mu^{(4)\text{EW}} \left(\begin{array}{c} [e, u, d] \\ [\mu, c, s] \end{array} \right)_{\text{LNC}} \simeq -\frac{\sqrt{2}G_\mu m_\mu^2}{16\pi^2} \frac{\alpha}{\pi} \times 25.74 \simeq -6.97(20)(30) \times 10^{-11}, \tag{4.101}$$

obtained here for the 1st plus 2nd family, is close to the very simple estimate (4.80) based on separating L.D. and S.D. by a cut-off in the range 1 to 2 GeV.

(Footnote 30 continued)

$$F_T(m_\mu^2/M_\rho^2) = -\ln \frac{M_\rho^2}{M_Z^2} - \frac{2}{3} \frac{m_\mu^2}{M_\rho^2} \ln \left(\frac{M_\rho^2}{m_\mu^2} + 1 \right) + O \left((m_\mu^2/M_\rho^2)^2 \right).$$

Up to terms $O(m_\mu^2/M_Z^2)$ the result reads

$$\begin{aligned}
F_T\left(\frac{1}{x_\rho}\right) &= \frac{1}{6} \left\{ (x_\rho^2 - 6x_\rho) \ln x_\rho - 2x_\rho - 6 \ln a + 9 - x_\rho r_\rho \ln(-2/(r_\rho - x_\rho + 2)) \right. \\
&\quad \left. - r_\rho \ln((x_\rho^4 - r_\rho(x_\rho^3 - 6x_\rho^2 + 10x_\rho - 4) - 8x_\rho^3 + 20x_\rho^2 - 16x_\rho + 2)/2) \right\},
\end{aligned}$$

with $x_\rho = M_\rho^2/m_\mu^2$, $r_\rho = \sqrt{x_\rho^2 - 4x_\rho}$ and $a = m_\mu^2/M_Z^2$.

Perturbative Residual Fermion–loop Effects

So far unaccounted are sub-leading contributions which come from diagrams (c), (d), (e) and (f) in Fig. 4.19. They have been calculated in [148] and we distinguish the non-Higgs dependent ones with the result³¹

$$a_{\mu;f\text{-rem,no H}}^{(4)\text{EW}} = -\frac{\sqrt{2}G_\mu m_\mu^2}{16\pi^2} \frac{\alpha}{\pi} \left\{ \frac{1}{2s_W^2} \left[\frac{5}{8} \frac{m_t^2}{M_W^2} + \ln \frac{m_t^2}{M_W^2} + \frac{7}{3} \right] \right\} \\ \simeq -4.12(3) \times 10^{-11}, \quad (4.102)$$

and the Higgs dependent ones

$$a_{\mu;t\text{-rem,H}\gamma}^{(4)\text{EW}} = -\frac{\sqrt{2}G_\mu m_\mu^2}{16\pi^2} \frac{\alpha}{\pi} \Delta C^{tH} \quad (4.103)$$

where ΔC^{tH} is the coefficient from diagram (f)

$$\Delta C^{tH} = \begin{cases} \frac{16}{9} \ln \frac{m_t^2}{m_H^2} + \frac{104}{27} + \frac{m_H^2}{m_t^2} \left(\frac{4}{15} \ln \frac{m_t^2}{m_H^2} + \frac{104}{225} \right), & m_H \ll m_t \\ \frac{32}{3} \left(1 - \frac{1}{\sqrt{3}} \text{Cl}_2(\pi/3) \right), & m_H = m_t \\ \frac{m_t^2}{m_H^2} \left(8 + \frac{8}{9} \pi^2 + \frac{8}{3} \left(\ln \frac{m_H^2}{m_t^2} - 1 \right)^2 \right) - \frac{m_t^4}{m_H^4} \frac{32}{3} \left(\ln \frac{m_H^2}{m_t^2} + 1 \right), & m_H \gg m_t \end{cases}$$

with typical values $\Delta C^{tH} = (7.74, 4.42, 4.19)$ contributing to (4.109) by $(-2.10, -1.20, -1.13) \times 10^{-11}$, respectively, for $m_H = (60, m_t, 300)$ GeV. Given the Higgs mass of about 125 GeV the middle option should be a reasonable approximation.

The result is improvable. In the calculation [148] the approximation $s_W^2 \approx 1/4$ has been used for terms suppressed by a factor $(1 - 4s_W^2)$, in particular the Higgs–Z diagram (f) and the Z– γ diagram (b) of Fig. 4.19 were neglected. Some improvements have been discussed in [153]. Only recently, in [179], the exact Higgs mass dependent contribution ΔC^{tH} has been worked out. There are two Higgs-dependent diagrams represented by Fig. 4.19f, with either a photon or a Z-boson in the outer loop. Accordingly, we may write

$$a_{\mu;f\text{-rem,H}}^{(4)\text{EW}} = \sum_f \left[a_{\mu;f\text{-rem,H}\gamma}^{(4)\text{EW}}(f) + a_{\mu;f\text{-rem,HZ}}^{(4)\text{EW}}(f) \right], \quad (4.104)$$

³¹This is the sum of contributions Eqs. (13)–(15), (21) and (27) from diagrams (a)–(c) and (e) of Fig. 1 of [148], corresponding to diagrams (d), (e) and (c) of our Fig. 4.19. Interestingly, the Z vacuum polarization diagram (c) is the only place where a small neutrino fluctuation contribution comes in. Note that the Higgs-ghost contribution Eq. (22) of [148] accompanying their diagram (d) (our diagram (a)) is absent in our bookkeeping, as we treated diagram (a) in the unitary gauge [153, 155, 165] where ghosts are absent.

where the sum extends over the SM fermions; the relevant ones are $f = t, b, c, \tau$. Contributions from $f = e, \mu, u, d, s$ are below 10^{-14} and thus negligible. Figure 4.19f type diagrams have been calculated by Barr and Zee [180]. One calculates the inner loop first and then inserts the result into the outer loop. As a result one finds [179]

$$\begin{aligned} a_{\mu;f\text{-rem},H\gamma}^{(4)\text{EW}}(f) &= \frac{\sqrt{2}G_\mu m_\mu^2}{16\pi^2} \frac{\alpha}{\pi} N_{cf} Q_f^2 2 f_{H\gamma}(x_{fH}), \\ a_{\mu;f\text{-rem},HZ}^{(4)\text{EW}}(f) &= \frac{\sqrt{2}G_\mu m_\mu^2}{16\pi^2} \frac{\alpha}{\pi} N_c Q_f \frac{v_f}{4c_W^2 s_W^2} (1 - 4s_W^2) f_{HZ}(x_{fH}, x_{fZ}), \end{aligned} \quad (4.105)$$

with $x_{fH} = m_f^2/M_H^2$ and $x_{fZ} = m_f^2/M_Z^2$. v_f the weak vector current coefficient (4.36). The loop functions can be written in terms of one-dimensional integral representations or in terms of dilogarithms:

$$\begin{aligned} f_{H\gamma}(x) &= \int_0^1 dw x \frac{2w^2 - 2w + 1}{w^2 - w + x} \log \frac{w(1-w)}{x} \\ &= x [f_H(x) - 4], \end{aligned} \quad (4.106)$$

$$\begin{aligned} f_{HZ}(x, z) &= \int_0^1 dw x z \frac{2w^2 - 2w + 1}{w^2 - w + z} \left[\frac{\log \frac{w(1-w)}{x}}{w^2 - w + x} + \frac{\log \frac{x}{z}}{x - z} \right] \\ &= \frac{xz}{x - z} [f_H(z) - f_H(x)]. \end{aligned} \quad (4.107)$$

The dilogarithms are contained in the function $f_H(x)$, defined as

$$\begin{aligned} f_H(x) &= \frac{4x-2}{y} \left[\text{Li}_2\left(1 - \frac{1-y}{2x}\right) - \text{Li}_2\left(1 - \frac{1+y}{2x}\right) \right] - 2 \log x; \quad x < 1/4, \quad y = \sqrt{1-4x} \\ &= \frac{4x-2}{y} \text{Im} \left[\text{Li}_2\left(1 - \frac{1-iy}{2x}\right) - \text{Li}_2\left(1 - \frac{1+iy}{2x}\right) \right] - 2 \log x; \quad x > 1/4, \quad y = \sqrt{4x-1} \end{aligned} \quad (4.108)$$

The first version applies for the lighter fermions $4m_f^2 \leq m_H^2, M_Z^2$ the second for the top quark where $4m_t^2 > m_H^2, M_Z^2$ and the dilogarithm is complex of the complex arguments. Note that the real part of the difference $\text{Re} \left[\text{Li}_2\left(1 - \frac{1-iy}{2x}\right) - \text{Li}_2\left(1 - \frac{1+iy}{2x}\right) \right] = 0$ vanishes, obviously the integrals above are real for real $x, z > 0$.

Table 4.13 illustrates the relative size of the contributions from the top quark loop solely and including b, c and τ as well, the $H - Z$ contribution is suppressed by an order of magnitude for not too light Higgs boson masses. The approximation (4.104) is more than poor for $m_H = 300$ GeV, and apparently is valid only for much heavier Higgs bosons. For $m_H = 125 \pm 1$ GeV the exact result from the Higgs-dependent fermion loops we obtain

$$a_{\mu;f\text{-rem},H}^{(4)\text{EW}} = -\frac{\sqrt{2}G_\mu m_\mu^2}{16\pi^2} \frac{\alpha}{\pi} \Delta C^{fH} = -1.504(12) \times 10^{-11}, \quad (4.109)$$

Table 4.13 Higgs-dependent contributions ΔC^{tH} with closed fermion loops Fig. 4.19f

Fermion	$m_H = 60 \text{ GeV}$				$m_H = m_t$				$m_H = 300 \text{ GeV}$			
	$H\gamma$	HZ	sum	(4.104)	$H\gamma$	HZ	sum	(4.104)	$H\gamma$	HZ	sum	(4.104)
t	7.75	1.27		7.74	4.42	0.08		4.42	2.99	0.06		4.19
t, b, c, τ	7.99	1.29	8.12	7.67	4.47	0.09	4.56	4.42	3.01	0.06	3.08	4.19

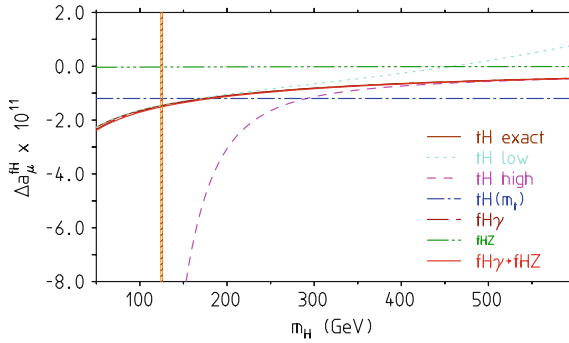


Fig. 4.23 Comparison of the Higgs boson mass dependence of the contribution from Fig. 4.19f in various approximations: the first four curves show the top quark only contribution exact, low Higgs mass expansion, high Higgs mass expansion and the value for $m_H = m_t$. Curves five and six show the results including all relevant fermions for $fH\gamma$ and fHZ . The last curve represents the sum of the previous two. The vertical band shown the mass range $m_H = 125 \pm 1 \text{ GeV}$

in agreement with [179]. Figure 4.23 shows the numerical result as a function of the Higgs boson mass and compares it with the numerical approximations from [148] supplemented by one more term in the expansions as given by (4.104). The $tH\gamma$ contribution, as expected, is clearly dominant.

Other subleading two-loop effects from the $Z - \gamma$ mixing diagram Fig. 4.19b have been estimated by RG methods first in [152] and confirmed in [153]. The result is part of the LL result (4.56) most terms of which are included in results of the refined analysis. The $Z - \gamma$ mixing yields

$$a_{\mu;f\text{-rem},Z}^{(4)EW} = \frac{\sqrt{2}G_\mu m_\mu^2}{16\pi^2} \frac{\alpha}{\pi} \sum_f N_{cf} Q_f \left[\frac{4}{9} g_V^\mu g_V^f \right] \ln \frac{M_Z}{m_{f'}} ,$$

with $m_{f'} \equiv \max[m_f, m_\mu]$ and $g_V^f = 2v_f$ the neutral vector current coefficient (4.36). Quarks here are taken in the quark parton model. Using the low energy effective weak mixing parameter $\sin^2 \Theta_{\text{eff}}(0) = 0.237855$ we obtain

$$a_{\mu;f\text{-rem},Z}^{(4)EW} = -\frac{\sqrt{2}G_\mu m_\mu^2}{16\pi^2} \frac{\alpha}{\pi} \times 0.4361 = -0.1181 \times 10^{-11}$$

Actually, this includes a substantial contribution (0.4178 out of 0.4361) from the strongly interacting quarks and the result has been obtained by adopting effective quark masses $m_u = m_d = m_s = 0.1$ GeV as an educated guess. The sensitivity to such a choice is quite dramatic in view of the range of light quark masses from their current quark mass values (chiral symmetry breaking), about 5 MeV for u and d quark, to the constituent quark masses of about 1/3 of the proton mass (about 300 MeV). The sensitivity come from the large logarithms $\propto \ln M_Z/m_q$ and perturbative calculations loose their sense when low scale quark masses come into play. It is therefore necessary to evaluate the hadronic part by non-perturbative methods using e^+e^- -data in a dispersion relation for a reliable evaluation. The approach introduced in Sect. 3.8 and will be discussed in detail in the next Chap. 5.

Digression on the Hadronic $\gamma - Z$ Mixing

Hadronic effects from the $Z - \gamma$ mixing diagram Fig. 4.19b enter via the renormalized γZ vacuum polarization amplitude. The latter may be written (one of the electromagnetic currents j_μ^{em} in the definition of $\Pi'_{\gamma\gamma}(q^2)$ has to be replaced by the current J_μ^Z (4.34) which couples to the Z boson field with neutral current coupling coefficients (4.36)) as

$$\frac{c_W}{s_W} \Pi'_{\gamma Z}(q^2) = \Delta\alpha(q^2) - \Delta\alpha_2(q^2), \quad (4.110)$$

where $\Delta\alpha(q^2)$ is the shift of the fine structure constant $\alpha = e^2/4\pi$ and $\Delta\alpha_2(q^2)$ the corresponding shift of the weak $SU(2)$ coupling $\alpha_2 = g^2/4\pi$, between $q^2 = 0$ and any non-zero q^2 . For what is required in our case, in perturbation theory at large space-like $q^2 = -M_Z^2$, we have in leading log approximation

$$\begin{aligned} \Delta\alpha(-M_Z^2) &\approx \frac{2\alpha}{3\pi} \sum_f N_{cf} Q_f^2 \ln \frac{M_Z}{m_f}, \\ \Delta\alpha_2(-M_Z^2) &\approx \frac{\alpha_2}{3\pi} \sum_f N_{cf} T_{3f} Q_f \ln \frac{M_Z}{m_f}, \end{aligned} \quad (4.111)$$

such that we may write

$$\begin{aligned} \frac{c_W}{s_W} \Pi'_{\gamma Z}(-M_Z^2) &= \Delta\alpha(-M_Z^2) - \Delta\alpha_2(-M_Z^2) \\ &\approx -\frac{\alpha}{3\pi} \frac{1}{s_W^2} \sum_f N_{cf} (T_{3f} Q_f - 2 Q_f^2 s_W^2) \ln \frac{M_Z}{m_f} \end{aligned} \quad (4.112)$$

This is by the way precisely the vacuum polarization contribution to the shift of the effective weak mixing parameter in the running from the zero momentum transfer to q^2 :

$$\sin^2 \Theta_{\text{eff}}(q^2) = \left\{ \frac{1 - \Delta\alpha_2(q^2)}{1 - \Delta\alpha(q^2)} + \dots \right\} \sin^2 \Theta_{\text{eff}}(0) .$$

The ellipses stand for additional radiative corrections not of interest here. For the hadronic shift we thus may use the results provided in [133, 137, 181]. Using an up-to-date compilation of data we obtain

$$\Delta\alpha_{\text{had}}^{(5)}(-M_Z^2) - \Delta\alpha_{2\text{had}}^{(5)}(-M_Z^2) = 2.695(20)(5)[21] \times 10^{-2} ,$$

where the low energy effective value $\sin^2 \Theta_{\text{eff}}(0) = 0.237855(230)$ has been used to set $\alpha_2 = \alpha / \sin^2 \Theta_{\text{eff}}(0)$. It corresponds to the LEP/SLD value $\sin^2 \Theta_{\text{eff}}(M_Z^2) = 0.23153(16)$ by taking into account its running to low energies [137]. In the on-shell renormalization scheme with G_μ , M_W and M_Z as input parameters, one is using $\sin^2 \Theta_W = 1 - M_W^2/M_Z^2 = 0.22290(29)$ as the weak mixing parameter. Our result may be adapted to any value of this parameter using the reference values

$$\Delta\alpha_{\text{had}}^{(5)} = 0.02749(16) \text{ and } \Delta\alpha_{2\text{had}}^{(5)} = 0.05444(35) , \quad (4.113)$$

with the errors 100% correlated. Adapted to a different $\sin^2 \theta$ one may use

$$\Delta\alpha_{2\text{had}}^{(5)} = \Delta\hat{\alpha}_{2\text{had}}^{(5)} / \sin^2 \theta ,$$

where (now independent of $\sin^2 \theta$) we have

$$\Delta\hat{\alpha}_{2\text{had}}^{(5)} = 0.05444(35) \times 0.23153 = 1.2605(82) \times 10^{-2} . \quad (4.114)$$

One should be aware that when evaluated via a dispersion relation of e^+e^- -data the correct α or α_2 in front of the dispersion integral like (3.144) is the zero momentum value. However, in deriving (4.112) from (4.111) one is using the relation $\alpha = s_W^2 \alpha_2$. So one should take properly care of this. The main uncertainties from the e^+e^- -data. The errors of $\Delta\alpha$ and $\Delta\alpha_2$ are 100% correlated and thus cancels largely in the difference. Relative to the hadronic uncertainty, the one of $\Delta\alpha_2$ coming from the uncertainty of $\sin^2 \Theta_W$ is a factor of four smaller. In [153] an estimate of $-\frac{2}{3} \sum_{q=u,d,s,c,b} N_q (T_q Q_q - 2Q_q^2 s_W^2) \times \ln \frac{M_Z}{m_q} \rightarrow -6.88(50)$ has been used. The relative normalization factor is $\frac{\alpha}{2\pi s_W^2}$, such that our result corresponds to $-5.87(4)$ in place of $-6.88(50)$, the latter has been adopted in the recent electroweak update [179].

$$a_{\mu;5\text{-had},Z}^{(4)\text{EW}} = -\frac{\sqrt{2}G_\mu m_\mu^2}{16\pi^2} \alpha \left[\frac{\pi}{\alpha} s_W^2 \frac{8}{3} \left(\Delta\alpha_{\text{had}}^{(5)} - \Delta\hat{\alpha}_{2\text{had}}^{(5)} / s_W^2 \right) (1 - 4s_W^2) \right] \quad (4.115)$$

End of the Digression

The non-perturbatively improved result now reads

$$\begin{aligned}
 a_{\mu;f\text{-rem},Z}^{(4)\text{EW}} &= -\frac{\sqrt{2}G_\mu m_\mu^2}{16\pi^2} \frac{\alpha}{\pi} \left[\left(\frac{8}{9} \ln \frac{M_Z}{m_\mu} + \frac{4}{9} \ln \frac{M_Z}{m_\tau} \right) (1 - s_W^2)^2 \right. \\
 &\quad \left. + \frac{4}{3} \times 5.87(4) (1 - 4s_W^2) \right] = -\frac{\sqrt{2}G_\mu m_\mu^2}{16\pi^2} \frac{\alpha}{\pi} \times 0.9402(121)(59) \\
 &= -0.2547(33)(16)[37] \times 10^{-11} .
 \end{aligned} \tag{4.116}$$

Of the 0.9402 only 0.0912 comes from the leptons, 0.8490 is the hadronic part. The result is extremely sensitive to the value of $\sin^2 \theta$ utilized. Our result is for the on-shell scheme with $s_W^2 = \sin^2 \Theta_W$. For $s_W^2 = \sin^2 \Theta_{\text{eff}}(0)$ this contribution would be reduced to $-0.1018(21) \times 10^{-11}$, i.e., a 6.3% change in $\sin^2 \theta$ (scheme dependence) causes the result to change by a factor 2.5, essentially the change in the overall factor $1 - 4s_W^2$. Needless to say that all the contributions from the different diagrams have to be calculated consistently in the same renormalization scheme.

Finally, the renormalization of the weak mixing parameter (see e.g. [133] for more details)

$$\sin^2 \Theta_f = \left(1 + \frac{\cos^2 \Theta_W}{\sin^2 \Theta_W} \Delta\rho \right) \sin^2 \Theta_W = \sin^2 \Theta_W + \Delta\rho \cos^2 \Theta_W$$

in the one-loop result (4.47) entering via diagram Fig. 4.18 (b) contributes a substantial correction here because of the dominating m_t^2 contribution to $\Delta\rho$ (4.40) yields³²

$$\begin{aligned}
 \delta a_\mu^{(2)\text{EW}}(Z) &= -\frac{\sqrt{2}G_\mu m_\mu^2}{16\pi^2} \frac{\alpha}{\pi} \frac{\cos^2 \Theta_W}{2 \sin^2 \Theta_W} (1 - 4 \sin^2 \Theta_W) \frac{m_t^2}{M_W^2} \\
 &= -\frac{\sqrt{2}G_\mu m_\mu^2}{16\pi^2} \frac{\alpha}{\pi} \times 0.877(11)(8) = -0.238(4) \times 10^{-11} ,
 \end{aligned} \tag{4.117}$$

³²With

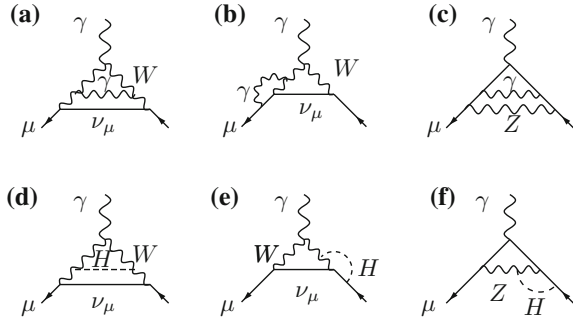
$$a_\mu^{(2)\text{EW}}(Z) = \frac{\sqrt{2}G_\mu m_\mu^2}{16\pi^2} \frac{(1 - 4 \sin^2 \Theta_W)^2 - 5}{3}$$

and $\sin^2 \Theta_W \rightarrow \sin^2 \Theta_W + \delta \sin^2 \Theta_W$ we have

$$\begin{aligned}
 \delta a_\mu^{(2)\text{EW}}(Z) &= \frac{\sqrt{2}G_\mu m_\mu^2}{16\pi^2} \frac{2}{3} (1 - 4 \sin^2 \Theta_W) \times -4 \delta \sin^2 \Theta_W \\
 &= -\frac{\sqrt{2}G_\mu m_\mu^2}{16\pi^2} \frac{8}{3} (1 - 4 \sin^2 \Theta_W) \cos^2 \Theta_W \Delta\rho
 \end{aligned}$$

with $\Delta\rho = \frac{\sqrt{2}G_\mu m_\mu^2}{16\pi^2} 3 m_t^2$. Using the tree level relation $\sqrt{2}G_\mu = \pi\alpha \frac{1}{M_W^2 \sin^2 \Theta_W}$ (see (4.42)) and hence $\frac{\sqrt{2}G_\mu}{16\pi^2} = \frac{\alpha}{\pi} \frac{1}{16} \frac{1}{M_W^2 \sin^2 \Theta_W}$ the result follows.

Fig. 4.24 Sample bosonic electroweak two-loop diagrams in the unitary gauge. Among the bosonic corrections are the photonic corrections to the weak one-loop diagrams Fig. (4.18). Furthermore, important are diagrams exhibiting virtual Higgs boson exchange with heavy W and Z bosons



again in agreement with [179]. The first error reflects the uncertainty of M_W , the second the one of m_t .

As a summary Eqs. (4.102), (4.116) and (4.117) represent our reminder (usually called NLL) estimate

$$a_{\mu;f\text{-rem,all}}^{(4)\text{EW}} = -4.61(3) \times 10^{-11} . \tag{4.118}$$

Results for the Bosonic Contributions

Full electroweak bosonic corrections have been calculated in [154]. At the two-loop level there are 1678 diagrams (fermion loops included) in the linear't Hooft gauge, and the many mass scales involved complicate the exact calculation considerably. A sample of diagrams showing purely bosonic decorations of the muon line are depicted in Fig. 4.24. Besides, photonic corrections of the weak one-loop diagrams, we have a class of diagrams with Higgs boson exchange interactions between the W and Z bosons and the muon. The latter bring in the leading Higgs boson contribution to the muon $g-2$, which was dramatically suppressed (very tiny coupling to light fermions) at the one-loop level. However, the heavy masses M_W , M_Z and m_H , which appear in the corresponding propagators, reveal these particles to be essentially static, and one may perform asymptotic expansions in $(m_\mu/M_V)^2$ and $(M_V/m_H)^2$, such that the calculation simplifies considerably. A further approximation is possible taking advantage of the smallness of the NC vector couplings, which are suppressed like $(1-4 \sin^2 \Theta_W) \sim 0.1$ for quarks and $(1-4 \sin^2 \Theta_W)^2 \sim 0.01$ for leptons, i.e., in view of the experimental value $\sin^2 \Theta_W \sim 0.23$ we may take $\sin^2 \Theta_W = 1/4$ as a good approximation. This remarkable calculation was performed by Czarnecki, Krause and Marciano in 1995 [154]. Altogether, they find for the two-loop electroweak corrections

$$a_{\mu;\text{bos}}^{(4)\text{EW}} = \frac{\sqrt{2}G_\mu m_\mu^2}{16\pi^2} \frac{\alpha}{\pi} \left(\sum_{i=-1}^2 \left[a_{2i} s_W^{2i} + \frac{M_W^2}{m_H^2} b_{2i} s_W^{2i} \right] + O(s_W^6) \right) \tag{4.119}$$

$$\simeq -21.4_{-1.0}^{+4.3} \times 10^{-11}$$

for $M_W = 80.392$ GeV ($\sin^2 \Theta_W = 1 - M_W^2/M_Z^2$) and $m_H = 250$ GeV ranging between $m_H = 100$ GeV and $m_H = 500$ GeV. The expansion coefficients may be found in [154]. The result from this expansion is displayed in Fig. 4.25 together with the known exact bosonic two-loop result. Since $m_H \approx 125$ GeV, the large $m_H \gg M_W$ expansion still provides a good crosscheck for the exact result, but is not expected to yield a good approximation at the physical Higgs mass. The on mass-shell renormalization prescription has been used. Part of the two-loop bosonic corrections have been absorbed into the lowest order result, by expressing the one-loop contributions in (4.47) in terms of the muon decay constant G_μ .³³ For the lower Higgs masses the heavy Higgs mass expansion is not accurate and an exact calculation has been performed by Heinemeyer, Stöckinger and Weiglein [183] and by Gribouk and Czarnecki [184]. The result has the form

$$a_{\mu;\text{bos}}^{(4)\text{EW}} = -\frac{\sqrt{2}G_\mu m_\mu^2}{16\pi^2} \frac{\alpha}{\pi} \left(c_L^{\text{bos},2L} \ln \frac{M_W^2}{m_\mu^2} - c_0^{\text{bos},2L} \right), \quad (4.120)$$

where the coefficient of the large logarithm $\ln \frac{M_W^2}{m_\mu^2} \sim 13.27$ is given by the simple expression

$$c_L^{\text{bos},2L} = \frac{1}{18} [107 + 23 (1 - 4s_W^2)^2] \sim 5.96.$$

In contrast to the leading term the Higgs mass dependent function $c_0^{\text{bos},2L}$ in its exact analytic form is rather unwieldy and therefore has not been published. It has been calculated numerically first in [183]. The result was confirmed in [184] which also presents a number of semi-analytic intermediate results which give more insight into the calculation. After knowing the Higgs mass to have a value $m_H \sim M_V$ rather than $M_V/m_H \ll 1$ it was important to work out the exact Higgs mass dependence of $c_0^{\text{bos},2L}$. An updated result has been presented by Gnendiger, Stöckinger and Stöckinger-Kim [179] recently.

In the range of interest, $m_H = 50$ GeV to $m_H = 350$ GeV, say, one may expand the result as a function of the Higgs mass in terms of Tschebycheff polynomials defined on the interval $[-1,1]$, for example. With

$$x = (2m_H - 400 \text{ GeV})/(300 \text{ GeV})$$

³³In [182] using asymptotic expansions and setting $m_H \sim M_W$ and $\sin^2 \Theta_W \sim 0$ an approximate form for the bosonic corrections

$$a_{\mu;\text{bos}}^{(4)\text{EW}} = -\frac{\sqrt{2}G_\mu m_\mu^2}{16\pi^2} \frac{\alpha}{\pi} \left[\frac{65}{9} \ln \frac{M_W^2}{m_\mu^2} + O(\sin^2 \Theta_W \ln \frac{M_W^2}{m_\mu^2}) \right]$$

was given, which is not too far from the result (4.119).

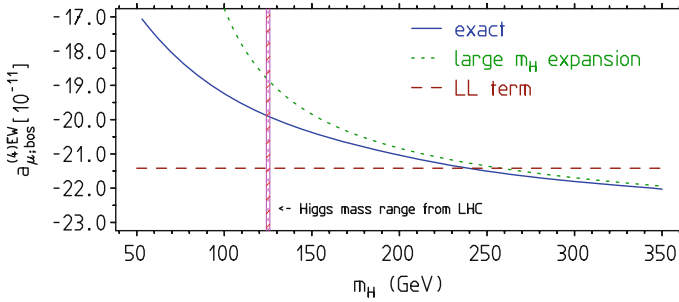


Fig. 4.25 Exact result for the bosonic correction [183, 184] versus the asymptotic expansion (4.119) and the LL approximation (first term of (4.120))

and the polynomials

$$t_1 = 1, \quad t_2 = x, \quad t_{i+2} = 2xt_{i+1} - t_i, \quad i = 1, \dots, 4$$

we may approximate (4.120) in the given range by³⁴

$$a_{\mu; bos}^{(4)EW} \simeq -\frac{\sqrt{2}G_\mu m_\mu^2}{16\pi^2} \frac{\alpha}{\pi} \sum_{i=1}^6 a_i t_i(x) \quad (4.121)$$

with the coefficients $a_1 = 75.3204$, $a_2 = 8.12415$, $a_3 = -2.79504$, $a_4 = 0.940354$, $a_5 = -0.336949$ and $a_6 = 0.132004$. The result is plotted in Fig. 4.25 and using the recent value obtained for the Higgs mass (3.34) one gets [179]

$$a_{\mu; bos}^{(4)EW} = (-19.97 \pm 0.3) \times 10^{-11}. \quad (4.122)$$

Note that

$$c_0^{\text{bos}, 2L} \simeq 5.34(12) \quad (4.123)$$

has the same value for the electron. The uncertainty is obtained by varying m_H by ± 1.5 GeV and M_W by ± 15 MeV. The exact result exhibits a much more moderate Higgs mass dependence at lower Higgs masses. The previous uncertainty caused by the unknown Higgs mass with the discovery of the Higgs by ATLAS [123] and CMS [124] has essentially disappeared. Recent results yield $m_H = 125.1 \pm 0.3$ GeV for the Higgs mass, with a surprisingly narrow error band.

³⁴In the previous calculations [183, 184] of the bosonic part an overall electroweak coupling $G_\mu \alpha(m_\mu)$ had been used. A recent careful reanalysis by Gnendiger, Stöckinger and Stöckinger-Kim [179] finds that the correct overall coupling must read $G_\mu \alpha$, i.e., the previous results have to be rescaled by the factor $\alpha/\alpha(m_\mu) \simeq 0.992934$ as included in the coefficients of Eq. (4.121).

Table 4.14 Summary of weak 2-loop effects in units 10^{-11} . Fermion triangle loops: 1st, 2nd and 3rd family LO, fermion loops NLO without Higgs boson, fermion loops NLO involving the Higgs boson, and bosonic loops (with equation numbers). The first line collects the results discussed in the text, the second shows the results [179] for comparison

$a_\mu^{(4)EW}(e, \mu, u, c, d, s)$	$a_\mu^{(4)EW}(\tau, t, b)$	$a_{\mu;f\text{-rem,H}}^{(4)EW}$	$a_{\mu;f\text{-rem,no H}}^{(4)EW}$	$a_{\mu;bos}^{(4)EW}$
Eq. (4.101)	Eq. (4.70)	Eq. (4.109)	Eq. (4.118)	Eq. (4.122)
-6.96 ± 0.36	-8.19 ± 0.08	-1.50 ± 0.01	$-4.61 \pm 0.03^{+0.00}_{-0.15}$	-19.97 ± 0.03
-6.91 ± 0.36	-8.21 ± 0.10	-1.50 ± 0.01	-4.64 ± 0.10	-19.97 ± 0.03

Summary of the Results for the Weak Contributions

We finally compare our results with the very recent reanalysis of [185]: combining the results of the full EW 2-loop calculation, updated in [179], with the results involving the hadronic effects from Refs. [148, 153, 155, 165]. The various weak contributions are collected in Table 4.14 and add up to the total weak 2-loop contribution

$$a_\mu^{(4)EW} \simeq (-41.23 \pm 0.22[m_H, m_t] \pm 0.72[\text{had}]) \times 10^{-11}. \quad (4.124)$$

The previous dominating Higgs mass uncertainty now appears reduced by an order of magnitude due to the now known Higgs mass value (3.34).

Three-loop effects have been estimated by RG methods first in [152] and confirmed in [153] with the result³⁵

$$\begin{aligned} a_{\mu LL}^{(6)EW} &\simeq a_{\mu LL}^{(4)EW} \left(\frac{\alpha(\mu)}{\alpha} - 1 \right) \left(-0.8 \frac{\alpha}{\pi} \ln \frac{M_Z}{m_\mu} \right) \\ &\simeq a_{\mu LL}^{(4)EW} \frac{\alpha}{\pi} \left(\frac{2}{3} \ln \frac{m_\mu}{m_e} - 0.8 \ln \frac{M_Z}{m_\mu} \right), \end{aligned}$$

where we used $\alpha(m_\mu)$ to leading order given by (3.48). Then using (4.57) one obtains

$$a_{\mu LL}^{(6)EW} \simeq (0.16 \pm 0.2) \times 10^{-11} \quad (4.125)$$

where the error stands for uncalculated 3-loop contributions.

By adding up (4.49), (4.124) and (4.125) we find the result

$$a_\mu^{EW} = (153.42 \pm 0.72[\text{had}] \pm 0.22[m_H, m_t, 3\text{-loop}]) \times 10^{-11}. \quad (4.126)$$

³⁵In [152] $a_{\mu LL}^{(4)EW}$ is represented by our Eq. (4.56) but with prefactor $G_\mu \alpha(m_\mu)$ in place of our $G_\mu \alpha$. The extra 3-loop correction coming from the replacement $\alpha \rightarrow \alpha(m_\mu)$ largely cancels the correction factor $-0.8 \frac{\alpha}{\pi} \ln \frac{M_Z}{m_\mu}$, which alone would yield $a_{\mu LL}^{(6)EW} \simeq 0.46 \times 10^{-11}$. By accident, in our parametrization the two contributions essentially compensate each other.

based on [153, 155, 179, 183, 184].³⁶ The electroweak error is dominated by the missing 3-loop contribution. The results also agrees well with the recent reevaluation $a_\mu^{\text{EW}} = (153.6 \pm 1.0) \times 10^{-11}$ in [179], from which we also took the Higgs boson mass dependent results (4.109) and (4.122).

We note that after the discovery of the Higgs [122] and given its mass (3.34), the uncertainty of the weak contribution has been substantially reduced. While the one-loop Higgs boson contribution is completely negligible (tiny Higgs to Muon Yukawa coupling y_μ), at the two-loop level the Higgs interaction with the heavy states W , Z and the top quark t reveal a much higher sensitivity of a_μ to the virtual Higgs exchange. Results are within uncertainties with most of the ones presented in [7].

4.2.3 Two-Loop Electroweak Contributions to a_e

The dominant electroweak 1-loop contributions Eq. (4.47) scale with high precision with an overall factor $x_{(e\mu)} = (m_e/m_\mu)^2$, up to terms which are suppressed with higher powers up to logarithms, like the contribution from the Higgs Eq. (4.48). Thus

$$a_e^{(2)\text{EW}} = x_{(e\mu)} a_\mu^{(2)\text{EW}} = 45.50(0) \times 10^{-15}. \quad (4.127)$$

At two loops various contributions do not scale in this simple way [144, 148, 154]. We therefore present a set of modified formulas, which allow us to calculate $a_e^{(4)\text{EW}}$. Apart from the overall factor

$$\frac{\sqrt{2}G_\mu m_e^2}{16\pi^2} \frac{\alpha}{\pi} = x_{(e\mu)} \frac{\sqrt{2}G_\mu m_\mu^2}{16\pi^2} \frac{\alpha}{\pi} \simeq 6.33563742 \times 10^{-17}, \quad (4.128)$$

the logarithmically enhanced as well as some constant terms change according to Eq. (4.52), adapted for the electron. We only present those terms which do not scale trivially. The QPM results Eqs. (4.53) and (4.54) are modified to

$$a_e^{(4)\text{EW}}_{((e, u, d)\text{QPM})} \simeq -\frac{\sqrt{2}G_\mu m_e^2}{16\pi^2} \frac{\alpha}{\pi} \left[\ln \frac{M_u^8}{m_e^6 M_d^2} + \frac{47}{6} - \frac{8\pi^2}{9} \right] \simeq -2.36 \times 10^{-15}, \quad (4.129)$$

³⁶The result is essentially the same as

$$a_\mu^{\text{EW}} = (154 \pm 1[\text{had}] \pm 2[\text{m}_H, \text{m}_t, 3\text{-loop}]) \times 10^{-11}$$

of Czarnecki, Marciano and Vainshtein [153], which also agrees numerically with the one

$$a_\mu^{\text{EW}} = (152 \pm 1[\text{had}]) \times 10^{-11}$$

obtained by Knecht, Peris, Perrottet and de Rafael [155].

$$a_e^{(4)\text{EW}}([\mu, c, s])_{\text{QPM}} \simeq -\frac{\sqrt{2}G_\mu m_e^2}{16\pi^2} \frac{\alpha}{\pi} \left[\ln \frac{M_c^8}{m_\mu^6 M_s^2} \right] \simeq -1.15 \times 10^{-15}, \quad (4.130)$$

for the 1st and 2nd family, respectively. The EFT/QPM estimates used in Eq. (4.80) now read

$$a_e^{(4)\text{EW}}([\mu, d, s]; p < M_\Lambda)_{\text{EFT}} = \frac{\sqrt{2}G_\mu m_e^2}{16\pi^2} \frac{\alpha}{\pi} \left[\frac{4}{3} \ln \frac{M_\Lambda^2}{m_e^2} + \frac{2}{3} \right] \simeq 1.39 \times 10^{-15},$$

$$a_e^{(4)\text{EW}}([\mu, d, s]; p > M_\Lambda)_{\text{QPM}} = \frac{\sqrt{2}G_\mu m_e^2}{16\pi^2} \frac{\alpha}{\pi} \left[2 \ln \frac{M_Z^2}{M_\Lambda^2} \right] \simeq 1.04 \times 10^{-15},$$

and together with

$$a_e^{(4)\text{EW}}([e, \mu, c])_{\text{QPM}} = -\frac{\sqrt{2}G_\mu m_e^2}{16\pi^2} \frac{\alpha}{\pi} \left[3 \ln \frac{M_Z^2}{m_e^2} + 3 \ln \frac{M_Z^2}{m_\mu^2} - 4 \ln \frac{M_Z^2}{M_c^2} + \frac{23}{6} - \frac{8}{9} \pi^2 \right]$$

$$\simeq -\frac{\sqrt{2}G_\mu m_e^2}{16\pi^2} \frac{\alpha}{\pi} \times 75.32 \simeq -4.77 \times 10^{-15},$$

yield the complete estimate for the 1st plus 2nd family

$$a_e^{(4)\text{EW}}\left(\begin{matrix} [e, u, d] \\ [\mu, c, s] \end{matrix}\right) = -\frac{\sqrt{2}G_\mu m_e^2}{16\pi^2} \frac{\alpha}{\pi} \left[\frac{5}{3} \ln \frac{M_\Lambda^2}{m_e^2} + 3 \ln \frac{M_\Lambda^2}{m_\mu^2} - 4 \ln \frac{M_\Lambda^2}{M_c^2} + \frac{19}{6} - \frac{8}{9} \pi^2 \right]$$

$$\simeq -\frac{\sqrt{2}G_\mu m_e^2}{16\pi^2} \frac{\alpha}{\pi} \times 36.85 \quad (46) \simeq -2.33 \quad (3) \times 10^{-15}. \quad (4.131)$$

The large N_c QCD inspired LMD result Eq. (4.99) for the 1st family translates into

$$a_e^{(4)\text{EW}}([e, u, d]) \simeq -\frac{\sqrt{2}G_\mu m_e^2}{16\pi^2} \frac{\alpha}{\pi} \left\{ \frac{1}{3} \left(-r_\pi (r_\pi + 2) \sqrt{1 - \frac{4}{r_\pi}} \left[\ln \frac{-2}{r_\pi \sqrt{1 - \frac{4}{r_\pi}} - r_\pi + 2} \right] \right. \right.$$

$$\left. \left. + r_\pi^2 \ln r_\pi - 2r_\pi - 3 \right) + \ln \frac{M_\rho^2}{m_e^2} - \frac{M_\rho^2}{M_{a_1}^2 - M_\rho^2} \ln \frac{M_{a_1}^2}{M_\rho^2} - \frac{8\pi^2}{9} + \frac{11}{6} \right\}$$

$$\simeq -\frac{\sqrt{2}G_\mu m_e^2}{16\pi^2} \frac{\alpha}{\pi} \times 29.41 \quad (2.56) = -1.86 \quad (16) \times 10^{-15}, \quad (4.132)$$

with $r_\pi = m_\pi^2/m_e^2$. For the 2nd family Eq. (4.100) reads

$$a_e^{(4)\text{EW}}([\mu, c, s]) \simeq -\frac{\sqrt{2}G_\mu m_e^2}{16\pi^2} \frac{\alpha}{\pi} \left[\frac{2}{3} \ln \frac{M_\phi^2}{M_{\eta'}^2} - \frac{2}{3} \ln \frac{M_\eta^2}{m_\eta^2} \right.$$

$$\left. + \frac{1}{3} \frac{M_\phi^2 - m_\eta^2}{M_{f_1}^2 - M_\phi^2} \ln \frac{M_{f_1}^2}{M_\phi^2} + 4 \ln \frac{M_c^2}{M_\phi^2} + 3 \ln \frac{M_\phi^2}{m_\mu^2} + 2 \right]$$

$$\simeq -\frac{\sqrt{2}G_\mu m_e^2}{16\pi^2} \frac{\alpha}{\pi} \times 18.19 \quad (1.16) \simeq -1.15 \quad (7) \times 10^{-15}. \quad (4.133)$$

The LL approximation Eq. (4.56) for a_e is given by

$$\begin{aligned}
 a_{e\text{LL}}^{(4)\text{EW}} &= -\frac{\sqrt{2}G_\mu m_e^2}{16\pi^2} \frac{\alpha}{\pi} \left\{ \left[\frac{161}{9} + \frac{27}{9}(1-4s_W^2)^2 \right] \ln \frac{M_Z}{m_e} \right. \\
 &\quad \left. - \sum_{f \in F} N_{cf} Q_f \left[12 T_f^3 Q_f - \frac{8}{9} (T_f^3 - 2Q_f s_W^2) (1-4s_W^2) \right] \ln \frac{M_Z}{m_f} \right\} \\
 &\simeq -14.64 \times 10^{-15}, \tag{4.134}
 \end{aligned}$$

where the sum extends over $F = \mu, \tau, u, d, s, c, b$.

Also (4.116) does not simply scale with the prefactor. Instead we have

$$\begin{aligned}
 a_{e;\text{f-rem,Z}}^{(4)\text{EW}} &= -\frac{\sqrt{2}G_\mu m_e^2}{16\pi^2} \frac{\alpha}{\pi} \left[\left(\frac{4}{9} \ln \frac{M_Z}{m_e} + \frac{4}{9} \ln \frac{M_Z}{m_\mu} + \frac{4}{9} \ln \frac{M_Z}{m_\tau} \right) (1-s_W^2)^2 \right. \\
 &\quad \left. + \frac{4}{3} \times 5.87(4) (1-4s_W^2) \right] = -\frac{\sqrt{2}G_\mu m_e^2}{16\pi^2} \frac{\alpha}{\pi} \times 0.968(121)(59) \\
 &= -0.0613(9) \times 10^{-15}. \tag{4.135}
 \end{aligned}$$

Note that the contributions Eqs. (4.70), (4.109), (4.102) and (4.117) scale with $x_{(e\mu)}$. The bosonic contributions only depend on the external fermion mass and we may use the full 2-loop result Eq. (4.122) together with Eq. (4.120). Denoting the prefactors (4.50) and (4.128) by $\mathcal{K}_{2\mu}$ and \mathcal{K}_{2e} , respectively, we have

$$c_0^{\text{bos},2L} = c_L^{\text{bos},2L} \ln \frac{M_W^2}{m_\mu^2} + a_{\mu;\text{bos}}^{(4)\text{EW}} / \mathcal{K}_{2\mu}$$

such that

$$a_{e;\text{bos}}^{(4)\text{EW}} = -\mathcal{K}_{2e} \left(c_L^{\text{bos},2L} \ln \frac{M_W^2}{m_e^2} - c_0^{\text{bos},2L} \right) = x_{(e\mu)} a_{\mu;\text{bos}}^{(4)\text{EW}} - \mathcal{K}_{2e} c_L^{\text{bos},2L} \ln \frac{m_\mu^2}{m_e^2}, \tag{4.136}$$

which evaluates to $a_{e;\text{bos}}^{(4)\text{EW}} = (-8.70 \pm 0.01) \times 10^{-15}$. Results are collected in Table 4.15.

Table 4.15 Summary of weak 2-loop effects contributing to a_e in units 10^{-15} . Fermion triangle loops: 1st, 2nd and 3rd family LO, fermion loops NLO without Higgs boson, fermion loops NLO involving the Higgs boson, and bosonic loops (with equation numbers)

$a_e^{(4)\text{EW}}(e, \mu, u, c, d, s)$	$a_e^{(4)\text{EW}}(\tau, t, b)$	$a_{e;\text{f-rem,H}}^{(4)\text{EW}}$	$a_{e;\text{f-rem,no H}}^{(4)\text{EW}}$	$a_{e;\text{bos}}^{(4)\text{EW}}$
Eqs. (4.132) + (4.133)	Eq. (4.70)	Eq. (4.109)	Eq. (4.118)	Eq. (4.122)
-3.01 ± 0.17	-1.91 ± 0.02	-0.35 ± 0.00	-1.06 ± 0.01	-8.70 ± 0.01

As a result we obtain the total weak 2–loop contribution

$$a_e^{(4)\text{EW}} \simeq (-15.04 \pm 0.02[m_H, m_t] \pm 0.23[\text{had}]) \times 10^{-15}. \quad (4.137)$$

The total weak contribution thus is given by

$$a_e^{\text{EW}} \simeq (30.53 \pm 0.02[m_H, m_t] \pm 0.23[\text{had}]) \times 10^{-15}. \quad (4.138)$$

This is very close to $a_e(\text{weak}) = 29.73(52) \times 10^{-15}$ used in [6, 45]. The value corrects the result estimated in [7].

Note that the leading log approximation in Eq. (4.134) utilizing constituent quarks in this case is very close to the result in Eq. (4.137). Using this approximation we would get the value $a_e^{\text{EW}} \simeq 30.95 \times 10^{-15}$, which often has been adopted in the past.

References

1. T. Kinoshita, B. Nizic, Y. Okamoto, Phys. Rev. D **41**, 593 (1990)
2. T. Kinoshita, W.J. Marciano, in *Quantum Electrodynamics*, ed. by T. Kinoshita (World Scientific, Singapore, 1990), pp. 419–478
3. G.W. Bennett et al., Muon (g-2) Collab. Phys. Rev. Lett. **92**, 161802 (2004)
4. B.L. Roberts, Nucl. Phys. B (Proc. Suppl.) **131** 57 (2004); R.M. Carey et al., Proposal of the BNL Experiment E969 (2004), www.bnl.gov/henp/docs/pac0904/P969.pdf; J-PARC Letter of Intent L17, B.L. Roberts contact person
5. B.E. Lautrup, E. de Rafael, Nucl. Phys. B **70**, 317 (1974)
6. P.J. Mohr, B.N. Taylor, Rev. Mod. Phys. **77**, 1 (2005); P.J. Mohr, B.N. Taylor, D.B. Newell, Rev. Mod. Phys. **84**, 1527 (2012)
7. F. Jegerlehner, A. Nyffeler, Phys. Rept. **477**, 1 (2009)
8. A. Petermann, Helv. Phys. Acta **30**, 407 (1957); Nucl. Phys. **5**, 677 (1958)
9. C.M. Sommerfield, Phys. Rev. **107**, 328 (1957); Ann. Phys. (NY) **5**, 26 (1958)
10. B.E. Lautrup, E. De Rafael, Nuovo Cim. A **64**, 322 (1969)
11. H. Suura, E. Wichmann, Phys. Rev. **105**, 1930 (1957); A. Petermann, Phys. Rev. **105**, 1931 (1957)
12. H.H. Elend, Phys. Lett. **20**, 682 (1966); Erratum-ibid **21**, 720 (1966)
13. M. Passera, J. Phys. G **31** R75 (2005); Phys. Rev. D **75**, 013002 (2007)
14. G. Li, R. Mendel, M.A. Samuel, Phys. Rev. D **47**, 1723 (1993)
15. J.A. Mignaco, E. Remiddi, Nuovo Cim. A **60**, 519 (1969); R. Barbieri, E. Remiddi, Phys. Lett. B **49**, 468 (1974); Nucl. Phys. B **90**, 233 (1975); R. Barbieri, M. Caffo, E. Remiddi, Phys. Lett. B **57**, 460 (1975); M.J. Levine, E. Remiddi, R. Roskies, Phys. Rev. D **20**, 2068 (1979); S. Laporta, E. Remiddi, Phys. Lett. B **265**, 182 (1991); S. Laporta, Phys. Rev. D **47**, 4793 (1993); Phys. Lett. B **343**, 421 (1995); S. Laporta, E. Remiddi, Phys. Lett. B **356**, 390 (1995)
16. S. Laporta, E. Remiddi, Phys. Lett. B **379**, 283 (1996)
17. T. Kinoshita, Phys. Rev. Lett. **75**, 4728 (1995)
18. T. Kinoshita, Nuovo Cim. B **51**, 140 (1967)
19. B.E. Lautrup, E. De Rafael, Phys. Rev. **174**, 1835 (1968); B.E. Lautrup, M.A. Samuel, Phys. Lett. B **72**, 114 (1977)
20. S. Laporta, Nuovo Cim. A **106**, 675 (1993)
21. S. Laporta, E. Remiddi, Phys. Lett. B **301**, 440 (1993)

22. J.H. Kühn, A.I. Onishchenko, A.A. Pivovarov, O.L. Veretin, *Phys. Rev. D* **68**, 033018 (2003)
23. M.A. Samuel, G. Li, *Phys. Rev. D* **44**, 3935 (1991) [Errata-ibid. *D* **46**, 4782 (1992); *D* **48**, 1879 (1993)]
24. A. Czarnecki, M. Skrzypek, *Phys. Lett. B* **449**, 354 (1999)
25. S. Friot, D. Greynat, E. De Rafael, *Phys. Lett. B* **628**, 73 (2005)
26. B.E. Lautrup, M.A. Samuel, *Phys. Lett. B* **72**, 114 (1977)
27. T. Kinoshita, *Phys. Rev. Lett.* **61**, 2898 (1988)
28. M.A. Samuel, *Phys. Rev. D* **45**, 2168 (1992)
29. R. Barbieri, E. Remiddi, *Nucl. Phys. B* **90**, 233 (1975)
30. R. Barbieri, E. Remiddi, *Phys. Lett. B* **57**, 273 (1975)
31. J. Aldins, T. Kinoshita, S.J. Brodsky, A.J. Dufner, *Phys. Rev. Lett.* **23**, 441 (1969); *Phys. Rev. D* **1**, 2378 (1970)
32. M. Caffo, S. Turrini, E. Remiddi, *Phys. Rev. D* **30**, 483 (1984); E. Remiddi, S.P. Sorella, *Lett. Nuovo Cim.* **44**, 231 (1985); R.N. Faustov, A.L. Kataev, S.A. Larin, V.V. Starshenko, *Phys. Lett. B* **254**, 241 (1991); D.J. Broadhurst, A.L. Kataev, O.V. Tarasov, *Phys. Lett. B* **298**, 445 (1993)
33. S. Laporta, *Phys. Lett. B* **312**, 495 (1993)
34. P.A. Baikov, D.J. Broadhurst, Three-loop QED Vacuum Polarization and the Four-loop Muon Anomalous Magnetic Moment, in *New Computing Techniques in Physics Research IV. International Workshop on Software Engineering and Artificial Intelligence for High Energy, Nuclear Physics*, ed by B. Denby, D. Perret-Gallix (World Scientific, Singapore 1995), pp. 167–172, [arXiv:hep-ph/9504398](https://arxiv.org/abs/hep-ph/9504398)
35. J.P. Aguilar, D. Greynat, E. De Rafael, *Phys. Rev. D* **77**, 093010 (2008)
36. T. Kinoshita, W.B. Lindquist, *Phys. Rev. Lett.* **47**, 1573 (1981)
37. T. Kinoshita, W.B. Lindquist, *Phys. Rev. D* **27**, 867 (1983); *Phys. Rev. D* **27**, 877 (1983); *Phys. Rev. D* **27**, 886 (1983); *Phys. Rev. D* **39**, 2407 (1989); *Phys. Rev. D* **42**, 636 (1990)
38. T. Kinoshita, in *Quantum Electrodynamics*, ed. by T. Kinoshita (World Scientific, Singapore, 1990), pp. 218–321
39. T. Kinoshita, *Phys. Rev. D* **47**, 5013 (1993)
40. V.W. Hughes, T. Kinoshita, *Rev. Mod. Phys.* **71**, S133 (1999)
41. T. Kinoshita, M. Nio, *Phys. Rev. Lett.* **90**, 021803 (2003); *Phys. Rev. D* **70**, 113001 (2004)
42. T. Kinoshita, *Nucl. Phys. B (Proc. Suppl.)* **144**, 206 (2005)
43. T. Kinoshita, M. Nio, *Phys. Rev. D* **73**, 013003 (2006)
44. T. Aoyama, M. Hayakawa, T. Kinoshita, M. Nio, *Phys. Rev. Lett.* **99**, 110406 (2007)
45. T. Aoyama, M. Hayakawa, T. Kinoshita, M. Nio, *Phys. Rev. Lett.* **109**, 111807 (2012). doi:[10.1103/PhysRevLett.109.111807](https://doi.org/10.1103/PhysRevLett.109.111807)
46. T. Aoyama, M. Hayakawa, T. Kinoshita, M. Nio, *Phys. Rev. Lett.* **109**, 111808 (2012). doi:[10.1103/PhysRevLett.109.111808](https://doi.org/10.1103/PhysRevLett.109.111808)
47. S. Laporta, [arXiv:1704.06996](https://arxiv.org/abs/1704.06996) [hep-ph]
48. T. Aoyama, M. Hayakawa, T. Kinoshita, M. Nio, *Phys. Rev. D* **91**, 033006 (2015). doi:[10.1103/PhysRevD.91.033006](https://doi.org/10.1103/PhysRevD.91.033006)
49. G.P. Lepage, *J. Comput. Phys.* **27**, 192 (1978)
50. T. Kinoshita, *I.E.E.E. Trans. Instrum. Meas.* **44**, 498 (1995)
51. T. Kinoshita, *I.E.E.E. Trans. Instrum. Meas.* **46**, 108 (1997)
52. V.W. Hughes, T. Kinoshita, *Rev. Mod. Phys.* **71**, S133 (1999); T. Kinoshita, *IEEE Trans. Instrum. Meas.* **50**, 568 (2001)
53. T. Kinoshita, Recent Developments of the Theory of Muon and Electron $g-2$, in *In Memory of Vernon Willard Hughes*, ed. by E.W. Hughes, E. Iachello (World Scientific, Singapore, 2004), pp. 58–77
54. T. Aoyama, M. Hayakawa, T. Kinoshita, M. Nio, *Nucl. Phys. B* **740**, 138 (2006)
55. T. Aoyama, M. Hayakawa, T. Kinoshita, M. Nio, *Nucl. Phys. B* **796**, 184 (2008)
56. S. Laporta, *Int. J. Mod. Phys. A* **15**, 5087 (2000)
57. S. Laporta, *Phys. Lett. B* **504**, 188 (2001)
58. S. Laporta, *Phys. Lett. B* **523**, 95 (2001)

59. S. Laporta, *Acta Phys. Polon. B* **34**, 5323 (2003)
60. S. Laporta, P. Mastrolia, E. Remiddi, *Nucl. Phys. B* **688**, 165 (2004)
61. S. Laporta, *Int. J. Mod. Phys. A* **23**, 5007 (2008)
62. S. Laporta, *Subnucl. Ser.* **45**, 409 (2009)
63. M. Caffo, S. Turrini, E. Remiddi, *Phys. Rev. D* **30**, 483 (1984)
64. M.A. Samuel, *Lett. Nuovo Cim.* **21**, 227 (1978)
65. M.L. Laursen, M.A. Samuel, *J. Math. Phys.* **22**, 1114 (1981)
66. J. Calmet, A. Peterman, *Phys. Lett. B* **56**, 383 (1975)
67. M.A. Samuel, C. Chlouber, *Phys. Rev. Lett.* **36**, 442 (1976); C. Chlouber, M.A. Samuel, *Phys. Rev. D* **16**, 3596 (1977)
68. T. Aoyama, M. Hayakawa, T. Kinoshita, M. Nio, *Phys. Rev. D* **77**, 053012 (2008). doi:[10.1103/PhysRevD.77.053012](https://doi.org/10.1103/PhysRevD.77.053012)
69. S. Laporta, P. Mastrolia, E. Remiddi, *Nucl. Phys. B* **688** (2004) 165; P. Mastrolia, E. Remiddi, *Nucl. Phys. B (Proc. Suppl.)* **89**, 76 (2000)
70. A.L. Kataev, *Phys. Rev. D* **86**, 013010 (2012)
71. P.A. Baikov, K.G. Chetyrkin, C. Sturm, *Nucl. Phys. Proc. Suppl.* **183**, 8 (2008)
72. P.A. Baikov, K.G. Chetyrkin, J.H. Kühn, C. Sturm, *Nucl. Phys. B* **867**, 182 (2013)
73. R. Lee, P. Marquard, A.V. Smirnov, V.A. Smirnov, M. Steinhauser, *JHEP* **1303**, 162 (2013)
74. A. Kurz, T. Liu, P. Marquard, M. Steinhauser, *Nucl. Phys. B* **879**, 1 (2014)
75. A. Kurz, T. Liu, P. Marquard, A.V. Smirnov, V.A. Smirnov, M. Steinhauser, *Phys. Rev. D* **92**, 073019 (2015)
76. T. Kinoshita, M. Nio, *Phys. Rev. D* **73**, 053007 (2006)
77. T. Aoyama, M. Hayakawa, T. Kinoshita, M. Nio, N. Watanabe, *Phys. Rev. D* **78**, 053005 (2008)
78. T. Aoyama, M. Hayakawa, T. Kinoshita, M. Nio, *Phys. Rev. D* **78**, 113006 (2008)
79. T. Aoyama, M. Hayakawa, T. Kinoshita, M. Nio, *Phys. Rev. D* **82**, 113004 (2010)
80. T. Aoyama, K. Asano, M. Hayakawa, T. Kinoshita, M. Nio, N. Watanabe, *Phys. Rev. D* **81**, 053009 (2010)
81. T. Aoyama, M. Hayakawa, T. Kinoshita, M. Nio, *Phys. Rev. D* **83**, 053003 (2011)
82. T. Aoyama, M. Hayakawa, T. Kinoshita, M. Nio, *Phys. Rev. D* **83**, 053002 (2011)
83. T. Aoyama, M. Hayakawa, T. Kinoshita, M. Nio, *Phys. Rev. D* **84**, 053003 (2011)
84. T. Aoyama, M. Hayakawa, T. Kinoshita, M. Nio, *Phys. Rev. D* **85**, 033007 (2012)
85. T. Aoyama, M. Hayakawa, T. Kinoshita, M. Nio, *Phys. Rev. D* **85**, 093013 (2012)
86. P. Baikov, A. Maier, P. Marquard, *Nucl. Phys. B* **877**, 647 (2013)
87. P.A. Baikov, A. Maier, P. Marquard, *Acta Phys. Polon. B* **44**, 2267 (2013)
88. S.G. Karshenboim, *Phys. Atom. Nucl.* **56**, 857 (1993) [*Yad. Fiz.* **56N6**, 252 (1993)]
89. A.L. Kataev, *Nucl. Phys. Proc. Suppl.* **155**, 369 (2006), [arXiv:hep-ph/0602098](https://arxiv.org/abs/hep-ph/0602098); *Phys. Rev. D* **74**, 073011 (2006)
90. S. Laporta, *Phys. Lett. B* **328**, 522 (1994)
91. A. Kurz, T. Liu, P. Marquard, A. Smirnov, V. Smirnov, M. Steinhauser, *Phys. Rev. D* **93**, 053017 (2016)
92. P. Nogueira, Automatic feynman graph generation. *J. Comput. Phys.* **105**, 279 (1993)
93. J.A.M. Vermaseren, [arXiv:math-ph/0010025](https://arxiv.org/abs/math-ph/0010025)
94. J. Kuipers, T. Ueda, J.A.M. Vermaseren, J. Vollinga, *Comput. Phys. Commun.* **184**, 1453 (2013)
95. M. Tentyukov, J.A.M. Vermaseren, *Comput. Phys. Commun.* **181**, 1419 (2010)
96. M. Steinhauser, T. Ueda, J.A.M. Vermaseren, *Nucl. Part. Phys. Proc.* **261–262** 45
97. R.H. Lewis, Fermat s User Guide, <http://www.bway.net/~lewis/>
98. A. Pak, A. Smirnov, *Eur. Phys. J. C* **71**, 1626 (2011)
99. B. Jantzen, A.V. Smirnov, V.A. Smirnov, *Eur. Phys. J. C* **72**, 2139 (2012)
100. M. Beneke, V.A. Smirnov, *Nucl. Phys. B* **522**, 321 (1998)
101. V.A. Smirnov, *Springer Tracts Mod. Phys.* **177**, 1 (2002)
102. V.A. Smirnov, *Springer Tracts Mod. Phys.* **250**, 1 (2012)
103. A.V. Smirnov, *Comput. Phys. Commun.* **189**, 182 (2015)

104. P. Marquard, D. Seidel, unpublished
105. K.G. Chetyrkin, F.V. Tkachov, Nucl. Phys. B **192**, 159 (1981)
106. L.V. Avdeev, Comput. Phys. Commun. **98**, 15 (1996)
107. V.A. Smirnov, Phys. Lett. B **460**, 397 (1999)
108. J.B. Tausk, Phys. Lett. B **469**, 225 (1999)
109. M. Czakon, Comput. Phys. Commun. **175**, 559 (2006)
110. A.V. Smirnov, Comput. Phys. Commun. **185**, 2090 (2014)
111. D.H. Bailey, A Portable High Performance Multiprecision Package. NASA Ames Research Center, RNR Technical Report RNR-90-022 (E-mail: dbailey@nas.nasa.gov); H.R.P. Ferguson, D.H. Bailey, S. Arno, Analysis of PSLQ, An Integer Relation Finding Algorithm. Math. Comput. **68**, 351–369 (1999)
112. A.V. Kotikov, Phys. Lett. B **254**, 158 (1991)
113. E. Remiddi, Nuovo Cim. A **110**, 1435 (1997)
114. T. Gehrmann, E. Remiddi, Nucl. Phys. B **580**, 485 (2000)
115. S. Laporta, E. Remiddi, Nucl. Phys. B **704**, 349 (2005)
116. M.Y. Kalmykov, JHEP **0604**, 056 (2006)
117. G.A. Baker, Jr., J.L. Gammel, J.G. Wills, J. Math. Anal. Appl. **2**, 405 (1961); G.A. Baker, Jr., *Essentials of Pad ϵ Approximants*, Academic Press (1975)
118. S.L. Glashow, Nucl. Phys. B **22**, 579 (1961); S. Weinberg, Phys. Rev. Lett. **19**, 1264 (1967); A. Salam, Weak and electromagnetic interactions, in *Elementary Particle Theory*, ed by N. Svartholm (Amquist and Wiksells, Stockholm, 1969), pp. 367–377
119. G. 't Hooft, Nucl. Phys. B **33**, 173 (1971); **35**, 167 (1971); G. 't Hooft, M. Veltman, Nucl. Phys. B **50**, 318 (1972)
120. R. Jackiw, S. Weinberg, Phys. Rev. D **5**, 2396 (1972); I. Bars, M. Yoshimura, Phys. Rev. D **6**, 374 (1972); G. Altarelli, N. Cabibbo, L. Maiani, Phys. Lett. B **40**, 415 (1972); W.A. Bardeen, R. Gastmans, B. Lautrup, Nucl. Phys. B **46**, 319 (1972); K. Fujikawa, B.W. Lee, A.I. Sanda, Phys. Rev. D **6**, 2923 (1972)
121. P.W. Higgs, Phys. Lett. **12B**, 132 (1964); Phys. Rev. Lett. **13**, 508 (1964); Phys. Rev. **145**, 1156 (1966); F. Englert, R. Brout, Phys. Rev. Lett. **13**, 321 (1964); G.S. Guralnik, C.R. Hagen, T.W.B. Kibble, Phys. Rev. Lett. **13**, 585 (1964); T.W.B. Kibble, Phys. Rev. **155**, 1554 (1967)
122. F. Gianotti (the ATLAS Collab.). CERN Seminar, July 4th, 2012; J. Incandela (the CMS Collab.). CERN Seminar, July 4th, 2012
123. G. Aad et al., [ATLAS Collab.], Phys. Lett. B **716**, 1 (2012). Science **338**, 1576 (2012)
124. S. Chatrchyan et al., [CMS Collab.], Phys. Lett. B **716**, 30 (2012). Science **338**, 1569 (2012)
125. N. Cabibbo, Phys. Rev. Lett. **10**, 531 (1963). M. Kobayashi, K. Maskawa, Prog. Theor. Phys. **49**, 652 (1973)
126. B. Pontecorvo, Sov. Phys. JETP **6**, 429 (1957) [Zh. Eksp. Teor. Fiz. **33**, 549 (1957)]; Sov. Phys. JETP **26**, 984 (1968) [Zh. Eksp. Teor. Fiz. **53**, 1717 (1967)]; Z. Maki, M. Nakagawa, S. Sakata, Prog. Theor. Phys. **28**, 870 (1962)
127. S.L. Glashow, J. Iliopoulos, L. Maiani, Phys. Rev. D **2**, 1285 (1970)
128. W.J. Marciano, A. Sirlin, Phys. Rev. Lett. **61**, 1815 (1988)
129. T. van Ritbergen, R.G. Stuart, Phys. Rev. Lett. **82**, 488 (1999)
130. M. Avramik, M. Czakon, Phys. Lett. B **568**, 48 (2003)
131. M. Veltman, Nucl. Phys. B **123**, 89 (1977); M.S. Chanowitz et al., Phys. Lett. **78B**, 1 (1978); M. Consoli, S. Lo Presti, L. Maiani, Nucl. Phys. B **223**, 474 (1983); J. Fleischer, F. Jegerlehner, Nucl. Phys. B **228**, 1 (1983)
132. M. Consoli, W. Hollik, F. Jegerlehner, Phys. Lett. B **227**, 167 (1989)
133. F. Jegerlehner, Renormalizing the Standard Model, in *Testing the Standard Model*, ed. by M. Cvetič, P. Langacker (World Scientific, Singapore, 1991), pp. 476–590, <http://www-com.physik.hu-berlin.de/~fjeger/books.html>
134. F. Jegerlehner, Prog. Part. Nucl. Phys. **27**, 1 (1991), <http://www-com.physik.hu-berlin.de/~fjeger/books.html>
135. S. Schael et al., [ALEPH and DELPHI and L3 and OPAL and SLD and LEP Electroweak Working Group and SLD Electroweak Group and SLD Heavy Flavour Group Collab.s], Phys. Rept. **427**, 257 (2006)

136. J. Fleischer, F. Jegerlehner, Phys. Rev. D **23**, 2001 (1981)
137. F. Jegerlehner, Nuovo Cim. C **034S1**, 31 (2011)
138. A. Francis, G. von Hippel, H.B. Meyer, F. Jegerlehner, PoS LATTICE **2013**, 320 (2013), [arXiv:1312.0035](https://arxiv.org/abs/1312.0035) [hep-lat]
139. F. Burger, K. Jansen, M. Petschlies, G. Pientka, JHEP **1511**, 215 (2015)
140. A. Francis, V. Gülpers, G. Herdoza, H. Horch, B. Jäger, H.B. Meyer, H. Wittig, PoS LATTICE **2015**, 110 (2015), [arXiv:1511.04751](https://arxiv.org/abs/1511.04751) [hep-lat]
141. F. Jegerlehner, Precision Tests of Electroweak-Interaction Parameters, in *Testing the Standard Model*, ed. by M. Zrałek, R. Mañka (World Scientific, Singapore, 1988), pp. 33–108
142. A. Czarnecki, W.J. Marciano, Phys. Rev. D **53**, 1066 (1996); Int. J. Mod. Phys. A **15**, 2365 (2000)
143. J. Erler, M.J. Ramsey-Musolf, Phys. Rev. D **72**, 073003 (2005)
144. T.V. Kukhto, E.A. Kuraev, A. Schiller, Z.K. Silagadze, Nucl. Phys. B **371**, 567 (1992)
145. S.L. Adler, Phys. Rev. **177**, 2426 (1969); J.S. Bell, R. Jackiw, Nuovo Cim. **60A**, 47 (1969); W.A. Bardeen, Phys. Rev. **184**, 1848 (1969)
146. C. Bouchiat, J. Iliopoulos, P. Meyer, Phys. Lett. **38B**, 519 (1972); D. Gross, R. Jackiw, Phys. Rev. D **6**, 477 (1972); C.P. Korhals Altes, M. Perrottet, Phys. Lett. **39B**, 546 (1972)
147. S. Peris, M. Perrottet, E. de Rafael, Phys. Lett. B **355**, 523 (1995)
148. A. Czarnecki, B. Krause, W. Marciano, Phys. Rev. D **52**, R2619 (1995)
149. F. Jegerlehner, Nucl. Phys. (Proc. Suppl.) C **51**, 131 (1996)
150. E. D'Hoker, Phys. Rev. Lett. **69**, 1316 (1992)
151. T. Sterling, M.J.G. Veltman, Nucl. Phys. B **189**, 557 (1981)
152. G. Degrossi, G.F. Giudice, Phys. Rev. **58D**, 053007 (1998)
153. A. Czarnecki, W.J. Marciano, A. Vainshtein, Phys. Rev. D **67**, 073006 (2003) [Erratum-ibid. D **73**, 119901 (2006)]
154. A. Czarnecki, B. Krause, W.J. Marciano, Phys. Rev. Lett. **76**, 3267 (1996)
155. M. Knecht, S. Peris, M. Perrottet, E. de Rafael, JHEP **0211**, 003 (2002); E. de Rafael, *The muon g - 2 revisited*, [arXiv:hep-ph/0208251](https://arxiv.org/abs/hep-ph/0208251)
156. A. Czarnecki, W.J. Marciano, A. Vainshtein, Acta Phys. Polon. B **34**, 5669 (2003)
157. S.L. Adler, W.A. Bardeen, Phys. Rev. **182**, 1517 (1969)
158. J. Wess, B. Zumino, Phys. Lett. B **37**, 95 (1971)
159. E. Witten, Nucl. Phys. B **223**, 422 (1983)
160. F. Jegerlehner, O.V. Tarasov, Phys. Lett. B **639**, 299 (2006)
161. J. Mondejar, K. Melnikov, Phys. Lett. B **718**, 1364 (2013)
162. G. 't Hooft, Recent Developments in Gauge Theories, in *Proceedings of the Summer-Institute, Cargèse, France, 1979*, ed. by G. 't Hooft, et al. NATO Advanced Study Institute Series B: Physics, vol. 59 (Plenum Press, New York, 1980)
163. L. Rosenberg, Phys. Rev. **129**, 2786 (1963)
164. A. Vainshtein, Phys. Lett. B **569**, 187 (2003)
165. M. Knecht, S. Peris, M. Perrottet, E. de Rafael, JHEP **0403**, 035 (2004)
166. J. Gasser, H. Leutwyler, Annals Phys. **158**, 142 (1984); Nucl. Phys. B **250**, 465 (1985)
167. M. Gell-Mann, R.J. Oakes, B. Renner, Phys. Rev. **175**, 2195 (1968)
168. J. Gasser, H. Leutwyler, Phys. Rept. **87**, 77 (1982)
169. K.G. Wilson, Phys. Rev. **179**, 1499 (1969); K.G. Wilson, J.B. Kogut, Phys. Rept. **12**, 75 (1974); V.A. Novikov, M.A. Shifman, A.I. Vainshtein, V.I. Zakharov, Nucl. Phys. B **249**, 445 (1985) [Yad. Fiz. **41**, 1063 (1985)]
170. M.A. Shifman, World Sci. Lect. Notes Phys. **62**, 1 (1999) (Chap. 1,2)
171. B.L. Ioffe, A.V. Smilga, Nucl. Phys. B **232**, 109 (1984)
172. S. Peris, M. Perrottet, E. de Rafael, JHEP **9805**, 011 (1998); M. Knecht, S. Peris, M. Perrottet, E. de Rafael, Phys. Rev. Lett. **83**, 5230 (1999); M. Knecht, A. Nyffeler, Eur. Phys. J. C **21**, 659 (2001)
173. J. Bijnens, L. Girlanda, P. Talavera, Eur. Phys. J. C **23**, 539 (2002)
174. G. Ecker, J. Gasser, A. Pich, E. de Rafael, Nucl. Phys. B **321**, 311 (1989)
175. G. Ecker, J. Gasser, H. Leutwyler, A. Pich, E. de Rafael, Phys. Lett. B **223**, 425 (1989)

176. G. 't Hooft, Nucl. Phys. B **72**, 461 (1974); *ibid.* **75**, 461 (1974)
177. A.V. Manohar, Hadrons in the $1/N$ Expansion, in *At the frontier of Particle Physics*, ed M. Shifman, vol. 1 (World Scientific, Singapore 2001), pp. 507–568
178. E. de Rafael, Phys. Lett. B **322**, 239 (1994)
179. C. Gnendiger, D. Stöckinger, H. Stöckinger-Kim, Phys. Rev. D **88**, 053005 (2013)
180. S.M. Barr, A. Zee, Phys. Rev. Lett. **65**, 21 (1990) [Erratum-*ibid.* **65**, 2920 (1990)]
181. F. Jegerlehner, Z. Phys., C **32**, 195 (1986)
182. V.A. Smirnov, Mod. Phys. Lett. A **10**, 1485 (1995)
183. S. Heinemeyer, D. Stöckinger, G. Weiglein, Nucl. Phys. B **699**, 103 (2004)
184. T. Gribouk, A. Czarnecki, Phys. Rev. D **72**, 053016 (2005)
185. H.G. Fargnoli, C. Gnendiger, S. Paßehr, D. Stöckinger, H. Stöckinger-Kim, PoS LL **2014**, 067 (2014)

Chapter 5

Hadronic Effects

The basic problems we are confronted with when we have to include the non-perturbative hadronic contributions to $g - 2$, we have outlined in Sect. 3.2.1 p. 183ff and in Sect. 4.2.2 p. 298ff, already. We will distinguish three types of contributions, which will be analyzed in different subsections below:

(i) The most sizable hadronic effect is the $O(\alpha^2)$ hadronic vacuum polarization (HVP) insertion in the internal photon line of the leading one-loop muon vertex diagram Fig. 5.1.

The hadronic “blob” can be calculated with help of the method discussed in Sect. 3.7.1. While perturbation theory fails and ab initio non-perturbative lattice QCD calculations are not yet ready at the required precision, it may be obtained via a DR from the measured cross section $e^+e^- \rightarrow$ hadrons via (3.143) and (3.142). Here 1 independent amplitude is to be determined by one specific data channel. Global fits based on the Resonance Lagrangian Approach (RLA), specifically, the Hidden Local Symmetry (HLS) phenomenological Lagrangian, allow to improve the data-driven evaluations.

(ii) An order of magnitude smaller but still sizable are the HVP insertions contributing at order $O(\alpha^3)$. They are represented by diagrams exhibiting one additional VP insertion, leptonic or hadronic, in the photon line or by diagrams with an additional virtual photon attached in all possible ways in Fig. 5.1. As long as hadronic effects enter via photon vacuum polarization only, they can be safely evaluated in terms of experimental data via the basic DR (3.143). The errors of the data here appear suppressed by one power in α relative to the leading hadronic contribution and therefore are not problematic concerning the required precision. Also the order $O(\alpha^4)$ effect involving HVP insertions is known with sufficient accuracy.

(iii) More involved and problematic is the hadronic light-by-light (HLbL) contribution, represented by the diagram Fig. 5.2, and entering at $O(\alpha^3)$. Here, a low energy Effective Field Theory (EFT) approach beyond Chiral Perturbation Theory (CHPT) (see p. 305) is needed and some model assumptions are unavoidable. Unfortunately,

Fig. 5.1 Leading hadronic contribution to $g - 2$

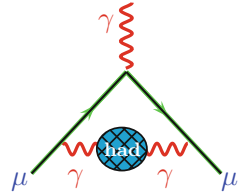
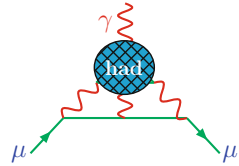


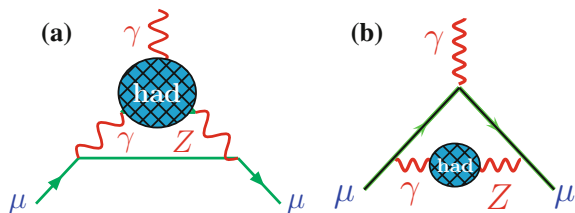
Fig. 5.2 Leading hadronic light-by-light scattering contribution to $g - 2$



as we will see, corresponding predictions depend on these model assumptions and give raise to non-negligible uncertainties. What saves the day at present is the fact that the size of the unsureness is smaller than the size of the uncertainty of the leading HVP contribution. Therefore, a rough estimate only cannot spoil the otherwise reliable prediction. For the future it remains a real challenge for theory since further progress in $g - 2$ precision physics depends on progress in putting this calculation on a safer theoretical basis. Attempts to evaluate the HLbL effects in terms of dispersion relation and $\gamma\gamma \rightarrow \text{hadrons}$ data (as well as data from crossed channels) have been considered more recently. About 19 independent amplitudes are to be determined by as many independent data sets, fortunately not all are equally important numerically. Lattice QCD calculations of the HLbL contribution are expected to be possible at the 10% level in not too far future.

(iv) Less a problem are the hadronic electroweak (HEW) contribution, represented by the diagrams Fig. 5.3, and entering at $O(\alpha G_F m_\mu^2)$. Since the leading HEW corrections Fig. 5.3a are due to quark triangle diagrams and since triple vector amplitudes vanish by Furry's theorem only the axial part of the $f\bar{f}Z$ -vertex contributes. Therefore the HEW contribution is given by the ABJ anomaly, which is perturbative and non-perturbative at the same time, i.e. the leading effects are calculable. The anomaly cancellation condition intimately relates quark and lepton contributions and the potentially large leading corrections cancel, such that hadronic corrections are well under control. The VP type EW corrections Fig. 5.3b are suppressed by a factor m_μ^2/M_Z^2 . The hadronic electroweak effects have been discussed in detail in Sect. 4.2.

Fig. 5.3 Leading hadronic electroweak contribution to $g - 2$



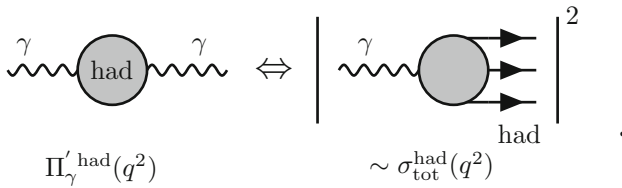
Since the HVP and HLbL type of contributions are confronted with different kinds of problems, which require a detailed discussion in each case, we will consider them in turn in the following two sections.

5.1 Hadronic Vacuum Polarization

5.1.1 Vacuum Polarization Effects and e^+e^- Data

Fortunately vacuum polarization effects may be handled via dispersion relations together with available $e^+e^- \rightarrow$ hadrons data (see p. 13 for remarks on the early history). The tools which we need to overcome the main difficulties we have developed in Sect. 3.7.1 and at the end of Sect. 3.8. For the evaluation of the leading order contribution the main problem is the handling of the experimental e^+e^- -annihilation data and in particular of their systematic errors. The latter turn out to be the limiting factor for the precision of the theoretical prediction of a_μ .

To leading order in α the hadronic “blob” in Fig. 5.1 has to be identified with the photon self-energy function $\Pi'_\gamma{}^{\text{had}}(s)$ which we relate to the cross section $e^+e^- \rightarrow$ hadrons by means of the DR (3.164) based on the correspondence:



The interrelationship is based on unitarity (optical theorem) and causality (analyticity), as elaborated before. Remember that $\Pi'_\gamma{}^{\text{had}}(q^2)$ is a one particle irreducible (1PI) object, represented by diagrams which cannot be cut into two disconnected parts by cutting a single photon line. At low energies the imaginary part is related to intermediate hadronic states like $\pi^0\gamma, \rho, \omega, \phi, \dots, \pi\pi, 3\pi, 4\pi, \dots, \pi\pi\gamma, \dots, KK, \dots \pi\pi Z, \dots, \pi\pi H, \dots$ (at least one hadron plus any strong, electromagnetic or weak interaction contribution), which in the DR correspond to the states produced in e^+e^- -annihilation via a virtual photon (at energies sufficiently below the point where $\gamma - Z$ interference comes into play).

At low energies, near flavor thresholds and in domains exhibiting resonances $\sigma_{\text{tot}}^{\text{had}}(q^2)$ cannot be calculated from first principles, because at present we lack appropriate non-perturbative methods to perform calculations in the time-like region.¹

Fortunately, the cross sections required are available in form of existing experimental data. Since the leading hadronic contribution is rather large, an elaborate

¹It is important to remember that there exist alternatives to the representation (3.163), which is based on the s -channel hadronic cross section, per se a time-like quantity. Exploiting analyticity, we get the representations (3.165) in terms of the space-like photon vacuum polarization function

handling of the experimental data is mandatory because the experimental errors are substantial and of course limit the precision of the “theoretical” prediction of a_μ . Like the deep inelastic electron–nucleon scattering experiments, the e^+e^- –annihilation experiments played an eminent role in establishing QCD as the underlying theory of the strong interaction and they have a long history. Touschek initiated the construction of an e^+e^- storage ring accelerator in the early 1960s at Frascati near Rome. Improved e^+e^- storage ring facilities and first cross section measurements followed at Orsay, Novosibirsk and Frascati. The observed rise in the total hadronic cross section at these times looked very puzzling, as actually a drop as $1/E^2$ was expected at high energies from unitarity arguments. The CEA experiment [1], however, which operated at slightly higher energy, left no room for doubts that the cross section was far higher than theoretical expectations at these times. Apart from its role in explaining Bjorken scaling in deep inelastic ep –scattering [2], QCD, for the first time, predicted a cross section enhanced by the color multiplicity factor $N_c = 3$, which was clearly favored by experiment and as we know in the sequel revolutionized strong interaction physics [3–5]. SLAC and DESY, reaching higher energies, followed and unexpectedly new states were discovered at SLAC, the τ lepton, the charm quark c and the bottom quark b . The highest energies so far were reached with LEP at CERN going up to 200 GeV. Important for the evaluation of the hadronic contributions to $g - 2$ are recent and ongoing hadronic cross section measurements at Novosibirsk, Frascati, Stanford and Beijing which provided much more accurate e^+e^- data. Table 5.1 gives a more complete overview of the history of e^+e^- machines and experiments and the maximum center of mass energy they reached. Unfortunately, some of the energy ranges have been covered only by old experiments with typically 20% systematic errors. The situation though, could be improved substantially by exclusive channel measurement with BaBar as well as with inclusive measurements with BES-II and KEDR. For a precise evaluation of the hadronic effects we need to combine data sets from many experiments of very different quality and performed in different energy intervals. The key problem here is the proper handling of the systematic errors, which are of different origin and depend on the experiment (machine and detector) as well as on theory input like radiative corrections. The statistical errors commonly are assumed to be Gaussian and hence may be added in quadrature. A problem here may be the low statistics of many of the older experiments which may not always justify this treatment. In the low energy region particularly important for $g - 2$, however, data have improved dramatically in recent years (CMD-2, CMD-3 SND/Novosibirsk, BES-II, BES-III/Beijing, CLEO/Cornell, KLOE/Frascati, BaBar/SLAC) and the statistical errors are a minor problem now.

(Footnote 1 continued)

$\Pi_\gamma^{\text{had}}(-Q^2)$ and (3.166) in terms of the space–like Adler–function $D(Q^2)$, which at low energies are accessible to non–perturbative lattice QCD simulations. At higher energies pQCD is applicable (see Sect. 2.8). Lattice QCD for the non–perturbative part together with perturbation theory will allow us to calculate a_μ^{had} from the QCD Lagrangian. Several lattice QCD groups have made impressive progress in the past decade and LQCD results are expected to get competitive with the data–driven approach in the near future.

Table 5.1 Chronology of e^+e^- facilities

Year	Accelerator	E_{\max} (GeV)	Experiments	Laboratory
1961–1962	AdA	0.250		LNF Frascati (Italy)
1965–1973	ACO	0.6–1.1	DM1	Orsay (France)
1967–1970	VEPP-2	1.02–1.4	'spark chamber'	Novosibirsk (Russia)
1967–1993	ADONE	3.0	BCF, $\gamma\gamma$, $\gamma\gamma 2$, MEA, $\mu\pi$, FENICE	LNF Frascati (Italy)
1971–1973	CEA	4,5		Cambridge (USA)
1972–1990	SPEAR	2.4–8	MARK I, CB, MARK 2	SLAC Stanford (USA)
1974–1992	DORIS	–11	ARGUS, CB, DASP 2, LENA, PLUTO	DESY Hamburg (D)
1975–1984	DCI	3.7	DM1,DM2,M3N,B \bar{B}	Orsay (France)
1975–2000	VEPP-2M	0.4–1.4	OLYA, CMD, CMD-2, ND, SND	Novosibirsk (Russia)
1978–1986	PETRA	12–47	PLUTO, CELLO, JADE, MARK-J, TASSO	DESY Hamburg (D)
1979–1985	VEPP-4	–11	MD1	Novosibirsk (Russia)
1979–2008	CESR/CESR-C	9–12	CLEO, CUSB	Cornell (USA)
1980–1990	PEP	–29	MAC, MARK-2	SLAC Stanford (USA)
1987–1995	TRISTAN	50–64	AMY, TOPAZ, VENUS	KEK Tsukuba (Japan)
1989	SLC	90 GeV	SLD	SLAC Stanford (USA)
1989–2005	BEPC	2.0–4.8	BES, BES-II	IHEP Beijing (China)
1989–2000	LEP I/II	110/210	ALEPH, DELPHI, L3, OPAL	CERN Geneva (CH)
1994–	VEPP-4M	12	KEDR	Novosibirsk (Russia)
1999–2007	DA ϕ NE	Φ factory	KLOE	LNF Frascati (Italy)
1999–2008	PEP-II	B factory	BABAR	SLAC Stanford (USA)
1999–2010	KEKB	B factory	Belle	KEK Tsukuba (Japan)
2008–	BEPC-II		BES-III	IHEP Beijing (China)
2010–	VEPP-2000	2	SND, CMD-3	Novosibirsk (Russia)
2015–	SuperKEKB	B factory		KEK Tsukuba (Japan)

The main uncertainty, related to the systematic errors of the experimental data, is evaluated via a certain common sense type error handling, which often cannot be justified unambiguously. This “freedom” of choice has led to a large number of estimates by different groups which mainly differ by individual taste and the level of effort which is made in the analysis of the data. Issues here are: the completeness of the data utilized, interpolation and modeling procedures, e.g. direct integration of the data by applying the trapezoidal rule versus fitting the data to some smooth functional form before integration, separation of energy ranges where data or theory (pQCD and/or hadronic models) are considered to be more reliable, combining the data before or after integration etc.

A reliable combination of the data requires to know more or less precisely what experiments have actually measured and what they have published. As mentioned earlier, hadronic cross section data are represented usually by the cross section ratio²

$$R_{\gamma}^{\text{had}}(s) \equiv \frac{\sigma(e^{+}e^{-} \rightarrow \gamma^{*} \rightarrow \text{hadrons})}{\sigma(e^{+}e^{-} \rightarrow \gamma^{*} \rightarrow \mu^{+}\mu^{-})}, \quad (5.1)$$

which measures the hadronic cross section in units of the leptonic point cross-section. One of the key questions here is: what is the precise definition of $R(s)$ as a “measured” quantity? In theory we would consider (5.1), which also may be written in terms of lowest order cross sections, with respect to QED effects. In short notation

$$R_{\gamma}^{\text{had}}(s) \equiv \frac{\sigma_{\text{had}}(s)}{\sigma_{\mu\mu}(s)} = \frac{\sigma_{\text{had}}^0(s)}{\sigma_{\mu\mu}^0(s)}$$

which reveals $R(s)$ defined in this way as an *undressed* $R(s)$ quantity, since in the ratio common effects, like dressing by VP effects (iterated VP insertions), normalization³ (luminosity measurement) and the like, cancel from the ratio automatically. While the

²Definitions of R ratios like (3.142) may differ slightly modulo subleading corrections. Often we simply denote it as $R(s)$. In fact the standard definition (5.1) has to be corrected for the $\sigma(e^{+}e^{-} \rightarrow \gamma^{*} \rightarrow \mu^{+}\mu^{-})$ specific effects like phase space and final state radiation. One has always to keep in mind that it is the undressed hadronic cross section $\sigma(e^{+}e^{-} \rightarrow \gamma^{*} \rightarrow \text{hadrons}) |\alpha/\alpha(s)|^2$ which matters in the DR for the hadronic contribution to the photon vacuum polarization. So in fact (3.142) is more precisely what is meant when we write the basic DR (3.136) in the form (3.143). We also should be aware that it is the pseudo-observable $\sigma(e^{+}e^{-} \rightarrow \gamma^{*} \rightarrow \text{hadrons})$ which is required for the DR, which has to be extracted from what is actually measurable, namely $\sigma(e^{+}e^{-} \rightarrow \text{hadrons})$. But also this total hadronic cross section is the result of a complicated “interpretation” of what has been seen in the detector, by disentangling the raw data from detector specific features. Practically, in the most relevant low energy regime, the one photon exchange approximation $\sigma(e^{+}e^{-} \rightarrow \text{hadrons}) \approx \sigma(e^{+}e^{-} \rightarrow \gamma^{*} \rightarrow \text{hadrons})$ is an excellent approximation before at about 40 GeV Z boson exchange mixes in. As included in Fig. 5.8, box diagram contributions exhibiting two photon exchange are taken into account as radiative corrections. The latter are not really understood when photons couple to hadrons composed of quarks.

³Note that the *initial state radiation* (ISR) bremsstrahlung only cancels if the same cuts are applied to hadro-production and to $\mu^{+}\mu^{-}$ pair production, a condition, which usually is not satisfied. We should keep in mind that experimentally it is not possible to distinguish an initial state photon from a final state photon.

dressed⁴ physical cross sections $\sigma_{\text{had}}(s)$ and $\sigma_{\mu\mu}(s)$ are proportional to the modulus square of the effective running fine structure constant $\alpha(s)$ (see (3.121) and Fig. 3.13) the “bare” or “undressed” ones $\sigma_{\text{had}}^0(s)$ and $\sigma_{\mu\mu}^0(s)$ are proportional to the square of the classical fine structure constant α determined at zero momentum transfer. The ratio obviously is insensitive to dressing by vacuum polarization. For the leading diagram Fig. 5.1 “dressed” would mean that the full photon propagator is inserted, “undressed” means that just the 1PI photon self-energy is inserted.

In principle, one could attempt to treat self-energy insertions in terms of the full photon propagator according to (3.154), however, vertices cannot be resummed in a similar way such that working consistently with full propagators and full vertices as building blocks, known as the “skeleton expansion”, is technically not feasible. One should avoid as much as possible treating part of the contributions in a different way than others. One has to remind that many fundamental properties of a QFT like gauge invariance, unitarity or locality, only can be controlled systematically order by order in perturbation theory. We therefore advocate to stick as much as possible to an order by order approach for what concerns the expansion in the electromagnetic coupling α , i.e. we will use (3.154) only in expanded form, which allows one to perform a systematic order by order treatment in α . In contrast, the strong interaction effects are non-perturbative and appear as hadronic “blobs”, which, with respect to the perturbative electroweak sector, follow the counting in orders of α : HVP insertions are $O(\alpha)$ and HLbL insertions are $O(\alpha^2)$, as they represent electromagnetic current correlators of two and four currents, respectively.

It turns out that at the level of accuracy we are aiming at, the quantity $R(s)$ we need is not really the ratio (5.1). We have seen that some unwanted effects cancel but others do not. In particular all kinds of electromagnetic radiation effects do not cancel in the ratio. This is obvious if we consider the low energy region, particularly important for the a_μ^{had} evaluation, where $\pi^+\pi^-$ -production dominates and according to (5.1) should be compared with $\mu^+\mu^-$ -production. Neither the final state radiation (FSR) bremsstrahlung contributions nor the phase spaces are commensurate and drop out, and the $\mu^+\mu^-$ -production phase space in the threshold region of $\pi^+\pi^-$ -pair production is certainly in the wrong place here. What we need is the hadronic contribution to $\text{Im}\Pi'_\gamma(s)$, which is what enters in the DR for $\Pi'_\gamma(s)$. Thus, what one has to extract from the measurements for the use in the DR is

$$R_\gamma^{\text{had}}(s) = 12\pi\text{Im}\Pi'_\gamma^{\text{had}}(s) \quad (5.2)$$

as accurately as possible, where $\Pi'_\gamma^{\text{had}}(s)$ is the hadronic component of the 1PI photon self-energy.

⁴The terminus “dressed” refers to the inclusion of higher order effects which are always included in measured quantities.

In fact the high energy asymptotic form of $\sigma_{\mu\mu}(s)$ is the quantity appropriate for the normalization:

$$R_{\gamma}^{\text{had}}(s) = \sigma(e^+e^- \rightarrow \text{hadrons}) / \frac{4\pi|\alpha(s)|^2}{3s} . \quad (5.3)$$

This is equivalent to

$$R_{\gamma}^{\text{had}}(s) = \sigma(e^+e^- \rightarrow \text{hadrons}) / \sigma(e^+e^- \rightarrow \mu^+\mu^-)|_{m_{\mu}=0} ,$$

or

$$R_{\gamma}^{\text{had}}(s) = \sigma(e^+e^- \rightarrow \text{hadrons}) / \sigma(e^+e^- \rightarrow \mu^+\mu^-) \cdot R_{\mu}(s) ,$$

where $R_{\mu}(s)$ to lowest order is given by (3.140). At first, the cross section here must have been corrected for bremsstrahlung effects, because the latter are process and detector dependent and are of higher order in α . The detector dependence is due to finite detector resolution and other so called *cuts* which we have discussed in Sect. 2.6.6. Cuts are unavoidable as real detectors by construction have some blind zones, e.g. the beam tube, and detection thresholds where events get lost. This requires *acceptance* and *efficiency* corrections. As a matter of fact a total cross section can be obtained only by extrapolations and theory or some modeling assumptions may be required to extract the quantity of interest.

There are two types of total cross section “measurements”. At low energies, in practice up to 1.4–2.1 GeV, one has to identify individual final states, because there is no typical characteristic “stamp”, which allows the experimenter to discriminate between hadronic and non-hadronic events unambiguously. One has to identify individual states by mass, charge, multiplicity, the number of final state particles. At high energies the primary quark pair produced hadronizes into two or more bunches, called jets, of hadrons of multiplicity increasing with energy. With increasing energy one passes more and more multi-hadron thresholds, like the ones of the n pion channels: $\pi^+\pi^-$, $\pi^+\pi^-\pi^0$, $\pi^+\pi^-\pi^+\pi^-$, $\pi^+\pi^-\pi^0\pi^0$ and so on, and the energy available distributes preferably into many-particle states if the corresponding phase space is available (see Fig. 5.4). The non-perturbative nature of the strong interaction is clearly manifest here since a perturbative order by order hierarchy is obviously absent on the level of the hadrons produced. In contrast, created lepton pairs can be easily identified in a detector as a two-body state and other non-hadronic states are down in the rate at least by one order in α . Therefore, at high enough energy one may easily separate leptons from hadrons because they have clearly distinguishable signatures, first and foremost the multiplicity. This allows one to carry out an *inclusive* measurement of the total cross section, all hadronic states count and there is no need for identification of individual channels. Such measurements are available⁵ above about 1.4 GeV

⁵Identifying the many channel (see Fig. 5.4) is difficult in particular when neutrals are involved. There is plenty of problems both with missing events or double counting states.

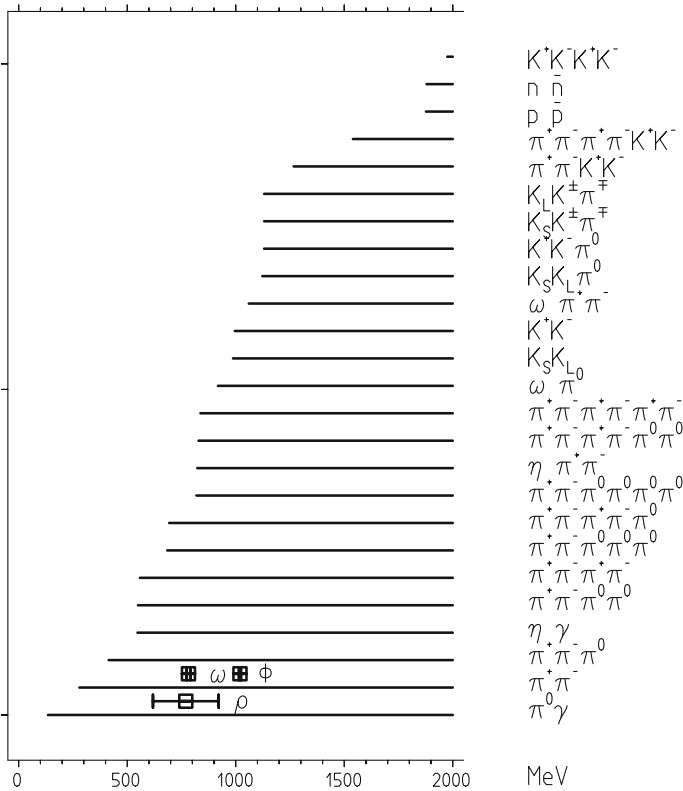


Fig. 5.4 Thresholds for exclusive multi particle channels below 2 GeV

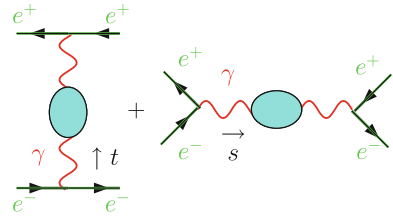
(MEA, $\gamma\gamma 2$). Above 2.1 GeV inclusive measurements are standard. The amazing fact is that at the level of the inclusive cross section, for high enough energies when the effective strong coupling constant α_s is small enough (see Fig. 3.3), perturbative QCD starts to work well away from threshold regions, where resonances show up, in the sense of hadron-quark duality:

$$\sigma(e^+e^- \rightarrow \text{hadrons})(s) = \sum_{X_h} \sigma(e^+e^- \rightarrow X_h)(s) \simeq \sum_q \sigma(e^+e^- \rightarrow q\bar{q})(s),$$

where the sums go over all states which are possible by conservation laws and phase space. The sum over quarks q is subject to the constraint $4m_q^2 \ll s$. The quark-pair production cross section is calculable in pQCD. Here the asymptotic freedom of QCD (see p. 155) comes into play in a way similar to what is familiar from deep inelastic ep -scattering and Bjorken scaling.

At low energies an inclusive measurement of the total hadronic cross sections is not possible and pQCD completely fails. Experimentally, it becomes a highly

Fig. 5.5 VP dressed tree level Bhabha scattering in QED



non-trivial task to separate muon-pairs from pion-pairs, neutral pions from photons, $\pi^+\pi^-\pi^0$ from $\pi^+\pi^-\gamma$ etc. Here only *exclusive* measurements are possible, each channel has to be identified individually and the cross section is obtained by adding up all possible channels. Many channels, e.g. those with π^0 's are not easy to identify and often one uses isospin relations or other kind of theory input to estimate the total cross section.

Experimentally, what is determined is of the form (see (2.107))

$$R_\gamma^{\text{had exp}}(s) = \frac{N_{\text{had}} (1 + \delta_{\text{RC}})}{N_{\text{norm}} \varepsilon} \frac{\sigma_{\text{norm}}(s)}{\sigma_{\mu\mu,0}(s)},$$

where N_{had} is the number of observed hadronic events, N_{norm} is the number of observed normalizing events, ε is the detector efficiency-acceptance product of hadronic events while δ_{RC} are radiative corrections to hadron production. $\sigma_{\text{norm}}(s)$ is the physical cross section for normalizing events (including all radiative corrections integrated over the acceptance used for the luminosity measurement) and $\sigma_{\mu\mu,0}(s) = 4\pi\alpha^2/3s$ is the normalization. In particular this shows that a precise measurement of R requires precise knowledge of the relevant radiative corrections.

For the normalization mostly the Bhabha scattering process is utilized [or $\mu\mu$ itself in some cases]. In general, it is important to be aware of the fact that the effective fine structure constant $\alpha(\mu)$ enters radiative correction calculations with different scales μ in “had” and “norm” and thus must be taken into account carefully.⁶ Care

⁶Bhabha scattering $e^+(p_+) e^-(p_-) \rightarrow e^+(p'_+) e^-(p'_-)$ has two tree level diagrams Fig. 5.5 the t - and the s -channel. With the positive c.m. energy square $s = (p^+ + p^-)^2$ and the negative momentum transfer square $t = (p_- - p'_-)^2 = -\frac{1}{2}(s - 4m_e^2)(1 - \cos\theta)$, θ the e^- scattering angle, there are two very different scales involved. The VP dressed lowest order cross section is

$$\frac{d\sigma}{d\cos\Theta} = \frac{s}{48\pi} \sum_{ik} |A_{ik}|^2$$

in terms of the tree level helicity amplitudes A_{ik} , $i, k = \text{L,R}$ denoting left- and right-handed electrons. The dressed transition amplitudes, in the approximation of vanishing electron mass, read

$$|A_{\text{LL,RR}}|^2 = \frac{3}{8} (1 + \cos\theta)^2 \left| \frac{e^2(s)}{s} + \frac{e^2(t)}{t} \right|^2$$

$$|A_{\text{LR,RL}}|^2 = \frac{3}{8} (1 - \cos\theta)^2 \left| \frac{e^2(s)}{s} + \frac{e^2(t)}{t} \right|^2.$$

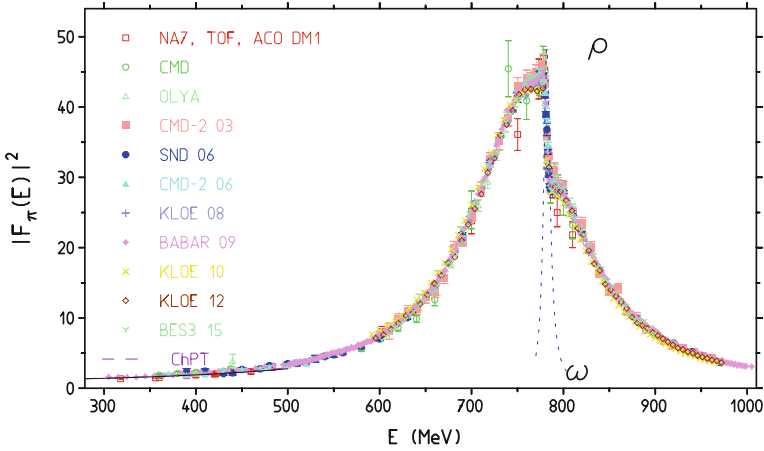


Fig. 5.6 The dominating low energy tail is given by the channel $e^+e^- \rightarrow \pi^+\pi^-$ which forms the ρ -resonance. The $\rho - \omega$ mixing caused by isospin breaking ($m_u - m_d \neq 0$) is distorting the ideal Breit–Wigner resonance shape of the ρ

also is needed concerning the ISR corrections because cuts for the Bhabha process ($e^+e^- \rightarrow e^+e^-$) typically are different from the ones applied to $e^+e^- \rightarrow$ hadrons. Usually, experiments have included corresponding uncertainties in their systematic errors, if they not have explicitly accounted for all appropriate radiative corrections.

The most important contribution for calculating a_μ^{had} comes from the low energy region below about 1 GeV. In Fig. 5.6 we show a compilation of the measurements of the square of the pion form factor $|F_\pi(s)|^2 = 4 R_{\pi\pi}(s)/\beta_\pi^3$ with $\beta_\pi = (1 - 4m_\pi^2/s)^{1/2}$ the pion velocity.

A collection of e^+e^- -data above 1 GeV is shown in Fig. 5.7 [6] (see also [7]), an up-to-date version of earlier compilations [8–16] by different groups. For detailed references and comments on the data we refer to [8] and the more recent experimental $R(s)$ measurements by MD-1 [17], BES-II [18] and KEDR [19]. Data for the very important $\pi\pi$ channel include the measurements from Novosibirsk (NSK) [20–22], Frascati (KLOE) [23–25], SLAC (BaBar) [26] and Beijing (BES-III) [27].

A lot of effort went into the perturbative QCD calculation of $R(s)$. The leading term is given by the Quark Parton Model (QPM) result

$$R(s)^{\text{QPM}} \simeq N_c \sum_q Q_q^2, \tag{5.4}$$

(Footnote 6 continued)

Preferably one uses small angle Bhabha scattering (small $|t|$) as a normalizing process which is dominated by the t -channel $\sim 1/t$, however, detecting electrons and positrons along the beam axis often has its practical limitations.

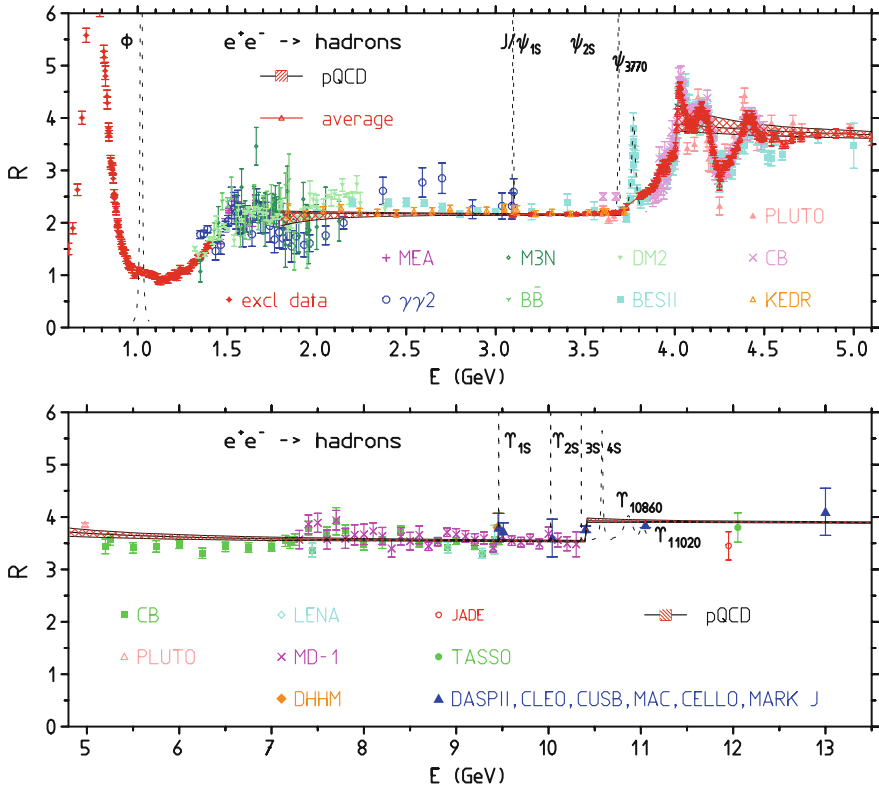


Fig. 5.7 Experimental results for $R_{\gamma}^{\text{had}}(s)$ in the range $1 \text{ GeV} < E = \sqrt{s} < 13 \text{ GeV}$, obtained at the e^+e^- storage rings listed in Table 5.1. The perturbative quark–antiquark pair–production cross section is also displayed (pQCD). Parameters: $\alpha_s(M_Z) = 0.1185 \pm 0.0006$, $m_c = 1.275 \pm 0.025 \text{ GeV}$, $m_b = 4.18 \pm 0.03 \text{ GeV}$ and $\mu \in (\frac{\sqrt{s}}{2}, 2\sqrt{s})$

where the sum extends over quarks q with $4m_q^2 \ll s$. Thus depending on the number of quark thresholds passed $R = 2$, $10/3$ and $11/3$ for $N_q = 3$, 4 and 5, respectively. In Fig. 5.7 one may nicely observe the jumps in R when a new threshold is passed. The higher order corrections are very important for a precise calculation of the contributions from the perturbative regions. Fortunately they are moderate sufficiently far above the thresholds. In pQCD the $\overline{\text{MS}}$ scheme (see Sect. 2.6.5) is generally adopted and normal order by order calculations are always improved by RG resummations. Corrections are known to $O(\alpha_s^4)$ [4, 28–30]. The $O(\alpha_s^3)$ term was first obtained by Gorishnii, Kataev, Larin and Surguladze, Samuel [29] in the massless limit, and then extended to include the mass effect and $O(\alpha_s^4)$ contributions by Baikov, Chetyrkin, Kühn et al. [30]. The state of the art was implemented in the program RHAD by Harlander and Steinhauser [31] (see also [32]). Away from the resonance regions the agreement between theory and experiment looks fairly convincing, however, one has to keep in mind that the systematic errors, which vary widely between a few % up to

10% are not shown in the plot. Typically, the theory result is much more accurate than the experimental one, in regions where it applies. This is possible, because, the QCD parameters α_s and the charm and bottom quark masses relevant here are known from plenty of all kinds of experiments rather accurately now. Nevertheless, it is not obvious that applying pQCD in place of the data, as frequently done, is not missing some non-perturbative contributions. The non-perturbative quark condensate terms ($1/Q^4$ power corrections) which enter the OPE are not a real problem in our context as they are small at energies where pQCD applies [33]. There are other kinds of NP phenomena like bound states, resonances, instantons and in particular the hadronization of the quarks. In applying pQCD to describe real physical cross sections of hadro-production one needs a “rule” which bridges the asymptotic freedom regime with the confinement regime, since the hadronization of the colored partons produced in the hard kicks into color singlet hadrons eludes a quantitative understanding. The rule is referred to as *quark hadron duality*⁷ [35, 36], which states that for large s the average non-perturbative hadron cross section equals the perturbative quark cross section:

$$\overline{\sigma(e^+e^- \rightarrow \text{hadrons})}(s) \simeq \sum_q \sigma(e^+e^- \rightarrow q\bar{q})(s), \quad (5.5)$$

where the averaging extends from threshold up to the given s value which must lie far enough above a threshold (global duality). Approximately, such duality relations then would hold for energy intervals which start just below the last threshold passed up to s . Qualitatively, such a behavior is visible in the data, however, for precise reliable predictions it has not yet been possible to quantify the accuracy of the duality conjecture. A quantitative check would require much more precise cross section measurements than the ones available today. Ideally, one should attempt to reach the accuracy of pQCD predictions. In addition, in dispersion integrals the cross sections are weighted by different s -dependent kernels, while the duality statement is claimed to hold for weight unity. One procedure definitely is contradicting duality reasonings: to “take pQCD plus resonances” or to “take pQCD where $R(s)$ is smooth and data in the complementary ranges”. Also adjusting the normalization of experimental data to conform with pQCD within energy intervals (assuming local duality) has no solid foundation.

In view of the problematic quality of the data in some regions a “theory-driven” approach replacing data by pQCD results in smaller or larger intervals [37–39] may well be adequate to reduce the hadronic uncertainties. However, the uncertainty of the pQCD results evaluated by varying just the QCD parameters $\alpha_s(\mu)$, the quark masses $m_q(\mu)$ and the renormalization scale μ , conventionally, in a range $\mu \in (\frac{\sqrt{s}}{2}, 2\sqrt{s})$, generally does not account for possible non-perturbative uncertainties, related to the hadronization process. Thus the problem of the theory driven approach is a reliable error estimate, and not the shift in the central value, which may well be shifted in the right direction. In the following we generally present a conservative approach of

⁷Quark-hadron duality was first observed phenomenologically for the structure function in deep inelastic electron-proton scattering [34].

the evaluation of the hadronic effects, taking the data and directly integrating them in all regions where pQCD cannot be trusted in the sense as advocated in [31].

The following *data integration procedure* has been used for the evaluation of the dispersion integral:

1. Take data as they are and apply the trapezoidal rule (connecting data points by straight lines) for integration.
2. To combine results from different experiments: (i) integrate data for individual experiments and combine the results, (ii) combine data from different experiments before integration and integrate the combined “integrand”. Check consistency of the two possible procedures to estimate the reliability of the results.
3. Error analysis: (1) statistical errors are added in quadrature, (2) systematic errors are added linearly for different experiments, (3) combined results are obtained by taking weighted averages. (4) all errors are added in quadrature for “independent” data sets. We assume this to be allowed in particular for different energy regions and/or different accelerators. (5) best: apply the true covariance matrix if available, this is the case for the ISR measurements from meson factories.
4. The ρ -resonance region is integrated using the Gounaris–Sakurai (GS) parametrization of the pion form factor [40]. Other pronounced resonances have been parametrized by Breit–Wigner shapes with parameters taken from the Particle Data Tables [41, 42].

5.1.2 *Integrating the Experimental Data and Estimating the Error*

Here we briefly elaborate on procedures and problems related to the integration of the function $R(s)$ given in terms of experimental data sets with statistical and systematic errors. Obviously one needs some interpolation procedure between the data points. The simplest is to use the trapezoidal rule in which data points are joined by straight lines. This procedure is problematic if data points are sparse in relation to the functional shape of $R(s)$. Note that in pQCD $R(s)$ is close to piecewise constant away from thresholds and resonances (where pQCD fails) and the trapezoidal rule should work reliably. For resonances the trapezoidal rule is not very suitable and therefore one uses Breit–Wigner type parametrizations in terms of resonance parameters given in the particle data table. Here it is important to check which type of BW parametrization has been used to determine the resonance parameters (see [8] for a detailed discussion). Some analyses use other smoothing procedures, by fitting the data to some guessed functional form (see e.g. [43, 44]).

While statistical errors commonly are added in quadrature (Gaussian error propagation), the systematic errors of an experiment have to be added linearly, because they encode overall errors like normalization or acceptance errors. Usually the experiments give systematic errors as a relative systematic uncertainty and the systematic error to be added linearly is given by the central value times the relative uncertainty.

For data from different experiments the combination of the systematic errors is more problematic. If one would add systematic errors linearly everywhere, the error would be obviously overestimated since one would not take into account the fact that independent experiments have been performed. However, often experiments use common simulation techniques for acceptance and luminosity determinations and the same state-of-the-art calculations for radiative corrections such that correlations between different experiments cannot be excluded. Since we are interested in the integral over the data only, a natural procedure seems to be the following: for a given energy range (scan region) we integrate the data points for each individual experiment and then take a weighted mean, based on the quadratically combined statistical and systematic error, of the experiments which have been performed in this energy range. By doing so we have assumed that different experiments have independent systematic errors, which of course often is only partially true.⁸ The problem with this method is that there exist regions where data are sparse yet the cross section varies rapidly. The applicability of the trapezoidal rule is then not reliable, but taking other models for the extrapolation introduces another source of systematic errors. It was noticed some time ago in [45] that fitting data to some function by minimizing χ^2 may lead to misleading results. The problem may be circumvented by the appropriate definition of the χ^2 to be minimized (see below). Fortunately, in the dominating ρ -resonance region the data base has been improving a lot during the past decade.

In order to start from a better defined integrand we do better to combine all available data points into a single dataset. If we would take just the collection of points as if they were from *one* experiment we not only would get a too pessimistic error estimate but a serious problem could be that scarcely distributed precise data points do not get the appropriate weight relative to densely spaced data point with larger errors. What seems to be more adequate is to take for each point of the combined set the weighted average of the given point and the linearly interpolated points of the other experiments:

$$\bar{R} = \frac{1}{w} \sum_i w_i R_i ,$$

with total error $\delta_{tot} = 1/\sqrt{w}$, where $w = \sum_i w_i$ and $w_i = 1/\delta_{i\ tot}^2$. By $\delta_{i\ tot} = \sqrt{\delta_{i\ sta}^2 + \delta_{i\ sys}^2}$ we denote the combined error of the individual measurements. In addition, to each point a statistical and a systematic error is assigned by taking weighted averages of the squared errors:

$$\delta_{sta} = \sqrt{\frac{1}{w} \sum_i w_i \delta_{i\ sta}^2} , \quad \delta_{sys} = \sqrt{\frac{1}{w} \sum_i w_i \delta_{i\ sys}^2} .$$

⁸If there are known common errors, like the normalization errors for experiments performed at the same facility, one has to add the common error after averaging. In some cases we correct for possible common errors by scaling up the systematic error appropriately.

There is of course an ambiguity in separating the well-defined combined error into a statistical and a systematic one. We may also calculate separately the total error and the statistical one and obtain a systematic error $\delta_{\text{sys}} = \sqrt{\delta_{\text{tot}}^2 - \delta_{\text{sta}}^2}$. Both procedures give very similar results. We also calculate $\chi^2 = \sum_i w_i (R_i - \bar{R})^2$ and compare it with $N - 1$, where N is the number of experiments. Whenever $S = \sqrt{\chi^2/(N - 1)} > 1$, we scale the errors by the factor S , unless there are plausible arguments which allow one to discard inconsistent data points.

In order to extract the maximum of information, weighted averages of different experiments at a given energy are calculated. The solution of the averaging problem may be found by minimizing χ^2 as defined by

$$\chi^2 = \sum_{n=1}^{N_{\text{exp}}} \sum_{i,j=1}^{N_n} (R_i^n - \bar{R}_i) (C_{ij}^n)^{-1} (R_j^n - \bar{R}_j),$$

where R_i^n is the R measurement of the n th experiment at energy $\sqrt{s_i}$, N_{exp} the number of experiments, C_{ij}^n is the covariance matrix between the i th and j th data point of the n th experiment, and \bar{R} is the average to be determined. The covariance matrix is given by

$$C_{ij}^n = \begin{cases} (\delta_{i \text{ sta}}^n)^2 + (\delta_{i \text{ sys}}^n)^2 & \text{for } j = i \\ \delta_{i \text{ sys}}^n \cdot \delta_{j \text{ sys}}^n & \text{for } j \neq i \end{cases}, \quad i, j = 1, \dots, N_n,$$

where $\delta_{i \text{ sta}}^n$ and $\delta_{i \text{ sys}}^n$ denote the statistical and systematic error, respectively, of R_i^n . The minimum condition $\frac{d\chi^2}{d\bar{R}_i} = 0$, for all i yields the system of linear equations

$$\sum_{n=1}^{N_{\text{exp}}} \sum_{j=1}^{N_n} (C_{ij}^n)^{-1} (R_j^n - \bar{R}_j) = 0, \quad i = 1, \dots, N_n.$$

The inverse covariance matrix \bar{C}_{ij}^{-1} between the calculated averages \bar{R}_i and \bar{R}_j is the sum over the inverse covariances of every experiment

$$\bar{C}_{ij}^{-1} = \sum_{n=1}^{N_{\text{exp}}} (C_{ij}^n)^{-1}.$$

This procedure, if taken literally, would yield reliable fits only if the errors would be small enough, which would require in particular sufficiently high statistics. In fact, many of the older experiments suffer from low statistics and uncertain normalization and the fits obtained in this manner are biased towards too low values (compare [43] with [44], for example). The correct χ^2 minimization requires to replace the experimental covariance matrices C_{ij}^n by the ones of the fit result \bar{C}_{ij} [45]. This is possible by iteration with the experimental covariance as a start value.

Often one attempts to model a number N_{exp} of given different measurements $R^n = \{R_i^n, i = 1, \dots, N_n, n = 1, \dots, N_{\text{exp}}\}$ by theoretical expectation $M(\mathbf{a}) = \{M_i, i = 1, \dots, N_n\}$ weighted by the error covariance matrix C^n provided together with the data. The vector \mathbf{a} denoting the unknown internal model parameter list, is determined by minimizing

$$\chi^2 = \sum_{n=1}^{N_{\text{exp}}} \sum_{i,j=1}^{N_n} [R^n - M(\mathbf{a})]_i^T (C_{ij}^n)^{-1} [R^n - M(\mathbf{a})]_j, \quad (5.6)$$

with respect to \mathbf{a} which is providing the optimum value \mathbf{a}_0 . This approach has been exercised for the case of low energy $e^+e^- \rightarrow$ hadrons data in [44] using some phenomenologically inspired shape functions and more recently in [46] adopting the HLS phenomenological Lagrangian model, for example.

The notorious normalization uncertainties of data sets may pose a serious problem and therefore should be analyzed carefully too. This has been done in [47] again within the framework of the HLS model. A constant global scale uncertainty can be written $\beta = 1 + \lambda$, where λ is a random variable with range on $] -1, +\infty[$. As the expectation values are $E(\lambda) = 0$ and $E(\lambda^2) = \sigma^2$ with $\sigma \ll 1$, the Gaussian approximation for λ is safe [48]. A data sample subject to a global scale uncertainty provides an individual contribution to an effective global χ_{glob}^2 , which is of the form

$$\chi^2 = \sum_{n=1}^{N_{\text{exp}}} \sum_{i,j=1}^{N_n} [R^n - M(\mathbf{a}) - \lambda A]_i^T (C_{ij}^n)^{-1} [R^n - M(\mathbf{a}) - \lambda A]_j + \frac{\lambda^2}{\sigma^2}, \quad (5.7)$$

where R, M, C and \mathbf{a} have the same meaning as before, while λ and σ are the new elements. As for A , even if intuitively one may prefer $A = R$, the choice $A = M(\mathbf{a})$ has been shown to drop out any biasing issue⁹ [45, 48]. As $M(\mathbf{a})$ is unknown at the start of the fitting, $A = R$ is the initial setting and $A \approx M(\mathbf{a})$ is achieved by iteration. Assuming that the unknown scale factor λ is solely of experimental origin – and, then, independent of the model parameters \mathbf{a} – the solution to $\partial\chi^2/\partial\lambda = 0$ provides its most probable value λ_0 . After substituting the solution into (5.7) the latter becomes

$$\chi^2 = \sum_{n=1}^{N_{\text{exp}}} \sum_{i,j=1}^{N_n} [R^n - M(\mathbf{a})]_i^T (\tilde{C}_{ij}^n)^{-1} [R^n - M(\mathbf{a})]_j \quad \text{with} \quad \tilde{C} = C + \sigma^2 A A^T, \quad (5.8)$$

which exhibits a modified error covariance matrix \tilde{C} and only depends on the (physics) model parameters. More precisely, the single recollection of the scale uncertainties λ shows up in its variance σ^2 in the modified covariance matrix \tilde{C} . A detailed analysis of the low energy e^+e^- data has been performed recently in [47] where also more details on the implementation of the method may be found.

⁹This does not mean that the choice $A = R$ necessarily leads to a significantly biased solution.

5.1.3 The Cross-Section $e^+e^- \rightarrow \text{Hadrons}$

The total cross section for hadron production in e^+e^- -annihilation (a typical s -channel process) may be written in the form

$$\begin{aligned}\sigma_{\text{had}}(s) &= \frac{\alpha}{s} \frac{4\pi}{\sqrt{1 - \frac{4m_e^2}{s}}} \left(1 + \frac{2m_e^2}{s}\right) \text{Im} \Pi_\gamma^{\text{had}}(s) \\ &\simeq \frac{4\pi\alpha}{s} \text{Im} \Pi_\gamma^{\text{had}}(s), \quad \text{since } s \geq 4m_\pi^2 \gg m_e^2,\end{aligned}$$

where $\Pi_\gamma^{\text{had}}(s)$ is the hadronic part of the photon vacuum polarization with (see (3.139) and Sect. 3.7.1)

$$\text{Im} \Pi_\gamma^{\text{had}}(s) = \frac{e^2}{12\pi} R_\gamma^{\text{had}}(s).$$

From (2.179) we easily get the lowest order quark/antiquark pair-production cross section encoded in

$$R_\gamma^{\text{pQCD}}(s) = \sum_q N_{cq} Q_q^2 \sqrt{1 - \frac{4m_q^2}{s}} \left(1 + \frac{2m_q^2}{s}\right), \quad (5.9)$$

which however is a reasonable approximation to hadro-production only at high energies away from thresholds and resonances (see below) and to the extent that quark-hadron duality (5.5) holds. At low energies $4m_\pi^2 < s < 9m_\pi^2$ the $\pi\pi$ -production channel is the dominant hadro-production process. The pion-pair production is commonly parametrized in terms of a non-perturbative amplitude, the pion form factor $F_\pi(s)$,

$$R_\gamma^{\text{had}}(s) = \frac{1}{4} \left(1 - \frac{4m_\pi^2}{s}\right)^{\frac{3}{2}} |F_\pi^{(0)}(s)|^2, \quad s < 9m_\pi^2. \quad (5.10)$$

For point-like pions we would have $F_\pi(s) = F_\pi(0) = 1$. At this point it is important to remind the reader that we have been deriving a set of relations and formulas to leading order $O(\alpha^2)$ in QED in Sect. 2.7. For a precise analysis of the hadronic effects higher order QED corrections are important as well. Furthermore, we have assumed that the center of mass energy $E = \sqrt{s}$ is small enough, typically, $E \leq 12$ GeV say, such that virtual Z exchange contributions $e^+e^- \rightarrow Z^* \rightarrow \text{hadrons}$ or $e^+e^- \rightarrow Z^* \rightarrow \mu^+\mu^-$ are sufficiently suppressed relative to virtual γ^* exchange at the precision we are aiming at. Since a_μ^{had} is rather insensitive to the high energy tail such a condition is not a problem.

In order to obtain the observed cross section, we have to include the QED corrections, the virtual, soft and hard photon effects. The basic problems have been

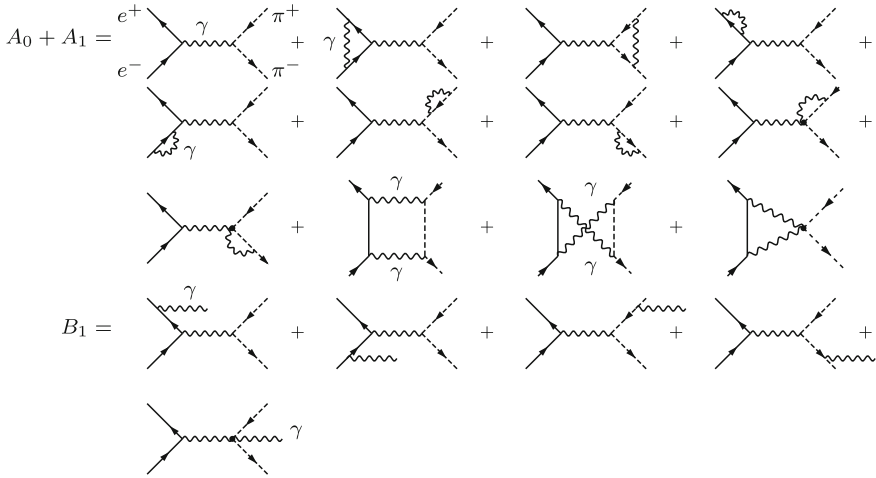


Fig. 5.8 One-loop sQED radiative corrections to pion-pair production assuming point-like pions. A_0 is the $e^+e^- \rightarrow \pi^+\pi^-$ Born amplitude, A_1 is the 1-loop virtual photon correction and B_1 the real photon emission $e^+e^- \rightarrow \pi^+\pi^-\gamma$ amplitude

discussed in Sect. 2.6.6. For the important $\pi\pi$ channel, assuming scalar QED for the pions (see Fig. 2.13 for the Feynman rules) the one-loop diagrams are depicted in Fig. 5.8. In calculating the corrected cross section one starts with point-like pions and replaces the point form-factor $F_\pi^{\text{point}}(s) \equiv 1$ (strong interaction switched off) by the strong interaction dressed one with $F_\pi(s)$ a generic function of s . At least to $O(\alpha^2)$ this is possible due to the simple structure (see (5.11) below) of the observed cross section [49–51].

Particularly important is the Initial State Radiation (ISR), which may lead to huge corrections in the shape of the cross section. The most dramatic effects are of kinematical nature and may be used for cross section measurements by the *radiative return* (RR) mechanism shown in Fig. 5.9: in the radiative process $e^+e^- \rightarrow \pi^+\pi^-\gamma$, photon radiation from the initial state reduces the invariant mass from s to $s' = s(1 - k)$ of the produced final state, where k is the fraction of energy carried away by the photon radiated from the initial state. This may be used to measure $\sigma_{\text{had}}(s')$ at all energies $\sqrt{s'}$ lower than the fixed energy \sqrt{s} at which the accelerator is running [52]. This is particularly interesting for machines running on-resonance like the ϕ - and B -factories, which typically have huge event rates as they are running on top of a peak [53–55]. A radiative return measurement is a next to leading order approach. On the theory side one expects that the handling of the photon radiation requires one order in α more than the scan method for obtaining the same accuracy. The precise calculation of radiative corrections is mandatory for unfolding the experimental information of interest from raw data. In particular the development and continuous improvement of the Monte Carlo generator program PHOKHARA [55], together with improved tools for luminosity measurements like the BABAYAGA [56], BH-WIDE [57] and MCGPJ [58], allowed to preform ISR cross section measurements at the half percent

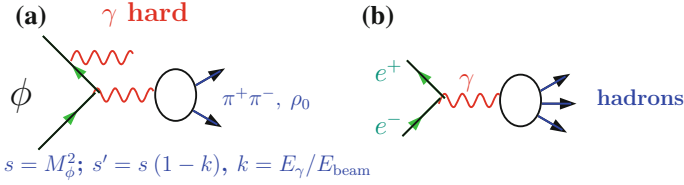


Fig. 5.9 **a** Radiative return measurement of the $\pi^+\pi^-$ cross-section by KLOE at the ϕ -factory DAΦNE. At the B -factory at SLAC, using the same principle, BABAR has measured many other channels at higher energies. Recently also BES-III at BEPC-II has applied the ISR mechanism to measure the $\pi^+\pi^-$ cross-section; **b** Standard measurement of σ_{had} in an energy scan as performed at Novosibirsk (CMD-2, CMD-3, SND, KEDR) and Beijing (BES-II) by tuning the beam energy

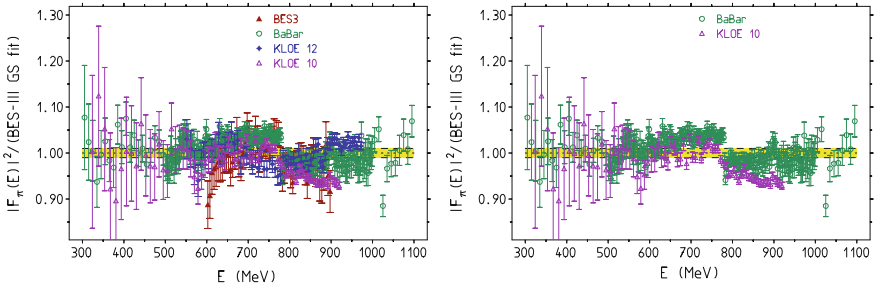


Fig. 5.10 Comparison of ISR $\pi\pi$ data: ratio $|F_\pi(E)|^2$ in units of a GS fit from BES-III. *Left panel* all sets. *Right panel* BaBar versus KLOE10, which exhibits the largest relative deviations

level [59, 60] at the end. The first dedicated radiative return experiment has been performed by KLOE at DAΦNE/Frascati, by measuring the $\pi^+\pi^-$ cross-section [23] (see Fig. 5.6). Based on the ISR method, meson factories have been able to improve the low energy $\pi\pi$ cross-sections database dramatically. Measurements from KLOE, BABAR and lately also from BES-III allowed to reduce errors by almost a factor ten. The measurements are very challenging and unfortunately there is quite some tension between the different data set as shown in Fig. 5.10. KLOE data lie higher below the ρ^0 and lower above the ρ^0 , with deviations at the few % level at the boundaries of the measured energy range. For a recent review of hadron production via e^+e^- collisions with initial state radiation see [61] or the earlier [62].

The “observed” cross section at $O(\alpha^2)$ may be written in the form

$$\begin{aligned} \sigma^{\text{obs}}(s) &= \sigma_0(s) [1 + \delta_{\text{ini}}(\omega) + \delta_{\text{fin}}(\omega)] \\ &+ \int_{4m_\pi^2}^{s-2\omega\sqrt{s}} ds' \sigma_0(s') \rho_{\text{ini}}(s, s') + \sigma_0(s) \int_{4m_\pi^2}^{s-2\omega\sqrt{s}} ds' \rho_{\text{fin}}(s, s'), \quad (5.11) \end{aligned}$$

which also illustrates the unfolding problem one is confronted with in determining the cross section of interest $\sigma_0(s)$. This “bare” cross section, undressed from electromagnetic effects, is formally given by the point cross-section (2.261) times the absolute square of the pion form factor which encodes the strong interaction effects

$$\sigma_0(s) = |F_\pi(s)|^2 \sigma^{\text{point}}(s) = \frac{\pi\alpha^2}{3s} \beta_\pi^3 |F_\pi(s)|^2. \quad (5.12)$$

The parameter ω is an IR cut-off as introduced in Sect.2.6.6 and by $\beta_\pi = (1 - 4m_\pi^2/s)^{1/2}$ we denote the pion velocity. It drops out in the sum (5.11). The initial state corrections, in the approximation neglecting $O(\alpha m_e^2/m_\pi^2)$ terms, are given by the following virtual+soft (V+S) and hard (H) parts:

$$\delta_{\text{ini}}(\omega) = \ln\left(\frac{2\omega}{\sqrt{s}}\right) B_e(s) + \frac{\alpha}{\pi} \left[-2 + \frac{\pi^2}{3} + \frac{3}{2} L_e \right],$$

where $L_e = \ln\left(\frac{s}{m_e^2}\right)$ and $B_e(s) = \frac{2\alpha}{\pi} [L_e - 1]$. The hard ISR radiator function reads

$$\rho_{\text{ini}}(s, s') = \frac{1}{s} \left[\frac{B_e(s)}{1-z} - \frac{\alpha}{\pi} (1+z) (L_e - 1) \right],$$

with $z = s'/s$. The final state corrections again we separate into a virtual+soft part and a hard part:

$$\begin{aligned} \delta_{\text{fin}}(\omega) = & \ln\left(\frac{2\omega}{\sqrt{s}}\right) B_\pi(s, s') + \frac{\alpha}{\pi} \left\{ \frac{3s - 4m_\pi^2}{s\beta_\pi} \ln\left(\frac{1 + \beta_\pi}{1 - \beta_\pi}\right) - 2 \right. \\ & - \frac{1}{2} \ln\left(\frac{1 - \beta_\pi^2}{4}\right) - \frac{3}{2} \ln\left(\frac{s}{m_\pi^2}\right) - \frac{1 + \beta_\pi^2}{2\beta_\pi} \left[\ln\left(\frac{1 + \beta_\pi}{1 - \beta_\pi}\right) \right. \\ & \left. \left[\ln\left(\frac{1 + \beta_\pi}{2}\right) + \ln(\beta_\pi) \right] + \ln\left(\frac{1 + \beta_\pi}{2\beta_\pi}\right) \ln\left(\frac{1 - \beta_\pi}{2\beta_\pi}\right) \right. \\ & \left. \left. + 2\text{Li}_2\left(\frac{2\beta_\pi}{1 + \beta_\pi}\right) + 2\text{Li}_2\left(-\frac{1 - \beta_\pi}{2\beta_\pi}\right) - \frac{2}{3}\pi^2 \right] \right\}, \end{aligned}$$

where $\text{Li}_2(x)$ is the dilogarithm (Spence function) and

$$B_\pi(s, s') = \frac{2\alpha}{\pi} \frac{s'\beta_\pi(s')}{s\beta_\pi(s)} \left[\frac{1 + \beta_\pi^2(s')}{2\beta_\pi(s')} \ln\left(\frac{1 + \beta_\pi(s')}{1 - \beta_\pi(s')}\right) - 1 \right].$$

The hard FSR radiator function is given by

$$\rho_{\text{fin}}(s, s') = \frac{1}{s} \left[\frac{B_\pi(s, s')}{1-z} + \frac{2\alpha}{\pi} (1-z) \frac{\beta_\pi(s')}{\beta_\pi^3(s)} \right].$$

At the level of precision of interest also higher order corrections should be included. The $O(\alpha^2)$ corrections are partially known only and we refer to [51] and references therein for more details.

The crucial point is that the radiator functions $\rho_{\text{ini}}(s, s')$ and to some extent also $\rho_{\text{fin}}(s, s')$ are calculable in QED. Pion pair production is C -invariant and it is very

important that experimental angular cuts, which always have to be applied, are symmetric such that C invariance is respected. Then, as in (5.11) for the total cross section, at the one-loop level initial-final state (IFS) interference terms are vanishing, also for the cut cross-sections. Generally, the IFS interference derives from the box diagrams of Fig. 5.8 and the cross terms

$$\left(\begin{array}{c} \text{---} \\ \diagup \quad \diagdown \\ \text{---} \end{array} \right) \times \left(\begin{array}{c} \text{---} \\ \diagdown \quad \diagup \\ \text{---} \end{array} \right)$$

which are obtained in calculating the transition probability $|T|^2$. Under this condition the cross section factorizes into initial state and final state radiation as in (5.11). Still we have a problem, the FSR is not calculable from first principles [63, 64, 173]. Hence $\rho_{\text{fin}}(s, s')$ is model-dependent, only the soft photon part of it is well modeled by sQED.¹⁰ Our Fig. 5.38 below provides a pretty reliable appraisal concerning the range of validity up to about 1 GeV of sQED in our context.

One other important point should be added here. A look at Fig. 5.11 tells us that there are two factors of e in the related matrix element, the absolute square of which determines the hadronic cross section. One from the initial $e^+e^-\gamma^*$ -vertex the other from the hadronic vertex, connected by the full photon propagator. Since the object of interest is the 1PI hadronic “blob” we have to subtract the VP-effects included in the full photon propagator.

5.1.4 Photon Vacuum Polarization and the Complex $\alpha_{\text{QED}}(s)$

Since the full photon propagator is complex in the time-like region, it is convenient to work with a complex $\alpha(s)$ to represent the complex full photon propagator and define

¹⁰In radiative return measurements at low energy one looks at the $\pi^+\pi^-$ invariant mass distribution $\left(\frac{d\sigma}{ds'}\right)$ plus any photon. Once s' is fixed the missing energy $s - s'$ is fixed and an “automatic” unfolding is obtained. Using the pion form factor ansatz:

$$\left(\frac{d\sigma}{ds'}\right)_{\text{sym-cut}} = |F_\pi(s')|^2 \left(\frac{d\sigma}{ds'}\right)_{\text{ini, sym-cut}}^{\text{point}} + |F_\pi(s)|^2 \left(\frac{d\sigma}{ds'}\right)_{\text{fin, sym-cut}}^{\text{point}},$$

we may directly resolve for the pion form factor as

$$|F_\pi(s')|^2 = \frac{1}{\left(\frac{d\sigma}{ds'}\right)_{\text{ini, sym-cut}}^{\text{point}}} \left\{ \left(\frac{d\sigma}{ds'}\right)_{\text{sym-cut}} - |F_\pi(s)|^2 \left(\frac{d\sigma}{ds'}\right)_{\text{fin, sym-cut}}^{\text{point}} \right\}.$$

This is a remarkable equation since it tells us that the inclusive pion-pair invariant mass spectrum allows us to get the pion form factor unfolded from photon radiation directly as for fixed s and a given s' the photon energy is determined. The point cross-sections are assumed to be given by theory and $d\sigma/ds'$ is the observed experimental pion-pair spectral function.

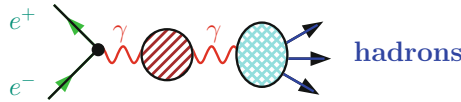


Fig. 5.11 Structure of hadroproduction in e^+e^- -annihilation. The hadronic current at the hadro-production vertex is connected to the e^+e^- -vertex by e^2 times the full photon propagator, represented by $\alpha(k^2)/k^2$ (see Eq. (3.120)). Thus $\sigma(e^+e^- \rightarrow \gamma^* \rightarrow \text{hadrons}) \propto |\alpha(k^2) T(\gamma^* \rightarrow \text{hadrons})(k^2)|^2$, where $T(\gamma^* \rightarrow \text{hadrons})$ denotes the hadronic matrix-element associated with the hadronic current (i.e. without factor e). k^μ is the four-momentum carried by the photon and $s = k^2$ the c.m. energy square of the hadron production process. The irreducible hadronic “blob” is obtained by dividing out the full photon propagator and replacing it with the lowest order one

$$\alpha(s) = \frac{\alpha}{1 - \Delta\alpha} \quad ; \quad \Delta\alpha = -(\Pi'_\gamma(s) - \Pi'_\gamma(0)) \quad . \quad (5.13)$$

The imaginary part of $\Delta\alpha$ is given by $-\text{Im} \Pi'_\gamma(s) = -\frac{\alpha}{3} R(s)$ (see Eq. (3.139)) and is relevant in particular near narrow resonances. The physical hadronic cross section is proportional to $|\alpha(s) T(\gamma^* \rightarrow \text{hadrons})(s)|^2$, because in the physical cross section the full photon propagator including all radiative corrections contributes in the measurement, as discussed in Sect. 3.7.1. In order to obtain the 1PI photon self-energy, which is our building-block for systematic order by order (in α) calculations, we have to undress the physical cross section from multiple 1PI insertions, which make up the dressed propagator. This requires to replace the running $\alpha(s)$ by the classical Thomson limit $\alpha(0) \equiv \alpha$. Usually it is sufficient to work with the approximation $|\alpha(s)|^2 |T(\gamma^* \rightarrow \text{hadrons})(s)|^2$ such that the dressed (physical) cross section σ is related to its undressed version $\sigma^{(0)}$ by

$$\sigma_{\text{tot}}^{(0)}(e^+e^- \rightarrow \text{hadrons}) = \sigma_{\text{tot}}(e^+e^- \rightarrow \text{hadrons}) \left| \frac{\alpha}{\alpha(s)} \right|^2 \quad . \quad (5.14)$$

Using this together with (3.146), we obtain

$$\Pi_\gamma^{\text{had}}(s) - \Pi_\gamma^{\text{had}}(0) = \frac{s}{4\pi^2\alpha} \int_0^\infty ds' \frac{\sigma_{\text{tot}}^{(0)}(e^+e^- \rightarrow \text{hadrons})(s')}{(s' - s - i\varepsilon)} \quad , \quad (5.15)$$

as a basic relation for the evaluation of the HVP effects in terms of e^+e^- -data.

Note that using the physical cross section in the DR gives a nonsensical result, since in order to get the photon propagator we have to subtract in any case the external charge at the right scale. Thus while

$$\frac{s}{4\pi^2\alpha} \int_0^\infty ds' \frac{\sigma_{\text{tot}}(e^+e^- \rightarrow \text{hadrons})(s')}{(s' - s - i\varepsilon)}$$

is double counting the VP effects, and therefore does not represent something meaningful, the linearly $|\alpha/\alpha(s)|$ -rescaled cross section

$$\frac{s}{4\pi^2} \int_0^\infty ds' \frac{1}{|\alpha(s')|} \frac{\sigma_{\text{tot}}(e^+e^- \rightarrow \text{hadrons})(s')}{(s' - s - i\varepsilon)},$$

yields the hadronic shift in the full photon propagator. Only at least once VP-subtracted physical cross sections are useful in DRs! However, this amounts to resumming electromagnetic effects to all orders in α , and is not useful in a systematic order by order approach. Hence we stick to the basic DR (5.15) in all what follows.

In general we know the experimental physical cross section $\sigma_{\text{tot}}(e^+e^- \rightarrow \text{hadrons})$ as well as the complex $\alpha(s)$, such that we can extract the required undressed $\sigma_{\text{tot}}^{(0)}(e^+e^- \rightarrow \text{hadrons})$ via (5.14). However, $\alpha(s)$ we only know after we know σ_{had} , so usually we can determine $\sigma_{\text{had}}^{(0)}(s)$ only by iteration, provided this iteration converges. In most cases experiments do not directly extract the R -ratio (5.1) as a ratio of measured cross sections. The reason is that luminosity is usually monitored by Bhabha-scattering and because $\sigma_{\mu\mu}(s)$ is much smaller than $\sigma_{\text{had}}(s)$ and has much lower statistics especially in resonance regions. In case (5.1) is available we have

$$\text{Im } \Pi'_\gamma{}^{\text{had}}(s) = \frac{\alpha}{3} R^{\text{had}}(s) = \frac{\sigma_{\text{had}}(s)}{\sigma_{\mu\mu}(s)} \quad (5.16)$$

experimentally, which allows us the obtain

$$\text{Re } \Pi'_{\gamma \text{ ren}}(s) = \text{Re } \Pi'_\gamma(s) - \Pi'_\gamma(0) = \frac{s}{\pi} \text{Re} \int_{s_0}^\infty ds' \frac{\text{Im } \Pi'_\gamma(s')}{s'(s' - s - i\varepsilon)}$$

directly, such that $\Pi'_{\gamma \text{ ren}}$ is determined. However, what is measured when looking at σ_{had} in isolation (via normalization to Bhabha events) is $\sigma_{\text{had}}(s) = \frac{4\pi\alpha}{s} \text{Im } \Pi'_\gamma{}^{\text{had}}(s) |1/(1 + \Pi'_{\gamma \text{ ren}}(s))|^2$ and thus

$$\text{Im } \Pi'_\gamma{}^{\text{had}}(s) = \frac{s}{4\pi\alpha} |1 + \Pi'_{\gamma \text{ ren}}(s)|^2 \sigma_{\text{had}}(s), \quad (5.17)$$

where $\Pi'(s) = \Pi'^{\text{lep}} + \Pi'^{\text{had}}$ is the full *irreducible* photon self-energy including the leptonic contributions, which is well known in perturbation theory. In terms of data alone to determine the two quantities $\text{Im } \Pi'(s)$ and $\text{Re } \Pi'(s)$ we need two measurements besides σ_{had} ideally also $\sigma_{\mu\mu}$, as performed recently in [65]. This works locally point by point for each energy. If only $\sigma_{\text{had}}(s)$ is known, the standard procedure is to expand (5.17) in Π' , which then allows to solve iteratively for $\Pi'(s)$ with the real part determined by the DR (5.15). This requires to know $\sigma_{\text{had}}(s)$ for all $s \geq s_0$ and is thus not a local procedure. This works well when $|\Pi'(s)| \ll 1$, which

is what we usually expect for an e.m. correction. Unfortunately, in the vicinity of some resonances the convergence condition $|\Pi'(s)| < 1$ is badly violated.

HVP Subtraction of $R_\gamma^{\text{had}}(s)$: a Problem of the DR Method?

So far we have not addressed the question what happens if $|\hat{\Pi}'_\gamma(s)| \geq 1$. The problem has been addressed recently in [6] and we include the discussion here. The full photon propagator (2.165) is usually obtained by Dyson resummation (2.162) of the 1PI part $x = \Pi'_\gamma(s)$. As we know this is a geometric series $1 + x + x^2 + \dots = 1/(1 - x)$ which only converges iff $|x| < 1$. Including the external e.m. couplings and renormalization we have

$$i e^2 D'_\gamma(q^2) = \frac{-i}{q^2} \frac{e^2}{1 + \Pi'_{\gamma \text{ ren}}(q^2)} .$$

The complex effective charge thus is given by the well-known expression

$$\frac{e^2}{1 + \Pi'_{\gamma \text{ ren}}(s)} = \frac{e^2}{1 - \Delta\alpha(s)} = e^2(s) .$$

Usually, $\Delta\alpha(s)$ is a correction i.e. $|\Delta\alpha(s)| \ll 1$ and the Dyson series converges well. Indeed for any type of perturbative effects no problem is encountered (besides possible Landau poles). For non-perturbative strong interaction physics there are exceptions. One would expect that, if there are problems, one would encounter them at low energy, but for the ρ , the ω and the ϕ , in spite of huge resonance enhancements, the HVP contributions to the running charge are small relative to unity, as the effect is suppressed by the e.m. coupling e^2 . The exception, surprisingly, we find at pretty high energies, at the very narrow Okubo–Zweig–Iizuka (OZI) suppressed resonances,¹¹ which are extremely sharp, because they lie below corresponding $q\bar{q}$ -thresholds. For these Extremely Narrow Resonances (ENR) the strong interaction appears heavily suppressed (3 gluons exchange) and the electromagnetic channel (1 photon exchange) appears almost as strong as the strong one (see Fig. 5.12). Actually, Γ_{ee} is not much smaller than Γ_{QCD} (i.e. strong decays). This phenomenon shows up for the resonances J/ψ , ψ_2 , Υ_1 , Υ_2 and Υ_3 . The imaginary parts from the narrow resonances read

$$\text{Im } \Pi'_\gamma(s) = \frac{\alpha}{3} R_\gamma(s) = \frac{3}{\alpha} \frac{\Gamma_{ee}}{\Gamma} ; \quad s = M_R^2$$

¹¹The OZI rule formulated in 1963 independently by Okubo, Zweig and Iizuka [66], explains why certain hadron decay channels appear substantially suppressed. Later it turned out to be a simple consequence of QCD. Diagrams representing OZI suppressed processes can be cut into an initial and a final state part by cutting gluon lines solely (see Fig. 5.12). An example is ϕ decay: since ϕ is essentially a $\bar{s}s$ state, the decay into strange meson states $\phi \rightarrow K^+K^-, \bar{K}^0K^0$ is dominating (83%), while the decay into non-strange mesons $\phi \rightarrow \pi^+\pi^-\pi^0$ is suppressed (15%), in spite of the much larger phase space available.

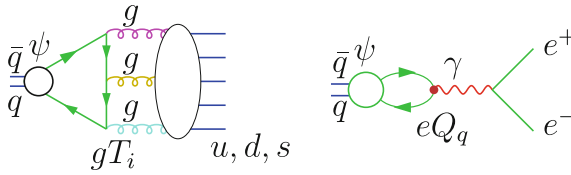


Fig. 5.12 OZI suppressed strong decays let e.m. interaction look to be almost of equal strength

at peak, causing the sharp spikes, which are seen only by appropriate high resolution scans, as we know. Let $\alpha(s)$ denotes the real $\alpha(s) = \alpha/(1 + \text{Re } \Pi'_{\gamma\text{ren}}(s))$, we note that,

$$|1 + \Pi'_{\gamma\text{ren}}(s)|^2 - (\alpha/\alpha(s))^2 = (\text{Im } \Pi'_{\gamma}(s))^2,$$

and at $\sqrt{s} = M_R$ values for the different resonances are given by 1.23×10^{-3} (ρ), 2.76×10^{-3} (ω), 1.56×10^{-2} (ϕ), 594.81 (J/ψ), 9.58 (ψ_2), 2.66×10^{-4} (ψ_3), 104.26 (Υ_1), 30.51 (Υ_2) and 55.58 (Υ_3). This shows that near OZI suppressed resonances the Dyson series cannot converge. So we have a problem with the dispersive approach, which requires $R_{\gamma}(s) \propto \text{Im } \Pi'_{\gamma}(s)$ as an input. What is measured by an experiment is the full propagator, the summed up Dyson series, $Z = |1/(1 + x + iy)|^2$, but we cannot extract y from that since for $|x + iy| \geq 1$ the observable Z has no representation in terms of x and y . Remember that the object required in the DR is the undressed $R_{\gamma}(s)$ in (5.3), which cannot be measured itself, rather we have to extract

$$R_{\gamma}^{\text{bare}} = R_{\gamma}^{\text{phys}} |1 + \Pi'_{\gamma\text{ren}}(s)|^2.$$

Locally, near OZI suppressed resonances, the usual iterative procedure of getting R_{γ}^{bare} does not converge! The way out usually practiced is to utilize the smooth space-like charge, i.e. $\bar{R}_{\gamma}^{\text{bare}} = R_{\gamma}^{\text{phys}} |1 + \Pi'_{\gamma\text{ren}}(-s)|^2$, expected to do the undressing “in average”. This actually does not look too wrong as we see in Fig. 5.13. Nevertheless, I see a problem her, not only for the interpretation of resonance data, where one would wish to be able to disentangle electromagnetic from strong interaction effects.

For what concerns the proper extraction of the hadronic effects contributing to the running of α_{QED} and to a_{μ}^{had} , I see no proof that this cannot produce non-negligible shifts! In the ENR regions, it is therefore indispensable to measure $R(s)$ via the experimental ratio (5.1) corrected for the difference in the phase spaces and in final state radiation, in order to get the proper undressed cross section needed in the DR approach. Cross-sections measured by normalizing to Bhabha events (which is what most experiments have been doing except from the more recent BaBar and KLOE12 ones) have the problem that one has to perform corrections which are not under control perturbatively. Note that from measuring (5.17) with $(1 + \Pi')(1 + \Pi'^{*}) = 1 + 2\text{Re } \Pi' + (\text{Re } \Pi')^2 + (\text{Im } \Pi')^2$ in the denominator, we cannot determine $\text{Im } \Pi'(s)$ and $\text{Re } \Pi'(s)$ locally unless we measure $\sigma_{\mu\mu}(s)$ as well.

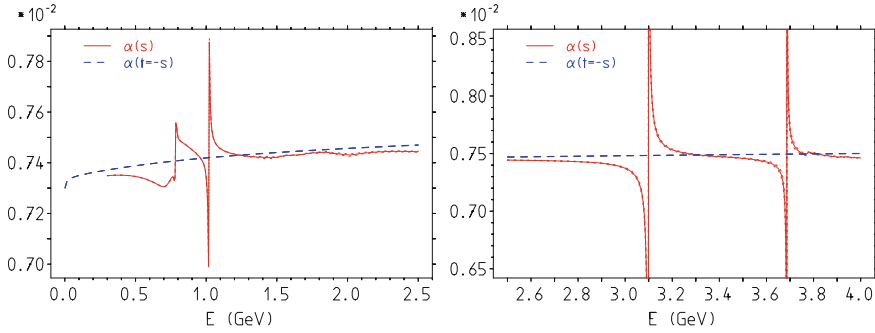


Fig. 5.13 Time-like versus space-like effective fine-structure constant α as a function of the energy E : $\alpha(s)$ in the mean follows $\alpha(t = -s)$ ($s = E^2$). Note that the smooth space-like effective charge agrees rather well with the non-resonant “background” above the ϕ (kind of duality)

The measurement of the $\mu\mu$ -pair production cross section normalized to the Monte Carlo event generation where the VP has been switched off yields

$$\frac{\sigma_{\text{data}}(e^+e^- \rightarrow \mu^+\mu^-)(s)}{\sigma_{\text{MC}}^0(e^+e^- \rightarrow \mu^+\mu^-)(s)} = \left| \frac{\alpha(s)}{\alpha} \right|^2 = \left| \frac{1}{1 + \Pi'_{\gamma\text{ren}}(s)} \right|^2. \tag{5.18}$$

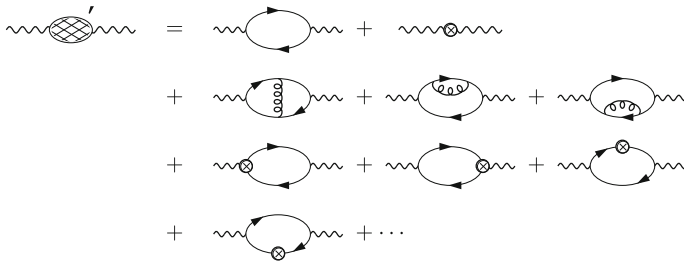
From this measurement together with $\text{Im } \Pi^{\text{had}}(s)$ from (5.16) we have a completely non-perturbative determination of the complex $\alpha(s)$. Fortunately, experimental progress is in sight here: KLOE 2015 [65] has a first direct measurements of the time-like complex running $\alpha_{\text{QED}}(s)$ (more further below)! Similar measurements for the J/ψ and other ultra-narrow resonances should be possible with BES-III. It is a fundamental problem! An interesting possibility in this respect is a novel approach to determine a_{μ}^{had} from a direct space-like measurement of $\alpha(-Q^2)$ as proposed in [67, 68] (see also [69]), recently. This novel approach would completely avoid the problem we have addressed here, as in the spacelike region corrections are perturbative everywhere.

5.1.5 $R(s)$ in Perturbative QCD

Due to the property of *asymptotic freedom*, which infers that the effective strong interaction constant $\alpha_s(s)$ becomes weaker the higher the energy scale $E = \sqrt{s}$, we may calculate the hadronic current correlators in perturbation theory as a power series in α_s/π . According to the general analysis presented above, the object of interest is

$$\rho(s) = \frac{1}{\pi} \text{Im} \Pi_{\gamma}(s) ; \quad \Pi_{\gamma}(q) : \text{wavy line} \text{---} \text{blob} \text{---} \text{wavy line} . \tag{5.19}$$

The QCD perturbation expansion diagrammatically is given by



Lines $\sim\sim\sim$ show external photons, \longrightarrow propagating quarks/antiquarks and \curvearrowright propagating gluons. See Fig. 2.14 for the Feynman rules of QCD. The vertices \otimes are marking renormalization counter term insertions. They correspond to subtraction terms which render the divergent integrals finite.

In QED (the above diagrams with gluons replaced by photons) the phenomenon of vacuum polarization was discussed first by Dirac [70] and finalized at the one-loop level by Schwinger [71] and Feynman [72]. Soon later Jost and Luttinger [73] presented the first two-loop calculation.

In 0th order in the strong coupling α_s , we have

$$2 \operatorname{Im} \left[\text{photon loop diagram} \right] = \left| \text{photon splitting diagram} \right|^2,$$

which is proportional to the free quark-antiquark production cross section [5] in the so called *Quark Parton Model* (QPM), which is describing quarks with the strong interaction turned off. The QPM provides an approximation which gets the better the higher the energy. As it is common practice, rather than considering the total hadronic production cross section $\sigma_{\text{tot}}(e^+e^- \rightarrow \gamma^* \rightarrow \text{hadrons})$ itself, we again use

$$R(s) \doteq \frac{\sigma_{\text{tot}}(e^+e^- \rightarrow \gamma^* \rightarrow \text{hadrons})}{\frac{4\pi\alpha^2}{3s}} = 12\pi^2 \rho(s), \tag{5.20}$$

which for sufficiently large s can be calculated in QCD perturbation theory. The result is given by [4, 28, 29, 74]

$$R(s)^{\text{pert}} = N_c \sum_f Q_f^2 \frac{v_f}{2} (3 - v_f^2) \Theta(s - 4m_f^2) \times \{1 + ac_1(v_f) + a^2c_2 + a^3c_3 + a^4c_4 + \dots\} \tag{5.21}$$

where $a = \alpha_s(s)/\pi$ and, assuming $4m_f^2 \ll s$, i.e. in the massless approximation

$$c_1 = 1$$

$$c_2 = C_2(R) \left\{ -\frac{3}{32}C_2(R) - \frac{3}{4}\beta_0\zeta(3) - \frac{33}{48}N_f + \frac{123}{32}N_c \right\}$$

$$= \frac{365}{24} - \frac{11}{12}N_f - \beta_0\zeta(3) \simeq 1.9857 - 0.1152N_f$$

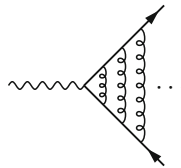
$$c_3 = -6.63694 - 1.20013N_f - 0.00518N_f^2 - 1.2395 \left(\sum_f Q_f \right)^2 / \left(3 \sum_f Q_f^2 \right)$$

$$c_4 = -156.61 + 18.77N_f - 0.7974N_f^2 + 0.0215N_f^3$$

in the \overline{MS} scheme. $N_f = \sum_{f:4m_f^2 \leq s} 1$ is the number of active flavors. The mass dependent threshold factor in front of the curly brackets is a function of the velocity $v_f = \left(1 - \frac{4m_f^2}{s}\right)^{1/2}$ and the exact mass dependence of the first correction term

$$c_1(v) = \frac{2\pi^2}{3v} - (3 + v) \left(\frac{\pi^2}{6} - \frac{1}{4} \right)$$

is singular (Coulomb singularity due to soft gluon final state interaction) at threshold. The singular terms of the n -gluon ladder diagrams



exponentiate and thereby remove the singularity [75]:

$$1 + x \rightarrow \frac{2x}{1 - e^{-2x}} ; \quad x = \frac{2\pi\alpha_s}{3v}$$

$$\left(1 + c_1(v) \frac{\alpha_s}{\pi} + \dots \right) \rightarrow \left(1 + c_1(v) \frac{\alpha_s}{\pi} - \frac{2\pi\alpha_s}{3v} \right) \frac{4\pi\alpha_s}{3v} \frac{1}{1 - \exp\left\{-\frac{4\pi\alpha_s}{3v}\right\}} .$$

Applying renormalization group improvement, the coupling α_s and the masses m_q have to be understood as running parameters

$$R\left(\frac{m_{0f}^2}{s_0}, \alpha_s(s_0)\right) = R\left(\frac{m_f^2(\mu^2)}{s}, \alpha_s(\mu^2)\right) ; \quad \mu = \sqrt{s} .$$

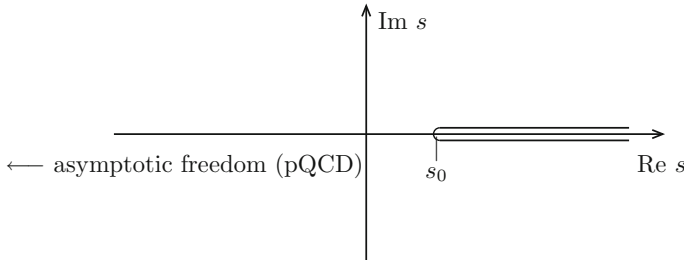


Fig. 5.14 Analyticity domain for the photon vacuum polarization function. In the complex s -plane there is a cut along the positive real axis for $s > s_0 = 4m^2$ where m is the mass of the lightest particles which can be pair-produced. If we include internal e.m. effects, we have $\pi^0\gamma$ as a channel with the lowest threshold $s_0 = m_{\pi^0}^2$

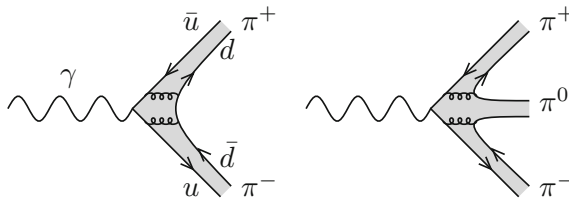


Fig. 5.15 Hadron production in low energy e^+e^- -annihilation: the primarily created quarks must hadronize. The shaded zone indicates strong interactions via gluons which confine the quarks inside hadrons

where $\sqrt{s_0}$ is a reference energy. Mass effects are important once one approaches a threshold from the perturbatively safe region sufficiently far above the thresholds where mass effects may be safely neglected. They have been calculated up to three loops by Chetyrkin, Kühn and collaborators [30] and have been implemented in the FORTRAN routine RHAD by Harlander and Steinhauser [31].

Where can we trust the perturbative result? Perturbative QCD is supposed to work best in the deep Euclidean region away from the physical region characterized by the cut in the analyticity plane Fig. 5.14. Fortunately, the physical region to a large extent is accessible to pQCD as well provided the energy scale is sufficiently large and one looks for the appropriate observable.

The imaginary part (total cross section) corresponds to the jump of the vacuum polarization function $\Pi(q^2)$ across the cut. On the cut we have the thresholds of the physical states, with lowest lying channels: $\pi^+\pi^-$, $\pi^0\pi^+\pi^-$, ... and resonances ρ , ω , ϕ , J/ψ ... , Υ ... , ... QCD is confining the quarks (a final proof of confinement is yet missing) in hadrons. In any case the quarks *hadronize* (see Fig. 5.15), a highly non-perturbative phenomenon which is poorly understood in detail. Neither the physical *thresholds* nor the *resonances* are obtained with perturbation theory! In particular, the perturbative quark-pair thresholds in (5.21) do not nearly approximate the physical thresholds for the low energy region below about 2 GeV, say. At higher energies pQCD works sufficiently far away from thresholds and resonances, i.e. in

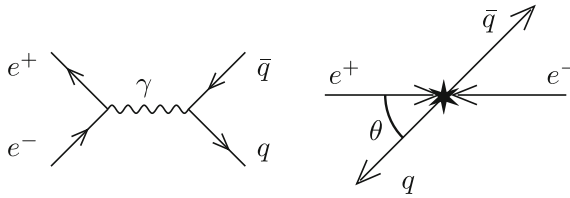


Fig. 5.16 Fermion pair production in e^+e^- -annihilation. The lowest order Feynman diagram (*left*) and the same process in the c.m. frame (*right*). The arrows represent the spacial momentum vectors and θ is the production angle of the quark relative to the electron in the c.m. frame

regions where $R(s)$ is a slowly varying monotonically decreasing function. This may be learned from Fig. 5.7 where the e^+e^- -data are shown together with the perturbative QCD prediction. Less problematic is the space-like (Euclidean) region $-q^2 \rightarrow \infty$, since it is away from thresholds and resonances. The best monitor for a comparison between theory and experiment has been proposed by Adler [76] long time ago: the so called *Adler-function*, up to a normalization factor, the derivative of the vacuum polarization function in the space-like region, introduced in (3.167) (see Fig. 5.18). In any case one has to ask the e^+e^- -annihilation data and to proceed in a semi-phenomenological way.

At higher energies highly energetic *partons*, quarks and/or gluons, are produced and due to asymptotic freedom perturbative QCD should somehow be applicable. As we will see this in fact manifests itself, for example, in the correct prediction of $\sigma_{\text{tot}}(e^+e^- \rightarrow \gamma^* \rightarrow \text{hadrons})$ in non-resonant regions at high enough energies, in the sense of quark-hadron duality (5.5). However, the consequences of the validity of pQCD are more far-reaching. According to perturbation theory the production of hadrons in e^+e^- -annihilation proceeds via the primary creation of a quark-antiquark pair (see Figs. 5.15, 5.16) where the quarks hadronize. The elementary process tells us that in a high energy collision of positrons and electrons (in the center of mass frame) q and \bar{q} are produced with high momentum in opposite directions (back-to-back).

The differential cross section, up to a color factor the same as for $e^+e^- \rightarrow \mu^+\mu^-$, reads

$$\frac{d\sigma}{d\Omega}(e^+e^- \rightarrow q\bar{q}) = \frac{3}{4} \frac{\alpha_s^2}{s} \sum Q_f^2 (1 + \cos^2 \theta) ,$$

typical for an angular distribution of a spin 1/2 particle. Indeed, the quark and the anti-quark seemingly hadronize individually in that they form *jets* [77]. Jets are bunches of hadrons which concentrate in a relatively narrow angular cone. This in spite of the fact that the quarks have unphysical charge and color, true physical states only can have integer charge and must be color singlets. Apparently, while charge and color have enough time to recombine into color singlets of integer charge, the momentum apparently has not sufficient time to distribute isotropically. The extra quarks needed to form physical states are virtual pairs created from the vacuum and carried

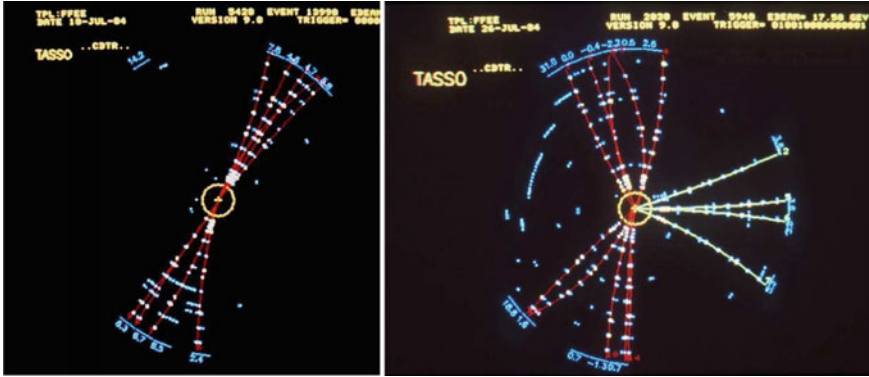


Fig. 5.17 Two and three jet event first seen by TASSO at DESY in 1979 [Resource DESY]

along by the primary quarks. As a rule pQCD is applicable to the extent that “hard partons”, quarks or gluons, may be interpreted as jets. Fig. 5.17 illustrates such $q\bar{q}$ (two-jet event) and $q\bar{q}g$ (three-jet event) jets. Three jet events produced with the electron positron storage ring PETRA at DESY in 1979 revealed the existence of the gluon. The higher the energy the narrower the jets, quite opposite to expectations at pre-QCD times when most people believed events with increasing energy will be more and more isotropic multi-hadron states.

5.1.6 Non-Perturbative Effects, Operator Product Expansion

The non-perturbative (NP) effects are parametrized as prescribed by the operator product expansion of the electromagnetic current correlator [78]

$$\begin{aligned}
 \Pi_{\gamma}^{\text{NP}}(Q^2) = & \frac{4\pi\alpha}{3} \sum_{q=u,d,s} Q_q^2 N_{cq} \cdot \left[\frac{1}{12} \left(1 - \frac{11}{18}a \right) \frac{\langle \frac{\alpha_s}{\pi} GG \rangle}{Q^4} \right. \\
 & + 2 \left(1 + \frac{a}{3} + \left(\frac{11}{2} - \frac{3}{4}l_{q\mu} \right) a^2 \right) \frac{\langle m_q \bar{q}q \rangle}{Q^4} \\
 & \left. + \left(\frac{4}{27}a + \left(\frac{4}{3}\zeta_3 - \frac{257}{486} - \frac{1}{3}l_{q\mu} \right) a^2 \right) \sum_{q'=u,d,s} \frac{\langle m_{q'} \bar{q}'q' \rangle}{Q^4} \right] + \dots
 \end{aligned} \tag{5.22}$$

where $a \equiv \alpha_s(\mu^2)/\pi$ and $l_{q\mu} \equiv \ln(Q^2/\mu^2)$. $\langle \frac{\alpha_s}{\pi} GG \rangle$ and $\langle m_q \bar{q}q \rangle$ are the scale-invariantly defined condensates. Sum rule estimates of the condensates yield typically (large uncertainties) $\langle \frac{\alpha_s}{\pi} GG \rangle \sim (0.389 \text{ GeV})^4$, $\langle m_q \bar{q}q \rangle \sim -(0.098 \text{ GeV})^4$ for $q = u, d$, and $\langle m_q \bar{q}q \rangle \sim -(0.218 \text{ GeV})^4$ for $q = s$. Note that the above expansion is just a parametrization of the high energy tail of NP effects associated with the

existence of non-vanishing condensates. The dilemma with the OPE in our context is that it works for large enough Q^2 only and in this form fails to describe NP physics at lower Q^2 . Once it starts to be numerically relevant pQCD starts to fail because of the growth of the strong coupling constant. In $R(s)$ NP effects as parametrized by (5.22) have been shown to be small in [33, 38, 79]. Note that the quark condensate, the vacuum expectation value (VEV) $\langle O_q \rangle$ of the dimension 3 operator $O_q \doteq \bar{q}q$, is a well defined non-vanishing order parameter in the chiral limit of QCD. In pQCD it is vanishing to all orders. In contrast the VEV of the dimension 4 operator $O_G \doteq \frac{\alpha_s}{\pi} GG$ is non-vanishing in pQCD but ill-defined at first as it diverges like Λ^4 in the UV cut-off. O_G contributes to the trace of the energy momentum tensor¹² [80–82]

$$\Theta_\mu^\mu = \frac{\beta(g_s)}{2g_s} GG + (1 + \gamma(g_s)) \{m_u \bar{u}u + m_d \bar{d}d + \dots\} \quad (5.23)$$

where $\beta(g_s)$ and $\gamma(g_s)$ are the RG coefficients (2.290) and in the chiral limit

$$\varepsilon_{\text{vac}} = - \left\{ \frac{\beta_0}{32} + O(\alpha_s) \right\} \langle O_G \rangle$$

represents the vacuum energy density which is not a bona fide observable in a continuum QFT.¹³ In the Shifman–Vainshtein–Zakharov (SVZ) approach [78] it is treated to represent the soft part with respect to the renormalization scale μ , while the corresponding OPE coefficient comprises the hard physics from scales above μ . Note that in the chiral limit $m_q \rightarrow 0$ the trace (5.23) does not vanish as expected on the classical level. Thus scale invariance (more generally conformal invariance) is broken in any QFT unless the β -function has a zero. This is another renormalization anomaly, which is a quantum effect not existing in a classical field theory. The renormalization group is another form of encoding the broken dilatation Ward identity.

¹²In a QFT a symmetric energy momentum tensor $\Theta_{\mu\nu}(x)$ should exist such that the generators of the Poincaré group are represented by (see (2.6), (2.7))

$$P_\mu = \int d^3x \Theta_{0\mu}(x), \quad M_{\mu\nu} = \int d^3x (x_\mu \Theta_{0\nu} - x_\nu \Theta_{0\mu})(x).$$

This corresponds to Noether’s theorem for the Poincaré group (see (2.94)). In a strictly renormalizable massless QFT which exhibits only dimensionless couplings classically one would expect the theory to be conformally invariant. The energy momentum tensor then would also implement infinitesimal dilatations and special conformal transformations. That is, the currents

$$D_\mu(x) = x^\rho \Theta_{\mu\rho}; \quad K_{\mu\nu} = 2 x^\rho x_\nu \Theta_{\mu\rho} - x^2 \Theta_{\mu\nu}$$

ought to be conserved, which requires the trace of the energy momentum tensor to vanish $\Theta_\mu^\mu = 0$. This only can be if the coupling g_s has a particular value g_s^* at which $\beta(g_s^*) = 0$.

¹³Usually, questions about non-perturbative features can be answered by lattice QCD. The problem in this case is that the continuum limit does not exist after the renormalization of the parameters and fields, but requires an extra subtraction specific to the quantity we want to determine itself. So it remains ill defined as a matter of principle. In contrast, the quark condensates are well defined by PCAC and GMOR type relations as (4.75) and fixed by the low lying hadron masses [83].

It's role for the description of the asymptotic behavior of the theory under dilatations (scale transformations) has been discussed in Sect. 2.6.5, where it was shown that under dilatations the effective coupling is driven into a zero of the β -function. For an asymptotically free theory like QCD we reach the scaling limit in the high energy limit. At finite energies we always have scaling violations, as they are well known from deep inelastic electron nucleon scattering. In e^+e^- -annihilation the scaling violation are responsible for the energy dependence (via the running coupling) on $R(s)$ in regions where mass effects are negligible.

As mentioned earlier the Adler-function is a good monitor to compare the pQCD as well as the NP results with experimental data, Fig. 5.18 shows that pQCD in the Euclidean region works very well for $\sqrt{Q^2} \gtrsim 2.5$ GeV [79]. The NP effects just start to be numerically significant where pQCD starts to fail. Thus, no significant NP effects can be established based on e^+e^- -data. This also has been confirmed in a recent analysis [85].

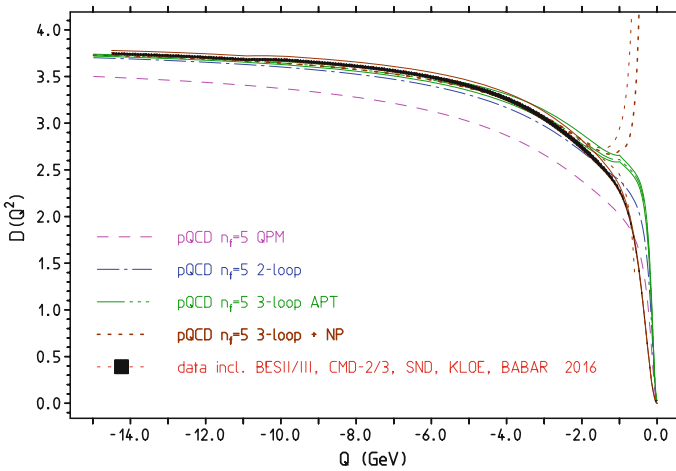


Fig. 5.18 “Experimental” Adler-function versus theory (pQCD + NP) in the low energy region (as discussed in [79]). Note that the error includes both statistical and systematic ones, in contrast to Fig. 5.7 where only statistical errors are shown. The massive 3-loop pQCD prediction includes 4- and 5-loop effects in the massless limit as well, which improves result where mass effects get small (*long-dash dot dot dot*). In the perturbative region the curvature is largely a result of the mass effects only. This is also illustrated by the QPM result (*dashed*). Below about 2 GeV pQCD fails, even if one attempts to remove the Landau pole by freezing the strong coupling as e.g. advocated by Analytic Perturbation Theory (APT) [84]. Including Non-Perturbative (NP) effects represented by power corrections as derived by OPE, these start to diverge as soon as they get numerically significant towards lower energies (*dotted*). The 2-loop massive QCD result shown large deviations from the data over the whole range displayed (*long-dash dot long-dash*)

5.1.7 Leading Hadronic Contribution to $(g - 2)$ of the Muon

We now are going to evaluate the hadronic vacuum polarization effects coming from the 5 “light” quarks $q = u, d, s, c, b$ in terms of the experimental e^+e^- data.¹⁴ Quarks contribute to the electromagnetic current according to their charge

$$j_{\text{em}}^\mu{}^{\text{had}} = \sum_c \left(\frac{2}{3} \bar{u}_c \gamma^\mu u_c - \frac{1}{3} \bar{d}_c \gamma^\mu d_c - \frac{1}{3} \bar{s}_c \gamma^\mu s_c + \frac{2}{3} \bar{c}_c \gamma^\mu c_c - \frac{1}{3} \bar{b}_c \gamma^\mu b_c + \frac{2}{3} \bar{t}_c \gamma^\mu t_c \right).$$


The hadronic electromagnetic current $j_{\text{em}}^\mu{}^{\text{had}}$ is a color singlet and hence includes a sum over colors indexed by c . Its contribution to the electromagnetic current correlator (3.133) defines $\Pi_\gamma^{\text{had}}(s)$, which enters the calculation of the leading order hadronic contribution to a_μ^{had} , diagrammatically given by Fig. 5.1. The representation as a dispersion integral has been developed in Sect. 3.8 on p. 233 (see also p. 224). Using (3.164) a_μ^{had} may be directly evaluated in terms of $R_\gamma(s)$ defined in (5.3). More precisely we may write

$$a_\mu^{\text{had}} = \left(\frac{\alpha m_\mu}{3\pi} \right)^2 \left(\int_{m_\pi^2}^{E_{\text{cut}}^2} ds \frac{R_\gamma^{\text{data}}(s) \hat{K}(s)}{s^2} + \int_{E_{\text{cut}}^2}^\infty ds \frac{R_\gamma^{\text{pQCD}}(s) \hat{K}(s)}{s^2} \right), \quad (5.24)$$

with a cut E_{cut} in the energy, separating the non-perturbative part to be evaluated from the data and the perturbative high energy tail to be calculated using pQCD.¹⁵ The kernel $K(s)$ is represented by (3.149) discarding the factor α/π . This integral can be performed analytically. Written in terms of the variable

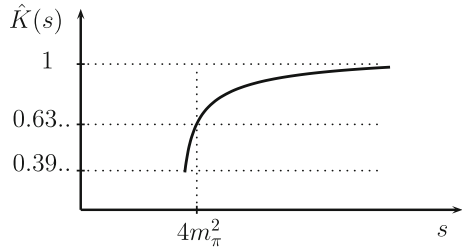
$$x = \frac{1 - \beta_\mu}{1 + \beta_\mu}, \quad \beta_\mu = \sqrt{1 - 4m_\mu^2/s}$$

¹⁴The heavy top quark of mass $m_t \simeq 173.21(0.87)$ GeV we certainly may treat perturbatively, as at the scale m_t the strong interaction coupling is weak (see Fig. 3.3). Actually, the top quark t is irrelevant here since, as we know, heavy particles decouple in QED in the limit $m_t \rightarrow \infty$ and contribute like a VP τ -loop with an extra factor $N_c Q_t^2 = 4/3$, thus

$$a_\mu^{(4)}(\text{vap, top}) = \frac{4}{3} \left[\frac{1}{45} \left(\frac{m_\mu}{m_t} \right)^2 + \dots \right] \left(\frac{\alpha}{\pi} \right)^2 \sim 5.9 \times 10^{-14}.$$


¹⁵Actually, a_μ^{had} , and therefore a_μ itself, is only a safely predictable quantity by virtue of asymptotic freedom of QCD. Otherwise the high energy tail would remain in the dark. In spite of the $1/s^2$ kernel we would be confronted with the question of a Landau pole, which in the “whatever non-QCD strong interaction world” could show up elsewhere. It may be interesting to note that within the SM from the $SU(3)_c \otimes SU(2)_L \otimes U(1)_Y$ gauge couplings only the weak hypercharge coupling g' is not asymptotically free, what then shows up in the QED sector as well. The corresponding growth of the coupling with energy is however very moderate even up to the Planck scale. Surprisingly, within the SM also the top quark Yukawa coupling y_t as well as the Higgs boson self-coupling λ show AF behavior, i.e. they get weaker the higher the energy (see e.g. [86]).

Fig. 5.19 Graph of weight function $\hat{K}(s)$ of the $g - 2$ dispersion integral



the result reads [87]

$$K(s) = \frac{x^2}{2} (2 - x^2) + \frac{(1 + x^2)(1 + x)^2}{x^2} \left(\ln(1 + x) - x + \frac{x^2}{2} \right) + \frac{(1 + x)}{(1 - x)} x^2 \ln(x) . \tag{5.25}$$

The representation (5.25) of $K(s)$ is valid for the muon (or electron) where we have $s > 4m_\mu^2$ in the domain of integration $s > 4m_\pi^2$, and x is real, and $0 \leq x \leq 1$. For the τ (5.25) applies for $s > 4m_\tau^2$. In the region $4m_\pi^2 < s < 4m_\tau^2$, where $0 < r = s/m_\tau^2 < 4$, we may use the form

$$K(s) = \frac{1}{2} - r + \frac{1}{2}r (r - 2) \ln(r) - \left(1 - 2r + \frac{1}{2}r^2 \right) \varphi/w \tag{5.26}$$

with $w = \sqrt{4/r - 1}$ and $\varphi = 2 \arctan(w)$. Note that the $\pi^+\pi^-$ channel exhibiting the threshold $4m_\pi^2$, although the by far dominating one contributing to (5.24), is not the channel with the lowest threshold. Since also the e.m. $\pi^0\gamma$ channel contributes to $R(s)$ the lowest threshold is $m_{\pi^0}^2 < 4m_\mu^2$ and between $m_{\pi^0}^2 < s < 4m_\mu^2$ the kernel there is given by (5.26) with $r = s/m_\mu^2 < 4$.

We have written the integral (5.24) in terms of the rescaled function

$$\hat{K}(s) = \frac{3s}{m_\mu^2} K(s)$$

which is slowly varying only in the range of integration. It increases monotonically from 0.63...[0.39...] at $\pi\pi[\pi\gamma]$ threshold $s = 4m_\pi^2[m_{\pi^0}^2]$ to 1 at $s = \infty$. The graph is shown in Fig. 5.19.

It should be noted that for small x the calculation of the function $K(s)$, in the form given above, is numerically unstable and we instead use the asymptotic expansion (used typically for $x \leq 0.0006$)

$$K(s) = \left(\frac{1}{3} + \left(\frac{17}{12} + \left(\frac{11}{30} + \left(-\frac{1}{10} + \frac{3}{70}x \right) x \right) x \right) x + \frac{1+x}{1-x} x^2 \ln(x) \right) .$$

Other representations of $K(s)$, like the simpler-looking form

$$K(s) = \frac{1}{2} - r + \frac{1}{2}r(r-2) \ln(r) + \left(1 - 2r + \frac{1}{2}r^2\right) \ln(x)/\beta_\mu, \quad (5.26)$$

with $r = s/m_\mu^2$, are much less suitable for numerical evaluation because of much more severe numerical cancellations.

Note the $1/s^2$ -enhancement of contributions from low energies in a_μ . Thus the $g-2$ kernel gives very high weight to the low energy range, in particular to the lowest lying resonance, the ρ^0 . Thus, this $1/E^4$ magnification of the low energy region by the a_μ kernel-function together with the existence of the pronounced ρ^0 resonance in the $\pi^+\pi^-$ cross-section are responsible for the fact that pion pair production $e^+e^- \rightarrow \pi^+\pi^-$ gives the by far largest contribution to a_μ^{had} .¹⁶ The ρ is the lowest lying vector-meson resonance and shows up in $\pi^+\pi^- \rightarrow \rho^0$ at $M_\rho \sim 770$ MeV (see Fig. 5.6). This dominance of the low energy hadronic cross section by a single simple two-body channel is good luck for a precise determination of a_μ , although a very precise determination of the $\pi^+\pi^-$ cross-section is a rather difficult task. Below about 810 MeV $\sigma_{\text{tot}}^{\text{had}}(s) \simeq \sigma_{\pi\pi}(s)$ to a good approximation but at increasing energies more and more channels open (see Fig. 5.4) and “measurements of R ” get more difficult, before above about 2 GeV inclusive R measurements become reliable. In the light sector of $q = u, d, s$ quarks, besides the ρ there is the ω , which is mixing with the ρ , and the ϕ resonance, essentially a $\bar{s}s$ bound system. In the charm region we have the pronounced $\bar{c}c$ -resonances, the $J/\psi_{1S}, \psi_{2S}, \dots$ resonance series and in

¹⁶As we need the VP-undressed hadronic cross section in the DR, the physical form factor $F_\pi(s)$ which includes VP effects has to be corrected accordingly:

$$|F_\pi^{(0)}(s)|^2 = |F_\pi(s)|^2 |\alpha/\alpha(s)|^2. \quad (5.27)$$

Figure 5.25 shows $\text{Re } \Delta\alpha(s) = 1 - \text{Re } \alpha/\alpha(s)$ in the time-like region. The resonances lead to pronounced variations of the effective charge (shown in the $\rho - \omega, \phi$ and J/ψ region).

For an order by order in α procedure of including corrections in a systematic manner, final state radiation should be subtracted as suggested in Sect. 5.1.3. The initial state radiation must and can be subtracted in any case, the final state radiation should be subtracted if possible. Note that measurements unavoidably include all virtual plus the unobserved soft photons. However, the hard virtual part for hadronic final states cannot be calculated in a model-independent manner, such that the subtraction seems not possible. It is therefore better to include as much as possible all photons in an inclusive measurement. The KLN theorem (see Sect. 2.6.6) infers that the inclusive cross section of virtual, soft plus hard real photons is $O(\alpha)$ without any logarithmic enhancement. Which also means a moderate model-dependence of the FSR correction, as a consequence of the absence of potentially large logs. We thus include the FSR (including full photon phase space) as

$$|F_\pi^{(\gamma)}(s)|^2 = |F_\pi^{(0)}(s)|^2 \left(1 + \eta(s) \frac{\alpha}{\pi}\right) \quad (5.28)$$

to order $O(\alpha)$, where $\eta(s)$ (5.1.12) is a known correction factor in sQED [203] (see p. 425 below). Here $F_\pi^{(0)}(s)$ is obtained from the measured cross section by subtracting photonic effects using sQED under consideration of the applied experimental cuts on the real photons.

the bottom region the $\bar{b}b$ -resonances $\Upsilon_{1S}, \Upsilon_{2S}, \dots$. Many of the resonances are very narrow as indicated in Fig. 5.7.

For the evaluation of the basic leading order (LO) integral (5.24) we take $R(s)$ -data up to $\sqrt{s} = E_{cut} = 5.2$ GeV and for the Υ resonance-region between 9.46 and 11.5 GeV and apply perturbative QCD from 5.2 to 9.46 GeV and for the high energy tail above 11.5 GeV. The available data which are included we have discussed in Sect. 3.2.1 p.185 already (see also Figs. 5.6, 5.7). The result of the evaluation is [6]

$$a_{\mu}^{\text{had}(1)} = (688.07 \pm 4.14)[688.77 \pm 3.38] \times 10^{-10} \quad (5.29)$$

based on e^+e^- -data [incl. τ -decay spectra [88]]. For the electron anomaly the LO contribution evaluates to $a_e^{\text{had}(1)} = 1.846(12) \times 10^{-12}$.

The contributions and errors from different energy regions is shown in Table 5.2. Most noticeable about this result are three features (see also Table 3.1)

- the experimental errors of the data lead to a substantial theoretical uncertainty, which is about 2/3 of the present experimental error of the BNL $g - 2$ experiment; as the upcoming Fermilab muon $g - 2$ experiment will reduce the present experimental error by a factor four the error of the HVP needs to be reduced further as much as possible;
- the low energy region is dominated by the $\pi\pi$ -channel and the ρ -resonance contributions is dramatically enhanced: $\sim 74\%$ [$\sim 79\%$ including the ω] of the con-

Table 5.2 Results for $a_{\mu}^{\text{had}} \times 10^{10}$ from different energy ranges. Given are statistical, systematic and the total error, the relative precision in % [rel] and the contribution to the final error² in % [abs]

Final state	Range (GeV)	Result	(Stat)	(Syst)	[Tot]	Rel (%)	Abs (%)
ρ	(0.28, 1.05)	506.02	(0.77)	(2.52)	[2.64]	0.5	40.6
ω	(0.42, 0.81)	35.23	(0.42)	(0.95)	[1.04]	3.0	6.3
ϕ	(1.00, 1.04)	34.31	(0.48)	(0.79)	[0.92]	2.7	5.0
J/ψ		8.94	(0.42)	(0.41)	[0.59]	6.6	2.0
Υ		0.11	(0.00)	(0.01)	[0.01]	6.8	0.0
had	(1.05, 2.00)	61.32	(0.20)	(2.65)	[2.65]	4.3	41.0
had	(2.00, 3.20)	21.63	(0.12)	(0.92)	[0.93]	4.3	5.0
had	(3.20, 3.60)	3.81	(0.02)	(0.03)	[0.04]	1.9	0.0
had	(3.60, 5.20)	7.59	(0.04)	(0.05)	[0.07]	0.0	0.0
pQCD	(5.20, 9.46)	6.27	(0.04)	(0.06)	[0.07]	0.1	0.0
had	(9.46, 11.50)	0.87	(0.00)	(0.05)	[0.05]	5.7	0.0
pQCD	(11.50, ∞)	1.96	(0.00)	(0.00)	[0.00]	0.0	0.0
Data	(0.28, 11.50)	679.84	(1.11)	(3.99)	[4.14]	0.6	98.8
Total		688.07	(1.11)	(3.99)	[4.14]	0.6	100.0

tribution and $\sim 41\%$ [$\sim 47\%$ including the ω] of error of a_μ^{had} comes from region $2m_\pi < \sqrt{s} < M_\phi$.

- the “intermediate” energy region, between 1 and 2 GeV, still gives a substantial contribution of about 9% [14% including the ϕ]. Unfortunately, because of the lower quality of the R -data in the region, it contributes 41% [46% including the ϕ] of the total error, i.e. errors come in equal parts from below 1 GeV and from 1 to 2 GeV, and together are the main source of uncertainty in the theoretical determination of a_μ .

Integration of various exclusive channels yields the results of Table 5.3, which illustrates the relative weight of different channels in the region of exclusive channel measurements. Inclusive measurements are available above 1.2 GeV, however, recent progress in this problematic range comes from measurements based on the *radiative return* mechanism by BABAR [7, 89–92] for the exclusive channels $e^+e^- \rightarrow \pi^+\pi^-\pi^0$, $\pi^+\pi^-\pi^+\pi^-$, K^+K^- , $K_L K_S$, $K^+K^-\pi^+\pi^-$, $K_L K_S \pi^+\pi^-$, $K_S K_S \pi^+\pi^-$, $2(K^+K^-)$, $K_S K_S K^+K^-$, $3(\pi^+\pi^-)$, $2(\pi^+\pi^-\pi^0)$, $K^+K^-2(\pi^+\pi^-)$ and $\bar{p}p$. These data cover a much broader energy interval and extend to much higher energies than previous experiments. Together with recent scan data from VEPP-2000 [93–97] remarkable progress has been achieved in this difficult range.

The sum of the exclusive channels from Table 5.3 is 637.73(3.69) which together with the sum of contributions from energies $E > 2$ GeV 51.08(1.10) from Table 5.2 yields a slightly higher value 688.81(3.85) than the 687.04(4.21) we get by including also the inclusive data below 2 GeV. Results are well within errors and this is a good consistency test. Note that resonances like ω and ρ contribute to the exclusive channels according to their branching fractions. When parametrized as relativistic Breit–Wigner shapes with a s -dependent width we have (see e.g. [98])

$$\begin{aligned} \Gamma_\omega(s) &= \Gamma(\omega \rightarrow 3\pi, s) + \Gamma(\omega \rightarrow \pi^0\gamma, s) + \Gamma(\omega \rightarrow 2\pi, s) \\ &= \frac{s}{M_\omega^2} \Gamma_\omega \left\{ Br(\omega \rightarrow 3\pi) \frac{F_{3\pi}(s)}{F_{3\pi}(M_\omega^2)} + Br(\omega \rightarrow \pi^0\gamma) \frac{F_{\pi\gamma}(s)}{F_{\pi\gamma}(M_\omega^2)} + Br(\omega \rightarrow 2\pi) \frac{F_{2\pi}(s)}{F_{2\pi}(M_\omega^2)} \right\}, \\ \Gamma_\phi(s) &= \Gamma(\phi \rightarrow K^+K^-, s) + \Gamma(\phi \rightarrow K_S K_L, s) + \Gamma(\phi \rightarrow 3\pi, s) + \Gamma(\phi \rightarrow \pi^0\gamma, s) + \Gamma(\phi \rightarrow \eta\gamma, s) \\ &= \frac{s}{M_\phi^2} \Gamma_\phi \left\{ Br(\phi \rightarrow K^+K^-) \frac{F_{K^+K^-}(s)}{F_{K^+K^-}(M_\phi^2)} + Br(\phi \rightarrow K_S K_L) \frac{F_{K_S K_L}(s)}{F_{K_S K_L}(M_\phi^2)} \right. \\ &\quad \left. + Br(\phi \rightarrow 3\pi) \frac{F_{3\pi}(s)}{F_{3\pi}(M_\phi^2)} + Br(\phi \rightarrow \pi^0\gamma) \frac{F_{\pi\gamma}(s)}{F_{\pi\gamma}(M_\phi^2)} + Br(\phi \rightarrow \eta\gamma) \frac{F_{\eta\gamma}(s)}{F_{\eta\gamma}(M_\phi^2)} \right\}. \quad (5.30) \end{aligned}$$

The factors $Br(V \rightarrow X)$ denote the branching fraction for the channel X and $F_X(s)$ is the phase space function for the corresponding channel normalized such that $F_X(s) \rightarrow \text{const}$ for $s \rightarrow \infty$. For the two-body decays $V \rightarrow P_1 P_2$ we have $F_{P_1 P_2}(s) = (1 - (m_1 + m_2)^2/s)^{3/2}$. The channel $V \rightarrow 3\pi$ is dominated by $V \rightarrow \rho\pi \rightarrow 3\pi$ and this fact is used when calculating $F_{3\pi}(s)$.

Table 5.3 Exclusive channel contributions to $a_{\mu}^{\text{had}} \times 10^{10}$ and $\Delta\alpha_{\mu}^{(5)}(-s_0) \times 10^4$, $\sqrt{s_0} = 2$ GeV, from the energy region $0.318 \text{ GeV} < E < 2 \text{ GeV}$. $X^* = X(\rightarrow \pi^0\gamma)$, $is, o =$ evaluated using isospin relations

Channel X	a_{μ}^X	%	$\Delta\alpha^X$	%	Channel X	a_{μ}^X	%	$\Delta\alpha^X$	%
$\pi^0\gamma$	4.00 ± 0.16	0.58	0.35 ± 0.01	0.56	$\omega\pi^+\pi^-[*]$	0.09 ± 0.00	0.01	0.02 ± 0.00	0.03
$\pi^+\pi^-$	502.16 ± 2.44	73.10	29.88 ± 0.14	46.80	$K^+K^-\pi^0$	0.35 ± 0.00	0.05	0.07 ± 0.00	0.11
$\pi^+\pi^-\pi^0$	44.32 ± 1.48	6.45	3.83 ± 0.14	6.00	$[K_S^0 K_L^0 \pi^0]_{\text{iso}}$	0.35 ± 0.00	0.05	0.07 ± 0.00	0.11
$\eta\gamma$	0.56 ± 0.02	0.08	0.06 ± 0.00	0.09	$K_S^0 K_{\pm}^{\pm} \pi^{\mp}$	1.08 ± 0.00	0.16	0.21 ± 0.00	0.33
$\pi^+\pi^-2\pi^0$	19.69 ± 2.32	2.87	3.34 ± 0.41	5.23	$[K_L^0 K_{\pm}^{\pm} \pi^{\mp}]_{\text{iso}}$	1.08 ± 0.00	0.16	0.21 ± 0.00	0.33
$2\pi^+2\pi^-$	14.80 ± 0.36	2.15	2.56 ± 0.06	4.01	$K^+K^-\pi^+\pi^-$	0.98 ± 0.04	0.14	0.22 ± 0.01	0.34
$\pi^+\pi^-3\pi^0$	0.85 ± 0.00	0.12	0.16 ± 0.00	0.25	$K^+K^-\pi^0\pi^0$	1.85 ± 0.00	0.27	0.37 ± 0.00	0.58
$2\pi^+2\pi^-\pi^0$	1.29 ± 0.00	0.19	0.25 ± 0.00	0.39	$K_S K_L \pi^+ \pi^-$	0.13 ± 0.01	0.02	0.03 ± 0.00	0.05
$2\pi^+2\pi^-\eta$	0.11 ± 0.01	0.02	0.02 ± 0.00	0.04	$K_S K_S \pi^+ \pi^-$	0.22 ± 0.03	0.03	0.05 ± 0.01	0.08
$\pi^+\pi^-4\pi^0$	0.08 ± 0.00	0.01	0.02 ± 0.00	0.03	$[K \bar{K} \pi \pi]_{\text{iso}}$	0.05 ± 0.00	0.01	0.01 ± 0.00	0.02
$\eta\pi^+\pi^-[*]$	0.43 ± 0.00	0.06	0.08 ± 0.00	0.12	$K^+K^-\pi^+\pi^-\eta$	0.09 ± 0.01	0.01	0.02 ± 0.00	0.03
$2\pi^+2\pi^-2\pi^0$	1.70 ± 0.00	0.25	0.35 ± 0.00	0.55	$p\bar{p}$	0.07 ± 0.00	0.01	0.02 ± 0.00	0.03
$3\pi^+3\pi^-$	0.31 ± 0.00	0.05	0.07 ± 0.00	0.11	$n\bar{n}$	0.06 ± 0.01	0.01	0.01 ± 0.00	0.02
$\omega\pi^0[*]$	0.81 ± 0.07	0.12	0.12 ± 0.01	0.18	$\omega \rightarrow \text{missing}$	0.09 ± 0.00	0.01	0.01 ± 0.00	0.01
K^+K^-	21.99 ± 0.61	3.20	2.56 ± 0.07	4.00	$\phi \rightarrow \text{missing}$	0.03 ± 0.00	0.00	0.00 ± 0.00	0.00
$K_S^0 K_L^0$	13.10 ± 0.41	1.91	1.46 ± 0.05	2.29	sum	639.60 ± 3.71	100.00	53.28 ± 0.46	100.00
					tot [sum in %]	688.07	[92.88]	64.09	[83.13]

Table 5.4 Some evaluations of $a_\mu^{(4)}$ (vap, had) since 2003

$a_\mu^{(4)}$ (vap, had) $\times 10^{10}$	Data	Year	Group	Ref.
696.3[7.2]	e^+e^-	2003	DEHZ03	[113]
711.0[5.8]	$e^+e^- + \tau$	2003	DEHZ03	[113]
694.8[8.6]	e^+e^-	2003	GJ03	[114]
690.9[4.4]	e^+e^-	2006	DEHZ06	[119]
689.4[4.6]	e^+e^-	2006	HMNT06	[128]
692.1[5.6]	e^+e^-	2006	FJ06	[15]
705.3[4.5]	$e^+e^- + \tau$	2009	DHea09	[129]
692.3[4.2]	e^+e^{-**}	2010	DHMZ10	[26, 130]
691.0[4.6]	$e^+e^- + \tau^{**}$	2011	JS11	[88]
694.4[3.7]	e^+e^{-**}	2011	HLMNT11	[131]
687.7[4.6]	HLS global fit	2012	BDDJ12	[132]
691.0[4.7]	e^+e^{-**}	2012	FJ12	[88]
693.2[3.7]	$e^+e^- + \tau^{**}$	2012	DHMZ10/JS11	[88, 130]
692.3[4.2]	e^+e^-	2016	DHMZ16	[7]
701.5[4.6]	$e^+e^- + \tau$	2016	DHMZ16	[7]
681.9[3.2]	$e^+e^- + \tau$ HLS fit	2016	BDDJ15	[47]
689.5[3.2]	$e^+e^- + \tau + \pi\pi$ phases	2017	Our estimate	(5.100)

Some of the most recent evaluations are collected in Table 5.4. Figure 5.20 illustrates how estimates developed as data have been improving over time. Differences in errors come about mainly by utilizing more “theory-driven” concepts: use of selected data sets only, extended use of perturbative QCD in place of data [assuming local duality], sum rule methods, low energy effective methods [120–122]. In some analyses (as indicated) τ data from ALEPH, OPAL, CLEO and Belle [123–127] have been combined with the e^+e^- data (see below). There have been many independent evaluations of a_μ^{had} in the past¹⁷ [12, 15, 16, 88, 113–119] and some of the more recent ones are shown in Fig. 7.2. For more detailed explanations of the differences see the comments to Fig. 7.1.

The compilation of the e^+e^- -data is shown in Fig. 5.6 in the most important low energy region and in Fig. 5.7 for the higher energies. The relative importance of various regions is illustrated in Fig. 5.21. The possibility of using hadronic τ -decay data was briefly discussed in Sect. 3.2.1 on p. 187 (see Fig. 5.22). More details are given as an Addendum Sect. 5.1.10 to this section. After applying the appropriate

¹⁷The method how to calculate hadronic vacuum polarization effects in terms of hadronic cross sections was developed long time ago by Cabibbo and Gatto [133]. First estimations were performed in [99–101]. As cross section measurements made further progress much more precise estimates became possible in the mid 80s [107–111]. A more detailed analysis based on a complete up-to-date collection of data followed about 10 years later [8].

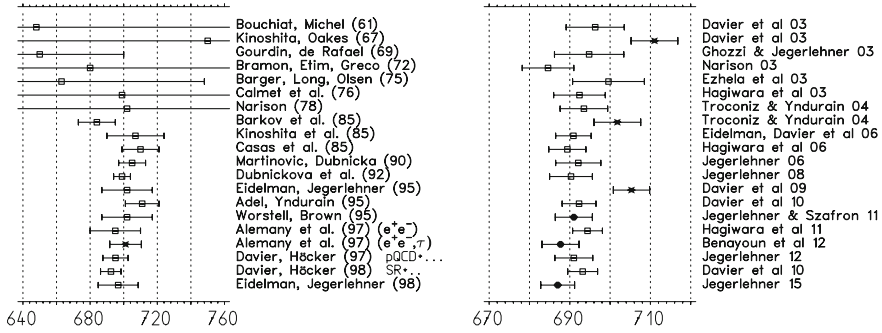


Fig. 5.20 History of evaluations before 2000 (*left*) [8–11, 99–112], and some more recent ones (*right*) [15, 113–119]; open squares = e^+e^- -data based, cross marked ($e^+e^- + \tau$) = in addition include data from τ spectral functions but without taking into account $\gamma - \rho^0$ mixing, these are obsolete now; *filled circles* ($e^+e^- + \tau$) including $\gamma - \rho^0$ mixing (see text)

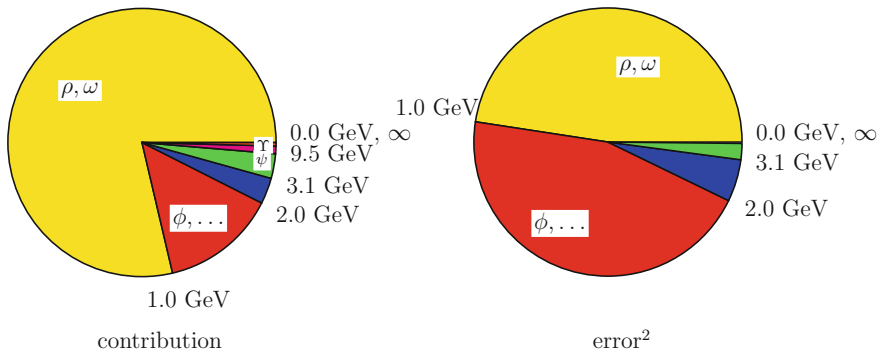
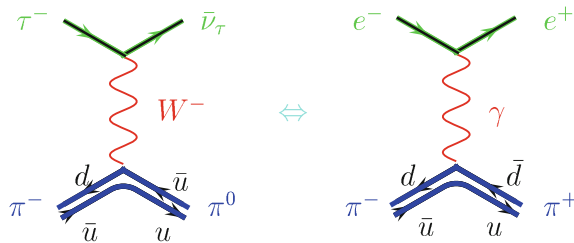


Fig. 5.21 The distribution of contributions (*left*) and errors² (*right*) in % for a_μ^{had} from different energy regions. The error of a contribution i shown is $\delta_{i,\text{tot}}^2 / \sum_i \delta_{i,\text{tot}}^2$ in %. The total error combines statistical and systematic errors in quadrature

Fig. 5.22 τ -decay versus e^+e^- -annihilation: the involved hadronic matrix-elements $\langle \text{out } \pi^+ \pi^- | j_\mu^{I=1}(0) | 0 \rangle$ and $\langle \text{out } \pi^0 \pi^- | J_{V\mu}^-(0) | 0 \rangle$ are related by an isospin rotation



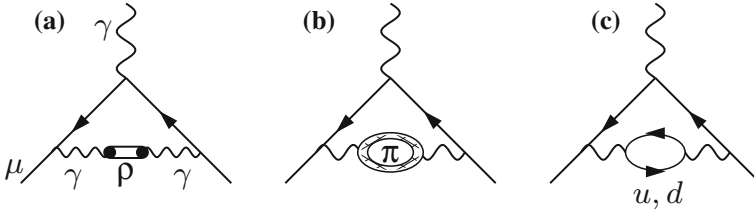


Fig. 5.23 Low energy effective graphs (a) and (b) and high energy graph (c)

Table 5.5 Low energy effective estimates of the leading vacuum polarization effects $a_\mu^{(4)}$ (vap). For comparison: 5.8420×10^{-8} for μ -loop, 5.9041×10^{-6} for e -loop

Data [280, 810] MeV	ρ^0 -exchange	π^\pm -loop	[u, d] quark loops	
			Constituent quarks	Current quarks
4.2666×10^{-8}	4.2099×10^{-8}	1.4154×10^{-8}	2.2511×10^{-8}	4.4925×10^{-6}

isospin breaking corrections, hadronic τ -decay spectra may be used to improve the data sample. The τ versus e^+e^- discrepancy which has been persisting for some time found its resolution in the missing $\rho^0 - \gamma$ mixing correction of the τ -data [88, 132]. Results which include τ -data are indicated in Table 5.4 (see also Table 3.2) and Fig. 7.2.

Digression: Exercises on the Low Energy Contribution

One important question we may ask here is to what extent are we able to understand and model the low energy hadronic piece theoretically? This excursion is mainly thought to shed light on what has a chance to work and what not in modeling low-energy hadronic effects. It is a kind of preparation for the discussion of the hadronic light-by-light scattering. As a starting point for understanding strong interaction physics at the muon mass scale one could attempt to use chiral perturbation theory, the low energy effective description of QCD, where quarks and gluons are replaced by hadrons, primarily the pions, the quasi Nambu-Goldstone bosons of spontaneous chiral symmetry breaking. One would then calculate π^\pm -loops as shown in Fig. 5.23, and as discussed earlier in Sect. 2.7.

The charged spin 0 pions π^\pm are assumed to couple to photons via minimal coupling, assuming the pions to be point-like as a leading approximation (see Sect. 2.7). However, the result given in Table 5.5 is underestimating the effect by about a factor 3. The main parameter for the size of the contribution is the mass and the coefficient $N_{ci} Q_i^2$, for color and charge of a particle species i (see (2.178)). If we would treat the quarks like leptons, switching off strong interactions and hence using the quark parton model (which is a good approximation only at sufficiently high energies) we would get for the sum of u and d quarks the result given in last entry which is similar in size to the contribution from an electron, about a factor 100 too large! The large

difference between the π^\pm result and the (u, d) doublet result illustrates the dilemma with naive perturbative approaches. The huge contribution on the quark level was obtained using the current quark masses $m_u \sim 3 \text{ MeV}$, $m_d \sim 8 \text{ MeV}$, which appear in the QCD Lagrangian as chiral symmetry breaking parameters. Strong interactions lead to dressed quarks with effective “constituent quark masses”, a concept which is not very well-defined e.g. if we choose $m_u \sim m_d \sim 300 \text{ MeV}$ (about 1/3 of the proton mass) one gets now a result which, this time, is a factor of two too small. In any case it is much closer to reality. This illustrates how sensitive these perturbative results are to the precise choice of the values of the quark masses. The failure of these trials is that one main non-perturbative effect is missing, namely, the ρ^0 -resonance: a neutral spin 1 vector-meson, produced in $e^+e^- \rightarrow \rho^0 \rightarrow \pi^+\pi^-$. Spin 1 vector-mesons can be incorporated in the framework of CHPT (see p. 305) which leads to the RLA [134, 135]. The result obtained by integrating the corresponding non-relativistic Breit-Wigner ρ^0 resonance in the range (280, 810) MeV gives a remarkably good result if we compare it with what we get using experimental data (see the first entry in Table 5.5). This also shows that adding up the ρ -exchange and the π^\pm -loop as independent effects would lead to a wrong answer. This is not so surprising since working with pions and vector-mesons as independent fields necessarily at some point produces a double counting problem, because the ρ may be understood as a $\pi^+\pi^-$ resonance. A much more reasonable approach would be to apply the low energy effective theory up to an energy scale Λ (long distance (L.D.) part) and pQCD above the same cut off Λ (short distance (S.D.) part). For more educated estimations of a_μ^{had} in low energy effective theory see [136] (see also [137]). We have been discussing the various possibilities in order to get some feeling about the reliability of such estimates, because in higher orders in general we will not be able to resort to experimental data to estimate the non-perturbative effect.

Fortunately, firm theoretical predictions are not only possible for the perturbative high energy tail. Also the low energy tail is strongly constrained, by the low energy effective CHPT briefly introduced on p. 305 in Sect. 4.2.2. The quantity of interest here is the vector form factor, defined by the hadronic pion pair production matrix element

$$\langle \text{out } \pi^+(p_+) \pi^-(p_-) | V_\mu(0) | 0 \rangle = -i (p_+ - p_-)_\mu F_V(s), \quad (5.31)$$

where $V_\mu(x)$ is the isovector current and $s = (p_+ + p_-)^2$. $F_V(s)$ has been calculated in CHPT in [138, 139] (one-loop), [140] (two-loop numerical) and [141] (two-loop analytical). The last reference gives a compact analytical result

$$F_V(s) = 1 + \frac{1}{6} \langle r_\pi^2 \rangle_V s + c_V^\pi s^2 + f_V^U \left(\frac{s}{m_\pi^2} \right), \quad (5.32)$$

and a fit to the space-like NA7 data [142] with the expression (5.32) leaving the square pion charge radius $\langle r_\pi^2 \rangle_V$ and c_V^π as free parameters, and including the theoretical error, leads to

$$\begin{aligned}\langle r_\pi^2 \rangle_V &= 0.431 \pm 0.020 \pm 0.016 \text{ fm}^2, \\ c_V^\pi &= 3.2 \pm 0.5 \pm 0.9 \text{ GeV}^{-4},\end{aligned}\tag{5.33}$$

where the first and second errors indicate the statistical and theoretical uncertainties, respectively. The central value of c_V^π is rather close to the value obtained by resonance saturation, $c_V^\pi = 4.1 \text{ GeV}^{-4}$ [140]. Since, on one hand experimental $\pi\pi$ production data below 300 MeV are sparse and of low statistics and on the other hand the key integral (5.24) exhibits a $1/E^4$ enhancement of the low energy tail, special attention is necessary for this threshold region. In this context (5.32) provides an important and firm parametrization of the low energy region and makes possible a reliable evaluation of the contribution to a_μ^{had} , as has been shown in [8] or [113]. A simple phenomenological fit of low energy $\pi\pi$ data, using a third order polynomial in s , yields

$$F_\pi(s) \approx 1 + c_1 s + c_2 s^2 + c_3 s^3$$

(structurally consistent with CHPT) yields $c_1 = 6.35046 \text{ GeV}^{-2}$, $c_2 = -22.5567 \text{ GeV}^{-4}$ and $c_3 = 140.482 \text{ GeV}^{-6}$ with a fractional error of 0.012358.

The crucial point here is that the threshold behavior is severely constrained by the chiral structure of QCD via the rather precise data for the pion form factor in the space-like region. The space-like fit provides a good description of the data in the time-like region. Pure chiral perturbation theory is able to make predictions only for the low energy tail of the form factor.

The electromagnetic form factor of the pion $F_\pi(s)$ usually is defined in an idealized world of strong interactions with two quark flavors (u and d) only, and electroweak interactions switched off. $F_\pi(s)$ has an isovector part $I = 1$ as well as an isoscalar part $I = 0$. The latter is due to isospin breaking by the mass difference of the u and d quarks: $m_u - m_s \neq 0$, which leads to $\rho - \omega$ mixing:

$$|\rho\rangle = |\rho_0\rangle - \varepsilon|\omega_0\rangle, \quad |\omega\rangle = |\omega_0\rangle + \varepsilon|\rho_0\rangle,$$

where $|\omega_0\rangle$ and $|\rho_0\rangle$ are the pure isoscalar and isovector states, respectively, and ε is the $\rho - \omega$ mixing parameter. Then, in the energy region close to the $\rho(770)$ and $\omega(782)$ meson masses, the form factor can be written as

$$\begin{aligned}F_\pi(s) &\simeq \left[\frac{F_\rho}{s - M_\rho^2} + \varepsilon \frac{F_\omega}{s - M_\omega^2} \right] \left[\frac{F_\rho}{-M_\rho^2} + \varepsilon \frac{F_\omega}{-M_\omega^2} \right]^{-1} \\ &\approx -\frac{M_\rho^2}{s - M_\rho^2} \left[1 + \varepsilon \frac{F_\omega(M_\omega^2 - M_\rho^2)s}{F_\rho M_\omega^2(s - M_\omega^2)} \right],\end{aligned}\tag{5.34}$$

where we only keep the terms linear in ε . The quantities M_ω and M_ρ are complex and contain the corresponding s -dependent widths. Including the higher resonances ρ' and ρ'' , (5.34) can be cast into the standard form

$$F_\pi(s) = \frac{\text{BW}_{\rho(770)}(s) \cdot \left(1 + \delta \frac{s}{M_\omega^2} \text{BW}_\omega(s)\right) + \beta \text{BW}_{\rho(1450)}(s) + \gamma \text{BW}_{\rho(1700)}(s)}{1 + \beta + \gamma}, \quad (5.35)$$

in terms of Breit–Wigner (BW) amplitudes (2.270) with s -dependent widths (5.30) and complex mixing parameters α , β , γ and δ . The $\pi^\pm\pi^0$ isovector form factor in the charged channels is obtained by setting $\delta = 0$ (switching off the ω) and with the parameters and pion velocities appropriate for the CC case.

The mixing is responsible for the typical distortion of the ρ -resonance (see Fig. 5.6), which originally would be a pure isospin $I = 1$ Breit–Wigner type resonance. The pion form factor (5.34) is the basic ansatz for the Gounaris–Sakurai formula [40] which is often used to represent experimental data by a phenomenological fit (see e.g. [20]).

However, theory in this case can do much more by exploiting systematically *analyticity*, *unitarity* and the properties of the *chiral limit*. A key point is that the phase of the pion form factor is determined by the $\pi\pi$ -scattering phase shifts [143]. Known experimental $\pi\pi$ -scattering data [144–146] together with progress in theory (combining two-loop CHPT and dispersion theory) lead to much more precise pion scattering lengths a_0^0 and a_0^2 [147, 148]. As a consequence, combining space-like data, $\pi\pi$ -scattering phase shifts and time-like data one obtains severe theoretical constraints on the pion form factor $F_\pi(s)$ for $s \leq 2M_K$ [120, 121]. A similar approach has been used previously in [109, 118, 149]. Recently, this approach has been applied in order to get a better control of the low energy tail, where cross sections tend to be rather small and therefore difficult to be measured precisely. The large uncertainty of the $\pi\pi$ contribution to a_μ from energies below 0.63 GeV motivated [122] to investigate it theoretically in a framework based on the analyticity and unitarity properties of the pion form factor. The main idea was to use, instead of the poorly known modulus, the phase of the form factor, which is equal by the Fermi–Watson theorem [150, 151] to the $\pi\pi$ scattering P -wave phase shift, and which has been calculated with high precision from Chiral Perturbation Theory (ChPT) and Roy equations [147, 152–154]. Above the inelastic threshold s_{in} , where the Fermi–Watson theorem is no longer valid and the phase of the form factor is not known, the analysis uses an integral condition

$$\frac{1}{\pi} \int_{s_{\text{in}}}^{\infty} ds \rho(s) |F(s)|^2 \leq I$$

on the form-factor modulus, derived using the measurements of the the $\pi\pi$ cross section by the BaBar experiment [26] up to 3 GeV and the asymptotic behavior of the form factor predicted by perturbative QCD [155–157] above that energy. Adopting the high energy asymptotic weight function $\rho(s) = 1/s$ a value $I = 0.578 \pm 0.022$ has been estimated in [122] and the contribution to a_μ from below 0.63 GeV obtained is

$$a_\mu^{\pi\pi(\gamma),\text{LO}}[2m_\pi, 0.63 \text{ GeV}] = (133.258 \pm 0.723) \times 10^{-10}, \quad (5.36)$$

a 40% reduction of the error estimated in a standard calculation in terms of e^+e^- data which yields $132.57(055)(0.93)[1.19] \times 10^{-10}$.

To be more specific, the corresponding electromagnetic vector current form factor $F_\pi(s)$ has the following properties:

(1) $F_\pi(s)$ is an analytic function of s in the whole complex s -plane, except for a cut on the positive real axis for $4m_\pi^2 \leq s < \infty$. If we approach the cut from above $s \rightarrow s + i\varepsilon$, $\varepsilon > 0$, $\varepsilon \rightarrow 0$ the form factor remains complex and is characterized by two real functions, the modulus and the phase

$$F_\pi(s) = |F_\pi(s)| e^{i\delta(s)} ; \quad \text{Arg}[F(s + i\varepsilon)] = \delta(s) \quad (5.37)$$

(2) analyticity relates $\text{Re } F_\pi(s)$ and $\text{Im } F_\pi(s)$ by a DR, which may be expressed as a relation between modulus and phase $\delta(s) = \arctan(\text{Im } F_\pi(s)/\text{Re } F_\pi(s))$, known as the Omnès representation [143]

$$F_\pi(s) = G_1(s) P(s) , \quad G_1(s) = \exp \left\{ \frac{s}{\pi} \int_{4m_\pi^2}^{\infty} ds' \frac{\delta(s')}{s'(s' - s)} \right\} , \quad (5.38)$$

where $P(s)$ is a polynomial, which determines the behavior at infinity, or, equivalently, the number and position of the zeros;

(3) charge conservation $F_\pi(0) = 1$, which fixes $P(0) = 1$; also $\left[\frac{dF(s)}{ds} \right]_{s=0} = \frac{1}{6} \langle r_\pi^2 \rangle_V$.

(4) $F_\pi(s)$ is real below the 2 pion threshold ($-\infty < s < 4m_\pi^2$), which implies that $P(s)$ must be a polynomial with real coefficients;

(5) the inelastic threshold is $s_{\text{in}} = 16m_\pi^2$, since for $I = 1$ the next threshold is the 4π one;

(6) finally, we have to take into account the isospin breaking by another factor which accounts for the $I = 0$ contribution:

$$P(s) \rightarrow G_\omega(s) \cdot G_2(s) , \quad (5.39)$$

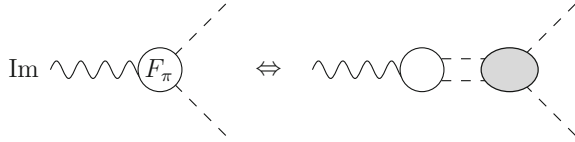
where $G_\omega(s)$ accounts for the ω -pole contribution due to $\rho - \omega$ -mixing with amplitude ε :

$$G_\omega(s) = 1 + \varepsilon \frac{s}{s_\omega - s} + \dots \quad s_\omega = (M_\omega - \frac{1}{2}i\Gamma_\omega)^2 . \quad (5.40)$$

In order to get it real below the physical thresholds we use an energy dependent width

$$\Gamma_\omega \rightarrow \Gamma_\omega(s) = \sum_X \Gamma(\omega \rightarrow X, s) = \frac{s}{M_\omega^2} \Gamma_\omega \left\{ \sum_X \text{Br}(\omega \rightarrow X) \frac{F_X(s)}{F_X(M_\omega^2)} \right\} , \quad (5.41)$$

Fig. 5.24 Final state interaction due to $\pi\pi \rightarrow \pi\pi$ scattering



where $Br(V \rightarrow X)$ denotes the branching fraction for the channel $X = 3\pi, \pi^0\gamma, 2\pi$ and $F_X(s)$ is the phase space function for the corresponding channel normalized such that $F_X(s) \rightarrow \text{const}$ for $s \rightarrow \infty$ [98].

The representation (5.38) tells us that once we know the phase on the cut and the location of the zeros of $G_2(s)$ the form factor is calculable in the entire s -plane. In the elastic region $s \leq s_{\text{in}}$ Watson’s theorem,¹⁸ exploiting unitarity, relates the phase of the form factor to the P wave phase shift of the $\pi\pi$ scattering amplitude with the same quantum numbers, $I = 1, J = 1$:

$$\left. \begin{aligned} \delta(s) &= \delta_1^1(s) \\ \eta_1(s) &\equiv 1 \end{aligned} \right\} \quad \text{for } s \leq s_{\text{in}} = 16m_\pi^2, \quad (5.43)$$

where $\eta_1 = |F_\pi(s)|$ is the elasticity parameter. However, it is an experimental fact that the inelasticity is negligible until the quasi two-body channels $\omega\pi, a_1\pi$, are open, thus in practice one can take (5.43) as an excellent approximation up to about 1 GeV (while $\sqrt{s_{\text{in}}} \simeq 0.56$ GeV). Actually, the phase difference (5.43) satisfies the bound [158]

$$\sin^2(\delta(s) - \delta_1^1(s)) \leq \frac{1}{2} [1 - \sqrt{1 - r^2(s)}], \quad r(s) = \frac{\sigma_{\text{non-}2\pi}^{I=1}}{\sigma_{e^+e^- \rightarrow \pi^+\pi^-}} \quad (5.44)$$

and $\eta_1 \leq (1 - r)/(1 + r)$, provided $r < 1$, which holds true below 1.13 GeV (below 1 GeV $r < 0.143 \pm 0.024$, or $\delta - \delta_1^1 \lesssim 6^\circ$, strongly decreasing towards lower energies).

¹⁸The pion isovector form factor is defined by the matrix element (5.31). The $\pi^+\pi^-$ state in this matrix element, in order not to vanish, must be in a $I = 1, J = 1$ (P wave) state, J the angular momentum. If we look at the charge density j_0 , time-reversal (T) invariance tells us that

$$\langle \text{out } \pi^+\pi^- | j_0(0) | 0 \rangle = \langle \text{in } \pi^+\pi^- | j_0(0) | 0 \rangle^*, \quad (5.42)$$

as for fixed J only “in” and “out” get interchanged. The complex conjugation follows from the fact that T must be implemented by an anti-unitary transformation. Now, with S the unitary scattering operator, which transforms in and out scattering states according to $|X \text{ out}\rangle = S^+ |X \text{ in}\rangle$ (X the label of the state) we have (using (5.42))

$$\langle \text{out } \pi^+\pi^- | j_0(0) | 0 \rangle = \langle \text{in } \pi^+\pi^- | S j_0(0) | 0 \rangle = e^{2i\delta_{\pi\pi}} \langle \text{out } \pi^+\pi^- | j_0(0) | 0 \rangle^*$$

which implies $F_\pi(s) = e^{2i\delta_{\pi\pi}} F_\pi^*(s)$. As two pions below the inelastic thresholds may scatter elastically only, by unitarity the S -matrix must be a pure phase in this case. The factor 2 is a convention, $\delta_{\pi\pi}(s)$ is the $\pi\pi$ -scattering phase shift.

The $\pi\pi$ scattering phase shift is due to elastic re-scattering of the pions in the final state (*final state interaction*) as illustrated by Fig. 5.24. The $\pi\pi$ scattering P -wave phase shift $\delta_1^1(s)$ (data are displayed in Fig. 5.40) has been studied some time ago in the framework of the Roy equations, also exploiting chiral symmetry [147]. As a result it turns out that $\delta_1^1(s)$ is constrained to a remarkable degree of accuracy up to about $E_0 = 0.8$ GeV (matching point). The behavior of $\delta_1^1(s)$ in the region below the matching point is controlled by three parameters: two S -wave scattering lengths a_0^0, a_0^2 and by the boundary value $\phi \equiv \delta_1^1(E_0)$. One may treat ϕ as a free parameter and rely on the very accurate predictions for a_0^0, a_0^2 from chiral perturbation theory. This information may be used to improve the accuracy of the pion form factor and thus to reduce the uncertainty of the hadronic contribution to the muon $g - 2$.

The remaining function $G_2(s)$ represents the smooth background that contains the curvature generated by the remaining singularities. The 4π channel opens at $s = 16 m_\pi^2$ but phase space strongly suppresses the strength of the corresponding branch point singularity of the form $(1 - s_{\text{in}}/s)^{9/2}$ – a significant inelasticity only manifests itself for $s > s_{\text{in}} = (M_\omega + m_\pi)^2$. The conformal mapping

$$z = \frac{\sqrt{s_{\text{in}} - s_1} - \sqrt{s_{\text{in}} - s}}{\sqrt{s_{\text{in}} - s_1} + \sqrt{s_{\text{in}} - s}} \quad (5.45)$$

maps the plane cut along $s > s_{\text{in}}$ onto the unit disk in the z -plane. It contains a free parameter s_1 - the value of s which gets maps into the origin. $G_2(s)$ may be approximated by a polynomial in z :

$$G_2(s) = 1 + \sum_{i=1}^{n_p} c_i (z^i - z_0^i), \quad (5.46)$$

where z_0 is the image of $s = 0$. The shift of z by $z \rightarrow z - z_0$ is required to preserve the charge normalization condition $G_2(0) = 1$. The form of the branch point singularity $(1 - s_{\text{in}}/s)^{9/2}$ imposes four constraints on the polynomial; a non-trivial contribution from $G_2(s)$ thus requires a polynomial of fifth order at least. An important issue is the need for a normalization point at the upper end of the energy range under consideration ($M_\rho \cdot \cdot \cdot 2M_K$). In fact, the present dispersion in the $\pi\pi$ -data (see Fig. 5.6) makes it difficult to fully exploit this approach as it seems not possible to get a convincing simultaneous fit to the different data sets. Details have been worked out in [120, 121].

For $\pi\pi \rightarrow \pi\pi$ scattering amplitudes of definite isospin I in the s -channel, one writes a partial wave decomposition

$$F^{(I)}(s, t) = \frac{8}{\pi} \sum_{\ell} (2\ell + 1) P_{\ell}(\cos \theta) t_{\ell}^{(I)}(s), \quad (5.47)$$

$$t_{\ell}^{(I)}(s) = \frac{\sqrt{s}}{2k} \hat{f}_{\ell}^{(I)}(s), \quad \hat{f}_{\ell}^{(I)}(s) = \frac{\eta_{\ell}^{(I)}(s) e^{2i\delta_{\ell}^{(I)}(s)} - 1}{2i},$$

where $\delta_\ell^{(I)}(s)$ and $\eta_\ell^{(I)}(s)$ are the phase shift and inelasticity of the I, ℓ partial wave, respectively, ℓ is the angular momentum, and k is the center of mass momentum. In the elastic case, $\eta = 1$ and

$$\hat{f}_\ell^{(I)}(s) = \sin \delta_\ell^{(I)}(s) e^{i\delta_\ell^{(I)}(s)}. \quad (5.48)$$

Given $I = 0, 1, 2$ we note that whenever I is even (odd) then ℓ is even (odd). The scattering lengths and slope parameters $a_\ell^{(I)}$ and $b_\ell^{(I)}$ are defined by the threshold parameters, which are the coefficients of the amplitude expansion in powers of center of mass (CM) momenta around threshold:

$$\frac{s^{1/2}}{2M_\pi k^{2\ell+1}} \hat{f}_\ell^{(I)}(s) \simeq a_\ell^{(I)} + b_\ell^{(I)} k^2 + O(k^4). \quad (5.49)$$

The Roy equations are DRs for the $\pi\pi$ scattering amplitudes. Roy's representation [152] for the partial wave amplitudes t_ℓ^I of elastic $\pi\pi$ scattering reads

$$t_\ell^I(s) = k_\ell^I(s) + \sum_{I'=0}^2 \sum_{\ell'=0}^{\infty} \int_{4M_\pi^2}^{\infty} ds' K_{\ell\ell'}^{II'}(s, s') \text{Im } t_{\ell'}^{I'}(s'), \quad (5.50)$$

where I and ℓ denote isospin and angular momentum, respectively and $k_\ell^I(s)$ is the partial wave projection of the subtraction term. It shows up only in the S - and P -waves,

$$k_\ell^I(s)\alpha = \alpha a_0^I \delta_\ell^0 + \frac{s - 4M_\pi^2}{4M_\pi^2} (2a_0^0 - 5a_0^2) \left(\frac{1}{3} \delta_0^I \delta_\ell^0 + \frac{1}{18} \delta_1^I \delta_\ell^1 - \frac{1}{6} \delta_2^I \delta_\ell^0 \right).$$

The kernels $K_{\ell\ell'}^{II'}(s, s')$ are explicitly known functions [147, 152].

5.1.8 Addendum I: The Hadronic Contribution to the Running Fine Structure Constant

By the same procedure, we have evaluated a_μ^{had} , the renormalized VP function can be calculated. The latter is identical to the shift in the fine structure constant, which encodes the charge screening:

$$\Delta\alpha(s) \equiv -\text{Re} [\Pi'_\gamma(s) - \Pi'_\gamma(0)]. \quad (5.51)$$

For the evaluation of the hadronic contribution we apply the DR (3.143). The integral to be evaluated is

$$\Delta\alpha_{\text{had}}^{(5)}(s) = -\frac{\alpha_s}{3\pi} \operatorname{Re} \left(\int_{m_{\pi^0}^2}^{E_{\text{cut}}^2} ds' \frac{R_{\gamma}^{\text{data}}(s')}{s'(s' - s - i\epsilon)} + \int_{E_{\text{cut}}^2}^{\infty} ds' \frac{R_{\gamma}^{\text{PQCD}}(s')}{s'(s' - s - i\epsilon)} \right). \quad (5.52)$$

Since, in this case the kernel behaves like $1/s$ (as compared to $1/s^2$ for a_{μ}) data from higher energies are much more important here. The hadronic contribution due to the 5 light quarks $\Delta\alpha_{\text{had}}^{(5)}(s)$ supplemented by the leptonic contribution is presented in Fig. 5.25. A particularly important parameter for precision physics at the Z -resonance (LEP/SLD experiments) is the precise value of the effective fine structure constant at the Z mass scale $\sqrt{s} = M_Z = 91.1876$ GeV $\alpha(M_Z^2)$. The hadronic contribution to the shift is

$$\Delta\alpha_{\text{hadrons}}^{(5)}(M_Z^2) = 0.027738 \pm 0.000190 \quad (5.53)$$

which together with the leptonic contribution (3.123) and using (3.121) yields

$$\alpha^{-1}(M_Z^2) = 128.929 \pm 0.026 \quad (5.54)$$

With more theory input, based on the Adler–function method [15, 79, 112], we obtain (see Fig. 5.18)

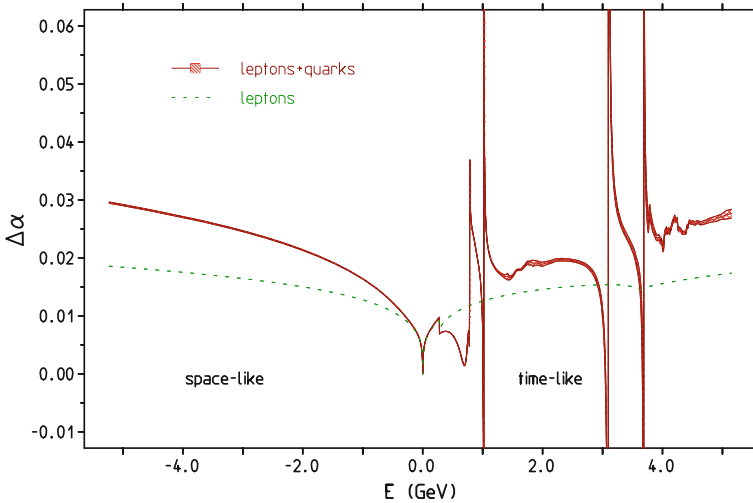


Fig. 5.25 Shift of the effective fine structure constant $\Delta\alpha$ as a function of the energy scale in the time-like region $s > 0$ ($E = \sqrt{s}$) versus the space-like region $-s > 0$ ($E = -\sqrt{-s}$). The band indicates the uncertainties

$$\begin{aligned}\Delta\alpha_{\text{hadrons}}^{(5)}(M_Z^2) &= 0.027555 \pm 0.000127 \\ \alpha^{-1}(M_Z^2) &= 128.965 \pm 0.017 .\end{aligned}\tag{5.55}$$

The leptonic shift has been calculated analytically to three loops in [159] and to four loops in [160]. At the Z mass the numerical result reads

$$\begin{aligned}\Delta\alpha_{\text{lep}}(M_Z^2) &= \left(\frac{\alpha}{\pi}\right) 13.52631(8) + \left(\frac{\alpha}{\pi}\right)^2 14.38553(6) + \left(\frac{\alpha}{\pi}\right)^3 84.8285(7) \\ &+ \left(\frac{\alpha}{\pi}\right)^4 [810.65(1)_{\text{NS}} - 39.8893(5)_{\text{SI}}] + \mathcal{O}(\alpha^5) ,\end{aligned}$$

where NS comes from non-singlet and SI from singlet diagrams, respectively. For the CODATA value $\alpha = 7.2973525698(24) \times 10^{-3}$ one obtains

$$\begin{aligned}\Delta\alpha_{\text{lep}}(M_Z^2) &= 0.0314192\dots + 0.00007762\dots + 0.00000106\dots + 0.00000002\dots \\ &= 3.14979(2) \times 10^{-2}\end{aligned}$$

Comment on the experimental determination of $\alpha(s)$ as a complex analytic function:

As noted earlier the effective fine structure constant shown in Fig. 5.25 is very important also for removing the VP effects from the physical cross section in order to get the undressed one which is needed in the DR (5.55). The dressed (physical) cross section measures the full photon self-energy the undressed (bare) extracts the one-particle irreducible self-energy. The precise relationship (3.117) between the full photon propagator and the 1PI self-energy $\Pi'_\gamma(s)$, discussed earlier in Sects. 2.6.1 and 3.7, is given by the Dyson summation formula (2.162). Here it is important to keep in mind that the photon vacuum polarization function is a complex analytic function. It is real on the negative real axis (space-like region) and has an imaginary part above the production threshold on the positive real axis (time-like region). This suggests to generalize the definition of the real effective e.m. fine structure constant to a complex analytic function. The complex effective fine structure constant is defined by (5.51) and (5.52) by omitting the “Re” prescription. What can be measured is

$$\frac{\sigma(e^+e^- \rightarrow \mu^+\mu^-)}{\sigma(e^+e^- \rightarrow \mu^+\mu^-)_{\text{pt}}} = |\alpha(s)/\alpha(0)|^2$$

where $\sigma(e^+e^- \rightarrow \mu^+\mu^-)$ is the experimental muon pair production cross section and $\sigma(e^+e^- \rightarrow \mu^+\mu^-)_{\text{pt}}$ the Monte Carlo cross section provided by theory with the VP effects switched off. The result of the KLOE measurement is shown in Fig. 5.26.

Then, using $\alpha(s) = \alpha(0)/(1 - \Delta\alpha)$ we have

$$Z \equiv |\alpha(0)/\alpha(s)|^2 = (1 - \Delta\alpha)(1 - \Delta\alpha)^* = 1 - 2\text{Re } \Delta\alpha + (\text{Re } \Delta\alpha)^2 + (\text{Im } \Delta\alpha)^2 .$$

Furthermore, separating the leptonic and the hadronic part $\Delta\alpha = \Delta\alpha_{\text{lep}} + \Delta\alpha_{\text{had}}$, the leptonic part $\Delta\alpha_{\text{lep}}(s)$ is well known from perturbative QED, given by (3.123) at one

loop and (3.124) at two loops. The analytic three loop result for $\Delta\alpha_{\text{lep}}(s)$ has been implemented in the `alphaQED` package [161]. The four loop leptonic corrections turn out to be negligible for our purpose. Using this information, the experiment allows one to determine $\Delta\alpha_{\text{had}}$. The second experimental input is $\text{Im } \Delta\alpha_{\text{had}}$ which is determined by $\sigma_{\text{had}}(s)$. Given $Z = (1 - x)^2 + y^2$ and y we extract $1 - x = \sqrt{Z - y^2}$ and hence

$$\text{Re } \Delta\alpha = x = 1 - \sqrt{Z - y^2} ; \quad \text{Im } \Delta\alpha = y , \tag{5.56}$$

the latter obtained from the R measurement. Then $\alpha(s) = \alpha(0)/(1 - x - iy)$ is the complex electromagnetic fine structure constant. The non-perturbative hadronic shifts, displayed in Fig. 5.27, follow as

$$\text{Re } \Delta\alpha_{\text{had}} = \text{Re } \Delta\alpha - \text{Re } \Delta\alpha_{\text{lep}} ; \quad \text{Im } \Delta\alpha_{\text{had}} = \text{Im } \Delta\alpha - \text{Im } \Delta\alpha_{\text{lep}} . \tag{5.57}$$

This measurement has been performed recently with the KLOE detector at the Φ factory DAΦNE at Frascati [65]. The experiment has measured the running of the effective QED coupling constant $\alpha(s)$ in the time-like region $0.6 < \sqrt{s} < 0.975$ GeV using the Initial State Radiation process $e^+e^- \rightarrow \mu^+\mu^-\gamma$. It represents the first measurement of the running of $\alpha(s)$ in this energy region. The results show a more than 5σ significance of the hadronic contribution to the running of $\alpha(s)$, which is the strongest direct evidence both in time- and space-like regions achieved in a single measurement. By using the $e^+e^- \rightarrow \pi^+\pi^-$ cross section previously measured at KLOE the real and imaginary parts of the shift $\Delta\alpha(s)$ has been extracted and is found to agree very well with the dispersive evaluation (5.52) based on the weighted

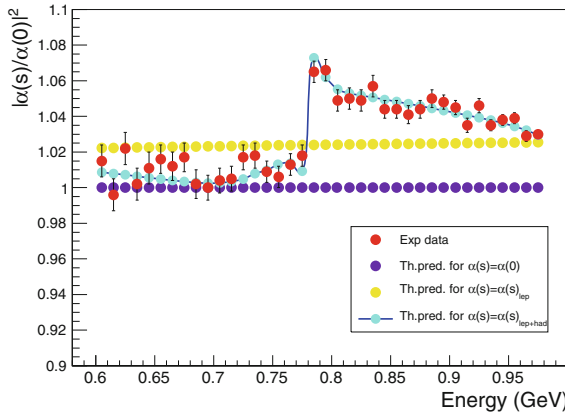


Fig. 5.26 A first direct measurement of the modulus square of the effective fine structure constant $|\alpha(s)/\alpha(0)|^2$ in the time-like region around the ρ resonance with the KLOE detector confirms the typical strong energy dependence on the vacuum polarization screening in the vicinity of a hadronic resonance. Courtesy of the KLOE-2 Collaboration. Reprinted from [65], <http://dx.doi.org/10.1016/j.physletb.2016.12.016>, (License: CC-BY-4.0)

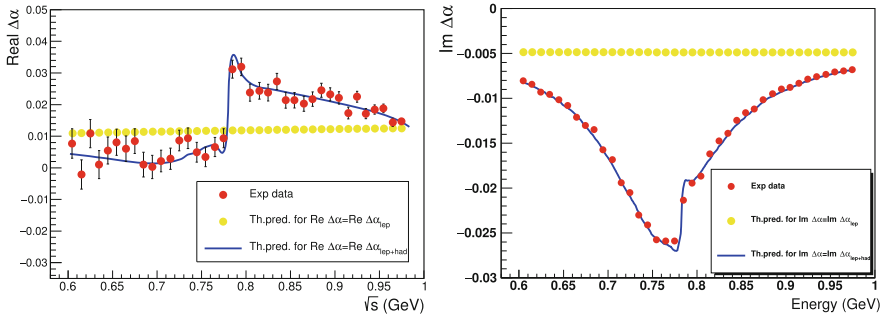
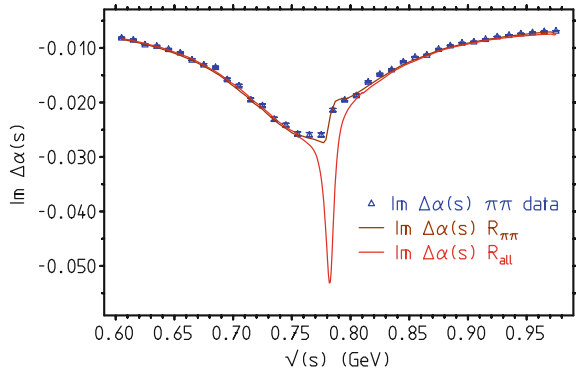


Fig. 5.27 Combining cross section measurements of $\sigma(e^+e^- \rightarrow \mu^+\mu^-)$ and $\sigma(e^+e^- \rightarrow \pi^+\pi^-)$ and subtracting the leptonic contributions obtained by QED calculations (see (3.123) and (3.124)) one is able to extract the real and the imaginary parts of the hadronic shift $\Delta\alpha_{\text{had}}(s) = 1 - \alpha(0)/\alpha(s) - \Delta\alpha_{\text{lep}}(s)$ separately. Courtesy of the KLOE-2 Collaboration. Reprinted from [65], <http://dx.doi.org/10.1016/j.physletb.2016.12.016> (License: CC-BY-4.0)

Fig. 5.28 Including the missing 3π channel changes $\text{Im } \Delta\alpha_{\text{had}}$ substantially at the ω resonance, which is not included in Fig. 5.27



average of the shown in Fig. 5.25. We mention that in the imaginary part is only included the $\pi\pi$ part measured in the same experiment (KLOE). The 3π channel could have been added from other experiments which have measured that channel. The effect is illustrated in Fig. 5.28. In contrast Fig. 5.26 includes the effects from all channels.

5.1.9 Addendum II: The Hadronic Contribution to the Running $SU(2)_L$ Gauge Coupling

Within the SM hadronic vacuum polarization effects not only appear in the photon self energy but also in other gauge boson self-energies (see e.g. [33]), in particular in $\gamma - Z$ mixing as discussed following p. 327, where it appears as a weak interaction contribution (see Sect. 4.2). It amounts to evaluate the running gauge coupling $\alpha_2 =$

$\frac{g^2}{4\pi}$ which together with the running $\alpha = \frac{e^2}{4\pi}$ determines the running of the effective weak mixing parameter $\sin \Theta_{\text{eff}} = \sin_g^2 = e^2/g^2$ defined in (4.42).

According to the SM gauge structure and factoring out the gauge couplings, the non-perturbative hadronic correction in the $\gamma\gamma$, γZ and ZZ self-energies, decompose as

$$\begin{aligned} \Pi^{\gamma\gamma} &= e^2 \hat{\Pi}^{\gamma\gamma} ; \quad \Pi^{Z\gamma} = \frac{eg}{c_g} \hat{\Pi}_V^{3\gamma} - \frac{e^2 s_g}{c_g} \hat{\Pi}_V^{\gamma\gamma} ; \\ \Pi^{ZZ} &= \frac{g^2}{c_g^2} \hat{\Pi}_{V-A}^{33} - 2 \frac{e^2}{c_g^2} \hat{\Pi}_V^{3\gamma} + \frac{e^2 s_g^2}{c_g^2} \hat{\Pi}_V^{\gamma\gamma} , \end{aligned} \quad (5.58)$$

where $s_g = \sin_g = e/g$, $c_g = (1 - s_g^2)^{1/2}$, and with $\hat{\Pi}(s) = \hat{\Pi}(0) + s \hat{\Pi}'(s)$

$$\begin{aligned} \Delta\alpha_{\text{had}}(s) &= -e^2 \left[\text{Re} \hat{\Pi}'^{\gamma\gamma}(s) - \hat{\Pi}'^{\gamma\gamma}(0) \right] , \\ \Delta\alpha_{2\text{had}}(s) &= -\frac{e^2}{s_g^2} \left[\text{Re} \hat{\Pi}'^{3\gamma}(s) - \hat{\Pi}'^{3\gamma}(0) \right] , \end{aligned} \quad (5.59)$$

which exhibit the leading hadronic non-perturbative parts, i.e. the ones involving the photon field including its mixing with the weak neutral current.¹⁹

Unlike the photon VP, which is directly related to to $e^+e^- \rightarrow \gamma^* \rightarrow \text{hadrons}$ process, other relevant combinations are not related in a similar simple direct way to a physical process. However, such HVP effects obey simple approximate relationships as they differ mainly by the different flavor weighting given by overall charge assignments. In the large- N_c terminology (see p. 152) in the planar approximation the relation would be given by the valence quark charges/couplings ratios. As flavor reweighting will play a role in some places below we briefly consider the interrelations between the electromagnetic and the weak neutral current here.

On Hadronic Currents and Correlators:

In QCD the hadronic currents in terms of the quark field (current are color singlets i.e. color diagonal in the quark fields and color is summed over) are the electromagnetic current:

$$j_{\text{em}}^\mu = \frac{2}{3} \bar{u}\gamma^\mu u - \frac{1}{3} \bar{d}\gamma^\mu d - \frac{1}{3} \bar{s}\gamma^\mu s + \dots \quad (5.60)$$

and the neutral isovector current as it shows up in the weak interactions

$$j_3^\mu = \frac{1}{2} \bar{u}\gamma^\mu u - \frac{1}{2} \bar{d}\gamma^\mu d - \frac{1}{2} \bar{s}\gamma^\mu s + \dots \quad (5.61)$$

¹⁹The leading hadronic contributions are available from the FORTRAN package `alphaQED` [161] $\Delta\alpha_{\text{had}}$ is named `dcr` and $\Delta\alpha_{2\text{had}}$ is given by `deg`.

In current correlators, one has to distinguish valence quark connected and disconnected contributions, where the latter need not be diagonal in flavor space and give rise to OZI suppressed transitions. In case the latter would be small relative to the flavor diagonal ones one would obtain a flavor weighting as in pQCD. The separation of the ud part based on isospin considerations not assuming OZI violating terms to be small leads to a different reweighting, however, and which actually turns out to be a much better approximation, as has been checked against lattice QCD simulations [162, 163].

In the $SU(3)_{\text{flavor}}$ limit of the light quarks we have $\Pi^{ss} \simeq \Pi^{dd} \simeq \Pi^{uu}$ and $\Pi^{ds} \simeq \Pi^{us} \simeq \Pi^{ud}$ ($m_s \simeq m_d \simeq m_u$), which implies

$$\hat{\Pi}_{(uds)}^{\gamma\gamma} \simeq \frac{2}{3} (\Pi^{uu} - \Pi^{ud}) ; \hat{\Pi}_{(uds)}^{3\gamma} \simeq \frac{1}{3} (\Pi^{uu} - \Pi^{ud}) ; \hat{\Pi}_{(uds)}^{33} \simeq \frac{3}{16} (\Pi^{uu} - \Pi^{ud}) + \frac{1}{16} \Pi^{ud}$$

These assumptions imply

$$\hat{\Pi}^{3\gamma} \simeq \frac{1}{2} \hat{\Pi}_{(uds)}^{\gamma\gamma} + \frac{3}{8} \hat{\Pi}_{(c)}^{\gamma\gamma} + \frac{3}{4} \hat{\Pi}_{(b)}^{\gamma\gamma} \quad (5.62)$$

and further assuming $|\Pi^{ud}| \ll 3 (\Pi^{uu} - \Pi^{ud})$ we have

$$\hat{\Pi}^{33} \simeq \frac{9}{32} \hat{\Pi}_{(uds)}^{\gamma\gamma} + \frac{9}{64} \hat{\Pi}_{(c)}^{\gamma\gamma} + \frac{9}{16} \hat{\Pi}_{(b)}^{\gamma\gamma} . \quad (5.63)$$

An attempt to proceed similarly in the $SU(2)_{\text{flavor}}$ limit of the light quarks with $\Pi^{dd} \simeq \Pi^{uu}$ ($m_d \simeq m_u$), we find no simple relation unless one assumes OZI suppressed terms to be negligible (see below). This leads to the reweighting as in perturbation theory, and leads to a 5% mismatch when compared with lattice simulations.

At low energy the VP effects are related to hadrons and a corresponding note the reader may find on page p. 152 in Sect.2.8. For energies where exclusive hadro-production channels are available i.e. below 2 GeV one may perform *flavor separation by hand*:

since final state e.m. interactions violate isospin, we skip all final states involving photons like: $\pi^0\gamma$, $\eta\gamma$, $\eta'\gamma$ etc. (see Table 5.3)

- as ud , $I = 0$ we include states with odd number of pions, incl. the ω meson
- as ud , $I = 1$ we include states with even number of pions, incl. the ρ meson
- as $\bar{s}s$ we count all states with Kaons, incl. the ϕ meson

States ηX with X some other hadrons are collected separately, and then split into $q = u, d$ and s components by appropriate mixing.

For the resonance contributions in the spirit of the large- N_c vector meson dominance picture we proceed as follows: in terms of single quark currents j^q , where $j_\mu^q = \bar{q}\gamma_\mu q$, we may define currents associated with the resonances $j^\rho = \frac{1}{2} (j^u - j^d)$, $j^\omega = \frac{1}{6} (j^u + j^d)$ and $j^\phi = -\frac{1}{3} j^s$, which corresponds to the ideally mixed $J^{PC} = 1^{--}$ states ρ_0 , ω_0 and ϕ_0 , we may write

$$\begin{aligned}
j^\gamma &= j^\rho + j^\omega + j^\phi + j^{J/\psi} + j^\Upsilon \\
j^3 &= \frac{1}{2} j^\rho + \frac{3}{4} j^\phi + \frac{3}{8} j^{J/\psi} + \frac{3}{4} j^\Upsilon
\end{aligned} \tag{5.64}$$

Denoting the diagonal amplitudes by $\Pi^{(V)}$ we obtain

$$\begin{aligned}
\hat{\Pi}^{\gamma\gamma} &\simeq \Pi^{(\rho)} + \Pi^{(\omega)} + \Pi^{(\phi)} + \Pi^{(J/\psi)} + \Pi^{(\Upsilon)} \\
\hat{\Pi}^{3\gamma} &\simeq \frac{1}{2} \Pi^{(\rho)} + \frac{3}{4} \Pi^{(\phi)} + \frac{3}{8} \Pi^{(J/\psi)} + \frac{3}{4} \Pi^{(\Upsilon)} \\
\hat{\Pi}^{33} &\simeq \frac{1}{4} \Pi^{(\rho)} + \frac{9}{16} \Pi^{(\phi)} + \frac{9}{64} \Pi^{(J/\psi)} + \frac{9}{16} \Pi^{(\Upsilon)}
\end{aligned} \tag{5.65}$$

provided mixing is small. For the combination $3\hat{\Pi}^{33} - \hat{\Pi}^{3\gamma} = -\frac{1}{2}\Pi^{\rho\omega} + \frac{3}{8}\Pi^{(\phi)} - \frac{3}{32}\Pi^{(J/\psi)} + \dots$ the (ud) contribution is solely due to $\rho - \omega$ mixing, as an example. In any case we apply the resonance reweighting for corresponding contributions of Table 5.2.

Besides the flavor $SU(3)$ inspired weighting

$$\Pi_{uds}^{3\gamma} = \frac{1}{2} \Pi_{uds}^{\gamma\gamma}$$

the ρ dominance (exact in the isospin limit) assignment

$$\Pi_{ud}^{3\gamma} = \frac{1}{2} \Pi_{ud}^{\gamma\gamma} ; \quad \Pi_s^{3\gamma} = \frac{3}{4} \Pi_s^{\gamma\gamma}$$

which agrees well with lattice data.

Note that the “wrong” perturbative weighting

$$\Pi_{ud}^{3\gamma} = \frac{9}{20} \Pi_{ud}^{\gamma\gamma} ; \quad \Pi_s^{3\gamma} = \frac{3}{4} \Pi_s^{\gamma\gamma}$$

has been proven to clearly mismatch lattice results, while the correction $\frac{9}{20} \Rightarrow \frac{10}{20}$ is in good agreement. This also means the OZI suppressed contributions should be at the 5% level and not negligibly small.

Note that in the 1985 $SU(3)$ flavor separation scheme [33] we assigned to non- ϕ (non-resonant) s component the weight 1/2, while in the updated scheme we assign the weight 3/4 as for resonant ϕ . We take the difference as a systematic uncertainty.

SM gauge boson self-energy contributions are expressed in terms of $J_3^\mu = \frac{1}{2} j_3^\mu$ such that $\hat{\Pi}'^{3\gamma}(s) - \hat{\Pi}'^{3\gamma}(0) \Leftrightarrow \frac{1}{2} \Pi^{3\gamma}$ and $\hat{\Pi}'^{33}(s) - \hat{\Pi}'^{33}(0) \Leftrightarrow \frac{1}{4} \Pi^{33}$. That we are using the proper recipe has been checked in lattice QCD calculations [162, 163]. The running weak mixing parameter has been displayed in Fig. 4.17 in Sect. 4.2.

5.1.10 Addendum III: τ Spectral Functions versus e^+e^- Annihilation Data

In 1997 precise τ -spectral functions became available [123–127] which, to the extent that flavor $SU(2)$ in the light hadron sector is a good symmetry, allows one to obtain the isovector part of the e^+e^- cross-section [164]. The idea to use the τ spectral data to improve the evaluation of the hadronic contributions a_μ^{had} was realized by Alemany, Davier and Höcker [11]. The isovector part of $\sigma(e^+e^- \rightarrow \text{hadrons})$ may be calculated by an isospin rotation, like $\pi^0\pi^- \rightarrow \pi^+\pi^-$, from τ -decay spectra, to the extent that the so-called conserved vector current (CVC) would be exactly conserved (which it is not, see below). In the following we will explicitly consider the dominating 2π channel only. The relation we are looking for may be derived by comparing the relevant lowest order diagrams Fig. 5.29, which for the e^+e^- case translates into

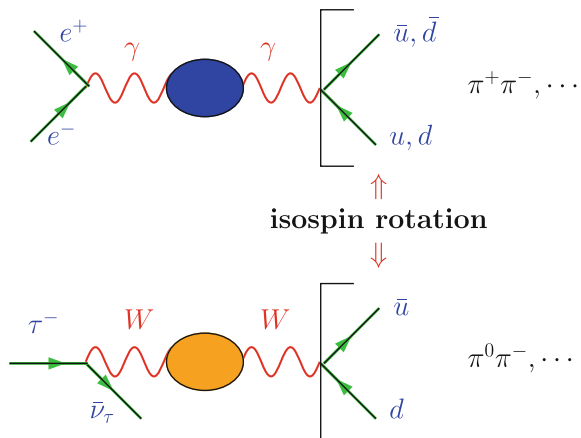
$$\sigma_{\pi\pi}^{(0)} \equiv \sigma_0(e^+e^- \rightarrow \pi^+\pi^-) = \frac{4\pi\alpha^2}{s} v_0(s) \tag{5.66}$$

and for the τ case into

$$\begin{aligned} \frac{1}{\Gamma} \frac{d\Gamma}{ds}(\tau^- \rightarrow \pi^-\pi^0\nu_\tau) &= \frac{6|V_{ud}|^2 S_{EW}}{m_\tau^2} \frac{B(\tau^- \rightarrow \nu_\tau e^- \bar{\nu}_e)}{B(\tau^- \rightarrow \nu_\tau \pi^-\pi^0)} \\ &\times \left(1 - \frac{s}{m_\tau^2}\right)^2 \left(1 + \frac{2s}{m_\tau^2}\right) v_-(s) \end{aligned} \tag{5.67}$$

where $|V_{ud}| = 0.97425 \pm 0.00022$ [41] denotes the CKM weak mixing matrix element and $S_{EW} = 1.01907 \pm 0.0003$ accounts for electroweak radiative corrections [113, 165–169]. The spectral functions are obtained from the corresponding invariant mass distributions. The $B(i)$'s are branching ratios. $SU(2)$ symmetry (CVC) would imply

Fig. 5.29 τ -decay data may be combined with $I=1$ part of e^+e^- annihilation data after isospin rotation [$\pi^-\pi^0 \Leftrightarrow \pi^-\pi^+$] and applying isospin breaking (IB) corrections (e.m. effects, phase space, isospin breaking in masses, widths, $\rho^0 - \omega$ mixing etc.)



$$v_-(s) = v_0(s) \quad (5.68)$$

The indices $i = 0, -$ denote the neutral $\pi^- \pi^+$ and the charged $\pi^- \pi^0$ channel, respectively. The spectral functions $v_i(s)$ are related to the pion form factors $F_\pi^i(s)$ by

$$v_i(s) = \frac{\beta_i^3(s)}{12} |F_\pi^i(s)|^2 \quad ; \quad (i = 0, -) \quad (5.69)$$

where $\beta_i(s)$ is the pion velocity: $\beta_0 = \beta_{\pi^- \pi^+}$, $\beta_- = \beta_{\pi^- \pi^0}$. The difference in phase space of the pion pairs gives rise to the relative factor β_-^3/β_0^3 .

Before a precise comparison via (5.68) is possible the various sources of isospin breaking effects have to be taken into account. An example of isospin breaking are the different final state radiation as illustrated in Fig. 5.30. As mentioned earlier, this has been investigated in [169, 170] for the most relevant $\pi\pi$ channel. The corrected version of (5.68) (see [169, 170] for details) may be written in the form

$$\sigma_{\pi\pi}^{(0)} = \left[\frac{K_\sigma(s)}{K_\Gamma(s)} \right] \frac{d\Gamma_{\pi\pi[\gamma]}}{ds} \times \frac{R_{IB}(s)}{S_{EW}} \quad (5.70)$$

with

$$K_\Gamma(s) = \frac{G_F^2 |V_{ud}|^2 m_\tau^3}{384\pi^3} \left(1 - \frac{s}{m_\tau^2}\right)^2 \left(1 + 2 \frac{s}{m_\tau^2}\right); \quad K_\sigma(s) = \frac{\pi\alpha^2}{3s},$$

the prefactor of the final state $\pi\pi$ -system of Fig. 5.29, and the isospin breaking correction

$$R_{IB}(s) = \frac{1}{G_{EM}(s)} \frac{\beta_{\pi^- \pi^+}^3}{\beta_{\pi^- \pi^0}^3} \left| \frac{F_\pi^0(s)}{F_\pi^-(s)} \right|^2 \quad (5.71)$$

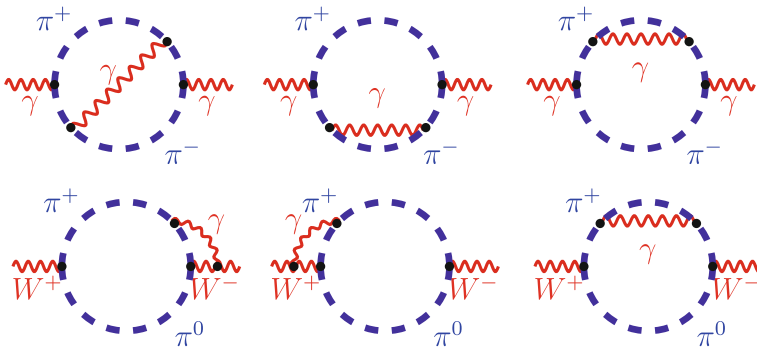


Fig. 5.30 Sample photonic correction which differ between the neutral and the charged channel. The cut diagrams represent the 2π states incl. FSR

includes the QED corrections to $\tau^- \rightarrow \nu_\tau \pi^- \pi^0$ decay with virtual plus real soft and hard photon radiation, integrated over all phase space.

However, photon radiation by hadrons is poorly understood theoretically. The commonly accepted recipe is to treat radiative corrections of the pions by scalar QED, except for the short distance (SD) logarithm proportional the $\ln M_W/m_\pi$ which is replaced by the quark parton model result and included in S_{EW} by convention. This SD log is present only in the weak charged current transition $W^{*+} \rightarrow \pi^+ \pi^0$ (γ), while in the charge neutral electromagnetic current transition $\gamma^* \rightarrow \pi^+ \pi^-$ (γ) this type of leading log is absent. In any case there is an uncertainty in the correction of the isospin violations by virtual and real photon radiation which is hard to quantify. However, the $\gamma\gamma \rightarrow \pi^- \pi^+$, $\pi^0 \pi^0$ data strongly suggest that sQED applies quite well below about 1 GeV.

Originating from (5.69), $\beta_{\pi^- \pi^+}^3 / \beta_{\pi^- \pi^0}^3$ is a phase space correction due to the $\pi^\pm - \pi^0$ mass difference. $F_\pi^0(s)$ is the NC vector current form factor, which exhibits besides the $I = 1$ part an $I = 0$ contribution. The latter represents the $\rho - \omega$ mixing term which originates from the $SU(2)$ breaking ($m_d - m_u$ mass difference). Finally, F_π^- is the CC $I = 1$ vector form factor. One of the leading isospin breaking effects is the $\rho - \omega$ mixing correction included in $|F_\pi^0(s)|^2$. The form factor corrections, in principle, also should include the electromagnetic shifts in the masses and the widths of the ρ 's.²⁰ Up to this last mentioned effect, discussed in [114], which was considered to be small, all the corrections were applied in [113] (see Fig. 5.34) but were not able to eliminate the observed discrepancy between $v_-(s)$ and $v_0(s)$. The deviation is starting at the peak of the ρ and is increasing with energy to about 10–20%. The origin of this difference is $\rho^0 - \gamma$ mixing, which occurs in the neutral $e^+ e^-$ channel, but obviously is absent in the charged τ^- -decay. This will be discussed next.

5.1.11 A Minimal Model: VMD + sQED Resolving the τ versus $e^+ e^-$ Puzzle

To come to the point, the “model” we apply here is a widely accepted model, with the difference that previous models of the pion form factor in the neutral channel, known as the Gounaris–Sakurai model, have been missing to take into account the one-loop diagrams in the $\rho^0 - \gamma$ mixing amplitude. When modeling the pion form factor as a strong interaction object, photon radiation by the pions is usually not accounted for. The latter is considered as an isospin breaking correction. Recently, in [88] an

²⁰Because of the strong resonance enhancement, especially in the ρ region, a small isospin breaking shift in mass and width between ρ^0 and ρ^\pm , typically $\Delta M_\rho = M_{\rho^\pm} - M_{\rho^0} \sim 2.5$ MeV and $\Delta \Gamma_\rho = \Gamma_{\rho^\pm} - \Gamma_{\rho^0} \sim 1.5$ MeV and similar for the higher resonances ρ' , ρ'' , ... and the mixings of these states, causes a large effect in the tails by the kinematic shift this implies. Such large parameter shifts can mimic to some extent a $\gamma - \rho^0$ mixing effect (see Fig. 5.33) and is included by Davier et al. [129, 171] as part of the “normal” IB, as an alternative to $\gamma - \rho^0$ mixing. Theory arguments yield a small $\Delta M_\rho \sim 0.8$ MeV only.

attempt has been made to take into account more systematically the effect of the electromagnetic interaction of the pions. This requires an effective model specifying the electromagnetic interaction of the pions. As we know in the SM photons couple to quarks and the radiation of bound systems like pions is a complicated problem of non-perturbative nature. As in the case of FSR at lower energies scalar QED treating the pions as point-like objects should be a good starting point. Thus the manifestly electromagnetically gauge invariant version of the VMD model is to be combined with scalar QED. The effective Lagrangian then reads

$$\begin{aligned}\mathcal{L} &= \mathcal{L}_{\gamma\rho} + \mathcal{L}_{\pi}, \\ \mathcal{L}_{\pi} &= D_{\mu}\pi^{+}D^{+\mu}\pi^{-} - m_{\pi}^2\pi^{+}\pi^{-}, \quad D_{\mu} = \partial_{\mu} - ieA_{\mu} - ig_{\rho\pi\pi}\rho_{\mu}, \\ \mathcal{L}_{\gamma\rho} &= -\frac{1}{4}F_{\mu\nu}F^{\mu\nu} - \frac{1}{4}\rho_{\mu\nu}\rho^{\mu\nu} + \frac{M_{\rho}^2}{2}\rho_{\mu}\rho^{\mu} + \frac{e}{2g_{\rho}}\rho_{\mu\nu}F^{\mu\nu}.\end{aligned}\quad (5.72)$$

We then are able to calculate self-energy (SE) effects which have to be included mandatory in order to get the $\rho \rightarrow \pi^{+}\pi^{-}$ decay correctly. In fact, the self-energy corrections to $e^{+}e^{-} \rightarrow \pi^{+}\pi^{-}$ in particular account for the energy dependent width of the ρ in the Gounaris–Sakurai parametrization of $F_{\pi}(s)$. As the ρ^0 mixes with the γ one has to take into account SE effects consistently in the $\rho - \gamma$ coupled system as represented in Fig. 5.31. The missing effect so far (above) was the energy dependent self-energy effects, the pion loops, in the $\rho - \gamma$ mixing propagator.²¹ The bare $\gamma - \rho$ transverse self-energy functions are given by

$$\Pi_{\gamma\gamma} = \frac{e^2}{48\pi^2}f(q^2), \quad \Pi_{\gamma\rho} = \frac{eg_{\rho\pi\pi}}{48\pi^2}f(q^2) \quad \text{and} \quad \Pi_{\rho\rho} = \frac{g_{\rho\pi\pi}^2}{48\pi^2}f(q^2), \quad (5.73)$$

Explicitly, in the $\overline{\text{MS}}$ scheme (μ the $\overline{\text{MS}}$ renormalization scale)

$$h(q^2) \equiv f(q^2)/q^2 = 2/3 + 2(1-y) - 2(1-y)^2G(y) + \ln\frac{\mu^2}{m_{\pi}^2}, \quad (5.74)$$

where $y = 4m_{\pi}^2/s$ and $G(y) = \frac{1}{2\beta_{\pi}}(\ln\frac{1+\beta_{\pi}}{1-\beta_{\pi}} - i\pi)$, for $q^2 > 4m_{\pi}^2$ (see (2.257)).

Mass eigenstates are obtained by diagonalization and renormalization. Renormalization conditions are such that the matrix is diagonal and of residue unity at the photon pole $q^2 = 0$ and at the ρ resonance $s = M_{\rho}^2$:

²¹In The GS model the approximation $-i\Pi_{\gamma\rho}^{\mu\nu(\pi)}(q) = \text{---}\text{---}\text{---}\text{---}\text{---}$ is adopted. Furthermore, the naive VMD Lagrangian

$$\mathcal{L}_{\gamma\rho} = -\frac{eM_{\rho}^2}{g_{\rho}}\rho_{\mu}A^{\mu}.$$

is used, which is not manifestly e.m. gauge invariant.

Fig. 5.31 Irreducible self-energy contributions at one-loop

$$\begin{aligned}
 -i \Pi_{\gamma}^{\mu\nu}(\pi)(q) &= \text{diagram 1} + \text{diagram 2} \\
 -i \Pi_{\gamma\rho}^{\mu\nu}(\pi)(q) &= \text{diagram 3} + \text{diagram 4} \\
 -i \Pi_{\rho\rho}^{\mu\nu}(\pi)(q) &= \text{diagram 5} + \text{diagram 6}
 \end{aligned}$$

$$\Pi_{\gamma\gamma}^{\text{ren}}(q^2) = \Pi_{\gamma\gamma}(q^2) - q^2 \Pi'_{\gamma\gamma}(0) \doteq q^2 \Pi'_{\gamma\gamma}{}^{\text{ren}}(q^2) \quad (5.75)$$

$$\Pi_{\gamma\rho}^{\text{ren}}(q^2) = \Pi_{\gamma\rho}(q^2) - \frac{q^2}{M_\rho^2} \text{Re} \Pi_{\gamma\rho}(M_\rho^2) \quad (5.76)$$

$$\Pi_{\rho\rho}^{\text{ren}}(q^2) = \Pi_{\rho\rho}(q^2) - \text{Re} \Pi_{\rho\rho}(M_\rho^2) - (q^2 - M_\rho^2) \text{Re} \frac{d\Pi_{\rho\rho}}{ds}(M_\rho^2) \quad (5.77)$$

where we have used $\Pi_{\rho\rho}(0) = 0$, $\Pi'_{\gamma\gamma}(q^2) = \Pi_{\gamma\gamma}(q^2)/q^2$, which is inferred by electromagnetic gauge invariance.

The propagators are given by the inverse of the 2×2 self-energy matrix

$$\hat{D}^{-1} = \begin{pmatrix} q^2 + \Pi_{\gamma\gamma}(q^2) & \Pi_{\gamma\rho}(q^2) \\ \Pi_{\gamma\rho}(q^2) & q^2 - M_\rho^2 + \Pi_{\rho\rho}(q^2) \end{pmatrix} \quad (5.78)$$

and read

$$\begin{aligned}
 D_{\gamma\gamma} &= \frac{1}{q^2 + \Pi_{\gamma\gamma}(q^2) - \frac{\Pi_{\gamma\rho}^2(q^2)}{q^2 - M_\rho^2 + \Pi_{\rho\rho}(q^2)}} \\
 D_{\gamma\rho} &= \frac{-\Pi_{\gamma\rho}(q^2)}{(q^2 + \Pi_{\gamma\gamma}(q^2))(q^2 - M_\rho^2 + \Pi_{\rho\rho}(q^2)) - \Pi_{\gamma\rho}^2(q^2)} \\
 D_{\rho\rho} &= \frac{1}{q^2 - M_\rho^2 + \Pi_{\rho\rho}(q^2) - \frac{\Pi_{\gamma\rho}^2(q^2)}{q^2 + \Pi_{\gamma\gamma}(q^2)}}.
 \end{aligned} \quad (5.79)$$

Resonance parameters derive from the location s_P of the pole of the propagator

$$s_P - M_{\rho^0}^2 + \Pi_{\rho^0\rho^0}(s_P) - \frac{\Pi_{\gamma\rho^0}^2(s_P)}{s_P + \Pi_{\gamma\gamma}(s_P)} = 0, \quad (5.80)$$

with $s_P = \tilde{M}_{\rho^0}^2$ complex:

$$\tilde{M}_\rho^2 \equiv (q^2)_{\text{pole}} = M_\rho^2 - i M_\rho \Gamma_\rho. \quad (5.81)$$

By diagonalization the physical ρ acquires a direct coupling to the electron

$$\begin{aligned}\mathcal{L}_{\text{QED}} &= \bar{\psi}_e \gamma^\mu (\partial_\mu - i e_b A_{b\mu}) \psi_e \\ &= \bar{\psi}_e \gamma^\mu (\partial_\mu - i e A_\mu + i g_{\rho ee} \rho_\mu) \psi_e\end{aligned}\quad (5.82)$$

with $g_{\rho ee} = e(\Delta_\rho + \Delta_0)$, where

$$\Delta_0 = \frac{\Pi_{\gamma\rho}(0)}{M_\rho^2}; \quad \Delta_\rho = \frac{\text{Re}\Pi_{\gamma\rho}(M_\rho^2) - \Pi_{\gamma\rho}(0)}{M_\rho^2}.$$

For our model $\Delta_0 = 0$ and $\Delta_\rho = e/g_\rho$ to leading order.

$F_\pi(s)$ with $\rho - \gamma$ Mixing at One-Loop

The $e^+e^- \rightarrow \pi^+\pi^-$ matrix element in sQED is given by

$$\mathcal{M} = -i e^2 \bar{v}(p_2) \gamma^\mu u(p_1) (p_1 - p_2)_\mu F_\pi(q^2) \quad (5.83)$$

with $F_\pi(q^2) = 1$. In our extended VMD model we have four terms Fig. 5.32 and hence

$$F_\pi(s) \propto e^2 D_{\gamma\gamma} + e g_{\rho\pi\pi} D_{\gamma\rho} - g_{\rho ee} e D_{\rho\gamma} - g_{\rho ee} g_{\rho\pi\pi} D_{\rho\rho},$$

and properly normalized (VP subtraction: $e^2(s) \rightarrow e^2$) the undressed pion form factor is given by:

$$F_\pi(s) = [e^2 D_{\gamma\gamma} + e(g_{\rho\pi\pi} - g_{\rho ee}) D_{\gamma\rho} - g_{\rho ee} g_{\rho\pi\pi} D_{\rho\rho}] / [e^2 D_{\gamma\gamma}]. \quad (5.84)$$

Phenomenological constraints (see below) typically yield couplings

$$g_{\rho\pi\pi}^{\text{bare}} = 5.8935, \quad g_{\rho\pi\pi}^{\text{ren}} = 6.1559, \quad g_{\rho ee} = 0.018149, \quad x = g_{\rho\pi\pi}/g_\rho = 1.15128.$$

We note that the precise s -dependence of the effective ρ -width is obtained by evaluating the imaginary part of the ρ self-energy:

$$\text{Im} \Pi_{\rho\rho} = \frac{g_{\rho\pi\pi}^2}{48\pi} \beta_\pi^3 s \equiv M_\rho \Gamma_\rho(s), \quad (5.85)$$

which yields

$$\Gamma_\rho(s)/M_\rho = \frac{g_{\rho\pi\pi}^2}{48\pi} \beta_\pi^3 \frac{s}{M_\rho^2}; \quad \Gamma_\rho/M_\rho = \frac{g_{\rho\pi\pi}^2}{48\pi} \beta_\pi^3; \quad g_{\rho\pi\pi} = \sqrt{48\pi \Gamma_\rho / (\beta_\pi^3 M_\rho)}. \quad (5.86)$$

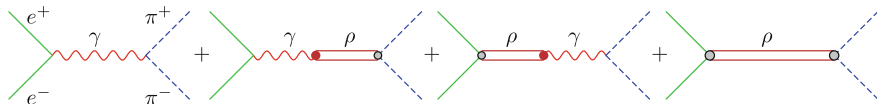


Fig. 5.32 Diagrams contributing to the process $e^+e^- \rightarrow \pi^+\pi^-$. One-loop self-energies of Fig. 5.31 are to be included

In our model, in the given approximation, the ρ on-shell form factor reads

$$F_\pi(M_\rho^2) = 1 - i \frac{g_{\rho ee} g_{\rho\pi\pi}}{e^2} \frac{M_\rho}{\Gamma_\rho} ; \quad |F_\pi(M_\rho^2)|^2 = 1 + \frac{36}{\alpha^2} \frac{\Gamma_{ee}}{\beta_\rho^3 \Gamma_\rho} , \quad (5.87)$$

$$\Gamma_{\rho ee} = \frac{1}{3} \frac{g_{\rho ee}^2}{4\pi} M_\rho ; \quad g_{\rho ee} = \sqrt{12\pi \Gamma_{\rho ee} / M_\rho} . \quad (5.88)$$

Note that there is no new parameter involved in this model, the only parameter which affects the $\rho^0 - \gamma$ mixing is $g_{\rho ee}$, which is entirely fixed by the electronic width $\Gamma_{\rho ee}$ of the ρ^0 .

Compared with the Gounaris–Sakurai (GS) formula

$$F_\pi^{\text{GS}}(s) = \frac{-M_\rho^2 + \Pi_{\rho\rho}^{\text{ren}}(0)}{s - M_\rho^2 + \Pi_{\rho\rho}^{\text{ren}}(s)} ; \quad \Gamma_{\rho ee}^{\text{GS}} = \frac{2\alpha^2 \beta_\rho^3 M_\rho^2}{9 \Gamma_\rho} (1 + d \Gamma_\rho / M_\rho)^2 , \quad (5.89)$$

we observe that the GS formula does not involve $g_{\rho ee}$ resp. $\Gamma_{\rho ee}$ in a direct way, as the normalization is fixed by applying an overall factor $1 + d \Gamma_\rho / M_\rho \equiv 1 - \Pi_{\rho\rho}^{\text{ren}}(0) / M_\rho^2 \simeq 1.089$ to enforce $F_\pi(0) = 1$, which in our approach is automatic by manifest gauge invariance.²²

In order to compare our “theory” with experimental $e^+e^- \rightarrow \pi^+\pi^-$ data we have to subtract from the data effects not included in our model. What we are interested in is the $I = 1$ component of the form factor, which is the part which can be confronted with results from τ -decay spectra. Our simple model does not include the isospin breaking $I = 0$ part, i.e. the $\omega \rightarrow \pi\pi$ contribution, and hence we have to perform comparisons with the $I = 1$ isovector part only. In standard parametrization based on the GS formula also higher resonances ρ' and ρ'' and even a ρ''' (e.g. in [26]) are taken into account, to represent the data by a fit and for extracting resonance parameters and their mixings [21, 26, 172]. By setting ω and higher ρ mixing amplitudes to zero in a fit, we obtain the parameters: $M_\rho = 775.5$ MeV, $\Gamma_\rho = 143.85$ MeV, $\mathcal{B}[(\rho \rightarrow ee)/(\rho \rightarrow \pi\pi)] = 4.67 \times 10^{-5}$, $e = 0.302822$, $g_{\rho\pi\pi} = 5.92$, $g_{\rho ee} = 0.01826$ from a fit to our model. For a detailed comparison the ratio:

$$r_{\rho\gamma}(s) \equiv \frac{|F_\pi(s)|^2}{|F_\pi(s)|_{D_{\gamma\rho}=0}^2} \quad (5.90)$$

is the precise measure for the so far unaccounted energy dependence of the $\rho - \gamma$ mixing. We have plotted it in Fig. 5.33. If mixing is not included in $F_0(s)$ already (as was standard in the past) the total correction formula to the spectral functions reads

$$v_0(s) = r_{\rho\gamma}(s) R_{\text{IB}}(s) v_-(s) \quad (5.91)$$

²²Note that electromagnetic gauge invariance is more than charge conservation $F_\pi(0) = 1$, and in fact the self-energy correction used in the standard GS formula does not respect gauge invariance [88].

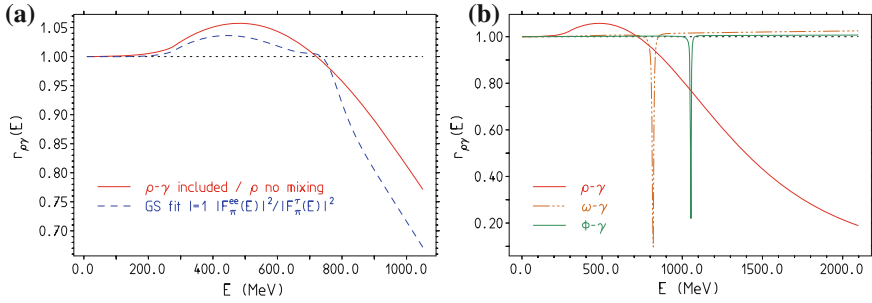


Fig. 5.33 **a** Ratio of $|F_\pi(E)|^2$ with mixing normalized to the no mixing case. The same ratio based on e^+e^- versus τ GS fits is also shown. $|F_\pi^{ee}(E)|^2$ I=1 part only, i.e. ω subtracted, no FSR and $|F_\pi^\tau(E)|^2$ after IB corrections, but without $\rho - \gamma$ mixing correction. **b** The same mechanism scaled up by the branching fraction $\Gamma_V/\Gamma(V \rightarrow \pi\pi)$ for $V = \omega$ and ϕ . In the $\pi\pi$ channel the effects for resonances $V \neq \rho$ are tiny if not very close to resonance

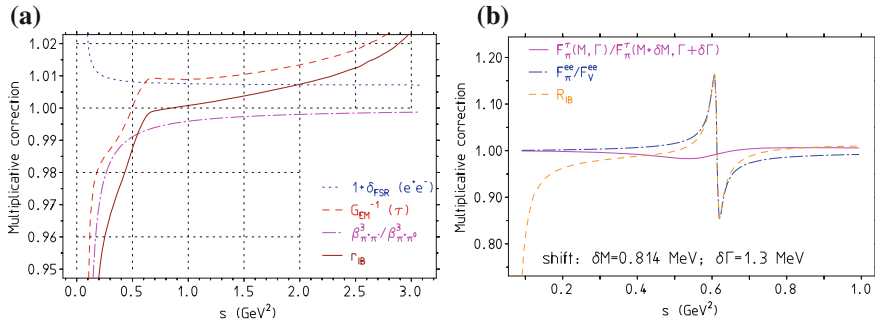


Fig. 5.34 Isospin breaking corrections. *Left* The final state radiation (FSR) contributing to $F_\pi^{ee}(s)$, τ -decay related photon radiation G_{EM}^{-1} , phase space correction $\beta_0^3/\beta_\pm^3(s)$ related to the pion mass difference, and the product of them r_{IB} . *Right* effects related to the shift in the ρ parameters, and from $\rho - \omega$ mixing, which contributes to the $I = 0$ part of $F_\pi^{ee}(s)$ (see also [171])

with

$$R_{IB}(s) = \frac{1}{G_{EM}(s)} \frac{\beta_0^3(s)}{\beta_\pm^3(s)} \left| \frac{F_0(s)}{F_-(s)} \right|^2 \quad (5.92)$$

given by (5.71). As discussed earlier $G_{EM}(s)$ is the electromagnetic radiative corrections, $\beta_0^3(s)/\beta_\pm^3(s)$ the phase space modification by the pion mass difference $m_{\pi^0} \neq m_{\pi^\pm}$ and $|F_0(s)/F_-(s)|^2$ includes shifts in masses, widths and correction due to $\rho - \omega$ mixing (Figs. 5.34, 5.35 and 5.36).

After subtracting final state radiation correction $\eta(s)$ (16), vacuum polarization effects $|\alpha/\alpha(s)|^2$ (16) and the $I = 0$ component represented by the $\rho - \omega$ mixing

Fig. 5.35 Total IB correction without and including the $\gamma - \rho$ mixing correction

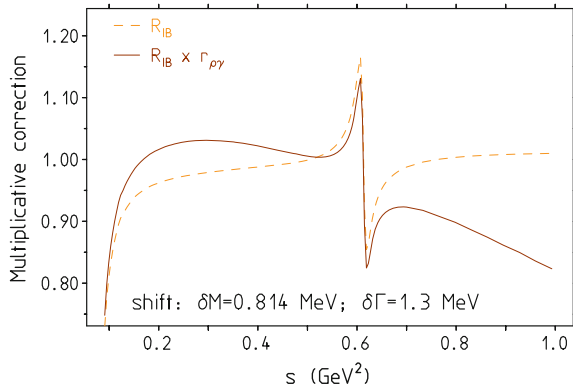
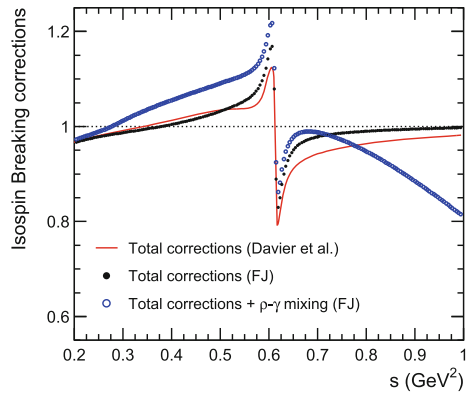


Fig. 5.36 Total IB correction to be applied to the τ decay spectra. Corrections applied by Davier et al. [129, 171] are compared with the corrections as discussed in the text (labeled FJ). Courtesy of Z. Zhang [171], <http://dx.doi.org/10.1051/epjconf/201611801036> (License: CC-BY-4.0)



(5.34) from the e^+e^- -data, we can compare isospin breaking corrected τ data with the e^+e^- data. In Fig. 5.37 we show the “data” normalized relative to a CMD-2 Gounaris–Sakurai fit.²³

Including the missing $\rho^0 - \gamma$ mixing effect clearly brings τ spectra into good agreement with the e^+e^- data. As illustrated in Fig. 5.33, in the vicinity of the ρ mass $r_{\rho\gamma}(s)$ can be mimicked by taking larger shifts of mass and width of the ρ as they are obtained by comparing the GS fits of the I=1 part of $F_{\pi}^{ee}(s)$ with the GS fit of $F_{\pi}^{\tau}(s)$ [114]. This however, is missing the true reason for the difference of the corresponding spectra, which resulted in the τ vs e^+e^- discrepancy.

Applications: a_{μ} and $B_{\pi\pi^0}^{\text{CVC}} = \Gamma(\tau \rightarrow \nu_{\tau}\pi\pi^0)/\Gamma_{\tau}$

How does the new correction affect the evaluation of the hadronic contribution to a_{μ} ? To lowest order in terms of e^+e^- -data, represented by $R(s)$, we have

$$a_{\mu}^{\text{had,LO}}(\pi\pi) = \frac{\alpha^2}{3\pi^2} \int_{4m_{\pi}^2}^{\infty} \frac{ds}{s} R_{\pi\pi}^{(0)}(s) K(s) , \tag{5.93}$$

²³The choice of the normalizing function is arbitrary, in particular at higher energies as there are no CMD-2 data above about 1 GeV.

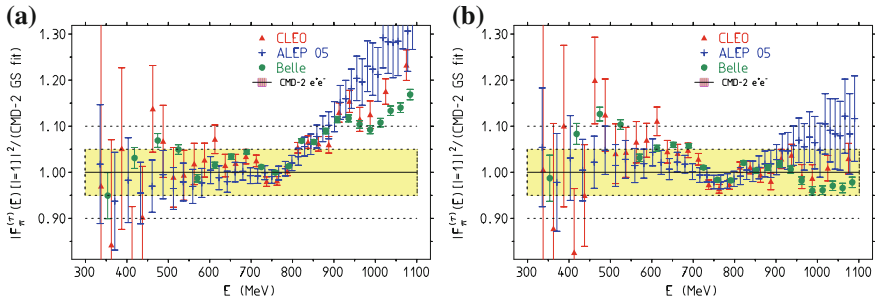


Fig. 5.37 $|F_\pi(E)|^2$ in units of $e^+e^- I = 1$ (CMD-2 GS fit): **a** τ data uncorrected for $\rho - \gamma$ mixing, and **b** after correcting for mixing

with the well-known kernel $K(s)$ and

$$R_{\pi\pi}^{(0)}(s) = (3s\sigma_{\pi\pi})/(4\pi\alpha^2(s)) = 3v_0(s) .$$

Note that the $\rho - \gamma$ interference is included in the measured e^+e^- -data, and so it is part of the contribution to a_μ^{had} , as it has to be. In fact a_μ^{had} is an intrinsically e^+e^- -based “observable” i.e. a neutral current channel quantity.

How to utilize τ data as an enhancement of the e^+e^- data set? In addition to applying the standard CVC violating corrections $v_-(s) \rightarrow v_0(s) = R_{\text{IB}}(s) v_-(s)$ we now have to include the new $\rho - \gamma$ correction

$$v_-(s) \rightarrow v_0(s) = r_{\rho\gamma}(s) R_{\text{IB}}(s) v_-(s) \quad (5.94)$$

As a result for the $I=1$ part of $a_\mu^{\text{had}}[\pi\pi]$ we find

$$\delta a_\mu^{\text{had}}[\rho\gamma] \simeq (-5.1 \pm 0.5) \times 10^{-10} . \quad (5.95)$$

as a correction applied for the range $[0.63, 0.96]$ GeV. The correction is not too large, but at the level of 1σ and thus non-negligible. Indeed the discrepancy between τ based and e^+e^- based evaluations is removed, as [88]:

$$\begin{aligned} a_\mu^{\text{had}}[ee \rightarrow \pi\pi] &= 353.82(0.88)(2.17)[2.34] \times 10^{-10} \\ a_\mu^{\text{had}}[\tau \rightarrow \pi\pi\nu] &= 354.25(1.24)(0.61)[1.38] \times 10^{-10} \\ a_\mu^{\text{had}}[ee + \tau] &= 354.14(0.82)(0.86)[1.19] \times 10^{-10} , \end{aligned}$$

which improves the LO HVP as given in (5.29).

An important independent cross-check is provided by the $\tau \rightarrow \pi^0 \pi \nu_\tau$ branching fraction $B_{\pi\pi^0} = \Gamma(\tau \rightarrow \nu_\tau \pi \pi^0)/\Gamma_\tau$, another key quantity which can be directly measured. This “ τ -observable”, a genuine charged channel quantity, can be evaluated in terms of the $I = 1$ part of the $e^+e^- \rightarrow \pi^+\pi^-$ cross section, after taking into

account the IB correction

$$v_0(s) \rightarrow v_-(s) = v_0(s) / (R_{\text{IB}}(s) r_{\rho\gamma}(s)) . \quad (5.96)$$

i.e. here we have to “undo” the $\rho^0 - \gamma$ mixing in the e^+e^- data, which is absent in the charged isovector channel. The branching fraction is thus given by

$$B_{\pi\pi^0}^{\text{CVC}} = \frac{2S_{\text{EW}} B_e |V_{ud}|^2}{m_\tau^2} \int_{4m_\pi^2}^{m_\tau^2} ds R_{\pi^+\pi^-}^{(0)}(s) \left(1 - \frac{2}{m_\tau^2}\right)^2 \left(1 + \frac{2s}{m_\tau^2}\right) \frac{1}{r_{\rho\gamma}(s) R_{\text{IB}}(s)} , \quad (5.97)$$

The shift we find is

$$\delta B_{\pi\pi^0}^{\text{CVC}}[\rho\gamma] = +0.62 \pm 0.06 \% \quad (5.98)$$

a remarkable shift, which again eliminates the former clash: τ data combined $B_{\pi\pi^0} = 25.3 \pm 0.1$ versus $e^+e^- + \text{CVC } ee$ data combined $B_{\pi\pi^0}^{\text{CVC}} = 24.6 \pm 0.3 \xrightarrow{\rho\gamma} 25.2 \pm 0.3$ in good agreement. Altogether we can say that the $\rho - \gamma$ mixing at one-loop perfectly matches the pattern of the τ versus e^+e^- puzzle, and thus removes it.

One question remains though: is our model, assuming point-like pions, realistic? There is no doubt it works at low energies when photons are relatively soft. Scalar QED in fact has been utilized to account for radiative corrections involving the charged pions in the final state, like the FSR correction (5.128), (5.129). Direct experimental studies of the FSR spectrum at intermediate energies are poorly available [173–175], and as far as studies exist they seem to support sQED [60, 176], which however, obviously has to break down in the hard photon regime. Here, di-pion production in $\gamma\gamma$ fusion is able to shed more light on that problem. Di-pion production cross sections are available from Crystal Ball, Mark II, JADE, PLUTO, CELLO and Belle [177–184]. The processes $\gamma\gamma \rightarrow \pi^+\pi^-$ and $\gamma\gamma \rightarrow \pi^0\pi^0$ provide an excellent laboratory to study scalar excitations a_0, f_0', f_0, \dots and their properties [185–189]. They also play a role in the context of hadronic light-by-light scattering as we will see later. In Fig. 5.38 we see that at low energies photons see the pions. The $\pi^+\pi^-$ cross section is large at threshold while the $\pi^0\pi^0$ one is tiny. Photons do not see the composite structure if they are not hard enough. The $\pi^0\pi^0$ final state is then available via strong rescattering only (see Fig. 5.39). As the energy of the $\pi\pi$ system increases the strong tensor meson resonance $f_2(1270)$ shows up in both the charged and the neutral channels. Rates only differ by the isospin weight factor 2. Apparently now photons directly probe the quarks. Figure 5.38 also illustrated that utilizing isospin relations to evaluate missing contributions to $a_\mu^{\text{had,LO}}$ from unseen channels may be rather misleading, since we are dealing with hadron production mediated by one photon exchange and electromagnetic interaction obviously can violate isospin by close to 100%.

What do we learn? (i) photons seem to see pions below 1 GeV; (ii) photons definitely look at the quarks in and above the $f_2(1270)$ resonance region. Above we applied sQED up to 0.975 GeV, the most relevant region for determining a_μ . Therefore our model should be pretty reliable. Nevertheless, to be on the conservative side we

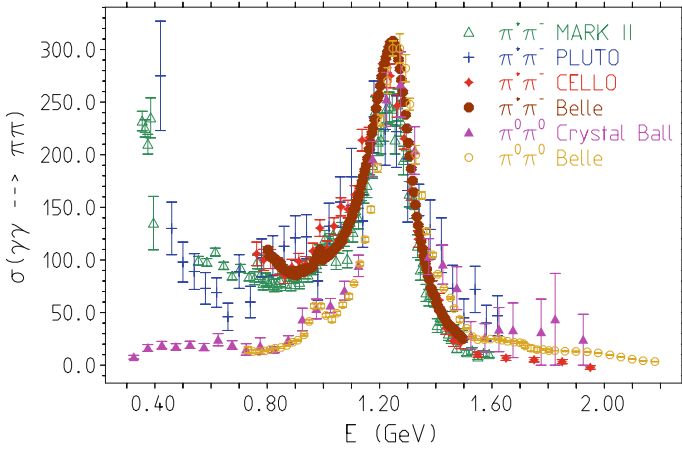


Fig. 5.38 How do photons couple to pions? This is obviously probed in reactions like $\gamma\gamma \rightarrow \pi^+\pi^-, \pi^0\pi^0$. Data infer that below about 1 GeV photons couple to pions as point-like objects (i.e. to the charged ones overwhelmingly), at higher energies the photons see the quarks exclusively and form the prominent tensor resonance $f_2(1270)$. The $\pi^0\pi^0$ cross section in this figure is enhanced by the isospin symmetry factor 2, by which it is reduced in the true data

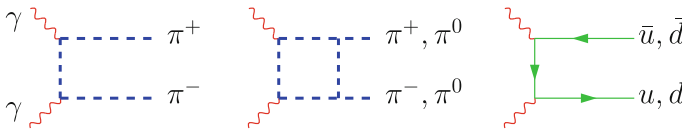


Fig. 5.39 Di-pion production in $\gamma\gamma$ fusion. At low energy we have direct $\pi^+\pi^-$ production and by strong rescattering $\pi^+\pi^- \rightarrow \pi^0\pi^0$, however with very much suppressed rate. With increasing energy, above about 1 GeV, the strong $q\bar{q}$ resonance $f_2(1270)$ appears produced equally at expected isospin ratio $\sigma(\pi^0\pi^0)/\sigma(\pi^+\pi^-) = \frac{1}{2}$. This demonstrates convincingly that we may safely work with point-like pions below 1 GeV

assume a 10% model uncertainty of the correction. One thing should be clear, not taking into account properly the electromagnetic interaction of pions, is definitely not a realistic approximation in trying to describe what we see in $e^+e^- \rightarrow \pi^+\pi^-$.

There is another important check of our result, namely, a comparison of the $\pi\pi$ rescattering as obtained in our model with the one obtained by Colangelo, Leutwyler in their “from first principles approach” which we described at the end of the previous subsection. One of the key ingredients in this approach is the strong interaction phase shift $\delta_1^1(s)$ of $\pi\pi$ (re)scattering in the final state. We compare the phase of $F_\pi(s)$ in our model with the one obtained by solving the Roy equation with $\pi\pi$ -scattering data as input. We notice that the agreement is surprisingly good up to about 1 GeV as shown in Fig. 5.40. It is not difficult to replace our phase by the more precise exact one. As a main conclusion we can say that using properly corrected τ spectral data yield the same result as the e^+e^- data and we can actually combine and hence improve the results: in view of the observed discrepancies in the $e^+e^- \rightarrow \pi\pi$ data

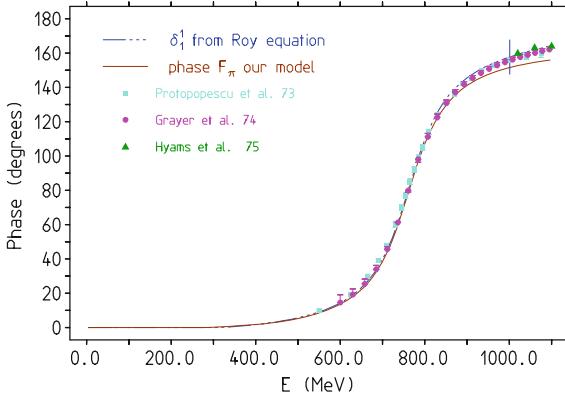


Fig. 5.40 The phase of $F_\pi(E)$ as a function of the c.m. energy E . We compare the result of the elaborate Roy equation analysis of [120, 121, 147] with the one due to the sQED pion-loop. The solution of the Roy equation depends on the normalization at a high energy point (typically 1 GeV). In our calculation we could adjust it by varying the coupling $g_{\rho\pi\pi}$. Data from [144–146]

from BaBar and KLOE it is certainly a good idea to take $\tau \rightarrow \pi\pi\nu_\tau$ data information into account, and we will take our best estimate

$$a_\mu^{\text{had}(1)} = (688.77 \pm 3.38) \times 10^{-10}, \quad (5.99)$$

which is based on a direct integration of all available $e^+e^- \rightarrow \text{hadrons}$, as well as the IB and $\gamma - \rho$ mixing corrected $\tau^\pm \rightarrow \pi^\pm\pi^0\nu_\tau$ -data in the range 0.63–0.96 GeV plus pQCD for the perturbatively save region between 5.2 and 9.46 GeV and for the high energy tail above 11.5 GeV. Taking into account the improvement obtained in [122], by using the precise $\pi\pi$ scattering phase shift data [144–146] to constrain $|F_\pi|^2$ below 0.63 GeV (see (5.36)) one obtains

$$a_\mu^{\text{had}(1)} = (689.46 \pm 3.25) \times 10^{-10}, \quad (5.100)$$

as a best estimate.

The recent analysis [92] reports 516.2 ± 3.5 for $e^+e^- + \tau$ in comparison to 506.9 ± 2.6 for e^+e^- for the range from threshold to 1.8 GeV. As below about 1 GeV the $\gamma - \rho$ mixing correction can be evaluated reliably via (5.95), it is determined by the electronic width of the ρ solely, we get 511.1 ± 3.5 and $a_\mu^{\text{had}/\text{LO}} = 692.6 \pm 3.3 \times 10^{-10}$ for e^+e^- [92] becomes $a_\mu^{\text{had}/\text{LO}} = 696.8 \pm 4.0 \times 10^{-10}$ for $e^+e^- + \tau$ after the $\gamma - \rho$ mixing correction.

We understand the EFT “VMD+sQED” as the low energy tail of the more appropriate resonance Lagrangian approach [134] or alternatives like the HLS model, which attempts to treat the spin 1 resonances ρ^\pm, ρ^0, ω and ϕ in a similar way as the massive gauge bosons W^\pm and Z in the electroweak SM (see below). Once more a systematic Lagrangian quantum field theory approach turns out to provide a

Table 5.6 Results for $a_\mu^{\text{had}} \times 10^{10}$ obtained by combining information from $\tau \rightarrow \pi\pi\nu_\tau$ decays in order to improve the evaluation of $a_\mu^{\text{had}(1)}$. Uncertainties given are the statistical, systematic and the total ones

a_μ^{had} contribution	Energy range	Result	(Stat)	(Syst)	[Tot]
$\pi\pi$ -data $e^+e^- I = 1$	(0.63, 0.96) GeV	353.82	(0.88)	(2.17)	[2.34]
$\pi\pi$ -data τ	(0.63, 0.96) GeV	354.25	(1.24)	(0.61)	[1.38]
$\pi\pi (I = 1) ee + \tau$	(0.63, 0.96) GeV	354.14	(0.82)	(0.86)	[1.19]
Total e^+e^-	(m_π, ∞)	687.04	(1.12)	(4.06)	[4.21]
Total $e^+e^- + \tau$	(m_π, ∞)	687.74	(0.83)	(3.34)	[3.44]

more reliable framework for understanding particle physics processes, while the relatively ad hoc phenomenological models, like the Gounaris–Sakurai ansatz, easily can miss some important effects.²⁴ Taking into account one-loop self-energy corrections systematically is mandatory and leads to substantial quantum interference effects. Equally important is the proper energy dependence of amplitudes off the resonances, which automatically implies decoupling of heavier states and a better match to a high energy behavior in accord with QCD.

Furthermore, we note that the $\rho - \gamma$ correction function $r_{\rho\gamma}(s)$ entirely fixed from neutral channel, which means that the τ data indeed provide independent additional information on the pion form factor. We now have a fairly reliable model to include τ data to improve a_μ^{had} and there is no τ versus e^+e^- alternative of a_μ^{had} . Result given in [88] are included in Fig. 7.2.

Extended Models: Resonance Lagrangian Approach and Global Fit Strategies

Including $\omega, \phi, \rho', \rho'', \dots$ requires to go to low-energy effective chiral Lagrangians with vector mesons [134, 135]. The resonance Lagrangian approach (RLA) provides an extension of low energy effective QCD as represented by chiral perturbation theory (CHPT) to energies up to about 1 GeV. Principles to be included are the chiral structure of QCD, the vector-meson dominance (VMD) model and electromagnetic gauge invariance. Specifically, we will consider the hidden local symmetry (HLS) version [190, 191], which is considered to be equivalent to alternative variants after implementing appropriate high energy asymptotic conditions [135, 192]. CHPT is the systematic and unambiguous approach to low energy effective QCD given by spontaneously broken chiral symmetry $SU(3) \otimes SU(3)$, with the pseudoscalars as Nambu-Goldstone bosons, together with a systematic expansion in low momenta and chiral symmetry breaking (SB) effects by the light quark masses, $m_q, q = u, d, s$. The limitation of CHPT is the fact that it ceases to converge for energies above about

²⁴We note that so far PDG parameters, masses, widths, branching fractions etc. of resonances like the ρ^0 are all extracted from data assuming GS like form factors or just some form of Breit–Wigner shapes and thus in general are model dependent!.

400 MeV, in particular it lacks to describe physics involving the vector resonances ρ , ω and ϕ .

The VMD is the effective theory implementing the direct coupling of the neutral spin 1 vector resonances ρ , ω , ϕ etc. to the photon. Such direct couplings are a consequence of the fact that the neutral spin 1 resonances like the ρ^0 are composed of charged quarks. The effect is well modeled by the VMD Lagrangian $\mathcal{L}_{\gamma\rho} = \frac{e}{2g_\rho} \rho_{\mu\nu} F^{\mu\nu}$ or $= -\frac{eM_\rho^2}{g_\rho} \rho_\mu A^\mu$, which has to be implement in low energy effective QCD in a way which is consistent with the chiral structure of QCD.

The construction of the HLS model may be outlined as follows: like in CHPT the basic fields are the unitary matrix fields $\xi_{L,R} = \exp[\pm i P/f_\pi]$, where $P = P_8 + P_0$ is the $SU(3)$ matrix of pseudoscalar fields, with P_0 and P_8 the basic singlet and octet fields, respectively. The pseudoscalar field matrix P is represented by

$$P_8 = \frac{1}{\sqrt{2}} \begin{pmatrix} \frac{1}{\sqrt{2}}\pi_3 + \frac{1}{\sqrt{6}}\eta_8 & \pi^+ & K^+ \\ \pi^- & -\frac{1}{\sqrt{2}}\pi_3 + \frac{1}{\sqrt{6}}\eta_8 & K^0 \\ K^- & \bar{K}^0 & -\sqrt{\frac{2}{3}}\eta_8 \end{pmatrix}, \quad (5.101)$$

$$P_0 = \frac{1}{\sqrt{6}} \text{diag}(\eta^0, \eta^0, \eta^0); \quad (\pi_3, \eta_8, \eta_0) \Leftrightarrow (\pi^0, \eta, \eta'). \quad (5.102)$$

The HLS ansatz is an extension of the CHPT *non-linear sigma model* to a *non-linear chiral Lagrangian* $[\text{Tr } \partial_\mu \xi^\pm \partial^\mu \xi]$ based on the symmetry pattern $G_{\text{global}}/H_{\text{local}}$, where $G = SU(3)_L \otimes SU(3)_R$ is the chiral group of QCD and $H = SU(3)_V$ the vector subgroup. The hidden local $SU(3)_V$ requires the spin 1 vector meson fields, represented by the $SU(3)$ matrix field V_μ , to be gauge fields. The needed covariant derivative reads $D_\mu = \partial_\mu - i g V_\mu$, and allows to include the couplings to the electroweak gauge fields A_μ , Z_μ and W_μ^\pm in a natural way. The vector field matrix is usually written as

$$V = \frac{1}{\sqrt{2}} \begin{pmatrix} (\rho^I + \omega^I)/\sqrt{2} & \rho^+ & K^{*+} \\ \rho^- & (-\rho^I + \omega^I)/\sqrt{2} & K^{*0} \\ K^{*-} & \bar{K}^{*0} & \phi^I \end{pmatrix}. \quad (5.103)$$

The unbroken HLS Lagrangian is then given by

$$\mathcal{L}_{\text{HLS}} = \mathcal{L}_A + \mathcal{L}_V; \quad \mathcal{L}_{A/V} = -\frac{f_\pi^2}{4} \text{Tr} [L \pm R]^2, \quad (5.104)$$

where $L = [D_\mu \xi_L] \xi_L^\dagger$ and $R = [D_\mu \xi_R] \xi_R^\dagger$. The covariant derivatives read

$$\begin{cases} D_\mu \xi_L = \partial_\mu \xi_L - i g V_\mu \xi_L + i \xi_L \mathcal{L}_\mu \\ D_\mu \xi_R = \partial_\mu \xi_R - i g V_\mu \xi_R + i \xi_R \mathcal{R}_\mu \end{cases}, \quad (5.105)$$

with known couplings to the Standard Model (SM) gauge bosons

$$\begin{cases} \mathcal{L}_\mu = eQA_\mu + \frac{g_2}{\cos\theta_W}(T_z - \sin^2\theta_W)Z_\mu + \frac{g_2}{\sqrt{2}}(W_\mu^+T_+ + W_\mu^-T_-) \\ \mathcal{R}_\mu = eQA_\mu - \frac{g_2}{\cos\theta_W}\sin^2\theta_W Z_\mu . \end{cases} \quad (5.106)$$

Like in the electroweak SM, masses of the spin 1 bosons may be generated by the Higgs-Kibble mechanism if one starts in place of the non-linear σ -model with the Gell-Mann–Levy linear σ -model by a shift of the σ -field.

In fact the global chiral symmetry G_{global} is well known not to be realized as an exact symmetry in nature, which implies that the ideal HLS symmetry evidently is not a symmetry of nature either. It evidently has to be broken appropriately in order to provide a realistic low energy effective theory mimicking low energy effective QCD. Corresponding to the strength of the breaking, usually, this is done in two steps, breaking of $SU(3)$ in a first step and breaking the isospin $SU(2)$ subgroup in a second step. Unlike in CHPT (perturbed non-linear σ -model) where one is performing a systematic low energy expansion, expanding in low momenta and the quark masses, here we introduce symmetry breaking as a phenomenological pattern with parameters to be fixed from appropriate data, since a systematic low energy expansion a lá CHPT ceases to converge at energies above about 400 MeV, while we attempt to model phenomenology up to including the ϕ resonance.

The broken HLS Lagrangian (BHLS) is then given by (see [132])

$$\mathcal{L}_{\text{BHLS}} = \mathcal{L}'_A + \mathcal{L}'_V + \mathcal{L}'_{\text{tHooft}} ; \quad \mathcal{L}'_{A/V} = -\frac{f_\pi^2}{4} \text{Tr} \{ [L \pm R] X_{A/V} \}^2 , \quad (5.107)$$

with 6 phenomenological chiral SB parameters. The phenomenological SB pattern suggests $X_I = \text{diag}(q_I, y_I, z_I)$, $|q_I - 1|, |y_I - 1| \ll |z_I - 1|$, $I = V, A$. There is also the parity odd anomalous sector, which is needed to account for reactions like $\gamma^* \rightarrow \pi^0\gamma$ and $\gamma^* \rightarrow \pi^+\pi^-\pi^0$ among others.

We note that this BHLS model would be a reliable low energy effective theory if the QCD scale Λ_{QCD} would be large relative to the scale of about 1 GeV up to which we want to apply the model, which in reality is not the case. Nevertheless, as a phenomenological model applied to low multiplicity hadronic processes (specified below) it seems to work pretty well, as we have demonstrated by a global fit of the available data in [132]. The major achievement is a simultaneous consistent fit of the $e^+e^- \rightarrow \pi^+\pi^-$ data from CMD-2 [21], SND [22], KLOE [23–25], BaBar [26] and BES-III [27], and the $\tau \rightarrow \pi^-\pi^0\nu_\tau$ decay spectral functions by ALEPH [123], OPAL [125], CLEO [126] and Belle [127]. The $e^+e^- \rightarrow \pi^-\pi^+$ channel gives the dominant hadronic contribution to the muon $g - 2$. Isospin symmetry $\pi^-\pi^0 \Leftrightarrow \pi^-\pi^+$ allows one to include existing high quality τ -data as advocated long time ago in [11].

We note that as long as higher order corrections are restricted to the mandatory pion- and Kaon-loop effects in the vector boson self-energies, renormalizability is

not an issue. These contributions behave as in a strictly renormalizable theory and correspond to a reparametrization only.

A suitable extension of the HLS model which covers most channels in the range up to just above the ϕ resonance has been worked out and has been applied for an evaluation of a_μ^{had} in [132, 193, 194]. The idea is to constrain the effective Lagrangian by fitting available data from all possible channels. Thereby uncertainties may be reduced by consistency with effective field theory concepts. In [132] 45 different data sets in the range up to $E_0 = 1.05$ GeV (6 annihilation channels and 10 partial width decays) are used to constrain the effective Lagrangian couplings. The phenomenologically constrained effective theory then is applied to predict the cross sections for the channels $\pi^+\pi^-$, $\pi^0\gamma$, $\eta\gamma$, $\eta'\gamma$, $\pi^0\pi^+\pi^-$, K^+K^- , $K^0\bar{K}^0$, which account for 83.4% of a_μ^{had} . The missing part, the channels 4π , 5π , 6π , $\eta\pi\pi$, $\omega\pi$ and the energy range $E > E_0$ is evaluated using data directly and pQCD for perturbative regions and the tail. As we know, including self-energy effects is mandatory. They affect the neutral channel mixing between γ , ρ^0 , ω and ϕ as dynamical effects and provide the proper decay widths with proper phase space and energy dependence etc.

In the region covered by the HLS model the leading order HVP is obtained by summing over the channels:

$$\begin{cases} a_\mu^{\text{had}}[\text{HLS}] = \sum_i a_\mu(H_i) \\ a_\mu(H_i) = \frac{1}{4\pi^3} \int_{s_{H_i}}^{s_{\text{cut}}} ds K(s) \sigma_{H_i}(s) \end{cases}, \quad (5.108)$$

which relates the hadronic intermediate state contributions $\{H_i, i = 1 \dots n\}$ to the annihilation cross sections $\sigma(e^+e^- \rightarrow H_i) \equiv \sigma_{H_i}(s)$. $K(s)$ is the known kernel which is enhancing the weight of the threshold region between s_{H_i} and $s_{\text{cut}} = (1.05 \text{ GeV})^2$. The full LO a_μ^{had} is obtained by adding to $a_\mu^{\text{had}}[\text{HLS}]$ the missing channels below 1.05 GeV, plus the remainder from energies above the model breakpoint, obtained by the standard approach (see [47] for details).

According to [132] the method indeed works in reducing uncertainties by using indirect constraints. This approach is able to reveal inconsistencies in the data. A key point is that no inconsistencies between τ data and e^+e^- data show up. In contrary τ data, which are not subject to complicated mixing effects, help to fix more precisely the Lagrangian couplings and thus allow to reduce uncertainties of the predictions. We have included the result of this global fit in Fig. 7.2. Typically, some data sets get low weight as they conflict with the HLS global fit. This in particular concerns the BaBar di-pion data which after taking into account standard IB corrections seem to agree well with the Belle τ -spectra, while not accounted for neutral channel mixing effects, like $\gamma - \rho^0$ mixing, predict a substantial difference. As BaBar data treated with equal weight enhance the contribution to a_μ^{had} by about $\delta a_\mu^{\text{had}} \simeq 6 \times 10^{-10}$ the HLS fit reduces this enhancement and yields a lower central value at reduced uncertainty, which enhances the significance of $\delta a_\mu = a_\mu^{\text{exp}} - a_\mu^{\text{the}}$ to a 4–5 σ deviation.

Important points to notice from the global HLS fit: one obtains very accurate fits up to 1.05 GeV without including any higher resonances. A possible shift between the masses of the ρ^\pm and the ρ^0 is consistent with zero as well as with a shift $\delta M = 0.814$ GeV, which one obtains by assuming the leading electromagnetic shift of the mass squares (Cottingham formula) to be spin independent, i.e.,

$$M_{\rho^\pm}^2 - M_{\rho^0}^2 \approx m_{\pi^\pm}^2 - m_{\pi^0}^2 . \tag{5.109}$$

In any case singling out phenomenologically a viable effective resonance Lagrangian by global fits is expected to help in improving EFT calculations of hadronic light-by-light scattering (see Sect. 5.2 below).

Concluding remark: it should be mentioned here that the τ vs e^+e^- problem, which lead to inconsistent results between the charged channel isovector τ -decay spectral functions and the e^+e^- cross sections [113, 129, 171], has been solved [6, 88, 132]. The origin of the problem has been unaccounted mixing effects between the ρ^0 and the γ mainly, an effect which is absent in the charged channel but has to be corrected for. If done properly τ data may be included and are consistent with the e^+e^- data. The quality of the consistency is illustrated in Fig. 5.41, which displays the fit of the τ -spectral functions only, supplemented by the isospin breaking effects (with the latter provided by the review of particle properties (RPP) [42]) in comparison with the $e^+e^- \rightarrow \pi^+\pi^-$ spectra. There exist a number of other analyses [195–198], (see [199, 200] for an early outline of the method) which we have not discussed. One should keep in mind that the following schemes have **no** justification:

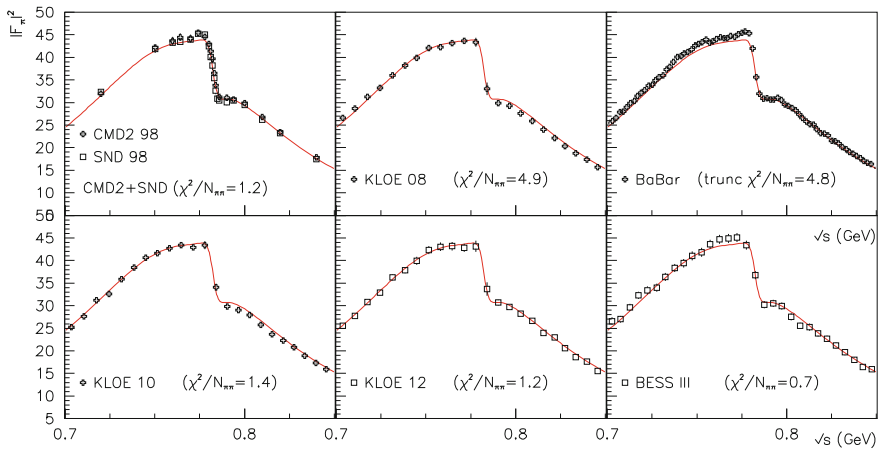
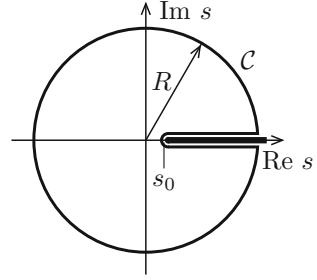


Fig. 5.41 Comparing the τ +PDG prediction (red curve) of the pion form factor in e^+e^- annihilation in the $\rho - \omega$ interference region. Reprinted from [47], <http://dx.doi.org/10.1140/epjc/s10052-015-3830-x> (License: CC-BY-4.0)

Fig. 5.42 Integral contour

- $\sigma_{\text{had}} = \sigma_{\text{pQCD}} + \sigma_{\text{resonances}}$
- local duality: i.e., duality (5.5) applied to relatively narrow energy intervals (resonance regions).

There are also some pitfalls in the use of dispersion relations. Often one encounters arguments of the following type: consider a function, like $\Pi'_{\text{ren}}(s) = \Delta\Pi'(s) = \Pi'(s) - \Pi'(0)$ in our case, which is an analytic function order by order in perturbation theory. Analyticity then infers that the contour integral along a path shown in Fig. 5.42 vanishes. Considering $f(s) \equiv K(s)\Delta\Pi'(s)$, where $K(s)$ is an analytic kernel function, such the $f(s)$ is analytic, then by *Cauchy's theorem* on the one hand we have

$$f(0) = \frac{1}{\pi} \int_{4m_\pi^2}^{\mu_0^2} \frac{ds}{s - i\epsilon} \text{Im } f(s) + \frac{1}{2\pi i} \oint_{|s|=\mu_0^2} \frac{ds}{s} f(s), \quad (5.110)$$

and by the *optical theorem* on the other hand, with $(s = \mu_0^2 e^{i\theta})$ and

$$R(s) = \frac{1}{2\pi i} \lim_{\epsilon \rightarrow 0_+} [\Pi'(s + i\epsilon) - \Pi'(s - i\epsilon)],$$

we have

$$f(0) = \frac{1}{12\pi^2} \int_{4m_\pi^2}^{\mu_0^2} \frac{ds}{s} K(s) R(s) + \frac{1}{2\pi} \int_0^{2\pi} d\theta f(\theta). \quad (5.111)$$

Therefore, for the renormalized VP function $f(s) = \Delta\Pi'(s)$, in particular, with $f(0) = 0$ we get

$$\int_{\text{cut}} \frac{ds}{s} \Delta\Pi'(s) = - \int_{\text{circle}} \frac{ds}{s} \Delta\Pi'(s), \quad (5.112)$$

and for a large enough circle one is tempted to apply pQCD on the right hand side and thus obtain the integral of our interest, which exhibits the non-perturbative physics. What is usually forgotten is that the uncertainty is of the order of $\delta = 2\pi R\varepsilon$ with ε being the small error expected from the truncation of the perturbative series. δ easily can turn out to be large (due to R large) such that we are not able to make a safe estimate for the wanted integral. Since analyticity is true order by order in perturbation theory, we precisely reproduce the perturbative answer for the left hand side if we use perturbation theory on the right hand side. Taking into account $\Pi_\gamma^{\text{NP}}(s)$ in (5.22), known as an asymptotic OPE only, based on not too well constrained condensates does not make the estimate much more reliable (see Sect. 5.1.6). Also, it is not true that from the asymptotic expansion of a function one can get back the original function via this approach. While analyticity is a very powerful theoretical concept it is difficult to be applied in numerical problems, because, small perturbations in one place typically cause large variations at remoter locations. In any case, non-perturbative physics cannot be accessed in this way in terms of the perturbative QCD expansion.

In this context, exploiting analyticity, other tricks have been advocated in [196]: splitting off the most problematic low energy part of the dispersion integral (the remainder estimated by standard means)

$$a_\mu^{\text{had,LO}}(s_1) = \int_0^{s_1} \tilde{K}(s)R(s) ds , \quad (5.113)$$

and noting (see Sect. 3.7) that $R(s) = 12\pi \text{Im } \hat{\Pi}'_\gamma(s)$ and $2i \text{Im } \Pi(s) = \Pi(s + i\varepsilon) - \Pi(s - i\varepsilon)$ on the cut yields $\Pi(s)$ away from the cut. By Cauchy's theorem

$$\int_0^{s_1} p(s)R(s) ds - 6\pi i \oint_{|s|=s_1} p(s)\hat{\Pi}'_\gamma(s) ds = 0 , \quad (5.114)$$

where $p(s)$ is an arbitrary analytic function. Therefore,

$$a_\mu^{\text{had,LO}}(s_1) = \int_0^{s_1} [\tilde{K}(s) - p(s)]R(s) ds + 6\pi i \oint_{|s|=s_1} p(s)\hat{\Pi}'_\gamma(s) ds . \quad (5.115)$$

We know that in the region between 1 and 2 GeV $R(s)$ extracted from the available e^+e^- data still carries large uncertainties, which limits an accurate evaluation of (5.113). Reference [196] advocates to fix $p(s)$ such that the contribution from this region gets minimized by minimizing

$$\text{Max} \left| \frac{\tilde{K}(s) - p(s)}{\tilde{K}(s)} \right| , \quad \sqrt{s} \in I \equiv [1 \text{ GeV}, 1.8 \text{ GeV}] \quad (5.116)$$

on the expense of an extra contribution from the circle. In [196] $p(s)$ is chosen to be of the form $p(s) = a + bs$ and on the circle $\hat{\Pi}'_\gamma(s)|_{|s|=s_1}$ is approximated by $\Pi_{\text{OPE}}(s)$ which is proportional to (5.22) (see Sect. 5.1.6): $e^2 \Pi_{\text{OPE}}(s) = \Pi'_\gamma{}^{\text{NP}}(s = -Q^2)$. By this the available information on $R(s)$ in the interval I gets erased (suppressed by a factor 2.5) and gets transported onto the circle as a weight factor which multiplies Π_{OPE} , a quantity which is not well determined as we learn from Fig. 5.18 and the discussion there. Even so the information on $R(s)$ in the interval I is unsatisfactory, it is hard to believe that suppressing the available true information at the end should provide a more reliable estimate of $a_\mu^{\text{had,LO}}(s_1)$.

5.1.12 Hadronic Higher Order Contributions

At next-to-leading (NLO) order, $O(\alpha^3)$, there are several classes of hadronic contributions with typical diagrams shown in Fig. 5.43. They have been estimated first in [105]. Classes (a) to (c) involve leading HVP insertions and may be treated using DRs together with experimental e^+e^- -annihilation data. Class (d) involves leading QED corrections of the charged hadrons and related problems were discussed at the end of Sect. 5.1.7 on p. 379, already. The last class (e) is a new class of non-perturbative contributions, the *hadronic light-by-light scattering* which is constrained by experimental data only for one exceptional line of phase space. The evaluation of this contribution is particularly difficult and it will be discussed in the next section.

The $O(\alpha^3)$ hadronic contributions from classes (a), (b) and (c) may be evaluated without particular problems as described in the following.

At the three-loop level all diagrams of Fig. 4.3 which involve closed muon-loops are contributing to the hadronic corrections when at least one muon-loop is replaced by a quark-loop dressed by strong interactions mediated by virtual gluons.

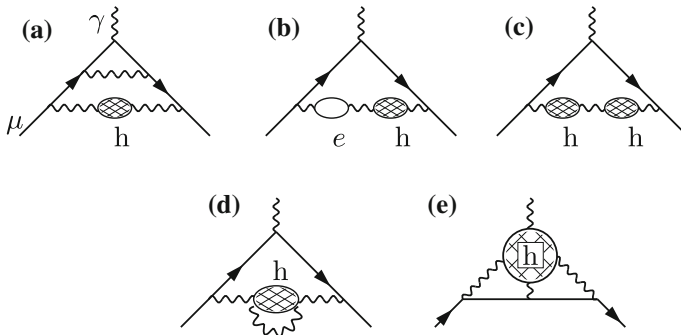


Fig. 5.43 Hadronic higher order contributions: **a–c** involving LO vacuum polarization, **d** involving HO vacuum polarization and **e** involving light-by-light scattering

Class (a) consists of a subset of 12 diagrams of Fig. 4.3: diagrams (7)–(18) plus 2 diagrams obtained from diagram (22) by replacing one muon-loop by a hadronic “bubble”, and yields a contribution of the type

$$a_{\mu}^{(6)\text{had}_{(a)}} = \left(\frac{\alpha}{\pi}\right)^3 \frac{2}{3} \int_{4m_{\pi}^2}^{\infty} \frac{ds}{s} R(s) K^{[(a)]}(s/m_{\mu}^2), \quad (5.117)$$

where $K^{[(a)]}(s/m_{\mu}^2)$ is a QED function which was obtained analytically by Barbieri and Remiddi [201]. The kernel function is the contribution to a_{μ} of the 14 two-loop diagrams obtained from diagrams (1)–(7) of Fig. 4.2 by replacing one of the two photons by a “heavy photon” of mass \sqrt{s} . The convolution (5.117) then provides the insertion of a photon self-energy part into the photon line represented by the “heavy photon” according to the method outlined in Sect. 3.8. Explicitly, the kernel is given by

$$\begin{aligned} K^{[(a)]}(b) = & -\frac{139}{144} + \frac{115}{72} b + \left(\frac{19}{12} - \frac{7}{36} b + \frac{23}{144} b^2 + \frac{1}{b-4}\right) \ln b \\ & + \left(-\frac{4}{3} + \frac{127}{36} b - \frac{115}{72} b^2 + \frac{23}{144} b^3\right) \frac{\ln y}{\sqrt{b(b-4)}} \\ & + \left(\frac{9}{4} + \frac{5}{24} b - \frac{1}{2} b^2 - \frac{2}{b}\right) \zeta(2) + \frac{5}{96} b^2 \ln^2 b \\ & + \left(-\frac{1}{2} b + \frac{17}{24} b^2 - \frac{7}{48} b^3\right) \frac{\ln y}{\sqrt{b(b-4)}} \ln b \\ & + \left(\frac{19}{24} + \frac{53}{48} b - \frac{29}{96} b^2 - \frac{1}{3b} + \frac{2}{b-4}\right) \ln^2 y \\ & + \left(-2b + \frac{17}{6} b^2 - \frac{7}{12} b^3\right) \frac{D_p(b)}{\sqrt{b(b-4)}} \\ & + \left(\frac{13}{3} - \frac{7}{6} b + \frac{1}{4} b^2 - \frac{1}{6} b^3 - \frac{4}{b-4}\right) \frac{D_m(b)}{\sqrt{b(b-4)}} \\ & + \left(\frac{1}{2} - \frac{7}{6} b + \frac{1}{2} b^2\right) T(b), \end{aligned} \quad (5.118)$$

where

$$y = \frac{\sqrt{b} - \sqrt{b-4}}{\sqrt{b} + \sqrt{b-4}},$$

and

$$\begin{aligned}
 D_p(b) &= \text{Li}_2(y) + \ln y \ln(1-y) - \frac{1}{4} \ln^2 y - \zeta(2) , \\
 D_m(b) &= \text{Li}_2(-y) + \frac{1}{4} \ln^2 y + \frac{1}{2} \zeta(2) , \\
 T(b) &= -6 \text{Li}_3(y) - 3 \text{Li}_3(-y) + \ln^2 y \ln(1-y) \\
 &\quad + \frac{1}{2} (\ln^2 y + 6 \zeta(2)) \ln(1+y) + 2 \ln y (\text{Li}_2(-y) + 2\text{Li}_2(y)) .
 \end{aligned}$$

Again $\text{Li}_2(y) = -\int_0^y \frac{dt}{t} \ln(1-t)$ is the dilogarithm and $\text{Li}_3(y) = \int_0^y \frac{dt}{t} \text{Li}_2(t)$ the trilogarithm defined earlier in (3.40). Limiting cases are

$$\begin{aligned}
 K^{[a]}(0) &= \frac{197}{144} + \frac{1}{2} \zeta(2) - 3\zeta(2) \ln 2 + \frac{3}{4} \zeta(3) , \\
 K_\infty^{[a]}(b) &\stackrel{b \rightarrow \infty}{=} -\frac{1}{b} \left(\frac{23}{36} \ln b + 2\zeta(2) - \frac{223}{54} \right) .
 \end{aligned}$$

For the subclass which corresponds to the leading HVP graph Fig. 5.1 decorated in all possible ways with an additional virtual photon the result reads

$$\begin{aligned}
 \Delta K^{[a]}(b) &= \frac{35}{36} + \frac{8}{9} b + \left(\frac{4}{3} - \frac{1}{9} b - \frac{5}{18} b^2 \right) \ln b \\
 &\quad + \left(-\frac{4}{3} + \frac{19}{9} b + \frac{4}{9} b^2 - \frac{15}{8} b^3 \right) \frac{\ln y}{\sqrt{b(b-4)}} \\
 &\quad + \left(1 + \frac{1}{3} b - \frac{1}{6} b^2 - \frac{2}{b} \right) \zeta(2) + \left(\frac{1}{2} + \frac{1}{6} b - \frac{1}{12} b^2 - \frac{1}{3b} \right) \ln^2 y \\
 &\quad + \left(\frac{16}{3} - \frac{4}{3} b - \frac{4}{3} b^2 + \frac{1}{3} b^3 \right) \frac{D_m(b)}{\sqrt{b(b-4)}} . \tag{5.119}
 \end{aligned}$$

Krause [202] has given an expansion up to fourth order, which reads

$$\begin{aligned}
 K^{[a]}(s/m^2) &= \frac{m^2}{s} \left\{ \left[\frac{223}{54} - 2\zeta(2) - \frac{23}{36} \ln \frac{s}{m^2} \right] \right. \\
 &\quad + \frac{m^2}{s} \left[\frac{8785}{1152} - \frac{37}{8} \zeta(2) - \frac{367}{216} \ln \frac{s}{m^2} + \frac{19}{144} \ln^2 \frac{s}{m^2} \right] \\
 &\quad + \frac{m^4}{s^2} \left[\frac{13072841}{432000} - \frac{883}{40} \zeta(2) - \frac{10079}{3600} \ln \frac{s}{m^2} + \frac{141}{80} \ln^2 \frac{s}{m^2} \right] \\
 &\quad \left. + \frac{m^6}{s^3} \left[\frac{2034703}{16000} - \frac{3903}{40} \zeta(2) - \frac{6517}{1800} \ln \frac{s}{m^2} + \frac{961}{80} \ln^2 \frac{s}{m^2} \right] \right\} . \tag{5.120}
 \end{aligned}$$

Here m is the mass of the external lepton $m = m_\mu$ in our case. The expanded approximation is more practical for the evaluation of the dispersion integral, because it is numerically more stable in general.

Class (b) consists of 2 diagrams only, obtained from diagram (22) of Fig. 4.3, and one may write this contribution in the form

$$a_\mu^{(6) \text{ had}_{(b)}} = \left(\frac{\alpha}{\pi}\right)^3 \frac{2}{3} \int_{4m_\pi^2}^{\infty} \frac{ds}{s} R(s) K^{(b)}(s/m_\mu^2), \quad (5.121)$$

with

$$K^{(b)}(s/m_\mu^2) = \int_0^1 dx \frac{x^2 (1-x)}{x^2 + (1-x)s/m_\mu^2} \left[-\hat{\Pi}'_\gamma e \left(-\frac{x^2}{1-x} \frac{m_\mu^2}{m_e^2} \right) \right],$$

where we have set $\Pi' = \frac{\alpha}{\pi} \hat{\Pi}'$. Using (2.178) with $z = -\frac{x^2}{1-x} \frac{m_\mu^2}{m_e^2}$ one obtains

$$\hat{\Pi}'_\gamma e(z) = -2 \int_0^1 dy y (1-y) \ln(1-zy(1-y)) = \frac{8}{9} - \frac{\beta^2}{3} + \left(\frac{1}{2} - \frac{\beta^2}{6}\right) \beta \ln \frac{\beta-1}{\beta+1},$$

with $\beta = \sqrt{1 + 4 \frac{1-x}{x^2} \frac{m_\mu^2}{m_e^2}}$.

Here the kernel function is the contribution to a_μ of the 2 two-loop diagrams obtained from diagrams (8) of Fig. 4.2 by replacing one of the two photons by a “heavy photon” of mass \sqrt{s} .

In diagram (b) $m_f^2/m^2 = (m_e/m_\mu)^2$ is very small and one may expand β in terms of this small parameter. The x -integration afterwards may be performed analytically. Up to terms of order $\mathcal{O}(\frac{m_f^2}{m^2})$ the result reads [202]

$$\begin{aligned} K^{(b)}(s) = & - \left(\frac{5}{9} + \frac{1}{3} \ln \frac{m_f^2}{m^2} \right) \times \left\{ \frac{1}{2} - (x_1 + x_2) \right. \\ & \left. + \frac{1}{x_1 - x_2} \left[x_1^2 (x_1 - 1) \ln \left(\frac{-x_1}{1-x_1} \right) - x_2^2 (x_2 - 1) \ln \left(\frac{-x_2}{1-x_2} \right) \right] \right\} \\ & - \frac{5}{12} + \frac{1}{3} (x_1 + x_2) + \frac{1}{3(x_1 - x_2)} \left\{ x_1^2 (1-x_1) \left[\text{Li}_2 \left(\frac{1}{x_1} \right) - \frac{1}{2} \ln^2 \left(\frac{-x_1}{1-x_1} \right) \right] \right. \\ & \left. - x_2^2 (1-x_2) \left[\text{Li}_2 \left(\frac{1}{x_2} \right) - \frac{1}{2} \ln^2 \left(\frac{-x_2}{1-x_2} \right) \right] \right\}, \end{aligned} \quad (5.122)$$

with $x_{1,2} = \frac{1}{2}(b \pm \sqrt{b^2 - 4b})$ and $b = s/m^2$. The expansion to fifth order is given by

$$\begin{aligned}
K^{[b]}(s) = & \frac{m^2}{s} \left\{ \left(-\frac{1}{18} + \frac{1}{9} \ln \frac{m^2}{m_f^2} \right) \right. \\
& + \frac{m^2}{s} \left(-\frac{55}{48} + \frac{\pi^2}{18} + \frac{5}{9} \ln \frac{s}{m_f^2} + \frac{5}{36} \ln \frac{m^2}{m_f^2} - \frac{1}{6} \ln^2 \frac{s}{m_f^2} + \frac{1}{6} \ln^2 \frac{m^2}{m_f^2} \right) \\
& + \frac{m^4}{s^2} \left(-\frac{11299}{1800} + \frac{\pi^2}{3} + \frac{10}{3} \ln \frac{s}{m_f^2} - \frac{1}{10} \ln \frac{m^2}{m_f^2} - \ln^2 \frac{s}{m_f^2} + \ln^2 \frac{m^2}{m_f^2} \right) \\
& - \frac{m^6}{s^3} \left(\frac{6419}{225} - \frac{14}{9} \pi^2 + \frac{76}{45} \ln \frac{m^2}{m_f^2} - \frac{14}{3} \ln^2 \frac{m^2}{m_f^2} - \frac{140}{9} \ln \frac{s}{m_f^2} + \frac{14}{3} \ln^2 \frac{s}{m_f^2} \right) \\
& \left. - \frac{m^8}{s^4} \left(\frac{53350}{441} - \frac{20}{3} \pi^2 + \frac{592}{63} \ln \frac{m^2}{m_f^2} - 20 \ln^2 \frac{m^2}{m_f^2} - \frac{200}{3} \ln \frac{s}{m_f^2} + 20 \ln^2 \frac{s}{m_f^2} \right) \right\} \\
& + \frac{m_f^2}{m^2} \left[\frac{m^2}{s} - \frac{2}{3} \frac{m^4}{s^2} - \frac{m^6}{s^3} \left(-2 \ln \frac{s}{m^2} + \frac{25}{6} \right) - \frac{m^8}{s^4} \left(-12 \ln \frac{s}{m^2} + \frac{97}{5} \right) \right. \\
& \left. - \frac{m^{10}}{s^5} \left(-56 \ln \frac{s}{m^2} + \frac{416}{5} \right) \right]. \tag{5.123}
\end{aligned}$$

Class (c) includes the double HVP insertion, which is given by

$$a_\mu^{(6) \text{ had}_{[c]}} = \left(\frac{\alpha}{\pi} \right)^3 \frac{1}{9} \int_{4m_\pi^2}^{\infty} \frac{ds ds'}{s s'} R(s) R(s') K^{[c]}(s, s'), \tag{5.124}$$

where

$$K^{[c]}(s, s') = \int_0^1 dx \frac{x^4 (1-x)}{[x^2 + (1-x)s/m_\mu^2][x^2 + (1-x)s'/m_\mu^2]}.$$

This integral may be performed analytically. Setting $b = s/m^2$ and $c = s'/m^2$ one obtains for $b \neq c$

$$\begin{aligned}
K^{[c]}(s, s') = & \frac{1}{2} - b - c - \frac{(2-b)b^2 \ln(b)}{2(b-c)} - \frac{b^2(2-4b+b^2) \ln\left(\frac{b+\sqrt{-(4-b)b}}{b-\sqrt{-(4-b)b}}\right)}{2(b-c)\sqrt{-(4-b)b}} \\
& - \frac{(-2+c)c^2 \ln(c)}{2(b-c)} + \frac{c^2(2-4c+c^2) \ln\left(\frac{c+\sqrt{-(4-c)c}}{c-\sqrt{-(4-c)c}}\right)}{2(b-c)\sqrt{-(4-c)c}}, \tag{5.125}
\end{aligned}$$

and for $b = c$

$$K^{[c]}(s, s') = \frac{1}{2} - 2c + \frac{c}{2} (-2 + c - 4 \ln(c) + 3c \ln(c)) + \frac{c(-2 + 4c - c^2)}{2(-4 + c)} + \frac{c(12 - 42c + 22c^2 - 3c^3) \ln\left(\frac{c + \sqrt{(-4+c)c}}{c - \sqrt{(-4+c)c}}\right)}{2(-4 + c) \sqrt{(-4 + c)c}}. \quad (5.126)$$

In fact we may utilize (3.153) together with (3.165) in order to get the much simpler expression

$$a_\mu^{(6)\text{had}[c]} = \frac{\alpha}{\pi} \int_0^1 dx (1-x) \left(\Delta\alpha_{\text{had}}^{(5)}(-Q^2(x)) \right)^2, \quad (5.127)$$

where $Q^2(x) \equiv \frac{x^2}{1-x} m_\mu^2$ is the space-like square momentum-transfer. An accurate numerical evaluation of this integral is much simpler as it involves the integration over $R(s)$ once only.

Class (d) exhibits 3 diagrams (diagrams 19)–(21) of Fig. 4.3 and corresponds to the leading hadronic contribution with $R(s)$ corrected for final state radiation. We thus may write this correction by replacing

$$R(s) \rightarrow R(s) \eta(s) \frac{\alpha}{\pi} \quad (5.128)$$

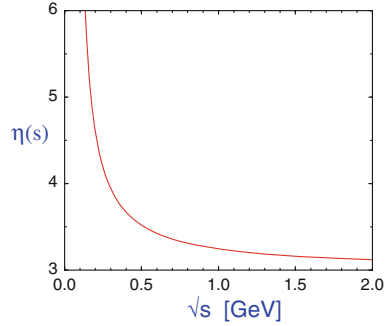
in the basic integral (5.24). This correction is particularly important for the dominating two pion channel²⁵ for which $\eta(s)$ may be calculated in scalar QED (treating the pions as point-like particles) [203, 204] and the result reads

$$\begin{aligned} \eta(s) = & \frac{1 + \beta_\pi^2}{\beta_\pi} \left\{ 4\text{Li}_2\left(\frac{1 - \beta_\pi}{1 + \beta_\pi}\right) + 2\text{Li}_2\left(-\frac{1 - \beta_\pi}{1 + \beta_\pi}\right) \right. \\ & - 3 \log\left(\frac{2}{1 + \beta_\pi}\right) \log\left(\frac{1 + \beta_\pi}{1 - \beta_\pi}\right) - 2 \log(\beta_\pi) \log\left(\frac{1 + \beta_\pi}{1 - \beta_\pi}\right) \left. \right\} \\ & - 3 \log\left(\frac{4}{1 - \beta_\pi^2}\right) - 4 \log(\beta_\pi) \\ & + \frac{1}{\beta_\pi^3} \left[\frac{5}{4} (1 + \beta_\pi^2)^2 - 2 \right] \log\left(\frac{1 + \beta_\pi}{1 - \beta_\pi}\right) + \frac{3}{2} \frac{1 + \beta_\pi^2}{\beta_\pi^2}, \end{aligned} \quad (5.129)$$

and provides a good measure for the dependence of the observables on the pion mass. Neglecting the pion mass is obviously equivalent to taking the high energy limit

²⁵Note that $R(s) \approx R^{\pi\pi}(s)$ up to about 0.81 GeV. Figure 5.38 suggests that sQED should work reliably up to not far below 1 GeV.

Fig. 5.44 The FSR correction factor $\eta(s)$ as a function of the center of mass energy



$$\eta(s \rightarrow \infty) = 3 .$$

In Fig. 5.44 the correction $\eta(s)$ is plotted as a function of the center of mass energy. It can be realized that for energies below 1 GeV the pion mass leads to a considerable enhancement of the FSR corrections. Regarding the desired precision, ignoring the pion mass would therefore lead to wrong results. Close to threshold for pion pair production ($s \simeq 4m_\pi^2$) the Coulomb forces between the two final state pions play an important role. In this limit the factor $\eta(s)$ becomes singular [$\eta(s) \rightarrow \pi^2/2\beta_\pi$] which means that the $O(\alpha)$ result for the FSR correction cannot be trusted anymore. Since these singularities are known to all orders of perturbation theory one can resum these contributions, which leads to an exponentiation [203] (see Sect. 5.1.5 p. 371):

$$R^{(\pi\pi\gamma)}(s) = R^{\pi\pi}(s) \left(1 + \eta(s) \frac{\alpha}{\pi} - \frac{\pi\alpha}{2\beta_\pi} \right) \frac{\pi\alpha}{\beta_\pi} \times \left[1 - \exp\left(-\frac{\pi\alpha}{\beta_\pi}\right) \right]^{-1} . \quad (5.130)$$

Above a center of mass energy of $\sqrt{s} = 0.3$ GeV the exponentiated correction to the Born cross section deviates from the non-exponentiated correction less than 1 %. The corresponding $O(\alpha)$ sQED contribution to the anomalous magnetic moment of the muon is

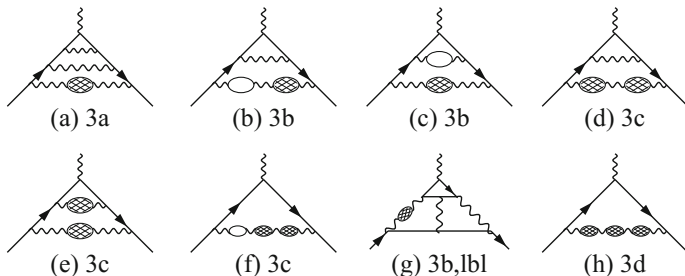
$$\delta^\gamma a_\mu^{\text{had}} = (38.6 \pm 1.0) \times 10^{-11} , \quad (5.131)$$

where we added a guesstimated error which of course is not the true model error, the latter remaining unknown.²⁶ In the inclusive region above typically 2 GeV, the FSR corrections are well represented by the inclusive photon emission from quarks. However, since in inclusive measurements experiments commonly do not subtract

²⁶One could expect that due to $\gamma - \rho^0$ mixing (VMD type models [205], see below) the sQED contribution gets substantially reduced. However, due to the low scales $\sim m_\mu, m_\pi$ involved, here, in relation to M_ρ the photons essentially behave classically in this case. Also, the bulk of the VP contribution at these low scales comes from the neutral ρ^0 -exchange Fig. 5.23, which does not directly produce FSR, the latter thus being due to the dissociated charged $\pi^+\pi^-$ intermediate state as assumed in sQED. In fact the main contribution comes from very low energies (Fig. 5.44).

Table 5.7 Higher order contributions from diagrams (a)–(c) (in units 10^{-11})

$a_\mu^{(2a)}$		$a_\mu^{(2b)}$		$a_\mu^{(2c)}$		$a_\mu^{\text{had}(2)}$		Ref.
-199	(4)	107	(3)	2.3	(0.6)	-90	(5)	[108]
-211	(5)	107	(2)	2.7	(0.1)	-101	(6)	[202]
-209	(4)	106	(2)	2.7	(1.0)	-100	(5)	[11]
-207.3	(1.9)	106.0	(0.9)	3.4	(0.1)	-98	(1)	[117]
-207.5	(2.0)	104.2	(0.9)	3.0	(0.1)	-100.3	(2.2)	[15]
-206.13	(1.30)	103.49	(0.63)	3.37	(0.05)	-99.27	(0.67)	[6, 88]

**Fig. 5.45** A sample of leading NNLO hadronic vacuum polarization diagrams

FSR, the latter is included already in the data and no additional contribution has to be taken into account. In more recent analyses this contribution is usually included in the leading hadronic contribution (5.29) as the $\pi^+\pi^-\gamma$ channel (see Table 5.3).

Results obtained by different groups, for so far unaccounted higher order vacuum polarization effects, are collected in Table 5.7. We will adopt the estimate

$$a_\mu^{\text{had}(2)} = (-99.27 \pm 0.67) \times 10^{-11} \quad (5.132)$$

obtained with the compilation [16]. For the electron only group (2a) yields a significant contribution [202]: $a_e^{(2a)} = -0.2210(12) \times 10^{-11}$.

5.1.13 Next-to-Next Leading Order Hadronic Contributions

Recently the next-to-next-to-leading order (NNLO), $O(\alpha^4)$, HVP contributions have been evaluated for the first time by [206–208] (see also [209]). The relevant kernels have been calculated by appropriate asymptotic expansion methods. The kernels have been calculated for the following groups of diagrams displayed in Fig. 5.45:

- K(3a): one hadronic insertion; up to two additional photons to the LO Feynman diagram; contains also the contributions with one or two closed muon loops and the light-by-light-type diagram with a closed muon loop.

Table 5.8 NNLO contributions diagrams (a)–(h) (in units 10^{-11})

$a_\mu^{(3a)}$	$a_\mu^{(3b)}$	$a_\mu^{(3b,1bl)}$	$a_\mu^{(3c)}$	$a_\mu^{(3d)}$	$a_\mu^{\text{had}(3)}$	Ref.
8.0	-4.1	9.1	-0.6	0.005	12.4 (1)	[206]
7.834 (61)	-4.033 (28)	9.005 (63)	-0.569 (5)	0.00518 (12)	12.24 (10)	[6]

- K(3b): one hadronic insertion and one or two closed electron loops and additional photonic corrections; the external photon couples to the muon.
- K(3b, 1bl): light-by-light-type contribution with closed electron loop and one hadronic insertion; the external photon couples to the electron.
- K(3c): two hadronic insertions and additional photonic corrections and/or closed electron or muon loops.
- K(3d): three hadronic insertions.

Class (3d) includes the leading triple HVP insertion, which is given by

$$a_\mu^{(8)\text{had}[(3d)]} = \left(\frac{\alpha}{\pi}\right)^4 \frac{1}{27} \int_{m_\pi^2}^{\infty} \frac{ds}{s} \frac{ds'}{s'} \frac{ds''}{s''} R(s) R(s') R(s'') K^{[(3d)]}(s, s', s''), \quad (5.133)$$

where

$$K^{[(3d)]}(s, s', s'') = \int_0^1 dx \frac{x^6 (1-x)}{[x^2 + (1-x)s/m_\mu^2][x^2 + (1-x)s'/m_\mu^2][x^2 + (1-x)s''/m_\mu^2]}.$$

Again we may utilize (3.153) and (3.165) in order to get the much simpler expression

$$a_\mu^{(8)\text{had}[(3d)]} = \frac{\alpha}{\pi} \int_0^1 dx (1-x) \left(\Delta\alpha_{\text{had}}^{(5)}(-Q^2(x)) \right)^3, \quad (5.134)$$

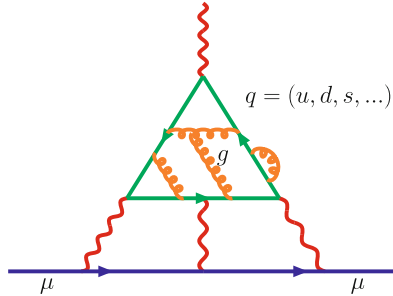
where $Q^2(x) \equiv \frac{x^2}{1-x} m_\mu^2$ is the space-like square momentum-transfer. An accurate numerical evaluation of this integral is much simpler as it involves the integration over $R(s)$ once only, which also allows for a standard error estimate.

Table 5.8 lists the different NNLO contributions obtained by Kurz et al. [206] together with my own evaluations based on my compilation of data discussed above evaluated with kernels from [206].

For the electron only group (3a) yields a significant contribution [206]: $a_e^{(3a)} = 0.0279(2) \times 10^{-12}$.

5.2 Hadronic Light-by-Light Scattering

In perturbation theory hadronic light-by-light scattering diagrams are like leptonic ones with leptons replaced by quarks which, however, exhibit strong interactions via gluons, which at low energies lead to a breakdown of perturbation theory.



Nevertheless, it is instructive to ask what quark-loop contributions would look like, if strong interactions would be weak or turned off. Quark loops, of course, play a role in estimating the S.D. effects above a certain energy scale. We may check which energy scales contribute relevant to the LbL integrals in the case of a muon loop and cutting off high energy contributions by a cut-off Λ . Typically, one obtains

Λ [GeV]	0.5	0.7	1.0	2.0
$a_\mu \times 10^{10}$	24	26	38	45

which illustrates that even for the muon the LbL contribution is rather sensitive to contributions from unexpectedly high scales. Only when the cut-off exceeds about 2 GeV the correct result $a_\mu^{(6)}(\text{lbl}, \mu) \simeq 46.50 \times 10^{-10}$ is well approximated. A constituent quark loop would yield the results summarized in Table 5.9. For the light quarks the numerical results are certainly more trustable while for the heavier quarks, like the c , the asymptotic expansion (4.13) becomes more reliable (see [108]; results taken from TABLE I).²⁷

Certainly, quark loops are far from accounting for the bulk of the HLbL effects. Actually, it is the spontaneous breakdown of the nearby chiral symmetry of QCD, an intrinsically non-perturbative phenomenon, which shapes the leading hadronic effects to be evaluated. While the non-perturbative effects which show up in the hadronic vacuum polarization may be reliably evaluated in terms of measured

²⁷In the free quark model (parton model) with current quark masses given in (3.38) one would get $a_\mu^{(6)}(\text{lbl}, u + d) = 8229.34 \times 10^{-11}$ and $a_\mu^{(6)}(\text{lbl}, s) = 17.22 \times 10^{-11}$ by adapting color, charge and mass in (4.11) and (3.50), respectively. Apart from the fact that pQCD makes no sense here, one should note that results are very sensitive to the precise definition of the quark masses used. Also note that the chiral limit $m_q \rightarrow 0$ of (4.11) [with $m_e \rightarrow m_q$ ($q = u, d, s$)] is IR singular. This also demonstrates the IR sensitivity of the LbL scattering contribution.

Table 5.9 CQM estimates of $a_\mu^{(6)}(\text{lbl}, q) \times 10^{11}$

0.3GeV lepton	[<i>ud</i>]	<i>s</i>	<i>c</i>	[<i>uds</i>]	[<i>udsc</i>]	Reference/method
79.0	49.7	1.1	2.1	50.8	52.9	[108] numerical
81.0	51.0	1.2	2.2	52.1	54.4	Eq. (4.13)
					62 (3)	[210]

hadronic cross sections $\sigma_{\text{tot}}(e^+e^- \rightarrow \gamma^* \rightarrow \text{hadrons})$, which allows us to obtain the full photon propagator $\langle 0|T\{A^\mu(x_1)A^\nu(x_2)\}|0\rangle$, for the light-by-light scattering Green function

$$\langle 0|T\{A^\mu(x_1)A^\nu(x_2)A^\rho(x_3)A^\sigma(x_4)\}|0\rangle$$

we have little direct experimental information when photons are off-shell. The perturbative QCD and QED corrections to the fermion-loop contributions to light-by-light scattering, $\gamma\gamma \rightarrow \gamma\gamma$, are available from [211] in the ultrarelativistic limit where the kinematic invariants are much larger than the masses of the charged fermions. For the contribution to $g - 2$ we need the light-by-light scattering amplitude with one photon real ($k^2 = 0$), or more precisely, its first derivative $\partial/\partial k^\mu$ evaluated at $k^\mu = 0$, equivalent to $E_\gamma \rightarrow 0$. But, the other three momenta are off-shell and to be integrated over the full phase space of the two remaining independent four-vectors. Unfortunately, the object in question cannot be calculated from first principles at present. Perturbation theory fails and CHPT is limited to the very low energy tail only. Lattice QCD in principle allows for an *ab initio* numerical calculation, which however is very challenging. Recent progress looks very promising [212–216] and a 10% evaluation should be possible within a few years. A very different approach, based on numerically solving the truncated tower of Dyson–Schwinger equations (DSE) in conjunction with the Bethe–Salpeter equations of QCD (see the end of Sect. 2.3.1 and Fig. 2.4 for the much simpler case of QED [no gauge self-interactions]), attempts a first principle prediction in a very different way [217–220]. While the data-driven dispersive approach is standard for evaluating HVP, dispersive methods have not been considered to be very constructive until recently. The machinery to exploit HLbL specific experimental data in a model independent way has now been developed by Colangelo, Hoferichter, Passera and Stoffer [CHPS] in [221, 222] for light-by-light scattering in general and by Pauk and Vanderhaeghen [PV] in [223] (also see [224, 225]) more specifically tailored to the muon $g - 2$. These approaches require experimental input which is largely missing at present. In any case much more experimental input is mandatory to make substantial progress in determining HLbL in the future.

At present one has to resort to models which are inspired by known properties of QCD as well as known phenomenological facts. One fact we already know from the HVP discussion, the ρ meson is expected to play an important role in the game. It looks natural to apply a vector-meson dominance (VMD) like model. Electromagnetic interactions of pions treated as point-particles would be described by scalar QED, as a first step in the sense of a low energy

expansion. Note that in photon–hadron interactions the photon mixes with hadronic vector–mesons like the ρ^0 . The naive VMD model attempts to take into account this hadronic dressing by replacing the photon propagator as

$$\frac{i g^{\mu\nu}}{q^2} + \dots \rightarrow \frac{i g^{\mu\nu}}{q^2} + \dots - \frac{i (g^{\mu\nu} - \frac{q^\mu q^\nu}{q^2})}{q^2 - M_\rho^2} = \frac{i g^{\mu\nu}}{q^2} \frac{M_\rho^2}{M_\rho^2 - q^2} + \dots, \quad (5.135)$$

where the ellipses stand for the gauge terms. Of course real photons $q^2 \rightarrow 0$ in any case remain undressed and the dressing would go away for $M_\rho^2 \rightarrow \infty$. The main effect is that it provides a damping at high energies with the ρ mass as an effective cut–off (physical version of a Pauli–Villars cut–off). However, the naive VMD model does not respect chiral symmetry properties.

More precisely, the hypothesis of *vector–meson dominance* [205] relates the matrix element of the hadronic part of the electromagnetic current $j_\mu^{\text{had}}(x)$ to the matrix element of the source density $J^{(\rho)}(x)$ of the neutral vector meson ρ^0 by

$$\langle B | j_\mu^{\text{had}}(0) | A \rangle = - \frac{M_\rho^2}{2\gamma_\rho} \frac{1}{q^2 - M_\rho^2} \langle B | J_\mu^{(\rho)}(0) | A \rangle, \quad (5.136)$$

where $q = p_B - p_A$, p_A and p_B the four momenta of the hadronic states A and B , respectively, M_ρ is the mass of the ρ meson. So far our VMD ansatz only accounts for the isovector part, but the isoscalar contributions mediated by the ω and the ϕ mesons may be included in exactly the same manner, as shown in Fig. 5.46. The key idea is to treat the vector meson resonances like the ρ as elementary fields in a first approximation. Free massive spin 1 vector bosons are described by a Proca field $V_\mu(x)$ satisfying the Proca equation $(\square + M_V^2) V_\mu(x) - \partial_\mu (\partial_\nu V^\nu) = 0$, which is designed such that it satisfies the Klein–Gordon equation and at the same time eliminates the unwanted spin 0 component: $\partial_\nu V^\nu = 0$. In the interacting case this equation is replaced by a *current–field identity* (CFI) [205]

$$(\square + M_V^2) V_\mu(x) - \partial_\mu (\partial_\nu V^\nu) = g_V J_\mu^{(V)}(x), \quad (5.137)$$

where the r.h.s. is the source mediating the interaction of the vector meson and g_V the coupling strength. The current should be conserved $\partial^\mu J_\mu^{(V)}(x) = 0$. The CFI then implies

$$\langle B | V_\mu(0) | A \rangle = - \frac{g_V}{q^2 - M_V^2} \langle B | J_\mu^{(V)}(0) | A \rangle,$$

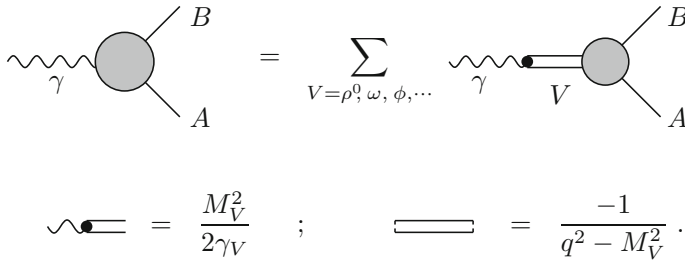


Fig. 5.46 The vector meson dominance model. A and B denote hadronic states

where terms proportional to q^μ have dropped due to current conservation. The VMD assumes that the hadronic electromagnetic current is saturated by vector meson resonances²⁸

$$j_\mu^{\text{had}}(x) = \sum_{V=\rho^0, \omega, \phi, \dots} \frac{M_V^2}{2\gamma_V} V_\mu(x), \tag{5.138}$$

such that, e.g.

$$\langle \rho(p) | j_\mu^{\text{had}}(0) | 0 \rangle = \varepsilon(p, \lambda)_\mu \frac{M_\rho^2}{2\gamma_\rho}, \quad p^2 = M_\rho^2.$$

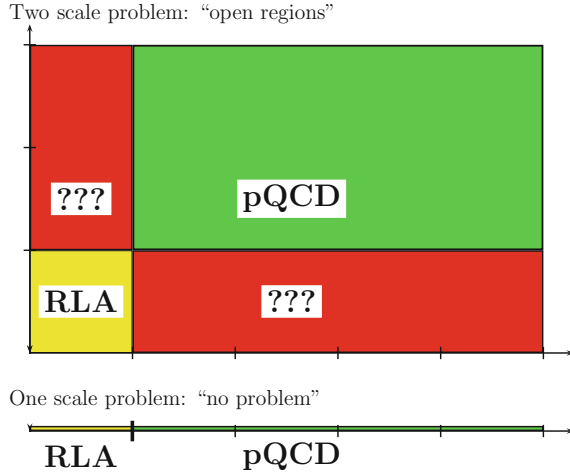
The mass-dependent factor M_V^2 must be there for dimensional reasons, γ_V is a coupling constant introduced in this form by convention. The VMD relation (5.136) thus derives from the CFI and ansatz (5.138). The VMD model is known to describe the gross features of the electromagnetic properties of hadrons quite well, most prominent example are the nucleon form factors. For recent phenomenological applications see [230].

A way to incorporate vector-mesons $\rho, \omega, \phi, \dots$ in accordance with the basic symmetries of QCD is the Resonance Lagrangian Approach (RLA) [134, 135]. The latter implements an extended version of CHPT (see p. 305) which incorporates VMD modeling in accord with the chiral structure of QCD. Alternative versions of the RLA

²⁸In large- N_c QCD [226–228] all hadrons become infinitely narrow, since all widths are suppressed by powers of $1/N_c$, and the VMD model becomes exact with an infinite number of narrow vector meson states. The large- N_c expansion attempts to approach QCD ($N_c = 3$) by an expansion in $1/N_c$. In leading approximation in the $SU(\infty)$ theory $R(s)$ would have the form [229]

$$R(s) = \frac{9\pi}{\alpha^2} \sum_{i=0}^{\infty} \Gamma_i^{ee} M_i \delta(s - M_i^2).$$

Fig. 5.47 Multi-scale strong interaction problems. For two and more scales some regions are neither modeled by low energy effective nor by perturbative QCD



are the HLS²⁹ [190] or massive YM [191] models and the ENJL [231] model. They are basically equivalent [135, 191, 192] in the context of our application.

A new quality of the problem encountered here is the fact that the integrand depends on 3 invariants q_1^2, q_2^2, q_3^2 , where $q_3 = -(q_1 + q_2)$. In contrast, the HVP correlator or the VVA triangle with an external zero momentum vertex only depend on a single invariant q^2 . In the latter case, the invariant amplitudes (form factors) may be separated into a low energy part $q^2 \leq \Lambda^2$ (soft) where the low energy effective description applies and a high energy part $q^2 > \Lambda^2$ (hard) where pQCD works. In multi-scale problems, however, there are mixed soft-hard regions (see Fig. 5.47), where no answer is available in general, unless we have data to constrain the amplitudes in such regions. In our case, only the soft region $q_1^2, q_2^2, q_3^2 \leq \Lambda^2$ and the hard region $q_1^2, q_2^2, q_3^2 > \Lambda^2$ are under control of either the low energy EFT and of pQCD,

²⁹In this approach the vector part $SU(2)_V$ of the global chiral group $SU(2)_L \otimes SU(2)_R$, realized as a non-linear σ model for the pions (see (4.73)), is promoted to a local symmetry and the ρ -mesons become the corresponding gauge vector bosons, as they do in the massive Yang-Mills (YM) approach. Together with the electromagnetic $U(1)_Q$ local group one obtains the symmetry pattern: $[SU(2)_L \otimes SU(2)_R / SU(2)_V]_{\text{global}} \otimes [SU(2)_V]_{\text{hidden}} \otimes U(1)_Q$, where the local group is broken by the Higgs mechanism to $U(1)_{\text{em}}$, with $Q_{\text{em}} = Q + T_3^{\text{hidden}}$, essentially as in the electroweak SM. Unlike in the massive YM ansatz the gauge bosons here are considered as collective fields ($V^\mu = \bar{q}\gamma^\mu q$ etc.) as in the Extended Nambu-Jona-Lasinio (ENJL) model. The generalization to $SU(3)$ is obvious. Similar to the pseudoscalar field $\phi(x)$ (4.72), the $SU(3)$ gauge bosons conveniently may be written as a 3×3 matrix field

$$V_\mu(x) = \sum_i T_i V_{\mu i} = \begin{pmatrix} \frac{\rho^0}{\sqrt{2}} + \frac{\omega_8}{\sqrt{6}} & \rho^+ & K^{*+} \\ \rho^- & \frac{-\rho^0}{\sqrt{2}} + \frac{\omega_8}{\sqrt{6}} & K^{*0} \\ K^{*-} & \bar{K}^{*0} & -2\frac{\omega_8}{\sqrt{6}} \end{pmatrix}_\mu$$

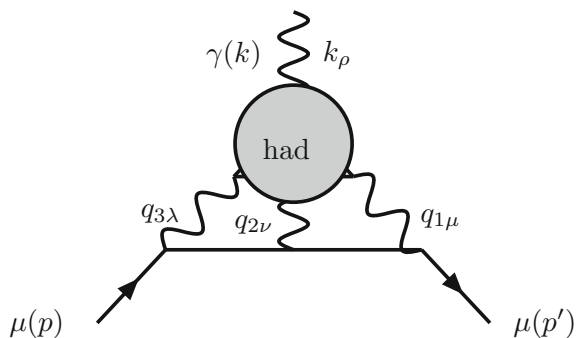
respectively. In the other domains operator product expansions and/or soft versus hard factorization “theorems” à la Brodsky-Farrar [232] may be applied.

Another problem of the RLA is that the low energy effective theory is non-renormalizable and thus has unphysical UV behavior, while QCD is renormalizable and has the correct UV behavior (but in pQCD fails to encompass the IR behavior). As a consequence of the mismatch of the functional dependence on the cut-off, one cannot match the two pieces in a satisfactory manner and one obtains a cut-off dependent prediction. Unfortunately, the cut-off dependence of the sum is not small even if one varies the cut-off only within “reasonable” boundaries around about 1 or 2 GeV, say. Of course the resulting uncertainty just reflects the model dependence and so to say parametrizes our ignorance. An estimate of the real model dependence is difficult as long as we are not knowing the true solution of the problem. In CHPT and its extensions, the low energy constants parametrizing the effective Lagrangian are accounting for the appropriate S.D. behavior, usually. Some groups however prefer an alternative approach based on the fact that the weakly coupled large- N_c QCD, i.e., $SU(N_c)$ for $N_c \rightarrow \infty$ under the constraint $\alpha_s N_c = \text{constant}$, is theoretically better known than true QCD with $N_c = 3$. It is thus tempting to approximate QCD as an expansion in $1/N_c$ [226–228]. Of course, also when applying a large- N_c expansion one has to respect the low energy properties of QCD as encoded by CHPT [233]. In CHPT the effective Lagrangian has an overall factor N_c , while the U matrix, exhibiting the pseudoscalar fields, is N_c independent. Each additional meson field has a $1/F_\pi \propto 1/\sqrt{N_c}$. In the context of CHPT the $1/N_c$ expansion thus is equivalent to a semiclassical expansion. The chiral Lagrangian can be used at tree level, and loop effects are suppressed by powers of $1/N_c$.

5.2.1 Calculating the Hadronic LbL Contribution

Let us start now with a setup of what one has to calculate actually. The hadronic light-by-light scattering contribution to the electromagnetic vertex is represented by the diagram Fig. 5.48. According to the diagram, a complete discussion of the

Fig. 5.48 Setup for the calculation of the hadronic contribution of the light-by-light scattering to the muon electromagnetic vertex



hadronic light-by-light contributions involves the full rank-four hadronic vacuum polarization tensor³⁰

$$\begin{aligned} \Pi_{\mu\nu\lambda\rho}(q_1, q_2, q_3) &= \int d^4x_1 d^4x_2 d^4x_3 e^{i(q_1x_1+q_2x_2+q_3x_3)} \\ &\times \langle 0 | T \{ j_\mu(x_1) j_\nu(x_2) j_\lambda(x_3) j_\rho(0) \} | 0 \rangle . \end{aligned} \quad (5.139)$$

Momentum k of the external photon is incoming, while the q_i 's of the virtual photons are outgoing from the hadronic “blob”. Here $j_\mu(x)$ denotes the light quark part of the electromagnetic current

$$j_\mu(x) = \frac{2}{3}(\bar{u}\gamma_\mu u)(x) - \frac{1}{3}(\bar{d}\gamma_\mu d)(x) - \frac{1}{3}(\bar{s}\gamma_\mu s)(x) \equiv \bar{q} \hat{Q} \gamma_\mu q(x) . \quad (5.140)$$

It includes a summation over color of the color and flavor diagonal quark bilinears. Since the electromagnetic current $j_\mu(x)$ is conserved, the tensor $\Pi_{\mu\nu\lambda\rho}(q_1, q_2, q_3)$ satisfies the Ward-Takahashi identities

$$\{q_1^\mu; q_2^\nu; q_3^\lambda; k^\rho\} \Pi_{\mu\nu\lambda\rho}(q_1, q_2, q_3) = 0 , \quad (5.141)$$

with $k = (q_1 + q_2 + q_3)$. Taking the derivative $\frac{\partial}{\partial k^\rho}$ of $k^\rho \Pi_{\mu\nu\lambda\rho}(q_1, q_2, k - q_1 - q_2) = 0$ implies

$$\Pi_{\mu\nu\lambda\rho}(q_1, q_2, k - q_1 - q_2) = -k^\sigma (\partial/\partial k^\rho) \Pi_{\mu\nu\lambda\sigma}(q_1, q_2, k - q_1 - q_2) , \quad (5.142)$$

and thus tells us that the object of interest is linear in k when we go to the static limit $k^\mu \rightarrow 0$ in which the anomalous magnetic moment is defined.

Up to one-loop the electromagnetic $\bar{\ell}\ell\gamma$ -vertex has been discussed in Sect. 2.6.3, its general structure in Sect. 3.3. Here we adopt the notation of Knecht and Nyfeler [234] ($q \rightarrow k, p_1 \rightarrow p$ and $p_2 \rightarrow p'$). From the diagram we easily read off the contribution of $\Pi_{\mu\nu\lambda\sigma}(q_1, q_2, q_3)$ to the electromagnetic vertex which is given by

$$\begin{aligned} \langle \mu^-(p') | (ie) j_\rho(0) | \mu^-(p) \rangle &= (-ie) \bar{u}(p') \Pi_\rho(p', p) u(p) \\ &= \int \frac{d^4q_1}{(2\pi)^4} \frac{d^4q_2}{(2\pi)^4} \frac{(-i)^3}{q_1^2 q_2^2 (q_1 + q_2 - k)^2} \frac{i}{(p' - q_1)^2 - m^2} \frac{i}{(p - q_1 - q_2)^2 - m^2} \\ &\times (-ie)^3 \bar{u}(p') \gamma^\mu (\not{p}' - \not{q}_1 + m) \gamma^\nu (\not{p} - \not{q}_1 - \not{q}_2 + m) \gamma^\lambda u(p) \\ &\times (ie)^4 \Pi_{\mu\nu\lambda\rho}(q_1, q_2, k - q_1 - q_2) , \end{aligned} \quad (5.143)$$

³⁰We remind that the light-by-light scattering Green function is overall convergent due to the Abelian gauge symmetry. The latter implies that integrals converge better than they look like by naive power counting (see the Footnote p. 66).

with $k_\mu = (p' - p)_\mu$. For the contribution to the form factors

$$\bar{u}(p') \Pi_\rho(p', p) u(p) = \bar{u}(p') \left[\gamma_\rho F_E(k^2) + i \frac{\sigma_{\rho\tau} k^\tau}{2m_\mu} F_M(k^2) \right] u(p), \quad (5.144)$$

Equation (5.142) implies that $\Pi_\rho(p', p) = k^\sigma \Pi_{\rho\sigma}(p', p)$ with

$$\begin{aligned} \bar{u}(p') \Pi_{\rho\sigma}(p', p) u(p) &= -ie^6 \times \\ &\int \frac{d^4 q_1}{(2\pi)^4} \frac{d^4 q_2}{(2\pi)^4} \frac{1}{q_1^2 q_2^2 (q_1 + q_2 - k)^2} \frac{1}{(p' - q_1)^2 - m^2} \frac{1}{(p - q_1 - q_2)^2 - m^2} \\ &\times \bar{u}(p') \gamma^\mu (\not{p}' - \not{q}_1 + m) \gamma^\nu (\not{p} - \not{q}_1 - \not{q}_2 + m) \gamma^\lambda u(p) \\ &\times \frac{\partial}{\partial k^\rho} \Pi_{\mu\nu\lambda\sigma}(q_1, q_2, k - q_1 - q_2). \end{aligned} \quad (5.145)$$

The WT-identity takes the form $k^\rho k^\sigma \bar{u}(p') \Pi_{\rho\sigma}(p', p) u(p) = 0$, which implies $\delta^{\text{lbl}} F_E(0) = 0$ and, in the terminology introduced at the end of Sect. 3.5, we have $V_\rho(p) = \Pi_\rho(p', p)|_{k=0} = 0$ and $T_{\rho\sigma}(p) = \Pi_{\rho\sigma}(p', p)|_{k=0}$. Thus, using the projection technique outlined in Sect. 3.5, the hadronic light-by-light contribution to the muon anomalous magnetic moment is equal to

$$F_M(0) = \frac{1}{48m} \text{Tr} \{ (\not{p} + m) [\gamma^\rho, \gamma^\sigma] (\not{p} + m) \Pi_{\rho\sigma}(p, p) \}. \quad (5.146)$$

The basic trace of Dirac matrices to be evaluated thus is

$$\text{Tr} \{ (\not{p} + m) [\gamma^\rho, \gamma^\sigma] (\not{p} + m) \gamma^\mu (\not{p}' - \not{q}_1 + m) \gamma^\nu (\not{p} - \not{q}_1 - \not{q}_2 + m) \gamma^\lambda \} \quad (5.147)$$

such that finally

$$\begin{aligned} F_M(0) &= \frac{-ie^6}{48m} \int \frac{d^4 q_1}{(2\pi)^4} \frac{d^4 q_2}{(2\pi)^4} \frac{1}{q_1^2 q_2^2 (q_1 + q_2)^2} \frac{1}{(p - q_1)^2 - m^2} \frac{1}{(p - q_1 - q_2)^2 - m^2} \\ &\times \text{Tr} \{ (\not{p} + m) [\gamma^\rho, \gamma^\sigma] (\not{p} + m) \gamma^\mu (\not{p} - \not{q}_1 + m) \gamma^\nu (\not{p} - \not{q}_1 - \not{q}_2 + m) \gamma^\lambda \} \\ &\times \left(\frac{\partial}{\partial k^\rho} \Pi_{\mu\nu\lambda\sigma}(q_1, q_2, k - q_1 - q_2) \right)_{k=0}. \end{aligned} \quad (5.148)$$

This is what we actually need to calculate. The integral to be performed is 8 dimensional. Thereof 3 integrations can be done analytically. In general, one has to deal with a 5 dimensional non-trivial integration over 3 angles and 2 moduli.

As mentioned before, the hadronic tensor $\Pi_{\mu\nu\lambda\sigma}(q_1, q_2, k - q_1 - q_2)$ we have to deal with, is a problematic object, because it has an unexpectedly complex structure as we will see, in no way comparable with the leptonic counterpart. The general covariant decomposition involves 138 Lorentz structures [235, 236]:

$$\begin{aligned}
 \Pi^{\mu\nu\alpha\beta}(p_1, p_2, p_3) \equiv & \Pi^1(p_1, p_2, p_3) g^{\mu\nu} g^{\alpha\beta} + \Pi^2(p_1, p_2, p_3) g^{\mu\alpha} g^{\nu\beta} \\
 & + \Pi^3(p_1, p_2, p_3) g^{\mu\beta} g^{\nu\alpha} \\
 & + \Pi^{1jk}(p_1, p_2, p_3) g^{\mu\nu} p_j^\alpha p_k^\beta + \Pi^{2jk}(p_1, p_2, p_3) g^{\mu\alpha} p_j^\nu p_k^\beta \\
 & + \Pi^{3jk}(p_1, p_2, p_3) g^{\mu\beta} p_j^\nu p_k^\alpha + \Pi^{4jk}(p_1, p_2, p_3) g^{\nu\alpha} p_j^\mu p_k^\beta \\
 & + \Pi^{5jk}(p_1, p_2, p_3) g^{\nu\beta} p_j^\mu p_k^\alpha + \Pi^{6jk}(p_1, p_2, p_3) g^{\alpha\beta} p_j^\mu p_k^\nu \\
 & + \Pi^{ijkm}(p_1, p_2, p_3) p_i^\mu p_j^\nu p_k^\beta p_m^\alpha, \tag{5.149}
 \end{aligned}$$

where $i, j, k, m = 1, 2$ or 3 and repeated indices are summed. The functions are scalar functions of all possible invariant products $p_i \cdot p_j$. By the WT identities and the kinematical constraint $k^\mu \rightarrow 0$ the number of amplitudes contributing to $g - 2$ reduces to 32. In four dimensions two of the structures are linearly dependent on the others [220]. In fact as shown recently in [237] the number of amplitudes contributing to $g - 2$ can be reduced to 19 independent ones, if one takes into account the symmetry of the integral under permutations of the three virtual photons.

Fortunately, this tensor is dominated by the pseudoscalar exchanges $\pi^0, \eta, \eta', \dots$ (see Figs. 3.6 and 5.49), described by the Wess–Zumino–Witten (WZW) effective Lagrangian [238, 239]

$$\mathcal{L}_{\text{WZW}} = \frac{\alpha}{\pi} \frac{N_c}{12F_\pi} \left(\pi^0 + \frac{1}{\sqrt{3}} \eta_8 + 2\sqrt{\frac{2}{3}} \eta_0 \right) \tilde{F}_{\mu\nu} F^{\mu\nu}. \tag{5.150}$$

This fact rises hope that a half-way reliable estimate should be possible. Generally, the perturbative QCD expansion only is useful to evaluate the short distance tail,

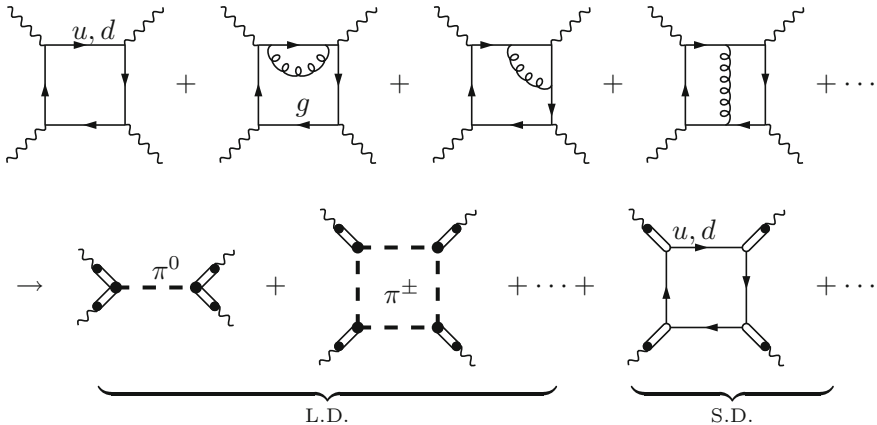
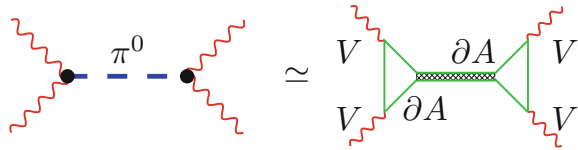


Fig. 5.49 Hadronic light-by-light scattering is dominated by π^0 -exchange in the odd parity channel, pion loops etc. at long distances (L.D.) and quark loops including hard gluonic corrections at short distances (S.D.). The photons in the effective theory couple to hadrons via $\gamma - \rho^0$ mixing

Fig. 5.50 Hadronic degrees of freedom (effective theories) versus quark gluon picture (QCD); example π^0 exchange

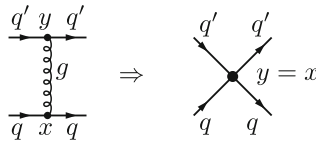


while the dominant long distance part must be evaluated using some low energy effective model which includes the pseudoscalar Nambu–Goldstone bosons as well as the vector mesons as shown in Fig. 5.49.

Note that, in spite of the fact that in pQCD our hadronic tensor $\Pi_{\mu\nu\lambda\sigma}(q_1, q_2, k - q_1 - q_2)$ only involves parity conserving vector interactions (γ^μ -type), in full QCD the parity violating axial–vector interactions ($\gamma^\mu\gamma_5$ -type) are ruling the game. Thereby the existence of the Adler–Bell–Jackiw (ABJ) anomaly [240] related via PCAC to the pseudoscalar states plays the key role. This connection may be illustrated as in³¹ Fig. 5.50.

5.2.2 Sketch on Hadronic Models

One way to “derive” the low energy structure of QCD starting from the QCD Lagrangian is to integrate out the S.D. part of the gluonic degrees of freedom,



which implies effective four quark interactions and a model very similar to the Nambu–Jona–Lasinio (NJL) model [241] (compare also the linear σ -model [242]), however, with nucleons replaced by *constituent quarks*. Practically, this is done via the regulator replacement,

$$\frac{1}{Q^2} \rightarrow \int_0^{1/\Lambda^2} d\tau e^{-\tau Q^2} , \tag{5.151}$$

in the gluon propagator and an expansion in $1/\Lambda^2$. In the leading $1/N_c$ limit this leads to the Lagrangian

³¹Formally, a $\gamma_5^2 = 1$ appears inserted at one of the vertices and one of the γ_5 's then anticommuted to one of the other vertices. The “quark–loop picture” is not kind of resummed pQCD, which does not know pions, rather an ENJL type diagram.

$$\begin{aligned} \mathcal{L}_{\text{ENJL}} = & \bar{q}^i \{i\gamma^\mu (\partial_\mu - iv_\mu - ia_\mu\gamma_5) - (\mathcal{M} + s - ip\gamma_5)\} q^i \\ & + 2g_S \sum_{i,j} (\bar{q}_R^i q_L^j) (\bar{q}_L^j q_R^i) - g_V \sum_{i,j} \left[(\bar{q}_L^i \gamma^\mu q_L^j) (\bar{q}_L^j \gamma_\mu q_L^i) + (L \rightarrow R) \right], \end{aligned} \quad (5.152)$$

with $q \equiv (u, d, s)$, defining the so called ENJL model (see [243] for a comprehensive review). v_μ, a_μ, s, p are the usual external vector, axial-vector, scalar and pseudoscalar matrix sources as used in CHPT. \mathcal{M} is the quark mass-matrix. Summation over colors between brackets in (5.152) is understood, i, j are flavor indices, $q_{R,L} \equiv (1/2)(1 \pm \gamma_5) q$ are the chiral quark fields and

$$g_V \equiv \frac{8\pi^2 G_V(\Lambda)}{N_c \Lambda^2}, \quad g_S \equiv \frac{4\pi^2 G_S(\Lambda)}{N_c \Lambda^2} \quad (5.153)$$

are Fermi type coupling parameters. The couplings $G_S(\Lambda)$ and $G_V(\Lambda)$ are dimensionless and $O(1)$ in the $1/N_c$ expansion and to leading order the constraint

$$G_S = 4G_V = \frac{\alpha_s}{\pi} N_c, \quad \text{i.e. } \alpha_s = O(1/N_c) \quad (5.154)$$

should be satisfied at scales where pQCD applies. The ENJL model exhibits the same symmetry pattern, the spontaneously broken chiral symmetry which is inferring the existence of non-vanishing quark condensates ($\langle \bar{u}u \rangle, \langle \bar{d}d \rangle, \langle \bar{s}s \rangle \neq 0$) and of the Nambu–Goldstone modes, the pions (π^0, π^\pm), the η and the Kaons in the $SU(3)$ (u, d, s) quark sector. The Lagrangian $\mathcal{L}_{\text{QCD}}^\Lambda$ includes only low frequency (less than Λ) modes of quark and gluon fields.

In the ENJL model quarks get dressed to constituent quarks in place of the much lighter current quarks which appear in the QCD Lagrangian. The constituent quark masses are obtained as a solution of the gap equation³² Fig. 5.51 and typically take values (4.54) for $\Lambda \simeq 1.16 \text{ GeV}$, depending on the cut-off (phenomenological adjustment).

Constituent quark–antiquark pair correlators $\langle (\bar{q}\Gamma_i q')(x) (\bar{q}\Gamma_j q')(y) \rangle$ ³³ via iterated four-fermion interactions as illustrated in Fig. 5.52 form meson propagators

³²The quark propagator in the ENJL model to leading order in $1/N_c$ is obtained by Dyson–Schwinger resummation according to Fig. 5.51. There is no wave function renormalization to this order in $1/N_c$ and the mass can be self-consistently determined from the Dyson–Schwinger equation. To leading order in N_c , this leads to the condition

$$M_i = m_i - g_S \langle \bar{q}q \rangle_i; \quad \langle \bar{q}q \rangle_i \equiv \langle 0 | \bar{q}_i q_i | 0 \rangle, \quad (5.155)$$

$$\langle \bar{q}q \rangle_i = -4 N_c M_i \int_\Lambda \frac{d^4 p}{(2\pi)^4} \frac{i}{p^2 - M_i^2}. \quad (5.156)$$

Here i denotes the quark flavor. The constituent quark mass M_i is independent of the momentum and only a function of G_S, Λ and the current mass m_i .

³³The Γ_i 's denote a 4×4 matrix in spinor space (see Eq. (2.22)) times a 2×2 matrix in isospin space (Pauli matrices), which specifies the channel: spin, parity, isospin, charge etc.

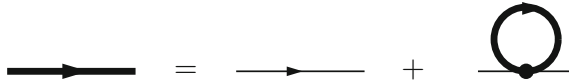


Fig. 5.51 Dyson–Schwinger equation for the inverse quark propagator (see Sect. 2.6.2 (2.184)), which at zero momentum leads to the gap equation (5.155). *Free lines* without endpoints denote inverse propagators; *thick line* dressed or constituent quark; *thin line* free current quark

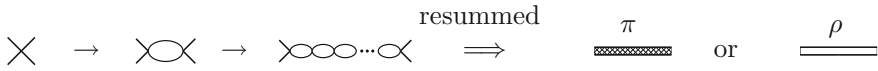


Fig. 5.52 ENJL meson propagators

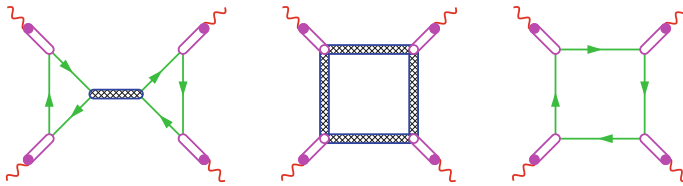


Fig. 5.53 ENJL model graphs: π^0 -exchange, pion-loop and quark-loop dressed by $\rho - \gamma$ transitions

such that one obtains the Fig. 5.53 type of ENJL diagrams which implies a VMD like dressing between mesons, quarks and the virtual photons. It should be clear that the ENJL model does not allow us to make predictions from first principles, since although it is “derived” from QCD by “integrating out the gluons” in the functional integral such a derivation is not possible on a quantitative level, because the non-perturbative aspects are not under control with presently available methods. What emerges is a particular structure of an effective theory, sharing the correct low energy properties of QCD, with effective couplings and masses of particles to be taken from phenomenology.

In fact, in order to work with the model one has to go one step further and introduce the collective fields describing the hadrons, like the pseudo-scalars and the vector-mesons and this leads back to the RLA or HLS type of approaches where the meson fields are put in by hand from the very beginning, just using the symmetries and the symmetry breaking patterns to constrain the effective Lagrangian. However, this does not fix the Lagrangian completely. For example, a special feature of the HLS Lagrangian [190] is the absence of a $\rho^0 \rho^0 \pi^+ \pi^-$ term, which is present in the extended chiral Lagrangian as well as in the VMD ansatz.

The spectrum of states, which eventually should be taken into account, together with the quantum numbers are given in the following Table 5.10. Nonet symmetry would correspond to states

$$\psi_8 = \frac{1}{\sqrt{6}}(u\bar{u} + d\bar{d} - 2s\bar{s}) ; \quad \psi_1 = \frac{1}{\sqrt{3}}(u\bar{u} + d\bar{d} + s\bar{s}) , \quad (5.157)$$

Table 5.10 Low lying mesons (hadrons) in the quark model [42]. θ is the phenomenological flavor mixing angle (see the text)

$n^{2s+1}\ell_J$	J^{PC}	$I = 1$		$I = \frac{1}{2}$	$I = 0$	$I = 0$	θ [$^\circ$]
		$u\bar{d}, d\bar{u}, \frac{1}{\sqrt{2}}(d\bar{d} - u\bar{u})$	$u\bar{s}, s\bar{u}, d\bar{s}, s\bar{d}$	f'	f		
1^1S_0	0^{-+}	π^+, π^-, π^0	K^+, K^-, K^0, \bar{K}^0	η	$\eta'(958)$		-24.5
1^3S_1	1^{--}	$\rho(770)$	$K^*(892)$	$\phi(1020)$	$\omega(782)$		36.4
1^3P_0	0^{++}	$a_0(1450)$	$K_0^*(1430)$	$f_0(1710)$	$f_0(1370)$		
1^3S_1	1^{++}	$a_1(1260)$	$K_1(1270)$	$f_1(1420)$	$f_1(1285)$		
1^3P_2	2^{++}	$a_2(1320)$	$K_2^*(1430)$	$f_2(1525)$	$f_2(1270)$		30.5

Table 5.11 Decay amplitudes $\mathcal{A}(\lambda_1, \lambda_2)$ in units of c_l and two-photon decay width (reduced with $\tilde{\Gamma}_{\gamma\gamma}$ for 1^+) in units of d_l (see text for the definition of c_l, d_l). Table from [244]

J^P	$\mathcal{A}(+-)$	$\mathcal{A}(++)$	$\mathcal{A}(+0)$	$\mathcal{A}(00)$	$\Gamma_{\gamma\gamma}$
0^-	0	\sqrt{X}	0	0	4
0^+	0	$\frac{2(X+\nu W^2)}{\sqrt{3}W}$	0	$\frac{-2}{\sqrt{3}}\sqrt{q_1^2}\sqrt{q_2^2}W$	144
1^+	0	$\frac{-\sqrt{2}\nu}{W}(q_1^2 - q_2^2)$	$\sqrt{2}\sqrt{q_2^2}(\nu - q_1^2)$	0	32
2^+	$2W\nu$	$\sqrt{\frac{2}{3}}\frac{\nu(q_1^2+q_2^2)+2q_1^2q_2^2}{W}$	$\sqrt{2}\sqrt{q_2^2}(\nu + q_1^2)$	$2\sqrt{\frac{2}{3}}W\sqrt{q_1^2}\sqrt{q_2^2}$	192/5

where ψ_1 is the ideal flavor singlet state. This symmetry is broken and the physical states are mixed through a rotation

$$f' = \psi_8 \cos \theta - \psi_1 \sin \theta ; \quad f = \psi_8 \sin \theta + \psi_1 \cos \theta \quad (5.158)$$

and the mixing angle has to be determined by experiment. For $\tan \theta = 1/\sqrt{2} \simeq 35.3^\circ$ the state f' would be a pure $s\bar{s}$ state. This is realized to good accuracy for $\omega - \phi$ mixing where ϕ is almost pure $s\bar{s}$.

A key quantity in the production of resonances in $\gamma\gamma \rightarrow$ hadron reactions is the two-photon width $\Gamma_{\gamma\gamma}$. The decay of a $C = +1$ resonance R into two photons $R(p) \rightarrow \gamma^*(q_1)\gamma^*(q_2)$ has a decay width [244]

$$\Gamma_{\gamma\gamma}[J^P] = \frac{1}{2J+1} \frac{1}{32\pi M} \sum_{\lambda_1, \lambda_2=\pm 1} |\mathcal{A}(\lambda_1, \lambda_2)|^2 . \quad (5.159)$$

in terms of appropriately normalized helicity amplitudes $\mathcal{A}(\lambda_1, \lambda_2)$, which are listed in Table 5.11 in units of $c_l = \sqrt{3/M} e_Q^2 16\pi\alpha R_{nl}^{(l)}(0) Y_{l0}(0, 0)/D^{l+1}$ where $Y_{lm}(\theta, \phi)$ are the spherical harmonics, $D = W^2/4 - m^2 - \nu$. Here, $R_{nl}^{(l)}(0)$ is the l -th derivative of the radial wave function $R_{nl}(r) = \psi_{nlm}(\mathbf{r})/Y_{lm}(\theta, \phi)$ of the bound state at $r = 0$. $W = \sqrt{p^2}$ denotes the two-photon energy, $\nu = q_1 \cdot q_2$ and $X = \nu^2 - q_1^2 q_2^2$. The photon helicities can take on the values $\lambda_i = \pm 1, 0$. The remaining helicity amplitudes can be obtained using the relations

$$\begin{aligned}\mathcal{A}(\lambda_1, \lambda_2) &= \eta_R \mathcal{A}(-\lambda_1, -\lambda_2) \\ \mathcal{A}(\lambda_1, \lambda_2) &= (-1)^J \mathcal{A}(\lambda_2, \lambda_1)|_{q_1 \leftrightarrow q_2},\end{aligned}$$

where $\eta_R = 1$ (-1) for mesons of the “normal” (“abnormal”) J^P series $J^P = 0^+, 1^-, 2^+, \dots$ ($J^P = 0^-, 1^+, 2^-, \dots$). Here we have defined $d_l = 3e_Q^4 \alpha^2 |R_{nl}^{(l)}(0)|^2 / M^{2(l+1)}$. In the case of the 1^+ meson the entry defines the reduced width $\tilde{\Gamma}_{\gamma\gamma}$. This is the transverse–transverse two-photon width divided by a factor $[(q_1^2 - q_2^2)/(2\nu)]^2$, which shows that $\Gamma_{\gamma\gamma}[1^P]$ is zero, in agreement with the Landau–Yang theorem.

At low energies, the interaction of a neutral pion with photons is described by the WZW Lagrangian (5.150). Since this is a non–renormalizable interaction, employing it in loop calculations generally results in ultraviolet divergences, which have to be eliminated by renormalization.

A simple and commonly adopted option is to introduce a Form Factor (FF) at the $\pi^0\gamma\gamma$ interaction vertex, which tames the contributions of highly virtual photons. This is not just a model: the VMD mechanism is a physical process, well established phenomenologically. This results in the following $\pi^0\gamma\gamma$ interaction vertex:

$$V_{\pi^0\gamma\gamma}^{\mu\nu}(q_1, q_2) = \frac{\alpha N_c}{3\pi F_\pi} F_{\pi^0\gamma^*\gamma^*}(m_\pi^2, q_1^2, q_2^2) i \epsilon^{\mu\nu\alpha\beta} q_{1\alpha} q_{2\beta}, \quad (5.160)$$

with $F_{\pi^0\gamma\gamma}(m_\pi^2, 0, 0) = 1$ and where $q_{1,2}$ denote the momenta of the two outgoing photons, and $F_{\pi^0\gamma^*\gamma^*}(m_\pi^2, q_1^2, q_2^2)$ falling off like $1/q_i^2$ in general (see below).

The part of the RLA Lagrangian (see [46, 132] for the complete effective HLS Lagrangian) relevant for us here includes the terms containing the neutral vector–meson $\rho^0(770)$, and the charged axial–vector mesons $a_1^\pm(1260)$ and π^\pm , as well as the photon:

$$\begin{aligned}\mathcal{L}_{\text{int}}^{\text{HLS}} &= -eg_\rho A^\mu \rho_\mu^0 - i g_{\rho\pi\pi} \rho_\mu^0 (\pi^+ \overleftrightarrow{\partial}^\mu \pi^-) - i g_{\gamma\pi\pi} A_\mu (\pi^+ \overleftrightarrow{\partial}^\mu \pi^-) \\ &+ (1-a) e^2 A^\mu A_\mu \pi^+ \pi^- + 2e g_{\rho\pi\pi} A^\mu \rho_\mu^0 \pi^+ \pi^- - e \frac{g_\rho}{F_\pi} A^\mu (V_{a_1\mu}^+ \pi^- - V_{a_1\mu}^- \pi^+) \\ &+ \dots\end{aligned} \quad (5.161)$$

where masses and couplings are related by

$$\begin{aligned}M_\rho^2 &= ag_V^2 F_\pi^2, & g_\rho &= ag_V F_\pi^2, \\ g_{\rho\pi\pi} &= \frac{1}{2} ag_V, & g_{\gamma\pi\pi} &= \left(1 - \frac{a}{2}\right) e.\end{aligned}$$

The parameter a is not fixed by the symmetry itself. A good choice is $a = 2$ which conforms with the phenomenological facts **(i)** universality of the ρ coupling $g_{\rho\pi\pi} = g_V$, **(ii)** $g_{\gamma\pi\pi} = 0$, which is the ρ meson dominance of the pion form factor, and **(iii)** the KSFR relation [245] $M_\rho^2 = 2g_{\rho\pi\pi}^2 F_\pi^2$. The corresponding Feynman rules are listed in Fig. 5.54 and supplement the sQED ones in Fig. 2.13. Also included we have the WZW term (5.150) and the vector–boson propagators read

$$i\Delta_V^{\mu\nu}(q, M_V) = \frac{-i}{(q^2 - M_V^2)} \left\{ g^{\mu\nu} - \frac{q^\mu q^\nu}{q^2} \right\} \quad (5.162)$$

where M_V is the mass.

As mentioned at the beginning of this section already, for the models presented so far one is confronted with the problem that one has to complement a non-renormalizable effective theory with renormalizable perturbative QCD above a certain cut-off. This generally results in a substantial cut-off dependence of the results. In order to avoid this matching problem, the most recent estimations attempt to resort to quark-hadron duality for matching L.D. and S.D. physics. This duality can be proven to hold in the large- N_c limit of QCD and this may be exploited in an $1/N_c$ expansion approach to QCD. However, once more the $N_c \rightarrow \infty$ limit, in which the hadrons turn out to be an infinite series of vector resonances, is not under quantitative control [226, 227]. Hence, a further approximation must be made by replacing the infinite series of narrow resonances by a few low lying states which are identified with existing hadronic states. As a result one obtains a modeling of the hadronic amplitudes, the simplest one being the lowest meson dominance (LMD) or minimal hadronic ansatz (MHA) approximation to large- N_c QCD [246, 247]. An examples of this type of ansatz has been discussed on p. 321 in Sect. 4.2.2. For a detailed discussion the reader should consult the articles [246–248].

The various HLbL contributions in the effective theory are shown in Fig. 5.55 and the corresponding $1/N_c$ and chiral $O(p)$ counting is given in Table 5.12.

Based on effective hadronic models, major efforts in estimating a_μ^{LbL} were made by Hayakawa, Kinoshita and Sanda (HKS 1995) [210], Bijnsens, Pallante and Prades (BPP 1995) [235] (see [249] for a recent update) and Hayakawa and Kinoshita (HK 1998) [250]. In 2001 Knecht and Nyffeler (KN 2001) [234, 251] presented a consequent large- N_c QCD inspired approach which implemented the proper QCD large momentum asymptotics such that cut-off matching is avoided as a matter of principle. They thereby also discovered a sign mistake in the π^0, η, η' exchange

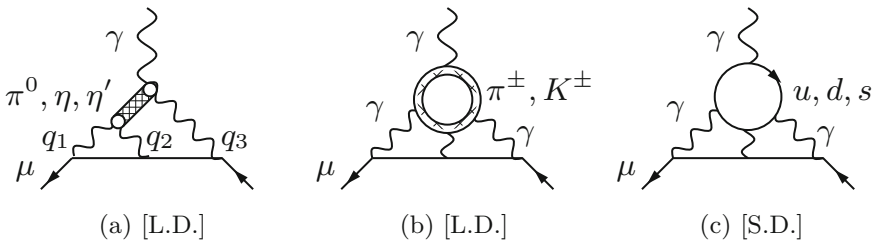


Fig. 5.55 Hadronic light-by-light scattering diagrams in a low energy effective model description. Diagrams **a** and **b** represent the long distance (L.D.) contributions at momenta $p \leq \Lambda$, diagram **c** involving a quark loop which yields the leading short distance (S.D.) part at momenta $p \geq \Lambda$ with $\Lambda \sim 1-2$ GeV as UV cut-off. Internal photon lines are dressed by $\rho - \gamma$ mixing. Note that, in view of multiple scale nature of the problem (see Fig. 5.47), the classification into L.D. and S.D. as used here is very sloppy

Table 5.12 Orders with respect to $1/N_c$ and chiral small p expansion of typical leading contributions shown in Fig. 5.55

Diagram	$1/N_c$ expansion	p expansion	Type
Figure 5.55a	N_c	p^6	π^0, η, η' exchange
Figure 5.55a	N_c	p^8	a_1, f_1, f_1' exchange
Figure 5.55b	1	p^4	Meson loops (π^\pm, K^\pm)
Figure 5.55c	N_c	p^8	Quark loops

contribution (see also [252, 253]), which changed the central value by $+167 \times 10^{-11}$! More recently Melnikov and Vainshtein (MV 2004) [254] found additional inconsistencies in previous calculations, this time in the short distance constraints (QCD/OPE) used in matching the high energy behavior of the effective models used for the π^0, η, η' exchange contribution. Knecht and Nyffeler restrict their analysis to pion-pole approximation. At least one vector state (V) has to be included in addition to the leading one in order to be able to match the correct high energy behavior. The resulting ‘‘LMD+V’’ parametrization has been worked out for the calculation of the LbL π^0 -pole contribution in [234] and was used later in [254] with modified parameter h_2 (see below) at the internal vertex and with a constant pion-pole form factor at the external vertex. Explicit models of form factors will be considered later.

As we will see a lot of effort is required to tune models such that they satisfy QCD large momentum asymptotics, which should ease the matching of models with true QCD. However, if a model is providing a good description of all available data up to 1 GeV say, but fails to have the correct high energy behavior, it does not mean that the model is obsolete in estimating the contribution for the range of its validity, provided it is parametrizing physics well there.

In the following we will discuss the various contributions classified in Table 5.12 in some detail. Special attention will be given to the leading pion-exchange. After a summary of the results the novel multi channel dispersive approach will be overviewed. The chapter will end with an account of the lattice QCD method and results (HVP and HLbL). Needless to say that only the original literature can provide full details on the various aspects and attempts to provide reliable results for these challenging calculations.

5.2.3 Pion-Exchange Contribution

Here we discuss the dominating hadronic contribution which is due to the neutral pion-exchange diagrams shown in Fig. 5.56. The key object here is the $\pi^0\gamma\gamma$ form factor $\mathcal{F}_{\pi^0\gamma^*\gamma^*}(m_\pi^2, q_1^2, q_2^2)$ which is defined by the matrix element

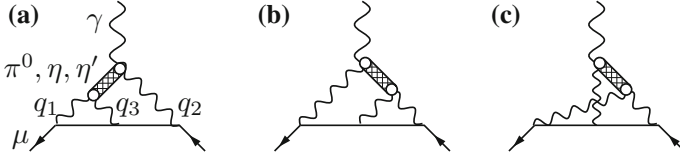


Fig. 5.56 Leading hadronic light-by-light scattering diagrams. Internal photons lines are dressed by $\rho - \gamma$ mixing

$$i \int d^4x e^{iq \cdot x} \langle 0 | T \{ j_\mu(x) j_\nu(0) \} | \pi^0(p) \rangle = \varepsilon_{\mu\nu\alpha\beta} q^\alpha p^\beta \mathcal{F}_{\pi^0 \gamma^* \gamma^*}(m_\pi^2, q^2, (p-q)^2). \quad (5.163)$$

It is Bose symmetric $\mathcal{F}_{\pi^0 \gamma^* \gamma^*}(s, q_1^2, q_2^2) = \mathcal{F}_{\pi^0 \gamma^* \gamma^*}(s, q_2^2, q_1^2)$ of course, as the two photons are indistinguishable. This holds for off-shell pions as well. An important point we should notice is that in the Feynman integral corresponding to one of the diagrams of Fig. 5.56 the pion is **not** necessarily near the pole, although pole-dominance might be expected to give a reasonable approximation. For clarity we therefore define the form factor not by the matrix element (5.163), but by the vertex function

$$i \int d^4x e^{iq \cdot x} \langle 0 | T \{ j_\mu(x) j_\nu(0) \tilde{\varphi}_{\pi^0}(p) \} | 0 \rangle = \varepsilon_{\mu\nu\alpha\beta} q^\alpha p^\beta \mathcal{F}_{\pi^0 \gamma^* \gamma^*}(p^2, q^2, (p-q)^2) \times \frac{i}{p^2 - m_\pi^2}, \quad (5.164)$$

with $\tilde{\varphi}(p) = \int d^4y e^{ipx} \varphi(y)$ the Fourier transformed π^0 -field.

The π^0 -exchange contributions to $\Pi_{\mu\nu\lambda\rho}(q_1, q_2, q_3)$, according to Fig. 5.56 takes the form

$$\begin{aligned} i \Pi_{\mu\nu\lambda\rho}^{(\pi^0)}(q_1, q_2, q_3) = & \frac{\mathcal{F}_{\pi^0 \gamma^* \gamma^*}(q_2^2, q_1^2, q_3^2) \mathcal{F}_{\pi^0 \gamma^* \gamma^*}(q_2^2, q_2^2, k^2)}{q_2^2 - m_\pi^2} \varepsilon_{\mu\lambda\alpha\beta} q_1^\alpha q_3^\beta \varepsilon_{\nu\rho\sigma\tau} q_2^\sigma q_2'^\tau \\ & + \frac{\mathcal{F}_{\pi^0 \gamma^* \gamma^*}(q_1^2, q_2^2, q_3^2) \mathcal{F}_{\pi^0 \gamma^* \gamma^*}(q_1^2, q_1^2, k^2)}{q_1^2 - m_\pi^2} \varepsilon_{\mu\rho\alpha\beta} q_1^\alpha q_1'^\beta \varepsilon_{\nu\lambda\sigma\tau} q_2^\sigma q_3^\tau \\ & + \frac{\mathcal{F}_{\pi^0 \gamma^* \gamma^*}(q_3^2, q_1^2, q_2^2) \mathcal{F}_{\pi^0 \gamma^* \gamma^*}(q_3^2, q_3^2, k^2)}{q_3^2 - m_\pi^2} \varepsilon_{\mu\nu\alpha\beta} q_1^\alpha q_2^\beta \varepsilon_{\lambda\rho\sigma\tau} q_3^\sigma q_3'^\tau \end{aligned}$$

with $q'_i = q_i + k$. To compute $a_{\mu}^{\text{LbL};\pi^0} \equiv F_{\text{M}}(0)|_{\text{LbL};\pi^0}$, we need

$$\begin{aligned}
\text{i} \frac{\partial}{\partial k^{\rho}} \Pi_{\mu\nu\lambda\sigma}^{(\pi^0)}(q_1, q_2, k - q_1 - q_2) = & \\
& \frac{\mathcal{F}_{\pi^0*\gamma*\gamma^*}(q_2^2, q_1^2, q_3^2) \mathcal{F}_{\pi^0*\gamma*\gamma}(q_2^2, q_2^2, 0)}{q_2^2 - m_{\pi}^2} \varepsilon_{\mu\lambda\alpha\beta} q_1^{\alpha} q_2^{\beta} \varepsilon_{\nu\sigma\rho\tau} q_2^{\tau} \\
& + \frac{\mathcal{F}_{\pi^0*\gamma*\gamma^*}(q_1^2, q_2^2, q_3^2) \mathcal{F}_{\pi^0*\gamma*\gamma}(q_1^2, q_1^2, 0)}{q_1^2 - m_{\pi}^2} \varepsilon_{\mu\sigma\tau\rho} q_1^{\tau} \varepsilon_{\nu\lambda\alpha\beta} q_1^{\alpha} q_2^{\beta} \\
& + \frac{\mathcal{F}_{\pi^0*\gamma*\gamma^*}(q_3^2, q_1^2, q_2^2) \mathcal{F}_{\pi^0*\gamma*\gamma}(q_3^2, q_3^2, 0)}{q_3^2 - m_{\pi}^2} \varepsilon_{\mu\nu\alpha\beta} q_1^{\alpha} q_2^{\beta} \varepsilon_{\lambda\sigma\rho\tau} q_3^{\tau} \\
& + O(k). \tag{5.165}
\end{aligned}$$

Here, we may set $k^{\mu} = 0$ such that $q_3 = -(q_1 + q_2)$. Inserting this last expression into (5.145) and computing the corresponding Dirac traces, one obtains [234]

$$\begin{aligned}
a_{\mu}^{\text{LbL};\pi^0} = & -e^6 \int \frac{d^4 q_1}{(2\pi)^4} \frac{d^4 q_2}{(2\pi)^4} \frac{1}{q_1^2 q_2^2 (q_1 + q_2)^2 [(p + q_1)^2 - m^2] [(p - q_2)^2 - m^2]} \\
& \times \left[\frac{\mathcal{F}_{\pi^0*\gamma*\gamma^*}(q_2^2, q_1^2, q_3^2) \mathcal{F}_{\pi^0*\gamma*\gamma}(q_2^2, q_2^2, 0)}{q_2^2 - m_{\pi}^2} T_1(q_1, q_2; p) \right. \\
& \left. + \frac{\mathcal{F}_{\pi^0*\gamma*\gamma^*}(q_3^2, q_1^2, q_2^2) \mathcal{F}_{\pi^0*\gamma*\gamma}(q_3^2, q_3^2, 0)}{q_3^2 - m_{\pi}^2} T_2(q_1, q_2; p) \right], \tag{5.166}
\end{aligned}$$

with

$$\begin{aligned}
T_1(q_1, q_2; p) = & \frac{16}{3} (p \cdot q_1) (p \cdot q_2) (q_1 \cdot q_2) - \frac{16}{3} (p \cdot q_2)^2 q_1^2 \\
& - \frac{8}{3} (p \cdot q_1) (q_1 \cdot q_2) q_2^2 + 8(p \cdot q_2) q_1^2 q_2^2 - \frac{16}{3} (p \cdot q_2) (q_1 \cdot q_2)^2 \\
& + \frac{16}{3} m^2 q_1^2 q_2^2 - \frac{16}{3} m^2 (q_1 \cdot q_2)^2, \tag{5.167}
\end{aligned}$$

$$\begin{aligned}
T_2(q_1, q_2; p) = & \frac{16}{3} (p \cdot q_1) (p \cdot q_2) (q_1 \cdot q_2) - \frac{16}{3} (p \cdot q_1)^2 q_2^2 \\
& + \frac{8}{3} (p \cdot q_1) (q_1 \cdot q_2) q_2^2 + \frac{8}{3} (p \cdot q_1) q_1^2 q_2^2 \\
& + \frac{8}{3} m^2 q_1^2 q_2^2 - \frac{8}{3} m^2 (q_1 \cdot q_2)^2. \tag{5.168}
\end{aligned}$$

Two of the three diagrams give equal contributions and T_2 has been symmetrized with respect to the exchange $q_1 \leftrightarrow -q_2$. At this stage everything is known besides the $\pi^0\gamma\gamma$ off-shell form factors.

For later reference it is interesting to note that the imaginary part obtained by applying (2.141) to the pion propagator (unitarity cut) is given by

$$\begin{aligned}
\text{Im} \left(i \frac{\partial}{\partial k^\rho} \Pi_{\mu\nu\lambda\sigma}^{(\pi^0)}(q_1, q_2, k - q_1 - q_2) \right) = \\
-\pi \delta(q_2^2 - m_\pi^2) \mathcal{F}_{\pi^0 * \gamma^* \gamma^*}(m_\pi^2, q_1^2, q_3^2) \mathcal{F}_{\pi^0 * \gamma^* \gamma}(m_\pi^2, m_\pi^2, 0) \varepsilon_{\mu\lambda\alpha\beta} q_1^\alpha q_2^\beta \varepsilon_{\nu\sigma\rho\tau} q_2^\tau \\
-\pi \delta(q_1^2 - m_\pi^2) \mathcal{F}_{\pi^0 * \gamma^* \gamma^*}(m_\pi^2, q_2^2, q_3^2) \mathcal{F}_{\pi^0 * \gamma^* \gamma}(m_\pi^2, m_\pi^2, 0) \varepsilon_{\mu\sigma\tau\rho} q_1^\tau \varepsilon_{\nu\lambda\alpha\beta} q_1^\alpha q_2^\beta \\
-\pi \delta(q_3^2 - m_\pi^2) \mathcal{F}_{\pi^0 * \gamma^* \gamma^*}(m_\pi^2, q_1^2, q_2^2) \mathcal{F}_{\pi^0 * \gamma^* \gamma}(m_\pi^2, m_\pi^2, 0) \varepsilon_{\mu\nu\alpha\beta} q_1^\alpha q_2^\beta \varepsilon_{\lambda\sigma\rho\tau} q_3^\tau \\
+ O(k). \tag{5.169}
\end{aligned}$$

in terms of the on-shell π^0 transition form factors.

The result in (5.166) does not depend on the direction of the muon momentum vector p such that we may average in Euclidean space over the directions \hat{P} :

$$\langle \dots \rangle = \frac{1}{2\pi^2} \int d\Omega(\hat{P}) \dots \tag{5.170}$$

using the technique of Gegenbauer polynomials (hyperspherical approach), see [255]. Since all p dependent terms are independent of the pseudoscalar form factors one may perform the integrations in general. After reducing numerators of the amplitudes T_i against the denominators of the propagators one is left with the following integrals ((4) $\equiv (P + Q_1)^2 + m_\mu^2$ and (5) $\equiv (P - Q_2)^2 + m_\mu^2$ with $P^2 = -m_\mu^2$)

$$\begin{aligned}
\left\langle \frac{1}{(4)} \frac{1}{(5)} \right\rangle &= \frac{1}{m_\mu^2 R_{12}} \arctan \left(\frac{zx}{1 - z\tau} \right), \\
\left\langle (P \cdot Q_1) \frac{1}{(5)} \right\rangle &= -(Q_1 \cdot Q_2) \frac{(1 - R_{m2})^2}{8m_\mu^2}, \\
\left\langle (P \cdot Q_2) \frac{1}{(4)} \right\rangle &= (Q_1 \cdot Q_2) \frac{(1 - R_{m1})^2}{8m_\mu^2}, \\
\left\langle \frac{1}{(4)} \right\rangle &= -\frac{1 - R_{m1}}{2m_\mu^2}, \\
\left\langle \frac{1}{(5)} \right\rangle &= -\frac{1 - R_{m2}}{2m_\mu^2}, \tag{5.171}
\end{aligned}$$

where $R_{mi} = \sqrt{1 + 4m_\mu^2/Q_i^2}$ and $(Q_1 \cdot Q_2) = Q_1 Q_2 \tau$ with $\tau = \cos \theta$, θ the angle between the two Euclidean four-vectors Q_1 and Q_2 . Note that $\int d\Omega(\hat{Q}_1) d\Omega(\hat{Q}_2) = 4\pi^4$. Denoting $x = \sqrt{1 - \tau^2}$, we have $R_{12} = Q_1 Q_2 x$ and

$$z = \frac{Q_1 Q_2}{4m_\mu^2} (1 - R_{m1})(1 - R_{m2}).$$

We have thus eliminated all momentum dependences up to the three which also show up in the hadronic form factors Q_1^2 , Q_2^2 , and Q_3^2 or equivalently on $(Q_1 \cdot Q_2) = Q_1 Q_2 \cos \theta$ and end up with a 3-dimensional integral over $Q_1 = |Q_1|$, $Q_2 = |Q_2|$

and $\tau = \cos \theta$:

$$a_{\mu}^{\text{LbL};\pi^0} = -\frac{2\alpha^3}{3\pi^2} \int_0^{\infty} dQ_1 dQ_2 \int_{-1}^{+1} d\tau \sqrt{1-\tau^2} Q_1^3 Q_2^3 \times [F_1 P_6 I_1(Q_1, Q_2, \tau) + F_2 P_7 I_2(Q_1, Q_2, \tau)], \quad (5.172)$$

where $P_6 = 1/(Q_2^2 + m_{\pi}^2)$, and $P_7 = 1/(Q_3^2 + m_{\pi}^2)$ denote the Euclidean single particle exchange propagators. The integration kernels I_1 and I_2 , which factorize from the dependence on the hadronic form factors in F_1 and F_2 , are given by

$$\begin{aligned} I_1(Q_1, Q_2, \tau) &= X(Q_1, Q_2, \tau) \left(8 P_1 P_2 (Q_1 \cdot Q_2) \right. \\ &\quad - 2 P_1 P_3 (Q_2^4/m_{\mu}^2 - 2 Q_2^2) - 2 P_1 (2 - Q_2^2/m_{\mu}^2 + 2 (Q_1 \cdot Q_2)/m_{\mu}^2) \\ &\quad + 4 P_2 P_3 Q_1^2 - 4 P_2 - 2 P_3 (4 + Q_1^2/m_{\mu}^2 - 2 Q_2^2/m_{\mu}^2) + 2/m_{\mu}^2 \Big) \\ &\quad - 2 P_1 P_2 (1 + (1 - R_{m1}) (Q_1 \cdot Q_2)/m_{\mu}^2) \\ &\quad + P_1 P_3 (2 - (1 - R_{m1}) Q_2^2/m_{\mu}^2) + P_1 (1 - R_{m1})/m_{\mu}^2 \\ &\quad + P_2 P_3 (2 + (1 - R_{m1})^2 (Q_1 \cdot Q_2)/m_{\mu}^2) + 3 P_3 (1 - R_{m1})/m_{\mu}^2, \\ I_2(Q_1, Q_2, \tau) &= X(Q_1, Q_2, \tau) \left(4 P_1 P_2 (Q_1 \cdot Q_2) \right. \\ &\quad + 2 P_1 P_3 Q_2^2 - 2 P_1 + 2 P_2 P_3 Q_1^2 - 2 P_2 - 4 P_3 - 4/m_{\mu}^2 \Big) \\ &\quad - 2 P_1 P_2 - 3 P_1 (1 - R_{m2})/(2m_{\mu}^2) - 3 P_2 (1 - R_{m1})/(2m_{\mu}^2) \\ &\quad + P_1 P_3 (2 + 3 (1 - R_{m2}) Q_2^2/(2m_{\mu}^2) + (1 - R_{m2})^2 (Q_1 \cdot Q_2)/(2m_{\mu}^2)) \\ &\quad + P_2 P_3 (2 + 3 (1 - R_{m1}) Q_1^2/(2m_{\mu}^2) + (1 - R_{m1})^2 (Q_1 \cdot Q_2)/(2m_{\mu}^2)) \\ &\quad - P_3 (2 - R_{m1} - R_{m2})/(2m_{\mu}^2), \end{aligned} \quad (5.173)$$

where we used the notation $P_1=1/Q_1^2$, $P_2=1/Q_2^2$, and $P_3 = 1/Q_3^2$ for the Euclidean propagators and introduced the auxiliary function

$$X(Q_1, Q_2, \tau) = \frac{1}{Q_1 Q_2 x} \arctan \left(\frac{zx}{1 - z\tau} \right), \quad (5.174)$$

which has the following asymptotic expansion for small x , near the forward and backward points:

$$X(Q_1, Q_2, \tau) = \frac{1}{Q_1 Q_2} \begin{cases} \frac{z}{1-z} \left(1 + \frac{1}{6} \frac{z(z-3)}{(1-z)^2} x^2 \right) + O(x^3) & \text{for } \tau > 0 \\ \frac{z}{1+z} \left(1 + \frac{1}{6} \frac{z(z+3)}{(1+z)^2} x^2 \right) + O(x^3) & \text{for } \tau < 0 \end{cases}.$$

Equation (5.172) provides the general set up for studying any type of single particle exchange contribution as a 3–dimensional integral representation. The non-perturbative factors according to (5.166) are given by

$$\begin{aligned} F_1 &= \mathcal{F}_{\pi^0 \ast \gamma \ast \gamma \ast}(-Q_2^2, -Q_1^2, -Q_3^2) \mathcal{F}_{\pi^0 \ast \gamma \ast \gamma}(-Q_2^2, -Q_2^2, 0), \\ F_2 &= \mathcal{F}_{\pi^0 \ast \gamma \ast \gamma \ast}(-Q_3^2, -Q_1^2, -Q_2^2) \mathcal{F}_{\pi^0 \ast \gamma \ast \gamma}(-Q_3^2, -Q_3^2, 0), \end{aligned} \quad (5.175)$$

and will be considered next. Note that F_2 is symmetric under the exchange $Q_1 \leftrightarrow Q_2$. We used this property to write $I_2(Q_1, Q_2, \tau)$ in (5.173) in a symmetric way.

5.2.4 The $\pi^0 \gamma \gamma$ Transition Form Factor

Experimental Constraints

Above we have formally reduced the problem of calculating the π^0 –exchange contribution diagrams Fig. 5.56 to the problem of calculating the integral (5.172). The non-perturbative aspect is now confined in the form factor function $\mathcal{F}_{\pi^0 \ast \gamma \ast \gamma \ast}(s, s_1, s_2)$, which is not known as well as it would be desirable. For the time being we have to use one of the hadronic models introduced above together with pQCD as a constraint on the high energy asymptotic behavior. Fortunately some experimental data are also available. The constant $\mathcal{F}_{\pi^0 \gamma \gamma}(m_\pi^2, 0, 0)$ is well determined as

$$\mathcal{F}_{\pi^0 \gamma \gamma}(m_\pi^2, 0, 0) = \frac{1}{4\pi^2 F_\pi}, \quad (5.176)$$

by the $\pi^0 \rightarrow \gamma \gamma$ decay rate. The invariant matrix element reads

$$\begin{aligned} \mathcal{M}[\pi^0(q) \rightarrow \gamma(p_1, \lambda_1) \gamma(p_2, \lambda_2)] &= \\ e^2 \varepsilon^{\mu \ast}(p_1, \lambda_1) \varepsilon^{\nu \ast}(p_2, \lambda_2) \varepsilon_{\mu \nu \alpha \beta} p_1^\alpha p_2^\beta \mathcal{F}_{\pi^0 \ast \gamma \ast \gamma \ast}(q^2, p_1^2, p_2^2). \end{aligned} \quad (5.177)$$

The on-shell transition amplitude in the chiral limit follows from the WZW Lagrangian (5.150) and is given by

$$M_{\pi^0 \gamma \gamma} = e^2 \mathcal{F}_{\pi^0 \gamma \gamma}(0, 0, 0) = \frac{e^2 N_c}{12\pi^2 F_\pi} = \frac{\alpha}{\pi F_\pi} \approx 0.025 \text{ GeV}^{-1},$$

and with $F_\pi \simeq 92.4 \text{ MeV}$ and quark color number $N_c = 3$, rather accurately predicts the experimental result

$$|M_{\pi^0 \gamma \gamma}^{\text{exp}}| = \sqrt{64\pi \Gamma_{\pi^0 \gamma \gamma} / m_\pi^3} = 0.025 \pm 0.001 \text{ GeV}^{-1}.$$

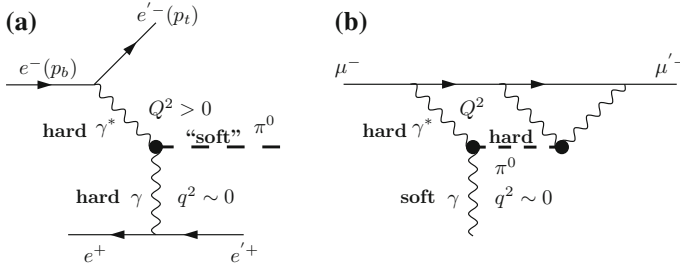


Fig. 5.57 **a** Measurement of the π^0 form factor $\mathcal{F}_{\pi^0\gamma^*\gamma}(m_\pi^2, -Q^2, 0)$ at high space-like Q^2 , **b** needed at external vertex is $\mathcal{F}_{\pi^0\gamma^*\gamma}(-Q^2, -Q^2, 0)$

At leading order QED the $\pi^0 \rightarrow \gamma\gamma$ decay width is given by

$$\Gamma_{\pi^0\gamma\gamma} = \frac{\pi\alpha^2 m_\pi^3}{4} |\mathcal{F}_{\pi^0\gamma\gamma}(m_\pi^2, 0, 0)|^2 \tag{5.178}$$

and its experimental measurement is

$$\Gamma_{\pi^0\gamma\gamma} = 7.73(16) \text{ eV} . \tag{5.179}$$

Additional experimental information is available for $\mathcal{F}_{\pi^0\gamma^*\gamma}(m_\pi^2, -Q^2, 0)$ coming from experiments $e^+e^- \rightarrow e^+e^-\pi^0$ (see Fig. 5.57) where the electron (positron) gets tagged, i.e., selected according to appropriate kinematic criteria, such that $Q^2 = -(p_b - p_t)^2 = 2E_b E_t (1 - \cos \Theta_t)$ is large. p_b is the beam electron (positron) four-momentum, p_t the one of the tagged electron (positron) and Θ_t is the angle between \mathbf{p}_t and \mathbf{p}_b . The differential cross section

$$\frac{d\sigma}{dQ^2}(e^+e^- \rightarrow e^+e^-\pi^0)$$

is then strongly peaked towards zero momentum transfer of the untagged positron (electron) which allows experiments to extract the form factor.

Note that the production of an on-shell pion at large $-q_1^2 = Q^2$ is only possible if the real photon is highly energetic, i.e., $q_2^0 = |\mathbf{q}_2|$ large. This is different from the $g - 2$ kinematical situation at the external photon vertex, where the external photon has zero four-momentum. By four-momentum conservation thus only $\mathcal{F}_{\pi^0\gamma^*\gamma}(-Q^2, -Q^2, 0)$ and **not** $\mathcal{F}_{\pi^0\gamma^*\gamma}(m_\pi^2, -Q^2, 0)$ can enter at the **external** vertex. However, for a “far off-shell pion” the effective theory breaks down altogether. Indeed, $\mathcal{F}_{\pi^0\gamma^*\gamma}(-Q^2, -Q^2, 0)$ is not an observable quantity away from the pion-pole and in particular not for large $Q^2 \gg m_\pi^2$.

For the **internal** vertex both photons are virtual, and luckily, experimental data on $\mathcal{F}_{\pi^0\gamma^*\gamma}(m_\pi^2, -Q^2, 0)$ is available from CELLO [256] and CLEO [257]. This is **one** of the “question marks region” of Fig. 5.47 which is actually controlled by experimental

data. Experiments fairly well confirm the Brodsky-Lepage [258] evaluation of the large Q^2 behavior

$$\lim_{Q^2 \rightarrow \infty} \mathcal{F}_{\pi^0 \gamma^* \gamma}(m_\pi^2, -Q^2, 0) \sim \frac{2F_\pi}{Q^2}. \tag{5.180}$$

In this approach the transition form factor is represented as a convolution of a hard scattering amplitude (HSA) and the soft non-perturbative meson wave function and the asymptotic behavior follows from a pQCD calculation of the HSA. Together with the constraint from π^0 decay

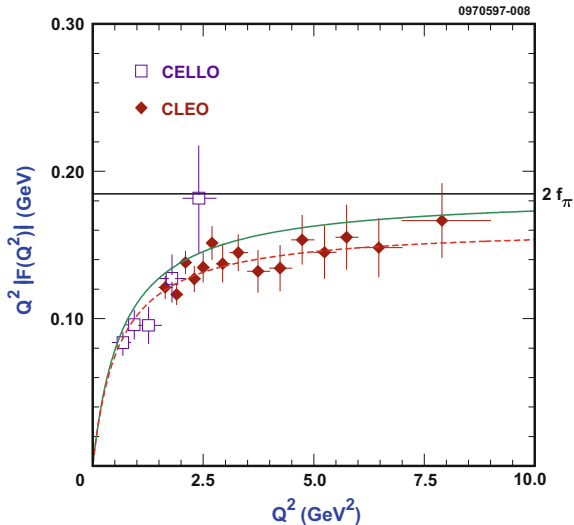
$$\lim_{Q^2 \rightarrow 0} \mathcal{F}_{\pi^0 \gamma^* \gamma}(m_\pi^2, -Q^2, 0) = \frac{1}{4\pi^2 F_\pi} \tag{5.181}$$

an interpolating formula

$$\mathcal{F}_{\pi^0 \gamma^* \gamma}(m_\pi^2, -Q^2, 0) \simeq \frac{1}{4\pi^2 F_\pi} \frac{1}{1 + (Q^2/8\pi^2 F_\pi^2)} \tag{5.182}$$

was proposed, which in fact gives an acceptable fit to the data shown in Fig. 5.58. Refinements of form factor calculations/models were discussed and compared with the data in [257] (see also [259–267]). Recently new experiments have determined this form factor. The results from BaBar [268] and Belle [269] are included in Fig. 5.59. While BaBar data seem to indicate a “violation” of the Brodsky-Lepage bound (at least at the high end of the explored energy range), newer Belle data suggest a perfect matching with this behavior.

Fig. 5.58 $\mathcal{F}_{\pi^0 \gamma^* \gamma}(m_\pi^2, -Q^2, 0)$ data from CLEO and CELLO. Shown is the Brodsky-Lepage prediction (5.182) (solid curve) and the phenomenological fit by CLEO (dashed curve) [Reprinted with permission from [257]. Copyright (2007) by the American Physical Society]



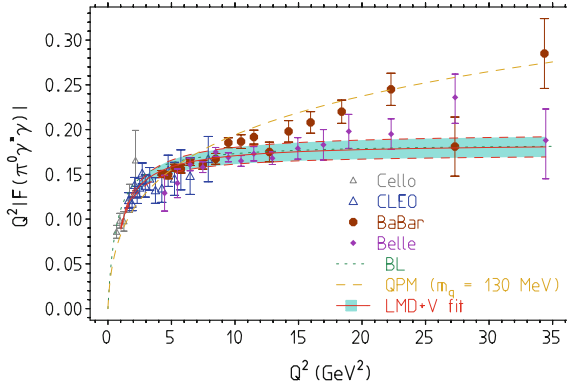


Fig. 5.59 An update of Fig. 5.58 including the new data from BaBar and Belle, which reach much higher energy transfers. The BaBar data seem to suggest a violation of the Brodsky-Lepage (BL) bound, but could be fitted by a CQM fit with a quark mass of 130 MeV. Actually, a best LMD+V fit (aqua band) of the weighted average yields a perfect compatibility with the BL behavior. The LMD+V form factor (5.218) best fit we obtain with $h_5 = -7.66(50) \text{ GeV}^4$ adopting the VMD inspired values $M_1 = M_\rho = 0.77526(25) \text{ GeV}$ and $M_2 = M_{\rho'} = 1.455(25) \text{ GeV}$. The terms proportional to m_π^2 are negligible in the fit and we take $h_3, h_4, h_6 \approx 0$. Note that the LMD+V fit is not a free fit as the general form is theory (QCD+OPE) driven and as the corresponding constrained fit is required to satisfy additional conditions (see text below)

Transition form factor measurements have also been performed for η and η' [256, 257, 268, 270–272]. They provide important constraints for the evaluation of the corresponding $g - 2$ contributions below.

It is important to note here that the L.D. term $\mathcal{F}_{\pi^0\gamma\gamma}(m_\pi^2, 0, 0)$, which is unambiguously determined by the anomaly, gets screened at large Q^2 , in spite of the fact that in the chiral limit

$$\mathcal{F}_{\pi^0\gamma^*\gamma^*}(q_3^2, q_1^2, q_2^2)|_{m_q=0} = \mathcal{F}_{\pi^0\gamma\gamma}(0, 0, 0)|_{m_q=0} = \frac{1}{4\pi^2 F_0} . \quad (5.183)$$

The $1/Q^2$ behavior is in common with the one of the quark loops when $m_q \neq 0$, as we will discuss next. A seemingly plausible approximation which helps to simplify the calculation is to assume *pion-pole dominance* in the sense that one takes the form factor on the pion mass shell and uses $\mathcal{F}_{\pi^0\gamma^*\gamma^*}$ everywhere. This pole approximation apparently has been used by all authors (HKS, BPP, KN) in the past, but has been criticized in [273]. The first analyses taking the off-shellness into account has been presented in [274, 275].

Here an important point comes into play: modeling of the non-perturbative effects one has to distinguish carefully whether one is considering the *soft-soft* regime where a low energy effective theory like ENJL or HLS is adequate or whether one is attempting to model the *soft-hard* ranges of Fig. 5.47, which is what Knecht-Nyffeler [234] and Melnikov-Vainshtein [254] are considering. It makes a difference since the RLA type models predict a VMD dressing of all off-shell photon lines,

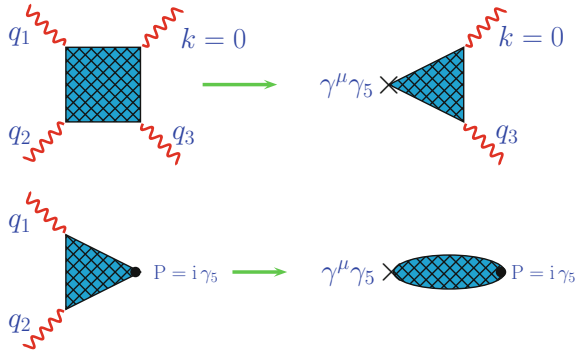


Fig. 5.60 The OPE for the photon–photon scattering Green function, for $q_1 \approx -q_2 \gg q_3 = -(q_1 + q_2)$ the triangle “blob” is dominated by pseudoscalar exchanges but also accounts for whatever QCD permits. In the sum of all hadronic states it is given by the perturbatively calculable triangle anomaly. *Upper panel* Melnikov–Vainshtein considering the $\gamma\gamma \rightarrow \gamma\gamma$ amplitude (see p. 480 below). *Lower panel* Knecht–Nyffeler considering the $\gamma\gamma \rightarrow \pi^0$ form factor (see p. 459 below). The subsequent $\pi^0 \rightarrow \gamma\gamma$ transition is taken into account in a second step

while QCD asymptotics predicts that the form factor at the external vertex has to be constant. This is also the case in the large- N_c inspired approach if consequently applied, as in [274]. It also seems not to be a surprise that (MV) and (JN) get a different asymptotic constant, the first given by the triangle anomaly, the second by the magnetic susceptibility. MV consider the full $\gamma^*\gamma^* \rightarrow \gamma^*\gamma$ ($k^\mu = 0$) amplitude Fig. 5.60, while KN/JN consider the Green function of two currents with a pion field as a starting point. The “discrepancy” is actually a matter of splitting the problem into sub-problems/sub-processes as suggested by Fig. 5.55 where different effects may be taken into account in different ways. We also should keep in mind that the MV approach is focusing on a specific kinematic constraint where OPE can be applied (Fig. 5.47). One also should note that in the low energy regime the spontaneous breaking of the chiral symmetry implies the existence of quark condensates, which have no trace in pQCD and in the *hard–hard* range the true short distance behavior should be that of the unbroken phase i.e. by pQCD.

The point is that the form factor sitting at the external photon vertex in the pole approximation [read $\mathcal{F}_{\pi^0\gamma^*\gamma}(m_\pi^2, -Q^2, 0)$] for $-Q^2 \neq m_\pi^2$ violates four-momentum conservation $k^\mu = 0$. The latter requires $\mathcal{F}_{\pi^0\gamma^*\gamma}(-Q^2, -Q^2, 0)$ as discussed before. In the chiral limit the only consistent choice for the form factor in the pole approximation is $\mathcal{F}_{\pi^0\gamma\gamma}(0, 0, 0)$ which is a constant given by (5.181); this model is advocated by Melnikov and Vainshtein, and leads to a substantially larger contribution, due to the lack of damping of the high energy modes. But, what we really need is $\mathcal{F}_{\pi^0\gamma^*\gamma}(-Q^2, -Q^2, 0)$ and the question is how it behaves at high energies. Definitely, no direct experimental information is available here. In principle a fully dispersive approach as advocated in [222] would avoid such problems, but the approach requires more experimental data from $\gamma^*\gamma^* \rightarrow$ hadron processes than what is presently

available. Although very challenging, lattice QCD is expected to give unambiguous answers here in future.

Theoretical Considerations

Apart from these experimental constraints, any satisfactory model for the off-shell form factor $\mathcal{F}_{\pi^0\gamma^*\gamma^*}((q_1 + q_2)^2, q_1^2, q_2^2)$ should match at large momentum with short-distance constraints from QCD that can be calculated using the OPE. In [234, 247] the short-distance properties for the three-point function $\langle VVP \rangle$ in (5.164) in the chiral limit and assuming octet symmetry have been worked out in detail (see also [246] for earlier partial results). At least for the pion the chiral limit should be a not too bad approximation,³⁴ however, for the η and, in particular, for the non-Nambu-Goldstone boson η' further analysis will be necessary.

(1) Lessons from CQM:

Let us consider first the behavior of $\mathcal{F}_{\pi^0\gamma^*\gamma^*}$ in the CQM, where it is given by a quark triangular loop (see (2.147) and [250])³⁵

$$\begin{aligned} F_{\pi^0\gamma^*\gamma^*}^{\text{CQM}}(q_3^2, q_1^2, q_2^2) &= 2m_q^2 C_0(m_q, m_q, m_q; q_3^2, q_1^2, q_2^2) \\ &\equiv \int [d\alpha] \frac{2m_q^2}{m_q^2 - \alpha_2\alpha_3q_1^2 - \alpha_3\alpha_1q_2^2 - \alpha_1\alpha_2q_3^2}, \end{aligned} \quad (5.184)$$

where $[d\alpha] = d\alpha_1 d\alpha_2 d\alpha_3 \delta(1 - \alpha_1 - \alpha_2 - \alpha_3)$ and m_q is a quark mass ($q = u, d, s$). We are adopting the normalization $F_{\pi^0\gamma^*\gamma^*}^{\text{CQM}} = \mathcal{F}_{\pi^0\gamma^*\gamma^*} / \mathcal{F}_{\pi^0\gamma^*\gamma^*}^{\text{WZW}}$ here, such that $\mathcal{F}_{\pi^0\gamma^*\gamma^*}^{\text{CQM}} = \frac{N_c}{12\pi^2 F_\pi} F_{\pi^0\gamma^*\gamma^*}^{\text{CQM}}$. For $q_1^2 = q_2^2 = q_3^2 = 0$ we obtain $F_{\pi^0\gamma^*\gamma^*}^{\text{CQM}}(0, 0, 0) = 1$. Note the symmetry of C_0 under permutations of the arguments (q_3^2, q_1^2, q_2^2) . C_0 is a known function in terms of logs and dilogs for arbitrary values of the arguments. For our purpose it is sufficient to calculate it at one of the square momenta set to zero. One finds

$$F_{\pi^0\gamma^*\gamma^*}^{\text{CQM}}(0, q_1^2, q_2^2) = \frac{-m_q^2}{q_1^2 - q_2^2} \left\{ \ln^2 \frac{\sqrt{4m_q^2 - q_1^2} - \sqrt{-q_1^2}}{\sqrt{4m_q^2 - q_1^2} + \sqrt{-q_1^2}} - (q_1^2 \rightarrow q_2^2) \right\}. \quad (5.185)$$

³⁴As pointed out in [276], the integrals (5.166) are infrared safe for $m_\pi \rightarrow 0$. This can also be seen within the EFT approach to light-by-light scattering proposed in [251, 253] to be discussed later in Sect. 5.2.4.

³⁵We actually first consider a current quark loop which is related via PCAC to the triangle anomaly (see below). Non-perturbative strong interactions effects transmute it into a constituent quark loop ($m_q \rightarrow M_q$, the latter being non-vanishing in the chiral limit). See also the recent advocacy of the constituent chiral quark model (C χ QM) for evaluating hadronic contributions to a_μ in [277, 278].

For large q_1^2 at $q_2^2 \sim 0$, $q_3^2 \sim 0$ the asymptotic behavior is given by

$$F_{\pi^{0*}\gamma^*\gamma^*}^{\text{CQM}}(0, q_1^2, 0) \sim \frac{m_q^2}{-q_1^2} \left\{ \ln^2 \left(\frac{-q_1^2}{m_q^2} \right) \right\}. \quad (5.186)$$

For large $q_1^2 \sim q_2^2$ at $q_3^2 \sim 0$ we have

$$F_{\pi^{0*}\gamma^*\gamma^*}^{\text{CQM}}(0, q_1^2, q_1^2) \sim 2 \frac{m_q^2}{-q_1^2} \left\{ \ln \left(\frac{-q_1^2}{m_q^2} \right) \right\} \quad (5.187)$$

and the same behavior follows for $q_3^2 \sim q_1^2$ at $q_2^2 \sim 0$. Note that in all cases we have the same power behavior $\sim m_q^2/q_1^2$ modulo logarithms. It is important to note that in the chiral limit $F_{\pi^{0*}\gamma^*\gamma^*}^{\text{CQM}} \xrightarrow{m_q \rightarrow 0} 0$ if $(q_3^2, q_1^2, q_2^2) \neq (0, 0, 0)$. Thus our consideration seems to be not quite relevant, as it says that the chiral corrections at high energies are damped by a $1/Q^2$ behavior in all the possible directions. The dominant terms come from the chiral limit, but, surprisingly, the CQM calculation also sheds light on the leading contribution, as we are going to discuss now. The singular behavior of $F_{\pi^{0*}\gamma^*\gamma^*}^{\text{CQM}}$ under exchange of limits:

$$\begin{aligned} \lim_{m_q \rightarrow 0} F_{\pi^{0*}\gamma^*\gamma^*}^{\text{CQM}}(q_3^2, q_1^2, q_2^2) &\equiv 0 \text{ for all } (q_3^2, q_1^2, q_2^2) \neq (0, 0, 0) \\ \lim_{(q_3^2, q_1^2, q_2^2) \rightarrow (0, 0, 0)} F_{\pi^{0*}\gamma^*\gamma^*}^{\text{CQM}}(q_3^2, q_1^2, q_2^2) &\equiv 1 \text{ for all } m_q \neq 0 \end{aligned} \quad (5.188)$$

implies that the chiral limit is either zero **or** unity,

$$\lim_{m_q \rightarrow 0} \lim_{(q_3^2, q_1^2, q_2^2) \rightarrow (0, 0, 0)} F_{\pi^{0*}\gamma^*\gamma^*}^{\text{CQM}}(q_3^2, q_1^2, q_2^2) \equiv 1, \quad (5.189)$$

depending on whether $(q_3^2, q_1^2, q_2^2) \neq (0, 0, 0)$ or $(q_3^2, q_1^2, q_2^2) = (0, 0, 0)$, respectively. This singular behavior is an alternative form of expressing the ABJ anomaly and the non-renormalization theorem. For the pseudoscalar vertex the latter just means that the last identity (5.189) to all orders of perturbation theory yields a constant, which always may be renormalized to unity by an appropriate renormalization of the axial current. The divergence of the latter being the interpolating field of the pseudoscalar Nambu–Goldstone mode involved.³⁶ Amazingly, the pseudoscalar vertex (at one loop, in the real world of non-vanishing quark masses) is UV finite and regularized independent; the two vector currents are trivially conserved, because of the $\varepsilon_{\mu\nu\alpha\beta} q_1^\alpha q_2^\beta$ tensor structure in (5.177), and we obtain the ABJ anomaly as a IR phenomenon (see also [279]) and not as a UV renormalization effect as it appears if one looks at the VVA matrix element. Since the anomaly is exact to all orders

³⁶The anomaly cancellation required by renormalizability of a gauge theory here just would mean the absence of a non-smooth chiral limit.

and at all energy scales, it is not surprising that it may be obtained from the IR region as well. Note that with the exception of the WZW point form-factor, all other models considered (see e.g. (5.211) or (5.214), below) share the property of the CQM that they yield the anomaly at $(0, 0, 0)$ while dropping for large p_i^2 like $1/p_i^2$ if $(q_1^2, q_2^2, p_3^2) \neq (0, 0, 0)$. But likely only the CQM may be a half-way reasonable model for the configuration $(-Q^2, -Q^2, 0)$ needed at the external vertex.

(2) Lessons from QCD:

The key object which enters the Feynman diagrams is the **off-shell** $\pi^0\gamma\gamma$ form factor $\mathcal{F}_{\pi^0\gamma^*\gamma^*}((q_1 + q_2)^2, q_1^2, q_2^2)$ which is defined, up to small mixing effects with the states η and η' , via the Green's function $\langle VVP \rangle$ in QCD

$$\int d^4x d^4y e^{i(q_1 \cdot x + q_2 \cdot y)} \langle 0 | T \{ j_\mu(x) j_\nu(y) P^3(0) \} | 0 \rangle \\ = \varepsilon_{\mu\nu\alpha\beta} q_1^\alpha q_2^\beta \frac{i \langle \bar{\psi}\psi \rangle}{F_\pi} \frac{i}{(q_1 + q_2)^2 - m_\pi^2} \mathcal{F}_{\pi^0\gamma^*\gamma^*}((q_1 + q_2)^2, q_1^2, q_2^2), \quad (5.190)$$

where $P^3 = \bar{\psi}i\gamma_5 \frac{\lambda^3}{2} \psi = (\bar{u}i\gamma_5 u - \bar{d}i\gamma_5 d)/2$. By $\langle \bar{\psi}\psi \rangle$ we denoted the **single flavor** bilinear quark condensate. By $\langle \bar{\psi}\psi \rangle_0$ we will denote the same quantity in the chiral limit. Here again the low energy effective structure of QCD as encoded in CHPT is relevant. The vacuum condensates are a consequence of the spontaneous breakdown of chiral symmetry. A first example where quark condensates entered the game we encountered in (4.76) on p. 309. The existence of an order parameter like the quark condensate makes the high energy behavior different from naive pQCD expectations. It is important to notice that the Green function $\langle VVP \rangle$ is an order parameter of chiral symmetry. It vanishes to all orders in perturbative QCD in the chiral limit as the d quark and the u quark contributions making up P^3 cancel. As a consequence the behavior at short distances is smoother than expected from naive power counting arguments. Several limits are of interest. In the first case, the two momenta become simultaneously large, which in position space describes the situation where the space-time arguments of all the three operators tend towards the same point at the same rate. To leading order and up to corrections of order $\mathcal{O}(\alpha_s)$ one obtains the following behavior for the form factor [234]

$$\lim_{\lambda \rightarrow \infty} \mathcal{F}_{\pi^0\gamma^*\gamma^*}((\lambda q_1 + \lambda q_2)^2, (\lambda q_1)^2, (\lambda q_2)^2) = -\frac{F_0}{3} \frac{1}{\lambda^2} \frac{q_1^2 + q_2^2 + (q_1 + q_2)^2}{q_1^2 q_2^2} + \mathcal{O}\left(\frac{1}{\lambda^4}\right).$$

The factor F_0 in the chiral limit accounts for the factor $1/F_\pi$ in the definition of $\mathcal{F}_{\pi^0\gamma^*\gamma^*}$ (5.190) above.

In order to discuss the other limits of interest let us introduce the QCD octet of vector and axial currents and the octet of pseudoscalar densities

$$\begin{aligned}
V_\mu^a(x) &= : \bar{\psi}(x) \gamma_\mu \frac{\lambda^a}{2} \psi(x) : \\
A_\mu^a(x) &= : \bar{\psi}(x) \gamma_\mu \gamma_5 \frac{\lambda^a}{2} \psi(x) : \\
P^a(x) &= : \bar{\psi}(x) i \gamma_5 \frac{\lambda^a}{2} \psi(x) :
\end{aligned}$$

where λ^a are the Gell-Mann matrices, $\frac{\lambda^a}{2} = T^a$ are the $SU(3)$ generators for the three-flavor case. Although the non-perturbative QCD vacuum due to the spontaneous breaking of the chiral symmetry is non-trivial we denote it by $|0\rangle$ simply. We furthermore define the following two-point functions: one is $\langle AP \rangle$ of the axial currents with the pseudoscalars (see p. 309 and (4.76))

$$\int d^4x e^{i p x} \langle 0 | T \{ A_\mu^a(x) P^b(0) \} | 0 \rangle \equiv \delta^{ab} \langle \bar{\psi} \gamma_\mu \psi \rangle_0 \frac{P_\mu}{p^2}, \quad (5.191)$$

which is dominated by the pion-pole, $1/p^2$ being the chiral limit of the pion-propagator $1/(p^2 - m_\pi^2 + i\varepsilon)$; and the other the two-point function $\langle VT \rangle$ of the vector current and the antisymmetric tensor density,

$$\int d^4x e^{i p x} \langle 0 | T \{ V_\mu^a(x) (\bar{\psi} \sigma_{\rho\sigma} \frac{\lambda^b}{2} \psi)(0) \} | 0 \rangle \equiv \delta^{ab} (\Pi_{VT})_{\mu\rho\sigma}(p), \quad (5.192)$$

with $\sigma_{\rho\sigma} = \frac{i}{2} [\gamma_\rho, \gamma_\sigma]$. Conservation of the vector current and invariance under parity then give

$$(\Pi_{VT})_{\mu\rho\sigma}(p) = (p_\rho g_{\mu\sigma} - p_\sigma g_{\mu\rho}) \Pi_{VT}(p^2). \quad (5.193)$$

We also note that the corresponding correlator between the axial current and the tensor density vanishes as a consequence of invariance under charge conjugation.

The reason for introducing the $SU(3)$ octet currents is that they satisfy the simple orthogonality conditions (5.191) and (5.192). The electromagnetic current can be expressed in terms of the $SU(3)$ currents as

$$j_\mu(x) = : \bar{\psi}(x) \gamma_\mu \frac{\lambda^3}{2} \psi(x) : + \frac{1}{6} : \bar{\psi}(x) \gamma_\mu \lambda^0 \psi(x) :, \quad (5.194)$$

where λ^0 is the unit matrix, which corresponds to the $SU(3)$ singlet.

Digression on the asymptotic behavior of the pion transition form factor

The object we are considering here is the three-point function

$$(\Pi_{VVP})_{\mu\nu}(q_1, q_2) = \int d^4x d^4y e^{i(q_1 x + q_2 y)} \langle 0 | T \{ j_\mu(x) j_\nu(y) P^3(0) \} | 0 \rangle$$

where $j_\mu(x) = \bar{q} \hat{Q}_q \gamma_\mu q = Q_u \bar{u}(x) \gamma_\mu u(x) + Q_d \bar{d}(x) \gamma_\mu d(x)$: is the electromagnetic current and $P^3(x) = \bar{q} \frac{\lambda_3}{2} i \gamma_5 q = \frac{1}{2} (: \bar{u}(x) i \gamma_5 u(x) - \bar{d}(x) i \gamma_5 d(x) :)$ the pion

interpolating field. Both \hat{Q} and the Gell-Mann matrix λ^3 are diagonal matrices in flavor space. The conserved electromagnetic current implies the WT-identities

$$q_1^\mu (\Pi_{VVP})_{\mu\nu}(q_1, q_2) = q_2^\nu (\Pi_{VVP})_{\mu\nu}(q_1, q_2) = 0.$$

As a parity odd object $\langle VVP \rangle$ must have the tensor structure

$$(\Pi_{VVP})_{\mu\nu}(q_1, q_2) = \varepsilon_{\mu\nu\rho\sigma} q_1^\rho q_2^\sigma \mathcal{H}_V(q_1^2, q_2^2, (q_1 + q_2)^2).$$

We are going to study the high energy behavior when two of the three fields approach each other in x -space. The object of interest is the time-ordered product

$$\begin{aligned} T \{ J_{\Gamma_1}(x) J_{\Gamma_2}(y) \} &= : \bar{\psi}(x) \Gamma_1 \psi(x) \bar{\psi}(y) \Gamma_2 \psi(y) : \\ &+ : \bar{\psi}(x) \Gamma_1 S_F(x-y) \Gamma_2 \psi(y) : + : \bar{\psi}(y) \Gamma_2 S_F(y-x) \Gamma_1 \psi(x) : \\ &- \text{Tr} [S_F(y-x) \Gamma_1 S_F(x-y) \Gamma_2] \end{aligned} \quad (5.195)$$

of a pair of fermion bilinears

$$J_\Gamma =: \bar{\psi}(x) \Gamma \psi(x) : .$$

The free Feynman propagators

$$S_F(x) = i \int \frac{d^4 q}{(2\pi)^4} e^{-iqx} \frac{\not{q} + m}{q^2 - m^2 + i\varepsilon}$$

are color and flavor diagonal spinor space matrices and the trace is over spinor, color and flavor indices. The normal ordering means the self-contractions (tadpoles) are absent. The structure holds beyond perturbation theory if propagators are full propagators and vertices dressed ones. We thus have the structure discussed in Sect. 4.2.2 p. 316, graphically represented by Eq. (4.83) with appropriately chosen coupling matrices.

In the chiral limit the quark mass is zero. We also have to expand the fields. In the Schwinger-Fock gauge the gluon fields satisfy $x^\mu G_\mu(x) = 0$ and we have

$$\psi(x) = \psi(y) + (x-y)^\mu (D_\mu \psi)(y) + \dots ,$$

where the second term is a gluonic correction (see Eq. 4.80) which is subleading and we will neglect it in the following.

We first consider (see Fig. 5.60)

$$\begin{aligned} \lim_{\lambda \rightarrow \infty} (\Pi_{VVP})_{\mu\nu}(\lambda q_1, q - \lambda q_1) &= \int d^4 y e^{iqy} \lim_{\lambda \rightarrow \infty} \int d^4 x e^{i\lambda q_1(x-y)} \langle 0 | T \{ j_\mu(x) j_\nu(y) \} P^3(0) \rangle | 0 \rangle \\ &= \int d^4 y e^{iqy} \lim_{\lambda \rightarrow \infty} \int d^4 z e^{i\lambda q_1 z} \langle 0 | T \{ j_\mu(y+z) j_\nu(y) \} P^3(0) \rangle | 0 \rangle , \end{aligned}$$

where we have used translation invariance and changed the integration variable $x \rightarrow z = x - y$ and use that operators commute under the T -product and pairwise T -contractions can be done in any order. As $\langle 0|P^3(0)|0\rangle = 0$ the last, potentially most singular term, will not contribute and the first term of (5.195) is regular as $x \rightarrow y$ so we have to consider the second plus third term only, with $\Gamma_1 = \hat{Q}\gamma_\mu$ and $\Gamma_2 = \hat{Q}\gamma_\nu$. Then

$$\begin{aligned} & \lim_{\lambda \rightarrow \infty} \int d^4z e^{i\lambda q_1 z} \langle 0|T \{T \{j_\mu(y+z)j_\nu(y)\} P^3(0)\} |0\rangle \\ &= \frac{i}{\lambda} \frac{q_1^\rho}{q_1^2} \langle 0|T \left\{ : \bar{\psi}(0) (\gamma_\mu \gamma_\rho \gamma_\nu - \gamma_\nu \gamma_\rho \gamma_\mu) \hat{Q}^2 \psi(0) : P^3(0) \right\} |0\rangle + \mathcal{O}(1/\lambda^2) \end{aligned}$$

and using the Chisholm identity

$$\gamma_\mu \gamma_\rho \gamma_\nu = (g_{\mu\rho} g_{\nu\sigma} + g_{\nu\rho} g_{\mu\sigma} - g_{\mu\nu} g_{\rho\sigma}) \gamma^\sigma - i \varepsilon_{\mu\rho\nu\sigma} \gamma^\sigma \gamma_5,$$

which exhibits a symmetric and an anti-symmetric part (the first cancels while the second doubles) we get

$$\gamma_\mu \gamma_\rho \gamma_\nu - \gamma_\nu \gamma_\rho \gamma_\mu = 2i \varepsilon_{\mu\nu\rho\sigma} \gamma^\sigma \gamma_5$$

and hence

$$\lim_{\lambda \rightarrow \infty} (\Pi_{VV P})_{\mu\nu}(\lambda q_1, p - \lambda q_1) = \frac{i}{\lambda} \frac{q_1^\rho}{q_1^2} 2i \varepsilon_{\mu\nu\rho\sigma} \langle 0|T \left\{ : \bar{\psi}(y) \gamma^\sigma \gamma_5 \hat{Q}^2 \psi(y) : P^3(0) \right\} |0\rangle + \mathcal{O}(1/\lambda^2).$$

The factored out two point function in the chiral limit reads

$$i \int d^4y e^{iqy} \langle 0|T \left\{ : \bar{\psi}(y) \gamma^\sigma \gamma_5 \hat{Q}^2 \psi(y) : : \bar{\psi}(0) \frac{\lambda^3}{2} i \gamma_5 \psi(0) : \right\} |0\rangle = \langle \bar{\psi}\psi \rangle_0 \frac{q^\sigma}{q^2},$$

such that

$$\lim_{\lambda \rightarrow \infty} (\Pi_{VV P})_{\mu\nu}(\lambda q_1, q - \lambda q_1) = \frac{i}{\lambda} \frac{q_1^\rho q^\sigma}{q_1^2 q^2} 2i \varepsilon_{\mu\nu\rho\sigma} \langle \bar{\psi}\psi \rangle_0 + \mathcal{O}(1/\lambda^2).$$

This has to be compared with the exact three-point function (5.190). In the isospin symmetry limit for the u and d quarks we have for the two electromagnetic currents each a factor $Q_u + Q_d = 1/3$ and an overall color factor $N_c = 3$, and we obtain the results

$$\mathcal{F}_{\pi^0 * \gamma^* \gamma^*}(q^2, (\lambda q_1)^2, (q - \lambda q_1)^2) = -\frac{2F_0}{3} \frac{1}{\lambda^2} \frac{1}{q^2}, \quad (5.196)$$

where we used $i/((\lambda q_1 + q - \lambda q_1)^2 - m_\pi^2 + i\varepsilon) = i/(q^2 - m_\pi^2 + i\varepsilon) \rightarrow i/q^2$ in the chiral limit.

The second case of interest concerns

$$\lim_{\lambda \rightarrow \infty} (\Pi_{VV P})_{\mu\nu}(\lambda q_1, q_2) = \int d^4 y e^{iq_2 y} \lim_{\lambda \rightarrow \infty} \int d^4 x e^{i\lambda q_1 x} \langle 0|T \left\{ T \left[j_\mu(x) P^3(0) \right] j_\nu(y) \right\} |0\rangle,$$

where again we have used that operators commute under the T -product and pairwise T -contractions can be done in any order. Since $\langle 0|j_\nu(y)|0\rangle = 0$ the contribution from the last term of (5.195) is absent, while the first term is regular as $x \rightarrow 0$, such that we have to consider the second plus third term only, with $\Gamma_1 = \hat{Q}\gamma_\mu$ and $\Gamma_2 = \frac{\lambda^3}{2} i\gamma_5$. Then

$$\begin{aligned} & \lim_{\lambda \rightarrow \infty} \int d^4 x e^{i\lambda q_1 x} \langle 0|T \left\{ T \left[j_\mu(x) P^3(0) \right] j_\nu(y) \right\} |0\rangle \\ &= \frac{i}{\lambda} \frac{q_1^\rho}{q_1^2} \langle 0|T \left\{ : \bar{\psi}(0) (\gamma_\mu \gamma_\rho i\gamma_5 - i\gamma_5 \gamma_\rho \gamma_\mu) \hat{Q} \frac{\lambda^3}{2} \psi(0) : j_\nu(y) \right\} |0\rangle + \mathcal{O}(1/\lambda^2), \end{aligned}$$

and using

$$\{\gamma_\mu, \gamma_5\} = 0, \quad \gamma_\mu \gamma_\rho = g_{\mu\rho} - i\sigma_{\mu\rho}, \quad \sigma_{\mu\rho} = \frac{i}{2} [\gamma_\mu, \gamma_\rho], \quad \sigma_{\mu\rho} \gamma_5 = \frac{i}{2} \varepsilon_{\mu\rho\alpha\beta} \sigma^{\alpha\beta},$$

we get

$$\gamma_\mu \gamma_\rho i\gamma_5 - i\gamma_5 \gamma_\rho \gamma_\mu = 2\sigma_{\mu\rho} \gamma_5 = i\varepsilon_{\mu\rho\alpha\beta} \sigma^{\alpha\beta},$$

and hence

$$\lim_{\lambda \rightarrow \infty} (\Pi_{VV P})_{\mu\nu}(\lambda q_1, q_2) = \frac{i}{\lambda} \frac{q_1^\rho}{q_1^2} i\varepsilon_{\mu\rho\alpha\beta} \langle 0|T \left\{ : \bar{\psi}(0) \sigma^{\alpha\beta} \hat{Q} \frac{\lambda^3}{2} \psi(0) : j_\nu(y) \right\} |0\rangle + \mathcal{O}(1/\lambda^2).$$

Now the vector-tensor (VT) vacuum expectation value unlike in pQCD does not vanish due to the spontaneous breakdown of chiral symmetry (chiral quark condensates). So we define

$$\begin{aligned} & i \int d^4 y e^{iq_2 y} \langle 0|T \left\{ : \bar{\psi}(0) \sigma^{\alpha\beta} \hat{Q} \frac{\lambda^3}{2} \psi(0) :: \bar{\psi}(y) \hat{Q} \gamma_\nu \psi(y) : \right\} |0\rangle \equiv (\Pi_{VT})_\nu^{\alpha\beta}(q_2) \\ (\Pi_{VT})_\nu^{\alpha\beta}(q_2) &= (q_2^\alpha \delta_\nu^\beta - q_2^\beta \delta_\nu^\alpha) \Pi_{VT}(q_2^2) = q_2^\sigma (\delta_\sigma^\alpha \delta_\nu^\beta - \delta_\sigma^\beta \delta_\nu^\alpha) \Pi_{VT}(q_2^2). \end{aligned} \quad (5.197)$$

Thus

$$\begin{aligned} \lim_{\lambda \rightarrow \infty} (\Pi_{VVP})_{\mu\nu}(\lambda q_1, q_2) &= \int d^4y e^{iq_2 y} \lim_{\lambda \rightarrow \infty} \int d^4x e^{\lambda q_1 x} \langle 0 | T \left\{ T \left[j_\mu(x) P^3(0) \right] j_\nu(y) \right\} | 0 \rangle \\ &= -2 \frac{1}{\lambda} \frac{q_1^\rho q_2^\sigma}{q_1^2} \varepsilon_{\mu\nu\rho\sigma} \Pi_{VT}(q_2^2). \end{aligned} \quad (5.198)$$

This has to be compared with the exact three-point function (5.190), which defined the pion Transition Form Factor (TFF) $\mathcal{F}_{\pi^0 \gamma^* \gamma^*}(p_\pi^2, q_1^2, q_2^2)$. Then using $i/((\lambda q_1 + q_2)^2 - m_\pi^2 + i\varepsilon) \rightarrow i/(\lambda^2 q_1^2)$, again, in the isospin symmetry limit for the u and d quarks we have for the two electromagnetic currents each a factor $Q_u + Q_d = 1/3$ and an overall color factor $N_c = 3$, and we obtain the results

$$\mathcal{F}_{\pi^0 \gamma^* \gamma^*}((\lambda q_1 + q_2)^2, (\lambda q_1)^2, q_2^2) = -\frac{2}{3} \frac{F_\pi}{\langle \bar{\psi} \psi \rangle} \Pi_{VT}(q_2^2). \quad (5.199)$$

End of the Digression

In summary: the short-distance behavior of the form factor then reads

$$\lim_{\lambda \rightarrow \infty} \mathcal{F}_{\pi^0 \gamma^* \gamma^*}(q^2, (\lambda q_1)^2, (q - \lambda q_1)^2) = -\frac{2F_0}{3} \frac{1}{\lambda^2} \frac{1}{q^2} + \mathcal{O}\left(\frac{1}{\lambda^3}\right), \quad (5.200)$$

when the space-time arguments of the two vector currents in $\langle VVP \rangle$ approach each other and

$$\lim_{\lambda \rightarrow \infty} \mathcal{F}_{\pi^0 \gamma^* \gamma^*}((\lambda q_1 + q_2)^2, (\lambda q_1)^2, q_2^2) = -\frac{2}{3} \frac{F_0}{\langle \bar{\psi} \psi \rangle_0} \Pi_{VT}(q_2^2) + \mathcal{O}\left(\frac{1}{\lambda}\right), \quad (5.201)$$

when the space-time argument of one of the vector currents approaches the one of the pseudoscalar density.

In particular, at the external vertex in light-by-light scattering in (5.166), the following limit is relevant [274]

$$\lim_{\lambda \rightarrow \infty} \mathcal{F}_{\pi^0 \gamma^* \gamma^*}((\lambda q_1)^2, (\lambda q_1)^2, 0) = -\frac{2}{3} \frac{F_0}{\langle \bar{\psi} \psi \rangle_0} \Pi_{VT}(0) + \mathcal{O}\left(\frac{1}{\lambda}\right). \quad (5.202)$$

Note that there is no fall-off in this limit, unless $\Pi_{VT}(0)$ vanishes. As pointed out in [280], the value of $\Pi_{VT}(p^2)$ at zero momentum is related to the quark condensate magnetic susceptibility χ of QCD in the presence of a constant external electromagnetic field. It has been introduced in [281]

$$\langle 0 | \bar{q} \sigma_{\mu\nu} q | 0 \rangle_F = e Q_q \chi \langle \bar{\psi} \psi \rangle_0 F_{\mu\nu}, \quad (5.203)$$

with $Q_u = 2/3$ and $Q_d = -1/3$ and $F_{\mu\nu}$ the e.m. field strength tensor. With our definition of Π_{VT} in (5.192) one then obtains the relation (see also [282])

$$\Pi_{\text{VT}}(0) = -\frac{\langle \bar{\psi}\psi \rangle_0}{2} \chi. \quad (5.204)$$

Remember that χ has been introduced in (4.93) in a different context already.

The matrix element which determines $\Pi_{\text{VT}}(0)$ we have encountered in Sect. 4.2.2 p. 316. The one-loop diagram shown in Eq. (4.83) (last diagram), and corresponding Eqs. (4.85), (4.90) and (4.91), which yields (as we consider external currents in place of an on-shell photon here the photon polarization vectors in $f_{\alpha\beta} = k_\alpha \varepsilon_\beta - k_\beta \varepsilon_\alpha = (k_\alpha g_{\beta\rho} - k_\beta g_{\alpha\rho}) \varepsilon^\rho$ has to be replaced by unity) [283]

$$\chi = -\frac{N_c}{4\pi^2 F_\pi^2} = -8.9 \text{ GeV}^{-2}. \quad (5.205)$$

Unfortunately, there is no agreement in the literature on what the actual value of χ should be. In comparing different results one has to keep in mind that χ actually depends on the renormalization scale μ . In [281] the estimate $\chi(\mu = 0.5 \text{ GeV}) = -(8.16_{-1.91}^{+2.95}) \text{ GeV}^{-2}$ was given in a QCD sum rule evaluation of nucleon magnetic moments. This value was confirmed by the recent reanalysis [284] which yields $\chi = -(8.5 \pm 1.0) \text{ GeV}^{-2}$. Various results have been presented in [247, 280, 285–289]. A more detailed discussion may be found in [275].

Further important information on the (on-shell) pion form factor (5.163) has been obtained in [290] based on higher-twist terms in the OPE and worked out in [291]. We consider the $\pi^0 \rightarrow \gamma\gamma$ transition amplitude (5.163) with $j_\mu = \frac{2}{3}\bar{u}\gamma_\mu u - \frac{1}{3}\bar{d}\gamma_\mu d$ the relevant part of the electromagnetic current. In the chiral limit, the first two terms of $\mathcal{F}_{\pi^0\gamma^*\gamma^*}(0, -Q^2, -Q^2)$ for large Euclidean momentum $Q^2 \rightarrow \infty$ read [290]

$$\mathcal{A}^{\mu\nu}(\pi^0 \rightarrow \gamma^*\gamma^*) = i\frac{1}{3} \varepsilon^{\mu\nu\alpha\beta} \langle 0 | \frac{q_\alpha}{q^2} j_{5\beta}^{(3)} - \frac{8}{9} \frac{q_\alpha}{q^4} \tilde{j}_\beta^{(3)} | \pi^0(p) \rangle, \quad (5.206)$$

where $j_{5\mu}^{(3)} = \bar{\psi}\lambda^3\gamma_\mu\gamma_5\psi$ and $\tilde{j}_\mu^{(3)} = g_s \bar{\psi}\lambda^3\gamma^\rho T^a \tilde{G}_{\rho\mu}^a \psi$. The matrix elements are parametrized as follows: $\langle 0 | j_{5\mu}^{(3)}(0) | \pi^0(p) \rangle = 2i F_0 p_\mu$ and $\langle 0 | \tilde{j}_\mu^{(3)}(0) | \pi^0(p) \rangle = -2i F_0 p_\mu \delta^2$. For the pion form factor this implies

$$\frac{\mathcal{F}_{\pi^0\gamma^*\gamma^*}(0, -Q^2, -Q^2)}{\mathcal{F}_{\pi^0\gamma\gamma}(0, 0, 0)} = \frac{8}{3}\pi^2 F_0^2 \left\{ \frac{1}{Q^2} - \frac{8}{9} \frac{\delta^2}{Q^4} + \mathcal{O}\left(\frac{1}{Q^6}\right) \right\}, \quad (5.207)$$

and the sum rule estimate performed in [291] yields $\delta^2 = (0.2 \pm 0.02) \text{ GeV}^2$.

Hadronic Form Factors: The Large- N_c QCD Inspired Approach

To remind, the large- N_c framework attempts to make use of the structural simplification of QCD when the number of colors goes to infinity. G. 't Hooft [226] (see also

[227]) has shown that one gets perfect quark–hadron duality with a hadron spectrum given by an infinite tower of zero width vector boson states. Although the limit is not known as an exact solution with a numerically fixed mass spectrum it is complementary to the true low energy QCD, represented by CHPT, which is missing the spin 1 states like the ρ , which we know play a major role as contributions to $g - 2$. By combining large- N_c counting from the $1/N_c$ expansion with the chiral counting in powers of momentum and current quark masses, low energy hadron physics can be extended beyond CHPT in a controlled way towards higher energies [228]. This framework puts states like $\rho, \omega, \phi, \dots$ in place, which play a key role in strong interaction physics below 1–2 GeV aside of the pions and Kaons. In practice one replaces the infinite series of spin 1 bosons with the phenomenologically known low lying hadron spectrum. In the context of HVP and HLbL de Rafael has been promoting this point of view since 1994 [136] and triggered the so far only complete calculations [210] (HSK using HLS) and [235] (BPP using ENJL) as well as many improvements (KN, MV) since.

When we attempt to model the one–particle exchange form factors in a way which bridges the low energy hadron spectrum (CHPT, VMD, HLS/ENJL) with QCD high energy constraints, the large- N_c QCD inspired [233] approach developed by the Marseille group [234, 246, 247] provides well founded method in parametrizing hadronic form factors. The free parameters are to be fixed by data (if available) and by QCD asymptotics (CHPT and/or pQCD).

As mentioned already before, in this context it is very important to specify in which domain of Fig. 5.47 the model is supposed to be valid. So CHPT and the VMD, HLS and ENJL models attempt a modeling the *soft–soft* domain up to a scale of 1–2 GeV where pQCD is supposed to become applicable. The low energy models typically are not renormalizable and thus lead to a mismatch in the region where we need to match the low energy effective theory with QCD. However, it turns out that the cutoff dependence usually is not too strong although not weak either. Here the large- N_c QCD approach definitely has its merits to bridge the *soft–soft* with the *soft–hard* regions. Still, it seems that also this strategy of approaching the problem is not unambiguous, as the mentioned discrepancy in the QCD large momentum behavior between the Knecht–Nyffeler and the Melnikov–Vainshtein (see Fig. 5.60) approach shows. The reason is that the first approach approaches the problem from a low energy effective point of view from a specific channel $\pi^0 \rightarrow \gamma\gamma$ (a sub-space of the Hilbert space of hadrons), while the second looks at it from the overall $\gamma\gamma \rightarrow \text{hadrons} \rightarrow \gamma\gamma$ setting, which means that different contributions are taken into account by adopting a different bookkeeping.

Here we briefly present some typical $\pi^0\gamma\gamma$ transition form factors, which have been used in evaluations of the HLbL contribution in the past. With $\gamma^*\gamma^* \rightarrow \pi^0 \rightarrow \gamma^*\gamma^*$ replacing the full amplitude, and in the pion–pole approximation, Knecht and Nyffeler [234, 276] were able to reduce the problem of evaluating the leading HLbL contribution analytically to a 2–dimensional integral representation over the moduli of the Euclidean photon momenta

$$a_{\mu}^{\text{LbL};\pi^0} = \int_0^{\infty} dQ_1 \int_0^{\infty} dQ_2 \sum_{i=1,2} w_i(Q_1, Q_2) f_i(Q_1, Q_2), \quad (5.208)$$

which may be integrated numerically without problems. In the pole approximation the weight functions w_i are model independent (rational functions, square roots and logarithms). The model dependence (form factors) resides in the f_i 's. The representation permits a transparent investigation of the form factor dependencies. For the general π^0 -exchange diagrams we are left with the 3-dimensional integral representation (5.172) and numerically the analysis gets more involved as discussed in [275].

(1) The **pion-pole** case:

As most existing evaluations of the one-particle exchange contributions are considering the pole approximation (the FFs evaluated as the residues at the pion propagator pole), we first focus here on this case, i.e., with q_1 and q_2 the two photon momenta and $q_3 = -(q_1 + q_2)$ the pion momentum we take the pion to be on-shell $q_3^2 = m_{\pi}^2$. In order to get an idea about different possibilities we consider the following four cases here: (see also [248, 292])³⁷

$$\mathcal{F}_{\pi^0 \ast \gamma \ast \gamma}^{\text{WZW}}(q_3^2, q_1^2, q_2^2) = \frac{N_c}{12\pi^2 F_{\pi}}, \quad (5.209)$$

which leads, however, to a divergent result in the equivalent integrals (5.166), (5.208) and (5.172),³⁸ since there is no damping at high energies. One can use some momentum cutoff around 1 – 2 GeV, but this procedure is completely arbitrary. Nevertheless, the WZW form factor serves as a physical normalization to the $\pi^0 \rightarrow \gamma\gamma$ decay rate and all models satisfy the constraint

$$\mathcal{F}_{\pi^0 \gamma \gamma}(m_{\pi}^2, 0, 0) = \mathcal{F}_{\pi^0 \gamma \gamma}^{\text{WZW}}(m_{\pi}^2, 0, 0) = \frac{N_c}{12\pi^2 F_{\pi}} = 0.274 \text{ GeV}^{-1}. \quad (5.210)$$

One way to implement a damping at high momentum is the VMD prescription ($\gamma - \rho$ mixing) which works reasonably well in many applications to low-energy hadronic physics. It follows automatically in the HLS model which was used in [210, 250] to evaluate the full hadronic light-by-light scattering contribution. The HLS models implements VMD in a consistent way, respecting chiral symmetry and electromagnetic gauge invariance. It leads to the VMD dressed WZW form factor

³⁷In fact all the seemingly very differently motivated models collected in Table 5.13 below, marginally differ from each other. All are normalized to the WZW on-shell point and in general behave as $1/Q^2$ at large momentum transfer, implementing variants of the VMD mechanism.

³⁸Actually, the contribution involving the term T_2 in (5.166) is finite even for a constant form factor, see [234, 250]. The numerical value is in fact always much smaller, less than 5%, than the results obtained for the part with T_1 with more realistic form factors.

$$\mathcal{F}_{\pi^0\gamma^*\gamma^*}^{\text{VMD}}(q_3^2, q_1^2, q_2^2) = \frac{N_c}{12\pi^2 F_\pi} \frac{M_V^2}{(M_V^2 - q_1^2)} \frac{M_V^2}{(M_V^2 - q_2^2)}. \quad (5.211)$$

Note that the on- and off-shell VMD form factors are identical, since they do not depend on the momentum q_3^2 which flows through the pion-leg. The problem with the VMD form factor is that the damping is now too strong as it behaves like $\mathcal{F}_{\pi^0\gamma^*\gamma^*}(m_\pi^2, -Q^2, -Q^2) \sim 1/Q^4$, instead of $\sim 1/Q^2$ deduced from the OPE, see (5.200). This actually means that the proper form factor cannot factorize, i.e. a structure $\mathcal{F}_{\pi^0\gamma^*\gamma^*}(m_\pi^2, q_1^2, q_2^2) = F(q_1^2)F(q_2^2)$ is excluded in any case. Rather than a behavior $M^4/(q_1^2 q_2^2)$ a behavior like $M^2/(q_1^2 + q_2^2)$ (see the CQM behavior (5.185)) seems to be at work.

One may attempt to rectify the high energy behavior of the VMD case by the Leading Meson Dominance (LMD) ansatz [246]

$$\mathcal{F}_{\pi^0\gamma^*\gamma^*}^{\text{LMD}}(m_\pi^2, q_1^2, q_2^2) = \frac{F_\pi}{3} \frac{c_V - q_1^2 - q_2^2}{(M_V^2 - q_1^2)(M_V^2 - q_2^2)}. \quad (5.212)$$

The on-shell vertex condition fixes c_V to

$$c_V = \frac{N_c}{4\pi^2} \frac{M_V^4}{F_\pi^2}.$$

However, also this LMD model fails as it misses to satisfy the Brodsky-Lepage QCD asymptotics if $q_1^2 = -Q^2 \gg M_V^2$ while $q_2^2 \approx 0$. Note that the prefactor

$$\frac{F_\pi}{3} = 0.0308 \text{ GeV} \quad (5.213)$$

is the result of the OPE from the leading large Q^2 asymptotic behavior (5.191).

(2) The **on- and off-shell** pion case, with proper QCD asymptotics:

In order to satisfy QCD asymptotics at least one additional vector meson has to be included [246]. One also should relax from assuming the pion to be on-shell. This leads to the LMD+V ansatz

$$\begin{aligned} \mathcal{F}_{\pi^0\gamma^*\gamma^*}^{\text{LMD+V}}(p_\pi^2, q_1^2, q_2^2) &= \frac{F_\pi}{3} \frac{\mathcal{P}(q_1^2, q_2^2, p_\pi^2)}{\mathcal{Q}(q_1^2, q_2^2)}, \\ \mathcal{P}(q_1^2, q_2^2, p_\pi^2) &= h_0 q_1^2 q_2^2 (q_1^2 + q_2^2 + p_\pi^2) + h_1 (q_1^2 + q_2^2)^2 + h_2 q_1^2 q_2^2 + h_3 (q_1^2 + q_2^2) p_\pi^2 \\ &\quad + h_4 p_\pi^4 + h_5 (q_1^2 + q_2^2) + h_6 p_\pi^2 + h_7, \\ \mathcal{Q}(q_1^2, q_2^2) &= (M_{V_1}^2 - q_1^2) (M_{V_2}^2 - q_1^2) (M_{V_1}^2 - q_2^2) (M_{V_2}^2 - q_2^2), \end{aligned} \quad (5.214)$$

with $p_\pi^2 \equiv (q_1 + q_2)^2$. The parameters are to be fixed by asymptotic conditions via OPE or by data where available. In the Euclidean region with $q_1^2 < 0$, $q_2^2 < 0$ and $p_\pi^2 < 0$ the form factor is expected fall off monotonically and not to increase beyond

the WZW value $\mathcal{F}_{\pi^0\gamma\gamma}(0, 0, 0)$ (which fixes h_7) in exceptional directions. This let us expect $h_0, h_5, h_6 \leq 0$, while $h_2, h_3 + h_4, h_7 \geq 0$, as we will see $h_1 = 0$ is one of the asymptotic conditions to be satisfied. Indeed, this pattern is confirmed to the extend that we have constraints by OPE or data. In spite of the fact that with presently available experimental data we are not able to constrain unambiguously all parameters, we advocate to use the LMD+V **off-shell** form factor [234] for the numerical evaluation of the pion-exchange contribution.

Note that in the pion-pole approximation in the chiral limit the parameters h_3, h_4 and h_6 are absent. The parameters of the off-shell pion form factor are fixed by the following conditions: the low energy limit is given by

$$\mathcal{F}_{\pi^0\gamma\gamma}(0, 0, 0) = \frac{F_\pi}{3} \frac{h_7}{M_1^4 M_2^4} = \frac{1}{4\pi^2 F_\pi} \Rightarrow h_7 = \frac{3 M_1^4 M_2^4}{4\pi^2 F_\pi^2}$$

and fixes h_7 . From the leading large q^2 behavior in the different possible configurations we obtain

$$h_0 = -1,$$

is fixed by the all virtualities large OPE condition (5.191). The Brodsky-Lepage asymptotics requires

$$\begin{aligned} \mathcal{F}_{\pi^0*\gamma*\gamma}(p_\pi^2, q^2, 0) &\sim \frac{F_\pi}{3} \frac{h_1}{M_1^2 M_2^2} + \dots \Rightarrow h_1 = 0 \\ \mathcal{F}_{\pi^0*\gamma*\gamma}(q^2, q^2, 0) &\sim \frac{F_\pi}{3} \frac{h_3 + h_4}{M_1^2 M_2^2} + \dots = \frac{F_0}{3} \chi \Rightarrow h_4 = -h_3 + M_1^2 M_2^2 \chi, \end{aligned}$$

where we used (5.202) and (5.204) and $F_0 \approx F_\pi$. Note that values for χ in the literature range from -2.2 GeV^{-2} to -8.9 GeV^{-2} . We know that the pion exchange picture is effective when two adjacent currents and hence **one** quark propagator of the original LbL quark-box Fig. 5.49 (see also Eq. 5.237 below), carries large momentum, the pion momentum remaining close to the pion mass shell. For the diagram Fig. 5.56a this means $q_1^2 \sim q_2^2 \gg q_3^2$ and the OPE infers the pion dominance picture. The pion acquires large virtuality whenever $q_3^2 \gg m_\pi^2$ in fact the pion dominance picture is expected to break down. In particular $q_1^2 \sim q_3^2 \gg q_2^2$ requires **two** adjacent quark propagators of the original LbL quark-box to carry large momentum, this shrinks the two propagators to a contact term (as illustrated in Fig. 5.61), which carries a $\sim 1/q^2$.

Nevertheless, using the above constraints we have

$$\mathcal{F}_{\pi^0*\gamma*\gamma}(p_\pi^2, q^2, q^2) \sim -\frac{2F_\pi}{3} \frac{1}{q^2} + \frac{F_\pi}{3} (h_2 - 4(M_1^2 + M_2^2) - m_\pi^2) \frac{1}{q^4} + \dots,$$

where the leading term has been fixed a priori to satisfy (5.207) obtained by the OPE. For the next-to-leading term (5.207) implies

$$\begin{aligned}
 h_2 - 4(M_1^2 + M_2^2) - m_\pi^2 &= -\frac{16}{9}\delta^2 \simeq -(0.36 \pm 0.04) \text{ GeV}^2 \\
 \Rightarrow h_2 &= 4(M_1^2 + M_2^2) + m_\pi^2 - \frac{16}{9}\delta^2 \simeq 10.53(29) \text{ GeV}^2
 \end{aligned}
 \tag{5.215}$$

assuming $p_\pi^2 \approx m_\pi^2$. Furthermore, the leading term of

$$\begin{aligned}
 \mathcal{F}_{\pi^0\gamma^*\gamma}(m_\pi^2, -Q^2, 0) &\sim -\frac{F_\pi}{3} \frac{h_5 + h_3 m_\pi^2}{M_1^2 M_2^2} \frac{1}{Q^2} + \frac{F_\pi}{3} X \frac{1}{Q^4} + \dots \\
 X &= \frac{h_4 m_\pi^4 + (h_3(M_1^2 + M_2^2) + h_6) m_\pi^2 + h_5(M_1^2 + M_2^2) + h_7}{M_1^2 M_2^2}
 \end{aligned}$$

is constrained by the CLEO, CELLO, BaBar and Belle data, which is fairly well represented by the Brodsky-Lepage estimate (5.182)

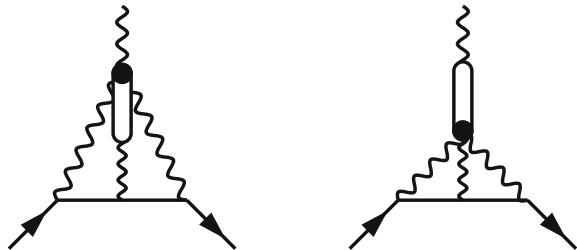
$$-\frac{F_\pi}{3} \frac{h_5 + h_3 m_\pi^2}{M_1^2 M_2^2} \sim 2F_\pi \Rightarrow h_5 + h_3 m_\pi^2 = -6(M_1^2 M_2^2) \simeq -7.62 \text{ GeV}^4 \tag{5.216}$$

In fact a fit to the weighed average of all data Fig. 5.59 yields

$$h_5 = -7.66(50) \text{ GeV}^4, \tag{5.217}$$

more than consistent with the theory driven result. Note that the fit quality is not great although not too bad either in view of the data quality. With the new data from BaBar and Belle the old CLEO fit $h_5 = -6.93(26) \text{ GeV}^4$ is outdated. We assumed $M_1 = M_\rho = 0.77562 \text{ GeV}$ and $M_2 = M_{\rho'} = 1.455 \text{ GeV}$ and checked that letting float the masses does not improve the LMD+V fit. The precise fit function to be applied is

Fig. 5.61 Contraction scheme for two adjacent high momentum quark propagators



$$\mathcal{F}_{\pi^0\gamma^*\gamma}(m_\pi^2, -Q^2, 0) = \frac{1}{4\pi^2 F_\pi} \frac{M_1^2}{M_1^2 + Q^2} \frac{M_2^2}{M_2^2 + Q^2} - \frac{F_\pi}{3} \frac{(h_5 Q^2 + h_3 m_\pi^2 Q^2 - h_4 m_\pi^4 - h_6 m_\pi^2)}{M_1^2 M_2^2 (M_1^2 + Q^2)(M_2^2 + Q^2)} \quad (5.218)$$

where the first term provides the correct on-shell limit. The terms proportional to m_π^2 are negligible in the range where data exist, such that h_3 , h_4 and h_6 cannot be fitted and therefore are set to zero (no need for them). These terms are absent in the chiral limit anyway. Actually, $h_6 \approx -m_\pi^2 h_4$ in order that the $Q^2 \rightarrow 0$ limit is given by the first term. It should be noted that h_7 has been fixed neglecting m_π^2 terms. We always assume that within the uncertainties we do not distinguish between the on-shell transition form factor and its chiral limit. In any case we must require the bound

$$|h_6 + m_\pi^2 h_4| \ll \frac{3M_1^4 M_2^4}{4\pi^2 F_\pi^2 m_\pi^2} \approx 794.2 \text{ GeV}^4 \sim (5.3 \text{ GeV})^4, \quad (5.219)$$

which is not a very good bound but it is a true bound.

Finally, the configuration at the external vertex

$$\mathcal{F}_{\pi^0\gamma^*\gamma}(-Q^2, -Q^2, 0) = \frac{F_\pi}{3} \frac{h_3 + h_4}{M_1^2 M_2^2} - \frac{F_\pi}{3} \left[\frac{h_5 + h_6}{M_1^2 M_2^2} + \frac{h_3 + h_4}{M_1^2 M_2^2} (M_1^2 + M_2^2) \right] \frac{1}{Q^2} + \dots$$

to leading order has been fixed by the magnetic susceptibility above already. The next to leading term exhibits the so far unknown parameter h_6 on which we have no information, except the bound just given. In addition, also $h_3 + h_4$ only is constrained, so essentially h_3 and h_6 remain free parameters. Since except from [274, 275] nobody has done an analysis beyond the pole-approximation, where at least in the chiral limit h_3 , h_4 as well as h_6 are absent, related problems have never been taken seriously. As it turned out, the results [275] agree within errors with the results obtained in the pole approximation, the difference is mainly in the larger uncertainty. For the pole approximation the parameters of the LMD+V ansatz [234, 254, 274] are rather well under control, and we will also adopt it in the following. One should add here that in the dispersive approach, to be discussed below in Sect. 5.2.11, everything is fixed in principle by physical data and off-shell extrapolations are controlled by analyticity, as far as analyticity helps to extrapolate data fixed only within given uncertainties.

We would like to point out that using the off-shell LMD+V form factor at the external vertex leads to a short-distance behavior which qualitatively agrees with the OPE constraints derived by Melnikov and Vainshtein in [254]. As a matter of fact, taking first $q_1^2 \sim q_2^2 \gg q_3^2$ and then q_3^2 large, one obtains, together with the pion propagator in (5.166), an overall $1/q_3^2$ behavior for the pion-exchange contribution, as expected from (5.251), since, according to (5.202), $\mathcal{F}_{\pi^0\gamma^*\gamma}^{\text{LMD+V}}(q_3^2, q_3^2, 0) \sim \text{const}$ for large q_3^2 . This also qualitatively agrees with the $1/q_3^2$ fall-off obtained for the quark-box diagram in light-by-light scattering derived in [254].

Whatever model for $\mathcal{F}_{\pi^0\gamma^*\gamma^*}(m_\pi^2, q_1^2, q_2^2)$ is adopted, the low energy constraint given by $\mathcal{F}_{\pi^0\gamma^*\gamma^*}(m_\pi^2, 0, 0)$ is unambiguous. The WZW form factor is a constant and if used at both vertices leads to a divergent result. This is not so surprising as physics requires some kind of VMD mechanism as we know. The LMD form factor as well as the HLS and the ENJL model do not satisfy the large momentum asymptotics required by QCD. Using these models thus leads to cut-off dependent results, where the cut-off is to be varied between reasonable values which enlarges the model error of such estimates. Nevertheless it should be stressed that such approaches are perfectly legitimate³⁹ and the uncertainties just reflect the lack of precise understanding of this kind of physics. For the large- N_c inspired form factors the proper high energy behavior can only be implemented by introducing at least two vector mesons: the $\rho(770)$ and the $\rho'(1465)$, which is denoted by LMD+V. One may consider the two VMD masses as effective masses to be fitted from the data, however the available data are not precise enough to establish better fits. For a discussion of form factors beyond the pole-approximation we refer also to [248].

Even if we adopt to utilize the LMD+V type form factor, there have been three different version of implementations at the two vertices where it enters. In the notation adapted to the first diagram of Fig. 5.56 the possibilities are:

- $\mathcal{F}_{\pi\gamma^*\gamma^*}^{\text{LMD+V}}(m_\pi^2, q_1^2, q_2^2) \cdot \mathcal{F}_{\pi\gamma^*\gamma}^{\text{LMD+V}}(m_\pi^2, q_3^2, 0)$,

as advocated by KN. It implements the pion-pole approximation with VMD damping at internal and external vertex, but violates four momentum conservation at external vertex.

- $\mathcal{F}_{\pi\gamma^*\gamma^*}^{\text{LMD+V}}(m_\pi^2, q_1^2, q_2^2) \cdot \mathcal{F}_{\pi\gamma^*\gamma}^{\text{WZW}}(m_\pi^2, 0, 0)$,

as advocated by MV. At the internal vertex the LMD+V form factor is adopted, while the OPE analysis (considered below) predicts the constant WZW form factor for the external vertex. The OPE argument here is based on the asymptotics of the full LbL quark-loop box diagram which refers to the *hard-hard* regime of Fig. 5.47. VMD damping in this case we have at internal vertex only. In a way this looks puzzling. How can it be that the off-shell photon at the external vertex does not mix with the ρ , which would necessarily dress the form factor and provide a $1/Q^2$ behavior?

- $\mathcal{F}_{\pi^*\gamma^*\gamma^*}(q_3^2, q_1^2, q_2^2) \cdot \mathcal{F}_{\pi^*\gamma^*\gamma}(q_3^2, q_3^2, 0)$,

as advocated by JN. This implements VMD damping for off-shell photons at both vertices and preserves four momentum conservation at the external vertex. The OPE argument used here refers to the *soft-hard* regime. Admittedly, the second factor representing a far off-shell pion form factor at spacelike momentum transfer looks obsolete, as not related to any directly observable feature. Why should quarks form a pion at such kinematic circumstances? But, it does not look unreasonable to expect that it is qualitatively well described by the CQM form factor (see also [278]), which includes the WZW term, but, beyond the chiral limit, exhibits $1/q^2$ screening

³⁹Suppose we have a perfect RLA parametrization of all data up to an energy Λ above which pQCD is applicable. Then of course one gets a fully acceptable result even though the RLA is non-renormalizable and its application may not make any sense beyond Λ . This is known to work perfectly in case of the HVP (see e.g. [46]). In the HLbL case it is the mixed soft-hard regions where new kinds of problems arise, and where the OPE analysis comes into play.

of the latter, similar to the Brodsky-Lepage formula. If one argues with the chiral limit (no dependence on parameters h_3, h_4 and h_6 which otherwise just enhance the uncertainty) actually the three alternatives lead to compatible results. The chiral limit is expected to provide a viable approximation within the uncertainties usually assigned.

A new constraint on the pion TFF $\mathcal{F}_{\pi\gamma^*\gamma^*}(m_\pi^2, -Q_1^2, -Q_2^2)$ has been obtained by a recent lattice QCD calculation [293, 294] for the $(0, -Q^2, -Q^2)$ configuration, for which any information has been missing so far. Lattice data clearly see a $1/Q^2$ behavior for increasing Q^2 . This evidently rules out the naive VMD form factors, and together with the Brodsky-Lepage bound, largely confirmed by the available experimental data, only leaves the LMD+V ansatz as a viable parametrization. What remains an open problem is the $(-Q^2, -Q^2, 0)$ configuration relevant at the external vertex which is related to the problem of the magnetic susceptibility, which we addressed before.

As an upshot of our elaboration we have sufficient evidence that the large- N_c inspired LMD+V parametrization should provides a reliable estimation of the leading π^0 exchange contribution to a_μ^{HLbL} . Simpler parametrizations look to be obsolete by now. With the parameters constrained above (including an updated $\pi^0\gamma\gamma$ form factor fit of the data (see Fig. 5.59) and the recent lattice QCD constraint [293, 294]) the updated LMD+V result from [275] now reads

$$a_\mu^{\text{LbL}}(\pi^0) = (64.68 \pm 12.40) \times 10^{-11} \quad (5.220)$$

The central value and error have been estimated by a scan in the LMD+V off-shell form factor parameter space. By varying those parameters which in the LMD+V ansatz remain only weakly constrained or are not unconstrained in the ranges $\chi = -3.3 \pm 1.1 \text{ GeV}^{-2}$, $h_3, h_4 = -10, 0, +10 \text{ GeV}^2$ with the constraint $h_3 + h_4 = m_\pi^2 m_\pi^2 \chi$ and $h_6 = -10, -5, 0 \text{ GeV}^4$. Corresponding energy scales in GeV units read $674 \text{ MeV} \geq 1/\sqrt{\chi} \geq 335 \text{ MeV}$, $\sqrt{h_{3,4}} \leq 3.2 \text{ GeV}$ and $(h_6)^{1/4} \leq 1.8 \text{ GeV}$.

Higher Pseudoscalar Contributions

The higher pseudoscalars η and η' may be included in a way similar to the π^0 . We thus need the TFFs corresponding (5.175) and the adapted master integral (5.172). By the PCAC relation the interpolating fields of the PS mesons are proportional to the divergence of the axial currents. It is convenient to decompose the axial current into the different possible flavor channels and write it as a linear combination of isospin $j_{5\mu}^{(3)} = \bar{q}\lambda_3\gamma_\mu\gamma_5q$, hypercharge $j_{5\mu}^{(8)} = \bar{q}\lambda_8\gamma_\mu\gamma_5q$ and the $SU(3)$ singlet $j_{5\mu}^{(0)} = \bar{q}\lambda_0\gamma_\mu\gamma_5q$, where $\lambda_3 = \text{diag}(1, -1, 0)$ and $\lambda_8 = \text{diag}(1, 1, -2)$ are the diagonal Gell-Mann matrices of flavor $SU(3)$ and λ_0 is the unit matrix. Then

$$j_{5\mu} = \sum_{a=3,8,0} c_a j_{5\mu}^{(a)}, \quad c_a = \frac{\text{Tr}[\lambda_a \hat{Q}^2]}{\text{Tr}[\lambda_a^2]} = (3, 1, 4)/18. \quad (5.221)$$

The relative weight factors $W^{(a)}$ for the contributions from different $SU(3)$ flavor states follow from the flavor–decomposition (5.221) at the two pseudoscalar vertices $W^{(a)} \sim c_a^2$ multiplied by $\text{Tr}[\lambda_a^2](= 2, 6, 3)$ as $1/\sqrt{\text{Tr}[\lambda_a^2]}$ is needed for the normalization of the states: $\pi^0 = (u\bar{u} - d\bar{d})/\sqrt{2}$, $\eta_8 = (u\bar{u} + d\bar{d} - 2s\bar{s})/\sqrt{6}$, and $\eta_0 = (u\bar{u} + d\bar{d} + s\bar{s})/\sqrt{3}$. Thus

$$W^{(a)} = \frac{(\text{Tr}[\lambda_a \hat{Q}^2])^2}{\text{Tr}[\lambda_a^2]\text{Tr}[\hat{Q}^4]} ; \quad W^{(3)} = \frac{1}{4}, \quad W^{(8)} = \frac{1}{12}, \quad W^{(0)} = \frac{2}{3}. \quad (5.222)$$

where $\text{Tr}[\hat{Q}^4] = 2/9$ is the overall normalization such that $\sum_a W^{(a)} = 1$.

The additional complication is the mixing of the pseudoscalar states. In the nonet symmetry limit (see (5.157)) the relative weight factors are given by (5.222), which also follow from the WZW Lagrangian (5.150). Taking into account mixing of η_8 and η_0 into the physical states η and η' is complicated by the fact that there is a gluonic anomaly contribution $\frac{\alpha_s}{\pi} G\tilde{G}$ in the divergence of the axial singlet current

$$\partial^\mu \bar{q}_i \gamma_\mu \gamma_5 q_i = 2m_i \hat{q}_i i \gamma_5 q_i + \frac{\alpha_s}{\pi} G\tilde{G}.$$

As we know this implies that η_0 unlike the other pseudoscalars is not a Nambu–Goldstone boson in the chiral limit. The proper treatment of mixing in this case requires **two** angles to specify the projections from the unmixed sates to mixed ones η and η' [233]:

$$\begin{aligned} F_\eta^8 &= \cos \theta_8 F_8, & F_{\eta'}^8 &= \sin \theta_8 F_8 \\ F_\eta^0 &= -\sin \theta_0 F_0, & F_{\eta'}^0 &= \cos \theta_0 F_0. \end{aligned} \quad (5.223)$$

The parameters can be estimated in theory, using for instance large– N_c estimates together with the chiral expansion [233], or phenomenologically, using the decay widths $\Gamma(\eta \rightarrow \gamma\gamma) = 0.510 \pm 0.025$ keV and $\Gamma(\eta' \rightarrow \gamma\gamma) = 4.30 \pm 0.15$ keV and two more experimental constraints [295, 297] as an input.

Note on the determination of the couplings as they derive from the decays widths

$$\Gamma(\eta \rightarrow \gamma\gamma) = \frac{\alpha^2 m_\eta^3}{64\pi^3 F_\pi^2} r_\eta^2, \quad (\eta \rightarrow \eta \text{ or } \eta')$$

where, in the $SU(3)$ octet-singlet basis [233, 297], with $c_0 = \cos \theta_0$, $s_0 = \sin \theta_0$ etc. one obtains

$$\begin{aligned} r_\eta &= \frac{F_\pi c_0/F_8 - 2\sqrt{2}s_8/F_0}{\sqrt{3} c_0 c_8 + s_8 s_0}, \\ r_{\eta'} &= \frac{F_\pi s_0/F_8 + 2\sqrt{2}c_8/F_0}{\sqrt{3} c_0 c_8 + s_8 s_0}. \end{aligned}$$

In the equivalent q_s -mixing scheme [295], starting from states $|\eta_q\rangle \sim |u\bar{u} + d\bar{d}\rangle/\sqrt{2}$ and $|\eta_s\rangle \sim |s\bar{s}\rangle$, one may write

$$\begin{aligned} r_\eta &= \frac{F_\pi}{C_\pi} \left[\frac{C_q}{F_q} \cos \phi - \frac{C_s}{F_s} \sin \phi \right], \\ r_{\eta'} &= \frac{F_\pi}{C_\pi} \left[\frac{C_q}{F_q} \sin \phi + \frac{C_s}{F_s} \cos \phi \right] \end{aligned}$$

where $C_\pi = 1/(3\sqrt{2})$, $C_q = 5/(9\sqrt{2})$ and $C_s = 1/9$ are charge factors. The angle ϕ in leading order of flavor breaking is given by

$$\sin \phi = \sqrt{((m_{\eta'}^2 - m_{ss}^2)(m_\eta^2 - m_{qq}^2))/((m_{\eta'}^2 - m_\eta^2)(m_{ss}^2 - m_{qq}^2))}$$

with $m_{qq}^2 = m_\pi^2$, $m_{ss}^2 = 2M_K^2 - m_\pi^2$, $F_q = F_\pi$ and $F_s = \sqrt{2F_K^2 - F_\pi^2}$. The last two parameters can be directly determined from the experimental 2γ widths of η and η' . The relative weights $W^{(a)}$ thus are given by $(1, r_\eta^2, r_{\eta'}^2)$ since we normalized to $r_{\pi^0} = 1$.

The results obtained typically read

$$F_8 = (1.26 \pm 0.05) F_\pi \quad \text{and} \quad F_0 = (1.17 \pm 0.04) F_\pi \quad (5.224)$$

with mixing angles $\theta_8 = -21.2^\circ \pm 1.8^\circ$ $\theta_0 = -9.2^\circ \pm 2.1^\circ$. In the VMD type screening we replace ρ, ρ' by ω, ω' or ϕ, ϕ' . The mass effects alone $m_\pi \rightarrow m_\eta \rightarrow m_{\eta'}$ yields $a_{\mu}^{\text{LbL};\pi^0} = 59.55 \times 10^{-11} \rightarrow 15.53 \times 10^{-11} \rightarrow 10.09 \times 10^{-11}$. Together with the π^0 exchange result (5.220), taking into account the different couplings and weights as described yields

$$a_{\mu}^{\text{LbL}}(\pi^0, \eta, \eta') = (95.45[64.68 + 14.87 + 15.90] \pm 12.40) \times 10^{-11}. \quad (5.225)$$

We are now ready to summarize the results for the pseudoscalar contributions obtained by the different groups. A comparison of the different results also sheds light on the difficulties and the model dependencies in the theoretical estimations achieved so far.

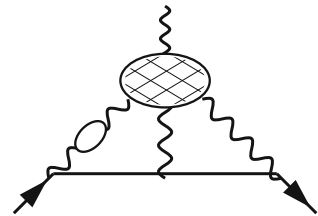
A very recent lattice QCD simulation [293, 294] of the doubly virtual $\pi^0 \rightarrow \gamma^*\gamma^*$ form factor is well consistent with the LMD+V parametrization under consideration of other more or less well established constraints yields $a_{\mu;\text{LMD+V}}^{\text{HLbL};\pi^0} = (65.0 \pm 8.3) \times 10^{-11}$. It is not surprising that the VMD form factor cannot be in agreement with the lattice data, while the LMD+V form factor can be matched.

Table 5.13 collects results obtained by other groups, the main differences are due to the implementation of additional S.D. constraints.

Table 5.13 Various model predictions of the π^0 and PS exchange contribution. In units 10^{-10}

Model	$a_\mu(\pi^0)$	$a_\mu(\pi^0, \eta, \eta')$	Ref.
HLS	5.7 ± 0.4	8.3 ± 0.6	[210] HKS
ENJL	5.9 ± 0.9	8.5 ± 1.3	[235] BPP
LMD+V (on-shell, $h_2 = -10 \text{ GeV}^2$)	6.3 ± 1.0	8.8 ± 1.2	[234] KN
LMD+V (on-shell, WZW at external vertex)	7.7 ± 0.7	11.4 ± 1.0	[254] MV
LMD+V (off-shell, $\chi = -(3.3 \pm 1.1) \text{ GeV}^{-2}$)	7.2 ± 1.2	9.9 ± 1.6	[274, 275] N/JN
linearized ENJL	8.2 ± 1.6	9.5 ± 1.7	[296]
RLA – VV'P model	6.7 ± 0.2	10.5 ± 0.5	[298]
RLA resonance saturation	6.6 ± 1.2		[299]
Non-local quark model	5.0 ± 0.4	5.9 ± 0.9	[300, 301]
Chiral Quark Model	6.8 ± 0.3		[278]
AdS/QCD inspired FF	6.9	10.7	[302]
AdS/QCD inspired FF	6.5 ± 0.3		[303]
DSE (truncated Dyson–Schwinger equations)	5.8 ± 1.0	8.1 ± 1.2	[220]
Padéized data		9.43 ± 0.53	[304]
LMD+V (on-shell, lattice QCD constraint)	6.5 ± 0.8		[293]
LMD+V (5.225)	6.5 ± 1.2	9.5 ± 1.3	[275] JN updated

Fig. 5.62 A hadronic light-by-light (see next section) next to leading order correction, which is of the same order as the NNLO corrections



Higher order HLbL contributions have been evaluated recently in [209]. The pion-pole contribution enhanced by an electron loop in one of the photon lines is estimated to yield

$$a_\mu^{\pi^0\text{-pole,NLO}} = 1.5 \times 10^{-11}$$

using a simple VMD form factor, which yields $a_\mu^{\pi^0\text{-pole,LO}} = 57.2 \times 10^{-11}$. Including other contributions, which sum up to what is represented by Fig. 5.62 [209] gives an estimate:

$$a_\mu^{\text{HLbL, NLO}} = (3 \pm 2) \times 10^{-11}$$

as an additional correction.

Besides the methods elaborated so far various other approaches have been applied to evaluate the pion-pole contribution. In Table 5.13 we compare the various predictions. The agreement of many results is not an accident: all models must satisfy the $\pi^0 \rightarrow \gamma\gamma$ decay constraint and assume a VMD type $\propto 1/Q^2$ behavior for large Q^2 . This latter constraint is implemented differently at the external vertex: in [254] and [274] (see also [282, 299]) a high energy boundary term is included such that the Brodsky-Lepage (VMD) $\propto 1/Q^2$ behavior is replaced by $\propto \text{const}$ at the external vertex. Corresponding evaluations lead to about 30% larger values which are supposed to include the quark loop tail.

Before we are going to discuss the evaluation of the yet missing HLbL contributions below in Sect. 5.2.5, we will discuss some more theoretical aspects in order to shed more light on light-by-light.

An Effective Field Theory Approach to HLbL

Analytic calculations of $a_\mu^{\text{LbL;had}}$ based on simplified (non-RLA) *Effective Field Theory* also provided instructive results: these studies are based on the $O(N_c, p^8)$ WZW Lagrangian

$$\mathcal{L}_{WZW} = \frac{\alpha N_c}{24\pi F_\pi} \varepsilon_{\mu\nu\alpha\beta} F^{\mu\nu} F^{\alpha\beta} \left(\pi^0 + \frac{1}{\sqrt{3}} \eta \right) + \dots,$$

the $O(p^6)$ chiral Lagrangian and assuming scalar QED for the interaction of the photon with the charged pseudoscalars. The leading diagrams are shown in Fig. 5.63. Diagrams (a) and (b) in this approach are divergent and renormalized by the effective counter term Lagrangian

$$\mathcal{L}^{(6)} = (\alpha^2/4\pi^2 F_0) \delta\chi \bar{\psi} \gamma_\mu \gamma_5 \psi \partial^\mu \pi^0 + \dots \quad (5.226)$$

generating diagrams (d) and (e). Diagram (c) is finite. The overall divergence requires a lowest order anomalous magnetic moment type diagram (f). The effective Lagrangian thus must include a term of type (3.84), with $a_\mu \rightarrow \delta a_\mu$. Strictly speaking this spoils the predictive power of the effective theory by an overall subtraction, unless the divergence is removed by some other mechanism like the VMD model again, for example. Including the pion and Kaon loops of Fig. 5.55, the result may be cast into the form [251]

$$a_\mu^{\text{LbL;had}} = \left(\frac{\alpha}{\pi} \right)^3 \left\{ N_c \left(\frac{m_\mu^2}{16\pi^2 F_\pi^2} \frac{N_c}{3} \right) \left[\ln^2 \frac{\mu_0}{m_\mu} + c_1 \ln \frac{\mu_0}{m_\mu} + c_0 \right] \right. \\ \left. + f \left(\frac{m_{\pi^\pm}}{m_\mu}, \frac{M_{K^\pm}}{m_\mu} \right) + O \left(\frac{m_\mu^2}{\mu_0^2} \times \log s, \frac{m_\mu^4}{\mu_0^4} N_c \times \log s \right) \right\}. \quad (5.227)$$

Since $F_\pi = O(\sqrt{N_c})$, the leading term is $O(N_c)$ (see Table 5.12) and exhibits a \log^2 term with universal coefficient $C = (N_c^2 m_\mu^2)/(48\pi^2 F_\pi^2) \simeq 0.025$ for $N_c = 3$ [251].

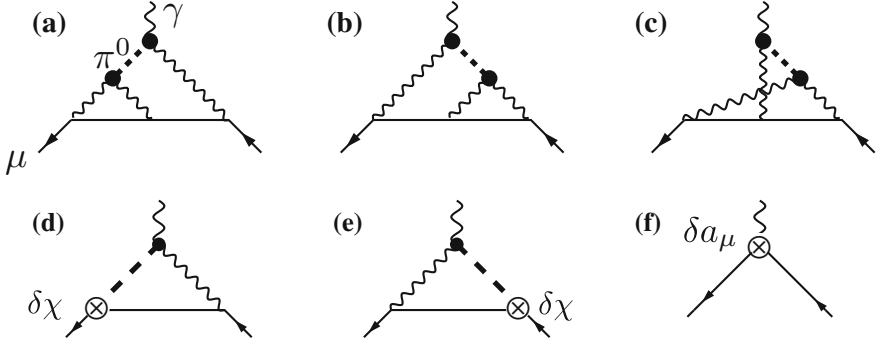


Fig. 5.63 Diagrams contributing to $a_\mu^{\text{LbL};\pi^0}$ in EFT. \otimes denotes a renormalization counter term insertion. Counter terms $\delta\chi$ are needed to render the triangular subgraphs of (a) and (b) finite, δa_μ is needed to remove the remaining overall two-loop divergence

The scale $\overline{\mu}_0$, originally represents the cut-off $\mu_0 = \Lambda$ or, in dimensional regularization, the $\overline{\text{MS}}$ scale or after imposing a subtraction (= renormalization) condition it is the renormalization scale. Again the VMD model (5.211) is the simplest possibility to introduce a physical cut-off $\mu_0 = M_\rho$, such that

$$a_{\mu;\text{VMD}}^{\text{LbL};\pi^0} = \left(\frac{\alpha}{\pi}\right)^3 C X_{\pi^0} = \left(\frac{\alpha}{\pi}\right)^3 C \left[\ln^2 \frac{M_\rho}{m_\mu} + c_1 \ln \frac{M_\rho}{m_\mu} + c_0 \right]. \quad (5.228)$$

In this case the diagrams Fig. 5.63 exhibit three well separated scales:

$$m_\pi^2 - m_\mu^2 \ll m_\mu^2 \ll M_\rho^2,$$

and based on this hierarchy an expansion in $\delta \equiv (m_\pi^2 - m_\mu^2)/m_\mu^2$ and m_μ^2/M_ρ^2 is possible. The expansion in δ is especially simple and reduces to the *Taylor expansion* of the pion propagator. The expansion in m_μ^2/M_ρ^2 is a *Large Mass Expansion*. The result obtained in [252] is given by

$$\begin{aligned} X_{\pi^0} = & L^2 + \left(\frac{1}{2} - \frac{\pi}{\sqrt{3}}\right)L - \frac{277}{216} + \frac{2\pi}{\sqrt{3}}S_2 - \frac{17\pi}{72\sqrt{3}} + \frac{57}{8}S_2 - \frac{\zeta_3}{6} - \frac{11\pi^2}{324} \\ & + \frac{m_\mu^2}{M_\rho^2} \left[\frac{155}{27}L^2 - \left(\frac{65}{27} + \frac{3\pi}{\sqrt{3}}\right)L - \frac{11915}{1296} + \frac{2\pi}{\sqrt{3}}S_2 + \frac{4\pi}{3\sqrt{3}} + \frac{117}{4}S_2 - \frac{1}{6}\zeta_3 + \frac{347\pi^2}{1944} \right] \\ & + \delta \left[\left(\frac{2}{3} - \frac{2\pi}{3\sqrt{3}}\right)L - \frac{1}{27} + \frac{5}{2}\frac{\pi}{\sqrt{3}}S_2 - \frac{11\pi}{18\sqrt{3}} - \frac{1}{8}S_2 - \frac{2}{9}\zeta_3 + \frac{53\pi^2}{648} \right] + \mathcal{O}\left(\frac{m_\mu^4}{M_\rho^4}, \delta^2\right), \end{aligned} \quad (5.229)$$

where $L = \log(M_\rho/m_\mu)$, $\zeta_3 \simeq 1.202057$ and $S_2 = \frac{4}{9\sqrt{3}}\text{Cl}_2\left(\frac{\pi}{3}\right) \simeq 0.260434$. The numerical evaluation in terms of the known physical parameters yields

$$a_{\mu; \text{VMD}}^{\text{LbL}; \pi^0} = [136 - 112 + 30] \times 10^{-11} = +54 \times 10^{-11},$$

and agrees with the LMD+V model result [234]. Note that there are large cancellations between leading and subleading terms, although the leading log is sizable $\ln(M_\rho/m_\mu) \simeq 1.98$. Nyffeler obtained $a_{\mu; \text{VMD}}^{\text{LbL}; \pi^0} = [123 - 103 + 34] \times 10^{-11} = +54 \times 10^{-11}$ [305] confirming this pattern, by a fit of (5.228) to the representation (5.208) for the VMD model.

An alternative possibility to renormalize the EFT model is to use data from a related process, like a $P \rightarrow \ell^+ \ell^-$ decay, to fix the counterterms, as performed in [253]. The effective Lagrangian for this process reads

$$\mathcal{L}_{P\ell^+\ell^-} = -\frac{N_c \alpha^2}{48\pi^2 F_\pi} \chi \bar{\mu}_\ell \gamma^\lambda \gamma_5 \mu_\ell \left(\partial_\lambda \pi^0 + \frac{1}{\sqrt{3}} \partial_\lambda \eta \right) + \dots,$$

where μ_ℓ denotes a lepton spinor, and using the $P\ell^+\ell^-$ constraint, one obtains result similar to (5.228) with $c_1 = -2/3 \delta\chi(\mu_0) + 0.237 = -0.93_{-0.83}^{+0.67}$. The value of $\delta\chi$ here has been determined from the $\eta \rightarrow \mu^+ \mu^-$ branching fraction, taken as a renormalization condition. This also provides the overall counterterm δa_μ required to get a finite prediction. In this way one can avoid to refer to the VMD model for eliminating the overall counterterm and use an experimental constraint instead. The result obtained is $a_{\mu; P\ell^+\ell^-}^{\text{LbL}; \pi^0} = (57_{-60}^{+50}) \times 10^{-11}$. The bare pion and Kaon loops (with undressed photons) as expected yield a subleading correction with $f\left(\frac{m_{\pi^\pm}}{m_\mu}, \frac{M_{K^\pm}}{m_\mu}\right) = -0.038$ or $\delta a_{\mu; \text{sQED}}^{\text{LbL}}(\pi^\pm, K^\pm - \text{loops}) \simeq -48 \times 10^{-11}$. This also agrees (as it should) with known undressed sQED results. Note that the uncertainties in this approach are very large in general, as far as they have been estimated.

Hadronic Light-by-Light Scattering and the Triangle Anomaly

In order to develop a systematic framework to include also other single hadron exchange contributions we need some more insight into the mechanism of hadroproduction in LbL scattering. To this end it is instructive to follow the approach advocated in [254] (MV's OPE approach). The alternative way to look at the problem is to use the anomalous PCAC relation (5.232) and to relate $\pi^0 \gamma \gamma$ directly with the ABJ anomaly (Bell–Jackiw approach). The profile of the ABJ anomaly we have discussed in Sect. 4.2.2 on p. 299 within the context of the weak hadronic effects. Here we are interested in the role of the triangle anomaly in the context of the hadronic light-by-light contribution. We therefore consider the VVA three-point function

$$\mathcal{W}_{\mu\nu\rho}(q_1, q_2) = i \int d^4 x_1 d^4 x_2 e^{i(q_1 \cdot x_1 + q_2 \cdot x_2)} \langle 0 | T\{V_\mu(x_1) V_\nu(x_2) A_\rho(0)\} | 0 \rangle \quad (5.230)$$

of the flavor and color diagonal fermion currents

$$V_\mu = \bar{\psi} \gamma_\mu \psi, \quad A_\mu = \bar{\psi} \gamma_\mu \gamma_5 \psi, \quad (5.231)$$

where $\psi(x)$ is a quark field. The vector currents are strictly conserved $\partial_\mu V^\mu(x) = 0$, while the axial vector current satisfies a PCAC relation plus the anomaly (indexed by $_0$ are bare parameters),

$$\partial_\mu A^\mu(x) = 2 i m_0 \bar{\psi} \gamma_5 \psi(x) + \frac{\alpha_0}{4\pi} \varepsilon_{\mu\nu\rho\sigma} F^{\mu\nu} F^{\rho\sigma}(x). \quad (5.232)$$

To leading order the correlator of interest is associated with the one-loop triangle diagram plus its crossed ($q_1, \mu \leftrightarrow q_2, \nu$) partner Fig. 4.20. The covariant decomposition of $\mathcal{W}_{\mu\nu\rho}(q_1, q_2)$ into invariant functions has four terms

$$\mathcal{W}_{\mu\nu\rho}(q_1, q_2) = \frac{1}{8\pi^2} \left\{ w_L(q_1^2, q_2^2, q_3^2) (q_1 + q_2)_\rho \varepsilon_{\mu\nu\alpha\beta} q_1^\alpha q_2^\beta + 3 \text{ transversal} \right\}.$$

The longitudinal part is entirely fixed by the anomaly,

$$w_L(q_1^2, q_2^2, q_3^2) = -\frac{2N_c}{q_3^2}, \quad (5.233)$$

which is exact to all orders of perturbation theory, the famous Adler-Bardeen non-renormalization theorem.

Specifically, the WT identities restrict the covariant decomposition of $\mathcal{W}_{\mu\nu\rho}(q_1, q_2)$ to four invariant functions⁴⁰

$$\begin{aligned} \mathcal{W}_{\mu\nu\rho}(q_1, q_2) = & -\frac{1}{8\pi^2} \left\{ w_L(q_1^2, q_2^2, q_3^2) (q_1 + q_2)_\rho \varepsilon_{\mu\nu\alpha\beta} q_1^\alpha q_2^\beta \right. \\ & \left. + w_T^{(+)}(q_1^2, q_2^2, q_3^2) t_{\mu\nu\rho}^{(+)}(q_1, q_2) + w_T^{(-)}(q_1^2, q_2^2, q_3^2) t_{\mu\nu\rho}^{(-)}(q_1, q_2) + \tilde{w}_T^{(-)}(q_1^2, q_2^2, q_3^2) \tilde{t}_{\mu\nu\rho}^{(-)}(q_1, q_2) \right\}, \end{aligned} \quad (5.234)$$

with the transverse tensors given by

$$\begin{aligned} t_{\mu\nu\rho}^{(+)}(q_1, q_2) &= q_{1\nu} \varepsilon_{\mu\rho\alpha\beta} q_1^\alpha q_2^\beta - q_{2\mu} \varepsilon_{\nu\rho\alpha\beta} q_1^\alpha q_2^\beta - (q_1 \cdot q_2) \varepsilon_{\mu\nu\rho\alpha} (q_1 - q_2)^\alpha \\ &\quad + (q_1^2 + q_2^2 - q_3^2)/q_3^2 \varepsilon_{\mu\nu\alpha\beta} q_1^\alpha q_2^\beta (q_1 + q_2)_\rho, \\ t_{\mu\nu\rho}^{(-)}(q_1, q_2) &= [(q_1 - q_2)_\rho - (q_1^2 - q_2^2)/(q_1 + q_2)^2 (q_1 + q_2)_\rho] \varepsilon_{\mu\nu\alpha\beta} q_1^\alpha q_2^\beta, \\ \tilde{t}_{\mu\nu\rho}^{(-)}(q_1, q_2) &= q_{1\nu} \varepsilon_{\mu\rho\alpha\beta} q_1^\alpha q_2^\beta + q_{2\mu} \varepsilon_{\nu\rho\alpha\beta} q_1^\alpha q_2^\beta - (q_1 \cdot q_2) \varepsilon_{\mu\nu\rho\alpha} (q_1 + q_2)^\alpha. \end{aligned}$$

⁴⁰We closely follow the notation of [306].

Bose symmetry ($q_1, \mu \leftrightarrow q_2, \nu$) implies

$$\begin{aligned} w_T^{(+)}(q_2^2, q_1^2, q_3^2) &= +w_T^{(+)}(q_1^2, q_2^2, q_3^2), \\ w_T^{(-)}(q_2^2, q_1^2, q_3^2) &= -w_T^{(-)}(q_1^2, q_2^2, q_3^2), \\ \tilde{w}_T^{(-)}(q_2^2, q_1^2, q_3^2) &= -\tilde{w}_T^{(-)}(q_1^2, q_2^2, q_3^2). \end{aligned}$$

In [306] the following three chiral symmetry relations between amplitudes were derived in pQCD:

$$\begin{aligned} &\left[w_T^{(+)} + w_T^{(-)} \right] (q_1^2, q_2^2, q_3^2) - \left[w_T^{(+)} + w_T^{(-)} \right] (q_3^2, q_2^2, q_1^2) = 0, \\ &\left[\tilde{w}_T^{(-)} + w_T^{(-)} \right] (q_1^2, q_2^2, q_3^2) + \left[\tilde{w}_T^{(-)} + w_T^{(-)} \right] (q_3^2, q_2^2, q_1^2) = 0, \\ &\left[w_T^{(+)} + \tilde{w}_T^{(-)} \right] (q_1^2, q_2^2, q_3^2) + \left[w_T^{(+)} + \tilde{w}_T^{(-)} \right] (q_3^2, q_2^2, q_1^2) = w_L(q_3^2, q_2^2, q_1^2) \\ &\quad - 2 \left[\frac{(q_2^2 + q_1 \cdot q_2)}{q_1^2} w_T^{(+)}(q_3^2, q_2^2, q_1^2) - \frac{q_1 \cdot q_2}{q_1^2} w_T^{(-)}(q_3^2, q_2^2, q_1^2) \right], \end{aligned}$$

involving the transverse part of the $\langle VVA \rangle$ correlator $\mathcal{W}_{\mu\nu\rho}(q_1, q_2)$, and which hold for all values of the momentum transfers q_1^2, q_2^2 and q_3^2 .

In the kinematic configuration relevant for $g-2$ calculations, $q_1 = k \pm q$, $q_2 = -k$, expanding to linear order in k and noting that $\tilde{t}_{\mu\nu\rho}^{(-)}(q_1, q_2) \sim t_{\mu\nu\rho}^{(+)}(q_1, q_2) = q^2 \varepsilon_{\mu\nu\rho\sigma} k^\sigma - q_\mu \varepsilon_{\nu\rho\alpha\beta} q^\alpha k^\beta - q_\rho \varepsilon_{\mu\nu\alpha\beta} q^\alpha k^\beta + O(k^2)$ and $t_{\mu\nu\rho}^{(-)}(q_1, q_2) = O(k^2)$, for $Q^2 = -q^2$, the relations (5.235) imply Vainshtein's [283] non-renormalization theorem: the amplitudes

$$\begin{aligned} w_L(Q^2) &\equiv w_L(-Q^2, 0, -Q^2), \\ w_T(Q^2) &\equiv w_T^{(+)}(-Q^2, 0, -Q^2) + \tilde{w}_T^{(-)}(-Q^2, 0, -Q^2), \end{aligned}$$

in the chiral limit satisfy

$$w_T(Q^2)_{\text{pQCD}}|_{m=0} = \frac{1}{2} w_L(Q^2)|_{m=0}, \quad (5.235)$$

valid to all orders of perturbative QCD in the kinematic limit relevant for the $g-2$ contribution.

In order to obtain the coupling to pseudoscalars we have to take the derivative as required by the PCAC relation, and using (5.233) we obtain

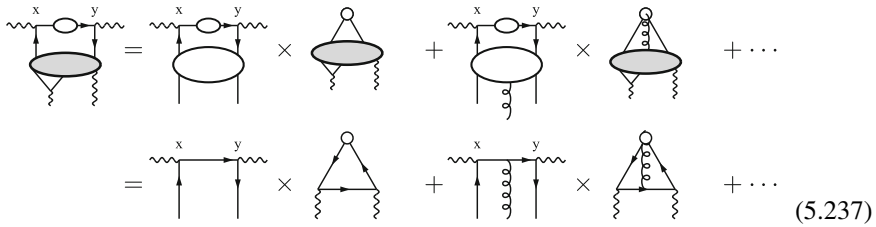
$$\begin{aligned} (q_1 + q_2)^\rho \mathcal{W}_{\mu\nu\rho}(q_1, q_2) &= \frac{1}{8\pi^2} \varepsilon_{\mu\nu\alpha\beta} q_1^\alpha q_2^\beta w_L(q_1^2, q_2^2, q_3^2) q_3^2 \\ &= -\frac{N_c}{4\pi^2} \varepsilon_{\mu\nu\alpha\beta} q_1^\alpha q_2^\beta. \end{aligned} \quad (5.236)$$

This holds to all orders and for arbitrary momenta. It should be stressed that the pole in the amplitude w_L is just a kinematical singularity stemming from the covariant decomposition of the tensor amplitude and by dimensional counting. Thus, in general, the VVA correlator does not exhibit physical one particle poles and in observables all kinematical singularities must cancel out in any case.

A crucial question is the one about the correct high energy behavior of $\mathcal{F}_{\pi^0 \rightarrow \gamma^* \gamma^*}$. It is particularly this far off-shell behavior which enters in a relevant manner in the integral (5.166). This high energy behavior has to be fixed somehow in all the evaluations and was reconsidered by Knecht and Nyffeler [234, 246] and later by Melnikov and Vainshtein [254]. The latter authors criticized all previous evaluations in this respect and came up with a new estimation of the correct asymptotic behavior. Key tool again is the OPE in order to investigate the short distance behavior of the four-current correlator in (5.139), which may be written as [254]

$$\langle 0 | T \{ j_\mu(x_1) j_\nu(x_2) j_\lambda(x_3) \} | \gamma(k) \rangle,$$

taking into account that the external photon is in a physical state. A look at the first of the diagrams of Fig. 5.56, and taking into account the pole-dominance picture, shows that with q_1 and q_2 as independent loop integration momenta the most important region to investigate is $q_1^2 \sim q_2^2 \gg q_3^2$, which is related to a short distance expansion of $T \{ j_\mu(x_1) j_\nu(x_2) \}$ for $x_1 \rightarrow x_2$. Thus the OPE again is of the form (4.82), however, now for two electromagnetic currents $T \{ j_\mu(x) j_\nu(y) X \}$ and with a “state” X the third electromagnetic current $j_\lambda(z)$ times the physical external photon state $|\gamma(k)\rangle$:



Note that this time the first term of (4.83) is absent due to C -invariance (Furry’s theorem). As usual the result of an OPE is a product of a perturbative *hard* “short distance coefficient function” times a non-perturbative *soft* “long distance matrix element”. Surprisingly, for the leading possible term here, the non-perturbative factor is just given by the ABJ anomaly diagram, which is known to be given by the perturbative one-loop result, exact to all orders in the massless limit. This requires of course that the leading operator in the short distance expansion must involve the divergence of the axial current, as the VVV triangle is identically zero by Furry’s theorem. This is how the pseudoscalar pion comes into the game in spite of the fact that LbL scattering externally involves vector currents only. Indeed, in leading order one obtains

$$i \int d^4 x_1 \int d^4 x_2 e^{i(q_1 x_1 + q_2 x_2)} T\{j_\mu(x_1) j_\nu(x_2) X\} = \int d^4 z e^{i(q_1 + q_2)z} \left\{ \frac{2i}{\hat{q}^2} \varepsilon_{\mu\nu\alpha\beta} \hat{q}^\alpha T\{j_5^\beta(z) X\} + \frac{2m_q}{\hat{q}^2} g_{\mu\nu} T\{S(z) X\} + \dots \right\}, \quad (5.238)$$

with $j_5^\mu = \bar{q} \hat{Q}^2 \gamma^\mu \gamma_5 q$ the relevant axial current and $\hat{q} = (q_1 - q_2)/2 \approx q_1 \approx -q_2$ represents a large momentum transfer. The second chirally suppressed term allows for a scalar $S = \bar{q} \hat{Q}^2 q$ transition. The momentum flowing through the axial vertex is $q_1 + q_2$ and in the limit $k^\mu \rightarrow 0$ of our interest $q_1 + q_2 \rightarrow -q_3$, which is assumed to be much smaller than \hat{q} ($q_1^2 - q_2^2 \sim -2q_3 \hat{q} \sim 0$). The ellipses stand for terms suppressed by higher powers of $\Lambda_{\text{QCD}}/\hat{q}$. After the perturbative large q_1, q_2 behavior has been factored out the remaining soft matrix element to be calculated is

$$T_{\lambda\beta} = i \int d^4 z e^{i q_3 x_3} \langle 0 | T\{j_\lambda(x_3) j_{5\beta}(0)\} | \gamma(k) \rangle, \quad (5.239)$$

which by the LSZ reduction formula is equivalent to

$$T_{\lambda\beta} = -i e \varepsilon^\rho(k) T_{\rho\lambda\beta},$$

where $\varepsilon_\mu(k)$ is the polarization vector for the external photon and

$$T_{\rho\lambda\beta} = - \int d^4 x d^4 y e^{i(qx - ky)} \langle 0 | T\{j_\rho(y) j_\lambda(x) j_{5\beta}(0)\} | 0 \rangle, \quad (5.240)$$

which is precisely the famous VVA triangle correlator. In fact the anomalous PCAC relation relates the WZW $\pi^0 \gamma \gamma$ vertex directly with the ABJ anomaly (Bell–Jackiw approach), and the WZW effective Lagrangian in flavor $SU(3)$ space follows as given by (5.150). So, Eqs. (5.233), (5.235) and (5.236) summarize the most relevant features related to the triangle diagram.

We may check this by calculating perturbatively a massive fermion–loop to leading order

$$w_L^{1\text{-loop}}(Q^2) = 2w_T^{1\text{-loop}}(Q^2) = \sum_f 2N_{cf} \int_0^1 \frac{dx x(1-x)}{x(1-x)Q^2 + m_f^2} \\ m_f^2 \ll Q^2 \sum_f 2N_{cf} \left[\frac{1}{Q^2} - \frac{2m_f^2}{Q^4} \ln \frac{Q^2}{m_f^2} + O\left(\frac{1}{Q^6}\right) \right], \quad (5.241)$$

where w_T is the transversal amplitude which survives in linear order when one of the external vector momenta approaches zero (the configuration relevant for all $g - 2$ applications, see below). N_{cf} is 1 for leptons 3 for quarks. This indeed confirms the above stated assertions, but of course does not say that it is true beyond perturbation theory.

Using the $SU(3)$ flavor decomposition (5.221) of the current and the tensor decomposition (5.234), the matrix–element (5.239) we are interested in may be written as [254]

$$\begin{aligned} T_{\lambda\beta}^{(a)} &= -\frac{i e N_c \text{Tr}[\lambda_a \hat{Q}^2]}{4\pi^2} \left\{ w_L^{(a)}(q_3^2) q_{3\beta} q_3^\sigma \tilde{f}_{\sigma\lambda} \right. \\ &\quad \left. + w_T^{(a)}(q_3^2) \left(-q_3^2 \tilde{f}_{\lambda\beta} + q_{3\lambda} q_3^\sigma \tilde{f}_{\sigma\beta} - q_{3\beta} q_3^\sigma \tilde{f}_{\sigma\lambda} \right) \right\}, \\ q_3^\beta T_{\lambda\beta}^{(a)} &= \frac{i e N_c \text{Tr}[\lambda_a \hat{Q}^2]}{2\pi^2} q_3^\sigma \tilde{f}_{\sigma\lambda}, \end{aligned} \quad (5.242)$$

where $w_L^{(a)}(q_3^2) q_3^2 = -2$ has been used and where $\tilde{f}_{\alpha\beta}$ is the dual of $f_{\alpha\beta} = k_\alpha \varepsilon_\beta - k_\beta \varepsilon_\alpha$ with $\varepsilon_\alpha = \varepsilon_\alpha(k)$ the (external) photon polarization vector. The result follows by noticing that the LbL scattering tensor required in (5.145) is $\frac{\partial}{\partial k^\rho} \Pi_{\mu\nu\lambda\sigma} \simeq \frac{2i}{\hat{q}^2} \varepsilon_{\mu\nu\alpha\beta} \hat{q}^\alpha T_{\lambda\beta}[\tilde{f}] + \text{permutations}$ with $\tilde{f}_{\alpha\beta} \rightarrow \varepsilon_{\alpha\beta\gamma\delta} k^\gamma \varepsilon^\delta \rightarrow \varepsilon_{\alpha\beta\rho\sigma}$. In addition we have to use Shouten's identity

$$-q_3^2 \varepsilon_{\lambda\beta\rho\sigma} + q_{3\lambda} \varepsilon_{q_3\beta\rho\sigma} - q_{3\beta} \varepsilon_{q_3\lambda\rho\sigma} = q_{3\sigma} \varepsilon_{q_3\lambda\beta\rho} - q_{3\rho} \varepsilon_{q_3\lambda\beta\sigma}$$

and permutations thereof to simplify the coefficient of the transversal amplitude w_T .

Both amplitudes of (5.242), the longitudinal w_L as well as the transversal w_T , are calculable from the triangle fermion one–loop diagram. In the chiral limit they are given by (5.233) [283, 306–308]. At this stage of the consideration it looks like a real mystery what all this has to do with π^0 -exchange, as everything looks perfectly controlled by perturbation theory. The clue is that as a low energy object we may evaluate this matrix element at the same time perfectly well in terms of hadronic spectral functions by saturating it by a sum over intermediate states. For the positive frequency part we have

$$\langle 0 | j_{5\beta}^{(a)}(z) j_\lambda(0) | \gamma(k) \rangle = \int \frac{d^4 p_n}{(2\pi)^3} \sum_n \langle 0 | j_{5\beta}^{(a)}(z) | n \rangle \langle n | j_\lambda(0) | \gamma(k) \rangle,$$

where for $a = 3$ the lowest state contributing is the π^0 , the next to lowest the a_1 , followed by the f_2 , and so on. Thus

$$\begin{aligned} \langle 0 | j_{5\beta}^{(3)}(z) j_\lambda(0) | \gamma(k) \rangle &= \int \frac{d^3 p}{(2\pi)^3 2\omega_p} \times \left\{ \langle 0 | j_{5\beta}^{(3)}(z) | \pi^0(p) \rangle \langle \pi^0(p) | j_\lambda(0) | \gamma(k) \rangle \right. \\ &\quad \left. + \sum_s \langle 0 | j_{5\beta}^{(3)}(z) | a_1(p, s) \rangle \langle a_1(p, s) | j_\lambda(0) | \gamma(k) \rangle \right. \\ &\quad \left. + \sum_s \langle 0 | j_{5\beta}^{(3)}(z) | f_2(p, s) \rangle \langle f_2(p, s) | j_\lambda(0) | \gamma(k) \rangle + \dots \right\}. \end{aligned} \quad (5.243)$$

For the leading π^0 contribution we have the matrix elements

$$\begin{aligned}\langle 0|j_{5\beta}^{(3)}(z)|\pi^0(p)\rangle &= e^{ipz} 2iF_\pi p_\beta, \\ \langle \pi^0(p)|j_\lambda(0)|\gamma(k)\rangle &= -4e g_{\pi^0\gamma\gamma} p^\alpha \tilde{f}_{\alpha\lambda}.\end{aligned}$$

The first relation defines F_π , and using $N_c \text{Tr}[\lambda_3 \hat{Q}^2] = 1$ the second fixes the important $\pi^0\gamma\gamma$ coupling to

$$g_{\pi^0\gamma\gamma} = \frac{1}{16\pi^2 F_\pi} \quad (5.244)$$

by the anomaly in (5.242) in the chiral limit $m_\pi^2 \rightarrow 0$. Omitting subleading terms, as a result we find

$$\langle 0|j_{5\beta}^{(3)}(z)j_\lambda(0)|\gamma(k)\rangle = i \int \frac{d^4 p}{(2\pi)^3} \Theta(p^0) \delta(p^2 - m_\pi^2) 2F_\pi g_{\pi^0\gamma\gamma} p_\beta p^\alpha \tilde{f}_{\alpha\lambda} e^{ipz},$$

and finally for the time ordered correlation

$$\langle 0|T\{j_{5\beta}^{(3)}(z)j_\lambda(0)\}|\gamma(k)\rangle = i \int \frac{d^4 p}{(2\pi)^4} \frac{i}{p^2 - m_\pi^2 + i\varepsilon} 4F_\pi g_{\pi^0\gamma\gamma} p_\beta p^\alpha \tilde{f}_{\alpha\lambda} e^{ipz}.$$

Taking i times the Fourier transform we have

$$T_{\lambda\beta}(p, k) = -4 F_\pi g_{\pi^0\gamma\gamma} \frac{i}{p^2 - m_\pi^2 + i\varepsilon} p_\beta p^\alpha \tilde{f}_{\alpha\lambda}, \quad (5.245)$$

the non-perturbative correspondent for the longitudinal part of (5.242). The OPE argument together with the correspondence

$$\begin{aligned}\frac{-ie}{4\pi^2} w_L(q^2) q_\beta q^\sigma \tilde{f}_{\sigma\lambda} \\ \downarrow \\ \langle 0|j_{5\beta}^{(3)}(0)|\pi^0(q)\rangle \times \langle \pi^0(q)|j_\lambda(0)|\gamma(k)\rangle &= 2i F_\pi q_\beta \times -4e g_{\pi^0\gamma\gamma} q^\sigma \tilde{f}_{\sigma\lambda}\end{aligned} \quad (5.246)$$

establishes the π^0 exchange as a leading LbL scattering contribution and, as an important byproduct, we have **predicted** the basic $\pi^0\gamma\gamma$ coupling $g_{\pi^0\gamma\gamma}$, as first derived by Bell–Jackiw in [240]. Not very surprisingly, the “picture” developed here based on the OPE argument is neatly supported by recent lattice QCD calculations [309] supporting OPE premise that quark fields have to get close to each other in configuration space to catch the leading HLbL effects, confirming the single pion exchange dominance.

In order to point out the close relation to real light-by-light scattering Melnikov–Vainshtein consider the quasi S -matrix element

$$\begin{aligned} \mathcal{M} &= \alpha^2 N_c \text{Tr}[\hat{Q}^4] \mathcal{A} = \alpha^2 N_c \text{Tr}[\hat{Q}^4] \mathcal{A}_{\mu_1 \mu_2 \mu_3 \gamma \delta} \epsilon_1^{\mu_1} \epsilon_2^{\mu_2} \epsilon_3^{\mu_3} f^{\gamma \delta} \\ &= -e^3 \int d^4x d^4y e^{-i(q_1 x + q_2 y)} \epsilon_1^{\mu_1} \epsilon_2^{\mu_2} \epsilon_3^{\mu_3} \langle 0 | T \{ j_{\mu_1}(x) j_{\mu_2}(y) j_{\mu_3}(0) \} | \gamma \rangle, \end{aligned} \quad (5.247)$$

with the photon momenta q_i (incoming, $\sum q_i = 0$) and the photon polarization vectors ϵ_i . The first three photons are virtual, while the fourth one represents the external magnetic field and can be regarded as a real photon with vanishingly small momentum q_4 . The field strength tensor of the external soft photon is denoted by $f^{\gamma \delta} = q_4^\gamma \epsilon_4^\delta - q_4^\delta \epsilon_4^\gamma$. Since for a_μ only terms linear in q_4 are needed, see (5.142), one can set $q_4 = 0$ in the amplitude $\mathcal{A}_{\mu_1 \mu_2 \mu_3 \gamma \delta}$. For $q_1^2 \approx q_2^2 \gg q_3^2$ the above OPE applies (see Fig. 5.60) and with (5.242) one can therefore write the hadronic light-by-light scattering amplitude as follows

$$\begin{aligned} \mathcal{A}_{\mu_1 \mu_2 \mu_3 \gamma \delta} f^{\gamma \delta} &= \frac{8}{\hat{q}^2} \epsilon_{\mu_1 \mu_2 \delta \rho} \hat{q}^\delta \sum_{a=3,8,0} W^{(a)} \left\{ w_L^{(a)}(q_3^2) q_3^\rho q_3^\sigma \tilde{f}_{\sigma \mu_3} \right. \\ &\quad \left. + w_T^{(a)}(q_3^2) \left(-q_3^2 \tilde{f}_{\mu_3}^\rho + q_{3\mu_3} q_3^\sigma \tilde{f}_\sigma^\rho - q_3^\rho q_3^\sigma \tilde{f}_{\sigma \mu_3} \right) \right\} + \dots, \end{aligned} \quad (5.248)$$

where the weights $W^{(a)}$ are given by $W^{(3)} = \frac{1}{4}$, $W^{(8)} = \frac{1}{12}$ and $W^{(0)} = \frac{2}{3}$ (see (5.222)).

The expression in (5.248) is then extrapolated to arbitrary values of q_1^2, q_2^2 by writing $\mathcal{A} = \mathcal{A}_{\text{PS}} + \mathcal{A}_{\text{AV}} + \text{permutations}$, with the ansatz

$$\mathcal{A}_{\text{PS}} = \sum_{a=3,8,0} W^{(a)} \phi_L^{(a)}(q_1^2, q_2^2) w_L^{(a)}(q_3^2) (f_2^{\mu\nu} \tilde{f}_1^{\nu\mu}) (\tilde{f}^{\rho\sigma} f_3^{\sigma\rho}), \quad (5.249)$$

where $f_i^{\mu\nu} = q_i^\mu \epsilon_i^\nu - q_i^\nu \epsilon_i^\mu$ denote the field strength tensors. The form factors $\phi_L^{(a)}(q_1^2, q_2^2)$ account for the dependence of the amplitude on $q_{1,2}^2$, i.e. the internal interaction vertex in π^0 -exchange with two virtual photons, whereas the meson propagator together with the external interaction vertex comprise the triangle amplitude $w_L^{(a)}(q_3^2)$.

For the pion one obtains, outside the chiral limit,

$$w_L^{(3)}(q_3^2) = \frac{2}{q_3^2 + m_\pi^2}, \quad (5.250)$$

whereas the ABJ anomaly fixes $\phi_L^{(3)}(0, 0) = N_c / (4\pi^2 F_\pi^2)$. Defining the $\pi^0 \gamma^* \gamma^*$ form factor as follows $F_{\pi^0 \gamma^* \gamma^*}(q_1^2, q_2^2) = \phi_L^{(3)}(q_1^2, q_2^2) / \phi_L^{(3)}(0, 0)$, one finally obtains the result

$$\mathcal{A}_{\pi^0} = -\frac{N_c W^{(3)}}{2\pi^2 F_\pi^2} \frac{F_{\pi^0 \gamma^* \gamma^*}(q_1^2, q_2^2)}{q_3^2 + m_\pi^2} (f_2^{\mu\nu} \tilde{f}_1^{\nu\mu}) (\tilde{f}^{\rho\sigma} f_3^{\sigma\rho}) + \text{permutations}. \quad (5.251)$$

By relating the $\langle VVV|\gamma\rangle$ matrix element to the triangle amplitude $\langle AV|\gamma\rangle$, in particular to the invariant function $w_L^{(3)}(q_3^2)$, Melnikov and Vainshtein deduce that no form factor $F_{\pi^0\gamma^*\gamma}(q_3^2, 0)$ should be used at the external vertex, but only a constant factor, as comprised in (5.251). They rightly point out that such a form factor violates momentum conservation at the external vertex and criticize the procedure adopted in earlier works [210, 234, 235, 250]. However, it is obvious from their expressions (reproduced above), that they only consider the on-shell pion form factor $\mathcal{F}_{\pi^0\gamma^*\gamma}(q_1^2, q_2^2) \equiv \mathcal{F}_{\pi^0\gamma^*\gamma}(m_\pi^2, q_1^2, q_2^2)$ (e.g. at the internal vertex) and not the off-shell pion form factor $\mathcal{F}_{\pi^0\gamma^*\gamma}(q_3^2, q_1^2, q_2^2)$. Therefore, contrary to the claim in their paper, they only consider the **pion-pole** contribution to hadronic light-by-light scattering. Actually, also a second argument by Melnikov and Vainshtein in favor of a constant form factor at the external vertex was based on the use of on-shell form factors. Since $\mathcal{F}_{\pi^0\gamma^*\gamma}(q_3^2, 0) \equiv \mathcal{F}_{\pi^0\gamma^*\gamma}(m_\pi^2, q_3^2, 0) \sim 1/q_3^2$, for large q_3^2 , according to Brodsky-Lepage, the use of a (non-constant) on-shell form factor at the external vertex would lead to an overall $1/q_3^4$ behavior which contradicts (5.251).

Next we will have to consider the other possible one-particle exchanges. The subleading terms of (5.243) is dominated by axial vector-meson exchange and will be discussed below.

The second term of (5.238) is much simpler and describes the exchange of scalars, which within a $\langle VVVV\rangle$ correlator is not possible in the massless limit. In the OPE replacing $\partial^\mu j_{5\mu}$ by the scalar $m_q S$, where m_q is a short distance mass i.e. a current quark mass. In place of the VVA triangle we now have the VVS correlator

$$T_{\rho\lambda} = - \int d^4x d^4y e^{i(qx-ky)} \langle 0|T\{j_\rho(y) j_\lambda(x) S(0)\}|0\rangle$$

with a covariant decomposition

$$T^{\rho\lambda}(q, k) = (g^{\rho\lambda} q \cdot k - k^\rho q^\lambda) w_S(q^2, k^2, (q - k)^2)$$

and by LSZ

$$T_\lambda = i \int d^4z e^{iq_3x_3} \langle 0|T\{j_\lambda(x_3) S(0)\}|\gamma(k)\rangle = -i e \varepsilon^\rho(k) T_{\rho\lambda} = -i e \varepsilon_\lambda(k) kq w_S(q^2).$$

Scalar contributions will be discussed later.

Digression on the Adler-Bardeen non-renormalization theorem

Here a remark on the Adler-Bardeen non-renormalization theorem [310] of the triangle anomaly is in order: our discussion seems to contradict this theorem. The latter is often misinterpreted, however. It is not true that higher order corrections are absent altogether, rather, explicit calculations show that higher order corrections are **proportional** to the lowest order (triangle) result, and this only for the appropriately renormalized axial current. In the chiral limit this is even true for the full correlator (5.234) up to two loops as shown in [307]. The result is a consequence of

conformal invariance, which holds at tree level in the massless limit. In any quantum field theory conformal invariance is broken unless its renormalization group (RG) β -function is zero, which is not the case for generic coupling constants in general. As a consequence at three and more loops the general AVV amplitudes, besides the longitudinal one, which is protected by the non-renormalization theorem of the axial anomaly, appear renormalized by extra terms proportional to the β -function [308, 311]. What it means is that the radiative corrections are renormalized away by imposing the proper normalization for the topological axial current [239] which is subject to winding numbers and all that. Also the singlet axial current $J_5^\mu = A^\mu$ (5.231) has to be non-trivially renormalized in order that the axial anomaly conserves its leading one-loop value. It is known [312] that in addition to the standard ultraviolet renormalization constant $Z_{\overline{\text{MS}}}$ which reads $Z_{\overline{\text{MS}}} = 1$ in our case (as $Z_{\overline{\text{MS}}} - 1 = O(\alpha_s^2)$), one has to apply a finite renormalization constant Z_5 in order that renormalized and bare currents are related by a multiplicative renormalization

$$(J_\mu^5)_{\text{ren}} = Z_5 Z_{\overline{\text{MS}}} (J_\mu^5)_0. \quad (5.252)$$

Indeed the counterterms coming from the wave function renormalization of the quark fields and the ultraviolet renormalization of the axial and vector currents cancel. A finite renormalization constant which is known up to three loops [313] remains, however.

In order to understand more precisely what is the problem let us consider the anomalous PCAC relation for the singlet current (5.232) in QCD (notation as in Sect. 2.8) in the chiral limit, where it takes the form

$$\partial_\mu J_5^\mu = \frac{\alpha_s}{4\pi} \frac{1}{2} n_f G\tilde{G} \quad (5.253)$$

where $G\tilde{G} = \varepsilon^{\mu\nu\rho\sigma} G_{\mu\nu}^i G_{\rho\sigma}^i$ and $G_{\mu\nu}^i$ is the non-Abelian gluonic field strength tensor (2.275). The divergence of the current $\partial_\mu J_5^\mu$ gets renormalized multiplicatively as the current J_5^μ itself. However, the operator $G\tilde{G}$ mixes under renormalization:

$$(G\tilde{G})_{\text{ren}} = Z_{G\tilde{G}} (G\tilde{G})_0 + Z_{GJ} (\partial_\mu J_5^\mu)_0. \quad (5.254)$$

One could expect that it also mixes with the gauge-variant field $\partial_\mu G_i^\mu$, however, the explicit calculation reveals that this does not happen [314]. Larin has shown to three loops that the anomalous PCAC relation (5.232) only preserves its form provided the current is non-trivially renormalized by the specific finite Z_5 factor

$$Z_5 = 1 - 4 C_F a + \left(22 C_F^2 - \frac{107}{9} C_A C_F + \frac{31}{18} C_F n_f \right) a^2, \quad (5.255)$$

where $C_F = 4/3$ and $C_A = 3$ are the Casimir operators of the defining and the adjoint representations of the color group and n_f is the number of quark flavors. Here $a = \alpha_s/(4\pi)$ where α_s is the QCD coupling.

In our light-by-light scattering context the axial current is a dynamically generated internal current showing up in the light-by-light scattering single particle exchange sub-processes. The corrections exhibited in the constant Z_5 are true corrections, which we cannot get rid of. If we renormalize the current as usual we get the constant back as a contribution to the Wilson coefficient, and thus it is not true that radiative corrections are completely absent in the $\langle VVVV \rangle$ correlator. For an explicit two-loop calculation see [211]. The corrections in the high energy limit turned out to be small, however. True, there is no extra infinity beyond the SM counter terms. The non-perturbative constant Z_5 as usual is not known. Note that the “prediction” of the WZW Lagrangian argued above is in fact a perturbative argument based on the one-loop triangle approximation. Fortunately, the prediction of the $\pi^0 \rightarrow \gamma\gamma$ decay rate based on the WZW Lagrangian is an excellent approximation, such that apparently the perturbative results for Z_5 are not far from the possible non-perturbative answer.

Overall, in the light-by-light scattering amplitude, pQCD must give the right answer for what concerns the UV renormalization. So what we have been discussing is the question of how to redistribute renormalization factors between the soft and the hard matrix element obtained when applying the OPE.

End of the Digression

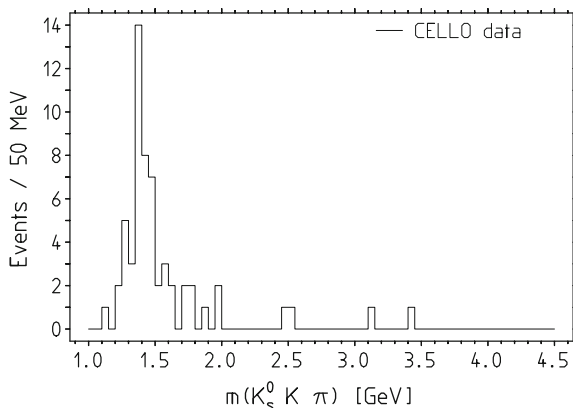
5.2.5 Exchanges of Axial-Vector Mesons

While the pseudoscalar exchanges are related to the longitudinal amplitude w_L in the decomposition (5.242), the axial–vector exchange contributions correspond to the transversal amplitudes w_T (see Fig. 5.56 with π^0, η, η' replaced by a_1, f_1, f_1'). In the corresponding one meson exchange integral (5.172) we have to work out the appropriate kernels I_1 and I_2 , as given below, and $F_1 P_6$ and $F_2 P_7$ have to be replaced by the corresponding axial vector-meson exchange expressions.⁴¹

After a reevaluation of the axial contributions in the seminal paper [254] by Melnikov and Vainshtein one has been confronted with the question why is $a_\mu[a_1, f_1', f_1] \sim 25 \times 10^{-11}$ so large? Indeed, experimentally looking at (i) untagged $\gamma\gamma \rightarrow f_1(1420)$ no signal is seen! while (ii) single-tag $\gamma^*\gamma \rightarrow f_1(1420)$ reveals a strong peak at $Q^2 \gg m_{f_1}^2$ (see Fig. 5.64). So far only sparse data is available and new measurements are very important, in particular the momentum dependence of $a_1 \rightarrow \gamma\gamma^*$, for example. These channels are special: by the Landau–Yang theorem $\mathcal{F}_{A\gamma\gamma}(M_A^2, 0, 0) = 0$, so one has to get the effective couplings from the off-shell data on $\mathcal{F}_{A\gamma\gamma}(M_A^2, -Q^2, 0)$ with the problem that at low Q^2 states with $J \neq 1$ dominate.

⁴¹The Landau–Yang theorem [315] forbids AVV transitions but this is true for real photons only. The f_1 e.g. is clearly seen in one photon tag events in e^+e^- annihilation, like single tagged $\gamma\gamma^* \rightarrow K_s^0 K \pi$ [316–318] (see the PDG note on f_1 [244, 319, 320]).

Fig. 5.64 $\sigma(\gamma^*\gamma \rightarrow f_1 \rightarrow K_s^0 K \pi)$ from CELLO 1989 [316] (see also the more recent [317, 318, 321]). This also illustrates the quality of the data available for many of the relevant $\gamma\gamma$ physics channels



The cross section for a resonance R of mass M , spin J , charge conjugation C and width Γ reads:

$$\sigma_{\gamma\gamma \rightarrow R} = 8\pi (2J + 1) \frac{\Gamma_{\gamma\gamma} \Gamma}{(W^2 - M^2)^2 + \Gamma^2 M^2} |\mathcal{F}_{J^{PC}}(Q^2)|^2,$$

where W is the two-photon mass, $\Gamma_{\gamma\gamma}$ the two-photon width and $|\mathcal{F}_{J^{PC}}(Q^2)|^2$ the square of the form factor. For the f_1 the $\gamma\gamma$ coupling parameter is defined as

$$\Gamma_{\gamma\gamma}(f_1) = \lim_{Q^2 \rightarrow 0} \frac{M^2}{Q^2} \Gamma_{\gamma\gamma}^{TS},$$

with $\Gamma_{\gamma\gamma}^{TS}$ the partial width for the transverse-scalar two-photon interaction. The form factors are parametrized by

$$\frac{\mathcal{F}_{0^{-+}}(Q^2)}{\mathcal{F}_{0^{-+}}(0)} = \frac{1}{(1 + Q^2/\Lambda_0^2)^2},$$

and

$$\frac{\mathcal{F}_{0^{++}}(Q^2)}{\mathcal{F}_{0^{++}}(0)} = \frac{Q^2}{M^2} \left(1 + \frac{Q^2}{2M^2}\right) \frac{2}{(1 + Q^2/\Lambda_1^2)^4},$$

where the parameters Λ_i are expected to be given by the ρ mass by VMD dressing.

A model in the large- N_c spirit it is to take the axial-meson propagators (in the Feynman gauge) and dress it (by subtraction of a vector-meson state as a physical version of a Pauli-Villars cut-off) by the corresponding vector-mesons such that they satisfy the appropriate high energy behavior as predicted by the OPE at the external vertex. At the internal vertex a VMD ansatz is adopted. This is the model

advocated by Melnikov and Vainshtein (for a more detailed consideration see a similar application in Sect.4.2.2 p. 316). In contrast to the well established $\pi^0\gamma\gamma$ coupling the corresponding direct experimental information is lacking for the $a_1\gamma\gamma$ vertex, which is absent in the effective Lagrangians. However, the mechanism to fix the coupling strength is similar to the one described in Sect.5.2.4 for the pion exchange which determines $g_{\pi\gamma\gamma}$. What helps is the Vainshtein relation $w_T(q^2) = w_L(q^2)/2 = -1/q^2$, which holds in the chiral limit. It amounts to replace the pion decay constant F_π by f_A defined by $\langle 0|j_{S\beta}^{(3)}(0)|a_1(p)\rangle = \varepsilon_\beta(p) f_A M_A^2$, where $\varepsilon_\beta(p)$ is the spin polarization vector of the axial meson. The correspondence (5.246) now reads

$$\begin{aligned} & \frac{-ie}{4\pi^2} w_T(q^2) \left(-q^2 \tilde{f}_{\lambda\beta} + q_\lambda q^\sigma \tilde{f}_{\sigma\beta} - q_\beta q^\sigma \tilde{f}_{\sigma\lambda} \right) \\ & \quad \downarrow \\ & \langle 0|j_{S\beta}^{(3)}(0)|a_1(q, s)\rangle \times \langle a_1(q, s)|j_\lambda(0)|\gamma(k)\rangle \\ & \quad \parallel \\ & f_A M_A^2 \varepsilon_{A\beta}(q, s) \times \frac{-e}{M_A} g_{A\gamma\gamma} \varepsilon_{A\beta'}^*(q, s) \left(-q^2 \tilde{f}_{\lambda\beta'} + q_\lambda q^\sigma \tilde{f}_{\sigma\beta'} - q_{\beta'} q^\sigma \tilde{f}_{\sigma\lambda} \right) \end{aligned} \quad (5.256)$$

with $\sum_s \varepsilon_{A\beta}(q, s) \varepsilon_{A\beta'}^*(q, s) = -g_{\beta\beta'} + q_\beta q_{\beta'}/M_A^2$, where the second part due to the transversality of the tensor structure does not contribute. In the chiral limit $w_T(q^2) = w_L(q^2)/2 = -1/q^2$ is known and we obtain

$$\frac{1}{q^2 - m_\pi^2} \rightarrow \frac{1}{2} \frac{-g_{\beta\beta'}}{q^2 - M_A^2} \quad \text{and} \quad g_{A\gamma\gamma} = \frac{1}{4\pi^2 f_A M_A}. \quad (5.257)$$

Note that in contrast to F_π the vector type coupling f_A is dimensionless and in fact F_π appears replaced by $M_A f_A$ which like F_π is non-vanishing in the chiral limit. Relative to the π^0 -exchange the a_1 -exchange picks a factor

$$N_A = \frac{1}{4} r_A, \quad r_A = \left(\frac{F_\pi}{f_A M_A} \right)^2 \simeq 0.5, \quad (5.258)$$

where we note that the same normalization factor holds for each of the two $a_1\gamma\gamma$ vertices. The factor 1/4 takes care of the relative factor 1/2 between w_L and w_T and the undressed axial-vector propagator now will have weight 1 i.e. $1/(q^2 - M_A^2)$. Experimentally $f_A = 0.097 \pm 0.022$, is not very well known, however, is well compatible with $f_A = f_V/2$ [$f_V = 0.195$] which holds in the complete VMD scenario (corresponding to $a = 2$ in the HLS model and $g_A = 1/2$ in the ENJL model [248, 322]). One may use relations like the first Weinberg sum rule [323, 324]

$$F_\pi^2 = f_V^2 M_V^2 - f_A^2 M_A^2 \quad \text{and} \quad F_\pi^2 m_\pi^2 = f_V^2 M_V^4 + f_A^2 M_A^4,$$

in order to further check the reliability of our estimate of f_A . As a best choice we will adopt $r_A \sim 0.5 \pm 0.1$ for the numerical evaluation. We finally specify the products

corresponding to $\mathcal{F}_{\pi^0 \gamma^* \gamma^*}(q_3^2, q_1^2, q_2^2) \mathcal{F}_{\pi^0 \gamma^* \gamma^*}(q_3^2, q_3^2, 0)/(q_3^2 - m_\pi^2)$ of (5.166) which reads $F_2 P_7(Q_3^2, Q_1^2, Q_2^2)$ in (5.172). These contributions have been discussed by Melnikov and Vainshtein [254] and more recently by Pauk and Vanderhaeghen [325]. While MV find a large contribution in particular from the f_1 , which is enhanced by a large coefficients, so that the result looked plausible and actually was adopted in several estimates of the HLbL contribution (see Table 5.14). More recent analyses as [325] e.g. find smaller results in agreement with older estimates (HKS, BPP). In the MV calculation the form factors motivated by large- N_c and OPE arguments are missing to be antisymmetric in the two photon virtualities, which is required by overall (form factor times the kinematic coefficients) Bose symmetry (Landau–Yang theorem). We adopt the MV form factors but antisymmetrize them such that the Landau–Yang suppression is manifest (see [244, 320]). The construction of the form factors again follows the scheme outlined on p. 190. For each flavor sector one is taking into account the states of appropriate quantum numbers together with virtual photons dressed by the corresponding vector states and adopting the narrow width approximation one constructs

$$\text{Im } w_T = \pi \sum_i g_i \delta(s - m_i^2),$$

where the weight factors g_i satisfy

$$\sum_i g_i = 1, \quad \sum_i g_i m_i^2 = 0,$$

in order to reproduce (4.97) in the chiral limit. Beyond the chiral limit the corrections (4.96) should be implemented by modifying the second constraint to match the coefficient of the second terms in the OPE.

Accordingly, we write the axial meson form factors in the form

$$\begin{aligned} w_T^{(3)} &= \frac{1}{M_{a_1}^2 - M_\rho^2} \left[\frac{M_{a_1}^2 - m_\pi^2}{Q_3^2 + M_\rho^2} - \frac{M_\rho^2 - m_\pi^2}{Q_3^2 + M_{a_1}^2} \right] \frac{Q_3^2}{Q_3^2 + M_\rho^2} \simeq \left(\frac{1}{Q_3^2} - \frac{m_\pi^2}{Q_3^4} + \dots \right) \\ \Phi_3 &= \frac{\text{asym}(Q_2^2, Q_1^2) M_\rho^4}{(Q_1^2 + M_\rho^2)(Q_2^2 + M_\rho^2)}, \quad W_3 = \frac{1}{4}, \\ w_T^{(ud)} &= \frac{1}{M_{f_1}^2 - M_\omega^2} \left[\frac{M_{f_1}^2 - m_\eta^2/5}{Q_3^2 + M_\omega^2} - \frac{M_\omega^2 - m_\eta^2/5}{Q_3^2 + M_{f_1}^2} \right] \frac{Q_3^2}{Q_3^2 + M_\omega^2} \simeq \left(\frac{1}{Q_3^2} - \frac{m_\eta^2/5}{Q_3^4} + \dots \right) \\ \Phi_{ud} &= \frac{\text{asym}(Q_2^2, Q_1^2) M_\omega^4}{(Q_1^2 + M_\omega^2)(Q_2^2 + M_\omega^2)}, \quad W_8 = \frac{2}{3}, \quad W_{ud}^{\text{ideal}} = \frac{25}{36}, \\ w_T^{(s)} &= \frac{1}{M_{f_1'}^2 - M_\phi^2} \left[\frac{M_{f_1'}^2 - m_\eta^2}{Q_3^2 + M_\phi^2} - \frac{M_\phi^2 - m_\eta^2}{Q_3^2 + M_{f_1'}^2} \right] \frac{Q_3^2}{Q_3^2 + M_\phi^2} \simeq \left(\frac{1}{Q_3^2} - \frac{m_\eta^2}{Q_3^4} + \dots \right) \\ \Phi_s &= \frac{\text{asym}(Q_2^2, Q_1^2) M_\phi^4}{(Q_1^2 + M_\phi^2)(Q_2^2 + M_\phi^2)}, \quad W_0 = \frac{1}{12}, \quad W_s^{\text{ideal}} = \frac{1}{18}, \end{aligned} \quad (5.259)$$

where

$$\text{asym}(Q_2^2, Q_1^2) \equiv (Q_2^2 - Q_1^2)/(Q_2^2 + Q_1^2) \quad (5.260)$$

is the factor restoring overall Bose symmetry and the relative weight factors for the different channels are given by (5.221) in the **nonet symmetry** limit (see (5.157)). The “asym” factor is taken from the 1^+ entry of Table 5.11. The expanded forms for w_T indicated allow for a direct comparison with the structure of the OPE and reveal that the residues of the poles have been chosen correctly (see Sects. 4.2.2). The overall factor 4 accounts for the fact that we have normalized to the π^0 -exchange contribution and not to $W^{(3)} = 1/4$. Written as a three-fold integral representation (5.172) we identify

$$F_2 P_7(Q_3^2, Q_1^2, Q_2^2) = 4 N_A \left(W_3 w_T^{(3)} \Phi_3 + W_{ud} w_T^{(ud)} \Phi_{ud} + W_s w_T^{(s)} \Phi_s \right)$$

and $F_1 P_6(Q_2^2, Q_1^2, Q_3^2)$ is obtained from $F_2 P_7$ by exchanging $Q_3^2 \leftrightarrow Q_2^2$. The relevant integration kernels I_1 and I_2 may be found as follows:

we extract the coefficient from the (5.238) together with the three-point correlator in (5.240), which we expand according to (5.234) for $g - 2$ kinematics to first order in the external photon momentum k . This yields the expressions of the form (5.242) as a decomposition in terms of w_L and w_T . Alternatively, we may write the amplitude as a one-particle exchange amplitude with two general axial vector-meson (A) form factors

$$T_A^{\mu\nu\tau}(q_1, q_2) = i P_\alpha Q_\beta \left\{ Q^\tau \varepsilon^{\mu\nu\alpha\beta} F_A(q_1^2, q_2^2) + \{(Pq_1) Q^\mu - (Qq_1) P^\mu\} \varepsilon^{\nu\alpha\beta\tau} F'_A(q_1^2, q_2^2) \right. \\ \left. + \{(Pq_2) Q^\nu - (Qq_2) P^\nu\} \varepsilon^{\mu\alpha\beta\tau} F''_A(q_1^2, q_2^2) \right\}$$

with $P = (q_1 + q_2)$, $Q = (q_1 - q_2)/2$. We then calculate

$$T_A^{\mu\nu\tau}(q_1, q_2) T_A^{*\rho\lambda\tau'}(k, k + q_3) (-g_{\tau\tau'} + P_\tau P_{\tau'}/[q_3^2]) \frac{1}{q_3^2 - M_A^2}$$

plus two similar terms corresponding to the three diagrams of Fig. 5.56 with pseudoscalars (π^0, η, η') replaced by the axial mesons (a_1, f_1, f'_1). In the $g - 2$ limit only the products of the first form factor F_A like $F_A(q_1^2, q_2^2) F_A(0, q_3^2)$ contribute, and according to Melnikov–Vainshtein we identify $F_A(q_1^2, q_2^2) \propto \Phi_i(Q_1^2, Q_2^2)$ and $F_A(0, q_3^2) \rightarrow w_T^{(i)}(Q_3^2)$. Above we also have used (5.257) and we find that only the $g_{\tau\tau'}$ part of the propagator contributes (transversality). The kinematic factors again can be averaged (5.170) over the muon momentum direction and in the notation introduced in (5.171) one obtains

$$\begin{aligned}
I_1(Q_1, Q_2, \tau) = & X(Q_1, Q_2, \tau) \left(-8 P_1 P_2 (Q_1 \cdot Q_2) + 4 P_1 P_3 Q_2^2 \right. \\
& - 2 P_1 \left(6 - \frac{2(Q_1 \cdot Q_2) - Q_2^2}{m_\mu^2} \right) - 4 P_2 P_3 Q_1^2 + 4 P_2 - 2 P_3 \left(4 + \frac{Q_1^2}{m_\mu^2} \right) + \frac{6}{m_\mu^2} \Big) \\
& + P_1 P_2 \left(4 + 2(1 - R_{m1})(1 + \frac{1}{4}(1 - R_{m1})) \frac{(Q_1 \cdot Q_2)}{m_\mu^2} \right) \\
& - P_1 P_3 \left((1 - R_{m2})^2 \frac{(Q_1 \cdot Q_2)}{m_\mu^2} \right) - P_1 \frac{((1 - R_{m1}) - 4(1 - R_{m2}))}{m_\mu^2} \\
& - P_2 P_3 \left(4 + (1 - R_{m1}) \frac{Q_1^2}{m_\mu^2} - \frac{1}{2}(1 - R_{m1})^2 \frac{(Q_1 \cdot Q_2)}{m_\mu^2} \right) \\
& + P_2 \frac{(1 - R_{m1})}{m_\mu^2} - 2 P_3 \frac{(1 - R_{m2})}{m_\mu^2} ,
\end{aligned}$$

$$\begin{aligned}
I_2(Q_1, Q_2, \tau) = & X(Q_1, Q_2, \tau) \left(+4 P_1 P_2 (Q_1 \cdot Q_2) - 2 P_1 P_3 Q_2^2 \right. \\
& - P_1 \left(2 + \frac{Q_2^2}{m_\mu^2} \right) - 2 P_2 P_3 Q_1^2 - P_2 \left(2 + \frac{Q_1^2}{m_\mu^2} \right) + 4 P_3 - \frac{4}{m_\mu^2} \Big) \\
& + P_1 P_3 \left(2 + \frac{1}{4} ((1 - R_{m1})^2 + (1 - R_{m2})^2) \frac{(Q_1 \cdot Q_2)}{m_\mu^2} + \frac{1}{2} (1 - R_{m2}) \frac{Q_2^2}{m_\mu^2} \right) \\
& - P_1 \frac{((1 - R_{m1}) + 3(1 - R_{m2}))}{2m_\mu^2} + P_2 P_3 \left(2 + \frac{1}{4} ((1 - R_{m1})^2 \right. \\
& + (1 - R_{m2})^2) \frac{(Q_1 \cdot Q_2)}{m_\mu^2} + \frac{1}{2} (1 - R_{m1}) \frac{Q_1^2}{m_\mu^2} \Big) - P_2 \frac{(3(1 - R_{m1}) + (1 - R_{m2}))}{2m_\mu^2} \\
& + P_3 \frac{(2 - R_{m1} - R_{m2})}{2m_\mu^2} - 2 P_1 P_2 .
\end{aligned}$$

For the numerical analysis, likely, a more realistic assumption is that of ideal mixing,⁴² which re-weights the f_1 and $f_{1'}$ contributions with the indicated weight factors. The numerical evaluation for ideal mixing yields

$$a_\mu^{\text{LbL}}(a_1, f_1, f_{1'}) = (7.55[1.89 + 5.19 + 0.47] \pm 2.71) \times 10^{-11} \quad (5.261)$$

while nonet symmetry would yield $7.58[1.89 + 4.98 + 0.70] \times 10^{-11}$ if we still use physical axial-meson masses. Table 5.14 collects results obtained in previous stud-

⁴²In this case (f'_j) = $\begin{pmatrix} \cos\theta & -\sin\theta \\ \sin\theta & \cos\theta \end{pmatrix} \begin{pmatrix} \psi_8 \\ \psi_1 \end{pmatrix}$ with $\tan\theta = 1/\sqrt{2}$ (f' pure $s\bar{s}$) and the nonet symmetry coupling weights (1, $1/\sqrt{3}$, $2\sqrt{2}/\sqrt{3}$) (see (5.150)) turns into (1, $-\sqrt{2}/3$, $5/3$) and the corresponding weights $W^{(a)}$ are proportional to the squares.

Table 5.14 Results for axial-vector (a_1 , f_1 and f_1') exchange contributions (assuming ideal mixing of f_1 and f_1') in units 10^{-11}

Model for $\overline{\mathcal{F}}_{A\gamma^*\gamma^*}$	$a_\mu(a_1)$	$a_\mu(a_1, f_1, f_1')$
ENJL[BPP] [235, 249, 327]	2.5 (1.0)	28 (5)
HLS [HKS,HK] [210, 250]	1.7 (1.0)	–
LMD[MV] [254]	5.7 (1.3)	22 (5)
LMD[PdRV] [328]	–	15 (10)
LMD[JN] [275]	7.0 (1.3)	22 (5)
LMD[PV] [325]	–	6.4 (2.0)
LMD [326] (2016 update)	1.9 (0.5)	7.6 (2.0)

ies [326]. The earlier studies only included the a_1 , other differences again are due to the S.D. constraints used and different implementation of f_1 , f_1' mixing.

5.2.6 Exchanges of Scalar Mesons

The scalar contribution indicated in (5.238) is chirally suppressed but nevertheless requires to be analyzed. We will consider the regular nonet $a_0(1450)$, $f_0(1370)$ and $f_0'(1710)$ and the second one $a_0(980)$, $f_0(600)[= \sigma]$ and $f_0'(980)$ as two manifestations of the same bare input states [329]. Not much is experimentally established about their $\gamma\gamma$ couplings, as the modes $S \rightarrow \gamma\gamma$ have not been seen, in general. The only exceptions are the $f_0(980)$ of mass $m_{f_0} = (980 \pm 10)$ MeV with $\Gamma_{f_0 \rightarrow \gamma\gamma} = (0.30 \pm 0.10)$ keV and the $a_0(980)$ of mass $m_{a_0} = (985.1 \pm 1.3)$ MeV with $\Gamma_{a_0 \rightarrow \gamma\gamma} = (0.29_{-0.09}^{+0.07})$ keV [42], which allows for a direct check of the effective coupling. In the VMD model one may use the relation $g_{SV\gamma} = \sqrt{2} \gamma_V / e g_{S\gamma\gamma}$, typically $\gamma_\rho = 2.51 \pm 0.02$. The widths $\Gamma(S \rightarrow \gamma\gamma) = 1/(64\pi) |g_{S\gamma\gamma}|^2 M_S^3$ estimated to be typically (1.5 – 2.6) keV using the VMD relation. Flavor decomposition follows the same pattern as the leading divergence of the axial current part with $\partial^\mu j_{5\mu}$ replaced by the scalar $m_q S$ and a current quark mass as a factor:

$$T_\lambda^{(a)} = -\frac{i e m_q N_c \text{Tr}[\lambda_a \hat{Q}^2]}{4\pi^2} \times \left\{ -w_S^{(a)}(q_3^2) (g_{\lambda\sigma} q_{3\rho} - g_{\lambda\rho} q_{3\sigma}) \frac{1}{2} f^{\sigma\rho} \right\}. \quad (5.262)$$

The OPE argument together with the correspondence

$$\begin{aligned} & \frac{i e m_q}{4\pi^2} \left\{ w_S(q^2) (g_{\lambda\sigma} q_\rho - g_{\lambda\rho} q_\sigma) \frac{1}{2} f^{\sigma\rho} \right\} \\ & \quad \downarrow \\ & \langle 0 | S^{(3)}(0) | \sigma(q) \rangle \times \langle \sigma(q) | j_\lambda(0) | \gamma(k) \rangle = 2i F_\sigma m_q \times -4 e g_{\sigma\gamma\gamma} q^\sigma f_{\sigma\lambda} \end{aligned} \quad (5.263)$$

establishes the $\sigma[a_0(600)]$ exchange. We note that, as in the case of the axial meson exchange, we have one invariant amplitude contributing at each vertex. For the first diagram $F_S(q_1^2, q_2^2) F_S(0, q_3^2)$. Accordingly, we again may write the scalar meson

form factors in the form of external \times an internal vertex amplitude á la Melnikov–Vainshtein

$$\begin{aligned}
 w_S^{(3)} &= \frac{1}{m_{a_0}^2 - M_\rho^2} \left[\frac{m_{a_0}^2 - m_\pi^2}{Q_3^2 + M_\rho^2} - \frac{M_\rho^2 - m_\pi^2}{Q_3^2 + m_{a_0}^2} \right] \simeq \left(\frac{1}{Q_3^2} - \frac{m_\pi^2}{Q_3^4} + \dots \right) \\
 \Phi_3 &= \frac{4 M_\rho^4}{(Q_1^2 + M_\rho^2)(Q_2^2 + M_\rho^2)}, \quad W_3 = \frac{1}{4}, \\
 w_S^{(ud)} &= \frac{1}{m_{f_0}^2 - M_\omega^2} \left[\frac{m_{f_0}^2 - m_\eta^2/5}{Q_3^2 + M_\omega^2} - \frac{M_\omega^2 - m_\eta^2/5}{Q_3^2 + m_{f_0}^2} \right] \simeq \left(\frac{1}{Q_3^2} - \frac{m_\eta^2/5}{Q_3^4} + \dots \right) \\
 \Phi_{ud} &= \frac{4 M_\omega^4}{(Q_1^2 + M_\omega^2)(Q_2^2 + M_\omega^2)}, \quad W_8 = \frac{2}{3}, \quad W_{ud}^{\text{ideal}} = \frac{25}{36}, \\
 w_S^{(s)} &= \frac{1}{m_{f_0'}^2 - M_\phi^2} \left[\frac{m_{f_0'}^2 - m_\eta^2}{Q_3^2 + M_\phi^2} - \frac{M_\phi^2 - m_\eta^2}{Q_3^2 + m_{f_0'}^2} \right] \simeq \left(\frac{1}{Q_3^2} - \frac{m_\eta^2}{Q_3^4} + \dots \right) \\
 \Phi_s &= \frac{4 M_\phi^4}{(Q_1^2 + M_\phi^2)(Q_2^2 + M_\phi^2)}, \quad W_0 = \frac{1}{12}, \quad W_s^{\text{ideal}} = \frac{1}{18}. \quad (5.264)
 \end{aligned}$$

The normalization factor may be written as

$$N_S = \frac{1}{2} N_A \left(\frac{1}{4\pi^2 F_0} \right)^2,$$

with N_A from (5.258) (see comments there). And we obtain

$$\begin{aligned}
 FF_S &= (m_u M_u W_3 w_S^{(3)} \Phi_3 + \frac{m_u + m_s}{2} \frac{M_u + M_s}{2} W_{ud} w_S^{(ud)} \Phi_{ud} \\
 &\quad + m_s M_s W_s w_S^{(s)} \Phi_s) N_S. \quad (5.265)
 \end{aligned}$$

Again, written as a three-fold integral representation (5.172) we identify

$$F_2 P_7(Q_3^2, Q_1^2, Q_2^2) = 4 N_A \left(W_3 w_S^{(3)} \Phi_3 + W_{ud} w_S^{(ud)} \Phi_{ud} + W_s w_S^{(s)} \Phi_s \right), \quad (5.266)$$

and $F_1 P_6(Q_2^2, Q_1^2, Q_3^2)$ is obtained from $F_2 P_7$ by exchanging $Q_3^2 \leftrightarrow Q_2^2$. The relevant integration kernels I_1 and I_2 are obtained as follows:

Here again we extract the coefficient from the (5.238) together with the three-point correlator in (5.240), replacing $2i \varepsilon_{\mu\nu\alpha\beta} \hat{q}^\alpha j_5^\beta(z) \rightarrow 2m_q g_{\mu\nu} S(z)$. One then has $2i m / [(q_1 - q_2)^2] g_{\mu\nu} T_{\rho\lambda}(-k, k + q_3)$ with $T^{\rho\lambda}(p_1, p_2) = (-g^{\rho\lambda}(p_1 p_2) + p_2^\rho p_1^\lambda - 1^\lambda) w_S(p_1, p_2)$ the scalar VVS loop contribution, which in contrast to the VVA loop exhibits radiative corrections. Again an expansion in the external soft photon momentum k to linear order in k is performed. Again from the structure “internal scalar vertex \times scalar propagator \times external scalar vertex”, three terms corresponding

to the diagrams of Fig. 5.56 with pseudoscalars (π^0, η, η') replaced by the scalar mesons (a_0, f_0, f'_0). The hadronic effects as before appear as form factor products $F_S(q_1^2, q_2^2) F_S(0, q_3^2)$ multiplied by the kinematic kernels, which we average over the muon momentum direction (5.170) again. With the notation introduced in (5.171) one obtains the weight functions:

$$I_1(Q_1, Q_2, \tau) = X(Q_1, Q_2, \tau) \left(16 P_1 P_3 \left(2 + \frac{Q_2^2}{m_\mu^2} \right) - 8 P_1 \frac{1}{m_\mu^2} - 8 P_3 \frac{1}{m_\mu^2} \right) \\ - 2 P_1 P_2 P_3 (1 - R_{m1})^2 \frac{(Q_1 \cdot Q_2)}{m_\mu^2} - 4 P_1 P_2 \frac{(1 - R_{m1})}{m_\mu^2} - 8 P_1 P_3 \frac{(R_{m1} - R_{m2})}{m_\mu^2} \\ + 4 P_2 P_3 \frac{(1 - R_{m1})}{m_\mu^2} ,$$

$$I_2(Q_1, Q_2, \tau) = X(Q_1, Q_2, \tau) \left(8 P_1 P_2 + 2 P_1 \frac{1}{m_\mu^2} + 2 P_2 \frac{1}{m_\mu^2} \right) \\ - P_1 P_2 P_3 \left(4 + ((1 - R_{m1})^2 + (1 - R_{m2})^2) \frac{(Q_1 \cdot Q_2)}{2m_\mu^2} \right) \\ + P_1 P_2 \frac{(2 - R_{m1} - R_{m2})}{m_\mu^2} - P_1 P_3 \frac{(1 - R_{m2})}{m_\mu^2} - P_2 P_3 \frac{(1 - R_{m1})}{m_\mu^2} .$$

The numerical evaluation adopting the $\eta - \eta'$ mixing scheme (including the gluonic component) yields

$$a_\mu^{\text{LbL}}(a_0, f_0, f'_0) = (-5.98[-0.17 - 2.96 - 2.85] \pm 1.20) \times 10^{-11} , \quad (5.267)$$

while nonet symmetry would give $-6.13[-0.17 - 4.99 - 0.99] \times 10^{-11}$ and ideal mixing $-6.01[-0.17 - 5.19 - 0.66] \times 10^{-11}$ if we still use physical scalar-meson masses.

When rescaling to the experimental $f_0(980) \rightarrow \gamma\gamma$ rate we find $-7.74(2.85)$ in place -5.98 . The average is -6.86 not much different from (5.267), which we will adopt as a best estimate. Table 5.15 collects results obtained in previous studies. Note that the scalar contribution has to be negative. In the dispersive approach, to be discussed below in Sect. 5.2.11, scalar contributions are expected to be included in the $\gamma\gamma \rightarrow \pi^+\pi^-, \pi^0\pi^0$ data (see e.g. [330]). A preliminary result for the $I = 0$ contribution is -8.8×10^{-11} [331, 332].

Table 5.15 Results for scalar (a_0 , f_0 and f'_0) exchange contributions (assuming a $\eta - \eta'$ type mixing scheme of f_0 and f'_0) in units 10^{-11}

Model for $\mathcal{F}_{S\gamma^*\gamma^*}$	$a_\mu(a_0)$	$a_\mu(a_0, f_0, f'_0)$
ENJL[BPP] [235, 249, 327]	–	–7 (2)
LENJL [296]	–	12.3 (2.4)
LMD[MV] [254]	–	–0 (0)
LMD[JN] [275]	–0.2 (0.1)	–7 (3)
LMD[PdRV] [328]	–	15 (10)
LMD[PV] [325]	–0.63 (0.1)	–3.1 (0.8)
N χ QM [301]	–	3.4 (4.8)
LMD [326] (2016 update)	–0.17 (0.1)	–6.0 (1.2)

5.2.7 Tensor Exchanges

The lowest tensor resonance is the spin 2 $f_2(1270)$ dominating in $\gamma\gamma \rightarrow \pi^+\pi^-, \pi^0\pi^0$ production as we see in Fig. 5.38. The f_2 parameters extracted are $M_f = 1275.1(1.2)$ MeV, $\Gamma_f = 185.1^{+2.9}_{-2.4}$ MeV and $\Gamma_{f\gamma\gamma}/\Gamma_f = (1.64 \pm 0.19) \times 10^{-5}$. The f_2 is at an energy where the often applied sQED clearly fails as the photons couple to the quarks and not any longer to point-like pions. Low energy effective methods are expected to fail at these energies and the only save approach is the newly advocated dispersive approach based directly on the data. Such analysis requires an elaborate data decomposition into partial waves the setup for which has been elaborated very recently in [222]. Preliminary attempts based on pole–approximation VMD form factors have been calculated first in [325], with the result

$$a_\mu[f'_2, f_2, a'_2, a_2] \sim (1.1 = [0.79 + 0.07 + 0.22 + 0.02] \pm 0.1) \times 10^{-11}. \quad (5.268)$$

Fortunately, the contribution turns out to be small enough, not to affect the total HLbL contribution substantially. Again this contribution in the dispersive approach (see Sect. 5.2.11 below) is directly included as part of a the $\gamma\gamma \rightarrow \pi^+\pi^-, \pi^0\pi^0$ data contribution. The result for the $I = 2$ contribution is 0.9×10^{-11} [331, 332].

If treated as single particle exchanges one has to cope with the following spin 2 particle structures: The massive spin 2 propagator has the form

$$D^{\mu\nu\alpha\beta}(k) = \frac{f^{\mu\nu\alpha\beta}}{k^2 - M^2 + i\varepsilon},$$

with

$$f^{\mu\nu\alpha\beta} = \frac{1}{2} \left(g^{\mu\alpha} g^{\nu\beta} + g^{\mu\beta} g^{\nu\alpha} - g^{\mu\nu} g^{\alpha\beta} \right) + \frac{1}{2} \left(g^{\mu\alpha} \frac{k^\nu k^\beta}{M^2} + g^{\nu\beta} \frac{k^\mu k^\alpha}{M^2} + g^{\mu\beta} \frac{k^\nu k^\alpha}{M^2} + g^{\nu\alpha} \frac{k^\mu k^\beta}{M^2} \right) + \frac{2}{3} \left(\frac{1}{2} g^{\mu\nu} + \frac{k^\mu k^\nu}{M^2} \right) \left(\frac{1}{2} g^{\alpha\beta} + \frac{k^\alpha k^\beta}{M^2} \right).$$

The $f\gamma^*\gamma^*$ tensor basis exhibits 5 invariant amplitudes

$$T_f^{\mu\nu\alpha\beta} = \sum_{k=1}^5 B_k^{\mu\nu\alpha\beta} F_k^f(q_1^2, q_2^2), \quad (5.269)$$

$$B_1^{\mu\nu\alpha\beta} = \{ Q^2 P^\mu P^\nu + P^2 Q^\mu Q^\nu - (PQ) [P^\mu Q^\nu + P^\nu Q^\mu] + [(PQ)^2 - P^2 Q^2] g^{\mu\nu} \} Q^\alpha Q^\beta,$$

$$B_2^{\mu\nu\alpha\beta} = [P^\mu P^\nu - P^2 g^{\mu\nu}] Q^\alpha Q^\beta + [(PQ)^2 - P^2 Q^2] g^{\mu\alpha} g^{\nu\beta} + \{ P^2 [Q^\mu g^{\nu\alpha} + Q^\nu g^{\mu\alpha}] - (PQ) [P^\mu g^{\nu\alpha} + P^\nu g^{\mu\alpha}] \} Q^\beta,$$

$$B_3^{\mu\nu\alpha\beta} = \left\{ \frac{1}{2} [P^\mu Q^\nu - P^\nu Q^\mu] - \frac{1}{4} P^\mu P^\nu + Q^\mu Q^\nu - (Q^2 - \frac{1}{4} P^2) g^{\mu\nu} \right\} Q^\alpha Q^\beta,$$

$$B_4^{\mu\nu\alpha\beta} = \{ [P^2 g^{\mu\nu} - P^\mu P^\nu] Q^2 - P^2 Q^\mu Q^\nu \} Q^\alpha Q^\beta + (PQ)^2 \left(\frac{1}{4} P^2 - Q^2 \right) g^{\mu\alpha} g^{\nu\beta} + \left\{ (PQ) Q^2 [P^\mu g^{\nu\alpha} + P^\nu g^{\mu\alpha}] + \frac{1}{2} P^2 [Q^\mu g^{\nu\alpha} - Q^\nu g^{\mu\alpha}] \right\} Q^\beta,$$

$$B_5^{\mu\nu\alpha\beta} = P^2 g^{\mu\nu} Q^\alpha Q^\beta - P^2 \left(\frac{1}{4} P^2 - Q^2 \right) g^{\mu\alpha} g^{\nu\beta} - \left\{ \frac{1}{2} P^2 [P^\mu g^{\nu\alpha} - P^\nu g^{\mu\alpha}] + P^2 [Q^\mu g^{\nu\alpha} + Q^\nu g^{\mu\alpha}] \right\} Q^\beta,$$

and one may proceed as for the other single particle exchanges.

5.2.8 The Pion-Loop

The π -loop in Fig. 5.49 contributes to HLbL via the diagram Fig. 5.55b. The simplest model is sQED exhibiting 6 box diagrams, 12 triangle diagrams and 3 bulb diagrams,

$$ie^4 \Pi_{\text{sQED}}^{\mu\nu\lambda\sigma} = 6 \times \text{[Box Diagram]} + 12 \times \text{[Triangle Diagram]} + 3 \times \text{[Bulb Diagram]}, \quad (5.270)$$

and which yields $a_{\mu \text{sQED}}^{\pi\text{-loop}} \simeq -40 \times 10^{-11}$. As an off-shell photon mixes with the ρ^0 (as well as with the ω , the ϕ etc.) VMD damping becomes effective (see Fig. 5.49). The bare sQED contribution gets modified according to

$$\Pi_{\text{sQED+VMD}}^{\mu\nu\lambda\sigma} = F_{\pi}^V(q_1^2) F_{\pi}^V(q_2^2) F_{\pi}^V(q_3^2) F_{\pi}^V(q_4^2) \Pi_{\text{sQED}}^{\mu\nu\lambda\sigma},$$

where $F_{\pi}^V(q^2)$ is the pion form factor. This simple VMD dressing yields a result $a_{\mu \text{sQED+VMD}}^{\pi\text{-loop}} \simeq -16 \times 10^{-11}$, a reduction by more than a factor two. This is also what is obtained by the Bern group [331]. With an ENJL inspired form factor BPP get $a_{\mu \text{sQED+VMD}}^{\pi\text{-loop}} \simeq -19 \times 10^{-11}$, while HKS estimated $a_{\mu \text{sQED+HLS}}^{\pi\text{-loop}} \simeq -4.5 \times 10^{-11}$ only, based on the HLS model type of implementing the VMD mechanism. The HLS approach in this context has been criticized in [236] and indeed there is an intrinsic ambiguity related to the HLS a -parameter on which the outcome depends sensitively. In full VMD the photons at the $\gamma\pi^+\pi^-$ as well as the $\gamma\gamma\pi^+\pi^-$ vertices get dressed by a factor

$$\frac{M_{\rho}^2 g^{\mu\nu} - q^{\mu} q^{\nu}}{M_{\rho}^2 - q^2},$$

while in the HLS model we get factors

$$g^{\mu\nu} - \frac{a}{2} \frac{q^2 g^{\mu\nu} - q^{\mu} q^{\nu}}{q^2 - M_{\rho}^2} \quad \text{for } \gamma\pi^+\pi^-,$$

$$g^{\mu\rho} g^{\nu\sigma} - g^{\mu\rho} \frac{a}{2} \frac{q_2^2 g^{\nu\sigma} - q_2^{\nu} q_2^{\sigma}}{q_2^2 - M_{\rho}^2} - g^{\nu\sigma} \frac{a}{2} \frac{q_1^2 g^{\mu\rho} - q_1^{\mu} q_1^{\rho}}{q_1^2 - M_{\rho}^2} \quad \text{for } \gamma\gamma\pi^+\pi^-.$$

The problem is that one attempts to use the HLS model at energies beyond the range of applicability (the *soft-hard* ranges issue). Missing the correct high energy constraint by the HLS model the corresponding pion-loop results [210, 250] should be considered obsolete.

The evaluation of the bare pseudoscalar loops actually is possible in terms of the large mass expansion in m_{μ}/M_P . The expansion in scalar QED, relevant for the charged pion contribution, is given by [333]

$$a_{\mu \text{sQED}}^{\pi\text{-loop}} = A_{2 \text{lbl}}^{(6)}(m_{\mu}/m_{\pi}) \left(\frac{\alpha}{\pi}\right)^3 \quad (5.271)$$

with

$$A_{2 \text{lbl}}^{(6)}(m_{\mu}/M) = \frac{m_{\mu}^2}{M^2} \left(\frac{1}{4} \zeta_3 - \frac{37}{96} \right)$$

$$+ \frac{m_{\mu}^4}{M^4} \left(\frac{1}{8} \zeta_3 + \frac{67}{6480} \zeta_2 - \frac{282319}{1944000} + \frac{67}{12960} L^2 + \frac{7553}{388800} L \right)$$

$$\begin{aligned}
& + \frac{m_\mu^6}{M^6} \left(\frac{19}{216} \zeta_3 + \frac{157}{36288} \zeta_2 - \frac{767572853}{7112448000} + \frac{1943}{725760} L^2 + \frac{51103}{7620480} L \right) \\
& + \frac{m_\mu^8}{M^8} \left(\frac{11}{160} \zeta_3 + \frac{943}{432000} \zeta_2 - \frac{3172827071}{37507050000} + \frac{8957}{6048000} L^2 + \frac{22434967}{7620480000} L \right) \\
& + \frac{m_\mu^{10}}{M^{10}} \left(\frac{17}{300} \zeta_3 + \frac{139}{111375} \zeta_2 - \frac{999168445440307}{14377502462400000} + \frac{128437}{149688000} L^2 \right. \\
& \quad \left. + \frac{1033765301}{691558560000} L \right) + O\left(\frac{m_\mu^{12}}{M^{12}}\right). \tag{5.272}
\end{aligned}$$

where $L = \ln(M^2/m_\mu^2)$, M denoting the pseudoscalar meson mass m_π, m_K, \dots and $\zeta_2 = \zeta(2) = \pi^2/6$, $\zeta_3 = \zeta(3)$. The numerical evaluation of the exact sQED contribution yielded $A_{2\text{lbl}}^{(6)}(m_\mu/m_\pi) = -0.0383(20)$ [108], more recently [333] obtains $A_{2\text{lbl}}^{(6)}(m_\mu/m_\pi) = -0.0353$ using the heavy mass expansion approach. With our choice of parameters using (5.272) we get $a_{\mu\text{sQED}}^{\pi\text{-loop}} \approx -45.3 \times 10^{-11}$.

For the dressed case $a_{\mu\text{sQED+VMD}}^{\pi\text{-loop}}$ an expansion in $\delta = (m_\mu - m_\pi)/m_\pi$ and $(m_\pi/M_\rho)^2$ has been given for the HLS model in [254]. For physical $m_\pi/M_\rho \sim 0.2$ this expansion is poorly convergent and therefore not of big help, as the ‘‘cut-off’’ M_ρ is too low.

More recently in [334, 335] it has been argued that the effect of pion polarizability has been missing in earlier calculations and that the effects could be sizable. The electric and magnetic polarizabilities of an extended object describe its rigidity against deformation by external electric and magnetic fields, respectively. A recent measurement in pion Compton scattering $\pi^- \gamma \rightarrow \pi^- \gamma$ at low energies by the COMPASS Collaboration [336] finds a result $\alpha_\pi = (2.0 \pm 0.6 \pm 0.7) \times 10^{-4} \text{ fm}^3$ in accord with CHPT predictions [186]. The calculations [334, 335] essentially are based on CHPT, which however, at NLO gives a divergent δa_μ . This means the results depend substantially on the extension towards higher energies. Adding VMD ($\gamma - \rho$ mixing) at the $\gamma\pi^+\pi^-$ vertex and a_1 -exchange at the $\gamma\gamma\pi^+\pi^-$ vertex, like

$$\mathcal{L}_I = -\frac{e^2}{4} F_{\mu\nu} \pi^+ \left(\frac{1}{D^2 + M_A^2} \right) F^{\mu\nu} \pi^- + \text{h.c.} + \dots; \quad D_\mu = \partial_\mu + ieQA_\mu,$$

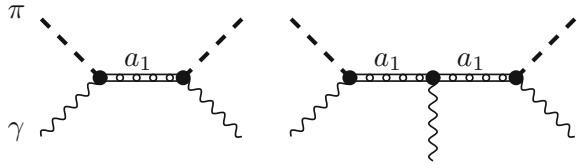
can provide the necessary damping to match OPE constraints in order to get a finite answer $a_{\mu\text{sQED+VMD+a}_1\text{-exchange}}^{\pi\text{-loop}} \sim -(11-71) \times 10^{-11}$.

Indeed the $\pi a_1 \gamma$ coupling is a standard RLA (see Fig. 5.54) vertex. A careful reconsideration of the pion polarizability issue, taking into account the a_1 -exchange effects as represented by Fig. 5.65, yields the result [236] (see also [337])

$$a_{\text{sQED+VMD+a}_1\text{-exchange}}^{\pi\text{-loop}} \simeq -(20 \pm 5) \times 10^{-11}, \tag{5.273}$$

when integrated up to a cut-off of order 1–2 GeV, i.e., the effects of pion polarizability is actually small, at the 10% level. Again one has to keep in mind that RLA type

Fig. 5.65 $\pi - a_1$ transition in the pion loop accounting for the pion polarizability



models have their limitations when applying them beyond the *soft-soft* (i.e. at energies beyond 1 GeV) regime if one is not enforcing the correct high energy behavior more or less by-hand, e.g. by adding additional states, as we have discussed in the context of the large- N_c inspired modeling in Sect. 5.2.4.

It should be noted that pion-loops and scalars are related and linked to $\gamma\gamma \rightarrow \pi^+\pi^-, \pi^0\pi^0$ reactions. Pioneering measurements by Crystal Ball, JADE, MARK II, PLUTO, CELLO [178–182] have been dramatically extended and improved at higher energies by Belle [183]. For theoretical aspects concerning these processes we refer to [185–189, 338]. While at low energies only the charged pions couple to the photons (charged pion loop only) at higher energies above 1 GeV photons see the quarks and $\pi^0\pi^0$ dramatically increases to $\frac{1}{2}$ (isospin symmetry factor) the rate of $\pi^+\pi^-$ and both channels are dominated by the huge tensor resonance $f_2(1270)$, which has been estimated in [325] to yield a small effect to the HLbL contribution (see Fig. 5.38). In this case the Dispersion Relation Approach (DRA) advocated in [221, 222] and [223] is expected to lead to more reliable results as pion loops, scalar and tensor contributions appear as a single contribution which can be obtained directly from the data.

A first result based on the DRA has been worked out in [332] now. The method used combines the dispersive description of the HLbL tensor with a partial-wave expansion and demonstrates that the known scalar-QED result is recovered after partial-wave resummation. Using dispersive fits to high-statistics data for the pion vector form factor, the evaluation of the full pion box yields $a_\mu^{\pi\text{-box}} = -15.9(2) \times 10^{-11}$. With suitable input for the $\gamma^*\gamma^* \rightarrow \pi\pi$ helicity partial waves based on a pion-pole left-hand cut it is shown that for the dominant charged-pion contribution this representation is consistent with the two-loop chiral prediction and the COMPASS measurement [336] for the pion polarizability (see also [337]). This allows for a reliably estimate of the S -wave rescattering effects to the full pion box and leads to the final estimate for the sum of these two contributions:

$$a_\mu^{\pi\text{-box}} + a_{\mu,J=0}^{\pi\pi,\pi\text{-pole LHC}} = -24(1) \times 10^{-11} . \quad (5.274)$$

It includes besides the pion-loop the contribution from the scalar $f_0(500)$: “the isospin-0 part of the result can be interpreted as a model-independent implementation

of the contribution from the $f_0(500)$ of about -9×10^{-11} to HLbL scattering contribution". The $\pi\pi$ -rescattering effects related to the pion-pole left-hand cut amounts to $a_{\mu, J=0}^{\pi\pi, \pi\text{-pole LHC}} = -8(1) \times 10^{-11}$, where the error is dominated by the uncertainties related to the asymptotic parts of the integral. The result agrees well with the other recent evaluations of the pion-loop, scalar and tensor contribution estimates but has a much smaller uncertainty and being directly data-driven is more reliable.

5.2.9 The Quark-Loop

The quark-loops in Fig. 5.49 contribute to HLbL as represented by diagram Fig. 5.55c. At first we expect a corresponding contribution from the *hard-hard* region of Fig. 5.47 separated by a cutoff Λ in the GeV range. However, whether a quark-loop contributions has to be taken into account or not very much depends on the framework in which one is evaluating the HLbL contribution. In the large- N_c approach a separate quark loop is absent unless one applies a cut-off by separating regions according to Fig. 5.47, which however is not in the spirit of this approach. In the RLA one has to separate regions by suitable cutoffs. The fermion-loop diagrams contribution is known analytically and not only depends heavily on the fermion mass (see Chap. 4, Sect. 4.1.3) but also on the cutoff if one applies one. For the muon loop we have already illustrated at the beginning of this Section that in order to catch the full contribution one has to choose a surprisingly high cutoff of about 3 GeV. For constituent quarks of mass about 300 MeV and a cutoff $\Lambda = 1[2]$ GeV one gets about 50[75]% of the complete quark-loop contribution. Which means that the contribution from the tail in the *hard-hard* region above typical cutoffs of 1 to 2 GeV which apply for low energy effective hadron models like HLS and ENJL is non-negligible (see Table 5.9).

In this context the ENJL model is special as it exhibits a constituent quarks sector as part of the effective Lagrangian. Thus a constituent quark contribution is tightly correlated with the meson sector by chiral symmetry. Results provided in [249] are collected in Table 5.16. The conclusion of [249] is that the quark-loop within the ENJL framework is about

Table 5.16 The quark-loop contribution $a_{\mu, \text{ENJL}}^{\text{quark-loop}}$, in units 10^{-10} , with VMD damping, for the ENJL model and with a heavy quark mass as cut-off Λ separating the low energy ENJL part and its high energy tail. As an effective quark mass for the tail $M_Q = \Lambda$ is chosen. Results from [249]

Λ GeV	VMD	ENJL (L.D.)	ENJL (S.D.)	ENJL (sum)
0.5	0.48	0.78	2.46	3.2
0.7	0.72	1.14	1.13	2.3
1.0	0.87	1.44	0.59	2.0
2.0	0.98	1.78	0.13	1.9
4.0	0.98	1.98	0.03	2.0
8.0	0.98	2.00	.005	2.0

$$a_{\mu \text{ENJL}}^{\text{quark--loop}} \simeq 20(4) \times 10^{-11} . \quad (5.275)$$

Note that the choice $M_Q = \Lambda$ looks difficult to be justified and probably underestimates the contribution from the tail. But for a cutoff of 8 GeV the contribution from the tail in any case is expected to be small and the result should be reliable. The sum of pion-loop + quark-loop is very similar for BPP and HKS, and therefore should be more reliable than the individual contributions, which turn out to be more model dependent.⁴³

At the beginning of this section we already discussed how sensitive bare LbL quark loops depend on the quark masses adopted and on a cutoff if applied. With small constituent quark masses, or in the extreme when using current quark masses (see Table 5.9 and Footnote 27), one can obtain much larger results. Also the implementation of the VMD type shielding leads the very different results. It is therefore interesting to have alternative approaches like solving numerically the non-perturbative Dyson–Schwinger equations of QCD (for QED the DSE have been presented at the end of Sect. 2.3.1). The DSE estimate of [219, 220] is $10.7(0.2) \times 10^{-10}$ by a factor 5 larger than the ENJL result and by a factor 2 larger than the CQM result. Similar size results are obtained in models with a low constituent quark mass when no VMD-like damping is included. Examples are the non local chiral quark model [339] with $11.0(0.9) \times 10^{-10}$ and a number of estimates within the chiral quark model $(7.6 - 8.9) \times 10^{-10}$ [278], $(11.8 - 14.8) \times 10^{-10}$ [340] and $(7.6 - 12.5) \times 10^{-10}$ [341] (also see [342]). The last three estimates are thought as estimates of the full HLbL contribution and completely ignore the intrinsic non-perturbative feature of the hadronic light-by-light scattering process being dominated by pseudoscalar meson exchanges.

As mentioned earlier, in the large- N_c resonance saturation approach (LMD+V) the S.D. behavior is incorporated as a boundary condition and no separate quark loops contributions has to be accounted for concerning the light quark sector. There remains the small c -quark contribution

$$a_{\mu \text{pQCD}}^{c\text{-quark}} \simeq 2.3 \times 10^{-11} \quad (5.276)$$

to be taken into account [328].

The results from pseudoscalar- and quark-loops of the various evaluations may be summarized as follows.

⁴³Note that within the ENJL framework quarks are constituent quarks and the constituent quark loop is subject to the VMD mechanism. This differs from simply applying pQCD to the *hard-hard* domain of Fig. 5.47.

Table 5.17 Light-by-Light: π^\pm, K^\pm & quark loops

Model $\pi^+\pi^-\gamma^*(\gamma^*)$	$a_\mu(\pi^\pm) \times 10^{11}$	$a_\mu(\pi^\pm, K^\pm) \times 10^{11}$	$a_\mu(\text{quarks}) \times 10^{11}$
Point	-45.3	-49.8	62 (3)
VMD	-16	-	-
HLS [HKS, HK]	-4 (8)	-4.5 (8.1)	9.7 (11.1)
ENJL[BPP]	-18 (13)	-19 (13)	21 (3)
Guesstimate [MV]	0 (10)	0 (10)	0
DR sQED+VMD [CHPS]	-16	-16.5	-

Table 5.18 Summary of the 2009 status of results for the various contributions to $a_\mu^{\text{HLbL:had}} \times 10^{11}$

Contribution	BPP	HKS	KN	MV	BP	PdRV	N/JN
π^0, η, η'	85 ± 13	82.7 ± 6.4	83 ± 12	114 ± 10	-	114 ± 13	99 ± 16
π, K loops	-19 ± 13	-4.5 ± 8.1	-	0 ± 10	-	-19 ± 19	-19 ± 13
Axial vectors	2.5 ± 1.0	1.7 ± 1.7	-	22 ± 5	-	15 ± 10	22 ± 5
Scalars	-6.8 ± 2.0	-	-	-	-	-7 ± 7	-7 ± 2
Quark loops	21 ± 3	9.7 ± 11.1	-	-	-	2.3	21 ± 3
Total	83 ± 32	89.6 ± 15.4	80 ± 40	136 ± 25	110 ± 40	105 ± 26	116 ± 39

5.2.10 A Summary of Results

As a reference we consider the 2009 status summarized in Table 13 of [275], which we reproduce as Table 5.18.

The main problem is that the separation into the different contributions is very much dependent on the effective models. It would be desirable to know what are the separate contributions from different regions in Fig. 5.47 for the different approaches. I still think that sticking together results obtained for different ranges separated by a standard cutoff, say 1 GeV, would be most useful. It is interesting to note that changing the high energy constraints of low energy effective models often affects the contribution from the range below 1 GeV by a substantial amount (for examples see [249]), which at least leaves doubts that one always has the right strategy. At present it is not easy to give a reliable estimate of the full a_μ^{HLbL} . There are many results for isolated sub-contributions, most for the isolated π^0 -pole, which however, although being the leading contribution, is not a good approximation for the full HLbL. The most reliable results seem to be the ones from the most complete analyses like the one from BPP [235] and the updates thereof. The second complete calculation by HKS [210] has not been reconsidered more recently.

- (a) According to Table 5.12 the diagram Fig. 5.55a yields the most important contribution but requires a model for its calculation. The results for this dominating contribution are collected in Table 5.13. The results from the related axial- and scalar-exchanges are listed in Tables 5.14 and 5.15, respectively.

- (b) Next in Table 5.12 are pion- and Kaon-loops Fig. 5.55b which only yields a subleading contribution again being model dependent. Results are given in the middle column of Table 5.17.
- (c) Third in Table 5.12 is the quark loop Fig. 5.55c which only appears as a S.D. complement of the ENJL and the HLS low energy effective models. Corresponding values are included in the last column of Table 5.17.

A number of improvements have been first considered in [254]:

- (1) the constraint on the twist four $(1/q^4)$ -term in the OPE requires $h_2 = -10 \text{ GeV}^2$ in the Knecht-Nyffeler form factor (5.214): $\delta a_\mu \simeq (+5 \pm 0) \times 10^{-11}$
- (2) the contributions from the f_1 and f'_1 isoscalar axial-vector mesons: $\delta a_\mu \simeq (+5.7 \pm 1.9) \times 10^{-11}$ (using dressed photons, corrected to satisfy Landau-Yang)
- (3) for the remaining effects: scalars (f_0) + dressed π^\pm , K^\pm loops + dressed quark loops: $\delta a_\mu \simeq (-5 \pm 13) \times 10^{-11}$
- (4) new S.D. constraint: WZW point form-factor at the external vertex: $\delta a_\mu \simeq (+14 \pm 7) \times 10^{-11}$

Further issues raised concern the pole-approximation in single particle exchanges [273] (i.e. in the usually adopted Euclidean approach the pion exchange is far off the pole, see Fig. 5.57), the new magnetic susceptibility constraint χ [274], pion polarizability [236, 334, 335, 337], Landau-Yang theorem issue in axial exchanges [224, 325, 326] and LbL at NLO [209]. Further improvements have been possible with new data on the pion TFF by BaBar and Belle (see Fig. 5.59), and by a new constraint by lattice data [293, 294].

More recent studies of single meson exchanges may be found in [224, 325]. The axial vector meson exchange contribution in this analysis is found to be substantially smaller than estimated in MV [254]. The analysis also evaluated the contribution of the tensor resonance $f_2(1270)$, with the result $1.1(0.9) \times 10^{-11}$. Note that as far as this application is concerned the ENJL and the HLS models are equivalent and in fact the HLS may be “derived” from the ENJL model by making a number of additional approximations [192, 231]. The uncertainties quoted include the changes due to the variation of the cut-off by 0.7–8 GeV for the ENJL model and by 1–4 GeV for the HLS model. For the LMD+V parametrization, the leading π^0 -exchange contribution does not involve an explicit cut-off dependence (large- N_c duality approach), but some of the parameters needed to characterize the off-shell form factor could not be fixed yet and have to be varied in a wide range producing a substantial uncertainty.

As our best estimate we take the sum of Eqs. (5.225), (5.261), (5.267), (5.273), (5.275), (5.276), (5.268) and (5.226):

$$a_\mu^{\text{HLbL}} = [95.45(12.40) + 7.55(2.71) - 5.98(1.20) + 20(5) - 20(4) + 2.3(0.2) + 1.1(0.1) + 3(2)] \times 10^{-11} = 103.4(28.8) \times 10^{-11},$$

where we added errors quadratically and multiplied the resulting error by a factor 2 to account for possible so far unaccounted model uncertainties.

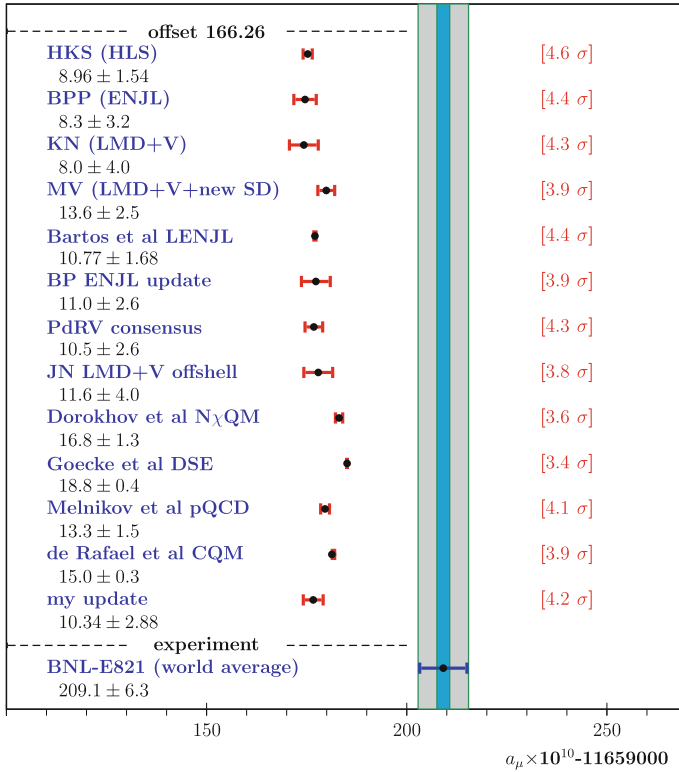


Fig. 5.66 Results from various HLbL calculations. The plot also illustrates the history of HLbL calculations. Some of the estimates do not attempt to provide any model uncertainties, which are generally not easy to estimate reliably. The narrow band illustrates the expected uncertainty from the next generation experiments

A selection of estimates for HLbL is presented in Fig. 5.66 and Table 5.19. Because of the increased accuracy of the experiments and the substantial reduction of the error on the other hadronic contributions also a reconsideration of the hadronic light-by-light contributions is needed. To what extent this is possible remains to be seen, however, some progress should be possible by taking into account various points which have been brought up in the more recent discussions. Further progress should be possible by the dispersive approach advocated recently, which however depends vitally on better experimental data. Better data are equally important for better model constraints. Lattice QCD is supposed to be the ultimate method to get a true QCD prediction and recent progress looks to be very promising.

Table 5.19 Summary of selected estimates for the different contributions to $a_\mu^{\text{HLbL}} \times 10^{11}$. For comparison, the first line shows some results when no form factors are used (undressed). The only complete calculations are HKS and BPP, but only the latter has been updated recently. Note: LMD+V [KN, JN] and (LMD+V, WZW) [MV] are applying the large- N_c concept plus OPE to different objects as illustrated in Fig. 5.60. (LMD+V, WZW) [MV] respect QCD asymptotics on the LbL scattering level which requires the external vertex to be the WZW point vertex, the quark loop contribution is then included already. LMD+V [KN, JN] apply the LMD+V transition form factor also at the external vertex, QCD asymptotics then requires an extra S.D. quark loop contribution

Model	π^0, η, η'	Axial-mesons	Scalars	π, K -loops	Quark-loop	Total	Ref.
QM	$+\infty$	–	–	–45	60	–	no FF
HLS [HKS]	82.7 (6.4)	1.7 (1.7)	–	–4.5 (8.1)	9.7 (11.1)	89.6 (15.4)	[210]
ENJL [BPP]	85 (13)	2.5 (1.0)	–6.8 (2.0)	–19 (13)	21 (3)	83 (32)	[235]
LMD+V [KN]	83 (12)	–	–	–	–	80 (40)	[234]
(LMD+V, WZW) [MV]	114 (10)	22 (5)	0 (10)	–	0	136 (25)	[254]
LENJL	95.5 (17.0)	–	–	12.3 (2.4)	0	107.7 (16.8)	[296]
ENJL update	–	–	–	–	–	110 (40)	[327]
PdRV consensus	114 (13)	15 (10)	–7 (7)	–19 (19)	2.3 [c-quark]	105 (26)	[328]
LMD+V [JN]	99 (16)	22 (5)	–7 (2)	–19 (13)	21 (3)	116 (40)	[274]
RLA	104.7 (5.4)	–	–	–	–	–	[298]
RLA	65.8 (5.4) [π^0]	–	–	–	–	–	[299]
N_χ QM	58.5 (8.7)	–	3.4 (4.8)	–	11 (9)	168 (13)	[339]
DSE	81 (2)	–	–	–	107 (2)	188 (4)	[218]
pQCD	–	–	–	–	–	118–148	[340]
CQM	68 (3) [π^0]	–	–	–	82 (6)	150 (3)	[278]
RLA	–	–	–	–	–(11 – 71)	–	[334]
ENJL+ a_1	–	–	–	–20 (5)	–	–	[236]
LMD [PV]	–	6.4 (2.0)	–3.1 (0.8)	–	–	–	[223]
LMD+V	95.5 (12.4)	7.6 (2.0)	–6.0 (1.2)	–20 (5)	22.3 (4)	103.4 (28.8)	[326]
DRA [CHPS]	–	–	–24 (1)	–	–	–	[332]

5.2.11 The Dispersive Approach

It is obvious from our discussion that one of the main problems concerning HLbL is the missing experimental data to constrain effective hadronic models needed for estimates of the HLbL contribution to a_μ . This also has been the motivation to attempt a dispersive approach similar to what is the standard way to evaluate the HVP contribution. Obviously, this multi-scale, multi-amplitude problem is very much more complicated, than determining a single scalar amplitude via data from a specific process like $e^+e^- \rightarrow \text{hadrons}$.⁴⁴ Quite recently an essentially data-driven Dispersion Relation Approach (DRA) has been set up independently by two groups Pauk

⁴⁴Although we only need to know one single function $R(s)$ one has to keep in mind that $R(s)$ comprises many different channels and is all but simple to be measured accurately.

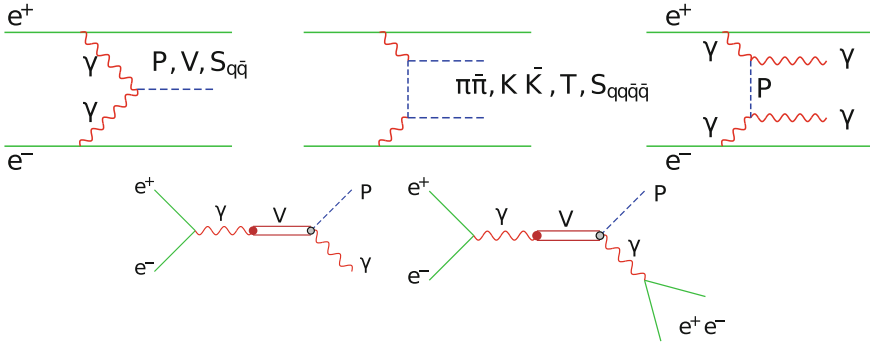


Fig. 5.67 Sample processes relevant for the dispersive approach

and Vanderhaeghen (PVdH) [223], focusing directly on the $g - 2$ vertex, and by Colangelo, Hoferichter, Procura and Stoffer (CHPS) [221, 222, 331], who more generally start from the four-point Green function of electromagnetic currents. We briefly sketch the main ideas in the following. Investigations about data-driven dispersive approach see also [343].

For future improvements of HLbL evaluations one urgently needs more information from $\gamma\gamma \rightarrow$ hadrons processes (see Fig. 5.67), together with the possible crossed channels. A comprehensive theoretical study of $\gamma\gamma$ -physics is [344]. Important aspect are investigated in [345–351] (see also [352–354]). The goal is to exploit possible new experimental data to better constrain the relevant physical amplitudes.

Mostly, experiments at e^+e^- -facilities investigate single-tag events (higher rates, lower background). New data are expected from KLOE [355], KEDR exhibiting taggers and from BaBar, Belle, BES-III which have high luminosity. More information is also expected from Dalitz-decay studies $\rho, \omega, \phi \rightarrow \pi^0(\eta)e^+e^-$ possible at Novosibirsk, CERN (NA60), JLab, Mainz, Bonn, Jülich and with BES. Unfortunately some of the interesting processes seem to be buried in the background. The background is a general problem in $\gamma\gamma \rightarrow$ hadrons physics.

The dispersive approach is able to allow for real progress since contributions which we have treated so far as separate contributions will be treated in an integral manner. An example is the $\gamma\gamma \rightarrow \pi\pi$ process which includes contributions attributed to the two-pion channel, the pion-loop, the scalar contribution as well as the tensor contribution. All-in-one can be gotten from the experimental data shown in Fig. 5.38. This also will settle such issues as the pion polarizability.

Cutting the $g - 2$ Vertex

In the PVdH approach we consider the off-shell Pauli form factor $F_M(k^2)$ (3.20), which we may write in terms of helicity amplitudes as

$$\begin{aligned}
F_2(k^2) &= e^6 \sum_{\lambda_1, \lambda_2, \lambda_3, \lambda} (-1)^{\lambda + \lambda_1 + \lambda_2 + \lambda_3} \int \frac{d^4 q_1}{(2\pi)^4} \int \frac{d^4 q_2}{(2\pi)^4} L_{\lambda_1 \lambda_2 \lambda_3 \lambda}(p, q_1, k - q_1 - q_2, q_2) \\
&\times \frac{\Pi_{\lambda_1 \lambda_2 \lambda_3 \lambda}(q_1, k - q_1 - q_2, q_2, k)}{q_1^2 q_2^2 (k - q_1 - q_2)^2 [(p + q_1)^2 - m^2] [(p + k - q_2)^2 - m^2]}, \quad (5.277)
\end{aligned}$$

which is the off-shell version of (5.148) derived earlier [with $q_2 \leftrightarrow q_3$]. Here, the Fourier transform of the four-current correlator (5.139) has been projected onto the helicity basis

$$\Pi_{\lambda_1 \lambda_2 \lambda_3 \lambda_4}(q_1, q_2, q_3) = \epsilon^\mu(q_1, \lambda_1) \epsilon^\nu(q_2, \lambda_2) \epsilon^\lambda(q_3, \lambda_3) \epsilon^\rho(q_4, \lambda_4) \Pi_{\mu\nu\lambda\rho}(q_1, q_2, q_3)$$

by means of the photon polarization vectors $\epsilon(q, \lambda)$, by inserting the completeness relation

$$\sum_{\lambda=\pm} \epsilon_\nu^*(p, \lambda) \epsilon_\mu(p, \lambda) = -g_{\mu\nu}$$

modulo gauge terms (see (2.26)). The complementary coefficients correspondingly read

$$\begin{aligned}
L_{\lambda_1 \lambda_2 \lambda_3 \lambda_4}(p, q_1, q_2, q_3) &= \epsilon_\mu^*(\lambda_1, q_1) \epsilon_\nu^*(\lambda_2, q_2) \epsilon_\lambda^*(\lambda_3, q_3) \epsilon_\sigma^*(\lambda_4, q_4) \\
&\times \text{Tr} \left[\Lambda^\sigma(p + q_1 + q_2, p) \gamma^\lambda(\not{p} + \not{q}_1 + \not{q}_2 + m) \gamma^\nu(\not{p} + \not{q}_1 + m) \gamma^\mu \right],
\end{aligned}$$

with projector (3.92) and (3.93):

$$\Lambda_\sigma(p', p) = \frac{m^2}{k^2(4m^2 - k^2)} (\not{p} + m) \left[\gamma_\sigma + \frac{k^2 + 2m^2}{m(k^2 - 4m^2)} (p' + p)_\sigma \right] (\not{p}' + m).$$

serves to insert the LbL scattering tensor into the magnetic form factor.

When analytically continued to complex values of the external photon's virtuality k^2 , the muon's electromagnetic vertex function possesses branch point singularities joining the physical production thresholds, as is dictated by unitarity⁴⁵ (see Sects. 3.7 and 3.8). Using Cauchy's integral theorem, the off-shell form factor $F_M(k^2)$ can be represented as an integral along a closed contour avoiding the cuts and extended to infinity. Assuming that the form factor vanishes uniformly when k^2 tends to infinity the contour integral reduces to an integral of the form factor's discontinuity $\text{Disc}_{k^2} F_M(k^2)$ along the cut in the k^2 -plane starting from the lowest branch point:

$$F_M(0) = \frac{1}{2\pi i} \int_0^\infty \frac{dk^2}{k^2} \text{Disc}_{k^2} F_M(k^2). \quad (5.278)$$

⁴⁵For the discussion of the anomalous thresholds of the three-point functions, located below the normal thresholds, see [222].

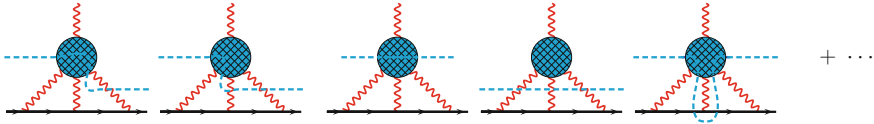


Fig. 5.68 Unitarity diagrams contributing to the imaginary part of the vertex function. The *cut* indicates the on-shell intermediate states. The ellipses stand for diagrams with photons attached to the muon line permuted

As can be seen from the structure of the two-loop integral in (5.277), the branch cuts of the Pauli form factor $F_M(k^2)$ are related to the propagators of virtual particles and non-analyticities of the HLbL tensor. The latter possesses two types of discontinuities, the corner (one-photon) and cross (two-photon) cuts (see Fig. 5.68). The corner cuts are related to a conversion of a photon to a hadronic state with negative C -parity, while the cross cuts are related to a two-photon production of a C -even hadronic state. As the dominant contributions originate from the lowest thresholds it is mainly governed by intermediate states involving pions. In particular, the lowest threshold in the C -odd channel is related to a $\pi^+\pi^-$ -pair production and in the C -even channel to a π^0 intermediate state. By virtue of unitarity, these discontinuities are related to amplitudes of physical hadron production processes. Experimentally, the amplitudes involved in the unitarity equation for the required discontinuities can be measured in two-photon and e^+e^- production processes (for references see [356]). The dispersive analysis of the two-pion production channel by a real and a virtual photon was recently discussed in [350].

Taking into account the analytical structure of the HLbL tensor, the discontinuity in (5.278) is obtained as a sum of nine topologically different contributions, which are graphically represented by unitarity diagrams in Fig. 5.68. On a practical level, the contribution of a particular unitarity diagram is obtained by replacing the cut virtual propagators in the two-loop integral by corresponding delta functions according to (2.141), and the cut vertices by their appropriate discontinuities. It is important to note that one obtains non-vanishing imaginary parts only if physical sub-processes are kinematically admitted, which requires a non-vanishing k^2 in our case. As an example for the first diagram in (see Fig. 5.68), it implies

$$\begin{aligned}
 \text{Disc } F_M(k^2) &= e^6 \sum_{\lambda_1, \lambda_2, \lambda_3, \lambda} (-1)^{\lambda+\lambda_1+\lambda_2+\lambda_3} \\
 &\int \frac{d^4 q_1}{(2\pi)^4} \int \frac{d^4 q_2}{(2\pi)^4} \frac{1}{q_1^2} \frac{1}{(k-q_1-q_2)^2} \frac{1}{(p+q_1)^2 - m^2} \frac{1}{(p+k-q_2)^2 - m^2} \\
 &\times L_{\lambda_1 \lambda_2 \lambda_3 \lambda}(p, q_1, k-q_1-q_2, q_2) (2\pi i) \delta(q_2^2) \\
 &\times \text{Disc}_{(k-q_2)^2} \Pi_{\lambda_1 \lambda_2 \lambda_3 \lambda}(q_1, k-q_1-q_2, q_2, k).
 \end{aligned} \tag{5.279}$$

Table 5.20 The contributions to a_μ (in units 10^{-10}) of two-particle (2p) and three-particle (3p) cuts for the two topologies (see Fig. 5.69) appearing in the pole approximation compared to the results of the conventional 2-loop integration of [234]. Note that total = 2 \times direct + crossed

	2p-cut	3p-cut	Total	Direct
Direct	4.91	-2.14	2.77	2.77
Crossed	-7.40	7.56	0.16	0.16
Total	2.42	3.28	5.70	5.70

The non-perturbative discontinuity function $\text{Disc}_{(k-q_2)^2} \Pi_{\lambda_1 \lambda_2 \lambda_3 \lambda}$ in (5.279) is directly related to amplitudes of processes $\gamma^* \gamma^* \rightarrow X$ and $\gamma^* \rightarrow \gamma X$, with X denoting a C -even hadronic state, which are accessible experimentally (Table 5.20).

To set up and test the technique for evaluating the phase space and dispersion integrals we consider a well-studied approximation for the contribution of a pseudoscalar meson (corresponding to π^0 , η and η' exchanges), based on the large- N_c inspired form factors [234] as discussed in Sect. 5.2.4 above. In this approximation, we have two-particle cuts (2p) and the three-particle cuts (3p) from diagrams Fig. 5.56, and the HLbL amplitude is approximated by a pole term of the form:

$$\begin{aligned} \Pi_{\text{pole}}(q_1^2, (k - q_1 - q_2)^2, q_2^2, k^2, (k - q_1)^2, (q_1 + q_2)^2) & \quad (5.280) \\ &= \frac{|\mathcal{F}_{\pi^0 \gamma \gamma}(m_\pi^2, 0, 0)|^2}{(q_1^2 - M_V^2)(q_2^2 - M_V^2)((k - q_1 - q_2)^2 - M_V^2)(k^2 - M_V^2)} \\ &+ \text{crossed terms.} \end{aligned}$$

Furthermore, for each diagram we have the two cuts as shown in Fig. 5.68, such that

$$F_M(0) = \frac{1}{2\pi i} \int_{M^2}^{\infty} \frac{dk^2}{k^2} \text{Disc}_2 F_M(k^2) + \frac{1}{2\pi i} \int_0^{\infty} \frac{dk^2}{k^2} \text{Disc}_3 F_M(k^2)$$

with $\text{Disc}_2 F_M(k^2)$ and $\text{Disc}_3 F_M(k^2)$ denoting the sum of two- and three-particle discontinuities. Interestingly, the different cuts yield contributions of opposite sign, and also the different topologies of the diagrams Fig. 5.56 (cut as illustrated in Fig. 5.69) yield results of opposite sign: We note that both time-like $e^+ e^- \rightarrow \gamma^* \rightarrow P\gamma$ and space-like $\gamma^* \gamma^* \rightarrow P$ data are needed as input. PVdH use both monopole (mon) and dipole (dip) parametrizations of the form:

$$\frac{\mathcal{F}_{M\gamma^*\gamma^*}^{\text{mon}}(q_1^2, q_2^2)}{\mathcal{F}_{M\gamma^*\gamma^*}(0, 0)} = \frac{1}{(1 - q_1^2/\Lambda_{\text{mon}}^2)} \frac{1}{(1 - q_2^2/\Lambda_{\text{mon}}^2)}, \quad (5.281)$$

$$\frac{\mathcal{F}_{M\gamma^*\gamma^*}^{\text{dip}}(q_1^2, q_2^2)}{\mathcal{F}_{M\gamma^*\gamma^*}(0, 0)} = \frac{1}{(1 - q_1^2/\Lambda_{\text{dip}}^2)^2} \frac{1}{(1 - q_2^2/\Lambda_{\text{dip}}^2)^2}, \quad (5.282)$$

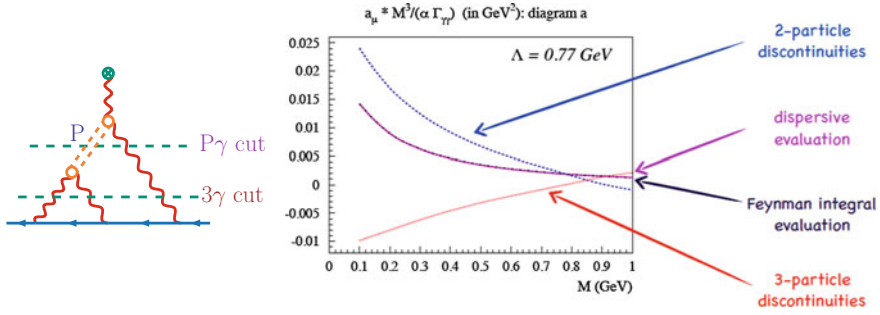


Fig. 5.69 The dispersive approach: the role of the different possible cut exemplified. The sum of all the individual cut contributions reproduces the Feynman diagram calculation, while the individual contributions are substantially off. Courtesy of V. Pauk and M. Vanderhaeghen. Reprinted with permission from [223], Copyright © (2014) by the American Physical Society

where Λ_{mon} (Λ_{dip}) are the monopole (dipole) mass parameters respectively, which are to be determined from phenomenology. These ansätze are just dressing the constant WZW form factor by single and double VMD and correspond to single parameter versions of (5.211) and (5.214), respectively, discussed in Sect. 5.2.4. This kind of very simple phenomenological modeling obviously must yield results in the ballpark of more elaborate approaches as long as they satisfy the WZW constraint together with the Brodsky–Lepage asymptotic behavior. Like the pseudoscalar threshold values $\mathcal{F}_{P\gamma\gamma}(0, 0)$ are fixed by the WZW effective Lagrangian or, equivalently, by the related widths $\Gamma(P \rightarrow \gamma\gamma)$ as in (5.178), one can use the experimental widths in cases where the couplings are not or less well known.

The required transition model form factors applied have been constrained by light-by-light scattering sum rules [224, 225], which actually can reveal inconsistencies like the ones of the axial exchanges when they violate the Landau–Yang theorem, as discussed above.

Here we summarize the estimates obtained in [223, 225]:

(i) Axial-vector mesons:

For axial mesons the Landau–Yang theorem predicts $\Gamma(A \rightarrow \gamma\gamma) \equiv 0$. Thus one has to define an effective width from the slope of the width obtained from an adapted Breit–Wigner type parametrization with one of the photons off-shell. Considering a decay into one quasi-real longitudinal photon (with virtuality Q_1^2) and a transverse (real) photon one defines

$$\tilde{\Gamma}_{\gamma\gamma} \equiv \lim_{Q_1^2 \rightarrow 0} \frac{M^2}{Q_1^2} \frac{1}{2} \Gamma(A \rightarrow \gamma_L^* \gamma_T), \tag{5.283}$$

which allows to express the FF normalization entering the $A\gamma^*\gamma$ vertex as [224]:

$$[\mathcal{F}_{\mathcal{A}\gamma^*\gamma^*}(0, 0)]^2 = \frac{3}{M} \frac{4}{\pi\alpha^2} \tilde{\Gamma}_{\gamma\gamma}. \tag{5.284}$$

Table 5.21 Data and results for a_μ in units 10^{-11} from the dispersive analysis [325]: present values [357] of the $f_1(1285)$ meson and $f_1(1420)$ meson masses M , their equivalent 2γ decay widths $\tilde{\Gamma}_{\gamma\gamma}$, defined according to (5.283), as well as their dipole masses Λ_{dip} entering the FF of (5.282). For $\tilde{\Gamma}_{\gamma\gamma}$, we use the experimental results from the L3 Collaboration: $f_1(1285)$ from [321], $f_1(1420)$ from [317]

	M [MeV]	$\tilde{\Gamma}_{\gamma\gamma}$ [keV]	Λ_{dip} [MeV]	a_μ
$f_1(1285)$	1281.8 ± 0.6	3.5 ± 0.8	1040 ± 78	5.0 ± 2.0
$f_1(1420)$	1426.4 ± 0.9	3.2 ± 0.9	926 ± 78	1.4 ± 0.7
Sum				6.4 ± 2.0

Results are collected in Table 5.21. They compare to the results obtained by applying antisymmetrization to the large- N_c type MV form factors. For the case of ideal mixing we estimated $a_\mu[a_1, f'_1, f_1] \sim (7.55 = [1.89 + 5.19 + 0.47] \pm 2.71) \times 10^{-11}$ in Sect. 5.2.5 above.

(ii) Scalar mesons

Taken into account here are the mesons $f_0(980)$, $f'_0(1370)$ and $a_0(980)$. The modulus square of the FF is given by

$$[\mathcal{F}_{S\gamma^*\gamma^*}(0, 0)]^2 = \frac{1}{M} \frac{4}{\pi\alpha^2} \Gamma_{\gamma\gamma}. \quad (5.285)$$

Results are collected in Table 5.22. The results compare with the expected contribution from $q\bar{q}$ scalars $a_\mu[a_0, f'_0, f_0] \sim (-5.98 = [-0.17 - 2.96 - 2.85] \pm 1.20) \times 10^{-11}$, which we have evaluated adopting the large- N_c inspired FF in Sect. 5.2.6 above.

(iii) Tensor mesons

The dominant tensor mesons produced in two-photon fusion processes are given by: $f_2(1270)$, $a_2(1320)$, $f_2(1565)$, and $a_2(1700)$, see Table 5.23. As described above, we will assume in our analysis that the tensor meson is only produced in a state of helicity 2. This allows to express the normalization of the dominant (helicity-2) FF entering the $\mathcal{T}\gamma^*\gamma^*$ vertex as [224]:

Table 5.22 Data and results from the dispersive analysis [325]: scalar meson pole contribution to a_μ in units $[10^{-11}]$ based on the present PDG values [357] of the scalar meson masses M and their 2γ decay widths $\Gamma_{\gamma\gamma}$ and the monopole ansatz (5.281)

	M [MeV]	$\Gamma_{\gamma\gamma}$ [keV]	a_μ ($\Lambda_{\text{mon}} = 1$ GeV)	a_μ ($\Lambda_{\text{mon}} = 2$ GeV)
$f_0(980)$	980 ± 10	0.29 ± 0.07	-0.19 ± 0.05	-0.61 ± 0.15
$f'_0(1370)$	$1200 - 1500$	3.8 ± 1.5	-0.54 ± 0.21	-1.84 ± 0.73
$a_0(980)$	980 ± 20	0.3 ± 0.1	-0.20 ± 0.07	-0.63 ± 0.21
Sum			-0.9 ± 0.2	-3.1 ± 0.8

Table 5.23 Data and results from the dispersive analysis [325] (see Sect. 5.2.11 below): tensor meson pole contribution to a_μ based on the present PDG values [357] of the tensor meson masses M and their 2γ decay widths $\Gamma_{\gamma\gamma}$. Resonances here are parametrized by a simple dipole form factor (5.282) with a cut-off $\Lambda_{\text{dip}} = 1.5$ GeV

Resonance	M [MeV]	$\Gamma_{\gamma\gamma}$ [keV]	a_μ [10^{-11}]
$f_2(1270)$	1275.1 ± 1.2	3.03 ± 0.35	0.79 ± 0.09
$f_2(1565)$	1562 ± 13	0.70 ± 0.14	0.07 ± 0.01
$a_2(1320)$	1318.3 ± 0.6	1.00 ± 0.06	0.22 ± 0.01
$a_2(1700)$	1732 ± 16	0.30 ± 0.05	0.02 ± 0.003
Sum			1.1 ± 0.1

$$[\mathcal{F}_{\mathcal{T}\gamma^*\gamma^*}(0, 0)]^2 = \frac{5}{M} \frac{4}{\pi\alpha^2} \Gamma_{\gamma\gamma}. \quad (5.286)$$

Results for the tensor contributions are collected in Table 5.23. Somewhat surprisingly, the contribution of the prominent $f_2(1270)$ resonance, displayed in Fig. 5.38, only yields a small contribution.

The estimates presented so far are based on simple VMD type FF models (which have been shown to violate proper QCD asymptotic behavior) and have been intended as a first approximation. The results have been useful as they revealed some inconsistencies with earlier estimates of the axial contributions. A realization of the “data + dispersion relation” paradigm remains to be done. At present the method is suffering from the lack of relevant data.

Cutting the $\gamma\gamma$ Scattering Green Function

This subsection provides an outline of the DRA advocated by Colangelo et al. [221, 222]. The attempt is to constrain the amplitudes of the four-point HLbL tensor by data with subsequent projection onto/into the $g - 2$ vertex. Here we can only sketch the main elements of the approach which is very elaborate also because of the many amplitudes of the four-photon Green function and the need to project it down and insert it into the $g - 2$ vertex as set up in Sect. 5.2.1. The basic minimal linearly independent covariant decomposition (5.149) has an unpleasant feature, the scalar amplitudes defined thereby unavoidably exhibit unphysical kinematic singularities (see Sect. 2.5.7). The latter can be eliminated by introducing appropriate additional (linearly dependent) tensor structures. How to do this one can learn from Bardeen, Tung [358], and Tarrach [359] (BTT). The reason why unphysical kinematic singularities show up are the kinematic tensor coefficients, which get contracted with external kinematic tensors when calculating observables. The scalar products of momenta which result after the contraction eliminate the singularities. In our case we have to contract with the Dirac trace (5.147) which projects the tensor onto $a_\mu^{\text{HLbL}} = F_M(0)$. Thereby, the scalar amplitudes get multiplied by $q_1 \cdot q_2$ or $q_3 \cdot q_4$ at most in square. Thereafter all possible singularities cancel. This means that the only possible singularities are (double or single) poles in $q_1 \cdot q_2$ or $q_3 \cdot q_4$. The precise

form of these poles can be easily determined: they correspond to degeneracies of the obtained basis of Lorentz structures in the limit $q_1 \cdot q_2 \rightarrow 0$ and/or $q_3 \cdot q_4 \rightarrow 0$. The additional structures, thus may be constructed to lift these degeneracies in these limits. In [222] 11 such structures have been found. The extended set of 54 structures exhibits all possible crossing symmetries in a manifest way.

Explicitly, the resulting representation of the HLbL tensor reads

$$\Pi^{\mu\nu\lambda\sigma} = \sum_{i=1}^{54} T_i^{\mu\nu\lambda\sigma} \Pi_i, \quad (5.287)$$

where seven of the tensor coefficients are listed in (5.315) in the Appendix which follows below. All the remaining structures are crossed versions of these seven ones. In order to compute the contribution to $(g_\mu - 2)$, one has to insert the specific tensor decompositions obtained into (5.146), which then may be written

$$\begin{aligned} a_\mu^{\text{HLbL}} = & -e^6 \int \frac{d^4 q_1}{(2\pi)^4} \frac{d^4 q_2}{(2\pi)^4} \frac{1}{q_1^2 q_2^2 (q_1 + q_2)^2} \frac{1}{(p + q_1)^2 - m^2} \frac{1}{(p - q_2)^2 - m^2} \\ & \times \sum_{i=1}^{19} \hat{T}_i(q_1, q_2; p) \hat{\Pi}_i(q_1, q_2, -q_1 - q_2), \end{aligned} \quad (5.288)$$

where

$$\begin{aligned} \hat{T}_i(q_1, q_2; p) = & \frac{1}{48m} \text{Tr} \left((\not{p} + m) [\gamma^\rho, \gamma^\sigma] (\not{p} + m) \gamma^\mu (\not{p} + \not{q}_1 + m) \gamma^\lambda (\not{p} - \not{q}_2 + m) \gamma^\nu \right) \\ & \times \left(\frac{\partial}{\partial k^\rho} \hat{T}_{\mu\nu\lambda\sigma}^i(q_1, q_2, k - q_1 - q_2) \right) \Big|_{k=0}. \end{aligned} \quad (5.289)$$

Computing the Dirac trace, which is the one (5.147) encountered earlier, and averaging over the direction of muon four momentum p_μ , as described in Sect. 5.2.3, yields the angular integrals (5.171), and one can immediately perform five of the eight integrations. This leads to the master formula for the HLbL contribution to a_μ :

$$a_\mu^{\text{HLbL}} = \frac{2\alpha^3}{3\pi^2} \int_0^\infty dQ_1 dQ_2 \int_{-1}^1 d\tau \sqrt{1 - \tau^2} Q_1^3 Q_2^3 \sum_{i=1}^{12} T_i(Q_1, Q_2, \tau) \bar{\Pi}_i(Q_1, Q_2, \tau), \quad (5.290)$$

which is the generalization of (5.172) derived in [275]. The hadronic scalar functions $\bar{\Pi}_i$ are linear combinations of the Π_i 's in (5.287) and are listed in (5.316) together with the integral kernels $T_i(Q_1, Q_2, \tau)$ (corresponding to our $I_i(Q_1, Q_2, \tau)$ (5.173)) in (5.317) in a following Appendix. They have to be evaluated for the reduced $g - 2$ vertex kinematics

$$\begin{aligned}
 s &= -Q_3^2 = -Q_1^2 - 2Q_1Q_2\tau - Q_2^2, & t &= -Q_2^2, & u &= -Q_1^2, \\
 q_1^2 &= -Q_1^2, & q_2^2 &= -Q_2^2, & q_3^2 &= -Q_3^2 = -Q_1^2 - 2Q_1Q_2\tau - Q_2^2, & k^2 &= q_4^2 = 0.
 \end{aligned}
 \tag{5.291}$$

It turns out that there are only 19 independent linear combinations of the structures $T_i^{\mu\nu\lambda\sigma}$ that contribute to $(g_\mu - 2)$ at first. However, because of the symmetries under the exchange of the momenta $q_1 \leftrightarrow -q_2$, only a subset of 12 of these functions appears in the master formula (5.290). The integral kernels T_i listed in [222] are fully general for any light-by-light process, while the scalar functions Π_i parametrize the hadronic content of the master formula. A corresponding formula has been worked out in [236], which also lists the required integral kernels, corresponding to the $T_i^{\mu\nu\lambda\sigma}$'s, but for the minimal decomposition (5.149).

The idea here is to get the Π_i 's from dispersion relations with appropriate experimental data as an input. Of course, as we have used it earlier, we as well can attempt to model the Π_i 's or try to get them from lattice QCD simulations.

How do we get the scalar amplitudes which are encoding all non-perturbative physics entering a_μ^{HLbL} ? The basic ideas of utilizing dispersion relations have been developed in Sect. 3.8 for the case of the HVP. Instead of calculating the hadronic ‘‘blobs’’, which we so far cannot do with needed precision, we relate them to the imaginary parts which correspond to cut diagrams, where a cut puts intermediate states to their mass shell, which in turn relates cut diagrams via on-shell T -matrix elements to physical cross sections. The possible cut diagrams in HLbL are shown in Fig. 5.70, which exhibit multi-hadron sub-processes which eventually are

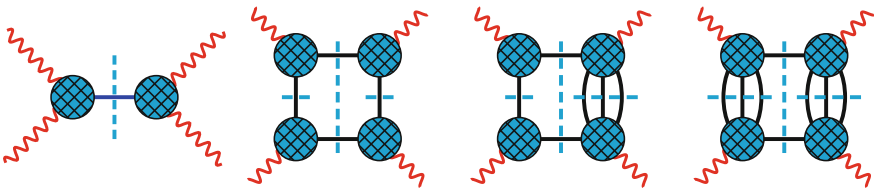


Fig. 5.70 Unitarity diagrams according to the Mandelstam representation. *Cuts* are represented by the dashed lines, where *cut lines* represent on-shell particles. Crossed diagrams have to be included as well

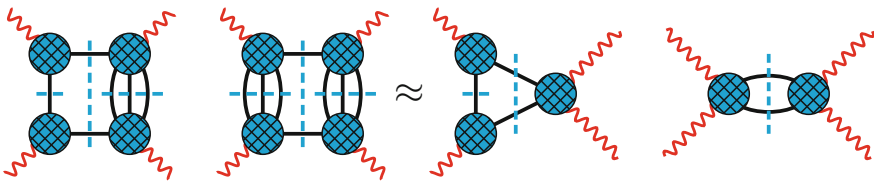


Fig. 5.71 Partial-wave approximation of multi-particle intermediate states by leading two-particle cut contributions

approximated by the two-particle intermediate states as illustrated in Fig. 5.71. In the two-to-two HLbL process we have crossing symmetric s -, t - and u -channels constrained by (see Fig. 2.5)

$$s + t + u = \sum_{i=1}^4 q_i^2 . \quad (5.292)$$

Amplitudes are related in this case to their imaginary parts by a Mandelstam representation [360, 361] of the scalar functions. One has to assume that the photon virtualities q_i^2 are fixed and small enough so that no anomalous thresholds are present (see [222]). Here it is important to remind that in the SM the four photon light-by-light scattering amplitude, due to the transversality of the external photons has an effective dimension $d(\Gamma)_{\text{eff}} = -4$ instead of 0 and thus is very well convergent. For the same reason, transversality of the photon self-energy, actually the photon propagator has $d(\Gamma)_{\text{eff}} = 0$ instead of 2. In both cases it is the Abelian gauge symmetry which makes integrals better convergent than they look like by naive power counting (see p. 65). Hence, for a generic scalar function Π_i , according to Fig. 5.70, one can write a fixed- t dispersion relation, a generalization of the DR derived in Sect. 3.7, here without any subtractions:

$$\begin{aligned} \Pi_i^t(s, t, u) &= c_i^t + \frac{\rho_{i;s}^t}{s - m_\pi^2} + \frac{\rho_{i;u}^t}{u - m_\pi^2} \\ &+ \frac{1}{\pi} \int_{4m_\pi^2}^{\infty} ds' \frac{\text{Im}_s \Pi_i^t(s', t, u')}{s' - s} + \frac{1}{\pi} \int_{4m_\pi^2}^{\infty} du' \frac{\text{Im}_u \Pi_i^t(s', t, u')}{u' - u}, \end{aligned} \quad (5.293)$$

where c_i^t is supposed to behave as $\lim_{t \rightarrow 0} c_i^t = 0$ and takes into account the t -channel pole, the s - and u - channel π^0 pole terms (all possible single particle exchanges in general), followed by s - and u -channel continuum from the two- and more-particle exchange contributions. The imaginary parts $\text{Im}_s \Pi_i$ and $\text{Im}_u \Pi_i$ are understood to be evaluated just above the corresponding cut of the s and u channels, respectively. The primed variables fulfill

$$s' + t + u' = \sum_{i=1}^4 q_i^2 \equiv \Sigma . \quad (5.294)$$

The DR (5.293) says that for any given value of t the full amplitude $\Pi_i^t(s, t, u)$ is determined for arbitrary s and u once the imaginary parts in the s -channel and the u -channel both are given. If we continue the fixed- t dispersion relation analytically in t , we have to replace the imaginary parts by the discontinuities (see Sect. 3.7), defined by

$$\begin{aligned}
D_{i;s}^t(s') &:= \frac{1}{2i} \left(\Pi_i^t(s' + i\epsilon, t, u') - \Pi_i^t(s' - i\epsilon, t, u') \right), \\
D_{i;u}^t(u') &:= \frac{1}{2i} \left(\Pi_i^t(s', t, u' + i\epsilon) - \Pi_i^t(s', t, u' - i\epsilon) \right),
\end{aligned} \tag{5.295}$$

hence

$$\begin{aligned}
\Pi_i^t(s, t, u) &= c_i^t + \frac{\rho_{i;s}^t}{s - m_\pi^2} + \frac{\rho_{i;u}^t}{u - m_\pi^2} \\
&\quad + \frac{1}{\pi} \int_{4m_\pi^2}^\infty ds' \frac{D_{i;s}^t(s')}{s' - s} + \frac{1}{\pi} \int_{4m_\pi^2}^\infty du' \frac{D_{i;u}^t(u')}{u' - u}.
\end{aligned} \tag{5.296}$$

Both the discontinuities as well as the pole residues are determined by s - or u -channel unitarity, which also defines their analytic continuation in t . While $\rho_{i;s,u}^t$ are due to a one-pion intermediate state, $D_{i;s,u}^t$ are due to multi-particle intermediate states, see Fig. 5.70.

Given the experience with estimating various contributions as discussed in previous sections, one may limit the further analysis in a first step to two-pion intermediate states and neglect the contribution of heavier intermediate states to the discontinuities. The leading one- and two-pion contributions are represented by the first diagram of Fig. 5.70 and the last of Fig. 5.71. As we know the leading contribution is expected to come from the pion-exchange. The contribution to the four photon tensor is given by (5.165), its one-pion cut by (5.169). These confront with the CHPS analysis: the pion-pole contribution in the dispersive approach is obtained by analyzing the unitarity relation of the S -matrix element for $\gamma\gamma \rightarrow \text{hadrons} \rightarrow \gamma\gamma$:

$$\begin{aligned}
\text{Im}_s \left(e^4 (2\pi)^4 \delta^{(4)}(q_1 + q_2 + q_3 - q_4) H_{\lambda_1 \lambda_2, \lambda_3 \lambda_4} \right) &= \sum_n \frac{1}{2S_n} \left(\prod_{i=1}^n \int d\mu(p_i) \right) \\
&\quad \times \langle \gamma^*(-q_3, \lambda_3) \gamma^*(q_4, \lambda_4) | n; \{p_i\} \rangle^* \langle \gamma^*(q_1, \lambda_1) \gamma^*(q_2, \lambda_2) | n; \{p_i\} \rangle,
\end{aligned} \tag{5.297}$$

where S_n is the symmetry factor of the intermediate state $|n\rangle$ and $d\mu(p_i) \equiv \frac{d^3 p_i}{2\omega_p (2\pi)^3}$ the invariant phase space element of particle i . Notice that $e^4 H_{\lambda_1 \lambda_2, \lambda_3 \lambda_4}$ is the T -matrix element according to (2.103) with

$$H_{\lambda_1 \lambda_2, \lambda_3 \lambda_4} = \epsilon_\mu^{\lambda_1}(q_1) \epsilon_\nu^{\lambda_2}(q_2) \epsilon_\lambda^{\lambda_3*}(-q_3) \epsilon_\sigma^{\lambda_4*}(k) \Pi^{\mu\nu\lambda\sigma}(q_1, q_2, q_3). \tag{5.298}$$

We consider now only the π^0 intermediate state in the sum:

$$\begin{aligned}
& \text{Im } \pi_s \left(e^4 (2\pi)^4 \delta^{(4)}(q_1 + q_2 + q_3 - q_4) H_{\lambda_1 \lambda_2, \lambda_3 \lambda_4} \right) \\
&= \frac{1}{2} \int d\mu(p) \langle \gamma^*(-q_3, \lambda_3) \gamma^*(q_4, \lambda_4) | \pi^0(p) \rangle^* \langle \gamma^*(q_1, \lambda_1) \gamma^*(q_2, \lambda_2) | \pi^0(p) \rangle.
\end{aligned} \tag{5.299}$$

After reducing the matrix elements and using the definition (5.163) of the pion TFF one obtains

$$\begin{aligned}
\text{Im } \pi_s \Pi^{\mu\nu\lambda\sigma} &= -\frac{1}{2} \int d\mu(p) (2\pi)^4 \delta^{(4)}(q_1 + q_2 - p) \epsilon^{\mu\nu\alpha\beta} \epsilon^{\lambda\sigma\gamma\delta} q_{1\alpha} q_{2\beta} q_{3\gamma} q_{4\delta} \\
&\quad \times \mathcal{F}_{\pi^0 \gamma^* \gamma^*}(q_1^2, q_2^2) \mathcal{F}_{\pi^0 \gamma^* \gamma^*}(q_3^2, q_4^2) \\
&= -\pi \delta(s - m_\pi^2) \epsilon^{\mu\nu\alpha\beta} \epsilon^{\lambda\sigma\gamma\delta} q_{1\alpha} q_{2\beta} q_{3\gamma} q_{4\delta} \mathcal{F}_{\pi^0 \gamma^* \gamma^*}(q_1^2, q_2^2) \mathcal{F}_{\pi^0 \gamma^* \gamma^*}(q_3^2, q_4^2).
\end{aligned} \tag{5.300}$$

By projecting onto the scalar functions Π_i , this leads to

$$\rho_{i;s}^t = \begin{cases} \mathcal{F}_{\pi^0 \gamma^* \gamma^*}(q_1^2, q_2^2) \mathcal{F}_{\pi^0 \gamma^* \gamma^*}(q_3^2, q_4^2) & i = 1, \\ 0 & i \neq 1, \end{cases} \tag{5.301}$$

and, analogously,

$$\rho_{i;u}^t = \begin{cases} \mathcal{F}_{\pi^0 \gamma^* \gamma^*}(q_1^2, q_4^2) \mathcal{F}_{\pi^0 \gamma^* \gamma^*}(q_2^2, q_3^2) & i = 3, \\ 0 & i \neq 3. \end{cases} \tag{5.302}$$

Pion-Pole Contribution

The total pion-pole contribution is given by

$$\Pi_i^{\pi^0\text{-pole}}(s, t, u) = \frac{\rho_{i;s}}{s - m_\pi^2} + \frac{\rho_{i;t}}{t - m_\pi^2} + \frac{\rho_{i;u}}{u - m_\pi^2}, \tag{5.303}$$

where the pole residues are products of pion TFFs $\rho_{i;s} = \rho_{i;s}^t$ (5.301) etc. This is the contribution represented by our Figs. 5.49(1st), 5.55a and 5.56, respectively. What is new is the way the hadronic $\pi^0 \rightarrow \gamma\gamma$ form factors will be determined from experimental data. With (5.303) and using the master formula (5.290), we recover the well-known result for the pion-pole contribution (5.172) derived in [234, 275]:

$$\begin{aligned}
a_\mu^{\pi^0\text{-pole}} &= \frac{2\alpha^3}{3\pi^2} \int_0^\infty dQ_1 dQ_2 \int_{-1}^1 d\tau \sqrt{1 - \tau^2} Q_1^3 Q_2^3 \\
&\quad \times \left(T_1(Q_1, Q_2, \tau) \bar{\Pi}_1^{\pi^0\text{-pole}}(Q_1, Q_2, \tau) + T_2(Q_1, Q_2, \tau) \bar{\Pi}_2^{\pi^0\text{-pole}}(Q_1, Q_2, \tau) \right),
\end{aligned} \tag{5.304}$$

with

$$\begin{aligned}\bar{\Pi}_1^{\pi^0}\text{-pole} &= -\frac{\mathcal{F}_{\pi^0\gamma^*\gamma^*}(-Q_1^2, -Q_2^2)\mathcal{F}_{\pi^0\gamma^*\gamma^*}(-Q_3^2, 0)}{Q_3^2 + m_\pi^2}, \\ \bar{\Pi}_2^{\pi^0}\text{-pole} &= -\frac{\mathcal{F}_{\pi^0\gamma^*\gamma^*}(-Q_1^2, -Q_3^2)\mathcal{F}_{\pi^0\gamma^*\gamma^*}(-Q_2^2, 0)}{Q_2^2 + m_\pi^2},\end{aligned}\tag{5.305}$$

where $Q_3^2 = Q_1^2 + 2Q_1Q_2\tau + Q_2^2$ and the integral kernels T_i coincide with the kernels I_i (5.173) in Sect. 5.2.3. This result agrees with the one of [234], which applied the pole approximation but differs from [275] in the arguments of the form factors. Possible parametrizations and available data for the pion TFF have been discussed extensively in Sect. 5.2.4. Corresponding results are listed in Table 5.13.

Pion-Box Contribution

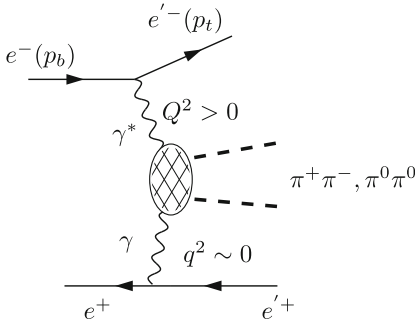
It concerns the contribution given by our Figs. 5.49 (2nd), 5.55b discussed in Sect. 5.2.8. The evaluation is based on sQED with off-shell photons dressed by the VMD pion vector form factors,⁴⁶ called FsQED by the Bern group in [222]. It is thus a Feynman diagram calculation as depicted in (5.270). What will be new is the way the effective hadronic FsQED couplings will be determined from experimental data. The latter concern the $\pi^0 \rightarrow \gamma\gamma$ as well as $\gamma\gamma \rightarrow \pi\pi$ subprocesses, direct as well as in the related crossed channels. Required is a determination of the HLbL amplitudes $\bar{\Pi}_i$, which show up in the covariant decomposition (5.287) in terms of their imaginary parts via the appropriate DRs. This is a quite elaborate task, which has been worked out in [237, 332]. Thereby, it is important to keep in mind that the tensor decomposition is not unambiguous and the individual amplitudes $\bar{\Pi}_i$ are not observables. At the end it is the projection onto an observable like a_μ , which is free from redundancies.

The dispersive representation for the pion box corresponds to the unitarity cut diagrams of Figs. 5.70 (2nd graph) and 5.71 (r.h.s.) where the cut lines are charged pions and the related physical processes are $\gamma^*\gamma^* \rightarrow \pi\pi$, which is a sub-process of

$$e^+(k_1)e^-(k_2) \rightarrow e^+(k_3)e^-(k_4)\gamma^*(q_1)\gamma^*(q_2) \rightarrow e^+(k_3)e^-(k_4)\pi^a(p_1)\pi^b(p_2),$$

where pions are on-shell in the direct and crossed channels [338, 362] (see also [244], for recent Belle data [184]). The e^+e^- -incident-based differential cross section is converted to that based on $\gamma^*\gamma$ -incident by dividing by the single-tag two-photon luminosity function $d^2L_{\gamma^*\gamma}/dWdQ^2$, which is a function of W , the c.m. energy of the incident $\gamma^*\gamma$ system, and Q^2 (see Fig. 5.72). The off-shell process

⁴⁶See Sect. 2.7 and Sect. 5.1.11.



$$\frac{d\sigma_{\gamma^*\gamma}}{d|\cos\theta^*|} = \frac{d^3\sigma_{ee}}{dWd|\cos\theta^*|dQ^2} \frac{f}{2 \frac{d^2L_{\gamma^*\gamma}}{dWdQ^2} (1+\delta)(\varepsilon/\varepsilon')\varepsilon'}.$$

The factors δ , ε , and f correspond to the radiative correction and ε' to the tagging efficiency.

Fig. 5.72 Extracting $\gamma^*\gamma \rightarrow \pi\pi$ from $e^+e^- \rightarrow e^+e^-\gamma^*\gamma \rightarrow e^+e^-\pi\pi$ in a single tag experiment like Belle [184]. Denoted by θ^* is the production angle of one of the π 's

$$\gamma^*(q_1, \lambda_1) \gamma^*(q_2, \lambda_2) \rightarrow \pi^a(p_1) \pi^b(p_2), \quad (5.306)$$

where $\lambda_{1,2}$ denote the helicities of the off-shell photons, is related to the tensor $W_{\mu\nu}^{ab}$ defined as the QCD matrix element

$$W_{ab}^{\mu\nu}(p_1, p_2, q_1) = i \int d^4x e^{-iq_1 \cdot x} \langle \pi^a(p_1) \pi^b(p_2) | T \{ j_{em}^{\mu had}(x) j_{em}^{\nu had}(0) \} | 0 \rangle. \quad (5.307)$$

With appropriate off-shell polarization vectors one may perform an off-shell LSZ reduction and define the connected part matrix element

$$\begin{aligned} & \langle \pi^a(p_1) \pi^b(p_2) | \gamma^*(q_1, \lambda_1) \gamma^*(q_2, \lambda_2) \rangle \\ &= ie^2 (2\pi)^4 \delta^{(4)}(p_1 + p_2 - q_1 - q_2) \epsilon_\mu^{\lambda_1}(q_1) \epsilon_\nu^{\lambda_2}(q_2) W_{ab}^{\mu\nu}(p_1, p_2, q_1). \end{aligned} \quad (5.308)$$

The helicity amplitudes are given by the contraction with polarization vectors as usual:

$$\epsilon_\mu^{\lambda_1}(q_1) \epsilon_\nu^{\lambda_2}(q_2) W_{ab}^{\mu\nu}(p_1, p_2, q_1) = e^{i(\lambda_1 - \lambda_2)\phi} H_{\lambda_1 \lambda_2}^{ab}, \quad (5.309)$$

with ϕ a free phase.

The unitarity relation exhibiting two-pion intermediate states reads

$$\begin{aligned} \text{Im}_s^{\pi\pi} \left(e^4 (2\pi)^4 \delta^{(4)}(q_1 + q_2 + q_3 - q_4) H_{\lambda_1 \lambda_2, \lambda_3 \lambda_4} \right) &= \frac{1}{2} \int d\mu(p_1) d\mu(p_2) \times \\ &\left[\langle \pi^+(p_1) \pi^-(p_2) | \gamma^*(-q_3, \lambda_3) \gamma^*(q_4, \lambda_4) \rangle^* \langle \pi^+(p_1) \pi^-(p_2) | \gamma^*(q_1, \lambda_1) \gamma^*(q_2, \lambda_2) \rangle \right. \\ &\left. + \frac{1}{2} \langle \pi^0(p_1) \pi^0(p_2) | \gamma^*(-q_3, \lambda_3) \gamma^*(q_4, \lambda_4) \rangle^* \langle \pi^0(p_1) \pi^0(p_2) | \gamma^*(q_1, \lambda_1) \gamma^*(q_2, \lambda_2) \rangle \right], \end{aligned} \quad (5.310)$$

and for the corresponding LbL four-tensor takes the form

$$\begin{aligned} \text{Im}_s^{\pi\pi} \Pi^{\mu\nu\lambda\sigma} &= \frac{1}{32\pi^2} \frac{\beta_\pi(s)}{2} \int d\Omega_s'' \left(W_{+-}^{\mu\nu}(p_1, p_2, q_1) W_{+-}^{\lambda\sigma*}(p_1, p_2, -q_3) \right. \\ &\left. + \frac{1}{2} W_{00}^{\mu\nu}(p_1, p_2, q_1) W_{00}^{\lambda\sigma*}(p_1, p_2, -q_3) \right), \end{aligned} \quad (5.311)$$

where the subscripts $\{+-, 00\}$ denote the pion charges and $\beta_\pi(s)$ is the pion velocity. This provides the basic s channel unitarity relation, which can be related to the $\gamma\gamma \rightarrow \pi\pi$ cross-sections. For details I refer to [237].

The off-shell photons have attached pion vector form factors [237]. Due to the high degree of crossing symmetry, this pion-box contribution can be expressed in terms of either fixed- s , $-t$, or $-u$ dispersion relations, or in a symmetrized form

$$\begin{aligned} \Pi_i^{\pi\text{-box}}(s, t, u) &= \frac{1}{3} \left[\frac{1}{\pi} \int_{4m_\pi^2}^{\infty} dt' \frac{\text{Im} \Pi_i^{\pi\text{-box}}(s, t', u')}{t' - t} \right. \\ &\left. + \frac{1}{\pi} \int_{4m_\pi^2}^{\infty} du' \frac{\text{Im} \Pi_i^{\pi\text{-box}}(s, t', u')}{u' - u} + \text{fixed-}t + \text{fixed-}u \right]. \end{aligned} \quad (5.312)$$

The relevant imaginary parts are obtained via a helicity state and partial-wave decomposition of the $\gamma\gamma \rightarrow \pi^+\pi^-$ data [237, 332]. The pion-box contribution to a_μ is given by

$$\begin{aligned} a_\mu^{\pi\text{-box}} &= a_\mu^{\text{FsQED}} = \frac{2\alpha^3}{3\pi^2} \int_0^\infty dQ_1 dQ_2 \int_{-1}^1 d\tau \sqrt{1-\tau^2} Q_1^3 Q_2^3 \times \\ &F_\pi^V(-Q_1^2) F_\pi^V(-Q_2^2) F_\pi^V(-Q_3^2) \times \sum_{i=1}^{12} T_i(Q_1, Q_2, \tau) \bar{\Pi}_i^{\text{sQED}}(Q_1, Q_2, \tau), \end{aligned} \quad (5.313)$$

where the functions $\bar{\Pi}_i$ are defined in (5.316). They are linear combinations of the scalar functions Π_i in the limit $k \rightarrow 0$.

The calculation of the off-shell sQED loop contribution includes the six box diagrams, twelve triangles, and three bulb diagrams of (5.270) yields

$$a_\mu^{\pi\text{box}} = -15.9 \times 10^{-11}$$

using a form factor $F_{\pi}^V(-Q^2)$ fitted to the available data. Adopting a VMD form factor the result is $a_{\mu}^{\pi\text{-box VMD}} = -16.4 \times 10^{-11}$. Including $\pi\pi$ rescattering effects in the $\gamma^*\gamma^* \rightarrow \pi^+\pi^-$ partial-wave analysis, which also includes the $f_0(500)$ scalar meson, the result obtained in [332] reads

$$a_{\mu}^{\pi\text{-box}} + a_{\mu, J=0}^{\pi\pi, \pi\text{-pole LHC}} = -24(1) \times 10^{-11}. \quad (5.314)$$

The results is in good agreement with other [236] recent estimates like (5.273), which however does not include a scalar contribution. This new result is considered to be more reliable as it is based on data directly. It also has a substantially smaller error.

The results have been briefly discussed within the context of other results at the end of Sect. 5.2.8. To fully exploit the sophisticated machinery developed we have to motivate experimenters to provide the data which enter the dispersion relations which are needed here [344, 350, 351]. Data are available as plotted in Figs. 5.58, 5.59 and 5.38. For $\gamma\gamma^* \rightarrow \pi^0, \eta, \eta'$ data see [256, 257, 268, 269, 272]. Related form factor theory considerations may be found in [258–267]. Experimental spectra of $\gamma\gamma^* \rightarrow \pi\pi$ are available from [178–183] at present. For theoretical studies and data analyzes I refer to [185–189]. One also has to be aware that better radiative correction calculations are mandatory for the reliable extraction of $\gamma^*\gamma^* \rightarrow$ hadrons data from $e^+e^- \rightarrow e^+e^-$ hadrons or related processes in crossed channels.

Appendix: Amplitudes and Integration Kernels for the General HLbL Tensor Structures

The structures collected here are needed for any calculation which goes beyond the one-particle exchange approximations, which are very much simpler and have been given above. As they represent the general $g - 2$ setup, I think it is useful the present them here for completeness. The somewhat lengthy formulas, which only represent the frame for the missing “picture”, which is the non-perturbative hadronic four-current “blob”, illustrate well the kinematic complexity of the HLbL issue.

The BTT extended covariant decomposition of the HLbL tensor (5.287) is based on the tensor coefficients [237]

$$\begin{aligned} T_1^{\mu\nu\lambda\sigma} &= \epsilon^{\mu\nu\alpha\beta} \epsilon^{\lambda\sigma\gamma\delta} q_{1\alpha} q_{2\beta} q_{3\gamma} q_{4\delta}, \\ T_4^{\mu\nu\lambda\sigma} &= (q_2^\mu q_1^\nu - q_1 \cdot q_2 g^{\mu\nu}) (q_4^\lambda q_3^\sigma - q_3 \cdot q_4 g^{\lambda\sigma}), \\ T_7^{\mu\nu\lambda\sigma} &= (q_2^\mu q_1^\nu - q_1 \cdot q_2 g^{\mu\nu}) (q_1 \cdot q_4 (q_1^\lambda q_3^\sigma - q_1 \cdot q_3 g^{\lambda\sigma}) + q_4^\lambda q_1^\sigma q_1 \cdot q_3 - q_1^\lambda q_1^\sigma q_3 \cdot q_4), \\ T_{19}^{\mu\nu\lambda\sigma} &= (q_2^\mu q_1^\nu - q_1 \cdot q_2 g^{\mu\nu}) (q_2 \cdot q_4 (q_1^\lambda q_3^\sigma - q_1 \cdot q_3 g^{\lambda\sigma}) + q_4^\lambda q_2^\sigma q_1 \cdot q_3 - q_1^\lambda q_2^\sigma q_3 \cdot q_4), \\ T_{31}^{\mu\nu\lambda\sigma} &= (q_2^\mu q_1^\nu - q_1 \cdot q_2 g^{\mu\nu}) (q_2^\lambda q_1 \cdot q_3 - q_1^\lambda q_2 \cdot q_3) (q_2^\sigma q_1 \cdot q_4 - q_1^\sigma q_2 \cdot q_4), \\ T_{37}^{\mu\nu\lambda\sigma} &= (q_3^\mu q_1 \cdot q_4 - q_4^\mu q_1 \cdot q_3) (q_3^\nu q_4^\lambda q_2^\sigma - q_4^\nu q_2^\lambda q_3^\sigma + g^{\lambda\sigma} (q_4^\nu q_2 \cdot q_3 - q_3^\nu q_2 \cdot q_4) \\ &\quad + g^{\nu\sigma} (q_2^\lambda q_3 \cdot q_4 - q_4^\lambda q_2 \cdot q_3) + g^{\lambda\nu} (q_3^\sigma q_2 \cdot q_4 - q_2^\sigma q_3 \cdot q_4)), \\ T_{49}^{\mu\nu\lambda\sigma} &= q_3^\sigma (q_1 \cdot q_3 q_2 \cdot q_4 q_4^\mu g^{\lambda\nu} - q_2 \cdot q_3 q_1 \cdot q_4 q_4^\nu g^{\lambda\mu} + q_4^\mu q_4^\nu (q_1^\lambda q_2 \cdot q_3 - q_2^\lambda q_1 \cdot q_3) \\ &\quad + q_1 \cdot q_4 q_3^\mu q_4^\nu q_2^\lambda - q_2 \cdot q_4 q_4^\mu q_3^\nu q_1^\lambda + q_1 \cdot q_4 q_2 \cdot q_4 (q_3^\nu g^{\lambda\mu} - q_3^\mu g^{\lambda\nu})) \\ &\quad - q_4^\lambda (q_1 \cdot q_4 q_2 \cdot q_3 q_3^\mu g^{\nu\sigma} - q_2 \cdot q_4 q_1 \cdot q_3 q_3^\nu g^{\mu\sigma} + q_3^\mu q_3^\nu (q_1^\sigma q_2 \cdot q_4 - q_2^\sigma q_1 \cdot q_4)) \end{aligned}$$

$$\begin{aligned}
& + q_1 \cdot q_3 q_4^\mu q_3^\nu q_2^\sigma - q_2 \cdot q_3 q_3^\mu q_4^\nu q_1^\sigma + q_1 \cdot q_3 q_2 \cdot q_3 \left(q_4^\nu g^{\mu\sigma} - q_4^\mu g^{\nu\sigma} \right) \\
& + q_3 \cdot q_4 \left(\left(q_1^\lambda q_4^\mu - q_1 \cdot q_4 g^{\lambda\mu} \right) \left(q_3^\nu q_2^\sigma - q_2 \cdot q_3 g^{\nu\sigma} \right) \right. \\
& \quad \left. - \left(q_2^\lambda q_4^\nu - q_2 \cdot q_4 g^{\lambda\nu} \right) \left(q_3^\mu q_1^\sigma - q_1 \cdot q_3 g^{\mu\sigma} \right) \right). \tag{5.315}
\end{aligned}$$

These structures satisfy the required crossing symmetries and all the remaining structures are just crossed versions of the above seven ones.

The hadronic scalar functions $\bar{\Pi}_i$, which appear in the $g - 2$ master integral formula (5.290), are linear combinations of the Π_i 's in (5.315) defined by [237]

$$\begin{aligned}
\bar{\Pi}_1 &= \Pi_1 + q_1 \cdot q_2 \Pi_{47}, \\
\bar{\Pi}_2 &= \Pi_2 - \frac{1}{2} \left(q_1^2 + q_1 \cdot q_2 \right) \left(2\Pi_{47} - \Pi_{50} - \Pi_{51} - \Pi_{54} \right), \\
\bar{\Pi}_3 &= \Pi_4 + \left(q_1^2 + q_1 \cdot q_2 \right) \Pi_{19} + \left(q_1 \cdot q_2 + q_2^2 \right) \Pi_{20} \\
&\quad + \left(q_1^2 + q_1 \cdot q_2 \right) \left(q_1 \cdot q_2 + q_2^2 \right) \Pi_{31} - \frac{s}{2} \left(2\Pi_{47} - \Pi_{50} - \Pi_{51} \right) + \frac{1}{2} \left(q_1^2 - q_2^2 \right) \Pi_{54}, \\
\bar{\Pi}_4 &= \Pi_5 - q_1 \cdot q_2 \Pi_{21} + \frac{1}{2} \left(q_1 \cdot q_2 + q_2^2 \right) \left(2\Pi_{22} - 2q_1 \cdot q_2 \Pi_{33} + \Pi_{50} + \Pi_{51} - \Pi_{54} \right) - q_2^2 \Pi_{47}, \\
\bar{\Pi}_5 &= \Pi_7 - \Pi_{19} - \left(q_1 \cdot q_2 + q_2^2 \right) \Pi_{31}, \\
\bar{\Pi}_6 &= \Pi_9 - \Pi_{22} + q_1 \cdot q_2 \Pi_{33}, \\
\bar{\Pi}_7 &= \Pi_{10} - \Pi_{21} - \left(q_1 \cdot q_2 + q_2^2 \right) \Pi_{33}, \\
\bar{\Pi}_8 &= \Pi_{16} + \Pi_{47} + \Pi_{54}, \\
\bar{\Pi}_9 &= \Pi_{17} + \Pi_{47} - \Pi_{50} - \Pi_{51}, \\
\bar{\Pi}_{10} &= \frac{1}{2} \left(\Pi_{39} + \Pi_{40} + \Pi_{46} \right), \\
\bar{\Pi}_{11} &= \Pi_{42} - \Pi_{47} + \frac{1}{2} \left(\Pi_{50} + \Pi_{51} + \Pi_{54} \right), \\
\bar{\Pi}_{12} &= \frac{1}{2} \left(\Pi_{50} - \Pi_{51} + \Pi_{54} \right). \tag{5.316}
\end{aligned}$$

As in the pion exchange case Sect. 5.2.3 one can reduce the general eight-dimensional integral to a three-dimensional representation by averaging over the directions of the muon momentum (5.170).

For the tensors (5.315) the following kernels are obtained [237]:

$$\begin{aligned}
T_1 &= \frac{Q_1^2 \tau (R_{m1} - 1) (R_{m1} + 5) + Q_2^2 \tau (R_{m2} - 1) (R_{m2} + 5) + 4Q_1 Q_2 (R_{m1} + R_{m2} - 2) - 8\tau m^2}{2Q_1 Q_2 Q_3^2 m^2} \\
&\quad + X \left(\frac{8(\tau^2 - 1)}{Q_3^2} - \frac{4}{m^2} \right), \\
T_2 &= \frac{Q_1 (R_{m1} - 1) \left(Q_1 \tau (R_{m1} + 1) + 4Q_2 (\tau^2 - 1) \right) - 4\tau m^2}{Q_1 Q_2 Q_3^2 m^2} + X \frac{8(\tau^2 - 1) (2m^2 - Q_2^2)}{Q_3^2 m^2},
\end{aligned}$$

$$\begin{aligned}
T_3 &= \frac{1}{Q_3^2} \left(-\frac{2(R_{m1} + R_{m2} - 2)}{m^2} - \frac{Q_1 \tau (R_{m1} - 1)(R_{m1} + 7)}{2Q_2 m^2} + \frac{8\tau}{Q_1 Q_2} \right. \\
&\quad \left. - \frac{Q_2 \tau (R_{m2} - 1)(R_{m2} + 7)}{2Q_1 m^2} + \frac{Q_1^2 (1 - R_{m1})}{Q_2^2 m^2} + \frac{Q_2^2 (1 - R_{m2})}{Q_1^2 m^2} + \frac{2}{Q_1^2} + \frac{2}{Q_2^2} \right) \\
&\quad + X \left(\frac{4}{m^2} - \frac{8\tau}{Q_1 Q_2} \right), \\
T_4 &= \frac{1}{Q_3^2} \left(\frac{4(\tau^2 (R_{m1} - 1) + R_{m2} - 1)}{m^2} - \frac{Q_1 \tau (R_{m1} - 5)(R_{m1} - 1)}{Q_2 m^2} + \frac{4\tau}{Q_1 Q_2} \right. \\
&\quad \left. - \frac{Q_2 \tau (R_{m2} - 3)(R_{m2} - 1)}{Q_1 m^2} + \frac{2Q_2^2 (R_{m2} - 1)}{Q_1^2 m^2} - \frac{4}{Q_1^2} \right. \\
&\quad \left. + X \left(-\frac{8Q_2^2 \tau^2}{m^2} - \frac{16Q_2 Q_1 \tau}{m^2} - \frac{8Q_1^2}{m^2} + \frac{16Q_2 \tau}{Q_1} + 16 \right) \right), \\
T_5 &= \frac{1}{Q_3^2} \left(Q_1^2 \left(\frac{\tau^2 (R_{m1} - 1)(R_{m1} + 3) + 4(R_{m1} + R_{m2} - 2)}{2m^2} - \frac{4}{Q_2^2} \right) - \frac{Q_2^2 \tau^2 (R_{m2} - 5)(R_{m2} - 1)}{2m^2} \right. \\
&\quad \left. + \frac{Q_1^3 \tau (R_{m1} - 1)(R_{m1} + 5)}{Q_2 m^2} + Q_1 \left(\frac{Q_2 \tau (R_{m1} + 5R_{m2} - 6)}{m^2} - \frac{12\tau}{Q_2} \right) + \frac{2Q_1^4 (R_{m1} - 1)}{Q_2^2 m^2} \right. \\
&\quad \left. - 4\tau^2 + X \left(Q_1 \left(8Q_2 (\tau^3 + \tau) - \frac{2Q_2^3 \tau}{m^2} \right) + Q_1^2 \left(32\tau^2 - \frac{4Q_2^2 (\tau^2 + 1)}{m^2} \right) \right. \right. \\
&\quad \left. \left. + Q_1^3 \left(\frac{16\tau}{Q_2} - \frac{10Q_2 \tau}{m^2} \right) - \frac{4Q_1^4}{m^2} \right) \right), \\
T_6 &= \frac{1}{Q_3^2} \left(\frac{Q_1^2 (\tau^2 ((R_{m1} - 22) R_{m1} - 8R_{m2} + 29) + 2(-5R_{m1} + R_{m2} + 4))}{2m^2} \right. \\
&\quad \left. + Q_1 \left(\frac{Q_2 \tau (2\tau^2 ((R_{m2} - 3)^2 - 4R_{m1}) - 26R_{m1} + R_{m2} (R_{m2} - 12) + 37)}{2m^2} - \frac{4\tau}{Q_2} \right) \right. \\
&\quad \left. + \frac{Q_2^2 (\tau^2 (-8R_{m1} + R_{m2} (5R_{m2} - 26) + 29) - 4(R_{m1} + 2R_{m2} - 3))}{2m^2} + \frac{Q_1^3 \tau (R_{m1} - 9)(R_{m1} - 1)}{2Q_2 m^2} \right. \\
&\quad \left. + \frac{Q_2^3 \tau (R_{m2} - 9)(R_{m2} - 1)}{Q_1 m^2} + \frac{8Q_2 \tau}{Q_1} + \frac{2Q_2^4 (1 - R_{m2})}{Q_1^2 m^2} + \frac{4Q_2^2}{Q_1^2} \right. \\
&\quad \left. + X \left(\frac{Q_2 Q_1^3 (8\tau^3 + 22\tau)}{m^2} + \frac{Q_1^4 (8\tau^2 - 2)}{m^2} + Q_1^2 \left(\frac{Q_2^2 (36\tau^2 + 18)}{m^2} - 8(\tau^2 + 1) \right) \right. \right. \\
&\quad \left. \left. + \frac{Q_2^4 (8\tau^2 + 4)}{m^2} + Q_1 \left(\frac{Q_2^3 (8\tau^3 + 34\tau)}{m^2} - 8Q_2 \tau (\tau^2 + 5) \right) \right. \right. \\
&\quad \left. \left. - 16Q_2^2 (2\tau^2 + 1) - \frac{16Q_2^3 \tau}{Q_1} \right) \right), \\
T_7 &= \frac{1}{Q_3^2} \left(\frac{Q_1^2 (2(R_{m1} + R_{m2} - 2) - \tau^2 ((R_{m1} + 10) R_{m1} + 8R_{m2} - 19))}{2m^2} \right. \\
&\quad \left. + Q_1 \left(\frac{Q_2 \tau (2\tau^2 (R_{m2} - 5)(R_{m2} - 1) - 2R_{m1} + R_{m2} (R_{m2} + 4) - 3)}{2m^2} - \frac{4\tau}{Q_2} \right) \right. \\
&\quad \left. + \frac{Q_2^2 \tau^2 (R_{m2} - 5)(R_{m2} - 1)}{2m^2} + \frac{Q_1^3 \tau (R_{m1} - 9)(R_{m1} - 1)}{2Q_2 m^2} + 4\tau^2 \right. \\
&\quad \left. + X \left(\frac{Q_2 Q_1^3 (8\tau^3 + 6\tau)}{m^2} + Q_1 \left(\frac{2Q_2^3 \tau}{m^2} - 8Q_2 (\tau^3 + \tau) \right) \right) \right)
\end{aligned}$$

$$\begin{aligned}
& + \frac{Q_1^4 (8\tau^2 - 2)}{m^2} + Q_1^2 \left(\frac{2Q_2^2 (6\tau^2 - 1)}{m^2} - 8(\tau^2 + 1) \right) \Big), \\
T_8 = & \frac{1}{Q_3^2} \left(Q_1^2 \left(\frac{4}{Q_2^2} - \frac{2(2\tau^2 + 1)(R_{m1} + R_{m2} - 2)}{m^2} \right) + Q_1 \left(\frac{4\tau}{Q_2} - \frac{4Q_2\tau(\tau^2 + 1)(R_{m2} - 1)}{m^2} \right) \right. \\
& - \frac{6Q_1^3\tau(R_{m1} - 1)}{Q_2m^2} + \frac{Q_1^4(2 - 2R_{m1})}{Q_2^2m^2} \\
& \left. + X \left(\frac{Q_1^4(8\tau^2 + 4)}{m^2} + Q_1^3 \left(\frac{8Q_2\tau(\tau^2 + 2)}{m^2} - \frac{16\tau}{Q_2} \right) + Q_1^2 \left(\frac{Q_2^2(8\tau^2 + 4)}{m^2} - 16\tau^2 \right) \right) \right), \\
T_9 = & Q_3^2 \left(\frac{R_{m1} - 1}{Q_2^2m^2} + \frac{R_{m2} - 1}{Q_1^2m^2} - \frac{2}{Q_1^2Q_2^2} \right) + X \left(-\frac{2Q_3^2}{m^2} + \frac{8Q_2\tau}{Q_1} + \frac{8Q_1\tau}{Q_2} + 8(\tau^2 + 1) \right), \\
T_{10} = & \frac{1}{Q_3^2} \left(-\frac{Q_1^2(\tau^2(R_{m1} - 1)(R_{m1} + 3) + 2(R_{m1} + R_{m2} - 2))}{m^2} - \frac{Q_2^3\tau(R_{m2} - 1)(R_{m2} + 3)}{Q_1m^2} \right. \\
& - \frac{Q_2^2(\tau^2(R_{m2} - 1)(R_{m2} + 3) + 2(R_{m1} + R_{m2} - 2))}{m^2} - \frac{Q_1^3\tau(R_{m1} - 1)(R_{m1} + 3)}{Q_2m^2} \\
& + Q_1 \left(\frac{8\tau}{Q_2} - \frac{Q_2\tau((R_{m1} + 4)R_{m1} + R_{m2}(R_{m2} + 4) - 10)}{m^2} \right) + \frac{8Q_2\tau}{Q_1} \\
& + 8\tau^2 + X \left(-16Q_1^2(\tau^2 - 1) - 16Q_2Q_1\tau(\tau^2 - 1) - 16Q_2^2(\tau^2 - 1) \right) \\
& \left. + X \left(\frac{4Q_2Q_1\tau}{m^2} + \frac{4Q_1^2}{m^2} + \frac{4Q_2^2}{m^2} \right) \right), \\
T_{11} = & \frac{1}{Q_3^2} \left(\frac{Q_1^2(\tau^2(R_{m1} - 5)(R_{m1} - 1) - 2(R_{m1} + 3R_{m2} - 4))}{m^2} \right. \\
& + \frac{Q_2^2(\tau^2((2 - 3R_{m2})R_{m2} + 1) + R_{m1} - 3R_{m2} + 2)}{m^2} - \frac{6Q_1^3\tau(R_{m1} - 1)}{Q_2m^2} \\
& + Q_1 \left(\frac{Q_2\tau((R_{m1} - 2)R_{m1} - 2R_{m2}(3R_{m2} + 8) + 23)}{2m^2} + \frac{12\tau}{Q_2} \right) - \frac{Q_2^3\tau(R_{m2} - 1)^2}{2Q_1m^2} \\
& + X \left(\frac{Q_2^2Q_1^2(8\tau^2 + 10)}{m^2} + \frac{28Q_2Q_1^3\tau}{m^2} + \frac{12Q_1^4}{m^2} - \frac{2Q_2^4}{m^2} + Q_2^2(8 - 8\tau^2) \right) + 8\tau^2 \Big), \\
T_{12} = & -\frac{Q_1\tau(R_{m1}^2 - 7)}{4Q_2m^2} + \frac{Q_2\tau(R_{m2}^2 - 7)}{4Q_1m^2} + \frac{2Q_1^2}{Q_2^2m^2} - \frac{2Q_2^2}{Q_1^2m^2} - \frac{4}{Q_1^2} + \frac{4}{Q_2^2} \\
& + \frac{1}{Q_3^2} \left(\frac{Q_2^2(4\tau^2R_{m1} + 2\tau^2R_{m2} + 3R_{m1} + R_{m2})}{2m^2} - \frac{Q_1^2(2\tau^2R_{m1} + 4\tau^2R_{m2} + R_{m1} + 3R_{m2})}{2m^2} \right. \\
& - \frac{11Q_1^3\tau R_{m1}}{2Q_2m^2} + \frac{11Q_2^3\tau R_{m2}}{2Q_1m^2} + \frac{11Q_1Q_2\tau(R_{m1} - R_{m2})}{2m^2} - \frac{2Q_1^4R_{m1}}{Q_2^2m^2} + \frac{2Q_2^4R_{m2}}{Q_1^2m^2} \\
& + X \left(\frac{Q_1^4(4\tau^2 + 3)}{m^2} - \frac{Q_2^4(4\tau^2 + 3)}{m^2} + Q_1^3 \left(\frac{14Q_2\tau}{m^2} - \frac{16\tau}{Q_2} \right) - \frac{14Q_2^3Q_1\tau}{m^2} \right. \\
& \left. - 4Q_1^2(7\tau^2 + 1) + Q_2^2(28\tau^2 + 4) + \frac{16Q_2^3\tau}{Q_1} \right) \Big), \tag{5.317}
\end{aligned}$$

where

$$\begin{aligned}
X &= \frac{1}{Q_1 Q_2 x} \arctan\left(\frac{zx}{1-z\tau}\right), \quad x = \sqrt{1-\tau^2}, \quad Q_3^2 = Q_1^2 + 2Q_1 Q_2 \tau + Q_2^2, \\
z &= \frac{Q_1 Q_2}{4m^2} (1 - R_{m1})(1 - R_{m2}), \quad R_{mi} = \sqrt{1 + \frac{4m^2}{Q_i^2}}.
\end{aligned} \tag{5.318}$$

These objects provide the integral kernel functions of the scalar HLbL amplitudes $\bar{\Pi}_i$ in the formula (5.290) (a corresponding representation for the tensors (5.149) are given in [236]). For general studies it may be useful to know the general kernels defined in (5.289). After calculating the trace and performing the contraction of the Lorentz indices one finds the following integral kernels:

$$\begin{aligned}
\hat{T}_1(q_1, q_2; p) &= -\frac{8}{3} \left((q_1 \cdot q_2)^2 - q_1^2 q_2^2 \right) m^2 - \frac{8}{3} q_2^2 (p \cdot q_1)^2 - \frac{8}{3} q_1^2 (p \cdot q_2)^2 \\
&\quad - \frac{4}{3} q_1^2 p \cdot q_2 (q_2^2 + q_1 \cdot q_2) + p \cdot q_1 \left(\frac{4}{3} (q_1^2 + q_1 \cdot q_2) q_2^2 + \frac{16}{3} p \cdot q_2 q_1 \cdot q_2 \right), \\
\hat{T}_2(q_1, q_2; p) &= -\frac{8}{3} \left((q_1 \cdot q_2)^2 - q_1^2 q_2^2 \right) m^2 - \frac{8}{3} q_1^2 (p \cdot q_2)^2 + p \cdot q_1 \left(\frac{8}{3} p \cdot q_2 q_1 \cdot q_2 - \frac{4}{3} q_2^2 q_1 \cdot q_2 \right) \\
&\quad + p \cdot q_2 \left(4q_1^2 q_2^2 - \frac{8}{3} (q_1 \cdot q_2)^2 \right), \\
\hat{T}_3(q_1, q_2; p) &= -\frac{8}{3} \left((q_1 \cdot q_2)^2 - q_1^2 q_2^2 \right) m^2 - \frac{8}{3} q_2^2 (p \cdot q_1)^2 + \frac{4}{3} q_1^2 p \cdot q_2 q_1 \cdot q_2 \\
&\quad + p \cdot q_1 \left(-4q_1^2 q_2^2 + \frac{8}{3} (q_1 \cdot q_2)^2 + \frac{8}{3} p \cdot q_2 q_1 \cdot q_2 \right), \\
\hat{T}_4(q_1, q_2; p) &= \frac{8}{3} q_1 \cdot q_2 (q_1^2 + q_2^2 + 2q_1 \cdot q_2) m^2 + \frac{8}{3} q_2^2 (p \cdot q_1)^2 + \frac{8}{3} q_1^2 (p \cdot q_2)^2 \\
&\quad - \frac{8}{3} p \cdot q_1 p \cdot q_2 (q_1^2 + q_2^2 + 4q_1 \cdot q_2), \\
\hat{T}_5(q_1, q_2; p) &= \frac{8}{3} (p \cdot q_1)^2 q_2^2 - \frac{8}{3} m^2 (q_1^2 + q_1 \cdot q_2) q_2^2 + \frac{8}{3} q_1^2 (p \cdot q_2)^2 - \frac{4}{3} p \cdot q_2 q_1 \cdot q_2 (3q_1^2 + 2q_1 \cdot q_2) \\
&\quad + p \cdot q_1 \left(\frac{4}{3} q_2^2 (3q_1^2 + 2q_1 \cdot q_2) - \frac{8}{3} p \cdot q_2 (q_1 \cdot q_2 - q_2^2) \right), \\
\hat{T}_6(q_1, q_2; p) &= \frac{8}{3} (p \cdot q_2)^2 q_1^2 - \frac{8}{3} m^2 (q_2^2 + q_1 \cdot q_2) q_1^2 - \frac{4}{3} p \cdot q_2 (3q_2^2 + 2q_1 \cdot q_2) q_1^2 \\
&\quad + \frac{8}{3} q_2^2 (p \cdot q_1)^2 + p \cdot q_1 \left(\frac{8}{3} p \cdot q_2 (q_1^2 - q_1 \cdot q_2) + \frac{4}{3} q_1 \cdot q_2 (3q_2^2 + 2q_1 \cdot q_2) \right), \\
\hat{T}_7(q_1, q_2; p) &= \frac{4}{3} q_1 \cdot q_2 (2q_1^4 + (q_2^2 + 4q_1 \cdot q_2) q_1^2 + (q_1 \cdot q_2)^2) m^2 - \frac{4}{3} q_2^2 (p \cdot q_1)^2 q_1 \cdot q_2 \\
&\quad + \frac{4}{3} q_1^2 (p \cdot q_2)^2 (2q_1^2 + q_1 \cdot q_2) - \frac{8}{3} p \cdot q_1 p \cdot q_2 (q_1^4 + 3q_1 \cdot q_2 q_1^2 + (q_1 \cdot q_2)^2), \\
\hat{T}_8(q_1, q_2; p) &= \frac{4}{3} q_1 \cdot q_2 (2q_2^4 + (q_1^2 + 4q_1 \cdot q_2) q_2^2 + (q_1 \cdot q_2)^2) m^2 - \frac{4}{3} q_1^2 (p \cdot q_2)^2 q_1 \cdot q_2 \\
&\quad + \frac{4}{3} q_2^2 (p \cdot q_1)^2 (2q_2^2 + q_1 \cdot q_2) - \frac{8}{3} p \cdot q_1 p \cdot q_2 (q_2^4 + 3q_1 \cdot q_2 q_2^2 + (q_1 \cdot q_2)^2), \\
\hat{T}_9(q_1, q_2; p) &= -\frac{4}{3} (q_1^2 + q_1 \cdot q_2) (2q_2^4 + (q_1^2 + 4q_1 \cdot q_2) q_2^2 + (q_1 \cdot q_2)^2) m^2 \\
&\quad + \frac{4}{3} q_1^2 (p \cdot q_2)^2 (q_1^2 + q_1 \cdot q_2) - \frac{4}{3} p \cdot q_2 (q_1^2 + q_1 \cdot q_2) (q_2^2 + q_1 \cdot q_2) (3q_1^2 + 2q_1 \cdot q_2) \\
&\quad + \frac{4}{3} (p \cdot q_1)^2 (2q_2^4 + (q_1^2 + 5q_1 \cdot q_2) q_2^2 + 2(q_1 \cdot q_2)^2) \\
&\quad + p \cdot q_1 \left(\frac{4}{3} (3q_1^2 + 2q_1 \cdot q_2) (q_2^2 + q_1 \cdot q_2)^2 + \frac{8}{3} p \cdot q_2 (q_2^2 (q_2^2 + 2q_1 \cdot q_2) - q_1^2 q_1 \cdot q_2) \right), \\
\hat{T}_{10}(q_1, q_2; p) &= -\frac{4}{3} (q_1^2 + q_1 \cdot q_2) (q_1^2 q_2^2 + (q_1 \cdot q_2)^2) m^2 + \frac{4}{3} q_1^2 (p \cdot q_2)^2 (q_1^2 - q_1 \cdot q_2)
\end{aligned}$$

$$\begin{aligned}
& -\frac{4}{3}q_1^2 p \cdot q_2 q_1 \cdot q_2 (3q_1^2 + 2q_1 \cdot q_2) + \frac{4}{3}(p \cdot q_1)^2 \left((q_1^2 + q_1 \cdot q_2) q_2^2 + 2(q_1 \cdot q_2)^2 \right) \\
& + p \cdot q_1 \left(\frac{4}{3} (3q_1^2 + 2q_1 \cdot q_2) (q_1 \cdot q_2)^2 + \frac{8}{3} p \cdot q_2 (q_1 \cdot q_2 - q_1^2) q_1 \cdot q_2 \right), \\
\hat{T}_{11}(q_1, q_2; p) &= -\frac{8}{3}m^2 q_1 \cdot q_2 (q_1^2 + q_1 \cdot q_2) q_1^2 - \frac{4}{3}p \cdot q_2 \left((q_2^2 + 2q_1 \cdot q_2) q_1^2 + 2(q_1 \cdot q_2)^2 \right) q_1^2 \\
& + p \cdot q_1 \left(\frac{8}{3} p \cdot q_2 (q_1^2 + q_1 \cdot q_2) q_1^2 + \frac{4}{3} q_1 \cdot q_2 \left((q_2^2 + 2q_1 \cdot q_2) q_1^2 + 2(q_1 \cdot q_2)^2 \right) \right), \\
\hat{T}_{12}(q_1, q_2; p) &= -\frac{4}{3} (q_2^2 + q_1 \cdot q_2) (2q_1^4 + (q_2^2 + 4q_1 \cdot q_2) q_1^2 + (q_1 \cdot q_2)^2) m^2 \\
& + \frac{4}{3} q_2^2 (p \cdot q_1)^2 (q_2^2 + q_1 \cdot q_2) - \frac{4}{3} p \cdot q_2 (q_1^2 + q_1 \cdot q_2)^2 (3q_2^2 + 2q_1 \cdot q_2) \\
& + \frac{4}{3} (p \cdot q_2)^2 (2q_1^4 + (q_2^2 + 5q_1 \cdot q_2) q_1^2 + 2(q_1 \cdot q_2)^2) \\
& + p \cdot q_1 \left(\frac{4}{3} (q_1^2 + q_1 \cdot q_2) (q_2^2 + q_1 \cdot q_2) (3q_2^2 + 2q_1 \cdot q_2) \right. \\
& \quad \left. + \frac{8}{3} p \cdot q_2 (q_1^4 + 2q_1 \cdot q_2 q_1^2 - q_2^2 q_1 \cdot q_2) \right), \\
\hat{T}_{13}(q_1, q_2; p) &= -\frac{4}{3} (q_2^2 + q_1 \cdot q_2) (q_1^2 q_2^2 + (q_1 \cdot q_2)^2) m^2 + \frac{4}{3} q_2^2 (p \cdot q_1)^2 (q_2^2 - q_1 \cdot q_2) \\
& - \frac{4}{3} p \cdot q_2 (q_1 \cdot q_2)^2 (3q_2^2 + 2q_1 \cdot q_2) + \frac{4}{3} (p \cdot q_2)^2 \left((q_2^2 + q_1 \cdot q_2) q_1^2 + 2(q_1 \cdot q_2)^2 \right) \\
& + p \cdot q_1 \left(\frac{4}{3} q_1 \cdot q_2 (3q_2^2 + 2q_1 \cdot q_2) q_2^2 + \frac{8}{3} p \cdot q_2 q_1 \cdot q_2 (q_1 \cdot q_2 - q_2^2) \right), \\
\hat{T}_{14}(q_1, q_2; p) &= -\frac{8}{3} m^2 q_1 \cdot q_2 (q_2^2 + q_1 \cdot q_2) q_2^2 + p \cdot q_2 \left(-\frac{8}{3} (q_1 \cdot q_2)^3 - \frac{4}{3} q_2^2 (q_1^2 + 2q_1 \cdot q_2) q_1 \cdot q_2 \right) \\
& + p \cdot q_1 \left(\frac{8}{3} p \cdot q_2 (q_2^2 + q_1 \cdot q_2) q_2^2 + \frac{4}{3} \left((q_1^2 + 2q_1 \cdot q_2) q_2^2 + 2(q_1 \cdot q_2)^2 \right) q_2^2 \right), \\
\hat{T}_{15}(q_1, q_2; p) &= \frac{8}{3} m^2 (q_1^2 + q_1 \cdot q_2) (q_2^2 + q_1 \cdot q_2) (q_1^2 + q_2^2 + 2q_1 \cdot q_2) - \frac{8}{3} p \cdot q_1 p \cdot q_2 (q_1^2 + q_2^2 + 2q_1 \cdot q_2)^2, \\
\hat{T}_{16}(q_1, q_2; p) &= \frac{8}{3} (q_1^2 + q_2^2 + q_1 \cdot q_2) (q_1^2 q_2^2 - (q_1 \cdot q_2)^2) m^2 - \frac{8}{3} q_2^2 (p \cdot q_1)^2 (q_1^2 + q_2^2 + q_1 \cdot q_2) \\
& - \frac{8}{3} q_1^2 (p \cdot q_2)^2 (q_1^2 + q_2^2 + q_1 \cdot q_2) + \frac{16}{3} p \cdot q_1 p \cdot q_2 q_1 \cdot q_2 (q_1^2 + q_2^2 + q_1 \cdot q_2), \\
\hat{T}_{17}(q_1, q_2; p) &= -\frac{4}{3} q_1^2 p \cdot q_2 (q_1^2 + q_1 \cdot q_2) q_2^2 + \frac{4}{3} m^2 (q_1^2 q_2^2 - (q_1 \cdot q_2)^2) q_2^2 \\
& - \frac{4}{3} (p \cdot q_1)^2 (q_2^2 + 6(q_1^2 + q_1 \cdot q_2)) q_2^2 + \frac{4}{3} q_1^2 (p \cdot q_2)^2 (q_2^2 + 2q_1 \cdot q_2) \\
& + p \cdot q_1 \left(\frac{4}{3} q_1^2 (q_2^2 + q_1 \cdot q_2) q_2^2 + \frac{8}{3} p \cdot q_2 q_1 \cdot q_2 (3q_1^2 + 2q_1 \cdot q_2) \right), \\
\hat{T}_{18}(q_1, q_2; p) &= -\frac{4}{3} q_2^2 p \cdot q_2 (q_1^2 + q_1 \cdot q_2) q_1^2 + \frac{4}{3} m^2 (q_1^2 q_2^2 - (q_1 \cdot q_2)^2) q_1^2 \\
& - \frac{4}{3} (p \cdot q_2)^2 (q_1^2 + 6(q_2^2 + q_1 \cdot q_2)) q_1^2 + \frac{4}{3} q_2^2 (p \cdot q_1)^2 (q_1^2 + 2q_1 \cdot q_2) \\
& + p \cdot q_1 \left(\frac{4}{3} q_1^2 (q_2^2 + q_1 \cdot q_2) q_2^2 + \frac{8}{3} p \cdot q_2 q_1 \cdot q_2 (3q_2^2 + 2q_1 \cdot q_2) \right), \\
\hat{T}_{19}(q_1, q_2; p) &= -\frac{4}{3} m^2 (q_1^2 - q_2^2) (q_1^2 (4q_1 \cdot q_2 + q_2^2) + q_1 \cdot q_2 (7q_1 \cdot q_2 + 4q_2^2)) \\
& - \frac{8}{3} p \cdot q_2 (q_1^2 - q_2^2) q_1 \cdot q_2 (q_1^2 + q_1 \cdot q_2) + \frac{4}{3} q_2^2 (p \cdot q_1)^2 (q_1^2 + 2q_1 \cdot q_2 + q_2^2) \\
& - \frac{4}{3} q_1^2 (p \cdot q_2)^2 (q_1^2 + 2q_1 \cdot q_2 + q_2^2) \\
& + p \cdot q_1 \left(\frac{16}{3} p \cdot q_2 (q_1^2 - q_2^2) (q_1^2 + 2q_1 \cdot q_2 + q_2^2) + \frac{8}{3} (q_1^2 - q_2^2) q_1 \cdot q_2 (q_1 \cdot q_2 + q_2^2) \right).
\end{aligned} \tag{5.319}$$

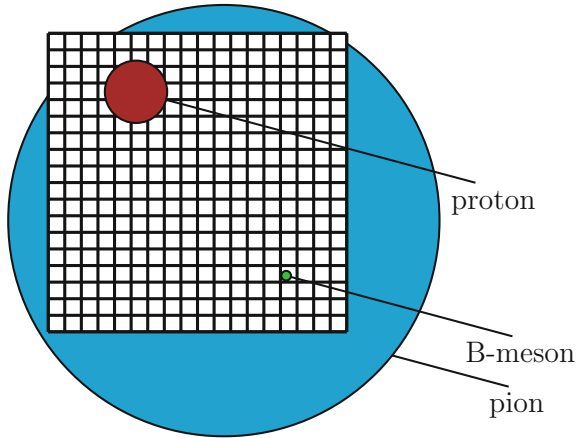


Fig. 5.73 Illustration of some basic issues in LQCD calculations: the role of the lattice resolution and the lattice size in relation to physical objects. Typically, while a proton gets reasonably resolved and reasonably fits into the volume, the much lighter pion is hard to be fit into the box (volume artifacts), while the much heavier B -meson is hard to be resolved sufficiently (lattice artifacts). Thus, the lattice discretization has to be chosen appropriate to the physical object but is constrained by the available computing resources

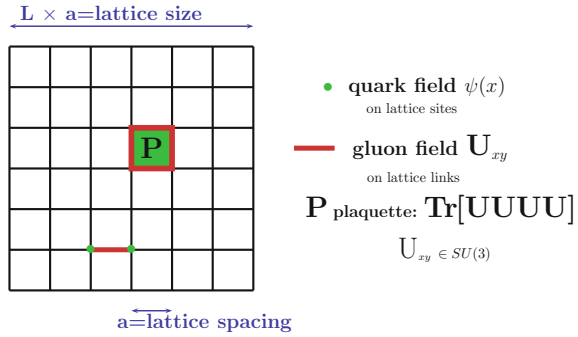
5.3 Lattice QCD

Lattice QCD results have been improving a lot in recent years and results get closer to be competitive with results obtained by the dispersive approach based on experimental data, which not always agree at a level which allow us to reduce uncertainties as desirable for future muon $g - 2$ experiments. In this section I briefly review (by far incomplete) some of the essentials (see e.g. [363] for a concise course in LQCD) of lattice QCD and the present status of its role in evaluating hadronic effects contributing to a_μ .

Lattice QCD, formulated first by Ken Wilson in 1974 [364], allows us to calculate non-perturbative strong interaction contributions from first principles. However, numerical simulations are only possible for systems with a finite number of degrees of freedom, which requires to replace the space–time continuum by a finite lattice of spacing a in a finite box of length L and one has to extrapolate to the continuum $a \rightarrow 0$ and perform the infinite volume limit $L \rightarrow \infty$. How to choose a and L when studying a physical problem is illustrated in Fig. 5.73. In addition, numerical simulation requires to work in Euclidean space (by the appropriate Wick rotation). The rules for going from Minkowski space (M) to Euclidean space we have fixed in Sect. 2.5.4:

$$x^0 \equiv t \rightarrow -ix^4 = -i\tau ; \quad p^0 \equiv E \rightarrow -ip^4$$

Fig. 5.74 Wilson’s lattice implementation of QCD. A plaquette P is an ordered product of four U ’s along a basic lattice face (closed 1×1 path in lattice units) and corresponds to the Yang–Mills action



such that all scalar product take a factor (-1) : $(xy)_M \rightarrow -(xy)_E, (pq)_M \rightarrow -(pq)_E$ and $(xq)_M \rightarrow -(xq)_E$, consistent with $g^{\mu\nu} = g_{\mu\nu} \rightarrow -\delta_{\mu\nu}$. Contravariant vectors correspond as $x^\mu = (x^0, x^i) \rightarrow (x^i, x^4) = (x_i, x_4)$ for $i = 1, 2, 3$, covariant one’s as $x_\mu = (x^0, -x^i) \rightarrow -(x^i, x^4) = -(x_i, x_4)$. Correspondingly, $d^4x = dx^0 dx^1 dx^2 dx^3 \rightarrow -i \Pi_{i=1}^4 dx_i$. In addition for the Dirac matrices we adopt the convention⁴⁷ $\gamma_4 = (\gamma_0)^M$ and $\gamma_i = i(\gamma_i)^M$ such that $\{\gamma_\mu, \gamma_\nu\} = 2\delta_{\mu\nu}$ and $\not{p}_M \rightarrow -i \not{p}_E$. Then we have the Euclidean e.m. current $J_\mu = (J_0, \mathbf{J}) = (j_0, \mathbf{j})$. A four vector in Euclidean configuration space is represented on the lattice by $x_\mu = an_\mu$ with $n_\mu \in Z^4$ a four-tuple of integers. Quark fields are represented by Dirac spinor fields ψ_x sitting on lattice points x while the gauge fields are $SU(3)_c$ matrix fields U_{xy} attached to the links $\langle xy \rangle$ as illustrated in Fig. 5.74. In terms of the gluon fields G_μ^i we have

$$U_{xy} = \mathcal{P} \exp \left\{ i g_0 \int_x^y T_i G_\mu^i(z) dz^\mu \right\},$$

where \mathcal{P} means path-ordering along the path from x to y and g_0 is the bare gauge coupling. On the lattice $dz^\mu = a \hat{\mu}$ and one denotes $U_{xy} = U_\mu(x)$ on the link at x in direction μ and $\hat{\mu}$ a unit vector in direction of μ i.e. $y = x + a\hat{\mu}$. Then in terms of the Hermitian Lie algebra valued gauge fields $\mathcal{G}_\mu = \sum_i T_i G_\mu^i$ on the lattice $U_\mu(x) = e^{i g_0 a \mathcal{G}_\mu(x+a\hat{\mu}/2)}$. Fields are statistically distributed with weight function

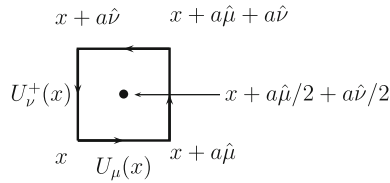
$$e^{-S(U, \psi, \bar{\psi})}$$

where S is the Euclidean action (energy \times Euclidean time):

$$S = \beta \sum_P \text{Tr}[UUUU] + \sum_{\langle xy \rangle} \bar{\psi}_x M(U)_{xy} \psi_y, \tag{5.320}$$

⁴⁷One has to translate the Dirac Lagrangian $\bar{\psi} (i\gamma^\mu \partial_\mu - m) \psi \rightarrow -\bar{\psi} (\gamma_\mu \partial_\mu + m) \psi$ noting that $\frac{\partial}{\partial x^0} \rightarrow i \frac{\partial}{\partial x^4}$ one infers that we have to set $\gamma^0 \rightarrow \gamma^4$ and then $\gamma^i \rightarrow i\gamma^i$ for the spatial components.

where $\beta \propto 1/g_0^2$. More specifically: consider the simplest Wilson loop (trace of product of U 's along a closed path), the 1×1 plaquette



$$\begin{aligned} U_{\mu\nu}(x) &\equiv W_{\mu\nu}^{1 \times 1} = U_\mu(x) U_\nu(x + a\hat{\mu}) U_\mu^+(x + a\hat{\nu}) U_\nu^+(x) \\ &= e^{i g_0 a (\mathcal{G}_\mu(x + a\hat{\mu}/2) + \mathcal{G}_\nu(x + a\hat{\mu} + a\hat{\nu}/2) - \mathcal{G}_\mu(x + \hat{\nu} + a\hat{\mu}/2) - \mathcal{G}_\nu(x + a\hat{\nu}/2))} \end{aligned}$$

and expand about the center of the plaquette $x + a\hat{\mu}/2 + a\hat{\nu}/2$ which yields

$$U_{\mu\nu} = 1 + i a^2 g_0 \mathcal{G}_{\mu\nu} - \frac{a^4 g_0^2}{2} \mathcal{G}_{\mu\nu} \mathcal{G}_{\mu\nu} + O(a^6),$$

where the commutator $\mathcal{G}_{\mu\nu} = [D_\mu, D_\nu]$ is the field-strength tensor and $D_\mu = \mathbf{1}\partial_\mu + i\mathcal{G}_\mu$ the covariant derivative (2.274). Hence, what corresponds to the Yang–Mills action is proportional to $\text{Re} (1 - U_{\mu\nu})$. One still has to sum over the directions. At each site x there are 6 distinct positively oriented plaquettes [$\mu < \nu$] to be summed over but then divided by 2 as one has been double counting. The gauge term for the $SU(3)$ Yang–Mills theory then may be written as

$$S_g = \beta \sum_{x, \mu < \nu} \left\{ 1 - \frac{1}{6} \text{Tr}[U_{\mu\nu} + U_{\mu\nu}^+] \right\}, \quad (5.321)$$

with $\beta = \frac{6}{g_0^2}$. For $a \rightarrow 0$ S_g represents the pure Yang–Mills action, the first term of (2.276) in Sect. 2.8. The quark field term is given by

$$S_F = a^4 \sum_x \bar{\psi}(x) (\not{D} + m_0) \psi(x), \quad (5.322)$$

with \not{D} the lattice version of the Dirac operator where D_μ is the covariant derivative and m_0 denotes the flavor diagonal bare quark mass matrix. The Wilson–Dirac operator is given by

$$\not{D} = \frac{1}{2} \{ \gamma_\mu (\nabla_\mu^* + \nabla_\mu) - a \nabla_\mu^* \nabla_\mu \}, \quad (5.323)$$

with ∇_μ^* and ∇_μ gauge covariant forward and backward n.n. difference operators:

$$\nabla_\mu \psi(x) = \frac{1}{a} [U_\mu(x) \psi(x + a\hat{\mu}) - \psi(x)]; \quad \nabla_\mu^* \psi(x) = \frac{1}{a} [\psi(x) - U_\mu(x - a\hat{\mu}) \psi(x - a\hat{\mu})].$$

The second term of (5.323), the so called Wilson term, is required to eliminate flavor doubling on the lattice on the expense that $-\frac{1}{2}a\nabla_\mu^*\nabla_\mu$ violates chiral symmetry, which only can be recovered in the continuum limit as $a \rightarrow 0$. This lattice implementation of QCD is fully gauge invariant and does not require any gauge fixing, as it is not formulated in terms of the gauge potentials.

A key problem on a finite lattice is the fact that the momenta are quantized, with values in the first Brillouin zone. Assuming L even and the lattice $V_{L,a}$ centered in configuration space about the origin with box size aL we have $Q_\mu = \frac{2\pi}{a(L+1)}(-\frac{L}{2} + n)$; $n = 0, 1, 2, \dots, L$ which defines a finite lattice $\Lambda_{L,a}$ in momentum space of lattice spacing $\frac{2\pi}{a(L+1)}$ and size $\frac{\pi}{a} \frac{2L}{L+1} \approx \frac{2\pi}{a}$ and thus $Q_{\mu \min} \approx \frac{2\pi}{aL}$ while $Q_{\mu \max} \approx \frac{\pi}{a}$.

Between the lattices $V_{L,a}$ and $\Lambda_{L,a}$ one has the relations

$$a^4 \sum_{x \in V_{L,a}} e^{-iqx} = a^4 N \delta_{q,0}^{(4)}; \quad q \in \Lambda_{L,a}, \quad \frac{1}{Na^4} \sum_{q \in \Lambda_{L,a}} e^{iqx} = \frac{1}{a^4} \delta_{x,0}^{(4)}; \quad x \in V_{L,a},$$

where $N = (L+1)^4$ is the number of lattice sites and the Fourier transforms back and forth read

$$\tilde{f}_q = a^4 \sum_{x \in V_{L,a}} e^{-iqx} f_x, \quad f_x = \frac{1}{Na^4} \sum_{q \in \Lambda_{L,a}} e^{iqx} \tilde{f}_q.$$

On the first Brillouin zone the inverse scalar propagator is given by

$$\tilde{G}_{a,q}^{-1} = m_0^2 + 4a^{-2} \sum_{i=1}^4 \sin^2 \frac{aq_i}{2}.$$

A free fermion propagators on a lattice (U=1) is given by⁴⁸

⁴⁸For the interacting case the Wilson fermion action usually is written in terms of redefined quark fields

$$\psi \rightarrow \sqrt{2\kappa}\psi; \quad \kappa = \frac{1}{2(m_0 + 4r)},$$

such that Wilson fermion action reads

$$S_F = \sum_{x,y} \bar{\psi}(x) D_F(x,y) \psi(y),$$

with

$$D_F(x,y) = \delta_{x,y} - \kappa \left\{ \sum_{\mu} (r - \gamma_{\mu}) U_{\mu}(x) \delta_{x+a\hat{\mu},y} + (r + \gamma_{\mu}) U_{\mu}^+(x - a\hat{\mu}) \delta_{x-a\hat{\mu},y} \right\},$$

here κ is called hopping parameter and $r = 1$ for the Wilson term specified earlier.

$$D_F(x, y) = \sum_{\mu=1}^4 \gamma_{\mu} \frac{\delta_{x+a\hat{\mu},y} - \delta_{x-a\hat{\mu},y}}{2a} + m_0 \delta_{xy},$$

which has dimension $n_{\text{sites}} \times n_{\text{color}} \times n_{\text{Dirac}} \times n_t$ rows and columns. The Fourier transform yields

$$\tilde{D}_F^{-1}(p) = \mathbf{1}m_0 + \frac{i}{a} \sum_{\mu=1}^4 \gamma_{\mu} \sin(ap_{\mu}),$$

where in the massless limit $\tilde{D}_F(p)$ has 16 poles in the Brillouin zone such that a naive Fermion has “doublers”. Besides the pole at $p_{\mu} = 0$, poles also sit at points where one or more of the components take values $p_{\mu} = \pi/a$ ($\mu = 1, 2, 3, 4$) in place of 0, by periodicity of the $\sin(ap_{\mu})$. The “doublers” are removed by adding the Wilson term which modifies the inverse Fermion propagator to

$$\tilde{D}_F^{-1} = \mathbf{1}m_0 + \frac{i}{a} \sum_{\mu=1}^4 \gamma_{\mu} \sin(ap_{\mu}) + \mathbf{1} \frac{1}{a} \sum_{\mu=1}^4 (1 - \cos(ap_{\mu})),$$

making “doublers” heavy of mass proportional to $1/a$ such that they get removed in the continuum limit.

Observables (physical quantities) are then obtained as weighted averages

$$\langle \mathcal{O} \rangle = \frac{1}{Z} \int \cdots \int \prod_x d\psi_x d\bar{\psi}_x \prod_{\langle xy \rangle} dU_{xy} \mathcal{O}(U, \psi, \bar{\psi}) e^{-S(U, \psi, \bar{\psi})},$$

where $Z = \langle 1 \rangle$ is the partition function which serves as a normalization here.

The high demand of computational resources is easy to understand if we count the many degrees of freedom involved. Per one gauge-field configuration $\{U\}$ (a configuration being the set of U 's on all links) one has 3^2-1 color degrees of freedom times the number of “links” (directions per site), which is 4, times the lattice size, i.e. $8 \times 4 \times L^3 \times T$, where T is the number of lattice points in Euclidean time (usually T is chosen bigger than L in order to have a better control of the Euclidean time evolution). Per one quark propagator M^{-1} we have a color-factor 3×3 times the spin multiplicity 4×4 times the square of the lattice size, i.e. $9 \times 16 \times L^6 \times T^2$. Thus the dimension of integrals is $D = 80 \times L^3 \times T$ (32 real parameters of the U 's, 2×12 real parameters for ψ 's and the same number for $\bar{\psi}$'s, which is 80 real entries per site. The dimension of the complex quark matrices is $N = 12 \times L^3 \times T$.

The method to deal with such incredibly high dimensional integrals is Monte Carlo integration together with the Metropolis “accept–reject” updating algorithm [365] and appropriate importance sampling. One generates a Markov chain of gauge configurations distributed according to the probability measure (see below)

$$[dU] e^{-S_g(U)} \prod_f \det(D(U) + m_f) . \tag{5.324}$$

Given the set of generated configurations, expectation values $\langle O(U, \psi, \bar{\psi}) \rangle$ are calculated by averaging over all configurations. For inverting the huge sparse matrices M the conjugate gradient algorithm [366] and improvements of it is applied. Substantial progress has been made and still is required by developing even better algorithms and methods of analysis as well as much faster computers.

One key problem of LQCD is the simulation with fermions (Grassmann fields = anti-commuting c-numbers). Fermions in comparison to bosons are much more difficult to simulate. As the action is bilinear in the Grassmann quark fields one can actually integrate out the fermions, which yields the fermion determinant in (5.324) as a weight factor of the remaining gauge configuration integrals. A generic correlation function then reads

$$\langle O_1(x_1) O_2(x_2) \rangle = \frac{1}{Z} \prod_{\langle xy \rangle} dU_{xy} e^{-S_g(U)} \det M_u \cdot \det M_d \cdots [O_1(x_1) O_2(x_2)]_{\text{Wick}} ,$$

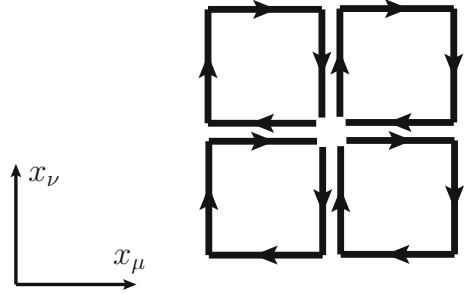
where the fermion fields in the correlator are pairwise Wick contracted to quark propagators M_u^{-1}, M_d^{-1} etc. This however is very difficult/expensive to evaluate and a direct numerical evaluation goes far beyond available computer resources. Fortunately, there are tricks to overcome the barrier: dynamical fermions are simulated by pseudofermions (auxiliary fermion fields with bosonic statistics) in the Hybrid Monte Carlo algorithm (molecular dynamics approach). Also statistical method requires large samples to be accurate. The accuracy $\sim \frac{1}{\sqrt{N}}$ can be improved substantially only by taking into account an enormous increase in computing time. Problem of auto-correlations and possible zero modes come in addition. Also, the extrapolations necessary (volume, lattice distance, parameters)! require to repeat simulations for different lattice spacings, different volumes and different physical parameters.

In order to improve the continuum extrapolation one may change the action in such a way that the limit $a \rightarrow 0$ scales with $O(a^2)$, rather than with $O(a)$ as in case of the Wilson action. Sheikholeslami and Wohlert [367] have introduced the $O(a)$ **improved action** by adding terms which also produces $O(a)$ effects as they are expected from dimension 5 operators:

$$\begin{aligned} S_{\text{eff}} &= S_{QCD} + aS_1 ; \quad S_1 = \int d^4x \mathcal{L}_1(x) \\ \mathcal{L}_1(x) &= \sum_i c_i(g_0) O_i , \quad \dim [O_i] = 5 . \end{aligned} \tag{5.325}$$

The equation of motion allows one to eliminate most of the possible operators such that $O(a)$ cut-off effects in on-shell matrix elements can be canceled by adding **one term** only to the Wilson action, namely a magnetic moment type term

Fig. 5.75 Sheikholeslami-Wohlert (SW) lattice implementation of the improvement term (5.326), which allows one to improve the Wilson lattice QCD action at $O(a)$ by tuning the constant c_{sw}



$$\mathcal{L}_1(x) = a^3 c_{\text{sw}} \sum_x \frac{i}{4} \bar{\psi}(x) \sigma_{\mu\nu} P_{\mu\nu}(x) \psi(x), \quad c_{\text{sw}} = 1 + O(g_0^2), \quad (5.326)$$

where

$$\begin{aligned} P_{\mu\nu}(x) = & \frac{1}{4} \left(U_\mu(x) U_\nu(x + a\hat{\mu}) U_\mu^+(x + a\hat{\nu}) U_\nu^+(x) \right. \\ & - U_\nu^+(x - a\hat{\nu}) U_\mu^+(x - a\hat{\mu} - a\hat{\nu}) U_\nu(x - a\hat{\mu} - a\hat{\nu}) U_\mu(x - a\hat{\mu}) \\ & + U_\nu(x) U_\mu^+(x - a\hat{\mu} + a\hat{\nu}) U_\nu^+(x - a\hat{\mu}) U_\mu(x - a\hat{\mu}) \\ & \left. - U_\mu(x) U_\nu^+(x + a\hat{\mu} - a\hat{\nu}) U_\mu^+(x - a\hat{\nu}) U_\nu(x - a\hat{\nu}) \right) \end{aligned}$$

is displayed in Fig. 5.75 the lattice version of the field strength tensor as for small a we have $P_{\mu\nu}(x) = a^2 \mathcal{G}_{\mu\nu} + O(a^4)$. This often applied technique, which is based on the universality of the continuum limit, improves the control of the lattice artifacts dramatically.

The bare coupling g_0 and the cutoff a are not independent quantities but are related by the renormalization group which we have discussed in Sect. 2.8 (see p. 155ff). On the lattice the renormalization scale μ in (2.293) on the bare level is to be identified by $1/a$ such that

$$\Lambda_{\text{QCD}} = \lim_{a \rightarrow 0} \frac{1}{a} \exp\left(-\frac{1}{2b_0 g_0^2(a)}\right) \left(\frac{b_0 g_0^2(a)}{1 + \frac{b_1}{b_0} g_0^2(a)}\right)^{-\frac{b_1}{2b_0^2}}, \quad (5.327)$$

where Λ_{QCD} is the non-perturbative scale of QCD, and b_0 and b_1 are the first two, scheme independent, coefficients of the β -function

$$b_0 = \frac{1}{(4\pi)^2} \left(11 - \frac{2}{3} N_f\right); \quad b_1 = \frac{1}{(4\pi)^4} \left(102 - \frac{38}{3} N_f\right),$$

here normalized differently from (2.290). In LQCD the strong interaction coupling conventionally appears as a prefactor $\beta \equiv 6/g_0^2$ in (5.321). LQCD parameters are determined by tuning predictions of f_π , m_π , M_K , M_D and M_B to their physical

(experimental) values. This fixes Λ_{QCD} (equivalent to α_s) and the quark masses $\hat{m} = (m_u + m_d)/2, m_s, m_c$ and m_b . Any other quantity calculated then is a prediction.

The need for ab initio calculations of a_μ^{had} is well motivated: – the problems to determine non-perturbative contributions to the muon $g - 2$ from experimental data at sufficient precision persists and is not easy to improve, – a model-independent extension of CHPT to the relevant energies ranges up to 2 GeV is missing while the new experiments E989 @ FNAL and E34 @ J-PARC require and improvement of the hadronic uncertainties by a factor of four.

The hope is that LQCD can deliver estimates of accuracies

$$\delta a_\mu^{\text{HVP}}/a_\mu^{\text{HVP}} < 0.5\% , \quad \delta a_\mu^{\text{HLbL}}/a_\mu^{\text{HLbL}} \lesssim 10\% \quad (5.328)$$

in the coming years.

The main advantage of lattice regulated QCD is its model-independence and the approximations are systematically improvable. With LQCD one may overcome the reliance on experimental data – except for simple hadronic quantities needed to fix the bare parameters. Also, LQCD can provide model independent results – except for chiral extrapolation and constraining the IR regime. One should note that lattice QCD calculations of a_μ^{HVP} and a_μ^{HLbL} in principle are very straight forward as no analytic continuation or the like is needed. As static quantities they are directly accessible by the Euclidean method. The challenge is the control of the approximations on which the method is based given the limitations of the computational resources.

5.3.1 Lattice QCD Approach to HVP

A very concise and inspiring status report has been given by Hartmut Wittig at the Lattice 2016 Conference [368], and I will follow his synopsis. We know that in the dispersive approach the HVP is dominated by the contribution of the ρ meson, which is characterized by its mass and width, on both of which the HVP depends sensitively. The lattice regularization has to be adapted accordingly and one has to keep in mind that the width is determined predominantly by the $\rho \rightarrow \pi\pi$ decay channel (see e.g. [369]). While in the time-like region the ρ peak is easy to catch, in the Euclidean regime, which is the one accessible to LQCD, the contribution appears smeared over a larger range. We expect that a reasonable LQCD approximation requires the ρ to be resolved sufficiently and at the same time two pions states should fit into the volume available. The primary object for calculating the HVP in LQCD is the electromagnetic current correlator in configuration space

$$\langle J_\mu(\mathbf{x}, t) J_\nu(\mathbf{0}, 0) \rangle , \quad (5.329)$$

where $J_\mu = \frac{2}{3}\bar{u}\gamma_\mu u - \frac{1}{3}\bar{d}\gamma_\mu d - \frac{1}{3}\bar{s}\gamma_\mu s + \dots$ in terms of the quark fields $u(x), d(x), s(x), \dots$. In principle, a Fourier transform

$$\Pi_{\mu\nu}(Q) = \int d^4x e^{iQx} \langle J_\mu(x) J_\nu(0) \rangle = (Q_\mu Q_\nu - \delta_{\mu\nu} Q^2) \Pi(Q^2) \quad (5.330)$$

yields the vacuum polarization function $\Pi(Q^2)$ needed to calculate

$$a_\mu^{\text{HVP}} = 4\alpha^2 \int_0^\infty dQ^2 f(Q^2) \{ \Pi(Q^2) - \Pi(0) \} . \quad (5.331)$$

The integration kernel in this representation is

$$f(Q^2) = w(Q^2/m_\mu^2)/Q^2 ; \quad w(r) = \frac{16}{r^2 (1 + \sqrt{1 + 4/r})^4 \sqrt{1 + 4/r}} \quad (5.332)$$

In our notation used in Sect. 5.1

$$a_\mu^{\text{had}} = \frac{\alpha}{\pi} \int_0^\infty dQ^2 f(Q^2) (-4\pi\alpha\hat{\Pi}(Q^2)) ,$$

where $-4\pi\alpha\hat{\Pi}(Q^2) = \Delta\alpha_{\text{had}}(-Q^2)$. Note that $\Delta\alpha_{\text{had}}(-Q^2)$ has been determined quite accurately by the DR in terms of e^+e^- data as shown in Fig. 3.13. It can be used for a direct comparison with lattice results. See e.g. Figure 1 of [370] which in our representations (3.165) and (3.166) translates into our Figs. 3.15 and 3.16, respectively. The contributions to a_μ^{had} from the ranges displayed in the left panel of Fig. 3.15 are the same. This is illustrated in Fig. 5.76. We note that in the representation (3.166), in terms of the Adler function, the contribution obtained for a given Q_{min} is substantially smaller than in the representations (3.165) or (5.331), which integrate the HVP function directly, with the disadvantage that an accurate value for $\Pi(0)$ is required, which is absent in the Adler function approach [371, 372] (see text following (3.166)). We note that the integrand is strongly peaked as a function of Q at about $(\sqrt{5} - 2)^{1/2} m_\mu \approx 55$ MeV, so the low momentum regime is particularly important.

As momenta are quantized on a finite lattice, the low momentum region is difficult to evaluate in lattice QCD, the minimum momentum on the lattice is $2\pi/L$ where L is the lattice box length. So the access of low momenta is via extrapolation to the infinite volume limit. Present simulations reach typically $Q_{\text{min}} = 2\pi/L$ with $m_\pi aL \gtrsim 4$ for $m_\pi \sim 200$ MeV, such that $Q_{\text{min}} \sim 314$ MeV. The integrand displayed in Fig. 5.76 reveals that about 44% of the low x contribution to a_μ^{had} is not covered by data yet (see e.g. [373]). The figures illustrate the role of extrapolations (especially the large volume limit) still required in order to obtain the bulk of a_μ^{had} . What is used is of course shape information from chiral perturbation theory and from vector meson dominance model type parametrizations which help to control the extrapolation fairly well (see e.g. [374]). The low Q^2 problematics is obvious when looking at Fig. 5.77 showing recent results of a true LQCD HVP simulation.

Fig. 5.76 The integrand of (5.331), which represents (3.165) as an integral over Q^2 . Ranges between $Q_i = 0.00, 0.15, 0.30, 0.45$ and 1.0 GeV and their percent contribution to a^{had} and the “LQCD sample” as in Fig. 1 of [370]. See Fig. 5.77 for a true LQCD result

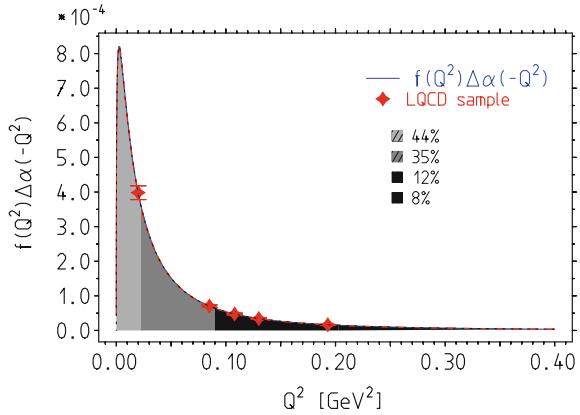
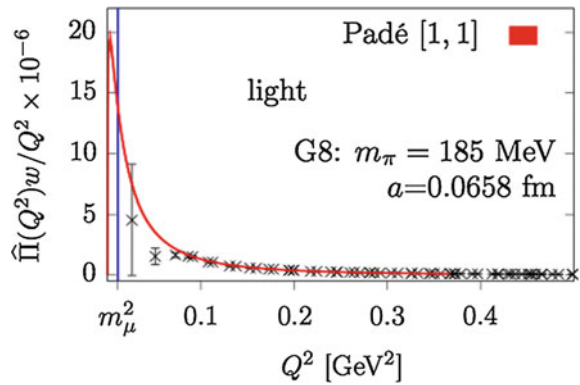


Fig. 5.77 Typical recent LQCD result for the integrand of (5.331) from the Mainz/CLS Collaboration. Reproduced with permission from [375]



One of the main problems is the fact that the statistical accuracy deteriorates as $Q \rightarrow 0$. A Fourier transformation of lattice data then is far from being straight forward and uncertainties due to fluctuations in general turn out to be large (see e.g. [376, 377]). On a finite lattice also the proper choice of the boundary conditions is important. In most cases in spatial directions periodic boundary conditions are used for gauge fields and anti-periodic ones for quark fields.

The low momentum gap of accessible lattice data requires appropriate extrapolation methods. Moment expansions are often the way out for getting more precise estimates of $\Pi(Q^2)$ below Q_{min} . Taylor expansion in conjunction with Padé approximants⁴⁹ as advocated in [380] is the simplest one can do. This approach has been

⁴⁹Suppose that of an analytic function $f(x)$ we only know its Taylor expansion polynomial $f(x) \approx \sum_{i=1}^N c_i x^i$. For growing x the approximation in general fails badly to represent $f(x)$. A Padé approximant $[m,n]$ for $f(x)$ is a rational function $f(x) \approx [m,n]_f(x)$, a ratio of two polynomials of degree m (in the numerator) and n (in the denominator) where the coefficients are determined such that its Taylor expansion to degree N is identical with the Taylor expansion of $f(x)$. The degrees m and n can be chosen such that $[m,n]$ matches with the large x behavior of $f(x)$ which we assume to be known as in the case of the HVP function $\Pi(Q^2)$ where the large Q^2 behavior

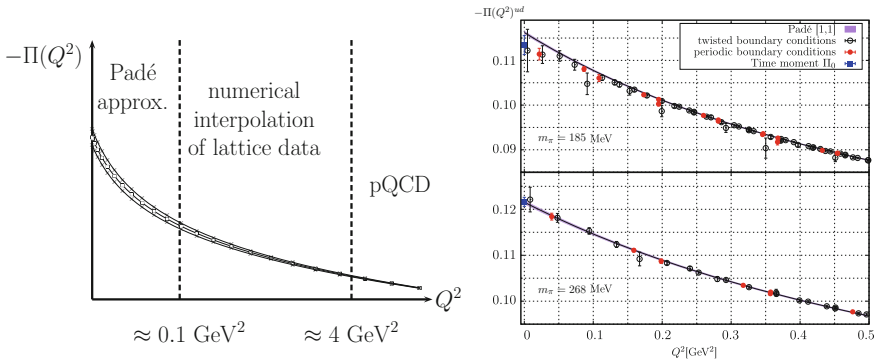


Fig. 5.78 *Left* Accessing the low momentum region with lattice data: lattice results available for $Q^2 > (2\pi/L)^2$ must be extrapolated to $Q^2 = 0$ in order to determine $\Pi(0)$. This may be done by Padé approximants [380]. A reasonable accuracy can be achieved with $Q^2_{\text{min}} \approx 0.1 \text{ GeV}^2$. Above about 2 GeV perturbative QCD is reliable. *Right* the u, d contributions to the vacuum polarization function in the range $0 < Q^2 \leq 0.5 \text{ GeV}^2$ for two ensembles from [387]. Data points corresponding to Fourier momenta are represented by *filled red circles*, while *open black circles* denote data points computed using twisted boundary conditions. The *curves* represent the fits using a Padé approximant of order [1, 1]. *Blue filled squares* indicate the value of $\Pi(0)$ determined from the second time moment. Reprinted with permission from [387]

used first in [381] for the case of the strange quark contribution and recently in [382] for the full HVP result (see also [383–385]). As momenta are quantized normal Taylor coefficient based Padé approximants may not be well determined for feasible lattice sizes and one has to resort to multi-point Padés [386]. What one has to do is suggested in Fig. 5.78.

The low momentum region is usually approached by time–moments in various ways:

- via the low energy expansion in Q^2 :

$$\Pi(Q^2) = \Pi_0 + \sum_{j=1}^N Q^{2j} \Pi_j,$$

- a study of the HVP for $Q = (\omega, \mathbf{0})$

$$\Pi_{kk}(\omega) = a^4 \sum_{x_0} e^{i\omega x_0} \sum_{\mathbf{x}} \langle J_k(x) J_k(0) \rangle,$$

(Footnote 49 continued)

is known from pQCD. As $\hat{\Pi}(Q^2)$ grows logarithmically with growing Q^2 [n-1,n] Padés are upper bound and [n,n] lower bounds for $\hat{\Pi}(Q^2)$. The number of coefficients of a Padé approximant $[m,n] = \sum_{k=0}^m a_k x^k / (1 + \sum_{k=1}^n b_k x^k)$ is $n + m + 1$ unless $a_0 = 0$ as in case of the renormalized HVP $\hat{\Pi}(Q^2)$ or the Adler function $D(Q^2)$, where it is $n + m$. Padés for $D(Q^2)/Q^2$ require $n + m + 1$ coefficients. For Stieltjes functions $f(x)$ Padé series $[n-1,n]_f(x)$ and $[n,n]_f(x)$ converge to $f(x)$ [378, 379].

- a study of the spatially summed vector correlator

$$G(x_0) = -a^3 \sum_{\mathbf{x}} \langle J_k(x) J_k(0) \rangle ,$$

- time moments

$$G_{2n} \equiv a \sum_{x_0} x_0^{2n} G(x_0) = (-1)^n \frac{\partial^{2n}}{\partial \omega^{2n}} \left\{ \omega^2 \hat{\Pi}(\omega^2) \right\} \Big|_{\omega^2=0} ,$$

where $\hat{\Pi}(Q^2) \equiv \Pi(Q^2) - \Pi(0)$ with the expansion coefficients

$$\Pi(0) \equiv \Pi_0 = \frac{1}{2} G_2 , \quad \Pi_j = (-1)^{j+1} \frac{G_{2j+2}}{(2j+2)!} ,$$

- Time-Momentum Representation (TMR)

$$\hat{\Pi}(Q^2) = \frac{1}{Q^2} \int_0^\infty dx_0 G(x_0) \left[Q^2 x_0^2 - 4 \sin^2 \left(\frac{1}{2} Q x_0 \right) \right] , \quad (5.333)$$

which are used for the evaluation of $\hat{\Pi}(Q^2)$ from its time moments in coordinate space. The point: here Q^2 is a tunable parameter and an extrapolation to $Q^2 = 0$ is not needed [376, 388, 389]. The advantage of the TMR is that one can separate long distance from short distance or intermediate range effects and take them into account separately.

Expanding the brace in (5.333) one obtains the time moments expansion which is mathematically identical to the Taylor expansion:

$$\begin{aligned} \frac{1}{Q^2} \int_{-\infty}^\infty dx_0 G(x_0) \sum_{k=1}^\infty (-1)^{k+1} \frac{(Q x_0)^{2k+2}}{(2k+2)!} &= \sum_{k=1}^\infty \frac{(-1)^{k+1}}{(2k+2)!} \underbrace{\int_{-\infty}^\infty dx_0 x_0^{2k+2} G(x_0)}_{\Pi_k} Q^{2k} \\ &= \sum_{k=1}^\infty \Pi_k Q^{2k} . \end{aligned}$$

On the level of the numerical analysis of extrapolating the truncated series one expects important improvement for the TMR. The extrapolation to low momenta is often performed by means of low order Padé approximants as advocated in [384, 386] (see also [373, 390]).

It is evident that different LQCD simulations work with different L and hence with different Q_{\min} . With progress in CPU power one can systematically lower Q_{\min} . Fortunately, the low Q behavior in the Euclidean region is accessible to low energy effective modeling by CHPT combined with VMD approach or simply by Padé

techniques. Various studies suggest that given lattice data down to about 0.1 GeV^2 is expected to be sufficient because the low energy tail is then under sufficient control to get a reliable result. An “expensive” point at low Q typically has a large statistical uncertainties and may not be very useful for constraining the tail. In the Euclidean approach it is not necessarily a serious problem if we have to get 40% say of the contribution by extrapolation to $Q \rightarrow 0$, when the extrapolation is reliable. This is very different from the time-like case, where missing a 40% contribution would be a more serious problem, in view of the threshold and resonance patterns.

Digression on Taylor coefficient based on e^+e^- data

Based on the identity

$$-\frac{\Pi(Q^2)}{Q^2} = \frac{\alpha}{3\pi} \int_{4m_\pi^2}^{\infty} \frac{ds}{s} \frac{R(s)}{s+Q^2}. \quad (5.334)$$

the Taylor coefficients can be calculated dispersively in the time-like approach via

$$\Pi_{n+1} = (-1)^{(n+1)} \frac{\alpha}{3\pi} \int_{4m_\pi^2}^{\infty} \frac{ds}{s} \frac{R(s)}{s^{n+1}}. \quad (5.335)$$

Using the present world average (WA) compilation of the e^+e^- data (as available from [161]) and the corresponding HLS model best fit (see Sect. 5.1.11) one finds [373]

n	WA compilation	HLS model
0	$1.01962131\text{E}+01 \pm 6.693577\text{E}-02$	$8.60436543\text{E}+00 \pm 1.303549\text{E}-02$
1	$2.38190432\text{E}-01 \pm 1.257508\text{E}-03$	$2.31974285\text{E}-01 \pm 3.137495\text{E}-04$
2	$8.89142868\text{E}-03 \pm 5.749533\text{E}-05$	$8.97346405\text{E}-03 \pm 1.138840\text{E}-05$
3	$4.99117005\text{E}-04 \pm 4.018536\text{E}-06$	$5.14676918\text{E}-04 \pm 6.561512\text{E}-07$
4	$3.78809709\text{E}-05 \pm 3.333508\text{E}-07$	$3.95581883\text{E}-05 \pm 5.245059\text{E}-08$
5	$3.53345581\text{E}-06 \pm 2.971228\text{E}-08$	$3.70101838\text{E}-06 \pm 6.216865\text{E}-09$
6	$4.06928851\text{E}-07 \pm 2.867316\text{E}-09$	$4.23990709\text{E}-07 \pm 1.378845\text{E}-09$
7	$6.51188814\text{E}-08 \pm 4.102998\text{E}-10$	$6.72641010\text{E}-08 \pm 4.547703\text{E}-10$
8	$1.59771291\text{E}-08 \pm 1.260996\text{E}-10$	$1.64295040\text{E}-08 \pm 1.722887\text{E}-10$
9	$5.43416738\text{E}-09 \pm 5.033454\text{E}-11$	$5.58818049\text{E}-09 \pm 6.967189\text{E}-11$
10	$2.17223798\text{E}-09 \pm 2.125434\text{E}-11$	$2.23581201\text{E}-09 \pm 2.941683\text{E}-11$
11	$9.33132065\text{E}-10 \pm 9.276033\text{E}-12$	$9.60971183\text{E}-10 \pm 1.283852\text{E}-11$

One should keep in mind that the predictable HLS channels ($\pi^+\pi^-$, $\pi^0\gamma$, $\eta\gamma$, $\pi^+\pi^-\pi^0$, K^+K^- , K_LK_S below 1.05 GeV) account for about 80% of a_μ^{had} only, i.e. the HLS result is incomplete. The non-HLS contribution including data at higher energies (beyond our 1.05 GeV breakpoint) are relevant for the lowest moments only. Higher

moments should agree as they are more and more low energy dominated. One also should be aware that higher moments are emphasising more and more the energy region below the ρ which is problematic not only for the LQCD approach but also from the point of view of experimental data needed in the dispersive approach. With the $n = 12$ coefficients one can calculate Padé approximants $[n-1,n]$ and $[n,n]$ up to $n = 4$. Padé improvements of $\Pi(Q^2)$ lattice data have been analyzed in [380]. Since for an analytic function, like $\Pi(Q^2)$, the Taylor coefficients, up to an alternating sign from the substitution $q^2 \rightarrow -Q^2$, are identical for the Euclidean $\Pi(Q^2)$ and the time-like $\Pi(q^2)$ the above Taylor coefficients directly compare with the ones obtained from lattice data, provided all effects included in the e^+e^- -data are included in the Euclidean regime as well.

An early lattice QCD result for the Adler function slope $\Pi_1 = 5.8(5) \text{ GeV}^{-2}$ has been obtained in [388, 389]. The value obtained lies low because the given lattice result essentially caught the dominant ρ contribution only, while the contributions from the region above about 1 GeV was not included. More recent calculations find results much close to the e^+e^- data based evaluations, as shown in Fig. 5.79.

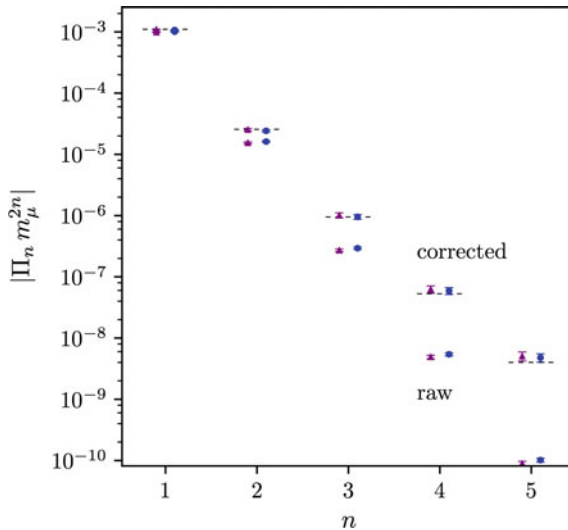


Fig. 5.79 Contributions to the hadronic vacuum polarization $\hat{\Pi}(q^2)$ at $q^2 = -m_\mu^2$ coming from individual Taylor coefficients Π_n with $n = 1, 2, \dots, 5$. Results are shown for corrected (above) and uncorrected (raw, below) coefficients coming from lattice QCD simulations with physical sea-quark masses from two different lattices, sets 3 and 8 of Table I in [382]. The corrected coefficients include two corrections (1) adding $\delta\Pi_n$ of Table IV in [382] and (2) replacing the pion mass from the simulation with the physical pion mass in the leading $\pi\pi$ loop. Contributions from s and c quarks to both the raw and corrected moments are included for $n = 1, \dots, 4$. The dashed lines are results derived from e^+e^- data: the data direct of Table 1 from [373]. The error estimates on the lattice results do not include contributions due to electromagnetic, isospin-violating, and disconnected contributions; (estimated to be around 2% for the $n = 1$ moment). Courtesy of the HPQCD Collaboration. Reprinted from [382]

Results presented as set 8[10] of Table II in [382], obtained for the point closest to the physical one: $\hat{\Pi}_1 = 0.0811(12)[0.0756(13)]$ in our convention read $\Pi_1 = 12\pi^2 \sum_{u,d,s,c} Q_f^2 \times \hat{\Pi}_1 = 10.67(17)[9.95(17)] \text{ GeV}^{-2}$. The most recent calculation presented in [391] evaluated the first two moments $\left[\hat{\Pi}_n \equiv \partial^n \hat{\Pi}(Q^2) / (\partial Q^2)^n \right]_{Q^2=0} / n!$ for the connected contribution as

$$\hat{\Pi}_1 [\text{GeV}^{-2}] = 0.0999(10)(9)(23)(13) \quad \text{and} \quad \hat{\Pi}_2 [\text{GeV}^{-4}] = -0.181(6)(4)(10)(2) .$$

The first two errors represent the lattice statistical and systematic the third from finite volume extrapolation and the fourth estimates the uncertainty of the isospin breaking corrections. This converts to

$$\Pi_1 [\text{GeV}^{-2}] = 10.22(30) \quad \text{and} \quad \Pi_2 [\text{GeV}^{-4}] = -0.207(14) ,$$

in our normalization. In [392] also the moments of the disconnected contribution have been calculated: $\Pi_1 [\text{GeV}^{-2}] = -1, 5(2)(1) \times 10^{-2}$, $\Pi_2 [\text{GeV}^{-4}] = 4.4(1.0)(0.4) \times 10^{-2}$.

The isospin breaking corrections are detailed below in Table 5.24.

End of the Digression

Correlated fits in the simplest cases are performed using the forms

$$\text{Padé [1,1]: } \Pi_{[1,1]}^{\text{fit}}(Q^2) = \frac{a_1 Q^2}{b_1 + Q^2} ,$$

$$\text{Padé [2,1]: } \Pi_{[2,1]}^{\text{fit}}(Q^2) = Q^2 \left(a_0 + \frac{a_1 Q^2}{b_1 + Q^2} \right) ,$$

$$\text{Polynomial: } \Pi^{\text{fit}}(Q^2) = a + b Q^2 ,$$

for extrapolations. The resulting renormalized HVP function is then represented by

$$Q^2 \leq Q_{\text{cut}}^2 : \Pi_{\text{ren}} = 4\pi^2 \left(\Pi_{[m,n]}^{\text{fit}}(Q^2) - \Pi_{[m,n]}^{\text{fit}}(0) \right) ,$$

$$Q^2 > Q_{\text{cut}}^2 : \Pi_{\text{ren}} = 4\pi^2 \left(\Pi^{\text{data}}(Q^2) - \Pi_{[m,n]}^{\text{fit}}(0) \right) ,$$

and the leading order HVP is given by

$$\begin{aligned} \text{integration of fit : } a_{\mu,<}^{\text{HLO}} &= Z_V \left(\frac{\alpha}{\pi}\right)^2 \int_0^{Q_{\text{cut}}^2} dQ^2 \hat{\Pi}_{<}(Q^2) \frac{w(Q^2/m_\mu^2)}{Q^2}, \\ \text{integration of data : } a_{\mu,>}^{\text{HLO}} &= Z_V \left(\frac{\alpha}{\pi}\right)^2 \int_{Q_{\text{cut}}^2}^{\infty} dQ^2 \hat{\Pi}_{>}(Q^2) \frac{w(Q^2/m_\mu^2)}{Q^2}, \end{aligned}$$

where the second integral includes the pQCD tail. The renormalization factor Z_V is required to correct for the non-conservation of the lattice version of the e.m. current, which is conserved in the continuum limit only in general.

Somewhat more ambitious parametrizations of the low Q^2 extrapolations have been applied by different Collaborations. Below an appropriately chosen Q_{match} , typically $Q_{\text{match}}^2 = 2 \text{ GeV}^2$, one may use a VMD model inspired ansatz [376, 393]

$$\Pi_{\text{low}}(Q^2) = \sum_{i=1}^M \frac{f_i^2}{m_i^2 + Q^2} + \sum_{j=0}^{N-1} a_j (Q^2)^j, \quad (5.336)$$

corrected for some low energy deviations, with coefficients fitted from the lattice data. This is not very different from the Padé approach [380]

$$\Pi(Q^2) = \Pi(0) - Q^2 \left(a_0 + \sum_{n=1}^N \frac{a_n}{b_n + Q^2} \right) \quad (5.337)$$

where coefficients are determined by [N-1,N] or [N,N] Padé approximants depending on whether a_0 is set to zero or is subject to the fit.

Another equally important extrapolation problem arises from the fact that computational expenses grow dramatically with decreasing light quark masses. Only recently simulation with physical pion masses became possible. Usually light quark masses have to be chosen to have unphysical values and corresponding pion masses are as large as 500 MeV. The chiral extrapolation to the physical mass value is then necessary. Such extrapolations can be based on CHPT, which predicts the functional form like

$$\begin{aligned} a_\mu^{\text{A}}(m_\pi^2, a) &= b_0 + b_1 m_\pi^2 + b_2 m_\pi^2 \ln m_\pi^2 + b_3 a, \\ a_\mu^{\text{B}}(m_\pi^2, a) &= b_0 + b_1 m_\pi^2 + b_2 m_\pi^4 + b_3 a, \end{aligned} \quad (5.338)$$

where the term linear in a are to be replaced by a^2 when simulating with improved actions. A typical result obtained by the Mainz/CLS Collaboration is shown in Fig. 5.80.

For the heavier flavors s and c the low Q^2 extrapolation is much less severe a problem and a chiral extrapolation is not required as simulation can be performed

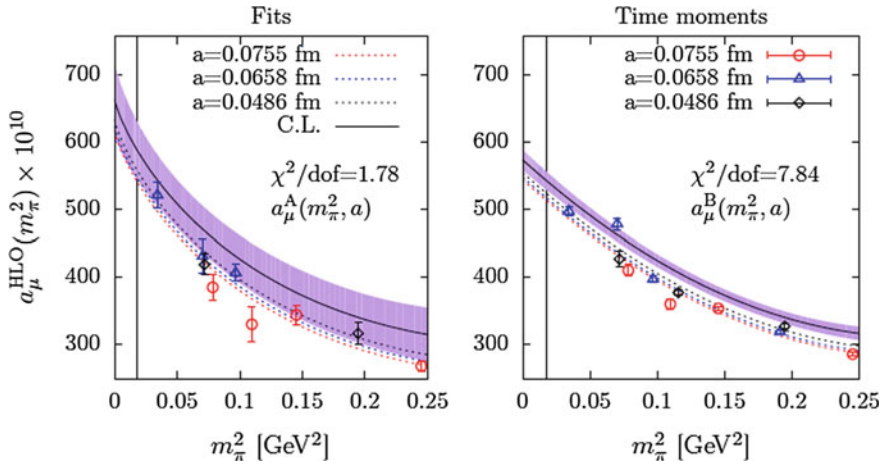


Fig. 5.80 Example for chiral extrapolation as a function of m_π^2 . Shown is the leading order HVP contribution to a_μ of the two light quarks as a function of m_π^2 for various lattice spacings a from the Mainz/CLS [394] obtained with $O(a)$ improved Wilson fermions. C.L. represents the continuum extrapolation. *Left panel* extrapolations using form $a_\mu^A(m_\pi^2, a)$ of (5.338) and using Padé fits. *Right panel* extrapolations using form $a_\mu^B(m_\pi^2, a)$ of (5.338) and using a time moment analysis (see text). Reproduced with permission from [375]

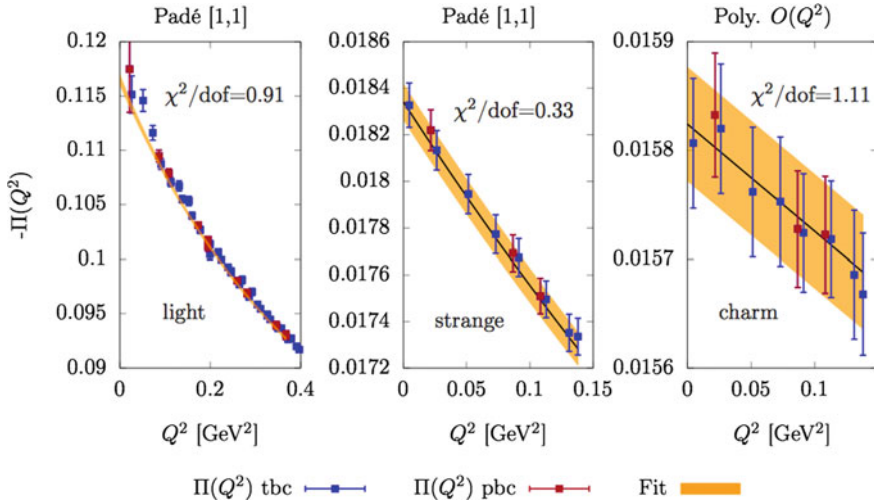
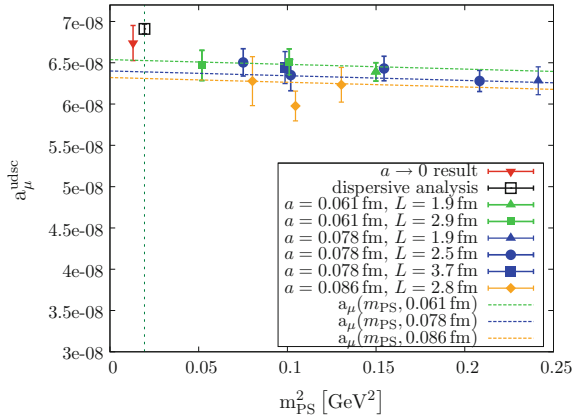


Fig. 5.81 A comparison of the lattice data end their extrapolation for (u, d) , s and c . Reproduced with permission from [375]

directly at the physical point. Still the continuum extrapolation has to be performed. In Fig. 5.81 the results for the different flavors are compared.

Fig. 5.82 $N_f = 2 + 1 + 1$ result a_μ^{udsc} as a function of m_{PS}^2 from the ETM Collaboration [396] for various a and L . Courtesy of the ETM Collaboration. Reprinted with permission from [396]



A different strategy for the $m_{PS} \rightarrow m_\pi^2$ extrapolation⁵⁰ has been adopted by the European Twisted Mass (ETM) Collaboration: a_μ^{HVP} is a very sensitive function of the pion mass and the chiral extrapolation of a_μ is not easy to control. The required extrapolation may be made easier by rescaling the weight–function argument in (5.331) in such a way that the modified definition

$$a_{\bar{\mu}}^{HVP} = \alpha^2 \int_0^\infty \frac{dQ^2}{Q^2} w \left(\frac{Q^2}{H^2} \frac{H_{phys}^2}{m_\mu^2} \right) \Pi_R(Q^2), \quad (5.339)$$

has a reduced sensitivity of the unphysical pion mass m_{PS} , for determining a_μ^{HVP} [374, 395]. Here, H stands for some hadronic scale that can be determined at unphysical values of the pion mass m_{PS} . It is required to have a well-defined limit at the physical pion mass, m_π , denoted H_{phys} which has to be known from experimental measurements for example. With such a choice, by definition $a_{\bar{\mu}}^{hvp} \rightarrow a_\mu^{hvp}$ when $H \rightarrow H_{phys}$. Inspired by the observation that the ρ -meson gives the dominant contribution to a_μ^{hvp} , the choice $H = m_V$ is appropriate where m_V denotes the ρ -meson mass for unphysical values of the light quark masses as determined by the simulation. The result is displayed in Fig. 5.82 and indeed the originally strong pion mass dependence appears substantially reduced. Note that the single meson VMD inspired m_ρ rescaling is expected to apply for the (u, d) part only, for which it has been tuned in the original $N_f = 2$ case [374, 395]. In the four flavor extension a more general VMD inspired form, including higher mass vector meson poles (5.336), has been adopted to extrapolate the low energy tail region $Q^2 \leq 2 \text{ GeV}^2$. It has been noticed that a naive application the ρ pole VMD ansatz, separately for the strange quark contribution, does not give the desired improvement [381], as expected. Consequently

⁵⁰The twisted mass action, like the clover action, avoids $O(a)$ lattice artifacts but violates chiral symmetry, which is corrected by the ansatz $a_\mu(m_{PS}, a) = A + B m_{PS}^2 + Ca^2$, correspondingly.

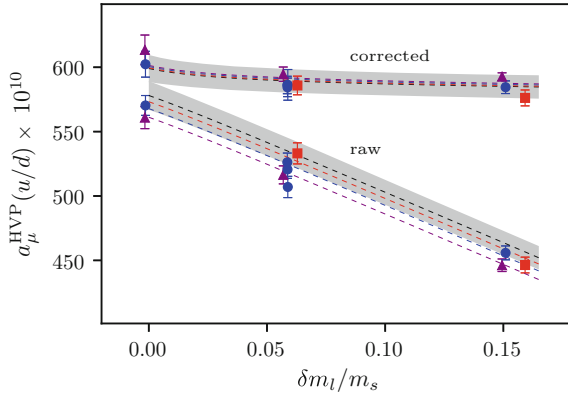
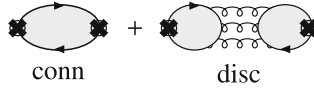


Fig. 5.83 Raw versus corrected lattice data of the HPQCD collaboration: shown is the $N_f = 2$ contribution to a_μ^{HVP} as a function of $\delta m_l/m_s$ where $\delta m_l = m_l - (m_u + m_d)/2$ is the excess of the unphysical light quark mass m_l over the physical light quark masses $m_u \simeq m_d$ and m_s the physical strange quark mass. Including $N_f = 2 + 1 + 1$ flavors the result obtained is $(a_\mu^{\text{HVP}})_{\text{con}} \times 10^{10} = 598 \pm 11(u, d) + 53.4 \pm 0.6(s) + 14.4 \pm 0.4(c)$ at $m_\pi^{\text{min}} L = 3.9$. Courtesy of the HPQCD Collaboration. Reprinted from [382]

the rescaling approach has been improved by appropriate flavor separation in [382].⁵¹ The achieved improvement is evident from Fig. 5.83 from the HPQCD Collaboration, which shows a_μ^{HVP} as a function of $\delta m_l/m_s$ (to which the pion mass square is proportional) before and after the correction.

So far we have considered the leading **connected** contribution. The disconnected contributions in LQCD from diagrams with disconnected quark loops



have to be evaluated separately. Disconnected contributions

$$\langle \text{Tr} \left(\gamma_\mu D_F^f(x, x) \right) \text{Tr} \left(\gamma_\nu D_F^{f'}(y, y) \right) \rangle,$$

also known as Okubo–Zweig–Iizuka (OZI) rule (1964) violating contributions, are responsible for some pronounced effects in hadron spectroscopy like the η' versus pion mass shift (the η' mass is not vanishing in the chiral limit) or at higher energies the OZI suppressed charmonium resonances J/ψ , ψ_1 and the bottomonium resonances Υ_1 to Υ_3 . Concerning the HVP, disconnected contributions are expected to be important, although suppressed. A rough estimate from just the extra charge weight factors $-1/(2(4 + 1))$ yield [397]

$$\hat{\Pi}^{\text{disc}}/\hat{\Pi}^{\text{conn}} = -1/10,$$

⁵¹Recent calculations as Refs. [382, 391] also include effects so far missing in lattice simulations, like isospin breaking and electromagnetic corrections, as discussed below.

which, however, does not take into account the different spectral content of the compared correlators. Taking into account higher CHPT corrections [398] one estimates a negative contribution at the few percent level. The corrections are large but not in the ratio. On the lattice, disconnected contributions $\hat{\Pi}^{\text{disc}}$ are very noisy, while the ratios $\hat{\Pi}^{\text{disc}}/\hat{\Pi}^{\text{conn}}$ is expected to be more quiet. A non-zero contributions could be resolved after appropriate noise reduction techniques have been applied [399–403]. Some recent estimates are:

group	Ref	$(a_\mu^{\text{HVP}})_{\text{disc}}/(a_\mu^{\text{HVP}})_{\text{conn}}$	$(a_\mu^{\text{HVP}})_{\text{disc}}$
HPQCD/Hadspec	[404]	$-0.14(5)\%$	-0.84×10^{-10}
RBC/UKQCD	[400]	$-1.6(7)\%$	$-(9.6 \pm 3.3 \pm 2.3) \times 10^{-10}$
Mainz/CLS	[399]	$< -1\%$	
Bali& Endrödi	[401]	$\Pi^{\text{disc}}/\Pi^{\text{conn}} = -(3.6 \pm 4.5) \times 10^{-4}$ at $Q^2 = 0.03 \text{ GeV}^2$.	

More solid results remain to be established. The disconnected contribution seem not to be substantial at the present level of accuracy. One should remember that when attempting a flavor separation of the flavor content in the e^+e^- data, discussed Sect. 5.1.9, one is expecting percent level OZI violating contributions as e.g. the $\phi \rightarrow 3\pi$ one. In a study of the Euclidean imaginary time correlators [162] it has been shown (see Fig. 1) that a simple flavor $SU(3)$ reweighting shows a convincing agreement with lattice data, while a perturbative reweighting of the flavor content (i.e. just assuming OZI violation to be negligible) misses to fit the lattice data at the 5% level. This has been confirmed independently by [163] (see Fig. 9).

The present status of HVP results from LQCD is shown in Fig. 5.84 together with the dispersive results based on e^+e^- data. Recent progress is impressive and comes closer to be competitive with the e^+e^- data based evaluations. At present the statistical accuracy is limited by the disconnected contributions, which are below 1%, typically finite volume effects range between 3 and 7% for physical $m_\pi = 140 \text{ MeV}$ and⁵² $m_\pi L \sim 4$. The strange quark contribution has been determined in [381] as $53.4(6) \times 10^{-10}$ and in [408] as $53.1(9)_{-3}^{+1} \times 10^{-10}$ in agreement and with accuracy better than 2%. The charm quark contribution evaluated in [381] as $14.4(4) \times 10^{-10}$ is at the 3% level.

The main issues of the LQCD determinations of a_μ are the following (see e.g. [368]):

- statistical accuracy at the sub-percent level required,
- reduction of the systematic uncertainty associated with small Q^2 region and closely related problems with an accurate determination of $\Pi(0)$,
- perform comprehensive study of finite volume effects,

⁵²These numbers refer to simulation parameters which have been reached in simulations presented in Fig. 5.84. Ongoing computations as e.g. [391] now reach $Lm_\pi = 4.2 \div 4.5$ in spatial directions and $Tm_\pi = 5.9 \div 7.7$ in the imaginary time direction, all with physical m_π . That converts to $L = 6.1 \dots 6.6 \text{ fm}$ and $T = 8.6 \dots 11.3 \text{ fm}$ which severely reduces corresponding extrapolation problems.

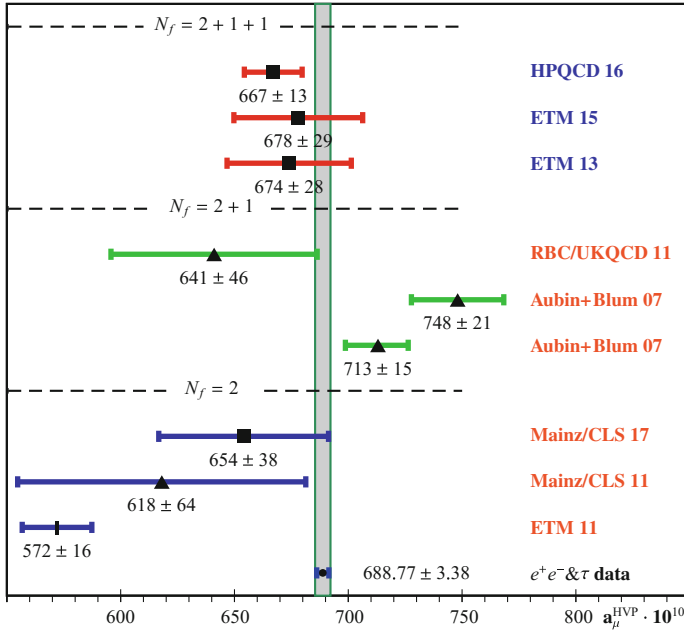


Fig. 5.84 Summary of recent LQCD results for the leading order a_μ^{HVP} , in units 10^{-10} . Labels: ■ marks u, d, s, c , ▲ u, d, s and ▮ u, d contributions. Individual flavor contributions from light (u, d) amount to about 90%, strange about 8% and charm about 2%. Results shown are from HPQCD 16 [382], ETM 15 [405], ETM 13 [396], RBC/UKQCD 11 [406], Aubin+Blum 07 [393], Mainz/CLS 17 [387], Mainz/CLS 11 [407] and ETM 11 [374]

- include quark–disconnected diagrams,
- include isospin breaking: $m_d \neq m_u$ and QED corrections.

For simulations, which do not include isospin breaking and QED effects one has to add corrections relative to what is included in the $R_\gamma(s)$ compilations of e^+e^- data in the dispersive approach. Table 5.24 lists a number of corrections to be applied when comparing LQCD results with experimental data. The focus is on the dominant $\pi\pi$ channel in the range between threshold and 1 GeV. A weighted average of data from the different experiments is represented by a Gounaris–Sakurai parametrization, which allows us to switch on and off the different effects.

Phenomenologically $I = 1$ and $I = 1 + 0$ only differ by $\rho - \omega$ mixing, which is attributed to isospin breaking by $m_u \neq m_d$. Whether what we call $I = 1$ here has some other $I = 0$ component one cannot say from inspection of the experimental data. Final state radiation (FSR) is to be applied to the full $e^+e^- I = 1 + 0$ form factor, while $\gamma - \rho$ mixing is a correction which applies to the $I = 1$ part only. We also applied the e.m. shift of the ρ mass $\delta M_\rho = 0.814$ MeV estimated using (5.109) from neutral to charged, and the shift of the width $\delta \Gamma_\rho = 0.2135$ MeV by applying the shift in m_π and M_ρ by $-\delta M_\rho$ to (5.86). Note that $|F_\pi|^2$ is affected via the change in the ρ mass and width. But, since we have to integrate the $R(s)$ ratio after all, there

Table 5.24 Neutral channel: missing effects in lattice QCD simulations performed in the isospin limit $m_d = m_u$ and without QED effects. Tabulated are the effects δa_μ in units 10^{-10} , integrated from 300 MeV to 1 GeV

Correction type	GS model	Shift	Eq.
$I = 1$ NC: GS fit of e^+e^- data, ω switched off	489.20*		(5.35)
$\omega - \rho$ mixing	491.91	+2.71	(5.35)
FSR of ee $I = 1 + 0$	496.13	+4.22	(5.28)
$\gamma - \rho$ mixing	486.46	-2.74	(5.90)
Elmag. shift $m_{\pi^0} \rightarrow m_{\pi^\pm}$	shift of *		
$I = 1$ NC $m_\pi = m_{\pi^0}$ in $ F_\pi ^2$	488.12	+1.08	(5.35)
apply $-\delta M, -\delta \Gamma$ (radiative shifts)	491.80	-2.60	(5.35)
$I = 1$ NC $m_\pi = m_{\pi^0}$ in $R(s)$ versus $ F_\pi ^2$ [$ F_\pi ^2$ fixed]	502.01	+12.81	(5.10)
Combined $m_\pi = m_{\pi^0}$	500.91		
Physical $m_\pi = m_{\pi^\pm}$ plus e.m. shift in mass and width	489.20	-11.17	
Elmag. channels [132]			
$\pi^0\gamma$	4.64 \pm 0.04		
$\eta\gamma$	0.65 \pm 0.01		
$\pi^+\pi^-\pi^0$ missing disconnected?	5.26 \pm 0.15		

is an additional correction from the pion velocity factor which relates $|F_\pi|^2(s)$ and $R(s)$ via (5.10) and from the shift of the integration threshold.

Another possible issue is the 3π channel dominated phenomenologically by the ω -decay in the ω region and by the ϕ -decay in the ϕ region. Because when extracting the resonances from the data one is subtracting a continuum background, there is also a direct 3π background (continuum) of states which are not counted as resonance decay products. The ω in the isospin limit is a pure 3π final state, absent in the isovector part. The $\phi \rightarrow 3\pi$ channel is OZI suppressed in the nonet-symmetry limit where ϕ is a pure $s\bar{s}$ state. The $\phi \rightarrow 3\pi$ decay then can only come from quark flavor disconnected diagrams. The total 3π contribution is 44.32 ± 1.48 (see Table 5.3) the ω contributes 35.23 ± 1.04 and the ϕ 34.31 ± 0.92 (see Table 5.2). The corresponding branching fractions are $89.2 \pm 0.7\%$ for $\omega \rightarrow 3\pi$ and $15.32 \pm 0.32\%$ for $\phi \rightarrow 3\pi$. Thus ω and ϕ decays contribute 36.68 ± 1.42 of 44.32 ± 1.48 to the 3π channel, the rest 7.64 ± 0.40 is counted as background. So in the connected $I = 1 + 0$ we expect a 3π contribution of 5.26 ± 0.15 should come from disconnected contributions. The isovector $I = 1$ part has no 3π component. So comparison of the isovector correlator with the e.m. current correlator allows one to check the size of the 3π channel in lattice simulations.

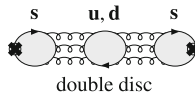
Table 5.25 Charged channel: missing effects in lattice QCD simulations performed in the isospin limit $m_d = m_u$ and without QED effects. Tabulated are the effects δa_μ in units 10^{-10} , integrated from 300 MeV to 1 GeV (see (5.71))

Correction type	GS model	Shift	Eq.
GS fit of τ data	505.32		(5.35)
$+\delta M_\rho, +\delta \Gamma_\rho$	501.44	-3.88	(5.71)
$1/G_{EM}$	504.62	-0.70	(5.71)
β^3/β_0^3	498.73	-6.59	(5.71)
$I = 1, \text{LQCD type}$	494.15	-11.17	

In summary: LQCD results in the isospin limit without e.m. effects and $m_\pi = m_{\pi^0}$ as a reference pion mass require a correction

$$\delta a_\mu = [-11.17 + 2.71 + 4.22 - 2.74 + 4.64 + 0.65] \times 10^{-10} = (-1.69 \pm 0.2) \times 10^{-10},$$

besides an eventual correction a for missing 3π contribution, depending on the approximations made. Note that in the time-like regime the OZI suppressed process of Fig. 5.12 with $\psi \rightarrow \phi, q\bar{q} \rightarrow s\bar{s}$ and the final state is a 3π state, has to be included. This requires to include double disconnected contributions of the type



where the u, d quark blob must include 3π intermediate states which would dominate.

Also in the charged isovector channel there are a number of corrections to be applied when one wants to compare results obtained by simulating in the isospin limit and QED effects absent with τ decay spectra. Corresponding corrections are listed in Table 5.25. The hadronic τ -decay spectral functions we have discussed in Sect. 5.1.10.

The vivid activity in the field is expected to produce results at the 1% level within the coming years and provide very important cross-checks for the dispersive approach.

5.3.2 Lattice QCD Approach to HLbL

Hadronic light-by-light scattering is much more complicated than HVP. One has to deal with complicated non-perturbative multi-scale physics. Hadronic models still have their limitations and uncertainties are difficult to quantify and the dispersive

formalism is much more involved than in the HVP case. A lattice calculation of the HLbL contribution is the big hope here, but is a challenge which goes far beyond the problems met when attempting an accurate HVP determination. Also on the lattice identifying dominant sub-processes like $\gamma^*\gamma^* \rightarrow \pi^0, \eta, \eta'$ is important and actually very much simpler than a full HLbL simulation.

Hadronic light-by-light scattering requires to compute the Euclidean four point correlator of electromagnetic currents. Taking into account that one photon four-momentum is vanishing ($k^\mu = 0$) one still is left with two independent momenta, which means that computational costs grow with the volume square. Various techniques have been proposed:

- QCD+QED simulations [409, 410]:

in this approach the matrix elements of the e.m. current between muon initial and final state

$$\begin{aligned} \langle \mu(\mathbf{p}', s') | J_\mu(0) | \mu(\mathbf{p}, s) \rangle &= \langle \mathbf{p}', s' | \sum_f Q_f \bar{\psi}_f(0) \gamma_\mu \psi_f(0) | \mathbf{p}, s \rangle \\ &= -e \bar{u}(\mathbf{p}', s') \left(\gamma_\mu F_E(Q^2) + i \frac{\sigma_{\mu\nu} Q_\nu}{2m_\mu} F_M(Q^2) \right) u(\mathbf{p}, s) \end{aligned}$$

is calculated directly in QED+QCD non-perturbatively. The wanted $O(\alpha^3)$ contribution $a_\mu = F_M(0)$ has to be extracted from the data. So the challenge is to subtract accurately the unwanted leading $O(\alpha^2)$ terms. This only works diagram by diagram and configuration by configuration in order to get the required noise reduction. First results obtained by this method which provide a proof on principle may be found in [410].

- QCD+ stochastic QED [309, 411]:

in this case QED is treated perturbatively. Exact Feynman gauge photon propagators

$$D_{\mu\nu}(x, y) = \frac{1}{VT} \delta_{\mu\nu} \sum_{k, |\mathbf{k}| \neq 0} \frac{e^{ik \cdot (x-y)}}{\hat{k}^2}; \quad \hat{k}^2 = \frac{4}{a^2} \sum_\rho \sin^2 \frac{ak_\rho}{2}$$

are inserted as illustrated in Fig. 5.85. Two internal photons at vertices x, y are selected stochastically and quark propagators are calculated from point sources at x and y . The current insertion \mathbf{x}_{op} at the external vertex and the third photon vertex z are explicitly summed over (see Fig. 5.85) in the simulation.

Standard 8-dimensional Monte Carlo integration over the two space-time points is applied. A dominant contribution is observed to come from the region where x and y are not far separated. This confirms that the single meson exchange contribution give the leading effects. It also is a direct non-perturbative confirmation that the OPE argumentation used in Sect. 5.2.4 is justified. First results obtained with a 139 MeV pion on a $48^3 \times 96$ lattice are

$$(a_\mu^{\text{HLbL}})_{\text{conn}} = (116.1 \pm 9.1) \times 10^{-11} \quad (m_\pi = 139 \text{ MeV}, a = 0.11 \text{ fm}),$$

for the connected, and

$$(a_\mu^{\text{HLbL}})_{\text{disc}} = (-56.0 \pm 12.6.1) \times 10^{-11},$$

for the leading disconnected contribution. The results are for $N_f = 2 + 1$ flavors, using domain wall fermions and the error is statistical only. The sum is

$$a_\mu^{\text{HLbL}} = (53.5 \pm 13.6) \times 10^{-11}.$$

These results are preliminary as it remains to investigate finite volume effects, lattice artifacts and additional disconnected diagrams. It should be noted that all disconnected diagrams with only one photon attached to the quark loop vanish in the flavor $SU(3)$ limit because the sum of the charges of the u , d and s quarks is zero.

- Light-by-light four point function with exact perturbative QED kernel avoiding power-law volume effects [213]:

According to Fig. 5.87 one can write a configuration space convolution

$$a_\mu^{\text{HLbL}} = F_M(0) = \frac{me^6}{3} \int d^4y \int d^4x \bar{\mathcal{L}}_{[\rho,\sigma];\mu\nu\lambda}(x, y) i \hat{\Pi}_{\rho;\mu\nu\lambda\sigma}(x, y)$$

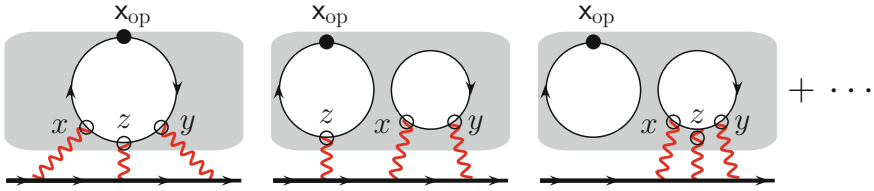


Fig. 5.85 Setup for the stochastic QED approach to HLbL. Connected and leading disconnected diagrams. Closed loops are quark loops decorated in all possible ways by non-perturbative gluon exchange. Photon vertices are to be permuted in all possible ways. One needs to make sure that the loops are connected by gluons, while vacuum blobs need to be subtracted, such that the diagrams are 1-particle irreducible. See also Fig. 5.86

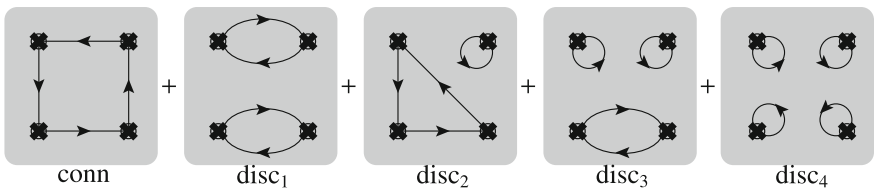
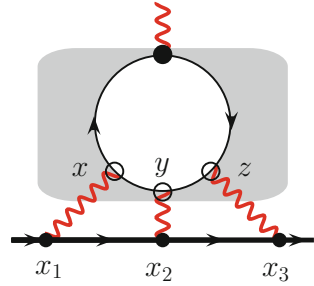


Fig. 5.86 Quark flavor connected and disconnected contributions to HLbL, which have to be calculated separately in LQCD. To be inserted into the muon vertex as in Fig. 5.85, i.e., three vertices are connected by photon propagators to the muon line, one vertex is external. Vertices permuted in all possible ways. Gray areas symbolize the non-perturbative glue cloud

Fig. 5.87 Configuration space kernel separation: the muon line together with the three photon propagators represent the integration kernel $\bar{\mathcal{L}}$ weighting the hadronic four current correlator $\hat{\Pi}$ which is directly accessible to LQCD



of a known perturbative QED Kernel with a moment of the non-perturbative QCD four current correlator in Euclidean space,

$$\hat{\Pi}_{\rho;\mu\nu\lambda\sigma}(x, y) = \int d^4z z_\rho \langle J_\mu(x+z) J_\nu(y+z) J_\sigma(z) J_\lambda(0) \rangle, \quad (5.340)$$

the primary object of any HLbL lattice calculation. The QED kernel function

$$\bar{\mathcal{L}}_{[\rho,\sigma];\mu\nu\lambda}(x, y)$$

may be obtained by rewriting (5.148) in configuration space. Writing⁵³

$$\begin{aligned} \left(\frac{\partial}{\partial k^\rho} \Pi_{\mu\nu\lambda\sigma}(q_1, q_2, k - q_1 - q_2) \right)_{k=0} &= \int_{x,y,z} e^{i(q_1(x-z)+q_2(y-z))} \Pi_{\rho;\mu\nu\lambda\sigma}(x, y, z) \\ &= \int_{x',y',z} e^{i(q_1x'+q_2y')} \Pi_{\rho;\mu\nu\lambda\sigma}(x' + z, y' + z, z) \\ \Pi_{\rho;\mu\nu\lambda\sigma}(x, y, z) &= i z_\rho \langle 0|T \{ j_\mu(x) j_\nu(y) j_\lambda(z) j_\sigma(0) \} |0 \rangle \end{aligned}$$

we have (denoting $x' \rightarrow x$ and $y' \rightarrow y$)

$$\hat{\Pi}_{\rho;\mu\nu\lambda\sigma}(x, y) = i \int_z z_\rho \langle 0|T \{ j_\mu(x+z) j_\nu(y+z) j_\lambda(z) j_\sigma(0) \} |0 \rangle,$$

which continued to Euclidean space reads (5.340). At first, still in Minkowski space, we have

$$F_M(0) = \frac{e^6}{48} \int_{x,y} \bar{\mathcal{L}}_{[\rho,\sigma];\mu\nu\lambda}(x, y) i \hat{\Pi}_{\rho;\mu\nu\lambda\sigma}(x, y),$$

where

⁵³Note that $e^{i(q_1x+q_2y+q_3z)} \stackrel{k=0}{=} e^{i(q_1(x-z)+q_2(y-z))}$. Also $\int_q \equiv \int \frac{d^4q}{(2\pi)^4}$ and $\int_x \equiv \int d^4x$.

$$\begin{aligned} \bar{\mathcal{L}}_{[\rho,\sigma];\mu\nu\lambda}(x, y) &\equiv i \int_{q_1, q_2} \frac{1}{q_1^2 q_2^2 (q_1 + q_2)^2} \frac{1}{(p - q_1)^2 - m^2} \frac{1}{(p - q_1 - q_2)^2 - m^2} \\ &\times \frac{1}{m} \text{Tr} \{ (\not{p} + m) [\gamma_\rho, \gamma_\sigma] (\not{p} + m) \gamma_\mu (\not{p} - \not{q}_1 + m) \gamma_\nu (\not{p} + \not{q}_3 + m) \gamma_\lambda \} e^{i(q_1 x + q_2 y)} \end{aligned}$$

is a known QED kernel function. Rotated to Euclidean space (for conventions see the begin of this Sect. 5.3) we have (all objects now in Euclidean metric)

$$\begin{aligned} \bar{\mathcal{L}}_{[\rho,\sigma];\mu\nu\lambda}(x, y) &\equiv \int_{q_1, q_2} \frac{1}{q_1^2 q_2^2 (q_1 + q_2)^2} \frac{1}{(p - q_1)^2 + m^2} \frac{1}{(p - q_1 - q_2)^2 + m^2} \\ &\times \frac{1}{m} \text{Tr} \{ (\not{p} + im) [\gamma_\rho, \gamma_\sigma] (\not{p} + im) \gamma_\mu (\not{p} - \not{q}_1 + im) \gamma_\nu (\not{p} + \not{q}_3 + im) \gamma_\lambda \} e^{-i(q_1 x + q_2 y)}, \end{aligned}$$

which we also may write as

$$\begin{aligned} \bar{\mathcal{L}}_{[\rho,\sigma];\mu\nu\lambda}(x, y) &= \\ &\frac{1}{m} \text{Tr} \{ (i\not{p} - m) [\gamma_\rho, \gamma_\sigma] (i\not{p} - m) \gamma_\mu (i\not{p} + \not{\partial}_x - m) \gamma_\nu (i\not{p} + \not{\partial}_x + \not{\partial}_y - m) \gamma_\lambda \} \mathcal{J}(\hat{\epsilon}, x, y), \\ \mathcal{J}(\hat{\epsilon}, x, y) &= \int_{q_1, q_2} \frac{1}{q_1^2 q_2^2 (q_1 + q_2)^2} \frac{1}{(p - q_1)^2 + m^2} \frac{1}{(p - q_1 - q_2)^2 + m^2} e^{-i(q_1 x + q_2 y)}. \end{aligned} \quad (5.341)$$

The Fourier integral \mathcal{J} is IR singular and required an IR regularization. It can be represented in terms of position space scalar propagators. Using

$$\frac{i}{q^2 + m^2} = \int_x \Delta_F(x) e^{-iqx}; \quad \Delta_F(x) = \frac{m^2}{4\pi^2} \frac{K_1(m|x|)}{m|x|}, \quad (5.342)$$

where $K_1(z)$ is a modified Bessel function (see (2.142)), one obtains [213]

$$\mathcal{J}(\hat{\epsilon}, x, y) = \int_{x_1, x_2, x_3} D(x_1 - x) D(x_2 - y) D(x_3) \Delta_F(x_1 - x_2) e^{-ip(x_1 - x_2)} \Delta_F(x_2 - x_3) e^{-ip(x_2 - x_3)},$$

where $\Delta_F(x_i - x_k)$ represent the Euclidean scalar muon propagator and $D(x_i)$ the Euclidean scalar photon propagator, which we may regularize by an infinitesimal photon mass. One can choose $p = -im\hat{\epsilon}$, where $\hat{\epsilon}$ is a unit vector in direction of the muon momentum, thus $p^2 = -m^2$ and then averaged over the muon direction

$$\bar{\mathcal{L}}_{[\rho,\sigma];\mu\nu\lambda}(x, y) = \frac{1}{2\pi^2} \int d\Omega_\epsilon \mathcal{L}_{[\rho,\sigma];\mu\nu\lambda}(\hat{\epsilon}, x, y) \equiv \langle \mathcal{L}_{[\rho,\sigma];\mu\nu\lambda}(\hat{\epsilon}, x, y) \rangle_{\hat{\epsilon}}. \quad (5.343)$$

The result only depends on $|x|$, $|y|$ and $x \cdot y = |x||y| \cdot \beta$ ($\beta = \cos\vartheta$; ϑ the angle between the Euclidean four-vectors x and y) and one gets the 3-dimensional integral representation in configuration space, with

$$\int_{x,y} f(|x|, |y|, \beta) = 8\pi^3 \int_0^\infty d|x||x|^3 \int_0^\infty d|y||y|^3 \int_0^\pi d\beta \sin^2 \beta f(|x|, |y|, \beta). \quad (5.344)$$

The configuration space kernel can be worked out once for all and may be found in [213]. I think this is a most promising approach to the HLbL problem and we are waiting for its realization in a dedicated lattice QCD simulation.

At present LQCD HLbL evaluations reach a statistical accuracy at the 10% level for the connected contribution, disconnected contributions are sizable and have larger statistical fluctuations at the 20% level but can be resolved. One expects to be able to constrain/check phenomenological models in not too far future.

Lattice QCD Calculation of the $\pi^0 \rightarrow \gamma^* \gamma^*$ Form Factor

Lattice calculation of dominant subprocesses as presented in [293, 412] are very useful to constrain meson TFFs. As discussed earlier the dominating contribution to HLbL is related to pseudoscalar meson exchange, which we have discussed in Sect. 5.2.4. A first lattice calculation of the dominant $\pi^0 \rightarrow \gamma^* \gamma^*$ subprocesses for doubly virtual photon configurations has been obtained in [293] recently. Such new lattice data are very useful as corresponding experimental data are missing so far.

In Minkowski space the relevant matrix element is defined by (5.163). In momentum space [412]

$$M_{\mu\nu}(p, q_1) = i \int d^4x e^{iqx} \langle 0 | T \{ j_\mu(x) j_\nu(0) \} | \pi^0(p) \rangle = \varepsilon_{\mu\nu\alpha\beta} q_1^\alpha q_2^\beta \mathcal{F}_{\pi^0 \gamma^* \gamma^*}(m_\pi^2; q_1^2, q_2^2),$$

with $p = q_1 + q_2$, defines the invariant on-shell pion form factor $\mathcal{F}_{\pi^0 \gamma^* \gamma^*}(m_\pi^2; q_1^2, q_2^2)$ for off-shell photons of virtualities q_1^2 and q_2^2 . On the Euclidean lattice one can calculate the electromagnetic current correlator [293]

$$M_{\mu\nu}^E(\omega_1, \mathbf{q}_1) = - \int d\tau e^{\omega_1 \tau} \int d^3z e^{-i\mathbf{q}_1 \mathbf{z}} \langle 0 | T \{ J_\mu(\mathbf{z}, \tau) J_\nu(\mathbf{0}, 0) \} | \pi(p) \rangle,$$

where ω_1 is a real parameter tuned such that $q_1 = (\omega_1, \mathbf{q}_1)$ is in the range $q_{1,2}^2 < M_V^2 = \min(M_\rho^2, 4m_\pi^2)$. A simulation of (5.190) is then obtained considering

$$\begin{aligned} M_{\mu\nu}^E &\sim C_{\mu\nu}^{(3)}(\tau, t_\pi; \mathbf{p}, \mathbf{q}_1, \mathbf{q}_2) \\ &= a^6 \sum_{\mathbf{x}, \mathbf{z}} \langle T \{ J_\mu(\mathbf{z}, t_i) J_\nu(\mathbf{0}, t_f) P^+(\mathbf{x}, t_0) \} \rangle e^{i\mathbf{p}\mathbf{x}} e^{-i\mathbf{q}_1 \mathbf{z}}, \end{aligned} \quad (5.345)$$

where $\tau = t_f - t_i$ is the time separation of the two currents and $t_\pi = \min(t_f - t_0, t_i - t_0)$ (see Fig. 5.88).

The projection to the pion pole is obtained in the large t_π limit:

$$A_{\mu\nu}(\tau) = \lim_{t_\pi \rightarrow \infty} C_{\mu\nu}^{(3)}(\tau, t_\pi) e^{E_\pi t_\pi},$$

Fig. 5.88 Three point correlator defining the $\pi^0 \rightarrow \gamma^* \gamma^*$ off-shell form factor. The three-momenta of the pion and the two photons are \mathbf{p} , \mathbf{q}_1 and \mathbf{q}_2 , t_π and τ the relative time arguments. Kinematics: $\mathbf{p} = 0$, $q_1^2 = \omega_1^2 - |\mathbf{q}_1|^2$, $q_2^2 = (m_\pi - \omega_1)^2 - |\mathbf{q}_1|^2$

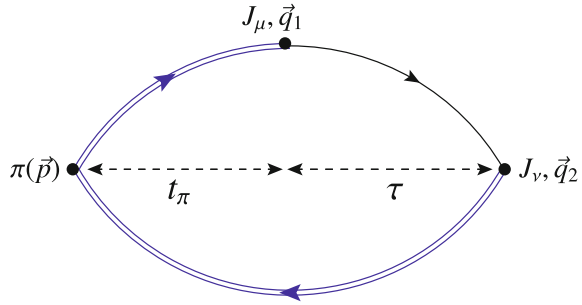


Table 5.26 Comparison of the lattice data LMD+V fit from [293] (1st line) with the estimate from the LMD+V fit Fig. 5.59 (2nd line)

$\tilde{h}_2 = h_2 \cdot F_\pi/3$	$\tilde{h}_5 = h_5/(M_1^2 M_2^2) \cdot F_\pi/3$	$\alpha = h_7/(M_1^4 M_2^4) \cdot F_\pi/3$	M_1	M_2
0.345 (167)(83)	-0.195 (70)(34)	0.273 (24)(7)	0.775	1.465
0.3243 (89)	-0.1852 (121)	0.2747 (4)	0.77526	1.455

and one obtains

$$M_{\mu\nu}^E = \frac{2E_\pi}{Z_\pi} \left(\int_{-\infty}^0 d\tau e^{\omega_1 \tau} A_{\mu\nu}(\tau) e^{-E_\pi \tau} + \int_0^\infty d\tau e^{\omega_1 \tau} A_{\mu\nu}(\tau) \right), \quad (5.346)$$

where the normalization factor Z_π is extracted from the asymptotic behavior of the pseudoscalar two point correlation function $\langle T \{ P(\mathbf{z}, t) P^+(\mathbf{0}, 0) \} \rangle$. For the pion TFF a simulation in the isospin sector of QCD is adequate. Thus $n_f = 2$ CLS (Coordinated Lattice Simulations) ensembles generated with $O(a)$ improved Wilson-Clover action for $m_\pi = 193$ MeV and $Lm_\pi > 4$ and three lattice spacings between 0.05 and 0.075 have been used to generate and analyze TFF data in [294]. Lattice data then have been parametrized by large- N_c type form factors VMD, LMD and LMD+V. Interestingly it turns out that only the LMD+V form factor is able to fit the doubly virtual data if other well established constraints⁵⁴ are taken into account as well. The LMD+V fit yields

$$\mathcal{F}_{\pi^0 \gamma \gamma}(m_\pi^2; 0, 0) = 0.273(24) \text{ GeV}^{-1}, \quad (5.347)$$

well in agreement with $\mathcal{F}_{\pi^0 \gamma^* \gamma^*}(m_\pi^2; 0, 0) = 1/(4\pi^2 F_\pi) = 0.274 \text{ GeV}^{-1}$ [293]. For the first time a constraint from $\mathcal{F}_{\pi^0 \gamma^* \gamma^*}(m_\pi^2; -Q^2, -Q^2)$ in the range $0 < Q^2 < 2 \text{ GeV}^2$ is available. Best fit with LMD+V ansatz (5.214), in clear conflict with VMD ansatz (5.211) yields the parameters Table 5.26 (see also Fig. 5.89).

The results for the pion-pole contribution base on the LQCD fit reads

⁵⁴These are $h_0 = -1$, $h_1 = 0$, the subleading term in the OPE (5.207) as well as the fit Fig. 5.59. In addition working in the chiral limit effectively $h_3, h_4, h_6 \approx 0$.

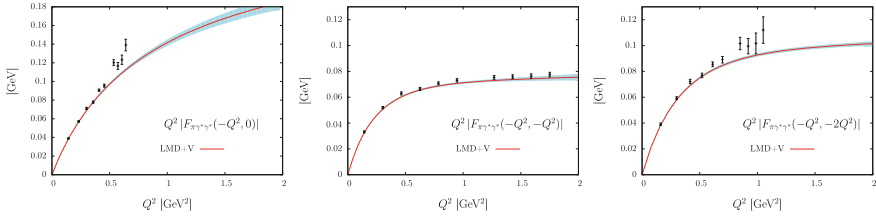


Fig. 5.89 LMD+V fit of pion TFF lattice QCD data from [293]. Courtesy of A. Gérardin, H.B. Meyer and A. Nyffeler. Reprinted with permission from [293], Copyright ©(2016) by the American Physical Society

$$a_{\mu}^{\text{HLbL}}(\pi^0) = (65.0 \pm 8.3) \times 10^{-11}, \quad (5.348)$$

well in agreement with phenomenological estimates. This pioneering calculation is very important as it for the first time provides information on the doubly virtual form factor and clearly rules out a number of usually accepted ansätze like the simple VMD ansatz.

More recently it has become fashionable to apply Padé approximants methods (see e.g. [304, 413] and references therein). Padé approximants are useful in cases where only an number of Taylor coefficients of an analytic function are available (via theory or via experimental data). However, as a purely mathematical tool, it does not provide any physics information (as e.g. physical functional shapes). So physics information is mandatory and if available it makes no sense to first expand it in moments in order to resum them by Padé approximants. For a data-driven approach this is problematic also because data are often sparse and not of very good quality in the low energy region and a low energy expansion may not be very reliable.⁵⁵ In HVP rational approximations do not match pQCD behavior, while in HLbL bivariant rational approximants are within the class of QCD motivated large- N_c LMD+V type TFFs, which have been constrained by the same data as well. In addition, the pseudoscalar TFFs are functions of three variable (not of two). The bivariant version assumes the pole approximation and information concerning the off-shell pion which is to be integrated over is missing. Similarly, the Padé method provides no information concerning the options of variants of the OPE constraints (e.g. Melnikov–Vainshtein versus Knecht–Nyffeler behavior). The method is not model independent as often claimed. Why then the uncertainty in [304] is only a fraction of that of other estimates remains unclear. Also, the Stieltjes function property often referred to, which if valid infers the convergence of Padé approximants series, only applies in the Euclidean regime and is of little help when low order Padés are considered. Suppose one would apply the same procedure not to $\gamma\gamma \rightarrow \pi^0$ Fig. 5.59 but to $\gamma\gamma \rightarrow \pi^+\pi^-$ and/or $\gamma\gamma \rightarrow \pi^0\pi^0$ Fig. 5.38 one would badly fail as the rational approximates never would

⁵⁵This is different from asymptotic expansion (low- or high-energy) and Padé resummations applied in the context of perturbative calculations, where the moment expansions are exact order by order in perturbation theory (see e.g. [79]).

reproduce the Breit–Wigner type shape of the $f_2(1270)$. We should keep in mind that after all what we want to know and understand is what QCD should tell us (lattice QCD).

References

1. A. Litke et al., Phys. Rev. Lett. 30, 1189 (1973); G. Tarnopolsky et al. Phys. Rev. Lett. **32**, 432 (1974)
2. H.D. Politzer, Phys. Rev. Lett. 30, 1346 (1973); D. Gross, F. Wilczek. Phys. Rev. Lett. **30**, 1343 (1973)
3. H. Fritzsch, M. Gell-Mann, H. Leutwyler, Phys. Lett. **47**, 365 (1973)
4. T. Appelquist, H. Georgi, Phys. Rev. D **8**, 4000 (1973); A. Zee. Phys. Rev. D **8**, 4038 (1973)
5. H. Fritzsch, Phys. Rev. D **10**, 1624 (1974); H. Fritzsch, H. Leutwyler, Report CALT-68-416 (1974)
6. F. Jegerlehner, EPJ Web Conf. **118**, 01016 (2016), [arXiv:1705.00263](https://arxiv.org/abs/1705.00263) [hep-ph]
7. M. Davier, A. Höcker, B. Malaescu, Z. Zhang, Adv. Ser. Direct. High Energy Phys. **26**, 129 (2016)
8. S. Eidelman, F. Jegerlehner, Z. Phys. C **67**, 585 (1995); F. Jegerlehner, Nucl. Phys. (Proc. Suppl.) C **51**, 131 (1996); J. Phys. G **29**, 101 (2003); Nucl. Phys. Proc. Suppl. **126**, 325 (2004)
9. K. Adel, F.J. Yndurain, [arXiv:9509378](https://arxiv.org/abs/9509378)
10. D.H. Brown, W.A. Worstell, Phys. Rev. D **54**, 3237 (1996)
11. R. Alemany, M. Davier, A. Höcker, Eur. Phys. J. C **2**, 123 (1998)
12. A.D. Martin, J. Outhwaite, M.G. Ryskin, Phys. Lett. B **492**, 69 (2000). Eur. Phys. J. C **19**, 681 (2001)
13. O.V. Zenin et al., [arXiv:hep-ph/0110176](https://arxiv.org/abs/hep-ph/0110176)
14. M.R. Whalley, J. Phys. G **29**, A1 (2003)
15. F. Jegerlehner, Nucl. Phys. Proc. Suppl. **162**, 22 (2006)
16. F. Jegerlehner, Acta Phys. Polon. B **44**(11), 2257 (2013)
17. A.E. Blinov et al., Z. Phys. C **70**, 31 (1996)
18. J.Z. Bai et al., [BES Collab.], Phys. Rev. Lett. **84**, 594 (2000); Phys. Rev. Lett. **88**, 101802 (2002); M. Ablikim et al., Phys. Lett. B **677**, 239 (2009)
19. V.V. Anashin et al., Phys. Lett. B **753**, 533 (2016), [arXiv:1610.02827](https://arxiv.org/abs/1610.02827) [hep-ex]
20. R.R. Akhmetshin et al., CMD-2 Collab. Phys. Lett. B **578**, 285 (2004)
21. V.M. Aulchenko et al., [CMD-2 Collab.], JETP Lett. **82**, 743 (2005) [Pisma Zh. Eksp. Teor. Fiz. **82**, 841 (2005)]; R.R. Akhmetshin et al., JETP Lett. **84**, 413 (2006) [Pisma Zh. Eksp. Teor. Fiz. **84**, 491 (2006). Phys. Lett. B **648**, 28 (2007)]
22. M.N. Achasov et al., [SND Collab.], J. Exp. Theor. Phys. **103**, 380 (2006) [Zh. Eksp. Teor. Fiz. **130**, 437 (2006)]
23. A. Aloisio et al., [KLOE Collab.], Phys. Lett. B **606**, 12 (2005); F. Ambrosino et al., [KLOE Collab.], Phys. Lett. B **670**, 285 (2009)
24. F. Ambrosino et al., KLOE Collab. Phys. Lett. B **700**, 102 (2011)
25. D. Babusci et al., KLOE Collab. Phys. Lett. B **720**, 336 (2013)
26. B. Aubert et al., [BABAR Collab.], Phys. Rev. Lett. **103**, 231801 (2009); J.P. Lees et al. Phys. Rev. D **86**, 032013 (2012)
27. M. Ablikim et al., BESIII Collab. Phys. Lett. B **753**, 629 (2016)
28. K.G. Chetyrkin, A.L. Kataev, F.V. Tkachov, Phys. Lett. B **85**, 277 (1979); M. Dine, J. Sapirstein, Phys. Rev. Lett. **43**, 668 (1979); W. Celmaster, R.J. Gonsalves, Phys. Rev. Lett. **44**, 560 (1980); K.G. Chetyrkin. Phys. Lett. B **391**, 402 (1997)
29. S.G. Gorishnii, A.L. Kataev, S.A. Larin, Phys. Lett. B **259**, 144 (1991); L. R. Surguladze, M.A. Samuel, Phys. Rev. Lett. **66**, 560 (1991); [Erratum-ibid. **66**, 2416 (1991)]

30. K.G. Chetyrkin, J.H. Kühn, Phys. Lett. B 342, 356 (1995); K.G. Chetyrkin, J.H. Kühn, A. Kwiatkowski, Phys. Rept. 277, 189 (1996); K.G. Chetyrkin, J.H. Kühn, M. Steinhauser, Phys. Lett. B 371, 93 (1996); Nucl. Phys. B 482(213) (1996); 505, 40 (1997); K.G. Chetyrkin, R. Harlander, J.H. Kühn, M. Steinhauser, Nucl. Phys. B 503, 339 (1997); K.G. Chetyrkin, R.V. Harlander, J.H. Kühn, Nucl. Phys. B 586, 56 (2000); [Erratum-ibid. B 634, 413 (2002)]; P.A. Baikov, K.G. Chetyrkin, J.H. Kühn, Phys. Rev. Lett. 101, 012002 (2008); P.A. Baikov, K.G. Chetyrkin, J.H. Kühn, J. Rittinger Phys. Rev. Lett. **108**, 222003 (2012)
31. R.V. Harlander, M. Steinhauser, Comput. Phys. Commun. **153**, 244 (2003); 2009 update at <http://www.rhad.de/>
32. K.G. Chetyrkin, J.H. Kühn, M. Steinhauser, Comput. Phys. Commun. 133, 43 (2000); B. Schmidt, M. Steinhauser. Comput. Phys. Commun. **183**, 1845 (2012)
33. F. Jegerlehner, Z. Phys. C **32**, 195 (1986)
34. E.D. Bloom, F.J. Gilman, Phys. Rev. Lett. 25, 1140 (1970). Phys. Rev. D **4**, 2901 (1971)
35. E.C. Poggio, H.R. Quinn, S. Weinberg, Phys. Rev. D **13**, 1958 (1976)
36. M.A. Shifman, *Quark-Hadron Duality*, arXiv:hep-ph/0009131
37. A.D. Martin, D. Zeppenfeld, Phys. Lett. B **345**, 558 (1995)
38. M. Davier, A. Höcker, Phys. Lett. B 419, 419 (1998). Phys. Lett. B **435**(427), 427 (1998)
39. J.H. Kühn, M. Steinhauser, Phys. Lett. B **437**, 425 (1998)
40. G.J. Gounaris, J.J. Sakurai, Phys. Rev. Lett. **21**, 244 (1968)
41. S. Eidelman et al., Particle Data Group, Phys. Lett. B **592**, 1 (2004)
42. W.M. Yao et al., Particle Data Group, J. Phys. G 33, 1 (2006); K.A. Olive et al., [Particle Data Group], Chin. Phys. C 38, 090001 (2014); C. Patrignani et al., [Particle Data Group. Chin. Phys. C **40**(10), 100001 (2016)
43. M.L. Swartz, SLAC-PUB-6710 (1994), arXiv:hep-ph/9411353 unpublished
44. M.L. Swartz, Phys. Rev. D **53**, 5268 (1996)
45. G. D'Agostini, Nucl. Inst. Meth. A **346**, 306 (1994)
46. M. Benayoun, P. David, L. DelBuono, F. Jegerlehner, Eur. Phys. J. C **73**, 2453 (2013)
47. M. Benayoun, P. David, L. DelBuono, F. Jegerlehner, Eur. Phys. J. C **75**(12), 613 (2015), <http://dx.doi.org/10.1140/epjc/s10052-015-3830-x>
48. V. Blobel, *Some Comments on χ^2 Minimization Applications*, eConf **C030908**, MOET002 (2003); *Dealing with systematics for chi-square and for log likelihood goodness of fit*, Banff International Research Station STATISTICAL INFERENCE PROBLEMS IN HIGH ENERGY PHYSICS, <http://www.desy.de/~blobel/banff.pdf> (2006)
49. A.B. Arbuzov, V.A. Astakhov, A.V. Fedorov, G.V. Fedotovitch, E.A. Kuraev, N.P. Merenkov, JHEP **9710**, 006 (1997)
50. V.A. Khoze, M.I. Konchatnij, N.P. Merenkov, G. Pancheri, L. Trentadue, O.N. Shekhovzova, Eur. Phys. J. C **18**, 481 (2001)
51. A. Hoefer, J. Gluza, F. Jegerlehner, Eur. Phys. J. C **24**, 51 (2002)
52. V.N. Baier, V.S. Fadin, Phys. Lett. B **27**, 223 (1968)
53. S. Spagnolo, Eur. Phys. J. C **6**, 637 (1999); A.B. Arbuzov, E.A. Kuraev, N.P. Merenkov, L. Trentadue, JHEP 12, 009 (1998); S. Binner, J.H. Kühn, K. Melnikov, Phys. Lett. B **459**, 279 (1999); M.I. Konchatnij, N.P. Merenkov, JETP Lett. **69**, 811 (1999); V.A. Khoze et al., Eur. Phys. J. C **18**, 481 (2001)
54. M. Benayoun, S.I. Eidelman, V.N. Ivanchenko, Z.K. Silagadze, Mod. Phys. Lett. A **14**, 2605 (1999)
55. H. Czyż, J.H. Kühn, Eur. Phys. J. C 18, 497 (2001); G. Rodrigo, A. Gehrmann-De Ridder, M. Guillaume, J.H. Kühn, Eur. Phys. J. C 22, 81 (2001); G. Rodrigo, H. Czyż, J.H. Kühn, M. Szopa, Eur. Phys. J. C 24, 71 (2002); H. Czyż, A. Grzelińska, J.H. Kühn, G. Rodrigo, Eur. Phys. J. C 27, 563 (2003); Eur. Phys. J. C 33, 333 (2004). Eur. Phys. J. C **39**, 411 (2005)
56. C.M. Carloni Calame, C. Lunardini, G. Montagna, O. Nicosini, F. Piccinini, Nucl. Phys. B **584**, 459 (2000); C.M. Carloni Calame, G. Montagna, O. Nicosini, F. Piccinini, Nucl. Phys. Proc. Suppl. **131**, 48 (2004); G. Balossini, C.M. Carloni Calame, G. Montagna, O. Nicosini, F. Piccinini, Nucl. Phys. B **758**, 227 (2006); C.M. Carloni Calame et al., Nucl. Phys. Proc. Suppl. **225-227**, 293 (2012)

57. S. Jadach, W. Placzek, B.F.L. Ward, Phys. Lett. B **390**, 298 (1997)
58. A.B. Arbuzov, G.V. Fedotovitch, F.V. Ignatov, E.A. Kuraev, A.L. Sibidanov, Eur. Phys. J. C **46**, 689 (2006)
59. A. Arbuzov et al., Phys. Lett. B **383**, 238 (1996)
60. S. Actis et al., Working Group on radiative corrections and Monte Carlo generators for low energies. Eur. Phys. J. C **66**, 585 (2010)
61. V.P. Druzhinin, S.I. Eidelman, S.I. Serednyakov, E.P. Solodov, Rev. Mod. Phys. **83**, 1545 (2011)
62. W. Kluge, Nucl. Phys. Proc. Suppl. **181–182**, 208 (2008)
63. S.K. Dubinsky, A.Y. Korchin, N.P. Merenkov, J. Exp. Theor. Phys. **99**, 225 (2004); [Zh. Eksp. Teor. Fiz. **126**, 259 (2004)]
64. S. Dubinsky, A. Korchin, N. Merenkov, G. Pancheri, O. Shekhovtsova, Eur. Phys. J. C **40**, 41 (2005)
65. A. Anastasi et al. [KLOE-2 Collab.], <http://dx.doi.org/10.1016/j.physletb.2016.12.016>
66. S. Okubo, Phys. Lett. **5**, 1975 (1963); G. Zweig, CERN Report No.8419/TH412 (1964); J. Iizuka. Prog. Theor. Phys. Suppl. **37**, 38 (1966)
67. C.M. Carloni Calame, M. Passera, L. Trentadue, G. Venanzoni, Phys. Lett. B **746**, 325 (2015); see also A.B. Arbuzov, D. Haidt, C. Matteuzzi, M. Paganoni, L. Trentadue. Eur. Phys. J. C **34**, 267 (2004)
68. G. Abbiendi et al., Eur. Phys. J. C **77**, 139 (2017)
69. G. Abbiendi et al., OPAL Collab. Eur. Phys. J. C **45**, 1 (2006)
70. P.A.M. Dirac, Théorie du positron, in *Septième Conseil de Physique Solvay: Structure et propriétés des noyaux atomique, October 22–29, 1933*, (Gauthier-Villars, Paris 1934), pp. 203–230; P.A.M. Dirac, Proc. Cambridge. Phil. Soc. **30**, 150 (1934)
71. J. Schwinger, Phys. Rev. **75**, 651 (1949)
72. R.P. Feynman, Phys. Rev. **76**, 749 (1949)
73. R. Jost, J.M. Luttinger, Helv. Phys. Acta **23**, 201 (1950)
74. P.A. Baikov, K.G. Chetyrkin, J.H. Kühn, Phys. Rev. Lett. **101**, 012002 (2008)
75. V.A. Novikov, L.B. Okun, M.A. Shifman, A.I. Vainshtein, M.B. Voloshin, V.I. Zakharov, Phys. Rept. **41**, 1 (1978)
76. S.L. Adler, Phys. Rev. D **10**, 3714 (1974); A. De Rujula, H. Georgi. Phys. Rev. D **13**, 1296 (1976)
77. G. Serman, S. Weinberg, Phys. Rev. Lett. **39**, 1436 (1977)
78. M.A. Shifman, A.I. Vainshtein, V.I. Zakharov, Nucl. Phys. B **147**, 385 (1979)
79. S. Eidelman, F. Jegerlehner, A.L. Kataev, O. Veretin, Phys. Lett. B **454**, 369 (1999)
80. R.J. Crewther, Phys. Rev. Lett. **28**, 1421 (1972)
81. M.S. Chanowitz, J.R. Ellis, Phys. Rev. D **7**, 2490 (1973)
82. S.L. Adler, J.C. Collins, A. Duncan, Phys. Rev. D **15**, 1712 (1977); J.C. Collins, A. Duncan, S.D. Joglekar. Phys. Rev. D **16**, 438 (1977)
83. J. Gasser. H. Leutwyler, Phys. Rept. **87**, 77 (1982)
84. D.V. Shirkov, I.L. Solovtsov, Phys. Rev. Lett. **79**, 1209 (1997); D.V. Shirkov. Phys. Part. Nucl. Lett. **10**, 186 (2013). (And references therein)
85. S. Bodenstein, C.A. Dominguez, S.I. Eidelman, H. Spiesberger, K. Schilcher, JHEP **1201**, 039 (2012)
86. F. Jegerlehner, Acta Phys. Polon. B **45**(6), 1167 (2014)
87. S.J. Brodsky, E. de Rafael, Phys. Rev. **168**, 1620 (1968)
88. F. Jegerlehner, R. Szafron, Eur. Phys. J. C **71**, 1632 (2011)
89. B. Aubert et al. [BABAR Collab.], Phys. Rev. D **70**, 072004 (2004); **71**, 052001 (2005); **73**, 012005 (2006); **73**, 052003 (2006)
90. B. Aubert et al. [BABAR Collab.], Phys. Rev. D **76**, 012008 (2007); *ibid.* 092005; *ibid.* 092006; D **77**, 092002 (2008)
91. J.P. Lees et al. [BaBar Collab.], Phys. Rev. D **85**, 112009 (2012); Phys. Rev. D **86**, 012008 (2012); Phys. Rev. D **87**, 092005 (2013); Phys. Rev. D **88**, 032013 (2013); Phys. Rev. D **89**, 092002 (2014); Phys. Rev. D **95**, 052001 (2017), [arXiv:1704.05009](https://arxiv.org/abs/1704.05009) [hep-ex]

92. M. Davier, Nucl. Part. Phys. Proc. **260**, 102 (2015), [arXiv:1612.02743](https://arxiv.org/abs/1612.02743) [hep-ph]
93. M.N. Achasov et al. [SND Collab.], Phys. Rev. D **88**(5), 054013 (2013); *ibid.* **90**(11), 112007 (2014)
94. V.M. Aulchenko et al., Phys. Rev. D **91**(5), 052013 (2015)
95. M.N. Achasov et al. [SND Collab.], Phys. Rev. D **93**(9), 092001 (2016); *ibid.* **94**(3), 032010; (9), 092002; (11), 112001; 112006 (2016)
96. R.R. Akhmetshin et al. [CMD-3 Collab.], Phys. Lett. B **723**, 82 (2013); *ibid.* **759**, 634 (2016) 634
97. E.A. Kozyrev et al., CMD-3 Collab. Phys. Lett. B **760**, 314 (2016)
98. F.M. Renard, Nucl. Phys. B **82**, 1 (1974); N.N. Achasov, N.M. Budnev, A.A. Kozhevnikov, G.N. Shestakov, Sov. J. Nucl. Phys. **23**, 320 (1976); N.N. Achasov, A.A. Kozhevnikov, M.S. Dubrovin, V.N. Ivanchenko, E.V. Pakhtusova. Int. J. Mod. Phys. A **7**, 3187 (1992)
99. C. Bouchiat, L. Michel, J. Phys. Radium **22**, 121 (1961)
100. L. Durand, III., Phys. Rev. **128**, 441 (1962); Erratum-*ibid.* **129**, 2835 (1963)
101. T. Kinoshita, R.J. Oakes, Phys. Lett. **25**, 143 (1967)
102. M. Gourdin, E. De Rafael, Nucl. Phys. B **10**, 667 (1969)
103. A. Bramòn, E. Etim, M. Greco, Phys. Lett. **39**, 514 (1972)
104. V. Barger, W.F. Long, M.G. Olsson, Phys. Lett. **60**, 89 (1975)
105. J. Calmet, S. Narison, M. Perrottet, E. de Rafael, Phys. Lett. B **61**, 283 (1976). Rev. Mod. Phys. **49**, 21 (1977)
106. S. Narison, J. Phys. G: Nucl. Phys. **4**, 1849 (1978)
107. L.M. Barkov et al., Nucl. Phys. B **256**, 365 (1985)
108. T. Kinoshita, B. Nizic, Y. Okamoto, Phys. Rev. Lett. **52**, 717 (1984). Phys. Rev. D **31**, 2108 (1985)
109. J.A. Casas, C. Lopez, F.J. Ynduráin, Phys. Rev. D **32**, 736 (1985)
110. Ľ. Martinovič, S. Dubnička, Phys. Rev. D **42**, 884 (1990)
111. A.Z. Dubničková, S. Dubnička, P. Strizenec, Dubna-Report, JINR-E2-92-28 (1992)
112. F. Jegerlehner, in *J*, ed. by Radiative Corrections Solà (World Scientific, Singapore, 1999), pp. 75–89
113. M. Davier, S. Eidelman, A. Höcker, Z. Zhang, Eur. Phys. J. C **27**, 497 (2003). Eur. Phys. J. C **31**, 503 (2003)
114. S. Ghozzi, F. Jegerlehner, Phys. Lett. B **583**, 222 (2004)
115. S. Narison, Phys. Lett. B **568**, 231 (2003)
116. V.V. Ezhela, S.B. Lugovsky, O.V. Zenin, arXiv:hep-ph/0312114
117. K. Hagiwara, A.D. Martin, D. Nomura, T. Teubner, Phys. Lett. B **557**, 69 (2003); Phys. Rev. D **69**, 093003 (2004). Phys. Lett. B **649**, 173 (2007)
118. J.F. De Troconiz, F.J. Yndurain, Phys. Rev. D **65**, 093001 (2002). Phys. Rev. D **71**, 073008 (2005)
119. S. Eidelman, *Status of $(g_\mu - 2)/2$ in Standard Model*, in *Proceedings of the 33rd International Conference on High Energy Physics 2006, "High Energy Physics, ICHEP'06"*, Moscow (Russia), ed. by A. Sissakian, G. Kozlov, E. Kolganova (World Scientific, Singapore, 2007), p. 547; M. Davier, Nucl. Phys. Proc. Suppl. **169**, 288 (2007)
120. H. Leutwyler, *Electromagnetic form factor of the pion*, in *Proceedings of the Continuous Advances in QCD 2002*, ed. by K.A. Olive, M.A. Shifman, M.B. Voloshin (World Scientific, Singapore, 2002). p. 646, [arXiv:hep-ph/0212324](https://arxiv.org/abs/hep-ph/0212324)
121. G. Colangelo, Nucl. Phys. Proc. Suppl. **131**, 185 (2004); *ibid.* **162**, 256 (2006)
122. B. Ananthanarayan, I. Caprini, D. Das, I.S. Imsong, Phys. Rev. D **89**, 036007 (2014). Phys. Rev. D **93**, 116007 (2016)
123. R. Barate et al. [ALEPH Collab.], Z. Phys. C **76**, 15 (1997); Eur. Phys. J. C **4**, 409 (1998); S. Schael et al. [ALEPH Collab.], Phys. Rept. **421**, 191 (2005)
124. M. Davier et al., Eur. Phys. J. C **74**, 2803 (2014)
125. K. Ackerstaff et al., OPAL Collab. Eur. Phys. J. C **7**, 571 (1999)
126. S. Anderson et al., CLEO Collab. Phys. Rev. D **61**, 112002 (2000)
127. M. Fujikawa et al., Belle Collab. Phys. Rev. D **78**, 072006 (2008)

128. K. Hagiwara, A.D. Martin, D. Nomura, T. Teubner, Phys. Lett. B **649**, 173 (2007); T. Teubner, Nucl. Phys. Proc. Suppl. **181–182**, 20 (2008)
129. M. Davier et al., Eur. Phys. J. C **66**, 127 (2010)
130. M. Davier, A. Höcker, B. Malaescu, Z. Zhang, Eur. Phys. J. C **71**, 1515 (2011); [Erratum-ibid. C **72**, 1874 (2012)]
131. K. Hagiwara, R. Liao, A.D. Martin, D. Nomura, T. Teubner, J. Phys. G G **38**, 085003 (2011)
132. M. Benayoun, P. David, L. DelBuono, F. Jegerlehner, Eur. Phys. J. C **72**, 1848 (2012). (And references therein)
133. N. Cabibbo, R. Gatto, Phys. Rev. Lett. **4**, 313, (1960). Phys. Rev. **124**, 1577 (1961)
134. G. Ecker, J. Gasser, A. Pich, E. de Rafael, Nucl. Phys. B **321**, 311 (1989)
135. G. Ecker, J. Gasser, H. Leutwyler, A. Pich, E. de Rafael, Phys. Lett. B **223**, 425 (1989)
136. E. de Rafael, Phys. Lett. B **322**, 239 (1994); J.S. Bell, E. de Rafael. Nucl. Phys. B **11**, 611 (1969)
137. B.V. Geshkenbein, V.L. Morgunov, Phys. Lett. B **352**, 456 (1995)
138. J. Gasser, H. Leutwyler, Ann. Phys. (NY) **158**, 142 (1984)
139. J. Gasser, H. Leutwyler, Nucl. Phys. B **250**, 517 (1985)
140. J. Gasser, U.-G. Meißner, Nucl. Phys. B **357**, 90 (1991)
141. G. Colangelo, M. Finkemeier, R. Urech, Phys. Rev. D **54**, 4403 (1996)
142. S.R. Amendolia et al., NA7 Collab. Nucl. Phys. B **277**, 168 (1986)
143. R. Omnès, Nuovo Cim. **8**, 316 (1958)
144. B. Hyams et al., Nucl. Phys. B **64**, 134 (1973)
145. G. Grayer et al., Nucl. Phys. B **75**, 189 (1974)
146. S.D. Protopopescu et al., Phys. Rev. D **7**, 1279 (1973)
147. B. Ananthanarayan, G. Colangelo, J. Gasser, H. Leutwyler, Phys. Rept. **353**, 207 (2001); G. Colangelo, J. Gasser, H. Leutwyler, Nucl. Phys. B **603**, 125 (2001); I. Caprini, G. Colangelo, J. Gasser, H. Leutwyler, Phys. Rev. D **68**, 074006 (2003); B. Ananthanarayan, I. Caprini, G. Colangelo, J. Gasser, H. Leutwyler. Phys. Lett. B **602**, 218 (2004)
148. H. Leutwyler, *On the Dispersion Theory of $\pi\pi$ Scattering*, [arXiv:hep-ph/0612111](https://arxiv.org/abs/hep-ph/0612111); $\pi\pi$ Scattering, [arXiv:hep-ph/0612112](https://arxiv.org/abs/hep-ph/0612112)
149. B.V. Geshkenbein, Phys. Rev. D **61**, 033009 (2000)
150. E. Fermi, Nuovo Cim. **2S1**, 17 (1955); [Riv. Nuovo Cim. **31**, 1 (2008)]
151. K.M. Watson, Phys. Rev. **95**, 228 (1954)
152. S.M. Roy, Phys. Lett. B **36**, 353 (1971). Helv. Phys. Acta **63**, 627 (1990)
153. I. Caprini, G. Colangelo, H. Leutwyler, Eur. Phys. J. C **72**, 1860 (2012)
154. R. Garcia-Martin, R. Kaminski, J.R. Pelaez, J. Ruiz de Elvira, F.J. Yndurain, Phys. Rev. D **83**, 074004 (2011)
155. G.R. Farrar, D.R. Jackson, Phys. Rev. Lett. **43**, 246 (1979)
156. G.P. Lepage, S.J. Brodsky, Phys. Lett. **87B**, 359 (1979)
157. B. Melic, B. Nizic, K. Passek, Phys. Rev. D **60**, 074004 (1999)
158. L. Łukaszuk, Phys. Lett. B **47**, 51 (1973); S. Eidelman, L. Łukaszuk. Phys. Lett. B **582**, 27 (2004)
159. M. Steinhauser, Phys. Lett. B **429**, 158 (1998). doi:[10.1016/S0370-2693\(98\)00503-6](https://doi.org/10.1016/S0370-2693(98)00503-6)
160. C. Sturm, Nucl. Phys. B **874**, 698 (2013). doi:[10.1016/j.nuclphysb.2013.06.009](https://doi.org/10.1016/j.nuclphysb.2013.06.009)
161. <http://www-com.physik.hu-berlin.de/~fjeger/alphaQED.tar.gz>; <http://www-com.physik.hu-berlin.de/~fjeger/alphaQED.pdf>
162. A. Francis, G. von Hippel, H.B. Meyer, F. Jegerlehner, PoS LATTICE **2013**, 320 (2013), [arXiv:1312.0035](https://arxiv.org/abs/1312.0035) [hep-lat]
163. F. Burger, K. Jansen, M. Petschlies, G. Pientka, JHEP **1511**, 215 (2015)
164. Y.S. Tsai, Phys. Rev. D **4**, 2821 (1971); [Erratum-ibid. D **13**, 771 (1976)]
165. W.J. Marciano, A. Sirlin, Phys. Rev. Lett. **61**, 1815 (1988)
166. E. Braaten, C.S. Li, Phys. Rev. D **42**, 3888 (1990)
167. R. Decker, M. Finkemeier, Nucl. Phys. B **438**, 17 (1995)
168. J. Erler, Rev. Mex. Fis. **50**, 200 (2004), [arXiv:hep-ph/0211345](https://arxiv.org/abs/hep-ph/0211345)
169. V. Cirigliano, G. Ecker, H. Neufeld, Phys. Lett. B **513**, 361 (2001); JHEP **0208**, 002 (2002)

170. F. Flores-Baez, A. Flores-Tlalpa, G. Lopez, Castro, G. Toledo Sanchez, Phys. Rev. D **74**, 071301 (2006); A. Flores-Tlalpa, F. Flores-Baez, G. Lopez Castro, G. Toledo Sanchez, Nucl. Phys. Proc. Suppl. **169**, 250 (2007); F.V. Flores-Baez, G.L. Castro, G. Toledo Sanchez. Phys. Rev. D **76**, 096010 (2007)
171. Z. Zhang, EPJ Web Conf. **118**, 01036 (2016). doi:[10.1051/epjconf/201611801036](https://doi.org/10.1051/epjconf/201611801036)
172. L.M. Barkov et al., (OLYA, CMD), Nucl. Phys. B **256**, 365 (1985); R.R. Akhmetshin et al. [CMD-2 Collab.], [arXiv:hep-ex/9904027](https://arxiv.org/abs/hep-ex/9904027); Phys. Lett. B **527**, 161 (2002); *ibid.* **578**, 285 (2004)
173. J. Gluza, A. Hoefler, S. Jadach, F. Jegerlehner, Eur. Phys. J. C **28**, 261 (2003)
174. H. Czyż, A. Grzelińska, J.H. Kühn, Phys. Lett. B **611**, 116 (2005)
175. G. Pancheri, O. Shekhovtsova, G. Venanzoni, Phys. Lett. B **642**, 342 (2006)
176. F. Ambrosino et al., [KLOE Collab.], Phys. Lett. B **634**, 148 (2006). Eur. Phys. J. C **49**, 473 (2007)
177. R. Brandelik et al., Tasso Collab. Z. Phys. C **10**, 117 (1981)
178. H. Marsiske et al. [Crystal Ball Collab.], Phys. Rev. D **41**, 3324 (1990); J.K. Bienlein, DESY-92-083B
179. T. Oest et al., JADE Collab. Z. Phys. C **47**, 343 (1990)
180. J. Boyer et al., for the MARK II Collab. Phys. Rev. D **42**, 1350 (1990)
181. C. Berger et al., PLUTO Collab. Z. Phys. C **26**, 199 (1984)
182. H.J. Behrend et al., CELLO Collab. Z. Phys. C **56**, 381 (1992)
183. H. Nakazawa et al. [Belle Collab.], Phys. Lett. B **615**, 39 (2005); S. Uehara et al., Phys. Rev. D **79**, 052009; (2009); Phys. Rev. D **78**, 052004 (2008); H. Nakazawa [Belle Collab.], Nucl. Part. Phys. Proc. **260**, 98 (2015)
184. M. Masuda et al., Belle Collab. Phys. Rev. D **93**(3), 032003 (2016)
185. G. Mennessier, Z. Phys. C **16**, 241 (1983); G. Mennessier, S. Narison, W. Ochs. Phys. Lett. B **665**, 205 (2008)
186. S. Bellucci, J. Gasser, M.E. Sainio, Nucl. Phys. B **423**, 80 (1994); [Erratum-*ibid.* B **431**, 413 (1994)]; J. Gasser, M.A. Ivanov, M.E. Sainio, Nucl. Phys. B **728**, 31 (2005). Nucl. Phys. B **745**, 84 (2006)
187. M. Knecht, B. Moussallam, J. Stern, Nucl. Phys. B **429**, 125 (1994); R. Garcia-Martin, B. Moussallam. Eur. Phys. J. C **70**, 155 (2010)
188. N.N. Achasov, G.N. Shestakov, Phys. Rev. D **77**, 074020 (2008); JETP Lett. **88**, 295 (2008); [Pisma Zh. Eksp. Teor. Fiz. **88**, 345 (2008)]
189. M.R. Pennington, T. Mori, S. Uehara, Y. Watanabe, Eur. Phys. J. C **56**, 1 (2008); M.R. Pennington, [arXiv:0906.1072](https://arxiv.org/abs/0906.1072)
190. M. Bando, T. Kugo, S. Uehara, K. Yamawaki, T. Yanagida, Phys. Rev. Lett. **54**, 1215 (1985); M. Bando, T. Kugo, K. Yamawaki, Phys. Rept. **164**, 217 (1988); M. Harada, K. Yamawaki, Phys. Rept. **381**, 1 (2003)
191. U.G. Meissner, Phys. Rept. **161**, 213 (1988); see also S. Weinberg. Phys. Rev. **166**, 1568 (1968)
192. J. Prades, Z. Phys. C **63**, 491 (1994); Erratum: Eur. Phys. J. C **11**, 571 (1999)
193. M. Benayoun, P. David, L. DelBuono, O. Leitner, H.B. O'Connell, Eur. Phys. J. C **55**, 199 (2008)
194. M. Benayoun, P. David, L. DelBuono, O. Leitner, Eur. Phys. J. C **65**, 211 (2010). Eur. Phys. J. C **68**, 355 (2010)
195. S. Bodenstein, C.A. Dominguez, K. Schilcher, Phys. Rev. D **85**, 014029 (2012); Erratum: [Phys. Rev. D **87**(7), 079902 (2013)]
196. S. Bodenstein, C.A. Dominguez, K. Schilcher, H. Spiesberger, Phys. Rev. D **88**(1), 014005 (2013)
197. P. Masjuan et al., [arXiv:1306.2045](https://arxiv.org/abs/1306.2045) [hep-ph]
198. A.V. Nesterenko, [arXiv:1701.00678](https://arxiv.org/abs/1701.00678) [hep-ph]
199. N.F. Nasrallah, N.A. Papadopoulos, K. Schilcher, Phys. Lett. **126B**, 379 (1983)
200. N.A. Papadopoulos, J.A. Penarrocha, F. Scheck, K. Schilcher, Nucl. Phys. B **258**, 1 (1985)
201. R. Barbieri, E. Remiddi, Phys. Lett. B **49**, 468 (1974). Nucl. Phys. B **90**, 233 (1975)
202. B. Krause, Phys. Lett. B **390**, 392 (1997)

203. J.S. Schwinger, *Particles, Sources, Fields*, vol. 3 (Addison–Wesley, Redwood City (USA) 1989), p. 99; see also: M. Drees, K.I. Hikasa, *Phys. Lett. B* **252**, 127 (1990); where a misprint in Schwinger’s formula is corrected
204. K. Melnikov, *Int. J. Mod. Phys. A* **16**, 4591 (2001)
205. J.J. Sakurai, *Ann. Phys. (NY)* **11**, 1 (1960); H. Joos, *Acta Phys. Austriaca Suppl.* **4** (1967); N.M. Kroll, T.D. Lee, B. Zumino, *Phys. Rev.* **157**, 1376 (1967)
206. A. Kurz, T. Liu, P. Marquard, M. Steinhauser, *Phys. Lett. B* **734**, 144 (2014)
207. A. Kurz, T. Liu, P. Marquard, M. Steinhauser, *PoS LL* **2014**, 051 (2014)
208. A. Kurz, T. Liu, P. Marquard, A.V. Smirnov, V.A. Smirnov, M. Steinhauser, *EPJ Web Conf.* **118**, 01033 (2016)
209. G. Colangelo, M. Hoferichter, A. Nyffeler, M. Passera, P. Stoffer, *Phys. Lett. B* **735**, 90 (2014)
210. M. Hayakawa, T. Kinoshita, A.I. Sanda, *Phys. Rev. Lett.* **75**, 790 (1995). *Phys. Rev. D* **54**, 3137 (1996)
211. Z. Bern, A. De Freitas, L.J. Dixon, A. Ghinculov, H.L. Wong, *JHEP* **0111**, 031 (2001)
212. M. Hayakawa, T. Blum, N.H. Christ, T. Izubuchi, L.C. Jin, C. Lehner, *PoS LATTICE* **2015**, 104 (2016), [arXiv:1511.01493](https://arxiv.org/abs/1511.01493) [hep-lat]
213. J. Green, O. Gryniuk, G. von Hippel, H.B. Meyer, V. Pascalutsa, *Phys. Rev. Lett.* **115**(22), 222003 (2015)
214. J. Green, N. Asmussen, O. Gryniuk, G. von Hippel, H.B. Meyer, A. Nyffeler, V. Pascalutsa, *PoS LATTICE* **2015**, 109 (2016), [arXiv:1510.08384](https://arxiv.org/abs/1510.08384) [hep-lat]; N. Asmussen, J. Green, H.B. Meyer, A. Nyffeler, [arXiv:1609.08454](https://arxiv.org/abs/1609.08454) [hep-lat]
215. T. Blum, N. Christ, M. Hayakawa, T. Izubuchi, L. Jin, C. Jung, C. Lehner, *Phys. Rev. Lett.* **118**(2), 022005 (2017)
216. L. Jin, T. Blum, N. Christ, M. Hayakawa, T. Izubuchi, C. Jung, C. Lehner, [arXiv:1611.08685](https://arxiv.org/abs/1611.08685) [hep-lat]
217. C.S. Fischer, T. Goecke, R. Williams, *Eur. Phys. J. A* **47**, 28 (2011), [arXiv:1009.5297](https://arxiv.org/abs/1009.5297) [hep-ph]
218. T. Goecke, C.S. Fischer, R. Williams, *Phys. Rev. D* **83**, 094006 (2011); [Erratum-ibid. **D 86**, 099901 (2012)]
219. T. Goecke, C.S. Fischer, R. Williams, *Phys. Rev. D* **87**, 034013 (2013)
220. G. Eichmann, C.S. Fischer, W. Heupel, R. Williams, *A.I.P. Conf. Proc.* **1701**, 040004 (2016), [arXiv:1411.7876](https://arxiv.org/abs/1411.7876) [hep-ph]
221. G. Colangelo, M. Hoferichter, B. Kubis, M. Procura, P. Stoffer, *Phys. Lett. B* **738**, 6 (2014)
222. G. Colangelo, M. Hoferichter, M. Procura, P. Stoffer, *JHEP* **1409**, 091 (2014)
223. V. Pauk, M. Vanderhaeghen, *Phys. Rev. D* **90**(11), 113012 (2014); <http://dx.doi.org/10.1103/PhysRevD.90.113012>
224. V. Pascalutsa, V. Pauk, M. Vanderhaeghen, *Phys. Rev. D* **85**, 116001 (2012)
225. I. Danilkin, M. Vanderhaeghen, [arXiv:1611.04646](https://arxiv.org/abs/1611.04646) [hep-ph]
226. G. ’t Hooft, *Nucl. Phys. B* **72**, 461 (1974); *ibid.* **75**, 461 (1974); E. Witten, *Nucl. Phys. B* **160**, 57 (1979)
227. A.V. Manohar, *Hadrons, in the 1/N expansion, in At the Frontier of Particle Physics*, ed. by M. Shifman, vol. 1, (World Scientific, Singapore, 2001), pp. 507–568
228. H. Leutwyler, *Nucl. Phys. Proc. Suppl.* **64**, 223 (1998); R. Kaiser, H. Leutwyler, *Eur. Phys. J. C* **17**, 623 (2000)
229. B.V. Geshkenbein, V.L. Morgunov, [arXiv:hep-ph/9410252](https://arxiv.org/abs/hep-ph/9410252)
230. E. Czerwinski et al., *MesonNet Workshop on Meson Transition Form Factors*, [arXiv:1207.6556](https://arxiv.org/abs/1207.6556) [hep-ph]
231. A. Dhar, R. Shankar, S.R. Wadia, *Phys. Rev. D* **31**, 3256 (1985); D. Ebert, H. Reinhardt, *Phys. Lett. B* **173**, 453 (1986)
232. S.J. Brodsky, G.R. Farrar, *Phys. Rev. Lett.* **31**, 1153 (1973). *Phys. Rev. D* **11**, 1309 (1975)
233. H. Leutwyler, *Nucl. Phys. Proc. Suppl.* **64**, 223 (1998); R. Kaiser, H. Leutwyler, [arXiv:hep-ph/9806336](https://arxiv.org/abs/hep-ph/9806336)
234. M. Knecht, A. Nyffeler, *Phys. Rev. D* **65**, 073034 (2002)
235. J. Bijnens, E. Pallante, J. Prades, *Phys. Rev. Lett.* **75**, 1447 (1995); [Erratum-ibid. **75**, 3781 (1995)]; *Nucl. Phys. B* **474**, 379 (1996); [Erratum-ibid. **626**, 410 (2002)]

236. J. Bijnens, J. Releford, [arXiv:1608.01454](https://arxiv.org/abs/1608.01454) [hep-ph]
237. G. Colangelo, M. Hoferichter, M. Procura, P. Stoffer, *JHEP* **1509**, 074 (2015)
238. J. Wess, B. Zumino, *Phys. Lett. B* **37**, 95 (1971)
239. E. Witten, *Nucl. Phys. B* **223**, 422 (1983)
240. S.L. Adler, *Phys. Rev.* **177**, 2426 (1969); J.S. Bell, R. Jackiw, *Nuovo Cim.* **60A**, 47 (1969); W.A. Bardeen. *Phys. Rev.* **184**, 1848 (1969)
241. Y. Nambu, G. Jona-Lasinio, *Phys. Rev.* **122**, 345 (1961); *ibid.* **124**, 246 (1961)
242. M. Gell-Mann, M. Levy, *Nuovo Cim.* **16**, 705 (1960)
243. J. Bijnens, *Phys. Rept.* **265**, 369 (1996)
244. G.A. Schuler, F.A. Berends, R. van Gulik, *Nucl. Phys. B* **523**, 423 (1998)
245. K. Kawarabayashi, M. Suzuki, *Phys. Rev. Lett.* **16**, 255 (1966); R. Fayyazuddin. *Phys. Rev.* **147**, 1071 (1966)
246. S. Peris, M. Perrottet, E. de Rafael, *JHEP* **9805**, 011 (1998); M. Knecht, S. Peris, M. Perrottet, E. de Rafael. *Phys. Rev. Lett.* **83**, 5230 (1999)
247. M. Knecht, A. Nyffeler, *Eur. Phys. J. C* **21**, 659 (2001)
248. J. Bijnens, E. Gamiz, E. Lipartia, J. Prades, *JHEP* **0304**, 055 (2003)
249. J. Bijnens, *EPJ Web Conf.* **118**, 01002 (2016); see also J. Bijnens, M.Z. Abyaneh, *EPJ Web Conf.* **37**, 01007 (2012); M.Z. Abyaneh, The Anatomy of the Pion Loop Hadronic Light by Light Scattering Contribution to the Muon Magnetic Anomaly, [arXiv:1208.2554](https://arxiv.org/abs/1208.2554) [hep-ph], master thesis
250. M. Hayakawa, T. Kinoshita, *Phys. Rev. D* **57**, 465 (1998); [Erratum-*ibid.* **D 66**, 019902 (2002)]
251. M. Knecht, A. Nyffeler, M. Perrottet, E. De Rafael, *Phys. Rev. Lett.* **88**, 071802 (2002)
252. I. Blokland, A. Czarnecki, K. Melnikov, *Phys. Rev. Lett.* **88**, 071803 (2002)
253. M. Ramsey-Musolf, M.B. Wise, *Phys. Rev. Lett.* **89**, 041601 (2002)
254. K. Melnikov, A. Vainshtein, *Phys. Rev. D* **70**, 113006 (2004)
255. J.L. Rosner, *Ann. Phys. (N.Y.)* **44**, 11 (1967); Implicitly, the Method of Gegenbauer Polynomials was Already used in the Following Papers: M. Baker, K. Johnson, R. Willey, *Phys. Rev.* **136**, B1111 (1964); **163**, 1699 (1967); M.J. Levine, R. Roskies, *Phys. Rev. D* **9**, 421 (1974); M.J. Levine, E. Remiddi, R. Roskies, *ibid.* **20**, 2068 (1979); R.Z. Roskies, E. Remiddi, M.J. Levine, in *Quantum Electrodynamics*, ed. by T. Kinoshita (World Scientific, Singapore, 1990) p. 162
256. H.J. Behrend et al., CELLO Collab. *Z. Phys. C* **49**, 401 (1991)
257. J. Gronberg et al., CLEO Collab. *Phys. Rev. D* **57**, 33 (1998)
258. G.P. Lepage, S.J. Brodsky, *Phys. Rev. D* **22**, 2157 (1980); S.J. Brodsky, G.P. Lepage. *Phys. Rev. D* **24**, 1808 (1981)
259. A.V. Efremov, A.V. Radyushkin, *Phys. Lett. B* **94**, 245 (1980); A.V. Radyushkin, R. Ruskov, *Phys. Lett. B* **374**, 173 (1996); A.V. Radyushkin. *Acta Phys. Polon. B* **26**, 2067 (1995)
260. S. Ong, *Phys. Rev. D* **52**, 3111 (1995); P. Kroll, M. Raulfs, *Phys. Lett. B* **387**, 848 (1996); A. Khodjamirian. *Eur. Phys. J. C* **6**, 477 (1999)
261. Y. Klopot, A. Oganesian, O. Teryaev, *Phys. Rev. D* **87**(3), 036013 (2013); Erratum: [*Phys. Rev. D* **88**(5), 059902 (2013)]; A.G. Oganesian, A.V. Pimikov, N.G. Stefanis, O.V. Teryaev. *Phys. Rev. D* **93**(5), 054040 (2016)
262. F. del Aguila, M.K. Chase, *Nucl. Phys. B* **193**, 517 (1981); E. Braaten, *Phys. Rev. D* **28**, 524 (1983); E.P. Kadantseva, S.V. Mikhailov, A.V. Radyushkin, *Yad. Fiz.* **44**, 507 (1986); [*Sov. J. Nucl. Phys.* **44**, 326 (1986)]
263. A.E. Dorokhov, [arXiv:1003.4693](https://arxiv.org/abs/1003.4693) [hep-ph]
264. S.V. Mikhailov, A.V. Pimikov, N.G. Stefanis, *Phys. Rev. D* **82**, 054020 (2010), [arXiv:1010.4711](https://arxiv.org/abs/1010.4711) [hep-ph]
265. P. Kroll, [arXiv:1012.3542](https://arxiv.org/abs/1012.3542) [hep-ph]
266. S.S. Agaev, V.M. Braun, N. Offen, F.A. Porkert, [arXiv:1012.4671](https://arxiv.org/abs/1012.4671) [hep-ph]
267. T.N. Pham, X.Y. Pham, [arXiv:1101.3177](https://arxiv.org/abs/1101.3177) [hep-ph]
268. B. Aubert et al., BaBar Collab. *Phys. Rev. D* **80**, 052002 (2009)
269. S. Uehara et al., Belle Collab. *Phys. Rev. D* **86**, 092007 (2012)
270. S. Uehara et al., Belle Collab. *Phys. Rev. D* **80**, 032001 (2009)

271. S. Uehara et al., Belle Collab. Phys. Rev. D **82**, 114031 (2010)
272. P. del Amo Sanchez et al., BABAR Collab. Phys. Rev. D **84**, 052001 (2011)
273. F. Jegerlehner, Acta Phys. Polon. B **38**, 3021 (2007)
274. A. Nyffeler, Phys. Rev. D **79**, 073012 (2009)
275. F. Jegerlehner, A. Nyffeler, Phys. Rept. **477**, 1 (2009)
276. A. Nyffeler, Nucl. Phys. (Proc. Suppl.) **116**, 225 (2003); Nucl. Phys. B (Proc. Suppl.) **131**, 162 (2004)
277. E. de Rafael, Phys. Lett. B **703**, 60 (2011)
278. D. Greynat, E. de Rafael, JHEP **1207**, 020 (2012)
279. A.D. Dolgov, V.I. Zakharov, Nucl. Phys. B **27**, 525 (1971)
280. V.M. Belyaev, Y.I. Kogan, Sov. J. Nucl. Phys. **40**, 659 (1984); [Yad. Fiz. **40**, 1035 (1984)]
281. B.L. Ioffe, A.V. Smilga, Nucl. Phys. B **232**, 109 (1984)
282. V. Mateu, J. Portoles, Eur. Phys. J. C **52**, 325 (2007)
283. A. Vainshtein, Phys. Lett. B **569**, 187 (2003)
284. S. Narison, Phys. Lett. B **666**, 455 (2008)
285. A.E. Dorokhov, Eur. Phys. J. C **42**, 309 (2005)
286. V.Y. Petrov, M.V. Polyakov, R. Ruskov, C. Weiss, K. Goeke, Phys. Rev. D **59**, 114018 (1999); K. Goeke, H.C. Kim, M.M. Musakhanov, M. Siddikov. Phys. Rev. D **76**, 116007 (2007)
287. I.I. Balitsky, A.V. Yung, Phys. Lett. B **129**, 328 (1983)
288. I.I. Balitsky, A.V. Kolesnichenko, A.V. Yung, Sov. J. Nucl. Phys. **41**, 178 (1985); [Yad. Fiz. **41**, 282 (1985)]
289. P. Ball, V.M. Braun, N. Kivel, Nucl. Phys. B **649**, 263 (2003)
290. E.V. Shuryak, A.I. Vainshtein, Nucl. Phys. B **199**, 451 (1982)
291. V.A. Novikov, M.A. Shifman, A.I. Vainshtein, M.B. Voloshin, V.I. Zakharov, Nucl. Phys. B **237**, 525 (1984)
292. J. Bijnens, F. Persson, *Effects of Different form-factors in meson photon photon transitions and the muon anomalous magnetic moment*, [arXiv:hep-ph/0106130](https://arxiv.org/abs/hep-ph/0106130)
293. A. Gérardin, H.B. Meyer, A. Nyffeler, Phys. Rev. D **94**, 074507 (2016); PoS LATTICE **2016**, 175 (2017)
294. G. Antoine, H.B. Meyer, A. Nyffeler, [arXiv:1611.02190](https://arxiv.org/abs/1611.02190) [hep-lat]
295. T. Feldmann, P. Kroll, B. Stech, Phys. Lett. B **449**, 339 (1999). Phys. Rev. D **58**, 114006 (1998)
296. E. Bartos, A.Z. Dubnickova, S. Dubnicka, E.A. Kuraev, E. Zemlyanaya, Nucl. Phys. B **632**, 330 (2002)
297. R. Escribano, J.M. Frère, JHEP **0506**, 029 (2005)
298. P. Roig, A. Guevara, G. Lpez, Castro. Phys. Rev. D **89**(7), 073016 (2014), [arXiv:1401.4099](https://arxiv.org/abs/1401.4099) [hep-ph]
299. K. Kampf, J. Novotny, Phys. Rev. D **84**, 014036 (2011)
300. A.E. Dorokhov, W. Broniowski, Phys. Rev. D **78**, 073011 (2008)
301. A.E. Dorokhov, A.E. Radzhabov, A.S. Zhevlakov, JETP Lett. **100**(2), 133 (2014); [Pisma Zh. Eksp. Teor. Fiz. **100**(2), 141 (2014)]
302. D.K. Hong, D. Kim, Phys. Lett. B **680**, 480 (2009)
303. L. Cappiello, O. Cata, G. D'Ambrosio, Phys. Rev. D **83**, 093006 (2011)
304. P. Masjuan, P. Sanchez-Puertas, Phys. Rev. D **95**, 054026 (2017)
305. A. Nyffeler, *Theoretical Status of the Muon $g - 2$* , [arXiv:hep-ph/0305135](https://arxiv.org/abs/hep-ph/0305135)
306. M. Knecht, S. Peris, M. Perrottet, E. de Rafael, JHEP **0403**, 035 (2004)
307. F. Jegerlehner, O.V. Tarasov, Phys. Lett. B **639**, 299 (2006)
308. J. Mondejar, K. Melnikov, Phys. Lett. B **718**, 1364 (2013)
309. T. Blum, N. Christ, M. Hayakawa, T. Izubuchi, L. Jin, C. Lehner, Phys. Rev. D **93**(1), 014503 (2016)
310. S.L. Adler, W.A. Bardeen, Phys. Rev. **182**, 1517 (1969)
311. E.J. Schreier, Phys. Rev. D **3**, 980 (1971)
312. T.L. Trueman, Phys. Lett. B **88**, 331 (1979)
313. S.A. Larin, Phys. Lett. B **303**, 113 (1993)

314. D. Espriu, R. Tarrach, Z. Phys. C **16**, 77 (1982)
315. L.D. Landau, Dokl. Akad. Nauk., USSR **60**, 207 (1948); C.N. Yang, Phys. Rev. **77**, 242 (1950)
316. H.J. Behrend et al., CELLO Collab. Z. Phys. C **42**, 367 (1989)
317. P. Achard et al. [L3 Collab.], JHEP **0703**, 018 (2007)
318. R. Ahohe et al., CLEO Collab. Phys. Rev. D **71**, 072001 (2005)
319. <http://pdg.lbl.gov/rpp/book/page1484.ps>
320. G. Köpp, T.F. Walsh, P.M. Zerwas, Nucl. Phys. B **70**, 461 (1974)
321. P. Achard et al., L3 Collab. Phys. Lett. B **526**, 269 (2002)
322. J. Bijnens, J. Prades, Z. Phys. C **64**, 475 (1994)
323. S. Weinberg, Phys. Rev. Lett. **18**, 507 (1967)
324. E.G. Floratos, S. Narison, E. de Rafael, Nucl. Phys. B **155**, 115 (1979)
325. V. Pauk, M. Vanderhaeghen, Eur. Phys. J. C **74**(8), 3008 (2014), <http://dx.doi.org/10.1140/epjc/s10052-014-3008-y>
326. F. Jegerlehner, talk presented at the workshop on Hadronic contributions to the muon anomalous magnetic moment: strategies for improvements of the accuracy of the theoretical prediction, 1–5 April 2014, Waldthausen Castle near Mainz
327. J. Bijnens, J. Prades, Mod. Phys. Lett. A **22**, 767 (2007)
328. J. Prades, E. de Rafael, A. Vainshtein, Advanced series on directions in high energy physics **20** (2009) 303, ed by B.L. Roberts, W. Marciano, [arXiv:0901.0306](https://arxiv.org/abs/0901.0306) [hep-ph] (2009)
329. S. Spanier, N.A. Törnqvist, *Note on Scalar Mesons in* [42]
330. Y. Mao, X.G. Wang, O. Zhang, H.Q. Zheng, Z.Y. Zhou, Phys. Rev. D **79**, 116008 (2009)
331. M. Procura, G. Colangelo, M. Hoferichter, P. Stoffer, EPJ Web Conf. **118**, 01030 (2016)
332. G. Colangelo, M. Hoferichter, M. Procura, P. Stoffer, [arXiv:1701.06554](https://arxiv.org/abs/1701.06554) [hep-ph]; [arXiv:1702.07347](https://arxiv.org/abs/1702.07347) [hep-ph]
333. J.H. Kühn, A.I. Onishchenko, A.A. Pivovarov, O.L. Veretin, Phys. Rev. D **68**, 033018 (2003)
334. K.T. Engel, H.H. Patel, M.J. Ramsey-Musolf, Phys. Rev. D **86**, 037502 (2012); see also J.F. Donoghue, B.R. Holstein, Phys. Rev. D **48**, 137 (1993)
335. K.T. Engel, M.J. Ramsey-Musolf, Phys. Lett. B **738**, 123 (2014); K.T. Engel, *Charged pion contribution to the anomalous magnetic moment of the muon*, Dissertation (Ph.D.), California Institute of Technology, <http://resolver.caltech.edu/CaltechTHESIS:05212013-160540441>
336. C. Adolph et al., COMPASS Collab. Phys. Rev. Lett. **114**, 062002 (2015)
337. L.Y. Dai, M.R. Pennington, Phys. Rev. D **94**(11), 116021 (2016)
338. H. Krasemann, J.A.M. Vermaseren, Nucl. Phys. B **184**, 269 (1981)
339. A.E. Dorokhov, A.E. Radzhabov, A.S. Zhevlakov, Eur. Phys. J. C **75**(9), 417 (2015)
340. R. Boughezal, K. Melnikov, Phys. Lett. B **704**, 193 (2011)
341. P. Masjuan, M. Vanderhaeghen, [arXiv:1212.0357](https://arxiv.org/abs/1212.0357) [hep-ph]
342. J. Erler, G. Toledo, Sanchez, Phys. Rev. Lett. **97**, 161801 (2006)
343. A. Nyffeler, EPJ Web Conf. **118**, 01024 (2016)
344. G. Mennessier, Z. Phys. C **16**, 241 (1983) 241
345. J. Bijnens, F. Cornet, Nucl. Phys. B **296**, 557 (1988)
346. M.R. Pennington, Mod. Phys. Lett. A **22**, 1439 (2007)
347. M.R. Pennington, T. Mori, S. Uehara, Y. Watanabe, Eur. Phys. J. C **56**, 1 (2008)
348. R. Garcia-Martin, B. Moussallam, Eur. Phys. J. C **70**, 155 (2010)
349. N.N. Achasov, G.N. Shestakov, Phys. Rev. D **81**, 094029 (2010)
350. B. Moussallam, Eur. Phys. J. C **73**, 2539 (2013)
351. L.Y. Dai, M.R. Pennington, Phys. Rev. D **90**(3), 036004 (2014)
352. D. Babusci et al., Eur. Phys. J. C **72**, 1917 (2012)
353. A. Nyffeler, PoS CD **12**, 045 (2013), [arXiv:1306.5987](https://arxiv.org/abs/1306.5987) [hep-ph]
354. C.F. Redmer, EPJ Web Conf. **130**, 01013 (2016)
355. G. Amelino-Camelia et al., Eur. Phys. J. C **68**, 619 (2010)
356. M. Benayoun et al., *Hadronic Contributions to the Muon Anomalous Magnetic Moment Workshop. $(g - 2)_\mu$: Quo vadis? Workshop. Mini Proceedings*, [arXiv:1407.4021](https://arxiv.org/abs/1407.4021) [hep-ph]
357. K. Nakamura et al. [Particle Data Group Collab.], J. Phys. G **37**, 075021 (2010)

358. W.A. Bardeen, W.K. Tung, Phys. Rev. **173**, 1423 (1968); Erratum: [Phys. Rev. D **4**, 3229 (1971)]
359. R. Tarrach, Nuovo Cim. A **28**, 409 (1975)
360. S. Mandelstam, Phys. Rev. **112**, 1344 (1958)
361. A.D. Martin, T.D. Spearman, *Elementary Particle Theory* (North-Holland Publishing Company, Amsterdam, 1970)
362. M. Poppe, Int. J. Mod. Phys. A **1**, 545 (1986)
363. F. Knechtli, M. Günther, M. Peardon, Lattice Quantum Chromodynamics, Practical Essentials, Springer Briefs in Physics. doi:[10.1007/978-94-024-0999-4](https://doi.org/10.1007/978-94-024-0999-4)
364. K.G. Wilson, Phys. Rev. D **10**, 2445 (1974)
365. N. Metropolis, A.W. Rosenbluth, M.N. Rosenbluth, A.H. Teller, E. Teller, Equation of state calculations by fast computing machines. J. Chem. Phys. **21**, 1087 (1953)
366. E. Stiefel, Über einige methoden der relaxationsrechnung. Z. Angew. Math. Phys. **3**, 1–33 (1952); M.R. Hestenes, E. Stiefel, Methods of conjugate gradients for solving linear systems. J. Res. Natl. Bur. Stand. **49**, 409–436 (1952)
367. B. Sheikholeslami, R. Wohlert, Nucl. Phys. B **259**, 572 (1985)
368. H. Wittig, Talk at Lattice (2016)
369. X. Feng, K. Jansen, D.B. Renner, Phys. Rev. D **83**, 094505 (2011)
370. C. Aubin, T. Blum, P. Chau, M. Golterman, S. Peris, C. Tu, Phys. Rev. D **93**, 054508 (2016)
371. A. Francis, G. Herdoíza, H. Horch, B. Jäger, H.B. Meyer, H. Wittig, PoS LATTICE **2014**, 163 (2014), [arXiv:1412.6934](https://arxiv.org/abs/1412.6934) [hep-lat]
372. M. Della Morte, A. Francis, G. Herdoíza, H. Horch, B. Jäger, A. Jüttner, H. Meyer, H. Wittig, PoS LATTICE **2014**, 162 (2014), [arXiv:1411.1206](https://arxiv.org/abs/1411.1206) [hep-lat]
373. M. Benayoun, P. David, L. DelBuono, F. Jegerlehner, [arXiv:1605.04474](https://arxiv.org/abs/1605.04474) [hep-ph]
374. X. Feng, K. Jansen, M. Petschlies, D.B. Renner, Phys. Rev. Lett. **107**, 081802 (2011)
375. H. Horch, Talk at Lattice 2016, in the leading order hadronic contribution of the anomalous magnetic moment of the muon with $O(a)$ -improved Wilson fermions with Padé approximants from fits and time moments. PoS LATTICE **2016**, 165 (2016)
376. X. Feng, S. Hashimoto, G. Hotzel, K. Jansen, M. Petschlies, D.B. Renner, Phys. Rev. D **88**, 034505 (2013)
377. K. Jansen, X. Feng, S. Hashimoto, G. Hotzel, M. Petschlies, D. Renner, PoS LATTICE **2013**, 464 (2014)
378. G.D. Allen, C.K. Chui, W.R. Madych, F.J. Narcowich, P.W. Smith, J. Approx. Theory **14**(4), 302–316 (1975)
379. Y.L. Luke, Comput. Math. Appl. **3**(4), 307–314 (1977)
380. C. Aubin, T. Blum, M. Golterman, S. Peris, Phys. Rev. D **86**, 054509 (2012)
381. B. Chakraborty et al., HPQCD Collab. Phys. Rev. D **89**, 114501 (2014)
382. B. Chakraborty, C.T.H. Davies, P.G. de Oliviera, J. Koponen, G.P. Lepage, [arXiv:1601.03071](https://arxiv.org/abs/1601.03071) [hep-lat]
383. M. Della Morte, B. Jäger, A. Jüttner, H. Wittig, JHEP **1203**, 055 (2012); A. Francis et al., [arXiv:1411.3031](https://arxiv.org/abs/1411.3031) [hep-lat]
384. K. Maltman, M. Golterman, S. Peris, PoS LATTICE **2014**, 126 (2014), [arXiv:1410.7068](https://arxiv.org/abs/1410.7068) [hep-lat]
385. E.B. Gregory, C. McNeile, PoS LATTICE **2015**, 113 (2016), [arXiv:1512.00331](https://arxiv.org/abs/1512.00331) [hep-lat]
386. M. Golterman, K. Maltman, S. Peris, Phys. Rev. D **90**(7), 074508 (2014)
387. M. Della Morte et al., [arXiv:1705.01775](https://arxiv.org/abs/1705.01775) [hep-lat]
388. D. Bernecker, H.B. Meyer, Eur. Phys. J. A **47**, 148 (2011)
389. A. Francis, B. Jäger, H.B. Meyer, H. Wittig, Phys. Rev. D **88**, 054502 (2013)
390. E. de Rafael, Phys. Lett. B **736**, 522 (2014)
391. S. Borsanyi et al., [arXiv:1612.02364](https://arxiv.org/abs/1612.02364) [hep-lat]; K. Miura et al. [Budapest-Marseille-Wuppertal Collab.], PoS LATTICE **2016**, 174 (2017)
392. T. Kawanai et al. [Budapest-Marseille-Wuppertal Collab.], PoS LATTICE **2016**, 171 (2017)
393. C. Aubin, T. Blum, Phys. Rev. D **75**, 114502 (2007)

394. M. Della Morte, G. Herdoíza, H. Horch, B. Jäger, H. Meyer, H. Wittig, PoS LATTICE **2015**, 111 (2015)
395. D.B. Renner, X. Feng, K. Jansen, M. Petschlies, PoS LATTICE **2011**, 022 (2012)
396. F. Burger et al. [ETM Collab.], JHEP **1402**, 099 (2014), [http://dx.doi.org/10.1007/JHEP02\(2014\)099](http://dx.doi.org/10.1007/JHEP02(2014)099)
397. M. Della Morte, A. Jüttner, JHEP **1011**, 154 (2010)
398. J. Bijnens, J. Releforts, [arXiv:1609.01573](https://arxiv.org/abs/1609.01573) [hep-lat]
399. V. Gülpers, A. Francis, B. Jäger, H. Meyer, G. von Hippel, H. Wittig, PoS LATTICE **2014**, 128 (2014)
400. T. Blum et al., Phys. Rev. Lett. **116**, 232002 (2016)
401. G. Bali, G. Endrödi, Phys. Rev. D **92**, 054506 (2015)
402. G.S. Bali, S. Collins, A. Schäfer, Comput. Phys. Commun. **181**, 1570 (2010)
403. T. Blum, T. Izubuchi, E. Shintani, Phys. Rev. D **88**, 094503 (2013)
404. B. Chakraborty, C.T.H. Davies, J. Koponen, G.P. Lepage, M.J. Peardon, S.M. Ryan, Phys. Rev. D **93**, 074509 (2016)
405. F. Burger, X. Feng, K. Jansen, M. Petschlies, G. Pientka, D.B. Renner, EPJ Web Conf. **118**, 01029 (2016)
406. P. Boyle, L. Del Debbio, E. Kerrane, J. Zanotti, Phys. Rev. D **85**, 074504 (2012)
407. M. Della Morte, B. Jäger, A. Jüttner, H. Wittig, JHEP **1203**, 055 (2012)
408. T. Blum et al. [RBC/UKQCD Collab.], JHEP **1604**, 063 (2016)
409. M. Hayakawa, T. Blum, T. Izubuchi, N. Yamada, PoS LAT **2005**, 353 (2006)
410. T. Blum, S. Chowdhury, M. Hayakawa, T. Izubuchi, Phys. Rev. Lett. **114**, 012001 (2015)
411. A. Duncan, E. Eichten, H. Thacker, Phys. Rev. Lett. **76**, 3894 (1996)
412. X. Feng, S. Aoki, H. Fukaya, S. Hashimoto, T. Kaneko, J.i. Noaki, E. Shintani. Phys. Rev. Lett. **109**, 182001 (2012)
413. P. Masjuan, P. Sanchez-Puertas, [arXiv:1504.07001](https://arxiv.org/abs/1504.07001) [hep-ph]

Chapter 6

The $g - 2$ Experiments

6.1 Overview on the Principle of the Experiment

The main concepts and early results from the CERN muon storage ring experiment have been summarized in [1]. There are a number of excellent reviews on this subject and I am following in parts the ones of Combley, Farley and Picasso [2, 3] and of Vernon Hughes [4]. See also the more recent overviews [5, 6]. Many details on the experimental setup of the E821 experiment may be found in [7, 8], texts which were also very helpful. New experiments are on the way: one at Fermilab (E989) [9–11] in the US and another one at J-PARC (E34) [12–14] in Japan. While the Fermilab experiment represents a major upgrade of the Brookhaven experiment operating with **ultra relativistic muons** (as the later CERN experiments), the J-PARC experiment is planned to use **ultra cold muons** and will be the first precise experiment using a very different approach with rather different systematics.

The principle of the BNL muon $g - 2$ experiment involves the study of the orbital and spin motion of highly polarized muons in a magnetic storage ring. This method has been applied in the last CERN experiment [15] already. The key improvements of the BNL experiment include the very high intensity of the primary proton beam from the proton storage ring AGS (Alternating Gradient Synchrotron), the injection of muons instead of pions into the storage ring, and a super-ferric storage ring magnet [16].

The muon $g - 2$ experiment at Brookhaven works as illustrated in Fig. 6.1 [17–19]. Protons (mass about 1 GeV, energy 24 GeV) from the AGS hit a target and produce pions (of mass about 140 MeV). The pions are unstable and decay into muons plus a neutrino where the muons carry spin and thus a magnetic moment which is directed along the direction of the flight axis. The longitudinally polarized muons from pion decay are then injected into a uniform magnetic field \mathbf{B} where they travel in a circle. The ring is a doughnut-shaped structure with a diameter of 14 m. A picture of the BNL muon storage ring is shown in Fig. 6.2. In the horizontal plane of the orbit the muons execute relativistic cyclotron motion with angular frequency ω_c . By the motion of the muon magnetic moment in the homogeneous magnetic field

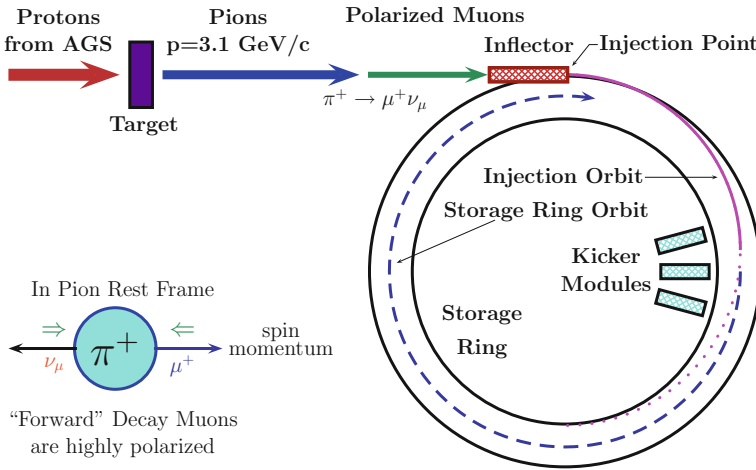


Fig. 6.1 The schematics of muon injection and storage in the $g - 2$ ring

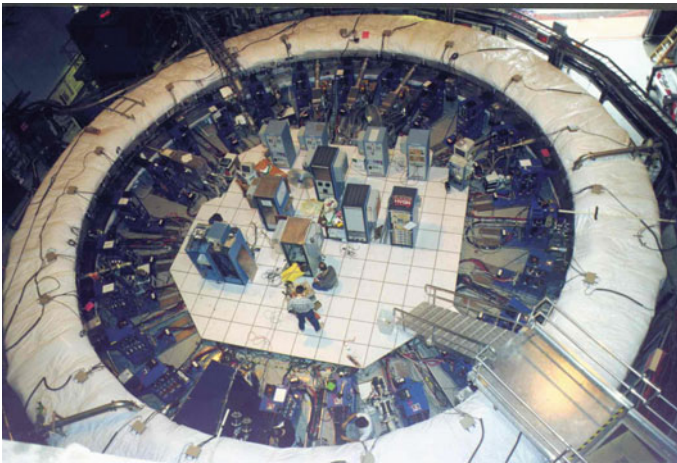


Fig. 6.2 The Brookhaven National Laboratory muon storage ring. The ring has a radius of 7.112 m, the aperture of the beam pipe is 90 mm, the field is 1.45 T and the momentum of the muon is $p_\mu = 3.094 \text{ GeV}/c$. Picture taken from the Muon $g - 2$ Collaboration Web Page <http://www.g-2.bnl.gov/> (Courtesy of Brookhaven National Laboratory)

the spin axis is changed in a particular way as described by the Larmor precession. After each circle the muon’s spin axis changes by 12’ (arc seconds), while the muon is traveling at the same momentum (see Fig. 3.1). The muon spin is precessing with angular frequency ω_s , which is slightly bigger than ω_c by the difference angular frequency $\omega_a = \omega_s - \omega_c$.

$$\begin{aligned}
\omega_c &= \frac{eB}{m_\mu c \gamma}, \\
\omega_s &= \frac{eB}{m_\mu c \gamma} + \frac{e}{m_\mu c} a_\mu B, \\
\omega_a &= \frac{e}{m_\mu c} a_\mu B,
\end{aligned} \tag{6.1}$$

where $a_\mu = (g_\mu - 2)/2$ is the muon anomaly and $\gamma = 1/\sqrt{1 - v^2/c^2}$ is the relativistic Lorentz factor, v the muon velocity.¹ In the experiment ω_a and B are measured. The muon mass m_μ is obtained from an independent experiment on muonium, which is a ($\mu^+ e^-$) bound system. Note that if the muon would just have its Dirac magnetic moment $g = 2$ (tree level) the direction of the spin of the muon would not change at all.

In order to retain the muons in the ring an electrostatic focusing system is needed. In reality in addition to the magnetic field \mathbf{B} an electric quadrupole field \mathbf{E} in the plane normal to the particle orbit is applied, which changes the angular frequency according to the Thomas-Bargmann–Michel–Telegdi (BMT) equation

$$\omega_a = \frac{e}{m_\mu c} \left(a_\mu \mathbf{B} - \left[a_\mu - \frac{1}{\gamma^2 - 1} \right] \frac{\mathbf{v} \times \mathbf{E}}{c^2} \right). \tag{6.2}$$

Interestingly, one has the possibility to choose γ such that $a_\mu - 1/(\gamma^2 - 1) = 0$, in which case ω_a becomes independent of \mathbf{E} . This is the so-called *magic* γ . The muons are rather unstable and decay spontaneously after some time. When running at the magic energy the muons are highly relativistic, they travel almost at the speed of light with energies of about $E_{\text{magic}} = \gamma m_\mu c^2 \simeq 3.098 \text{ GeV}$. This rather high energy is dictated by the need of a large time dilatation on one hand and by the requirement to minimize the precession frequency shift caused by the electric quadrupole superimposed upon the uniform magnetic field. The magic γ -factor is about $\gamma = \sqrt{1 + 1/a_\mu} = 29.3$; the lifetime of a muon at rest is $2.19711 \mu\text{s}$ (micro seconds), while in the ring it is $64.435 \mu\text{s}$ (theory) [$64.378 \mu\text{s}$ (experiment)]. Thus, with their lifetime being much larger than at rest, muons are circling in the ring many times before they decay into a positron plus two neutrinos: $\mu^+ \rightarrow e^+ + \nu_e + \bar{\nu}_\mu$. Since parity is violated maximally in this weak decay there is a strong correlation between the muon spin direction and the direction of emission of the positrons. The differential decay rate for the muon in the rest frame is given by (see also (2.47) and (6.57) below)

$$d\Gamma^\pm/\Gamma = N(E_e) \left(1 \pm \frac{2x - 1}{3 - 2x} \cos \theta \right) dx d \cos \theta, \tag{6.3}$$

in which E_e is the positron energy, x is E_e in units of the maximum energy $m_\mu/2$, Γ the total decay width (4.38), $N(E_e)$ is a normalization factor

¹Formulas like (6.1) presented in this first overview will be derived below.

$$N(E_e) = 2x^2(3 - 2x) ,$$

and θ the angle between the positron momentum in the muon rest frame and the muon spin direction. At tree level $\Gamma = \tau_\mu^{-1} = G_\mu^2 m_\mu^5 / 192\pi^3$. The μ^+ decay spectrum is peaked strongly for small θ due to the non-vanishing coefficient of $\cos \theta$

$$A(E_e) = \frac{2x - 1}{3 - 2x} ,$$

which is called asymmetry factor and reflects the *parity violation*.

The positron is emitted along the spin axis of the muon as illustrated in Fig. 6.3. The decay positrons are detected by 24 lead/scintillating fiber calorimeters spread evenly around inside the muon storage ring. These counters measure the positron energy and provide the direction of the muon spin. The number of decay positrons with energy greater than E_{th} emitted at time t after muons are injected into the storage ring is

$$N(t) = N_0(E_{th}) \exp\left(\frac{-t}{\gamma\tau_\mu}\right) [1 + A(E_{th}) \sin(\omega_a t + \phi(E_{th}))] , \quad (6.4)$$

where $N_0(E_{th})$ is a normalization factor, τ_μ the muon life time (in the muon rest frame), and $A(E_{th})$ is the asymmetry factor for positrons of energy $E > E_{th}$. A typical example for the time structure from the BNL experiment is shown in Fig. 6.4. As we see the exponential decay law for the decaying muons is modulated by the $g - 2$ angular frequency. In this way the angular frequency ω_a is neatly determined

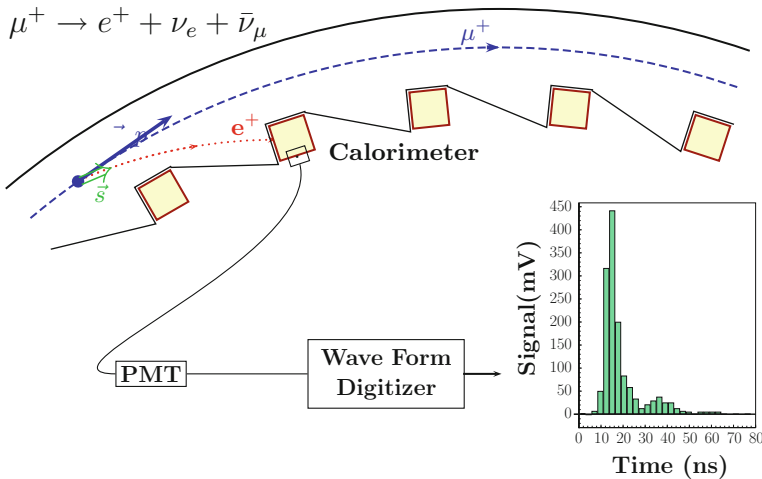


Fig. 6.3 Decay of μ^+ and detection of the emitted e^+ (PMT = Photomultiplier)

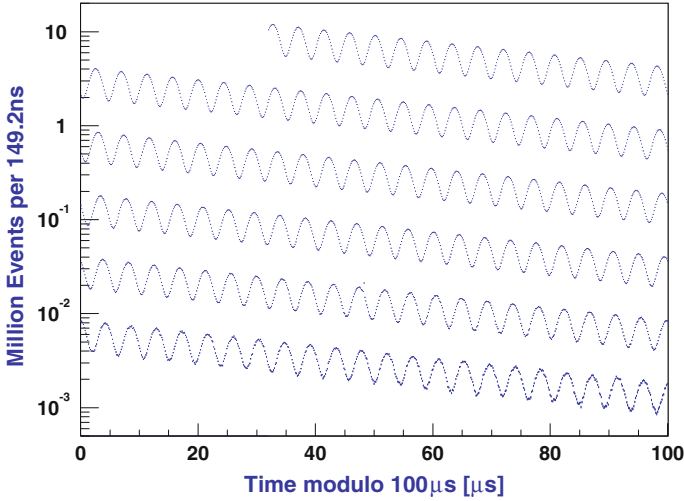


Fig. 6.4 Distribution of counts versus time for the 3.6 billion decays in the 2001 negative muon data-taking period. Courtesy of the E821 collaboration. Reprinted with permission from [16]. Copyright (2007) by the American Physical Society

from the time distribution of the decay positrons observed with the electromagnetic calorimeters [20–24].

The magnetic field is measured by *Nuclear Magnetic Resonance* (NMR) using a standard probe of H₂O [25]. This standard can be related to the magnetic moment of a free proton by

$$B = \frac{\hbar\omega_p}{2\mu_p}, \tag{6.5}$$

where ω_p is the Larmor spin precession angular velocity of a proton in water. Using this, the frequency ω_a from (6.4), (6.1) and $\mu_\mu = (1 + a_\mu) e\hbar/(2m_\mu c)$, one obtains

$$a_\mu = \frac{R}{\lambda - R}, \tag{6.6}$$

where

$$R = \omega_a/\omega_p \text{ and } \lambda = \mu_\mu/\mu_p. \tag{6.7}$$

The BNL experiment E-821 has determined

$$\bar{R} = \omega_a/\tilde{\omega}_p = 0.003\,707\,206\,4(20), \tag{6.8}$$

where \bar{R} , assuming CPT invariance, is the weighted average of the results obtained separately for positive and negative muons, and $\tilde{\omega}_p$ is the proton cyclotron frequency in the average magnetic field along the storage ring. The quantity λ appears because

the value of the muon mass m_μ is needed, and also because the B field measurement involves the proton mass m_p . Measurements of the microwave spectrum of ground state muonium (μ^+e^-) [26] at LAMPF at Los Alamos, in combination with the theoretical prediction of the Muonium hyperfine splitting $\Delta\nu$ [27–29] (and references therein), have provided the precise (new CODATA 2011 recommended) value [30]

$$\frac{\mu_\mu}{\mu_p} = \lambda = 3.183\,345\,107(84) \text{ (30 ppb)}, \quad (6.9)$$

which is to be used together with the E821 measurement of R to determine a_μ via (6.6). More details on the hyperfine structure of muonium will be given below in Sect. 6.6.

Since the spin precession frequency can be measured very well, the precision at which $g - 2$ can be measured is essentially determined by the possibility to manufacture a constant homogeneous magnetic field \mathbf{B} and to determine its value very precisely. An example of a field map from the BNL experiment is shown in Fig. 6.5. Important but easier to achieve is the tuning to the magic energy. Possible deviations may be corrected by adjusting the effective magnetic field appropriately.

In the following we will discuss various aspects mentioned in this brief overview in more detail: beam dynamics, spin precession dynamics, some theory background about the properties of the muon. This should shed some more light on the muon spin physics as it derives from the SM. A summary of the main experimental results and two short addenda on the ground state hyperfine structure of muonium and on single electron dynamics and the electron $g - 2$ will close this part on the experimental principles.

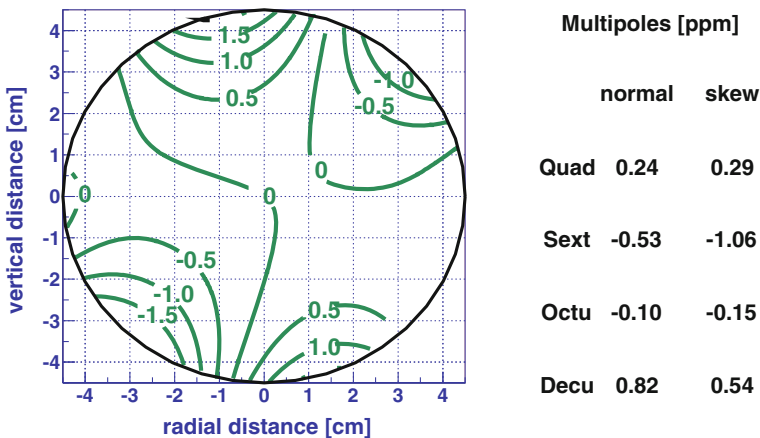


Fig. 6.5 Magnetic field profile. The contours are averaged over azimuth and interpolated using a multi-pole expansion. The circle indicates the storage aperture. The *contour lines* are separated by 1 ppm deviations from the central average. Courtesy of the E821 collaboration [16]

6.2 Particle Dynamics

The anomalous magnetic moment of both electrons and muons are measured by observing the motion of charged particles in a type of Penning trap, which consists of an electrical quadrupole field superimposed upon a uniform magnetic field. The configurations used in these experiments have axial symmetry. The orbital motion of charged particles in the storage ring may be discussed separately from the spin motion because the forces associated with the anomalous magnetic moment are very weak ($a_\mu \approx 1.16 \times 10^{-3}$) in comparison to the forces of the charge of the particle determining the orbital motion. The force \mathbf{F} on a particle of charge e of velocity \mathbf{v} in fields \mathbf{E} and \mathbf{B} is given by the Lorentz force

$$\mathbf{F} = \frac{d\mathbf{p}}{dt} = e (\mathbf{E} + \mathbf{v} \times \mathbf{B}) . \tag{6.10}$$

In a uniform magnetic field \mathbf{B} of magnitude B_0 the particle with relativistic energy E_0 moves on a circle of radius

$$r_0 = \frac{E_0}{ecB_0} , \quad E_0 = \gamma mc^2 . \tag{6.11}$$

Since we are interested in the dynamics of the muon beam in a ring, we consider a cylindrically symmetric situation. The cylindrical coordinates: $r = \sqrt{x^2 + y^2}$, θ , z are the radial, azimuthal and vertical coordinates of the particle position as shown in Fig. 6.6.

The relativistic equation of motion for the muon in the static cylindrical fields $\mathbf{B}(r, z)$ and $\mathbf{E}(r, z)$ takes the form

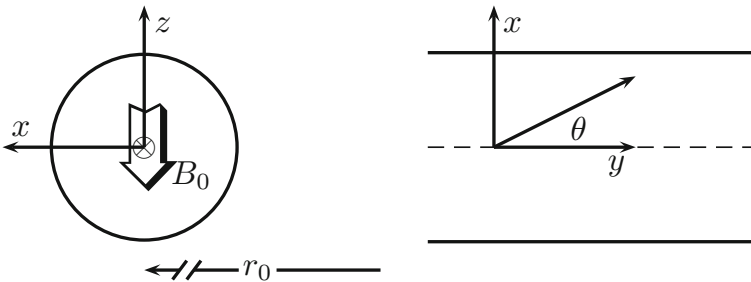


Fig. 6.6 Coordinates for the beam dynamics. View at the beam end (*left*) $x = r - r_0$ radial, z vertical, with B field in $-z$ direction; $(x, z) = (0, 0)$ is the beam position, the negative muon beam points into the plane. View from top (*right*) y is the direction along the beam

$$\frac{d}{dt} (m\dot{r}) = m r \dot{\theta}^2 - e r \dot{\theta} B_z + e E_r, \tag{6.12}$$

$$\frac{d}{dt} (m r^2 \dot{\theta}) = 0, \tag{6.13}$$

$$\frac{d}{dt} (m\dot{z}) = e r \dot{\theta} B_r + e E_z. \tag{6.14}$$

The general form of the electrostatic potential applied is

$$V(r, z) = \frac{V_0}{d^2} \left[r^2 - 2r_0^2 \ln \frac{r}{r_0} - r_0^2 - 2z^2 \right],$$

where r_0 is the radius of the circle on which $\partial V / \partial r = 0$. This potential is singular along the symmetry axis except in the case $r_0 = 0$. In the latter case

$$V(r, z) = \frac{V_0}{d^2} (r^2 - 2z^2), \tag{6.15}$$

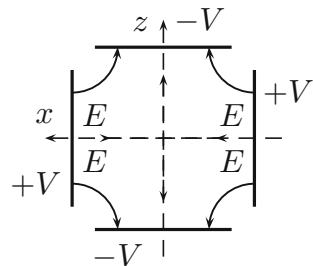
which is the potential used in an electron trap. Here $(r_0, 0)$ and $(0, z_0)$ are the coordinates of the plates and $d^2 = r_0^2 + 2z_0^2$ (for a symmetric trap $r_0 = \sqrt{2}z_0$).

In the muon $g - 2$ experiment $r \rightarrow x = r - r_0$ with $|x| \ll r_0$ (see Fig. 6.6) and weak focusing is implemented by a configuration of charged plates as shown in Fig. 6.7. In order to get a pure quadrupole field one has to use hyperbolic plates with end-caps $z^2 = z_0^2 + x^2/2$ and $z^2 = \frac{1}{2}(x^2 - x_0^2)$ on the ring. While the CERN experiment was using hyperbolic plates, the BNL one uses flat plates which produce 12- and 20-pole harmonics. The length of the electrodes is adjusted to suppress the 12-pole mode leaving a 2% 20-pole admixture. The electric field produces a restoring force in the vertical direction and a repulsive force in the radial direction:

$$\mathbf{E} = (E_r, E_\theta, E_z) = (\kappa x, 0, -\kappa z), \tag{6.16}$$

where $x = r - r_0$ and κ a positive constant. In order to keep the beam focused, the restoring force of the vertical magnetic field must be stronger than the repulsive force

Fig. 6.7 Electric quadrupole field E . The vertical direction is z , the radial x ($x_0 = \sqrt{2}z_0$); $V = V_0/2$ at the plates



of the electrical field in the radial direction:

$$0 < \frac{eV_0}{d^2} < \frac{e^2 B^2}{8mc} . \quad (6.17)$$

The radial force is

$$F_r = \frac{\gamma m v^2}{r} - \frac{e}{c} v B_z + e E_r , \quad (6.18)$$

and since on the equilibrium orbit $r = r_0$ and $E_r = 0$ we have

$$\frac{\gamma m v^2}{r_0} = \frac{e}{c} v B_z . \quad (6.19)$$

As r_0 is large relative to the beam spread, we may expand r about r_0 :

$$\frac{1}{r} = \frac{1}{r_0 + x} \simeq \frac{1}{r_0} \left(1 - \frac{x}{r_0} \right) .$$

Therefore, using (6.19) we may write

$$F_x = F_r = -e\beta B_z (1 - n) \frac{x}{r_0} \Rightarrow \gamma m \ddot{x} = -(1 - n) \frac{\gamma m v^2}{r_0^2} x , \quad (6.20)$$

where $\beta = v/c$ and n is the field index

$$n = \frac{\kappa r_0}{\beta B_0} , \quad B_0 = B_z . \quad (6.21)$$

For the vertical motion we have

$$F_z = -e\kappa z \Rightarrow \gamma m \ddot{z} = -e\kappa z , \quad (6.22)$$

and with $\omega_0 = v/r_0$, using (6.19) and (6.21), the equations of motion take the form

$$\begin{aligned} \ddot{x} + (1 - n) \omega_0^2 x &= 0 , \\ \ddot{z} + e\kappa z &= 0 , \end{aligned} \quad (6.23)$$

with the oscillatory solutions

$$\begin{aligned} x &= A \cos(\sqrt{1 - n} \omega_0 t) , \\ z &= B \cos(\sqrt{n} \omega_0 t) . \end{aligned} \quad (6.24)$$

We have used $e\kappa = n\omega_0^2$ following from (6.21). The amplitudes depend on the *initial condition* of the particle trajectory. This motion is called *betatron oscillation*. The betatron frequencies are $\omega_{y\text{BO}} = \sqrt{n}\omega_c$ and $\omega_{x\text{BO}} = \sqrt{1-n}\omega_c$ where $\omega_c = \omega_0 = v/r_0$ is the cyclotron frequency. In the experiment a lattice of quadrupoles is distributed along the ring. For the BNL experiment the lattice has a four-fold symmetry and the quadrupoles are covering 43% of the ring. The corresponding dynamics has to be calculated taking into account the geometry of the configuration, but follows the same principle.

The dynamics of an electron in a Penning trap and the principle of electron $g - 2$ experiments will be considered briefly in Sect. 6.7 at the end of this part of the book.

6.3 Magnetic Precession for Moving Particles

The precession of spinning particles in magnetic fields is a classic subject investigated long time ago [31]. Our exposition follows closely Bell's lecture. In a magnetic field \mathbf{B} the polarization \mathbf{P} of a particle changes according to

$$\frac{d\mathbf{P}}{dt} = g \frac{e}{2m} \mathbf{P} \times \mathbf{B} ,$$

the component of \mathbf{P} parallel to \mathbf{B} remains constant, while the part of \mathbf{P} perpendicular to \mathbf{B} rotates about \mathbf{B} with angular frequency

$$\omega = g \frac{e}{2m} B , \quad (6.25)$$

the non-relativistic cyclotron frequency. This holds in the rest frame O of the particle. For moving and even fast-moving particles we may get the motion in the laboratory system O' by a Lorentz transformation. In a pure L -transformation $x^{\mu'} = L^{\mu}_{\nu} x^{\nu}$ [$x^{\mu} = (ct, \mathbf{x})$] L has the form²

$$L = \begin{pmatrix} \gamma & -\gamma \frac{\mathbf{v}}{c} \\ -\gamma \frac{\mathbf{v}}{c} & \mathbf{1} + (\gamma - 1) \mathbf{n} \mathbf{n} \cdot \end{pmatrix} ,$$

where $\mathbf{n} = \mathbf{v}/v$ and $\gamma = 1/\sqrt{1 - v^2/c^2}$. For accelerated particles, the velocity is changing and in the next moment the velocity is $\mathbf{v}' = \mathbf{v} + \delta\mathbf{v}$. In the laboratory frame we thus have $x^{\mu'} = L^{\mu}_{\nu}(\mathbf{v})x^{\nu}$ and $x^{\mu''} = L^{\mu}_{\nu}(\mathbf{v}')x^{\nu}$ and expanding to linear order in $\delta\mathbf{v}$ one obtains the motion as seen in the laboratory frame as

$$\begin{aligned} t'' &= t' - \delta\mathbf{u}' \cdot \mathbf{x}' , \\ \mathbf{x}'' &= \mathbf{x}' + \delta\boldsymbol{\theta}' \times \mathbf{x}' - \mathbf{u}' t' , \end{aligned} \quad (6.26)$$

² L is a matrix operator acting on four-vectors. The \cdot operation at the right of the spacial submatrix means forming a scalar product with the spatial part of the vector on which L acts.

with

$$\begin{aligned}\mathbf{u}' &= \gamma \left(1 + \frac{\gamma - 1}{v^2} \mathbf{v} \cdot \mathbf{v} \right) \delta \mathbf{v}, \\ \delta \boldsymbol{\theta}' &= \frac{\gamma - 1}{v^2} (\delta \mathbf{v} \times \mathbf{v}),\end{aligned}\quad (6.27)$$

which tells us that from the two pure boosts we got an infinitesimal transformation which includes both a boost (pure if $\delta \boldsymbol{\theta}' = 0$) and a rotation (pure if $\mathbf{u}' = 0$). The transformation (6.26) is the infinitesimal law for transforming vectors in O' to vectors in O'' .

The precession equation for accelerated moving particles is then obtained as follows: Let O' be the observer for whom the particle is momentarily at rest. If the particle has no electric dipole moment, what we assume (see end of Sect. 3.3), an electric field does not contribute to the precession and only serves to accelerate the particle

$$\delta \mathbf{u}' = \frac{e}{m} \mathbf{E}' \delta t', \quad (6.28)$$

while the magnetic field provides the precession

$$\delta \mathbf{P}' = -g \frac{e}{2m} \mathbf{B}' \times \mathbf{P}' \delta t'. \quad (6.29)$$

In the laboratory frame O' the observed polarization is $\mathbf{P}' + \delta \mathbf{P}'$ where $\mathbf{P}' = \mathbf{P}$ is the polarization of the particle in its rest frame O . The observer O'' by a boost from O sees a polarization $\mathbf{P}'' + \delta \mathbf{P}''$ which differs by a rotation $\delta \boldsymbol{\theta}'$ from the previous one: (note that momentarily $\mathbf{P}'' = \mathbf{P}' = \mathbf{P}$)

$$\delta \mathbf{P}'' = \delta \mathbf{P}' + \delta \boldsymbol{\theta}' \times \mathbf{P}, \quad (6.30)$$

or

$$\delta \mathbf{P}'' = -g \frac{e}{2m} \mathbf{B}' \times \mathbf{P} \delta t' + \frac{(\gamma - 1)}{v^2} (\delta \mathbf{v} \times \mathbf{v}) \times \mathbf{P}. \quad (6.31)$$

The precession equation in the laboratory frame may be obtained by applying the L -transformations of coordinates and fields to the lab frame:

$$\begin{aligned}\delta t' &= \gamma \left(\delta t - \frac{\mathbf{v} \cdot \delta \mathbf{x}}{c^2} \right) = \gamma \delta t \left(1 - \frac{v^2}{c^2} \right) = \frac{1}{\gamma} \delta t, \\ \mathbf{B}' &= \gamma \left(\mathbf{B} - \frac{\mathbf{v} \times \mathbf{E}}{c^2} \right) + \frac{(1 - \gamma)}{v^2} \mathbf{v} \cdot \mathbf{B} \mathbf{v}, \\ \mathbf{E}' &= \gamma (\mathbf{E} + \mathbf{v} \times \mathbf{B}) + \frac{(1 - \gamma)}{v^2} \mathbf{v} \cdot \mathbf{E} \mathbf{v},\end{aligned}\quad (6.32)$$

and one obtains

$$\frac{d\mathbf{P}}{dt} = \boldsymbol{\omega}_s \times \mathbf{P}, \quad (6.33)$$

with

$$\boldsymbol{\omega}_s = \frac{\gamma - 1}{v^2} \frac{d\mathbf{v}}{dt} \times \mathbf{v} - g \frac{e}{2m} \left(\mathbf{B} - \frac{\mathbf{v} \times \mathbf{E}}{c^2} + \frac{1 - \gamma}{\gamma v^2} \mathbf{v} \cdot \mathbf{B} \mathbf{v} \right). \quad (6.34)$$

The first term, which explicitly depends on the acceleration, is called *Thomas precession*. The acceleration in the laboratory frame may be obtained in the same way from (6.28) together with (6.27) and (6.32)

$$\frac{d\mathbf{v}}{dt} = \frac{e}{\gamma m} (\mathbf{E} + \mathbf{v} \times \mathbf{B}) - \frac{e}{\gamma m c^2} \mathbf{v} \cdot \mathbf{E} \mathbf{v}, \quad (6.35)$$

which is just another form of the usual equation of motion³ (Lorentz force)

$$\frac{d\mathbf{p}}{dt} = \frac{d}{dt} (\gamma m \mathbf{v}) = e (\mathbf{E} + \mathbf{v} \times \mathbf{B}).$$

If one uses (6.35) to eliminate the explicit acceleration term from (6.34) together with $(\mathbf{v} \times \mathbf{B}) \times \mathbf{v} = \mathbf{B}v^2 - \mathbf{v} \cdot \mathbf{B} \mathbf{v}$ and $\mathbf{v} \times \mathbf{v} = 0$, one obtains

$$\boldsymbol{\omega}_s = -\frac{e}{\gamma m} \left\{ (1 + \gamma a) \mathbf{B} + \frac{(1 - \gamma)}{v^2} a \mathbf{v} \cdot \mathbf{B} \mathbf{v} + \gamma \left(a + \frac{1}{\gamma + 1} \right) \frac{\mathbf{E} \times \mathbf{v}}{c^2} \right\}, \quad (6.36)$$

where $a = g/2 - 1$ is the anomaly term.

6.3.1 $g-2$ Experiment and Magic Momentum

In the $g-2$ experiment one works with purely transversal fields: $\mathbf{v} \cdot \mathbf{E} = \mathbf{v} \cdot \mathbf{B} = 0$. Then using $(\mathbf{v} \times \mathbf{E}) \times \mathbf{v} = v^2 \mathbf{E}$ (when $\mathbf{v} \cdot \mathbf{E} = 0$) and $v^2/c^2 = (\gamma^2 - 1)/\gamma^2$ the equation of motion can be written

$$\frac{d\mathbf{v}}{dt} = \boldsymbol{\omega}_c \times \mathbf{v}, \quad \boldsymbol{\omega}_c = -\frac{e}{\gamma m} \left(\mathbf{B} + \frac{\gamma^2}{\gamma^2 - 1} \frac{\mathbf{E} \times \mathbf{v}}{c^2} \right). \quad (6.37)$$

³Note that $d\gamma = \gamma^3 \mathbf{v} \cdot d\mathbf{v}/c^2$ and the equation of motion implies

$$\mathbf{v} \cdot \frac{d(\gamma m \mathbf{v})}{dt} = m \gamma^3 \mathbf{v} \cdot \frac{d\mathbf{v}}{dt} = e \mathbf{v} \cdot \mathbf{E},$$

as $\mathbf{v} \cdot (\mathbf{v} \times \mathbf{B}) \equiv 0$. This has been used in obtaining (6.35).

The velocity \mathbf{v} thus rotates, without change of magnitude, with the relativistic cyclotron frequency ω_c . The precession of the polarization \mathbf{P} , which is to be identified with the muon spin \mathbf{S}_μ , for purely transversal fields is then

$$\omega_a = \omega_s - \omega_c = -\frac{e}{m} \left\{ a \mathbf{B} + \left(a - \frac{1}{\gamma^2 - 1} \right) \frac{\mathbf{E} \times \mathbf{v}}{c^2} \right\}. \quad (6.38)$$

This establishes the key formula for measuring a_μ , which we have used and discussed earlier. It was found by Bargmann, Michel and Telegdi in 1959 [31] (see also [32] for a recent reconsideration). Actually, the magnetic transversality condition $\mathbf{v} \cdot \mathbf{B} = 0$ due to electrostatic focusing is not accurately satisfied (pitch correction) such that the more general formula

$$\omega_a = -\frac{e}{m} \left\{ a \mathbf{B} - a \left(\frac{\gamma}{\gamma + 1} \right) \frac{\mathbf{v} \cdot \mathbf{B} \mathbf{v}}{c^2} + \left(a - \frac{1}{\gamma^2 - 1} \right) \frac{\mathbf{E} \times \mathbf{v}}{c^2} \right\}, \quad (6.39)$$

has to be used.

Since the anomalous magnetic moment for leptons is a very small quantity $a \approx 1.166 \times 10^{-3}$, electrons and muons in a pure magnetic field and initially polarized in the direction of motion ($\mathbf{P} \propto \mathbf{v}$) only very slowly develop a component of polarization transverse to the direction of motion. The observation of this development provides a sensitive measure of the small but theoretically very interesting anomalous magnetic moment.

In the original muon $g - 2$ experiments only a \mathbf{B} field was applied and in order to give some stability to the beam the \mathbf{B} was not quite uniform,⁴ and the particles oscillate about an equilibrium orbit. As a result one of the main limitations of the precision of those experiments was the difficulty to determine the effective average \mathbf{B} to be used in calculating a_μ from the observed oscillation frequencies. To avoid this, in the latest CERN experiment, as later in the BNL experiment, the field \mathbf{B} is chosen as uniform as possible and focusing is provided by transverse electric quadrupole fields. To minimize the effect of the electric fields on the precession of \mathbf{P} , muons with a special “magic” velocity are used so that the coefficient of the second term in (6.37) is small:

$$a_\mu - \frac{1}{\gamma^2 - 1} \approx 0,$$

corresponding to a muon energy of about 3.1 GeV. This elegant method for measuring a_μ was proposed by Bailey, Farley, Jöstlein, Picasso and Wickens and realized as the last CERN muon $g - 2$ experiment and later adopted by the experiment at BNL. The motion of the muons is characterized by the frequencies listed in Table 6.1.

Two small, but important, corrections come from the effect of the electric focusing field \mathbf{E} on the spin precession ω_a .

⁴Magnetic focusing using an inhomogeneous field $B_z = B_0 (r_0/r)^n$, which by Maxwell’s equation $\nabla \times \mathbf{B} = 0$ implies $B_r \simeq -n/r_0 B_0 z$ for $r \simeq r_0$, leads to identical betatron oscillation equations (6.23) as electrostatic focusing.

Table 6.1 Frequencies and time periods in the muon $g - 2$ experiment E821. The field index used is $n = 0.137$. It is optimized to avoid unwanted resonances in the muon storage ring

Type	$\nu_i = \omega_i/2\pi$	Expression	Frequency (MHz)	Period
Anomalous precession	ν_a	$\frac{ea_\mu B}{2\pi m}$	0.23	$4.37 \mu\text{s}$
Cyclotron	ν_c	$\frac{v}{2\pi r_0}$	6.71	149 ns
Horizontal betatron	ν_x	$\sqrt{1-n} \nu_c$	6.23	160 ns
Vertical betatron	ν_z	$\sqrt{n} \nu_c$	2.48	402 ns

The first is the *Radial Electric Field Correction*, the change in ω_a when the momentum p deviates from the magic value $p \neq p_m$ and hence $p = \beta\gamma m = p_m + \Delta p$. In fact, the beam is not monoenergetic and the momentum tune has a small uncertainty of about $\pm 0.5\%$. This effect can be corrected by a change in the effective magnetic field [15] used in extracting a_μ . In cylindrical coordinates Fig. 6.6 using $(\mathbf{v} \times \mathbf{E})_z = -v_y E_x = -v E_r$, as $E_y = 0$, we find $aB_z + (a - 1/(\beta^2\gamma^2)) v E_r/c^2$ or, with $B_0 = -B_z > 0$,

$$B_{0\text{eff}} = B_0 \left[1 - \beta \frac{E_r}{B_0} \left(1 - \frac{1}{a_\mu \beta^2 \gamma^2} \right) \right] \equiv C_E B_0 . \quad (6.40)$$

This directly translates into

$$\frac{\Delta\omega_a}{\omega_a} = C_E \simeq -2 \frac{\beta E_r}{B_0} \left(\frac{\Delta p}{p_m} \right) . \quad (6.41)$$

One may apply furthermore the relation $\Delta p/p_m = (1-n)(x_e/r_0)$, where x_e is the equilibrium position of the particle relative to the center of the aperture of the ring. For the BNL experiment typically

$$C_E \simeq 0.5 \text{ ppm} . \quad (6.42)$$

The second effect is the *Vertical Pitch Correction* arising from vertical betatron oscillations [3, 33]. The focusing force due to \mathbf{E} changes v_z at the betatron oscillation frequency $\omega_p = \omega_{z\text{BO}}$ ⁵ such that

$$\psi(t) = \psi_0 \sin \omega_p t . \quad (6.43)$$

The muon will follow a spiral path with pitch angle ψ (see Fig. 6.8) given by

⁵The pitch frequency here should not to be confused with the proton precession frequency ω_p appearing in (6.7).

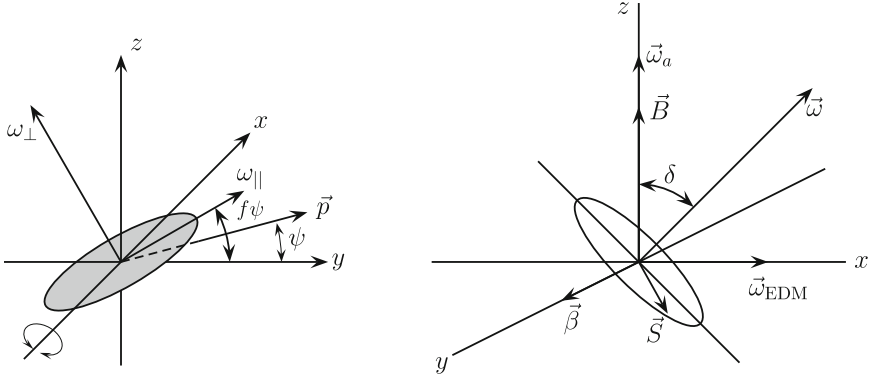


Fig. 6.8 *Left frame for pitch correction.* \mathbf{p} lies always in the yz -plane. The pitch angle ψ between \mathbf{p} and the y -axis (beam direction) oscillates. The spin \mathbf{S} then rotates about the x -axis through an angle $f\psi$, where for electric focusing $f = 1 + \beta^2\gamma a - \gamma^{-1}$; $f = 1$ at magic γ . *Right frame for EDM correction.* As $|\mathbf{E}| \ll |\mathbf{E}^*| = c|\boldsymbol{\beta} \times \mathbf{B}|$, $\boldsymbol{\omega}_{\text{EDM}}$ points along the x -axis while the unperturbed $\boldsymbol{\omega}_a$ points in z -direction. $\delta = \arctan \frac{\eta\beta}{2a} \simeq \frac{\eta}{2a}$

$$\frac{v_z}{v} = \sin \psi \simeq \psi, \tag{6.44}$$

and ω_a is changed. Now $\mathbf{v} \cdot \mathbf{B} \neq 0$, which persists as an effect from the focusing field also if running at the magic γ . The corresponding correction follows from (6.39), at $\gamma = \gamma_m$. The motion vertical to the main plane implies

$$\begin{aligned} \omega_{az} &= \frac{e}{m} a B_0 \left[1 - \left(\frac{\gamma}{\gamma + 1} \right) \beta_z^2 \right] \\ &= \omega_a \left[1 - \left(\frac{\gamma}{\gamma + 1} \right) \beta^2 \frac{v_z^2}{v^2} \right] = \omega_a \left[1 - \left(\frac{\gamma - 1}{\gamma} \right) \psi^2 \right], \end{aligned} \tag{6.45}$$

where ω_a is the ideal (unperturbed) precession frequency. Similarly,

$$\begin{aligned} \omega_{ay} &= -\frac{e}{m} a B_0 \left[1 - \left(\frac{\gamma}{\gamma + 1} \right) \beta_z \beta_y \right] \\ &= -\omega_a \left[1 - \left(\frac{\gamma}{\gamma + 1} \right) \beta^2 \frac{v_z v_y}{v^2} \right] = -\omega_a \left[1 - \left(\frac{\gamma - 1}{\gamma} \right) \psi \right], \end{aligned} \tag{6.46}$$

where we used

$$\frac{v_z}{v} = \sin \psi \simeq \psi, \quad \frac{v_y}{v} = \cos \psi \simeq 1.$$

The component of ω_a parallel to the tilted plane changes sign and in the time average has no effect. The perpendicular component is

$$\omega_{\perp} = \omega_a = \omega_z \cos \psi - \omega_y \sin \psi \simeq \omega_z - \omega_y \psi, \quad (6.47)$$

and hence

$$\omega'_a = \omega_a (1 - C_P) = \omega_a \left(1 - \frac{\psi^2}{2} \right). \quad (6.48)$$

In the time average by (6.43) $\overline{\psi^2} = \frac{1}{2} \psi_0^2$ and thus $C_P = \frac{1}{4} \psi_0^2$. This holds provided $\omega_a \ll \omega_p$ otherwise the correction reads [33]

$$C_P = \frac{1}{4} \psi_0^2 \beta^2 \left(1 - (a\beta\gamma)^2 \frac{\omega_p^2}{(\omega_a^2 - \omega_p^2)} \right), \quad (6.49)$$

with $(a\beta\gamma)^2 = 1/(\beta\gamma)^2$ at magic γ . For the BNL experiment the pitch corrections is of the order

$$C_P \simeq 0.3 \text{ ppm}. \quad (6.50)$$

A third possible correction could be due to an EDM of the muon. If a large enough *electric dipole moment*⁶

$$\mathbf{d}_e = \frac{\eta e}{2mc} \mathbf{S}, \quad (6.51)$$

(see (1.5), p. 34 in Sect. 2.1.2 and the discussion at the end of Sect. 3.3) would exist the applied electric field \mathbf{E} (which is vanishing at the equilibrium beam position) and the motional electric field induced in the muon rest frame $\mathbf{E}^* = \gamma \boldsymbol{\beta} \times \mathbf{B}$ would add an extra precession of the spin with a component along \mathbf{E} and one about an axis perpendicular to \mathbf{B} :

$$\omega_{a'} = \omega_a + \omega_{\text{EDM}} = \omega_a - \frac{\eta e}{2m_{\mu}} \left(\frac{\mathbf{E}}{c} + \boldsymbol{\beta} \times \mathbf{B} \right), \quad (6.52)$$

or

$$\Delta\omega_a = -2d_{\mu} (\boldsymbol{\beta} \times \mathbf{B}) - 2d_{\mu} \mathbf{E},$$

which, for $\beta \sim 1$ and $d_{\mu} \mathbf{E} \sim 0$, yields

$$\omega_{a'} = B \sqrt{\left(\frac{e}{m_{\mu}} a_{\mu} \right)^2 + (2d_{\mu})^2}. \quad (6.53)$$

Note that η is the dimensionless constant equivalent of magnetic moment g -factors. The result is that the plane of precession is no longer horizontal but tilted at an angle

⁶Remembering the normalization: the magnetic and electric dipole moments are given by $\mu = \frac{q}{2} \frac{e\hbar}{2mc}$ and $d = \frac{\eta}{2} \frac{e\hbar}{2mc}$, respectively.

$$\delta \equiv \arctan \frac{\omega_{\text{EDM}}}{\omega_a} = \arctan \frac{\eta \beta}{2a} \simeq \frac{\eta}{2a}, \quad (6.54)$$

and the precession frequency is increased by a factor

$$\omega'_a = \omega_a \sqrt{1 + \delta^2}. \quad (6.55)$$

The tilt gives rise to an oscillating vertical component of the muon polarization, and may be detected by recording separately the electrons which strike the counters above and below the mid-plane of the ring. This measurement has been performed in the last CERN experiment on $g - 2$, and has been repeated at BNL.

6.4 Theory: Production and Decay of Muons

For the ($g_\mu - 2$) experiments one needs polarized muons. Basic symmetries of the weak interaction of the muons make it relatively easy to produce polarized muons. What helps is the maximal parity violation of the charged current weak interactions, mediated by the charged W^\pm gauge bosons, which in its most pronounced form manifests itself in the “non-existence” of right-handed neutrinos ν_R . What it means more precisely is that right handed neutrinos are “sterile” in the sense that they do not interact with any kinds of the gauge bosons, which we know are responsible for electromagnetic (photon), weak (W - and Z -bosons) and strong (gluons) interactions of matter. It means that their production rate in ordinary weak reactions is practically zero which amounts to lepton number conservation for all practical purposes in laboratory experiments.⁷

Pion production may be done by shooting protons (accumulated in a proton storage ring) on a target material where pions are the most abundant secondary particles. The most effective pion production mechanism proceeds via decays of resonances. For pions it is dominated by the Δ_{33} isobar ($\Delta_{33} \rightarrow N\pi$) [basic processes $p + p \rightarrow p + n + \pi^+$ and $p + n \rightarrow p + p + \pi^-$]

$$p + (N, Z) \rightarrow \Delta^* + X \rightarrow “(N + 1, Z + 1 \mp 1)” + \pi^\pm,$$

where the ratio $\sigma(\pi^+)/\sigma(\pi^-) \rightarrow 1$ at high Z .⁸

⁷Only the recently established phenomenon of neutrino oscillations proves that lepton number in fact is not a perfect quantum number. This requires that neutrinos must have tiny masses and this requires that right-handed neutrinos (ν_R 's) must exist. In fact, the smallness of the neutrino masses explains the strong suppression of lepton number violating effects.

⁸At Brookhaven the 24 GeV proton beam extracted from the AGS with 60×10^{12} protons per AGS cycle of 2.5 s impinges on a Nickel target of one interaction length and produces amongst other debris-particles a large number of low energy pions. The pions are momentum selected and then decay in a straight section where about one third of the pions decay into muons. The latter are momentum selected once more before they are injected into the $g - 2$ storage ring.

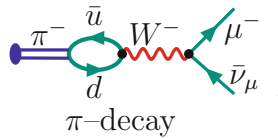
We now look more closely to the decay chain

$$\begin{aligned} \pi &\rightarrow \mu + \nu_\mu \\ &\quad \downarrow \\ &\quad e + \nu_e + \nu_\mu, \end{aligned}$$

producing the polarized muons which decay into electrons which carry along in their direction of propagation the knowledge of the muon’s polarization (for a detailed discussion see e.g. [34]).

(1) Pion decay:

The π^- is a pseudoscalar bound state $\pi^- = (\bar{u}\gamma_5 d)$ of a d quark and a u antiquark \bar{u} . The main decay channel is via the diagram:



In this two-body decay of the charged spin zero pseudoscalar mesons the lepton energy is fixed (monochromatic) and given by

$$E_\ell = \sqrt{m_\ell^2 + p_\ell^2} = \frac{m_\pi^2 + m_\ell^2}{2m_\pi}, \quad p_\ell = \frac{m_\pi^2 - m_\ell^2}{2m_\pi}.$$

Here the relevant part of the Fermi type effective Lagrangian reads

$$\mathcal{L}_{\text{eff,int}} = -\frac{G_\mu}{\sqrt{2}} V_{ud} (\bar{\mu}\gamma^\alpha (1 - \gamma_5) \nu_\mu) (\bar{u}\gamma_\alpha (1 - \gamma_5) d) + \text{h.c.},$$

where G_μ denotes the Fermi constant and V_{ud} the first entry in the CKM matrix. For our purpose $V_{ud} \sim 1$. The transition matrix-element reads

$$\begin{aligned} T &= \text{out} \langle \mu^-, \bar{\nu}_\mu | \pi^- \rangle_{\text{in}} \\ &= -i \frac{G_\mu}{\sqrt{2}} V_{ud} F_\pi (\bar{u}_\mu \gamma^\alpha (1 - \gamma_5) v_{\nu_\mu}) p_\alpha, \end{aligned}$$

where we used the hadronic matrix-element

$$\langle 0 | \bar{d} \gamma_\mu \gamma_5 u | \pi(p) \rangle \doteq i F_\pi p_\mu,$$

which defines the pion decay constant F_π . As we know the pion is a pseudoscalar such that only the axial part of the weak charged $V - A$ current couples to the pion. By angular momentum conservation, as the π^+ has spin 0 and the emitted neutrino is left-handed ($(1 - \gamma_5)/2$ projector) the μ^+ must be left-handed as well. Going to the

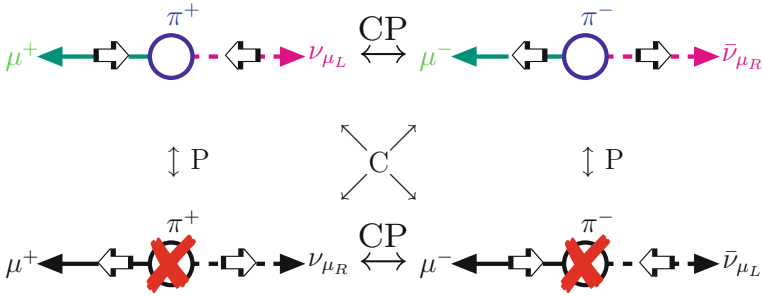


Fig. 6.9 Pion decay is a parity violating weak decay where leptons of definite handedness are produced depending on the given charge. CP is conserved while P and C are violated maximally (unique handedness). μ^- [μ^+] is produced with positive [negative] helicity $h = \mathbf{S} \cdot \mathbf{p}/|\mathbf{p}|$. The existing μ^- and μ^+ decays are related by a CP transformation. The decays obtained by C or P alone are nonexistent in nature

π^- not only particles have to be replaced by antiparticles (C) but also the helicities have to be reversed (P), since a left-handed antineutrino (essentially) does not exist. Note that the decay is possible only due to the non-zero muon mass, which allows for the necessary helicity flip of the muon. The handedness is opposite for the opposite charge. This is illustrated in Fig. 6.9.

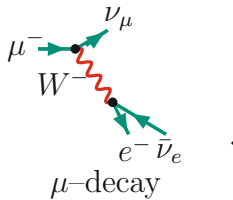
The pion decay rate is given by

$$\Gamma_{\pi^- \rightarrow \mu^- \bar{\nu}_\mu} = \frac{G_\mu^2}{8\pi} |V_{ud}|^2 F_\pi^2 m_\pi m_\mu^2 \left(1 - \frac{m_\mu^2}{m_\pi^2}\right)^2 \times (1 + \delta_{\text{QED}}) ,$$

with CKM matrix-element $V_{ud} \sim 1$ and δ_{QED} the electromagnetic correction.

(2) Muon decay:

Muon decay $\mu^- \rightarrow e^- \bar{\nu}_e \nu_\mu$ is a three body decay



The matrix element can be easily calculated. The relevant part of the effective Lagrangian reads

$$\mathcal{L}_{\text{eff,int}} = -\frac{G_\mu}{\sqrt{2}} (\bar{e} \gamma^\alpha (1 - \gamma_5) \nu_e) (\bar{\nu}_\mu \gamma_\alpha (1 - \gamma_5) \mu) + \text{h.c.} ,$$

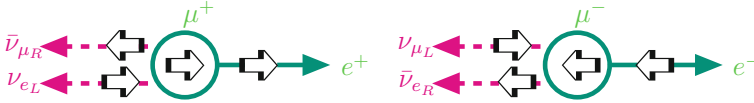


Fig. 6.10 In μ^- [μ^+] decay the produced e^- [e^+] has negative [positive] helicity, respectively

and thus

$$T = {}_{\text{out}} \langle e^-, \bar{\nu}_e \nu_\mu | \mu^- \rangle_{\text{in}} = \frac{G_\mu}{\sqrt{2}} (\bar{u}_e \gamma^\alpha (1 - \gamma_5) v_{\nu_e}) (\bar{u}_{\nu_\mu} \gamma_\alpha (1 - \gamma_5) u_\mu),$$

which proves that the μ^- and the e^- have both the same left-handed helicity [the corresponding anti-particles are right-handed] in the massless approximation. This implies the decay scheme Fig. 6.10 for the muon.

The positrons are thus emitted preferably in the direction of the muon spin, and measuring the direction of the positron momentum provides the direction of the muon spin.

After integrating out the two unobservable neutrinos, the polarized differential decay probability to find an e^\pm with energy between E_e and $E_e + dE_e$ emitted at an angle between θ and $\theta + d\theta$ reads (see also (2.47))

$$\frac{d^2 \Gamma}{dE_e d \cos \theta} = \frac{G_\mu^2}{12\pi^3} \frac{p_e}{E_\mu} \left\{ Q^2 (p_0 p_1) + 2 (Q p_0) (Q p_1) - (n_0 p_1) (Q^2 - 2 (Q p_1)) \right\}, \quad (6.56)$$

with p_0 the muon momentum, p_1 the positron/electron momentum, n_0 the muon polarization vector $n_0^2 = -1$, $n_0 p_0 = 0$ ($n_0 = (0, \mathbf{P}_\mu)$ in the muon rest frame) where $Q = p_0 - p_1$, $Q^2 = m_\mu^2 + m_e^2 - 2 (p_0 p_1)$. For a polarized muon $P_\mu = |\mathbf{P}_\mu| = 1$, in practice $P_\mu < 1$ describes the degree of polarization. As $(n_0 p_1)$ is L-invariant, its value is as given in the muon rest frame⁹: $(n_0 p_1) = -P_\mu \sqrt{E_e^2 - m_e^2} \cos \theta$. The asymmetry proportional to the coefficient of $(n p_0)$

$$A \propto \frac{(Q^2 - 2 (Q p_1))}{Q^2 (p_0 p_1) + 2 (Q p_0) (Q p_1)}$$

⁹Note that the original electron phase space element $dV_e \equiv \frac{d^3 p_1}{E_e}$ is L-invariant such that with $d^3 p_1 = -p_e^2 d p_e d \cos \theta d \varphi$, after integrating over the azimuthal angle φ , giving a factor 2π , and using $p_e d p_e = E_e d E_e$ we infer that $dV_e \rightarrow 2\pi \sqrt{E_e^2 - m_e^2} d E_e d \cos \theta$ is independent of the frame. While in the rest frame $u_0 p_1 = -\mathbf{P}_\mu \mathbf{p}_1 = -P_\mu p_e \cos \theta$ in the laboratory frame $u_0 = \left(1, \frac{\mathbf{p}_0}{E_0 - m}\right) \frac{\mathbf{p}_0 \mathbf{P}_\mu}{m}$ and thus $u_0 p_1 = \cos \theta_\mu \frac{p_\mu}{m} \left(E_e - \frac{p_\mu p_{1x}}{E_0 - m}\right)$.

is also independent of the frame. In the muon rest frame, in terms of the fractional positron/electron energy $x = E_e/W$ and $x_0 = m_e/W$ where $W = \max E_e = (m_\mu^2 + m_e^2)/2m_\mu$ we have¹⁰

$$\frac{d^2 \Gamma^\pm}{dx d \cos \theta} = \frac{G_\mu^2 m_\mu^5}{96\pi^3} \left(1 + \frac{m_e^2}{m_\mu^2}\right)^4 \sqrt{x^2 - x_0^2} \left\{ (3x - 2x^2 - x_0^2) \pm P_\mu \sqrt{x^2 - x_0^2} \left(2x - 1 - x_0 \frac{m_e}{m_\mu}\right) \cos \theta \right\},$$

or neglecting the electron mass

$$\frac{d^2 \Gamma^\pm}{dx d \cos \theta} = \frac{G_\mu^2 m_\mu^5}{192\pi^3} x^2 (3 - 2x \pm P_\mu (2x - 1) \cos \theta). \quad (6.57)$$

Typically, the μ -decay spectrum is strongly peaked at small angles θ , the e^\pm emission angle between the e momentum \mathbf{p}_e and the muon polarization vector \mathbf{P}_μ . The result above holds in the approximation $x_0 = m_e/W \sim 9.67 \times 10^{-3} \simeq 0$.

Assuming unit polarization, the μ^\pm decay spectrum may be written in the form Eq. (6.3) discussed earlier or equivalently

$$\begin{aligned} W^\pm(x, \cos \theta) dx d \cos \theta &= \tau_\mu^{-1} x^2 (3 - 2x) \left[1 \pm \frac{2x - 1}{3 - 2x} \cos \theta \right] \\ &= \tau_\mu^{-1} \frac{N(E_e)}{2} [1 + A(E_e) \cos \theta] dx d \cos \theta, \end{aligned}$$

where

$$N(E_e) = 2x^2(3 - 2x), \quad \left[\int_0^1 dx N(x) = 1 \right], \quad (6.58)$$

represents a normalizing spectrum and

$$A(E_e) = \frac{2x - 1}{3 - 2x}, \quad \left[\int_0^1 dx N(x) A(x) = 1/3 \right], \quad (6.59)$$

is the asymmetry which reflects the *parity violation* and strongly correlates the muon spin with the positron momentum direction. The asymmetry changes sign at $x = 1/2$.

Figure 6.11 shows energy spectrum $N(x)$ as a function of x where the positron energy from the normal μ^\pm -decay is $E_e = x \times 52.83$ MeV. $A(E_e)$ is the e^\pm energy dependent μ^\pm -decay asymmetry, the degree of correlation between e^\pm momentum and μ^\pm spin direction. For the μ^- decay $A(E_e)$ has the opposite sign. Also displayed is the weighted μ^+ decay asymmetry spectrum, the product of N and A^2 . The average asymmetry is

¹⁰With $Q^2 = m_\mu^2 + m_e^2 - 2p_0 p_1$, $Qp_0 = m_\mu^2 - p_0 p_1$, $Qp_1 = p_0 p_1 - m_e^2$, and $p_0 p_1 = m_\mu E_e$, $E_e = xW$, $m_\mu = 2W$ the curly bracket of (6.56) reads $\{\dots\} = 8W^4 x [(3 - 2x) + P_\mu \cos \theta (2x - 1)] + O(m_e^2/m_\mu^2)$.

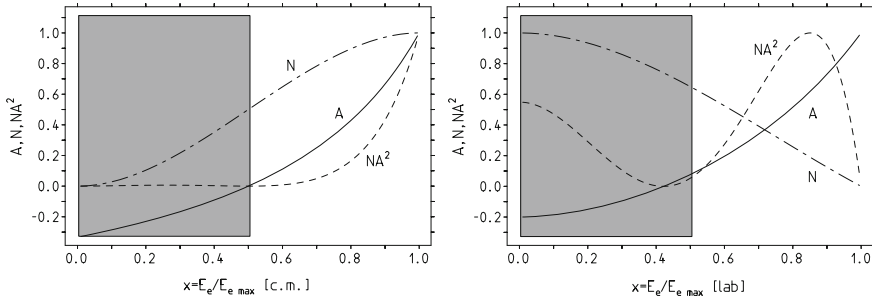


Fig. 6.11 Number of decay positrons per unit energy (Michel spectrum) N (arbitrary units), value of the asymmetry A , and relative yield NA^2 (arbitrary units) as a function of the positron energy in units of the maximal positron energy. The polarization is assumed to be unity. Events in the shaded region $E < E_{th}$ are not counted, since if all events are integrated the asymmetry gets largely canceled. *Left* as seen in the muon rest frame. *Right* as seen in the laboratory frame

$$A = \frac{\int_0^1 dx N(x) A(x)}{\int_0^1 dx N(x)} = \frac{1}{3} ; \quad \frac{W(\cos \theta)}{d \cos \theta} = \frac{1}{2} (1 + A \cos \theta) = \frac{1}{2} \left(1 + \frac{1}{3} \cos \theta \right) .$$

What we see in the laboratory frame we obtain by the transformation (see [2])

$$E'_e = \gamma (E_e + \beta p_{ex}) ; \quad p'_{ex} = \gamma (p_{ex} + \beta E_e) , \quad p'_{ey} = p_{ey} , \quad p'_{ez} = p_{ez} ,$$

where $\gamma = E/m$ and $\beta = p/E$ when $p'_\mu = p^{\text{lab}}_\mu = (E, p, 0, 0)$ boosted along the x -axis. Denoting θ' the positron emission angle in the laboratory frame, where the muon's spin precesses relative to the momentum vector such that one can identify

$$\cos \theta' \rightarrow \cos (\omega_a t + \phi) ,$$

up to a phase ϕ . Adopting polar coordinates (x, θ_μ, φ) in the rest frame with \mathbf{p}_μ as a x -axis and $\varphi = 0$ in the plane of the muon spin precession, then, if the spin is at angle $(\omega_a t)$ to the muon direction, then it is at angle θ (introduced above) with respect to the positron direction. In terms of (θ_μ, φ)

$$\cos \theta = \cos \theta_\mu \cos (\omega_a t) + \sin \theta_\mu \sin (\omega_a t) \cos \varphi ,$$

and integrating over those positrons emitted within a region R in the muon rest frame which can be detected in the laboratory frame we have

$$\begin{aligned} & \frac{1}{2\pi} \int_R 2\tau_\mu W(x, \cos \theta) dx d \cos \theta d\varphi \\ &= \frac{1}{2\pi} \int_R 2x^2 (3 - 2x) + 2x^2 (2x - 1) [\cos \theta_\mu \cos (\omega_a t) + \sin \theta_\mu \sin (\omega_a t) \cos \varphi] dx d \cos \theta d\varphi . \end{aligned}$$

Integrating over φ the second term in the square bracket vanishes, while the first gets a factor 2π , such that

$$N'_e = \int_x \int_{\cos\theta} 2x^2 (3 - 2x) dx d \cos \theta ; \quad N'_e A'_e = \int_x \int_{\cos\theta} 2x^2 (2x - 1) \cos \theta dx d \cos \theta .$$

What is the range R in $(x, \cos \theta)$ space which gets mapped to the positrons detected in the laboratory frame? In the laboratory frame the positron energy in units of $W \approx m_\mu/2$ takes values

$$x'_L = x \gamma_\mu (1 + \cos \theta_\mu) , \quad x'_T = x \sin \theta_\mu ,$$

where x'_L is the positron momentum along the boost direction and x'_T the one transverse to it. A **threshold energy** in the laboratory system fixes a lower bound for $x'^2_L + x'^2_T = x'^2_{th}$ such that

$$x^2 \gamma_\mu^2 (1 + \cos \theta_\mu)^2 + x^2 \sin^2 \theta_\mu \geq x'^2_{th}$$

together with $x \leq 1$. Since $\gamma_\mu \gg 1$ we may neglect the transversal term and get

$$\cos \theta_\mu \geq x'_{th}/x\gamma_\mu - 1 .$$

For $\cos \theta = 1 = x'_{th}/x_{\min}\gamma_\mu - 1$ thus $1 \geq x \geq b/2$ where $b = x'_{th}/\gamma_\mu$. Thus with $\int_{b/x}^1 d \cos \theta = 2 - b/x$ and $\int_{b/x}^1 \cos \theta d \cos \theta = b/x - b^2/2x^2$ and integrating $\int_{b/2}^1 dx \dots$ we obtain

$$N'_e = \left[2 - \frac{5b}{3} + \frac{b^3}{4} - \frac{b^4}{24} \right] ; \quad N'_e A'_e = \left[\frac{b}{3} - \frac{b^3}{4} + \frac{b^4}{12} \right] ,$$

where $b/2 \leq 1$. If we substitute $b = 2x_{th}$ and drop an overall factor $2/3$ we obtain [1]

$$N'_e = (x_{th} - 1)^2 (3 + x_{th} - x_{th}^2) ; \quad N'_e A'_e = x_{th} (2x_{th} + 1) (x_{th} - 1)^2 . \quad (6.60)$$

The above result may be obtained as an integral $I(x_{th}) = \int_{x_{th}}^1 dx \dots$ by taking the derivative $-dI(x_{th})/dx_{th}$ which yields

$$A(E) = P_\mu \frac{1 + x' - 8x'^2}{4x'^2 - 5x' - 5} ; \quad N(E) \propto (x' - 1)(4x'^2 - 5x' - 5)$$

with $x' = E/E_{\max}$, E the positron's laboratory energy and $E_{\max} = 3.098$ GeV. These equations correspond to the laboratory frame versions of (6.58) and (6.59).¹¹ Again, the positron number oscillation with time as a function of positron energy reads

$$N(t, E) = N_0(E) e^{-t/\gamma\tau} [1 + A(E) \cos(\omega_a t + \phi(E))] ,$$

which we have plotted in the right panel of Fig. 6.11. The phase ϕ comes from the initial spin polarization of the muons. By plotting the number of decay positrons observed as a function of time, one may extract ω_a by fitting the data to the simple 5-parameter function (6.62) below. Since the determination of ω_a is based on the number of counts, there is a statistical uncertainty on ω_a . In fitting N_0 , τ , ω_a and ϕ from $N(t)$, data-fitting statistics implies that the statistical error on ω_a is approximately [1]

$$\frac{\delta\omega_a}{\omega_a} \approx \frac{\sqrt{2}}{\omega_a \gamma\tau A \langle P \rangle \sqrt{N}} . \quad (6.61)$$

The factor $1/\sqrt{N}$ is statistical error of the data sample, the factor $1/A$ is obvious from $N^{-1}\delta N/\delta\omega_a \propto A$ and the factor $1/\omega_a\gamma\tau$ accounts for improvement of the accuracy with the number of oscillations per decay-time $\omega_a t/\frac{1}{\gamma\tau} = \omega_a\gamma\tau$. Also the average degree of the polarization $\langle P \rangle$ matters of course. The factor of $\sqrt{2}$ comes from the strong correlation between the phase ϕ and the frequency ω_a . Since both A and N depend on the energy-threshold and since one wishes to minimize the statistical uncertainty of ω_a , the energy-threshold is chosen such that the product NA^2 is maximized. Then counting all positrons above a threshold energy E_{th} the oscillation profile reads

$$N(t, E_{\text{th}}) = N_0(E_{\text{th}}) e^{-t/\gamma\tau} [1 + A(E_{\text{th}}) \cos(\omega_a t + \phi(E_{\text{th}}))] , \quad (6.62)$$

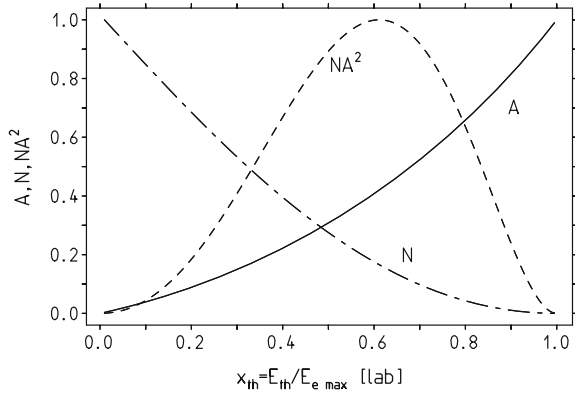
with (using (6.60))

$$A(E_{\text{th}}) = P_\mu \frac{x_{\text{th}}(2x_{\text{th}} - 1)}{3 + x_{\text{th}} - x_{\text{th}}^2} ; \quad N(E_{\text{th}}) \propto (x_{\text{th}} - 1)^2(3 + x_{\text{th}} - x_{\text{th}}^2) .$$

Figure 6.12 shows that the ‘‘figure of merit’’ NA^2 has a maximum at $x_{\text{th}} \approx 0.65$, which corresponds to about 2 GeV. Equation (6.62) represents the actual time structure which is confronted with the experimental data to extract the Larmor precession angular frequency ω_a .

¹¹Note that, this is not what one gets by writing (6.56) in terms of laboratory system variables. It is rather a matter of how the geometrical acceptance of the decay positrons/electrons is affected by boosting the system.

Fig. 6.12 Optimizing the quality $NA^2(E_{th})$ by an appropriate choice of the laboratory energy threshold E_{th} above which positrons/electrons are registered (see [1])



6.5 Muon $g - 2$ Results

First a historical note: before the E821 experiment at Brookhaven the last of a series of measurement of the anomalous g -factor $a_\mu = (g_\mu - 2)/2$ at CERN was published about 30 years earlier. At that time a_μ had been measured for muons of both charges in the Muon Storage Ring at CERN. The two results,

$$\begin{aligned} a_{\mu^-} &= 1165937(12) \times 10^{-9} , \\ a_{\mu^+} &= 1165911(11) \times 10^{-9} , \end{aligned} \tag{6.63}$$

are in good agreement with each other, and combine to give a mean

$$a_\mu = 1165924.0(8.5)10^{-9} \text{ [7 ppm]} , \tag{6.64}$$

which was very close to the theoretical prediction $1165921.0(8.3)10^{-9}$ at that time. The measurements thus confirmed the remarkable QED calculation plus hadronic contribution, and served as a precise verification of the CPT theorem for muons.

Measured in the experiments is the ratio $R = \omega_a/\omega_p$ of the muon precession frequency $\omega_a = \omega_s - \omega_c$ and the proton precession frequency ω_p , which together with the ratio of the magnetic moment of the muon to the one of the proton $\lambda = \mu_\mu/\mu_p$ determines the anomalous magnetic moment as

$$a_\mu = \frac{R}{\lambda - R} . \tag{6.65}$$

The CERN determination of a_μ utilized the value $\lambda = 3.1833437(23)$.

The BNL muon $g - 2$ experiment has been able to improve and perfect the method of the last CERN experiments in several respects and was able to achieve an impressive 14-fold improvement in precision. The measurements are $R_{\mu^-} = 0.0037072083(26)$ and $R_{\mu^+} = 0.0037072048(25)$ the difference being $\Delta R = (3.5 \pm$

Table 6.2 Summary of CERN and E821 results

Experiment	Year	Polarity	$a_\mu \times 10^{10}$	Precision [ppm]	References
CERN I	1961	μ^+	11 450 000 (220000)	4300	[35]
CERN II	1962–1968	μ^+	11 661 600 (3100)	270	[36]
CERN III	1974–1976	μ^+	11 659 100 (110)	10	[15]
CERN III	1975–1976	μ^-	11 659 360 (120)	10	[15]
BNL	1997	μ^+	11 659 251 (150)	13	[20]
BNL	1998	μ^+	11 659 191 (59)	5	[21]
BNL	1999	μ^+	11 659 202 (15)	1.3	[22]
BNL	2000	μ^+	11 659 204 (9)	0.73	[23]
BNL	2001	μ^-	11 659 214 (9)	0.72	[24]
	Average		11 659 208.0 (6.3)	0.54	[24]

$3.4) \times 10^{-9}$. Together with the updated muon-to-proton magnetic ratio¹² $\lambda = 3.183345107(84)$ [37] one obtains the new values

$$\begin{aligned} a_{\mu^-} &= 11659215(8)(3) \times 10^{-10}, \\ a_{\mu^+} &= 11659204(6)(5) \times 10^{-10}. \end{aligned} \quad (6.66)$$

Assuming CPT symmetry, as valid in any QFT, and taking into account correlations between systematic errors between the various data sets the new average $R = 0.0037072064(20)$ is obtained. From this result together with the updated λ (6.9) one obtains the new average value

$$a_\mu = 11659209.1(5.4)(3.3)[6.3] \times 10^{-10}, \quad (6.67)$$

with a relative uncertainty of 0.54 ppm [16]. Where two uncertainties are given the first is statistical and the second systematic, otherwise the total error is given where statistical and systematic errors have been added in quadrature. In Table 6.2 all results from CERN and E821 are collected. The new average is completely dominated by the BNL results. The individual measurements are shown also in Fig. 6.13. The comparison with the theoretical result is devoted to the next section. The achieved improvement and a comparison of the sensitivity to various kinds of physics effects has been shown earlier in Fig. 3.8 at the end of Sect. 3.2.1.

The following two sections are addenda, one on the determination of λ in (6.65) and the other a sketch of the electron $g - 2$ measurement technique.

¹²This value is replacing $\lambda = 3.18334539(10)$ used in [24].

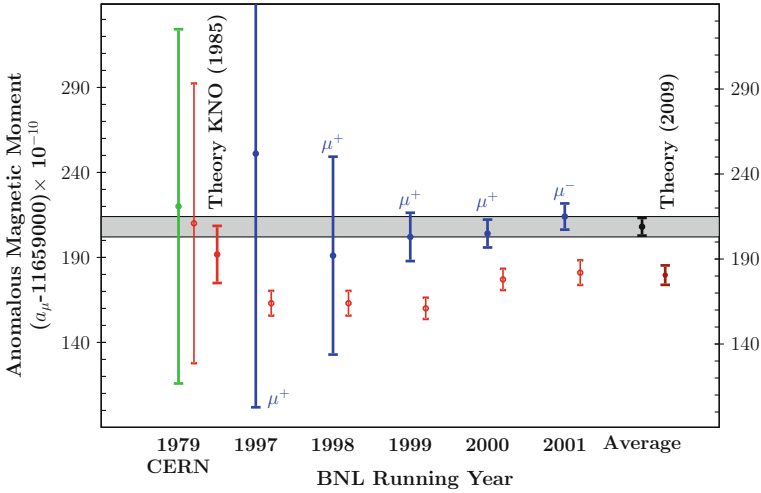


Fig. 6.13 Results for the individual E821 measurements, together with the new world average and the theoretical prediction. The CERN result is shown together with the theoretical prediction by Kinoshita et al. 1985, at about the time when the E821 project was proposed. The *dotted vertical bars* indicate the theory values quoted by the experiments

6.6 Ground State Hyperfine Structure of Muonium

The hyperfine and Zeeman levels of $^2S_{1/2}$ ground state Muonium are shown in Fig. 6.14. The energy levels are described by the Hamiltonian

$$\mathcal{H} = h \Delta\nu \mathbf{I}_\mu \cdot \mathbf{J} - \mu_B^\mu g'_\mu \mathbf{I}_\mu \cdot \mathbf{B} + \mu_B^e g_J \mathbf{J} \cdot \mathbf{B}, \tag{6.68}$$

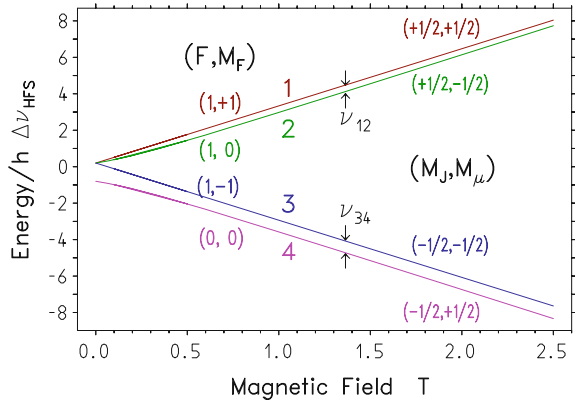
where \mathbf{I}_μ is the muon spin operator, \mathbf{J} is the electron total angular momentum operator and \mathbf{B} is the external static magnetic field. The total angular momentum is $\mathbf{F} = \mathbf{J} + \mathbf{I}_\mu$.

Microwave transitions ν_{12} and ν_{34} are measured in a strong magnetic field B of 1.6T. Also this experiment uses the parity violating correlation of the direction of the muon spin and the positron emission of μ -decay.

The hyperfine splitting (HFS) and the muon magnetic moment are determined from ν_{12} and ν_{34} .

$$\begin{aligned} \nu_{12} &= -\mu_\mu B + \frac{\Delta\nu}{2} \left[1 + x - \sqrt{1 + x^2} \right], \\ \nu_{34} &= +\mu_\mu B + \frac{\Delta\nu}{2} \left[1 - x + \sqrt{1 + x^2} \right], \end{aligned} \tag{6.69}$$

Fig. 6.14 Muonium ground state hyperfine structure Zeeman splitting (Breit-Rabi energy level diagram). At high fields the transitions ν_{12} and ν_{34} are essentially muon spin flip transitions



where $x = (g_J \mu_B^e + g'_\mu \mu_B^\mu) B / (h \Delta\nu)$ is proportional to the magnetic field strength B .¹³ The latest experiment at LAMPF at Los Alamos has measured these level splittings very accurately. The Larmor relation, $2\mu_p B = h\nu_p$, and NMR is used to determine B in terms of the free proton precession frequency ν_p and the proton magnetic moment μ_p . Using (6.69) and the measured transition frequencies ν_{12} and ν_{34} both $\Delta\nu$ and μ_μ/μ_p can be determined.

Note that the sum of (6.69) equals to the zero field splitting $\Delta\nu \equiv \Delta\nu_{\text{HFS}}$ independent of the field B , while for high fields the difference measures the magnetic moment μ_μ :

$$\Delta\nu = \nu_{12} + \nu_{34} ,$$

$$\mu_\mu B = \nu_{34} - \nu_{12} - \Delta\nu \left(\sqrt{1 + x^2} - x \right) \approx \nu_{34} - \nu_{12} - \frac{\Delta\nu}{2x} , \quad (x \gg 1) .$$

The magnetic moment was measured to be

$$\mu_\mu/\mu_p = 3.183\,345\,24(37) \text{ (120 ppb)} ,$$

which translates into a muon–electron mass ratio

$$m_\mu/m_e = \left(\frac{g_\mu}{2} \right) \left(\frac{\mu_p}{\mu_\mu} \right) \left(\frac{\mu_B^e}{\mu_p} \right) = 206.768\,276(24) \text{ (120 ppb)} ,$$

¹³The gyromagnetic ratios of the bound electron and muon differ from the free ones by the binding corrections [38]

$$g_J = g_e \left(1 - \frac{\alpha^2}{3} + \frac{\alpha^2}{2} \frac{m_e}{m_\mu} + \frac{\alpha^3}{4\pi} \right) , \quad g'_\mu = g_\mu \left(1 - \frac{\alpha^2}{3} + \frac{\alpha^2}{2} \frac{m_e}{m_\mu} \right) .$$

when using $g_\mu = 2(1 + a_\mu)$ with $a_\mu = 11\,659\,208.0(6.3) \times 10^{-10}$ and $\mu_p/\mu_B^e = 1.521\,032\,206(15) \times 10^{-3}$ [30]. The measured value of the zero field HFS is

$$\Delta\nu^{\text{exp}} = 4\,463\,302\,765(53) \text{ Hz (12 ppb)},$$

in good agreement with the theoretical prediction [27, 28, 30, 39–41]

$$\begin{aligned} \Delta\nu^{\text{the}} &= \frac{16}{3} c R_\infty \alpha^2 \frac{m_e}{m_\mu} \left(1 + \frac{m_e}{m_\mu}\right)^{-3} (1 + \delta\mathcal{F}(\alpha, m_e/m_\mu)) \\ &= 4\,463\,302\,905(272) \text{ Hz (61 ppb)}, \end{aligned}$$

where the error is mainly due to the uncertainty in m_μ/m_e . The correction $\delta\mathcal{F}(\alpha, m_e/m_\mu)$ depends weakly on α and m_e/m_μ ,

$$R_\infty = 10\,973\,731.568\,525(37) \text{ m}^{-1}$$

is the Rydberg constant $\alpha^2 m_e c / 2h$ [30]. A combined result was used to determine (6.9) used in the determination of a_μ (see also [42]).

6.7 Single Electron Dynamics and the Electron $g - 2$

The basic principle of a muon $g - 2$ experiment is in many respects very similar to the one of electron $g - 2$ experiments, although the scale of the experiment is very different and the electron $g - 2$ experiment uses atomic spectroscopy type methods to determine the frequencies. The particle dynamics considered in Sect. 6.2 applies to the single electron or single ion Penning trap shown in Fig. 6.15. Electron motion in a hyperboloid Penning trap in the *axial* (vertical) direction is a harmonic oscillation

$$z(t) = A \cos(\omega_z t),$$

with

$$\omega_z = 2\sqrt{eV_0/md^2},$$

(see (6.15)). In the *radial* direction it is an epicycloid motion with

$$\begin{aligned} x(t) &= +\rho_m \cos(\omega_m t) + \rho_c \cos(\omega'_c t), \\ y(t) &= -\rho_m \sin(\omega_m t) - \rho_c \sin(\omega'_c t). \end{aligned}$$

Here

$$\omega'_c = \omega_+ = \frac{1}{2}(\omega_c + \sqrt{\omega_c^2 - 2\omega_z^2}) \simeq \omega_c$$

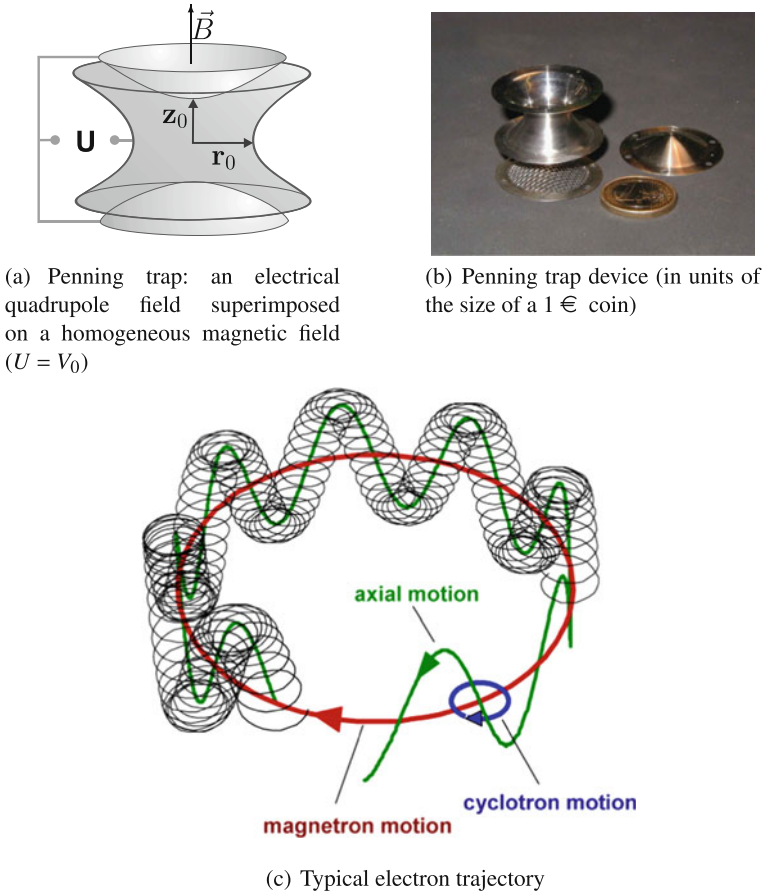


Fig. 6.15 Electron motion in a hyperbolic Penning trap Courtesy of G. Werth, Mainz [43]

is the *perturbed cyclotron frequency* and

$$\omega_m = \omega_- = \frac{1}{2}(\omega_c - \sqrt{\omega_c^2 - 2\omega_z^2}) = \omega_c - \omega'_c$$

the *magnetron frequency*. The frequencies are related by $\omega_c^2 = \omega_+^2 + \omega_-^2 + \omega_z^2$. Typical values for a positron in a magnetic field $B = 3$ T, $U = 10$ V and $d = 3.3$ mm are $\nu_c = 48$ GHz, $\nu_z = 64$ MHz, $\nu_m = 12$ kHz depending on the field strengths determined by B , U and d .

The observation of the splitting of the spin states requires a coupling of the cyclotron and spin motion of the trapped electron to the axial oscillation, which is realized by an extremely weak magnetic bottle modifying the uniform magnetic field by an inhomogeneous component (Dehmelt et al. [44]) (see Fig. 6.16). The latter is imposed by a ferromagnetic ring electrode, such that

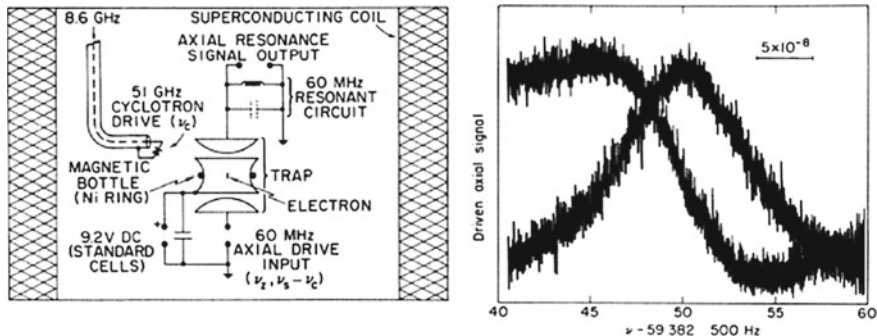


Fig. 6.16 *Left* schematic of the geonium apparatus (Dehmelt et al. [44]). Hyperbolic end caps and ring electrodes trap the electron axially while coupling the driven harmonic motion to an external LC circuit tuned to drive the axial frequency. Radial trapping of the electron is produced by the strong magnetic field from a superconducting solenoid. *Right* frequency shift in the axial resonance signal at ≈ 60 MHz. The signal-to-noise ratio of this ≈ 8 Hz wide line corresponds to a frequency resolution of 10 ppb. Reprinted with permission from [44]. Copyright (2007) by the American Physical Society

$$B = B_0 + B_2 z^2 + \dots, \quad (6.70)$$

which imposes a force

$$F = m_s g_e \mu_B \text{grad } B = m_s g_e \mu_B B_2 z$$

on the magnetic moment. Because of the cylindrical symmetry the force is linear in first order and the motion remains harmonic. The force adds or subtracts a component depending on $m_s = \pm 1/2$ and thus changes the axial frequency by

$$\Delta\omega_z = g_e \mu_B \frac{B_2}{m_e \omega_z}, \quad (6.71)$$

as shown in Fig. 6.16.

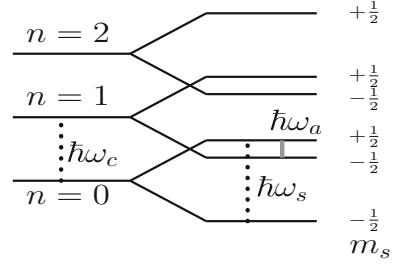
For a trap working at a temperature of $T = 4^\circ$ K the thermic energy is $E = kT = 3.45 \times 10^{-4}$ eV. The trapped electron occupies low quantum states, the cyclotron ($n = 0, 1, 2, \dots$) and spin ($m_s = \pm 1/2$) energy levels,

$$E(n, m_s) = \left(n + \frac{1}{2}\right) \hbar\omega'_c + \frac{g_e}{2} \hbar\omega_c m_s - \frac{\hbar}{2} \delta \left(n + \frac{1}{2} + m_s\right)^2, \quad (6.72)$$

for $\nu_c = 84$ GHz thus $\hbar\omega_c = 3.47 \times 10^{-4}$ eV which implies $n_c = 0, 1$ such that QM is at work (the axial motion corresponds to $n_z \simeq 1000$ and hence is classical).

In fact this is not quite true: Gabrielse has shown that in Dehmelt's experiment at 4° K, because of the spread in the thermic spectrum, still many higher states are populated and, in a field of a few Tesla, only at about $T = 0.1^\circ$ K one reaches the ground state [45]. The third term in (6.72) is the leading relativistic correction of

Fig. 6.17 Lowest electron quantum states in a Penning trap



size $\delta/\nu_c \equiv h\nu_c/(mc^2) \approx 10^{-9}$ [46], too small to be important at the present level of accuracy of the experiments. The radiation damping is

$$\frac{dE}{dt} = -\hat{\gamma}E, \quad \hat{\gamma} = \frac{e^2\omega^2}{6\pi\epsilon_0 mc^3}, \quad (6.73)$$

and with $\alpha\hbar c = e^2/(4\pi\epsilon_0) = 1.44 \text{ MeVfm}$ one has $\hat{\gamma}_c = 1.75 \text{ s}^{-1}$. The spontaneous damping by radiation is then $\hat{\gamma}_z \simeq \hat{\gamma}_c/10^6 \simeq 0.15$ per day. The $g - 2$ follows from the spin level splitting Fig. 6.17

$$\Delta E = g_e \mu_B B = \frac{g_e}{2} \hbar\omega_c \equiv \hbar\omega_s, \quad (6.74)$$

such that

$$a_e \equiv \frac{g_e - 2}{2} = \frac{\omega_s - \omega_c}{\omega_c} \equiv \frac{\omega_a}{\omega_c}. \quad (6.75)$$

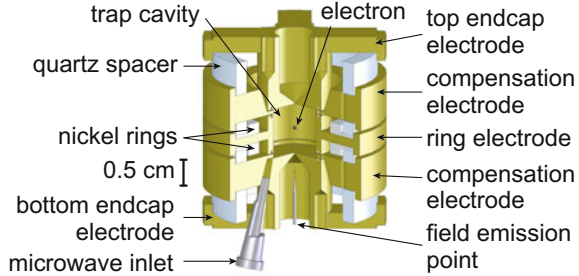
From the spin Larmor precession frequency $\hbar\omega_s = m_e g_e \mu_B B$ (μ_B the Bohr magneton) and the calibration of the magnetic field by the cyclotron frequency of a single ion in the Penning trap $\hbar\omega_c = q_{\text{ion}}/M_{\text{ion}} B$ one obtains

$$g_e = 2 \frac{\omega_s}{\omega_c} \frac{q_{\text{ion}}}{e} \frac{m_e}{M_{\text{ion}}}, \quad (6.76)$$

or if g_e is assumed to be known one may determine the electron mass very precisely. The most precise determination was obtained from g -factor experiments on $^{12}\text{C}^{5+}$ and $^{16}\text{C}^{7+}$ [47] with a cylindrical cryogenic double Penning trap in a magnetic field of 3.8 T [working at frequencies $\nu_c = 25 \text{ MHz}$, $\nu_z = 1 \text{ MHz}$, $\nu_m = 16 \text{ kHz}$].

The Harvard electron $g - 2$ experiment [48, 49] performs spectroscopy of a single electron in the lowest cyclotron and spin levels in a cylindrical Penning trap (see Fig. 6.18). The problem of a harmonic Penning trap is that it is a cavity and hence allows only certain electromagnetic frequencies. The damping by spontaneous emission affects the cyclotron frequency in a way which is not fully under control. The cylindrical trap which exhibits plenty of higher harmonics solves this problem as it can be operated at well selected frequencies. Working frequencies are

Fig. 6.18 Cylindrical Penning trap cavity used to confine a single electron and inhibit spontaneous emission. Reprinted with permission from [48]. Copyright (2008) by the American Physical Society, <http://dx.doi.org/10.1103/PhysRevLett.100.120801>



$\nu_s \approx \nu_c \approx 149$ GHz, $\nu_z \approx 200$ MHz, $\nu_m \approx 134$ kHz. For the first time it was possible to work with the lowest quantum states of (6.72) (see Fig. 6.17) in the determination of $g_e - 2$. The result has been discussed in Sect. 3.2.2.

6.8 The Upcoming Experiments: What Is New?

A new more precise experiment has to improve on the ingredients of (6.6) which more explicitly reads

$$a_\mu = \frac{\omega_a / \tilde{\omega}_p}{\mu_\mu / \mu_p - \omega_a / \tilde{\omega}_p}, \tag{6.77}$$

where ω_a is the muon spin precession frequency and $\tilde{\omega}_p$ the proton cyclotron frequency in the average magnetic field seen by the muons. Both frequencies will be provided by the new muon $g - 2$ experiments. One ingredient, the μ_μ / μ_p ratio, which has been obtained with the muonium HFS experiment at LAMPF, will be limited at 120 ppb.

The Fermilab experiment [9–11] will improve the present error of a_μ from 540 to 140 ppb by a more precise determination of ω_a / ω_p . The principle of the experiment is the same as described earlier in this chapter. The improvements concern

- ω_a : one of the main issues at BNL was the limited statistics. At Fermilab highly intense shots of polarized 3.094 GeV/c muons will be available (21 times BNL), which will turn the formerly statistics dominated measurement into a systematics dominated one. The final data sample will include 1.5×10^{11} events in the final fit. This will give $\delta\omega_a(\text{statistics}) = 110$ ppb. The background from hadronic decays is eliminated as all pions decay and protons are removed from the muon beam before injection into the storage ring. Further improvements include:
 - new injection and kicker system (the frequency at BNL was disturbingly close to the second harmonic of ω_a , which affected the BNL analysis).
 - Improved systematics to 70 ppb concerning pileup, gain and energy scale stability and muon losses.
 - Improved correction for electric field and pitch, better control of the beam profile.

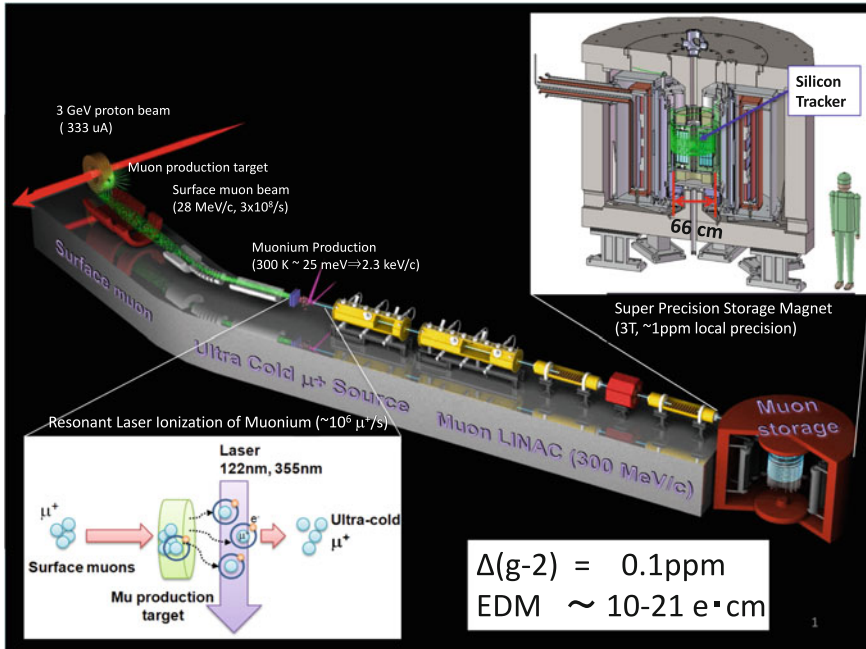


Fig. 6.19 Ultra-cold muon generation beam line and muon storage for the E34 experiment at J-PARC. Courtesy of the J-PARC $g-2$ Collaboration

- ω_p : better homogeneity and control/calibration of the homogeneous magnetic field i.e. improved $\tilde{\omega}_p$ at the 70 ppb level (factor 2 improvement over BNL).

The J-PARC experiment [12–14] planned to work with ultra cold muons represents a novel approach. Slow polarized muons are injected again into a homogeneous magnetic field filling a cylindrical trap free of any electrical fields. Thus the basic precession equation (6.2) again reduces to the simple $\omega_a = \frac{e}{m_\mu c} a_\mu B$ form. The size of the trap is almost a table top experiment. There is no electric beam focusing, meaning that muons need be injected at zero transverse momentum. The slow muons are living much shorter, by close to the factor $\gamma_{\text{magic}}/\gamma_{\text{cold}} \approx 10$ relative to the magic γ type experiments. However, muons are moving in a much smaller device. Smaller magnet fields intrinsically are more uniform. The principle is illustrated in Figs. 6.19 and 6.20. Data acquisition takes place within the small trap volume. The positron/electron number count again will be fitted to a function of the form (6.62). However, the completely different setup as a small low energy experiment implies rather different parameters in (6.62) and correspondingly in (6.61). On the one hand ω_a will be bigger because a bigger magnetic field will be applied, on the other hand $\gamma_{\text{magic}} \approx 30 \rightarrow \gamma_{\text{cold}} \approx 3$ such that $\gamma\tau$ appears reduced by a factor about 10 and is much smaller now. Also the degree of polarization expected to be about 50% (comparing to the expected 97% with E989) affects the statistical precision. The size

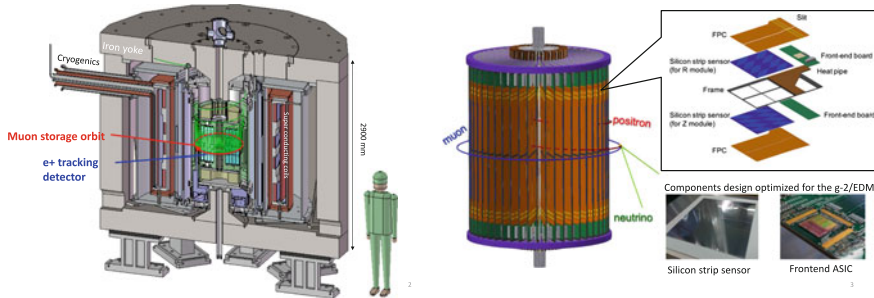


Fig. 6.20 *Left* magnet with storage ring and 3-dimensional spiral injection. *Right* Silicon tracker for positron detection. Courtesy of the J-PARC g-2 Collaboration. Private communication by T. Mibe

Table 6.3 Comparison of main parameters for the Fermilab and J-PARC $g - 2$ experiments. The parameters of the Fermilab experiment are identical with the ones of the Brookhaven experiment (except from the statistics: BNL registered about 3.6×10^9 events, and had $A = 0.3$)

Parameter	Fermilab E989	J-PARC E34
Muon lab energy	3.098 GeV	300 MeV
Radius	7.11 m	33.3 cm
Cyclotron period	149.1 ns	7.4 ns
Lifetime, $\gamma\tau$	64.4 μ s	6.6 μ s
Effective asymmetry A	0.4	0.4
Beam polarization	0.97	0.50
Magnetic field	1.45 T	3.0 T
Precession frequency ω_a	1.43 MHz	2.96 MHz
Events in final fit	1.8×10^{11}	8.1×10^{11}
Statistical goal	140 ppb	400 ppb

of the effective asymmetry may be tuned to be comparable. In a first step the E34 experiment attempts to reach the precision of the BNL experiment. In Table 6.3 we compare the main parameters between the Fermilab/Brookhaven and the J-PARC experiments. While the E989 experiment is expected to substantiate the present 3 to 4 σ deviation as a new physics effect, the E43 experiment in a first step will scrutinize possible unaccounted systematic effects in the comparison between theory and experiment. We should keep in mind that the basic BMT equation (6.2) does not include possible higher order real photon radiation effects¹⁴ which are very different for ultra relativistic and ultra cold muons.

¹⁴What I mean is that, as in Sect. 6.3, one solves the Dirac equation in an external field (the first of the QED field Eq. (3.1) with zero radiation field $A_\mu(x) \equiv 0$) rather than the coupled QED field equations.

References

1. J. Bailey et al., *Nuovo Cim. A* **9**, 369 (1972)
2. F. Combley, E. Picasso, *Phys. Rep.* **14C**, 1 (1974)
3. F.J.M. Farley, E. Picasso, in *Quantum Electrodynamics*, ed. by T. Kinoshita (World Scientific, Singapore 1990), p. 479; *Adv. Ser. Direct. High Energy Phys.* **7**, 479 (1990)
4. V.W. Hughes, The anomalous magnetic moment of the muon, in *International School of Sub-nuclear Physics: 39th Course: New Fields and Strings in Subnuclear Physics*, Erice, Italy, 29 Aug–7 Sep (2001); *Int. J. Mod. Phys. A* **18S1**, 215 (2003)
5. F.J.M. Farley, Y.K. Semertzidis, *Prog. Part. Nucl. Phys.* **52**, 1 (2004)
6. D.W. Hertzog, W.M. Morse, *Annu. Rev. Nucl. Part. Sci.* **54**, 141 (2004)
7. J.M. Paley, Measurement of the anomalous magnetic moment of the negative muon to 0.7 parts per million, Boston University Dissertation, 2004, Available from the UMI Thesis Server
8. J.P. Miller, E. de Rafael, B.L. Roberts, *Rep. Prog. Phys.* **70**, 795 (2007). doi:[10.1088/0034-4885/70/5/R03](https://doi.org/10.1088/0034-4885/70/5/R03)
9. J. Grange et al. [Muon $g-2$ Collab.], [arXiv:1501.06858](https://arxiv.org/abs/1501.06858) [physics.ins-det]
10. D.W. Hertzog, EPJ Web Conf. **118**, 01015 (2016). doi:[10.1051/epjconf/201611801015](https://doi.org/10.1051/epjconf/201611801015)
11. G. Venanzoni [Fermilab E989 Collab.], *Nucl. Part. Phys. Proc.* **273–275**, 584 (2016). doi:[10.1016/j.nuclphysbps.2015.09.087](https://doi.org/10.1016/j.nuclphysbps.2015.09.087); PoS EPS-HEP2015, 568 (2015)
12. N. Saito [J-PARC $g-2$ /EDM Collab.], *AIP Conf. Proc.* **1467**, 45 (2012). doi:[10.1063/1.4742078](https://doi.org/10.1063/1.4742078)
13. H. Iinuma [J-PARC muon $g-2$ /EDM Collab.], *J. Phys. Conf. Ser.* **295**, 012032 (2011). doi:[10.1088/1742-6596/295/1/012032](https://doi.org/10.1088/1742-6596/295/1/012032)
14. T. Mibe [J-PARC $g-2$ Collab.], *Nucl. Phys. Proc. Suppl.* **218**, 242 (2011). doi:[10.1016/j.nuclphysbps.2011.06.039](https://doi.org/10.1016/j.nuclphysbps.2011.06.039)
15. J. Bailey et al., *Nucl. Phys. B* **150**, 1 (1979)
16. G.W. Bennett et al. [Muon $g-2$ Collab.], *Phys. Rev. D* **73**, 072003 (2006)
17. G.T. Danby et al., *Nucl. Instrum. Methods Phys. Res. A* **457**, 151 (2001)
18. Y.K. Semertzidis, *Nucl. Instrum. Methods Phys. Res. A* **503**, 458 (2003)
19. E. Efsthathiadis et al., *Nucl. Instrum. Methods Phys. Res. A* **496**, 8 (2002)
20. R.M. Carey et al., *Phys. Rev. Lett.* **82**, 1632 (1999)
21. H.N. Brown et al. [Muon ($g-2$) Collab.], *Phys. Rev. D* **62**, 091101 (2000)
22. H.N. Brown et al. [Muon ($g-2$) Collab.], *Phys. Rev. Lett.* **86**, 2227 (2001)
23. G.W. Bennett et al. [Muon $g-2$ Collab.], *Phys. Rev. Lett.* **89**, 101804 (2002) [Erratum-ibid. **89**, 129903 (2002)]
24. G.W. Bennett et al. [Muon $g-2$ Collab.], *Phys. Rev. Lett.* **92**, 161802 (2004)
25. R. Prigl et al., *Nucl. Instrum. Methods Phys. Res. A* **374**, 118 (1996); X. Fei, V. Hughes, R. Prigl, *Nucl. Instrum. Methods Phys. Res. A* **394**, 349 (1997)
26. W. Liu et al., *Phys. Rev. Lett.* **82**, 711 (1999)
27. T. Kinoshita, M. Nio, *Phys. Rev. D* **53**, 4909 (1996); M. Nio, T. Kinoshita, *Phys. Rev. D* **55**, 7267 (1997); T. Kinoshita, [arXiv:hep-ph/9808351](https://arxiv.org/abs/hep-ph/9808351)
28. A. Czarnecki, S.I. Eidelman, S.G. Karshenboim, *Phys. Rev. D* **65**, 053004 (2002); S.G. Karshenboim, V.A. Shelyuto, *Phys. Lett. B* **517**, 32 (2001)
29. H. Lamm, *Phys. Rev. A* **95**(1), 012505 (2017)
30. P.J. Mohr, B.N. Taylor, *Rev. Mod. Phys.* **72**, 351 (2000); **77**, 1 (2005); P.J. Mohr, B.N. Taylor, D.B. Newell, *Rev. Mod. Phys.* **84**, 1527 (2012)
31. L.H. Thomas, *Phil. Mag.* **3**, 1 (1927); V. Bargmann, L. Michel, V.A. Telegdi, *Phys. Rev. Lett.* **2**, 435 (1959); B.W. Montague, *Phys. Rep.* **113**, 1 (1984); J.S. Bell, CERN-75-11, 38p (1975)
32. C. Duval, *Nucl. Phys. B* **912**, 450 (2016)
33. F.J.N. Farley, *Phys. Lett. B* **42**, 66 (1972)
34. F. Scheck, *Leptons, Hadrons and Nuclei* (North Holland, Amsterdam, 1983)
35. G. Charpak et al., *Phys. Rev. Lett.* **6**, 128 (1961); G. Charpak et al., *Nuovo Cim.* **22**, 1043 (1961)
36. J. Bailey et al., *Phys. Lett. B* **28**, 287 (1968); *Nuovo Cim. A* **9**, 369 (1972)

37. S. Eidelman et al. [Particle Data Group], Phys. Lett. B **592**, 1 (2004); K.A. Olive et al., Chin. Phys. C **38**, 090001 (2014); C. Patrignani et al., Chin. Phys. C **40**(10), 100001 (2016)
38. H. Grotch, R.A. Hegstrom, Phys. Rev. A **4**, 59 (1971); R. Faustov. Phys. Lett. B **33**, 422 (1970)
39. K. Pachucki, Phys. Rev. A **54**, 1994 (1996); *ibid.* **56**, 297 (1997); S.G. Karshenboim, Z. Phys. D **36**, 11 (1996); S.A. Blundell, K.T. Cheng, J. Sapirstein, Phys. Rev. Lett. **78**, 4914 (1997); M.I. Eides, H. Grotch, V.A. Shelyuto, Phys. Rev. D **58**, 013008 (1998)
40. K. Melnikov, A. Yelkhovsky, Phys. Rev. Lett. **86**, 1498 (2001)
41. R.J. Hill, Phys. Rev. Lett. **86**, 3280 (2001)
42. K.P. Jungmann, Nucl. Phys. News **12**, 23 (2002)
43. F.G. Major, V.N. Gheorghie, G. Werth, *Charged Particle Traps* (Springer, Berlin, 2005)
44. R.S. Van Dyck, P.B. Schwinberg, H.G. Dehmelt, Phys. Rev. D **34**, 722 (1986)
45. S. Peil, G. Gabrielse, Phys. Rev. Lett. **83**, 1287 (1999)
46. L.S. Brown, G. Gabrielse, Rev. Mod. Phys. **58**, 233 (1986)
47. T. Beier et al., Phys. Rev. Lett. **88**, 011603 (2002); Nucl. Instrum. Methods B **205**, 15 (2003)
48. D. Hanneke, S. Fogwell, G. Gabrielse, Phys. Rev. Lett. **100**, 120801 (2008). doi:[10.1103/PhysRevLett.100.120801](https://doi.org/10.1103/PhysRevLett.100.120801), <http://g2pc1.bu.edu/lept06/GabrielseTalk.pdf>
49. D. Hanneke, S.F. Hoogerheide, G. Gabrielse, Phys. Rev. A **83**, 052122 (2011). doi:[10.1103/PhysRevA.83.052122](https://doi.org/10.1103/PhysRevA.83.052122)

Chapter 7

Comparison Between Theory and Experiment and Future Perspectives

7.1 Experimental Results Confront Standard Theory

The anomalous magnetic moment of the muon provides one of the most precise tests of quantum field theory as a basic framework of elementary particle theory and of QED and the electroweak SM in particular. With what has been reached by the BNL muon $g - 2$ experiment (see Table 7.1), namely the reduction of the experimental uncertainty by a factor 14 to $\sim 63 \times 10^{-11}$, a new quality in “diving into the sea of quantum corrections” has been achieved: the four/five loop order QED [$\sim 381/5 \times 10^{-11}$] known thanks to the heroic efforts of Aoyama, Hayakawa, Kinoshita and Nio [3, 4] and Laporta [5], the weak correction up to 2nd order [$\sim 154 \times 10^{-11}$] and the hadronic light-by-light scattering [$\sim 100 \times 10^{-11}$] are now in the focus. The uncertainty of the weak corrections has been substantially reduced with the discovery of the Higgs boson, which revealed its mass within a small error band. The hadronic vacuum polarization effects which played a significant role already for the last CERN experiment now is a huge effect of more than 11 SD’s. As a non-perturbative effect it still has to be evaluated largely in terms of experimental data with unavoidable experimental uncertainties which yield the biggest contribution to the uncertainty of theoretical predictions. However, due to substantial progress in the measurement of total hadronic e^+e^- -annihilation cross sections, the uncertainty from this source has reduced to a remarkable $\sim 35 \times 10^{-11}$ only. This source of error now is only slightly larger than the uncertainty in the theoretical estimates of the hadronic light-by-light scattering contribution [$\sim 29 \times 10^{-11}$]. Nevertheless, we have a solid prediction with a total uncertainty of $\sim 45 \times 10^{-11}$, which is clearly below the experimental error of the muon $g - 2$ measurement. A graphical representation for the sensitivity and the weight of the various contributions is presented in Fig. 3.8 (see also Table 7.2 and Fig. 7.3). For another recent summary see [6]. We now have at the same time, a new very sensitive test of our current theoretical understanding of the fundamental forces and the particle spectrum, and a stringent bound on physics beyond the SM entering at scales below about 1 TeV. But, may be more important is the actual deviation between theory and experiment at the 4σ level which is a *clear*

Table 7.1 Progress from CERN 1979 to BNL 2006 [* = CPT assumed]

	CERN 1979 [1]	BNL 2006 [2]
a_{μ^+}	$1165911(11) \times 10^{-9}$	$11659204(7)(5) \times 10^{-10}$
a_{μ^-}	$1165937(12) \times 10^{-9}$	$11659214(8)(3) \times 10^{-10}$
a_{μ}^*	$1165924(8.5)10^{-9}$	$11659208(4)(3) \times 10^{-10}$
$(a_{\mu^+} - a_{\mu^-})/a_{\mu}$	$-(2.2 \pm 2.8) \times 10^{-5}$	$-(8.6 \pm 18.2) \times 10^{-7}$
d_{μ} (EDM) *	$(3.7 \pm 3.4) \times 10^{-19} e \cdot \text{cm}$	$< 2.7 \times 10^{-19} e \cdot \text{cm}$
a_{μ}^{the}	$1165921(8.3)10^{-9}$	$11659179.3(6.8)10^{-10}$
$a_{\mu}^{\text{the}} - a_{\mu}^{\text{exp}}$	$(-3.0 \pm 11.9) \times 10^{-9}$	$(-28.7 \pm 9.1) \times 10^{-10}$
$(a_{\mu}^{\text{the}} - a_{\mu}^{\text{exp}})/a_{\mu}^{\text{exp}}$	$-(2.6 \pm 10.2) \times 10^{-6}$	$-(2.5 \pm 0.8) \times 10^{-6}$

Table 7.2 Standard model theory and experiment comparison

Contribution	Value $\times 10^{10}$	Error $\times 10^{10}$	Reference
QED incl. 4-loops + 5-loops	11 658 471.886	0.003	[4, 5]
Hadronic LO vacuum polarization	689.46	3.25	(5.99)
Hadronic light-by-light	10.34	2.88	[9–13]
Hadronic HO vacuum polarization	-8.70	0.06	[7, 8]
Weak to 2-loops	15.36	0.11	[14–17]
Theory	11 659 178.3	3.5	–
Experiment	11 659 209.1	6.3	[2]
The. - Exp. 4.3 standard deviations	-30.6	7.2	–

indication of something missing. We have to remember that such high precision physics is extremely challenging for both experiment and for theory and it is not excluded that some small effect has been overlooked or underestimated at some place. To our present knowledge, it is hard to imagine that a 4σ shift could be explained by known physics. Thus New Physics seems a likely interpretation, if it is not an experimental fluctuation (3σ : 0.27% chance, 4σ : 0.0063% chance).

It should be noted that among all the solid precision tests, to my knowledge, the muon $g - 2$ shows the largest established deviation between theory and experiment. Actually, the latter has been persisting since the first precise measurement was released at BNL in February 2001 [18], and a press release announced “We are now 99 percent sure that the present Standard Model calculations cannot describe our data”. A 2.6σ deviation was found at that time for a selected choice of the hadronic vacuum polarization and with the wrong sign hadronic LbL scattering contribution.¹ In the meantime errors went further down experimentally as well as in theory,²

¹With the correct sign of the hadronic LbL term the deviation would have been 1.5σ based on the smallest available hadronic vacuum polarization. With larger values of the latter the difference would have been smaller.

²To mention the sign error and the issue of the high energy behavior in the LbL contribution or errors in the applied radiative corrections of e^+e^- -data or missing possible real photon radiation effects by the muons.

especially the improvement of the experimental e^+e^- -data, indispensable as an input for the “prediction” of the hadronic vacuum polarization, and the remedy of the wrong sign of the π^0 exchange LbL term has brought us forward a big step. The theoretical status, the main theme of this book, has been summarized in Sect. 3.2.3 (see Table 3.5 and Fig. 3.8) the experimental one in Sect. 6.5 (see Table 6.2 and Fig. 6.13). The jump in the precision is best reminded by a look at Table 7.1 which compares the results from the 1979 CERN final report [1] with the one’s of the 2006 BNL final report [2].

The CPT test has improved by an order of magnitude. Relativistic QFT in any case guarantees CPT symmetry to hold and we assume CPT throughout in taking averages or estimating new physics effects etc. The world average experimental muon magnetic anomaly, dominated by the very precise BNL result, now is [2]

$$a_\mu^{\text{exp}} = 1.16592091(54)(33) \times 10^{-3}, \quad (7.1)$$

with relative uncertainty 5.4×10^{-7} , which confronts the SM prediction

$$a_\mu^{\text{the}} = 1.16591783(35) \times 10^{-3}, \quad (7.2)$$

and agrees up to the small but non-negligible deviation

$$\Delta a_\mu = a_\mu^{\text{exp}} - a_\mu^{\text{the}} = 306 \pm 72 \times 10^{-11}, \quad (7.3)$$

which is a 4.3σ effect. Errors have been added in quadrature. Note that the experimental uncertainty is still statistics dominated.³ Thus just running the BNL experiment longer could have substantially improved the result. Originally the E821 goal was $\delta a_\mu^{\text{exp}} \sim 40 \times 10^{-11}$. Figure 7.1 illustrates the improvement achieved by the BNL experiment, status by end 2009. The theoretical predictions mainly differ by the L.O. hadronic effects, which also dominates the theoretical error.

More recent progress in the determination of the HVP has been achieved mainly by the ISR hadronic cross section measurements. Some recent evaluations are collected in Fig. 7.2. The last entry [19] is based on the evaluation of all data and pQCD is used only where it can be applied safely according to [20, 21] and as discussed in Sect. 5.1.7. Differences in errors come about mainly by utilizing more “theory-driven” concepts⁴: use of selected data sets only, extended use of perturbative QCD in place of data [assuming local duality], sum rule methods, low energy effective

³The small spread in the central values does not reflect this fact, however.

⁴The terminology “theory-driven” means that we are not dealing with a solid theory prediction. As in some regions only old data sets are available, some authors prefer to use pQCD in place of the data also in regions where pQCD is not supposed to work reliably. The argument is that even under these circumstances pQCD may be better than the available data. This may be true, but one has to specified what “better” means. In this approach non-perturbative effects are accounted for by referring to local quark-hadron duality in relatively narrow energy intervals. What is problematic is a reliable error estimate. Usually, only the pQCD errors are accounted for, essentially only the uncertainty in α_s is taken into account. It is *assumed* that no other uncertainties from non-perturbative effects exist; this is why errors in this approach are systematically lower than in more conservative data

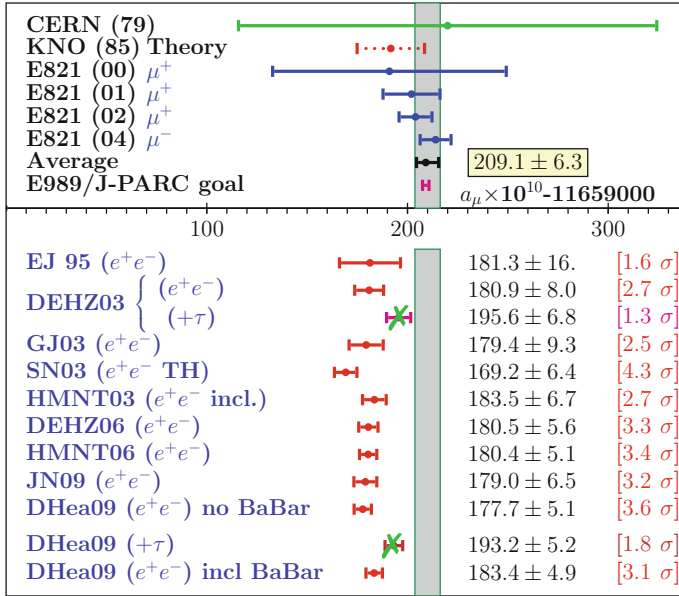


Fig. 7.1 Comparison between theory and experiment status 2009. Results differ by different L.O. hadronic vacuum polarizations and variants of the HLBL contribution (see Fig. 5.66). Some estimates include isospin rotated τ -data ($+ \tau$), which here are missing however $\gamma - \rho$ mixing corrections, why I marked them. EJ95 vs. JN09 illustrates the improvement of the e^+e^- -data between 1995 and 2009 (see also Table 5.4 and Fig. 6.13). E989 shows the expectation from the follow-up experiment of E821

methods [31–33]. The ** marked results include the most recent data from SND, CMD-2, KLOE, BaBar and BES-III [34–40].⁵ In some analyses (as indicated) τ data from ALEPH, OPAL, CLEO and Belle [44–48] have been combined with the e^+e^-

(Footnote 4 continued)

oriented approaches. Note that applying pQCD in any case *assumes* quark–hadron duality to hold in large enough intervals, ideally from threshold to ∞ (global duality). My “conservative” evaluation of a_μ^{had} estimates an error of 0.8%, which for the given quality of the data is as progressive as it can be, according to my standards concerning reliability. In spite of big progress in hadronic cross section measurements the agreement between different measurements is not as satisfactory as one would wish. Also more recent measurements often do not agree within the errors quoted by the experiments. Thus, one may seriously ask the question how such small uncertainties come about. The main point is that results in different energy ranges, as listed in Table 5.2 in Sect. 5.1.7, are treated as independent and all errors including the systematic ones are added in quadrature. By choosing a finer subdivision, like in the clustering procedure of [29], for example, one may easily end up with smaller errors (down to 0.6%). The subdivision I use was chosen originally in [30] and were more or less naturally associated with the ranges of the different experiments. The problem is that combining systematic errors is not possible on a commonly accepted basis if one goes beyond the plausible procedures advocated by the Particle Data Group.

⁵The analysis [41] does not include exclusive data in a range from 1.43 to 2 GeV; therefore also the new BaBar data are not included in that range. It also should be noted that CMD-2 and SND are not

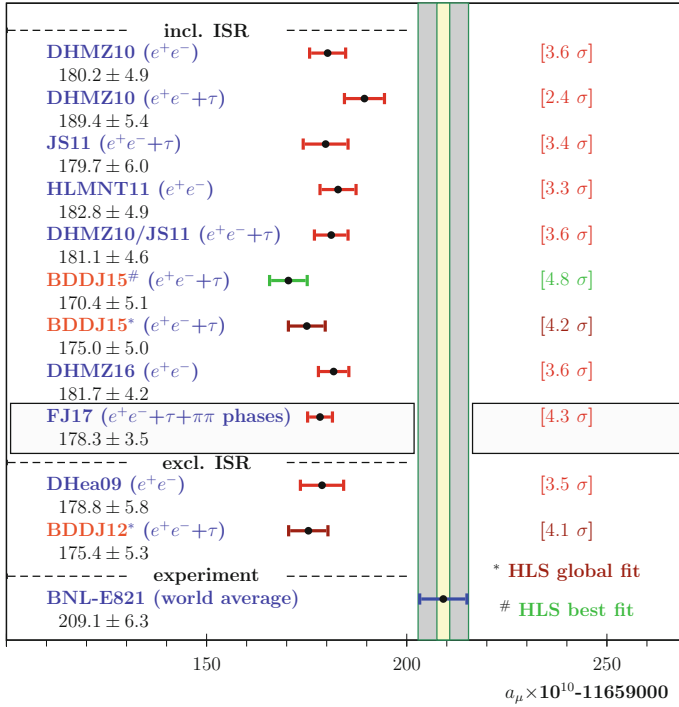


Fig. 7.2 Dependence of a_μ predictions on recent evaluations of $a_\mu^{\text{had,LO}}$. The HLS best fit BDDJ15# (NSK + KLOE10 + KLOE12) does not include BaBar $\pi\pi$ data [22], while BDDJ15* does. JS11/FJ16 [7, 8] is updated and include the new BES-III data. Further points are BDDJ12 [23], DHMZ10 [24], HLMNT11 [25] and DHea09 [26]. The DHMZ10 ($e^+e^-+\tau$) result is not including the $\rho - \gamma$ mixing correction, i.e. it misses important isospin breaking effects. In contrast, DHMZ10/JS11 is obtained by including this correction, which brings the point into much better agreement with standard analyses based on e^+e^- data alone, as for example the DHMZ10 (e^+e^-) result. (see also [27, 28]). FJ17 represents our result (5.100). The narrow vertical band illustrates the E989 expectation

data. Some points are based on phenomenological low energy effective Lagrangian (specifically HLS) global fits [22, 23], constrained by data from additional channels, in particular the τ ones, and reweighting by the global fit qualities, which leads to somewhat lower central values with smaller errors.

Figure 7.3 illustrates how different physics contributions add up to the final answer. We note that the theory error is about 30% smaller now than the experimental one. It is fully dominated by the hadronic uncertainties of the hadronic low energy cross

(Footnote 5 continued)

fully independent measurements; data are taken at the same machine and with the same radiative correction program. The radiative corrections play a crucial role at the present level of accuracy, and common errors have to be added linearly. In [42, 43] pQCD is used in the extended ranges 1.8–3.7 GeV and above 5.0 GeV; furthermore [43] excludes the KLOE data.

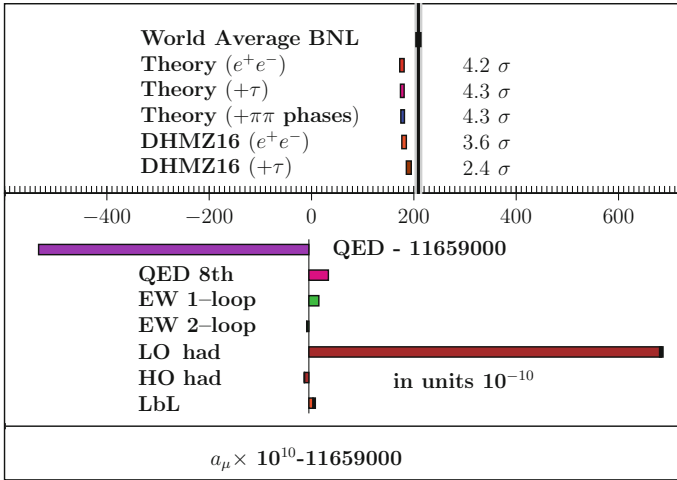


Fig. 7.3 All kinds of physics meet. Shown are the various contributions which add up to the theory prediction relative to the experimental result. The 8th order QED included in the QED part is shown separately. The 10th order QED is too small to be displayed here. For comparison also the extra contribution obtained by including the isospin rotated and isospin breaking corrected hadronic τ -decay data are shown. The “Theory” results are based on e^+e^- data (5.29), including τ after $\gamma - \rho$ mixing correction (5.99) and after including $\pi\pi$ phase shift data improvement [33] (5.100). The recent results DHMZ16 from [49] are also displayed. The second result DHMZ16 includes τ data without $\gamma - \rho$. The *black* heads on the bars represent the uncertainties. The *black vertical band* represents the future error band. Note that what seems to be a cancellation between “QED-11659000” and “LO had” is due to the QED off-set chosen. The complete QED and LO had are both positive and just add up. In any case the uncertainties and the deviation between theory and experiment look amazingly small in comparison to the various SM effect which are substantial for a precise prediction

section data on the one hand and not much less by the uncertainty of the hadronic light-by-light scattering contribution on the other hand. The history of muon $g - 2$ measurements together with the theory values with which results were compared are listed once more in Table 7.3.

7.2 New Physics in $g - 2$

The question about which unknown physics hides behind the SM was and is the main issue of theoretical particle physics since the emergence of the SM as *the* theory of “fundamental” particle interactions which we know today. Besides the SM’s main shortcoming, which is that it lacks to include gravity, it rises many other questions about its structure, its many vastly different mass scales, and the answers always are attempts of embedding the SM into an extended theory. While the SM is very well established and is able to explain a plenitude of experimental data, and this so well

Table 7.3 Progress in a_μ measurements. Theory values as quoted in References ($\mu\text{SR} = \text{Muon Storage Ring}$)

Laboratory	Year	Ref.		Result (error) $\times 10^3$	Precision	Theory $\times 10^3$
Columbia	1960	[50]		1.22 (8)		1.16
CERN cyclotron	1961	[51]	μ^+	1.145 (22)		1.165
CERN cyclotron	1962	[52]	μ^+	1.162 (05)		1.165
CERN 1st μSR	1966	[53]	μ^-	1.165 (03)		1.165
CERN 2nd μSR	1968	[54]	μ^\pm	1.166 16 (31)		1.1656
CERN 2nd μSR	1977	[55]	μ^\pm	1.165 9240 (85)	7 ppm	1.165 9210 (83)
BNL, 1997 data	1999	[56]	μ^+	1.165 925 (15)	13 ppm	1.165 9163 (8)
BNL, 1998 data	2000	[57]	μ^+	1.165 919 1 (59)	5 ppm	1.165 9163 (8)
BNL, 1999 data	2001	[18]	μ^+	1.165 920 2 (15)	1.3 ppm	1.165 9160 (7)
BNL, 2000 data	2002	[58]	μ^+	1.165 920 4 (9)	0.73 ppm	1.165 9177 (7)
BNL, 2001 data	2004	[59]	μ^-	1.165 921 4 (9)	0.72 ppm	1.165 918 1 (8)
World average	2004	[59]	μ^\pm	1.165 920 80 (63)	0.54 ppm	1.165 91793 (68)

that the more and more elaborate experimental efforts start to be a kind of frustrating, it is well known and as well established that the SM is *not* able to explain a number of facts, like the existence of non-baryonic Cold Dark Matter (CDM) (at most 5% of our universe's energy density is normal baryonic matter, about 21% are CDM), the matter-antimatter asymmetry in the universe, which requires baryon-number B and lepton-number L violation, the problem of the cosmological constant (see e.g. [60]) and so on. So, new physics must exist but how is it realized? What can the muon $g - 2$ tell us about new physics?⁶

New physics contributions, which, if they exist, are an integral part of the measured numbers, typically are expected to be due to states or interactions which have not been seen by other experiments, either by a lack of sensitivity or, at the high energy frontier, because experimental facilities like accelerators are below the threshold of energy needed for producing the new heavy states or because the signal was still buried in the background. At the high energy frontier LEP, the Tevatron and the LHC have set limits on many species of possible new particles predicted in a plenitude of models beyond the SM. A partial list of existing bounds is collected in Table 7.4. The simplest possibility is to add a 4th fermion family called sequential fermions, where the neutrino has to have a large mass (>45 GeV) as additional light (nearly massless) neutrinos have been excluded by LEP.

Another possibility for extending the SM is the Higgs sector where one could add scalar singlets, an additional doublet, a Higgs triplet and so on. Two Higgs doublet models (THDM or 2HDM) are interesting as they predict 4 additional physical spin 0 bosons one neutral scalar H^0 , a neutral pseudoscalar A , as well as the two charged

⁶The variety of speculations about new physics is mind-blowing and the number of articles on "physics beyond the SM" (BSM) almost uncountable. This short essay tries to reproduce a few of the main ideas for illustration, since a shift in one number can have many reasons and only in conjunction with other experiments it is possible to find out what is the true cause for an observed deviation from the SM prediction. My citations may be not very concise and I apologize for the certainly numerous omissions.

bosons H^\pm . Many new real and virtual processes, like $W^\pm H^\mp \gamma$ transitions, are the consequence. Any SUSY extension of the SM requires two Higgs doublets. Similarly, there could exist additional gauge bosons, like from an extra $U(1)'$. This would imply an additional Z boson, a sequential Z' which would mix with the SM Z and the photon. More attractive are extensions which solve some real or thought shortcomings of the SM. This includes Grand Unified Theories (GUT) [61] which attempt to unify the strong, electromagnetic and weak forces, which correspond to three different factors of the local gauge group of the SM, in one big simple local gauge group

$$G_{\text{GUT}} \supset SU(3)_c \otimes SU(2)_L \otimes U(1)_Y \equiv G_{\text{SM}},$$

which is assumed to be spontaneously broken in at least two steps

$$G_{\text{GUT}} \rightarrow SU(3)_c \otimes SU(2)_L \otimes U(1)_Y \rightarrow SU(3)_c \otimes U(1)_{\text{em}}.$$

Coupling unification is governed by the renormalization group evolution of $\alpha_1(\mu)$, $\alpha_2(\mu)$ and $\alpha_3(\mu)$, corresponding to the SM group factors $U(1)_Y$, $SU(2)_L$ and $SU(3)_c$, with the experimentally given low energy values, typically at the Z mass scale, as starting values evolved to very high energies, the GUT scale M_{GUT} where couplings should meet. Within the SM the three couplings do not unify, thus unification requires new physics as predicted by a GUT extension. Also extensions like the left–right (LR) symmetric model are of interest. The simplest possible unifying group is $SU(5)$ which, however, is ruled out by the fact that it predicts protons to decay faster than allowed by observation. GUT models like $SO(10)$ or the exceptional group E_6 not only unify the gauge group, thereby predicting many additional gauge bosons, they also unify quarks and leptons in a GUT matter multiplet. Now quarks and leptons directly interact via the *leptoquark* gauge bosons X and Y which carry color, fractional charge ($Q_X = -4/3$, $Q_Y = -1/3$) as well as baryon and lepton number. Thus GUTs are violating B as well as L , yet with $B - L$ still conserved. The proton may now decay via $p \rightarrow e^+ \pi^0$ or many other possible channels. The experimental proton lifetime $\tau_{\text{proton}} > 2 \times 10^{29}$ years at 90% C.L. requires the extra gauge bosons to exhibit masses of about $M_{\text{GUT}} > 10^{16}$ and excludes $SU(5)$ as it predicts unification at too low scales. M_{GUT} is the *GUT scale* which is only a factor 1000 below the Planck scale.⁷ In general GUTs also have additional normal gauge bosons, extra W 's and Z 's which mix with the SM gauge bosons.

⁷GUT extensions of the SM are not very attractive for the following reasons: the extra symmetry breaking requires an additional heavier Higgs sector which makes the models rather clumsy in general. Also, unlike in the SM, the known matter–fields are *not* in the fundamental representations, while an explanation is missing why the existing lower dimensional representations remain unoccupied. In addition, the three SM couplings (as determined from experiments) allow for unification only with at least one additional symmetry breaking step $G_{\text{GUT}} \rightarrow G' \rightarrow G_{\text{SM}}$. In non-SUSY GUTs the only possible groups are $G_{\text{GUT}} = E_6$ or $SO(10)$ and $G' = G_{LR} = SU(3)_c \otimes SU(2)_R \otimes SU(2)_L \otimes U(1)$ or $G_{PS} = SU(2)_R \otimes SU(2)_L \otimes SU(4)$ [62]. G_{LR} is the left–right symmetric extension of the SM and G_{PS} is the Pati–Salam model, where $SU(3)_c \otimes U(1)_Y$

Table 7.4 Present lower bounds on new physics states. Bounds are 95% C.L. limits from LEP (ALEPH, DELPHI, L3, OPAL), the Tevatron (CDF, D0) and the LHC (ATLAS, CMS)

Object	mass bound	comment
Heavy neutrino	$m_{\nu'}^M > 39$ GeV	Majorana- ν [$\nu \equiv \bar{\nu}$]
Heavy neutrino	$m_{\nu'}^D > 45$ GeV	Dirac- ν [$\nu \neq \bar{\nu}$]
Heavy lepton	$m_L > 100$ GeV	
4th family quark b'	$m_{b'} > 199$ GeV	$p\bar{p}$ NC decays
W'_{SM}	$M_{W'} > 800$ GeV	SM couplings
W_R	$M_{W_R} > 715$ GeV	right-handed weak current
Z'_{SM}	$M_{Z'} > 81.5$ TeV	SM couplings
Z_{LR} ($g_R = g_L$)	$M_{Z_{LR}} > 630$ GeV	of $G_{LR} = SU(2)_R \otimes SU(2)_L \otimes U(1)$
Z_χ ($g_\chi = e/\cos\Theta_W$)	$M_{Z_\chi} > 595$ GeV	of $SO(10) \rightarrow SU(5) \otimes U(1)_\chi$
Z_ψ ($g_\psi = e/\cos\Theta_W$)	$M_{Z_\psi} > 590$ GeV	of $E_6 \rightarrow SO(10) \otimes U(1)_\psi$
Z_η ($g_\eta = e/\cos\Theta_W$)	$M_{Z_\eta} > 620$ GeV	of $E_6 \rightarrow G_{LR} \otimes U(1)_\eta$
$h^0 \equiv H_1^0$ Higgs	$m_{H_1^0} > 92.8$ GeV	SUSY ($m_{H_1^0} < m_{H_2^0}$)
A^0 pseudoscalar Higgs	$m_A > 93.4$ GeV	THDM, MSSM
H^\pm charged Higgs	$m_{H^\pm} > 80.0$ GeV	THDM, MSSM
LHC results pp direct searches		
4th family quark b'	$m_{b'} > 755$ GeV	NC decays
4th family quark t'	$m_{t'} > 782$ GeV	NC decays
W'_{SM}	$M_{W'} > 3.71$ TeV	SM couplings
Z'_{SM}	$M_{Z'} > 2.9$ TeV	SM couplings
Z_{LR} ($g_R = g_L$)	$M_{Z_{LR}} > 1.16$ TeV	of $G_{LR} = SU(2)_R \otimes SU(2)_L \otimes U(1)$
Z_χ ($g_\chi = e/\cos\Theta_W$)	$M_{Z_\chi} > 2.62$ TeV	of $SO(10) \rightarrow SU(5) \otimes U(1)_\chi$
Z_ψ ($g_\psi = e/\cos\Theta_W$)	$M_{Z_\psi} > 2.57$ TeV	of $E_6 \rightarrow SO(10) \otimes U(1)_\psi$
Z_η ($g_\eta = e/\cos\Theta_W$)	$M_{Z_\eta} > 1.87$ TeV	of $E_6 \rightarrow G_{LR} \otimes U(1)_\eta$

In deriving bounds on New Physics it is important to respect constraints not only from a_μ and the direct bounds of Table 7.4, but also from other precision observables which are sensitive to new physics via radiative corrections. Important examples are the electroweak precision observables [64, 65]:

$$M_W = 80.385(15) \text{ GeV}, \quad (7.4)$$

(Footnote 7 continued)

of the SM is contained in the $SU(4)$ factor. Coupling unification requires the extra intermediate breaking scale to lie very high $M' \sim 10^{10}$ GeV for G_{LR} and $M' \sim 10^{14}$ GeV for G_{PS} . These are the scales of new physics in these extensions, completely beyond of being phenomenologically accessible. The advantage of SUSY GUTs is that they allow for unification of the couplings with the new physics scale being as low as M_Z to 1 TeV [63], and the supersymmetrized $G_{GUT} = SU(5)$ extension of the SM escapes to be excluded.

$$\sin^2 \Theta_{\text{eff}}^\ell = 0.23152(5), \quad \rho_0 = 1.00037(23), \quad (7.5)$$

which are both precisely measured and precisely predicted by the SM or in extensions of it. The SM predictions use the very precisely known independent input parameters α , G_μ and M_Z , but also the less precisely known top quark mass

$$m_t = 173.21 \pm 0.87 \text{ GeV}, \quad (7.6)$$

and the Higgs boson mass [66]

$$m_H = 125.09(24) \text{ GeV}, \quad (7.7)$$

are important.

The parameter ρ_0 is the tree level (SM radiative corrections subtracted) ratio of the low energy effective weak neutral to charged current couplings: $\rho = G_{\text{NC}}/G_{\text{CC}}$ where $G_{\text{CC}} \equiv G_\mu$. This parameter is rather sensitive to new physics. In the SM at tree level $\rho_0 \equiv 1$ independent of any free parameter. This is due to the custodial symmetry of the minimal SM Higgs sector and consequently ρ is a SM prediction very similar to the anomalous lepton moments. In general, extensions of the SM, like GUTs or models including Higgs triplets etc., violate the custodial symmetry and if ρ_0 depends on parameters of the extension then ρ becomes a tunable quantity and one has a fine tuning problem [67]. The fact that $\rho_0 = 1$ in the SM allowed one to predict the top quark mass from a precision measurement of $\Delta\rho$ (4.40) at LEP prior to the discovery of the top quark at the Tevatron. The leading top quark mass effect in $\Delta\rho \propto m_t^2$ is lost if $\rho_0 \neq 1$ and such extensions are disfavored (see e.g. [68]).

Equally important are constraints by the B -physics branching fractions [69]

$$\text{BR}(b \rightarrow s\gamma) = (3.43 \pm 0.22) \times 10^{-4}; \quad \text{BR}(B_s \rightarrow \mu^+ \mu^-) = 2.8_{-0.6}^{+0.7} \times 10^{-9}. \quad (7.8)$$

Concerning flavor physics, in particular the B factories Belle at KEK and BaBar at SLAC have set new milestones in confirming the flavor structure as inferred by the SM. In the latter Flavor-Changing Neutral Currents (FCNC) are absent at tree level due to the GIM mechanism and CP-violation and flavor mixing patterns seem to be realized in nature precisely as implemented by the three fermion-family CKM mixing scheme. Many new physics models have serious problems to accommodate this phenomenologically largely confirmed structure in a natural way. Therefore, the criterion of *Minimal Flavor Violation* (MFV) [70] has been conjectured as a framework for constructing low energy effective theories which include the SM Lagrangian without spoiling its flavor structure. The SM fermions are grouped into three families with two $SU(2)_L$ doublets (Q_L and L_L) and three $SU(2)_L$ singlets (U_R , D_R and E_R) and the largest group of unitary transformations which commutes

with the gauge group is $G_F = U(3)^5$ [71]. The latter may be written more specifically as

$$G_F = SU(3)_q^3 \otimes SU(3)_\ell^2 \otimes U(1)_B \otimes U(1)_L \otimes U(1)_Y \otimes U(1)_{PQ} \otimes U(1)_{E_R}$$

with $SU(3)_q^3 = SU(3)_{Q_L} \otimes SU(3)_{U_R} \otimes SU(3)_{D_R}$ and $SU(3)_\ell^2 = SU(3)_{L_L} \otimes SU(3)_{E_R}$. The SM Yukawa interactions break the subgroup $SU(3)_q^3 \otimes SU(3)_\ell^2 \otimes U(1)_{PQ} \otimes U(1)_{E_R}$. However, one may introduce three dimensionless auxiliary fields

$$Y_U \sim (3, \bar{3}, 1)_{SU(3)_q^3}, \quad Y_D \sim (3, 1, \bar{3})_{SU(3)_q^3}, \quad Y_E \sim (3, \bar{3})_{SU(3)_\ell^2}$$

which provide a convenient bookkeeping for constructing MFV effective theories. Formally the auxiliary fields allow to write down MFV compatible interactions as G_F invariant effective interactions. The MFV criterion requires that a viable dynamics of flavor violation is completely determined by the structure of the ordinary SM Yukawa couplings. Most of the promising and seriously considered new physics models, which we will consider below, belong to the class of MFV extensions of the SM. Examples are the R-parity conserving two doublet Higgs models, the R-parity conserving minimal supersymmetric extension of the SM [72] and the Littlest Higgs model without T-parity.

Another important object is the electric dipole moment which is a measure of CP-violation and was briefly discussed at the end of Sect. 3.3. Since extensions of the SM in general exhibit additional sources of CP violation, EDMs are very promising probes of new physics. An anomalously large EDM of the muon d_μ would influence on the a_μ extraction from the muon precession data as discussed at the end of Sect. 6.3.1. We may ask whether d_μ could be responsible for the observed deviation in a_μ . In fact (6.55) tells us that a non-negligible d_μ would increase the observed a_μ , and we may estimate

$$|d_\mu| = \frac{1}{2} \frac{e}{m_\mu} \sqrt{(a_\mu^{\text{exp}})^2 - (a_\mu^{\text{SM}})^2} = (2.53 \pm 0.31) \times 10^{-19} e \cdot \text{cm}. \quad (7.9)$$

This also may be interpreted as an upper limit as given in Table 7.1. Recent advances in experimental techniques will allow to perform much more sensitive experiments for electrons, neutrons and neutral atoms [73]. For new efforts to determine d_μ at much higher precision see [74, 75]. In the following we will assume that d_μ is in fact negligible, and that the observed deviation has other reasons.

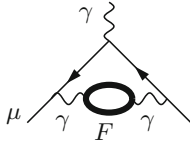
As mentioned many times, the general form of contributions from states of mass $M_{\text{NP}} \gg m_\mu$ takes the form

$$a_\mu^{\text{NP}} = \mathcal{C} \frac{m_\mu^2}{M_{\text{NP}}^2} \quad (7.10)$$

where naturally $\mathcal{C} = O(\alpha/\pi)$, like for the weak contributions (4.47), but now from interactions and states not included in the SM. New fermion loops may contribute in the same way as a τ -lepton

Table 7.5 Typical New Physics scales required to satisfy $\Delta a_\mu^{\text{NP}} = \Delta a_\mu$ (7.3)

\mathcal{C}	1	α/π	$(\alpha/\pi)^2$
M_{NP}	$2.0^{+0.4}_{-0.3}$ TeV	100^{+21}_{-13} GeV	5^{+1}_{-1} GeV



$$a_\mu^{(4)}(\text{vap}, F) = \sum_F Q_F^2 N_{cF} \left[\frac{1}{45} \left(\frac{m_\mu}{m_F} \right)^2 + \dots \right] \left(\frac{\alpha}{\pi} \right)^2,$$

which means $\mathcal{C} = O((\alpha/\pi)^2)$. Note that the τ contribution to a_μ is 4.2×10^{-10} only, while the 3σ effect we are looking for is 28.7×10^{-10} . As the direct lower limit for a sequential fermion is about 100 GeV (see Table 7.4) such effects cannot account for the observed deviation. A 100 GeV heavy lepton only yields the tiny contribution⁸ 1.34×10^{-13} .

A rough estimate of the scale M_{NP} required to account for the observed deviation is given in Table 7.5. An effective tree level contribution would extend the sensibility to the very interesting 2 TeV range, however, no compelling scenario I know of exists for this case (see below).

⁸It should be noted that heavy sequential fermions are constrained severely by the ρ -parameter (NC/CC effective coupling ratio), if doublet members are not nearly mass degenerate. A doublet (ν_L, L) with $m_{\nu_L} = 45$ GeV and $m_L = 100$ GeV only contributes $\Delta\rho \simeq 0.0008$, which however is violating already the limit from LEP electroweak fits (7.5). Not yet included is a similar type contribution from the 4th family (t', b') doublet mass-splitting, which also would add a large positive term

$$\Delta\rho = \frac{\sqrt{2}G_\mu}{16\pi^2} 3 m_{t'}^2 \left(1 + \frac{m_{b'}^2}{m_{t'}^2} \ln \frac{m_{b'}}{m_{t'}} \right) + \dots$$

in case of a large mass splitting $m_{t'}^2 \gg m_{b'}^2$, or a small correction $\Delta\rho = \frac{\sqrt{2}G_\mu}{16\pi^2} \frac{2\Delta^2}{\Sigma}$, which vanishes for small mass splitting $\Delta = |m_{t'}^2 - m_{b'}^2| \ll \Sigma = m_{t'}^2 + m_{b'}^2$. In this context it should be mentioned that the so called *custodial symmetry* of the SM which predicts $\rho_0 = 1$ at the tree level (independent of any parameter of the theory, which implies that it is not subject to subtractions due to parameter renormalization) is one of the severe constraints on extensions of the SM. Virtual top effect contributing to the radiative corrections of ρ allowed a determination of the top mass prior to the discovery of the top by direct production at Fermilab in 1995. The LEP precision determination of $\Delta\rho = \frac{\sqrt{2}G_\mu}{16\pi^2} 3 m_t^2$ (up to subleading terms) from precision measurements of Z resonance parameters yields $m_t = 172.3^{+10.2}_{-7.6}$ GeV in excellent agreement with the direct determination $m_t = 171.4(2.1)$ GeV at the Tevatron and with the recent determinations $m_t = 172.84(0.70)$ GeV [76] from ATLAS and $m_t = 172.44(0.13)(0.47)$ GeV [77] from CMS (for CDF and D0 see [78]). In extensions of the SM in which ρ depends on physical parameters on the classical level, like in GUT models or models with Higgs triplets etc. one largely loses this prediction and thus one has a fine tuning problem [67]. But, also “extensions” which respect custodial symmetry like simply adding a 4th family of fermions should not give a substantial contribution to $\Delta\rho$, otherwise also this would spoil the indirect top mass prediction.

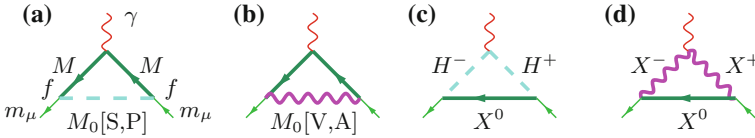


Fig. 7.4 Possible New Physics contributions. Neutral boson exchange: **a** scalar or pseudoscalar and **b** vector or axialvector, flavor changing or not. New charged bosons: **c** scalars or pseudoscalars, **d** vector or axialvector

7.2.1 Generic Contributions from Physics Beyond the SM

It is important to remember that the fermion anomalous magnetic moments are predictions only within the framework of a renormalizable theory. Therefore, extensions based on dimension 5 or higher operators in general lose most of the predictive power we have in the SM and they will not be considered in the following, except for a short account on anomalous gauge couplings.

Common to many of the extensions of the SM are predictions of new states: scalars S , pseudoscalars P , vectors V or axialvectors A , neutral or charged. They contribute via one-loop lowest order type diagrams shown in Fig. 7.4. Here, we explicitly assume all fermions to be Dirac fermions. Besides the SM fermions, μ in particular, new heavy fermions F of mass M may be involved, but fermion number is assumed to be conserved, like in $\Delta\mathcal{L}_S = f\bar{\psi}_\mu\psi_F S + \text{h.c.}$, which will be different in supersymmetric (SUSY) extensions discussed below, where fermion number violating Majorana fermions necessarily must be there.

Note that massive spin 1 boson exchange contributions in general have to be considered within the context of a gauge theory, in order to control gauge invariance and unitarity. We will present corresponding contributions in the unitary gauge calculated with dimensional regularization. We first discuss neutral boson exchange contributions from diagrams (a) and (b). Exotic neutral bosons of mass M_0 coupling to muons with coupling strength f would contribute [79, 80]

$$\Delta a_\mu^{\text{NP}} = \frac{f^2}{4\pi^2} \frac{m_\mu^2}{M_0^2} L, \quad L = \frac{1}{2} \int_0^1 dx \frac{Q(x)}{(1-x)(1-\lambda^2 x) + (\epsilon\lambda)^2 x}, \quad (7.11)$$

where $Q(x)$ is a polynomial in x which depends on the type of coupling:

- Scalar : $Q_S = x^2 (1 + \epsilon - x)$
- Pseudoscalar : $Q_P = x^2 (1 - \epsilon - x)$
- Vector : $Q_V = 2x (1 - x) (x - 2 (1 - \epsilon)) + \lambda^2 (1 - \epsilon)^2 Q_S$
- Axialvector : $Q_A = 2x (1 - x) (x - 2 (1 + \epsilon)) + \lambda^2 (1 + \epsilon)^2 Q_P$

with $\epsilon = M/m_\mu$ and $\lambda = m_\mu/M_0$. As an illustration we first consider the regime of a heavy boson of mass M_0 and m_μ , $M \ll M_0$ for which one gets

$$\begin{aligned}
 L_S &= \frac{M}{m_\mu} \left(\ln \frac{M_0}{M} - \frac{3}{4} \right) + \frac{1}{6} \stackrel{M=m_\mu}{=} \ln \frac{M_0}{m_\mu} - \frac{7}{12}, \\
 L_P &= -\frac{M}{m_\mu} \left(\ln \frac{M_0}{M} - \frac{3}{4} \right) + \frac{1}{6} \stackrel{M=m_\mu}{=} -\ln \frac{M_0}{m_\mu} + \frac{11}{12}, \\
 L_V &= \frac{M}{m_\mu} - \frac{2}{3} \stackrel{M=m_\mu}{=} \frac{1}{3}, \\
 L_A &= -\frac{M}{m_\mu} - \frac{2}{3} \stackrel{M=m_\mu}{=} -\frac{5}{3}.
 \end{aligned}
 \tag{7.12}$$

In accordance with the MFV requirement it is more realistic to assume a flavor conserving neutral current $M = m_\mu$ as given by the second form. Typical contributions are shown in Fig. 7.5. Taking the coupling small enough such that a perturbative expansion in f makes sense, we take $f/(2\pi) = 0.1$, only the scalar exchange could account for the observed deviation with a scalar mass $480 \text{ GeV} < M_0 < 690 \text{ GeV}$. Pseudoscalar and axialvector yield the wrong sign. The vector exchange is too small. We learn that substantial pseudoscalar, vector or axialvector contribution are stringently limited, in principle, unless enhanced scalar contributions cancel them.

As we will see later, in SUSY and littlest Higgs extensions the leading contributions actually come from the regime $m_\mu \ll M, M_0$ with $M \sim M_0$, which is of enhanced FCNC type, and thus differs from the case just presented in (7.12). For the combinations of fixed chirality up to terms of order $O(m_\mu/M)$ one gets

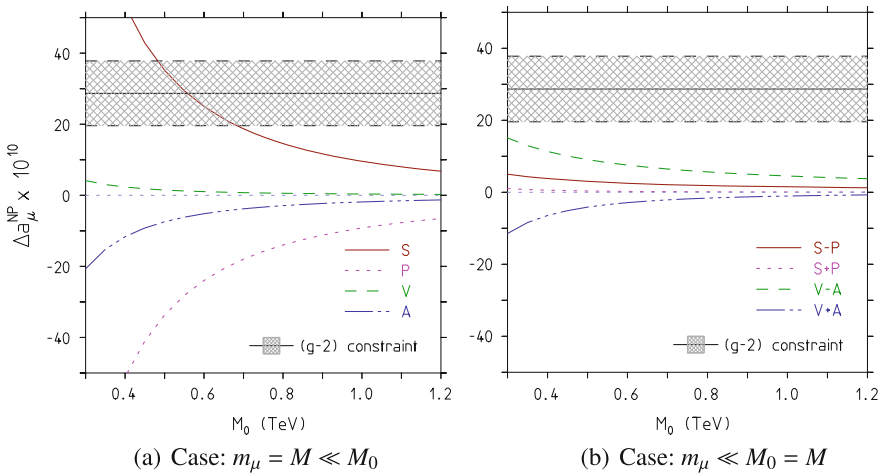


Fig. 7.5 Single particle one-loop induced NP effects for $f^2/(4\pi^2) = 0.01$ (Note, a typical EW SM coupling would be $e^2/(4\pi^2 \cos^2 \Theta_W) = 0.003$). S, P, V, A denote scalar, pseudoscalar, vector and axialvector exchange. Panel **a** shows (7.12) for $M = m = m_\mu$, panel **b** the chiral combinations (7.13) for $m = m_\mu$ and $M = M_0$, with the large combinations $L_S - L_P$ and $L_V - L_A$ rescaled by the muon Yukawa coupling m_μ/v in order to compensate for the huge prefactor M/m_μ (see text)

$$\begin{aligned}
L_S + L_P &= \frac{1}{6(1-z)^4} \left[2 + 3z - 6z^2 + z^3 + 6z \ln z \right] = \frac{1}{12} F_1^C(z), \\
L_S - L_P &= \frac{-M}{2m_\mu(1-z)^3} \left[3 - 4z + z^2 + 2 \ln z \right] = \frac{M}{3m_\mu} F_2^C(z), \\
L_V + L_A &= \frac{-1}{6(1-z)^4} \left[8 - 38z + 39z^2 - 14z^3 + 5z^4 - 18z^2 \ln z \right] = -\frac{13}{12} F_3^C(z), \\
L_V - L_A &= \frac{M}{2m_\mu(1-z)^3} \left[4 - 3z - z^3 + 6z \ln z \right] = \frac{M}{m_\mu} F_4^C(z), \tag{7.13}
\end{aligned}$$

where $z = (M/M_0)^2 = O(1)$ and the functions F_i^C are normalized to $F_i^C(1) = 1$. The possible huge enhancement factors M/m_μ , in some combination of the amplitudes, typical for flavor changing transitions, may be compensated due to radiative contributions to the muon mass (as discussed below) or by a corresponding Yukawa coupling $f \propto y_\mu = \sqrt{2} m_\mu/v$, as it happens in SUSY or little Higgs extensions of the SM.

The second class of possible new physics transitions due to charged S, P, V and A modes are represented by the diagrams (c) and (d) in Fig. 7.4. It amounts to replace L in (7.11) according to

$$\Delta a_\mu^{\text{NP}} = \frac{f^2}{4\pi^2} \frac{m_\mu^2}{M_0^2} L, \quad L = \frac{1}{2} \int_0^1 dx \frac{Q(x)}{(\epsilon\lambda)^2 (1-x)(1-\epsilon^{-2}x) + x}, \tag{7.14}$$

where again $Q(x)$ is a polynomial in x which depends on the type of coupling:

$$\begin{aligned}
\text{Scalar} &: Q_S = -x(1-x)(x+\epsilon) \\
\text{Pseudoscalar} &: Q_P = -x(1-x)(x-\epsilon) \\
\text{Vector} &: Q_V = 2x^2(1+x-2\epsilon) - \lambda^2(1-\epsilon)^2 Q_S \\
\text{Axialvector} &: Q_A = 2x^2(1+x+2\epsilon) - \lambda^2(1+\epsilon)^2 Q_P
\end{aligned}$$

Again, results for V and A are in the unitary gauge calculated with dimensional regularization. For a heavy boson of mass M_0 and m_μ , $M \ll M_0$ one finds

$$\begin{aligned}
L_S &= -\frac{1}{4} \frac{M}{m_\mu} - \frac{1}{12} \stackrel{M=m_\mu}{=} -\frac{1}{3}, \quad L_P = \frac{1}{4} \frac{M}{m_\mu} - \frac{1}{12} \stackrel{M=m_\mu}{=} \frac{1}{6}, \\
L_V &= -\frac{M}{m_\mu} + \frac{5}{6} \stackrel{M=m_\mu}{=} -\frac{1}{6}, \quad L_A = \frac{M}{m_\mu} + \frac{5}{6} \stackrel{M=m_\mu}{=} \frac{11}{6}. \tag{7.15}
\end{aligned}$$

The second form given is for a flavor conserving charged current transition with $M = m_\mu$.

Also for the charged boson exchanges the regime $m_\mu \ll M, M_0$ with $M \sim M_0$ is of interest in SUSY and littlest Higgs extensions of the SM and we find

$$\begin{aligned}
L_S + L_P &= \frac{-1}{6(1-z)^4} \left[1 - 6z + 3z^2 + 2z^3 - 6z^2 \ln z \right] = -\frac{1}{12} F_1^N(z), \\
L_S - L_P &= \frac{-M}{2m_\mu(1-z)^3} \left[1 - z^2 + 2z \ln z \right] = -\frac{M}{6m_\mu} F_2^N(z), \\
L_V + L_A &= \frac{1}{6(1-z)^4} \left[10 - 43z + 78z^2 - 49z^3 + 4z^4 + 18z^3 \ln z \right] = \frac{5}{3} F_3^N(z), \\
L_V - L_A &= \frac{-M}{m_\mu(1-z)^3} \left[4 - 15z + 12z^2 - z^3 - 6z^2 \ln z \right] = -\frac{2M}{m_\mu} F_4^N(z), \quad (7.16)
\end{aligned}$$

where $z = (M/M_0)^2 = O(1)$ and the functions F_i^N are normalized to $F_i^N(1) = 1$. For a general study of this kind of effects in view of the LHC mass limits see [81].

Another simple illustration of the one-loop sensitivity to new physics are heavier gauge bosons with SM couplings. From direct searches we know that they must be at least as heavy as 800 GeV. Contributions then follow from the weak one-loop contributions by rescaling with $(M_W/M_{W_{SM}})^2 \sim 0.01$ and hence 1% of 19.5×10^{-10} only, an effect much too small to be of relevance.

At $O((\alpha/\pi)^2)$ new physics may enter via vacuum polarization and we may write corresponding contributions as a dispersion integral (3.150):

$$\Delta a_\mu^{\text{NP}} = \frac{\alpha}{\pi} \int_0^\infty \frac{ds}{s} \frac{1}{\pi} \text{Im} \Delta \Pi_\gamma^{\text{NP}}(s) K(s).$$

Since, we are looking for contributions from heavy yet unknown states of mass $M \gg m_\mu$, and $\text{Im} \Delta \Pi_\gamma^{\text{NP}}(s) \neq 0$ for $s \geq 4M^2$ only, we may safely approximate $K(s) \simeq \frac{1}{3} \frac{m_\mu^2}{s}$ for $s \gg m_\mu^2$ such that, with $\frac{1}{\pi} \text{Im} \Delta \Pi_\gamma^{\text{NP}}(s) = \frac{\alpha(s)}{\pi} R^{\text{NP}}(s)$

$$\Delta a_\mu^{\text{NP}} = \frac{1}{3} \frac{\alpha}{\pi} \left(\frac{m_\mu}{M} \right)^2 L, \quad \frac{L}{M^2} = \frac{\alpha}{3\pi} \int_0^\infty \frac{ds}{s^2} R^{\text{NP}}(s).$$

An example is a heavy lepton mentioned before. A heavy narrow vector meson resonance of mass M_V and electronic width $\Gamma(V \rightarrow e^+e^-)$ (which is $O(\alpha^2)$) contributes $R_V(s) = \frac{9\pi}{\alpha^2} M_V \Gamma(V \rightarrow e^+e^-) \delta(s - M_V^2)$ such that $L = \frac{3\Gamma(V \rightarrow e^+e^-)}{\alpha M_V}$ and hence

$$\Delta a_\mu^{\text{NP}} = \frac{m_\mu^2 \Gamma(V \rightarrow e^+e^-)}{\pi M_V^3} = \frac{4\alpha^2 \gamma_V^2 m_\mu^2}{3M_V^2}. \quad (7.17)$$

Here we have applied the Van Royen-Weisskopf formula [82], which for a $J^{PC} = 1^{--}$ vector state predicts

$$\Gamma(V \rightarrow e^+e^-) = 16\pi\alpha^2 Q_q^2 \frac{|\psi_V(0)|^2}{M_V^2} = \frac{4}{3} \pi \alpha^2 \gamma_V^2 M_V,$$

where $\psi_V(0)$ is the meson wave function at the origin (dim 3) and γ_V is the dimensionless effective photon vector–meson coupling defined by $j_{\text{em}}^\mu(x) = \gamma_V M_V^2 V^\mu(x)$ with $V^\mu(x)$ the interpolating vector–meson field. γ_V characterizes the strong interaction properties of the $\gamma - V$ coupling and typically has values 0.2 for the ρ to 0.02 for the Υ . For $\gamma_V = 0.1$ and $M_V = 200$ GeV we get $\Delta a_\mu \sim 2 \times 10^{-13}$. The hadronic contribution of a 4th family quark doublet assuming $m_{b'} = m_{t'} = 200$ GeV would yield $\Delta a_\mu \sim 5.6 \times 10^{-14}$ only. Unless there exists a new type of strong interactions like Technicolor⁹ [83–85]. New strong interaction resonances are not expected, because new heavy sequential quarks would be too shortlived to be able to form resonances. As we know, due to the large mass and the large mass difference $m_t \gg m_b$, the top quark is the first quark which decays, via $t \rightarrow Wb$, as a bare quark before it has time to form hadronic resonances. This is not so surprising as the top Yukawa coupling responsible for the weak decay is stronger than the strong interaction constant.

New physics effects here may be easily buried in the uncertainties of the hadronic vacuum polarization. In any case, we expect $O((\alpha/\pi)^2)$ terms from heavy states not yet seen to be too small to play a role here. Possible light dark states are discussed later in Sect. 7.2.6.

In general the effects related to single diagrams, discussed in this paragraph, are larger than what one expects in a viable extension of the SM, usually required to be a renormalizable QFT¹⁰ and to exhibit gauge interactions which typically cause large cancellations between different contributions. But even if one ignores possible cancellations, all the examples considered so far show how difficult it actually is to reconcile the observed deviation with NP effects not ruled out already by LEP, Tevatron and LHC new physics searches. Apparently a more sophisticated extension of the SM is needed which is able to produce substantial radiative corrections in

⁹Searches for Technicolor states like color–octet techni– ρ were negative up to 260–480 GeV depending on the decay mode.

¹⁰Of course, there are more non-renormalizable extensions of the SM than renormalizable ones. For the construction of the electroweak SM itself renormalizability was the key guiding principle which required the existence of neutral currents, of the weak gauge bosons, the quark–lepton family structure and last but not least the existence of the Higgs. However, considered as a low energy effective theory one expects all kinds of higher dimension transition operators coming into play at higher energies. Specific scenarios are anomalous gauge couplings, little Higgs models, models with extra space–dimensions à la Kaluza–Klein. In view of the fact that non-renormalizable interactions primarily change the high energy behavior of the theory, we expect corresponding effects to show up primarily at the high energy frontier. The example of anomalous $W^+W^-\gamma$ couplings, considered in the following subsection, confirms such an expectation. Also in non-renormalizable scenarios, effects are of the generic form (7.10) possibly with M_{NP} replaced by a cut-off Λ_{NP} . On a fundamental level we expect the Planck scale to provide the cut–off, which would imply that effective interactions of non-renormalizable character show up at the 1 ppm level at about 10^{16} GeV. It is conceivable that at the Planck scale a sort of cut-off theory which is modeling an “ether” is more fundamental than its long distance tail showing up as a renormalizable QFT [86]. Physics-wise such an effective theory, which we usually interpret to tell us the fundamental laws of nature, is different in character from what we know from QCD where chiral perturbation theory or the resonance Lagrangian type models are non-renormalizable low energy tails of a known renormalizable theory, as is Fermi’s non-renormalizable low energy effective current–current type tail within the SM.

the low energy observable a_μ while the new particles have escaped detection at accelerator facilities so far and only produce small higher order effects in other electroweak precision observables. In fact supersymmetric extensions of the SM precisely allow for such a scenario, as we will discuss below.

7.2.2 Flavor Changing Processes

We already have seen that flavor changing processes could give large contributions to a_μ . As pointed out in [87, 88] taking into account just the vertex diagrams could be very misleading. The argument is that the same interactions and heavy states which could contribute to a_μ^{NP} according to Fig. 7.4 would contribute to the muon self energy, via the diagrams Fig. 7.6. By imposing chiral symmetry to the SM, i.e. setting the SM Yukawa couplings to zero, lepton masses could be radiatively induced by flavor changing $f\bar{\psi}_\mu\psi_F S + \text{h.c.}$ and $f\bar{\psi}_\mu i\gamma_5\psi_F P + \text{h.c.}$ interactions (F a heavy fermion, S a scalar and P a pseudoscalar) in a hierarchy $m_\mu \ll M_F \ll M_S, M_P$. Then with $m_\mu \propto f^2 M_F$ and $a_\mu \propto f^2 m_\mu M_F / M_{S,P}^2$ one obtains $a_\mu = \mathcal{C} m_\mu^2 / M_{S,P}^2$ with $\mathcal{C} = O(1)$, and the interaction strength f has dropped from the ratio. The problem is that a convincing approach of generating the lepton/fermion mass spectrum by radiative effects is not easy to accommodate. Of course it is a very attractive idea to replace the Yukawa term, put in by hand in the SM, by a mechanism which allows us to understand or even calculate the known fermion mass-spectrum, exhibiting a tremendous hierarchy of about 13 orders of magnitude of vastly different couplings/masses [from m_{ν_e} to m_t]. The radiatively induced values must reproduce this pattern and one has to explain why the same effects which make up the muon mass do not contribute to the electron mass. Again the needed hierarchy of fermion masses is only obtained by putting it in by hand in some way. In the scenario of radiatively induced lepton masses one has to require the family hierarchy like $f_e^2 M_{F_e} / f_\mu^2 M_{F_\mu} \simeq m_e / m_\mu$, $f_P \equiv f_S$ in order to get a finite cut-off independent answer, and $M_0 \rightarrow M_S \neq M_P$, such that $m_\mu = \frac{f_\mu^2 M_{F_\mu}}{16\pi^2} \ln \frac{M_S^2}{M_P^2}$ which is positive only provided $M_S > M_P$. It looks one tries to replace one puzzle with another. But of course new fields exhibiting new interactions affect radiative corrections also through mass effects.

Another aspect of flavor changing transition in the lepton sector is the following: after neutrino oscillations and herewith right-handed singlet neutrinos and neutrino

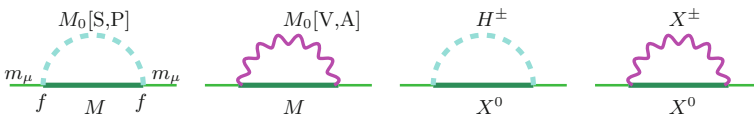


Fig. 7.6 Lepton self-energy contributions induced by the new interactions appearing in Fig. 7.4 may generate m_μ as a radiative correction effect

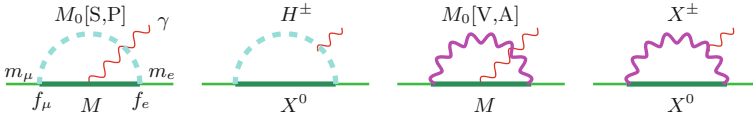


Fig. 7.7 $\mu \rightarrow e\gamma$ transitions by new interactions (overall flavor changing version of Fig. 7.4)

masses have been established, also lepton flavor violating (LFV) transitions like $\mu^\pm \rightarrow e^\pm\gamma$, see Fig. 7.7, are in the focus of further searches. The corresponding contributions here read

$$L_S^\mu \simeq \frac{1}{6}, \quad L_P^\mu \simeq \frac{1}{6}, \quad L_V^\mu \simeq \frac{2}{3}, \quad L_A^\mu \simeq -\frac{2}{3},$$

$$L_S^e \simeq \frac{m_\mu}{m_e} \left(\ln \frac{M_0}{m_\mu} - \frac{3}{4} \right), \quad L_P^e \simeq -\frac{m_\mu}{m_e} \left(\ln \frac{M_0}{m_\mu} - \frac{3}{4} \right), \quad L_V^e \simeq \frac{m_\mu}{m_e}, \quad L_A^e \simeq -\frac{m_\mu}{m_e}.$$

The latter flavor changing transitions are strongly constrained, first by direct rare decay search experiments which were performed at the Paul Scherrer Institute (PSI) and second, with the advent of the much more precise measurement of a_e . For example, for a scalar exchange mediating $e \rightarrow \mu \rightarrow e$ with $f^2/(4\pi^2) \simeq 0.01$ and $M_0 \simeq 100$ GeV we obtain $\Delta a_e^{NP} \simeq 33 \times 10^{-11}$ which is ruled out by (3.72) $|a_e^{\text{exp}} - a_e^{\text{the}}| \lesssim 1 \times 10^{-12}$. Either M_0 must be heavier or the coupling smaller: $f^2/(4\pi^2) < 0.0003$. The present limit for the branching fraction $Br(\mu \rightarrow e\gamma)$ from the MEG experiment at PSI is 4.2×10^{-13} (at 90% C.L.) [89] (see also [90]). Other LFV processes have been searched for are $\tau \rightarrow e\gamma$, $\tau \rightarrow \mu\gamma$, $\mu \rightarrow eee$, $\tau \rightarrow \mu\mu\mu$ and since no signal was observed stringent limits were derived. Note that

$$\Gamma(\mu \rightarrow e\gamma) = \frac{e^2 f_\mu^2 f_e^2}{16\pi^2} m_\mu^5 (|F_M^L|^2 + |F_M^R|^2), \quad (7.18)$$

where $F_M^{L,R}$ are the left- and right-handed zero-momentum transfer magnetic $\mu e\gamma$ form factors. In the SM

$$Br(\mu \rightarrow e\gamma) \propto \frac{\alpha^3}{G_\mu^2} \frac{(\Delta m_\nu^2)_{\mu e}^2}{M_W^8}, \quad (7.19)$$

is extremely tiny. Only new physics can give rates in experimentally interesting ranges. In the quark sector CKM flavor mixing via the charged current is comparably huge and the $b \rightarrow s\gamma$ transitions is an established effect. This process also acquires enhanced SUSY contributions which makes it an excellent monitor for new physics [90], as we will see below. For a recent review see [92] and references therein. The detailed review [93] is focusing on the compatibility of the present and future constraints from Δa_μ and from the bound on $\mu \rightarrow e\gamma$ flavor violation for a variety of extensions of the SM as they contribute to the effective Lagrangian of the magnetic and electric dipole moment form (3.22).

7.2.3 Anomalous Couplings

Besides new states with new interactions also possible anomalous couplings of SM particles are very interesting. In particular the non-Abelian gauge boson self-interactions have to be checked for possible deviations. In the SM these couplings are dictated by the local gauge principle of Yang-Mills, once the interaction between the gauge bosons and the matter-fields (4.37) is given. For $g = 2$ in particular the anomalous W -boson couplings are of interest, which occur in the 1st of the weak one-loop diagrams in Fig. 4.18. Possible is an anomalous magnetic dipole moment (see [94] and references therein)

$$\mu_W = \frac{e}{2m_W}(1 + \kappa + \lambda), \quad (7.20)$$

and an anomalous electric quadrupole moment

$$Q_W = -\frac{e}{2m_W}(\kappa - \lambda). \quad (7.21)$$

In the SM local gauge symmetry, which is mandatory for renormalizability of the SM, requires $\kappa = 1$ and $\lambda = 0$. The contribution to a_μ due to the deviation from the SM may be calculated and as a result one finds [95]

$$a_\mu(\kappa, \lambda) \simeq \frac{G_\mu m_\mu^2}{4\sqrt{2}\pi^2} \left[(\kappa - 1) \ln \frac{\Lambda^2}{m_W^2} - \frac{1}{3} \lambda \right]. \quad (7.22)$$

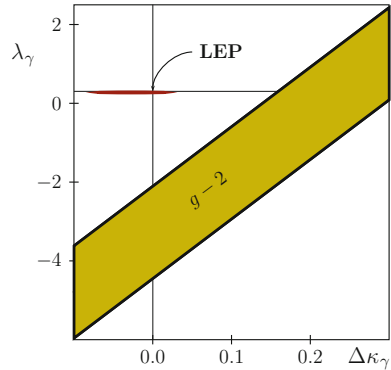
Actually, the modification spoils renormalizability and one has to work with a cut-off Λ in order to get a finite answer and the result has to be understood as a low energy effective answer. For $\Lambda \simeq 1$ TeV the BNL constraint (7.3) would yield

$$\kappa - 1 = 0.24 \pm 0.08, \quad \lambda = -3.58 \pm 1.17 \quad (\text{BNL 04}), \quad (7.23)$$

on the axes of the $(\Delta\kappa, \lambda)$ -plane. Of course from one experimental number one cannot fix two or more parameters. In fact arbitrary large deviations from the SM are still possible described by the band Fig. 7.8: $\lambda = 3 \ln \frac{\Lambda^2}{m_W^2} \Delta\kappa - \tilde{a}_\mu$ with $\tilde{a}_\mu = \frac{12\sqrt{2}\pi^2 \delta a_\mu}{G_\mu m_\mu^2} \simeq 3.58 \pm 1.17$, as an interval on the λ -axis and a slope of about 15.

This possibility again is already ruled out by $e^+e^- \rightarrow W^+W^-$ data from LEP [96, 97] $\kappa - 1 = -0.027 \pm 0.045$, $\lambda = -0.028 \pm 0.021$. Applying the LEP bounds we can get not more than $a_\mu(\kappa, 0) \simeq (-3.3 \pm 5.3) \times 10^{-10}$, $a_\mu(1, \lambda) \simeq (0.2 \pm 1.6) \times 10^{-10}$, and thus the observed deviation cannot be due to anomalous $WW\gamma$ couplings. The constraint on those couplings from $g = 2$ is at least an order of magnitude weaker than the one from LEP. Much more promising are the next examples, adding another Higgs doublet to the SM and the supersymmetrized SM.

Fig. 7.8 Bounds on triple gauge couplings in $WW\gamma$



7.2.4 Two-Higgs Doublet Models

The minimal SM Higgs structure is very special as it implies automatically a custodial symmetry which predicts $\rho_0 = F_{\text{NC}}/G_F = 1$ at tree level and FCNCs are automatically highly suppressed. After the discovery of the Higgs particle the search for additional scalars has moved increasingly into focus of present and future collider physics. One possibility of extending the SM is to modify the Higgs sector where one could add scalar singlets, an additional doublet, a Higgs triplet and so on. From a theoretical point of view the case with two Higgs doublets is very attractive. General Two Higgs Doublet Models (2HDM) are interesting as they predict 4 additional physical spin 0 bosons. Two Higgs doublets are needed in Minimal Supersymmetric extensions of the SM (MSSM). One reason is supersymmetry itself, the other is anomaly cancellation of the SUSY partners of the Higgs particles. Our interest here: models with two Higgs doublets give additional contributions to a_μ which could bridge the discrepancy Δa_μ (7.3) [98–102].

While in the SM the complex Higgs doublet field $\Phi_b(x)$ of hypercharge $Y = 1$ and its hypercharge conjugate field $\Phi_t(x) = i \tau_2 \Phi_b^*$ of hypercharge $Y = -1$ (τ_2 the second 2×2 Pauli matrix) are built with the same two complex fields φ^0 and φ^+ , in 2HDMs $\Phi_1(x)$ and $\Phi_2(x)$ are chosen to be two independent fields with hypercharges $Y = (-1, +1)$. A consequence is that 2HDMs exhibit tree level FCNCs, which are in contradiction with experimental findings [96]. In fact, the generic Yukawa Lagrangian with the SM fermionic content gives rise to FCNCs because the fermionic couplings of the two scalar doublets cannot be simultaneously diagonalized in flavor space. Conditions for the absence of FCNCs are well known [103–107] and interestingly FCNCs can be forbidden by a discrete Z_2 symmetry which exchanges the two doublets: $\Phi_1 \leftrightarrow \Phi_2$, the so called R-parity. The latter is also added as an additional selection rule in SUSY extension of the SM. R-parity in SUSY models implies the existence of a lightest SUSY particle (LSP), which is a dark matter candidate.

Here, one should keep in mind that the electroweak SM turned out to be the minimal renormalizable extension of “QED+charged weak current Fermi-theory”:

which required neutral currents, local Yang-Mills symmetry (gauge bosons), chiral symmetry, lepton-quark family structure, last but not least the existence of the Higgs boson. Most important in our context, in the SM tree level FCNCs are automatically absent. Not foreseeable was the third fermion family, which however as we know is required for CP violation the be possible the way it appears to be realized. Renormalizability is a natural property which is emergent as a low energy effective phenomenon if the underlying physical system exhibits a physical cut-off, which likely is to be identified with the Planck cut-off (see e.g. [108]). Symmetries like the R-parity, which do not affect renormalizability but are not required by minimality, in such a context are unnatural as they are not emergent as an unavoidable low energy feature, but introduced ad hoc (added by hand).

The scalar potential must share the symmetry $\Phi_2 \rightarrow -\Phi_2$. The most general renormalizable Higgs potential is then given by

$$V = m_{11}^2(\Phi_1^+\Phi_1) + m_{22}^2(\Phi_2^+\Phi_2) - m_{12}^2(\Phi_1^+\Phi_2 + \Phi_2^+\Phi_1) + \frac{\lambda_1}{2}(\Phi_1^+\Phi_1)^2 + \frac{\lambda_2}{2}(\Phi_2^+\Phi_2)^2 + \lambda_3(\Phi_1^+\Phi_1)(\Phi_2^+\Phi_2) + \lambda_4(\Phi_1^+\Phi_2)(\Phi_2^+\Phi_1) + \frac{\lambda_5}{2}[(\Phi_1^+\Phi_2)^2 + (\Phi_2^+\Phi_1)^2]. \quad (7.24)$$

A soft Z_2 symmetry breaking term $\propto m_{12}^2$ has been added. This implies finite Higgs-mediated FCNCs at one loop and one has a fine tuning problem. Vacuum stability requires

$$\lambda_{1,2} > 0, \quad \lambda_3 > -\sqrt{\lambda_1\lambda_2}, \quad |\lambda_5| < \lambda_3 + \lambda_4 + \sqrt{\lambda_1\lambda_2}.$$

Applicability of perturbation theory requires $|\lambda_i| < \lambda_{\max} \sim 4\pi$.

In terms of the components of the two doublet fields

$$\Phi_i = \begin{pmatrix} \phi_i^+ \\ (v_i + \eta_i + i\chi_i)/\sqrt{2} \end{pmatrix}; \quad (i = 1, 2)$$

of fixed hypercharge $Y_i = (-1, +1)$, the new physical scalars are the two scalars h and H , the pseudoscalar A and the charged Higgs bosons H^\pm . As an extension of the SM the 2HDM has to be in the broken phase in which both neutral components of the Φ_1 and the Φ_2 fields acquire a vacuum expectation value v_1 and v_2 and the physical states are the result of a mixing mechanism of the physical components of the Φ_i fields which requires diagonalizing the mass matrices. As a consequence mass squares m_{11}^2 and m_{22}^2 are functions of the λ_i 's, the v_i 's and the Z_2 symmetry breaking parameter m_{12}^2 [106]. The condition for the existence of a global minimum then reads

$$m_{12}^2 \left(m_{11}^2 - m_{22}^2 \sqrt{\lambda_2/\lambda_1} \right) (\tan \beta - (\lambda_1/\lambda_2)^{1/4}) > 0.$$

The parameter $\tan \beta$ is determined by

$$\tan \beta = \frac{v_2}{v_1} \equiv \frac{v_{\text{top}}}{v_{\text{bottom}}}, \quad 0 \leq \beta \leq \frac{\pi}{2},$$

where β is the rotation angle which rotates the original doublets into

$$\Phi'_1 = \begin{pmatrix} G^+ \\ (v + S_1 + i G^0)/\sqrt{2} \end{pmatrix}; \quad \Phi'_2 = \begin{pmatrix} H^+ \\ (S_2 + i A)/\sqrt{2} \end{pmatrix},$$

where Φ'_2 has a vanishing VEV. Φ'_1 may be identified with the SM Higgs field with vacuum expectation value $v = (v_1^2 + v_2^2)^{1/2}$. The fields G^\pm and G^0 can be gauged away and hence represent the unphysical SM Higgs ghosts, absent in the unitary gauge.

The physical scalars are the charged Higgses H^\pm , a pseudoscalar A and two physical scalars H and h which are given by mixing of η_1 and η_2 with mixing angle α :

$$\begin{aligned} H^\pm &= -\sin \beta \phi_1^\pm + \cos \beta \phi_2^\pm, & H &= \cos \alpha \eta_1 + \sin \alpha \eta_2, \\ A &= -\sin \beta \chi_1 + \cos \beta \chi_2, & h &= -\sin \alpha \eta_1 + \cos \alpha \eta_2. \end{aligned}$$

Accordingly, the neutral fields S_i

$$\begin{aligned} S_1 &= \cos(\alpha - \beta) H - \sin(\alpha - \beta) h, & H &= \cos(\beta - \alpha) S_1 - \sin(\beta - \alpha) S_2, \\ S_2 &= \sin(\alpha - \beta) H + \cos(\alpha - \beta) h, & h &= \sin(\beta - \alpha) S_1 + \cos(\beta - \alpha) S_2, \\ S_3 &= A, & A &= S_3 \end{aligned}$$

couple to the gauge bosons identical as the Higgs in the SM, and we easily find the couplings for H and h , which simply pick factors $\cos(\alpha - \beta)$ and $\pm \sin(\alpha - \beta)$ e.g. $VVH \rightarrow VVH \cos(\alpha - \beta) - VVh \sin(\alpha - \beta)$ ($V = W, Z$). The inverse transformation we write

$$\phi_i(x) = \mathcal{R}_{ij} S_j(x); \quad \phi_i(x) = h(x), H(x), A(x). \quad (7.25)$$

In the CP violating case h and H would also mix with A [109]. Whereas β only depends on the ratio of the vacuum expectation values, α depends on all the parameters of the Higgs potential, $\tan 2\alpha = \frac{v_1 v_2 (\lambda_3 + \lambda_4 + \lambda_5)}{2\lambda_2 v_2^2 - 2\lambda_1 v_1^2}$ ($-\frac{\pi}{2} \leq \alpha \leq 0$).

In the phenomenologically interesting region of enhanced $\tan \beta$ together with a light Higgs for the CP-even part of the Higgs sector we have $\beta - \alpha - \pi/2 \equiv \eta$ small. Actually, for $\beta - \alpha = \pi/2$ the two scalars h and H are completely separated in the two doublets Φ'_i , such that h has identical couplings as the SM Higgs boson and $\eta = 0$ is called the SM limit of a 2HDM. In this case the couplings of the light CP-even neutral Higgs h with the gauge bosons and fermions have the SM values. In fact, the measured signal strengths and production cross section of such a particle are in very good agreement with the corresponding SM predictions [110–122]. While h corresponds to the SM Higgs boson the second scalar is often denoted by H_1 in order to distinguish it from the SM Higgs boson H . Thus, $M_{H_1} > M_h$ and $M_h = m_H^{\text{SM}}$.

The 2HDM potential shares eight free parameters $\lambda_{i=1,\dots,5}$, m_{11}^2 , m_{22}^2 and m_{12}^2 , seven more than the SM Higgs potential, which has two free parameters λ and the VEV v . The Higgs mass is then given by $m_H^2 = \lambda v^2/3$. Now, the mass–coupling relations include the four scalar masses the two mixing parameters α and β and v and read [104–106, 123, 124]

$$\begin{aligned}\lambda_1 &= \frac{M_H^2 c_\alpha^2 + M_h^2 s_\alpha^2 - m_{12}^2 t_\beta}{v^2 c_\beta^2}, \\ \lambda_2 &= \frac{M_H^2 s_\alpha^2 + M_h^2 c_\alpha^2 - m_{12}^2 t_\beta^{-1}}{v^2 s_\beta^2}, \\ \lambda_3 &= \frac{(M_H^2 - M_h^2) c_\alpha s_\alpha + 2M_{H^\pm} s_\beta c_\beta - m_{12}^2}{v^2 s_\beta c_\beta}, \\ \lambda_4 &= \frac{(M_A^2 - 2M_{H^\pm}^2) s_\beta c_\beta + m_{12}^2}{v^2 s_\beta c_\beta}, \\ \lambda_5 &= \frac{m_{12}^2 - M_A^2 s_\beta c_\beta}{v^2 s_\beta c_\beta},\end{aligned}\tag{7.26}$$

where $s_\alpha = \sin \alpha$, $c_\alpha = \cos \alpha$, $s_\beta = \sin \beta$, $c_\beta = \cos \beta$ and $t_\beta = \tan \beta$. The potential minimum conditions fix the potential masses to values [106]

$$\begin{aligned}m_{11}^2 &= m_{12}^2 t_\beta - \frac{1}{2} v^2 [\lambda_1 c_\beta^2 + (\lambda_3 + \lambda_4 + \lambda_5) s_\beta^2], \\ m_{22}^2 &= m_{12}^2 t_\beta^{-1} - \frac{1}{2} v^2 [\lambda_2 s_\beta^2 + (\lambda_3 + \lambda_4 + \lambda_5) c_\beta^2].\end{aligned}$$

The vacuum stability and perturbativity $|\lambda_i| < \lambda_{\max}$ conditions put sever constraints on the admitted mass ranges, in particular the mass difference $M_H - M_{H^\pm}$ is severely constraint as a function of M_A (see e.g. Fig. 1 in [125]).

In 2HDMs many new real and virtual processes, like $W^\pm H^\mp \gamma$ transitions, are the consequence. The non–observation of processes like $\Upsilon \rightarrow H + \gamma$ sets stringent lower bounds on the scalar masses. Together with the LEP bounds this prevents large 2HDM contribution to a_μ . Present bounds on scalars are $M_{H^\pm} > 80$ GeV, $M_A > 93$ GeV and $M_{H_t} > 93$ GeV. In general, in type I models, fermions get contributions to their masses from the VEVs of both Higgs scalars. Phenomenologically preferred and most interesting are the type II models where a discrete symmetry guarantees that the upper and the lower entries of the fermion doublets get their masses from different VEVs ($m_t \propto v_2$, $m_b \propto v_1$) in order to prevent FCNCs [103]. Only the type II models satisfy the MFV criterion. Such models are also interesting because one easily may get $m_t \gg m_b$ without having vastly different Yukawa couplings. Anyway, the possibility of two Higgs doublets is an interesting option and therefore has been studied extensively [98, 99, 101, 102, 124–128] in the past. We assume couplings of the 2HDMs to be real (CP conserving case), for a discussion of the complex case see [129, 130].

The naming of 2HDMs has been changed recently [125, 131]: as already mentioned a major constraint on 2HDMs is the absence/suppression of FCNCs. Requiring “Natural Flavor Conservation” (NFC)¹¹ restricts the models to four different classes (so called aligned models A2HDMs) which differ by the manner in which the Higgs doublets couple to fermions [106, 129, 132]. They are organized via discrete symmetries like Z_2 under which different matter sectors, such as right-handed leptons or left-handed quarks, have different charge assignments.

For flavor conserving A2HDMs, the non-diagonal neutral couplings can be eliminated by requiring the alignment in flavor space of the Yukawa matrices [131]: the two Yukawa matrices which couple to a given type of right-handed fermions are assumed to be proportional to each other and can, therefore, be diagonalized simultaneously. The three proportionality parameters ζ_f ($f = u, d, l$) are arbitrary complex numbers and introduce new sources of CP violation. We consider the CP conserving case with real ζ 's only.

One considers type I, II, X and Y models depending on the possible implementations of the Yukawa couplings which we denote as $y_f^\phi \frac{m_f}{v} \bar{f} f \phi$ for the scalars $\phi = h, H$ and as $i y_f^A \frac{m_f}{v} \bar{f} \gamma_5 f A$ for the pseudoscalar A . In terms of the fermion mass-eigenstates fields, the Yukawa interactions of the A2HDM read

$$\begin{aligned} \mathcal{L}_Y = & \sqrt{2} H^+ (\bar{u} [V_{CKM} y_d^A P_R + y_u^A V_{CKM} P_L] d + \bar{\nu} y_l^A P_R l) \\ & - \sum_{i=h,H,A, f=u,d,l} \phi_i \bar{f} y_f^i P_R f + \text{h.c.}, \end{aligned} \quad (7.27)$$

where $P_{R,L} \equiv \frac{1 \pm \gamma_5}{2}$ are the right-handed and left-handed chirality projectors. The normalized Yukawa couplings are then given by $Y_{d,l}^i = \mathcal{R}_{i1} + (\mathcal{R}_{i2} + i \mathcal{R}_{i3}) \zeta_{d,l}$ and $Y_u^i = \mathcal{R}_{i1} + (\mathcal{R}_{i2} - i \mathcal{R}_{i3}) \zeta_u^*$ and the standard ones by

$$\begin{aligned} y_f^h &= \sin(\beta - \alpha) + \cos(\beta - \alpha) \zeta_f \\ y_f^H &= \cos(\beta - \alpha) - \sin(\beta - \alpha) \zeta_f. \\ y_{d,l}^A &= -\zeta_{d,l}, \quad Y_u^A = \zeta_u \end{aligned} \quad (7.28)$$

The Z_2 breaking parameter η affects only the couplings $Y_f^h = 1 + \eta \zeta_f$ and $Y_f^H = -\zeta_f + \eta$. The possibilities are listed in Table 7.6 For the type II model the relevant couplings read

$$\begin{aligned} H \bar{f} f, \quad f = b, t & \quad -\frac{g}{2} \left(\frac{m_b \cos \alpha}{M_W \cos \beta}, \frac{m_t \sin \alpha}{M_W \sin \beta} \right) \\ h \bar{f} f, \quad f = b, t & \quad -\frac{g}{2} \left(-\frac{m_b \sin \alpha}{M_W \cos \beta}, \frac{m_t \cos \alpha}{M_W \sin \beta} \right) \\ A \bar{f} i \gamma_5 f, \quad f = b, t & \quad -\frac{g}{2} \left(\frac{m_b}{M_W} \tan \beta, \frac{m_t}{M_W} \cot \beta \right) \\ H^+ \bar{t} b & \quad \frac{g}{\sqrt{2}} \left(\frac{m_b}{M_W} \tan \beta \frac{1+\gamma_5}{2} + \frac{m_t}{M_W} \cot \beta \frac{1-\gamma_5}{2} \right) V_{tb}. \end{aligned} \quad (7.29)$$

¹¹In my opinion “natural” here is misleading. Imposing ad hoc Z_2 selection rules have no natural explanation.

Table 7.6 The normalized Yukawa couplings of the neutral bosons to up- and down-type quarks and charged leptons. The usual Yukawa couplings are $y_f^i = Y_f^i m_f/v$

	$Y_u^A = \zeta_u$	$Y_d^A = -\zeta_d$	$Y_l^A = -\zeta_l$	Y_u^H	Y_d^H	Y_l^H	Y_u^h	Y_d^h	Y_l^h
Type I	$\cot \beta$	$-\cot \beta$	$-\cot \beta$	$\frac{\sin \alpha}{\sin \beta}$	$\frac{\sin \alpha}{\sin \beta}$	$\frac{\sin \alpha}{\sin \beta}$	$\frac{\cos \alpha}{\sin \beta}$	$\frac{\cos \alpha}{\sin \beta}$	$\frac{\cos \alpha}{\sin \beta}$
Type II	$\cot \beta$	$\tan \beta$	$\tan \beta$	$\frac{\sin \alpha}{\sin \beta}$	$\frac{\cos \alpha}{\cos \beta}$	$\frac{\cos \alpha}{\cos \beta}$	$\frac{\cos \alpha}{\sin \beta}$	$-\frac{\sin \alpha}{\cos \beta}$	$-\frac{\sin \alpha}{\cos \beta}$
Type X	$\cot \beta$	$-\cot \beta$	$\tan \beta$	$\frac{\sin \alpha}{\sin \beta}$	$\frac{\sin \alpha}{\sin \beta}$	$\frac{\cos \alpha}{\cos \beta}$	$\frac{\cos \alpha}{\sin \beta}$	$\frac{\cos \alpha}{\sin \beta}$	$-\frac{\sin \alpha}{\cos \beta}$
Type Y	$\cot \beta$	$\tan \beta$	$-\cot \beta$	$\frac{\sin \alpha}{\sin \beta}$	$\frac{\cos \alpha}{\cos \beta}$	$\frac{\sin \alpha}{\sin \beta}$	$\frac{\cos \alpha}{\sin \beta}$	$-\frac{\sin \alpha}{\cos \beta}$	$\frac{\cos \alpha}{\sin \beta}$

The masses in units of v : $m_f/v = \frac{g}{2} \frac{m_f}{M_W}$ with g the $SU(2)$ SM gauge coupling.

The SM Higgs contribution (4.48) is tiny, due to the fact that the $H\bar{\mu}\mu$ Yukawa coupling $y_\mu = \sqrt{2}m_\mu/v$ is very small because the SM Higgs VEV is large: $v = 246.221(1)$ GeV. In 2HDMs of type II and type X the Yukawa couplings may be enhanced by large factors $\tan \beta = v_2/v_1$. This is particularly important for the heavier fermions. It is evident that if 2HDMs are expected to explain Δa_μ , then only models of type II and X have a chance to do so.

The couplings for the other fermions are given by analogous expressions. For example, the coupling for the τ may be obtained by substituting $m_t \rightarrow 0$, $m_b \rightarrow m_\tau$.

A class of 2HDMs also exists where one of the Higgs doublets does not participate in the dynamics and remains *inert* [133, 134]. Finally, in the so-called type III models (previously type I) both up and down fermions couple to both Higgs doublets. A detailed analysis of flavor and CP violation in type III models can be found in [135] and references therein.

The parameter space compatible with collider and flavor physics data has been updated in [125]: the direct LEP bound is $M_{H^\pm} > 80$ GeV, however, given (7.8) the 2HDM calculation of the decay rates of the radiative quark-level transitions $b \rightarrow s\gamma$ $b \rightarrow d\gamma$ and their CP-conjugates for type II models yields a $\tan \beta$ -independent bound of $M_{H^\pm} > 580$ GeV [136]. Constraints from LHC data on the alignment parameters ζ_f are [121]:

$$0 < |\zeta_u| < 1.2, \quad 0 < |\zeta_d| < 50, \quad 0 < |\zeta_l| < 100. \tag{7.30}$$

The complete 1-loop result (see Fig. 7.9a) reads [79, 80, 137]

$$a_\mu^{(2)2\text{HDM}} = \frac{G_\mu m_\mu^2}{4\pi^2 \sqrt{2}} \sum_j (y_\mu^j)^2 r_\mu^j f_j(r_\mu^j), \tag{7.31}$$

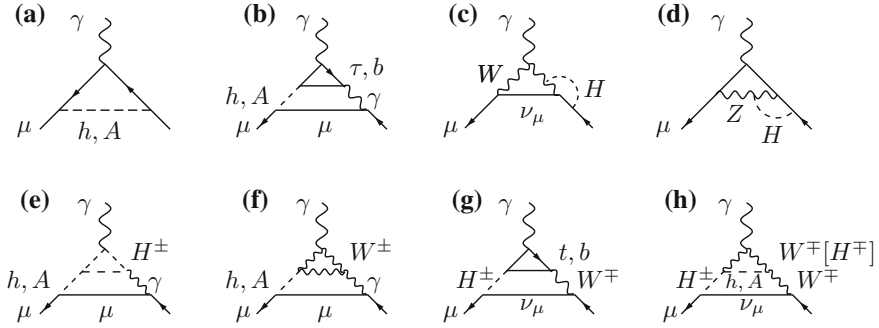


Fig. 7.9 Leading 2HDM graphs **a** and **b** contributing to a_μ . Diagrams **c** and **d**, with $H \rightarrow h, H, A$, are examples of subleading bosonic contributions which are modified with respect to the SM weak bosonic contributions due to the extended Higgs structure. Graphs **e–h** have been shown to give substantial contributions as well [109, 124]

where $j = \{h, H, A, H^\pm\}$, $r_\mu^j = m_\mu^2/M_j^2$, and

$$\begin{aligned}
 f_{h,H}(r) &= \int_0^1 dx \frac{x^2(2-x)}{1-x+rx^2} = -\ln r - 7/6 + O(r), \\
 f_A(r) &= \int_0^1 dx \frac{-x^3}{1-x+rx^2} = +\ln r + 11/6 + O(r), \\
 f_{H^\pm}(r) &= \int_0^1 dx \frac{-x(1-x)}{1-(1-x)r} = -1/6 + O(r).
 \end{aligned} \tag{7.32}$$

The normalized Yukawa couplings $y_\mu^{h,H,A}$ are listed in Table 7.6, and $y_\mu^{H^\pm} = y_\mu^A$. In any case we have $r \ll 1$ such that $f_{H^\pm}(r)$ is small relative to $f_{h,H,A}(r)$.

In case $\alpha \approx \beta$ the enhanced terms are (see (7.25))

$$\begin{aligned}
 a_\mu^{(2)\text{2HDM}}(h) &\simeq \frac{G_\mu m_\mu^2}{4\pi^2 \sqrt{2}} \tan^2 \beta \frac{m_\mu^2}{M_h^2} \left(\ln \frac{M_h^2}{m_\mu^2} - \frac{7}{6} \right) > 0, \\
 a_\mu^{(2)\text{2HDM}}(A) &\simeq \frac{G_\mu m_\mu^2}{4\pi^2 \sqrt{2}} \tan^2 \beta \frac{m_\mu^2}{M_A^2} \left(-\ln \frac{M_A^2}{m_\mu^2} + \frac{11}{6} \right) < 0, \\
 a_\mu^{(2)\text{2HDM}}(H^\pm) &\simeq \frac{G_\mu m_\mu^2}{4\pi^2 \sqrt{2}} \tan^2 \beta \frac{m_\mu^2}{M_{H^\pm}^2} \left(-\frac{1}{6} \right) < 0.
 \end{aligned} \tag{7.33}$$

Since we need a positive contribution M_A and M_{H^\pm} must be large (above 100 GeV) in order to make the negative contribution small and the contribution is entirely due to the light scalar h , the mass of which we identify with the 125 GeV resonance found at CERN. This then is the SM Higgs contribution (4.48) enhanced by $\tan^2 \beta$. If this should match Δa_μ it would require the unreasonably large value $\tan \beta \approx 380$.

When considering the case $\beta - \alpha \approx \pi/2$, in which h has the same couplings as the SM Higgs boson, h appears replaced by H relative to the $\sin(\beta - \alpha) \approx 0$ case of (7.33). In the decoupling limit, $M_H \simeq M_A \simeq M_{H^\pm}$ [the mass differences are of $O(M_Z^2/M_A)$] we then get

$$a_{\mu}^{(2)2\text{HDM}} \simeq \frac{G_{\mu} m_{\mu}^2}{4\pi^2 \sqrt{2}} \tan^2 \beta \frac{m_{\mu}^2}{M_A^2} \left(\frac{1}{2} - \frac{2m_{\mu}^2}{M_A^2} \ln \frac{M_A^2}{m_{\mu}^2} \right). \quad (7.34)$$

The contribution of h is not $\tan \beta$ -enhanced and is thus negligible and part of a_{μ}^{EW} already. For $100 \text{ GeV} < M_A < 1000 \text{ GeV}$, and $30 < \tan \beta < 100$, the 2HDM contribution to a_{μ} ranges from about 1.3×10^{-11} to 2.1×10^{-14} , which in the best case is two orders of magnitude below what is needed to explain the BNL measurement of a_{μ} .

At 2-loops the Barr-Zee diagrams Fig. 7.9 can yield an enhanced contribution, which can exceed the 1-loop result substantially. The enhancement factor m_b^2/m_{μ}^2 actually compensates the suppression by α/π as $(\alpha/\pi) \times (m_b^2/m_{\mu}^2) \sim 4 > 1$. For the type II case diagram Fig. 7.9b dominates and yields

$$a_{\mu}^{(4)2\text{HDM-BZ}}(h, A) = \frac{G_{\mu} m_{\mu}^2}{4\pi^2 \sqrt{2}} \frac{\alpha}{\pi} \sum_{i=h,H,A;f} N_{cf} Q_f^2 Y_{\mu}^i Y_f^i r_f^i g_i(r_{if}), \quad (7.35)$$

with $r_{if} = m_f^2/M_i^2$ ($i = h, H, A$) and

$$\begin{aligned} g_{h,H}(r) &= \int_0^1 dx \frac{2x(1-x) - 1}{x(1-x) - r} \ln \frac{x(1-x)}{r} = -2(\ln r + 2) + (2r - 1) g_A(r), \\ g_A(r) &= \int_0^1 dx \frac{1}{x(1-x) - r} \ln \frac{x(1-x)}{r} = \frac{2}{y} \left[\text{Li}_2 \left(1 - \frac{1-y}{2r} \right) - \text{Li}_2 \left(1 - \frac{1+y}{2r} \right) \right], \end{aligned} \quad (7.36)$$

with $y = \sqrt{1 - 4r}$.

In [109] the complete set of Barr-Zee type diagrams Fig. 7.9 have been calculated for the first time. Using the effective vertices from the previous section for calculating the second loop, ignoring suppressed terms proportional to higher powers of m_{μ}^2/M^2 (with M a heavy mass) in the numerator and the muon mass in the denominator, we obtain the various contributions to the anomalous magnetic moment of the muon:

$$\Delta a_{\mu}^{(b)} = \sum_{i,f} \frac{\alpha \sqrt{2} G_{\mu} m_{\mu}^2}{4 \pi^3} N_c^f Q_f^2 Y_f^i Y_l^i F^{(1)} \left(\frac{m_f^2}{M_i^2} \right), \quad (7.37)$$

$$\Delta a_{\mu}^{(e)} = \sum_i \frac{\alpha m_{\mu}^2}{8 \pi^3 M_i^2} Y_l^i \lambda_{\phi_i H^+ H^-} F^{(2)} \left(\frac{M_{H^\pm}^2}{M_i^2} \right). \quad (7.38)$$

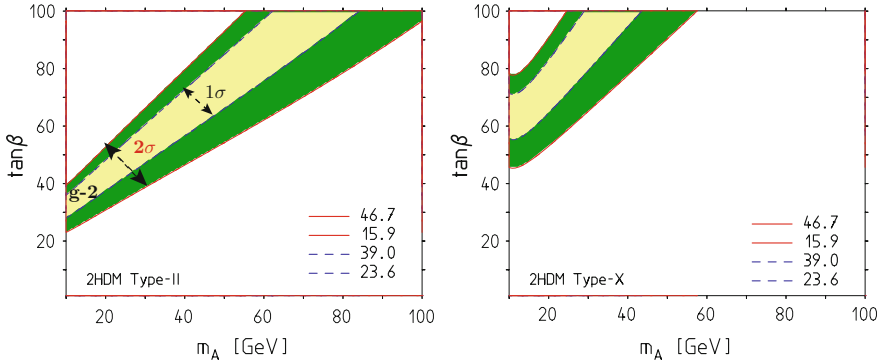


Fig. 7.10 Parameter ranges where the A2HDMs of type II or type X could explain Δa_μ . Predictions including relevant effects from leading Barr-Zee diagrams of Fig. 7.9 for $M_H = M_{H^\pm} = 500$ GeV. For small m_{12}^2 the perturbativity constraints $\lambda_1, \lambda_2 < 4\pi$ can barely be satisfied for large M_H, M_{H^\pm} . See [125] for details

$$\Delta a_\mu^{(f)} = \sum_i \frac{\alpha \sqrt{2} G_\mu m_\mu^2}{8 \pi^3} y_l^i \mathcal{R}_{i1} F^{(3)} \left(\frac{M_W^2}{M_i^2} \right). \quad (7.39)$$

$$\begin{aligned} \Delta a_\mu^{(g)} &= \frac{\alpha \sqrt{2} G_\mu m_\mu^2 N_c |V_{tb}|^2}{32 \pi^3 s_W^2 (M_{H^\pm}^2 - M_W^2)} \int_0^1 dx \left[Q_t x + Q_b (1-x) \right] \\ &\times \left[\zeta_d \zeta_l m_b^2 x (1-x) + \zeta_u \zeta_l m_t^2 x (1+x) \right] \left[\mathcal{G} \left(\frac{m_t^2}{M_{H^\pm}^2}, \frac{m_b^2}{M_{H^\pm}^2} \right) - \mathcal{G} \left(\frac{m_t^2}{M_W^2}, \frac{m_b^2}{M_W^2} \right) \right], \end{aligned} \quad (7.40)$$

$$\begin{aligned} \Delta a_\mu^{(h_1)} &= \frac{\alpha \sqrt{2} G_\mu m_\mu^2}{64 \pi^3 s_W^2 (M_{H^\pm}^2 - M_W^2)} \sum_i \left[\zeta_l (\mathcal{R}_{i2} - i \mathcal{R}_{i3}) \right] \int_0^1 dx x^2 \\ &\times \left[(M_{H^\pm}^2 + M_W^2 - M_i^2)(1-x) - 4M_W^2 \right] \left[\mathcal{G} \left(\frac{M_W^2}{M_{H^\pm}^2}, \frac{M_i^2}{M_{H^\pm}^2} \right) - \mathcal{G} \left(1, \frac{M_i^2}{M_W^2} \right) \right], \end{aligned} \quad (7.41)$$

$$\begin{aligned} \Delta a_\mu^{(h_2)} &= \frac{\alpha m_\mu^2}{64 \pi^3 s_W^2 (M_{H^\pm}^2 - M_W^2)} \sum_i \left[\zeta_l (\mathcal{R}_{i2} - i \mathcal{R}_{i3}) \right] \lambda_{\phi_i H^+ H^-} \int_0^1 dx x^2 (x-1) \\ &\times \left[\mathcal{G} \left(1, \frac{M_i^2}{M_{H^\pm}^2} \right) - \mathcal{G} \left(\frac{M_{H^\pm}^2}{M_W^2}, \frac{M_i^2}{M_W^2} \right) \right]. \end{aligned} \quad (7.42)$$

We denoted $s_W^2 = 1 - M_W^2/M_Z^2$. The needed loop functions are given by:

$$F^{(1)}(r) = \frac{r}{2} \int_0^1 dx \frac{2x(1-x) - 1}{x(1-x) - r} \ln(x(1-x)/r), \quad (7.43)$$

$$F^{(2)}(r) = \frac{1}{2} \int_0^1 dx \frac{x(x-1)}{x(1-x) - r} \ln(x(1-x)/r), \quad (7.44)$$

$$F^{(3)}(r) = \frac{1}{2} \int_0^1 dx \frac{x [3x(4x-1) + 10]r - x(1-x)}{x(1-x) - r} \ln(x(1-x)/r), \quad (7.45)$$

and

$$\mathcal{G}(r_a, r_b) = \frac{\ln \left(\frac{r_a x + r_b (1-x)}{x(1-x)} \right)}{x(1-x) - r_a x - r_b (1-x)}. \quad (7.46)$$

The triple Higgs couplings $\lambda_{\phi, H^+ H^-}$ deriving from the Higgs potential is given by [138]

$$\lambda_{hH^+H^-} = -\frac{1}{v} \left[\left(M_h^2 - \frac{m_{12}^2}{s_\beta c_\beta} \right) \frac{c_{\beta+\alpha}}{s_\beta c_\beta} + (2 M_{H^\pm}^2 - M_h^2) s_{\beta-\alpha} \right].$$

The first two contributions are the well known classical results [98–102, 123, 125, 137–141]. The analysis [125] has shown (see Fig. 7.10) that the parameter space of the A2HDMs allows for substantial contributions to the muon $g - 2$, when one of the neutral scalars is essentially degenerate with the charged scalar. The constraints from collider and flavor physics only admit the type X model to possibly explain Δa_μ .

A first complete 2-loop A2HDM calculation has been presented recently in [124]. The analysis confirms the results [109, 125] concerning the leading effects, just discussed. However, the bosonic correction calculated for the first time can contribute effects of the size of the future experimental accuracy:

$$a_\mu^B = (2 \dots 4) \times 10^{-10}$$

for $\eta = 0, 0.1$ constrained by 2×10^{-10} and $\eta = -0.1$ where the larger values are obtained.

As an illustration we present some values for 1-loop and 2-loop contributions separately and for the sum for selected parameters with $M_h = 125$ GeV and choosing $M_{H^\pm} = M_H$ in units of 10^{-11} :

$(M_A, M_H, \tan \beta)$	$a_\mu^{(2)}(H)$	$a_\mu^{(2)}(A)$	$a_\mu^{(4)}(H)$	$a_\mu^{(4)}(A)$	sum
(50, 125, 10)	0.32	-1.09	-2.14	7.19	4.26
(50, 250, 10)	0.17	-1.09	-1.29	7.19	4.96
(50, 500, 10)	0.09	-1.09	-0.77	7.19	5.40
(50, 250, 100)	16.84	-109.20	-129.40	718.79	496.94
(50, 500, 100)	8.86	-109.20	-77.16	718.79	541.25
(100, 500, 10)	0.09	-0.31	-0.77	2.70	1.69
(100, 125, 40)	5.11	-4.95	-34.23	43.19	9.06
(100, 250, 40)	2.69	-4.95	-20.70	43.19	20.20

Typically, 1-loop and 2-loop terms as well as CP-even and CP-odd ones enter with alternating signs and there are substantial cancellations. Substantial positive contributions require not only large $\tan \beta$ but also small M_A . The LEP bound is at 90 GeV, and $\tan \beta$ much larger than 40 look not very natural. It is rather unlikely the 2HDMs are the origin of the yet unexplained deviation. If $M_A \sim M_h$ the contributions largely cancel. Given M_h , to get a large $M_A - M_h$ mass splitting requires a large M_A , which however yields a large contribution of the disfavored negative sign. This means that the muon $g - 2$ constraint gives a bound on M_A which, however, strongly depends on $\tan \beta$ (see e.g. [101, 102, 128, 138, 142] for a more detailed discussion). Besides the dominant 2-loop contributions from Fig. 7.9b a 2-loop calculation of the 2HDM contributions, including diagrams like Figs. 7.9c, d, within the context of the MSSM has been presented in [15]. The contributions from diagrams Fig. 7.9e-h, depending on the parameters, can change the leading result by about 10%.

If one identifies M_h with m_H of the SM the correction is found to be small: $a_\mu^{\text{bos.2L}}(\text{MSSM} - \text{SM}) < 3 \times 10^{-11}$ in the parameter range $M_A \gtrsim 50$ GeV and $\tan \beta \lesssim 50$. In fact, in the LL approximation, the 2HDM sector in the MSSM at 2-loops does not change the SM result. The reason is that at the 1-loop level the electroweak SM result numerically remains practically unchanged, because the additional 2HDM diagrams all are suppressed by the small Yukawa coupling of the μ (like the SM Higgs contribution).

For an effective field theory approach to 2HDMs I refer to [143].

In summary: A2HDMs exhibit a special narrow corner in parameter space which would allow to explain Δa_μ , namely the type X alignment with a light A of mass about 50 GeV and essentially degenerate $M_H \sim M_{H^\pm}$ of about 200 GeV and a large $\tan \beta \gtrsim 50$. This is a boarder line case and may be excluded by corroborating the LEP limit $M_A > 93$ GeV.

7.2.5 Supersymmetry

Supersymmetry (SUSY) is a theoretically very attractive idea, however, should it be realized in nature as a property of the spectrum of elementary particles, the non-observation of any SUSY partner up the present collider energies, tells us that SUSY would be highly broken. Searches at the LHC have pushed up possible SUSY partner

mass limits to the TeV range. While in pre-LHC times SUSY looked to be the perfect candidate for explaining the Δa_μ deviation (7.3), this has changed after the first years of LHC running. Besides the fact that no new physics has been found, the discovery of the Higgs particle with mass 125 GeV has a great impact on SUSY extensions and essentially has excluded the most attractive constrained SUSY scenarios (see e.g. [144–146] and references therein). This does not exclude SUSY as a possible solution of the muon $g - 2$ deviation and we will discuss the possibilities in the following.

Supersymmetric extensions of the SM, in particular the Minimal Supersymmetric Standard Model (MSSM), are still a promising possibility for physics beyond the SM. Supersymmetry implements a symmetry mapping

$$\text{boson} \xleftrightarrow{Q} \text{fermion}$$

between bosons and fermions, by changing the spin by $\pm 1/2$ units [147]. The SUSY algebra [graded Lie algebra] reads

$$\{Q_\alpha, \bar{Q}_\beta\} = -2 (\gamma^\mu)_{\alpha\beta} P_\mu; P_\mu = (H, \mathbf{P}),$$

with P_μ the generators of space–time translations, Q_α four component Majorana (neutral) spinors and $\bar{Q}_\alpha = (Q^\dagger \gamma^0)_\alpha$ the Pauli adjoint. It represents the only possible non-trivial unification of internal and space–time symmetry in a quantum field theory. The Dirac matrices in the Majorana representation play the role of the structure constants. The SUSY extension of the SM associates with each SM state X a supersymmetric “sstate” \tilde{X} where sfermions are bosons and sbosons are fermions as shown in Table 7.7.

SUSY is a global symmetry imposed on the SM particle spectrum, the SM gauge group remains untouched and there are no new gauge bosons. Also the matter fields remain the same. SUSY and gauge invariance are compatible only if a second Higgs

Table 7.7 The particle spectrum of a MSSM

SM particles ($R_p = +1$)	SUSY partners ($R_p = -1$)	
$\begin{pmatrix} \nu_e \\ e^- \end{pmatrix}_L, \begin{pmatrix} \nu_\mu \\ \mu^- \end{pmatrix}_L, \begin{pmatrix} \nu_\tau \\ \tau^- \end{pmatrix}_L$ $\nu_{eR}, e_R, \nu_{\mu R}, \mu_R, \nu_{\tau R}, \tau_R$	$\begin{pmatrix} \tilde{\nu}_e \\ \tilde{e}^- \end{pmatrix}_L, \begin{pmatrix} \tilde{\nu}_\mu \\ \tilde{\mu}^- \end{pmatrix}_L, \begin{pmatrix} \tilde{\nu}_\tau \\ \tilde{\tau}^- \end{pmatrix}_L$ $\tilde{\nu}_{eR}, \tilde{e}_R, \tilde{\nu}_{\mu R}, \tilde{\mu}_R, \tilde{\nu}_{\tau R}, \tilde{\tau}_R$	Sneutrinos, sleptons
$\begin{pmatrix} u \\ d \end{pmatrix}_L, \begin{pmatrix} c \\ s \end{pmatrix}_L, \begin{pmatrix} t \\ b \end{pmatrix}_L$ $u_R, d_R, c_R, s_R, t_R, b_R$	$\begin{pmatrix} \tilde{u} \\ \tilde{d} \end{pmatrix}_L, \begin{pmatrix} \tilde{c} \\ \tilde{s} \end{pmatrix}_L, \begin{pmatrix} \tilde{t} \\ \tilde{b} \end{pmatrix}_L$ $\tilde{u}_R, \tilde{d}_R, \tilde{c}_R, \tilde{s}_R, \tilde{t}_R, \tilde{b}_R$	Squarks (stop, ...)
W^\pm, H^\pm	$\tilde{W}^\pm, \tilde{H}^\pm \rightarrow \tilde{\chi}_{1,2}^\pm$	Charginos
γ, Z, h^0, H^0, A^0	$\tilde{\gamma}, \tilde{Z}, \tilde{h}^0, \tilde{H}^0, \tilde{A}^0 \rightarrow \tilde{\chi}_{1,2,3,4}^0$	Neutralinos
g, G	\tilde{g}, \tilde{G}	Gluino, gravitino

doublet field is introduced where H_1 induces the masses of all down-type fermions and H_2 the masses of all up-type fermions. A second complex Higgs doublet is also required for the anomaly cancellation of the fermionic sboson sector. This means 4 additional scalars (H^0, A^0, H^\pm) and their SUSY partners. The lighter neutral scalar denoted by h^0 corresponds to the SM Higgs boson H . Both Higgs fields exhibit a neutral scalar and acquire vacuum expectation values v_1 and v_2 . The parameter $\tan \beta = v_2/v_1$ is one of the very important basic parameters as we will see. As $m_t \propto v_2$ and $m_b \propto v_1$ in such a scenario the large mass splitting $m_t/m_b \sim 40$ could be “explained” by a large ratio v_2/v_1 , which means a large $\tan \beta$. So values $\tan \beta \sim 40$ look natural.

Digression on Supergravity and SUSY Breaking

A very interesting question is what happens if one attempts to promote global SUSY to local SUSY. Since SUSY entangles internal with space-time symmetries of special relativity, local SUSY implies supergravity (SUGRA) as one has to go from global Poincaré transformation to local ones. This means general coordinate invariance which in turn relates to geometry and gravity according to Einstein’s general relativity. SUGRA must include the spin 2 graviton and its superpartner, the spin 3/2 gravitino. Such a QFT is necessarily non-renormalizable [148]. Nevertheless it is attractive to consider the MSSM as a low energy effective theory of a non-renormalizable SUGRA scenario with $M_{\text{Planck}} \rightarrow \infty$ [149]. SUSY is spontaneously broken in the hidden sector by fields with no $SU(3)_c \otimes SU(2)_L \otimes U(1)_Y$ quantum numbers and which couple to the observable sector only gravitationally. Denoting by M_{SUSY} the SUSY breaking scale, the gravitino acquires a mass

$$m_{3/2} \sim M_{\text{SUSY}}^2 / M_{\text{Planck}} ,$$

with M_{Planck} the inherent scale of gravity.¹² SUSY is not realized as a perfect symmetry in nature. SUSY partners of the known SM particles have not yet been observed because sparticles in general are heavier than the known particles. Like the SM local G_{SM} symmetry is broken by the electroweak symmetry breaking (EWSB), SUGRA is broken at some higher scale M_{SUSY} by a super-Higgs mechanism. The Lagrangian takes the form

$$\mathcal{L}^{\text{MSSM}} = \mathcal{L}_{\text{global}}^{\text{SUSY}} + \mathcal{L}_{\text{breaking}}^{\text{SUSY}}$$

with

$$\mathcal{L}_{\text{global}}^{\text{SUSY}} = \mathcal{L}^{\text{SUSY}}(SU(3)_c \otimes SU(2)_L \otimes U(1)_Y; W)$$

¹² $M_{\text{Pl}} = (G_N/c\hbar)^{-1/2} \simeq 1.22 \times 10^{19}$ GeV, G_N Newton’s gravitational constant, c speed of light, \hbar Planck constant.

with W the following gauge invariant and B and L conserving superpotential¹³

$$W = W_Y - \mu H_1 H_2; \quad W_Y = \sum_F (h_U \tilde{Q}_L \tilde{U}_L^c H_2 + h_D \tilde{Q}_L \tilde{D}_L^c H_1 + h_L \tilde{L} \tilde{E}_L^c H_1)$$

(Y = Yukawa; F = families) where¹⁴ \tilde{Q}_L and \tilde{L} denote the $SU(2)_L$ doublets (\tilde{U}_L, \tilde{D}_L), (\tilde{N}_L, \tilde{E}_L) and $\tilde{U}_L^c, \tilde{D}_L^c, \tilde{E}_L^c$ are the scalar partners of the right-handed quarks and leptons, written as left-handed fields of the antiparticle (c = charge conjugation). $SU(2)_L$ and $SU(3)_c$ indices are summed over. h_U, h_D and h_L are the Yukawa couplings, the complex 3×3 matrices in family space of the SM. In the Minimal Super Gravity (mSUGRA) scheme, also related to the less constrained ‘‘Constrained MSSM’’ (CMSSM) [150], one assumes universality of all soft parameters.¹⁵ The mSUGRA ansatz exhibits super gravity induced SUSY breaking with $m_{3/2} = m_0$ at the bare level. In addition the Kähler flat supergravity relation $B_0 = A_0 - m_0$ implies that $\tan \beta$ in mSUGRA is not a free parameter. So mSUGRA exhibits only 3 free parameters $m_{1/2}, m_0$ and A_0 . The LSP in this scenario barely can accommodate the observed dark matter relic density (see [150] and references therein). The CMSSM drops the relation between B_0 and A_0 and assumes B_0 and μ to be quantities related to the EW symmetry breaking scale. In addition there is no relation between m_0 and the gravitino mass.

In this case the SUSY breaking term has the form

$$\mathcal{L}_{\text{breaking}}^{\text{SUSY}} = -m^2 \sum_i |\varphi_i|^2 - M \sum_a \lambda_a \lambda_a + (A m W_Y - B m \mu H_1 H_2 + \text{h.c.}).$$

¹³One could add other gauge invariant couplings like

$$(\tilde{U}_L^c \tilde{D}_L^c \tilde{D}_L^c), (\tilde{Q}_L \tilde{L} \tilde{D}_L^c), m(\tilde{L} H_2), (\tilde{L} \tilde{L} \tilde{E}_L^c)$$

which violate either B or L , however. In the minimal model they are absent.

¹⁴We label $U = (u, c, t)$, $D = (d, s, b)$, $N = (v_e, \nu_\mu, \nu_\tau)$ and $E = (e, \mu, \tau)$.

¹⁵Even with the constraints mentioned, SUSY extensions of the SM allow for about 100 free symmetry breaking parameters. Free parameters typically are masses and mixings of the neutralinos, the higgsino mass μ (the $+\mu H_1 H_2$ term of the 2HDM Higgs potential) and $\tan \beta$. This changes if one merges GUT concepts with SUSY, in fact SUSY-GUTs (e.g. as based on $SU(5)$) are the only theories which allow for grand unification broken at a low scale (~ 1 TeV). This provides strong constraints on the SUSY breaking mechanism, specifically we distinguish the constrained CMSSM a SUSY-GUT with soft breaking masses universal at the GUT scale. The NUHM is as CMSSM with non-universal Higgs masses: • the CMSSM defined to have universal couplings at the GUT scale has the free parameters: $m_0, m_{1/2}, A_0, \tan \beta$ and $\text{sign}(\mu)$. • NUHM1 considers M_A as an additional free parameter at the EW scale. • NUHM2 in addition assumes μ to be independent at the EW scale. These models assume many degeneracies of masses and couplings in order to restrict the number of parameters. Typically, SM parameters are supplemented by $m_{1/2}$ (scalar-matter mass, like $m_{\tilde{q}}, m_{\tilde{l}}$), m_0 (the $U(1)_Y \otimes SU(2)_L$ gaugino masses, $m_{\tilde{\gamma}}, m_{\tilde{z}}, m_{\tilde{W}}$ and gluino mass $m_{\tilde{g}}$), $\text{sign}(\mu), \tan \beta, A$ (trilinear soft breaking term), and more for less constrained models.

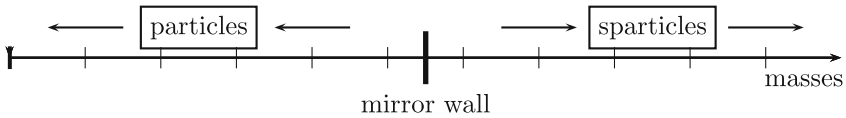
The essential new parameters are

- μ the supersymmetric higgsino mass
- m is the universal mass term for all scalars φ_i
- M is the universal mass term to all gauginos λ_a
- A, B are the breaking terms in the superpotential W .

Thus in addition to the SM parameters we have 5 new parameters

$$\mu, m, M, A \text{ and } B.$$

The SUSY breaking lifts the degeneracy between particles and sparticle and essentially makes all sparticles to be heavier than all particles.



This scenario leads to universal masses for all SUSY partners:

- s-matter: $m_{\tilde{q}} = m_{\tilde{l}} = m_{\tilde{H}} = m_{1/2}$
- gauginos: $M_3 = M_2 = M_1 = m_0$

where M_3, M_2 and M_1 are the mass scales of the spartners of the gauge bosons in $SU(3)_c, SU(2)_L$ and $U(1)_Y$, respectively. The non-observation of any sparticles so far requires a mass bound of about $m_{3/2}, m_{1/2}, m_0 \sim 100 \div 1000$ GeV, which is of the order of the weak scale 246 GeV or higher.

In general one expects different masses for the different types of gauginos:

- M' the $U(1)_Y$ gaugino mass
- M the $SU(2)_L$ gaugino mass
- $m_{\tilde{g}}$ the $SU(3)_c$ gluino mass.

However, the grand unification assumption

$$M' = \frac{5}{3} \tan^2 \Theta_W M = \frac{5}{3} \frac{\alpha}{\cos^2 \Theta_W \alpha_s} m_{\tilde{g}},$$

with $\sin^2 \Theta_W = 1 - M_W^2/M_Z^2$, leads back to the CMSSM scenario. A very attractive feature of this scenario is the fact that the known SM Yukawa couplings now may be understood by evolving couplings from the GUT scale down to low energy by the corresponding RG equations. One interesting outcome is that the Higgs mechanism gets triggered naturally as one of the running mass squares, the one of the Higgs boson, gets negative for appropriate regions in SUSY parameter space (there exist no-EWSB ranges as well). This also implies the form of the muon Yukawa coupling $y_\mu \propto \tan \beta$, as

$$y_\mu = \frac{m_\mu}{v_1} = \frac{m_\mu g_2}{\sqrt{2}M_W \cos \beta} \tag{7.47}$$

where $g_2 = e/\sin \Theta_W$ and $1/\cos \beta \approx \tan \beta$. This enhanced coupling is central for the discussion of the SUSY contributions to a_μ . In spite of the fact that SUSY and GUT extensions of the SM have completely different motivations and in a way are complementary, supersymmetrizing a GUT is very popular as it allows coupling constant unification together with a low GUT breaking scale which promises nearby new physics. Actually, supersymmetric $SU(5)$ circumvents the problems of the normal $SU(5)$ GUT and provides a viable phenomenological framework. The extra GUT symmetry requirement is attractive also because it reduces the number of independent parameters. The discovery of the Higgs boson of mass 125 GeV, which requires large squark masses in a SUSY extension of the SM, and the fact that no non-SM particle has been found at the LHC, largely rules out scenarios like the CMSSM. Nevertheless, such minimal scenarios may provide a viable starting point for proceeding with less constrained non-minimal SUSY models.

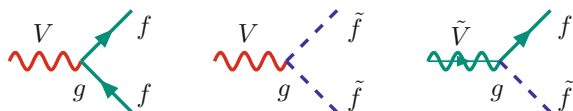
End of the Digression

While supersymmetrizing the SM fixes all gauge and Yukawa couplings of the sparticles (see Fig. 7.11), there are a lot of free parameters to fix the SUSY breaking and masses, such that mixings of the sparticles remain quite arbitrary: the mass eigenstates of the gaugino–Higgsino sector are obtained by unitary transformations which mix states with the same conserved quantum numbers (in particular the charge)

$$\chi_i^+ = V_{ij}\psi_j^+, \chi_i^- = U_{ij}\psi_j^-, \chi_i^0 = N_{ij}\psi_j^0 \tag{7.48}$$

where ψ_j^a denote the spin 1/2 sparticles of the SM gauge bosons and the two Higgs doublets. In fact, a SUSY extension of the SM in general exhibits more than 100 parameters, while the SM has 28 including masses and mixings parameters of the neutrinos. Also, in general SUSY extensions of the SM lead to tree level FCNCs and unsuppressed non-CKM type CP–violation, which both are absent in the SM, in agreement with observation. Actually, just a SUSY extension of the SM, while solving the pretended naturalness problem of the SM Higgs sector [151], creates its own naturalness problem as it leads to proton decay and the evaporation of baryonic matter in general. An elegant way to get rid of the latter problem is to impose the so called R –parity, which assigns $R_p = +1$ to all normal particles and $R_p = -1$ to all sparticles. If R –parity is conserved sparticles can only be produced in pairs and there must exist a stable Lightest Supersymmetric Particle (LSP), the lightest neutralino. Thus all sparticles at the end decay into the LSP plus normal matter. The LSP is

Fig. 7.11 Yukawa coupling = gauge coupling in the MSSM



a Cold Dark Matter (CDM) candidate [152] if it is neutral and colorless. From the precision mapping of the temperature and polarization anisotropies in the Cosmic Microwave Background (CMB), the Planck Collaboration has determined the relic density of cold dark matter to [96, 153, 154]

$$\Omega_{\text{CDM}} = \rho_{\text{CDM}}/\rho_{\text{crit}} = 0.1186(20)h^{-2} = 0.258(11). \quad (7.49)$$

This sets severe constraints on the SUSY parameter space [155–157]. Note that SUSY is providing a new source for CP–violation, which could help in understanding the matter–antimatter asymmetry $n_B = (n_b - n_{\bar{b}})/n_\gamma \simeq 6 \times 10^{-10}$ observed in our world.

However, what should cause R –parity to be conserved is another question. It just means that certain couplings one usually would assume to be there naturally are excluded. If R is not conserved sparticles may be produced singly and the LSP is not stable and would not provide a possible explanation of CDM. Then also (7.49) would not provide information on SUSY parameters.

The main theoretical motivation for a supersymmetric extension of the SM is the **hierarchy** or **naturalness** problem¹⁶ of the latter: chiral symmetry requires fermions to be massless, local gauge symmetries require the gauge bosons to be massless, so the only SM particle which is not required to be massless, before the spontaneous symmetry breaking by the Higgs mechanism, is the scalar Higgs boson, together with the mass–degenerate later Higgs–ghosts (all fields in the Higgs doublet). This argument, however, only is true in the symmetric phase. In the broken phase, triggered by a negative bare Higgs potential mass square term, all masses including the Higgs particle itself, exhibit a mass proportional to the Higgs VEV v according to (4.46). Therefore, the Higgs mass in the broken phase cannot be expected to be much larger than the heavier of the SM particles, unless the dimensionless Higgs self-coupling λ for unknown reasons would be much larger than the gauge couplings or the top quark Yukawa coupling. What is actually tuned when renormalizing the Higgs mass is λ because v is given as the universal electroweak scale, which is determined by the Fermi constant, an object independent of any SM interaction parameters at leading order or to all orders by definition. The Higgs VEV v is to be viewed as an orderparameter, which breaks the symmetry of the vacuum (by a collective long range order) and has no direct correlation to the short distance cutoff, which is the Planck mass if one equips the bare SM with a Planck cutoff (see [108, 151]).

¹⁶Stating that a small parameter (like a small mass) is unnatural unless the symmetry is increased by setting it to zero. The equivalent hierarchy problem addresses the fine–tuning problem encountered in Higgs mass renormalization: the renormalized (observed) low energy effective mass square

$$m_{\text{ren}}^2 = m_{\text{bare}}^2 - \delta m^2$$

is $O(v^2)$ of the order of the electroweak scale square, while in the bare theory exhibiting the Planck mass as a UV cutoff, m_{bare}^2 and the counterterm δm^2 are of order $\Lambda_{\text{Planck}}^2$. So the observed Higgs mass appears as a highly fine–tuned difference of two very large numbers. Exact supersymmetry eliminates the fine–tuning by canceling positive bosonic contributions to δm^2 exactly by negative fermionic ones, such that quadratic UV singularities are absent.

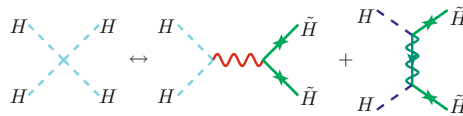
Table 7.8 Lower bounds (95% C.L.) on SUSY states. Bounds from LEP (ALEPH, DELPHI, L3, OPAL), Tevatron (CDF, D0) and LHC (ATLAS,CMS) [158, 159]

Object	Mass bound (GeV)		Comment	
Sleptons	$m_{\tilde{e},\tilde{\mu},\tilde{\tau}}$	>	98, 94, 82	$m_{\tilde{\mu}\tilde{\tau}} - m_{\tilde{\chi}_1^0} > 10, 15 \text{ GeV}$
Sbottom, stop	$m_{\tilde{b},\tilde{t}}$	>	600, 730	for $m_{\tilde{b},\tilde{t}} - m_{\tilde{\chi}_1^0} = 8, 10 \text{ GeV}$
Squarks $\neq \tilde{t}, \tilde{b}$	$m_{\tilde{q}}$	>	1450	
chargino	$m_{\tilde{\chi}_1^\pm}$	>	345	for $m_{\tilde{\nu}} > 300 \text{ GeV}$
Stable neutralino (LSP)	$m_{\tilde{\chi}_1^0}$	>	46	all $\tan \beta$, all Δm , all m_0
Unstable neutralino	$m_{\tilde{\chi}_1^0}$	>	380	$\tilde{\chi}_1^0 \rightarrow Z\tilde{G}$, GMSB ^a
Neutralinos $\tilde{\chi}_2^0, \tilde{\chi}_3^0, \tilde{\chi}_4^0$	$m_{\tilde{\chi}^0}$	>	345	
Charginos $\tilde{\chi}_1^\pm, \tilde{\chi}_2^\pm$	$m_{\tilde{\chi}^\pm}$	>	345	
Sneutrino $\tilde{\nu}$	$m_{\tilde{\nu}}$	>	94	
Gluino	$m_{\tilde{g}}$	>	1150	any $m_{\tilde{q}}[m_{\tilde{g}} = m_{\tilde{q}}]$

^aGauge mediated supersymmetry breaking (GMSB) is an elegant mechanism to transmit supersymmetry breaking from the hidden to the MSSM observable sector, which solves the supersymmetric flavor problem

In the symmetric phase the Higgs particles have a mass which is a truly free parameter, independent of it couplings. The only known symmetry which requires scalar particles to be massless in the symmetry limit is supersymmetry.¹⁷ Simply because a scalar is now always a supersymmetric partner of a fermion which is required to be massless by chiral symmetry. Thus only in a supersymmetric theory it is natural to have a “light” Higgs, so the commonly accepted jargon. In any case in a SUSY extension of the SM the lightest scalar h^0 , which corresponds to the SM Higgs, is bounded to have mass $m_{h^0} \leq M_Z$ at tree level.

It is one of the most striking consequences of supersymmetrizing the SM that the Higgs boson mass is a predicted quantity now, although depending on other new free parameters showing up in the SUSY extension. The basic reason is that supersymmetrizing the Higgs self-coupling $HHHH \leftrightarrow HH\tilde{H}\tilde{H}$ relates λ to the gauge and Yukawa couplings:



¹⁷Conformal symmetry would require severe fine tuning of parameters, just what we want to avoid in this context.

In the MSSM it implies constraints on the 2HDM potential (7.24):

$$\lambda_1 = \lambda_2 = -(\lambda_3 + \lambda_4 + \lambda_5) = \frac{1}{4} (g^2 + g'^2) ; \quad \lambda_4 = -\frac{1}{2}g^2 ; \quad \lambda_5 = 0 ,$$

and as a consequence, in the minimal SUSY models the masses of the extra Higgses at tree level are severely constrained by the following mass- and coupling-relationships:

$$M_{H^\pm}^2 = M_W^2 + M_A^2 , \quad M_{H,h}^2 = \frac{1}{2} \left(M_Z^2 + M_A^2 \pm \sqrt{(M_Z^2 - M_A^2)^2 + 4M_Z^2 M_A^2 \sin^2 2\beta} \right) ,$$

$$\tan(2\alpha) = \tan(2\beta) \frac{M_A^2 + M_Z^2}{M_A^2 - M_Z^2} , \quad \sin^2(\alpha - \beta) = \frac{M_H^2}{M_A^2} \frac{M_Z^2 - M_H^2}{M_Z^2 + M_A^2 - 2M_H^2} . \quad (7.50)$$

Only two independent parameters are left, which we may choose to be $\tan \beta$ and M_A .¹⁸ This tree level Higgs mass prediction receives large radiative corrections from the t/\tilde{t} sector (see Fig. 7.12), which changes the upper bound to [160]

$$m_{h^0}^2 \leq M_Z^2 + \frac{\sqrt{2}G_\mu}{2\pi^2 \sin^2 \beta} 3m_t^4 \ln \left(\frac{m_{\tilde{t}_1} m_{\tilde{t}_2}}{m_t^2} \right) + \dots \quad (7.51)$$

which in any case is well below 200 GeV. For improved bounds obtained by including higher order corrections¹⁹ I refer to [161, 162] (see also [163]). In the MSSM one

¹⁸In [138] the CP conserving 2HDM case is considered without imposing the $\Phi_2 \rightarrow -\Phi_2$ symmetry, which allows for two more terms in the potential $V \rightarrow V + [\lambda_6 (\Phi_1^\dagger \Phi_1) + \lambda_7 (\Phi_2^\dagger \Phi_2)] (\Phi_1^\dagger \Phi_2) + \text{h.c.}$. The CP-even mass matrix is of the form

$$\mathcal{M}^2 = \begin{pmatrix} \lambda_1 v^2 & \lambda_6 v^2 \\ \lambda_6 v^2 & M_A^2 + \lambda_5 v^2 \end{pmatrix}$$

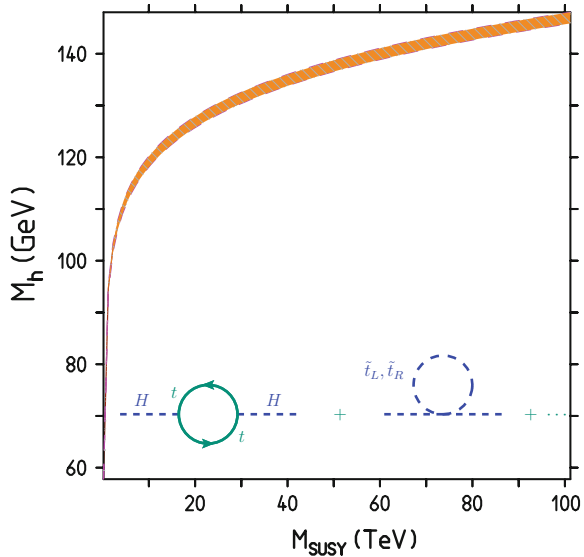
and one has to distinguish the following special limits:

- Decoupling limit: $M_A^2 \gg \lambda_1 v^2$ implying $M_h^2 \sim \lambda_1 v^2$ and $|c_{\beta-\alpha}| \ll 1$ and the lighter scalar h is the SM like one.
- Alignment limits: $\lambda_6 = 0$ with two possibilities:
 - (1) $\lambda_1 < \lambda_5 + M_A^2/v^2$ and again h is identical with the SM Higgs and $c_{\beta-\alpha} = 0$
 - (2) $\lambda_1 > \lambda_5 + M_A^2/v^2$ in which case H is identical with SM Higgs and $c_{\beta-\alpha} = 1$. This is an unexpected possibility, namely the discovered Higgs is to be identified the heavier scalar. The lighter would have masses in the range 20–90 GeV and would have escaped detection so far, because of suppressed couplings to SM states.

¹⁹Denoting by M_h^2 the corrected light Higgs on-shell mass, and by m_h^2 the tree level mass given in (7.50), then including leading logarithms in α_s and y_t up to 3 loops on finds

$$M_h^2 = m_h^2 + \hat{v}^2 \hat{y}_t^4 \left[12 L \kappa_L - 12 L^2 \kappa_L^2 \left(16 \hat{g}_3^2 - 3 \hat{y}_t^2 \right) \right. \\ \left. + 4 L^3 \kappa_L^3 \left(736 \hat{g}_3^4 - 240 \hat{g}_3^2 \hat{y}_t^2 - 99 \hat{y}_t^4 \right) + \dots \right] ,$$

Fig. 7.12 The MSSM lightest Higgs mass as a function of M_{SUSY} for $\tan \beta = 5$ and $m_A = 60$ GeV at 3 loops leading log order. Note that the M_{SUSY} independent “offset” LO value (7.50) depends substantially on m_A and $\tan \beta$, and thus also affects M_h . The stop mixing parameter X_t is chosen zero here. Inlaid diagrams: leading one-loop corrections to the Higgs pole mass



can reach $m_H \lesssim 135$ GeV, in non-minimal SUSY this limit can go up by 5 GeV or more [164]. In any case one has to relax from too much constraints on the SUSY parameter space to avoid conflict with phenomenological bounds. In Table 7.8 some important direct search bounds on sparticle masses are listed.

It is worthwhile to mention that in an exactly supersymmetric theory the anomalous magnetic moment must vanish, as observed by Ferrara and Remiddi in 1974 [165]:

$$a_\mu^{\text{tot}} = a_\mu^{\text{SM}} + \Delta a_\mu^{\text{SUSY}} = 0.$$

Thus, since $a_\mu^{\text{SM}} > 0$, in the SUSY limit, in the unbroken theory, we would have

$$\Delta a_\mu^{\text{SUSY}} = -a_\mu^{\text{SM}} < 0.$$

However, we know that SUSY must be drastically broken, not a single supersymmetric partner has been observed so far. All super-partners of existing particles seem to be too heavy to be produced up to now. If SUSY is broken a_μ may have either sign. In fact, the 3–4 standard deviation ($g_\mu - 2$)–discrepancy requires $\Delta a_\mu^{\text{SUSY}} > 0$, of the same sign as the SM contribution and of at least the size of the weak contribution [$\sim 200 \times 10^{-11}$] (see Fig. 3.8).

The leading SUSY contributions, like the weak SM contributions, are due to one-loop diagrams. Most interesting are the ones which get enhanced for large $\tan \beta$. Such supersymmetric contributions to a_μ stem from sneutrino–chargino and

(Footnote 19 continued)

with $L = \ln M_{\text{SUSY}}/M_t$, $\hat{v} = v^{\text{SM}}(M_t)$, $\hat{g}_3 = g_3^{\text{SM}}(M_t)$, $\hat{y}_t = y_t^{\text{SM}}(M_t)$ and $\kappa_L = 1/(16\pi^2)$. The 3-loop term is scheme dependent and depends on specific approximations made [161].

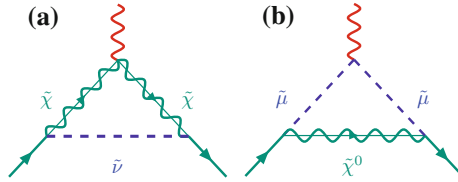


Fig. 7.13 Physics beyond the SM: leading SUSY contributions to $g - 2$ in a supersymmetric extension of the SM. Diagrams **a** and **b** correspond to diagrams **a** and **b** of Fig. 7.4, respectively

smuon–neutralino loops Fig. 7.13 and yield [166–169]:

$$\Delta a_\mu^{\text{SUSY (1)}} = a_\mu^{\chi^\pm} + a_\mu^{\chi^0} \tag{7.52}$$

with

$$a_\mu^{\chi^\pm} = \frac{m_\mu}{16\pi^2} \sum_k \left\{ \frac{m_\mu}{12m_{\tilde{\nu}_\mu}^2} (|c_k^L|^2 + |c_k^R|^2) F_1^C(x_k) + \frac{m_{\chi_k^\pm}}{3m_{\tilde{\nu}_\mu}^2} \text{Re}[c_k^L c_k^R] F_2^C(x_k) \right\}$$

$$a_\mu^{\chi^0} = \frac{m_\mu}{16\pi^2} \sum_{i,m} \left\{ -\frac{m_\mu}{12m_{\tilde{\mu}_m}^2} (|n_{im}^L|^2 + |n_{im}^R|^2) F_1^N(x_{im}) + \frac{m_{\chi_i^0}}{3m_{\tilde{\mu}_m}^2} \text{Re}[n_{im}^L n_{im}^R] F_2^N(x_{im}) \right\}$$

and $k = 1, 3$ and $i = 1, \dots, 4$ denote the chargino and neutralino indices, $m = 1, 2$ is the smuon index, and the couplings are given by

$$c_k^L = -g_2 V_{k1},$$

$$c_k^R = y_\mu U_{k2},$$

$$n_{im}^L = \frac{1}{\sqrt{2}} (g_1 N_{i1} + g_2 N_{i2}) U_{m1}^{\tilde{\mu}*} - y_\mu N_{i3} U_{m2}^{\tilde{\mu}*},$$

$$n_{im}^R = \sqrt{2} g_1 N_{i1} U_{m2}^{\tilde{\mu}} + y_\mu N_{i3} U_{m1}^{\tilde{\mu}},$$

with mixing matrices V_{ij} , U_{ij} and N_{ij} defined in (7.48). The kinematical variables are the mass ratios $x_k = m_{\chi_k^\pm}^2/m_{\tilde{\nu}_\mu}^2$, $x_{im} = m_{\chi_i^0}^2/m_{\tilde{\mu}_m}^2$, and the one-loop vertex functions read

$$F_1^C(x) = \frac{2}{(1-x)^4} [2 + 3x - 6x^2 + x^3 + 6x \ln x],$$

$$F_2^C(x) = \frac{3}{2(1-x)^3} [-3 + 4x - x^2 - 2 \ln x],$$

$$F_1^N(x) = \frac{2}{(1-x)^4} [1 - 6x + 3x^2 + 2x^3 - 6x^2 \ln x],$$

$$F_2^N(x) = \frac{3}{(1-x)^3} [1 - x^2 + 2x \ln x],$$

and are normalized to $F_i^J(1) = 1$. The functions $F_i^C(x)$ are the ones calculated in (7.13) and $F_i^N(x)$ in (7.16), respectively. The couplings g_i denote the $U(1)$ and $SU(2)$ gauge couplings $g_1 = e/\cos\Theta_W$ and $g_2 = e/\sin\Theta_W$, respectively, and y_μ is the muon's Yukawa coupling (7.47). The interesting aspect of the SUSY contribution to a_μ is that they are enhanced for large $\tan\beta$ in contrast to SUSY contributions to electroweak precision observables, which mainly affect $\Delta\rho$ which determines the ρ -parameter and contributes to M_W . The anomalous magnetic moment thus may be used to constrain the SUSY parameter space.

Simplifying (7.52) to include the most relevant terms only, we note that the leading SUSY contributions [167, 168] to the muon $g-2$ are given by the chargino–sneutrino loop

$$a_\mu^{\chi^\pm} = \frac{\alpha m_\mu^2 M_2 \mu \tan\beta}{4\pi \sin^2\theta_W m_{\tilde{\nu}_\mu}^2} \left(\frac{f_\chi(M_2^2/m_{\tilde{\nu}_\mu}^2) - f_\chi(\mu^2/m_{\tilde{\nu}_\mu}^2)}{M_2^2 - \mu^2} \right) \quad (7.53)$$

and the bino–smuon loop

$$a_\mu^{\chi^0} = \frac{\alpha m_\mu^2 M_1 (\mu \tan\beta - A_\mu)}{4\pi \cos^2\theta_W (m_{\tilde{\mu}_R}^2 - m_{\tilde{\mu}_L}^2)} \left(\frac{f_N(M_1^2/m_{\tilde{\mu}_R}^2)}{m_{\tilde{\mu}_R}^2} - \frac{f_N(M_1^2/m_{\tilde{\mu}_L}^2)}{m_{\tilde{\mu}_L}^2} \right) \quad (7.54)$$

where $m_{\tilde{\mu}_L}$ and $m_{\tilde{\mu}_R}$ are the smuon masses and

$$f_\chi(x) = \frac{x^2 - 4x + 3 + 2\ln x}{(1-x)^3}, \quad f_\chi(1) = -2/3,$$

$$f_N(x) = \frac{x^2 - 1 - 2x \ln x}{(1-x)^3}, \quad f_N(1) = -1/3.$$

For most of the MSSM parameter space $\Delta a_\mu^{\text{SUSY}}$ is dominated by the chargino–smuon contribution, which decouples for large $m_{\tilde{\nu}_\mu}^2$. However, this contribution can still be of the order of the SM weak contribution a_μ^{EW} even when the masses are much larger than M_W because of the $\tan\beta$ enhancement of the muon Yukawa coupling.

An expansion in $1/\tan\beta$ and because SUSY partners of SM particles are heavier than the latter one usually also expands in M_W/M_{SUSY} which is leading to the handy approximations

$$a_\mu^{\chi^\pm} = \frac{g_2^2}{32\pi^2} \frac{m_\mu^2}{M_{\text{SUSY}}^2} \text{sign}(\mu M_2) \tan\beta \left[1 + O(\tan\beta^{-1}, M_W/M_{\text{SUSY}}) \right],$$

$$a_\mu^{\chi^0} = \frac{g_1^2 - g_2^2}{192\pi^2} \frac{m_\mu^2}{M_{\text{SUSY}}^2} \text{sign}(\mu M_2) \tan\beta \left[1 + O(\tan\beta^{-1}, M_W/M_{\text{SUSY}}) \right],$$

where parameters have been taken to be real and M_1 and M_2 of the same sign. Provided all SUSY masses are about equal to M_{SUSY} and $\tan \beta$ has moderate values one then obtains

$$\Delta a_\mu^{\text{SUSY}} \simeq \text{sign}(\mu) \frac{\alpha(M_Z)}{8\pi \sin^2 \Theta_W} \frac{(5 + \tan^2 \Theta_W)}{6} \frac{m_\mu^2}{\tilde{m}^2} \tan \beta \left(1 - \frac{4\alpha}{\pi} \ln \frac{\tilde{m}}{m_\mu} \right) \quad (7.55)$$

\tilde{m} a typical SUSY loop mass and μ is the Higgsino mass. Here we also included the leading 2-loop QED logarithm as an RG improvement factor [170]. In Fig. 7.14 contributions are shown for various values of $\tan \beta$. Above $\tan \beta \sim 5$ and $\mu > 0$ the SUSY contributions from the diagrams Fig. 7.13 easily could explain the observed deviation (7.3) with SUSY states of masses in the interesting range 100 to 500 GeV. However, after the LHC experiments ATLAS and CMS have pushed up the limits on possible sparticles masses, we observe a possible conflict and previously favored SUSY scenarios like CMSSM are ruled out. Therefore one should look at the SUSY setup more closely. What matters are the sleptons, neutralinos and charginos which are to be light to explain the muon $g - 2$ discrepancy. In contrast squarks are favored to be rather heavy in order to explain the Higgs boson mass and to satisfy the LHC bounds. Indeed a hierarchy

$$m_{\tilde{q}} \gg m_{\tilde{\ell}}, m_{\tilde{\chi}^\pm}, m_{\tilde{\chi}^0}$$

still is perfectly in accord with the limits collected in Table 7.8. Perspectives for direct searches of neutralinos and sleptons at the LHC are discussed in [171].

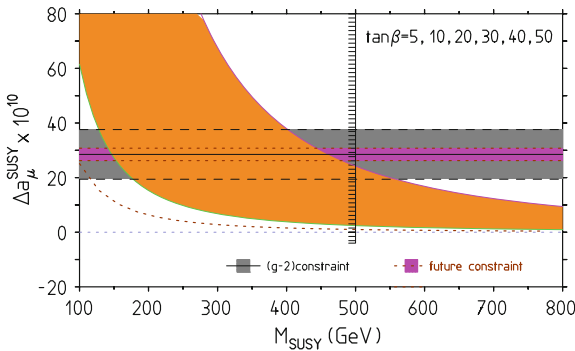


Fig. 7.14 Constraint on large $\tan \beta$ SUSY contributions as a function of M_{SUSY} . The horizontal band shows $\Delta a_\mu^{\text{NP}} = \Delta a_\mu$. The region left of $M_{\text{SUSY}} \sim 500$ GeV is excluded by LHC searches for CMSSM scenarios with M_{SUSY} a universal SUSY mass. For $m_h \sim 125$ GeV actually $M_{\text{SUSY}} > 800$ GeV depending on details of the stop sector ($\{\tilde{t}_1, \tilde{t}_2\}$ mixing and mass splitting) and weakly on $\tan \beta$. Orange shaded range $\tan \beta = 5 \div 50$

More recently, also the $\tan^2 \beta$ enhanced contributions have been calculated [172].²⁰ They arise from the $\tan \beta$ enhanced shift $\Delta_\mu \propto \alpha \tan \beta$ in the on mass-shell muon mass renormalization:

$$m_\mu \rightarrow m_\mu + \delta m_\mu = \frac{m_\mu}{1 + \Delta_\mu} + \text{non-}\tan \beta\text{-enhanced terms.} \quad (7.56)$$

In the case that all SUSY masses are equal and much larger than M_W the correction reads

$$\Delta_\mu \simeq -0.0018 \tan \beta \text{ sign}(\mu). \quad (7.57)$$

Extracting $\tan \beta$ from a_μ^{exp} , the resulting value would be smaller by about 10% when $\tan \beta \sim 50$. Corrections can be even larger in certain regions of SUSY parameter space. Typically, for large $\tan \beta$ they are larger than other 2-loop contributions. The contributions of the 2HDM sector of the MSSM have been discussed earlier in Sect. 7.2.4.

The very large $\tan \beta$ regime (motivated by the possibility that v_1 could be vanishing and the muon mass induced radiatively as advocated e.g. in [87]) has been studied in [173]. In the simplified case that all SUSY masses are equal to M_{SUSY} and $\tan \beta$ is moderate the one loop SUSY result takes the form

$$\Delta a_\mu^{\text{SUSY,1L}} \approx 13 \times 10^{-10} \text{ sign}(\mu) \tan \beta \left(\frac{100 \text{ GeV}}{M_{\text{SUSY}}} \right)^2.$$

For large $\tan \beta$ higher order terms change the linear behavior in $\tan \beta$. The higher order terms can be resummed [172] to

$$\Delta a_\mu^{\text{SUSY}} = \frac{\Delta a_\mu^{\text{SUSY,1L}}}{1 + \Delta_\mu},$$

which has finite limit

$$\Delta a_\mu^{\text{SUSY}} = \lim_{\tan \beta \rightarrow \infty} \frac{\Delta a_\mu^{\text{SUSY,1L}}}{\Delta_\mu} \approx -72 \times 10^{-10} \left(\frac{1 \text{ TeV}}{M_{\text{SUSY}}} \right)^2$$

still assuming degenerate SUSY masses. If we want to make SUSY effects responsible for positive deviation Δa_μ the case that all SUSY masses are of similar size is ruled out. In order to get a positive result one has to assume large mass splittings. Two possible regimes, which are not in conflict with bounds from other observables, have been considered in [173]:

- the $\tilde{B} \tilde{\mu}_L \tilde{\mu}_R$ contributions dominate for $M_1, m_L, m_R \ll \mu$: “large μ -limit”,
- the $\tilde{B} \tilde{H} \tilde{\mu}_L$ contributions dominate for $M_1, \mu, m_R \ll m_L$: “ $\tilde{\mu}_R$ -dominance”.

²⁰The highest power in $\tan \beta$ at a given order L in the loop expansion is $\alpha^L \tan^L \beta$. As a correction only the leading one of order $\alpha^2 \tan^2 \beta$ is numerically significant.

We remind that gauginos are denoted by \tilde{W} for the $SU(2)$ and by \tilde{B} for the $U(1)_Y$ gauge groups. In both regimes the result changes to

$$\Delta a_{\mu \text{lim}}^{\text{SUSY}} \approx 37 \times 10^{-10} \left(\frac{1 \text{ TeV}}{M_{\text{SUSY}}} \right)^2,$$

assuming $M_A = 50 \text{ GeV}$. Typically, of order 1σ effects are obtained only for sufficiently small M_A and sufficiently large $\tan \beta$. This behavior is reflecting what happens in general two Higgs doublet models of type II and X, as discussed before.

A remarkable 2-loop calculation within the MSSM has been performed by Heinemeyer, Stöckinger and Weiglein [140]. They evaluated the exact 2-loop correction of the SM 1-loop contributions Figs. 4.1, and 4.18. These are all diagrams where the μ -lepton number is carried only by μ and/or ν_μ . In other words, SM diagrams with an additional insertion of a closed sfermion- or charginos/neutralino-loop. Thus the full 2-loop result from the class of diagrams with closed sparticle loops is known. This class of SUSY contributions is interesting because it has a parameter dependence completely different from the one of the leading SUSY contribution and can be large in regions of parameter space where the 1-loop contribution is small. The second class of corrections are the 2-loop corrections to the SUSY 1-loop diagrams Fig. 7.13, where the μ -lepton number is carried also by $\tilde{\mu}$ and/or $\tilde{\nu}_\mu$. This class of corrections is expected to have the same parameter dependence as the leading SUSY 1-loop ones and only the leading 2-loop QED corrections are known [170] as already included in (7.55). More recently, an extended more complete calculation has been presented in [174].

The prediction of $\Delta a_{\mu}^{\text{SUSY}}$ as a function of the mass of the Lightest Observable SUSY Particle $M_{\text{LOSP}} = \min(m_{\tilde{\chi}_1^\pm}, m_{\tilde{\chi}_2^0}, m_{\tilde{f}_i})$, from a MSSM parameter scan with $\tan \beta = 50$, including the 2-loop effects is shown in Fig. 7.15. Plotted is the maximum value of a_μ obtained by a scan of that part of SUSY parameter space which is allowed by the other observables like m_h , M_W and the b -decays. The 2-loop corrections in general are moderate (few %). However, not so for lighter M_{LOSP} in case of heavy smuons and sneutrinos when corrections become large (see also [175]). The remaining uncertainty of the calculation has been estimated to be below 3×10^{-10} , which is satisfactory in the present situation. This may however depend on details of the SUSY scenario and of the parameter range considered. A comprehensive review on supersymmetry, the different symmetry breaking scenarios and the muon magnetic moment has been presented by Stöckinger [169]. Low energy precision test of supersymmetry and present experimental constraints also are reviewed and discussed in [176].

The results for the SUSY contributions to a_μ up to two-loops may be found in [169, 172, 174], and may be written as

$$\begin{aligned} \Delta a_{\mu}^{\text{SUSY}} = & \Delta a_{\mu}^{\text{SUSY,1L}} \left(1 - \frac{4\alpha}{\pi} \log \frac{M_{\text{SUSY}}}{m_{\mu}} \right) \left(\frac{1}{1 + \Delta_{\mu}} \right) + a_{\mu}^{(\chi\gamma H)} + a_{\mu}^{(\tilde{f}\gamma H)} \\ & + a_{\mu}^{(\chi\{W,Z\}H)} + a_{\mu}^{(\tilde{f}\{W,Z\}H)} + a_{\mu}^{\text{SUSY,ferm,2L}} + a_{\mu}^{\text{SUSY,bos,2L}} + \dots \quad (7.58) \end{aligned}$$

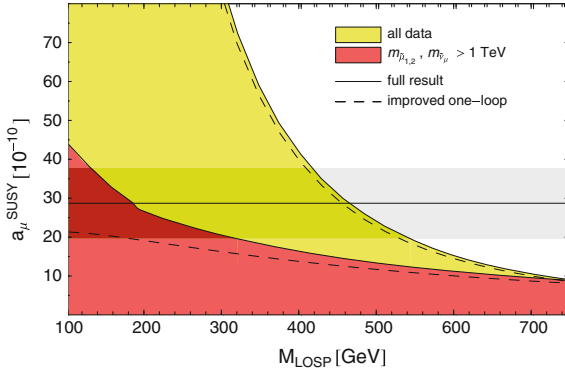


Fig. 7.15 Allowed values of MSSM contributions to a_μ as a function of the mass of the Lightest Observable SUSY Particle M_{LOSP} , from an MSSM parameter scan with $\tan\beta = 50$. The 1σ region corresponding to the deviation (7.3) is indicated as a horizontal band. The *yellow* region corresponds to all input parameter points that satisfy the experimental constraints from b -decays, m_h (here prior to the Higgs discovery) and $\Delta\rho$. In the *red* region, smuons and sneutrinos are heavier than 1 TeV. The *dashed lines* correspond to the contours that arise from ignoring the 2-loop corrections from chargino/neutralino- and sfermion-loop diagrams. Courtesy of D. Stöckinger [169]

The labels ($\chi\gamma H$) etc. identify contributions from Fig. 7.9b type diagrams which would be labeled by $(\tau h\gamma)$, with possible replacements $\gamma \rightarrow V = \gamma, Z, W^\pm, h \rightarrow H = h, H, A, H^\pm$ and $\tau^\mp \rightarrow X = \chi^\mp, \chi^0, \tilde{f}$. Contributions (XVV) correspond to Fig. 4.19a, d with corresponding substitutions. The remaining terms $a_\mu^{\text{SUSY, ferm. 2L}}$ and $a_\mu^{\text{SUSY, bos. 2L}}$ denote small terms like the fermionic contribution Fig. 7.9b and the bosonic contributions Fig. 7.9c, d, which differ from the SM result due to the modified Higgs structure. The ellipsis denote the known but negligible 2-loop contributions as well as the missing 2-loop and higher order contributions. As in the 2HDM case, all leading terms come from Barr-Zee type diagrams. In terms of the functions $F_{h,H}(z) = z g_{h,H}(z)$ and $F_A(z) = z g_A(z)$ with $g_i(z)$ given by (7.36), the results read [98, 99, 139, 141, 175, 177]

$$a_\mu^{(\chi\gamma H)} = \frac{\sqrt{2}G_\mu m_\mu^2}{8\pi^2} \frac{\alpha}{\pi} \sum_{k=1,2} \left[\text{Re}[\lambda_\mu^A \lambda_{\chi_k^+}^A] F_A(m_{\chi_k^+}^2/m_A^2) + \sum_{S=h,H} \text{Re}[\lambda_\mu^S \lambda_{\chi_k^+}^S] F_h(m_{\chi_k^+}^2/m_S^2) \right],$$

$$a_\mu^{(\tilde{f}\gamma H)} = \frac{\sqrt{2}G_\mu m_\mu^2}{8\pi^2} \frac{\alpha}{\pi} \sum_{\tilde{f}=\tilde{t},\tilde{b},\tilde{\tau}} \sum_{i=1,2} \left[\sum_{S=h,H} (N_c Q^2)_{\tilde{f}} \text{Re}[\lambda_\mu^S \lambda_{\tilde{f}_i}^S] F_{\tilde{f}}(m_{\tilde{f}_i}^2/m_S^2) \right],$$

with $F_{\tilde{f}}(z) = z(2 + \ln z - F_A(z))/2$ and couplings (see Eqs. (7.29, 7.48))

$$\begin{aligned}\lambda_{\mu}^{h,H,A} &= (-\sin \alpha / \cos \beta, \cos \alpha / \cos \beta, \tan \beta), \\ \lambda_{\chi_k^+}^{h,H,A} &= \sqrt{2} M_W / m_{\chi_k^+} (U_{k1} V_{k2} (\cos \alpha, \sin \alpha, -\cos \beta) + U_{k2} V_{k1} (-\sin \alpha, \cos \alpha, -\sin \beta)), \\ \lambda_{\tilde{t}_i}^{h,H} &= 2m_{\tau} / (m_{\tilde{t}_i}^2 \cos \beta) (-\mu^* (\cos \alpha, \sin \alpha) + A_{\tau} (-\sin \alpha, \cos \alpha)) (U^{\tilde{t}_{i1}})^* U^{\tilde{t}_{i2}}.\end{aligned}$$

The last expression given for the \tilde{t} applies to the \tilde{b} with $\tau \rightarrow b$ everywhere, and for the \tilde{t} with $\tau \rightarrow t$ together with $(\mu, \cos \beta, \cos \alpha, \sin \alpha) \rightarrow (-\mu, \sin \beta, \sin \alpha, -\cos \alpha)$.

For the potentially enhanced Barr-Zee type contributions the following simple approximations have been given [15, 169]:

$$\begin{aligned}a_{\mu}^{(\chi^{VH})} &\approx 11 \times 10^{-10} \left(\frac{\tan \beta}{50} \right) \left(\frac{100 \text{ GeV}}{M_{\text{SUSY}}} \right)^2 \text{sign}(\mu M_2), \\ a_{\mu}^{(\tilde{\gamma}^H)} &\approx -13 \times 10^{-10} \left(\frac{\tan \beta}{50} \right) \left(\frac{m_t}{m_{\tilde{t}}} \right) \left(\frac{\mu}{20 M_H} \right) \text{sign}(X_t), \\ a_{\mu}^{(\tilde{b}^H)} &\approx -3.2 \times 10^{-10} \left(\frac{\tan \beta}{50} \right) \left(\frac{m_b \tan \beta}{m_{\tilde{b}}} \right) \left(\frac{A_b}{20 M_H} \right) \text{sign}(\mu).\end{aligned}$$

The parameter X_t is determined by the SUSY breaking parameter A_f , μ and $\tan \beta$ by $X_t = A_t - \mu^* \cot \beta$. Like for the leading 1-loop case, the first approximation applies if all SUSY masses are approximately equal (e.g. $\mu \sim M_2 \sim m_A$) (but the relevant masses are different in the two cases), and the second and third are valid if the stop/sbottom mixing is large and the relevant stop/sbottom and Higgs masses are of similar size. We refer to the review by Stöckinger [169] for a more detailed presentation of the higher order SUSY effects. The latter have been reconsidered and updated recently in [174].

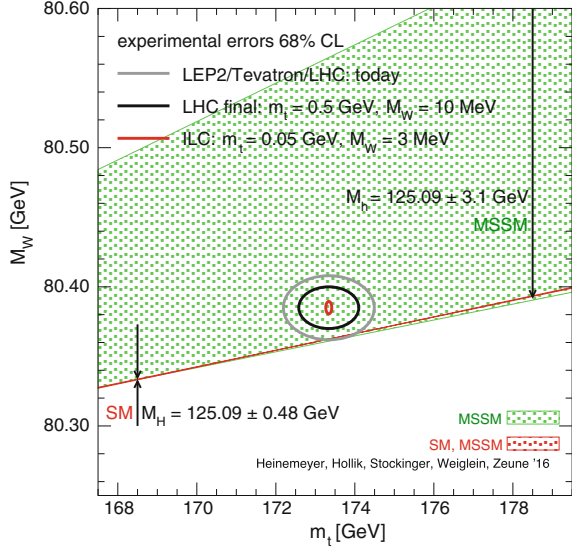
Constraints from M_W

Here we are looking at SM precision observables like G_F (muon lifetime), Z observables M_Z , Γ_Z , g_V , g_A , $\sin^2 \Theta_{\text{eff}}$ (LEP1/SLD) W boson and t quark observables M_W , Γ_W , m_t and Γ_t (LEP2/Tevatron/LHC). An important observable is the W mass predicted to satisfy

$$M_W^2 \left(1 - \frac{M_W^2}{M_Z^2} \right) = \frac{\pi \alpha}{\sqrt{2} G_F} (1 + \Delta r), \quad (7.59)$$

where $\Delta r = f(\alpha, G_F, M_Z, m_t, \dots)$ represents the radiative correction to the tree level mass-coupling relation, which depends on the independent parameters of the theory. They differ from the SM by additional contributions in extensions of the SM and thus allow to constrain the parameter space of the extended model. In SUSY models M_W is sensitive to the top/stop sector parameters and actually M_W is essentially the only observable which tends to slightly improve the fit when including MSSM

Fig. 7.16 Prediction for M_W as a function of m_t . The green region shows the allowed region for the MSSM M_W prediction. It has been obtained by scanning over the MSSM parameters as described in [178]. The cuts $m_{\tilde{\tau}_2}/m_{\tilde{\tau}_1} < 2.5$ and $m_{\tilde{b}_2}/m_{\tilde{b}_1} < 2.5$ are applied. The red strip indicates the overlap region of the SM and the MSSM, with $M_M^{\text{SM}} = 125.6 \pm 0.7$ GeV. The two arrows indicate the possible size of the slepton and the chargino (and neutralino) contributions. Courtesy of S. Heinemeyer et al. Reproduced from [178]



contributions. This is shown in Fig. 7.16. In contrast, the other well controlled precision observable $\sin^2 \Theta_{\text{eff}}$, as defined in terms of the Z boson NC couplings (4.36),

$$\sin^2 \Theta_{\text{eff}} = \frac{1}{4} \left(1 - \text{Re} \frac{v_{\text{eff}}}{a_{\text{eff}}} \right), \quad (7.60)$$

remains unaffected when including SUSY effects [181] (see Figs. 14 and 15 of [182] and Fig. 1 of [183] and Fig. 4 of [181]). The global fit of LEP data [184] does not improve when going from the SM to the MSSM, i.e. SUSY effects are strongly constrained here. MSSM results merge into SM results for larger SUSY masses, as decoupling is at work.

In comparison to $(g_\mu - 2)$, the SM prediction of M_W [185, 186], as well as of other electroweak observables, as a function of m_t for given α , G_μ and M_Z , is in much better agreement with the experimental result (at 1σ), although the MSSM prediction for suitably chosen MSSM parameters is slightly favored by the data, as shown in Fig. 7.16. The very recent M_W determination by ATLAS moves results closer towards the SM prediction as shown in Fig. 7.17. Thus large extra corrections to the ones of the SM are not tolerated. The radiative shift of M_W is represented by (4.42) and the leading SUSY contributions mainly come in via $\Delta\rho$. As we know, $\Delta\rho$ is most sensitive to weak isospin splitting and in the SM is dominated by the contribution from the (t, b) -doublet. In the SUSY extension of the SM these effects are enhanced by the contributions from the four SUSY partners $\tilde{t}_{L,R}, \tilde{b}_{L,R}$ of t, b , which can be as large as the SM contribution itself for $m_{1/2} \ll m_t$ [light SUSY], and tends to zero for $m_{1/2} \gg m_t$ [heavy SUSY]. It is important to note that these contributions are not enhanced by $\tan \beta$. Thus, provided $\tan \beta$ enhancement is at

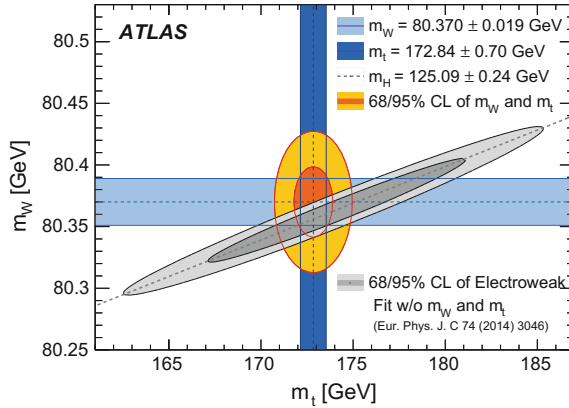


Fig. 7.17 The 68 and 95% confidence-level contours of the M_W and m_t indirect determination from the global electroweak fit [179] are compared to the 68 and 95% confidence-level contours of the ATLAS measurements of the top-quark and W-boson masses. The determination from the electroweak fit uses as input the LHC measurement of the Higgs-boson mass, $m_H = 125.09 \pm 0.24$ GeV [66]. Reprinted from [180], CERN-EP-2016-305: ©2016-2017 CERN (License: CC-BY-4.0)

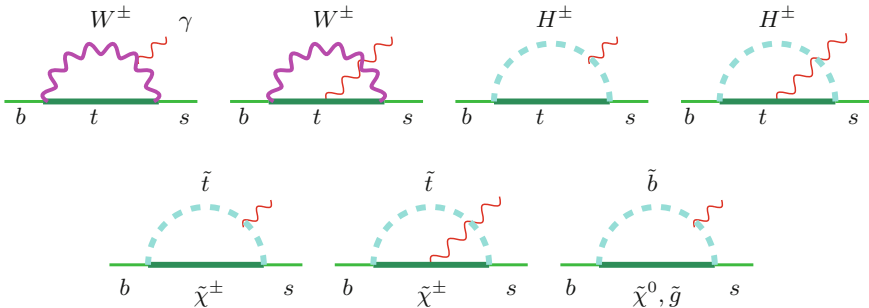


Fig. 7.18 Leading graphs in $b \rightarrow s\gamma$. SM, 2HDM and SUSY specific contributions

work, it is quite natural to get a larger SUSY contribution to $(g_\mu - 2)$ than to M_W , otherwise some tension between the two constraints would be there as M_W prefers the heavy SUSY domain.

Constraints from B -physics

Data on the penguin loop induced $B \rightarrow X_s \gamma$ transition (see Fig. 7.18) yields another strong constraint on deviations from the SM [187]. Indeed, the SM prediction [70, 188, 189] $\text{BR}(b \rightarrow s\gamma)_{\text{NNLL}} = (3.15 \pm 0.23) \times 10^{-4}$ is consistent within 1.2σ with the experimental result [96, 190] $\text{BR}(b \rightarrow s\gamma) = (3.43 \pm 0.22) \times 10^{-4}$. It implies that SUSY requires heavier $m_{1/2}$ and/or m_0 in order not to spoil the good agreement.

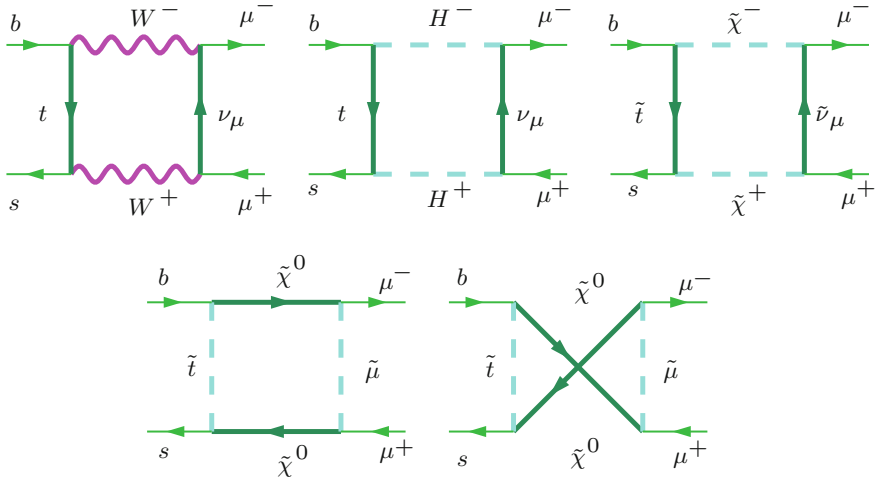


Fig. 7.19 Leading graphs in $B_s \rightarrow \mu^+ \mu^-$. SM, 2HDM and SUSY specific contributions

The very rare box loop induced decay $B_s \rightarrow \mu^+ \mu^-$ (see Fig. 7.19) is very interesting because SUSY contributions (box contributions with W 's replaced by charged Higgses H^\pm) are able to enhance the SM value $\text{BR}(B_s \rightarrow \mu^+ \mu^-) = (3.1 \pm 1.4) \times 10^{-9}$ by two orders of magnitude, especially in scenarios with non-universal Higgs masses (NUHM). A first measurement recently by LHCb [96, 191] found $\text{BR}(B_s \rightarrow \mu^+ \mu^-) = 2.8_{-0.6}^{+0.7} \times 10^{-9}$, in agreement with the SM value. Again this is limiting significant effects from physics beyond the SM.

Since the SM predictions are in good agreement with the experimental values (7.8), only small extra radiative corrections are allowed (1.5σ). Generally, in SUSY extensions of the SM [192], this excludes light $m_{1/2}$ and m_0 , requiring larger values depending on $\tan \beta$. Reference [188] also illustrates the updated $b \rightarrow s \gamma$ bounds on M_{H^\pm} (> 295 GeV for $2 \leq \tan \beta$) in the 2HDM (Type II) [193]. Important constraints also come from $B_u \rightarrow \tau \nu$ [194].

Constraints from CDM

In R -parity conserving SUSY extensions which provide a dark matter candidate the CDM constraint (7.49) can have a tough impact on the SUSY scenario, as can be observed in Fig. 7.20 where the different constraints are combined. The upper panel illustrates the pre-LHC situation when the Higgs mass has been assumed to lie at most little above the LEP limit $m_H \simeq 114$ GeV. It was truly remarkable that in spite of the different highly non-trivial dependencies on the MSSM parameters, with $g - 2$ favoring definitely $\mu > 0$, $\tan \beta$ large and/or light SUSY states, there is a common allowed range, although a quite narrow one, depending strongly on $\tan \beta$.

Before the Higgs discovery and LHC mass bounds, assuming the CMSSM scenario, besides the direct limits from LEP and Tevatron, the most important constraints were coming from $(g_\mu - 2)$, $b \rightarrow s \gamma$ and from the dark matter relic density (cosmo-

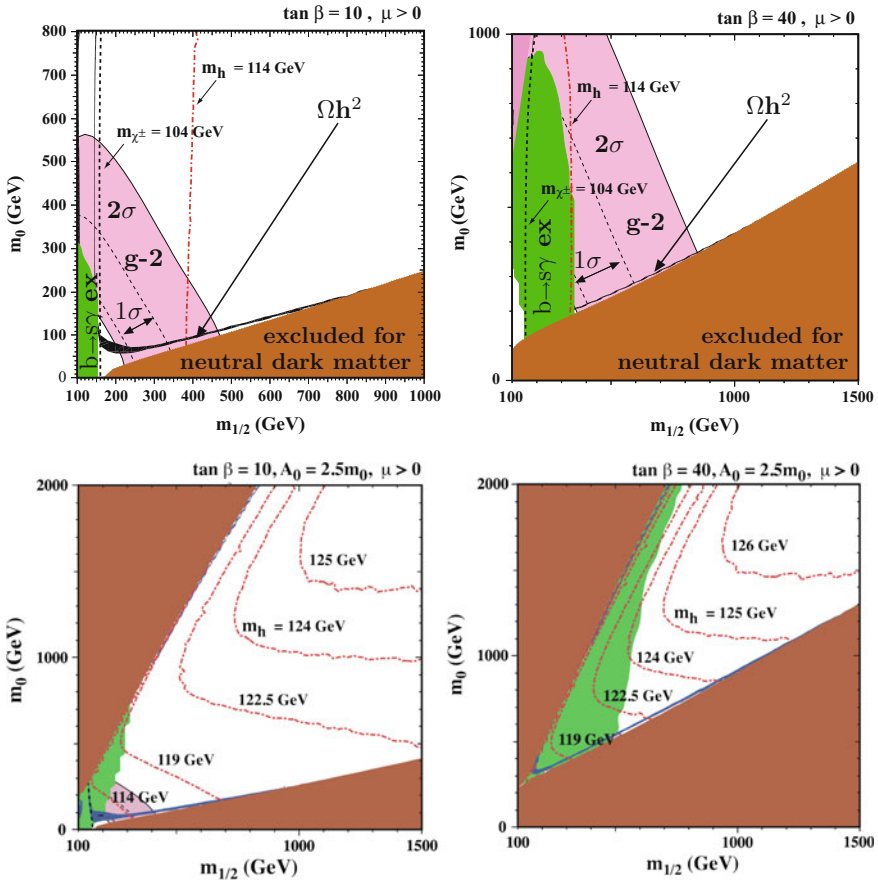


Fig. 7.20 *Top row* the pre-LHC case. The $(m_0, m_{1/2})$ plane for $\mu > 0$ for **a** $\tan \beta = 10$ and **b** $\tan \beta = 40$ in the CMSSM scenario. The allowed region by the cosmological neutral dark matter constraint (7.49) is shown by the *black/blue* parabolic shaped region. The disallowed region where $m_{\tilde{\tau}_1} < m_\chi$ has *brown* shading. The regions excluded by $b \rightarrow s\gamma$ have *green* shading (*left*). The $(g_\mu - 2)$ favored region at the 2σ [$(287 \pm 182) \times 10^{-11}$] (between dashed lines the 1σ [$(287 \pm 91) \times 10^{-11}$] band) level has *pink* shading. The LEP constraint on $m_{\chi^\pm} = 104$ GeV and $m_h = 114$ GeV are shown as near vertical lines excluding the region left of it. *Bottom row* after LHC run I. The Higgs discovery has changed it all. Plot courtesy of K. Olive updated from [155] upper part and from [157], with kind permission of The European Physical Journal (EPJ) [lower part]

logical bound on CDM given in (7.49) [155, 156]. Due to the precise value of Ω_{CDM} the lightest SUSY fermion (sboson) of mass m_0 is given as a function of the lightest SUSY boson (sfermion) with mass $m_{1/2}$ within a narrow band. This is illustrated in Fig. 7.20 together with the constraints from $(g_\mu - 2)$ (7.3) and $b \rightarrow s\gamma$ (7.8). Since m_h for given $\tan \beta$ is fixed by $m_{1/2}$ via (7.51) with $\min(m_{\tilde{\tau}_i}; i = 1, 2) \sim m_{1/2}$, the allowed region is to the right of the (almost vertical) line $m_h = 114$ GeV which is the direct LEP bound. Again there is an interesting tension between the SM like

lightest SUSY Higgs mass m_h which in case the Higgs mass goes up from the present limit to higher values requires heavier sfermion masses and/or lower $\tan \beta$, while a_μ prefers light sfermions and large $\tan \beta$. Another lower bound from LEP is the line characterizing $m_{\chi^\pm} > 104$ GeV. The CDM bound gives a narrow hyperbola like shaped band. The cosmology bound is harder to see in the $\tan \beta = 40$ plot, but it is the strip up the $\chi - \tilde{\tau}$ degeneracy line, the border of the excluded region (dark) which would correspond to a charged LSP which is not allowed. The small shaded region in the upper left is excluded due to no-EWSB there. The latter must be tuned to reproduce the correct value for M_Z . The $\tan \beta = 40$ case is much more favorable, since $(g_\mu - 2)$ selects the part of the (pre-Planck) WMAP strip which has a Higgs above the LEP bound. Within the CMSSM the discovery of the Higgs and the determination of its mass essentially is fixing m_0 and $m_{1/2}$. So far the very encouragingly looking pre-LHC setting.²¹

However, the Higgs boson discovery by ATLAS and CMS at the LHC revealing $m_H \simeq 125$ GeV dramatically changed this to situation as illustrated in the bottom panel of Fig. 7.20 [157]. The change of a single number m_H by about 9% was able to spoil the very attractive CMSSM scenario and the assumption of universal masses is ruled out as a candidate to accommodate the different phenomenological facts simultaneously.

As we have seen, the present LHC data have a quite dramatic impact on SUSY scenarios. The main lesson is that in constrained models like mSUGRA, CMSSM, NUHM1 or NUHM2 (see e.g. [196]) all allowed parameter points with $m_h \sim 125$ GeV are inconsistent with the observed $(g_\mu - 2)$ [197–199]. However, unconstrained SUSY extensions of the SM can be tuned to accommodate Δa_μ [145]. Only direct searches for sneutrino, chargino, smuon and neutralino states (or corresponding mass bounds) can lead to definite conclusions. The muon $g - 2$ can also be reconciled with the Higgs boson mass of 125 GeV by extending the MSSM so that extra contributions to the Higgs potential appear [200] (see also [201]). Also GMSB models remain in the game [202]. In SUSY scenarios there are plenty of possibilities to escape yesterdays constraints. Clearly, if the $(g_\mu - 2)$ discrepancy is taken serious, any scenario assuming universal squark–slepton masses is ruled out. Therefore acceptable global fits are possible only by detaching squarks and gluinos from the other electroweak superpartners. Such scenarios are the phenomenological pMSSM's [203] and a recent analysis adopting an 8 parameter pMSSM8 scenario: with one 3rd generation squark mass parameters $m_{\tilde{q}3}$, three slepton mass parameters $m_{\tilde{l}_{1,2,3}}$, a gaugino masses M_2 , the trilinear coupling A_t , Higgs sector parameters M_A and $\tan \beta$ and the Higgs mixing parameter μ , allows one to fit reasonably well all relevant observables [196, 198] (see also [158, 159]).

While the searches for SUSY states at the LHC have produced heavy constraints on colored superpartners the squarks and gluinos with limits of 1.5 TeV at 95% C.L., for the muon $g - 2$ a key problem remains. The searches for charginos ($\tilde{\chi}_1^\pm$), neutralinos ($\tilde{\chi}_2^0$), and sleptons ($\tilde{L}_L = \tilde{e}_L, \tilde{\mu}_L$) through direct electroweak production. These channels face the difficulty that their production cross sections are much lower, resulting

²¹For scenarios beyond the CMSSM see [169, 195].

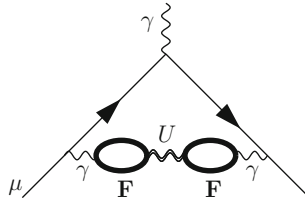


Fig. 7.21 Dark Photon U exchange providing a shift in a_μ . The dark photon is mixing with the photon through loops of very heavy fermions F charged under both the SM $U(1)_Y$ and the dark $U(1)_D$

in much weaker exclusion bounds. For the interesting mass ranges around the EW scale, the $\tilde{\chi}^\pm$ coannihilation (like $\chi \tilde{\tau}^\pm \rightarrow \tau^\pm \gamma / Z^0$, $\chi_1^0 \tilde{l}_1 \rightarrow \tau / \mu \gamma$, $\chi^0 \chi^0 \rightarrow f \bar{f}$ etc.) region exhibits a dense population of states (compressed spectrum) and thus is hard to be disentangled at the LHC (see e.g. [204, 205] and references therein). So possibly only a future e^+e^- collider will be able to resolve such possible opaque spots.

7.2.6 Dark Photon/Z and Axion Like Particles

With mass bounds on possible new particles going up, the $(g_\mu - 2)$ deviation becomes harder to accommodate given the scaling law (7.10), which requires relatively light new states of the order of the electroweak scale $v = 246$ GeV. But what about light hidden states which could have escaped detection? Certainly, such states should be neutral and couple to SM fermions only by mixing with the photon, similar to the ρ 's coupling to leptons. If the new state is light, with mass of order m_μ say, this “dark photon” can be very weakly coupling to muons and still accommodate Δa_μ . The dark photon or U boson was originally motivated by cosmology [206–208]. It mediates a force originating from an extra $U(1)_D$ local gauge group factor, which thus is neutral (dark) relative to the SM gauge interactions, but couples to SM fermions via mixing mediated by new very heavy charged fermions F (see Fig. 7.21). Such higher-order $\gamma - U$ effective interaction is modeled by the effective Lagrangian²²

$$\mathcal{L}_{\text{mix}} = -\epsilon F_Y^{\mu\nu} F_{\mu\nu D}, \quad (7.61)$$

where $F_Y^{\mu\nu}$ is the $U(1)_Y$ field strength tensor and $F_D^{\mu\nu}$ is $U(1)_D$ counterpart. The parameter ϵ represents the mixing strength and is the ratio of the dark and electromagnetic coupling constants. U boson searches typically can be studied in processes like $e^+e^- \rightarrow U\gamma$ and subsequent decay like $U \rightarrow e^+e^-$. The phenomenology of

²²It resembles the VMD type II Lagrangian (5.72), which describes the effective interaction of the neutral ρ meson with the photon. The role of the quarks is assumed to be played by new charged very heavy Fermions F .

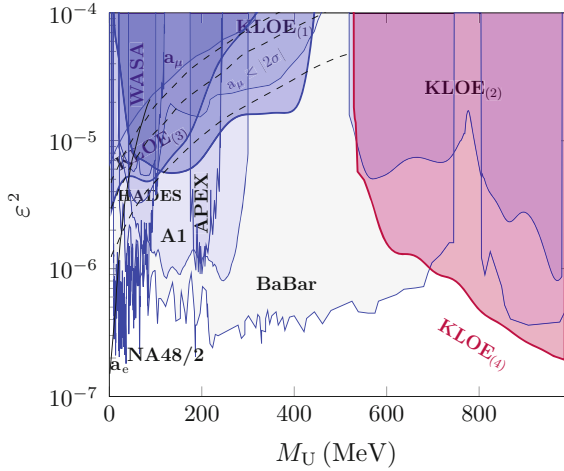
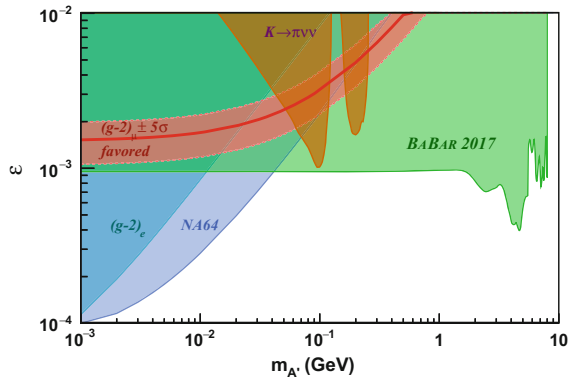


Fig. 7.22 Exclusion limits on the kinetic mixing parameter squared, ϵ^2 , as a function of the U boson mass. The red curve labeled KLOE(3) shows the exclusion boundary from [221, 222], while the curves labeled KLOE(1) and KLOE(2) indicate the previous KLOE results. Also shown are the exclusion limits provided by E141, E774, Apex, WASA, HADES, A1, BaBar, and NA48/2. The gray band delimited by the dashed white lines indicates the mixing level and m_U parameter space that could explain the discrepancy observed between the measurement and SM calculation of the muon $(g - 2)_\mu$. Courtesy of the KLOE-2 Collaboration. Reprinted from [222], <http://dx.doi.org/10.1016/j.physletb.2016.04.019>

Fig. 7.23 Exclusion plot from BaBar [218] ϵ as a function of the “dark Z boson” mass $m_{A'}$ together with the NA64 [220] contour. BaBar essentially rules out dark photons as a source of the muon $g - 2$ discrepancy. Courtesy of the BaBar Collaboration. Reprinted from [218]



such “dark Z” models has been analyzed in [209] (and references therein). Present limit are summarized in Figs. 7.22 and 7.23 along with the indirect limits from the measurements of $(g_e - 2)$ and $(g_\mu - 2)$ at 5σ , shown with dashed curves. Limits from direct searches are shown as shaded regions and solid curves: E141 [210], E774 [210], KLOE($\phi \rightarrow \eta U$, $U \rightarrow e^+e^-$) [211], Apex [212], WASA [213], HADES [214], A1 [215], KLOE($e^+e^- \rightarrow U\gamma$, $U \rightarrow \mu^+\mu^-$) [216], BaBar [217, 218], NA48/2 [219], NA64 [220] and KLOE($e^+e^- \rightarrow U\gamma$, $U \rightarrow e^+e^-$) [221].

The $g - 2$ contribution is given by

$$a_{\mu}^{\text{dark photon}} = \frac{\alpha}{2\pi} \epsilon^2 F(M_U/m_{\mu}) \quad (7.62)$$

where $F(x) = \int_0^1 2z(1-z)^2/[(1-z)^2+x^2z] dz$. For values of $\epsilon \sim 1-2 \times 10^{-3}$ and $M_U \sim 10-100$ MeV, this could explain the muon $g-2$ discrepancy. Searches for the dark photon signals are going on. Another scenario is the “dark Higgs” or “axion-like” one.²³ Contributions of axion-like particles to lepton dipole moments have been discussed in [226]. For a pseudoscalar (a) and scalar (s) axion the interaction Lagrangian considered reads

$$\mathcal{L} = \frac{1}{4} g_{a\gamma\gamma} a F^{\mu\nu} \tilde{F}_{\mu\nu} + g_{a\psi} a \bar{\psi} i \gamma_5 \psi + \frac{1}{4} g_{s\gamma\gamma} s F^{\mu\nu} F_{\mu\nu} + g_{s\psi} s \bar{\psi} \psi. \quad (7.63)$$

For recent account of the phenomenology see [227–229] and references therein. Contributions of a spin 0 axion-like particle (ALP) to lepton dipole moments, $g-2$ and EDMs, have been examined. Barr-Zee (BZ),²⁴ light-by-light and vacuum polarization loop effects yield (see also [126, 230, 231])

$$\begin{aligned} a_{\ell,a}^{\text{BZ}} &\simeq \left(\frac{m_{\ell}}{4\pi^2} \right) g_{a\gamma\gamma} y_{a\ell} \ln \frac{\Lambda}{m_a}, \\ a_{\ell,a}^{\text{LbL}} &\simeq 3 \frac{\alpha}{\pi} \left(\frac{m_{\ell} g_{a\gamma\gamma}}{4\pi} \right)^2 \ln^2 \frac{\Lambda}{m_a}, \\ a_{\ell,a}^{\text{VP}} &\simeq \frac{\alpha}{\pi} \left(\frac{m_{\ell} g_{a\gamma\gamma}}{12\pi} \right)^2 \ln \frac{\Lambda}{m_a}, \end{aligned}$$

from a light pseudoscalar ALP. The BZ and the LbL contributions are found to be capable of resolving the long-standing muon $g - 2$ discrepancy at the expense of relatively large ALP– $\gamma\gamma$ couplings. In fact, for a new pseudoscalar a the contribution to a_{μ} requires four parameters $g_{a\gamma\gamma}$, $y_{a\mu}$, m_a and Λ to be constrained, including two new mass scales not correlated to any known physics.

A pseudoscalar ALP would show up in $e^+e^- \rightarrow \gamma^* \rightarrow \gamma a$, analogous to $\pi^0\gamma$ production, which is characterized by the differential cross section

²³One of the biggest unsolved problems of the SM is the non-observation of strong CP violation which would be provided by a non-vanishing $\frac{\theta}{32\pi^2} G_{\mu\nu} \tilde{G}^{\mu\nu}$ term supplementing the QCD Lagrangian with $G_{\mu\nu}$ the gluon field strength tensor and $\tilde{G}^{\mu\nu}$ its dual. For non-zero quark masses this term predicts observable CP violation in strong interactions “the strong CP problem”. A fairly convincing answer could be provided by the Peccei-Quinn [223–225] extension of the SM by a $U(1)$ approximate global symmetry, which is spontaneously broken at some low scale f_a . The axion a is the pseudo Nambu-Goldstone boson of this symmetry of mass $m_a \ll \Lambda_{\text{QCD}}$.

²⁴The Barr-Zee diagram Fig. 7.9b, typically found in 2HDMs, here appears reduced to a one-loop diagram, where the lepton/quark (τ , b) triangle in the heavy mass limit is shrunk to a point, now the $g_{a\gamma\gamma}$ effective coupling. The h , A muon coupling here is $y_{a\ell}$.

$$\frac{d\sigma}{d\cos\theta} = \frac{\alpha}{64} g_{a\gamma\gamma}^2 \left(1 - \frac{m_a^2}{s}\right)^3 (1 + \cos^2\theta),$$

where θ is the angle between the ALP and the beam axis in the center-of-mass. As one believes to include all states $e^+e^- \rightarrow$ anything other than leptons, attributed to hadrons usually, within uncertainties it would just mean that the error estimates have been missing a substantial contribution. Bounds on such effects are provided by e^+e^- annihilation facilities like LEP, KLOE [222], CMD, SND, BaBar, Belle and BES. For details I refer to [226]. For a comprehensive review see [232].

These dark hidden states scenarios are particularly interesting because they can naturally bridge to the dark matter problem, one of the most mysterious missing parts of present day particle physics. However, some possibilities like the dark Z scenario are essentially ruled out by data already.

There are numerous other beyond the SM scenarios (see e.g. [233–235]), which exhibit new particles that could be contributing to the muon $g - 2$, and where parameters are limited by phenomenology. From the examples we have discussed we learned that it is by far not simple to obtain a 3 to 4 σ effects in a_μ . Most of the models yield contributions represented by diagrams either of the generic 1-loop type or by Barr-Zee type 2-loop diagrams only the masses and the couplings are specific as far as they are known. For little Higgs models the correction to a_μ have been computed in Ref. [236] and were found to be negligible $a_\mu^{LH} \approx 1 \times 10^{-10}$. An interesting new physics option are extra dimension scenarios, which however yield negative contributions of order $a_\mu^{(2)KK} \approx -1 \times 10^{-10}$ from the Kaluza-Klein excitations [237, 238]. Short summaries of these topics and more references may be found in [13].

7.3 Outlook on the Upcoming Experiments

Next generation muon ($g - 2$) experiments are going to happen soon. The two experiments under construction E989 at Fermilab [239–242] and E34 at J-PARC [243–245], both measure the difference between the spin precession and the cyclotron motion for a muon in a magnetic field. In order to reach a high precision experiments have to be setup such that the equation of motion

$$\boldsymbol{\omega}_a = \frac{e}{m_\mu c} \left(a_\mu \mathbf{B} - \left[a_\mu - \frac{1}{\gamma^2 - 1} \right] \frac{\mathbf{v} \times \mathbf{E}}{c^2} \right), \quad (7.64)$$

takes the form of a linear relation between the Larmor precession frequency and the homogeneous magnetic field:

$$\boldsymbol{\omega}_a = \frac{e}{m_\mu c} a_\mu \mathbf{B}. \quad (7.65)$$

The main point is to get rid of the effect from the electric field. This requires to work at magic γ by tuning the beam energy such that $a_\mu - 1/(\gamma^2 - 1) = 0$ or alternatively

to avoid any external electric field. The two experiments are complementary since they are using alternative possibilities. E989 is a traditional “magic γ ” experiment working with highly relativistic muons of magic energy $E \approx 3.1$ GeV. The muon energy determines the size of the storage ring diameter to about 14 m for a field of 1.5 Tesla, which is what can be reached in practice. So the ring of the BNL experiment can and actually is being used by the Fermilab experiment. The novel E34 experiment working with slow muons ($E \sim 300$ MeV) is a much smaller experiment (diameter of muon orbit 70 cm) working with a magnetic muon trap, with the main challenge to rule out any external electric field. Needless to say that the two approaches have very different systematic uncertainties. The E989 experiment will reduce the experimental error by a factor four to

$$\delta a_\mu = 16 \times 10^{-11}. \quad (7.66)$$

The BNL experimental error was statistics dominated, the Fermilab experiment will provide a factor of 20 more in statistics, more muons at higher injection rate. There will be much less background from pion decays by having a longer beam line which also helps improving the polarization. Further improvements concern a more uniform magnetic field, a more precise magnetic field calibration probe and a better centered beam using an improved focusing system. In addition, the signal processing will be improved by segmented detectors, by pileup and muon loss reduction (using better kickers), and by applying refined methods of analysis.

While the Fermilab experiment uses an approach which has been used and further developed since the 1970s in the CERN experiment, the J-PARC experiment is a new “from scratch” design, where the most critical part seems to be the shielding of electric fields. In contrast to the Fermilab experiment the J-PARC experiment works without the need of beam focusing. As a big advantage one should note that it is much easier to provide a homogeneous magnetic field when the fiducial volume is very much smaller. A shortcoming of an experiment with slow muons is that the degree polarization appears reduced, which evidently reduces the signal. Still, one can expect that a precision at the level of the BNL experiment can be reached such that the E34 experiment can provide a very important cross check of the BNL result.

In any case, the next generation experiments will scrutinize the presently seen deviation in $(g_\mu - 2)$. If the deviation is confirmed at least a 5σ significance will be reached. If the deviation would get reduced one would have one more precision test of the SM and a severe constraint on possible SM extensions. The E989 experiment is scheduled to begin data taking in early 2017 and a new measurement can be expected in about one year later.

7.4 Perspectives for the Future

The electron’s spin and magnetic moment were evidenced from the deflection of atoms in an inhomogeneous magnetic field and the observation of fine structure by optical spectroscopy [246, 247]. Ever since, magnetic moments and g -values of

particles in general and the $g - 2$ experiments with the electron and the muon in particular, together with high precision atomic spectroscopy, have played a central role in establishing the modern theoretical framework for particle physics: relativistic quantum field theory in general and quantum electrodynamics in particular, the prototype theory which developed further into the SM of electromagnetic, weak and strong interactions based on a local gauge principle and spontaneous symmetry breaking, with local gauge group $SU(3)_c \otimes SU(2)_L \otimes U(1)_Y$ spontaneously broken to $SU(3)_c \otimes U(1)_{em}$. Not only particle physics, also precision atomic physics and nuclear theory are based on relativistic QFT methods.²⁵

New milestones have been achieved not too long ago with the BNL muon $g - 2$ experiment together with the Harvard electron $g - 2$ experiment. Both experiments exploited all ingenuity to reach the next level of precision, and together with theory efforts maybe the next level of understanding of how it works. On the theory side, what we learned from the BNL experiment and what we will learn from the upcoming experiments depends a lot on how well we can corroborate the theoretical prediction. There is certainly common agreement that the hadronic light-by-light scattering contribution is the most problematic one, since no theoretically established method so far allowed us to calculate this contribution in a model independent way and with a satisfactorily controlled precision.

A very promising novel access of the HLbL is the data-driven dispersive approach advocated in [248–250]. The detailed theoretical framework has been developed in [251]. The method could improve the reliability of HLbL estimates dramatically, provided the data basis can be ameliorated by dedicated experiments of hadron production in light-by-light processes. More experimental information is also important for better modeling by effective theories. A typical example where data is missing is the $\pi^0\gamma^*\gamma^*$ form factor for both photons off-shell or direct light-by-light scattering in $e^+e^- \rightarrow e^+e^-\gamma^*\gamma^* \rightarrow e^+e^-\gamma\gamma$ or $e^+e^-\gamma^*\gamma$ with the virtual final state photon converting to a pair.

Another big hope for the long term future are the non-perturbative calculations of electromagnetic current correlators by means of lattice QCD [252–255]. This has to go in steps from two-point amplitudes (vacuum polarization and/or Adler function) to three-point form factors (non-perturbative effects in VVA correlators) and the four-point function linked to light-by-light scattering.

The hadronic vacuum polarization in principle may be substantially improved by continuing $e^+e^- \rightarrow$ hadrons cross-section measurements with higher precision. Substantial differences in the dominating $e^+e^- \rightarrow \pi\pi$ channel (at the few % level) between the KLOE results on the one hand and the BaBar result²⁶ on the other hand

²⁵Not to forget the role of QFT for other systems of infinite (large) numbers of degrees of freedom: condensed matter physics and critical phenomena in phase transitions (Ken Wilson 1971). The Higgs mechanism as a variant of the Ginzburg-Landau effective theory of superconductivity (1950) and the role QFT and the renormalization group play in the theory of phase transitions are good examples for synergies between elementary particle physics and condensed matter physics.

²⁶The KLOE and BaBar measurements have been obtained via the radiative return method which is a next to leading order approach. On the theory side one expects that the handling of the photon radiation requires one order in α more than the scan method for obtaining the same accuracy.

are persisting. Still, data taken with BaBar and Belle before the facilities were shut down are being analyzed. Fortunately, ongoing measurements with BES-III [260] and at the VEPP-2000 [261] facility are improving the data collection, such that the error of the HVP estimates continues to get smaller. Here, the ab initio lattice QCD results are getting closer to the data-driven dispersion relations results. Soon competitive results will be available and provide important cross checks.

Another previously disturbing problem, the deviations at the 10% level between e^+e^- -data and the isospin violations corrected hadronic τ -decay spectral functions, fortunately could be resolved in the meantime [7, 23]. If one corrects τ data for missing $\rho^0 - \gamma$ mixing, the τ data based results are in good agreement with the e^+e^- data based ones.

An interesting possibility in this respect is a novel approach to determine a_μ^{had} via a direct space-like measurement of $\alpha(-Q^2)$ in μe scattering as proposed in [262], recently (see also [263]). This approach completely avoids a number of problems one encounters with the standard time-like approach. In the latter case collecting hadron production data, applying radiative corrections to hadron production, vacuum polarization subtraction and problems related to thresholds and resonances are rather challenging. In contrast, a single space-like process like μe scattering is much simpler and the needed radiative corrections are under much better control of perturbation theory.

There is no doubt that performing doable improvements on both the theory and the experimental side allows to substantially sharpen (or diminish) the apparent gap between theory and experiment. Yet, even the present situation gives ample reason for speculations. No other experimental result has as many problems to be understood in terms of SM physics. One point should be noted in this context, however. An experiment at that level of accuracy, going one order of magnitude beyond any previous experiment, is a real difficult enterprise and only one such experiment has been performed so far. There is also a certain possibility to overlook some new problem which only shows up at higher precision and escaped the list of explicitly addressed problems by the experiment. It is for instance not 100% clear that what is measured in the experiment is precisely what theoreticians calculate. For example, it is believed that, because radiative corrections in $g - 2$ are infrared finite to all orders, real photon radiation can be completely ignored, in spite of the fact that we know that due to the electric interaction via charges a naive S -matrix in QED does not exist. Muons, like any charged particles, produce and absorb continuously photon radiation and therefore are dressed by a photon cloud which is thought not to affect the $g - 2$

(Footnote 26 continued)

Presently a possible deficit is on the theory side. What is urgently needed are full $O(\alpha^2)$ QED calculations, for Bhabha luminosity monitoring, μ -pair production as a reference and test process, and π -pair production in sQED as a first step and direct measurements of the final state radiation from hadrons. The CMD-3 and SND measurements take data at the same accelerator (same luminosity/normalization uncertainties) and use identical radiative corrections, such that for that part they are strongly correlated and this should be taken into account appropriately in combining the data. The present state-of-the-art event generator is PHOKHARA [256] for radiative return events and BABAYAGA [257] for the Bhabha channel (see also [258, 259]).

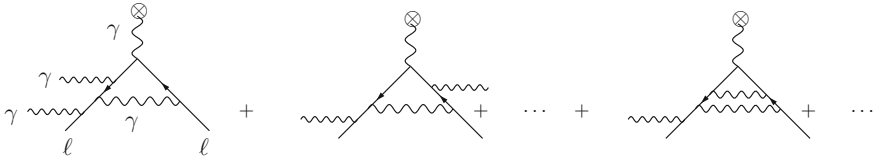


Fig. 7.24 Does soft real radiation affect the muon $g - 2$ measurement with highly relativistic muons? Could real radiation yield IR finite correction to the helicity flip amplitude? To LO (with one real photon) a helicity flip is not possible (Steinmann 2002)

measurement. The question has been addressed to leading order by Steinmann [264] (see also [265]). Possible effects at higher orders have not been estimated to my knowledge. Such possible multiple interactions with the external field usually are not accounted for, beyond the classical level. One also should keep in mind that the muon is unstable and the on-shell projection technique (see Sect. 3.5) usually applied in calculating a_μ in principle has its limitation. As $\Gamma_\mu \simeq 3 \times 10^{-16}$ MeV $\ll m_\mu \simeq 105.658$ MeV, it is unlikely that treating the muon to be stable could cause any problem. However, note that the Bargmann-Michel-Telegdi (BMT) equation is obtained by solving the Dirac equation (1st eq. below) as a relativistic one-particle problem with $A_\mu(x) \equiv 0$ only. What is missing, is a derivation of the BMT equation by solving the coupled QED field equations

$$\begin{aligned} (i\hbar\gamma^\mu\partial_\mu + Q_\ell\frac{e}{c}\gamma^\mu(A_\mu(x) + A_\mu^{\text{ext}}(x)) - m_\ell c)\psi_\ell(x) &= 0 \\ (\square g^{\mu\nu} - (1 - \xi^{-1})\partial^\mu\partial^\nu)A_\nu(x) &= -Q_\ell e\bar{\psi}_\ell(x)\gamma^\mu\psi_\ell(x), \end{aligned}$$

including the electromagnetic radiation field (see Fig. 7.24). Often it is argued that in case of the $(g_e - 2)$ one has an almost perfect agreement between theory and experiment, so no substantial effect can be missing. However, the measurement of a_e has been performed in a quantum regime where it is possible to essentially control single photon transitions. It is then conceivable that there are no problems with preparing quasi-isolated electron states. In the magic γ type $(g_\mu - 2)$ experiments the setup is not comparable at all and real radiation effects could be significant. In this context the J-PARC experiment [243–245] is a very promising novelty as it will work with ultra-cold muons instead of ultra-hot ones. So if radiation effects would play a role effects obviously would be very different.

Another question one may ask is whether the measurement of the magnetic field strength could not change the magnitude of the field by a tiny but non-negligible amount.²⁷ On the theory side one should be aware that the important 4-loop contribution has not been crosschecked by a completely independent calculation. Nonetheless, according to the best of our knowledge, the present status of both theory and experiment is as reflected by the systematic errors which have been estimated. Therefore most probably, the difference must be considered as a real indication of a missing piece on the theory side.

²⁷Of course such questions have been carefully investigated, and a sophisticated magnetic probe system has been developed by the E821 collaboration.

The anomalous magnetic moment of the muon is a beautiful example of “the closer we look the more we see”,²⁸ however, the efforts to dig even deeper into the structure of matter remains a big adventure also in future.

The $g - 2$ measurement is like a peek through the keyhole, you see at the same time an overlay of all things to a certain depth in one projection, but to make sure that what you see is there, you have to open the door and go to check. This will be a matter of accelerator physics, and an ILC would be the preferred and ideal facility to clarify the details. Of course and luckily, the LHC will tell us much sooner the gross direction new physics will go and is able to reach the physics at much higher scales. But, it is not the physics at the highest scales you see first in $g - 2$ as we learned in this book.

The Muon Storage Ring experiment on $(g_\mu - 2)$ and similarly the Penning Trap experiment on $(g_e - 2)$ are like microscopes which allow us to look into the subatomic world and the scales which we have reached with a_μ is about 100 GeV, i.e., the scale of the weak gauge bosons W and Z which is the LEP energy scale. As a_μ is effectively by a factor $(m_\mu/m_e)^2 \cdot \delta a_e^{\text{exp}}/\delta a_\mu^{\text{exp}} \simeq 19$ more sensitive to new heavy physics the mass scale which is tested by a_e is about $100/\sqrt{19} \sim 23$ GeV only, an energy region which we think we know very well as it has been explored by other means. We should keep in mind that the fact that the experiments measuring a_μ and a_e , respectively, hardly can be directly compared from the point of view of the experimental setup and the technical challenges they have to meet. This makes them two rather independent experimental entities. Therefore, the electron $(g_e - 2)$, if not be used to determine α , is the ideal complementary probe of the SM or its failure.

Remember that at LEP-I by electron–positron annihilation predominantly “heavy light” particles Z or at LEP-II predominantly W^+W^- -pairs have been produced, states which were produced in nature mostly in the very early universe.²⁹ Similarly, the Tevatron acted as a $t\bar{t}$ factory and the LHC reached the Higgs production stage and is hunting for the “new” in the TeV energy range, considerably above the SM spectrum.

Particle accelerators and storage rings are microscopes which allow us to investigate the nature in the subatomic range at distance $< 10^{-15}$ m and at the same time

²⁸ which is not always true, for example if we read a newspaper or if you read this book.

²⁹ An energy or an equivalent mass may always be translated into a temperature by means of the Boltzmann constant k which relates $1^\circ\text{K} \equiv 8.6 \times 10^{-5}\text{eV}$. Thus $T = E/k$ is the temperature of an event at energy E . As we know the universe expands and thereby cools down, thus looking at higher temperatures means looking further back in the history of the universe. By solving Friedmann’s cosmological equations with the appropriate equations of state backwards in time, starting from the present with a cosmic microwave background radiation temperature of 2.728°K and assuming the matter density to be the critical one $\Omega_{\text{tot}} = 1$, one may calculate the time at which temperatures realized at LEP with 100 to 200 GeV of center of mass energy where realized. This time is given by $t = 2.4/\sqrt{N(T)}$ (1 MeV/ kT)² sec, with $N(T) = \sum_{\text{bosons } B} g_B(T) + \frac{7}{8} \sum_{\text{fermions } F} g_F(T)$, the effective number of degrees of freedom excited at temperature T (see Eq. (19.43) in [266]). For LEP energies $m_b \ll kT \simeq M_W$ the numbers $g_{B/F}(T)$ counting spin, color and charge of bosonic/fermionic states in the massless limit include all SM particles except W^\pm, Z, H and t one obtains $N(T) = 345/4$. Thus LEP events happened to take place in nature $t \sim 0.3 \times 10^{-10}$ sec after the Big Bang for $T \sim 100$ GeV. With the LHC we reach $t_{\text{LHC}} \sim 1.66 \times 10^{-15}$ sec.

have the aim to directly produce new forms of matter, by pair creation, for example. The size of such machines is essentially determined by two parameters: the energy which determines the resolution $\lambda = hc/E_{c.m.} \simeq 1.2\text{GeV}/E_{c.m.}(\text{GeV}) \times 10^{-15} \text{ m}$ and the collision rate $\Delta N/\Delta t = L \times \sigma \simeq 10^{32} \sigma(\text{cm}^2)/\text{cm}^2 \text{ sec}$ (luminosity L as it has been reached LEP as an example). Usually projectiles must be stable particles or antiparticles like electrons, positrons and protons and antiprotons. The Muon Storage Ring experiments work with the rather unstable muons which are boosted to highly relativistic quasi-stable muons well selected in energy and polarization before they are injected into the storage ring. The ring in this case more acts as a detector rather than an accelerator as it usually does in the case of typical high energy machines. This allows to study the motion of the muons at incredible precision with very little background.

With the advent of the Large Hadron Collider (LHC) many things already have found a new direction, as we have mentioned several times. Experiments at the LHC take place under extreme conditions. At the LHC one is producing enormous amounts of events, billions per second, of which the overwhelming part of events are too complex to be understood and the interesting “gold plated” events which will tell us about new physics one has to dig out like “searching for a needle in a haystack”. Nevertheless, the physics accessible there hopefully will be found, which could tell us what we see in the $(g_\mu - 2)$ discrepancy. At LEP a big machine was able to measure about 20 different observables associated with different final states at the level of 0.1%. The strength of the LHC is that it is able to go far beyond what we have reached so far in terms of the energy scale. But as important, the LHC also is capable of producing milestones in precision physics, like the amazingly precise determination of the Higgs boson mass, the study of the Higgs bosons decay pattern or substantially improving the W and the top quark mass measurements. Other milestones have been achieved in rare processes, like the first observation of $B_s \rightarrow \mu^+ \mu^-$ events by the LHCb detector. The exclusion limits for many hypothetical new particles already have been moving up to much higher energies, such that several new physics scenarios could be ruled out.

The most remarkable event at the LHC has been the discovery of the Higgs particle. More surprising than its existence was the specific value of its mass found. This has to do with the stability bound of Higgs potential in the SM which has been addressed many times in the past. In 1995 the discovery of the top quark at the Tevatron also revived its mass and Hambye and Riesselmann (HR) in 1996 [267] (see also references therein) analyzed the stability bound as a function of the yet unknown Higgs boson mass, which is reproduced in Fig. 7.25. The Higgs boson mass at that time has been the only relevant parameter which was not yet known.³⁰ In a first 2-loop analysis, knowing m_t , HR estimated an upper bound of $M_H < 180 \text{ GeV}$, below which an extrapolation of the SM Higgs system up to the Planck scale $M_{\text{Planck}} \simeq 1.22 \times 10^{19} \text{ GeV}$ was possible within a small window. In fact the parameters m^2 and λ in the Higgs potential

³⁰A 95% CL lower bound of 77.5 GeV had been estimated by the LEP Collaborations [268] at that time.

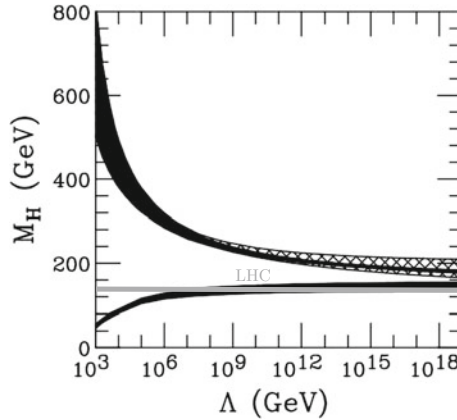


Fig. 7.25 The SM Higgs potential remains perturbative up to the Planck scale $\Lambda = M_{\text{Planck}}$, provided the Higgs boson is light enough (upper bound = avoiding a Landau pole) and the Higgs potential remains stable ($\lambda > 0$) if the Higgs boson is not too light. Parameters used: $m_t = 175[150 - 200]$ GeV ; $\alpha_s = 0.118$. The ATLAS and CMS discovery band has been overlaid. [Reprinted with permission from Ref. [267] <http://dx.doi.org/10.1103/PhysRevD.55.7255>. Copyright (1996) by the American Physical Society]

$$V(H) = \frac{m^2}{2} H^2 + \frac{\lambda}{24} H^4, \tag{7.67}$$

decide about the stability of the SM, maybe also about the stability of our universe. The fact that the Higgs mass falls quite precisely into that window is one of the most intriguing findings of recent particle physics.³¹

The Higgs mass just fits into the window of SM parameters which allows for a stable vacuum of the Higgs potential up to the Planck scale. Now all relevant parameters of the SM are known and we can predict how parameters of the SM evolve when we solve the RG up the Planck scale. This also applies to the effective Higgs boson mass, which can be predicted as a function of the renormalization scale μ :

$$m_{\text{Higgs,bare}}^2(\mu) = m_{\text{Higgs,ren}}^2 + \delta m^2(\mu)$$

$$\delta m^2(\mu) = \frac{M_{\text{Planck}}^2}{(16\pi^2)} C(\mu) ; C(\mu) = \left(\frac{5}{2} \lambda(\mu) + \frac{3}{2} g'^2(\mu) + \frac{9}{2} g^2(\mu) - 12 y_t^2(\mu) \right).$$

³¹Some analyses [270–272] claim a failure of vacuum stability i.e. $\lambda(\mu)$ has a zero and gets negative at about 10^9 GeV, and find a metastable vacuum instead, just missing stability. This have been questioned in [273] later. A final answer depend on the precise knowledge of the top Yukawa coupling and related problems have been analyzed in [274].

The bare mass here appears as a function of μ as we keep the observed mass as a boundary condition (bottom up approach).³² Taking into account the running of the SM parameters, at the Planck scale we obtain

$$m_{\text{eff}}^2 \sim \delta m^2 \simeq \frac{M_{\text{Planck}}^2}{32\pi^2} C(\mu = M_{\text{Planck}}) \simeq (0.0295 M_{\text{Planck}})^2 \simeq (3.6 \times 10^{17} \text{ GeV})^2,$$

and indeed the effective Higgs potential mass $m(M_{\text{Planck}})$ reaches a huge value which stays clearly below M_{Planck} , however. The non-vanishing quartically enhanced vacuum energy $V(0) = \langle V(H(x)) \rangle$ provides a cosmological constant density

$$\begin{aligned} \rho_{\Lambda \text{ bare}} &= \rho_{\Lambda \text{ ren}} + \delta\rho(\mu) \\ \delta\rho(\mu) &= \frac{M_{\text{Planck}}^4}{(16\pi^2)^2} X(\mu); \quad X(\mu) = \left(5\lambda + 3g^2 + 9g^2 - 24y_t^2\right). \end{aligned}$$

With SM running parameters at the Planck scale

$$\rho_{\text{eff}} \simeq \delta\rho \sim (1.28 M_{\text{Planck}})^4 \sim (1.57 \times 10^{19} \text{ GeV})^4.$$

Surprisingly, because the bosonic couplings and the top quark Yukawa have a different energy dependence both counterterms $\delta m^2(\mu)$ and $\delta\rho(\mu)$ vanish at a scale $\mu = \mu_{\text{CC}}$, which for the specific parameter set happens at

$$\mu_{\text{CC}} \approx 3.1 \times 10^{15} \text{ GeV} \tag{7.68}$$

clearly below the Planck scale again. There the effective mass changes sign and triggers the Higgs mechanism and the Higgs field acquires a non-vanishing VEV $\langle H(x) \rangle = v(\mu)$, which vanishes identically at higher energies $\mu > \mu_{\text{CC}}$.

Above the Higgs phase transition point μ_{CC} we start to see the bare theory i.e. a SM with its bare short distance effective parameters, so in particular a very heavy Higgs boson, which can be moving at most very slowly, and thus naturally satisfies the slow roll condition that the potential energy dominates the kinetic energy $\frac{1}{2}\dot{H}^2$. Note that the Higgs boson contributes to energy momentum tensor in Einstein's equations a pressure and energy density (\dot{H} the time derivative of H)

$$p = \frac{1}{2} \dot{H}^2 - V(H); \quad \rho = \frac{1}{2} \dot{H}^2 + V(H),$$

which then appear in Friedmann's cosmological solutions. As we approach the Planck scale (bare theory) the slow-roll condition $\frac{1}{2} \dot{H}^2 \ll V(H)$ comes into play as we

³²As we have consider the SM to exhibit at cutoff of the size of the Planck mass, we can also calculate the vacuum energy $V(0) \equiv \langle V(H) \rangle$ as a large but finite number. At high energies near the Planck scale the SM is in the symmetric phase i.e. $\langle H \rangle = 0$, while $\langle H^2 \rangle$ and $\langle H^4 \rangle$ are non-vanishing. This requires a Wick reordering of the potential [60] which is shifting the effective mass such that the coefficient proportional to λ changes from 2 to 5/2.

reach $p \approx -V(H)$, $\rho \approx +V(H)$ and hence $p = -\rho$, which is the equation of state of **DARK ENERGY**. The SM Higgs boson in the early universe provides a huge dark energy, which triggers inflation. That inflation has happened in the early universe is an established fact. The so called hierarchy problem is not a problem it is the solution which promotes the Higgs boson to be the natural candidate for the inflaton. This however only works if no SUSY or GUT is sitting in-between us and the Planck scale, and provided vacuum stability is holds within the SM.

Inflation tunes the total density to $\Omega_{\text{tot}} = 1$ or $\rho_{\text{tot}} = \rho_{\text{crit}} = (0.00216 \text{ eV})^4$. The presently observed dark energy density must be a part of it and actually has the value $\rho_{\Lambda} = (0.002 \text{ eV})^4$ the known 74% of the total.

Still, dark matter remains a mystery although there are a number of candidates like axions [275], or an extra $SU(4)$ version of QCD forming bound states which could provide bosonic dark matter [276]. So we hope we may soon add more experimentally established terms to the SM Lagrangian and extent our predictions to include the yet unknown. That's how it worked in the past with minimal extensions on theoretical grounds. Why this works so successfully nobody really knows. One observes particles, one associates with them a field, interactions are the simplest non-trivial products of fields (triple and quartic) at a spacetime point, one specifies the interaction strength, puts everything into a renormalizable relativistic QFT and predicts what should happen and it "really" happened essentially without exception. Maybe the muon $g - 2$ is the most prominent exception!

This book tried to shed light on the physics encoded in a single real number. Such a single number in principle encodes an infinity of information, as each new significant digit (each improvement should be at least by a factor ten in order to establish the next significant digit) is a new piece of information. It is interesting to ask, what would we know if we would know this number to infinite precision. Of course one cannot encode all we know in that single number. Each observable is a new view to reality with individual sensitivity to the deep structure of matter. All these observables are cornerstones of *one reality* unified self-consistently to our present knowledge by the knowledge of the Lagrangian of a renormalizable quantum field theory. Theory and experiments of the anomalous magnetic moment are one impressive example what it means to understand physics at a fundamental level. The muon $g - 2$ reveals the major ingredients of the SM and as we know now maybe even more.

On the theory part the fascinating thing is the technical complexity of higher order SM (or beyond) calculations of in the meantime thousands of diagrams which can only be managed by the most powerful computers in analytical as well as in the numerical part of such calculations. This book only gives little real insight into the technicalities of such calculation. Performing higher order Feynman diagram calculation could look like formal nonsense but at the end results in a number which experimenters indeed measure. Much of theoretical physics today takes place beyond the Galilean rules, namely that sensible predictions must be testable. For anomalous magnetic moment at least we still follow the successful tradition set up by Galileo Galilei, we definitely can check it, including all the speculations about it.

A next major step in this field of research would be establishing experimentally the electric dipole moment. This seems to be within reach thanks to a breakthrough in the

experimental techniques. The electric dipole moments are an extremely fine monitor for CP violation beyond the SM which could play a key role for understanding the origin of the baryon matter–antimatter asymmetry in the universe.

And now we are waiting for the new results on the muon $g - 2$ and for new data from the LHC to tell us where we go!

References

1. J. Bailey et al., Nucl. Phys. B **150**, 1 (1979)
2. G.W. Bennett et al., Muon $g-2$ Collab. Phys. Rev. D **73**, 072003 (2006)
3. T. Kinoshita, M. Nio, Phys. Rev. D **73**, 053007 (2006)
4. T. Aoyama, M. Hayakawa, T. Kinoshita, M. Nio, Phys. Rev. Lett. **109**, 111808 (2012)
5. S. Laporta, [arXiv:1704.06996](https://arxiv.org/abs/1704.06996) [hep-ph]
6. M. Knecht, EPJ Web Conf. **118**, 01017 (2016)
7. F. Jegerlehner, R. Szafron, Eur. Phys. J. C **71**, 1632 (2011)
8. F. Jegerlehner, EPJ Web Conf. **118**, 01016 (2016), [arXiv:1705.00263](https://arxiv.org/abs/1705.00263) [hep-ph]
9. J. Bijnens, E. Pallante, J. Prades, Phys. Rev. Lett. **75**, 1447 (1995) [Erratum-ibid. **75**, 3781 (1995)]; Nucl. Phys. B **474**, 379 (1996) [Erratum-ibid. **626**, 410 (2002)]
10. M. Hayakawa, T. Kinoshita, Phys. Rev. D **57**, 465 (1998) [Erratum-ibid. D **66**, 019902 (2002)]
11. M. Knecht, A. Nyffeler, Phys. Rev. D **65**, 073034 (2002)
12. K. Melnikov, A. Vainshtein, Phys. Rev. D **70**, 113006 (2004)
13. F. Jegerlehner, A. Nyffeler, Phys. Rep. **477**, 1 (2009)
14. A. Czarnecki, W.J. Marciano, A. Vainshtein, Phys. Rev. D **67**, 073006 (2003) [Erratum-ibid. D **73**, 119901 (2006)]; M. Knecht, S. Peris, M. Perrottet, E. de Rafael, JHEP **0211**, 003 (2002); E. de Rafael, *The muon $g-2$ revisited*, [arXiv:hep-ph/0208251](https://arxiv.org/abs/hep-ph/0208251)
15. S. Heinemeyer, D. Stöckinger, G. Weiglein, Nucl. Phys. B **699**, 103 (2004)
16. T. Gribouk, A. Czarnecki, Phys. Rev. D **72**, 053016 (2005)
17. C. Gnendiger, D. Stöckinger, H. Stöckinger-Kim, Phys. Rev. D **88**, 053005 (2013)
18. H.N. Brown et al., Muon ($g-2$) Collab. Phys. Rev. Lett. **86**, 2227 (2001)
19. F. Jegerlehner, Nucl. Phys. Proc. Suppl. **162**, 22 (2006)
20. K.G. Chetyrkin, J.H. Kühn, Phys. Lett. B **342**, 356 (1995); K.G. Chetyrkin, J.H. Kühn, A. Kwiatkowski, Phys. Rept. **277**, 189 (1996); K.G. Chetyrkin, J.H. Kühn, M. Steinhauser, Phys. Lett. B **371**, 93 (1996); Nucl. Phys. B **482**, 213 (1996); **505**, 40 (1997); K.G. Chetyrkin, R. Harlander, J.H. Kühn, M. Steinhauser, Nucl. Phys. B **503**, 339 (1997) K.G. Chetyrkin, R.V. Harlander, J.H. Kühn, Nucl. Phys. B **586**, 56 (2000) [Erratum-ibid. B **634**, 413 (2002)]
21. R.V. Harlander, M. Steinhauser, Comput. Phys. Commun. **153**, 244 (2003)
22. M. Benayoun, P. David, L. DelBuono, F. Jegerlehner, Eur. Phys. J. C **75**, 613 (2015)
23. M. Benayoun, P. David, L. DelBuono, F. Jegerlehner, Eur. Phys. J. C **72**, 1848 (2012) and references therein
24. M. Davier, A. Höcker, B. Malaescu, Z. Zhang, Eur. Phys. J. C **71**, 1515 (2011) [Erratum-ibid. C **72**, 1874 (2012)]
25. K. Hagiwara, R. Liao, A.D. Martin, D. Nomura, T. Teubner, J. Phys. G G **38**, 085003 (2011)
26. M. Davier et al., Eur. Phys. J. C **66**, 127 (2010)
27. M. Davier [BaBar Collab.], Nucl. Part. Phys. Proc. **260**, 102 (2015)
28. Z. Zhang, EPJ Web Conf. **118**, 01036 (2016)
29. K. Hagiwara, A.D. Martin, D. Nomura, T. Teubner, Phys. Lett. B **557**, 69; Phys. Rev. D **69**(2004), 093003 (2003)
30. S. Eidelman, F. Jegerlehner, Z. Phys. C **67**, 585 (1995); F. Jegerlehner, in *Radiative Corrections*, ed. by J. Solà (World Scientific, Singapore, 1999) p. 75

31. H. Leutwyler, Electromagnetic form factor of the pion, in *Continuous Advances in QCD 2002: Proceedings* ed. by K.A. Olive, M.A. Shifman, M.B. Voloshin (World Scientific, Singapore 2002) p. 646, [arXiv:hep-ph/0212324](https://arxiv.org/abs/hep-ph/0212324)
32. G. Colangelo, Nucl. Phys. Proc. Suppl. **131**, 185 (2004); *ibid.* **162**, 256 (2006)
33. B. Ananthanarayan, I. Caprini, D. Das, I.S. Imsong, Phys. Rev. D **93**, 116007 (2016)
34. V. M. Aulchenko et al. [CMD-2 Collab.], JETP Lett. **82**, 743 (2005) [Pisma Zh. Eksp. Teor. Fiz. **82**, 841 (2005)]; R. R. Akhmetshin et al., JETP Lett. **84**, 413 (2006) [Pisma Zh. Eksp. Teor. Fiz. **84**, 491 (2006)]; Phys. Lett. B **648**, 28 (2007)
35. M.N. Achasov et al. [SND Collab.], J. Exp. Theor. Phys. **103**, 380 (2006) [Zh. Eksp. Teor. Fiz. **130**, 437 (2006)]
36. A. Aloisio [KLOE Collab.], Phys. Lett. B 606 (2005) 12; F. Ambrosino et al. et al., KLOE Collab. Phys. Lett. B **670**, 285 (2009)
37. F. Ambrosino et al., KLOE Collab. Phys. Lett. B **700**, 102 (2011)
38. D. Babusci et al., KLOE Collab. Phys. Lett. B **720**, 336 (2013)
39. B. Aubert et al., [BABAR Collab.], Phys. Rev. Lett. **103**, 231801 (2009); J.P. Lees et al. Phys. Rev. D **86**, 032013 (2012)
40. M. Ablikim et al., BESIII Collab. Phys. Lett. B **753**, 629 (2016)
41. K. Hagiwara, A.D. Martin, D. Nomura, T. Teubner, Phys. Lett. B **649**, 173 (2007)
42. M. Davier, S. Eidelman, A. Höcker, Z. Zhang, Eur. Phys. J. C **27**, 497 (2003); Eur. Phys. J. C **31**, 503 (2003)
43. S. Eidelman, in Proceedings of the XXXIII International Conference on High Energy Physics, July 27–August 2 2006 (World Scientific, Moscow (Russia) to appear); M. Davier, Nucl. Phys. Proc. Suppl. **169**, 288 (2007)
44. R. Barate et al., [ALEPH Collab.], Z. Phys. C **76**, 15 (1997); Eur. Phys. J. C **4**, 409 (1998); S. Schael et al., [ALEPH Collab.], Phys. Rept. **421**, 191 (2005)
45. M. Davier et al., Eur. Phys. J. C **74**, 2803 (2014)
46. K. Ackersstaff et al., OPAL Collab. Eur. Phys. J. C **7**, 571 (1999)
47. S. Anderson et al., CLEO Collab. Phys. Rev. D **61**, 112002 (2000)
48. M. Fujikawa et al., Belle Collab. Phys. Rev. D **78**, 072006 (2008)
49. M. Davier, [arXiv:1612.02743](https://arxiv.org/abs/1612.02743) [hep-ph]
50. R.L. Garwin, D.P. Hutchinson, S. Penman, G. Shapiro, Phys. Rev. **118**, 271 (1960)
51. G. Charpak, F.J.M. Farley, R.L. Garwin, T. Muller, J.C. Sens, V.L. Telegdi, A. Zichichi, Phys. Rev. Lett. **6**, 128 (1961); G. Charpak, F.J.M. Farley, R.L. Garwin, T. Muller, J.C. Sens, A. Zichichi, Nuovo Cimento **22**, 1043 (1961)
52. G. Charpak, F.J.M. Farley, R.L. Garwin, T. Muller, J.C. Sens, A. Zichichi, Phys. Lett. B **1**, 16 (1962); Nuovo Cimento **37**, 1241 (1965)
53. F.J.M. Farley, J. Bailey, R.C.A. Brown, M. Giesch, H. Jöstlein, S. van der Meer, E. Picasso, M. Tannenbaum, Nuovo Cimento **45**, 281 (1966)
54. J. Bailey et al., Phys. Lett. B **28**, 287 (1968); Nuovo Cimento A **9**, 369 (1972)
55. J. Bailey [CERN Muon Storage Ring Collab.], Phys. Lett. B **55**, 420 (1975); Phys. Lett. B **67**, 225 (1977) [Phys. Lett. B **68**, 191 (1977)]; J. Bailey et al., CERN-Mainz-Daresbury Collab. Nucl. Phys. B **150**, 1 (1979)
56. R.M. Carey et al., Muon (g-2) Collab. Phys. Rev. Lett. **82**, 1632 (1999)
57. H.N. Brown et al., Muon (g-2) Collab. Phys. Rev. D **62**, 091101 (2000)
58. G.W. Bennett et al. [Muon (g-2) Collab.], Phys. Rev. Lett. **89**, 101804 (2002) [Erratum-*ibid.* **89**, 129903 (2002)]
59. G.W. Bennett et al., Muon (g-2) Collab. Phys. Rev. Lett. **92**, 161802 (2004)
60. F. Jegerlehner, Acta Phys. Polon. B **45**(6), 1215 (2014)
61. J.C. Pati, A. Salam, Phys. Rev. Lett. **31**, 661 (1973); Phys. Rev. D **8**, 1240 (1973); H. Georgi, S.L. Glashow, Phys. Rev. Lett. **32**, 438 (1974); H. Fritzsch, P. Minkowski, Ann. Phys. **93**, 193 (1975)
62. A. Galli, Nuovo Cim. A **106**, 1309 (1993)
63. J.R. Ellis, S. Kelley, D.V. Nanopoulos, Phys. Lett. B **249**, 441 (1990); *ibid.* **260**, 131 (1991); U. Amaldi, W. de Boer, H.Fürstenauf, Phys. Lett. B **260**, 447 (1991); P. Langacker, M.x. Luo. Phys. Rev. D **44**, 817 (1991)

64. LEP Electroweak Working Group (LEP EWWG), <http://lepewwg.web.cern.ch/LEPEWWG/plots/summer2006> [ALEPH, DELPHI, L3, OPAL, SLD Collab.s], *Precision electroweak measurements on the Z resonance*, Phys. Rept. **427**, 257 (2006), [arXiv:0509008](https://arxiv.org/abs/0509008) [hep-ex/0509008]; <http://lepewwg.web.cern.ch/LEPEWWG/Welcome.html>
65. J. Erler, P. Langacker, Electroweak model and constraints on new physics in W. M. Yao, et al., Particle Data Group. J. Phys. G **33**, 1 (2006)
66. G. Aad et al., ATLAS and CMS Collab. Phys. Rev. Lett. **114**, 191803 (2015)
67. M. Czakon, J. Gluza, F. Jegerlehner, M. Zralek, Eur. Phys. J. C **13**, 275 (2000)
68. F. Jegerlehner, Prog. Part. Nucl. Phys. **27**, 1 (1991)
69. Heavy Flavor Averaging Group (HFAG), <http://www.slac.stanford.edu/xorg/hfag/>, <http://www-cdf.fnal.gov/physics/new/bottom/bottom.html>
70. G. D'Ambrosio, G.F. Giudice, G. Isidori, A. Strumia, Nucl. Phys. B **645**, 155 (2002)
71. R.S. Chivukula, H. Georgi, Phys. Lett. B **188**, 99 (1987)
72. W. Altmannshofer, A.J. Buras, D. Guadagnoli, JHEP **0711**, 065 (2007)
73. I.B. Khriplovich, S.K. Lamoreaux, *CP Violation Without Strangeness: Electric Dipole Moments of Particles, Atoms and Molecules* (Springer, Berlin, 1997)
74. F.J.M. Farley et al., Phys. Rev. Lett. **93**, 052001 (2004); M. Aoki et al. [J-PARC Letter of Intent]: *Search for a Permanent Muon Electric Dipole Moment at the $\times 10^{-24}$ e·cm Level*, <http://www-ps.kek.jp/jhf-np/LOIlist/pdf/L22.pdf>
75. A. Adelmann, K. Kirch, [arXiv:hep-ex/0606034](https://arxiv.org/abs/hep-ex/0606034)
76. M. Aaboud et al., ATLAS collab. Phys. Lett. B **761**, 350 (2016)
77. V. Khachatryan et al., CMS collab. Phys. Rev. D **93**, 072004 (2016)
78. R. Schwienhorst [CDF and D0 Collab.s], [arXiv:1612.02311](https://arxiv.org/abs/1612.02311) [hep-ex]
79. B.E. Lautrup, A. Peterman, E. de Rafael, Phys. Rep. **3C**, 193 (1972)
80. J.P. Leveille, Nucl. Phys. B **137**, 63 (1978)
81. A. Freitas, J. Lykken, S. Kell, S. Westhoff, JHEP **1405**, 145 (2014) Erratum: [JHEP **1409**, 155 (2014)]
82. R. Van Royen, V.F. Weisskopf, Nuovo Cim. A **50**, 617 (1967) [Erratum-ibid. A **51**, 583 (1967)]
83. C.T. Hill, E.H. Simmons, Phys. Rep. **381**, 235 (2003) [Erratum-ibid. **390**, 553 (2004)]
84. E. Eichten, K. Lane, Phys. Lett. B **669**, 235 (2008)
85. R. Foadi, M.T. Frandsen, T.A. Ryttov, F. Sannino, Phys. Rev. D **76**, 055005 (2007); T.A. Ryttov, F. Sannino. Phys. Rev. D **76**, 105004 (2007)
86. F. Jegerlehner, Helv. Phys. Acta **51**, 783 (1978); F. Jegerlehner, The 'ether-world' and elementary particles, in *Theory of Elementary Particles* ed. by H. Dorn, D. Lüst, G. Weight (WILEY-VCH, Berlin, 1998) p. 386, [arXiv:hep-th/9803021](https://arxiv.org/abs/hep-th/9803021)
87. A. Czarnecki, W.J. Marciano, Phys. Rev. D **64**, 013014 (2001)
88. H. Okada, K. Yagyu, Phys. Rev. D **89**(5), 053008 (2014)
89. A.M. Baldini et al. [MEG Collab.], Eur. Phys. J. C **76**(8), 434 (2016)
90. R. Barbieri, L.J. Hall, Phys. Lett. B **338**, 212 (1994); R. Barbieri, L.J. Hall, A. Strumia, Nucl. Phys. B **445**, 219 (1995); J. Hisano, D. Nomura. Phys. Rev. D **59**, 116005 (1999)
91. W.C. Chiu, C.Q. Geng, D. Huang, Phys. Rev. D **91**, 013006 (2015)
92. P. Paradisi, EPJ Web Conf. **118**, 01026 (2016)
93. M. Lindner, M. Platscher, F.S. Queiroz, [arXiv:1610.06587](https://arxiv.org/abs/1610.06587) [hep-ph]
94. F. Jegerlehner, Nucl. Phys. B (Proc. Suppl.) **37**, 129 (1994)
95. P. Mery, S.E. Moubarik, M. Perrottet, F.M. Renard, Z. Phys. C **46**, 229 (1990)
96. W.M. Yao et al. [Particle Data Group], J. Phys. G **33**, 1 (2006); K.A. Olive et al., Chin. Phys. C **38**, 090001 (2014); C. Patrignani et al., Chin. Phys. C **40**(10), 100001 (2016)
97. LEP Electroweak Working Group (LEP EWWG), <http://lepewwg.web.cern.ch/LEPEWWG/lepww/tgc/>
98. D. Chang, W.F. Chang, C.H. Chou, W.Y. Keung, Phys. Rev. D **63**, 091301 (2001)
99. K.M. Cheung, C.H. Chou, O.C.W. Kong, Phys. Rev. D **64**, 111301 (2001)
100. F. Larios, G. Tavares-Velasco, C.P. Yuan, Phys. Rev. D **64**, 055004 (2001)
101. M. Krawczyk, Acta Phys. Polon. B **33**, 2621 (2002); PoS **HEP2005**, 335 (2006), [arXiv:0512371](https://arxiv.org/abs/0512371) [hep-ph/0512371]

102. K. Cheung, O.C.W. Kong, *Phys. Rev. D* **68**, 053003 (2003)
103. S.L. Glashow, S. Weinberg, *Phys. Rev. D* **15**, 1958 (1977)
104. A.G. Akeroyd, A. Arhrib, E.M. Naimi, *Phys. Lett. B* **490**, 119 (2000)
105. R. Santos, S.M. Oliveira, A. Barroso, [arXiv:hep-ph/0112202](https://arxiv.org/abs/hep-ph/0112202)
106. J.F. Gunion, H.E. Haber, *Phys. Rev. D* **67**, 075019 (2003)
107. I.F. Ginzburg, M. Krawczyk, *Phys. Rev. D* **72**, 115013 (2005)
108. F. Jegerlehner, *Acta Phys. Polon. B* **45**(6), 1167 (2014)
109. V. Ilisie, *JHEP* **1504**, 077 (2015)
110. C.-Y. Chen, S. Dawson, *Phys. Rev. D* **87**, 055016 (2013)
111. C.-Y. Chen, S. Dawson, M. Sher, *Phys. Rev. D* **88**, 015018 (2013)
112. J. Baglio, O. Eberhardt, U. Nierste, M. Wiebusch, *Phys. Rev. D* **90**, 015008 (2014)
113. O. Eberhardt, U. Nierste, M. Wiebusch, *JHEP* **1307**, 118 (2013)
114. X.D. Cheng, Y.D. Yang, X.B. Yuan, *Eur. Phys. J. C* **74**, 3081 (2014)
115. A. Barroso, P.M. Ferreira, R. Santos, M. Sher, J.P. Silva, [arXiv:1304.5225](https://arxiv.org/abs/1304.5225) [hep-ph]
116. S. Chang, S.K. Kang, J.P. Lee, K.Y. Lee, S.C. Park, J. Song, *JHEP* **1305**, 075 (2013)
117. G. Belanger, B. Dumont, U. Ellwanger, J. Gunion, S. Kraml, *Phys. Rev. D* **88**, 075008 (2013)
118. V. Barger, L.L. Everett, H.E. Logan, G. Shaughnessy, *Phys. Rev. D* **88**, 115003 (2013)
119. S. Chang, S.K. Kang, J.P. Lee, K.Y. Lee, S.C. Park, J. Song, *JHEP* **1409**, 101 (2014)
120. K. Cheung, J.S. Lee, P.-Y. Tseng, *JHEP* **1401**, 085 (2014)
121. A. Celis, V. Ilisie, A. Pich, *JHEP* **1312**, 095 (2013)
122. P.M. Ferreira, R. Guedes, J.F. Gunion, H.E. Haber, M.O.P. Sampaio, R. Santos, [arXiv:1407.4396](https://arxiv.org/abs/1407.4396) [hep-ph]
123. O.C.W. Kong, [arXiv:hep-ph/040210](https://arxiv.org/abs/1404.0210)
124. A. Cherchiglia, P. Kneschke, D. Stöckinger, H. Stöckinger-Kim, *JHEP* **1701**, 007 (2017)
125. A. Broggio, E.J. Chun, M. Passera, K.M. Patel, S.K. Vempati, *JHEP* **1411**, 058 (2014)
126. S.M. Barr, A. Zee, *Phys. Rev. Lett.* **65**, 21 (1990) [Erratum-ibid. **65**, 2920 (1990)]
127. M. Krawczyk, J. Zochowski, *Phys. Rev. D* **55**, 6968 (1997)
128. A. Wahab El Kaffas, P. Osland, O. Magne, OGREID, *Phys. Rev. D* **76**, 095001 (2007)
129. G.C. Branco, P.M. Ferreira, L. Lavoura, M.N. Rebelo, M. Sher, J.P. Silva, *Phys. Rept.* **516**, 1 (2012)
130. L. Basso, A. Lipniacka, F. Mahmoudi, S. Moretti, P. Osland, G.M. Pruna, M. Purmohammadi, *JHEP* **1211**, 011 (2012)
131. A. Pich, P. Tuzon, *Phys. Rev. D* **80**, 091702 (2009)
132. M. Aoki, S. Kanemura, K. Tsumura, K. Yagyu, *Phys. Rev. D* **80**, 015017 (2009)
133. E. Ma, Verifiable radiative seesaw mechanism of neutrino mass and dark matter. *Phys. Rev. D* **73**, 077301 (2006)
134. R. Barbieri, L.J. Hall, V.S. Rychkov, *Phys. Rev. D* **74**, 015007 (2006)
135. A. Crivellin, A. Kokulu, C. Greub, *Phys. Rev. D* **87**, 094031 (2013)
136. M. Misiak, M. Steinhauser, [arXiv:1702.04571](https://arxiv.org/abs/1702.04571) [hep-ph]
137. A. Dedes, H.E. Haber, *JHEP* **0105**, 006 (2001)
138. J.F. Gunion, *JHEP* **0908**, 032 (2009)
139. A. Arhrib, S. Baek, *Phys. Rev. D* **65**, 075002 (2002)
140. S. Heinemeyer, D. Stöckinger, G. Weiglein, *Nucl. Phys. B* **690**, 62 (2004); *ibid* **699**, 103 (2004)
141. K. Cheung, O.C.W. Kong, J.S. Lee, *JHEP* **0906**, 020 (2009)
142. J. Ellis, T. Hahn, S. Heinemeyer, K.A. Olive, G. Weiglein, *JHEP* **0710**, 092 (2007)
143. A. Crivellin, M. Ghezzi, M. Procura, *JHEP* **1609**, 160 (2016)
144. F. Jegerlehner, *Frascati Phys. Ser.* **54**, 42 (2012). [[arXiv:1203.0806](https://arxiv.org/abs/1203.0806) [hep-ph]]
145. P. Bechtle, H.E. Haber, S. Heinemeyer, O. Stål, T. Stefaniak, G. Weiglein, L. Zeune, *Eur. Phys. J. C* **77**, 67 (2017)
146. S. Heinemeyer, [arXiv:1612.08249](https://arxiv.org/abs/1612.08249) [hep-ph]
147. J. Wess, B. Zumino, *Nucl. Phys. B* **70**, 39 (1974); R. Haag, J. T. Lopuszanski, M. Sohnius, *Nucl. Phys. B* **88**, 257 (1975)

148. D.Z. Freedman, P. van Nieuwenhuizen, S. Ferrara, Phys. Rev. D **13**, 3214 (1976); S. Deser, B. Zumino. Phys. Lett. B **62**, 335 (1976)
149. H. P. Nilles, Phys. Rep. **110**, 1 (1984); H.E. Haber, G.L. Kane, Phys. Rep. **117**, 75 (1985); L. Ibáñez, Beyond the Standard Model, in CERN Yellow Report, CERN 92-06, 131–237 (1992)
150. E. Dudas, Y. Mambrini, A. Mustafayev, K.A. Olive, Eur. Phys. J. C **72**, 2138 (2012) Erratum: [Eur. Phys. J. C **73**, 2340 (2013)]
151. F. Jegerlehner, [arXiv:1305.6652](https://arxiv.org/abs/1305.6652) [hep-ph]; [arXiv:1503.00809](https://arxiv.org/abs/1503.00809) [hep-ph]
152. J.R. Ellis, J.S. Hagelin, D.V. Nanopoulos, K.A. Olive, M. Srednicki, Nucl. Phys. B **238**, 453 (1984)
153. C.L. Bennett et al., [WMAP Collab.], Astrophys. J. Suppl. **148**, 1 (2003); D.N. Spergel et al., [WMAP Collab.], Astrophys. J. Suppl. **148**, 175 (2003)
154. P.A.R. Ade et al., Planck collab. Astron. Astrophys. **594**, A13 (2016)
155. J.R. Ellis, K.A. Olive, Y. Santos, V.C. Spanos, Phys. Lett. B **565**, 176 (2003); Phys. Rev. D **71**, 095007 (2005)
156. H. Baer, A. Belyaev, T. Krupovnickas, A. Mustafayev, JHEP **0406**, 044 (2004); J. Ellis, S. Heinemeyer, K.A. Olive, G. Weiglein, *Indications of the CMSSM mass scale from precision electroweak data*, [arXiv:hep-ph/0604180](https://arxiv.org/abs/hep-ph/0604180)
157. J. Ellis, K.A. Olive, Eur. Phys. J. C **72**, 2005 (2012). doi:[10.1140/epjc/s10052-012-2005-2](https://doi.org/10.1140/epjc/s10052-012-2005-2)
158. G. Aad et al., [ATLAS Collab.], JHEP **1510**, 134 (2015)
159. V. Khachatryan et al., [CMS Collab.], JHEP **1610**, 129 (2016)
160. H.E. Haber, R. Hempfling, Phys. Rev. Lett. **66**, 1815 (1991); Y. Okada, M. Yamaguchi, T. Yanagida. Prog. Theor. Phys. **85**, 1 (1991)
161. P. Athron, J.h. Park, T. Stuedtner, D. Stöckinger, A. Voigt, JHEP **1701**, 079 (2017)
162. R. Hempfling, A.H. Hoang, Phys. Lett. B **331**, 99 (1994); H.E. Haber, R. Hempfling, A.H. Hoang, Z. Phys. C **75**, 539 (1997); S. Heinemeyer, W. Hollik, G. Weiglein, Phys. Lett. B **455**, 179 (1999); Phys. Rept. **425**, 265 (2006)
163. P. Bechtle, O. Brein, S. Heinemeyer, O. Stål, T. Stefaniak, G. Weiglein, K.E. Williams, Eur. Phys. J. C **74**, 2693 (2014)
164. P. Diessner, J. Kalinowski, W. Kotlarski, D. Stöckinger, Adv. High Energy Phys. **2015**, 760729 (2015)
165. S. Ferrara, E. Remiddi, Phys. Lett. B **53**, 347 (1974)
166. J.L. Lopez, D.V. Nanopoulos, X. Wang, Phys. Rev. D **49**, 366 (1994); U. Chattopadhyay, P. Nath. Phys. Rev. D **53**, 1648 (1996)
167. T. Moroi, Phys. Rev. D **53**, 6565 (1996) Erratum: [Phys. Rev. D **56**, 4424 (1997)]
168. S.P. Martin, J.D. Wells, Phys. Rev. D **64**, 035003 (2001)
169. D. Stöckinger, J. Phys. G: Nucl. Part. Phys. **34**, 45 (2007)
170. G. Degrassi, G.F. Giudice, Phys. Rev. D **58**, 053007 (1998)
171. M.A. Ajaib, B. Dutta, T. Ghosh, I. Gogoladze, Q. Shafi, Phys. Rev. D **92**, 075033 (2015)
172. S. Marchetti, S. Mertens, U. Nierste, D. Stöckinger, Phys. Rev. D **79**, 013010 (2009)
173. M. Bach, J.h. Park, D. Stöckinger, H. Stöckinger-Kim, JHEP **1510**, 026 (2015)
174. H. Fargnoli, C. Gnendiger, S. Paßehr, D. Stöckinger, H. Stöckinger-Kim, JHEP **1402**, 070 (2014)
175. T.F. Feng, X.Q. Li, L. Lin, J. Maalampi, H.S. Song, Phys. Rev. D **73**, 116001 (2006)
176. M.J. Ramsey-Musolf, S. Su, *Low Energy Precision Test of Supersymmetry*, [arXiv:hep-ph/0612057](https://arxiv.org/abs/hep-ph/0612057)
177. C.H. Chen, C.Q. Geng, Phys. Lett. B **511**, 77 (2001)
178. S. Heinemeyer, W. Hollik, G. Weiglein, L. Zeune, JHEP **1312**, 084 (2013)
179. M. Baak et al., Gfitter group. Eur. Phys. J. C **74**, 3046 (2014)
180. M. Aaboud et al., [ATLAS Collab.], [arXiv:1701.07240](https://arxiv.org/abs/1701.07240) [hep-ex]
181. O. Buchmueller et al., Phys. Lett. B **657**, 87 (2007)
182. S. Heinemeyer, W. Hollik, A.M. Weber, G. Weiglein, JHEP **0804**, 039 (2008)
183. O. Buchmueller et al., Phys. Rev. D **81**, 035009 (2010)

184. ALEPH, CDF, D0, DELPHI, L3, OPAL, SLD Collab.s, the LEP Electroweak Working Group, the Tevatron Electroweak Working Group and the SLD electroweak and heavy flavour groups, [arXiv:1012.2367](#) [hep-ex],
185. M. Awramik, M. Czakon, A. Freitas, G. Weiglein, Phys. Rev. D **69**, 053006 (2004)
186. S. Heinemeyer, W. Hollik, D. Stöckinger, A.M. Weber, G. Weiglein, JHEP **0608**, 052 (2006)
187. S. Bertolini, F. Borzumati, A. Masiero, G. Ridolfi, Nucl. Phys. B **353**, 591 (1991)
188. M. Misiak et al., Phys. Rev. Lett. **98**, 022002 (2007)
189. M. Misiak et al., Phys. Rev. Lett. **98**, 022002 (2007). M. Ciuchini, G. Degrossi, P. Gambino, G.F. Giudice, Nucl. Phys. B **534**, 3 (1998); G. Degrossi, P. Gambino, G.F. Giudice, JHEP **0012**, 009 (2000); M.S. Carena, D. Garcia, U. Nierste, C.E.M. Wagner, Phys. Lett. B **499**, 141 (2001)
190. D. Asner et al., The Heavy Flavor Averaging Group, [arXiv:1010.1589](#) [hep-ex]
191. R. Aaij et al., LHCb collab. Phys. Rev. Lett. **111**, 101805 (2013)
192. R. Barbieri, G.F. Giudice, Phys. Lett. B **309**, 86 (1993); M. Carena, D. Garcia, U. Nierste, C.E.M. Wagner. Phys. Lett. B **499**, 141 (2001)
193. L.F. Abbott, P. Sikivie, M.B. Wise, Phys. Rev. D **21**, 1393 (1980); M. Ciuchini, G. Degrossi, P. Gambino, G.F. Giudice. Nucl. Phys. B **527**, 21 (1998)
194. G. Isidori, P. Paradisi, Phys. Lett. B **639**, 499 (2006); G. Isidori, F. Mescia, P. Paradisi, D. Temes. Phys. Rev. D **75**, 115019 (2007)
195. S.P. Martin, J.D. Wells, Phys. Rev. D **67**, 015002 (2003)
196. K.J. de Vries, *Global fits of supersymmetric models after LHC Run I*, Thesis; K.J. de Vries [MasterCode Collab.], Nucl. Part. Phys. Proc. **273–275**, 528 (2016)
197. H. Baer, V. Barger, A. Mustafayev, Phys. Rev. D **85**, 075010 (2012)
198. P. Bechtle et al., Nucl. Part. Phys. Proc. **273–275**, 589 (2016)
199. J. Ellis, [arXiv:1504.03654](#) [hep-ph]
200. M. Endo, K. Hamaguchi, S. Iwamoto, T. Yoshinaga, JHEP **1401**, 123 (2014)
201. M. Endo, K. Hamaguchi, S. Iwamoto, N. Yokozaki, Phys. Rev. D **85**, 095012 (2012); M. Endo, K. Hamaguchi, S. Iwamoto, K. Nakayama, N. Yokozaki. Phys. Rev. D **85**, 095006 (2012)
202. G. Bhattacharyya, B. Bhattacharjee, T.T. Yanagida, N. Yokozaki, Phys. Lett. B **730**, 231 (2014)
203. A. Djouadi et al., [MSSM Working Group], [arXiv:hep-ph/9901246](#)
204. T. Nihei, L. Roszkowski, R. Ruiz de Austri, JHEP **0207**, 024 (2002)
205. B. Dutta et al., Phys. Rev. D **91**, 055025 (2015)
206. P. Fayet, Phys. Rev. D **75**, 115017 (2007)
207. M. Pospelov, Phys. Rev. D **80**, 095002 (2009)
208. D. Tucker-Smith, I. Yavin, Phys. Rev. D **83**, 101702 (R) (2011)
209. H. Davoudiasl, H.S. Lee, W.J. Marciano, Phys. Rev. D **85**, 115019 (2012)
210. J.D. Bjorken et al., Phys. Rev. D **80**, 075018 (2009)
211. D. Babusci et al., KLOE-2 collab. Phys. Lett. B **720**, 111 (2013)
212. S. Abrahamyan et al., APEX collab. Phys. Rev. Lett. **107**, 191804 (2011)
213. P. Adlarson et al., WASA-at-COSY collab. Phys. Lett. B **726**, 187 (2013)
214. G. Agakishiev et al., HADES collab. Phys. Lett. B **731**, 265 (2014)
215. H. Merkel et al., A1 collab. Phys. Rev. Lett. **112**, 221802 (2014)
216. D. Babusci et al., KLOE-2 collab. Phys. Lett. B **736**, 459 (2014)
217. J.P. Lees et al., BaBar collab. Phys. Rev. Lett. **113**, 201801 (2014)
218. J.P. Lees et al., [BaBar Collab.], [arXiv:1702.03327](#) [hep-ex]
219. J.R. Batley et al., NA48/2 collab. Phys. Lett. B **746**, 178 (2015)
220. D. Banerjee et al., NA64 collab. Phys. Rev. Lett. **118**, 011802 (2017)
221. A. Anastasi et al., KLOE collab. Phys. Lett. B **750**, 633 (2015)
222. A. Anastasi et al., KLOE-2 collab. Phys. Lett. B **757**, 356 (2016). doi:[10.1016/j.physletb.2016.04.019](#)
223. R.D. Peccei, H.R. Quinn, Phys. Rev. Lett. **38**, 1440 (1977)
224. S. Weinberg, Phys. Rev. Lett. **40**, 223 (1978)

225. F. Wilczek, Phys. Rev. Lett. **40**, 279 (1978)
226. W.J. Marciano, A. Masiero, P. Paradisi, M. Passera, Phys. Rev. D **94**, 115033 (2016)
227. C.Y. Chen, H. Davoudiasl, W.J. Marciano, C. Zhang, Phys. Rev. D **93**, 035006 (2016)
228. L. Wang, X.F. Han, Phys. Lett. B **739**, 416 (2014); X.F. Han, L. Wang, [arXiv:1701.02678](https://arxiv.org/abs/1701.02678) [hep-ph]
229. D. Zhuridov, Phys. Rev. D **93**, 035025 (2016)
230. M. Knecht, A. Nyffeler, M. Perrottet, E. De Rafael, Phys. Rev. Lett. **88**, 071802 (2002)
231. N.N. Achasov, A.V. Kiselev, JETP Lett. **75**, 527 (2002) [Pisma Zh. Eksp. Teor. Fiz. **75**, 643 (2002)]. doi:[10.1134/1.1500713](https://doi.org/10.1134/1.1500713)
232. J.I. Collar et al., New light, weakly-coupled particles, in *Fundamental Physics at the Intensity Frontier*, J.L. Hewett et al. (ed.). doi:[10.2172/1042577](https://doi.org/10.2172/1042577), [arXiv:1205.2671](https://arxiv.org/abs/1205.2671) [hep-ex]
233. S.J. Brodsky, S.D. Drell, Phys. Rev. D **22**, 2236 (1980)
234. H. Chavez, J.A. Martins, Simoes. Nucl. Phys. B **783**, 76 (2007)
235. X. Calmet, H. Fritzsche, D. Holtmannspotter, Phys. Rev. D **64**, 037701 (2001)
236. S.C. Park, J.h. Song, Phys. Rev. D **69**, 115010 (2004)
237. T. Appelquist, B.A. Dobrescu, Phys. Lett. B **516**, 85 (2001)
238. G. Cacciapaglia, M. Cirelli, G. Cristadoro, Nucl. Phys. B **634**, 230 (2002)
239. B.L. Roberts Nucl. Phys. B (Proc. Suppl.) **131**, 157 (2004); R.M. Carey et al., Proposal of the BNL Experiment E969, 2004; J-PARC Letter of Intent L17
240. J. Grange et al., [Muon g-2 Collab.], [arXiv:1501.06858](https://arxiv.org/abs/1501.06858) [physics.ins-det]
241. D.W. Hertzog, EPJ Web Conf. **118**, 01015 (2016)
242. G. Venanzoni, [Fermilab E989 Collab.], Nucl. Part. Phys. Proc. **273–275**, 584 (2016). doi:[10.1016/j.nuclphysbps.2015.09.087](https://doi.org/10.1016/j.nuclphysbps.2015.09.087); PoS EPS -HEP2015, 568 (2015)
243. N. Saito, J-PARC g-2/EDM collab. AIP Conf. Proc. **1467**, 45 (2012). doi:[10.1063/1.4742078](https://doi.org/10.1063/1.4742078)
244. H. Iinuma, J-PARC muon g-2/EDM collab. J. Phys. Conf. Ser. **295**, 012032 (2011). doi:[10.1088/1742-6596/295/1/012032](https://doi.org/10.1088/1742-6596/295/1/012032)
245. T. Mibe, [J-PARC g-2 Collab.], Nucl. Phys. Proc. Suppl. **218**, 242 (2011). doi:[10.1016/j.nuclphysbps.2011.06.039](https://doi.org/10.1016/j.nuclphysbps.2011.06.039)
246. W. Gerlach, O. Stern, Zeits. Physik **8**, 110 (1924)
247. G.E. Uhlenbeck, S. Goudsmit, Naturwissenschaften **13**, 953 (1925). Nature **117**, 264 (1926)
248. G. Colangelo, M. Hoferichter, B. Kubis, M. Procura, P. Stoffer, Phys. Lett. B **738**, 6 (2014)
249. V. Pauk, M. Vanderhaeghen, Phys. Rev. D **90**, 113012 (2014)
250. G. Colangelo, M. Hoferichter, M. Procura, P. Stoffer, JHEP **1409**, 091 (2014)
251. G. Colangelo, M. Hoferichter, M. Procura, P. Stoffer, JHEP **1509**, 074 (2015)
252. T. Blum, S. Chowdhury, M. Hayakawa, T. Izubuchi, Phys. Rev. Lett. **114**, 012001 (2015)
253. J. Green, O. Gryniuk, G. von Hippel, H.B. Meyer, V. Pascalutsa, Phys. Rev. Lett. **115**, 222003 (2015)
254. T. Blum, N. Christ, M. Hayakawa, T. Izubuchi, L. Jin, C. Lehner, Phys. Rev. D **93**, 014503 (2016)
255. J. Green, N. Asmussen, O. Gryniuk, G. von Hippel, H.B. Meyer, A. Nyffeler, V. Pascalutsa, PoS LATTICE **2015**, 109 (2016), [arXiv:1510.08384](https://arxiv.org/abs/1510.08384)
256. H. Czyż, J.H. Kühn, Eur. Phys. J. C **18**, 497 (2001); H. Czyż, A. Grzebińska, J.H. Kühn, G. Rodrigo, Eur. Phys. J. C **39**, 411 (2005); H. Czyż, Int. J. Mod. Phys. Conf. Ser. **35**, 1460402 (2014). doi:[10.1142/S2010194514604025](https://doi.org/10.1142/S2010194514604025)
257. C.M. Carloni Calame, C. Lunardini, G. Montagna, O. Nicrosini, F. Piccinini, Nucl. Phys. B **584**, 459 (2000); C.M. Carloni Calame, G. Montagna, O. Nicrosini, F. Piccinini, Nucl. Phys. Proc. Suppl. **131**, 48 (2004); C.M. Carloni Calame et al., Nucl. Phys. Proc. Suppl. **225–227**, 293 (2012)
258. S. Actis et al., Working group on radiative corrections and Monte Carlo generators for low energies. Eur. Phys. J. C **66**, 585 (2010)
259. F. Jegerlehner, K. Kołodziej, [arXiv:1701.01837](https://arxiv.org/abs/1701.01837) [hep-ph]
260. F.A. Harris, Nucl. Phys. Proc. Suppl. **162**, 345 (2006)
261. S. Eidelman, Nucl. Phys. Proc. Suppl. **162**, 323 (2006)
262. G. Abbiendi et al., Eur. Phys. J. C **77**, 139 (2017)

263. C.M. Carloni Calame, M. Passera, L. Trentadue, G. Venanzoni, *Phys. Lett. B* **746**, 325 (2015)
264. O. Steinmann, *Commun. Math. Phys.* **237**, 181 (2003)
265. A.B. Arbuzov, T.V. Kopylova, *Phys. Part. Nucl. Lett.* **11**, 339 (2014); *EPJ Web Conf.* **125**, 04005 (2016)
266. K.A. Olive, J.A. Peacock, Big-Bang cosmology, in S. Eidelman, et al., Particle Data Group. *Phys. Lett. B* **592**, 191–201 (2004)
267. T. Hambye, K. Riesselmann, *Phys. Rev. D* **55**, 7255 (1997). doi:[10.1103/PhysRevD.55.7255](https://doi.org/10.1103/PhysRevD.55.7255)
268. P. Bock et al., [ALEPH, DELPHI, L3 and OPAL Collab.s], CERN-EP-98-046, CERN-EP-98-46
269. M. Baak et al., Gfitter group collab. *Eur. Phys. J. C* **74**, 3046 (2014)
270. F. Bezrukov, MYu. Kalmykov, B.A. Kniehl, M. Shaposhnikov, *JHEP* **1210**, 140 (2012)
271. S. Alekhin, A. Djouadi, S. Moch, *Phys. Lett. B* **716**, 214 (2012)
272. D. Buttazzo et al., *JHEP* **1312**, 089 (2013)
273. A.V. Bednyakov, B.A. Kniehl, A.F. Pikelner, O.L. Veretin, *Phys. Rev. Lett.* **115**, 201802 (2015)
274. F. Jegerlehner, M.Yu. Kalmykov, B.A. Kniehl, *Phys.Lett. B* **722**, 123 (2013); *J. Phys. Conf. Ser.* **608**, 012074 (2015)
275. R.D. Peccei, *J. Korean Phys. Soc.* **29**, S199 (1996), [arXiv:hep-ph/9606475](https://arxiv.org/abs/hep-ph/9606475)
276. T. Appelquist et al., Lattice strong dynamics (LSD) collab. *Phys. Rev. D* **89**, 094508 (2014)

Appendix A

List of Acronyms

ABJ	Adler–Bell–Jackiw (anomaly)
AF	Asymptotic Freedom
AGS	Alternating Gradient Synchrotron
ALP	Axion-Like Particle
BHLS	Broken Hidden Local Symmetry (Lagrangian)
BMT	Bargmann–Michel–Telegdi (equation)
BNL	Brookhaven National Laboratory
BO	Betatron Oscillations
BPP	Bijnens–Pallante–Prades
BW	Breit–Wigner (resonance)
BZ	Barr-Zee (diagrams)
C	Charge-conjugation
CC	Charged Current
CDM	Cold Dark Matter
CERN	European Organization for Nuclear Research
CHPT	Chiral Perturbation Theory
CHPS	Colangelo–Hoferichter–Procura–Stoffer
CKM	Cabibbo–Kobayashi–Maskawa (quark flavor mixing matrix)
C.L.	Confidence Level
CM or c.m.	Center of Mass
CP	parity \times charge-conjugation (symmetry)
CPT	time-reversal \times parity \times charge-conjugation (symmetry)
CQM	Constituent Quark Model
CS	Callan–Symanzik (equation)
CVC	Conserved Vector Current
DESY	Deutsches Elektronen-Synchrotron
DIS	Deep Inelastic Scattering
DR	Dispersion Relation/Dimensional Regularization
DRA	Dispersion Relation Approach (to HLbL)
DSE	Dyson-Schwinger Equation
ED	Extra Dimension ($D - 4 \geq 1$)

EDM	Electric Dipole Moment
EFT	Effective Field Theory
em or e.m.	Electromagnetic
ENJL	Extended Nambu–Jona-Lasinio (model)
ENR	Extremely Narrow Resonances
EW	Electro Weak
EWSB	Electro–Weak Symmetry Breaking
exp (suffix/index)	experimental
FCNC	Flavor Changing Neutral Currents
FNAL	Fermi National Accelerator Laboratory (Batavia, Illinois, USA)
FP	Faddeev–Popov (Lagrangian)
F.P.	Finite Part (integral)
FSR	Final State Radiation
GF	Gauge Fixing (Lagrangian)
GMOR	Gell-Mann, Oakes and Renner (relation)
GS	Gounaris–Sakurai (parametrization)
h.c.	Hermitian conjugate
HFS	Hyper Fine Structure
HK	Hayakawa–Kinoshita
HKS	Hayakawa–Kinoshita–Sanda
HLbL	Hadronic Light-by-Light
HLS	Hidden Local Symmetry
H.O. or HO	Higher Order
HVP	Hadronic Vacuum Polarization
ILC	International Linear Collider (future e^+e^- collider)
IR	InfraRed
ISR	Initial State Radiation
J-PARC	Japan Proton Accelerator Research Complex
KEK	High Energy Accelerator Research Organization, KEK, Japan
KLN	Kinoshita–Lee–Nauenberg (theorem)
KN	Knecht–Nyffeler
KNO	Kinoshita–Nizic–Okamoto
LAMPF	Los Alamos Meson Physics Facility
LbL	Light-by-Light
L.D. or LD	Long Distance
LEP	Large Electron Positron (collider)
LFV	Lepton Flavor Violation
LHC	Large Hadron Collider
LL	Leading Logarithm
LMD	Leading Meson Dominance
LNC	Large N_c
L.O. or LO	Lowest Order (Leading Order)
LOSP	Lightest Observable SUSY Particle
LSP	Lightest Supersymmetric Particle
LSZ	Lehmann, Symanzik, Zimmermann (reduction formalism)

MS	Minimal Subtraction
μ SR	Muon Storage Ring
MV	Melnikov–Vainshtein
NC	Neutral Current
NJL	Nambu–Jona-Lasinio (model)
NLL	Next to Leading Logarithm
NLO	Next to Leading Order
NNLO	Next-to-Next Leading Order
NMR	Nuclear Magnetic Resonance
NP	New Physics/Non-Perturbative
$N\chi$ QM	Non-Local Chiral Quark Model
1PI	One Particle Irreducible
OPE	Operator Product Expansion
OZI	Okubo–Zweig–Iizuka (rule)
P	Parity (Space-reflection)
PCAC	Partially Conserved Axialvector Current
PMT	Photo Multiplier Tube
pQCD	perturbative QCD
PSI	Paul Scherrer Institut
PV	Pauk–Vanderhaeghen
QCD	Quantum Chromodynamics
QED	Quantum Electrodynamics
QFT	Quantum Field Theory
QM	Quantum Mechanics
QPM	Quark Parton Model
RG	Renormalization Group
RLA	Resonance Lagrangian Approach
S.D. or SD	Short Distance
SD	Standard Deviation ($1\text{ SD} = 1\sigma$)
SLAC	Stanford Linear Accelerator Center
SM	Standard Model (of electroweak and strong interactions)
sQED	scalar QED
SSB	Spontaneous Symmetry Breaking
SUGRA	Supergravity
SUSY	Supersymmetry
SVZ	Shifman–Vainshtein–Zakharov
T	Time-reversal
TDHM	Two Doublet Higgs Model
TEVATRON	TeV Proton-Antiproton Collider at FNAL
TFF	Transition Form Factor
the (suffix/index)	<u>theoretical</u>
UV	UltraViolet
VEV	Vacuum Expectation Value
VMD	Vector Meson Dominance
VP	Vacuum Polarization

VVA	Vector-Vector-Axialvector (amplitude)
WMAP	Wilkinson Microwave Anisotropy Probe
WT	Ward–Takahashi (identity)
WZW	Wess–Zumino–Witten (Lagrangian)
YM	Yang–Mills

¹

¹KLOE, CMD, SND, MD, BaBar, Belle, BES, E821, NA7, CLEO, CELLO, TASSO are names of detectors, experiments or collaborations see Table 5.1. ALEPH, DELPHI, L3 and OPAL are LEP detector/collaborations, CDF and D0 are TEVATRON detectors/collaborations.

Index

A

- Accelerator
 - mass bounds, 615
- Adler–function, 234, 346, 373, 376
- Adler–Bell–Jackiw anomaly, 152, 190, 192, 288, 296, 297, 300
- a_e
 - experiment, 599–603
 - experimental value, 173, 194, 197
 - lowest order result, 116
 - QED prediction, 196
 - SM prediction, 196
 - theory, 193–198
- α –representation, 72
- a_μ , 11
 - experiment, 171, 571–576
 - experimental value, 595, 611
 - hadronic contribution
 - leading, 185, 188, 380, 412, 611
 - subleading, 188, 427
 - hadronic light–by–light scattering, 183, 190, 434–505
 - lowest order result, 116
 - QED prediction, 199, 249–273
 - SM prediction, 611
 - theory, 199–200
 - weak bosonic corrections, 330
 - weak contribution, 13, 191–193, 333
 - weak fermionic corrections, 296
- Analyticity, 73, 76–78
- Anapole moment, 203
- Annihilation operator, 26, 50, 56
- Anomalous dimension, 126
- Anomalous precession, 583
- Anomaly
 - cancellation, 192, 296, 300, 456, 641
- Anti–screening, 150

- Anti–unitarity, 32, 33, 390
- Anticommutation relations, 26
- Appell function, 240
- Appelquist–Carazzone theorem, *see* decoupling theorem
- Asymptotic condition, 56
- Asymptotic freedom, 8, 127, 150, 369
- Axion, 663
- Axion-like particle, 663

B

- Baryon number
 - conservation, 152
 - violation, 615
- Betatron oscillations, 583
- Bhabha scattering, 352
- Bloch–Nordsieck prescription, 131, 362
- Bohr magneton, 6, 7, 170
- Boost, 24, 41
- Bose condensate, 37
- Bosons, 26
- Bremsstrahlung, 131, 379
 - collinear, 138
 - cuts, 350
 - hard, 136, 363
 - soft, 132, 363
 - exponentiation, 137

C

- C , *see* charge conjugation
- Cabibbo–Kobayashi–Maskawa matrix, *see* CKM matrix
- Canonical scaling, 127
- Casimir operator, 41
- Causality, 73, 76, 184

- Einstein, 31
 - Charge conjugation, 8, 31
 - Chiral
 - currents, 305, 307
 - fields, 28
 - perturbation theory, 151, 189, 305–308, 343, 385, 432
 - symmetry, 152
 - symmetry breaking, 305
 - Chisholm identity, 313
 - Chronological products, *see* time ordered products
 - CKM matrix, 35, 204, 288, 400, 588
 - Clausen function, 220
 - Cold Dark Matter, 615, 644–658
 - Color, 46, 148
 - factor, 99, 288
 - Commutation relations, 26
 - Computer algebra, 12
 - Confinement, 150
 - Conformal invariance, 375
 - Conformal mapping, 100, 391
 - Constituent quarks, 305, 310, 386–439, 455
 - masses, 296, 297, 439
 - model, 296
 - Counter terms, 61
 - Covariant derivative, 48, 143, 148
 - CP*
 - strong CP problem, 663
 - symmetry, 8
 - violation, 204, 288, 619
 - CPT*
 - symmetry, 8, 9
 - theorem, 9
 - Creation operator, 26, 50, 56
 - Cross section, 58, 60
 - bremsstrahlung, 132
 - data, 353
 - differential, 58
 - dressed, 349, 365
 - exclusive, 135, 352
 - inclusive, 132, 136, 350
 - total, 59, 350
 - undressed, 348, 365, 379
 - Crossing
 - particle–antiparticle, 55, 56
 - Current
 - conserved, 108, 306
 - dilatation, 121
 - electromagnetic, 32, 377
 - partially conserved, 306
 - Current–field identity, 431
 - Current quarks, 305
 - masses, 175, 297
 - Custodial symmetry, 620
 - Cutkosky rules, 226, 304
 - CVC, 306, 400
 - Cyclotron frequency, 172, 583
 - Cyclotron motion, 571
- D**
- D’Alembert equation, 27
 - Dark photon, 661
 - Decay law, 59
 - Decay rate, 58, 59
 - Decoupling, 250
 - Decoupling theorem, 120, 180
 - Deep inelastic scattering, 127
 - Detector acceptance, 350
 - Detector efficiency, 350
 - Dilatation current, 375
 - Dilogarithm, 236
 - Dipole moment, 5
 - non–relativistic limit, 205
 - Dirac
 - algebra, 28
 - helicity representation, 45
 - standard representation, 28
 - equation, 27, 163
 - field, 26, 31
 - matrices, 28
 - spinor, 27, 30
 - adjoint, 29
 - Dispersion integral, 184
 - Dispersion relation, 214, 215
 - Dispersive approach to HLbL, 495, 496, 500, 506
 - Dispersive approach, 145
 - Duality
 - quark–hadron, 355
 - quark–lepton, 296, 316
 - Dyson
 - series, 92
 - summation, 92, 217
 - Dyson–Schwinger equations, 54, 430
- E**
- Electric dipole moment, 5, 9, 10, 36, 171, 203, 204, 289, 586, 619
 - Electromagnetic
 - current, 32, 48, 216
 - hadronic, 377
 - vertex, 108
 - Electron
 - charge, 48

- EDM, 204
 - mass, 174
- Electron–positron annihilation, 184
- Elliptic integrals, 240
- e^+e^- cross-section, 353
 - in pQCD, 369–372
- e^+e^- -data, 184, 185, 345–359
 - flavor separation, 396
- Equation of motion, 163–168
- Error
 - correlations, 356
 - propagation, 356
- Euclidean field theory, 73
- Exclusion principle, 31
- Exponentiation
 - Coulomb singularity, 371
 - soft photon, 135, 137
- Extremely narrow resonances, 367

- F**
- Factorization, 135, 434
- Faddeev–Popov
 - ghosts, 149, 294
 - term, 149
- Fermion, 26
 - flavor, 99
 - loops, 53
 - strings, 52
- Feynman propagator, 50, 73
- Feynman rules, 50
 - EFT, 442
 - QCD, 149
 - QED, 51, 62
 - resonance Lagrangian, 442
 - sQED, 143
- Field
 - left-handed, 28
 - right-handed, 28
- Field strength tensor
 - Abelian, 26
 - dual, 300, 316
 - electromagnetic, 26
 - non-Abelian, 148, 301
- Final state radiation, 136, 379, 426, 548
- Fine structure constant, 60, 174
 - complex, 364
 - effective, 216, 221, 365, 392–394
- Flavor
 - conservation, 289
 - mixing, 288, 627
 - violation, 288
- Foldy–Wouthuysen transformation, 164

- Four-momentum, 27
 - conservation, 56
- Four-spinor, 27
- Fourier transformation, 27

- G**
- G-parity, 155
- g -factor, 6, 170, 580, 598, 602
- $\gamma\gamma \rightarrow \pi\pi$, 410, 500, 507, 519
- $\gamma - \rho$ mixing, 381, 407, 548
- Gauge
 - coupling, 48, 148, 289, 291, 628, 644
 - Feynman, 92, 105, 106, 112, 297
 - fixing, 149
 - group, 47, 148
 - invariance, 30, 47, 191, 204
 - Landau, 122, 123
 - parameter, 48, 149
 - symmetry, 204
 - unitary, 37, 192, 204, 294, 297
- Gauge boson
 - masses, 174, 291
- Gauge theory
 - Abelian, 8
 - non-Abelian, 8
- Gauge transformation
 - Abelian, 30
- $\gamma - Z$ mixing, 289, 327, 396
- Gell-Mann Low formula, 50
- Gluons, 46, 148, 183, 304, 315, 319, 370, 438
 - jet, 374
- GMOR relation, 308, 320
- Gordon identity, 114, 202
- Gram determinant, 91
- Grand Unified Theory, 616–617, 644
 - scale, 616, 643
- Green function, 49, 57
 - time ordered, 77

- H**
- Hadronic
 - light-by-light scattering, 420
- Hadronic contribution, 233
- Hadronic effects, 13
- Hadronization, 372
- Hadrons
 - baryons, 152
 - mesons, 151
 - spectrum, 151
- Handedness, *see* helicity
- Harmonic polylogarithms, 239

- Helicity, 11, 37, 301, 589, 590
 Helicity amplitudes, 507
 Hermitian transposition, 32
 Hierarchy problem, 645
 Higgs, 175, 193, 289, 294
 boson, 191, 287
 contribution, 295, 331, 332
 dark energy, 673
 ghosts, 204, 294
 inflation, 673
 mass, 175, 291, 331
 mechanism, 36, 150, 204
 phase, 204
 two doublet model, 641
 vacuum expectation value, 289, 641
 Hilbert space, 25
 HLS model, 412
 Hypergeometric functions, 240
- I**
- Imaginary time, 73, 75
 Infrared behavior, 127
 Infrared problem, 47, 55, 103, 113, 116
 Infrared safe, 139
 Initial state radiation, 136, 348, 361, 363, 379
 Integral
 box integral, 87
 contour, 74, 214
 form factor, 86
 self-energy, 86
 tadpole, 86
 Interaction
 electromagnetic, 47
 final state, 391
 hadronic, 183, 343
 strong, 148, 183
 weak, 191, 287
 Invariance
 C , P , T , 33
 dilatation, 121
 gauge, 47
 relativistic, 24
 scale, 375
 Isospin
 symmetry, 400
 symmetry breaking, 402, 548
 Isospin violation, 187
- J**
- Jarlskog invariant, 204
 Jets, 373
 gluon jet, 374
 Sterman-Weinberg formula, 139
- K**
- Kinematical singularity, 89, 91, 513
 Kinoshita-Lee-Nauenberg, 135, 379
 Klein-Gordon equation, 27, 78
- L**
- Λ QCD, 156
 Landau pole, 129, 130, 231
 large- N_c , 434
 large- N_c expansion, 152
 Larmor precession, 171
 Lattice QCD, 77, 151, 157, 345, 430, 666
 Lepton
 flavor violation, 288
 masses, 174
 quantum numbers, 288
 Lepton flavor violation, 627
 Lepton-quark family, 288, 296, 300
 Lepton number
 violation, 615
 Leptons, 192
 Leptoquarks, 616
 LHC
 Higgs discovery, 639
 mass bounds, 639
 Lifetime, 59
 Light-by-light scattering, 180
 hadronic, 189, 429-505
 pion-pole dominance, 453
 Logarithm
 leading, 120
 Sudakov, 135
 Long distance behavior, 127
 Lorentz
 boost, 29, 44, 164
 contraction, 24
 factor, 573
 force, 577, 582
 invariant distance, 24
 transformation, 24, 580
 LSZ reduction formula, 56, 302
 Luminosity, 59
- M**
- Magnetic susceptibility, 318, 454
 Magnetic moment, 5, 167
 anomalous, 116, 170
 Mandelstam

plane, 58
 variables, 58
 Meson
 exchange, 321
 pseudoscalar (spin 0), 154
 vector (spin 1), 154
 Minimal
 coupling, 47
 substitution, 143
 Minimal subtraction, 68, 70
 scheme, 86
 Momenta
 non-exceptional, 118
 μ^\pm -decay, 589
 Muon
 decay rate, 573, 590
 decay width, 290
 EDM, 205, 619
 life time, 4, 290
 magic momentum, 582
 magnetic precession, 580–582
 mass, 4, 174
 orbital motion, 577–580
 storage ring, 13, 172
 Muonium, 172
 hyperfine splitting, 597

N
 Nambu–Goldstone bosons, 306, 308, 385
 Nambu–Jona–Lasinio, 438
 Naturalness problem, 645
 Non-perturbative effects, 315, 355, 374
 Non-relativistic limit, 163–168, 205–206
 Nonet symmetry, 154
 Nuclear magnetic resonance, 172, 575

O
 Okubo–Zweig–Iizuka rule, 154
 Omnès representation, 389
 One-particle irreducible, 54, 91
 One loop integrals
 scalar, 85, 86
 Operator Product Expansion (OPE), 307,
 311–320, 355, 374, 480
 IPI, *see* one-particle irreducible
 Optical theorem, 184
 Orderparameter, 319
 Oscillations
 betatron, 580
 magnetron, 600
 OZI rule, 367

P
 Padé approximants, 273, 284
 Parity, 8, 24, 31
 violation, 288, 574
 Partial-wave expansion, 391
 Particles
 axion-like, 663
 Partons, 373
 Pauli
 equation, 163, 167
 matrices, 28
 term, 10, 66, 173
 PCAC, 306, 479
 Penning trap, 173, 599
 cylindrical, 602
 Perturbation expansion, 50
 π^\pm -decay, 588
 Pion
 charge radius, 386
 decay constant, 307
 form factor, 356, 360, 362, 363, 379,
 385–391
 Brodsky-Lepage, 452
 data, 353
 mass, 175
 scattering, 390
 lengths, 391
 phase shift, 390
 Pion transition form factors, 450
 $\pi\pi$ -scattering, 411
 lengths, 388, 392
 phase shifts, 388, 391
 Pitch correction, 586
 Planck scale, 641, 645
 Poincaré group, 24
 ray representation, 25
 Polarization, 29, 589, 590
 Polarization vector
 photon, 30
 Pole mass, 102
 Polylogarithms, 176
 Power-counting theorem
 Dyson, 118
 Weinberg, 118
 Precession frequency, 172

Q
 QED in external field, 163
 QPM, *see* quark parton model
 Quantum Chromodynamics (QCD)
 asymptotic freedom, 185, 351
 perturbative, 185, 351
 renormalization group, 155

running coupling, 183
 Quantum Electrodynamics, 4, 47–49
 Quantum field theory, 3, 23–47
 Quantum mechanics
 state space, 25
 time evolution, 25
 transition probability, 25
 Quark, 46, 148, 183, 192, 315, 370
 condensates, 306, 308, 319, 355, 374
 quantum numbers, 288
 Quark parton model, 183, 296, 370

R

Radial electric field correction, 584
 Radiation
 final state, 363, 379, 425, 548
 initial state, 136, 348, 361, 363, 379
 Radiative corrections, 91, 135, 169, 249
 Radiative return, 361, 381
 Regularization, 51, 60
 Renormalizability, 66, 148, 173, 192, 287, 625
 Renormalization, 51, 60
 charge, 108
 coupling constant, 61
 group, 120
 mass, 60
 MS scheme, 129
 on-shell scheme, 129
 scale, 87
 theorem, 61
 wave function, 61, 217
 Renormalization group, 120, 179, 298
 QCD, 155
 QED, 129
 SM, 157
 Representation
 finite dimensional, 41
 fundamental, 39, 288, 616
 non-unitary, 41
 unitary, 41
 Resonance, 185, 372
 Breit–Wigner, 146
 narrow width, 145
 ρ -meson, 185
 $\rho - \gamma$ mixing, 381, 407
 $\rho - \omega$ mixing, 353, 387, 548
 ρ -parameter, 290, 620, 650
 Rotation, 24, 41
 R-parity, 629, 645
 Running
 charge, 120, 217

 couplings, 157
 fine structure constant, 128
 mass, 120, 156
 Running α_s , 157, 183

S

Scaling, 126
 s -channel, 352, 360
 Schwinger–Dyson equations, 54, 430
 Self-energy
 lepton, 101
 photon, 91
 Short distance behavior, 125
 Shouten’s identity, 482
 S -matrix, 49, 55, 390
 Space-like, 221, 233, 346, 373
 Space-reflection, *see* parity
 Special Lorentz transformation, *see* boost
 Spectral condition, 26
 Spectral function, 222
 Spence function, 236
 Spin, 7, 36–47
 operator, 6, 167
 Spinor
 representation, 31
 Spontaneous symmetry breaking, 204, 319, 385
 Standard Model, 4, 13, 51, 287, 300
 Strong CP problem, 663
 Supersymmetry, 639–658

T

T , *see* time-reversal
 Tadpole, 95
 τ -data, 186, 400–402
 τ vs. e^+e^- puzzle, *see* resolved
 t -channel, 352
 Tensor
 antisymmetric, 25
 decomposition, 69
 energy momentum, 375
 integral, 88
 metric, 24
 permutation, 28
 vacuum polarization, 91
 Theorem
 Adler–Bardeen non-renormalization, 299, 304, 478
 Cauchy’s, 214
 CPT, 33
 decoupling, 120, 180, 250
 Furry’s, 53

- Kinoshita-Lee-Nauenberg, 135, 379
 - Noether's, 49
 - optical, 144, 184, 224, 227
 - Osterwalder-Schrader, 75
 - particle-antiparticle crossing, 31
 - renormalization, 61
 - spin-statistics, 31, 42
 - Watson's, 390
 - Thomas-Bargmann-Michel-Telegdi equation, 573
 - Thomas precession, 582
 - Thomson limit, 63, 217
 - Threshold, 98, 372
 - Time-like, 98
 - Time-reversal, 8, 24, 31
 - Time dilatation, 5, 172, 573
 - Time ordered products, 49
 - T -matrix, 56
 - element, 57
 - Translation, 24
 - Trilogarithm, 236
- U**
- Ultraviolet behavior, 125
 - Ultraviolet problem, 60, 64
 - Unitarity, 49, 184, 390
- V**
- Vacuum, 26
 - Vacuum expectation value, 37, 289
 - Vacuum polarization, 91, 100, 178, 216
 - hadronic, 183, 345-428
 - leptonic, 100, 218
 - Vacuum stability, 671
 - Van Royen-Weisskopf formula, 624
 - Vector-meson, 321, 379
 - dominance, 147, 189, 426
- Vertex**
- dressed, 53
 - electromagnetic, 53
- Vertex functions, 117**
- VMD model, 426, 430, 440, 469, 470**
- W**
- Ward-Takahashi identity, 64, 108
 - Wave function, 27
- Weak**
- gauge bosons, 191
 - hadronic effects, 296, 299
 - hypercharge, 288
 - interaction, 287
 - isospin, 288
- Wess-Zumino-Witten Lagrangian, 190, 309**
- Wick**
- ordering, 48, 50
 - rotation, 73, 74
- Wigner state, 26**
- Y**
- Yang-Mills
 - structure, 191
 - theory, 8, 287, 294
 - Yennie-Frautschi-Suura, 135, 137
- Yukawa**
- coupling, 37, 643, 644
 - interaction, 37, 642
- Z**
- Zeeman effect, 6
 - anomalous, 6
 - ζ -values, 236